WOODHEAD PUBLISHING SERIES IN ENERGY

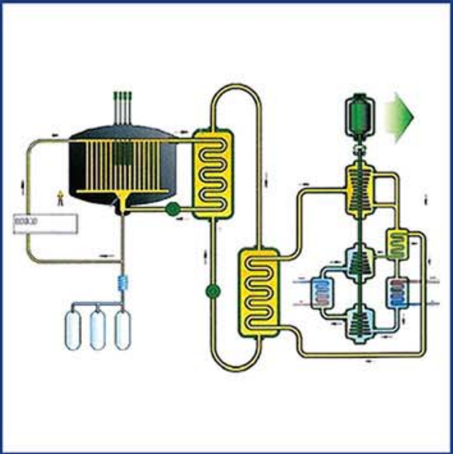

# Molten Salt Reactors and Thorium Energy

Edited by Thomas J. Dolan

WP
WOODHEAD
PUBLISHING

# Molten Salt Reactors and Thorium Energy

## Related titles

*Handbook of Small Nuclear Reactors*
(ISBN: 978-0-85709-851-1)

*Molten Salts Chemistry: From Lab to Applications*
(ISBN: 978-0-12-398538-5)

*Small Modular Reactors: Fad or Future*
(ISBN: 978-0-08-100252-0)

Woodhead Publishing Series in Energy

# Molten Salt Reactors and Thorium Energy

*Edited by*

## *Thomas J. Dolan*

ELSEVIER
WP
WOODHEAD
PUBLISHING
An imprint of Elsevier

Woodhead Publishing is an imprint of Elsevier
The Officers' Mess Business Centre, Royston Road, Duxford, CB22 4QH, United Kingdom
50 Hampshire Street, 5th Floor, Cambridge, MA 02139, United States
The Boulevard, Langford Lane, Kidlington, OX5 1GB, United Kingdom

Copyright © 2017 Elsevier Ltd. All rights reserved.

No part of this publication may be reproduced or transmitted in any form or by any means, electronic or mechanical, including photocopying, recording, or any information storage and retrieval system, without permission in writing from the publisher. Details on how to seek permission, further information about the Publisher's permissions policies and our arrangements with organizations such as the Copyright Clearance Center and the Copyright Licensing Agency, can be found at our website: www.elsevier.com/permissions.

This book and the individual contributions contained in it are protected under copyright by the Publisher (other than as may be noted herein).

**Notices**
Knowledge and best practice in this field are constantly changing. As new research and experience broaden our understanding, changes in research methods, professional practices, or medical treatment may become necessary.

Practitioners and researchers must always rely on their own experience and knowledge in evaluating and using any information, methods, compounds, or experiments described herein. In using such information or methods they should be mindful of their own safety and the safety of others, including parties for whom they have a professional responsibility.

To the fullest extent of the law, neither the Publisher nor the authors, contributors, or editors, assume any liability for any injury and/or damage to persons or property as a matter of products liability, negligence or otherwise, or from any use or operation of any methods, products, instructions, or ideas contained in the material herein.

**British Library Cataloguing-in-Publication Data**
A catalogue record for this book is available from the British Library

**Library of Congress Cataloging-in-Publication Data**
A catalog record for this book is available from the Library of Congress

ISBN: 978-0-08-101126-3 (print)
ISBN: 978-0-08-101243-7 (online)

For information on all Woodhead Publishing publications
visit our website at https://www.elsevier.com/books-and-journals

ELSEVIER
Book Aid
International
Working together
to grow libraries in
developing countries

www.elsevier.com • www.bookaid.org

*Publisher:* Joe Hayton
*Acquisition Editor:* Maria Convey
*Editorial Project Manager:* Charlotte Kent
*Production Project Manager:* Debasish Ghosh
*Designer:* Matt Limbert

Typeset by MPS Limited, Chennai, India

# Vision

We envision a world where almost every country has affordable molten salt reactors burning thorium, uranium, and spent fuel actinides, producing electricity, hydrogen, and desalinized water with no serious accidents.

# Contents

This page intentionally left blank

# List of Contributors

**Michel Allibert** Centre national de la recherche scientifique, Paris, France

**Charalampos Andreades** University of California, Berkeley, CA, United States

**A.S. Bakai** National Academy of Sciences of Ukraine, Kharkiv, Ukraine

**Stephen Boyd** Aufbau Laboratories, LLC, Blue Point, NY, United States

**Wayne Boyes** Steenkampskraal Thorium Limited, Centurion, South Africa

**Mariya Brovchenko** Institut de Radioprotection et de Sûreté Nucléaire, France

**Antonio Cammi** Polytechnic University of Milan, Milan, Italy

**Konrad Czerski** Institute for Solid-State Nuclear Physics, Berlin, Germany; University of Szczecin, Szczecin, Poland

**Zhimin Dai** Shanghai Institute of Applied Physics (SINAP), Shanghai, China

**Alexey M. Degtyarev** NRC "Kurchatov Institute", Moscow, Russia

**Sylvie Delpech** Centre national de la recherche scientifique, Paris, France

**Lindsay Dempsey** Generation Solutions, Auckland, New Zealand

**Leslie Dewan** Transatomic Power Corporation, Cambridge, MA, United States

**Valentino Di Marcello** Polytechnic University of Milan, Milan, Italy; Karlsruhe Institute of Technology—KIT, Karlsruhe, Germany

**Elling Disen** Norwegian Reactor facility at Halden, Norway

**Thomas J. Dolan** University of Illinois at Urbana-Champaign, Champaign, IL, United States

**I.V. Dulera** Bhabha Atomic Research Centre, Mumbai, Maharashtra, India

**Victor Dykin** Chalmers University of Technology, Gothenburg, Sweden

**Lyndon Edwards** Australian Nuclear Science and Technology Organisation (ANSTO), Sydney, Australia

**L. Berrin Erbay** Eskişehir Osmangazi University, Eskişehir, Turkey

**Yu S. Fedorov** Petersburg State Technological Institute (Technical University), St. Petersburg, Russia

**Charles Forsberg** Massachusetts Institute of Technology, Cambridge, MA, United States

**Kazuro Furukawa** High Energy Accelerator Research Organization, ITMSF, Tsukuba, Japan

**Stephan Gottlieb** Institute for Solid-State Nuclear Physics, Berlin, Germany

**Sophie Grape** Uppsala University, Uppsala, Sweden

**Eduardo D. Greaves** Simón Bolívar University, Caracas, Venezuela

**Carl Hellesen** Uppsala University, Uppsala, Sweden

**Fabian Herrmann** Institute for Solid-State Nuclear Physics, Berlin, Germany

**Daniel Heuer** Centre national de la recherche scientifique, Paris, France

**Yasuo Hirose** Retired, the former Institute of Research and Innovation, Kashiwa, Chiba-ken, Japan

**Zara Hodgson** National Nuclear Laboratory, Warrington, United Kingdom

**Boris Hombourger** Paul Scherrer Institute (PSI), Villigen, Switzerland; Laboratory for Reactor Physics and Systems Behaviour, EPFL Lausanne, Switzerland

**Armin Huke** Institute for Solid-State Nuclear Physics, Berlin, Germany

**Ahmed Hussein** Institute for Solid-State Nuclear Physics, Berlin, Germany; University of Northern British Columbia, Prince George, BC, Canada

**Yongjin Jeong** Ulsan National Institute of Science and Technology, Ulsan, Republic of Korea

**Lars Jorgensen** ThorCon Energy, Stevenson, WA, USA

**Motoyasu Kinoshita** The University of Tokyo, Tokyo, Japan; International Thorium Molten-Salt Forum, Yokohama, Japan

**Esben Klinkby** Seaborg Technologies, Copenhagen, Denmark

**Jan L. Kloosterman On behalf of the SAMOFAR consortium** Delft University of Technology, Delft, The Netherlands

**Jiří Křepel** Paul Scherrer Institute (PSI), Villigen, Switzerland

**John Kutsch** Thorium Energy Alliance, Harvard, IL, United States

**Vince Lackowski** Thorium Energy Alliance, Harvard, IL, United States

**Axel Laureau** Centre national de la recherche scientifique, Paris, France

**David LeBlanc** Terrestrial Energy, Inc., Oakville, ON, Canada

**Deokjung Lee** Ulsan National Institute of Science and Technology, Ulsan, Republic of Korea

**A.A. Lizin** State Research Centre—Research Institute of Atomic Reactors, Dimitrovgrad, Russia

**Lelio Luzzi** Polytechnic University of Milan, Milan, Italy

**Mark Massie** Transatomic Power Corporation, Cambridge, MA, United States

**Elsa Merle** Centre national de la recherche scientifique, Paris, France

**Andrey A. Myasnikov** NRC "Kurchatov Institute", Moscow, Russia

**Sergii Nichenko** Paul Scherrer Institute (PSI), Villigen, Switzerland

**Andreas Pautz** Paul Scherrer Institute (PSI), Villigen, Switzerland; Laboratory for Reactor Physics and Systems Behaviour, EPFL Lausanne, Switzerland

**Imre Pázsit** Chalmers University of Technology, Gothenburg, Sweden

**Thomas J. Pedersen** Copenhagen Atomics, Denmark

**Alessandro Pini** Polytechnic University of Milan, Milan, Italy

**Leonid I. Ponomarev** A.A. Bochvar High Technology Research Institute of Inorganic Materials, Moscow, Russia

**Michael Prasser** Paul Scherrer Institute (PSI), Villigen, Switzerland; Laboratory of Nuclear Energy Systems, ETH Zürich, Switzerland

**Magdi Ragheb** University of Illinois at Urbana-Champaign, Champaign, IL, United States

**A. Rama Rao** Bhabha Atomic Research Centre, Mumbai, Maharashtra, India

**Andrei Rineiski** Karlsruhe Institute of Technology, Germany

**Sean Robertson** Transatomic Power Corporation, Cambridge, MA, United States

**Cyril Rodenburg** Terrestrial Energy, Inc., Oakville, ON, Canada

**Götz Ruprecht** Institute for Solid-State Nuclear Physics, Berlin, Germany

**Laszlo Sajo-Bohus** Universidad Simón Bolívar, Caracas, Venezuela

**Raluca Scarlat** University of Madison-Wisconsin, Madison, WI, United States

**Troels Schønfeldt** Seaborg Technologies, Copenhagen, Denmark

**Ian Scott** Moltex Energy, London, United Kingdom

**Yoichiro Shimazu** University of Fukui, Fukui, Japan

**R.K. Sinha** Bhabha Atomic Research Centre, Mumbai, Maharashtra, India

**Stephen Smith** Transatomic Power Corporation, Cambridge, MA, United States

**Christopher Taylor** DNV GL, Oslo, Norway

**SAMOFAR consortium** Delft University of Technology, Delft, The Netherlands

**S.V. Tomilin** State Research Centre—Research Institute of Atomic Reactors, Dimitrovgrad, Russia

**Jan Uhlíř** Research Centre Řež, Husinec - Řež, Czech Republic

**Evgeny P. Velikhov** Kurchatov Institute, Moscow, Russia

**P.K. Vijayan** Bhabha Atomic Research Centre, Mumbai, Maharashtra, India

**Abdul Waris** Bandung Institute of Technology, Bandung, Indonesia

**Daniel Weißbach** Institute for Solid-State Nuclear Physics, Berlin, Germany

**Ritsuo Yoshioka** International Thorium Molten-Salt Forum (ITMSF), Yokohama, Japan

This page intentionally left blank

# Preface

There is growing awareness that nuclear energy is needed to complement intermittent energy sources and to avoid pollution from fossil fuels. Light-water reactors are complex, expensive, and vulnerable to core melt, steam explosions, and hydrogen explosions, so better technology is needed. Thorium energy and molten salt reactors could make nuclear energy safer and less expensive, so this book describes the current state of the art. It has the following sections:

- Motivation—why are we interested?
- Technical issues—reactor physics, thermal hydraulics, materials, environment, etc.
- Generic designs—thermal, fast, solid fuel, liquid fuel, etc.
- Specific designs—aimed at electrical power, actinide incineration, thorium utilization, etc.
- Worldwide activities in 23 countries.
- Conclusions.

This book is a collaboration of many authors from around the world. It can serve as a reference for engineers and scientists, and it can be used as a textbook for graduate students and advanced undergrads. We hope that leaders of governments and industry will recognize the great potential benefits and provide appropriate research support. Appendix A provides a list of about 450 abbreviations used in this field, since technical readers often suffer from excessive use of abbreviations (EUA). I am grateful to Professor Ritsuo Yoshioka, International Thorium Molten Salt Forum, for guidance in organizing and writing the book.

**Thomas J. Dolan**

杜蘭

# Introduction

# 1

*Thomas J. Dolan*
University of Illinois at Urbana-Champaign, Champaign, IL, United States

## Chapter Outline

The sections of this book are Motivation, Technical Issues, Generic Reactor Designs, Specific Reactor Designs, Research Activities, and Conclusions.

## 1.1 Need for MSR

Most nuclear power plants today use light water reactors (LWRs), which have the following disadvantages:

- New fuel must be added every 1–3 years, due to low fissile breeding by $^{238}$U;
- $^{239}$Pu in used fuel is a proliferation concern, whether it is reprocessed or disposed of as waste. (In this book we designate isotopes either as Pu-239 or as $^{239}$Pu);
- Temperature usually limits thermal efficiency to $<35\%$;
- High-pressure coolant → danger of pressure vessel failure;
- Danger of steam explosion (Chernobyl accident);
- High core radioactivity → large source term in accidents;
- High-level waste disposal problems;
- High core afterheat during accidents → danger of fuel melting (Three Mile Island, Fukkushima);
- Radiation damage limits to fuel and clad life;
- Potential hydrogen generation during accidents (Fukushima accident);

**Molten Salt Reactors and Thorium Energy. DOI: http://dx.doi.org/10.1016/B978-0-08-101126-3.00001-4**

- $^{135}$Xenon poisoning requires high excess core reactivity and careful power control;
- Present once-through fuel cycles utilize $<2\%$ of potential uranium energy and produce large volumes of high-level radioactive waste.

If successful, the molten salt reactor (MSR) could alleviate all of these problems. Water coolants and gaseous coolants must operate at high pressures, creating high stresses and failure risk. Liquid metal coolants can operate at low pressures, but can react chemically with water or air. Molten salt coolants can operate at low pressure with less chemical reactivity than liquid metals. Their operating temperatures are limited by compatibility with the structural material.

## 1.2 MSR origin and research curtailment

Eugene Wigner and Alvin Weinberg proposed a liquid fuel reactor in 1945, where aqueous water would be circulating with $^{233}$U-Th fuel. After Wigner left ORNL, Weinberg realized this concept as the Homogeneous Reactor Experiment (HRE) by using light water, and it generated 150 KW electricity in 1953. In parallel with the HRE development, ORNL investigated a nuclear application to aircraft jet engines. Since they needed 870°C temperature, solid fuel and water could not be adopted. They soon reached a design concept of liquid fuel reactor using molten salt instead of water, and they proposed molten fluoride, owing to the suggestion by Ray Briant. The Aircraft Reactor Experiment operated successfully for 100 hours in 1954, until it was shutdown. However, aerial refueling and ICBMs became available, and a nuclear-powered plane crash would have serious consequences.

Uranium-235 was thought to be in too short a supply for the anticipated nuclear build, and fissile fuel breeding was judged necessary. Alvin Weinberg, H.G. MacPherson, and their colleagues recognized that MSRs could be used to breed U-233 from thorium, greatly extending the nuclear fuel supply. A Molten Salt Reactor Experiment (MSRE) using Hastelloy N structure (Table 1.1) with LiF-BeF2 (“FLiBe”) salt and $UF_4$ fuel (U-235) operated successfully at ORNL from 1965–1969 (MacPherson, 1985; Weinberg, 1994).

It was also operated using U-233 fuel (derived from thorium elsewhere) in 1969. The MSRE operated 87% of the time during 15 months’ operation, paving the way for a Molten Salt Breeder Reactor (MSBR) proposal. In spite of the MSRE success, two other concepts had more political support in 1972:

- Admiral Hyman Rickover led the US program to develop LWRs for nuclear submarines. After the *Nautilus* nuclear submarine operated successfully in 1955, a commercial nuclear power plant of similar design was demonstrated at Shippingport, PA, in 1957. Then LWRs became popular for both civilian nuclear power and military applications.
- President Nixon, Republicans, and Democrats all supported development of the $U^{238}$-$Pu^{239}$ Liquid Metal Fast Breeder Reactor concept, rather than the $Th^{232}$-$U^{233}$ MSBR advocated by ORNL. The Clinch River Breeder Reactor project was begun.

**Table 1.1** **Nominal components of Hastelloy N, weight percent (Haynes International, 2002)**

| | |
|---|---|
| Nickel | 71 |
| Molybdenum | 16 |
| Chromium | 7 |
| Iron | 5 |
| Silicon | ≤ 1 |
| Manganese | ≤ 0.8 |
| Carbon | ≤ 0.08 |
| Cobalt | ≤ 0.20 |
| Copper | ≤ 0.35 |
| Tungsten | ≤ 0.50 |
| Aluminum + titanium | ≤ 0.35 |

The Government terminated the MSRE program, in spite of advice from Weinberg. "It was a triumph of Rickover's worldview of unrelenting competition between implacable nuclear-armed enemies over Weinberg's vision of a peaceful and prosperous age fueled by beneficial, broadly shared nuclear technology, specifically using thorium." (Martin, 2012).

Chapter 11, Liquid fuel, thermal neutron spectrum reactors provides more details of the ORNL research. Nowadays several organizations are helping to promote MSRs thorium energy.

## 1.3 MSR activities

The International Thorium Energy Organization was established "to make Thorium Energy a reality through a thriving community fostering innovation, cooperation and competition." It is a nonprofit, independent international organization, which holds Thorium Energy Conferences (London 2010; Washington 2012; Shanghai 2012; Geneva 2013; Mumbai 2015) (http://www.itheo.org/).

Ritsuo Yoshioka organized the International Thorium Molten Salt Forum, which provides information and advice about thorium research (http://msr21.fc2web.com/english.html).

The Thorium Energy Alliance, organized by John Kutsch in the USA, also promotes MSR research and holds annual conferences (www.thoriumenergyalliance.com/).

The Generation-IV International Forum started with over 100 reactor concepts and chose 6 for further detailed study, including a molten salt-cooled reactor. Currently there are two types, one with molten salt fuel, and the other, with solid fuel (Serp, 2014).

The Alvin Weinberg Foundation in London promotes research, organizes activities, and provides information about MSR (http://www.the-weinberg-foundation.org/).

Many groups are studying MSR reactor designs and prospects, including Terrestrial Energy, LFTR Energy, SAMOFAR, Transatomic Power, Copenhagen Atomics, Seaborg, ThorCon, Moltex Energy, Martingale, Dual Fluid Reactor, and universities.

India has large thorium resources, which motivates their MSR research. India developed both nuclear weapons and civilian nuclear power. The three-stage plan is (Martin, 2012):

1. Production of Pu-239 in pressurized heavy water reactors;
2. Using the Pu-239 to fuel thorium → U-233 breeders;
3. Advanced heavy water reactors operating on the thorium/U-233 fuel cycle.

The Bhabha Atomic Research Center in Mumbai hosted the 15th Thorium Energy Conference in October, 2015.

China has 500 people working on MSR. They are building a 2 MWth MSR solid fuel reactor cooled with molten salt (2017) and a 2 MWth liquid fuel MSR (2020) (Chinese Academy of Sciences, 2012).

Current progress in many countries is described in Chapter 25, Worldwide activities.

## 1.4 Fissile fuels

The term “fissile” refers to materials that can sustain chain reactions initiated by low-energy neutrons. The main fissile isotopes are $^{233}$U, $^{235}$U, and $^{239}$Pu. Natural uranium contains 0.72% U-235 and the rest is U-238, which is nonfissile. Isotopic separation processes are used to “enrich” the U-235 fraction to 3–5% for LWR power plant fuels, and research reactors may use up to 20% enrichment, limited by the nonproliferation treaty. Pu-239 is produced by neutron absorption in U-238 via the following reaction chain (Moir and Manheimer, 2014):

$$n + {}^{238}\mathrm{U} \rightarrow {}^{239}\mathrm{U} - \frac{\beta^{-}}{24\,\mathrm{min}} - > {}^{239}\mathrm{Np} - \frac{\beta^{-}}{2.4d} - > {}^{239}\mathrm{Pu} \ \left[{}^{238}\mathrm{U}(n,\gamma + 2\beta^{-}){}^{239}\mathrm{Pu}\right]$$

where the symbols $(n, \gamma)$ mean that a neutron is absorbed and a gamma ray is emitted; $\beta$ indicates beta decay (electron emission), and the 24 minutes and 2.4 days are the half-lives of the two beta decays. The brackets show the condensed notation for this reaction.

Similarly, fertile $^{232}$Th can breed fissile $^{233}$U by the reactions

$$n + {}^{232}\mathrm{Th} \rightarrow {}^{233}\mathrm{Th} - \frac{\beta^{-}}{24\,\mathrm{min}} - > {}^{233}\mathrm{Pa} - \frac{\beta^{-}}{2.4d} - > {}^{233}\mathrm{U} \ \left[{}^{232}\mathrm{Th}(n,\gamma + 2\beta^{-}){}^{233}\mathrm{U}\right]$$

$^{238}$U and $^{232}$Th are called “fertile,” meaning that they can be transmuted into fissile fuels by neutron absorption followed by two beta decays. In some cases the $^{233}$Pa may undergo the following reaction before it decays by beta emission:

$$^{233}\mathrm{Pa} + \mathrm{fast}\ n \rightarrow {}^{232}\mathrm{Pa} + n + n \ \ [{}^{233}\mathrm{P}a(n, 2n){}^{232}\mathrm{Pa}]$$

Then the $^{232}$P decays to $^{232}$U. The decay chain of $^{232}$U emits a 2.6 MeV gamma ray, which makes it difficult to handle. For a breeder reactor the $^{233}$Pa may be removed from the blanket salt to prevent the $(n,2n)$ reaction. On the other hand, for nonproliferation reasons it may be desirable to promote the ($n$,2$n$) reaction and generation of $^{232}$U to “spike” the uranium fuel, making it less suitable for weapons use.

The simplest reactor could have a core containing both fissile and fertile materials dissolved in a molten salt. Excess neutrons from fission would be used to sustain the chain reaction and to breed more fissile fuel.

## 1.5 Thorium fuel advantages

Approaches to a thorium reactor include:

- Molten thorium salt fuel, such as $ThF_4$ or $ThCl_4$;
- A driven subcritical molten salt system using fusion or accelerator-generated neutrons;
- Use of a graphite moderated, He cooled pebble bed reactor;
- The use of a seed and blanket solid fuel with an LWR cycle.

This book discusses the first two, because they involve molten salt.

The $Th^{232}-U^{233}$ *breeder* fuel cycle has the following advantages over the $U^{238}-Pu^{239}$ *breeder* fuel cycle:

- Th$^{232}$ is about four times as abundant as U$^{238}$ in the earth’s crust (Chapter 9: Environment, waste, and resources).
- Almost all the thorium can be converted to fissile U-233, but it is more difficult to convert U-238 to Pu-239 with high efficiency. (See also Hargraves and Moir 2010).
- Breeding is possible in thorium with both slow and fast neutrons. The regeneration factor $\eta$ is the number of fission neutrons emitted per neutron absorbed in the fuel. Values of $\eta \geq 2.2$ are needed for good breeding. In $^{233}$U of $\eta \sim 2.24$ (thermal neutrons) and 2.30 (typical fast neutron spectrum) (Fig. 1.1). In $^{239}$Pu these values are 2.01 (thermal, unsatisfactory) and 2.45 (fast), which requires a fast neutron spectrum.
- The delayed neutron fraction $\beta$ is 0.0026 in $^{233}$U, compared to 0.0020 in $^{239}$Pu. The larger value of $^{233}$U makes it easier to control the $^{233}$U core.

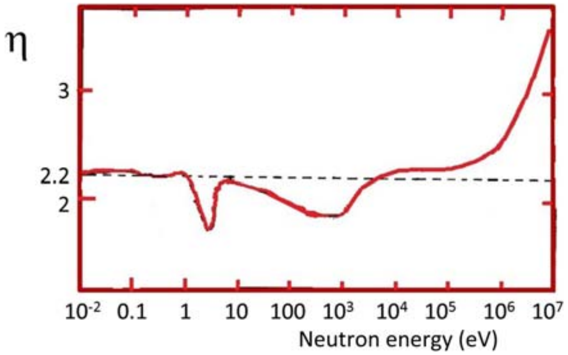

**Figure 1.1** Variation of $\eta$ with neutron energy for $^{233}$U, where $\eta$ is the number of fission neutrons emitted per neutron absorbed in fuel.
*Source*: See also Teller, E., 1981. Editor, Fusion, Vol 1, Part B, R. W. Moir, Chapter 15, The Fusion-Fission Fuel Factory, Academic Press, NY, Teller (1981).

## 1.6 Liquid fuel MSR

A single-fluid liquid fuel MSR is illustrated in Fig. 1.2.

A two-fluid reactor may have a core with fissile fuel (U-233, U-235, or Pu-239) sustaining the chain reaction surrounded by a blanket, where neutrons leaking out of the core would be captured by fertile material (Th-232 or U-238) to breed more fissile fuel.

Consider an example case with FLiBe salt containing $^{233}UF_4$ fuel. The reactor could have a core surrounded by a breeder blanket containing $ThF_4$ in FLiBe, as illustrated in Fig. 1.3. The core liquid circulates to a heat exchanger. A secondary coolant flows to an energy conversion system that generates electricity, such as a Rankine cycle or Brayton cycle.

The ionization states of the fertile breeder salt are controlled using $F_2$ gas. The intermediate $^{233}Pa$ could also be removed by the blanket processing system to prevent neutron absorption in $^{233}Pa$, which generates nonfissile $^{232}U$.

$ThF_4$ is gradually added to the blanket salt to compensate for losses. The fuel processing system could (optionally) remove fission products to keep the core radioactivity low and to reduce nonfissile neutron captures. Other fluoride or chloride salts could be used instead of $^7LiF\text{-}BeF_2$.

In a thermal neutron spectrum reactor, graphite blocks could be used to moderate the core neutrons for better neutron economy (Chapter 11: Liquid fuel, thermal neutron spectrum reactors). Other reactors could operate with fast neutrons and no graphite (Chapter 12: Fast spectrum liquid fueled reactors). Tritium bred by neutron absorption in lithium and other elements must be managed carefully to prevent

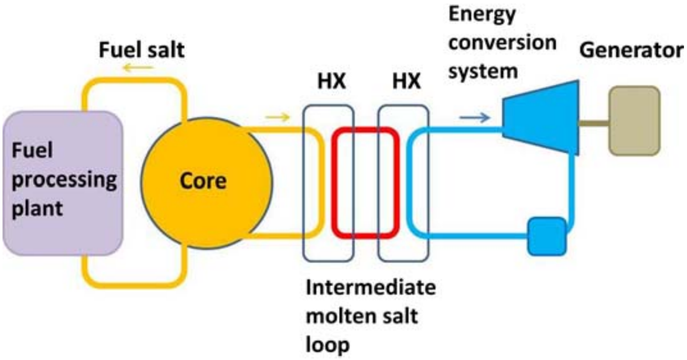

**Figure 1.2** Simplified view of a single-fluid liquid fuel MSR power plant. HX = heat exchangers. The fuel salt (yellow) could be FLiBe containing $UF_4$ and $ThF_4$. The fissile materials in the fuel salt would sustain the chain reaction, and the extra neutrons emitted could breed $^{233}U$ from the $^{232}Th$. The fuel processing plant (lavender) could separate U, Pu, Th, and Pa; adjust fuel salt composition to maintain reactivity; and remove fission products to reduce core radioactivity. The intermediate loop (red) could be a molten salt without U or Pu. Pumps, reheaters, and condensers are not shown. The energy conversion system (blue) could be either Rankine (steam), Brayton (gas), or supercritical fluid.

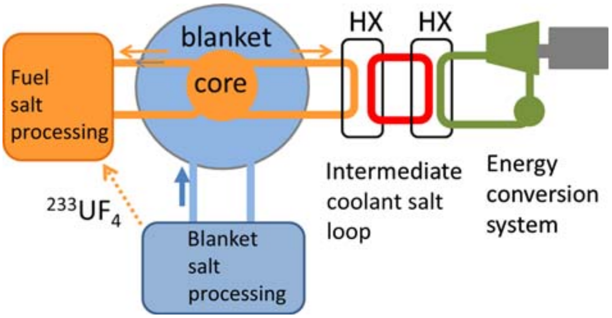

**Figure 1.3** A two-fluid liquid fuel reactor. The fission reactions occur mainly in the central core (orange) containing $^7LiF\text{-}BeF_2\text{-}^{233}UF_4$ molten salt. Hot fuel salt flows to a heat exchanger HX, where intermediate coolant salt (red) carries the heat to the energy conversion system (green), which generates electricity. The blanket region (blue) contains $^7LiF\text{-}BeF_2\text{-}ThF_4$ molten salt, where neutrons leaking from the core breed $^{233}U$. It becomes $^{233}UF_4$, which is extracted from the blanket salt and inserted into the fuel salt at a rate that helps control core reactivity. An additional heat exchanger (not shown) extracts heat from the blanket salt.

escape to the environment, because tritium is a radioactive gas that can pose a health hazard if ingested or inhaled at too great a concentration.

Liquid fuels offer many potential advantages over solid fuels (Hargraves, 2012).

## 1.7 Advantages of liquid fuel MSR

*Liquid fuel MSRs* would have the following advantages over *LWRs*.

### 1.7.1 Safety advantages

- Can operate at *low pressure*, avoiding the safety issues of high-pressure reactor vessels and huge containment domes.
- No concern about *clad* leaking fission products. There is no need for cladding. (Zirconium clad plus water at high temperatures generated hydrogen and explosions at Fukushima.)
- No danger of *fuel melting*. The fuel is already molten. (Solid fuel melting occurred at Three Mile Island and Fukushima, releasing radioactivity.)
- Continuous *online refueling* and reactivity adjustment.
- Lower core *excess reactivity* can be maintained. This makes control easier and safer.
- Continuous removal of *fission products* (optional) could keep core radioactivity low. Radioisotopes like Cs-137 could be removed and stored safely, or used for commercial processes. Low core radioactivity means that less radioactivity could be released during a severe accident. (The worst contaminant released at Chernobyl and Fukushima was Cs-137.)
- Easy removal of *noble gases* (xenon and krypton) avoids control problems of xenon poisoning. (Xenon poisoning contributed to the control problem at Chernobyl.)

- Core overheating could melt the *drain plugs*; the liquid core would drain into passively air-cooled tanks and slowly solidify, trapping radioactivity.
- Lower core *heat emission* after shutdown. Emergency core *cooling* would be easier, perhaps unnecessary. (Inadequate cooling was a major issue at Three Mile Island and Fukushima.)
- No *steam explosions* from core, since no water is there. (A major problem at Chernobyl.)
- The self-regulating core can *follow demand* loads with minimal or no use of control rods.
- Fluorine salts are *stable* in high radiation fields, with *boiling* temperatures ~1400°C, so boiling will not occur.

## 1.7.2 Economic advantages

- Low pressure and high heat capacity facilitate *compact*, less expensive reactor cores.
- Huge *containment* buildings might not be required.
- Compact reactors could be *mass produced*, shipped to the reactor sites, and installed underground. (This advantage will also be available in some future LWRs.)
- Core could operate at *high temperature* (~700°C), improving electrical generation efficiency (over 44%, compared with ~33% for current LWRs.)
- High temperature facilitates *compact Brayton cycle* systems.
- *Air-cooled* energy conversion systems could be used in arid or cold regions, because MSR can provide higher-temperature coolants (Chapter 2: Electricity production).
- Peak *wind energy* could be stored as compressed air, which could be heated by a thorium MSR to drive an open cycle air turbine, increasing the Brayton cycle efficiency without requiring cooling water. Rankine cycles would not couple as well as high-temperature compressed air Brayton (Chapter 2: Electricity production).
- No need for *manufacture* of fuel pellets, rods, and precise core structure.
- No need to continually test the core for *leaking* fuel pins.
- No need to *shut down* for refueling.
- Could be started up using fissile materials from *used LWR fuel*.
- After thorium reactors were breeding sufficient U-233, U-235 *enrichment plants* would not be required.
- *Fuel lifetime* is not limited by radiation damage.
- Liquid fuel reactors could be produce electricity *cheaper than coal* (Hargraves, 2012).
- U-233 bred from thorium can be *removed* from the molten salt by fluorine gas bubbles, which convert the salt $UF_4$ to gaseous $UF_6$, which bubbles out of the molten salt. The purified uranium can be converted back to $UF_4$ by exposure to $H_2$ and returned to the core. (The HF can be electrolytically separated into $H_2$ and $F_2$, which are recycled.) Chemical processing of liquid fuel is discussed in Chapter 8, Chemical processing of liquid fuel (See also Langworth 2015.)

## 1.7.3 Environmental advantages

- Thorium is four times as *abundant* as uranium, so thorium utilization would expand the world supply of nuclear fuel.
- *Recycling* of actinides (elements 89–103) into liquid fuel would reduce waste production, compared with once-through LWRs where they are not recycled.
- Fast spectrum MSRs, or even thermal spectrum MSRs could *incinerate* actinides from LWR used fuel, reducing their waste disposal requirements.

- Higher efficiency of electrical power generation (due to high coolant temperature) means less *waste heat* rejected to the environment.
- Liquid fuel reactors would generate less than 1% of LWR long-lived high-level *radioactive wastes*. After 500 years the radioactivity of thorium reactor wastes would be even lower than the radioactivity of the thorium ore from which the fuel was derived (Hargraves, 2012).
- Waste would contain such low concentrations of fissile isotopes that accidental *criticality* would not be a concern.
- Thorium is available from *rare-earth mining* streams and is less radioactive than uranium.

### 1.7.4 Nonproliferation advantages

- Bred Pu-239 could be *recycled and burned* in the core without leaving the site. The *Pu inventory* on site could be kept low.
- U-232 generated by (*n*,2*n*) reactions in Pa mixes with U-233 and, in sufficient quantity, could make it undesirable for weapons use (called *spiked*). Bred U-233 could also be diluted with U-238 to produce low-enriched fuel not suitable for weapons, called *denatured* fuel.
- Fissile materials stay at the secure *reactor site*. It would be very difficult to steal the securely stored, highly radioactive molten salt without interference from security forces.
- Could be used to consume Pu-239 from *dismantled nuclear weapons* without the problems of MOX fuel manufacture and control in LWRs.

Nonproliferation issues are discussed further in Chapter 10, Non-proliferation and safeguards aspects of the MSR fuel cycle.

These potential safety, economic, environmental, and nonproliferation advantages have inspired renewed interest in liquid fuel research and development in

**Table 1.2 Economics, regulatory, and public acceptance issues for new power plants (Dolan, 2014)**

| **Economics** |
|---|
| Simplicity<br>Capital cost of plant<br>Construction time—modular and factory built<br>Plant lifetime<br>Fuel cycle—cost, availability<br>Reliability, availability, maintainability<br>Load following<br>Investment risk and finance availability<br>Plant staff—size, training, availability<br>Market—proximity to load center<br>Transmission grid—capacity and stability<br>Resources<br>Natural hazards—seismic activity, fires, floods, wind storms, lightning |

(*Continued*)

**Table 1.2** **(Continued)**

| |
|---|
| Waste—chemical, radioactive<br>Decommissioning<br>International sales |
| **Regulatory simplicity** |
| Regulations—stability, retrofitting, reporting requirements<br>Law suits<br>Safety<br>Emergency planning—off-site evacuation plan required?<br>Emissions<br>Worker exposure<br>Licensing—lifetime power plant license (licensing may be slow in countries with no MSR experience). |
| **Public acceptance** |
| Public understanding<br>Environmental regulations—cooling water, archeological sites, protected species<br>Waste heat<br>Passive safety<br>Emissions—toxic metals, chemicals, radioactivity<br>Radwaste—minimization, benign disposal<br>Public concerns and perception<br>Nonproliferation of nuclear weapons |

*Source*: MSR designs could meet most of these goals Moir, R.W., 2008. Recommendations for a restart of molten salt reactor. Convers. Manage. 49 (2008), 1849−1858 (Moir, 2008).

many countries. We also need to consider the goals that must be met for successful deployment of new power plants (Table 1.2).

## 1.8 MSR development issues

Several issues could limit MSR *performance*:

- Fuel flowing out of the reactor continues to emit *delayed neutrons* in the surrounding pipes and valves. The neutron emission rate is a reactor dynamics issue (Chapter 5: Kinetics, dynamics, and neutron noise in stationary MSRs).
- These neutrons make the plumbing radioactive, so *remote maintenance* is required.
- Fission product *tellurium* caused cracking in MSRE, which could be reduced by controlling the $UF_3/UF_4$ ratio.
- Neutron irradiation produces *helium* accumulation. An increase of ultimate tensile stress produced by irradiation, called radiation hardening, is accompanied by a reduction of *ductility*. This could be alleviated by adjustment of the carbon content and by shielding the vessel wall, such as with a thorium blanket.
- *Corrosion* of structure, pipes, valves, and pumps. (Hastelloy N has corrosion resistance up to about 760°C in FLiBe.)

The MSRE developed control systems, drain tanks, salt heaters, Hastelloy, and instrumentation. For MSR power plants the following developments are needed:

- Better corrosion-resistant, high-temperature materials for reactor vessel and piping, and redox potential control techniques (Chapter 7: Materials, Chapter 8: Chemical processing of liquid fuel);
- Pumps and valves;
- Remote handling equipment, such as hot cells and robotics, are developed, but may need further modification;
- Heat exchangers for high-temperature molten salt, such as steam generators and molten salt to air heaters;
- Energy conversion systems (Brayton, Rankine, supercritical, or combined cycle) are in use for present power plants, but need further development to achieve higher efficiency and reliability at very high temperatures (Chapter 2: Electricity production);
- Chemical systems to separate uranium, plutonium, thorium, molten salts, fission products, and tritium, in a highly radioactive environment. This is a major issue requiring extensive, long-term development (Chapter 8: Chemical processing of liquid fuel);
- Lithium isotope separation methods. (It is desirable to remove $^{6}$Li, in order to minimize tritium generation.)

## 1.9 Tritium issues

Natural lithium is 7.42% Li-6 and 92.58% Li-7. Tritium ($^{3}$H) is produced by neutron absorption via the reactions:

$$^{6}\mathrm{Li} + n(\mathrm{thermal}) \rightarrow {}^{4}\mathrm{H}e(1.05\ \mathrm{MeV})\ + {}^{3}\mathrm{H}(2.73\ \mathrm{MeV})$$

$$^{7}\mathrm{Li} + n(\mathrm{fast}) \rightarrow {}^{3}\mathrm{H} + {}^{4}\mathrm{He} + n$$

The Li-7 reaction is endothermic, requiring a neutron energy >2.47 MeV, so most of the tritium production occurs in Li-6. Li-6 is a strong neutron absorber, which affects the reactor neutron economy, requiring extra fissile material in reactors using FLiBe. The reactor would function more efficiently if most of the Li-6 were removed by *isotope separation*, which is expensive (Chapter 7: Materials).

Tritium is a weak beta emitter (average energy 6 keV). These electrons cannot penetrate the skin, but tritium can form tritiated water inside the body if tritium is ingested or inhaled. This radioactive water can damage cells, posing a *health hazard* if tritium gas escapes into the environment. In the USA the Annual Limit for Intake (ALI) is 80 mCi (3 GBq) and the Committed Effective Dose Equivalent in soft tissue is 64 mrem per mCi ($1.7 \times 10^{-11}$ Sv/Bq) ingested. Thus, the ALI corresponds to a dose of about 0.05 Sv (Idaho State University, 2015).

The tritium hazard could be alleviated by

- removing some tritium from FLiBe by bubbling He gas through the FLiBe (sparging);
- removing some tritium from FLiBe in a vacuum disengager (spray into vacuum);

- tritium removal from an intermediate molten salt coolant loop;
- using tritium impermeable barriers on heat exchanger tubes;
- removing most of the Li-6 from the lithium (isotope separation);
- using molten salts that do not contain lithium, such as NaF;
- after tritium ingestion, drinking fluids that decrease the biological half-life of tritium in the body from 9.6 days to a few days, or by using dialysis for severe cases.

Although tritium is a concern, much technology has been developed to ensure its safe handling, especially in Canada, where the CANDU reactors produce large amounts if tritium.

## References

Chinese Academy of Sciences and US Department of Energy, 2012. Cooperating in Nuclear Energy Sciences and Technologies, First Executive Committee Meeting, Shanghai.

Dolan, T.J. (Ed.), 2014. Magnetic Fusion Technology. Springer, London.

Hargraves, R., Moir, R., 2010. Liquid fluoride thorium reactors, an old idea in nuclear power gets reexamined. Am. Sci. 98, 304–313.

Hargraves, R., 2012. Thorium, Energy Cheaper than Coal, 1 Robert Hargraves, Hanover, NH.

Haynes International, HASTELLOY®-N alloy, Kokomo, IN, 2002. Accessed in 2015 at: <https://www.haynesintl.com/pdf/h2052.pdf>.

Idaho State University, Radiation Information Network's Tritium Information Section. Accessed in 2015 at: <http://www.physics.isu.edu/radinf/tritium.htm>.

Langworth, G.R., The DMSR Book, How Africa Can Achieve Regional Energy Security with Molten Salt Nuclear Power Technology, 2015.

MacPherson, H.G., 1985. The molten salt reactor adventure. Nucl. Sci. Eng. 90, 374–380.

Martin, R., 2012. Superfuel, Thorium, the Green Energy Source for the Future. Palgrave Macmillan, New York, NY.

Moir, R.W., 2008. Recommendations for a restart of molten salt reactor. Convers. Manage. 49 (2008), 1849–1858.

Moir, R.W., Manheimer, W., 2014. Fusion-Fission Hybrids, Chapter 14 of Dolan, T. J. Magnetic Fusion Technology, Springer, London.

Serp, J. et al., 2014. The molten salt reactor (MSR) in generation IV: Overview and perspectives, Progress in Nuclear Energy Vol. 77, pp. 308–319. <www.elsevier.com/locate/pnucene>.

Teller, E., 1981. Editor, Fusion, Vol 1, Part B, R. W. Moir, Chapter 15, The Fusion-Fission Fuel Factory, Academic Press, NY.

Weinberg, A.M., 1994. The First Nuclear Era, the Life and Times of a Technological Fixer. American Institute of Physics Press.

# Electricity production

# 2

*Lindsay Dempsey*[1], *Charles Forsberg*[2] *and Thomas J. Dolan*[3]
[1]Generation Solutions, Auckland, New Zealand, [2]Massachusetts Institute of Technology, Cambridge, MA, United States, [3]University of Illinois at Urbana-Champaign, Champaign, IL, United States

## Chapter Outline

Magnetohydrodynamic (MHD) generators, thermoelectric convertors, and thermionic convertors have low efficiencies, so they are not considered here.

## 2.1 Heat engines

The efficiency of a heat engine, which converts thermal energy into electrical energy, is always less than the Carnot efficiency

$$\eta_c = 1 - T_c/T_h$$

where $T_h$ and $T_c$ are the coolant temperatures entering and leaving the engine, in degrees Kelvin. Sterling cycles are being developed for small-scale applications, but are not competitive with Rankine and Brayton cycles. Calculation of heat engine efficiencies is described by El-Wakil (1978).

Carnot cycle efficiency represents the maximum possible efficiency of any heat engine system between specified temperature limits. The efficiency of power conversion systems used in the real world is always inferior to the Carnot cycle

**Molten Salt Reactors and Thorium Energy. DOI: http://dx.doi.org/10.1016/B978-0-08-101126-3.00002-6**

efficiency. However, increasing the high-temperature within the cycle or decreasing in the low-temperature in the cycle generally increases the overall cycle efficiency or provides an opportunity to do so.

Some desirable features of heat engines are shown in Table 2.1.

As part of the flexibility characteristic a heat engine should also be able to vary its output to meet changing demand, which in some jurisdictions is affected by solar power plant output. For example, solar output is high in the midday, so less power is then needed from other sources to the grid. The "Cal ISO Duck" shown in Fig. 2.1 is an extreme case of grid demand for peaking power versus time.

Usually natural gas turbines are used to achieve fast peaking power ramp rates. Molten salt reactors (MSRs) can also be used, because some of the thermal energy

**Table 2.1** **Desirable characteristics of heat engines (Dempsey, 2015)**

Safe
Efficient—thermodynamically, financially, and in the use of all resources
Reliable
High availability
Robust—fault tolerant
Low maintenance and easy to maintain
Cheap—low first cost
Diversity of supply—multiple vendors
Flexible—load following, ramping, peaking
Scalable—works well in a range of sizes
Adaptable—can be upgraded/updated
Compatible with the nuclear island
Environmentally benign during all stages of its life cycle

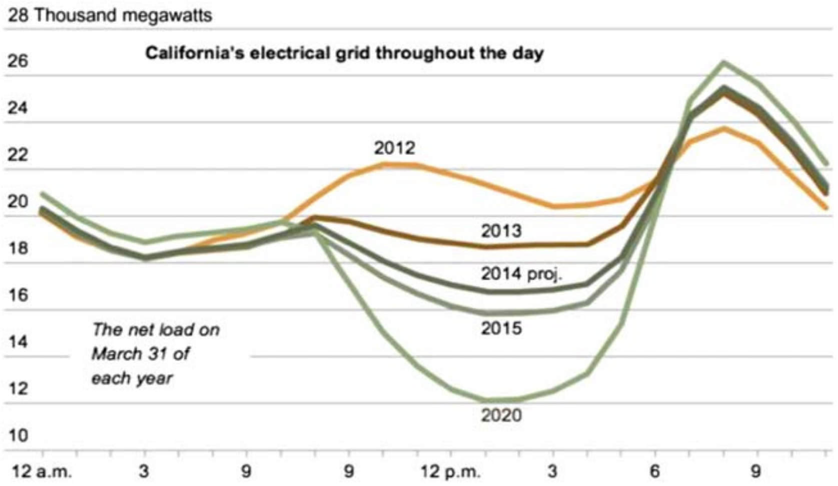

**Figure 2.1** Electrical peaking power demand versus time of day caused by large-scale solar and wind power (California ISO 2013).

**Table 2.2** **Some heat engine options**

- Steam turbine (Rankine cycle)
- Helium Brayton cycle
- Combined cycle, Brayton and Rankine together (CCGT)
- Supercritical $CO_2$
- Unusual cycles
  - Binary mercury/steam
  - Boiling aluminum chloride
  - Air-breathing hybrid CCGT
  - Air-breathing open cycle Brayton

stored in the molten salt can be converted by a heat engine for rapid power increases. An MSR with thermal storage designed to deliver electricity to the grid in accordance with the 2020 curve in Fig. 2.1 would be designed to have a load factor of ~50% and a fast ramping rate of ~10% per minute. In a theoretical example; for an average 1000 MWe, a plant following the 2020 curve would deliver a minimum of 278 MWe and a maximum of 1859 MWe over a 24-hour cycle.

Table 2.2 lists some heat engines for consideration, to be discussed in the following sections.

## 2.2 Rankine cycles

Steam cycles are well developed, widely used, and available in sizes from 5 kW to 1750 MW. The efficiencies are typically ~64% of Carnot, but can be higher in large, multicomponent systems. Fossil fuelled Rankine cycle power stations without $CO_2$ capture have efficiencies in the range of 36–46% on a lower heating value (LHV) basis, but the underlying efficiency of the Rankine cycle power island is higher, typically in the range of 40–49%. The lower figure for overall station efficiency is due to thermal losses in the boiler and the additional auxiliary load required to operate the boiler, including fuel and ash handling, forced draft and induced draft fans, and flue gas cleanup systems. Commercially available Rankine cycle turbines at the time of writing can be specified for steam conditions as high as 300 bar 600°C with steam reheat to 620°C. Advanced Rankine cycle turbine designs contemplate steam conditions as high at 350 bar 700°C with steam reheat to 720°C, but are not commercially available today.

Modern Rankine cycle turbines are very reliable and durable if operated and maintained in accordance with the manufacturer's recommendations. A service life of 300,000 hours (38 years at 90% service factor) or more is achievable for modern turbines. They are available from multiple vendors, so a competitive procurement process works well. The turbine island comprises the steam turbine, the generator, the condenser, the moisture separator, reheaters, and auxiliary equipment needed to convert steam produced at the nuclear reactor into electrical energy. The Flamanville EPR turbine island was contracted at about 200 Euro per kW (Alstom Company, 2006). Steam turbines perform best with a low-temperature heat sink.

The cooling requirements for Rankine cycles can consume a lot of cooling water, and many countries are restricting the use of once-through cooling, the least costly and most efficient cooling arrangement. The molten salt temperature would be limited to about 700°C, and 8 stages of feedwater heating would be needed to achieve highest efficiency. The biggest challenge would be development of a reliable steam generator that is resistant to freezing of the molten salt and that can recover from a salt freeze.

## 2.3 Helium Brayton cycles

Helium Brayton closed loop cycles can use high-temperature primary coolants and can achieve up to 54% efficiency at 900°C with triple pressure-recuperation and intercooling. (Assuming $T_c \sim 100°C$ the Carnot efficiency would be 68%.) The turbines have more stages (blade rows) than normal gas turbines. They are not widely used, and the largest commercial plant is 50 MWe at Oberhausen II. They may have multiple expansion steps, as illustrated in Fig. 2.2.

Fig. 2.3 shows the thermodynamic cycle of a multistage Brayton cycle system.

This particular system was designed for a fusion reactor blanket, but it could also be used with a MSR heat source. The hot, high-pressure helium at $p = 18$ MPa and temperature $T_1 \sim 650°C$ (point 1) spins the turbine and draft shaft, which turns the three compressors and the electrical power generator (not shown). After expansion through the turbine, part of the heat remaining in the gas is removed in the recuperator (points 2 to 3 on the T-S diagram) to preheat the gas entering the intermediate heat exchanger (IHX). The gas is further cooled in the heat rejection heat exchanger (HX) (points 3 to 4). This is the minimum temperature and pressure point of the cycle. It is compressed in three stages, with cooling between each stage to facilitate further compression (points 4 to 9). The preheating of the gas by the

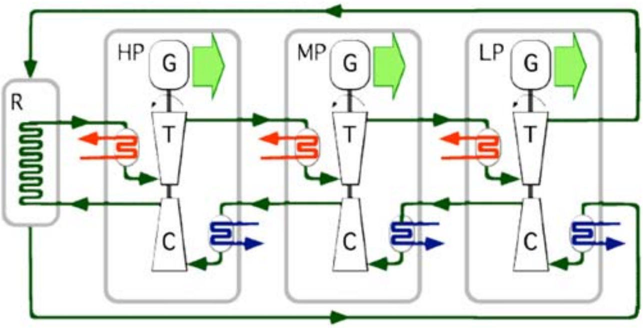

**Figure 2.2** Schematic flow diagram for a three-expansion-stage cycle, using high-pressure (HP), medium-pressure (MP), and low-pressure (LP) stages. Each stage has a generator (G), turbine (T), compressor (C), and heater and cooler heat exchangers, with a recuperator (R) located in a fourth vessel (Zhao and Peterson, 2004).

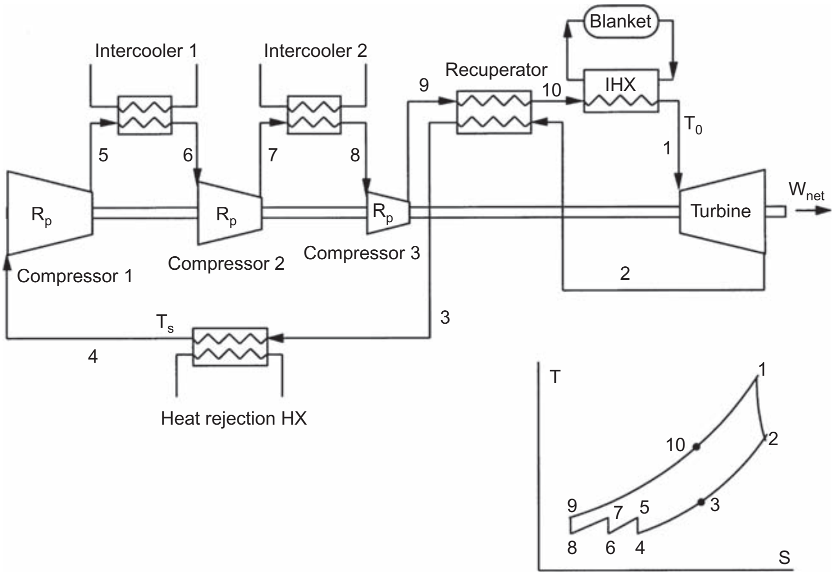

**Figure 2.3** A high-pressure Brayton cycle with intercoolers and recuperator (Malang, 1998, Figure 3).

recuperator (points 9 to 10) greatly boosts the starting temperature of the coolant going through the IHX, where the molten salt heats it up to $T_1$. If $T_1 = 650°\text{C}$, pressure = 18 MPa, and the recuperator efficiency

$$\eta_x = (T_{10} - T_9)/(T_2 - T_9)$$

were ~96%, then the conversion efficiency of thermal energy into electricity could be ~46%, which is comparable to that of a corresponding Rankine cycle. (Malang, 1998) (If $T_c \sim 100°\text{C}$, then the Carnot efficiency would be 60%).

Helium Brayton cycles are reasonably compact and efficient. They can be used with dry cooling and for desalination where water is scarce. High heat rejection temperatures $T_c$ would reduce cooling tower costs, and the absence of a steam cycle would remove a major pathway of tritium leakage.

There is not much industrial experience with high-power helium turbines. Helium Brayton cycles need high-pressure (~10 MPa), which makes it difficult to prevent leaks. The turbine operates at high speed, often >60 Hz. Impurities in helium attack some metals at high temperatures, so the helium must be kept pure.

In a combined cycle system the heat rejected by the Brayton cycle could drive a Rankine cycle. The efficiency would be improved, but the additional complexity might not be cost-effective.

Deficiencies of energy conversion systems using He, He + N, and $CO_2$ gases are discussed by Oh (2006).

## 2.4 Supercritical $CO_2$ Brayton cycles

At pressures above the triple point a fluid is a “supercritical” fluid, no longer a liquid or gas. A simple supercritical cycle at 550°C could achieve a net efficiency ~37%, so additional features are desirable to improve the efficiency. After considering several options (precompression, recompresion, partial cooling, recuperation) a recompression system with recuperation was found to be best (Dostal, 2004). Such a system is illustrated in Fig. 2.4.

Fig. 2.5 shows the thermodynamic cycle. Supercritical $CO_2$ drives the turbine (points 5 to 6) which drives the electrical power generator and the compressor shaft. The fluid is compressed (1 to 2) and (8 to 3) up to 12–20 MPa. The precooler and

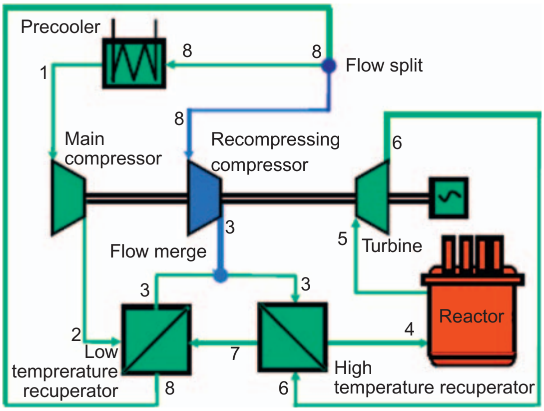

**Figure 2.4** A supercritical $CO_2$ system with recompression (Dostal, 2004).

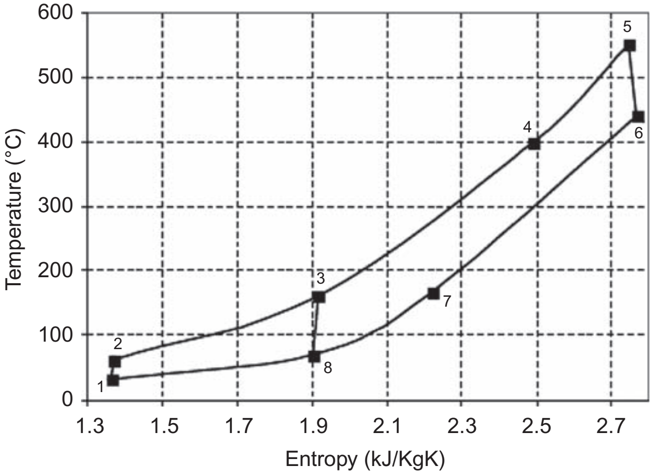

**Figure 2.5** The temperature–entropy diagram of a recompression Brayton cycle (Dostal, 2004).

recuperators improve the thermodynamic efficiency of the cycle. Then the highly compressed fluid is heated by the molten salt heat source (4 to 5) and recycled to the turbine. The cycle requires a good recuperator and a low-temperature heat sink (~10°C).

Fig. 2.6 shows the calculated efficiencies for supercritical $CO_2$ systems as functions of temperature and pressure.

The supercritical $CO_2$ cycle can operate at lower temperature than the Brayton cycle (550°C vs 850°C), but higher pressure (20 MPa vs 8 MPa), while achieving comparable efficiency of 45%. Higher temperatures could raise the efficiency above 50%. The turbomachinery is high speed and very compact. A 246-MWe turbine would be only 1.2 m diameter and 0.55 m long, compared with about 5 m long for a helium Brayton turbine and much larger for steam turbines.

The compact size makes turbine material strength and blade tip clearances significant issues. The high turbine speed requires high-speed reduction gearboxes or large-scale sophisticated frequency conversion. The high-pressure requires HXmaterials with good strength, and the turbine inlet temperatures will be limited by materials issues. The supercritical $CO_2$ cycle is potentially promising, but is still in a developmental stage. Sandia National Laboratory has successfully operated a supercritical $CO_2$ turbine/compressor loop with equipment rated around 100 kW. Supercritical cycles with other fluids, such as ammonia, are also possible.

In a comparison with the helium Brayton cycle, the supercritical steam cycle, and superheated steam cycle, "the supercritical $CO_2$ cycle dominates in the range of medium temperatures (500–700°C) over all three other considered cycles. Its high efficiency, simplicity, compactness and low capital cost is very attractive." (Dostal, 2004).

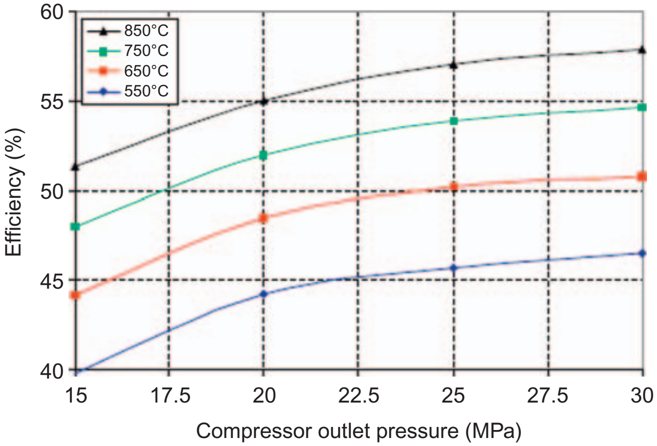

**Figure 2.6** Effect of turbine inlet temperature and compressor outlet pressure on efficiency for the recompression cycle (Dostal, 2004).

## 2.5 Metal vapor combined cycles

### 2.5.1 Mercury/water binary cycle

A high-temperature mercury vapor would drive a turbine, and the exhaust mercury vapor would condense on a steam generator. The steam cycle would be driven by the waste heat of the mercury vapor cycle to achieve higher efficiency. The Schiller mercury-vapor/steam plant at Portsmouth, New Hampshire, produced about 40 MW (15 from mercury and 25 from steam) in the 1950s. Mercury is highly toxic, so its large-scale use is no longer acceptable.

### 2.5.2 Potassium/steam binary cycle

Chambers, Fraas, and Ozisik did a preliminary design study of a potassium/steam binary cycle coupled to a MSR with fuel outlet temperature 982°C (1100°F). The fuel salt flows through an IHX, heating an inert salt to 926°C. A temperature drop of 56°C is assumed in both salt circuits. The intermediate salt loop heats a potassium boiler, sending potassium vapor to a turbine at 838°C (1540°F). The vapor condenses on a steam generator at 593°C, generating steam at 566°C (1050°F) and 28 MPa, with reheats to 566°C (parameters of the Philadelphia Electric Company Eddystone Plant). Fig. 2.7 illustrates the T-s diagram for the high-temperature binary cycle. The combined system could achieve an efficiency of 54% (Chambers, 1964).

The required potassium vapor turbines and heat exchangers, which must withstand corrosion from hot metal vapor and molten salts, have not yet been developed and tested. Potassium is not toxic, but it is highly reactive with air and water. Cesium and rubidium would also be suitable for vapor turbines, but they are rare and expensive. Estimates of the required materials and components for the binary cycle indicated that it could be cost-competitive (Chambers, 1964).

## 2.6 Nuclear air Brayton power cycles

In the 1950s the United States initiated the Aircraft Nuclear Propulsion program to couple a nuclear reactor to a jet engine to create a nuclear-powered bomber with unlimited range. The program resulted in the initial development of the MSR at Oak Ridge National Laboratory. The salt coolants were designed to deliver high-temperature nuclear heat to jet engines. The program was canceled with the development of intercontinental ballistic missiles. The MSR development continued for another decade to create a nuclear power plant coupled to a steam power cycle because at that time gas turbine technology was not sufficiently developed to be a practical power system for utility applications.

In the last 50 years there have been extraordinary developments in utility gas turbines burning natural gas. F Class gas turbines were introduced in the 1990's, that technology had advanced sufficiently to enable coupling a salt-cooled reactor to a nuclear air-Brayton combined cycle (NACC) power conversion system. Because of

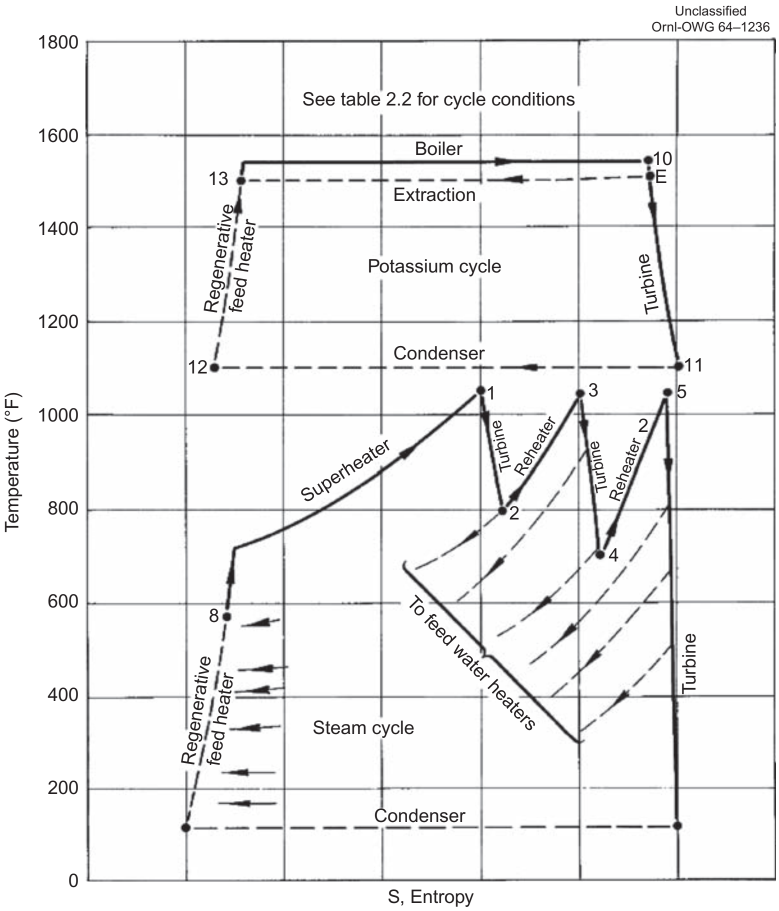

**Figure 2.7** The T-s diagram for a binary potassium-steam cycle, with potassium turbine inlet temperature 1540°F (838°C) and steam turbine inlet temperature 566°C (1050°F) (Chambers, 1964).

advances in gas turbine technology, this power cycle enables nuclear base-load electricity with additional peak electricity produced by using auxiliary natural gas or stored heat with incremental heat-to-electricity efficiencies of 66—70%. This capability enables a salt-cooled reactor with NACC to be the enabling technology for a low-carbon nuclear-renewable grid and increases revenue in deregulated electricity markets by 50—100% after subtracting the cost of natural gas relative to a base-load nuclear plant.

In a modern utility combined-cycle gas turbine the exit temperature of the compressed air from the front-end compressor is between 400 and 500°C; thus, the reactor coupled to NACC must deliver heat in the 600—700°C range. Salt coolants are the only coolants designed to deliver heat in this temperature range.

### 2.6.1 Nuclear Air-Brayton combined cycle

Advances in gas turbine technology now enable coupling a high-temperature reactor to a NACC (Andreades, June 2014, July 2014, 2015; Zohuri, 2015). Such a power system can operate in two modes: base-load and peak electricity (Fig. 2.8). Nuclear heat is used for base-load electricity production. Additional heat for peak electricity production can be provided by natural gas (near-term), stored heat, or ultimately hydrogen. During base-load operation of an NACC, atmospheric air is filtered, the air is compressed, heat is added from the reactor through a coiled-tube heat exchanger, the hot compressed air goes through turbine to produce electricity, the air is reheated and goes through a second turbine to produce electricity, the warm air exiting the gas turbine goes through a heat recovery steam generator (HRSG) to generate steam that is used to produce added electricity, and the air is exhausted to the stack. This power cycle is similar to that used in natural gas combined-cycle plants. If coupled to a salt-cooled reactor delivering heat between 600 and 700°C, heat-to-electricity efficiency is 42%.

The base-load NACC temperatures, determined by heat-exchanger material constraints, are far below allowable peak gas turbine temperatures. Thus, there is the option of adding heat after the nuclear heating to further raise compressed gas temperatures before entering a power turbine—a topping cycle. The incremental heat-to-electricity efficiency depends upon the design, ranging from 66–70%. This is the most efficient system known to convert incremental heat to electricity based on existing technology.

A commercial fluoride-salt-cooled high-temperature reactor (FHR) point design (Andreades, September 2014, Summer 2015) with NACC has been developed with a base-load output of 100 MWe to match the capabilities of the GE 7FB gas turbine—the largest rail-transportable gas turbine made by General Electric. The FHR uses solid fuel with clean salt coolant and delivers heat to the power cycle between 600 and 700°C. The power cycle can be coupled to an MSR delivering heat over the same temperature range. Utility combined-cycle gas turbines are growing rapidly in size and the new H-Class gas turbines have more than twice the output of the F-Class gas turbines and much larger gas turbines are expected to be available by the time any salt-cooled reactor is commercialized. The option exists to couple multiple turbines to a single reactor.

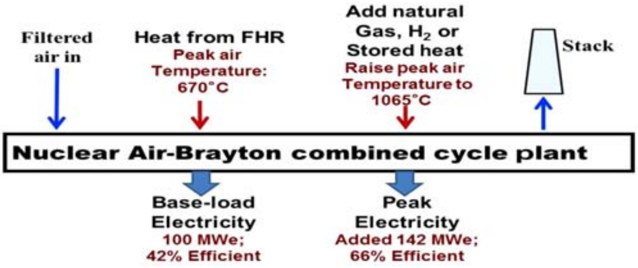

**Figure 2.8** Nuclear Air-Brayton combined cycle (NACC).

Fig. 2.9 shows in more detail FHR NACC point design with auxiliary heat provided by natural gas, hydrogen, or a Firebrick Resistance Heated Energy Storage (FIRES) system. In the power cycle, external air is filtered, compressed, heated by hot salt from the FHR while going through a coiled tube air heater (CTAH) to 670°C, sent through a turbine producing electricity, reheated in a second CTAH to the same gas temperature, and sent through a second turbine producing added electricity. Warm low-pressure air flow from the gas turbine system exhaust drives a HRSG, which provides steam to either an industrial steam distribution system for process heat sales or a Rankine cycle for additional electricity production. The air from the HRSG is exhausted up the stack to the atmosphere.

Added electricity (Fig. 2.10) can be produced by injecting fuel (natural gas, hydrogen, etc.) or adding stored heat after nuclear heating by the second CTAH. This boosts temperature to 1065°C in the compressed gas stream going to the second turbine that is exhausted to the HRSG. The specific design was optimized for

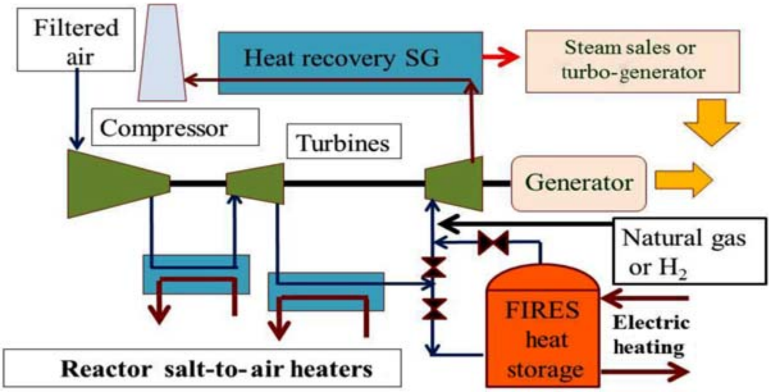

**Figure 2.9** Nuclear Air-Brayton combined cycle (NACC) with FIRES.

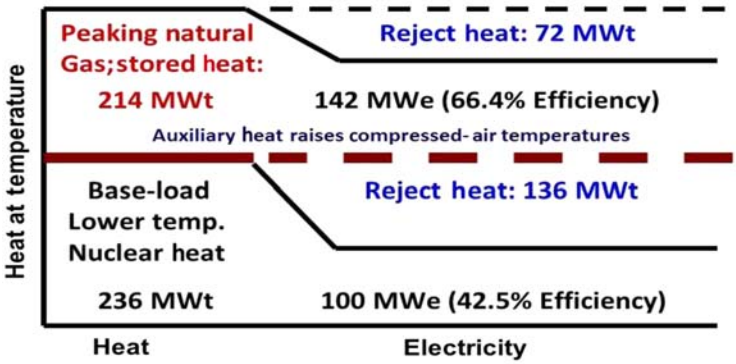

**Figure 2.10** Heat and electricity balance for NACC and FIRES.

base-load electricity production. The incremental natural gas, hydrogen, or stored heat-to-electricity efficiency is 66.4%—far above the best standalone natural gas plants because the added heat is a topping cycle. For comparison, the same GE 7FB combined cycle plant running on natural gas has a rated efficiency of 56.9%. Higher peaking efficiencies can be achieved by optimizing the design for peak electricity production and/or increasing peak turbine temperatures using active cooling blades with peak turbine temperatures above 1300°C.

The reason for these high incremental natural gas or stored heat-to-electricity efficiencies is that this high-temperature heat is added on top of "low-temperature" 670°C nuclear heat. For a modular 100 MWe FHR coupled to a GE 7FB modified gas turbine that added natural gas or stored heat produces an additional 142 MWe of peak electricity. The concept of a topping cycle for efficient conversion of fossil fuels to electricity is not new. The Indian Point I nuclear power plant built in the 1970s was a pressurized water reactor where the steam was sent to an oil-fired superheater to increase peak temperatures. It was at the time the most efficient oil to electricity plant in the world but was shut down after the oil embargo that made burning oil uneconomic.

The adoption of NACC as a power cycle has other major implications. The water-cooling requirements for combined cycle plants are ~40% of a light-water reactor because much of the heat rejection is by warm air versus cooling towers from other power cycles.

### 2.6.2 Heat storage

The heat storage system consists of high-temperature firebrick heated to high temperatures with electricity at times of low or negative electric prices (Stack, 2016,2017). The hot firebrick is an alternative to heating with natural gas. The firebrick, insulation systems, and most other storage system components are similar to high-temperature industrial recuperators. The round-trip storage efficiency from electricity to heat to electricity is ~66% based on ~100% efficiency in resistance electric conversion of electricity to heat and 66% efficiency in conversion of heat to electricity. That efficiency could be above 70% by 2030 with improving gas turbines.

Much of the technology to integrate FIRES into a gas turbine is being developed by Project Adele, a joint project of General Electric and RWE (a German utility). The goal is to develop an adiabatic compressed air storage system for deployment in Germany that is a lower cost alternative to battery and pumped storage of electricity. When electricity prices are low, air is (1) compressed 70 bar with the adiabatic compression raising the compressed air temperature to 600°C, (2) cooled to 40°C by flowing through a brick recuperator, and (3) stored as compressed air in salt domes deep underground. The compressed air must be cooled to avoid overheating the salt and causing structural failures of the underground works. When electricity prices are high, the compressed air flows back through the firebrick, is reheated and enters a turbine where it produces electricity before being exhausted to the atmosphere. The first demonstration project is to be completed in several years. As a result of this project, a firebrick recuperator is being incorporated into a modern large gas turbine. There are differences. For NACC with FIRES the gas temperatures are higher, the peak pressures are lower, and the firebrick is heated electrically. However, much of the technology is being developed, including how to integrate a gas turbine with a firebrick recuperator.

### 2.6.3 Economics

An economic analysis (Forsberg, 2014, 2016) was done of the performance of an FHR with NACC in California and Texas using natural gas to produce peak electricity. These states have deregulated electricity markets. The peaking capability increased the plant yearly revenue by about 50% after subtracting the cost of the natural gas compared to a base-load nuclear plant. Because NACC is more efficient than a standalone natural-gas combined cycle plant in converting natural gas to electricity (uses less natural gas), its electricity production costs for peak electricity are less than a standalone natural gas plant; thus, it earns large profits when electricity prices are set by natural gas plants.

Concerns about climate change from emissions of greenhouse gases have resulted in various policies to replace fossil fuel generation of electricity with nuclear and renewables. If the goal is a low-carbon electrical grid, the economics of salt-cooled reactors with NACC substantially improve and salt-cooled reactors with NACC may become the enabling technology for large-scale use of renewables.

Renewables are nondispatchable. The addition of wind and solar results in significant hours per year with very low electricity prices—near zero at times of high wind or solar input (Massachusetts Institute of Technology, 2015; Forsberg, 2015; Mills and Wiser, 2012). Fig. 2.11 shows an electricity price curve for fossil generation sources (existing; blue bars) and zero-carbon electricity grids in a deregulated market, where the horizontal axis has the wholesale price of electricity ($/MWh) and the vertical axis shows how many hours per year electricity could

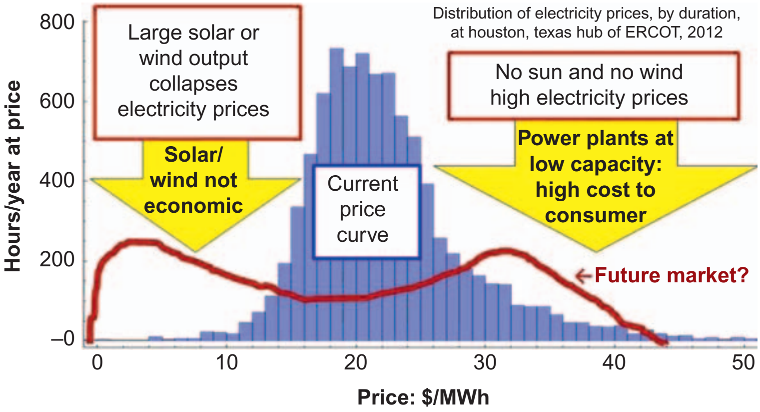

**Figure 2.11** Electricity price curve for fossil and low-carbon electricity grids.

be bought at a particular price. This specific example (blue bars) uses wholesale electricity price data from the Texas market in 2012. The price curve for an electrical grid primarily based on generating electricity from fossil fuels is approximately a bell-shaped curve. At times of low demand the power plants with the lowest operating costs are producing electricity and thus the market price of electricity is low. At times of high electricity demand, old inefficient units or units that burn more expensive fossil fuels are brought on line at high cost and set the wholesale price of electricity—resulting in high electricity prices at those times. There is an apparent minimum price of electricity. This is set by the cost of fossil fuels used to produce electricity. Sales of electricity below this price occur at times of very low demand when hydroelectric, nuclear, or wind plants set the price of electricity.

The red curve is a notational curve that shows what happens if one adds large quantities of renewables or nuclear and removes electricity generation by fossil fuel sources with no other changes. For example, if significant solar is added, the price of electricity will drop to zero in the middle of the day when there is high solar input and some solar output is curtailed due to the lack of markets. The incremental cost of solar production is near zero and solar producers will bid down hourly electricity prices to continue sales. The same happens for large wind input on windy days. To use an analogy, it's like selling tomatoes in August when everyone's tomatoes turn red at the same time—there is a glut on the market that results in price collapse. Electricity price collapse limits the large-scale use of these resources—even if there are large decreases in the costs of these technologies because all such plants provide output to the grid at the same time, independent of electricity demand.

When the wind stops or the sun does not shine, other power generators must be used to provide electricity. If these plants are used only half the time when the sun is down or the wind is not blowing, replacement plants will not be built unless the price of electricity doubles when they sell electricity to the grid to cover their costs. The long-term electricity price curve becomes bimodal—a fundamentally different price curve for electricity. This price collapse without storage technologies becomes economically significant when solar contributes $\sim 10\%$ of all electricity produced in a solar−fossil system, wind contributes $\sim 20\%$ of all electricity produced in a wind−fossil system, or nuclear contributes $\sim 70\%$ in a nuclear−fossil system. Revenue collapse discourages further investment in capacity of the very-low-carbon generating technologies in a free market. Subsidies can increase solar, wind, and nuclear capacities, but added capacity decreases revenue from the sale of electricity so subsidies have to increase as low-carbon technologies are added. Regulators can modify market rules so price collapse does not appear—but that does not change the costs to society—it just hides them as subsidies that increase the total cost of energy to society.

Constraints on the use of fossil fuels will dramatically improve the economics of NACC and create large incentives to add FIRES for heat storage to buy electricity when prices are low and produce added electricity when prices are high. In such an environment NACC becomes an enabling technology for renewables by providing

(1) a large market for electricity at times of low prices to charge FIRES and (2) peak power when required.

### 2.6.4 Observations

The concept of coupling a nuclear reactor to a jet engine (Brayton cycle) is from the 1950s; however, only in the last 15 years have the improvements in natural gas combined-cycle power plants made this a credible option. The advances in gas turbines are rapidly improving this power cycle option with time. If there are serious constraints on the burning of fossil fuels and significant use of renewables, the traditional base-load market for electricity will shrink with a corresponding growth in the demand for variable dispatchable electricity. Salt-cooled reactors with NACC can meet that market requirement.

## 2.7 Summary

MSRs can provide high coolant outlet temperatures, which enable high efficiency of electrical power generation. Rankine cycles can achieve up to about 49% efficiency at high steam temperatures. A helium-cooled Brayton cycle at $T_h = 650°C$, could achieve about 40%. A supercritical $CO_2$ Brayton cycle at 20 MPa, 700°C might achieve about 50%, and the turbine could be relatively small, but the technology is still under development. The NACC is just beginning development, but it could offer several advantages at 670°C:

- flexibility to provide either base load or peak power at low cost;
- base load efficiency ~42%;
- peak load (natural gas assisted) efficiency ~66%;
- reduced need for water;
- compatible with dry climates;
- compatible with hot firebrick thermal energy storage.

## References

Alstom Company, 2006. Flamanville Nuclear. France accessed at: <http://www.power-technology.com/projects/flamanvillenuclear/>.

Andreades, C., et al., 2014. Reheating Air-Brayton combined cycle power conversion design and performance under normal ambient conditions. J. Eng. Gas Turb. Power. 136.

Andreades, C., et al., September 2014. Technical Description of the “Mark 1” Pebble-Bed Fluoride-Salt-Cooled High-Temperature Reactor (PB-FHR) Power Plant, UCBTH-14-002. University of California at Berkeley. <http://fhr.nuc.berkeley.edu/>.

Andreades, C., Dempsey, L., Peterson, P.F., 2014. Reheating Air-Brayton combined cycle power conversion off-normal and transient performance. J. Eng. Gas Turb. Power. 136.

Andreades, C., Summer 2015. Nuclear Air-Brayton Combined Cycle Power Conversion Design, Physical Performance Estimation and Economic Assessment, PhD Thesis (Nuclear Engineering). University of California at Berkeley.

Chambers, W.R., Fraas, A.P., Ozisik, M.N., 1964. A potassium-steam binary cycle for nuclear power plants, ORNL-3584, UC-80-Reactor Technology, TID-4500 (29th ed.).

Dempsey, L., 2015. Power Conversion Options and Solutions for LFTR & MSR. Thorium Energy Alliance Conference, Palo Alto, CA, 3−4 June.

Dostal, V., Driscoll, J., Hejzlar, P., 2004. A supercritical carbon dioxide cycle for next generation nuclear reactors, MTI-ANP-TR-100, March 10, 2004.

El-Wakil, M.M., 1978. Nuclear Energy Conversion. American Nuclear Society, LaGrange Park, Illinois, USA.

Forsberg, C.W., et al., 2014. Fluoride-Salt-Cooled High-Temperature Reactor (FHR) Commercial Basis and Commercialization Strategy, MIT-ANP-TR-153. Massachusetts Institute of Technology, Cambridge, MA, December 2014.

Forsberg, C.W., 2015. Strategies for a Low-Carbon Electricity Grid With Full Use of Nuclear, Wind and Solar Capacity to Minimize Total Costs, MIT-ANP-162, Department of Nuclear Science and Engineering. Massachusetts Institute of Technology, Cambridge, Massachusetts, August 2015.

Forsberg, C.W., Peterson, P.F., 2016, Basis for Fluoride-salt-cooled High-temperature Reactors with Nuclear Air-Brayton Combined Cycles and Firebrick Resistance-Heated Energy Storage, *Nuclear Technology,* **196**, 13-33, October 2016.

Malang, S., Schnauder, H., Tillack, M.S., 1998. Combination of a self-cooled liquid metal breeder blanket with a gas turbine power conversion system. Fusion Engineering and Design. 41, 561−567.

Massachusetts Institute of Technology, 2015. Future of Solar Energy, Cambridge, MA.

Mills, A., Wiser, R., 2012. Changes in the Economic Value of Variable Generation at High Penetration Levels: A Pilot Case Study of California, LBNL-5445E.

Oh, C.H., Barner, R.B., Davis, C.B., Hawkes, B.D., Morton, J.D., 2006. Energy Conversion Advanced Heat Transport Loop and Power Cycle, INL/EXT-06-11681, August.

Petr, V., Kolovratnik, M., Hanzal, V., On the Use of $CO_2$ Gas Turbine in Power Engineering (in Czech)", Czech Technical University in Prague, Department of Fluid Dynamics and Power Engineering, Division of Power Engineering, Departmental report Z-530/99, January, (1999).

Stack, D., et al., 2016. Conceptual Design and Market Assessment of Firebrick Resistance Heated Energy Storage (FIRES) − Avoiding Wind and Solar Electricity Price Collapse to Improve Nuclear, Wind, and Solar Economics", Proc. International Congress on Advanced Nuclear Power Plants (ICAPP 2016), San Francisco, California, April 17−20, 2016.

Stack, D., 2017 Conceptual Design and Performance Characteristics of Firebrick Resistance-Heated Energy Storage for Industrial Heat Supply and Variable Electricity Production, MS Thesis, Department of Nuclear Science and Engineering, Massachusetts Institute of Technology, February.

Zhao and Peterson, 2004. A Reference 2400 MW(t) Power Conversion System Point Design for Molten-Salt-Cooled Fission and Fusion Energy Systems, University of California−Berkeley Report UCBTH-03-002, February 25.

Zohuri, B., McDaniel, P.J., DeOliveira, C.R., 2015. Advanced nuclear open Air-Brayton cycles for highly efficient power conversion. Nucl. Technol. 192, 48−60, October 2015, <http://dx.doi.org/10.13182/NT14-42>.

# Chemical fundamentals and applications of molten salts

# 3

*Stephen Boyd*[1] *and Christopher Taylor*[2]
[1]Aufbau Laboratories, LLC, Blue Point, NY, United States, [2]DNV GL, Oslo, Norway

## Chapter Outline

**Molten Salt Reactors and Thorium Energy. DOI:** http://dx.doi.org/10.1016/B978-0-08-101126-3.00003-8

## 3.1 Introduction

This book and this chapter focus on the many aspects of (mostly fluoride) molten-salt reactors (MSRs). This particular chapter serves as a general overview of the physicochemical properties of molten salts and describes some of the high-value applications that their unique properties enable. Topics discussed include the issues of containment materials, fluid mechanics, advanced Lewis-salt "pH" considerations, and the chemical properties of the salts themselves. Binary and ternary molten salts of many chemical classes (nitrates, chlorides, fluorides, etc.) have been studied for decades due to their unique, thermoelectrolytic and thermodynamic properties including density, viscosity, heat capacity, and thermal conductivity (Bloom et al., 1965), and each could form the subject matter of a chapter all on their own. These properties directly bear on applications of MSRs, including the production of electricity and the many high-temperature chemosynthetic applications that MSRs can facilitate.

An ideal working fluid should possess the following properties, as summarized by Saltarella et al. (2004):

- High boiling point;
- Low vapor pressure;
- High specific heat;
- High thermal conductivity;
- High density at low pressures.

In the first section that follows, the physical and chemical properties of molten salts will be introduced along with the theories that can be used to model or describe their behavior. In the subsequent sections various high-value applications for molten salts will be described across a broad range of industries, from the refining of hydrocarbons through to nuclear water processing and desalination.

## 3.2 Fundamental physicochemical properties of molten salts

### *3.2.1 Molten salts as working fluids in thermochemical processes*

Despite myriad advances in both inorganic and organic chemical catalysis, many chemical processes still require high temperatures to drive endothermic[1] reactions, such as ammonia production, as described later in this chapter.

---

[1] Endothermic: A part of a chemical reaction pathway that requires energy input to proceed. Conversely, an exotherm or an exothermic reaction is one that yields energy.

The high operating temperatures of MSR designs are in the 650°C–800°C range. Modern designs proffered by several start-up companies around the world exploit the high energy density of the salt to achieve MSR modularity, with the capacity for mobility and remote operation, focused mainly on electrical production.

A molten-salt fuel may contain isotopes of Th, U, Pa, Np, Pu, and the resultant fission products, which emit radioactive decay heat. Modern materials selection and corrosion retardation are required for molten-salt loops (Srinagar et al., 2008). Here, we will describe the properties of fluoride molten salts, their use in primary and secondary loops, and their potential applications for cost-effective, high-temperature chemical processes. (Chloride salts are also considered in some designs.)

Some clarification may be helpful to the reader at this point. Salts that characteristically melt at high temperatures are classically considered "molten salts." These systems have ionic bonds, often point charges, where much energy is needed to break those ionic bonds, hence the high melting points. Ionic liquids are a different type of salt that are liquids at room temperature (Marsh et al., 2004). Like molten salts, they have formal charges (+1, −1, etc.), but the charges are distributed among a group of other atoms that make up some substituent (a ring, a whole molecule, or what have you). Deep eutectics are a third class of compounds, where formal charges are assigned to two (or more) species, yet the interaction between them yields a system with an extremely lower melting point than the two compounds.

### 3.2.2 Chemistry, bonding, and electronic structure of molten salts

Molten salts have a unique electron landscape. In the solid state, most crystalline materials are held together ionically, with only *some* covalent bonding, depending on the system. Covalent character does exist in the solid state; however, two counter-examples are diamond (completely covalent) and silicon carbide (SiC), whose ionic character is only approximately 13% (Boyd et al., 2013). Their ionic (Coulombic) intermolecular bonding properties in the molten state interplay with the covalent bonding that emerges as a result of the phase change (from solid to liquid) in complex ways. This covalent/ionic ratio changes as one goes down and to the right in the periodic table; moving to the right increases the valence electrons' effective nuclear charge or $Z_{\mathrm{eff}}$[2], which decreases the ionic radius. The shift in electron density is due to distribution higher orbital involvement (4d, 5s, etc., as a function of higher atomic number), similar energies and symmetries, and decreasing cationic radius. These properties often permit more covalence (Nb, W, Ta, etc.), multiple oxidation states, and similar structure in the solid state and sometimes,

---

[2] Effective nuclear charge*:* The effective positive charge that binds an atom's valence electrons to the nucleus, denoted $Z_{\mathrm{eff}}$. Because core electrons shield valence electrons from the full positive charge of the nucleus, $Z_{\mathrm{eff}=}Z-S$, where $Z$ is the number of protons in the nucleus, and $S$ is the number of shielding electrons between the nucleus and the outermost electrons.

similar chemical behavior in either state, e.g., $TaBr_5$, $NbBr_5$, again depending on molecular symmetry.

Thus, a combination of ionic and covalent interactions occurs in the molten-salt bath. These interactions shift, depending on Lewis pH[3] and temperature. Coupled with molecular−orbital hybridization, covalently and loosely, ionically bound oligomers can and do occur in the molten state, depending on the species. This has been studied extensively computationally, and with good predictive results in several systems, but in pure form, namely, systems without all species contained within a working MSR model (Thoma, 1962; Thoma et al., 1963, 1968; Cantor, 1973; Madden et al., 2016). Lanthanide contraction[4] also substantively assists in ionic network calculations because of its predictability and stability under a wide range of molten-salt systems (Thoma, 1962). Scientists working on MSRs quickly discovered the role that eutectics, their deviations, and changes in Lewis pH played on thermal conductivity and melting points.

These larger species (salts with higher molecular weight metal centers,namely, in the lower row of the periodic table) form ionic networks in molten-salt systems (Salanne et al., 2008; Madden et al., 2016). Complications arise due to the fluctuating degree of both covalency and ionicity in the bath, however; shifting Lewis pH resulting from increasing fission-product production, necessary addition of fluorine, offgassing, and multispecies oligo/polymerization[5] all contribute to the complexity of the primary and secondary loops. The original MSRE experiments were managed by daily maintenance of the optimal, noninteger $U^{4+}/U^{3+}$ ratio, an extensive property of the system. This control is more difficult in MSRs larger than the original MSRE, such as those being proposed by several companies in this book (Discussions with Richard Engel, 2013).

### 3.2.3 Phase transformations in molten salts

Fig. 3.1 demonstrates the substantial eutectic and peritectic changes observed with even small changes in mol% concentrations and small temperature windows (Cantor, 1973; Madden et al., 2016). It does not, however, reflect the changes in

---

[3] Lewis acids−bases: A classification system where the Lewis acid is a recipient of electron pairs and the Lewis base is an electron pair donor. This system is more pragmatic in inorganic systems than the Brønsted system, since Brønsted acids and bases deal solely with hydrogen and hydroxyl ($OH^-$) exchanges.

[4] Lanthanide contraction: The filling of electron orbitals distinguishes the lanthanides and actinides from other blocks of elements. An atom's radius is determined by its outermost electrons, i.e., those with the highest principal quantum number. The radii of lanthanides and actinides are determined by their 6s and 7s electrons, respectively. Because f electrons do not effectively shield outer electrons from the nuclear charge, an increasing atomic number substantially increases outer electrons' attraction to the nucleus, whose increasing positive charge is only minimally shielded by the addition of an intermediate 4f or 5f electron. The result is an increasing Zeff and a contracting atomic radius when moving left-to-right across an f-block period.

[5] Oligo/polymerization: The joining of similar molecules in short (oligo) or long (poly) chains, usually as a result of ionocovalent bonding where (typically) halogens serve as the shared bridge between ionic species.

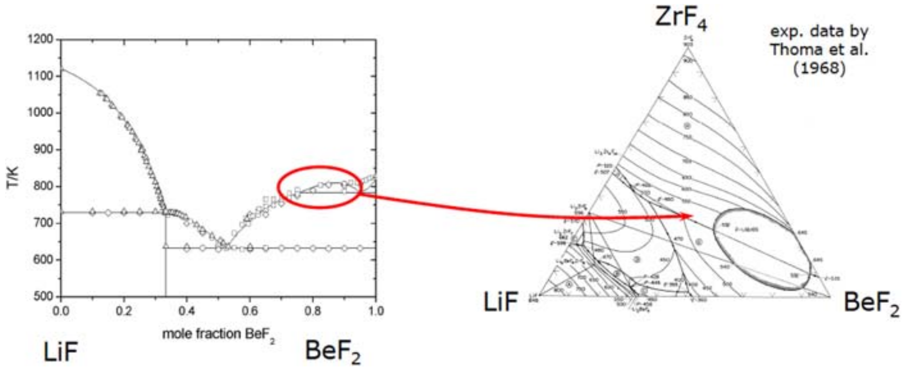

**Figure 3.1** LiF-BeF$_2$-ZrF$_4$ phase diagram. The extreme complexities of the large phase diagram (Left) are well-represented in the ternary phase detail (Right) (Thoma, 1962; Thoma et al., 1963, 1968).

density and viscosity that occur (Cantor, 1973). While *intrasystem* changes in density largely correlate negative-linearly in molten-salt fluoride mixtures as could be predicted, *intersystem* comparisons are not feasible, unless the eutectic salt compositions are the same and merely the mole percentages have changed. For example, addition of UF$_4$ in LiF-BeF$_2$-ZrF$_4$ mixtures studied by Cantor decreased the density, in comparison to the ternary LiF-BeF$_2$-ZrF$_4$ system (Cantor, 1973). The slight change shifted proportionally in mole percentage of the ternary group to accommodate the slight addition of UF$_4$. This negative-linear trend for density spans almost all salt mixtures, regardless of the anion as a function of temperature. Some substantive progress has been made regarding computationally derived density calculations (Herrmann et al., 2004; Quoining et al., 2011). Computed predictions of density, viscosity, and eutectic/peritectic points as a function of temperature and/or composition for different MSR and heat-exchanger component ratios are challenging, and computer modeling does not shed light on the dynamics that occur during MSR operation (to be discussed later). These critical parameters govern many aspects of heat-exchanger and core material construction. Geometry, effective thermal conductivity, and stresses should be incorporated into the heat exchanger design because of these changes to the candidate salt.

Poorly understood changes in viscosity, thermal capacity, and density are three disadvantages of the liquidus phase change. Fig. 3.1 is a clear example of the complexities associated with ternary eutectics due to Thoma's, as well as, Janz' early work in the late 1960s (Thoma et al., 1963, 1968; Janz et al., 1974). The following subsections explain some fundamental tools of crystal and molten-salt investigations.

Fluoride systems are the most extensively studied (Janz et al., 1974; Bale et al., 2002; Khosrow et al., 2009). Comparisons between different halogen salts that might emerge because of space-group symmetries or Lewis acids—base similarities are not available. The ORNL-MSR programs yielded a plethora of useful information, but no other systems were as extensively studied. NaCl-KCl ($NaKCl_2$), a strong candidate for fast reactors, is a good example of this incomparability. Fig. 3.1 exemplifies both the complexity and the extensive research conducted on binary, ternary, and n-ary fluoride salts throughout the decades of solid-state investigations. Janz et al., however, have amassed a substantive collection of empirical molten-salt data, predominantly on fluoride salts. Their work covers many salts, but of interest here are the fluorides and their thermodynamic properties (Janz et al., 1974).

Advances in solar thermal molten-salt systems have been aggressively explored, typically using the $KNO_3/NaNO_3$ pair as the working fluid (Born and Goeppert-Mayer, 1933; Edwards, 1970; Williams, 2006). The Rankine cycle is often employed, to varying degrees of success, depending mainly on the working fluid and the design architecture (Williams, 2006).

## 3.2.4 Crystallographic relations between the solid phase and persistent short-range order in molten salts

To understand the properties and behavior of a molten salt, one needs to first understand the solid state and then the solid/liquid transition. For MSRs these perspectives are important to understand eutectic and peritectic points. The rigidity and (quasi)periodicity of the crystal lattice is reduced in the ionocovalent, fluid molten phase during the transition, but quasilattice order is not lost.

The solid-state properties are partially reflected in the molten state. Sometimes, the crystallographic space groups[6] are of very low symmetry; molten states are of inherently low symmetry. The $LnF_3$ series are nine-coordinate in the solid state, for example. They reflect this in a six-ligand species in the molten state, with a formal charge of −3 ($LnF_6^{3-}$), implying a nine-coordinate system.

The lanthanide (Ln), lower transition, chalcogen[7] and actinide fluorides exemplify these complex symmetries. The solid state for many heterogeneous crystallographic systems adopts dimers, trimers, tetramers, and other examples of longer-range order, despite monomers occupying a single, crystallographic space group (Edwards, 1970). These n-mers can be seen in the ionocovalent networks of Madden's computer simulations (Madden, 2016). This is particularly true of the metalloid, lower-transition, lanthanide and actinide fluoride and halogen salts in the molten state (Edwards, 1969;

[6] Space group: A classification method for different atomic or molecular arrangements in crystals. The tallying of the atoms that represent the stoichiometry of the compound (e.g., $Al_2O_3$, $BaTiO_3$, NaCl), at various points in the most compact form possible. A finite number of motifs exist for the arrangement of atoms or molecules within the unit cell, such that dissimilar compounds can nevertheless be compared (see Fig. 3.6): different atoms or molecules in two different compounds can occupy the same spatial positions. High and low symmetry refer to the ease with which one atomic position can be translated to another. These are mathematical operations and are inversely related: the higher the number of operators, the lower the symmetry and, hence, the more complicated the unit cell.

[7] Chalcogen (pronounced kalkogen): A reference to Group XVI of the Periodic Table. The elements in this group all share specific and similar chemical properties. They form similar compounds as a result of their unique valence electron orbitals.

Edwards and Jones, 1977; Feigl, 1948; Wells, 1948). Well-known examples are the solid solutions of quartz, olivine, feldspar, and other silicates found in nature. One can also observe these phenomena in the quasihomogeneous mineralogic coexistence of tantalite and columbite in geologic deposits, which also contain lanthanides and actinides. The relative similarity in ionic radius and coordination number permits a seamless, often nonstoichiometric cationic substitution from one crystalline compound to the next, the hallmark of a solid solution (Graham and Thornber, 1974). The work done by Graham and Thornber (1974) demonstrates this well. For a good survey of foundational crystallographic principles, mathematics, and conventions that will help explain these phenomena, the reader can refer to West (1984).

Heat exchanger loop salts are based on simple salts, but with complex heat differentials, which present challenges to understanding liquid salt in the bulk and on intermolecular levels. The complexity of the ionic systems carries over to the molten state; covalence plays a substantial role and this is particularly true of core salts.

Crystallography plays a central role in understanding how the molecules interact in both their covalent and ionic states, and it serves as a vital tool to deduce the space group of the resultant eutectic(s) of any system. Central to the stabilization of any solid material is the concept of the crystal lattice energy. *Crystal lattice energy* or more commonly *lattice energy*, often abbreviated to $U_{\mathrm{pot}}$, is defined as the amount of energy required to separate the ions of a crystal to an infinite distance. The more modern convention is preferred: the energy required to form the bonds. The lattice energy is always negative, as is the usual convention for enthalpy, and represented using SI units ($\mathrm{kJ \cdot mol^{-1}}$). Since lattice energy cannot be derived empirically, extensive work has been done to develop different methods to calculate it, dating back to 1884 (Appell, 1884). Lattice energies are related to the Madelung constant (described below) due to the energy required to break those bonds. Lattice energies are a subset of the larger space of so-called *lattice sums*, which have many applications in charge-related fields of physics and chemistry where (quasi)periodic systems are investigated. Lattice sums are mathematical methods for calculation of lattice energies, and are beyond the scope of this chapter. Several authors have charted the development of the calculation of lattice sums (Borwein et al., 1985; Glasser and Zucker, 1980). Some standard calculations are shown in Fig. 3.2.

The *Madelung constant* (M, dimensionless) is a measure of the electrostatic potential of the ions within a crystallographic unit cell (Madelung, 1919; Osychenko et al., 2012; Hardin et al., 2014). It is usually a geometrically derived, dimensionless scalar. Often, however, the value must incorporate other potentials further away, whose electron densities are not spherically distributed (Streever and Caplan, 1973; Burns, 1993). The lattice energy is the amount of energy required to break the bonds between two atoms. Some simple M values are tabulated in Fig. 3.2. The calculation of M typically considers the Coulombic interactions between anions and cations as spherical, point charges within the crystal lattice. For highly symmetric crystals (e.g., cuboidal: rocksalt, rutile, fluorite, pyrochlore, KCl, LiF, NaCl, etc.), M for each varies only by sign, because the positions of the ions in the cell are the same and vary only by charge.

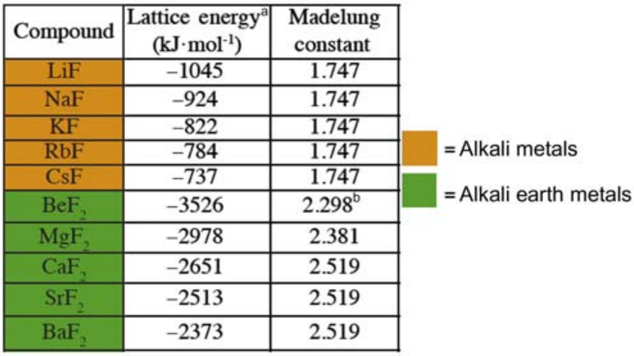

| Compound | Lattice energy[a] (kJ·mol$^{-1}$) | Madelung constant |
|---|---|---|
| LiF | −1045 | 1.747 |
| NaF | −924 | 1.747 |
| KF | −822 | 1.747 |
| RbF | −784 | 1.747 |
| CsF | −737 | 1.747 |
| $BeF_2$ | −3526 | 2.298[b] |
| $MgF_2$ | −2978 | 2.381 |
| $CaF_2$ | −2651 | 2.519 |
| $SrF_2$ | −2513 | 2.519 |
| $BaF_2$ | −2373 | 2.519 |

🟧 = Alkali metals

🟩 = Alkali earth metals

**Figure 3.2** Some crystallographic properties of simple, binary salts. [a]Calculated using Born-Haber Fajan cycle. [b]Trigonal structure used; BHFC method not used.

Indirectly, M is a measure of the complexity of a crystallographic unit cell, which often reveals useful information about the crystal. Each interatomic position within a low-symmetry unit cell has its own M, reflecting its local environment. This is due to the geometry, coordination number of the ions, molecular size, and the symmetry of the unit cell, and the distribution of the electronic charge on the ions themselves. Calculations of M diverge in lower symmetry crystals for several reasons, so more advanced mathematical tools must be used (Madelung, 1919; Streever and Caplan, 1973; Glasser and Zucker, 1980; Borwein et al., 1985; Burns, 1993).

In complex, inorganic crystals (such as $TaCl_5$) the bonds between the ions are not purely ionic, due to the large $Z_{\mathrm{eff}}$ on the valence electrons. Some covalent bonding is therefore present, which prohibits simple constants.

The electron density distributions of lower-transition metals often do not adopt spherical symmetry, which is assumed in calculating M in high-symmetry crystals, such as those listed in Fig. 3.2 (Streever and Caplan, 1973; Burns, 1993).

Researchers often use the “next-nearest neighbor” (NNN) protocol, because lower symmetry unit cells, which often contain high Z elements and/or complex ligands, have electronic effects beyond their immediate surroundings (Hoover et al., 1970; Brawer, 1980).

Trends are readily apparent in the data in Fig. 3.2. The more ionic a system is, the more negative the lattice energy. This is often partially estimated by the electronegativity of the element. Additionally, “ionicity" is influenced by the so-called $Z_{\mathrm{eff}}$ or the effective charge imposed on the *i*th electron in the valence orbital. Pure ionicity exists in some of the systems below.

In systems with modest ionicity and proximal, opposite charges in low-symmetry crystals, Coulombics and covalence are “felt” further away than merely NNN, thereby altering $U_{\mathrm{pot}}$. Finally, low-symmetry crystals often have high coordinate numbers for the metal center. The metal centers of the ligands attached have a range of interatomic distances, and often some of the total number of ligands are “shared” between nearby metal centers. To break these bonds, i.e., to change the phase of the system, multiple M values complicate the determination of the system

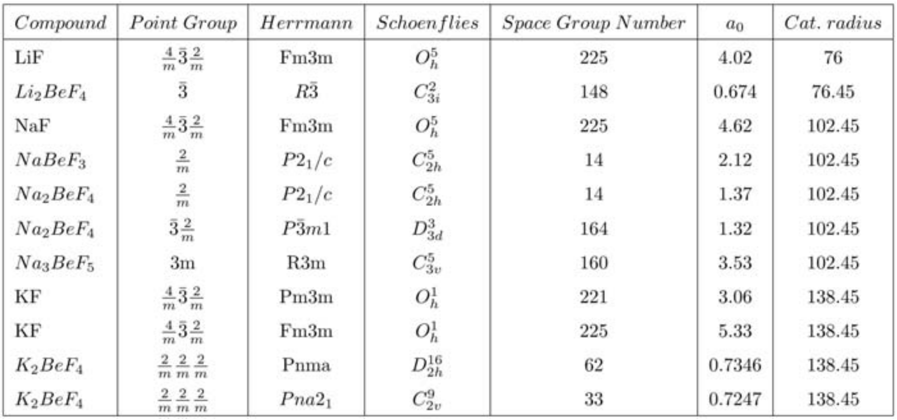

| *Compound* | *Point Group* | *Herrmann* | *Schoenflies* | *Space Group Number* | $a_0$ | *Cat. radius* |
|---|---|---|---|---|---|---|
| LiF | $\frac{4}{m}\bar{3}\frac{2}{m}$ | Fm3m | $O_h^5$ | 225 | 4.02 | 76 |
| $Li_2BeF_4$ | $\bar{3}$ | $R\bar{3}$ | $C_{3i}^2$ | 148 | 0.674 | 76.45 |
| NaF | $\frac{4}{m}\bar{3}\frac{2}{m}$ | Fm3m | $O_h^5$ | 225 | 4.62 | 102.45 |
| $NaBeF_3$ | $\frac{2}{m}$ | $P2_1/c$ | $C_{2h}^5$ | 14 | 2.12 | 102.45 |
| $Na_2BeF_4$ | $\frac{2}{m}$ | $P2_1/c$ | $C_{2h}^5$ | 14 | 1.37 | 102.45 |
| $Na_2BeF_4$ | $\bar{3}\frac{2}{m}$ | $P\bar{3}m1$ | $D_{3d}^3$ | 164 | 1.32 | 102.45 |
| $Na_3BeF_5$ | 3m | R3m | $C_{3v}^5$ | 160 | 3.53 | 102.45 |
| KF | $\frac{4}{m}\bar{3}\frac{2}{m}$ | Pm3m | $O_h^1$ | 221 | 3.06 | 138.45 |
| KF | $\frac{4}{m}\bar{3}\frac{2}{m}$ | Fm3m | $O_h^1$ | 225 | 5.33 | 138.45 |
| $K_2BeF_4$ | $\frac{2}{m}\frac{2}{m}\frac{2}{m}$ | Pnma | $D_{2h}^{16}$ | 62 | 0.7346 | 138.45 |
| $K_2BeF_4$ | $\frac{2}{m}\frac{2}{m}\frac{2}{m}$ | $Pna2_1$ | $C_{2v}^9$ | 33 | 0.7247 | 138.45 |

**Figure 3.3** Crystallographic parameters of some popular eutectic candidates, heat-exchanger salts and possible in situ variants for fluoride MSRs. [a]Most efficient unit-cell packing. [b]isomorphous; *c*/*a* ratios if *a*0 < 1; i.e: noncubic (hexagonal, rhombohedral); Cat. radius in picometers.
*Source*: Chase (1998); Mighell et al. (1977); Henry and Lonsdale (1965).

lattice energy. The valence orbital electron densities "searching" for the lowest energy configurations compound this view. This situation is described by ligand field theory[8]. Calculations are made as to the hybridized electron orbital occupancy, which affects the geometry of the unit cell, namely, structural changes in atomic positioning due to valence electron ordering to achieve the lowest energy. Though beyond the scope of this work, the reader can review the broad subject of crystal-field splitting theory and the derivations to understand ionic deviations from spherical symmetry (Streever and Caplan, 1973; Burns, 1993).

The crystallographic unit cell is a method of determining the most economic, formulaic representation of compounds like $MgF_2$, $BaTiO_3$, etc. The space group categorizes the complexity of a particular unit cell. Each crystalline compound may be classified into one of 230 space groups. Essentially, classification is determined by the way(s) one travels from one crystallographic point occupied by one atom or molecule within the unit cell to another by vector or geometric/algebraic operators such as rotations, translations, screw rotations, etc. In simple structures such as halite (table salt; cubic) or more complex ones ($TaCl_5$; monoclinic), these symmetries within the unit cell dictate the space group in which they fall. Several historical conventions have been adopted; both Schoenflies and Hermann-Mauguin conventions are used in Fig. 3.3 (Chase, 1998; Mighell et al., 1977; Henry and Lonsdale, 1965).

---

[8] Ligand field theory: A method of tallying and predicting transition-metal-based compounds based on the relative energies associated with (1) the oxidation state as it applies to the electron energies, (2) the hybridized molecular orbitals the valence electrons occupy, and (3) the relative energies of the bonding and antibonding energies of the metal and species to be bound, so as to exist in the lowest energy state possible that hybridization of the atomic orbitals allows.

In ionic systems, near-complete, formal, opposite charges are exerted on one another. The fewer electrons, the higher the $Z_{\text{eff}}$ and, therefore, the more negative the lattice energy. For less ionic or covalent crystals such as sugars or the classic compound *adamantane*, where van der Waals forces dominate, the lattice energies are much less negative.

### 3.2.5 Soft-sphere equations of state for the molten phase: The Helmholtz equation and proposed modifications resulting from molten-salt chemistry

Equations of state (EOS) are used to describe the thermodynamic properties of states of matter in the form of state functions. The EOS bears directly on the density and viscosity of the MSR system because the (dynamic) chemical components of the system dictate how the fluid(s) perform at temperature, pressure, internal energy, work, etc.

$$\text{Solid state} \pm \text{enthalpy of fusion} \rightarrow \text{Liquid state}$$

The enthalpy of fusion refers to the amount of the heat added to the system to promote the transition from solid to liquid ($\text{kJ} \cdot \text{mol}^{-1}$).

The chemical potentials for the entire set of species $\sum \mu_j \text{d}N_j$ (emergent and constant, so this is a simplistic, incomplete representation) should be considered. This term represents the chemical potential ($\mu_j$) or the interacting potential energy among the number of particles, $N$, and the different species $j$ within the system. This is particularly applicable to the MSR and the thermal behavior of both the primary and secondary loops, because the chemistries are dynamic, irreversible due to fission and offgassing (in the case of fuel salt), and not purely isochoric. Good data have been collated by Beneš and Konings on candidate eutectic mixtures in a review of previous work (Noh et al., 2014; Beneš and Konings, 2009).

The so-called soft sphere equation of state (SSEOS) for the liquidus transition was first explored in the 1970s. Hoover et al. used virial expansion to the 12th iteration (Hoover et al., 1970). This method proved reasonably accurate experimentally and roughly coincided with Monte Carlo simulations (Dai et al., 2016). Those Monte Carlo calculations, although state of the art for that era, proved to be only rough estimates. This was based mostly on the discontinuities found in the density curves as a result of changes to the system, namely, composition, Boltzmann temperature, etc., given that the density of the equations relied on viscosity of the system.

The best approach remains the Helmholtz version of the SSEOS (Hoover et al., 1970; Griffard et al., 2013a,b; Dai et al., 2016). The simplicity of space groups for binary salts in the solid state proved to be a critical tool for calculations of SSEOS in the liquid phase. Chen et al. described the EOS for $2\text{LiF} \cdot \text{BeF}_2$ or $\text{Li}_2\text{BeF}_4$ ("FLiBe") as a function of Boltzmann temperature (Chen et al., 1992). Their work demonstrated that any heat exchanger or MSR would encounter substantial changes in internal compression and, therefore, thermohydraulic performance with a closed system as a function of temperature (Dai et al., 2016). Their study of these basic compounds could be reasonably applied to secondary loops as well, since more substantial changes in temperature will be realized in heat exchangers on secondary loops. This bears directly on heat-exchanger performance (pumps, impellers, performance life) for so-called downstream hydrocarbon chemistry or any chemistry affected by secondary loops, and the MSR core itself.

As covalency begins to play a larger role in the molten phase, the geometry of rocksalt structures, typically with the cubic space groups or high-symmetry crystals, the unit cell begins to adopt a noncuboidal geometry, "bowing" out the otherwise ionic, linear bonds toward the molecular–orbital hybridization characteristic of covalent species.

Griffard et al. investigated the thermodynamic properties of some binary and ternary mixtures of fluoride salts, relying heavily on the high space-group symmetry of the fluoride salts (see Fig. 3.3) (Griffard et al., 2013a,b). While their conclusions produced accurate results, they were based on both computational and empirical data, but had four adjustable parameters (*n, Q m, d*) (see Fig. 3.4).

Griffard et al. also incorporated $BeF_2$, KF, NaF, and LiF into their molten-salt SSEOS (Griffard et al., 2013a,b; Dai et al., 2016). The effective modeling of $BeF_2$ is possibly due to its different thermodynamic properties, relative to metal fluorides adjacent to beryllium fluoride in the periodic table. It occupies an unusual niche spanning a low-temperature gap between LiF, NaF, and $MgF_2$.

Griffard's modifications to the modified Helmholz equation are the most advanced in the literature of molten salt thermodynamics (Griffard et al., 2013a,b; Dai et al., 2016). The Helmholtz EOS has historically been a useful tool for scientists, given its inherent flexibility and ability to incorporate other terms or derivations, such as the virial equation or the partition function. The weakness of this

$$\bar{f}(\bar{\nu},T) = Nk_BT\left[-\mathrm{in}\left(\frac{\bar{\nu}e}{N\lambda^3}\right) - \mathrm{din}\,(T) + C_n\rho^{\frac{n}{3}}\left(\frac{\epsilon}{k_BT}\right) + \frac{1}{2}(n+4)\,Q\rho^{\frac{n}{3}}\left(\frac{\epsilon}{k_BT}\right)^{\frac{1}{3}} - \rho^m\left(\frac{\epsilon}{k_BT}\right)\right] + E_{\mathrm{coh}}$$

$\bar{f}$ = molar Helmholtz energy
$\bar{\nu}$ = Volume specific
$N$ = Avogadro's number
$k_B$ = Boltzmann
$\lambda$ = deBroglie wavelength
$C_n$ = fcc madelung constant
$\rho$ = Density relative to closely packed fcc lattices
$\epsilon$ = Intermolecular potential energy
$n$ = Adjustable parameter in Soft – Sphere equation of state
$Q$ = Adjustable parameter in Soft – Sphere equation of state
$m$ = Adjustable parameter in Soft – Sphere equation of state
$d$ = Adjustable parameter in Soft – Sphere equation of state
*fcc* = Face - centered cubic
$E_{\mathrm{coh}}$ = Cohesive energy

**Figure 3.4** The Griffard equations and the parameters used therein.

approach is that a number of parameters, usually taking the exponential positions, as in the third, fourth, and fifth terms below, can be manipulated. The terms that they modify, however, carry little physical significance.

The Griffard equation could benefit from the incorporation of chemical modifications of Helmholtz parameters specific to solid-state chemistry, namely: $N$, $C_n$, $\epsilon$, $\rho$, bcc, and $E_{\mathrm{coh}}$. This would require extensive, computationally driven, molecular dynamics (MD) and density functional theory (DFT) assistance to be applicable to an MSR, as cited elsewhere (Noh et al., 2014; Dai et al., 2016).

The quantity $N_i$ of molecules of each molten salt constituent is constantly changing, due to the production of fission products and offgassing, excluding in situ or ex situ removal of waste products. This number, however, is calculable. The total number and mass of the fission products being produced and/or removed is known. Considering that a steady-state equilibrium is the goal of any nuclear system, a multicomponent tracking of offgassing could prove to be a reasonably accurate indicator of $\mathrm{d}N_i/\mathrm{d}t$, where $N_i$ represents the moles of each isotope being produced.

Given a known initial salt load, the neutron flux (location dependent), the core and ancillary geometries and the number of neutrons (in moles), and the statistical probability of a neutron uptake by a nuclide, these mathematics can be solved analytically.

The Madelung constant ($C_n$, $E_{\mathrm{coh}}$; third and external bracketed terms) for most crystals more complex than fcc (face-centered cubic) or bcc (body-centered cubic), will require heterogeneous, interatomic-specific Madelung values. For more complex species found in an MSR such as monomers or oligomers (as would normally be found for many of these species within an MSR), the complexity is challenging and yet feasible; eutectic and peritectic points are well-known for different salt compositions and those can be determined via scientific modalities that have been utilized for years.

In the solid state, these crystals are also of low symmetry, thereby expanding the Madelung component of $NbF_5$, $TeF_{4/6}$, $LnF_3$, etc., crystals, space groups, $\epsilon$, fcc, $\rho$, and $E_{\mathrm{coh}}$, as found in the Griffard equation.

For the more complex Madelung values, in contrast to the single constants found in the fcc and bcc space groups, the accompanying lattice energies will be affected as well. Empirical data may be useful, since M values for lower symmetry crystals either diverge or conditionally diverge, often because the "NNN" have a complex effect on the $M$ value of interest (Henry and Lonsdale, 1965; Borwein et al., 1985; Salanne et al., 2008). It may be more prudent to learn from the ab-initio work done by Dai et al. and Noh et al., using density functional theory (DFT). Their work incorporating the relative amounts of covalent bonding and phase change in the molten state with MD simulations, demonstrated that trimers and covalently bound clusters can form within the melt (Noh et al., 2014; Dai et al., 2016).

The density term, $\rho$, is specific to fcc in the Griffard case and relies on the high symmetry of the space groups to which these crystals belong. Packing in the solid and liquid states is calculable, since they follow the patterns of cubic close packing (CCP) or hexagonal close packing (HCP) motifs. This simplicity is lost for any molecules of lower symmetry, so both densities and viscosities will vary substantially while passing through a primary or secondary heat-exchanger loop.

Intermolecular potential energy (IPE) or $\epsilon$ according to Griffard could be more explicitly defined (Epsilon = intermolecular potential energy [induced ion dipole moment]). This challenging range of forces (dipole−dipole interactions; induced dipole, dispersion forces, etc.) combines in different, dynamic ways to permit $F$ exchange. $E_{\text{coh}}$ depends on lattice energy. Energetically below ionic and covalent bonding, primary IPE forces in either a primary or secondary MSR loop would predominantly be dipole−dipole and dipole−induced dipole interactions, particularly with tetravalent coordinated salts, $UF_x$ ($x = 3.x{-}4.x$) and the degrees of freedom these weak forces permit. Noninteger stoichiometries denote a flexibility in the system, often due to fluctuating Lewis pH, as in this case. In the liquid state, these forces apply and ionic forces play at least a moderate role. In contrast to $UF_x$, $ThF_4$ participates as a solvent, due to its strong ionic bonds, even in the molten state; very little fluorine loss or change in electronic distribution occurs.

The cohesive energy term ($E_{\text{coh}}$) returns to the Madelung values with $E_{\text{coh}}$ defined as:

$$E_{\text{coh}} = U_{\text{latt}} - (\overline{h}_{298} - \overline{h}_0) - (\overline{h}_{T_m} - \overline{h}_{298}) + vRT_{\text{m}}$$

As can be seen in the definition of $E_{\text{coh}}$, an expansion of the Madelung values to a Riemannian sum would be required, using the different melting points ($T_{\text{m}}$) of each component.

The complexities that accompany the phase change from the solid to the molten are the most vexing. Crystallographic properties affect the liquid phase, a largely ionic state, but with clear covalent influences affecting the mixture. These properties affect the interactive geometries observed in model systems, as shown in past studies of molten nitrate−chloride mixtures (Thoma, 1962).

Molecular ratios and cationic size play roles in the solid and molten states. $LnF_3$ (where lanthanides Ln = Y and the elements of the sixth row of the Periodic Table) are more complex in the solid state, but stand out as an important feature in MSR chemistry. A majority of the fission products are lanthanides, which can be well described by MD modeling (Salanne, et al., 2008; Madden et al., 2016; Dai et al., 2016). These models have strong theoretical origins, resting on the quasilinear relationships of lanthanides regarding cationic size and accommodation in the solid state (e.g., $LnF_6^{3-}$ octahedra) (Dai et al., 2016).

The definitions of eutectic and peritectic can point in specific directions, and some parallels can be made: eutectics are two crystallographic lattices being fused, where each sublattice that comprises the superlattice retains its respective space group. The space group of the two “fused” sublattices results in a new space group of lower symmetry. A peritectic solution involves a liquid and a solid that, when mixed, result in a new solid, again of lower symmetry. In a majority of historical cases, typified in the recent work of Capelli et al., solid solutions occur when the stoichiometries are noninteger, as in their investigations of the $LiF{-}CaF_2{-}ThF_4$ system (Capelli et al., 2015). The in-situ stoichiometries that occur in the molten salt eutectics/peritectics loosely reflect back on the two separate Hermann-Mauguin classifications depicted in Fig. 3.5 (Chen et al., 1992; Griffard et al., 2013a,b).

(A)

$$\underbrace{\pm\sum_{ab}(q_a+q_b)\,\beta_{ab}S_{ab}}_{\text{First term}}+\underbrace{\sum_{i,j}\frac{Q_kQ_l}{\epsilon R_{kl}}}_{\text{Second term}}+\underbrace{\sum_{r}^{occ.}\sum_{s}^{unocc.}\pm\sum_{s}^{occ.}\sum_{r}^{unocc.}\frac{2\left(\sum_{ab}c_{ra}c_{ab}\beta_{ab}\right)^2}{E_r\pm E_s}}_{\text{Third term}}$$

(B)

**$a_a, a_b$ = Electron densities for atomic orbitals $a,b$**

**$\beta,\ S$ = Resonance, overlap integrals**

**$Q_k, Q_l$ = Total local coulombic charges on atoms $k,l$**

**$\epsilon$ = Local dielectric constant**

**$R_{k,l}$ = The distance between atoms $k,l$**

**$R_{k,l}$ = The distance between atoms $k,l$**

**$C_{r,a}$ = Coefficient of atomic orbital a in moleclar orbital $r$**

**$r$ = Molecular orbitals on one molecule**

**$s$ = Molecular orbitals on a second molecule**

**$E_r$ = Energy molecular orbitals on one molecular $r$**

**$E_s$ = Energy molecular orbitals on one molecular $s$**

**Figure 3.5 (A)** The Salem-Klopman perturbation equation, (B) variable definitions for (A).

Consistent with cationic size, the species $LiNa(BeF_3)_2$ (not listed in Fig. 3.5) with the extremely small packing ($a_0 = 1.09Å$) are isostructural with $NaBeF_3$ and $Na_2BeF_2$. Despite being ternary, its small size is nonintuitive and accommodates two $BeF_3$ units. Thus, $BeF_n^{y-}$ n-mers mentioned previously can be reconciled with the information here.

As depicted, an SSEOS remains a static, isochoric system with no chemistry occurring. Further, terms three through five (see Fig. 3.3) all contain adjustable parameters that are chemical properties. Although complex, they are calculable, particularly when $\epsilon$, $\nu$, n, m, and $E_{coh}$ are included in the calculations. As with all chemical or physical systems, a steady-state equilibrium is the goal. With systems so massive and such wide-ranging (yet tractable) chemistries, like those found in primary and secondary loops, perhaps a more chemically dynamic perspective could be considered.

In MSR cases, the species are constantly changing radii, oligomerizing and exchanging anions (in the case of fluoride and chloride salts) with one another in the bath. The chloride salt system is somewhat different, in that the bath is Lewis acidic, because no Lewis base system appears to have been identified. $BeCl_2$, although studied and geometrically identical to $BeF_2$, does not appear to have been considered as a eutectic. The Lewis pH of these systems can be explored, but only systematically and with a combination of both empirical and quantum-chemical, computational assistance. Lewis pH changes initiate complex shifts in ionic bonding, n-meric geometries, and the like. It is computationally challenging to accommodate for these shifts in the Lanthanide (Ln) and actinide (An) rows, since relativistic effects on the valence electrons play an increasing role in their chemistries.

Despite careful investigation, Griffard et al., demonstrate the difficulties in predicting changes in density and viscosity, even for high-symmetry space-group systems (Griffard et al., 2013a,b). Their smallest calculated deviations from empirical data result from their thorough examinations of pure salts. Their temperatures were also fixed in their experiments, but substantial increases and decreases are expected in both the primary and secondary loops, due to fission products and temperature gradients in the heat exchangers. Their additional simplification regarding an isochoric state is impractical for real-world application.

Adding calculable (albeit very challenging at this level of complexity) dynamics and reactivity may diminish the variability in the Griffard equation, particularly as it pertains to terms three through five in the SSEOS (Fig. 3.4). It may even modify and/or restructure it. This could, in turn, be improved upon by inclusion of a modified *Salem-Klopman equation* Klopman (1968) (Fig. 3.5).

The Salem-Klopman equation (see Fig. 3.5), first proffered by the eponymous chemists in the 1960s, defined the chemical dynamics. The three terms in the Salem-Klopman equation have been satisfactory for use in density functional theory (DFT) calculations. With advances in computing power, DFT substantially accelerates understanding of complex molecular systems that involve both ionic and covalent interactions. To date, very few DFT calculations have been applied to MSR chemistry.

Solving these complex interactions could rely on DFT, as it is based on mean field theory (MFT). In this case, time-dependent MFT (TMFT) may be more appropriate, since an operating schedule and the nuclear fission rate are known, given predetermined parameters.

Crystallography again plays a role in shedding some light on optimal eutectic and peritectic points, and their accompanying stoichiometries. Direct comparisons between the solid and liquid phases can be drawn to some extent.

As the SSEOS name implies, the soft sphere is a sphere where the total spherical fluctuations of electron densities integrate to zero. These fluctuations are necessarily quasicovalent in the molten state, even with binary crystals that are highly ionic in the solid state, like NaF. The approach toward spherical geometry requires a "bowing" due to increasing, heat-driven, molecular hybridization, before lattice energy is broken. The most likely reason for the additional success with $BeF_2$ was the quasispherical shape of the total $2M^+ \cdot [BeF_4]^{2-}$ species in the molten state (Noh et al., 2014; Dai et al., 2016).

In the solid state, $BeF_2$ is four-coordinate, isostructural with β-cristoballite, and hence resides in the cubic Fd3(bar)m space group (Parthé, 1964). It adopts $sp^3$ hybridization, but with substantially covalent bonding, called dative bonding, or "coordinate, covalent" bonding, where two electrons stem from the same element or species. The ionic character is, therefore, significantly lower. Two fluorines bridge between neighboring Be atoms. Beryllium's high electronegativity causes deviation away from true, four-coordinate, "pure" ($\theta = 109.5$ degrees) $sp^3$ hybridization and geometry in $BeF_2$ (Dove et al., 1997; Swainson and Dove, 1993). This lends itself to a *mean* of 109.5 degrees, meaning bond angles and lengths are changing (Dove et al., 1997; Swainson and Dove, 1993). Dative bonding and nonrigid F—Be—F geometries and bond lengths promote the propensity for $BeF_2$ to form polymeric systems in the solid state, like the isostructural β-cristobalite and the many polymorphs of $SiO_2$ (Rakitin et al., 2015). Therefore, it appears highly likely that the *n*-mers seen in the molten state are at least partially due to these unusual characteristics for such a small molecule.

The $[BeF_4]^{2-}$ tetrahedron carries the formal −2 charge in the molten state. In the molten state, the two fluorines are donated to the $BeF_2$ from the two LiF molecules, making it a covalent, $[BeF_4]^{2-}$ tetrahedral anion, now $sp^3$ purely hybridized. With $2e^-$ density now distributed tetrahedrally among the four fluorines, the two lithium cations dynamically charge-compensate the negatively charged fluoride ligands, where the electron density is greatest. Critically, however, electron–electron repulsion will cause the electron density that forms the $-2$ charge to remain distributed among the four fluorines for a statistical majority of time within the anionic tetrahedron. The dynamics of these high-temperature, high-entropy systems will cause these tetrahedrally opposed densities ($e-/2$) to fluctuate quickly about the tetrahedron. Consistently, the loosely bound $Li^+$ also charge stabilizes in calculated DFT simulations for the dimers, trimers, and tetramers of $[BeF_4]^{2-}$:$[Be_2F_7]^{3-}$ and $[Be_3F_{10}]^{4-}$, respectively (Salanne et al., 2008; Noh et al., 2014; Dai et al., 2016). The flexibility of the $[Be_nF_{n+y(y=1,3,5...)}]^{n+1-}$ to form oligomers and to be sensitive to Lewis pH have an effect on the Lewis acid/base pair. This changes the viscosity and density of the fluid, because the networks of interacting $[Be_nF_{n+y(y=1,3,5...)}]^{n+1-}$ clusters increases. Given the increased presence of covalency in the molten state, these species (and larger clusters) of the parent $Li_2BeF_4$ are reasonable, so long as "global" charge compensation and MO hybridization are satisfied.

The argument remains the same for MF ($M_{>Li}$=Na, K, etc.). However, the masses of the $M_{>Li}$ cations are approximately 3.3 times (and greater) the mass of the lithium cations, which is why $2M_{>Li}F \cdot BeF_2$ fosters a good discussion regarding optimal eutectic salts. One could consider calling this charge compensation a "hopping" or stabilizing frequency for the sodium or potassium cation around the $[BeF_4]^{2-}$. This frequency is lower, in comparison to lithium, diminished by its mass. This is the rate at which the two $M_{\geq Li}$ cations per unit can charge-compensate the $[BeF_4]^{2-}$ tetrahedral anion in the liquid state.

All species in the first term of the S-K equation are known, given the initial salt load and at thermal/neutronic equilibrium. The resonance and overlap integrals can be estimated, since the total number of moles for every species can be calculated. In the molten state, these distances are either estimable or are already known. Furthermore, the chemical reaction rates of all species can also be calculated, because all reactions are predictable (it is a closed system).

The chemical potential ($\mu$) is the intermolecular potential energy, which is also a calculable term in the Griffard equation because in the S-K equation, Coulombic repulsion as a function of mean distance in the bath for all of the ions present can also be quantified.

As can be seen in the third term, below, the quadratic components ($\sum_{rs}$) refer to "occupied" and "unoccupied" and denote the HOMO and LUMO molecular orbitals. These terms include the Legendre polynomials or the geometry that the molecules adopt as a result of their covalent and ionic interactions.

The adjustable parameters modify terms 3–5 in the Griffard equation and the enthalpy terms found in $E_{coh}$, but they are modified, based on iterative estimates, predominantly modifying the density terms exponentially. So, even with simple fcc and/or bcc systems, changes in density affect the multiplicative terms substantially.

### 3.2.6 Summary of physicochemical properties of molten salts and theoretical considerations

Having a good understanding of the crystallographic basis for molten systems is essential to understand the solid-to-molten transition and the molten state.

Historically, the density of the solid state has been done pycnometrically (Viana et al., 2002).[9] The density of the liquid (molten) state has been done using more advanced equipment: thermogravimetric analysis (TGA) and differential scanning calorimetry (DSC). However, considering the challenges of these caustic systems, dedicated and long-term analysis with specialized systems is needed.

One needs a thorough understanding of the solid state in order to understand the molten state because:

- The complexity of the solid-state unit cell bears directly on the complexity of the resultant molecule in the molten state.
- The more geometrically complex the unit cell is, the greater the probable number of oligomeric, ionocovalent bonds will occur in the molten state.
- The Lewis acidity/basicity of simple, binary salts increase $\Delta S$ as a function of pseudo-spherical geometry, and their interference with salts that have differing Lewis pH.
- The lower the salt components are in the periodic table (e.g., involving tetrahedral and/or octahedral coordination of higher electronic orbitals) in the solid state necessarily increases the complexity of the resultant intermolecular, ionocovalent interactions in the molten state.
- Fermi-Dirac statistics (Boltzmann) add additional complexity to determining viscosity and/or equations of state, because the electronic populations of each molecular orbital change in number as f($T$).
- The relative interactions of the higher orbitals' changes within the d orbitals. Each d orbital will take prominence regarding the interactions of the surrounding molecules.

MSRs and their rich chemistries have been studied extensively since the 1950s. Their thermodynamic and thermochemical properties have been thoroughly investigated. Glassner, for example, covered a range of thermodynamic properties of the chlorides, oxides, and fluorides (Glassner, 1957). In addition to central station electric power, MSRs can have many other beneficial applications.

## 3.3 Remote power sources

### 3.3.1 Historical context

Policy makers have indicated interest in the prospect of remote power sources (RPS) since the 1970s (Carter, 1977; Martinez, 2002; Wiedemann et al., 2005; El-Genk, 2009). Many very radioactive isotopes could be harvested from MSRs for RPS applications.

---

[9] Pycnometrics: The practice used to determine density as a function of temperature. Pyrometric systems employ highly accurate temperature changes in order to plot density as a function of temperature.

### 3.3.2 Radioisotope thermoelectric generators and betavoltaic cells as RPSs: Extracting electrical work from MSR waste

Both Radioisotope Thermoelectric Generators (RTGs) and Betavoltaic Cells (BCs) have served as remote power sources for decades, from the well-known $^{238}$Pu (RTG, $\alpha$ emitter), to $^{90}$Sr, $^{90}$Y, $^{137}$Cs $^{147}$Pm, and $^{3}$H for BCs (Corliss and Harvey, 1964; Karam and Stein, 2009; Yakubov, 2010). Ex-situ billets of purified fission products can produce exceptional thermal output. The Soviets, e.g., used $^{90}$Sr to power their distant lighthouses positioned along the Arctic and White Seas. With an approximate half-life of 28.8 years and a theoretical power/mass ratio of 916 $\text{mW} \cdot \text{g}^{-1}$, this strong $\beta^{-}$ emitter served the Soviets well during the Cold War. Fig. 3.6 demonstrates NASA's substantial use of BCs and RTGs as power sources for a wide range of previous missions.

Although more difficult to work with due to its violent reactions with ambient water, $^{137}$Cs is also a strong $\beta^{-}$ emitter with a half-life of approximately 30.2 years. A theoretical yield of approximately $427\ \text{mW} \cdot \text{g}^{-1}$ makes it suitable as a source material for BCs. Fig. 3.7 depicts a partial list of RTG and BC materials.

Fig. 3.7 also depicts $^{1x}$Xe (x = 33,35,37,40) $^{85,\ 87\text{-}91}$Kr and $^{13z}$I ($z = 1-4$) as candidate materials for BCs. Although Kr can be made stable at room temperature on Earth

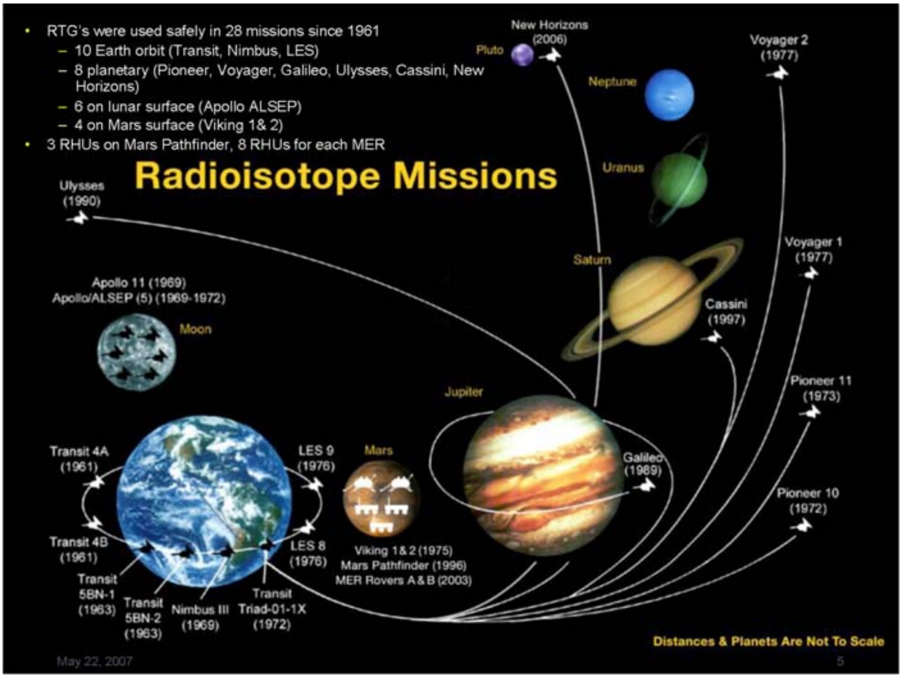

**Figure 3.6** Missions that relied on either Radioisotope Thermoelectric Generator (RTG) or Betavoltaic Cells (BCs) as the primary energy source.
*Source*: Image courtesy of JPL.

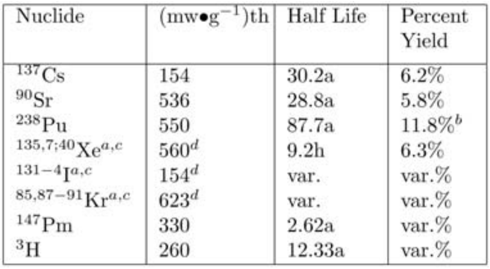

| Nuclide | $(\mathrm{mw} \bullet \mathrm{g}^{-1})\mathrm{th}$ | Half Life | Percent Yield |
|---|---|---|---|
| $^{137}Cs$ | 154 | 30.2a | 6.2% |
| $^{90}Sr$ | 536 | 28.8a | 5.8% |
| $^{238}Pu$ | 550 | 87.7a | 11.8%$^{b}$ |
| $^{135,7;40}Xe^{a,c}$ | 560$^{d}$ | 9.2h | 6.3% |
| $^{131-4}I^{a,c}$ | 154$^{d}$ | var. | var.% |
| $^{85,87-91}Kr^{a,c}$ | 623$^{d}$ | var. | var.% |
| $^{147}Pm$ | 330 | 2.62a | var.% |
| $^{3}H$ | 260 | 12.33a | var.% |

**Figure 3.7** Candidate Radioisotope Thermoelectric Generator/Betavoltaic Cell (RTG/BC) radioisotopes: $(12\% > x > 5\%)$ $x = \%$ fissile yield. Radioisotopic power (Specific Power) in $\mathrm{mw} \cdot \mathrm{g}^{-1}$ and accompanying half-life ($\sim 6\,\mathrm{h} < t_{1/2} < 90$ years). $^{a}$Fits criteria, but impractical for terrestrial use; $^{b}$Data based on 70%/30% $ThO_2$-$UO_2$ LWR production: 6 years at 87MW; $^{c}$Fast beta decay chains ending in stable isotopes; $^{d}$estimated, due to isotopic multiplicity.

with the application of fluorine chemistry ($KrF_n$; $n = 2, 4, 6, 8$), it is impractical to do so because the betas produced will engender radiolysis and decomposition (Ẑemva et al., 1975; Lutar et al., 1985; Sun et al., 2005; Anderson and Wong, 2005; Surapudi, 2011). $KrF_n$ is also unstable at STP. Gaseous source materials also present their own engineering difficulties. Nevertheless, it may be possible to use $^{1xy}Xe$ and $^{13z}I_2$ in novel BC, ion-drive and MPDT thruster configurations for space applications.

Additional research into materials and geometries would be required to accommodate such unusual BC systems (Sun et al., 2005; King et al., 2007). Some interesting configurations for the BC using the Xe/I combination could be imagined, however, taking advantage of the dramatic differences in melting/boiling points, the molar heat capacity differences and extremely high beta output. The fission gases Xe and Cs vapor were expelled into space with the TOPAZ design (Nguyen et al., 2001; Al-Shammari et al., 2014). Modern designs could more readily exploit waste gases through both BC and thermionic emission. A low but constant stream of high-energy offgases from an MSR on-board a space vehicle could serve as a strong BC source material. NASA investigated the Stirling RTG and BC (Nguyen et al., 2001; Wolverton, 2008; Yabukov, 2010), where a thermal gradient cools and heats an inert gas, such as helium. The differential induces mechanical motion of a cantilever, thereby converting a thermal differential into mechanical energy. Prototypes reached 23% efficiency and could theoretically reach 30% (Stine and Diver, 1999; Nguyen et al., 2001).

### 3.3.3 Space-based nuclear reactors as remote power sources

China and Russia have investigated space-based nuclear systems for more than a half century and the United States has done so intermittently (Wiedemann et al., 2005; El-Genk, 2009). The Soviet Union's RORSAT and COMOS lines of satellites employed nuclear reactors from 1970 to 1988, especially in the BUK MOX reactor model. (See Figs. 3.8, 3.9, and 3.10 for additional historical and technical detail for international deployment of space-based nuclear reactors.)

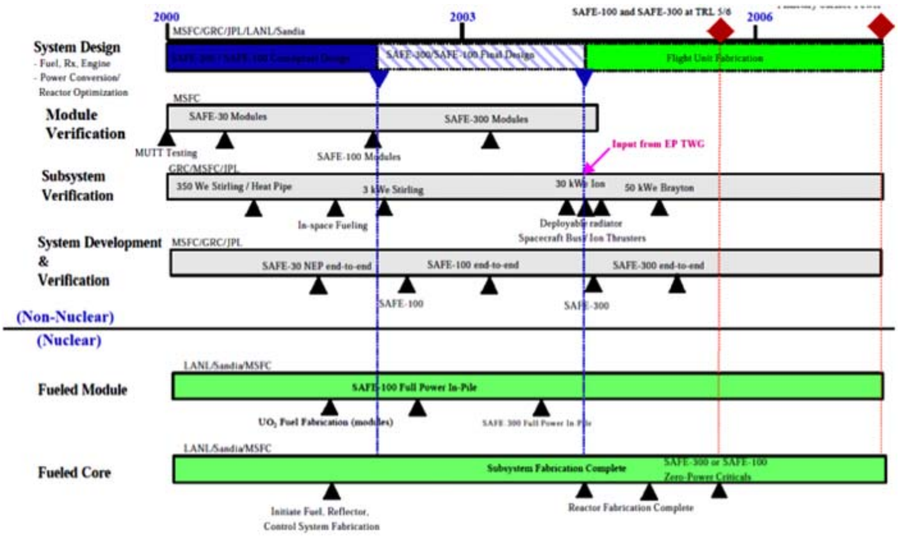

**Figure 3.8** SAFE construction and deployment proposed timeline.
*Source*: Adapted from Van Dyke et al. (2001).

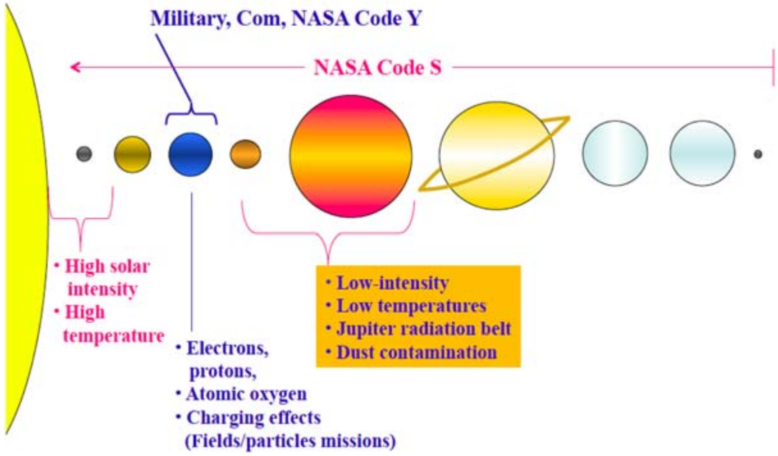

**Figure 3.9** NASA logistical considerations for short- and long-range energy sources (Van Dyke et al., 2001).
*Source*: Image courtesy JPL.

NASA/JPL work has continued on the SAFE nuclear reactor (Van Dyke et al., 2001; IAEA, 2005; Wangab and Chaohui, 2015) (see Fig. 3.8). NASA/JPL have set forth stringent conditions regarding extraterrestrial, lunar, and/or Martian use of nuclear reactors as RPSs:

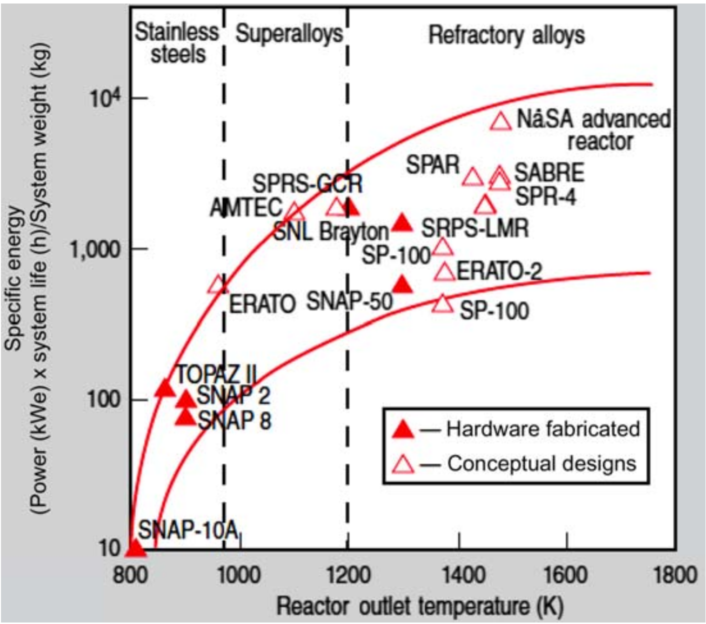

**Figure 3.10** Efforts and concepts, accompanying production temperatures and specific energies (estimated where appropriate) throughout the decades as categorized by material. Adapted from Yvon, P., Carré, F. Structural materials challenges for advanced reactor systems J. Nucl. Mater. 385 (2009) 217–222, copyright 2008 Elsevier.

- Acceptable mass/vehicle ratio;
- Materials suited to extreme thermal gradients;
- High energy density;
- Efficient fuel consumption, ideally with local, extraplanetary, harvestable fuel resources.

Nuclear reactors as RPSs can accommodate every need for remote, human exploration. Given the substantial distance between Earth and Mars (average distance: $2.25 \times 10^8$ km) a central question that has pervaded “Mars enthusiasts” is the issue of fuel. It is not feasible to bring large volumes of chemical fuel. The greater eccentricity of Mars’ orbit, its perigee, relative to Earth’s orbit, yields a minimum distance of $5.46 \times 10^7$ km.

Neither additional tanks, nor low-Earth orbit coupling (the so-called “sling-shot” effect) would suffice unless this were a one-way trip and the mission could refuel upon landing on the Martian surface—an option that an MSR RPS would offer. Note Figs. 3.9 and 3.10, where fission reactors feature prominently as high-energy, long-duration power sources (Van Dyke et al., 2001).

All BUK models used NaK alloy as the coolant. The BUK model, with the BUK 3 being the most often used, was deployed with all of the RORSAT launch vehicles bearing the COSMOS satellites, totaling 31 successful launches (Wiedemann et al., 2005; El-Genk, 2009). The satellites were boosted into high (800–100 km) orbit,

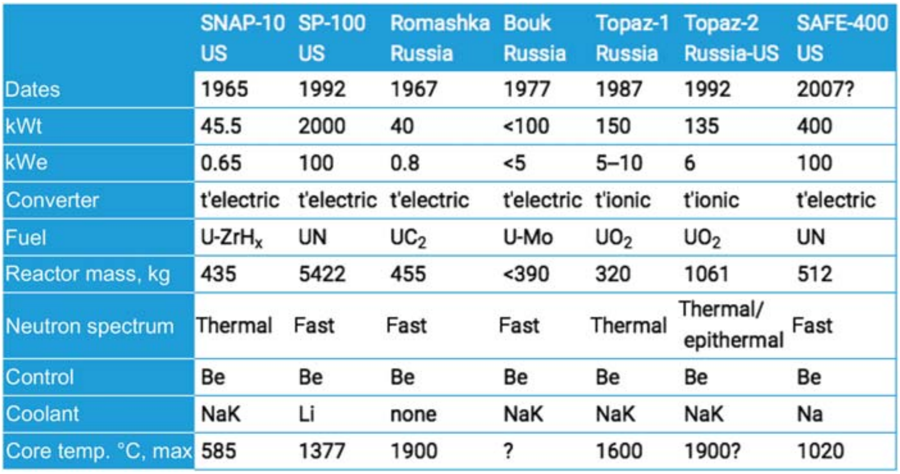

| | SNAP-10<br>US | SP-100<br>US | Romashka<br>Russia | Bouk<br>Russia | Topaz-1<br>Russia | Topaz-2<br>Russia-US | SAFE-400<br>US |
|---|---|---|---|---|---|---|---|
| Dates | 1965 | 1992 | 1967 | 1977 | 1987 | 1992 | 2007? |
| kWt | 45.5 | 2000 | 40 | <100 | 150 | 135 | 400 |
| kWe | 0.65 | 100 | 0.8 | <5 | 5–10 | 6 | 100 |
| Converter | t'electric | t'electric | t'electric | t'electric | t'ionic | t'ionic | t'electric |
| Fuel | $U\text{-}ZrH_x$ | UN | $UC_2$ | U-Mo | $UO_2$ | $UO_2$ | UN |
| Reactor mass, kg | 435 | 5422 | 455 | <390 | 320 | 1061 | 512 |
| Neutron spectrum | Thermal | Fast | Fast | Fast | Thermal | Thermal/ epithermal | Fast |
| Control | Be | Be | Be | Be | Be | Be | Be |
| Coolant | NaK | Li | none | NaK | NaK | NaK | Na |
| Core temp. °C, max | 585 | 1377 | 1900 | ? | 1600 | 1900? | 1020 |

**Figure 3.11** A series developmental timeline for the US and Russia: technical specifications (El-Genk, 2009).

however, sometimes with negative, unintended consequences. Most notably, the deactivation of these units resulted in solid NaK debris on the order of microns to centimeters in size. Sixteen COSMOS, Soviet-era nuclear satellites were discharged in such a way, from 1981 to 1988, thus complicating many space-based missions from then on (Wiedemann et al., 2005; El-Genk, 2009) (Fig. 3.11).

## 3.3.4 Materials considerations for a space-based MSR

A near complete absence of maintenance is one of the NASA requirements for space-based vehicles. This same goal holds true for Russian efforts for the better part of the last two decades. In particular, the Russians have investigated the use of magnetoplasma dynamic thrusters (MPDT) as a simple, but effective means of propulsion. (Ostrovsky et al., ДУК; Gorshkov et al., 2007). These parameters are perhaps also reflected in the short duration of the Soviet nuclear-powered RORSAT series of satellites, as the longest mission was only 135 days. Although not found in the literature, the extreme physical, neutronic, thermodynamic, and structural considerations likely played a central role in Soviet designs. NASA's intermittent attempts at designing nuclear-powered satellites are documented in the literature (see Figs. 3.8 and 3.10; Yvon and Carré, 2009; http://www.world-nuclear.org/information-library/non-power-nuclear-applications/transport/nuclear-reactors-for-space.aspx).

Austenitic and martensitic steels have been used successfully in Soviet missions for the reactor designs, including offgassing ports directly exposed to space. Fig. 3.12 depicts the choice of reactor materials as a function of temperature (Busby and Leonard, 2007; Yvon and Carré, 2009). The high chromium content of both materials would retard their use in MSRs due to the four available oxidation states of Cr with respect to fluorine; the enthalpy of formation for each ($-\Delta H_f$) of each ($CrF_{2-5}$) to form is feasible, but with varying $\Delta$Gs. Similar incompatibilities

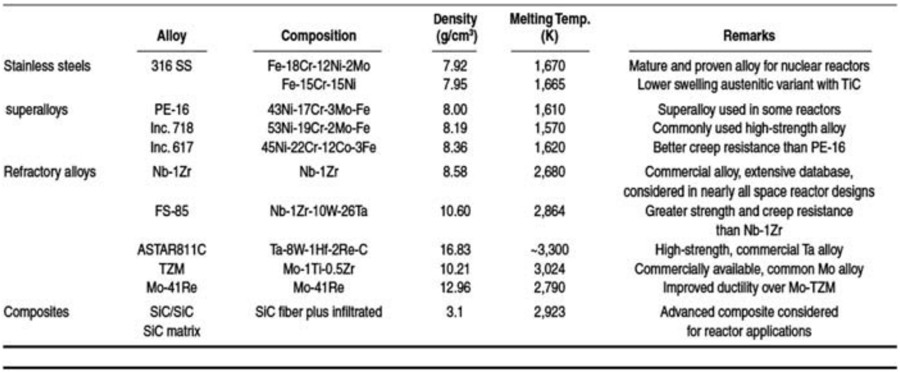

| | Alloy | Composition | Density ($g/cm^3$) | Melting Temp. (K) | Remarks |
|---|---|---|---|---|---|
| Stainless steels | 316 SS | Fe-18Cr-12Ni-2Mo | 7.92 | 1,670 | Mature and proven alloy for nuclear reactors |
| | | Fe-15Cr-15Ni | 7.95 | 1,665 | Lower swelling austenitic variant with TiC |
| superalloys | PE-16 | 43Ni-17Cr-3Mo-Fe | 8.00 | 1,610 | Superalloy used in some reactors |
| | Inc. 718 | 53Ni-19Cr-2Mo-Fe | 8.19 | 1,570 | Commonly used high-strength alloy |
| | Inc. 617 | 45Ni-22Cr-12Co-3Fe | 8.36 | 1,620 | Better creep resistance than PE-16 |
| Refractory alloys | Nb-1Zr | Nb-1Zr | 8.58 | 2,680 | Commercial alloy, extensive database, considered in nearly all space reactor designs |
| | FS-85 | Nb-1Zr-10W-26Ta | 10.60 | 2,864 | Greater strength and creep resistance than Nb-1Zr |
| | ASTAR811C | Ta-8W-1Hf-2Re-C | 16.83 | ~3,300 | High-strength, commercial Ta alloy |
| | TZM | Mo-1Ti-0.5Zr | 10.21 | 3,024 | Commercially available, common Mo alloy |
| | Mo-41Re | Mo-41Re | 12.96 | 2,790 | Improved ductility over Mo-TZM |
| Composites | SiC/SiC SiC matrix | SiC fiber plus infiltrated | 3.1 | 2,923 | Advanced composite considered for reactor applications |

**Figure 3.12** Overview of physical parameters for candidate materials (Busby and Leonard, 2007).
*Source*: Copyright 2008 Elsevier.

are seen for Mo and Fe in both alloys as well as in their facility for fluoride formation (Compere et al., 1975).

It is unlikely that refractory materials could be used extensively in a space-based MSR design with high-temperature gradients. Internal subsystems where such gradients do not exist and in which little or no salt bath exposure would occur could be feasible locations. Maintenance of their properties at high temperatures is a distinct advantage. Further research is needed on carbon—carbon composites or carbon—SiC composites, if prolonged heat and neutronic bombardment do not impact the SiC.

A one-way trip to Mars (called *Mars One*$^{©}$) basic exploration and colonization is slated for 2026. A small scientific team with the appropriate instrumentation could produce large quantities of information on all levels, including isotopic dating, areology, areophysics, and areochemistry. Seven candidates have been preliminarily chosen from a pool of over 78,000, but a minority are scientists.

MSRs as RPSs would satisfy both strict NASA/JPL requirements and offer the distinct option of round-trip missions to and from Mars for several reasons (see Fig. 3.13). Although logistically difficult, the transport of a small (50 $MW_e$) MSR is feasible, particularly if the MSR is used as the long-term propulsion needed for the space vehicle, and is then subsequently used as the power source for extended colonization. One field of engaging research is the prospect of using magnetoplasmadynamic thrusters (MPDT). This class of ion drive uses the Lorentz force, generating substantial thrust (Uribarri and Choueiri, 2009). The prospect of using an MPDT as primary, in-flight propulsion and possible landing suggests two possible advantages of using an MSR as an RPS. The first is that the high electricity requirement for this powerful class of drive (as high as 10 MW) can be met with an onboard MSR. Secondly, xenon has already been studied as an ion source, and iodine is an acceptable candidate as well (Uribarri and Choueiri, 2009; Ostrovsky et al., ДУК; Gorshkov et al., 2007). Xenon and iodine offgases (and to a lesser extent, Kr) from an MSR would serve as a continuously produced fuel source, and the

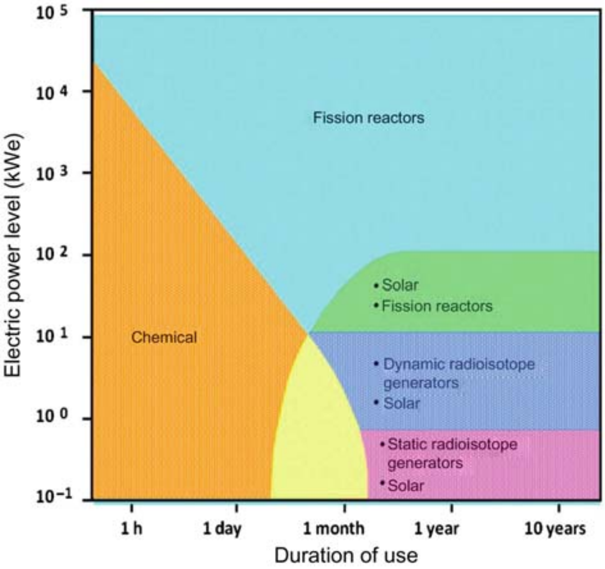

**Figure 3.13** Energy landscape and modalities as a function of source, average life span, and power output.
*Source*: Image courtesy of NASA.

corrosion of the thoriated tungsten cathode observed in the MPDT prototypes is moderated with higher mass ions (Uribarri and Choueiri, 2009).

MSR component shipments could be staggered to stay within the rocket load capacity, with some low-earth-orbit assembly required. Habitation, oxygen production, food production, machine mobility, and structural material construction could all be facilitated by a functional MSR with adequate fuel for sustained use.

### 3.3.5 Fueling the MSR on Mars and its employment as elemental production platform

During the increasingly advanced investigations conducted in the last decade, the presence of the elements that may be needed (U, F, Th, Cl) to produce fuel on Mars have all been detected. Candidate eutectic materials (Na, Zr, Ba, Li) were also found and in nontrivial quantities (Gooding, 1978; Griffith and Shock, 1995; Romulus, 2012; Moser, 2015). Although not directly observed, feldspar, olivine, Fayalite, Albite, and plagioclase have likely been found, based on collected geochemical data over the span of increasingly sophisticated Mars missions. This provides confidence that Cl, Be, B, P, Ni, Si, and other elements relevant to off-world MSR operations could be mined, if sufficient concentrations were found (Bandfield, 2002; Williams, 1997; McSween et al., 2001; Haynes, 2011; Ma et al., 2014). Figs. 3.14 and 3.15 depict relative concentrations on the Martian surface of U, Th, and F, respectively.

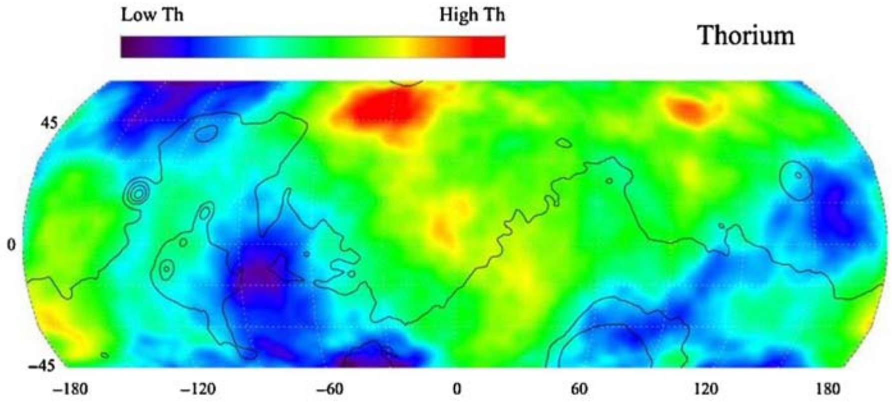

**Figure 3.14** Martian thorium and uranium abundance, mid-latitudes ( ± ∼45 degrees) (http://photojournal.jpl.nasa.gov/catalog/PIA04257).
*Source*: Image courtesy of JPL.

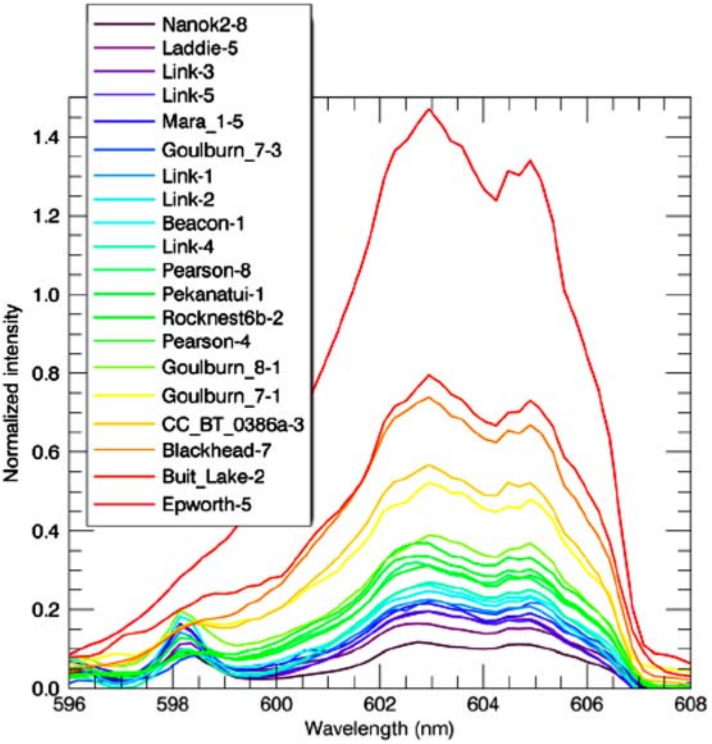

**Figure 3.15** Detection and relative intensity of fluorine-containing minerals on Mars (Moser, 2015).

In Fig. 3.15, the Epworth-5 line may be revealing. The data analysis that Forni et al. performed strongly suggests the presence of not only fluorite ($CaF_2$), but also the likely presence of fluorapatite ($Ca_5(PO_4)_3F$) and strontium fluoride ($SrF_2$) (Moser, 2015; Forni et al., 2015). Reduction of fluorine from the fluorapatite would also produce phosphate. As on Earth, the apatite-derived phosphate is then charge balanced with ammonium cation to produce fertilizer.

The logistical need for reduction of $CO_2$ to accommodate humans and plant growth is obviously met by the heavily $CO_2$-laden Martian atmosphere. Recent Mars missions have since confirmed the chemistry found within the Chassigny Nakhla Shergotty (CNS) meteorite, including phosphates, carbonates, and other species (Williams, 1997; McSween et al., 2001). MSRs could serve as the thermal and electrical power source for reduction of minerals into their constituent elements, including P, Si, K, Ca, Al, and others.

One critical issue for prospective travelers will be oxygen production for humans, plants, and likely animals. At an enthalpy of $532\,\mathrm{kJ \cdot mol^{-1}}$, the $sp^2$ hybridized oxygen bonds on the central carbon of $CO_2$ prove particularly robust (Haynes, 2011). Many attempts throughout the previous decades at low-energy reduction of the carbon to liberate the oxygen have failed, whether electrolytically, electrochemically, or thermoelectrochemically (Ren et al., 2015).

One group of researchers, however, recently published a molten-salt electrolytic method of carbon reduction with the added feature of generating carbon nanotubes at the cathode and pure oxygen at the anode (Yin and Moss, 1999; Ren et al., 2015). The operating temperature for this molten lithium carbonate ($Li_2CO_3$)-driven electrolytic process is 750°C. The researchers note that eutectics can bring the temperature lower, and addition of other metals (as catalysts) can tune the properties of the nanotubes. The $Li_2CO_3$ exists in equilibrium with the $CO_2$, thereby rendering the carbon available to reduction at the cathode (Yin and Moss, 1999).

As one of the main needs for prospective colonists, secondary MSR loops could provide a thermal platform to effect this oxygen production chemistry. Ample supplies of $CO_2$ exist in a $97+\%$ $CO_2$ Martian atmosphere. The $CO_2$ could be used in supercritical Rankine systems.

Despite the difficulty of Mars retaining atmospheric species, due to the absence of a magnetosphere, the relative atmospheric loss is slower than oxygen production would be, provided the rate of production exceeds $100\,\mathrm{g \cdot s^{-1}}$ (Dong et al., 2015; Neal-Jones et al., 2015).

Structural materials such as iron, titanium, and aluminum can also be produced at the temperatures at which an MSR operates on Mars. A 700°C minimum is needed for small-scale, electrolytic aluminum production, and 500°C for titanium using alternate processes (Jacobs, 1974; Kamali et al., 2008; Cuadros and Michalski, 2013). An appreciable current must also be available from the MSR for these high-temperature, electrolytic methods. To facilitate this aluminum production at lower temperatures, kaolinite must be used. This mineral has also been found on the Martian surface, and so have chlorine-containing minerals (Jacobs, 1974; Kamali et al., 2008; Hecht et al., 2009; Cuadros and Michalski, 2013). Aluminum chloride ($AlCl_3$) is synthesized, then used as a strongly Lewis-acidic, molten salt to dissolve the kaolinite and permit electrolytic reduction of aluminum. The use of kaolinite as the source mineral for aluminum (replacing bauxite), combined with the use of $AlCl_3$ permits the lower-temperature electrolytic method of aluminum reduction (Jacobs, 1974; Cuadros and Michalski, 2013).

To gauge exactly how much of a substantial remedy the presence of $CO_2$ and its interaction with plants, however, a unique experiment was undertaken in the Netherlands. Royal Dutch Shell participated in a trial, whereby $CO_2$ being emitted from one of their stacks was shuttled through an unused, underground pipe to a nexus of greenhouses approximately 85 km away (http://www.dw.com/en/dutch-farmers-boost-production-with-co2-waste/a-2214482; http://www.the-linde-group.com/en/clean_technology/clean_technology_portfolio/co2_applications/greenhouse_supply/index.html). The experiment proved a partial success, in that 400 greenhouses consumed 170 metric tons of $CO_2$. Another 100 greenhouses were added in 2006, but some $CO_2$ is released during plant decomposition. As of 2011, 350 metric tons have been used as a growth accelerant, with 25% faster growth for all species. $CO_2$ consumption is cyclic, tethered to the growth cycles of the plants. A more concerted effort toward staggered growth could be employed using atmospheric $CO_2$ on Mars as a nearly inexhaustible resource.

Figs. 3.10 and 3.13 clearly demonstrate a requisite need for a diverse energy landscape regarding space travel. As is well known, photon intensity varies as the inverse square of the distance. Accordingly, extended NASA missions beyond 4 AU (AU = Astronomical Unit = 149.6 M km = mean distance from the center of the Sun to the center of the Earth) are not practical using solar arrays as the primary power source. This, despite the superior efficiency of solar arrays (30%–40%) being produced in the new and growing field of multijunction cells (Sun et al., 2005; King et al., 2007). As with any energy production modality, solar arrays have an optimal usage window. Over time, solar arrays will likely succumb to the fine regolith dust that makes up the Martian landscape or, as noted in Fig. 3.12, exceed their practical usage window for prolonged and deeper space missions.

## 3.4 Heat exchangers and materials embrittlement challenges

Materials science, chemistry, neutronics, and heat transfer problems must all be solved for MSR heat exchanger design. Tube shapes, wall thickness, hoop stress, thermal stress, creep, swelling, embrittlement, and corrosion must be considered. A simple tube-within-a-tube design is trusted, minimizes surface area and is a natural choice, because larger bore sizes can stave off possible crystalline precipitation of less soluble species such as Pu, Np, and Ln. The concomitant drawback is that surface area *is* small, thereby leaving much heat remaining within the inner radial laminae ($r_{\max}-r_{\max-n}$). Since it is well known that the materials undergo slow changes over time, this means that the chemical potential of the materials themselves also changes. Early work on the examination of postexperimental materials demonstrated that *all* radionuclides exhibit some damage to the walls of the heat exchangers and, therefore, the core (http://www.world-nuclear.org/information-library/non-power-nuclear-applications/transport/nuclear-reactors-for-space.aspx). Some of the most aggressive nuclides are listed below.

### 3.4.1 Tellurium embrittlement

Chalcogens all exhibit a high electron affinity, being members of Group 16, and Te is third highest in the column at $190\,\mathrm{kJ \cdot mol^{-1}}$ (1.96 eV). The ground-state electronic configurations[10] for oxygen and tellurium ($\mathrm{O} = 1s^2\ 2s^2\ \mathbf{2p^4}$; $\mathrm{Te} = [\mathrm{Kr}]\ 4d^{10}\ 5s^2\ \mathbf{5p^4}$) both exhibit incomplete p orbitals ($\mathbf{np^4}$); a filled p orbital has six electrons. These incomplete p orbitals make chalcogens aggressive oxidizing agents, so as to close that deficit, namely, achieve a closed $\mathbf{np^6}$ (O, $n = 2$; Te, $n = 5$) orbital. For technical reasons beyond the scope of this discussion, sulfur, selenium, and tellurium can adopt higher oxidation states. In the case of tellurium in the MSR experiments conducted at ORNL, Te was found as $TeF_6$, a highly soluble form of a tellurium fluoride with a formal charge of $+6$. Early MSRE studies demonstrated the damage that Te inflicted on the inner surfaces of containment materials. In some cases fissures up to 300 μm deep were produced (Houtzeel and Dyer, 1972; McCoy, 1978). In a series of investigations, ORNL researchers examined the effects of $TeF_6$ and $TeF_6 + F_2$ exposure to a number of alloys, the most promising of which for use in an MSR (at the time) were Nickel 200 (99 + % pure Ni) and Monel K-500 (67%Ni, 32.x%Cu, balance other metals); Hastelloy was not included in these experiments. Both alloys were tested at approximately 500°C and for varying lengths of time. Both were found to have substantial Te-derived corrosion, both at the surface and intergranularly, although the Monel K-500 less so. One possibility is that, despite the presence of highly oxidizable Ti and Al in the Monel K-500 in a fluorinating environment such as in the molten-salt bath, the intermetallic, gamma prime precipitate ($Ni_3Al/Ti$, FCC crystal structure) may assist in corrosion resistance. When these alloys were exposed to $TeF_6$ and $F_2$, corrosion rates were reduced. It is possible that this reduction is attributable to $F_2$ being such a strong oxidizer, thereby maintaining $TeF_6$ in a fully oxidized, $+6$ state.$TeF_6$, the solubilized Te species, was readily reduced when exposed to these and other alloys. In fact, some metallic Te was detected on the Monel coupons, as well as CuTe. When investigated under x-ray crystallography, $NiTe_2$, NiTe and $NiF_2$ were all found in varying amounts on each coupon, supporting typical chalcogenic behavior where a Ch prefers a formal charge of $-2$. $Cu_{2\text{-}x}Te$ was also found on the Monel K-500, as would potentially have been predicted, given the percent balance that Cu makes as the Monel alloy. $Cu_{2\text{-}x}$ may also have been a logical prediction as a mixed system, given Cu's two oxidation states. This was, in part, because Te, like O, Se, S, all prefer a $Ch^{-2}$ (Ch = chalcogen) state, to close that p orbital. With this in mind, $Te^{-2}$

---

[10] Ground-state electron configuration: The total number of electrons in a neutral atom and the orbitals they occupy (s, p, d, f . . .). The geometries of these orbitals are Legendre polynomials.

then becomes stable and a much less aggressive oxidizer, given the high electron affinity[11] of $190\,\mathrm{kJ \cdot mol^{-1}}$ (1.96 eV), but at a cost of taking those two electrons from a Lewis base—among other species in the bath, the metal containment wall of the MSR. While the basicity explains the reactivity towards metals, the tellurium also has an affinity for grain boundaries in the alloy materials, and the mechanism of embrittlement has been shown to involve a decohesion effect, similar to the phenomenon of liquid metal embrittlement (Hemsworth et al., 1990; Všianska and Šob, 2011; Lu et al., 2016). Given that tellurium has a melting point ~450°C, it is highly likely that the tellurium embrittlement mechanism involves the formation of 2-D phases along grain boundaries with weak resistance to mechanical separation, potentially related to the $NiTe_x$ phases observed crystallographically (Jia et al., 2013).

Two solutions that ORNL researchers discovered were to (1) maintain a 95%/5% ratio of $UF_4/UF_3$, which engendered an overall reducing environment for the bath and (2) add small amounts of Nb to the containment materials. Addition of Nb suppressed the oxidizing behavior of Te by reducing the species to $Te^{2-}$ because Nb can stably oxidize to a +5 state, thereby affording a sacrificial electron sink without substantial materials changes in the bulk. The second was to maintain a reducing environment in the bath, which will be discussed in more detail further (Houtzeel and Dyer, 1972; McCoy, 1972; McCoy, 1978; Discussions with Richard Engel, 2nd time, 2013). Interestingly, niobium has also been shown to assist in the protection of zirconium-based alloys used in nuclear fuel element cladding with regards to embrittlement attack by iodine (produced radiolytically in the nuclear fuel element itself) (Edsinger and Murty, 2001).

With U being the most prevalent element, it is very reasonable that this rather precise measure of control can be effected. Because of this fortunate fact, one *possible* scenario behind the electronic reduction of Te (of which several can be construed) is offered below. It focuses on the redox interplay between neutral $UF_x$ species ($x = 2-4$), and their anions. This scenario has been compiled from information found in Thoma (1962), Houtzeel and Dyer (1972), and McCoy (1972).

ORNL investigators maintained a 5% level of $UF_3$ in the bath with $UF_4$ making up the balance, thereby oxidizing the $Te^{2-}$. ORNL found that this reduces the Te fission product with two additional electrons to $Te^{2-}$, the more stable anion in comparison to either $Te^0$ or $Te^-$.

Since the electrons are coming from the neutral $UF_x$ species or its anion ($x = 2-4$) to afford the electrons necessary, one needs to look at the possible mechanism(s) by which the electrons are ceded to Te. Li et al. (2013) proposed that the stability of the anions $UF_x^-$ ($x = 2-4$) lies along the following spectrum (see below), with $UF_2^-$ being the most stable. This series is an estimate, based on computationally driven valence shell electron analysis and photoelectron spectroscopy of the *gaseous* species, since no other data are available on the molten state (Mamantov and Manning, 1966; Batista et al., 2004; Hamel et al., 2007; Li et al., 2013): This is also consistent with ligand field theory. As more molecular orbitals

---

[11] Electron affinity: A measure of the energy exerted by a species to acquire an electron.

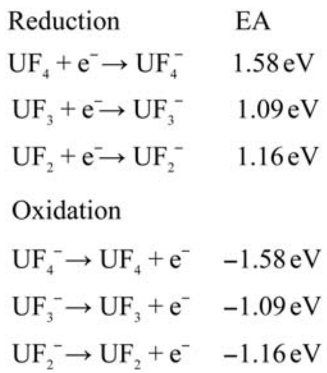

| Reduction | EA |
|---|---|
| $UF_4 + e^- \rightarrow UF_4^-$ | 1.58 eV |
| $UF_3 + e^- \rightarrow UF_3^-$ | 1.09 eV |
| $UF_2 + e^- \rightarrow UF_2^-$ | 1.16 eV |
| Oxidation | |
| $UF_4^- \rightarrow UF_4 + e^-$ | −1.58 eV |
| $UF_3^- \rightarrow UF_3 + e^-$ | −1.09 eV |
| $UF_2^- \rightarrow UF_2 + e^-$ | −1.16 eV |

**Figure 3.16** REDOX potentials for uranium fluoride species.
*Source*: Adapted from Li, W-L., Hu, H-S., Jian, T., Lopez, G.V., Su, J., Li, J., et al., 2013. Probing the electronic structures of low oxidation-state uranium fluoride molecules $UF_x$ ($x = 2, 4$). J. Chem. Phys. 139, 244303 and Batista, E.R., Martin, R.L., Hay, P.J., Peralta, J.E., Scuseria, G.E., 2004. Density functional investigations of the properties and thermochemistry of $UF_6$ and $UF_5$ using valence-electron and all-electron approaches. J. Chem. Phys. 121, 2144.

are involved, the bonds tend to become weaker, because additional electron density is needed to maintain the covalent bonds.

$$UF_2^- > UF_3^- > UF_4^-$$

The ability of an anion to release an electron to achieve a neutral species is known as the adiabatic detachment energy (ADE) follows a different pattern:

The negative values listed in Fig. 3.16 indicate that the $UF_4^- \rightarrow UF_4$ is an exothermic process. Redox reactions are clearly occurring in the absence of an applied voltage, yet the precise source of the initial electron from some sink is not completely understood (Mamantov and Manning, 1966; Hamel et al., 2007). Electrons would be obtained from other ions in the material, ions that have a lower reduction potential, thus facilitating a redox reaction. Therefore, the electron source may be a combination species: bridging fluorines (as will very often be the case), the presence of noble fission products, namely, metals (meaning less fluorine needed), or spontaneously from a less electronegative species that is soluble and prefers being a cation (Madden, 2016). Ba Sr, etc., were found, e.g., given the thermodynamics of the reaction at these temperatures (Hamel et al., 2007). Some evidence had been detected of Ba and Sr in the graphite and in the sparging gases, due to their gaseous precursors, but whether they were in the metallic or cationic state was not discussed, though it is entirely possible that Coulombics from the containment materials could stabilize cations. Nevertheless, the $UF_4^-$ species ceding the electron is an exothermic process under reducing conditions such as those produced.

The 95% $UF_4$ concentration that ORNL researchers maintained could likely be thought of as a LeChâtelier's principle push to the right. The low concentration of

$UF_x$ ($x = 2,3$), despite the lower exothermicity, may be made up for by the abundance of $UF_4$ in the bath, pushing $UF_3$ toward the anion. Li et al. (2013) had also reported that the electronic interaction of $UF_3$ and $UF_2$ species is complicated, highly dynamic and includes two-electron transfers in the transition from $UF_3$ to $UF_2$ and back (Mamantov and Manning, 1966; Hamel et al., 2007). In this possible scenario, the reduction of Te appears feasible.

### 3.4.2 Tritium embrittlement

As is well known, tritium ($^3H$ or T) was a continual problem with the MSRE. Under these extreme conditions, T can exist in a spectrum between cation, a neutral atom with one electron or the anion, the distinction of which cannot always be determined. The tritium anion's precise radius is difficult to quantify. The electron density of the anion is highly compressible, making quantification of the degree of covalency difficult to assess.

At MSR temperatures, T is easily formed, is a highly reactive species, and can attack metals prone to oxidation, forming tritides of the form $MT_x$, where M is the metal and T is behaving as the anion for the tritide to form. Migration into the walls ended up either contaminating the heat exchanger loop fluid or, due to the relatively short half-life (12.3 years), $^3He$ would be formed within the material bulk. Already described as an "electron sea," metals take on the electrons, thereby permitting the newly formed cations to flow freely within the bulk. An obvious, deleterious consequence of this would be *internal* structural flaws being formed. Internal and external assault would substantively shorten material lifetime. Tritium embrittlement—an extension of the well-known concept of hydrogen embrittlement—will also involve the two mechanisms of embrittlement described in the hydrogen stress-corrosion cracking literature: these are HEDE (hydrogen enhanced decohesion embrittlement) and HELP (hydrogen enhanced localized plasticity). In HEDE, hydrogen lowers the energy required to form a stable crack in the material through surface adsorption. In HELP, hydrogen interacts with the plastic dislocation fields in the material to modify the response of the deformation zone in the material to stress (Djukic et al., 2014).

A wide range of transition metals, including actinides and lanthanides, can all form tritides of varying Lewis strengths at these temperatures. Subsequent versions of Hastelloy, for example, contained less Ti, because of its greater capacity to form $TiT_x = (x \geq 3,4)$ over other metals in the alloy. These same liabilities hold true for other MSR materials that were considered at the time, particularly those with attractive neutronic or chemical characteristics such as Zr, Hf, Sc, and V at high temperatures and bath conditions. The chalcogens all form tritides under these conditions, $ChT_2$ (Ch = S, O, Se, Te), being satisfied in a −2 state with the closed p-orbital.

Tritium formation was due almost completely to the use of $^7LiF$-containing eutectics, with FLiBe being the most popular. The four 9s purity of $^7LiF$-containing eutectics still produced an appreciable amount of T (1170Ci/d) via $^7Li$ neutron capture, almost as much as the errant $^6Li$ (1210Ci/d) that remained in the purified

FLiBe (Houtzeel and Dyer, 1972; McCoy, 1978). According to ORNL documents, only about 19% of the total tritium produced would be removed via helium sparging (effusing as TF), with the bulk of the remainder unfortunately remaining, diffusing through the containment materials and, most predominantly, through the heat exchanger walls (Houtzeel and Dyer, 1972; McCoy, 1978; Discussions with Richard Engel, 2nd time, 2013). One slight advantage of having a reducing $UF_3$ environment in the bath is the production of $T_2$, thereby promoting some removal, along with Xe, Kr, and other gaseous fission compounds (McCoy, 1972).

Several mechanisms have been proposed to combat tritium migration:

1. $UF_3$ introduction serves dual roles of both Te and T reduction. It should therefore be monitored extremely carefully, and at its maximum level permissible in the bath.
2. Use sodium tetrafluoroborate ($NaBF_4$) in the heat-exchanger loop. This highly water-soluble salt, which could be introduced into the steam circuit, can irreversibly react with $T_2$ with a high affinity. Operators would have to take every safety measure possible, however, so as to contain any of the tritiated steam that may emerge as a result of a possible leak.
3. A cooled sink in a coffer tube could electrolytically remove T from the liquid state ($T_2O$ or HTO), offgassing the oxygen.
4. Offload tritiated steam into a sink, cool it to 0°C and take advantage of the higher freezing points of $T_2O$ at 4.5°C and $D_2O$ at 3.8°C, with temperature differences of THO, TDO, and TTO still appreciably different from $H_2O$.
5. If heat exchangers with thinner walls are used, a fourth option may be the installation of sacrificial exchangers, whereby parallel heat-exchanger systems are singly operated, permitting the shutdown of one exchanger loop to replace the other, with *de minimus* downtime.

Tritium control represents a complex engineering problem, but one that would certainly prolong the life and profitability of a commercial MSR as a high-temperature, chemistry production platform.

Many more designs and materials have been investigated over the decades. Forsberg et al. (2005) listed a few older promising candidates. A more thorough materials examination of heat exchangers was undertaken by Sridharan et al. in 2008 (Forsberg et al., 2005; Sridharan et al., 2008). The field is changing very rapidly as the commercial drive for improvement continues. The central question has always been whether the materials can stand up to prolonged exposure under these extreme conditions and to minimize corrosion, since it can never be eliminated. Avoiding embrittlement is also a problem, since the materials choice is so restricted by the operational environment. Given the small size and odd charge that tritium has, it probably poses a more vexing challenge than the other forms of systems deterioration.

## 3.5 High-temperature commercial applications

### 3.5.1 Ammonia production

In 1910, Fritz Haber and Carl Bosch developed an efficient, high-temperature, industrial-scale process for ammonia production by reacting hydrogen with nitrogen

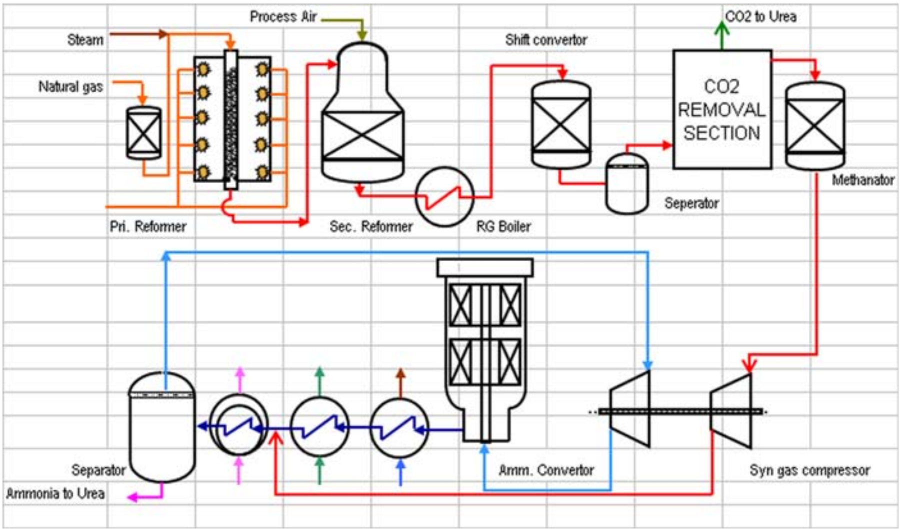

**Figure 3.17** Schematic and optimal production conditions for ammonia synthesis (Batista et al., 2004).

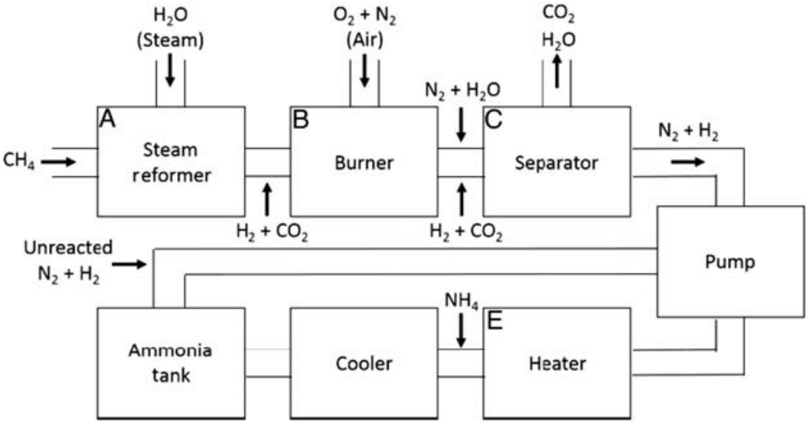

**Figure 3.18** Schematic and flow chart for ammonia production (Batista et al., 2004).

under certain conditions. (Haber and Bosch were awarded the Nobel Prize for Chemistry in 1918 and 1931, respectively.) At 450 million metric tons per year, ammonia production accounts for 2% of the world's energy demand, due to its increasing importance as a raw material for dye stuffs, nylon, nitric acid, and fertilizer (Nielsen, 1995) (see Fig. 3.17).

The Haber-Bosch process (Figs. 3.17 and 3.18) initially involves a steam reforming stage with methane to produce the hydrogen needed for the primary reaction:

$$CH_4 + H_2O \rightleftharpoons CO + 3H_2 \tag{3.1}$$

$$CO + H_2O \rightleftharpoons CO_2 + H_2$$

With methane ($CH_4$) being the typical commercial feedstock, this equation constitutes the endothermic, first phase of the Fischer-Tropsch (FT) process. The product is called *syngas* ($CO_2 + H_2$), in reference to the first requisite product produced during the FT process. Air, composed of 80% $N_2$ and 20% $O_2$, is reacted with hydrogen to remove the oxygen, producing water and $N_2$ (Eq. 3.2b). Oxygen cannot be present at more than picoliter levels, as unwanted side reactions occur with it present. After separating the product gases, a pure stream of $H_2$ and $N_2$ is fed into the primary reactor. The reactor is heated to approximately 450–500°C at ~20 MPa while in the presence of a catalyst (often $Fe_2O_3$—iron III oxide) and often promoters[12], such as aluminum III oxide ($Al_2O_3$) or "alumina" and potassium oxide ($K_2O$).

$$2H_2 + O_2 + N_2 \rightleftharpoons 2H_2O + N_2 \tag{3.2a}$$

$$N_2 + 3H_2 \rightleftharpoons 2NH_3 \tag{3.2b}$$

The ammonia is then cooled and liquefied for storage and transport. Due to the exothermicity of reaction 2b ($\Delta H = -92\ \text{kJ} \cdot \text{mol}^{-1}$), some industrial iterations transport the heat back to earlier stages of the process together with unreacted hydrogen and nitrogen. The constituent reagents ($H_2$, $N_2$) are reintroduced to the reaction column for recycling.

Fig. 3.19 depicts the poor yield given the pressure and temperatures involved, and this same trend is seen in Fig. 3.12: green curves are at ~20 MPa and purple curves are at ~400 KPa; the increase in yield is evident (Nielsen, 1995). It appears from the graph that higher yield is obtainable with lower pressure and higher temperature. This is not the case, however. Fig. 3.18 depicts the mol% yield as a function of the thermodynamics (Averill and Eldridge, 2014). Eqs. 3.2a and 3.2b both reflect the fact that these reactions are actually in equilibrium (note the double arrows) and do not go to completion as is typically thought of in chemistry. Reagents and products, therefore, have to be managed to produce an optimum yield, where pressure and temperature are the primary physics tools at hand. This entails "pushing the reaction to the right," by employing LeChâtelier's principles to effect changes in concentration, temperature, or pressure (in this case, volume is fixed). The boiling point of ammonia (−33°C) is higher than that of hydrogen (−252°C) or nitrogen (−196°C). Ammonia can then be continuously removed in liquid form. This is LeChâtelier's principle in practice (lowering concentration of a product) making additional production possible.

---

[12] Promoter: A compound that, in itself, is not a catalyst. It assists the catalyst on a molecular level, facilitating (and accelerating) catalytic activity. The electronic interactions and precise mechanism(s) that occur between the catalyst and promoter vary, depending on the promoter. All catalysts and promoters are polycrystalline materials, usually prepared in a fashion to maximize surface area.

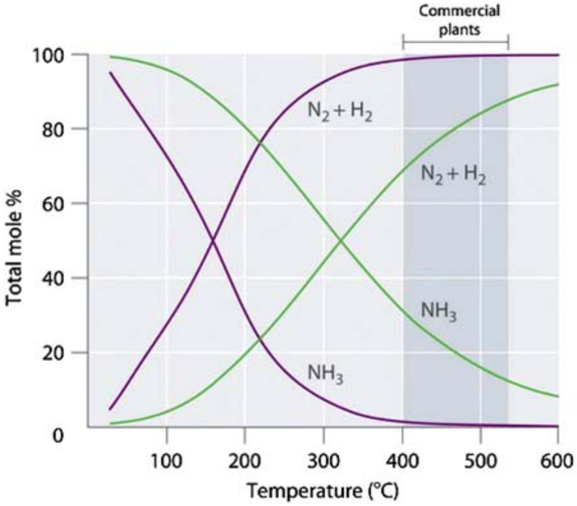

**Figure 3.19** Pressure—temperature—yield graph for products and reagents in the Haber process (Averill and Eldridge, 2014).

From Figs. 3.16, 3.17,and 3.18, several heating stages exist as opportunities for an MSR thermal platform to support their operation. On industrial scales, an MSR would also simultaneously serve as an electrical source needed for such extensive transport, at pressure, of the reagents and products involved. Heat exchangers can transport the residual salt temperature of between 400°C and 600°C and could either assist in the steam reforming process or supply the entire heat energy required for the primary reaction in the "heater" stage. Excess heat to bring secondary loops from the heat exchangers can be shuttled to several places where needed: Fig. 3.17A, B, C, E, respectively: FT-driven syngas production, namely, steam reformation (A, B), separator (C), and heater (E). It is significant to note that MSRs can be scaled to fit the needs of the industrial process. This feature would be attractive to any industrial effort. Capital expenditure (CAPEX) can be amortized over long periods and operational expenditure (OPEX) would most likely be under contract with the company that owns the MSR. In this fashion, corporate liability is minimized between both parties.

Nielsen provides a more thorough treatment of the thermodynamics, interactions of crystalline catalytic materials, and the equilibrium management techniques involved in industrial-scale ammonia production (Averill and Eldridge, 2014).

## 3.5.2 Hydrogen production

### 3.5.2.1 Hydrogen derived from fossil fuels

Hydrogen has long been suggested as a suitable alternative energy carrier in the proposed "hydrogen economy" (Turner and 1999, 2004; US Department of Energy

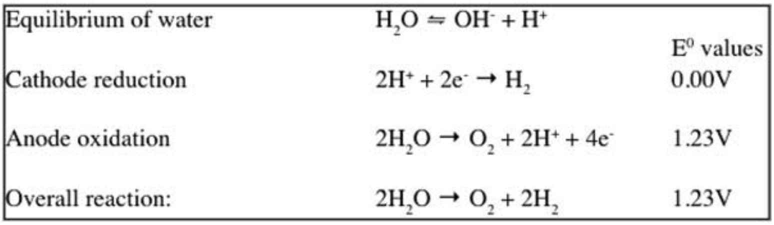

| | | |
|---|---|---|
| Equilibrium of water | $H_2O \leftrightharpoons OH^- + H^+$ | |
| | | $E^0$ values |
| Cathode reduction | $2H^+ + 2e^- \rightarrow H_2$ | 0.00V |
| Anode oxidation | $2H_2O \rightarrow O_2 + 2H^+ + 4e^-$ | 1.23V |
| Overall reaction: | $2H_2O \rightarrow O_2 + 2H_2$ | 1.23V |

**Figure 3.20** Electrolytic reduction potentials for water.

and Office of Basic Energy Sciences, 2004; The Hydrogen Economy, 2004). Although the most plentiful element in the universe, hydrogen on planets is sequestered within crystals, organic matter, and water and never found in elemental form. Currently, 96% of the world's hydrogen is commercially produced via steam reforming from natural gas (Olah et al., 2009). As mentioned above, this is, again, the FT method for production of syngas. The process typically employs a nickel-based catalyst, which converts methane into the desired products at approximately 500°C (the top process seen in Fig. 3.18). As with FT, the product stream is then recirculated to produce additional hydrogen and carbon dioxide.

While steam reforming is an established process reaching efficiencies of 80%, fuel combustion and cement manufacture alone produced slightly more than nine billion tons of $CO_2$ in 2010 (Peters et al., 2012). Emissions of $CO_2$ in 2007 amounted to 29.7 $\mathrm{Gt \cdot year^{-1}}$, with FT-derived $CO_2$ making up a significant fraction of that (Maitlis and de Klerk, 2013).

### 3.5.2.2 Hydrogen derived from electrolysis

Water electrolysis presents a clean alternative to steam reforming, producing zero greenhouse gases and supplying 4% of the world's hydrogen (Fig. 3.20). Currently, water electrolysis is tasked with supplying high-purity hydrogen for high-end applications such as rocket fuel. Although the process is efficient, it is expensive and traditionally involves a platinum catalyst.

As can be seen in Fig. 3.20, electrolytic reduction of water demands a substantial energy commitment as can be seen in the reduction potentials[13]. One advantage of this method, however, lies in the extremely high purity of the hydrogen produced (99.999%). Rocket fuels and the entire petroleum refinement industry both require high-purity hydrogen. The petroleum industry dominates the total annual consumption of hydrogen at 351 million $\mathrm{m^3 \cdot year^{-1}}$ (Maitlis and de Klerk, 2013; Hydrogen for Refineries, 2016). As an electrical platform, an MSR is well suited to the high-energy demands of electrolytic reduction of hydrogen, given the purportedly low cost of energy production ($\sim$0.02 ¢ $\cdot \mathrm{kwh^{-1}}$; this number is highly debated). This number is based on several cost estimates found in modern, nonacademic works.

---

[13] Reduction potentials: The voltage needed to liberate an electron at the anode (oxidation) and apply an electron to a target species at the cathode (reduction). The voltage depends on the binding energy associated with the nth electron.

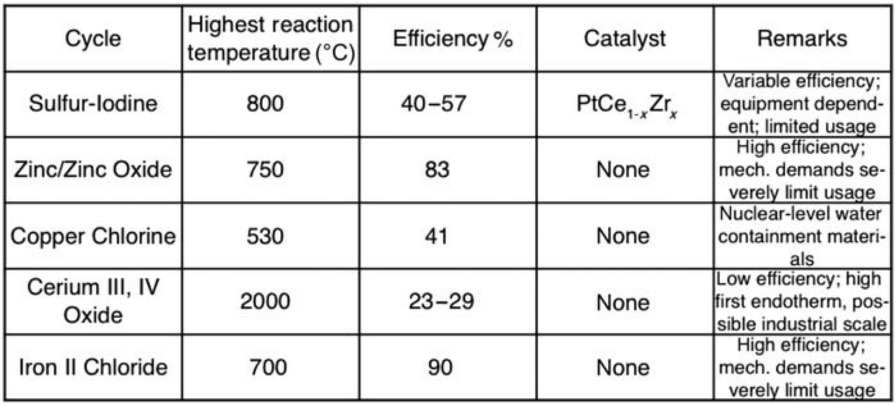

| Cycle | Highest reaction temperature (°C) | Efficiency % | Catalyst | Remarks |
|---|---|---|---|---|
| Sulfur-Iodine | 800 | 40–57 | $PtCe_{1-x}Zr_x$ | Variable efficiency; equipment dependent; limited usage |
| Zinc/Zinc Oxide | 750 | 83 | None | High efficiency; mech. demands severely limit usage |
| Copper Chlorine | 530 | 41 | None | Nuclear-level water containment materials |
| Cerium III, IV Oxide | 2000 | 23–29 | None | Low efficiency; high first endotherm, possible industrial scale |
| Iron II Chloride | 700 | 90 | None | High efficiency; mech. demands severely limit usage |

**Figure 3.21** General description of some select thermochemical systems.

### 3.5.2.3 Thermochemically derived hydrogen

Several means of liberating hydrogen have been discovered and modified throughout the decades. As the name implies, however, they all require a heat source. This process often involves redox. The thermochemical production of hydrogen is seen to have the advantages of high efficiency, zero greenhouse gas emissions, and relatively pure hydrogen output.

Several proposed cycles are summarized in Fig. 3.21 and generally operate between 500°C and 800°C (Kodama and Gokon, 2007). Nuclear heat sources are attractive for high, continuous, emissions-free heat with available, continuous voltage and current (Yalcuücin et al., 1989). See Fig. 3.22 for a good example of heat demand to effect hydrogen liberation. Research began in earnest for the HTGR (high-temperature gas reactor) as an effective heat source for thermochemical reactions. The HTGR preceded the restart of MSR research (Yalcücin, 1989; Nelson et al., 2007).

Hundreds of investigations on these materials and many others, and variations therein have been conducted over the decades. As noted in Fig. 3.21, almost all processes involve an initial thermochemical step, followed by or included with one or more redox reactions[14], namely, many are also electrochemically driven (Maitlis and de Klerk, 2013). Examples of reduction potentials are found in Fig. 3.20.

## 3.5.3 Catalytic cracking

Catalytic cracking is arguably the most important, high-temperature hydrocarbon chemistry performed (http://www.digitalrefining.com/article/1000787,Naphtha_catalytic_

---

[14] Redox reaction: A method of representing the simultaneous oxidation and reduction of compounds, such that the target species is reduced to elemental form. In the cases illustrated here, as well as in classic examples, redox reactions involve electron transfer according to the following mnemonic: OIL RIG: oxidation is loss; reduction is gain. Since hydrogen almost always exists as a cation (H + ), the goal is to reduce hydrogen to its diatomic, elemental form (H2), thereby requiring two electrons to complete the single valence shell.

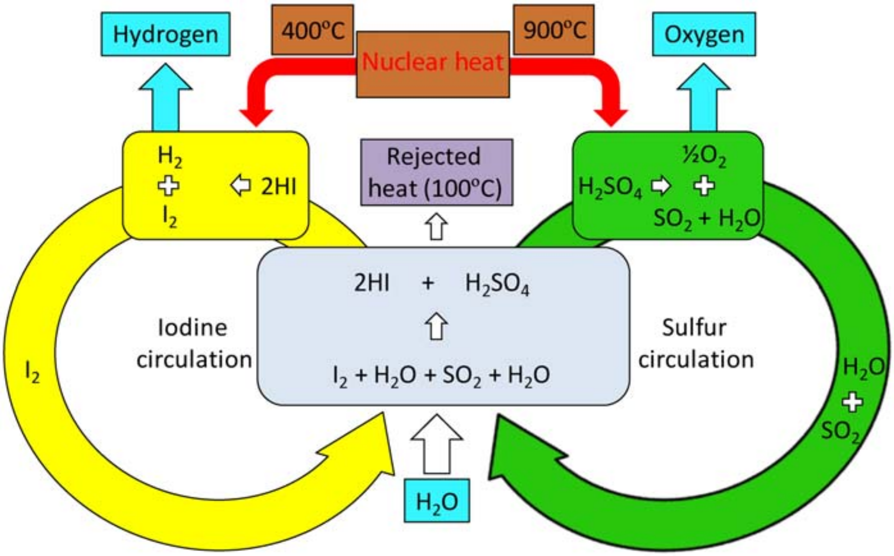

Figure 3.22 One possible sulfur—iodine thermochemical reduction scheme.

cracking_for_propylene_production.html#.VSxSeic_590; Nelson et al., 2007; Al-Shammari et al., 2014). In this process, long-chain hydrocarbons (C7—C23; C = carbon) are broken down into propylene ($C_3H_6$; propene) and ethylene ($C_2H_4$; ethene).

The consumer, commercial and industrial significance of this process is the production of carbon = carbon double bonds, marked "a" and "b" in Fig. 3.23 and cannot be understated. These double bonds are formed during the cracking process. The compounds serve as the precursors to the well-known polymers polypropylene and polyethylene and the scores of variants thereafter, and the polymerization stems from the presence of the double bonds. Fig. 3.21 shows the top 10 ethylene producers, amounting to $1.4 \times 10^7$ ton year$^{-1}$ (Fig. 3.24).

The chemical *reduction* of the carbon—carbon single bond to double bonds (recall that reduction is a gain of electrons) requires a high endotherm (400°C) to effect this chemistry. Cracking requires catalysis and, like thermochemical means of hydrogen production, hundreds of catalytic candidate variants have been investigated over the decades. Some representative catalysts are zeolite-HZSM-5, zeolite-Y, and mordenite. Most used on an industrial scale are the zeolite class of catalytic compounds and other types of naturally occurring minerals, which all share similar crystallographic elements. Appearing cage-like on the crystallographic level, zeolite chemistry occurs on the inside and edges of the cage. Intense spectroscopic methods are used to identify the many changes that occur to the complex crystallographic unit cell as a result of researchers' efforts to improve catalytic efficiency, but these changes present new characterization challenges. Changing the ratio of key elements, for example, Si-Al, slightly alters the Madelung and lattice energy

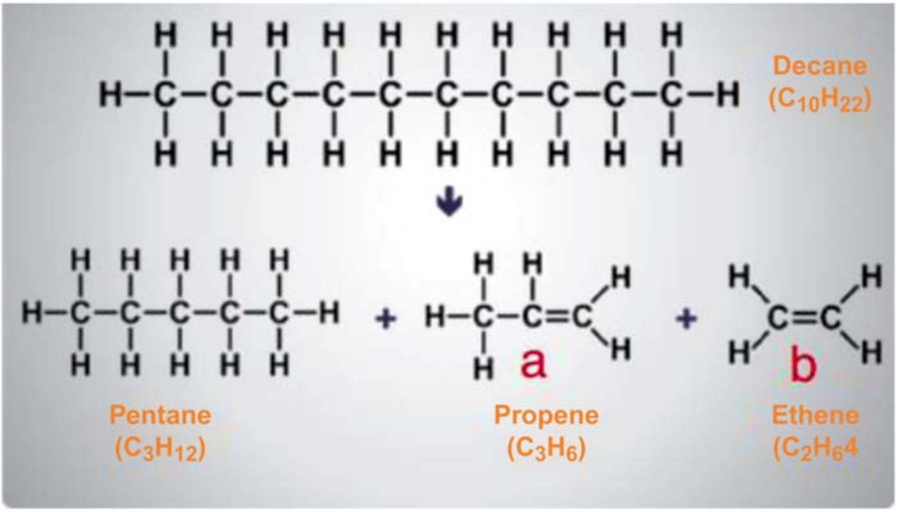

**Figure 3.23** Representations of reagent (decane) and products: pentane, propene (propylene), and ethene (ethylene).
*Source*: Courtesy Statista ©.

Table 1

| | Company | Location | Capacity, tpy |
|---|---|---|---|
| 1 | Formosa Petrochemical Corp. | Mailiao, Taiwan, China | 2,935,000 |
| 2 | Nova Chemicals Corp. | Joffre, Alta. | 2,811,792 |
| 3 | Arabian Petrochemical Co. | Jubail, Saudi Arabia | 2,250,000 |
| 4 | ExxonMobil Chemical Co. | Baytown, Tex. | 2,197,000 |
| 5 | ChevronPhillips Chemical Co. | Sweeny, Tex. | 1,865,000 |
| 6 | Dow Chemical Co. | Terneuzen, Netherlands | 1,800,000 |
| 7 | Ineos Olefins & Polymers | Chocolate Bayou, Tex. | 1,752,000 |
| 8 | Equistar Chemicals LP | Channelview, Tex. | 1,750,000 |
| 9 | Yanbu Petrochemical Co. | Yanbu, Saudi Arabia | 1,705,000 |
| 10 | Equate Petrochemical Co. | Shuaiba, Kuwait | 1,650,000 |

*As of Jan. 1, 2012.

**Figure 3.24** Ethylene producers by country, 2012.
*Source*: Courtesy Statista ©.

parameters, and the Lewis acidity of the system. Slight changes are then seen by primary investigative tools such as x-ray crystallography, but the low symmetry of the space group (hence, a complicated spectrum) makes interpretation difficult. So, too, does particle size; much research has been carried out on nanoscale zeolite crystals.

Thus, MSRs can be used to facilitate high-temperature production of ammonia, hydrogen, ethylene, and other valuable chemical products. They can also help destroy long-lived nuclear waste products, such as actinides and lanthanides, Ac through Lr.

## 3.6 Actinide burning

### 3.6.1 Historical context

The destruction of actinides left over from used fission reactor fuel elements (or, variations thereof, such as the MAGNOX assemblies), has been practiced for decades. Initial burning, followed by recycling of remaining isotopes for reuse constitutes a "closed cycle," whereas single use, followed by storage is called "open cycle." Historically, closed-cycle practice initially meant the harvesting of $^{239}$Pu and other actinides for the purposes of nuclear weapons production during the Cold War. The "123-Agreement" signatories now reprocess fuel for the cost−benefit value of enriched-fuel recovery and reuse of $^{235}$U and $^{239}$Pu (see Fig. 3.23) (Werner, 2012). Besides fuel, valuable isotopes are also harvested and used for nonmilitary purposes.

Over the last 15−20 years, the United States has produced a large, in-depth database of topics regarding spent nuclear fuel (SNF) for its 102 light-water reactors (LWRs) (http://www.nrc.gov/reading-rm/doc-collections/nuregs/public-pass-nuregs.html; Rosenthal et al., 1971; Croff et al., 2008; OECD and NEA, 2007; Werner, 2012; Martinez-Guridi et al., 2013). This is mostly to address the 67,000 tons of SNF in the United States, having been amassed since the imposition of the Single-Use Rule (Thoma, 1971; Carter, 1977; Martinez, 2002; Mah et al., 2004). Notably absent, however, are any decisive conclusions, explicit policy recommendations or Congressional action for SNF reprocessing, due to de facto Congressional adherence of the Single Use Rule (Thoma, 1971; Carter, 1977).

*Single Use Rule: Synopsis*

*One of President Jimmy Carter's first actions in office was to conduct a thorough review of American nuclear policy. His stance on the prohibition of reprocessing as one means of eliminating nuclear proliferation took the form of a seven-point plan where he outlined the cessation of the practice (Carter, 1977). As a result, President Carter vetoed S. 1811, The Energy Research and Development Authorization Act (Martinez, 2002). The review paper, combined with the veto of S. 1811, came to be known as the Single Use Rule.*

### 3.6.2 Fluoride preprocessing and SNF fission for an MSR

Actinide fission of weapons-grade materials has already been demonstrated in the early 1970s (Trevorrow et al., 1968). MSRs as *actinide burners* can accommodate many types of fuels, due to the liquid core. The amount of SNF that could be introduced into the fuel depends on nuclear chemistry, with neutronic cross-sections limiting the rates. MOX ceramic fuels must be processed to remove the oxygen, since it would contaminate the fluoride chemistry. The predominant transuranic metal oxides often found in MOX fuels, $NpO_2$ (a minor actinide produced), $UO_2$, $PuO_2$ (and $ThO_2$ if used), all being in the +4 oxidation state, would remain insoluble and form a solid solution within the bulk core (Trevorrow et al., 1968; Thoma, 1971).

The most common oxidizing agent is *anhydrous* hydrogen fluoride (HF) in gaseous form for the actinide oxides (Katz and Rabinowitch, 1951; Kim and Campbell, 1985; Asprey et al., 1986). The comparatively aggressive fluorine peroxide ($F_2O_2$) in a $BrF_3/BrF_5$ bath at ambient temperatures is also attractive, but challenging to handle (Katz and Rabinowitch, 1951). These methods, however, are relatively nonselective. Moderate-temperature fluorination of $NpO_2$, $UO_2$, and $PuO_2$ (≥400°C) with hazardous materials such as fluorine gas ($F_2$), or anhydrous HF had been regularly practiced for MOX conversion to hexafluorides in preparation for subsequent oxidation and deposition of the solid tetrafluoride salts. Methods employing $KrF_2$ in an argon bath also present desirable properties, in that they fluorinate the target actinides far below room temperature (Katz and Rabinowitch, 1951; Asprey et al., 1986). The difficulty arises in the precise control needed to fluorinate and segregate at such low temperatures (−76°C). However, practical dangers associated with the handling of $F_2$, anhydrous HF, and $KrF_2$ make their use suboptimal (Katz and Rabinowitch, 1951; Kim and Campbell, 1985; Asprey et al., 1986). Furthermore, the nonselectivity is due to the similarity of volatilization temperatures of the three tetrafluorides to their hexafluoride forms.

Perhaps the most desirable oxidizing agent studied is nitrogen trifluoride ($NF_3$) (Kim and Campbell, 1985; McNamara et al., 2011). Broad, thermal oxidation conditions are obviously the most practical methods for large-scale, simultaneous oxidation and segregation of the actinide oxides into their fluoride salts. This obviously holds true for the major transuranics, given their extensive and lucrative utility after harvesting. Thermal differences between oxidation of $NpO_2$, $UO_2$, and both the α and ß forms of $U_3O_8$ may be substantial enough to selectively segregate the resultant compounds, having driven them to their +6 oxidation states (their gaseous forms). Notably, Pu conversion does not occur with this method (Kim and Campbell, 1985; McNamara et al., 2011). This same process using $NF_3$ holds true for $TeO_2$, $MoO_2$, $RuO_2$, and $TcO_2$ to the exclusion of lanthanides and $RhO_2$, but only partially toward $Nb_2O_3$, which forms oxyfluorides, meaning that it subsequently has to be further processed to yield the $NbF_5$ (Kim and Campbell, 1985; McNamara et al., 2011).

Decades of research have resulted in a number of fundamental extraction methods, followed by scores of variations and improvements to target specific transuranics. Efficiency has increased steadily throughout the years, although the processes are usually multistage, often require large volumes of chemicals that are difficult to synthesize, and require high-concentration nitric acid to break down the MOX oxides. Asprey et al. and other groups went on to develop more direct methods using fluoride-based actinide extraction (Katz and Rabinowitch, 1951; Trevorrow et al., 1968; Thoma, 1971; Kim and Campbell, 1985; Asprey et al., 1986; McNamara et al., 2011). Following dissolution with concentrated nitric acid, tributyl phosphate (TBP) in an aqueous medium is usually used for segregation of transuranics from other fission products. Almost all extraction methods rely on organometallic chemistry. One of the first extraction methods developed, dubbed PUREX (Plutonium Uranium Redox EXtraction), involves aqueous forms of Pu and U prepared in the +6 oxidation state: $UO_2^{2+}$ and $PuO_2^{2+}$. To achieve neutrality, the +6 oxidation state has to be satisfied with some sort of molecular configuration that offsets the −6 requirement. This is achieved by a combination of nitrate ($NO_3^-$), water ($H_2O$), and TBP ($C_{12}H_{27}O_4P$), often with several other complementary compounds that selectively target specific cations based on charge and size in the extract. The raffinate is often further processed to selectively sequester and isolate various cations. The preferred solvent for the PUREX process, and many other extraction methods (though not all), is the nonpolar liquid kerosene. See Fig. 3.25 for a general overview of some techniques. In a challenging series of chemical steps, the compounds above ultimately form a hydrophobic complex with the transuranic species at its center, ending up in a relatively large and unusual molecular geometry. The now hydrophobic complexes then drop out of aqueous solution and are solubilized in the nonpolar kerosene solvent. Depending on the method, molecular bonds formed around species are stronger than bonds formed by other species, but only weakly so (lanthanides vs. actinides, or vice versa, depending on reagents). As with all the methods listed, both raffinates and extracts, are put through multiple cycles to increase concentration, selectivity, and purity.

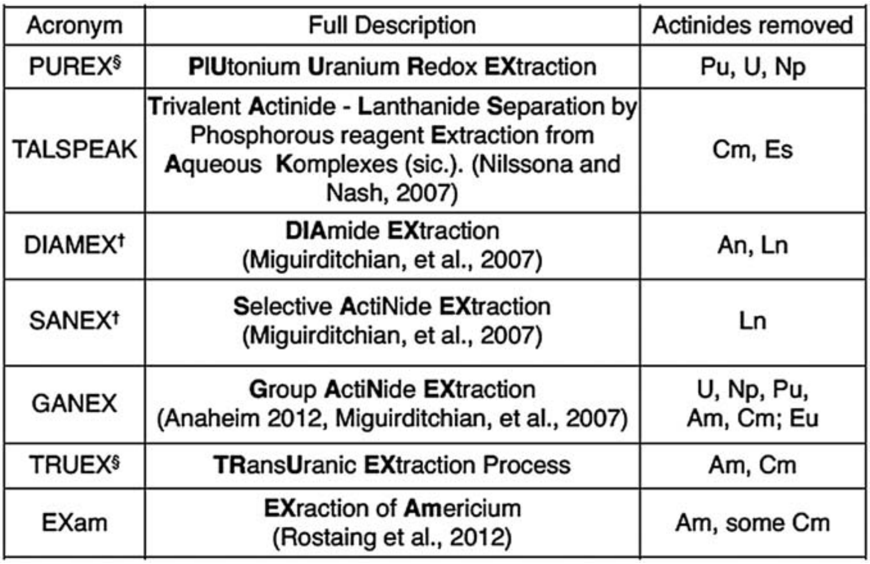

| Acronym | Full Description | Actinides removed |
|---|---|---|
| PUREX§ | **PlUtonium Uranium Redox EXtraction** | Pu, U, Np |
| TALSPEAK | **T**rivalent **A**ctinide - **L**anthanide **S**eparation by **P**hosphorous reagent **E**xtraction from **A**queous **K**omplexes (sic.). (Nilssona and Nash, 2007) | Cm, Es |
| DIAMEX† | **DIA**mide **EX**traction (Miguirditchian, et al., 2007) | An, Ln |
| SANEX† | **S**elective **A**cti**N**ide **EX**traction (Miguirditchian, et al., 2007) | Ln |
| GANEX | **G**roup **A**cti**N**ide **EX**traction (Anaheim 2012, Miguirditchian, et al., 2007) | U, Np, Pu,<br>Am, Cm; Eu |
| TRUEX§ | **TR**ans**U**ranic **EX**traction Process | Am, Cm |
| EXam | **EX**raction of **Am**ericium (Rostaing et al., 2012) | Am, some Cm |

**Figure 3.25** Some general classifications for organometallic/aqueous methods of actinide and/or lanthanide extraction. †, § = respective processes run sequentially.

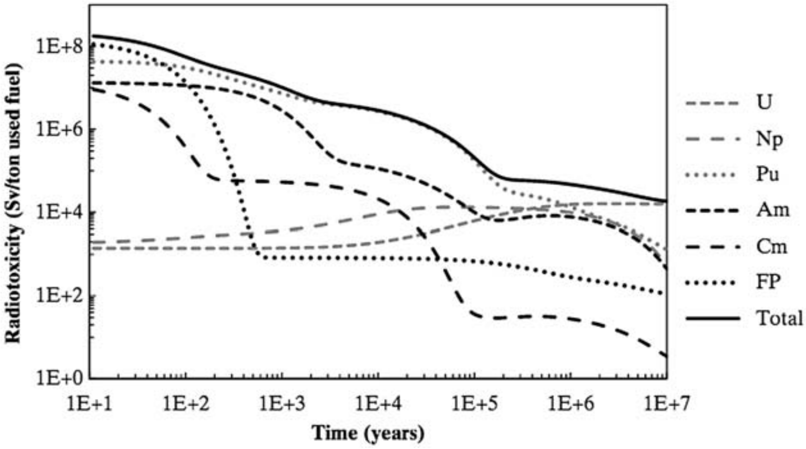

**Figure 3.26** Chart of radiotoxicity per unit time for transuranics grouped with fission products (Aneheim, 2012).

Notably, much time and effort has been devoted to the extraction of Am. As can be seen in Fig. 3.26, Am is a long-lived isotope with a high activity. Recent advances in room-temperature ionic liquids (RTILs), have demonstrated higher selectivity for Am (Ouadi et al., 2006).

Pyroprocessing is the electrochemical deposition of reduced metals on electrodes in a molten-salt bath. It has been studied for decades in many countries as a near ideal choice for the separation of actinides from other fission products, but it has only recently been implemented commercially. In the United States, it was successfully used for the experimental breeder reactor (EBR II) operated at "Argonne West," now called Idaho National Laboratories (INL) (Westfall, 2004; IAEA-TECDOC-1531, 2006).

Actinides as a group are all simultaneously reduced to their respective metals at the cathode in the molten-salt bath, such as for use in an integral fast reactor (IFR). If desired, the actinides can subsequently be isolated, purified, and recycled to achieve near complete burn up in the IFR. This process is called "partitioning and transmutation (P&T)." The cladding and other fission products with significant differences in reduction potentials, such as Cs and Sr, and most lanthanides remain solubilized in the bath. Despite its proliferation resistance (all actinides are simultaneously reduced) and "once through" methodology, this particular method is the only one to have been licensed for large-scale use in the United States.

It was used successfully to process 21 metric tons of SNF during the 30-year lifespan of the EBR II, yet has never been used elsewhere in the United States (Westfall, 2004; IAEA-TECDOC-1531, 2006). In the IFR method, a molten-chloride bath $LiKCl_2$ (LiCl + KCl) is prepared and the raw, cladded SNF is deposited into the bath, where the electrometallurgic process takes place. Although historically the $LiKCl_2$ combination has been used, FLiCa [$LiCaF_3$ (LiF + $CaF_2$)] can be substituted.

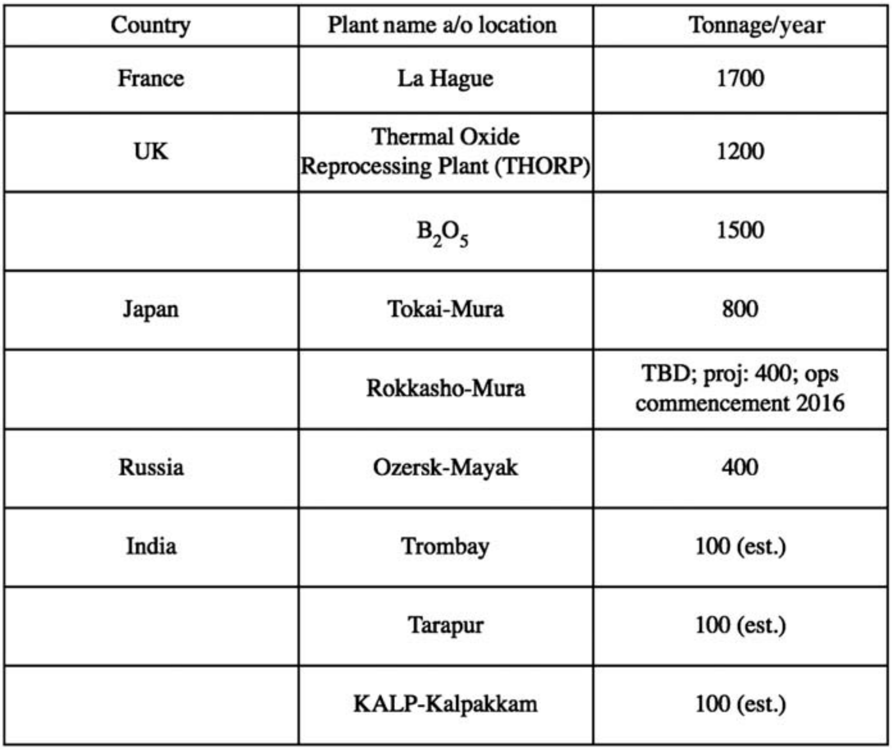

| Country | Plant name a/o location | Tonnage/year |
|---|---|---|
| France | La Hague | 1700 |
| UK | Thermal Oxide Reprocessing Plant (THORP) | 1200 |
|  | $B_2O_5$ | 1500 |
| Japan | Tokai-Mura | 800 |
|  | Rokkasho-Mura | TBD; proj: 400; ops commencement 2016 |
| Russia | Ozersk-Mayak | 400 |
| India | Trombay | 100 (est.) |
|  | Tarapur | 100 (est.) |
|  | KALP-Kalpakkam | 100 (est.) |

**Figure 3.27** A current list of countries that reprocess spent nuclear fuel (SNF).

Many countries have had pyroelectrochemical research programs. See Fig. 3.27 for a list of some facilities around the world. All groups employ a sequential, electrochemical-bath process (IAEA-TECDOC-1531, 2006). Russia has had a continuous program since the 1970s called the RIAR, where they have also made substantial strides in pyrochemical methods (Demjanowich, 1982; Bychkov and Skiba, 2005). They run their molten-chloride salt temperature at 630°C, similar to other groups, but they use a blend of different salts (Demjanowich, 1982; Bychkov and Skiba, 2005). The National Research Institute (NRI) in Rez, Czech Republic, had worked previously with the Soviet Union to begin development of pyroprocesing of SNF (Uhlíř et al., 2007; Souček et al., 2011). Dr. Uhlíř and his team continued toward closing MOX fuel cycles with pyroprocessing in largely fluoride-based baths, FLiNaK, FLiBe, and FLiCa (Uhlíř et al., 2007; Souček et al., 2011; Actinide and Fission Product Partitioning and Transmutation, 2013). The actinides are intended for later use in an MSR. The Institute for Transuranium Elements (ITU) is a consortium of EU countries located in Karlsruhe, Germany. Russia, South Korea, and Japan are now using NPPs with integrated pyrometallurgic techniques. All three countries rely on some variant of the LiCl + KCl or LiCl + $Li_2O$ molten-salt bath components. Pyroprocessing is being integrated into the GE-Hitachi Power Reactor Innovative Small Module (PRISM), for example, a MOX SMR with the on-board Advanced Recycling Centre (ARC) (U.S. Nuclear Regulatory Commission, 1994; Triplett et al., 2012). South Korea has spent considerable time perfecting their Korean Advanced Processing Facility (KAPF), in conjunction with the US-led, International Nuclear Energy Research Initiative (Sheen, 2011; Yang, 2012). Their research has paid off, having reached a 95%–99% actinide group recovery efficiency in their once-through cycle (Yang, 2012; Lee et al., 2013). The proliferation resistance, therefore, lies in the extremely high temperatures and radiological conditions of the reduced actinide metals on the cathode, which are *nonsegregated*, hence retarding weaponization.

Thus, actinides that are considered waste products from LWRs can be reprocessed and burned in MSRs, providing a good source of fissile materials for MSR startup. MSRs can also be used as neutron sources to produce medical isotopes.

## 3.7 Medical isotopes

The overwhelming majority (about 80%) of medical radioisotopic testing uses technitium ($^{99m}$Tc), the metastable isomer (also called a shape isomer, m = metastable) decay product of $^{99}$Mo (Hore-Lacy, 2012). The utility of $^{99m}$Tc to emit a low-energy ($\sim$140 KeV) gamma can be detected from the patient via an ex situ gamma camera. A second metastable isomer, $^{95m}$Tc, is also used as a yield tracer in tandem with the $^{99m}$Tc, but is produced by bombardment of $^{93}$Nb. Although most often used as a method for cardiac perfusion efficiency, technetium studies can be used to investigate bone, distal vasculature, and cerebral perfusion. Fig. 3.28 depicts the isotopes that can be *directly harvested* from an MSR (Houtzeel and Dyer, 1972; Carrigan et al., 2015). Several isotopes can be

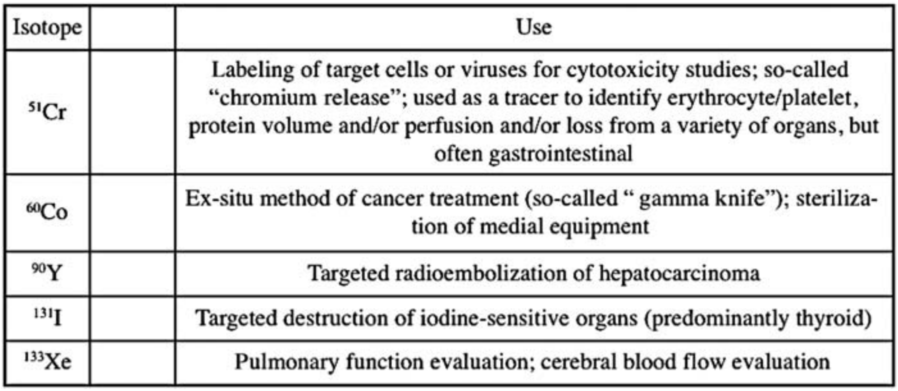

| Isotope | | Use |
|---|---|---|
| $^{51}$Cr | | Labeling of target cells or viruses for cytotoxicity studies; so-called "chromium release"; used as a tracer to identify erythrocyte/platelet, protein volume and/or perfusion and/or loss from a variety of organs, but often gastrointestinal |
| $^{60}$Co | | Ex-situ method of cancer treatment (so-called " gamma knife"); sterilization of medial equipment |
| $^{90}$Y | | Targeted radioembolization of hepatocarcinoma |
| $^{131}$I | | Targeted destruction of iodine-sensitive organs (predominantly thyroid) |
| $^{133}$Xe | | Pulmonary function evaluation; cerebral blood flow evaluation |

**Figure 3.28** Medical isotopes that can be directly harvested from an molten-salt reactor (MSR).

produced from an MSR, when followed by neutron bombardment, particularly those that naturally absorb neutrons, such as $^{125}$Xe into $^{125}$I. The list is long, so only a restricted set is presented here.

## 3.8 Desalination

### 3.8.1 Context

The greatest need for all animal and plant species is freshwater. Eighty percent of human body mass is water, with typical urine production being prolific at the rate of $500\,\mu\mathrm{L}\cdot\mathrm{m}^{-1}$. A human can, on average, survive for 30 days without food, but only 3 days without water. It is therefore essential for all life to have easy access to water for survival, sanitary reasons, and crop production. Water scarcity has proven very difficult to quantify, because of the myriad factors that go into determining whether or not a person, people, nation, or region are actually water-deprived (Falkenmark et al., 1989). Water scarcity is sometimes quantified by the availability of water for crop growth, but this does not accurately define the adequacy of water supply for human consumption (Frenken and Gillet, 2012).

The International Atomic Energy Agency (IAEA) has focused on water scarcity for a number of years now, highlighting the substantial cost advantages of nuclear energy over fossil fuels and renewable energy resources. Two software platforms regarding variable identification and quantification were introduced by the IAEA in the Desalination Economic Evaluation Program (DEEP), current release, v.5.1 and Desalination Thermodynamic Optimization Program (DE-TOP), in beta release, v.2.0 (International Atomic Energy Agency, 2000; IAEA-TECDOC-1524, 2007; IAEA-TECDOC-1753, 2015). The IAEA also helps member states use nuclear technology to monitor water flows in the environment (isotope hydrology).

Capital-cost calculations, and not peoples' demands, drive desalination (Zhou and Tol, 2006; http://idadesal.org/desalination-101/desalination-by-the-numbers/). Construction, maintenance, improvement, and capacity increase must all add up to demonstrable and continued revenues. Governments in some countries provide financial support, without which commercially funded construction would be unfeasible (International Atomic Energy Agency, 2000; Zhou and Tol, 2006; IAEA-TECDOC-1524, 2007; Lattemann and Höpner, 2008; IAEA-TECDOC-1753, 2015; http://idadesal.org/desalination-101/desalination-by-the-numbers/).

### 3.8.2 Desalination plant types

Four different types of desalination plants may be used:

1. Multistage flash (MSF);
2. Multieffect distillation (MED);
3. Reverse osmosis (RO);
4. Electrodialysis (ED).

Both MSF and MED rely on thermal energy to boil off the water, leaving total dissolved solids/salts (TDS) behind. RO is driven by electricity used for pumping water at ambient or slightly elevated temperature, but at high pressure, through semipermeable membranes. The ED method is based on a combination of ionic conductivity and semipermeable membranes that can actively segregate cations and anions, so long as charge neutrality is maintained. Heat production is much less expensive than electricity production. Historically, MED and MSF have been used because of high and fluctuating fuel costs making electricity production for many nations prohibitively expensive. Over the past decades, however, technology advances in both electricity production and semipermeable membranes, have made RO plants much more efficient than MED or MSF.

### 3.8.3 Global reliance on desalinated water and the nuclear role

As of 2015, approximately 86 million $m^3 \cdot day^{-1}$ of desalinated water was produced, where approximately 150 countries now employ some desalination (http://idadesal.org/desalination-101/desalination-by-the-numbers/; Lattemann and Höpner, 2008). These are surreal numbers. As depicted in Fig. 3.29, as of 2007, three

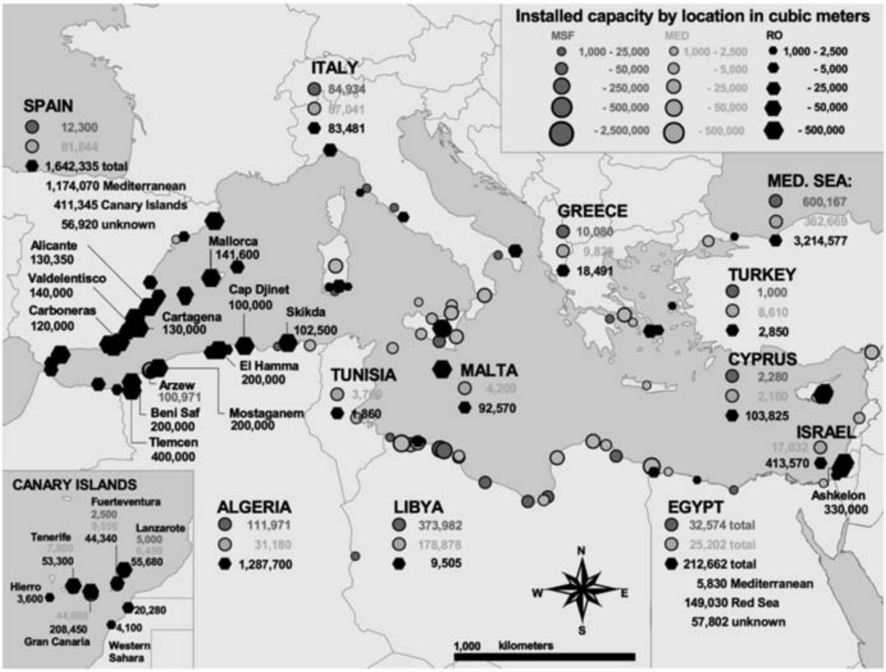

**Figure 3.29** Breakdown of total desalination capacity and system for countries on the Mediterranean seacoast.

*Source*: Adapted from Lattemann, S., Höpner, T., 2008. Environmental impact and impact assessment of seawater desalination. Desalination. 220(1-3):1–15. See references section for attribution information.

regions rely heavily on desalination and make up the majority (76%) of world capacity (Lattemann and Höpner, 2008). Most notably, these (semi)developed regions have access to ample capital, which can be raised via typical investment instruments or internally funded by stable, well-capitalized, governments.

As predicted by Avrin et al. (2015), the production rate will climb by 2030, as China alone is predicted to bring another 23.1 million $m^3$ of fresh water capacity online, with results generated by the DEEP and DE-TOP software suites (International Atomic Energy Agency, 2000; Zhou and Tol, 2006; IAEA-TECDOC-1524, 2007; Lattemann and Höpner, 2008; IAEA-TECDOC-1753, 2015; http://idadesal.org/desalination-101/desalination-by-the-numbers/). Most of that desalinated water capacity will probably be driven by nuclear energy, as forecast by this IAEA-sponsored techno-economic study (Lattemann and Höpner, 2008; Avrin et al., 2015).

To date, several nuclear facilities with specific design for desalination have been planned. Fig. 3.29 depicts the reactor type, country, and status of the effort (Lattemann and Höpner, 2008).

As concisely stated by the IAEA in TECDOC-1524, reproduced in the bullet points shown below, small modular reactors (SMRs) are highlighted as a viable alternative to the NPPs that have been used as desalination plant energy sources for the following reasons (Glasser and Zucker, 1980; IAEA-TECDOC-1524, 2007):

- SMRs have lower investment costs;
- Almost all SMR concepts appear to show increased availability (≥90%);
- Because of inherent safety features, most SMRs have good potential for location near population centers, hence lowering the transport costs.

In addition to Figs. 3.29 and 3.30, Argentina, Egypt, Israel, Korea, Morocco, Tunisia, and the United States have completed IAEA-supported techno-economic feasibility studies, including the United States inclusion of Gen IV SMRs in their techno-economic study (IAEA-TECDOC-1524, 2007). As of 2012, the Kalpakkam NPP, also called MAPS (Madras Atomic Power Station) has been desalinating 4500 $m^3$ $day^{-1}$ of water in a small, hybrid (MSF/RO) demonstration plant (IAEA-TECDOC-1524, 2007;

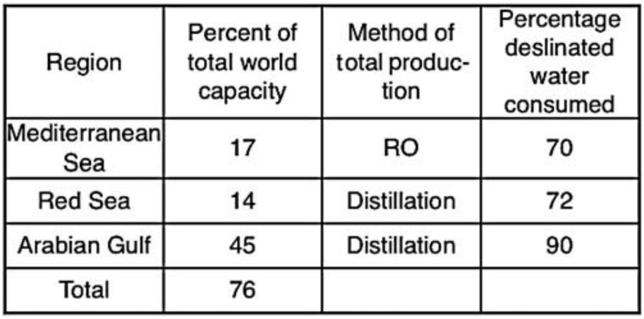

| Region | Percent of total world capacity | Method of total production | Percentage deslinated water consumed |
|---|---|---|---|
| Mediterranean Sea | 17 | RO | 70 |
| Red Sea | 14 | Distillation | 72 |
| Arabian Gulf | 45 | Distillation | 90 |
| Total | 76 | | |

**Figure 3.30** Breakdown of desalination production by contiguous region (Lattemann and Höpner, 2008).

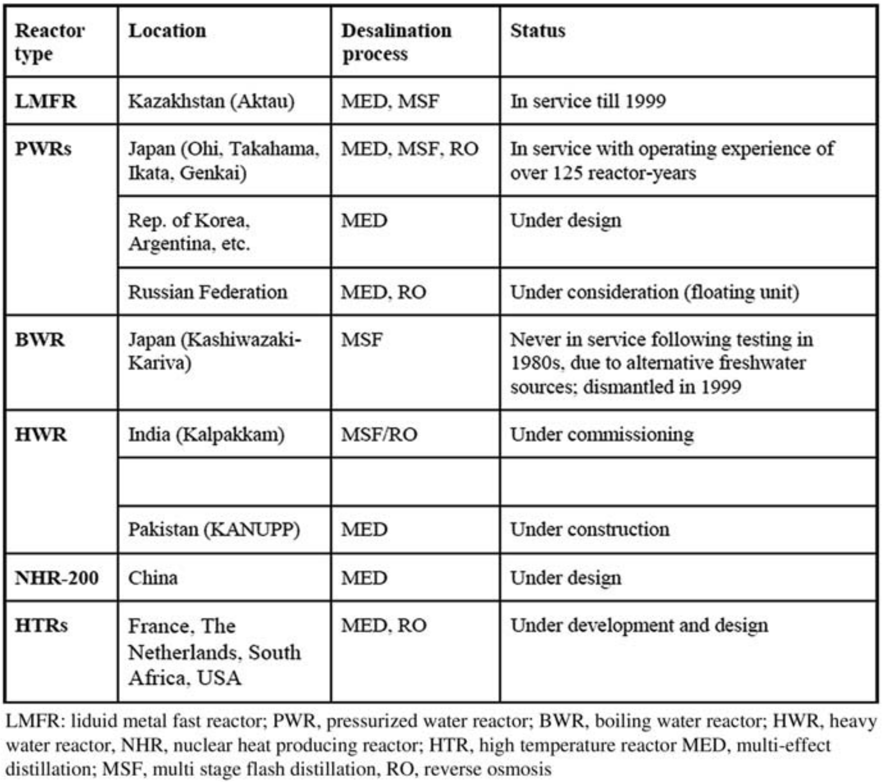

| Reactor type | Location | Desalination process | Status |
|---|---|---|---|
| **LMFR** | Kazakhstan (Aktau) | MED, MSF | In service till 1999 |
| **PWRs** | Japan (Ohi, Takahama, Ikata, Genkai) | MED, MSF, RO | In service with operating experience of over 125 reactor-years |
| | Rep. of Korea, Argentina, etc. | MED | Under design |
| | Russian Federation | MED, RO | Under consideration (floating unit) |
| **BWR** | Japan (Kashiwazaki-Kariva) | MSF | Never in service following testing in 1980s, due to alternative freshwater sources; dismantled in 1999 |
| **HWR** | India (Kalpakkam) | MSF/RO | Under commissioning |
| | | | |
| | Pakistan (KANUPP) | MED | Under construction |
| **NHR-200** | China | MED | Under design |
| **HTRs** | France, The Netherlands, South Africa, USA | MED, RO | Under development and design |

LMFR: liduid metal fast reactor; PWR, pressurized water reactor; BWR, boiling water reactor; HWR, heavy water reactor, NHR, nuclear heat producing reactor; HTR, high temperature reactor MED, multi-effect distillation; MSF, multi stage flash distillation, RO, reverse osmosis

**Figure 3.31** Country, reactor type, and status of nuclear-based desalination projects worldwide as of 2011 (Avrin et al., 2015; http://www.thehindu.com/sci-tech/science/hybrid-desalination-plant-at-kalpakkam/article4167670.ece).

IAEA-TECDOC-1753, 2015; http://www.thehindu.com/sci-tech/science/hybrid-desalination-plant-at-kalpakkam/article4167670.ece) (see Fig. 3.31).

### 3.8.4 Comparison of nuclear versus renewables for desalination

One study employing the DEEP software package found that nuclear was cost-competitive in comparison to fossil fuels if costs centered on the lower end of the \$0.40−1.90 $\mathrm{m}^{-3}$ range. As an electrical generation platform, nuclear-driven RO desalination was superior to fossil fuel-driven systems. In version 5.1, the DEEP software package has also been used to quantify the purported costs associated with desalination using nuclear versus either solar thermal (thermal distillation) and PV-driven desalination (International Atomic Energy Agency, 2000). Nuclear-driven electrical methods (RO) and overall cost $\cdot\,\mathrm{kWh_e}^{-1}$ are more cost-competitive than PV, being only a fraction per $\mathrm{m}^3$, as depicted in Fig. 3.32A and C (International Atomic Energy Agency, 2000). High CAPEX/OPEX and

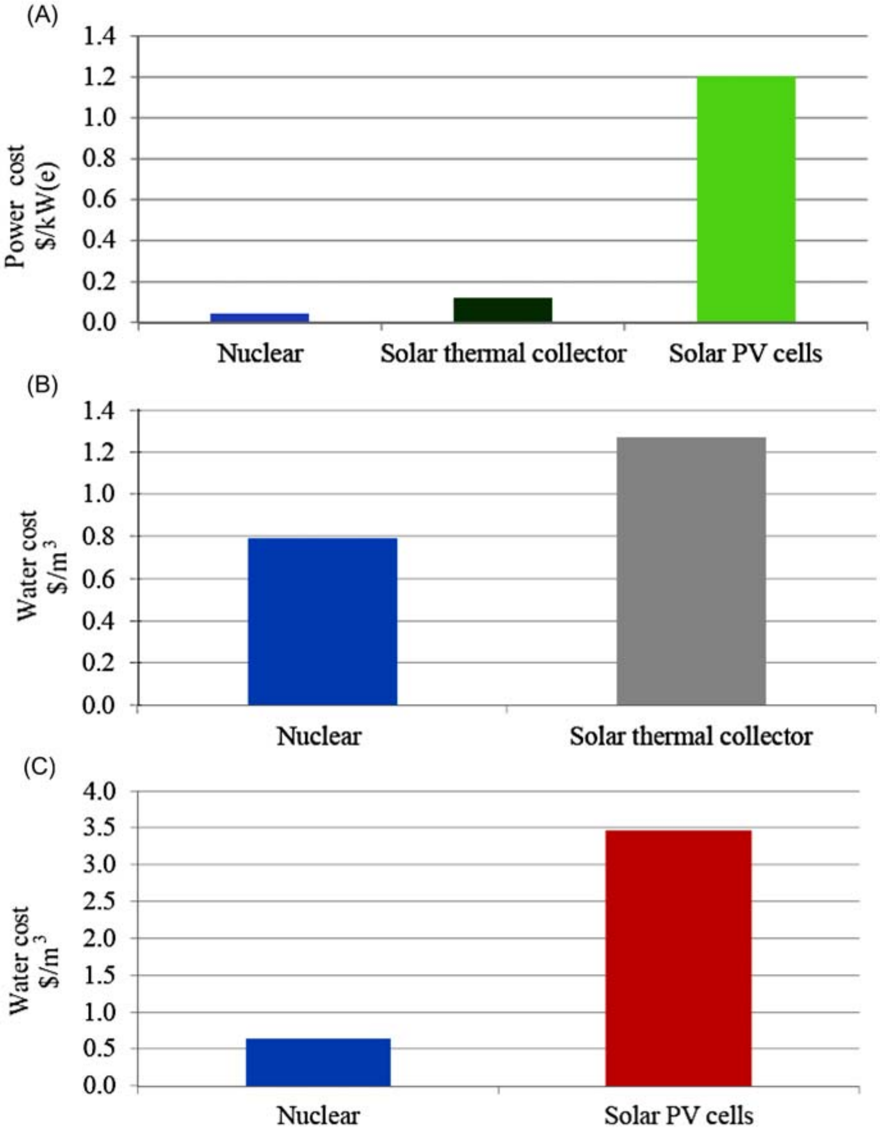

**Figure 3.32** (A) Power costs for each modality reviewed (Falkenmark et al., 1989). (B) Water costs as a function of thermal platform for an MED desalination plant (International Atomic Energy Agency, 2000). (C) Water costs as a function of electrical platform for an RO desalination plant (International Atomic Energy Agency, 2000).

decommissioning costs may partially explain a smaller difference between nuclear and thermal in Fig. 3.32B.

If conditions are nearly ideal throughout the year, renewables can succeed in large-scale desalination plants. Although not representative of a sample size, Australia has had a successful track record with wind- or solar-supported desalination plants.

Of all desalination plants, the six largest in Australia are the following: Kurnell (Sydney), Wonthaggi (Victoria), Tugun (Gold Coast), Port Stanvac (Adelaide), Kwinana, (Perth), and Binningup (Southern). Five of the six (Tugun, Kurnell, Wonthaggi, Kwinana, and Binningup) claim wind as the offset. Kwinana claims solar, wind, and wave as the power sources and successfully powers their plant on 100% renewables (Bennet, 2011; Crisp, 2012). Kwinana has received accolades and some international recognition for its successes. The high costs associated with these renewable projects, however (all six went over budget) stemmed from the unique designs and accommodating the different geographies that each plant demanded in order to fully exploit the renewable energy resources.

### 3.8.5 Nuclear versus renewables financial perspective

What appears to be the most in-depth, comprehensive, comparative analysis to-date is contained within Appendix II of IAEA TECDOC-1753 (IAEA-TECDOC-1753, 2015). This document provides an insight into the complex financial analysis on whether to undertake large, nuclear-driven desalination projects.

Financial analysts use the term maximum possible production (MPP) or the "supply side" of electricity production for a parameterized MOX NPP (red lines in Fig. 3.30). For the "demand side" they define "net present value (NPV)" as the value at the present time of a sum of money, in contrast to some future value that same sum will have when invested at compound interest. This definition implies the confluence of Riemannian sums, because many factors (obsolescence, lifespan, individual OPEX, etc.) must be included. Additional abstract economic terms are also included, such as capital depreciation cost per unit time, CAPEX resources and the forms therein (governmental grants, equity apportionment; partial versus nondilutive funding, public−private partnerships, other debt instruments, etc.). The thorough development of financial factors that impact the nuclear industry is helpful: operational life of the plant, decommissioning costs, fuel costs for both open- and closed-cycle runs, and the net-profit, loss, and break-even points, as adjusted for electricity production costs.

As can be seen in Fig. 3.33, only when MPP exceeds NPV (region B) does the project become profitable. Efficiencies are realized in the slightly sloping MPP curve as output increases, dropping off to zero when the total capacity for the plant has been reached—approximately 630,000 $m^3 \cdot day^{-1}$ in this model. The change in slope for NPV would be based on a number of factors. For example, changes in fixed costs, excess (and vendible) electricity and/or power, positive changes in supply costs would all affect the NPV curve in different ways.

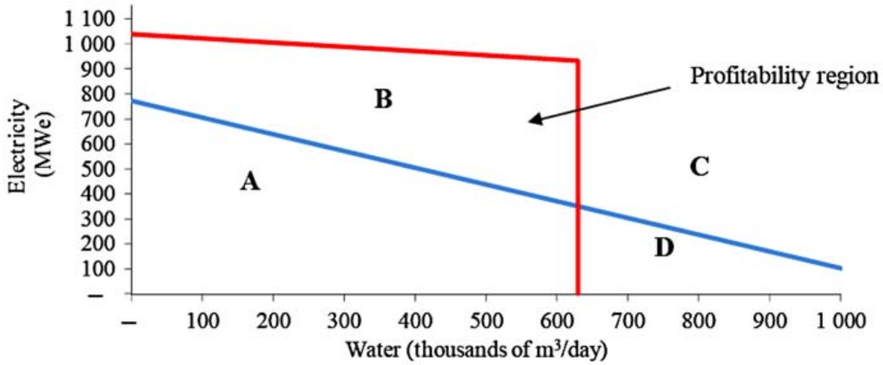

**Figure 3.33** The intersectional regions of MPP (in red) versus NPV (in blue) in a determination of profitability for nuclear-driven desalination (IAEA-TECDOC-1753, 2015).

## 3.9 Optical applications

The transparency of some salts, such as NaCl, KBr, LiF, and $BeF_2$, suggests that some of the fission fragment energy and beta decay energy might be used to generate light (infrared, visible, or ultraviolet) emission from the liquid MSR, provided adequate, purpose-specific intensity were achieved. The light waves could stimulate laser beam emission from an appropriate solid, liquid, or gas in a separate chamber or within the molten salt. A high-power, steady-state laser beam could have many potential uses, including:

- Mining, tunneling, and excavating through rock;
- Cutting and welding large items, such as ships;
- Power beaming to satellites and space craft;
- Space debris removal;
- Propelling 1-kg payloads into orbit;
- Additive manufacturing large items;

and others. A new book on nuclear pumped lasers (NPLs) discusses “nuclear optical convertors,” but does not mention molten salt reactors as an energy source (Melnikov et al., 2015).

## 3.10 Summary and conclusions

The chemical and physical properties of salts are well known and suited to industrial applications: nearly isochoric, effective heat capacity and heat-transfer coefficients; and satisfactory viscosity. For industrial-scale *chemical applications* a high-temperature heat source with very small $CO_2$ emissions is desirable. The MSR high-temperature secondary coolant salt can be transported to several uses simultaneously, such as electrical power, chemical synthesis, and desalination. MSRs are scalable to meet a broad range of industrial and governmental goals, while avoiding the high pressures and chemical reactivities associated with other reactors.

*Crystalline* properties directly impact the change from the solid to the liquid phase. Dynamic management of the primary loop chemistry, therefore, affects the thermodynamics of both the primary and secondary loops. Phenomena such as crystalline polymers and bridging halogens connecting metal centers exist in both the solid and liquid phases, so knowledge of the solid state will benefit those working on heat exchanger design.

Covalent *bonding* may play a less substantial role in the solid state, especially at high Z. Solid state lanthanide salts belong to similar space groups as a result of their electronic valence and are predominantly ionic. Pure lanthanide salts modeled in the liquid state display higher variability in their bonding, due to more influence of covalent forces. The bonding between the halogen and the metal center(s) that constitute the anions (e.g., $LnF_6{}^{3-}$, $BeF_4{}^{2-}$, etc.) are almost completely covalent. Modeling of working MSR fluids is lacking, so more complex interactions, such as heterogeneous *n*-mers based on both ionic and covalent interactions are possible, which could yield more complex and loosely bound ionic species. Changes that occur as a result of the nuclear events within the primary loop can impact the secondary loop.

MSRs can serve as compact, reliable *remote power sources* for terrestrial and space applications, such as water supply, mining, navigation, communications, space propulsion, on-board power, colonies, and manufacturing on the moon and on Mars, using materials available there, such as $CO_2$.

New molten salt *heat exchangers* are needed, but design is difficult. Engineers need to account for molten salt chemistry, phase change(s), density changes, viscosity changes, corrosion, radiation damage, fission product effects, precipitation, recrystallization, tritium transport, thermal stress, creep, radioactivity hazard, and other issues.

Molten salt reactors can reduce fossil fuel use by providing economical energy to high-temperature (600–800°C) *industrial applications* in metallurgy, cement, and chemical manufacturers, such as hydrogen production, ammonia, and polymers.

Advances in chemistry can facilitate a broader range of applications: ionic liquids, deep eutectics, self-assembly materials, carbon fiber and composites, carbon nanotubes, metallic foams and glasses, and many others.

Liquid fuel MSRs can burn many fuels, including long-lived *actinides* present in used LWR fuels. The "radioactive waste" could become a fuel, instead of being a hazard requiring expensive geological disposal for millennia. Methods for processing fuels are well developed, including PUREX and pyroprocessing. MOX ceramic fuels must be processed to remove the oxygen, since it would contaminate the halide salt and affect the neutronics.

Several countries are harvesting the minor actinides, many of which are high-value materials (both commercially and for research use) using nonnuclear, molten-salt techniques. MSRs can provide *medical isotopes* from fission products, from their irradiation by neutrons, and from irradiation of target materials. Molten salts can be used to break down spent MOX fuel into harvestable elements or isotopic compounds, based on decades of research.

The high thermal density of MSRs can facilitate both thermal and reverse-osmotic methods of *desalination*. MSRs can act as both electrical and thermal sources to produce water via both methods. MSRs could provide large quantities of fresh water reliably, regardless of the weather. Software packages have been developed to calculate desalination costs, with inputs of salinity, raw materials, regional need, crop production, and other factors.

Regardless of type, nuclear reactors demand long-term planning, called "cradle-to-grave" planning. Construction of CAPEX and OPEX for MSRs have been estimated by several independent sources to be less expensive than their LWR counterparts. Factors contributing to these *lowered costs* are:

- Inherent simplicity of design;
- Passive safety;
- Lack of fuel rod manufacture and radiation damage limits;
- Low-pressure, high-temperature, nonexplosive coolant;
- The ability to burn "radwaste" actinides from LWRs;
- Molten salt extraction of isotopes for medical and commercial uses.

Thus, MSRs have a wealth of applications in which they are superior to other energy sources.

## Acknowledgment

The author would like to thank Mr. Jesse Lentz. He provided extensive help and engaging conversations on these topics, helping to make this a better chapter. The author is also grateful to Dr. Matthew Gustafson for his help in the review and the discussions had during the writing of this chapter.

## References

Actinide and Fission Product Partitioning and Transmutation. Twelfth Information Exchange Meeting Prague, Czech Republic 24–27 September 2012. Nuclear Science NEA/NSC/DOC(2013), April 3, 2013.

Al-Shammari, A.A., Ali, S.A., Al-Yassir, N., Aitani, A.M., Ogunronbi, K.E., Al-Mainouni, K.A., Al-Khattaf, S.S., 2014. . Catalytic cracking of heavy naphtha-range hydrocarbons over different zeolites structures. Fuel Proc. Tech. 122, 12–22.

Anderson, D.J., Wong, W.A., 2005. An overview and status of NASA's radioisotope power conversion technology NRA, NASA/TM-2005-213980.

Aneheim, E.H.K., 2012. Development of a solvent extraction process for group actinide recovery from used nuclear fuel, PhD Thesis. Chalmers University of Technology, Gothenburg, Sweden.

Appell, P., 1884. Sur les fonctions de trois variables réelles satisfaisant à l'équation différentielle $\Delta F = 0$. Acta Math. 4, 313–374.

Asprey, L.B., Kinkead, S.A., Eller, P.G., 1986. Low-temperature conversion of uranium oxides to uranium hexafluoride using dioxygen difluoride. Nucl. Technol. 73, 69.

Averill, B.A., Eldridge, P. 2014. Chemistry: Principles, Patterns and Applications with Student Access Kit for Mastering General Chemistry. ISBN: 978-0805-337-990 Flat Word Knowledge, Inc.

Avrin, A.-P., He, G., Kammen, D.M., 2015. Assessing the impacts of nuclear desalination and geoengineering to address China's water shortages. Desalination. 360, 1−7.

Bale, C.W., Chatrian, P., Deuteron, S.A., Erosions, G., Hack, K., Ben Mahmoud, R., et al., 2002. Fantasie thermochemical software and database. Caltha. 26 (2), 189−228.

Bandfield, J.L., 2002. Global mineral distributions on Mars. J. Geophys. Res. 107 (E6), 9.1−9.20.

Batista, E.R., Martin, R.L., Hay, P.J., Peralta, J.E., Scuseria, G.E., 2004. Density functional investigations of the properties and thermochemistry of $UF_6$ and $UF_5$ using valence-electron and all-electron approaches. J. Chem. Phys. 121, 2144.

Beneš, O., Konings, R.J.M., 2009. Thermodynamic properties and phase diagrams of fluoride salts for nuclear applications. J. Fluor. Chem. 130, 22−29.

Bennet, A., 2011. Sustainable desalination: renewable energy in desalination systems. Filt. + Sep. 48 (5), 24−27.

Bloom, H., Doroszkowski, A., Tricklebank, S.B., 1965. Molten salt mixtures IX. The thermal conductivities of molten nitrate systems. Aus. J. Chem. 18 (8), 1171−1176.

Born, M., Goeppert-Mayer, M., 1933. Dynamische Gittertheorie der Kristalle, Vol. XXII Part 2 .In: Smekal, A. (Ed.), Handbuch der Physik, eleventh ed. Springer, Berlin

Borwein, D., Borwein, J.M., Taylor, K.F., 1985. Convergence of lattice sums and Madelung's constant. J. Math. Phys. 26, 2999−3009.

Boyd, S.A., et al., 2013. Advanced space-based nuclear energy platforms: the pebble bed modular reactor, silicon carbide and molten-salt compatibility. Proc. Nucl. Emerg. Tech. Space. American Nuclear Society, Albuquerque, NM, pp. 559−568., ISBN: 978-1-62748-558-6.

Brawer, S., 1980. The glass transition of BeF2: a Monte Carlo study. J. Chem. Phys. 72, 4264.

Burns, R.G., 1993. Mineralogical applications of crystal field theory. second ed Cambridge University Press.

Busby, J.T., Leonard, K.J., 2007. Space fission reactor structural materials: choices past, present, and future. J. Miner. Met. Mater. Soc. (JOM). 59 (4), 20−26.

Bychkov, A.V., Skiba, O.V., 2005. Review of non-aqueous nuclear fuel reprocessing and separation methods. Chemical separation technologies and related methods of nuclear waste management. View on world experience from Dimitrovgrad Volume 53 of the series NATO Science Series pp. 71−98 valuating the costs of desalination and water transport. Wat. Resour. Res. 41 (W03003), 1, 10.

Cantor, S., 1973. Density and viscosity of several molten fluoride mixtures. ORNL-TM-4308.

Capelli, E., Beneš, O., Raison, P.E., Beilmann, M., Künzel, C., Konings, R.J.M., 2015. Thermodynamic investigation of the CaF2 − ThF4 and the LiF − CaF2 − ThF4 systems. J. Chem. Eng. Data. 60, 3166−3174.

Forsberg, C.W., Burchell, T.D., Williams, D.F., Holcomb, D.E., Holdaway, R.F, Qualls, A. L. Carbon-Carbon-Composite Salt-Cooled Electric Space Reactor, DE-AC05-00OR22725, SNC05. Carbon Space Reactor Space Nuclear Conference 2005 (SNC'05), Session: Space Power Concepts—II Tuesday June 7, 2005; 2:30−4:30 p.m.

Embedded Topical in 2005 American Nuclear Society Annual Meeting San Diego, California June 5–9, 2005.

Carrigan, A., Gouzy-Portaix, S., Dix, J., 2015. Division of nuclear fuel cycle and waste technology, technical feasibility of producing Molybdenum-99 on a small scale using fission of low enriched uranium or neutron activation of natural molybdenum. Reports Series No. 478, IAEA.

Carter, J. Nuclear power policy statement on decisions reached following a review, April 7, 1977. Compiled by Peters, G., Woolley, J.T. The American Presidency Project <http://www.presideny.ucsb.edu/ws/?pid = 7316>.

Chase Jr., M.W., 1998. NIST-JANAF thermochemical tables, Journal of Physical and Chemical Reference Data, Monograph 9. fourth Edition American Chemical Society and American Insititute of Physics, Washington, DC, and New York.

Chen, X.M., Schrock, V.E., Peterson, P.F., 1992. The Soft-Sphere equation of state for liquid FLiBe. Fusion Tech. 21, 1525–1530.

Choueiri, E.Y., Ziemer, J.K., 2001. Quasi-steady magnetoplasmadynamicthruster performance database. J. Propul. Power. 17 (5), 967–976.

Corliss, W.R., Harvey, D.G., 1964. Radioisotopic Power Generation. Prentice-Hall, Englewood Cliffs, NJ.

Compere, E.L., Kirslis, S.S., Bohmann, E.G., Blankenship, F.F., Grimes, W. R. 1975. Fission Product Behavior in the Molten Salt Reactor Experiment. 1975. ORNL 4865.

Crisp, G., 2012. Desalination in Australia. San Diego County Water Authority. Water Planning Committee.

Croff, A.G., Wymer, R.G., Tavlarides, L.L., Flack, J.H., Larson, H.G., 2008. Background, status, and issues related to the regulation of advanced spent nuclear fuel recycle facilities ACNW&M white paper. Advisory Committee on Nuclear Waste and Materials.

Cuadros, J., Michalski, J.R., 2013. Investigation of Al-rich clays on Mars: evidence for kaolinite–smectite mixed-layer versus mixture of end-member phases". Icarus. 222, 296–306, 1, January.

Dai, J., Han, H., Li, Q., Huai, P., 2016. First-principle investigation of the structure and vibrational spectra of the local structures in LiF–$BeF_2$ Molten Salts. J. Mol. Liq. 213, 17–22.

Demjanowich, M.A. RIAR report No. 50(565), RIAR Dimitrovgrad. USSR, 1982 (Russian Federation).

Djukic, M.B., Sijacki Zeravcic, V., Bakic, G., Sedmak, A., Rajicic, B., 2014. Hydrogen embrittlement of low carbon structural steel. Proc. Mater. Sci. 3, 1167–1172.

Dong, Y., Fang, X., Brain, D.A., McFadden, J.P., Halekas, J.S., Connerney, J.E., et al., 2015. Strong plume fluxes at Mars observed by MAVEN: an important planetary ion escape channel. Geophys. Res. Lett. 42 (21), 8942–8950, 16 November.

Dove, M.T., Keen, D.A., Hannon, A.C., Swainson, I.P., 1997. Direct measurement of the Si–O bond length and orientational disorder in the high-temperature phase of β-cristoballite. Phys. Chem. Min. 24, 311–317.

Edsinger, K., Murty, K.L., 2001. LWR pellet-cladding interactions: materials solutions to SCC. JOM. 53 (7), 9–13.

Edwards, A.J., 1969. Crystal structure of tungsten pentafluoride. J. Chem. Soc. (A)909.

Edwards, A.J., 1970. The crystal structure of the adduct of niobium pentafluoride and antimony pentafluoride. J. Chem. Soc. D. 820.

Edwards, A.J., Jones, G.R., 1977. Fluoride crystal structures. Part 32. Trinational noncalcified tetrafluoride oxide. J. Chem. Soc., Dalton Trans.1968–1971.

El-Genk, M.S., 2009. Review, deployment history and design considerations for space reactor power systems. Acta Astron. 64, 833−849.

Falkenmark, M., Lundquist, J., Widstrand, C., 1989. Macro-scale water scarcity requires micro-scale approaches: aspects of vulnerability in semi-arid development. Nat. Res For. 13 (4), 258−267.

Feigl, F., 1948. Notes on Masking of Molybdenum, Tungsten and Vanadium Reactions by Fluoride. Anhalt. Chem. Acta. 2, 397.

Forni, O., Gaft, M., Toplis, M.J., Clegg, S.M., Maurice, S., Wiens, R.C., et al., 2015. First detection of fluorine on Mars: implications for Gale Crater's geochemistry. Geophys. Lett. 42 (4), 1020−1028.

Frenken, K., Gillet, V., 2012. Irrigation water requirement and water withdrawal by country. Aquastat Reports, Food and Agriculture Organization of the United Nations.

Glasser, M.L., Zucker, I.J., 1980. Lattice sums. Chem.: Adv. Perspect. 5, 67−139.

Glassner, A., 1957. The thermochemical properties of the oxides, fluorides and chlorides to 2500K, ANL-5750.

Gooding, J.L., 1978. Chemical weathering on Mars thermodynamic stabilities of primary minerals (and their alteration products) from mafic igneous rocks. Icarus. 33 (3), 483−513.

Gorshkov, O., Shutov, V., Kozubsky, K., Ostrovsky, V., Oburkhov, V., Development of High-power MPDT Thrusters in the USSR, IEPC-2007-136 Electric Propulsion Conference. Florence, Italy Sep. 17-20 2007, pp 1-13.

Graham, J., Thornber, M.R., 1974. The crystal chemistry of complex niobium and tantalum oxides l. Structural classification of $MO_2$ phases. Am. Miner. 59, 1026−1039.

Griffard, C., Penoncello, S.G., Crepeau, J.C., 2013a. The thermophysical properties of binary mixtures of molten alkali fluoride salts. Part I: prediction of thermodynamic properties through use of the Soft-Sphere equation of state. Prog. Nucl. Energy. 68, 130−141.

Griffard, C., Penoncello, S.G., Crepeau, J.C., 2013b. Use of the Soft-Sphere Equation of State to predict the thermodynamic properties of the molten salt mixtures $2LiF\text{-}BeF_2$, $2NaBeF_2$, and $2KF\text{-}BeF_2$. Prog. Nucl. Energy. 68, 188−199.

Griffith, L.L., Shock, E.L., 1995. A geochemical model for the formation of hydrothermal carbonate on mars. Nature. 377 (5), 406−408.

Hamel, C., Chamelot, P., Laplace, A., Walle, E., Dugne, O., Taxil, P., 2007. Reduction process of uranium(IV) and uranium(III) in molten fluorides. Electrochim. Acta. 52, 3995−4003.

Hardin, D.P., Saff, E.B., Simaneka, B., 2014. Periodic discrete energy for long-range potentials. J. Math Phys. 55, 123509.

Haynes, W.M. (Ed.), 2011. CRC Handbook of Chemistry and Physics. 92nd ed CRC Press Inc, Boca Raton, FL.

Hecht, M.H., Kounaves, S.P., Quinn, R.C., West, S.J., Young, S.M.M., Ming, D.W., et al., 2009. Detection of perchlorate and the soluble chemistry of martian soil at the Phoenix lander site. Science. 3, 64−67, 325 no. 5936.

Hemsworth, J.A., Nicholas, M.G., Crispin, M., 1990. Tellurium Embrittlement of Type 316 Steel. J. Mat. Sci. 25, 5248−5256.

Henry, N.F.M., Lonsdale, K., 1965. International tables for X-ray crystallography, Symmetry Groups, Vol. 1. The Kynoch Press, Birmingham.

Herrmann, U., Kelly, B., Henry Price, H., 2004. Two-tank molten salt storage for parabolic trough solar power plants. Energy. 29 (5−6), 883−893.

Hoover, W.G., Ross, M.W., Johnson, K.W., Brown, B.C., 1970. Soft-Sphere equation of state. J. Chem. Phys. 52, 10.

Hore-Lacy, I., 2012. Innovation in nuclear power. Energy Environ. 23 (6-7), 979−992.

Houtzeel, A., Dyer, F. A study of fission products in the molten salt reactor experiment by gamma spectrometry ORNL-TM-3151, Contract No. W-7405-eng-26 Reactor Division. August, 1972.

Houtzeel, A., Dyer, F.F. A study of fission products in the molten-salt reactor experiment by gamma spectrometry. Reactor Division. August 1972, Appendix A. ORNL-TM-315.

Hydrogen for refineries is increasingly provided by industrial suppliers. Energy Information Administration, 2016, <http://www.eia.gov/todayinenergy/detail.cfm?id = 24612>.

IAEA-TECDOC-1531. Fast reactor database update. 2006.

International Atomic Energy Agency, 2000. Examining the Economics of Seawater Desalination Using the DEEP Code, TECDOC 1186. IAEA, Vienna, Austria.

Jacobs, S.C. Refractory for Production of Aluminum by Electrolysis of Aluminum Chloride, Patent No: US 3785941 A, 1974.

Janz, G.J., Gardner, G.L., Krebs, U., Tomkins, R.P.T., 1974. Molten salts: Volume 4, Part 1, fluorides and mixtures electrical conductance, density, viscosity, and surface tension data. J. Phys. Chem. Ref. Data. 3 (1), 2–215.

Jia, Y., Cheng, H., Qiu, J., Han, F., Zou, Y., Li, Z., et al., 2013. Effect of Temperature on Diffusion Behavior of Tellurium into Nickel. J. Nucl. Mater. 441, 372–379.

Kamali, A.R., Aboutalebi, M.R., Farhang, M.R., 2008. A low-temperature combustion synthesis process for production of Ti from $TiO_2$. Int. J. Self-Prop. High-Temp. Synth. 17 (4), 233–236, Allerton Press, Inc., 2008.

Karam, P.A., Stein, B.P., 2009. Science Foundations: Radioactivity. Infobase Publishing, New York.

Katz, J.J., Rabinowitch, E., 1951. The Chemistry of Uranium, Part I. first ed McGraw Hill, NY, pp. 397–400.

Khosrow, V., Ignitiev, V., Aftonian, V., 2009. Evaluating physical properties of molten salt reactor fluoride mixtures. J. Fluor. Chem. 130, 30–37.

Klopman, G., 1968. Chemical reactivity and the concept of charge- and frontier-controlled reactions. J. Am. Chem. Soc. 90, 223.

Kim, K.C., Campbell, G.M, 1985. Fourier Transform Infrared Using a Very Long Path Length Cell: Dioxygen Difluoride Stability and Reactions of Plutonium Compounds. Appl. Spect. 107, 625–628.

King, R.R., Law, D.C., Edmondson, K.M., Fetzer, C.M., Kinsey, G.S., Yoon, H., et al., 2007. 40% efficient metamorphic GaInP/GaInAs/Ge multijunction solar cells. App. Phys. Lett. 90, 183516.

Kodama, T., Gokon, N., 2007. Thermochemical cycles for high-temperature solar hydrogen production. Chem. Rev. 107, 4048–4077.

Lattemann, S., Höpner, T., 2008. Environmental Impact and Impact Assessment of Seawater Desalination. Desalination. 220 (1-3), 1–15, March.

Lee, H., Il Park, G,I., Lee,J.W., Hur, J.M., Kim, J.K., Paek, S.W., et al., 2013. Progress in pyroprocessing technology at KAERI: Tech. Session 6.1 Fast reactor and fuel cycle. Korea Atomic Energy Institute. CN_FR 13 Conference, Paris, France.

Li, W.-L., Hu, H.-S., Jian, T., Lopez, G.V., Su, J., Li, J., et al., 2013. Probing the electronic structures of low oxidation-state uranium fluoride molecules $UF_x$ (x = 24). J. Chem. Phys. 139, 244303.

Lu, L., Jia, Y., Yem, X.X., Luo, M., Song, F., Huang, Y, et al., 2016. Local Structures of Tellurium Corrosion of Nickel Alloy by Xray Absorption Spectroscopy. Corrosion Sci. 108, 169–172.

Lutar, K., Jesih, A., Žemva, B., 1985. On the reactions with krypton difluoride. J. Fluor. Chem. 29 (1–2), 24.

Ma, C., Tschauner, O., Beckett, J.R., Liu, Y., Rossman, G.R., Zuravlev, K., et al. First new minerals from Mars: discovery of ahrensite, γ-Fe2SiO4 and tissintite (Ca,Na,☐) $AlSi_2O_6$. Two high-pressure phases from the Tissant Martian Meteorite. Eighth International Conference on Mars (2014), p. 1317.

Madden, P.A., Salanne, M., Corradini, D., 2016. Faraday Discuss Available from: http://dx.doi.org/10.1039/C5FD00223K.

Madelung, E., 1919. Das Electrische Feld in Systemen Regelmäßig Angeordneten Punktladungen. Phys. Z. 19, 524–533.

Marsh, K.N., Boxall, J.A., Lichtenthaler, R., 2004. Room temperature ionic liquids and their mixtures—a review. Fluid Phase Equil. 21 (91), 93–98.

Martinez, J.M., 2002. The Carter adminisration and the evolution of American nuclear non--proliferation policy 1977–1981. J. Pol. Hist. 14, 3.

Maitlis, P.M., de Klerk, A., 2013. Greener Fischer-Tropsch Processes for Fuels and Feedstocks. Wiley-VCH Verlag GmbH, ISBN: 978-3-527-32945-8.

Mamantov, G., Manning, D.L., 1966. Voltammetry and related studies of uranium in molten lithium fluoride–beryllium fluoride–zirconium fluoride. Anal. Chem. 38, 1494–1498.

Martinez-Guridi, G., Mubayi, V., Bari, R.A. Approaches for addressing risks in reprocessing facilities: an assessment. Presented at the ANS PSA 2013 International Topical Meeting on Probabilistic Safety Assessment and Analysis Columbia, SC September 22–26, 2013. BNL-100883-2013-CP.

McCoy, H.E. Materials for salt-containing vessels and piping, Chap. 7, p. 195, in The Development Status of Molten-Salt Breeders, ORNL-4812 (August 1972).

McCoy, Jr., E.H. Status of materials development for molten-salt reactors, ORNL/TM-5920 (January 1978).

McNamara, B.K.,Casella, A.M., Scheele, R.D., Kozelisky, A.E. Nitrogen trifluoride-based fluoride-volatility separations process: initial studies. 2011 FCR&D-SWF-2011-000390 PNNL-20775.

McSween, H.Y., Grove, T.L., Lentz, R.C.F., Dann, J.C., Holzheid, A.H., Riciputi, L.R., et al., 2001. Geochemical evidence for magmatic water within Mars from pyroxenes in the Shergotty meteorite. Nature. 409, 487–490.

Melnikov, S.P., et al., 2015. Lasers with Nuclear Pumping. Springer, Chapter 11.

Meslin, P.-Y., Hamara, D.K., Boynton, W.V., Sabroux, J.C., Gasnault, O. Analysis of uranium and thorium lines in Mars Odyssey gamma spectra, and refined mapping of atmospheric radon. 43rd Lunar and Planetary Science Conference (2012) 2852.

Mighell, A.D., Ondik, H.M., Molino, B.B., 1977. Crystal data space-group tables. J. Phys. Chem. Ref. Data. 6 (3).

Moser, D.E. Zirconium minerals from Mars, Moon and Earth indicate crustal ‘Refugia’ on early bombardment surfaces. Workshop on Early Solar System Impact Bombardment III, February 4–5, 2015 in Houston, Texas. LPI Contribution No. 1826, 3038.

Neal-Jones, N., Steigerwald, B. Scott, J. NASA mission reveals speed of solar wind stripping martian atmosphere. MAVEN. November 5, 2015, p. 15–217.

Nelson, P.F., Flores, A., Francüois, J.L., 2007. A design-phase PSA of a nuclear-powered hydrogen plant. Nucl. Eng. Des. 237, 219.

IAEA-TECDOC-1753, 2015. New technologies for seawater desalination using nuclear energy. Vienna, Austria.

Nguyen, V.M., Doherty, P.S., Riffat, S.B., 2001. Development of a prototype low-temperature Rankine cycle electricity generation system. Appl. Therm. Eng. 21, 169–181.

Nielsen, A. (Ed.), 1995. Ammonia: Catalysis and Manufacture. Springer-Verlag. Available from: http://dx.doi.org/10.1007/978-3-642-79197-0

Noh, S., Kwak, D., Lee, J., Kang, J., Byungchan Han, B., 2014. First-principles calculations of the thermodynamic properties of transuranium elements in a molten salt medium. J. Kor. Phys. Soc. 64 (6), 806−812.

OECD and NEA, 2007. Nuclear Energy Data 2007. OECD Publishing, Paris.

Olah, G.A., Goeppert, A., Surya Prakash, G.K., 2009. Beyond Oil and Gas: The Methanol Economy. second ed Wiley-VCH Verlag.

Ostrovsky, V.G., Smolentsev, A.A., Sokolov, B.A. RSC Energia experience in development of high-power electric thrusters. *ДУК* 621/455/32.

Osychenko, O.N., Astrakharchik, G.E., Boronot, J., 2012. Ewald method for polytropic potentials in arbitrary dimensionality. Mol. Phys. 110 (4), 227−247.

Ouadi, A., Gadenne, B., Hesemann, P., Moreau, J.J.E., Billard, I., Gaillard, C., et al., 2006. Task-Specific Ionic Liquids Bearing 2-Hydroxybenzylamine Units: synthesis and Americium-extraction studies. Chem: Eur. J. 12, 3074−3081.

Parthé, E., 1964. Crystal Chemistry of Tetrahedral Structures. Gordon and Breach, London, ISBN: 978-0677-00-700-7.

Peters, G.P., Marland, G., Le Quéré, C., Boden, T., Canadell, J.G., Raupach, M.R., 2012. Rapid growth in $CO_2$ emissions after the 2008−2009 global financial crisis. Nat. Clim. Change. 2, 2−4.

U.S. Nuclear Regulatory Commission. Office of Nuclear Reactor Regulation: Final Report, NUREG-1368, 1994.

Quoining, S., et al., 2011. Performance and design optimization of a low-cost solar organic Rankine cycle for remote power generation. Solar Energy. 85, 955−966.

Rakitin, M.S., Oganov, A.R., Niu, H., Esfahani, M.M.D., Zhou, X.-F., Qian, G.-R., et al., 2015. Novel phase of beryllium fluoride at high pressure. Phys. Chem. Chem. Phys. 17, 26283−26288.

Ren, J., Li, F.-F., Lau, J., González-Urbina, L., Licht, S., 2015. One-pot synthesis of carbon nanofibers from $CO_2$. Nano. Lett. 15, 6142−6148.

Romulus, S., 2012. Is boron a prebiotic element? A mini-review of the essentiality of boron for the appearance of life on earth. Prebio. Chem. Orig. Life Evol. Bios. 42 (1), 3−17.

Rosenthal, M.W., Haubenreich, P.N., McCoy, H.,E., McNeese, L.E., 1971. Recent progress in molten salt reactor development. Atom. Energy Rev., IX. 3, 601.

Salanne, M., Simon, C., Turq, P., Madden, P.A., 2008. Calculation of activities of ions in molten salts with potential application to the pyroprocessing of nuclear waste. J. Phys. Chem. B. 112 (4), 1177−1183.

Saltarella, P., Ott, L., Yonder, G., 2004. Physical properties and correlations for the molten salt FLIBE and their implementation in the RELAP5/ATHENA thermal-hydraulics code. Oakville National Laboratory Report, Nuclear Science and Technology Division, August, 2004.

Sheen, S., 2011. Nuclear sovereignty versus nuclear security: renewing the ROK-U.S. Atomic Energy Agreement. Kor. J. Def. Anal. 23 (2), 273−288.

Souček, P., Malmbeck, R., Nourry, C., Glatz, J.-P., 2011. Asian nuclear prospects 2010 pyrochemical reprocessing of spent fuel by electrochemical techniques using solid aluminium cathodes. Energy Proc. 7, 396−404.

Sridharan, K., Anderson, M., Corradini, M., Todd Allen, T., Olson, L., Ambrosek, J., et al. Final report molten salt heat transport loop: materials corrosion and heat transfer phenomena grant No.: DE-FC07-05ID14675 Project No.: 04-154, Final Report covering Period April 1, 2005 to March 31, 2008.

Srinagar, K., Anderson, M., Corroding, M., Allen, T., Olson, L., Ambrosine, J., et al., 2008. Molten salt heat transport loop: materials corrosion and heat transfer phenomena, Final Report, Nuclear Energy Research Initiative (NERI). University of Wisconsin, Madison, WI, July 9, 2008.

IAEA-TECDOC-1524, 2007. Status of nuclear desalination in IAEA member states.

Stine, W.B., Diver, R.B., 1999. A Compendium of Solar Dish/Stirling Technology, Contract No. 67-3678. Sandia National Laboratories, Livermore, CA.

Streever, R.L., Caplan, P.J., 1973. Nuclear-magnetic-resonance studies of $Er^{167}$ in erbium iron garnet. Phys. Rev. B. 8 (7), 3138−3144.

Sun, W., Kherani, N.P., Hirschman, K.D., Gadeken, L.L., Fauchet, P.M., 2005. A three-dimensional porous silicon p-n diode for betavoltaics and photovoltaics. Adv. Mat. 17, 1230−1233.

Surapudi, Subbarao, 2011. Overview of the Space Power Conversion and Energy Storage Technologies. NASA-Jet Propulsion Laboratory, Pasadena, CA, slide 15.

Swainson, I.P., Dove, M.T., 1993. Low-frequency floppy modes in β-cristoballite. Phys. Rev. Lett. 71, 1.

The Hydrogen Economy: opportunities, costs, barriers, and R&D needs. National Research Council, National Academies Press, Washington, DC (2004). Available from <http://www.nap.edu/catalog/10922.html>.

IAEA, June 2005. The role of nuclear power and nuclear propulsion in the peaceful exploration of space.

Thoma, R.E., 1962. Cation size effects in complex fluoride compound formation. Inorg. Chem. 1 (2), .

Thoma, R.E., 1971. Chemical aspects of MSRE operation. ORNL. 4658, 94−99.

Thoma, R.E., Hebert, G.M., Insley, H., Weaver, C.N., 1963. Phase equilibria in the system NaF-$YF_3$. Inorg. Chem. 2 (5), 1005−1011.

Thoma, R.E., Insole, H., Friedman, H.A., Hebert, G.M., 1968. Equilibrium phase diagram of the lithium fluoride-beryllium fluoride zirconium fluoride system. J. Nucl. Mater. 27 (2), 166−180.

Trevorrow, L.E., Gerding, T.J., Steindler, M.J., 1968. The fluorination of neptunium(IV) fluoride and neptunium(IV) oxide. J. Inorg. Nucl. Chem. 30 (10), 2671−2677.

Triplett, B.S., Loewen, E.P., Dooies, B.J., 2012. PRISM: a competitive small modular sodium-cooled reactor. Nucl. Tech. 17 (82), 186−200.

Turner, J.A., 1999. A reliazable renewable energy future. Science. 285, 687, Special Report: Toward a Hydrogen Economy, Science 305, 957 (2004).

Uhlíř, J., Mareček, M., Přeček, M. R&D on fluoride volatility method for reprocessing of LWR and FROxide-type Fuels. Proceedings of ICAPP 2007 Nice, France, May 13−18, 2007, Paper 7253.

Uribarri, L., Choueiri, E.Y., 2009. Creation of onset voltage hash by anode spots in a magnetoplasmadynamic thruster. J. Propul. Power. 25 (4), 949−957.

US Department of Energy, Office of Basic Energy Sciences, 2004. Basic Research Needs for the Hydrogen Economy. US DOE, Washington, DC. Available at: <http://www.sc.doe.gov/bes/hydrogen.pdf>.

Van Dyke, M et al., 2001. The Safe Affordable Fission Engine (SAFE) test series. NASA/JPL/MSFC/UAH 12th annual advanced space propulsion workshop.

Viana, M., Jouannin, P., Pontier, C., Chulia, D., 2002. About pycnometric density measurements. Talanta. 57, 583−593.

Všianska, M., Šob, M., 2011. The Effect of S-P Impurities, Grain Boundary and Surface Structure, Magnetism and Embrittlement in Nickel. Prog. Mat. Sci. 56, 817−840.

Wangab, S., Chaohui He, C., 2015. Subcritical space nuclear system without most movable control systems. J. Nucl. Sci. Tech. 52 (12), .

Wells, A.F., 1948. Structural Inorganic Chemistry, vol. 110. Oxford University Press, London.

Werner, J.D. Section research manager. U.S. Spent Nuclear Fuel Storage May 24, 2012. Congressional Research Service 7-5700 R42513.

West, A., 1984. Solid State Chemistry and its Applications. 2nd ed. Wiley and Sons.

Westfall, C., 2004. Vision and reality: the EBR-II story. Nuclear News25−32.

Weidemann, C., Oswald, M., Stabroth, S., Klinkrad, H., Vörsmann, P., 2005. Size Distribution of NaK Droplets Released During RORSAT Reactor Core Ejection. Adv. Space Res. 35, 1290−1295.

Williams, D.F. Assessment of candidate molten salt coolants for the NGNP/NHI heat-transfer loop ORNL/TM-2006/69 June 2006.

Williams, D.R. Preliminary Mars Pathfinder APXS results: elemental composition of rocks and soil, NSSDCA, NASA Goddard Space Flight Center. 1997 Report.

Wolverton, M., 2008. Stirling in deep space: to cut back on radioisotope fuel, NASA goes back 200 year. Sci. Am. 298, 22.

Yakubov, G., 2010. Nuclear Batteries with Tritium and Promethium-147 Radioactive Sources. Doctoral Thesis, University of Illinois at Urbana, Champaign.

Yalcuücin, S., 1989. A review of nuclear hydrogen production. Int. J. Hydrogen Energy. 14 (8), 551.

Yang, M.S., 2012. Korean Strategy for Sustainable Nuclear Energy Development. Korean Atomic Energy Research Institute.

Yin, X., Moss, J.R., 1999. Recent developments in the activation of carbon dioxide by metal complexes. Coord. Chem. Rev. 181, 27−59.

Yvon, P., Carré, F., 2009. Structural materials challenges for advanced reactor systems. J. Nucl. Mater. 385, 217−222.

Ẑemva, B., Slivnik, J., Andrej Ŝmalc, A., 1975. Krypton difluoride - vanadium pentafluoride adduct. J. Fluor. Chem. 6 (2), 191−193.

Zhou, Y., Tol, R.S.J., 2006. E172 Bouzgiemda, N., Nisan, S., Albouy, M. Financing of Nuclear Desalination Projects in Developing Countries, EUROMED 2006 Conference, Montpellier, France.

## Further Reading

Engel, J.R., Bauman, H.F., Dearing, J.F., Grimes, W.R., McCoy, E.H., Rhoades, W.A. Conceptual design characteristics of a denatured molten-salt reactor with once-through fueling. ORNL/TM-7207, July 1980.

Figure 29: Information compiled from IDA, IDA Worldwide Desalting Plant Inventory, No. 19 in MS Excel format, Media Analytics Ltd., Oxford, UK, 2006. Graphic of compilation appearing in: Lattemann, S., Höpner, T. Environmental impact and impact assessment of seawater desalination *Desalination* 220 (2008) 1−15. *Presented at the conference on Desalination and the Environment. Sponsored by the European Desalination Society and Center for Research and Technology Hellas (CERTH), Sani Resort, Halkidiki, Greece, April 22−25, 2007.* © 2006 Elsevier B.V. All rights reserved. Second version (colorized) appearing © 2009 Sabine Lattemann, Thomas Höpner, T. Third version: Lattermann, S. Development of an Environmental Impact assessment and

decision-support system for seawater desalination plants. Ph.D. dissertation. Delft University of Technology and of The Academic Board of the UNESCO-IHE Institute for Water Education. 9 February, 2010.

http://www.eia.gov/forecasts/ieo/index.cfm >

Gates, V.L., Atassi, B., Lewandowski, R.J., Ryu, R.K., Sato, K.F., Nemcek, A.A., Omary, R., Salem, R., 2007. Radioembolization with Y-90 Microspheres: Review of an Emerging Treatment for Liver Tumors. Fut. Onc. 3 (1), 73−81.

Mayorshin, A., Advances in reprocessing of spent fuel: partitioning. SSC RIAR, Russia. 004. General Conference-48, Nuclear Fuel Cycle Issues and Challenges. 48th Regular Session of the IAEA Generatl Conference. Sept. 21−22, 2004, Conference Room C.

Miguirditchian, M., Chareyre, L., Heres, X., Hill, C., Baron, P., Masson, M. GANEX: adaptation of the DIAMEX-SANEX process for the group actinide separation. Advanced nuclear fuel cycles and systems (GLOBAL 2007), Boise—Idaho, United States, September 9−13, 2007.

Nilssona, M., Nash, K.L., 2007. Review article: a review of the development and operational characteristics of the TALSPEAK process. Solvent Extr. Ion Exch. 25 (6), 665−701.

Ravichandran, R., Binukumar, J.P., Al Saadi, A., 2010. Estimation of effective half life of clearance of radioactive Iodine ($^{131}$I) in patients treated for hyperthyroidism and carcinoma thyroid. Indian J. Nucl. Med. 25 (2), 49−52.

Rostaing, C., Poinssot, C., Warin, D., Baron, P., Lorraina, B., 2012. Development and validation of the EXAm separation process for single Am recycling. Proc. Chem. 7, 367−373.

Salem, L., 1968. Intermolecular Orbital Theory of the Interaction between Conjugated Systems I. General Theory. J. Am. Chem. Soc. 90, 543, 553.

Smith, E.L., Abbott, A.P., Ryder, K.S., 2014. Deep Eutectic Solvents (DESs) and their applications. Chem. Rev. 114 (21), 11060−11082.

Welton, T., 1999. Room-temperature ionic liquids. Solvents for synthesis and catalysis. Chem. Rev. 99 (8), 2071−2084.

Woodrow, C., Isherwood, W., 2004. Distributed generation: remote power systems with advanced storage technologies. Energy Pol. 32, 1573−1589.

# Reactor physics of MSR

# 4

*Yoichiro Shimazu*
University of Fukui, Fukui, Japan

## Chapter Outline

## 4.1 Introduction

Reactor physics provides important information, such as power distribution, effective multiplication, and fuel composition changes with burnup. This chapter covers interaction of neutrons with matter, nuclear fission, multiplication factor, neutron spectrum, reaction rates, transport and diffusion equations of neutrons, criticality equation, and kinetic equations.

## 4.2 Interaction of neutrons with matter

Reactions of neutrons with nuclei are broadly classified into two classes, scattering and capture. In scattering reactions, the final result is merely an exchange of energy between the two colliding particles, and a neutron remains free after interaction. On the other hand, in capture reactions, the neutron is retained by the

**Molten Salt Reactors and Thorium Energy. DOI: http://dx.doi.org/10.1016/B978-0-08-101126-3.00004-X**

nucleus, forming a different isotope. There are four main kinds of neutron capture reactions:

1. The emission of gamma radiation $(n, \gamma)$;
2. The ejection of an alpha particle $(n, \alpha)$;
3. The ejection of a proton $(n, p)$; or
4. Fission $(n, f)$.

The radiative capture reaction is the most common, and it occurs with a wide variety of elements.

When a neutron is absorbed into a nucleus, the kinetic energy and the binding energy of the neutron are transferred to the compound nucleus, which will be left in an excited energy state. Part of the energy may be transferred to a neutron, which may be emitted from the nucleus, leaving the nucleus in a less excited energy state. This process is called "inelastic scattering" since part of the energy is left as internal energy of the nucleus.

Another possibility is that a neutron is scattered by a nucleus without changing nuclear internal energy, which is called "elastic scattering." The energy of the incoming neutron is distributed between the scattered neutron and the recoil nucleus. It is a classic hard-sphere collision with conservation of kinetic energy and momentum. Inelastic scattering can only occur for high-energy neutrons, while elastic scattering can occur for all neutron energies. The neutron collisions are summarized below:

$$\left.\begin{array}{l}\left.\begin{array}{l}\text{Fission [(n,f) reaction]}\\ \text{Capture [(n, gamma ray) reaction]}\end{array}\right\}\text{Absorption}\\ \text{(n,p) and (n, alpha) reactions}\\ \left.\begin{array}{l}\text{Elastic scattering [(n,n) reaction]}\\ \text{Inelastic scattering [(n,n') reaction]}\end{array}\right\}\text{Scattering}\\ \text{(n,2n) reaction}\end{array}\right\}\text{Collision}$$

## 4.2.1 Several processes can produce neutrons

1. Neutrons are easily obtained by reaction of alpha particles with some light elements, e.g., beryllium, boron, or lithium. The alpha-particle emitters may be polomium-210, radium-226, plutonium-239, or americium-241. These emitters emit alpha-particles according to their own decay constants. The energy of neutrons released in the (alpha, *n*) reaction ranges from about 1 to 10 MeV.
2. The reaction of gamma rays of energy about 2 MeV on the nuclei of deuterium or beryllium yields essentially mono energetic neutrons.
3. Some artificially produced heavy nuclides undergo spontaneous fission, emitting neutrons at an appreciable rate. Californium-252 decays with a half-life of 2.63 years and 3.1% of decays are spontaneous fissions.
4. Accelerated ion beams, such as protons or deuterons, bombarding targets such as tritiated titanium, lithium, or beryllium can yield $(p,n)$ and $(d,n)$ reactions. For example, the International Fusion Materials Irradiation Facility will use 40 MeV deuteron beams with a flowing lithium target.
5. High-energy accelerators ($\sim$1 GeV) striking a heavy metal target, such as Pb, can produce copious neutrons.
6. Fission reactions usually emit several neutrons.

## 4.3 Multiplication factor of chain reactions

When fissile nuclei, such as U 233, U-235, and Pu-239, absorb a neutron, the excited compound nucleus breaks up into two fission products and releases several high-energy ($\sim 1$ MeV) neutrons. When one of these neutrons is absorbed in another fissile nucleus, a chain reaction may begin.

In a hypothetical system of infinite size, neutrons do not leak out of the system. They are produced by fission and are removed only by absorption in the materials. The infinite multiplication factor is defined as

$$k_\infty = \frac{\text{Neutrons produced in one generation}}{\text{Neutrons absorbed in the preceding generation}} = \frac{\text{Rate of neutron production}}{\text{Rate of neutron absorption}} \tag{4.1}$$

The condition of criticality for stable self-sustaining fission chain reaction is that $k_\infty = 1$, in an infinite system without external neutron source.

In a system of finite size, some neutrons leak out of the system. The criticality condition must take into account the neutron leakage. The effective multiplication factor is given by

$$k_{\text{eff}} = \frac{\text{Rate of neutron production}}{\text{Rate of neutron absorption} + \text{neutron leakage}} \tag{4.2}$$

The requirement for criticality in a finite system without external neutron source is that $k_{\text{eff}} = 1$.

If $k_{\text{eff}} < 1$ then the system is subcritical. In such a case the population of neutrons will steadily decrease. In the presence of an external neutron source, however, a steady state can be maintained by the source. When $k_{\text{eff}} > 1$, the system is supercritical. In such a case the neutron production is larger than neutron loss, thus the population of neutrons will tend to increase exponentially with time. This increase could cause a nuclear explosion, or it could be limited by use of materials that absorb neutrons more strongly as they heat up, such as zirconium (or uranium-238).

## 4.4 Cross-sections

The microscopic cross-section, $\sigma$, for a particular reaction applies to a single nucleus. If the target material contains $N$ nuclei per a unit volume, the quantity $N\sigma$ is called the "macroscopic cross-section $\Sigma$" of the material:

$\Sigma = N\sigma \cdots (\text{m}^{-1})$,

For a mixture of elements or compounds containing several species the macroscopic cross-section is

$$\Sigma = N_1\sigma_1 + N_2\sigma_2 + \ \ldots \ + N_i\sigma_i + \ \ldots$$

where the values of $N_1$, $N_2$, etc., are dependent upon the composition of the mixture, the atomic weights, and densities of the constituents.

## 4.5 Reaction rate

Consider a mono-energetic neutron beam in which $n$ is the neutron density, i.e., the number of neutrons/m$^3$. If $v$ is the neutron speed, then $nv$ is the number of neutrons falling on 1 m$^2$ of target material per second. The product $\Sigma nv$ gives the number of interactions (between neutrons and nuclei) per m$^3$ of target material per second; thus,

$$\text{Reaction rate} = \Sigma nv \quad \text{interactions m}^{-3}\text{s}^{-1}$$

This expression gives the number of neutron interactions per second in 1 m$^3$ of material. The neutron flux is defined as the product of the neutron density and velocity:

$$\phi = nv \quad \text{neutrons m}^{-2}\text{s}^{-1}$$

and

$$\text{Reaction rate} = \Sigma\phi \quad \text{interactions m}^{-3}\text{s}^{-1}$$

The microscopic and macroscopic cross-sections are distinguished by adding a subscript for each reaction. For example, $\sigma_a$ for absorption, $\sigma_f$ for fission, $\sigma_s$ for scattering, and $\sigma_t$ for total cross-section.

## 4.6 Neutron energy distribution and maxwell–bolzmann distribution

The fission neutron energy distribution is shown in Fig. 4.1.

The average neutron energy is about 2 MeV, corresponding to a neutron speed of about 20,000 km/s. The fission probability increases at lower neutron energy, as shown in Fig. 4.2.

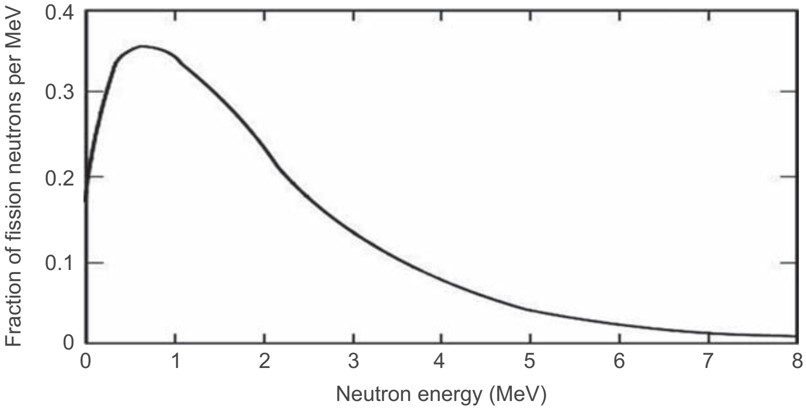

**Figure 4.1** Fission neutron energy spectrum for thermal fission of uranium-235 (Sekimoto, 2007).

Since the fission cross-section increases at low energies, most nuclear reactors use a moderator material to slow down the fission neutrons. The best moderators are light elements like hydrogen and carbon, because the recoil nucleus can absorb a large fraction of the neutron energy with each elastic collision. When the neutron energy is comparable to energies of the surrounding atoms, the neutron is called "thermalized." Reactors using mainly fission by thermal neutrons are called "thermal reactors." Nuclear reactors which use mainly fissions induced by fast neutrons are called "fast reactors." The difference is the energy distribution of neutrons in the reactor, as shown in Fig. 4.3.

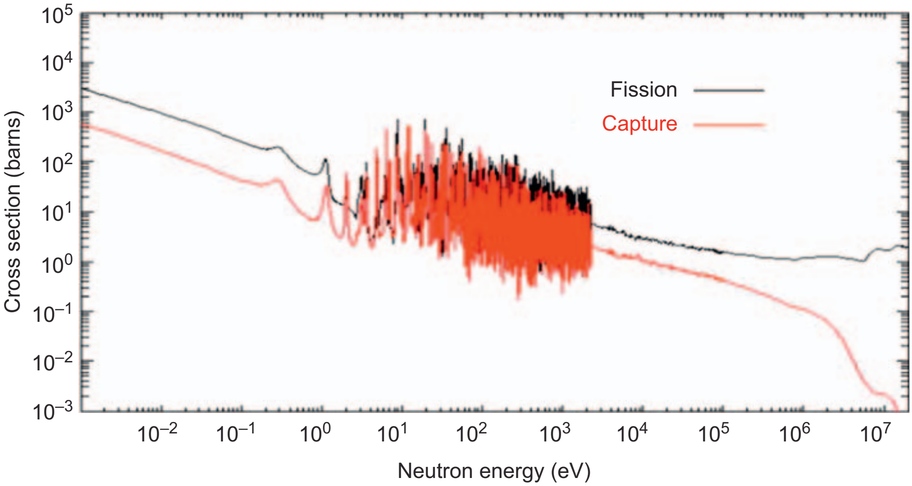

**Figure 4.2** Fission and capture cross-sections for $^{235}$U (Sekimoto, 2007).

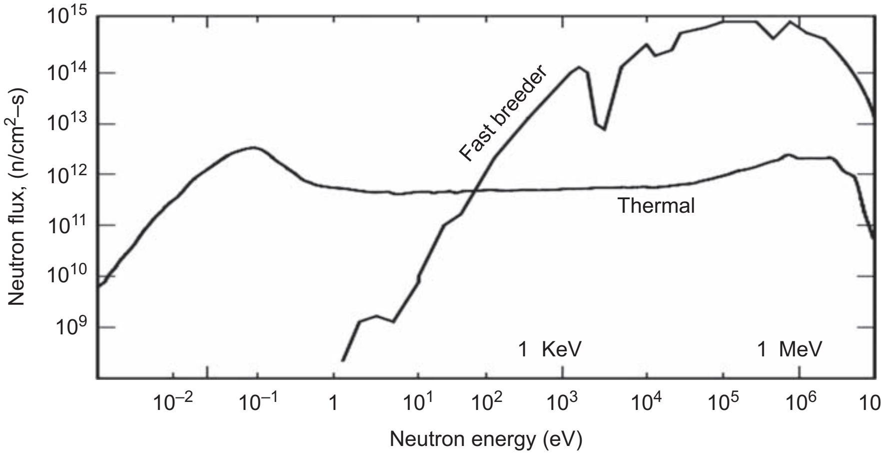

**Figure 4.3** Comparison of neutron flux spectra for thermal and fast reactors (DOE-HDBK-1019/1-93,1993).

If neutrons are introduced into an infinite, nonabsorbing scattering medium, from which neutrons are neither lost by escape nor by absorption, a state of thermal equilibrium will be attained. In this state, the probabilities are equal that a neutron will gain or lose energy in a collision with a scattering nucleus. The kinetic energies of the neutrons would then be represented by a “Maxwellian” distribution, characterized by the medium temperature.

## 4.7 Transport and diffusion of neutrons

Fission reactions generate heat, which must be removed by a coolant. The fission reaction rate depends on the neutron flux distribution, which can be calculated from the neutron transport equation (Boltzmann equation):

$$\begin{aligned}&\frac{1}{v}\frac{\partial}{\partial t}\Psi\big(\underline{r},E,\Omega,t\big)+\Sigma_t\big(\underline{r},E\big)\Psi\big(\underline{r},E,\Omega,t\big)+\Omega\cdot\nabla\Psi\big(\underline{r},E,\Omega,t\big)\\&\quad=\int_0^{\infty}dE'\int_0^{4\pi}d\Omega'\Sigma_s\big(\underline{r},E'\to E,\Omega'\cdot\Omega\big)\Psi\big(\underline{r},E',\Omega',\mathrm{t}\big)\\&+\frac{\chi(E)}{4\pi}\left(\int_0^{\infty}dE'\upsilon(E')\Sigma_f(\underline{r},E')\Phi(\underline{r},E',t)\right)+\frac{1}{4\pi}Q_{\mathrm{ext}}(\underline{r},E,t)\end{aligned}\tag{4.3}$$

where $\Psi(\underline{r},E,\Omega,t)$ Angular flux of neutrons at position $\underline{r}$ with energy $E$ moving in direction $\Omega$ at time $t$; $\Psi(\underline{r},E',\Omega',t)$ Angular flux of neutrons at position $\underline{r}$ with energy $E$’ moving in direction $\Omega'$ at time $t$; $\phi(\underline{r},E',t)$ Scalar flux at position $\underline{r}$ and neutron energy $E$’ at time $t$ defined as $\int_0^{4\pi} d\Omega\Psi\big(\underline{r},E',\Omega,t\big)$; $\Sigma_t\big(\underline{r},E\big)$ Total macroscopic cross-section for all interactions of energy $E$ at $\underline{r}$; $\Sigma_f\big(\underline{r},E\big)$ Macroscopic fission cross-section; $\Sigma_{\mathrm{s}}\big(\underline{r},E'\to E,\Omega'\cdot\Omega\big)$ Scattering macroscopic cross-section with neutrons of energy $E$’ moving in the direction $\Omega'$ to neutrons of energy $E$ and into the direction $\Omega$ at position $\underline{r}$; $Q(\underline{r},E,t)$ Isotropic neutron source at $\underline{r}$ of neutrons of energy $E$ at time $t$; $\chi(E)$ Fission neutron energy spectrum.

- The first term is the neutron density change rate.
- The second term is neutron loss due to all collisons.
- The third term is neutrons flowing out of the volume element.
- The fourth term is neutrons scattered into the volume element.
- The fifth term is neutrons generated by fission.
- The last term is neutrons from a neutron source.

All terms are defined at the position $r$, energy $E$, moving in direction $\Omega$ at time $t$, per unit volume per second.

The second and the third terms of the left hand side of the equation are neutrons lost and the right hand side is the neutron generation.

It is a differential/integral equation of neutron flux with seven independent variables (three spatial, two angular, energy, and time). It cannot be solved analytically except for very simplified cases. It is helpful to use discrete values of neutron flux, position, energy, angles, and time. Then the time-dependent problem reduces to a steady-state problem within each time step.

### 4.7.1 Energy discretization

The neutrons in a reactor have energy range from about 10 MeV down to less than 0.01 eV. The energy variable is handled by the *multigroup method*. The energy range of interest is divided in to G "groups" as shown in Fig. 4.4, where cross-sections are averaged in each energy group.

Group fluxes, group sources, and group fission spectra are also averaged in each energy group. We assume that the neutron flux may be represented by a product of angular flux and a function of energy *f(E)*.

$$\Psi\left(\underline{r}, E, \Omega\right) = \varphi\left(\underline{r}, \Omega\right) f(E), \tag{4.4}$$

where $f(E)$ is neutron energy spectrum $f(E)$.

Group cross-sections are defined as the average values for each energy group.

Using these discretizations and averages, a multigroup transport equation is obtained.

Multigroup transport equations are accurate under the following conditions:

1. Angular flux is separable with known spectrum $f(E)$
2. Cross-sections are constant within each energy interval.
3. Small intervals of energy, angle, space, and time are used

The unknowns in the multigroup transport equation are the group fluxes. Here, for simplicity, we consider a steady-state case (the time derivative term is omitted):

$$\begin{aligned}\Omega \cdot \nabla\Psi_g\left(\underline{r}, \Omega\right) + \Sigma_{t,g}\left(\underline{r}\right)\Psi\left(\underline{r}, \Omega\right) = \sum_{g'=1}^{G} \int_0^{4\pi} d\Omega' \Sigma_{s,g' \to g}(\underline{r}, \Omega' \to \Omega)\Psi_{g'}(\underline{r}, \Omega') \\ + \frac{\chi_g}{4\pi} \sum_{g'=1}^{G} \upsilon\Sigma_{f,g'}\left(\underline{r}\right)\Phi_{g'}\left(\underline{r}\right) + S_g(\underline{r}, \Omega)\end{aligned} \tag{4.5}$$

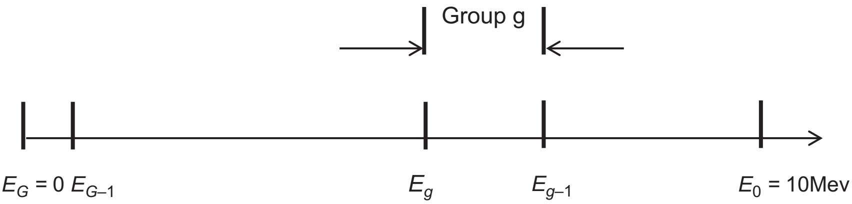

**Figure 4.4** Energy groups $E_g$.

This equation still has variables of position and angle. The angular flux may be expanded by spherical harmonics (PN method) or segmented in fixed angles (discrete-ordinate method or SN method).

### 4.7.2 One energy group approximation

We further approximate the above equation assuming monoenergetic neutrons. Then the equation becomes

$$\Omega\cdot\nabla\Psi(\underline{r},\Omega)+\Sigma_t(\underline{r})\Psi(\underline{r},\Omega)=\int_0^{4\pi}d\Omega'\Sigma_s(\underline{r},\Omega'\to\Omega)\Psi(\underline{r},\Omega')+\frac{1}{4\pi}\upsilon\Sigma_f(\underline{r})\phi(\underline{r})+S(\underline{r},\Omega) \tag{4.6}$$

In spherical harmonic expansion with only the initial two terms used, the flux is expressed as follows.

$$\phi(\underline{r},\Omega)=\frac{1}{4\pi}(\phi(\underline{r})+3\Omega\cdot J(\underline{r})) \tag{4.7}$$

where $\phi(\underline{r})$ : Total flux; $J(\underline{r})$ : Net current

Substituting this to the above equation, and with a tedious manipulation of equations, the following equations are obtained.

$$\begin{aligned}&\nabla\cdot J(\underline{r})+\Sigma_a(\underline{r})\phi(\underline{r})=S(\underline{r})\\&\frac{\nabla\phi(\underline{r})}{3}+\Sigma_{tr}(\underline{r})\,J(\underline{r})=S_1(\underline{r}),\end{aligned} \tag{4.8}$$

where $S_0(\underline{r})$: Isotorpic neutron source; $S_1(\underline{r})$: Anisotorpic neutron source

Assuming no anisotropic source, that is $S_1=0$, then

$$J(\underline{r})=-\frac{1}{3\Sigma_{tr}(\underline{r})}\nabla\phi(\underline{r}) \tag{4.9}$$

$\Sigma_a(r)=\Sigma_t(r)-\Sigma_s(r)$, $\Sigma_{tr}(r)=\Sigma_t(r)-\mu\Sigma_s(r)$, $\mu$ is average scattering angle cosine

This is called Fick's law, and it relates the neutron current to the neutron flux. Fick's law is used in many fields of physics, such as diffusion of atoms in gases and solids. The neutrons diffuse from high to low concentrations, and the diffiusion rate is proportional to the concentration gradient.

Fick's law is not accurate in regions such as

- Near a neutron source;
- Near a strong absorber of neutrons;
- At a reactor surface;
- In a zone where strong anisotropy exists.

In these cases, a full transport calculation is required. With these limitations in mind, neutron behavior can be approximated by the following diffusion equation.

$$-\nabla \cdot D(\underline{r})\nabla\phi(\underline{r}) + \Sigma_a(\underline{r})\phi(\underline{r}) = S, \tag{4.10}$$

where

$$D(\underline{r}) = \frac{1}{3\Sigma_{tr}(\underline{r})} \tag{4.11}$$

### 4.7.3 Calculation of nuclear group constants

Reactor physics calculations require nuclear group constants of both microscopic and macroscopic cross-sections. They are calculated thorough numerical programs using evaluated nuclear cross-section data libraries such as ENDF/B by USA, JEFF by NEA, or JENDL by Japan. Normally the calculations are done in two steps. In the first step, it is the cell or lattice calculation which provides a few-group constants library. These few-group constants include few-group micro- and macroscopic cross-sections and other information required for core calculations. Secondly, coupled neutron diffusion and thermal-hydraulics are usually carried out for a single- or quarter-assembly homogenized configuration for specially homogenized and energy group condensed few-group constants for whole core calculations.

### 4.7.4 Fuel burnup calculations

Fuel burnup calculations can be done to estimate composition changes with fuel burnup. In this calculation many reactions are taken into account, including radiation decay chains of all fuel components and fission products. These data are used to evaluate inventories of fuel and fission products with burnup.

## 4.8 Criticality equation

"Critical" means that $k_{\text{eff}} = 1$. Here we consider a simplified case with monoenergetic neutrons using the diffusion approximation for a homogeneous infinite slab with finite thickness. Homogeneous means that all the parameters are the same everywhere in the medium. The thickness $= a$ in the $x$ direction, but it is infinitely large in the $y$ and $z$ directions. The number of neutrons lost per unit volume per second is balanced by the production by nuclear fission as follows.

From the definition of $k_{\text{eff}}$ (Eq. (4.2)):

$$\begin{aligned}
\mathrm{k}_{\text{eff}} &= (\text{neutron source rate})/(\text{loss rate by scattering} + \text{loss rate by absorption}) \\
&= \left(\nu\sum\nolimits_{\mathrm{f}}\phi\right)\Big/\left(D\nabla^2\phi - \sum\nolimits_a\phi\right), \text{ or} \\
D\nabla^2\phi &- \Sigma_a\phi + \frac{\nu\Sigma_f}{k_{\text{eff}}}\phi = 0.
\end{aligned} \tag{4.12}$$

We define a diffusion length $L^2 = D/\Sigma_a$. Then,

$$\nabla^2\phi - \frac{1}{L^2}\phi + \frac{\nu\Sigma_f}{k_{\text{eff}}\Sigma_a}\phi = 0 \tag{4.13}$$

The last term can be rewritten by using infinite multiplication factor $k_\infty$ according to the definition as

$$\frac{\nu\Sigma_f}{\Sigma_a} = k_\infty,$$

where $k_\infty > 1.0$; otherwise no criticality is attainable.

Using these parameters the original equation is written as

$$\nabla^2\phi - \frac{1}{L^2}\left(1 - \frac{k_\infty}{k_{\text{eff}}}\right)\phi = 0 \tag{4.14}$$

Further it can be rewritten as

$$\nabla^2\phi + B^2\phi = 0, \text{ where } B^2 = \frac{1}{L^2}\left(\frac{k_\infty}{k_{\text{eff}}} - 1\right) \text{ and } B^2 > 0 \tag{4.15}$$

The solution of this equation is well known as

$$\phi(x) = A\sin(Bx) + C\cos(Bx) \tag{4.16}$$

As the original diffusion equation is a second-order differential equation, we need two boundary conditions to determine the constants, $A$ and $C$. We set the origin of the coordinate at the center of the slab reactor. The neutron flux must be real and positive in the reactor. One boundary condition is that the flux must be zero at the outer boundary. The other is that the flux distribution must be symmetric around the center plane of the reactor. Because of the second boundary condition the constant $A$ must be zero. Then the first boundary condition requires that

$$\phi\left(\pm\frac{a}{2}\right) = 0.$$

We assume the thickness of the reactor is $a$. Therefore,

$$\frac{B}{2}a = (2n+1)\frac{\pi}{2}. \tag{4.17}$$

Thus the general solution for the flux will be given as

$$\phi(x) = \sum_i A_i \cos\left((2n+1)\frac{\pi}{2}x\right) > 0. \tag{4.18}$$

However as the vibration of a string, the higher modes die out quickly and only the fundamental mode remains. Thus the final solution for the flux distribution is determined as

$$\phi(x) = C\cos\left(\frac{\pi}{a}x\right) \tag{4.19}$$

The remaining constant $C$ is determined from other conditions, such as power level.

As discussed above, the solution only exists when all of the boundary conditions are satisfied. In other words, the following condition must be satisfied.

$B = (\pi/a)$. This is called critical equation for an infinite slab of thickness $a$.

As

$$B^2 = \frac{1}{L^2}\left(\frac{k_\infty}{k_{\text{eff}}} - 1\right) \tag{4.20}$$

thus

$$k_{\text{eff}} = \frac{k_\infty}{1 + L^2B^2} \tag{4.21}$$

In the previous section, it is explained that $k_{\text{eff}} = k_\infty\ P_{\text{NL}}$.

Thus the nonleakage probability of infinite slab is given as

$$P_{\text{NL}} = \frac{1}{1 + L^2B^2},\ \text{and} \tag{4.22}$$

$$B^2 = \left(\frac{\pi}{a}\right)^2. \tag{4.23}$$

This is called geometrical buckling.

When the composition of a reactor is given, values of parameters of $k_\infty$ and $L^2$ are known. The required criticality condition is to satisfy the above condition, which means that the size or the thickness of the infinite slab reactor must be given as follows.

Since the reactor is critical, $k_{\text{eff}} = 1$, thus

$$1 + L^2B^2 = k_\infty \tag{4.24}$$

Thus,

$$B^2 = \frac{k_\infty - 1}{L^2}. \tag{4.25}$$

This is called material buckling. Generally speaking, the critical condition means that geometrical buckling and material buckling are identical.

Thus,

$$a = \pi L\sqrt{\frac{1}{k_\infty - 1}} \tag{4.26}$$

Geometrical buckling for the different geometry reactors are given as follows.

$$\text{Sphere;} \quad B^2 = \left(\frac{\pi}{R}\right) \tag{4.27}$$

$$\text{Cylinder;} \quad B^2 = \left(\frac{\pi}{H}\right)^2 + \left(\frac{2.405}{R}\right)^2 \tag{4.28}$$

$$\text{Rectangle;} \quad B^2 = \left(\frac{\pi}{a}\right)^2 + \left(\frac{\pi}{b}\right)^2 + \left(\frac{\pi}{c}\right)^2 \tag{4.29}$$

The sizes include extrapolation distance, which is as a correction to the diffusion approximation. In this section, such detailed discussion is neglected. Also neglected is the discussion of multiregion reactor, in which the boundary conditions are continuity of neutron flux and current at the boundary.

These analytical solutions can be obtained only for simple geometry and homogeneous media. In the actual situations, a reactor has three dimensions and the compositions are not homogeneous. In such cases, the solutions can be obtained only by numerical analysis. The solution methods are outside the scope of this chapter.

MSRs are operated on circulating liquid fuel. Thus, the fuel compositions are homogeneous in the reactor. The power distribution can be approximately expressed as Cosine and Bessel function for axial and radial distributions, respectively.

## 4.9 Kinetic equations

When a reactor is critical the reactor power stays constant. However, in order to change reactor power it is required to change effective multiplication of the reactor. When the effective multiplication factor is changed, how will the reactor power change? In order to answer this question, we need to know or solve reactor kinetic equations. Thus, in this section, a brief explanation of the derivation of the reactor kinetic equations is given, based on the diffusion equation of one energy group approximation model. Note that the following discussion assumes no fuel flow. Reactors with fuel flow are discussed in Chapter 5 of MSR kinetics and dynamics.

A subcritical reactor is not in a steady state without a neutron source in the system. In the diffusion approximation, Eq. (4.3) may reduced to the form

$$D\nabla^2\phi - \sum\nolimits_a \phi + S = \frac{dh}{dt} \tag{4.30}$$

In this equation, $S$ indicates neutron source, which is expressed as

$$S = k_\infty \Sigma_a \phi(1-\beta) + \lambda C \tag{4.31}$$

The first term indicates the prompt-neutron contribution and the second term indicates delayed neutron contribution. In the nuclear fission process, some neutrons are produced from fission products with some time delay. Usually they are classified into six groups but in our simplified discussion, they are treated as one group. Let $\beta$ present the fraction of fission neutrons which are delayed; then $(1-\beta)$ is the prompt-neutron fraction. The delayed neutrons are produced by radioactive decay of the precursors and expressed as $\lambda C$, where $\lambda$ is effective decay constant and $C$ represents the atomic density of the precursors.

Substituting the neutron source term into the Eq. (4.30),

$$D\nabla^2\phi - \Sigma_a\phi + k_\infty \Sigma_a \phi(1-\beta) + \lambda C = \frac{dn}{dt} \tag{4.32}$$

In this expression, neutron flux and precursor are both functions of time and space in a finite reactor. It will be assumed that the variables are separable, so the spatial distribution $\nabla^2\phi$ can be replaced by $-B^2\phi$, where $B^2$ is the geometrical buckling. This separation of variables leads to what is called the "point-reactor" model. Recalling that $\phi = nv$ and $D/\Sigma_a = L^2$,

$$\begin{aligned} &v\Sigma_a\left(-\tfrac{DB^2}{\Sigma_a} - 1 + k_\infty(1-\beta)\right)n + \lambda C \\ &= v\Sigma_a(-L^2B^2 - 1 + k_\infty(1-\beta))n + \lambda C \\ &= v\Sigma_a(1+L^2B^2)\left[\frac{k_\infty(1-\beta)}{1+L^2B^2} - 1\right] + \lambda C = \frac{dn}{dt} \end{aligned} \tag{4.33}$$

This equation can be simplified by introducing the following parameters.

$$\ell = \frac{1}{v\Sigma_a(1 + L^2B^2)} \tag{4.34}$$

This $\ell$ is called the finite medium prompt-neutron lifetime. Because the average distance that neutrons run without leaking from the medium is expressed as

$$x_{\mathrm{avg}} = \frac{1}{\Sigma_a(1 + L^2B^2)}, \tag{4.35}$$

thus the lifetime is obtained by dividing the distance by the neutron speed $v$.

Substituting the following relation,

$$k_{\mathrm{eff}} = \frac{k_\infty}{1 + L^2B^2} \tag{4.36}$$

finally, the following expression is obtained

$$\frac{k_{\mathrm{eff}}(1-\beta) - 1}{\ell} n + \lambda C = \frac{dn}{dt}$$

or

$$\frac{1 - \beta - 1/k_{\mathrm{eff}}}{\ell/k_{\mathrm{eff}}} n + \lambda C = \frac{(1 - 1/k_{\mathrm{eff}}) - \beta}{\ell/k_{\mathrm{eff}}} n + \lambda C = \frac{\rho - \beta}{\ell/k_{\mathrm{eff}}} n + \lambda C = \frac{dn}{dt} \tag{4.37}$$

where $\rho = (k_{\mathrm{eff}} - 1)/k_{\mathrm{eff}} \approx 1 - k_{\mathrm{eff}}$. The growth of precursors is estimated from

$$\frac{dC}{dt} = \beta k_\infty \Sigma_a \phi - \lambda C \tag{4.38}$$

Using the relation of

$$k_\infty v \Sigma_a = \frac{k_{\mathrm{eff}}}{\ell} \tag{4.39}$$

The following expression is obtained

$$\frac{dC}{dt} = k_{\mathrm{eff}} \frac{\beta}{\ell} n - \lambda C \tag{4.40}$$

These equations are further simplified by defining neutron generation time as

$$\Lambda = \frac{\ell}{k_{\mathrm{eff}}}. \tag{4.41}$$

Then, the final kinetic equations are expressed as

$$\begin{aligned} \frac{dn}{dt} &= \frac{\rho - \beta}{\Lambda} n + \lambda C \\ \frac{dC}{dt} &= \frac{\beta}{\Lambda} n - \lambda C \end{aligned} \quad . \tag{4.42}$$

In practice, neutron generation time and the prompt-neutron lifetime are almost identical because the $k_{\mathrm{eff}}$ is close to unity.

The discrete ordinates transport theory can be accurate for simple geometries, such as slabs and cylinders, but it is not practical to use it for complex geometrical shapes. For complicated geometries it is better to use the Monte Carlo method.

## 4.10 Monte Carlo method

The Monte Carlo method simulates a large number of individual particle trajectories, and then averages the results to determine the desired quantities, such as energy deposition. We will consider neutrons, keeping in mind that the technique applies also to gamma rays. To simulate a given neutron's history, a series of questions are posed, and the answer to each question is decided statistically. For example, if only two choices were available, and if they had equal probability, we could flip a coin to decide. In practice many choices are available, and they have probabilities determined by factors such as nuclear scattering cross-sections. Instead of flipping a coin, a random number generator is used. The random number generator is a computer algorithm (procedure) to generate decimal fractions randomly and uniformly between 0 and 1.

The random number is compared with the probability of an event to decide whether or not it occurs. For example, if the probability of an event were 0.300, we could decide that the event will occur if the random number is less than 0.300, and that it will not occur if the random number is greater than 0.300. A flow chart for Monte Carlo neutron simulations is shown in Fig. 4.5.

The neutron interactions are tallied (recorded) until it is absorbed or lost. Tracking thousands of neutron histories and averaging the results can provide accurate estimates of fission power, shielding, transmutations, and other phenomena. If the goal is to evaluate a result that has low probability, such as penetrating a thick shield, then large numbers of histories ($>10^5$) may be required to achieve high accuracy, but "variance reduction techniques" may be used to reduce the required number (Dolan, 1982).

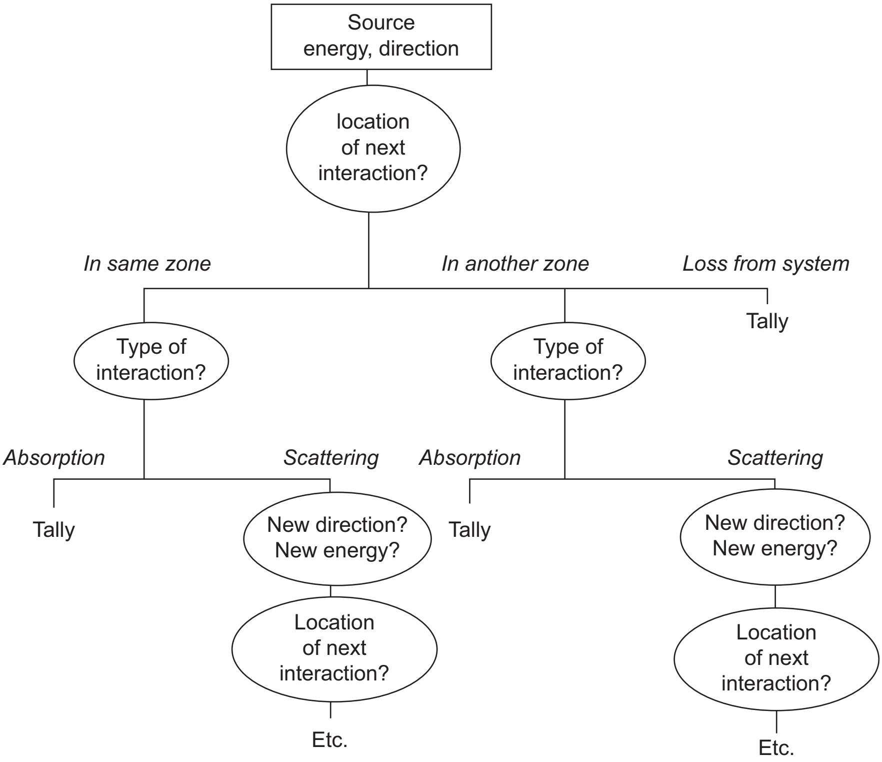

**Figure 4.5** Flow chart for Monte Carlo simulation of a neutron history (Dolan, 1982).

## 4.11 Conclusion

Nowadays reactor physics is a mature field of study in nuclear engineering. Neutronics studies for fission power plant studies produce information on

- Neutron energy spectra versus position;
- Nuclear fission rates and heating;
- Attenuation by shield;
- Neutron streaming through ducts;
- Radioisotope generation;
- Fissile fuel breeding;
- Decay heat after shutdown;
- Radioactivity of components and dose rates versus time after shutdown;
- Possibility of recycling or clearance of radioactive materials.

The recent trend in this field is to utilize large-scale computer facilities to analyze the reactor physical properties based on detailed and sophisticated calculation models. Neutron transport theory is accurate for simple geometries, and the diffusion approximation is easy to solve. Kinetics equations are needed to estimate the time variation of reactor power, and the Monte Carlo method is best for complex geometries.

# References

Dolan, T.J., 1982. Fusion Research. Pergamon Press, Elmsford, NY.

Sekimoto, H., 2007. Nuclear Reactor Theory. COE-INES textbook in Tokyo Institute of Technology. Available online. <http://www.nr.titech.ac.jp/coe21/eng/events/NuclReactorTheoryTextbook.pdf>.

This page intentionally left blank

# Kinetics, dynamics, and neutron noise in stationary MSRs

# 5

*Imre Pázsit and Victor Dykin*
Chalmers University of Technology, Gothenburg, Sweden

## Chapter Outline

## 5.1 Introduction

This chapter discusses the statics, kinetics, and dynamics of molten salt reactors. Naturally, MSRs differ from the traditional solid fuel reactors also with regards to their dynamic response to operational changes or disturbances, including start-up and shutdown. For instance, as will be shown in this chapter, the movement of the

**Molten Salt Reactors and Thorium Energy. DOI: http://dx.doi.org/10.1016/B978-0-08-101126-3.00005-1**

delayed neutron precursors in the core changes (enhances) the spatial neutronic coupling within the core, which naturally influences the space–time behavior of the reactor. Further, the time duration which the delayed precursors spend in the core and in the outer loop, respectively, influences the neutron balance in the core, and hence the dynamic response. Changes in the fuel velocity affect the criticality, and even small fluctuations of the velocity, including turbulence, might induce small neutron fluctuations. Further, similarly to how the propagation of temperature and density fluctuations in the coolant of a PWR, and two-phase flow in a BWR induce measurable neutron noise, similar perturbations (temperature fluctuations, void), as well as propagation of small inhomogeneities in the spatial distribution of the fuel concentration, the fission products and the delayed neutron precursors, will all lead to measurable neutron noise in an MSR. It is expected that similarly to traditional reactors, this neutron noise can be used for diagnostics and surveillance of the reactor status.

Although core physics and thermal hydraulics are tightly coupled even in solid fuel reactors, such as light-water reactors, it is obvious that the physics of MSRs is even more characterized by the strong interplay between the neutronic and the fluid fuel movement. Hence, methods aiming at a high-fidelity modeling of the space–time behavior of such systems must be based on a coupled core-physics—fluid flow model, and preferably on multiphysics modeling. A substantial volume of research has been performed along these lines (for an excellent summary see Krepel, 2006; Dulla, 2005; and Cammi et al., 2011), leading to the development of code systems such as Cinsf1D (Lecarpentier and Carpentier, 2003), DYN1D-MSR (Krepel, 2005, 2006), DYN3D-MSR (Krepel et al., 2007, 2008, 2014), and SIMMER-III (Wang et al., 2006). Much of this work was also performed with international cooperation, such as the European research projects MOST (Delpech et al., 2003) and EVOL (Merle-Lucotte et al.). A benchmark exercise was also performed for an intercomparison of the various computational tools (Delpech et al., 2003).

Apart from the full space–time diffusion and fluid flow approaches, kinetic approximations were also used, such as the adiabatic approximation (Wang and Cao, 2016b) and the quasistatic approximation (Dulla et al., 2004). The use of the point kinetic approximation was also attempted, but its application turned out to be much more problematic, as will be discussed in more detail later.

In this chapter the kinetics, dynamics, and neutron noise in an MSR will be treated in an utterly simple model of an MSR: a one-dimensional homogeneous bare system in one-group theory. The advantage of studying such a model is that it allows analytical solutions and hence good insight into the physics and neutronic behavior of such systems, while still retaining the key ingredients of the physics. Therefore, such studies were started at an early stage (Dulla, 2005), and pursued by several groups (Wang and Cao, 2015, 2016b). In addition, for enhanced insight, in such models some further simplifications can also be made, further enhancing the possibilities for insight and mathematical simplicity, such as the infinite fuel velocity assumption. As will be seen, such a simple model, and the considerations it allows, will be beneficial even for the solution and interpretation of the static case. The extension of the model to two-group theory is straightforward, such that all advantages with obtaining analytical results are preserved. Such results are found in the literature (Jonsson and Pázsit, 2011; Dykin and Pázsit, 2016); however, due to space limitations, these will not be described here.

A note is in order regarding the term “dynamics.” The usual distinction between reactor kinetics and dynamics is that the latter refers to the case when power feedback is included. In the model used in this chapter, no feedback effects such as temperature feedback, graphite expansion effect, etc. are accounted for. Accounting for power feedback makes it necessary to resort to numerical tools, as was done in the majority of the above-mentioned references (see also Wang et al.; Wang and Cao, 2016a). Hence, strictly speaking, only “kinetic” problems are considered here. However, in reactor noise terminology, it has become customary to refer to kinetics when the response of the system for a reactivity perturbation is calculated, without specifying the origin of the reactivity change, whereas when the neutronic response is due to a physical perturbation, modeled by a noise source, such a response is termed dynamic.

In the dynamic cases (according to the above terminology), both time and frequency behavior will be investigated, the emphasis being on the latter. The transient behavior during start-up will be investigated through the space and time dependence of the flux, whereas the kinetic and dynamic response of the reactor will be characterized by the space−frequency response to small stationary perturbations (fluctuations around the critical state). The emphasis will be on the dynamic properties that are specific to MSR and which therefore differ from those in solid fuel systems.

## 5.2 The MSR model

We assume a homogeneous unreflected slab reactor with one axial dimension along the $z$ axis. The flow of the fuel is also assumed to take place along this direction. The extrapolated system boundaries will lie at $z = 0$ and $z = H$, where thus the flux will vanish. We use one-group diffusion theory, and one average group of delayed neutron precursors will be assumed. The fuel, flowing axially with a velocity $u$, will be led back from the core outlet at $z = H$ to the core inlet at $z = 0$ through loop of length $L$. The total length $T$ of the recirculation will thus be $T = H + L$. The corresponding transit times will be denoted as $\tau_c = H/u$ for the passage through the core, $\tau_L = L/u$ in the external loop, and $\tau = \tau_c + \tau_L$ for the total recirculation time.

Actually, in a real MSR, the fuel velocities within the core and in the outer loop are unlikely to be equal. However, for convenience, a real MSR with a fuel velocity $u'$ different from the core velocity in the core, in an outer loop $T'$ can be rescaled such that one artificially chooses the loop length $L$ to be $L = u/u' \cdot T'$, such that the real outer recirculation time $\tau_L = L'/u' = L/u$ will be maintained.

It may be worth mentioning now that sometimes, and in particular in the cases when one has symmetry (e.g., with $u = 0$ and $u = \infty$, the latter will be discussed soon), it is practical to choose another coordinate system with spatial coordinate $x$, whose origin is in the middle of the reactor. In this case the core boundaries will lie at $x = \pm a$, and obviously one has $H = 2a$.

With these preliminaries, the equations that govern the MSR will read as

$$\frac{1}{v}\frac{\partial\phi(z,t)}{\partial t} = D\nabla^2\phi(z,t) + \left[\nu\Sigma_f(z,t)(1-\beta) - \Sigma_a(z,t)\right]\phi(z,t) + \lambda C(z,t) \tag{5.1}$$

$$\frac{\partial C(z,t)}{\partial t} + u\frac{\partial C(z,t)}{\partial z} = \beta\nu\Sigma_f(z,t)\phi(z,t) - \lambda C(z,t). \tag{5.2}$$

Regarding the boundary conditions, the flux is assumed to disappear at the extrapolated boundaries:

$$\phi(0,t) = \phi(H,t) = 0. \tag{5.3}$$

However, unlike for traditional systems, where one does not need to specify any boundary conditions for the nonmoving precursors, it is necessary to specify boundary conditions for an MSR due to the streaming of the fuel and hence that of the precursors. In a traditional system the precursor density would also vanish at the extrapolated boundary; however, the same condition cannot be prescribed in the MSR. Due to the flow, precursors generated in the whole volume of the core will leave on the exit, and will return to the inlet (diminished by the decay during the travel time). Hence the precursor density will not be zero at the boundaries. The only condition one can set is that the number density of delayed neutron precursors at the inlet is the same as that at the outlet with a time $\tau_L = L/u$ earlier, but decreased by the decay during this time:

$$C(0,t) = C(H,t-\tau_L)e^{-\lambda\tau_L}. \tag{5.4}$$

Even if the notion of the extrapolated boundary is a conceptual one, and one does not assume the flux physically to vanish at the extrapolation point, one might still discuss whether it is physically sound to treat equations even formally where the flux is zero and the precursor density is different from zero. However, it is easy to confirm that these boundary conditions lead to physically sound results. One way of doing this is to replace the zero boundary condition at the extrapolated boundary with logarithmic boundary conditions at the physical boundary. Such an investigation was performed by Pázsit et al. (2012) and the results showed a negligible quantitative difference. Hence in the continuation the above boundary conditions will be used.

## 5.3 The static equations

The static equations read as

$$D\nabla^2\phi_0(z) + (\nu\Sigma_f(1-\beta) - \Sigma_a(z))\phi_0(z) + \lambda C_0(z) = 0 \tag{5.5}$$

$$u\frac{dC_0(z)}{dz} = \beta\nu\Sigma_f\phi_0(z) - \lambda C_0(z) \tag{5.6}$$

with the boundary conditions corresponding to the stationary form of (5.4) which read

$$C_0(0) = C_0(H)e^{-\lambda\tau_L}. \tag{5.7}$$

Here, in addition to the streaming term for the precursors in Eq. (5.6), there is another crucial difference as compared to traditional static fuel reactors. Namely, in the latter, the delayed neutron precursors do not appear in the critical equations. This is always the case in one-group theory, whether one considers the transport equation or the diffusion approximation; and in energy-dependent cases it is still the case as long as the energy spectrum of the delayed neutrons is assumed to be equal to that of the prompt neutrons. As was noted already in Mattioda et al. (2000), in the case of an MSR, the delayed neutron precursors appear explicitly even in one-group diffusion theory, and cannot be eliminated from the static equations.

## 5.3.1 The adjoint property

Before continuing with the solution of this equation, it is worth taking a small deviation regarding an interesting property of the MSR equations. It is known that the transport equation, or the multigroup diffusion equations are not self-adjoint, but the one-group diffusion equations are self-adjoint. Not surprisingly, it turns out that in the case of an MSR, not even the one-group diffusion equations are self-adjoint (at finite fuel velocities). Similarly to the neutron streaming term of the diffusion equation, the reason for the nonadjoint property here is the streaming term of the precursors, i.e., the left-hand side of Eq. (5.6). Put a different way, the reason is the directed flow of the fuel in the core, which is not invariant for time-reversal.

To show the nonadjoint property and to show how the adjoint equation can be constructed, it is practical to write Eqs. (5.5) and (5.6) in matrix form

$$\hat{M}\vec{\phi}_0(z) = \begin{pmatrix} D\nabla^2 + \nu\Sigma_f(1-\beta) - \Sigma_a & \lambda \\ -\nu\Sigma_f\beta & u\dfrac{\partial}{\partial z} + \lambda \end{pmatrix} \begin{bmatrix} \phi_0(z) \\ C_0(z) \end{bmatrix} = 0, \tag{5.8}$$

where the matrix $\hat{M}$ and the vector $\vec{\phi}_0(z)$ are defined by the first equality. Then, it is easy to see that with an arbitrary flux function $\vec{\Psi}_0(z)$ one has

$$\left\langle \vec{\Psi}_0(z)\hat{M}\vec{\phi}_0(z)\right\rangle \neq \left\langle \vec{\phi}_0(z)\hat{M}\vec{\Psi}_0(z)\right\rangle \tag{5.9}$$

where the brackets indicate integration over the core, i.e.,

$$\langle \phi_0(z)\Psi_0(z)\rangle = \int_0^H \phi_0(z)\Psi_0(z)dz. \tag{5.10}$$

Except the convection term for the precursors, all other terms give equal contributions on the two sides of Eq. (5.9).

Similarly to the case of the transport equation, in order to construct the adjoint equation and the adjoint flux, it is not sufficient to construct an adjoint operator; one also needs to specify boundary conditions for the adjoint flux (in the present case for the precursor densities). Hence we seek a matrix $\hat{M}^\dagger$ and corresponding boundary conditions for the adjoint $\vec{\phi}_0^\dagger(z)$ such that

$$\left\langle \vec{\phi}_0(z)\hat{M}^\dagger\vec{\phi}_0^\dagger(z)\right\rangle = \left\langle \vec{\phi}_0^\dagger(z)\hat{M}\vec{\phi}_0(z)\right\rangle. \tag{5.11}$$

From considering that the adjoint equation is related to time-reversal, the adjoint operator can be written as

$$\hat{M}^\dagger = \begin{pmatrix} D\nabla^2 + \nu\Sigma_f(1-\beta) - \Sigma_a & -\nu\Sigma_f\beta \\ \lambda & -u\dfrac{\partial}{\partial z} + \lambda \end{pmatrix}, \tag{5.12}$$

whereas the boundary condition for the adjoint precursors will now read as

$$C_0^\dagger(H) = C_0^\dagger(0)e^{-\lambda\tau_L}. \tag{5.13}$$

It is easy to prove that with this construction, Eq. (5.11) holds. It is seen that the terms resulting from the off-diagonal and constants elements are equal, only the convection terms need to be checked. Taking the difference between the terms from the two sides of Eq. (5.11), one has

$$\begin{aligned} u\int_0^H \left\{C^\dagger(z)\frac{\mathrm{d}C(z)}{\mathrm{d}z} + C(z)\frac{\mathrm{d}C^\dagger(z)}{\mathrm{d}z}\right\}\mathrm{d}z &= [C(z)C^\dagger(z)_{z=0}^{H} = C(H)C^\dagger(H) - C^\dagger(0)C(0) \\ &= C(H)C^\dagger(H) - C(H)e^{\lambda\tau_L}C^\dagger(H)e^{-\lambda\tau_L} = 0. \end{aligned} \tag{5.14}$$

This proves that the adjoint property is fulfilled by the operator (5.12) and the boundary conditions for the adjoint precursor density (5.13).

It is also interesting to notice one major difference between the construction of the adjoint for the MSR as compared to the transport equation of traditional reactors, because it will have a bearing on the derivation of the point kinetic equations. In the transport equation, the construction of the adjoint incurs reversing the neutron velocity vectors, and specify different boundary conditions (in angle) *at the same place and at the same time*. As is seen from Eqs. (5.7) and (5.13), the direct and adjoint boundary conditions are relating the precursor densities at *different place and different time* (here, expressed by the decay terms). In the static case, this does not cause a problem since both the static and the adjoint precursor density are time-independent. However, as is seen from Eq. (5.4), in the time-dependent case the boundary conditions relate precursor densities at one place to another one at a different time and place, which will destroy the possibility of constructing a proper adjoint equation in the dynamic case. This point will be revisited later when discussing the point kinetic approximation.

### 5.3.2 Interpretation of the equation and some limiting cases

Similarly to the traditional systems, the equation for the precursor density can be solved to express $C_0(z)$ with $\phi_0(z)$, and one can derive an integro-differential equation for solely the flux. By integrating (5.6) one finds that

$$C_0(z) = e^{-\frac{z\lambda}{u}}\frac{\beta\nu\Sigma_f}{u}\left(\frac{1}{e^{\lambda\tau}-1}\int_0^H e^{\frac{z'\lambda}{u}}\phi_0(z)\mathrm{d}z' + \int_0^z e^{\frac{\lambda z'}{u}}\phi_0(z')\mathrm{d}z'\right), \tag{5.15}$$

where it is worth noting that only the full recirculation time $\tau$ appears. Hence one has a single integro-differential equation for the static flux in the form

$$\begin{aligned} &D\nabla^2\phi_0(z) + (\nu\Sigma_f(1-\beta) - \Sigma_a)\phi_0(z) \\ &\quad + e^{-\frac{z\lambda}{u}}\frac{\lambda\beta\nu\Sigma_f}{u}\left(\frac{1}{e^{\lambda\tau}-1}\int_0^H e^{\frac{z'\lambda}{u}}\phi_0(z)\mathrm{d}z' + \int_0^z e^{\frac{\lambda z'}{u}}\phi_0(z')\mathrm{d}z'\right) = 0. \end{aligned} \tag{5.16}$$

As can be seen, due to the indefinite integral in the last term, the characteristic equation is of third-order, making fully analytical solutions possible. However, before setting out to solve Eq. (5.16), it is worth analyzing Eq. (5.15) in some detail. By expanding the fraction multiplying the first integral on the r.h.s. as

$$\frac{1}{e^{\lambda\tau}-1} = \frac{e^{-\lambda\tau}}{1-e^{-\lambda\tau}} = e^{-\lambda\tau} + e^{-2\lambda\tau} + e^{-3\lambda\tau}\dots \tag{5.17}$$

and slightly rearranging, one obtains

$$C_0(z) = \frac{\beta\nu\Sigma_f}{u}\left(\sum_{n=1}^{\infty}\int_0^H e^{-\frac{\lambda}{u}(z-z')-n\lambda\tau}\phi_0(z')\mathrm{d}z' + \int_0^z e^{-\frac{\lambda}{u}(z-z')}\phi_0(z')\mathrm{d}z'\right). \tag{5.18}$$

This equation is suitable for an insight-giving interpretation. The second integral on the r.h.s. expresses the fact that all precursors generated at a rate $\beta\nu\Sigma_f\,\phi_0(z')$, between the core inlet and the observation point $z$, that is in all points $0 \le z' \le z$, will give a contribution to the total density at $z$, the exponential factor taking care of the decay due to the time $(z-z')/u$ it takes to get from $z'$ to $z$. The factor $1/u$ only corresponds to $\mathrm{d}t = \mathrm{d}z/u$. These precursors were hence generated in the last ("just actual") recirculation cycle. The infinite sum of the integrals in the first term on the r.h.s stands for a similar expression, but it is due to the precursors which were generated anywhere in the core with one, two, etc. full recirculation cycles earlier.

Hence it is seen that in Eq. (5.16), the first integral corresponds to the multiply recirculated precursors, whereas the second corresponds to the precursors which are "freshly" generated, and have not recirculated yet. This form also lends the possibility of introducing two different further simplifications which can be interpreted on physical terms, out of which one leads to exceptionally simple formulae that are also useful in the dynamic case.

### 5.3.3 The case of no recirculation

This case is only conceptionally interesting, because it does not lead to much simplification in mathematical terms. Assuming that the outer loop is infinitely long, so that all precursors decay before returning to the core, such that $\tau = \infty$, the first integral vanishes, and the equation simplifies to

$$D\nabla^2\phi_0(z) + (\nu\Sigma_f(1-\beta) - \Sigma_a)\phi_0(z) + \frac{\lambda\beta\nu\Sigma_f}{u}\int_0^z e^{\frac{\lambda(z-z')}{u}}\phi_0(z')\mathrm{d}z' = 0. \tag{5.19}$$

This equation could also have been obtained directly by simply setting $C(0) = 0$. Although in some practical cases it might prove a good approximation, from the calculational point of view, it does not bring much improvement. Despite the simplification in the form of the equation, its characteristic equation is still of third-order. The properties of such solutions were compared in Pázsit et al. (2012) with those where recirculation is significant, just in order to quantify the difference for various magnitude of recirculated precursors, depending on the recirculation time. This simplification will not be considered in the continuation.

### 5.3.4 The case of infinite fuel velocity

A much more interesting conceptual case is to consider high fuel velocities, in the limit of $u \to \infty$, which entails then $\tau = 0$ and $u\,\tau = T$ with $T$ being the total recirculation length $L + H$. Performing the limit, from (5.16) one obtains

$$D\nabla^2\phi_0(z) + (\nu\Sigma_f(1-\beta) - \Sigma_a)\phi_0(z) + \frac{\beta\nu\Sigma_f}{T}\int_0^H \phi_0(z')\mathrm{d}z' = 0. \tag{5.20}$$

Formally, the limiting procedure means that as the velocity increases, less and less precursors decay before returning to the core, and this leads to the dominance of the contribution from the multiply recirculated precursors [the first integral in (5.16)] over the precursors generated in the current cycle (the second integral). This happens when $\lambda\tau \ll 1$, i.e., the precursor decay during one recirculation cycle is negligible. This is not a completely unrealistic assumption. The results obtained by this approximation are therefore useful because they correspond to realistic cases reasonably well, whereas their solution is much simpler and transparent than that of the finite velocity case. Also, along with the case of zero fuel velocity (i.e., traditional reactors), it represents the other extreme of the scale of different fuel velocities (and similarly to the static fuel case, the equation is self-adjoint).

It has also to be added that when $u \to \infty$, the traditionally used MSR equations break down, in principle. This is since the flow of the fuel should require the presence of a streaming term also in Eq. (5.5) in the form (Zhang et al., 2009)

$$\frac{1}{v}\nabla \cdot (u\phi)$$

where $v$ stands for the neutron velocity. Since in practical cases $u \ll v$, this term is usually neglected. However, it is easy to confirm by quantitative calculations that the static and kinetic behavior of an MSR is practically the same at rather moderate velocities, such as $u = 300-400$ cm/s as what one obtains from the equations with $u = \infty$, which justifies the use of this approximation for conceptual studies.

Eq. (5.20) has an extremely simple solution. Since in this case both the static flux and the precursors are symmetric around $H/2$, it is practical to change the space variable to, $x = \left(z - \frac{H}{2}\right)$, which, as mentioned earlier, means that the system boundaries will lie at $x = \pm a$ instead of 0 and $H$. In this coordinate system the solution reads as

$$\phi_0(x) = A(\cos B_0 x - \cos B_0 a) \equiv A\varphi(x), \tag{5.21}$$

where

$$B_0^2 = \frac{\nu\Sigma_f(1-\beta) - \Sigma_a}{D}. \tag{5.22}$$

Since the static equation is homogeneous, the factor $A$ will remain arbitrary, but (5.21) with its argument (5.22) must fulfill the criticality condition to be a true solution. This condition can be obtained by putting (5.21) into (5.20). This shows that the solution has to fulfill the condition

$$-AB_0^2 \cos B_0 a = -\frac{\nu\Sigma_f\beta}{D}\frac{1}{T}\int_{-a}^{a}\phi(x')\mathrm{d}x' \equiv -\frac{\eta_0}{T}\int_{-a}^{a}\phi(x')\mathrm{d}x', \tag{5.23}$$

where the notation

$$\eta_0 = \frac{\nu\Sigma_f\beta}{D} \tag{5.24}$$

was introduced. Performing the integration yields the criticality equation

$$B_0^2 \cos B_0 a + \frac{2a\eta_0}{T}\cos B_0 a - \frac{2\eta_0}{TB_0}\sin B_0 a = 0. \tag{5.25}$$

Also, as is easily obtained from (5.15), one finds that the distribution of delayed neutron precursors is constant in space:

$$C_0(z) = \frac{\beta\nu\Sigma_f}{\lambda T}\int_0^H \phi_0(z')\mathrm{d}z' = A\frac{B_0^2 D}{\lambda}\cos B_0 a = C_0 \tag{5.26}$$

which is expected from physical intuition. Here in the second equality the form of the flux from Eq. (5.21) and the criticality Eq. (5.25) were utilized. It is thus seen that, similarly to a core with a static fuel, i.e., for $u = 0$, both the static flux and the delayed precursor density are symmetric around the origin, although the distribution of the precursors with moving fuel is very different from the case with a static fuel.

Some further interesting insight can be gained by considering the case of the infinite external loop, i.e., when $T \rightarrow \infty$, by keeping the core size $H = 2a$ constant. Physically, since in this case $H/T \rightarrow 0$, the fraction of the precursors that decay in the core, and indeed the precursor density itself everywhere in the loop tends to zero, one must have $C_0 = 0$, which is confirmed by (5.26). This also means that core must be critical only based on the prompt neutrons. This is indeed seen from Eq. (5.25), which shows that one must have $\cos(B_0 a) = 0$, i.e., in this case the MSR with moving fuel must have the same buckling as a traditional reactor of the same size. If the absorption cross-sections of the two reactors are the same, this means that, by virtue of (5.22), the MSR must have a higher fission cross-section. For finite $T$ values, some of the precursors will decay in the core, hence a lower fission cross-section is sufficient to keep the MSR critical, hence the buckling will be smaller than in the equivalent traditional core. This is generally valid also for finite fuel velocities.

### 5.3.5 The full solution

The full Eq. (5.16) can be solved by seeking the solution in form of expansion into the eigenfunctions of a traditional reactor with stationary fuel, i.e., in the eigenfunctions of a simple Helmholtz equation. This method converges fast, and is practical in quantitative work, hence it was used in several publications (Dulla, 2005; Pázsit and Jonsson, 2011). However, the equation can also be solved in a compact analytical form, as first suggested in Lapenta and Ravetto (2000). The same method can also be used in the time- and frequency-dependent calculations described in the forthcoming. Hence the principle of the calculations is briefly described here.

The closed analytical solution of (5.16) is obtained as follows (for the details we refer to Pázsit et al., 2012). By differentiating once with respect to $z$ and rearranging, one obtains a simple linear differential equation with constant coefficients in the form

$$\phi_0'''(z) + \frac{\lambda}{u}\phi_0''(z) + B_0^2\phi_0'(z) + \left(\frac{\lambda}{u}B_0^2 + C\right)\phi_0(z) = 0 \tag{5.27}$$

or, equivalently,

$$\phi_0'''(z) + \frac{\lambda}{u}\phi_0''(z) + B_0^2\phi_0'(z) + B_S^2\phi_0(z) = 0 \tag{5.28}$$

with

$$B_0^2 = \frac{\nu\Sigma_f(1-\beta) - \Sigma_a}{D}, \tag{5.29}$$

$$C = \frac{\lambda\beta\nu\Sigma_f}{Du} \tag{5.30}$$

and

$$B_S^2 = \frac{\lambda(\nu\Sigma_f - \Sigma_a)}{uD}. \tag{5.31}$$

Here, $B_S^2$ is equal to $\lambda/u$ times the static buckling of an equivalent traditional reactor with static fuel. The characteristic equation is a third-order polynomial in the variable $k$ (inverse length) obtained as

$$k^3 + \frac{\lambda}{u}k^2 + B_0^2 k + B_S^2 = 0. \tag{5.32}$$

Hence the characteristic equation has three roots. One can show that one root is real, and the other two are complex conjugates. In view of this, the solution can be written in the form

$$\phi_0(z) = A_1 e^{\alpha z}\sin(\beta z) + A_2 e^{\alpha z}\cos(\beta z) + A_3 e^{\gamma z}. \tag{5.33}$$

Of the three unknown coefficients, two can be eliminated by using the boundary conditions of vanishing flux at $z = 0$ and $z = H$, whereas substituting the resulting form, containing only one undetermined coefficient, will supply the criticality condition. Once the flux is found in an analytical form, the precursor density can easily be derived through Eq. (5.15).

### 5.3.6 Alternative solution of the MSR equations

An equivalent, alternative way of solving the MSR equations is to solve the coupled differential equations for the flux and the precursor density, without eliminating the delayed neutron precursors. This solution method, similar to the treatment of the two-group diffusion equations of a traditional system, brings out the different spatial behavior of the flux and the delayed neutron precursors in an MSR in a more transparent way than the method used above.

Then one starts with the matrix equation

$$\begin{pmatrix} \frac{\mathrm{d}^2}{\mathrm{d}z^2}+B_0^2 & \frac{\lambda}{D} \\ -\beta\nu\Sigma_f & u\frac{\mathrm{d}}{\mathrm{d}z}+\lambda \end{pmatrix} \begin{bmatrix} \phi_0(z) \\ C_0(z) \end{bmatrix} = 0. \tag{5.34}$$

The solution of this third-order differential equation can be written in the form

$$\begin{bmatrix} \phi_0(z) \\ C_0(z) \end{bmatrix} = A_1 \begin{bmatrix} 1 \\ c_1 \end{bmatrix} e^{k_1 z} + A_2 \begin{bmatrix} 1 \\ c_2 \end{bmatrix} e^{k_2 z} + A_3 \begin{bmatrix} 1 \\ c_3 \end{bmatrix} e^{k_3 z}, \tag{5.35}$$

where the roots $k_n$ are determined from the equation

$$\begin{vmatrix} k^2+B_0^2 & \frac{\lambda}{D} \\ -\beta\nu\Sigma_f & uk+\lambda \end{vmatrix} = (k^2+B_0^2)(uk+\lambda) + \frac{\lambda B\nu\Sigma_f}{D} = 0. \tag{5.36}$$

This characteristic equation, apart from having been multiplied by a factor $u$, is exactly the same as Eq. 5.32. The factors $c_n$ are determined by inserting the solution into (5.34), yielding

$$c_n = -\frac{D(k_n^2+B_0^2)}{\lambda} = \frac{\beta\nu\Sigma_f}{uk_n+\lambda}. \tag{5.37}$$

Two of the three amplitudes $A_n$ and the criticality equation are derived from the boundary conditions for the flux and the precursor density, respectively, leaving the amplitude of the solution undetermined.

Even without possession of a concrete solution, Eq. (5.35) shows that, since for $u \neq 0$ the $c_n$ are all different, the space dependence of the delayed neutron precursors is different from that of the static flux. This form is also suitable for deriving the solution with infinite fuel velocity. Taking the limit of Eq. (5.36) shows that one has

$$(k^2+B_0^2)k = 0 \tag{5.38}$$

and thus

$$k_{1,2} = \pm iB_0 \quad k_3 = 0 \tag{5.39}$$

and further

$$c_{1,2} = 0 \quad c_3 = -\frac{B_0^2 D}{\lambda}. \tag{5.40}$$

Switching again to the coordinate system with origin at the reactor center and boundaries at $x = \pm a$, the condition of zero flux at the extrapolated boundaries yields for the amplitudes

$$A_1 = A_2 \quad A_3 = -A_1(e^{iB_0a} + e^{-iB_0a}) \tag{5.41}$$

or

$$\phi_0(z) = A(\cos(B_0z) - \cos(B_0a)); \quad C_0(z) = A\frac{B_0^2D}{\lambda}\cos(B_0a) \equiv C_0, \tag{5.42}$$

which are identical with (5.21) and (5.26).

### 5.3.7 *Quantitative results*

Quantitative results are shown here for one core size with $H = 300$ cm, and extrapolation distance of 10 cm, corresponding to a power reactor. Following Dulla (2005), the numerical values used in this chapter correspond to a traditional U-fueled thermal system (the numerical data are shown in Table 5.1). The value of the neutron velocity $v$ was artificially chosen to have $\beta/\Lambda = 100$, where $\Lambda = 1/(v\ \nu\Sigma f)$, which is the customary value of the break frequency of the zero power reactor transfer function $G_0(\omega)$ in LWRs (more on that in Sections 5.5–5.7).

Calculations were made with different fuel velocities. Fig. 5.1 shows the neutron flux (Fig. 5.1A) and the delayed neutron precursors (Fig. 5.1B) in a large reactor, with different fuel velocities. Results are shown only for the physical reactor size, but not for the extrapolated boundary region. It is seen that the originally symmetric, cosine-shaped flux, which is symmetrical around the origin, gets distorted with increasing fuel velocities, the maximum being shifted towards the exit. At high velocities, when $\tau\cdot\lambda \ll 1$, the flux shape becomes symmetric again.

**Table 5.1** System parameters used in the calculations

| Parameter | Value used |
|---|---|
| $v$ | $\dfrac{100}{\beta\nu\Sigma_f}$ |
| $H$ | 50/300 cm |
| $L$ | 100/400 cm |
| $D$ | 0.33 cm |
| $\Sigma_a$ | 0.01 $\text{cm}^{-1}$ |
| $\nu\Sigma_\text{f}$ | $\Sigma_a + D\left(\dfrac{\pi}{H}\right)^2$ |
| $\beta$ | 0.0065 |
| $\lambda$ | 0.1 |

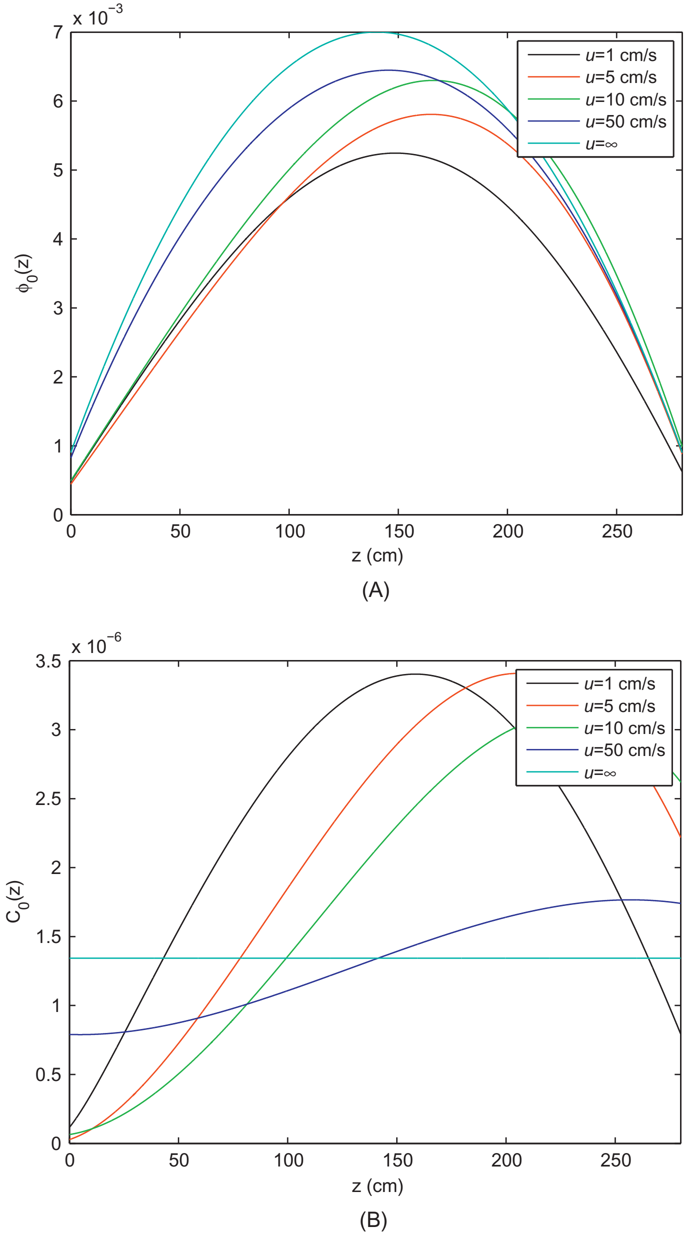

**Figure 5.1** Flux (A) and delayed neutron precursors (B) calculated with vanishing extrapolated flux boundary conditions, for several fuel velocities. Results are shown only for the physical size of the reactor.

The spatial distribution of the precursors changes much more significantly. For zero and low-fuel velocity, the distribution is similar to that of the static flux, with a maximum at or close the core center. With increasing liquid fuel velocities the maximum gets shifted towards the core exit, and at high velocities the maximum shifts all the way up to the core exit, such that the spatial dependence becomes monotonically increasing, before at ultrahigh fuel velocities it flattens out to approach the spatially constant distribution in the limit of $u \to \infty$.

The character of these results depends though partly on the effective delayed neutron fraction, which in the present calculations corresponds to a thermal system using U-235. By extrapolating the results of Dulla (2005), in an MSR containing thorium of minor actinides with a smaller value of $\beta$, the effect of the velocity on the static flux shape will be smaller.

The above-shown nonmonotonic change of the shape of the static flux, and the corresponding change in the dynamic transfer function, can be interpreted in simple terms. Starting with an MSR with static fuel and turning to static MSRs in equilibrium but with increasing fuel velocities, at low-fuel velocities all delayed neutron precursors which leave the core will decay in the external loop. This leads to a loss of reactivity and a spatial asymmetry in the flux and the precursor distributions. This tendency is monotonic up to a certain fuel velocity, when the return of the precursors to the core via recirculation starts to become significant. This will counteract the asymmetry in the flux, hence the nonmonotonic shape change. As was discussed in Wang and Cao (2015), this will also lead to a nonmonotonic behavior in the fraction $\alpha$ of the precursors that will decay in the core as compared to the total number of decays in the core and the external loop together.

However, as discussed in Mattioda et al. (2000), the dependence of the reactivity loss due to the recirculation on the fuel velocity is more involved. In addition to the fraction of the precursors which decay in the core, another contributing factor is the change of the importance function. As is seen in Fig. 5.1, the difference between the space dependence of the neutron flux and that of the precursors increases monotonically with increasing velocity. This indicates that with increasing velocity, most neutrons will decay at a place with a different importance than the place they were born. In practical cases this means that the dependence of the reactivity loss increases monotonically with increasing fuel velocity, as seen in the quantitative results in Dulla (2005) and Mattioda et al. (2000).

## 5.4 Space–time-dependent transient during start-up

In this section an outline is given, together with some asymptotic analysis, of how the formalism developed for the treatment of the space- and frequency-dependent response of the system, can also be used for calculating transients in systems with spatially homogeneous cross-sections. A typical case is considering a critical MSR, in which, however, initially the flux and/or the delayed neutron precursor distribution does not correspond to that in the stationary critical system. The starting example will consist of the following setting. We assume a critical homogeneous MSR, initially with stationary (nonmoving) fuel. Hence the equations will be the same as for a traditional reactor. Then, a hypothetical transient is created such that at time $t=0$, the fluid fuel velocity jumps instantaneously to a value $u>0$. Since an MSR core which is critical with a stationary fuel becomes subcritical when the fuel starts moving, some of the cross-sections need to be adjusted to a new value (e.g., the fission cross-section has to be changed to a higher value), to make the MSR critical with moving fluid fuel in the stationary case (which will be attained asymptotically). Hence, after an initial transient, the spatial distribution of the flux and the precursor density will tend to the shape corresponding to a critical MSR with the specified velocity. However, straight after $t=0$, there may be a mismatch, e.g., a deficit of neutrons from the decay of the delayed neutron precursors, which will cause a transient, whose duration is comparable with the mean life of the precursors. The amplitude of the final, asymptotic value of the flux will be not only different in shape, but also different in magnitude than that of the original critical flux. If no precursors were in the system initially, the final flux amplitude will be lower than the initial one.

### 5.4.1 The space–time-dependent equations for the transient

We shall first treat the case of starting with a critical traditional reactor, although the formalism is more general. Let us denote the material parameters of the initial core with static fuel with a zero index, and the static critical flux and precursor density as $\varphi_s(z)$ and $C_s(z)$. As will be seen soon, the static flux and precursor distributions will serve as starting values, or "source" terms, for the time-dependent calculations, which explain the choice of the subscript $s$. In principle, any nonnegative values can be chosen, not only those of a traditional critical system. We assume the same homogeneous one-dimensional system as in the foregoing, with extrapolated boundaries at $z=0$ and $z=H$ with assuming a vanishing flux at the extrapolated boundaries. With these notations, the static equations in this system read as

$$D_0\nabla^2\phi_s(z)+[\nu\Sigma_f^0-\Sigma_a]\phi_s(z)=0 \tag{5.43}$$

and

$$\beta\nu\Sigma_f^0\phi_s(z)=\lambda C_s(z) \tag{5.44}$$

with the boundary conditions $\phi_s(0)=\phi_s(H)=0$. The zero superscript of the fission cross-section indicates that this is the initial value at $t=-0$, which will be changed to a new one when the fuel starts moving at $t=+0$. The parameters of the system with a moving fuel will be denoted without an index, as before. This system is also homogeneous (cross-sections constant in space and time), and differ from the system with a static fuel only in the fission cross-section.

The static equations for such a slab reactor with fuel velocity $u$ in one-group diffusion theory with one-group of delayed neutrons, to which the reactor will asymptotically converge, are the same as in the previous section:

$$D\nabla^2\phi_0(z) + [\nu\Sigma_f(1-\beta) - \Sigma_a(z)]\phi_0(z) + \lambda C_0(z) = 0 \tag{5.45}$$

and

$$u\frac{dC_0(z)}{dz} = \beta\nu\Sigma_f\phi_0(z) - \lambda C_0(z) \tag{5.46}$$

with the boundary conditions

$$\phi_0(0) = \phi_0(H) = 0 \tag{5.47}$$

and

$$C_0(0) = C_0(H)e^{-\lambda\tau_L}, \tag{5.48}$$

where $\tau_L$ is the recirculation time in the outer loop. Here the subscript 0 was used, as before, to denote the static flux and precursor distributions, which will naturally be different from the $\phi_s(z)$ and $C_s(z)$ of the initial system with static fuel.

We assume now that at time $t=0$ the fuel instantaneously will get moving with a constant velocity $u$, and the fission cross-section is raised instantaneously from that of the static system, $\Sigma_f^0$, to that of the system with moving fuel, $\Sigma_f$ with which it is asymptotically critical. We also assume, however, that when the jump in the velocity and the cross-sections happens, the flux and the delayed neutron distributions belong to those of the static system:

$$\phi(z, t=0) = \phi_s(z); \quad \text{and} \quad C(z, t=0) = C_s(z). \tag{5.49}$$

Clearly, other choices are also possible (which will be considered later). Since these initial flux and precursor distributions do not correspond to the MSR with moving fuel, there will be a transient period, during which the flux and precursor distributions will be space- and time-dependent, but asymptotically will tend to a time-independent shape again. The goal is to calculate the transient. This can be achieved by analytical Laplace transform and numerical inverse Laplace transform methods.

The time-dependent equations read as

$$\frac{1}{v}\frac{\partial\phi(z,t)}{\partial t} = D\nabla^2\phi(z,t) + \left[(1-\beta)\nu\Sigma_f - \Sigma_a\right]\phi(z,t) + \lambda C(z,t), \tag{5.50}$$

and

$$\frac{\partial C(z,t)}{\partial t} + u\frac{\partial C(z,t)}{\partial z} = \beta\nu\Sigma_f\phi(z,t) - \lambda C(z,t). \tag{5.51}$$

The boundary conditions for the flux are given for all times $t \geq 0$ as

$$\phi(0,t) = \phi(H,t) = 0, \tag{5.52}$$

whereas for the precursors they will read

$$C(0,t) = C(H, t-\tau_L)e^{-\lambda\tau_L}. \tag{5.53}$$

Since, in agreement with the use of Laplace transform, all occurring time-dependent functions are zero for negative times, Eq. (5.53) is equivalent with

$$C(0,t)\begin{cases} 0 & \text{if} \quad t \leq \tau_L \\ C(H,t-\tau_L)e^{-\lambda\tau_L} & \text{if} \quad t > \tau_L \end{cases}. \tag{5.54}$$

which is also obvious on physical grounds. In the static MSR, there are no precursors in the external loop, hence after the start of the flow, it takes time $\tau_L$ before the precursors leaving the core exit will reach the core inlet, and during this time the precursor density at the inlet remains zero.

A temporal Laplace transform of (5.50) and (5.51), with the initial conditions (5.49) will yield

$$\frac{s}{v}\phi(z,s) - \frac{1}{v}\phi_s(z) = D\nabla^2\phi(z,s) + \left[(1-\beta)\nu\Sigma_f - \Sigma_a\right]\phi(z,s) + \lambda C(z,s) \tag{5.55}$$

and

$$sC(z,s) - C_s(z) + u\frac{\partial C(z,s)}{\partial z} = \beta\nu\Sigma_f\phi(z,s) - \lambda C(z,s), \tag{5.56}$$

whereas the Laplace transform of the boundary conditions will read

$$\phi(0,s) = \phi(H,s) = 0 \tag{5.57}$$

and

$$C(0,s) = C(H,s)e^{-(s+\lambda)\tau_L}. \tag{5.58}$$

The solution goes as for the static equations, by solving the precursor equations (5.56), using the boundary conditions (5.58), and substituting the solution back to the Laplace transformed equations for the flux, Eq. (5.55). The only difference is that, unlike in the static equations which refer to a critical system and hence are homogeneous, we have the additional inhomogeneous terms $\phi_s(z)$ and $C_s(z)$. Thus the solution of the precursor equations reads as

$$C(z,s) = e^{-\frac{\lambda+z}{u}}\frac{\beta\nu\Sigma_f}{u}\left[\frac{1}{e^{(\lambda+s)\tau}-1}\int_0^H e^{\frac{\lambda+z}{u}z'}\phi(z',s)\mathrm{d}z' + \int_0^z e^{\frac{\lambda+z}{u}z'}\phi(z',s)\mathrm{d}z'\right]$$
$$+\frac{e^{-\frac{\lambda+z}{u}}}{u}\left[\frac{1}{e^{(\lambda+s)\tau}-1}\int_0^H e^{\frac{\lambda+z}{u}z'}C_s(z')\mathrm{d}z' + \int_0^z e^{\frac{\lambda+z}{u}z'}C_s(z)\mathrm{d}z'\right]. \tag{5.59}$$

The last term, i.e., the second line of this equation, can actually be calculated analytically. Substituting this back to Eq. (5.55) yields, after a slight rearrangement

$$\nabla^2\phi(z,s) + B^2(s)\phi(z,s)$$
$$+\lambda e^{-\frac{\lambda+s}{u}}\frac{\beta\nu\Sigma_f}{uD}\left[\frac{1}{e^{(\lambda+s)\tau}-1}\int_0^H e^{\frac{\lambda+z}{u}z'}\phi(z',s)\mathrm{d}z' + \int_0^z e^{\frac{\lambda+z}{u}z'}\phi(z',s)\mathrm{d}z'\right] = F(z,s), \tag{5.60}$$

where

$$B^2(s) = \frac{(1-\beta)\nu\Sigma_f - \Sigma_a}{D} - \frac{s}{vD} = B_0^2 - \frac{s}{vD} \tag{5.61}$$

and the inhomogeneous (or source) term $F(z,s)$ is given as

$$F(z,s) = -\frac{\phi_s(z)}{vD} - \frac{\lambda e^{-\frac{\lambda+s}{u}z}}{uD}\left[\frac{1}{e^{(\lambda+s)\tau}-1}\int_0^H e^{\frac{\lambda+z}{u}z'}C_s(z')\mathrm{d}z' + \int_0^z e^{\frac{\lambda+z}{u}z'}C_s(z)\mathrm{d}z'\right]. \tag{5.62}$$

Since $F(z,s)$ is a known function, it will act as the inhomogeneous (source) term for the equations. Hence (5.60) can be written in condensed form as

$$\boldsymbol{L}(z,s)\phi(z,s) = F(z,s). \tag{5.63}$$

This equation can be solved by the Green's function technique: from (5.60) one defines

$$\boldsymbol{L}(z,s)G(z,z_0,s) = \delta(z-z_0) \tag{5.64}$$

and then the solution is given as

$$\phi(z,s) = \int_0^H G(z,z_0,s)F(z_0,s)\mathrm{d}z_0. \tag{5.65}$$

The strategy is to solve Eq. (5.64) analytically in the Laplace domain and then integrate it with $F(z, s)$ according to (5.65). The equation for the Green's function has exactly the same form as the one used in the neutron noise equations, which has already been determined in previous work (Pázsit and Jonsson, 2011), and which will be derived in detail in Section 5.5. One just has to replace $i\omega$ with $s$. Since the Green's function can be determined analytically, it can be integrated analytically with the $F(z, s)$ of Eq. (5.14).

The last remaining step to obtain the space−time dependence of the flux is to perform an inverse Laplace transform:

$$\phi(z,t) = \frac{1}{2\pi i}\int_{c-\mathrm{i}\infty}^{c+\mathrm{i}\infty} \phi(z,s)e^{st}\,\mathrm{d}s. \tag{5.66}$$

In the general case of finite fuel velocities $u$, the inverse transform cannot be obtained analytically. However, based on the analytical expression of $\phi(z, s)$, a numerical inverse Laplace transform method can be used. Such methods were used in the past for calculating the space−time behavior of neutron pulses injected to critical systems (Yoshioka et al., 1998). Here we will confine the treatment to the model case of infinite fuel velocity, and derive some asymptotic results analytically, which do not require an inverse transform.

## 5.4.2 Solution for $\mathrm{u} \to \infty$

By assuming infinite fuel velocity after $t = 0$, the corresponding equations will be very much simplified and suitable to give insight. At the same time, as will be seen, the case is somewhat pathological, and has to be taken with some cautiousness. Namely, at time $t = -0$, the distribution of the delayed neutron precursors in the core will be a cosine-shaped function, whereas in the outer loop there will be no precursors. Just after $t = +0$, at any given point in the core, the precursor density will oscillate with infinite speed between zero and the maximal value one had at $t = -0$ at the center of the reactor. However, formally, these oscillations are smoothed out to a constant value averaged over the whole loop. This constant amplitude will then change its magnitude when tending to the asymptotic value.

For the case of infinite fuel velocity, the inhomogeneous term $F(z, s)$ simplifies to

$$F(z,s) = -\frac{\phi_s(z)}{vD} - \frac{\lambda}{(\lambda+s)DT}\int_0^H C_s(z')\mathrm{d}z', \tag{5.67}$$

which, for later convenience, can be given in a coordinate system with its origin at the half-height of the reactor, and having $x$ as the variable in this system, the boundaries being at $x = \pm a = \pm H/2$:

$$F(x,s) = -\frac{\phi_s(x)}{vD} - \frac{\lambda}{(\lambda+s)DT}\int_{-a}^{a} C_s(x')\mathrm{d}x' \equiv -\frac{\phi_s(x)}{vD} - \frac{\lambda}{(\lambda+s)D}C_{s,0}. \tag{5.68}$$

Here the constant initial distribution $C_{s,0}$ of the delayed neutron precursors at $t = +0$ was introduced as

$$C_{s,0} = \frac{1}{T}\int_{-a}^{a} C_s(x')\mathrm{d}x'. \tag{5.69}$$

In the simple system under consideration, one has

$$\phi_s(x) = \cos(B_s x), \tag{5.70}$$

where, for simplicity, the amplitude of the static initial flux was normalized such that its maximum value is equal to unity. Further, $B_s = \pi/2\ a$, and

$$C_s(x) = \frac{\beta\nu\Sigma_f}{\lambda}\phi_s(x). \tag{5.71}$$

Putting (5.71) into (5.69) yields

$$C_{s,o} = \frac{\beta\nu\Sigma_f}{T\lambda}\int_{-a}^{a}\phi_s(x')\mathrm{d}x'. \tag{5.72}$$

The Green's function has also a simple analytical form, as given in Pázsit and Jonsson (2011) [however, note the sign error in the first term of the Green's function in Pázsit and Jonsson (2011), Eqs (5.47) and (5.50)]. Using the same coordinate system, one has

$$G(x,x_0,s) = -\frac{\eta(s)\varphi(x,s)\varphi(x_0,s)}{TK(s)B^2\cos Ba} - \frac{1}{B\sin 2Ba}\begin{cases}\sin B(a-x_0)\sin B(a+x) & x<x_0\\ \sin B(a+x_0)\sin B(a-x) & x>x_0\end{cases} \tag{5.73}$$

Here, $B \equiv B(s)$, the latter being defined through

$$B^2(s) = B_0^2 - \frac{s}{vD} \tag{5.74}$$

with $B_0^2$ having defined in (5.29) as $B_0^2 = (\nu\Sigma_f(1-\beta) - \Sigma_a)/D$. Further, in (5.73)

$$\varphi(x,s) = \cos B(s)x - \cos B(s)a, \tag{5.75}$$

$$\eta(s) = \frac{\lambda\eta_0}{\lambda + s} = \eta_0(1 - s/\lambda); \quad \eta_0 = \frac{\nu\Sigma_f\beta}{D} \tag{5.76}$$

and

$$K(s) = B^2(s)\cos B(s)a + \frac{2a\eta(s)}{T}\cos B(s)a - \frac{2\eta(s)}{TB(s)}\sin B(s)a. \tag{5.77}$$

It is worth noting that

$$K(0) = B_0^2 \cos B_0 a + \frac{2a\eta_0}{T} \cos B_0 a - \frac{2\eta_0}{TB_0} \sin B_0 a = 0 \tag{5.78}$$

since it is the criticality equation.

#### 5.4.2.1 Asymptotic values

With these preliminaries, one can calculate the initial values $\lim_{t\to 0} \phi(x, t)$ and $\lim_{t\to 0} C(x, t)$ from the Tauberian theorems. In an ordinary case one should just get back the initial conditions, hence this should be a mere check of the correctness of the formulae. However, due to the pathological character of this model (switching from zero to infinite fuel velocity during zero time), understandably, for the precursor distributions we will not obtain $\lim_{t\to 0} C(x, t) = C_s(x)$. Nevertheless, as will be seen, the result is completely consistent with the model.

According to the Tauberian theorems,

$$\lim_{t\to 0} \phi(x,t) = \lim_{s\to \infty} s\ \phi(x,s) \tag{5.79}$$

and similarly

$$\lim_{t\to 0} C(x,t) = \lim_{s\to \infty} s\ C(x,s). \tag{5.80}$$

*Initial values:* $t\to 0$

Since

$$B^2(s) \to -\frac{s}{vD} \quad \text{for} \quad s \to \infty \tag{5.81}$$

and hence

$$B(s) \to i\sqrt{\frac{s}{vD}} \quad \text{for} \quad s \to \infty, \tag{5.82}$$

one has

$$\sin B(s)x \to \frac{ie^{x\sqrt{\frac{x}{vD}}}}{2} \quad \text{and} \quad \cos B(s)x \to \frac{e^{x\sqrt{\frac{x}{vD}}}}{2} \quad \text{for} \quad s \to \infty. \tag{5.83}$$

For the calculation of the limit $t\to 0$, we shall use Eq. (5.65) (written in the $x$-coordinate system), i.e.,

$$\lim_{t\to 0} \phi(x,t) = \lim_{s\to \infty} s\ \phi(x,s) = \lim_{s\to \infty} s \int_{-a}^{a} G(x,x_0,s)F(x_0,s)\mathrm{d}x_0 \tag{5.84}$$

and calculate $\lim_{s\to\infty} F(x, s)$ and $\lim_{s\to\infty} s\, G(x, x_0, s)$ separately. One can then see that in this limit the second term of the $F(x, s)$ of Eq. (5.68) can be neglected, the first term is just being equal to

$$\lim_{s\to\infty} F(x,s) = -\frac{\phi_s(x)}{vD}. \tag{5.85}$$

Further, the first term of $s\, G(x, x_0, s)$ from Eq. (5.73) tends also to zero. This is because the sin and cos terms appear with equal powers in the numerator and the denominator (the term $K(s)$ contains a cos $B(s)\, a$), as well as $\eta(s) \sim 1/s$ in the numerator and $B^2(s) \sim s$ in the denominator. Regarding the remaining term, when expanding the terms in the numerator and the denominator, one notices that the terms

$$e^{2a\sqrt{\frac{s}{vD}}} \tag{5.86}$$

cancel in the numerator and the denominator, and the two terms for $x < x_0$ and $x \geq x_0$ are combined to

$$e^{-|x-x_0|\sqrt{\frac{s}{vD}}}. \tag{5.87}$$

Accounting for the limit

$$\lim_{s\to\infty} e^{-|x-x_0|\sqrt{\frac{s}{vD}}} = 2\frac{\delta(x-x_0)}{\sqrt{\frac{s}{vD}}} \tag{5.88}$$

one finds that

$$\lim_{s\to\infty} s\, G(x, x_0, s) = -v\ D\ \delta(x-x_0). \tag{5.89}$$

Substituting this into (5.84), also using (5.85) yields

$$\lim_{t\to 0} \phi(x,t) = \phi_s(x) \tag{5.90}$$

as expected.

For the delayed neutron precursors, the result is somewhat less trivial, but nonetheless it is rather interesting. For the case of infinite velocity, $u = \infty$, Eq. (5.59) reads as

$$C(x,s) = \frac{\beta\nu\Sigma_f}{(\lambda+s)T}\int_{-a}^{a}\phi(x',s)\mathrm{d}x' + \frac{1}{(\lambda+s)}\int_{-a}^{a} C_s(x')\mathrm{d}x'. \tag{5.91}$$

Taking the limit, since $\lim_{s\to\infty} s\,\phi(x, s)$ remains finite, only the second term gives a contribution, yielding

$$\lim_{t\to +0} C(x,t) = \lim_{s\to\infty} s\, C(x,s) = \frac{1}{F}\int_{-a}^{a} C_s(x')\mathrm{d}x' = C_{s,o}, \tag{5.92}$$

where $C_{s,0}$ was already defined in Eq. (5.69) as the constant distribution of the delayed neutron precursors at $t = +0$. This is not equal to $C_s(x)$, but it is what one actually expects on physical terms, based on the considerations at the beginning of this subsection. When the fuel flow recirculation starts at $t = +0$, the previously cosine-shaped distribution of the precursors gets “smeared out” over a spatial domain whose length equals to $T$, and in any given point in the core, the same average value $C_{s,0}$ of the precursor distribution, given by (5.92) prevails.

*Asymptotic values for $t \to \infty$*

In a similar manner, one can calculate the asymptotic form of the flux for $t \to \infty$ from the Tauberian theorem:

$$\lim_{t\to\infty} \phi(x,t) = \lim_{s\to 0} s\,\phi(x,s). \tag{5.93}$$

Using (5.65) (rewritten to the $x$-coordinate system), one has

$$\lim_{t\to\infty} \phi(x,t) \equiv \phi_\infty(x) = \lim_{s\to 0} s\,\phi(x,s) = \lim_{s\to 0} s \int_{-a}^{a} G(x,x_0,s)F(x_0,s)\mathrm{d}x_0. \tag{5.94}$$

Since $F(x,\ s\ =\ 0)$ is finite:

$$F(x,0) \equiv F(x) = -\frac{\phi_s(x)}{vD} - \frac{C_{s,0}}{D}, \tag{5.95}$$

it is sufficient to calculate only the limit

$$\lim_{s\to 0} s\,G(x,x_0,s). \tag{5.96}$$

Since the second term of (5.73) remains finite for $s \to 0$, we need to calculate

$$\lim_{s\to 0} -s\frac{\eta(s)\varphi(x,s)\varphi(x_0,s)}{T\ K(s)B^2\cos Ba} = -\mathrm{Res}\left[\frac{1}{K(s)}\right]_{s=0}\frac{\eta_0\varphi(x)\varphi(x_0)}{T\ B_0^2\cos B_0 a}. \tag{5.97}$$

where [c.f. Eqs. (5.21) and (5.75)],

$$\varphi(x) = \varphi(x, s=0) = \cos B_0(x) - \cos B_0(a) \tag{5.98}$$

Calculation of the residue yields

$$\begin{aligned}\mathrm{Res}\left[\frac{1}{K(s)}\right]_{s=0} &\equiv \mathrm{Res}(0) = \left\{\frac{1}{Dv}\left[\frac{B_0 a \sin B_0 a}{2} - \cos B_0 a\right]\right.\\ &\left.+\frac{2\eta_0}{T}\left[a\left(\frac{a}{2B_0 Dv}\sin B_0 a - \frac{\cos B_0}{\lambda}\right) - \frac{1}{B_0}\left(\frac{\sin B_0 a}{2B_0^2 Dv} - \frac{\sin B_0 a}{\lambda} - \frac{a}{2B_0 Dv}\cos B_o a\right)\right]\right\}^{-1},\end{aligned} \tag{5.99}$$

Using the above, one obtains the final result

$$\phi_\infty(x) = \frac{\mathrm{Res}(0)\eta_0\varphi(x)}{TB_0^2 \cos B_0 a}\int_{-a}^{a}\varphi(x')F(x')\mathrm{d}x' \equiv A\varphi_0(x) \tag{5.100}$$

with $F(x)$ defined in (5.95). In (5.100), the amplitude factor

$$A = \frac{\mathrm{Res}(0)\eta_0\varphi(0)}{TB_0^2 \cos B_0 a} \tag{5.101}$$

and the normalized (to unity at $x = 0$) shape function

$$\varphi_0(x) = \frac{\varphi(x)}{\varphi(0)} \tag{5.102}$$

were chosen in order for an easy comparison with the initial flux shape $\varphi_s(x)$, which, similarly to the shape function $\varphi_0(x)$, is normalized to unity at $x = 0$.

A comparison between $\phi_s(x)$ and $\varphi_0(x)$ is shown in Fig. 5.2. It is seen that with normalizing the two fluxes to the same value at $x = 0$ leads to a somewhat wider shape for $\phi_s(x)$, corresponding to the smaller buckling of the MSR case.

All quantities appearing in Eq. (5.101) are known analytically, hence not only the normalized shape of $\phi_\infty(x)$ can be obtained, but also its absolute value.

From (5.21) and (5.98) it is seen that the asymptotic flux shape is identical with the shape of the static flux of the MSR with $u = \infty$, and its amplitude is given concretely in terms of the initial values of the flux and the precursor density, $\phi_s(x)$ and

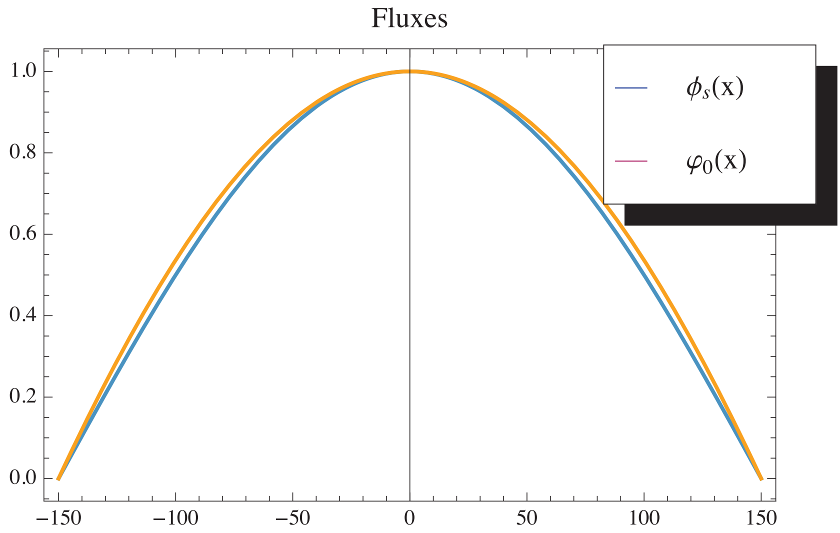

**Figure 5.2** Comparison of the static fluxes $\phi_s(x)$ and $\varphi_0(x)$

$C_s(x)$, respectively. This gives the possibility to calculate the change of the amplitude of the flux from the initial to the final state, without performing the numerical inverse Laplace transform. The ratio between the initial and final states will of course also depend on some parameters of the system, such as the ratio between the core height and the external loop (this will determine how large a fraction of the delayed neutrons is lost). A quantitative analysis and discussion are given in the next subsection.

In a similar manner, from (5.91) it is seen that for the asymptotic form of the precursor distribution, only the first term gives a contribution, and one obtains the result

$$C_\infty(x) = \frac{\beta\nu\Sigma_f}{T\lambda}\int_{-a}^{a}\phi_\infty(x')\ \mathrm{d}x' = C_\infty, \tag{5.103}$$

which shows a considerable resemblance to Eq. (5.72). This similarity will be used in the interpretation of the quantitative results of the next subsection.

### 5.4.2.2 Quantitative analysis

Some quantitative results are shown in Figs. 5.3 and 5.4, which will be discussed here. In these calculations, the data given in Table 5.1 were used as a starting point.

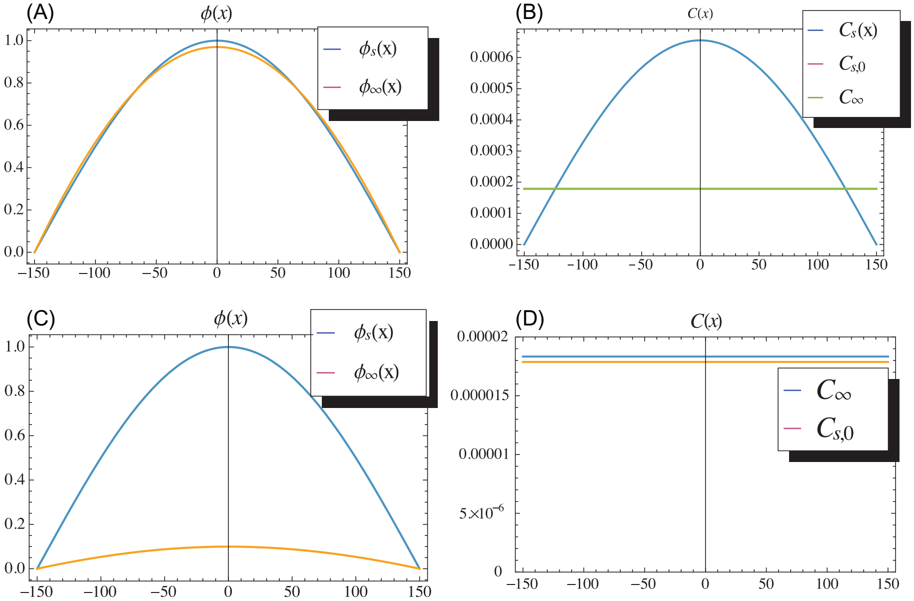

**Figure 5.3** The initial and final fluxes (A) and precursors (B) for initial conditions corresponding the traditional starting system. The initial and final fluxes (C) and precursors (D) for negligible initial precursors. All cases for $u = \infty$.

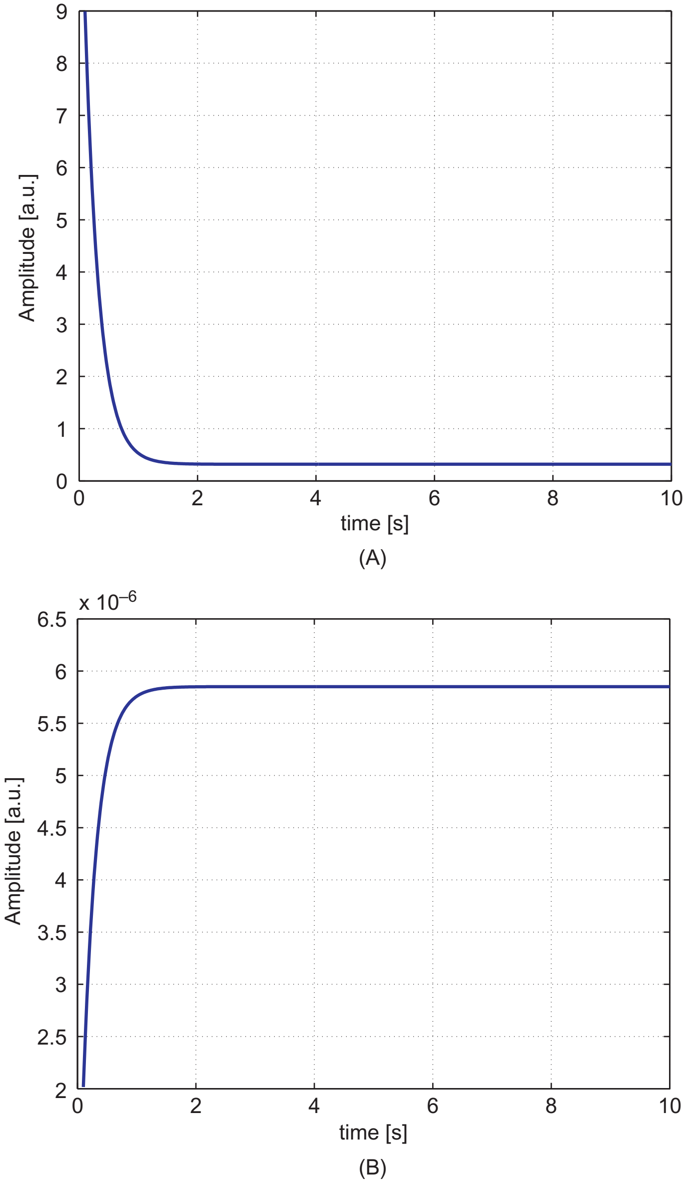

**Figure 5.4** The time evolution of the flux (A) and the delayed neutron precursors (B) from the start of the transient to the asymptotic value, at $x = 0$ (i.e., the core center) for $u = \infty$ cm/s.

The fission cross-section $\nu\Sigma_f^0$ of the MSR with the static fuel was calculated by the formula given in the table, leading to a critical traditional core. Thereafter a new, larger fission cross-section $\nu\Sigma_f$ was calculated from the criticality Eq. (5.23) to make the core critical with a moving fuel of infinite velocity.

First, the initial values $\phi_s(x)$ and $C_s(x)$ were chosen to correspond to the cosine-shape critical flux and precursor distribution of the static traditional core. With the material and geometrical data given, the constant value $C_{s,0}$ of the initial precursor distribution at $t=+0$ can be calculated from (5.92), and one obtains the value

$$C_{s,0} = 1.7874 \times 10^{-4} \tag{5.104}$$

The amplitude of the final (asymptotic) flux $A$ of Eq. (5.101), as well as the asymptotic value of the precursor distribution $C_\infty$ can also be calculated. With the numerical data one obtains

$$A = 0.97 \quad \text{and} \quad C_\infty = 1.78745 \times 10^{-4} \tag{5.105}$$

The initial and final distribution of the fluxes and the precursors are shown in Fig. 5.3(A, B), which illustrate the above. Fig. 5.3(B) shows the original cosine-shaped precursor distribution $C_s(x)$, as well as its the loop-averaged value $C_{s,0}$, existing at $t=+0$, and the asymptotic value $C_\infty$ (this latter cannot be distinguished from $C_{s,0}$ in the plot).

As is seen from both (5.104) and (5.105), as well as from the figures, the initial and final amplitudes of the flux and the precursor density differ extremely little. This may seem surprising at first, since after starting the fuel movement, the amount of delayed neutron precursors will be much less in the core than before. According to Eq. (5.92), the total amount in the core will be equal to $H/T = 300/700$, $<1/2$ times its value in the state of the core with static fuel [clearly demonstrated in Fig. 5.3(B)]; moreover, the worth of these precursors will also be less than in the original system, due to a less disadvantageous spatial distribution. Roughly, the worth of the delayed neutron precursors at $t = +0$ will be about one-third of that at $t=-0$. Hence, one would expect a significant decrease in the flux amplitude due to the deficit in the delayed neutron precursors.

The explanation for this apparent contradiction lies in the fact that an MSR with moving fuel is critical with a much lower amount (and worth) of precursors than a traditional system, and the difference is also about the same factor one-third (with the geometrical data used here). This is also seen from (5.72), which shows that since the shapes of the initial and asymptotic fluxes are very similar (c.f., Fig. 5.2), the level of the precursors needed if the initial flux $\phi_s(x)$ is replaced with the asymptotic flux in the critical MSR is also about the same as their initial value. Put it in a different way, the raising of the fission cross-section at $t=0$ brings the MSR with a moving fuel to very close to the asymptotic (critical) state with the already-existing precursors. The decrease of the maximum of the flux amplitude from the initial to final value will be about 3%, whereas the precursor distribution changes only in the sixth digit, due to the equality of the flux integrals.

These results indicate that if an MSR is started up such that it is first made critical with stationary fuel, then the fuel starts circulating and at the same time the reactivity of the system is increased by adding more fuel in the salt *approximately* at a proper pace, the arising transient should be expected to be mild.

A much more significant change in the flux and the precursor distributions can be seen if one assumes an initial nonzero flux, but no precursors being present in the core. Such a case was considered for a traditional reactor in Yoshioka et al. (1998), where the time evolution, and in particular the asymptotic value of the flux was calculated by injecting neutrons at $t = 0$ in form of a spatial Dirac-delta function into a critical, bare homogeneous system in which neither neutrons nor precursors were found for $t \leq 0$. It was shown that asymptotically, the initial flux will decrease approximately with a factor

$$\frac{\beta}{\Lambda\lambda} \approx 1000 \tag{5.106}$$

The same value can be derived with a back-of-an-envelope calculation from the point kinetic equations in one-group theory with one-group of precursors, which correspond to the case when the starting pulse had the same space dependence as the critical flux.

A similar scenario in our case is obtained by assuming $C_s(x) = C_{s,0} = 0$, which simply means that the second term on the right hand side of (5.91) as well as (5.95) will be 0. Eq. (5.100) can be used without changes other than a modified inhomogeneous term $F(x)$. Since in the previous case $F(x)$ was dominated by this term, in its absence the asymptotic value of the flux will be significantly lower, whereas the precursor distribution will grow from originally zero to its nonzero equilibrium value. Indeed, calculation of the asymptotic amplitude factor for this case will yield

$$A = 0.00275767 \tag{5.107}$$

This value is completely in line with the traditional results above, with the exception that the decrease of the original flux is not a factor of 1000, but only about 360. The reason for the difference is in line with the discussion above: the MSR considered here needs about one-third of the precursors compared to the traditional system, hence the deficit of precursors in the initial state of the MSR, as compared to what is needed to make the system critical, is also about three times less significant than in the traditional core. Hence the milder decrease of the flux amplitude from the initial to the final state.

Since, due to the large amplitude change, such a case is not amenable for illustration, we have selected a case with the starting flux being the same as in the previous example, whereas the initial value of the precursors was chosen as one-tenth of the value given in (5.104), i.e., the value $C_{s,0} = 1.7874 \times 10^{-5}$ was chosen. With this value, one obtains

$$A = 0.0994818 \quad \text{and} \quad C_\infty = 1.83318 \times 10^{-5} \tag{5.108}$$

That is, the initial flux amplitude decreases by about a factor 10 in the final state, whereas the precursor distribution increases slightly. This case is shown in Fig. 5.3C, D.

The time dependence of the flux and the precursors was calculated by numerical inverse Laplace transform methods. For illustration, Fig. 5.4 shows the time dependence of the flux and of the delayed neutron precursors from the start of the transient to the asymptotic, stationary value at the spatial point $x = 0$ (i.e., the core center). Here again, a low, but nonzero initial value of the precursors was chosen. It is seen that the neutron flux monotonically decreases, whereas the amplitude of the delayed neutron precursors monotonically increases until both reach the asymptotic value. Since, due to the infinite fuel velocity, there is no periodicity involved in the recirculation, there are no oscillations in either the flux or the precursor density.

Similar calculations can be performed also for finite fuel velocities, both for the asymptotic values and for the time dependence. For space limitations, these are not given here. Despite the possibility of analytical calculations in the Laplace domain, the complexity of these calculations leads to a loss of the main advantage of the analytical methods, i.e., transparency. For such cases the full numerical methods are more suitable, and many such scenarios were investigated and reported in the literature.

## 5.5 Dynamic equations in the frequency domain: neutron noise

From this section on, the dynamic response of the reactor will be investigated to small stationary perturbations. In particular, the properties of the neutron noise induced by small perturbations in the core will be calculated. [For a general overview of neutron noise theory in traditional systems, see Pázsit and Demazière (2010)].

As usual in noise theory, the perturbations are represented by the fluctuations of the cross-sections. In the overwhelming majority of the work performed in traditional systems in one-group theory, the noise source was assumed to be the fluctuations of the absorption cross-sections. For several important perturbations, such as density and temperature fluctuations of the coolant, vibration of control rods, this is naturally the case. Besides, modeling a physical perturbation (such as a vibrating control or fuel rod), leads to a very similar mathematical representation of the noise source due to the fluctuation of either of the cross-sections. As a consequence, apart from some minor trivial differences, the space- and frequency-dependence of the induced neutron noise will be very similar for both cases.

Due to the above, and also for simplicity of the description and compatibility with earlier work in traditional systems, the neutron noise due to the fluctuations of the absorption cross-sections will be elaborated and discussed also in the rest of this chapter. The justification of this choice is though not self-evident, and deserves some discussion. Not the least since space–time fluctuations of the fission cross-sections, due to the flow of the liquid fuel, will play a much more dominant role in an MSR than in traditional systems.

The justification is based on a recent work on this question, where the properties of neutron noise in an MSR, induced by the fluctuations of the fission cross-sections, were investigated (Dykin et al., 2016). It was shown that, although the mathematical representation of the noise source due to fission cross-section fluctuations in an MSR is indeed much more involved than, and rather different from, that due to the fluctuations of the absorption cross-sections, the neutron noise induced by propagating fission and cross-section fluctuations was very similar to each other both qualitatively and quantitatively. Given this fact and that the mathematical treatment of the neutron noise induced by fission cross-section fluctuations is much more complicated and less transparent, the choice of only considering fluctuations of the absorption cross-sections feels justified.

It is assumed that without the fluctuations of the cross-sections, the system is critical, with time-independent flux and precursor densities. The perturbation is represented by the space- and time-dependent stationary fluctuations of the cross-sections around their equilibrium (space- and time-independent, critical) values, hence the neutron flux and the precursor density will also exhibit small space- and time-dependent fluctuations. It is assumed that all fluctuating quantities are small, and in the linear theory which is customary to use in neutron noise theory, the product of any two fluctuating quantities can be neglected. This also means that no products of time-dependent quantities will occur, and hence a temporal Fourier-transform technique can be used for the solution.

One thus writes

$$\phi(z,t) = \phi_0(z) + \delta\phi(z,t), \tag{5.109}$$

$$C(z,t) = C_0(z) + \delta C(z,t) \tag{5.110}$$

and

$$\Sigma_a(z,t) = \Sigma_a + \delta\Sigma_a(z,t), \tag{5.111}$$

where $\phi_0$ and $C_0$ fulfill the critical equation with $\Sigma_a$. Putting these into the time-dependent equations (5.50) and (5.51), neglecting the second-order term $\delta\phi(z,t)\cdot\delta\Sigma_a(z,t)$, and subtracting the static equations yields

$$\frac{1}{v}\frac{\partial\delta\phi(z,t)}{\partial t} = D\nabla^2\delta\phi(z,t) + (\nu\Sigma_f(1-\beta) - \Sigma_a)\delta\phi(z,t) + \lambda\delta C(z,t) - \delta\Sigma_a(z,t)\phi_0(z) \tag{5.112}$$

$$\frac{\partial\delta C(z,t)}{\partial t} + u\frac{\partial\delta C(z,t)}{\partial z} = \beta\nu\Sigma_f\delta\phi(z,t) - \lambda\delta C(z,t) \tag{5.113}$$

with the boundary condition of vanishing flux fluctuations at the extrapolated boundaries and the condition for $\delta C$ in the form

$$\delta C(0,t) = \delta C(H, t-\tau_L)e^{-\lambda\tau_L}. \tag{5.114}$$

A Fourier transform of these expressions leads to

$$D\nabla^2\delta\phi(z,\omega) + \left(\nu\Sigma_f(1-\beta-\Sigma_a) - \frac{i\omega}{v}\right)\delta\phi(z,\omega) + \lambda\delta C(z,\omega) = \delta\Sigma_a(z,\omega)\phi_0(z) \tag{5.115}$$

$$i\omega\delta C(z,\omega) + u\frac{\partial\delta C(z,\omega)}{\partial z} = \beta\nu\Sigma_f\delta\phi(z,\omega) - \lambda\delta C(z,\omega) \tag{5.116}$$

$$\delta C(0,\omega) = \delta C(H,\omega)e^{-(i\omega+\lambda)\tau_L}. \tag{5.117}$$

The fluctuations of the precursor density can be eliminated the same way as in the static case, which leads to

$$\delta C(z,\omega) = e^{-\frac{(\lambda+i\omega)z}{u}}\frac{\lambda\beta\nu\Sigma_f}{u}\left(\frac{1}{e^{(\lambda+i\omega)\tau}-1}\int_0^H e^{\frac{(\lambda+i\omega)z'}{u}}\delta\phi(z',\omega)\mathrm{d}z' + \int_0^z e^{\frac{(\lambda+i\omega)z'}{u}}\delta\phi(z',\omega)\mathrm{d}z'\right) \tag{5.118}$$

and

$$\begin{aligned} &D\nabla^2\delta\phi(z,\omega) + \left(\nu\Sigma_f(1-\beta) - \Sigma_a - \frac{i\omega}{v}\right)\delta\phi(z,\omega) \\ &+ e^{-\frac{(\lambda+i\omega)z}{u}}\frac{\lambda\beta\nu\Sigma_f}{u}\left(\frac{1}{e^{(\lambda+i\omega)\tau}-1}\int_0^H e^{\frac{(\lambda+i\omega)z'}{u}}\delta\phi(z',\omega)\mathrm{d}z' + \int_0^z e^{\frac{(\lambda+i\omega)z'}{u}}\delta\phi(z',\omega)\mathrm{d}z'\right) \\ &= \delta\Sigma_a(z,\omega)\phi_0(z). \end{aligned} \tag{5.119}$$

This equation is a complete analog of Eq. (5.60), except that the source term is different (and that $i\omega$ replaces $s$). Eq. (5.60) corresponds to a transient in the time domain, whose source term is represented by the initial conditions. Eq. (5.119), on the other hand, gives a frequency domain representation of small, stationary fluctuations of the neutron flux, given rise by small, stationary fluctuations of the cross-section, which thus represents the "noise source."

### 5.5.1 The Green's function

Before turning to any particular case of the perturbation $\delta\Sigma_a(z,\omega)$, we will investigate the Green's function $G(z, z_0, \omega)$ of the problem, because it only reflects the properties of the system and not that of the particular perturbation. Often it is simpler to solve the corresponding equations for the Green's function than for the full noise equation.

Similarly to the case of the transient calculations, in order to get insight, it is interesting to consider the case of infinite fuel velocity first which allows closed form analytical solutions. Unlike for the transient case, the application of the infinite fuel velocity model is much less pathological. Since it is assumed that all perturbations started at $t = -\infty$, any possible transients have already decayed, and there is no physical contradiction in the application of infinite fuel velocity. The closed form analytical solutions will help in getting insight to the dynamics of reactors with circulating fuel, at least in a limiting case.

## *5.5.2 Solution for* $\mathrm{u} = \infty$

Performing the same limit of $u \to \infty$ and $\tau \to 0$ as in the previous case yields the equation for the neutron noise as

$$
\begin{aligned}
&D\nabla^2\delta\phi(z,\omega) + \left(\nu\Sigma_f(1-\beta) - \Sigma_a - \frac{i\omega}{v}\right)\delta\phi(z,\omega) + \frac{\lambda\beta\nu\Sigma_f}{(\lambda+i\omega)T}\int_0^H \delta\phi(z',\omega)\mathrm{d}z' \\
&\quad = \delta\Sigma_a(z,\omega)\phi_0(z).
\end{aligned}
\tag{5.120}
$$

For the calculation of the dynamic Green's function $G(x, x_0, \omega)$, first we define

$$
B^2(\omega) = B_0^2 - \frac{i\omega}{vD} = B_0^2\left(1 - \frac{i\omega}{v\nu\Sigma_f}\frac{\nu\Sigma_f}{\nu\Sigma_f - \Sigma_a - \nu\Sigma_f\beta}\right) = B_0^2\left(1 - \frac{i\omega\Lambda}{\rho\infty - \beta}\right)
\tag{5.121}
$$

and [c.f. Eq. (5.76)]

$$
\eta(\omega) = \frac{\lambda\eta_0}{\lambda + i\omega} \quad \text{with} \quad \eta_0 = \frac{\nu\Sigma_f\beta}{D}.
\tag{5.122}
$$

With these notations the equation for the Green's function of (5.120) with the shift of spatial variable from $z$ to $x$ reads as

$$
\nabla^2 G(x,x_0,\omega) + B^2(\omega)G(x,x_0,\omega) + \frac{\eta(\omega)}{T}\int_{-a}^{a} G(x,x_0,\omega)\mathrm{d}x' = \delta(x - x_0).
\tag{5.123}
$$

The details of the solution again can be found in Pázsit and Jonsson (2011). The result, analogously to (5.73), is found to be

$$
G(x,x_0,\omega) = -\frac{\eta(\omega)\varphi(x)\varphi(x_0)}{TK(\omega)B^2\cos B_a} - \frac{1}{B\sin 2Ba}\begin{cases}\sin B(a-x_0)\sin B(a+x) & x < x_0 \\ \sin B(a+x_0)\sin B(a-x) & x > x_0\end{cases},
\tag{5.124}
$$

where $B \equiv B(\omega)$,

$$\varphi(x) = \cos Bx - \cos Ba \tag{5.125}$$

[cf. Eq. (5.21)], and the factor $K(\omega)$ is defined as

$$K(\omega) = B^2 \cos Ba + \frac{2a\eta(\omega)}{T} \cos Ba - \frac{2\eta(\omega)}{TB} \sin Ba. \tag{5.126}$$

Note that $K(0) = 0$ because the r.h.s. of (5.126) reduces to the criticality Eq. (5.25). One notes the symmetry in $x$ and $x_0$: the fact that Eq. (5.120) is self-adjoint is reflected in the Green's function.

The second term in the Green's function is formally identical with the Green's function in traditional systems, where the first term is not present. The point kinetic behavior for traditional systems can be derived from the properties of this second term as $\omega$ tends to zero, because the term sin $2Ba$ tends to zero. In the present case, sin $2Ba$ does not tend to zero when $\omega$ tends to zero, and correspondingly, the point kinetic behavior will not be related to the second term, rather it will derive from the first one. Namely, taking the limit $\omega \to 0$, the second term of (5.124) will remain finite, whereas the first will diverge since $K(\omega) \to 0$, as mentioned above. Hence one has

$$G(x, x_0, \omega) \sim \frac{\eta_0 \varphi(x) \varphi(x_0)}{TK(\omega) B_0^2 \cos B_0 a}, \tag{5.127}$$

when $\omega \to 0$. Since the Green's function is now factorized with regards to frequency and space dependence, and the space dependence is further factorized into a product of the static flux at $x$ and $x_0$, respectively, it is shown that an MSR with infinite fuel velocity also shows point kinetic behavior at low frequencies. The analysis can be made similarly with considering systems of decreasing size instead of frequency, with a similar conclusion. However, the case of finite fuel velocity, which is not self-adjoint, will be considerably more complicated.

### 5.5.3 Quantitative analysis: comparison with traditional systems

The Green's function for infinite velocities was calculated in two different systems, for various frequencies, and compared to the case of a traditional reactor of the same size. The Greens's function of a traditional reactor is given as

$$G(x, x_0, \omega) = -\frac{1}{B(\omega) \sin 2B(\omega)a} \begin{cases} \sin B(\omega)(a+x) \sin B(\omega)(a-x_0) & x \le x_0; \\ \sin B(\omega)(a-x) \sin B(\omega)(a+x_0) & x > x_0, \end{cases} \tag{5.128}$$

where

$$B^2(\omega) = B_0^2\left(1 - \frac{1}{\left(1 - \frac{\Sigma_a}{\nu\Sigma_f}\right)G_0(\omega)}\right), \tag{5.129}$$

$$G_0(\omega) = \frac{1}{i\omega\left(\Lambda + \frac{\beta}{i\omega + \lambda}\right)} \tag{5.130}$$

and $B_0^2 = \pi/H$. We note that the basic formula for the MSR Green's function is the same as that for the traditional reactor, with an extra term added. Another difference is that to have both systems critical, they need to have slightly different material properties. The data used in the calculations are shown in Table 5.1.

The space dependence of the amplitude of the Green's functions of an MSR and a traditional system of power reactor size, for $x_0 = 0$ and for various frequencies, can be seen in Fig. 5.5.

At extremely low and high frequencies, the spatial form of the two Green's functions is the same, so they have the same asymptotic properties. At low frequencies, the noise has the same form as the static flux, indicating point kinetic behavior. However, the amplitude of the Green's function of the MSR is much larger than that in the traditional system. This can be related to the fact that the effective delayed neutron fraction is much smaller in the MSR than in a corresponding traditional reactor with the same nuclear constant $\beta$, due to the fact that a large portion of precursors decays outside the core in the MSR. It is easy to show for a traditional system that at plateau frequencies and below, the amplitude of the transfer system is proportional to $1/\beta$. For the MSR, a rough estimate is that the amplitude is proportional with $1/\beta_{\text{eff}}$, where $\beta_{\text{eff}}$ takes account the losses of the decays outside the core, and one can estimate it as

$$\beta_{eff} \sim \beta\frac{H}{L+H}.$$

With the present data, $H = 300$ cm and $L = 400$ cm, one obtains that the amplitude of the Green's function of an MSR is approximately 2.33 times larger than that of the corresponding traditional system. Fig 5.5A, B confirm this estimate quite well.

It has to be noted that in the present analysis an MSR with the parameters of a traditional thermal reactor fueled with U-235 was taken. A further difference is that an MSR will presumably run on fuel with a smaller fraction of delayed neutrons per fission, hence the difference will be even larger. Thus, the above observation has some relevance even outside the MSR systems and it is interesting in general for all fast reactor systems or for cores with MOX fuel, due to the smaller fraction of delayed neutrons. With some simplification it can be claimed that the amplitude of the neutron noise for the same perturbation can be expected to be larger in

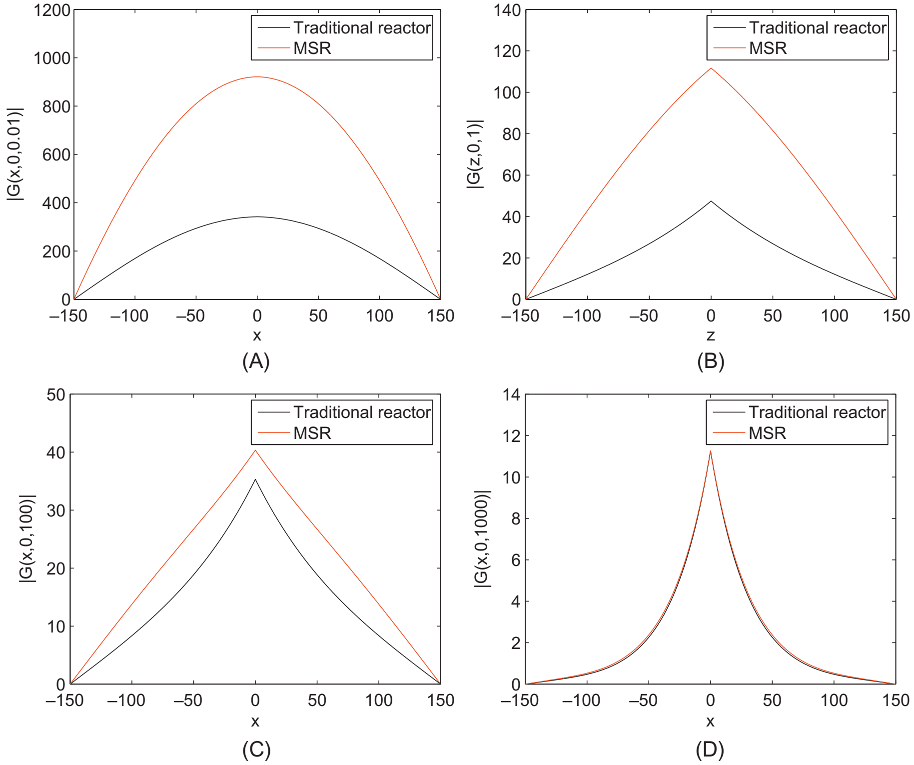

**Figure 5.5** Comparison between Green's functions for infinite and zero fuel velocity for various frequencies in a large system ($H = 300$ cm). (A) $\omega = 0.001$ rad/s; (B) $\omega = 1$ rad/s; (C) $\omega = 100$ rad/s; (D) $\omega = 1000$ rad/s.

Gen-IV systems than in traditional reactors, hence noise diagnostics of such systems will be effective.

One can also observe in Fig. 5.5A–D how the point kinetic behavior, expressed by the similarity of the space dependence of the Green's function with that of the static flux, gradually disappears and the system response to localized perturbations becomes localized. It is also seen that the MSR retains a point-kinetic behavior for larger frequencies than a traditional reactor. This can be attributed to the fact that the MSR is a more tightly coupled system than a traditional reactor, due to the movement of the fuel which, by transporting delayed neutron precursors from the place of their generation to their decay, establishes a neutronic coupling between different regions.

### 5.5.4 Results with finite velocity

The case of no recirculation will not be investigated here; as mentioned, its solution is not much easier than that of the full equation. This case was investigated in

Pázsit et al. (2012) and showed only predictable simple quantitative differences compared to the full recirculation treatment.

As mentioned in connection with the static and transient cases, the equation for the Green's function can either be solved by expansion into an orthogonal set of eigenfunctions of the static problem, as was done in Dulla et al. (2005), Dulla (2005), and Pázsit and Jonsson (2011), or by the analytical solution used earlier in this chapter both for the static case and for the transient problem. The latter way is preferred because such a solution can be convoluted with the noise source to arrive at analytical expressions for the induced neutron noise. The main task is again to determine the roots of the characteristic equation, with the only difference to the previous cases being that now not only some of the roots, but the equation itself becomes complex. The details are described in Pázsit et al. (2012), here we shall only restrict ourselves to present some quantitative results.

These are shown in Figs. 5.6 and 5.7. Fig. 5.6 shows the frequency dependence of the amplitude of the Green's function in the smaller system for various fuel velocities. At the lowest velocity, the frequency dependence is the same as that of the amplitude of the zero power transfer function $G_0(\omega)$: a plateau at medium frequencies, and an $1/\omega$ behavior at low and high frequencies. At higher frequencies, some multiple ripples appear. The frequencies where these appear correspond to the inverse of the recirculation time of the fuel. With higher velocities, these appear at higher frequencies. As will be shown shortly, it is these ripples which cannot be reproduced by a solution of the point kinetic equations.

Fig. 5.7 shows the space dependence of the amplitude of the Green's function in the large system, for $z_0 = H/2$ and a frequency of $\omega = 10$ rad/s, which is in the middle of the plateau region, for a few different velocities. For $u = 0$, that is a traditional reactor, the Green's function is relatively localized and indicates substantial deviation from the point kinetic behavior. For increasing fuel velocities, partly the

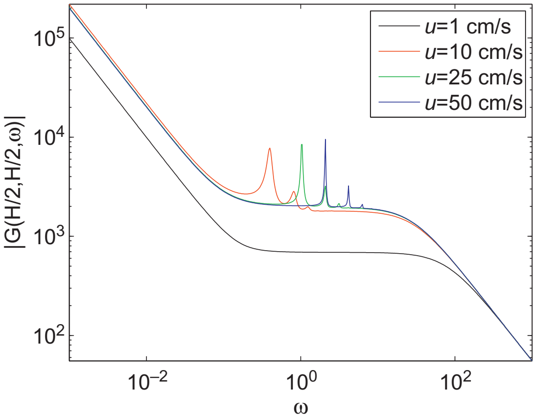

**Figure 5.6** Frequency dependence of the Green's function for a few different fuel velocities in the small system.

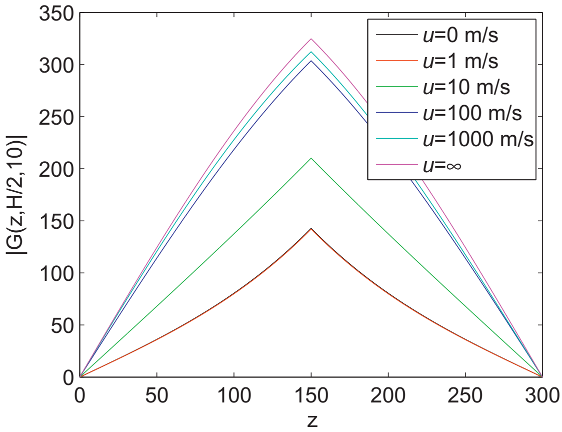

**Figure 5.7** The space dependence of the Green's function in a large system for a few different velocities, including $u = 0$ and $u = \infty$. $H = 300$ cm, $\omega = 10$ rad/s.

amplitude of the Green's function increases, and partly its shape is changed towards a more point-kinetic type behavior. The reasons for these effects were already touched upon; the increase of the amplitude is due to the loss of neutrons decaying from precursors outside the core, and the point kinetic behavior is due to the increased neutronic coupling between various parts of the core, due to the fuel flow and the movement of the precursors.

## 5.6 The point kinetic approximation and the point kinetic component

In this section the point kinetic approximation of the space–time-dependent MSR equations and derivation of the point kinetic component of the neutron noise will be discussed. This is yet another example where obvious, conceptual differences between the physics of traditional solid fuel reactors and the MSR will be revealed.

### *5.6.1 Introduction*

The point kinetic approximation is the simplest in the hierarchy of the various reactor kinetic approximations (Bell and Glasstone, 1970). Historically, the interest in the kinetic approximations arose because there was insufficient computer power to solve full space–time-dependent transient problems, especially to model large power excursions. Moreover, many of the available measurements were made in small, tightly coupled cores, where point-kinetic theory was expected to work fairly well.

In the late 1970s, the focus in reactor analysis was gradually shifting toward large commercial power reactor systems, where space-dependent effects were to play a much more significant role. Simultaneously, with the increase of computer power, more and more involved space−time-dependent calculations could be performed. As a result, the point-kinetic approximation has lost its original value and importance. Interestingly, however, the result of this approximation, i.e., the point kinetic component of the dynamic response, and in particular the point kinetic component of the neutron noise, kept its significance.

This is because with growing operational experience, the need for diagnostics of spatially dependent perturbations, such as unfolding the noise source properties (e.g., the position of a vibrating control rod or a channel blockage) arose. As it turns out, to design an effective unfolding procedure for locating a noise source, as well as to select optimum detector positions, it is useful to know the point-kinetic and pure space-dependent components of the neutron noise separately. Hence, the point-kinetic component of the induced neutron noise regained its significance in reactor calculations. The main emphasis of the discussion here is, therefore, to investigate the possibility of calculating the point-kinetic component in an MSR separately from the space-dependent component.

The point kinetic equations are usually derived from the space−time(−energy)-dependent diffusion or transport equations, with an assumption of factorizing the space−time-dependent flux into an amplitude factor $P(t)$ which is only dependent on time, and a normalized shape function $\psi(\mathrm{r}, t)$. This procedure is often referred to as the "Henry factorization" (Pázsit and Demazière, 2010). The goal of the point kinetic approximation is to derive the amplitude factor $P(t)$ from a set of simplified equations, which are obtained from the original space−time-dependent equations by a projection technique, i.e., integrating them with a weight function. In this process the coefficients of the arising point kinetic equation for $P(t)$ will depend on the unknown shape function. However, this dependence can either be neglected by replacing the shape function with the static flux or the static adjoint, or recalculating the shape function with time too, but with a substantially larger time-step.

As is described in Pázsit and Demazière (2010), the application of the point kinetic approximation is particularly useful in reactor noise theory, because, due to the use of linear ("first order") theory, allowing the neglection products of fluctuating quantities, the coefficients of the point kinetic equation will no longer contain the unknown shape function. In other words, the calculation of the amplitude and the shape function decouples, and the coefficients of the point kinetic equation become known constants.

Solution methods of the time-dependent equations of an MSR by way of the reactor kinetic approximations of traditional reactors, have been extensively discussed in the literature (MacPhee, 1958; Lapenta et al., 2001; Dulla et al., 2004, 2005; Dulla, 2005; Zhang et al., 2009). As is described in these publications, due to the different structure of the delayed neutron precursor equations for the MSR, the mathematical procedure of deriving the point kinetic equations is different from that of the traditional reactors. A modified, more involved form of the Henry factorization procedure has to be used, in which both the flux and the delayed neutron precursors need to be factorized. In accordance with this, the projection of the flux and the precursor equations requires two different weight functions, the static adjoints of both the flux and the precursors, each used with the corresponding equation.

Nevertheless, the above only represents a technical complication which can be handled. The more substantial problem, which became clear from the above investigations, is that in an MSR, even in the case of small stationary fluctuations of the neutron flux, the advantage of decoupling of the equations for the amplitude and the shape function disappears. It turns out that neglecting second-order terms, the point-kinetic parameters appearing in the point kinetic equations remain dependent in first order of the fluctuations of the unknown shape functions. This means that the correct solution (in first order) of the point kinetic equations requires simultaneous solutions for the shape functions, which will not be easier than the original full equations; in fact, due to the factorization procedure, it will even be more complicated. One can use various fixes to bring the point kinetic equations to a form which is independent from the shape function, but these result in solutions which, although not completely incorrect, do not reproduce some important features of the correct point kinetic component.

The underlying reason for this difference between traditional systems and the MSR is the contradiction between the propagating character included in the equation (for the transport of the precursors) and the very concept of point-kinetic behavior. The propagation incurs a nonseparable relationship between the spatial and temporal coordinates. This is in conflict with point kinetics, which assumes that the space and time dependence of the occurring functions can be factorized into a purely time- and a purely space-dependent function. As a partial consequence, in an MSR, the fulfilment of the adjoint property is possible only for the static quantities but cannot be achieved for the time-dependent quantities, such as the dynamic adjoint.

Hence, the easiest way to obtain the point kinetic component of the neutron noise is to first obtain the solution of the full space—time (or rather, space—frequency)-dependent equations, and extract the point kinetic component with the same projection techniques as one uses for the derivation of the point kinetic equations. Comparing the correct solution obtained that way with the solution of the “fixed” point kinetic approximation will reveal the deficiencies of the latter.

In the rest of this section an outline of the derivations, with proofs of the above statements will be given. For the details of the calculations the reader is referred to Pázsit et al. (2014).

## 5.6.2 Derivation of the linearized point kinetic equations

The kinetic approximations are defined through factorizing the space—time-dependent flux into an amplitude function $P(t)$ and a shape function $\psi(x, t)$ as

$$\phi(x,t) = P(t)\psi(x,t), \tag{5.131}$$

with the normalization condition

$$\frac{\partial}{\partial t}\int_{-a}^{a} W(x)\psi(x,t)\mathrm{d}x = 0. \tag{5.132}$$

Condition (5.132) makes the factorization unambiguous, but leaves a freedom in selecting different forms for the weight function $W(x)$. The choice of $W(x)$ will affect the actual form of the amplitude and the shape functions, as well as the structure of the equations for the amplitude function (the point kinetic equations) and for the shape function. In traditional systems with stationary fuel, the usual choice is to use the static adjoint as the weight function, i.e.,

$$\frac{\partial}{\partial t}\int_{-a}^{a}\phi_0^{\dagger}(x)\psi(x,t)\mathrm{d}x = 0. \tag{5.133}$$

This choice yields the traditional point kinetic equations, where the time evolution of the amplitude function $P(t)$ is driven by the reactivity perturbations. Once $P(t)$ is found, the point kinetic component of the space−time-dependent flux is obtained by replacing the shape function with the static flux, i.e.,

$$\phi_{p.k.}(x,t) = P(t)\phi_0(x). \tag{5.134}$$

Eq. (5.133) amounts to saying that the integral of the shape function and the weight function is constant, and one is free to choose this constant to be

$$\int_{-a}^{a}\phi_0^{\dagger}(x)\psi(x,t)\mathrm{d}x = \int_{-a}^{a}\phi_0^{\dagger}(x)\phi_0(x)\mathrm{d}x. \tag{5.135}$$

By way of this, the amplitude factor, and hence through (5.134) the point kinetic component of the noise, can be obtained from the full space−time-dependent flux as

$$P(t) = \frac{\int_{-a}^{a}\phi_0^{\dagger}(x)\phi(x,t)\mathrm{d}x}{\int_{-a}^{a}\phi_0^{\dagger}(x)\phi_0(x)\mathrm{d}x}. \tag{5.136}$$

The objective of this section is to show that for an MSR, the fluctuations of the amplitude factor can be obtained analytically by the above procedure, but there are no point kinetic equations available which would yield the same solution.

The derivation of the point kinetic equation starts with the space−time-dependent diffusion equations used in the foregoing, which are rewritten here for convenience:

$$\frac{1}{v}\frac{\partial\phi(x,t)}{\partial t} = D\frac{\partial^2\phi(x,t)}{\partial^2 x} + \left[(1-\beta)\nu\Sigma_f(x,t) - \Sigma_a(x,t)\right]\phi(x,t) + \lambda C(x,t), \tag{5.137}$$

$$\frac{\partial C(x,t)}{\partial t} + u\frac{\partial C(x,t)}{\partial x} = \beta\nu\Sigma_f(x,t)\phi(x,t) - \lambda C(x,t) \tag{5.138}$$

with the following boundary conditions:

$$\phi(-a,t)=\phi(a,t)=0, \tag{5.139}$$

$$C(-a,t)=C(a,t-\tau_L)e^{-\lambda\tau_L}. \tag{5.140}$$

The corresponding static equations read as

$$D\frac{\mathrm{d}^2\phi_0(x)}{\mathrm{d}^2x}+\left[(1-\beta)\nu\Sigma_f-\Sigma_a\right]\phi_0(x)+\lambda C_0(x)=0, \tag{5.141}$$

$$u\frac{\mathrm{d}C_0(x)}{\mathrm{d}x}=\beta\nu\Sigma_f\phi_0(x)-\lambda C_0(x), \tag{5.142}$$

with the boundary conditions

$$\phi_0(-a)=\phi_0(a)=0, \tag{5.143}$$

$$C_0(-a)=C_0(a)e^{-\lambda\tau_L}, \tag{5.144}$$

The corresponding static adjoint equations read as:

$$D\frac{\mathrm{d}^2\phi_0^\dagger(x)}{\mathrm{d}^2x}+\left[(1-\beta)\nu\Sigma_f-\Sigma_a\right]\phi_0^\dagger(x)-\beta\Sigma_f C_0^\dagger(x)=0, \tag{5.145}$$

$$u\frac{\mathrm{d}C_0^\dagger(x)}{\mathrm{d}x}\lambda\phi_0^\dagger(x)+\lambda C_0^\dagger(x), \tag{5.146}$$

with the corresponding adjoint boundary conditions

$$\phi_0^\dagger(-a)=\phi_0^\dagger(a)=0, \tag{5.147}$$

$$C_0^\dagger(a)=C_0^\dagger(-a)e^{-\lambda\tau_L}. \tag{5.148}$$

For simplicity, Eqs. (5.145) and (5.146) can be rewritten in a matrix form as

$$\begin{pmatrix} \dfrac{\mathrm{d}^2}{\mathrm{d}^2x}+B_0^2 & -\beta\dfrac{\nu\Sigma_f^0}{D} \\ \lambda & -u\dfrac{\mathrm{d}}{\mathrm{d}x}+\lambda \end{pmatrix}\begin{pmatrix} \phi_0^\dagger(x) \\ C_0^\dagger(x) \end{pmatrix}=0. \tag{5.149}$$

Since for the derivation of the point kinetic equations, both the flux and the delayed neutron precursor density has to be factorized into an amplitude factor and a shape function, the following factorization will be used:

$$\phi(x,t) = P(t)\psi(x,t), \tag{5.150}$$

and

$$C(x,t) = C(t)\varphi(x,t). \tag{5.151}$$

Accordingly, for both shape functions one has to specify a normalization condition, for which the static adjoints will be used as weight functions:

$$\frac{\partial}{\partial t}\int_{-a}^{a} \phi_0^\dagger(x)\psi(x,t)\mathrm{d}x = 0, \tag{5.152}$$

$$\frac{\partial}{\partial t}\int_{-a}^{a} C_0^\dagger(x)\varphi(x,t)\mathrm{d}x = 0. \tag{5.153}$$

With the above, the (nonlinearized) point kinetic equations can be derived by substituting Eqs. (5.150) and (5.151) into Eqs. (5.137) and (5.138), multiplying the resulting equations by the adjoint steady-state quantities $\phi_0^\dagger(x)$ and $C_0^\dagger(x)$, respectively, integrating for the whole reactor and subtracting the adjoint Eqs. (5.145) and (5.146) multiplied by $\psi(x, t)$ and $\varphi(x, t)$, correspondingly.

Then, define the fluctuations of the cross-sections as:

$$\nu\Sigma_f(x,t) = \nu\Sigma_f^0 + \delta\nu\Sigma_f(x,t), \tag{5.154}$$

$$\Sigma_a(x,t) = \Sigma_a^0 + \delta\Sigma_a(x,t). \tag{5.155}$$

However, our goal is to derive equations for the point kinetic component of the neutron noise, which is obtained as the fluctuation of the amplitude function. Hence we introduce the following linearization:

$$P(t) = P_0 + \delta P(t) = 1 + \delta P(t), \tag{5.156}$$

$$C(t) = C_0 + \delta C(t) = 1 + \delta C(t), \tag{5.157}$$

$$\psi(x,t) = \phi_0(x) + \delta\psi(x,t), \tag{5.158}$$

$$\varphi(x,t) = C_0(x) + \delta\varphi(x,t). \tag{5.159}$$

Then, using Eqs. (5.156)–(5.159) in the time-dependent and the static equations, neglecting the second-order terms and subtracting the static equations, the following point kinetic equations can be obtained:

$$\frac{\mathrm{d}}{\mathrm{d}t}\delta P(t) = -\frac{\overline{\beta}^{s}}{\Lambda}\delta P(t) + \overline{\lambda}^{s}\delta C(t) + \frac{\rho^{s}(t)}{\Lambda} + \lambda'(t) + \frac{\beta'(t)}{\Lambda}, \tag{5.160}$$

$$\frac{\mathrm{d}}{\mathrm{d}t}\delta C(t) + uS(t) = -\overline{\overline{\lambda}}^{s}\delta C(t) + \frac{\overline{\overline{\beta}}^{s}}{\Lambda}\delta P(t) + \beta\frac{\rho''^{s}(t)}{\Lambda} + \beta''(t) + \lambda''(t). \tag{5.161}$$

Here $\beta'(t)$, $\lambda'(t)$, $\beta''(t)$, and $\lambda''(t)$ depend on the fluctuations in the shape functions $\delta\psi(x,\ t)$ and $\phi(x,\ t)$ and defined as:

$$\lambda'(t) = \frac{\int_{-a}^{a}\phi_0^{\dagger}(x)\delta\varphi(x,t)\mathrm{d}x}{A_0}\lambda, \tag{5.162}$$

$$\beta'(t) = \frac{\int_{-a}^{a}C_0^{\dagger}(x)\delta\psi(x,t)\mathrm{d}x}{A_0}\beta, \tag{5.163}$$

$$\lambda''(t) = \frac{\int_{-a}^{a}\phi_0^{\dagger}(x)\delta\varphi(x,t)\mathrm{d}x}{E_0}\lambda, \tag{5.164}$$

$$\beta\lambda(t) = \frac{\int_{-a}^{a}C_0^{\dagger}(x)\delta\psi(x,t)\mathrm{d}x}{E_0}\beta, \tag{5.165}$$

with $A_0$ and $E_0$ being constants (Pázsit et al., 2014).

The above equations clearly show the difficulties described in the introduction. Although Eqs. (5.160) and (5.161) constitute a linear differential equation system for $\delta P(t)$ and $\delta C(t)$ from which, after a Fourier transform, $\delta P(\omega)$ can easily be expressed, this constitutes only a formal solution. As is seen, all functions in Eqs. (5.162)–(5.165) contain the fluctuations of the shape function in first order, which hence cannot be neglected, and which are unknowns. Thus, the solution cannot be calculated without making some assumptions about the unknown parameters. One such approximation is discussed in the next subsection.

It can also be shown (for the details, see Pázsit et al., 2014), that the reason for the presence of the first-order fluctuations of the shape function in the equations can be traced back to the nondisappearance of one term in the derivation, which arises due to the fact that the static adjoint does not fulfill the adjoint property with the time-dependent flux. Expressed with the shape function, this arises from the equality

$$\int_{-a}^{a}\phi_0^{\dagger}(x)\frac{\partial^2}{\partial^2 x}\psi(x,t)\mathrm{d}x = \int_{-a}^{a}\psi(x,t)\frac{\partial^2}{\partial^2 x}\phi_0^{\dagger}(x)\mathrm{d}x \tag{5.166}$$

$$\begin{aligned}\int_{-a}^{a} C_0^\dagger(x)\frac{\partial}{\partial x}\varphi(x,t)\mathrm{d}x &= [C_0^\dagger(x)\varphi(x,t)]_{-a}^{a} - \int_{-a}^{a}\varphi(x,t)\frac{\partial}{\partial x}C_0^\dagger(x)\mathrm{d}x \\ &= Q(t) - \int_{-a}^{a}\varphi(x,t)\frac{\partial}{\partial x}C_0^\dagger(x)\mathrm{d}x.\end{aligned} \tag{5.167}$$

One can easily show from the boundary conditions for the precursors, Eq. (5.140), reformulated to the shape function $\varphi(x, t)$ that $Q(t)$ is not zero, but it is more illuminating to discuss the same term at the level of the nonfactorized flux. The same equality reads then as

$$\int_{-a}^{a} C_0^\dagger(x)\frac{\partial}{\partial x}C(x,t)\mathrm{d}x = [C_0^\dagger(x)C(x,t)]_{-a}^{a} - \int_{-a}^{a} C(x,t)\frac{\partial}{\partial x}C_0^\dagger(x)\mathrm{d}x \tag{5.168}$$

and from the boundary conditions (5.140) and (5.148) this yields

$$[C_0^\dagger(x)C(x,t)]_{-a}^{a} = C_0^\dagger(a)[C(a,t) - C(a,t-\tau_L)] \neq 0. \tag{5.169}$$

In other words the static adjoint operator does not have the adjoint property against the time-dependent precursor distribution. It is also clear that if one replaces the space−time-dependent precursor distribution with the static one in (5.168), Eq. (5.169) becomes identically zero. In the time-dependent case, for the shape function, one obtains

$$[C_0^\dagger(x)\varphi(x,t)]_{-a}^{a} = \left[C_0^\dagger(a)\left[\varphi(a,t) - \varphi(a,t-\tau_L)\frac{C(t-\tau_L)}{C(t)}\right]\right] \neq 0. \tag{5.170}$$

### 5.6.3 Point kinetic equation with static fluxes

A straightforward way of deriving the point kinetic equations is to use the point kinetic approximation to the shape functions, that is to replace $\psi(x, t)$ and $\varphi(x, t)$ with the corresponding static fluxes $\phi_0(x)$ and $C_0(x)$, that is to assume (Lapenta et al., 2001)

$$\phi(x,t) = P(t)\phi_0(x), \tag{5.171}$$

and

$$C(x,t) = C(t)C_0(x). \tag{5.172}$$

In this case, the term $Q(t)$ in (5.167) becomes zero, but this is at the price that the boundary condition (5.140) cannot be fulfilled, since it would lead to

$$C(t)C_0(-a) = C(t-\tau_L)C_0(a)e^{-\lambda\tau_L}. \tag{5.173}$$

It is easy to show that in general this condition cannot be fulfilled and it cannot be imposed on the resulting point kinetic equations. The absence of the boundary conditions will be the reason for the absence of the characteristic structure of the amplitude function in the frequency domain, which will be seen in the exact solution. The fact that the boundary condition cannot be fulfilled is the result of the previously mentioned fact that the propagation property and the factorization of the space and time dependence are not compatible.

Turning now to the fluctuations of the amplitude functions, we split up the time-dependent quantities into expectation and fluctuating parts as

$$P(t) = P_0 + \delta P(t), \tag{5.174}$$

$$C(t) = C_0 + \delta C(t). \tag{5.175}$$

In view of Eqs. (5.171) and (5.172) one can assume $P_0 = 1$. The linearized point kinetic equations are obtained as

$$\frac{d}{dt}\delta P(t) = \frac{\rho^s(t)}{\Lambda} - \frac{\overline{\beta}^s}{\Lambda}\delta P(t) + \overline{\lambda}^s \delta C(t), \tag{5.176}$$

$$\frac{d}{dt}\delta C(t) = \frac{\overline{\overline{\beta}}^s}{\Lambda}\delta P(t) + \frac{\beta \rho''^s}{\Lambda} - \overline{\overline{\lambda}}^s \delta C(t). \tag{5.177}$$

After a temporal Fourier transform one arrives to the solution

$$\delta P(\omega) = G_0(\omega)(\rho^s(\omega) + \rho^{s1}), \tag{5.178}$$

where

$$G_0(\omega) = \frac{1}{\iota\omega\left(\Lambda + \dfrac{\overline{\beta}}{\iota\omega + \overline{\overline{\lambda}}}\right)} \tag{5.179}$$

$$\rho^{s1}(\omega) = \rho''^s(\omega)\frac{\lambda\beta}{\iota\omega + \overline{\overline{\lambda}}}. \tag{5.180}$$

It is seen that this solution contains a zero power transfer function whose frequency dependence is exactly the same as that of the traditional systems. The only difference is the appearance of an extra term in the expression of the reactivity. This solution will not be able to reproduce the periodic peaks of the true solution, which accounts for the return of the delayed neutron precursors to the core, and which were already seen in Fig. 5.6.

However, this solution is the only one which can be concretely calculated, hence it is the one which we will compare with the exact solution, derived from the full space–time (frequency)-dependent solution. It also has to be added that some empirical modifications of the point kinetic equations were introduced to account for this effect. For instance, in Lapenta et al. (2001) a term, similar in form to the neglected term in our Eq. (5.169) but expressed only with the amplitude function, was added. These do not supply a solution which is correct to the first order of the perturbation (Pázsit et al., 2009).

### 5.6.4 Derivation of the point kinetic component from the full solution

The fluctuations of the amplitude function can be determined from the full space–frequency-dependent solution by the Green's function technique. Actually, assuming a localized perturbation (in the form of a spatial Dirac-delta function) the induced noise will be proportional to the Green's function. Splitting the space–time-dependent quantities into a pure space-dependent mean value and a space–time-dependent fluctuating part, i.e.,

$$\Sigma_a(x,t) = \Sigma_a + \delta\Sigma_a(x,t) = \Sigma_a + \delta(x - x'), \tag{5.181}$$

$$\nu\Sigma_f(x,t) = \nu\Sigma_f + \delta\nu\Sigma_f(x,t), \tag{5.182}$$

$$\phi(x,t) = \phi_0(x) + \delta\phi(x,t), \tag{5.183}$$

$$C(x,t) = C_0(x) + \delta C(x,t). \tag{5.184}$$

Following the usual steps of substituting Eqs. (5.181)–(5.184) into (5.137) and (5.138), subtracting the static equations, neglecting second-order terms such as $\delta\Sigma a$ $(x,\ t)\delta\phi(x,\ t)$, and eliminating the equation for the precursor density by a temporal Fourier transform, one arrives at the following matrix noise equations:

$$\begin{pmatrix} \dfrac{\partial^2}{\partial^2 x} + B^2(\omega) & \dfrac{\lambda}{D} \\ -\beta\nu\Sigma_f^0 & u\dfrac{\partial}{\partial x} + (\iota\omega + \lambda) \end{pmatrix} \begin{pmatrix} \delta\phi(x,\omega) \\ \\ \delta c(x,\omega) \end{pmatrix} = \begin{pmatrix} \dfrac{\delta(x - x')\phi_0(x)}{D} \\ \\ 0 \end{pmatrix}, \tag{5.185}$$

where the frequency-dependent buckling $B^2(\omega)$ is defined as

$$B^2(\omega) = \frac{\nu\Sigma_f^0(1 - \beta) - \Sigma_a^0 - \dfrac{i\omega}{v}}{D}. \tag{5.186}$$

For simplicity, in the continuation it is assumed that only the absorption cross-section is perturbed. Then the corresponding matrix equation for the Green's function reads as

$$\begin{pmatrix} \dfrac{\partial^2}{\partial^2 x} + B^2(\omega) & \dfrac{\lambda}{D} \\ -\beta\nu\Sigma_f^0 & u\dfrac{\partial}{\partial x} + (\iota\omega + \lambda) \end{pmatrix} \begin{pmatrix} \delta G_\phi(x,\omega) \\ \delta G_C(x,\omega) \end{pmatrix} = \begin{pmatrix} \delta(x - x') \\ 0 \end{pmatrix}. \tag{5.187}$$

The solution to Eq. (5.187) can be obtained analytically, as described in the previous subsection with the usual techniques. Now, using the factorization (5.150)–(5.151) with the linearization (5.156)–(5.159), neglecting second-order terms, one obtains for the neutron noise

$$\delta\phi(x,\omega) = \delta P(\omega)\phi_0(x) + \delta\psi(x,\omega), \tag{5.188}$$

$$\delta C(x,\omega) = \delta C(\omega)C_0(x) + \delta\varphi(x,\omega). \tag{5.189}$$

Here the first term is the point kinetic component, and the second the space-dependent one. In order to obtain the point kinetic components, both sides of Eqs. (5.188)–(5.189) are multiplied by the adjoint fluxes $\phi_0^\dagger(x)$ and $C_0^\dagger(x)$, respectively. Then, integrating over the whole reactor and taking into account the normalization conditions (5.152)–(5.153), the following explicit expressions for $\delta P(\omega)$ and $\delta C(\omega)$ can be obtained:

$$\delta P(\omega) = \frac{\int_{-a}^{a} \phi_0^\dagger(x)\delta\phi(x,\omega)\mathrm{d}x}{\int_{-a}^{a} \phi_0^\dagger(x)\phi_0(x)\mathrm{d}x}, \tag{5.190}$$

$$\delta C(\omega) = \frac{\int_{-a}^{a} C_0^\dagger(x)\delta C(x,\omega)\mathrm{d}x}{\int_{-a}^{a} C_0^\dagger(x)C_0(x)\mathrm{d}x}. \tag{5.191}$$

These can be calculated with the usual techniques.

The above expressions can be evaluated quantitatively, since they only contain known quantities. The result can be compared with the solution (5.178) of the point kinetic equations.

Such a comparison is shown in Fig. 5.8, which displays the two zero power reactor transfer functions, i.e., the one calculated from the full space–frequency solution (for simplicity we call it $G_0^{Exact}$) and the one calculated from the point kinetic equations (see Eq. (5.178), for simplicity we call it $G_0^{Approx}$). The function $G_0^{Exact}$ shows the characteristic peaks at frequencies equal to the inverse of the *total* recirculation time $\tau_L$, as one can expect from the physics of the process. The solution $G_0^{Approx}$ is completely smooth and does not show any peaks. It can be mentioned that to compensate for this deficiency of the simplified point kinetic equations, an

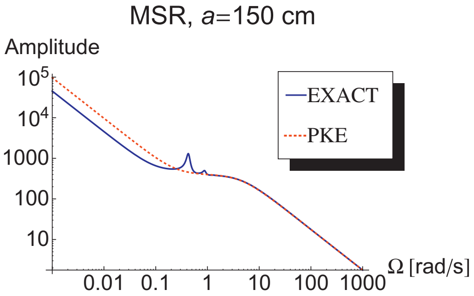

**Figure 5.8** Comparison between frequency dependence of amplitude of zero transfer functions as calculated from the full solution (red dotted line) and calculated from point kinetic equations (blue line) for H = 300 cm, $L = 400$ cm, $u = 50$ cm/s, $x = 0$ cm, $x_0 = 0$ cm (source position).

empirical form of the point kinetic equation was suggested in several publications (Dulla, 2005; Zhang et al., 2009). These equations indeed lead to a transfer function that has some minor peaks at certain frequencies. However, as was discussed in Pázsit et al. (2009), neither the position, nor the amplitude of those peaks correspond to the correct ones, given by the exact solution.

Another difference between the two transfer functions is that they differ by about a factor of 2 at low frequencies, and are equal to each other only at higher frequencies, from the upper part of the plateau region. This fact is due to the neglection of first-order terms when calculating the coefficients of the point kinetic equation.

It is thus seen that for the molten salt reactor equations, the derivation of the point kinetic equations for the neutron noise which supply results that are accurate in first order, faces some difficulties. A linearization of the equations obtained by the factorization technique leads to an equation in which certain terms contain the fluctuations of the shape functions, which are not known. If these terms are neglected, including the one which guarantees the fulfilment of the boundary conditions for the delayed neutron precursors, the solution becomes inaccurate. This latter was shown by calculating the point kinetic component from the full space—frequency-dependent solution by projecting it to the static adjoint flux. This shows that the molten salt reactor equations are not suitable to derive point kinetic equations which yield the correct point kinetic component.

## 5.7 The neutron noise in an MSR, induced by propagating perturbations

In traditional light-water reactors, the propagation of the coolant, through its non-completely homogeneous structure, represents a perturbation which has the property of propagating through the core. In pressurized water reactors (PWRs), the small fluctuations of the inlet temperature, affecting, e.g., the absorption cross-sections, represents a propagating perturbation whose effect on the neutron flux can be measured. Such propagating perturbations and their effect on the neutron noise were studied before (Kosály and Williams, 1971; Kosály and Meskó, 1972; Wach and Kosály, 1974). In these earlier works, the neutron noise was only calculated in the point kinetic approximation. The space dependence was calculated only very recently (Pázsit and Dykin, 2010). This interest was clearly triggered by the renewed interest in molten salt reactors, in which such perturbations will be present in a stronger form than in a PWR, since it will be the properties of the propagating fuel that will have some random variations in contrast to those of the coolant in a PWR. However, the neutronic response of the MSR will also be different, as we have already seen at the level of the Green's function. So the space-dependent neutron noise due to propagating perturbations is interesting both in traditional reactors and in the MSR.

The propagating perturbation can be represented as

$$\delta\Sigma_a(z,t) = \delta\Sigma_a(0, t - z/u), \tag{5.192}$$

and thus in the frequency domain one has

$$\delta\Sigma_a(z,\omega) = e^{-\frac{i\omega z}{u}}\delta\Sigma_a(0,\omega). \tag{5.193}$$

Here the process $\delta\Sigma_a(z=0,\ t)$, i.e., the perturbation at the inlet of the core, is usually considered as a white noise process, so the frequency dependence of its autospectrum is constant. This is often represented such that $\delta\Sigma_a(0,\ \omega)$ is taken as a constant, although strictly speaking it is only valid for its autospectrum. This latter is, however, calculated by the Wiener–Khinchin theorem as its own absolute value squared, so the assumption of $\delta\Sigma_a(0,\ \omega)$ being constant does not lead to any contradictions. Hence in the continuation we set $\delta\Sigma_a(0,\ \omega) = 1$.

As is known (Kosály and Meskó, 1972), the reactivity effect of such a perturbation, calculated as

$$\rho(\omega) = \frac{\int \phi_0^2(z)\delta\Sigma_a(z,\omega)\mathrm{d}z}{\nu\Sigma_f\int \phi_0^2(z)\mathrm{d}z} \tag{5.194}$$

shows a characteristic, periodic sink structure, i.e., it has zeros ("sinks") at

$$\omega = \frac{2\pi u}{H}n = \frac{2\pi}{\tau_c}n; \quad n = 2, 3\ldots, \tag{5.195}$$

where $\tau_c$ is the transit time of the fuel (coolant) through the core. This sink structure of the reactivity, which immediately affects the frequency dependence of the induced neutron noise, especially in the case of point kinetic behavior, will be used to interpret the results from the space-dependent calculations.

The space-dependent noise can be calculated by the help of Green's function, which we determined earlier. The noise is then given as

$$\delta\phi(z,\omega) = \int_{-a}^{a} G(z,z_0,\omega) e^{\frac{-i\omega z_0}{u}} \phi_0(z_0) \mathrm{d}z_0. \tag{5.196}$$

A few characteristic results will be shown for illustration. The frequency dependence of the noise in a small system is shown in Fig. 5.9 as measured in the center of the system. Such a small system is assumed to behave in a point kinetic manner up to high frequencies (especially in the MSR which, as it was noticed, behaves more point kinetically than a corresponding traditional system). Hence the resulting noise shows the sink structure of the reactivity, modulated by the frequency dependence of the transfer function, which is seen in Fig. 5.6. Also the ripples at low frequency can be seen, although less visibly, due to the linear plot in the x-axis in this figure. For the large system (Fig. 5.10), the situation is rather different. At low frequencies, the ripples due to the fuel recirculation are still visible. However, the sink structure at higher frequencies is rather different and less marked. Moreover, the frequency dependence is different in different parts of the reactor, as is seen in the figure which shows the noise in two different points of the reactor.

The diminishing of the sink structure is largely due to the less dominant contribution from the point kinetic components, since it is only this component which has the sink structure. The further deviations below the plateau frequencies can be partly understood from the interference between the point kinetic and space-dependent components of the induced noise, as was discussed in a companion paper, dealing with the space-dependent effect of propagating perturbations in traditional reactors (Pázsit and Dykin, 2010). This interference arises from the fact that

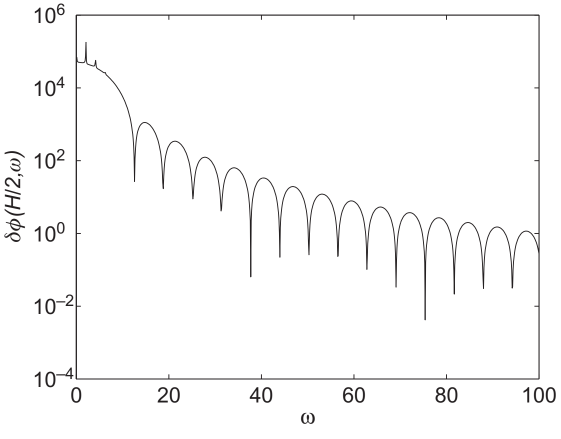

**Figure 5.9** The frequency dependence of the neutron noise induced by a propagating perturbation in a small system ($H = 50$ cm)

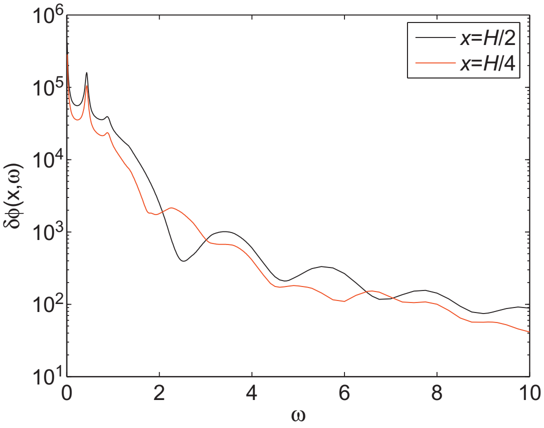

**Figure 5.10** The frequency dependence of the neutron noise induced by a propagating perturbation in two different points in a large system ($H = 300$ cm).

the point kinetic component has a uniform phase across the whole core, whereas the phase of the space-dependent term follows that of the perturbation. As seen from (5.193), the phase of the latter is

$$\varphi = \frac{\omega}{u} z,$$

i.e., it changes linearly with the position in the core. Hence the two components are at certain points in-phase, and at some other points out-of-phase, leading to constructive and destructive interference, respectively. The result is the somewhat complicated frequency behavior seen in Fig. 5.10.

Further insight can be gained by investigating the space dependence of the noise for different frequencies. We show this space dependence in the large system at four different frequencies. In Fig. 5.11A the space dependence is shown for a low frequency. At this frequency the system behaves in a point kinetic manner, hence the amplitude of the noise follows the shape of the static flux.

At the higher frequency of $\omega = 10$ rad/s (Fig. 5.11D), which is in the middle of the plateau region, the space dependence suddenly shows local maxima and minima, although the space dependence of both the point kinetic and the space-dependent parts is smooth and similar to the static flux. As was mentioned before and is discussed in detail in Pázsit and Dykin (2010), the maxima correspond to the core positions where the point kinetic and space-dependent terms are in-phase, and the local minima to the points where they are out-of-phase. The reason that no such nonmonotonic behavior is seen at low frequency is partly that at lower frequency the spatial oscillations of the phase of the space-dependent term are much slower, and more importantly, the point kinetic component dominates and hence the interference has no effect. At the plateau frequency, shown in Figs. 5.11C,D, the point

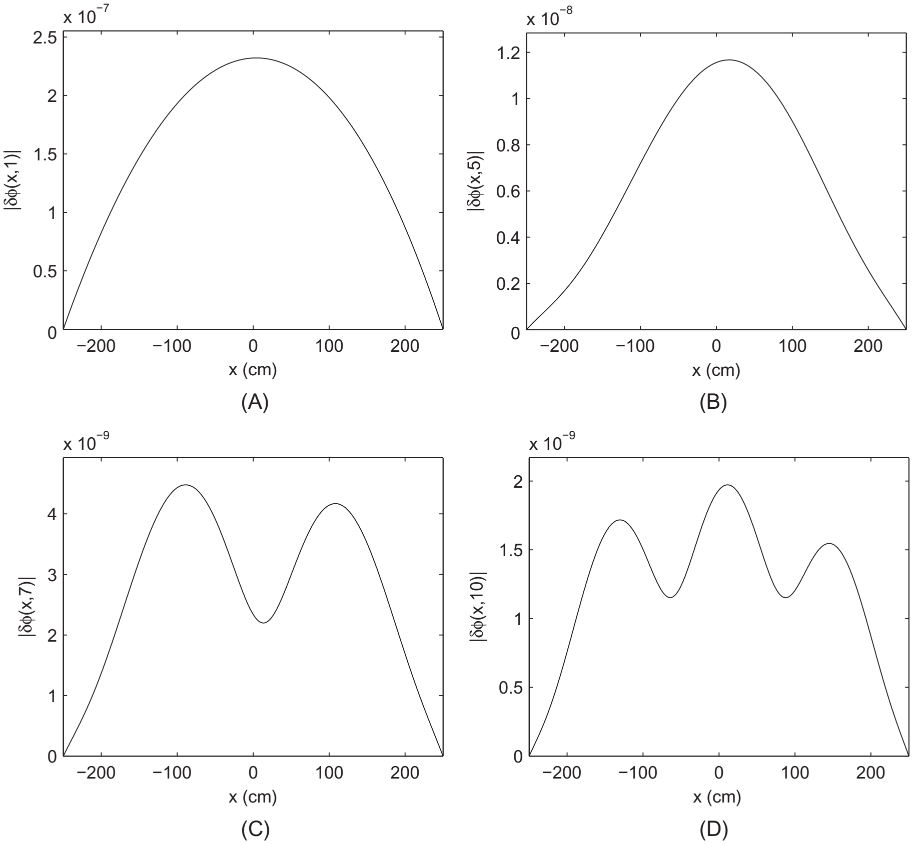

**Figure 5.11** Comparison between the neutron noise space dependence for different frequencies in a large system ($H = 500$ cm, $v = 250$ cm/s). (A) $\omega = 1$ rad/s; (B) $\omega = 5$ rad/s; (C) $\omega = 7$ rad/s; (D) $\omega = 10$ rad/s.

kinetic component has decreased such that the two components are comparable in amplitude. This is why the spatially oscillatory behavior of the noise is so marked. At even higher frequencies, the point kinetic term decreases further, and the spatial behavior becomes smooth again, because it is dominated by the space-dependent component alone.

It is also interesting to make a comparison with traditional systems. As is shown in Pázsit and Dykin (2010), in a traditional system of the same size, at the plateau frequency, the noise is dominated by the space-dependent component, hence the interference and the spatially oscillatory behavior of the noise is largely absent. It can only be observed at much lower frequencies in the large system. The fact that this interference of the two components exists at plateau frequencies in an MSR is a further indication of the fact that an MSR behaves in a more point kinetic manner than a corresponding traditional system.

## 5.8 Conclusions

As was seen, the physics and the dynamic behavior of an MSR comprises a number of interesting new questions and results. The spatial redistribution of the precursors and their partial decay outside the core has the effect that the noise level increases in the system, and the spatial coupling becomes tighter, leading to an increase in the contribution from the point kinetic component of the noise. While in a traditional power reactor the reactivity term is relatively insignificant at plateau frequencies, in an MSR of comparable size the point kinetic term is still comparable with the space-dependent one. This fact will influence the possibilities of the diagnostic methods, such as localizing noise sources, etc. The observation on increased noise amplitudes in an MSR has, by extrapolation, a relevance to all cores containing minor actinides with smaller fractions of delayed neutrons, in that higher noise amplitudes can be expected in all such systems.

It has to be emphasized that all deviations between a traditional system and an MSR in this study are solely due to the movement of the fuel, and not to the differing material composition of an MSR. In this simple study the two systems were compared by using similar material properties, to concentrate on the differences that are only attributed to the movement of the fuel. Further differences may be expected if the proper material properties of an MSR are taken into account, such as a smaller delayed neutron fraction. In a core with a fast spectrum, the present one-group treatment has to be replaced with a two-group approximation.

## Acknowledgment

The authors are indebted to Dr. Jiri Krepel of PSI, Prof. Piero Ravetto of the University of Turin, Prof. Jan Leen Kloosterman of TU Delft, and Prof. Xinrong Cao of Harbin Engineering University for interesting discussions and their useful advice regarding the manuscript, which is very much appreciated.

## References

Bell, G., Glasstone, S., 1970. Nuclear Reactor Theory. Van Nostrand Reinhold Company, New York.

Cammi, A., Di Marcello, V., Luzzi, L., Memoli, V., Ricotti, M.E., 2011. A multi-physics modelling approach to the dynamics of molten salt reactors. Ann. Nucl. Energy. 38 (6), 1356–1372.

Delpech, M., Dulla, S., Garzenne, C., Kóphazi, J., Krepel, J., Lebrun, C., et al., 2003. Benchmark of dynamic simulation tools for molten salt reactors. International Conference Global 2003, pp. 2182–2187, New Orleans, 2003. American Nuclear Society.

Dulla, S., 2005. Models and methods in the neutronics of fluid fuel reactors. PhD thesis. Graduate School of Nuclear Engineering, University of Turin.

Dulla, S., Ravetto, P., Rostagno, M.M., 2004. Neutron kinetics of fluid-fuel systems by the quasi-static method. Ann. Nucl. Energy. 31 (15), 1709.

Dulla, S., Ravetto, P., Rostagno, M.M., Bianchini, G., Carta, M., D'Angelo, A., 2005. On some features of spatial neutron kinetics for multiplying systems. Nucl. Sci. Eng. 1 (149), 88.

Dykin, V., Pázsit, I., 2016. The molten salt reactor point-kinetic component of neutron noise in two-group diffusion theory. Nucl. Technol. 193 (3), 404−415.

Dykin, V., Pázsit, I., Sanchez, R., 2016. Remark on the neutron noise induced by propagating perturbations in an MSR. Ann. Nucl. Energy. 90, 93−105.

Jonsson, A., Pázsit, I., 2011. Two-group theory of neutron noise in molten salt reactors. Ann. Nucl. Energy. 38 (6), 1219−1446.

Kosály, G., Meskó, L., 1972. Remarks on the transfer function relating inlet temperature fluctuations to neutron noise. Atomkernenergie. 20, 33.

Kosály, G., Williams, M.M.R., 1971. Point theory of the neutron noise induced by inlet temperature fluctuations and random mechanical vibrations. Atomkernenergie. 18, 203.

Krepel, J., 2006. Dynamics of Molten Salt Reactors. PhD thesis. Institute of Safety Research, Research Centre Rossendorf, Dresden.

Krepel, J., Grundmann, U., Rohde, U., Weiss, F.-P., 2005. DYN1D-MSR dynamics code for molten salt reactors. Ann. Nucl. Energy. 32 (17), 1799−1824.

Krepel, J., Rohde, U., Grundmann, U., Weiss, F.-P., 2007. DYN3D-MSR spatial dynamics code for molten salt reactors. Ann. Nucl. Energy. 34 (6), 449−462.

Krepel, J., Rohde, U., Grundmann, U., Weiss, F.-P., 2008. Dynamics of molten salt reactors. Nucl. Technol. 164 (15), 34−44.

Krepel, J., Hombourger, B., Fiorina, C., Mikityuk, K., Rohde, U., Kliem, S., et al., 2014. Fuel cycle advantages and dynamics features of liquid fueled MSR. Ann. Nucl. Energy. 64, 380−397.

Lapenta, G., Ravetto, P., 2000. Basic reactor physics problems in fluid-fuel recirculated reactors. Kerntechnik. 65 (5-6), 250−253.

Lapenta, G., Mattioda, F., Ravetto, P., 2001. Point kinetic model for fluid fuel systems. Ann. Nucl. Energy. 31 (15), 1709.

Lecarpentier, D., Carpentier, V., 2003. A neutronics program for critical and nonequilibrium study of mobile fuel reactors: the Cinsf1D code. Nucl. Sci. Eng. 143, 3346.

MacPhee, J., 1958. The kinetics of circulating fuel reactors. Nucl. Sci. Eng. 4, 588.

Mattioda, F., Ravetto, P., Ritter, G., 2000. Effective delayed neutron fraction for fluid-fuel systems. Ann. Nucl. Energy. 27 (16), 1523−1532.

Merle-Lucotte, E., Heuer, D., Allibert, M., Brovchenko, M., Capellan, N., Ghetta, V. Launching the thorium fuel cycle with the molten salt fast reactor. In ICAPP 2011 International Congress on Advances in Nuclear Power Plants (ICAPP 2011), Nice; France, May 2−5 2011. Paper No. 11190.

Pázsit, I., Jonsson, A., 2011. Reactor kinetics, dynamic response and neutron noise in molten salt reactors (MSR). Nucl. Sci. Eng. 167, 61−76.

Pázsit, I., Demazière, C., 2010. Noise Techniques in Nuclear Systems, volume 2 of Handbook of Nuclear Engineering. Springer Science.

Pázsit, I., Dykin, V., 2010. Investigation of the space-dependent noise induced by propagating perturbations. Ann. Nucl. Energy. 37 (10), 1329−1340.

Pázsit, I., Wihlstrand, G., Tambouratzis, T., Jonsson, A., Dahl, B., 2009. Research and development program in reactor diagnostics and monitoring with neutron noise methods, stages 14 and 15. Technical Report 2009:38, Swedish Radiation Safety Authority.

Pázsit, I., Jonsson, A., Pál, L., 2012. Analytical solutions of the molten salt reactor equations. Ann. Nucl. Energy. 50, 206−214.

Pázsit, I., Dykin, V., Sanchez, R., 2014. The point kinetic component of neutron noise in an MSR. Ann. Nucl. Energy. 64, 344–352.

Wach, D., Kosály, G., 1974. Investigation of the joint effect of local and global driving sources in incore-neutron noise measurements. Atomkernenergie. 23, 244.

Wang, J., Cao, X., 2015. Characters of neutron noise in full-size molten salt reactor. Ann. Nucl. Energy. 81, 179–187.

Wang, J., Cao, X., 2016a. Applicability of adiabatic approximation on neutron noise analysis in molten salt reactor. Ann. Nucl. Energy. 92, 295–303.

Wang, J., Cao, X., 2016b. Investigation on fluctuations in a full-size molten salt reactor with coupled neutronic/thermal-hydraulic model. Ann. Nucl. Energy. 92, 262–276.

Wang, J., Cao, X., Sun, X. Characters of coupled dynamics in molten salt reactor with perturbation theory. In *Proceedings of 23rd International Conference on Nuclear Engineering*, volume 104, p. 850, Chiba, Japan, May 17–21 2015. on CD-ROM.

Wang, S., Rineiski, A., Maschek, W., 2006. Molten salt related extensions of the SIMMER-III code and its application for a burner reactor. Nucl. Eng. Des. 236, 5801588.

Yoshioka, H., Pázsit, I., Otake, H., Nishina, K., 1998. Analysis of temporal and spatial decay of pulsed neutrons in single- and multiple-core systems. Ann. Nucl. Energy. 25 (14), 1169–1189.

Zhang, D., Rineiski, A., Qiu, S., 2009. Comparison of modeling options for delayed neutron precursor movement in a molten salt reactor. Trans. Am. Nucl. Society. 100, 639–640.

Zhang, D.L., Qiu, S.Z., Su, G.H., Liu, C.L., Qian, L.B., 2009. Analysis on the neutron kinetics for a molten salt reactor. Progr. Nucl. Energy. 51 (4-5), 624–636.

# Thermal hydraulics of liquid-fueled MSRs

# 6

*Lelio Luzzi*[1], *Antonio Cammi*[1], *Valentino Di Marcello*[1,2]
*and Alessandro Pini*[1]
[1]Polytechnic University of Milan, Milan, Italy, [2]Karlsruhe Institute of Technology—KIT, Karlsruhe, Germany

## Chapter Outline

## 6.1 Introduction

Liquid-fueled molten salt reactors (MSRs) are usually considered nonclassical reactor types because of the specific nature of the fuel, which is typically constituted by a molten fluoride salt mixture circulating in the primary circuit. The fission material (uranium and/or transuranium elements) is dissolved in the molten salt carrier, which also acts as coolant. Thanks to the potentialities of this liquid fuel, several MSR concepts were investigated at Oak Ridge National Laboratory in the past (see www.energyfromthorium.com/pdf/), and in recent years MSRs have been the subject of renewed interest in the framework of Generation IV nuclear reactors (GIF, 2002, 2014; Serp et al., 2014; IRSN, 2015). These concepts differ mainly by neutron balance (critical or subcritical), neutron spectra (thermal, epithermal, or fast), the presence/absence of the graphite matrix as moderator, and the fuel salt chemical composition.

The physics of circulating nuclear fuels involves a strong coupling between neutronics and thermo-hydrodynamics, which would require in general the adoption of a

**Molten Salt Reactors and Thorium Energy. DOI: http://dx.doi.org/10.1016/B978-0-08-101126-3.00006-3**

multiphysics modeling approach (e.g., see, Luzzi et al., 2012b, and also Chapter 25, Research activities of this book). However, in this chapter, analyses are performed assuming that the neutronic term is decoupled from fluid dynamics, and appears like a heat source within the fuel/coolant molten salt. The aim is to investigate only the thermo-hydrodynamic behavior. Reference is made to a simple axial-symmetric cylindrical geometry representative of a typical graphite-moderated MSR power channel, taking into account the thermodynamic and transport properties of the molten salt as well as its local flow conditions and heat transfer. Even if this assumption simplifies the equations to be solved, the thermo-hydrodynamic behavior of the molten salt remains complex. In this context, a preliminary analytic approach (Di Marcello et al., 2008) to evaluate the temperature radial profile in both fuel and graphite is reported in Sections 6.2 and 6.3, which are intended to offer the reader a useful validation framework for testing more sophisticated computer codes, in view of their adoption for more realistic and complex 3-D geometry analyses.

The circulating ″already molten″ fuel offers positive peculiarities to be exploited in the safety approach as well as in the fuel cycle of liquid-fueled MSRs (LeBlanc, 2010; Luzzi et al., 2012a; Křepel et al., 2014). For instance, the fluid nature of the fuel means that the reactor core meltdown is an irrelevant instance. Moreover, the reactor has almost no excess of nuclear reactivity, which reduces the risk of accidental reactivity insertion. On the contrary, the decay heat produced by the liquid fuel dissolved into the molten salt and distributed along a closed loop may impair the natural circulation features, leading to an undesired behavior of the reactor. Actually, natural circulation in the presence of internal heat generation (IHG) is characterized by a particular dynamics that needs to be carefully studied. In this context, Section 6.4 presents a preliminary investigation of IHG effects on natural circulation, with reference to the stability maps of single-phase rectangular loops.

## 6.2 Preliminary approach to thermo-hydraulics of internally heated molten salts

This section presents a preliminary approach to the thermo-hydraulics of internally heated molten salts useful to assess and compare the numerical solutions achievable by different computer codes. Below, we have chosen for the computational fluid dynamics (CFD) analyses a finite element software (COMSOL Multiphysics) and a finite volume software (FLUENT). The validation framework adopts the well-established analytic solution of flow in long smooth pipes, both in laminar and turbulent regimes, and has been set up in analogy with other works performed for innovative reactors, like the supercritical water reactor (Yang et al., 2007) and the accelerator-driven system (Cheng and Tak, 2006). It can be also an “excellent building-block case for testing turbulence models” (Wilcox, 2006), but such investigation is outside the scope of the present section.

### 6.2.1 Analytic Framework for Validation Purposes

We refer to the analytic solution of the radial temperature profile, in the presence of a volume-heat source within the fluid, for a circular-pipe system in cylindrical coordinates ($r$, $\theta$, $z$) in the case of both laminar and turbulent flow. The solution was found by Poppendiek (1954) under the following assumptions:

- Axial-symmetric conditions are taken into account.
- Thermal and hydrodynamic patterns are established (long pipes).
- Fluid axial conduction is neglected.
- Steady state exists.
- Uniform volume-heat source exists within the fluid.
- Physical properties are not a function of temperature.
- Heat is transferred uniformly to or from the fluid at the pipe wall.
- In the case of turbulent flow, an analogy exists between heat and momentum transfer.

Under the above assumptions, the differential Eq. (6.1) and the boundary conditions in Eqs. (6.2) and (6.3) describing the heat transfer in the pipe system for laminar or turbulent flow can be written according to the following 1-D formulation:

$$\frac{d}{dr}\left[(\alpha+\varepsilon)r\frac{dT(r)}{dr}\right]=\frac{u(r)}{u_m\rho c_P}\left[q'''-\frac{2}{r_0}q''_W\right]r-\frac{q'''r}{\rho c_P} \tag{6.1}$$

$$q''_W=-\lambda(dT/dr)\big|_{r=r_0} \tag{6.2}$$

$$T(r=r_D)=T_D \tag{6.3}$$

where $T$ is the fluid temperature, function of the radial coordinate $r$; $\alpha$, $\lambda$, $\rho$, and $c_P$ are the thermal diffusivity, the thermal conductivity, the density and the specific heat capacity of the fluid, respectively; $\varepsilon$ is the fluid eddy diffusivity, function of both the radial coordinate and the axial component of the fluid velocity $u(r)$; $u_m$ is the mean fluid velocity; $r_0$ is the pipe radius; $q'''$ and $q''_W$ are the volume-heat source and the uniform wall-heat flux, respectively. The second boundary condition, expressed by Eq. (6.3), is some reference temperature $T_D$ such as wall, center-line, or mixed-mean fluid temperature ($r_D$ being the radial coordinate at which $T_D$ is evaluated).

As far as CFD simulations are concerned, steady-state conditions are considered with reference to a 2-D axial-symmetric ($r$,$z$) computational domain. It is assumed that the fluid is incompressible, homogeneous, and its physical properties are not a function of temperature. Moreover, the action of gravity is neglected. For the analyses in turbulent regime, the standard *$k$—$\varepsilon$ model* has been selected, which is the two-equation model most widely used as reference among the several turbulence models available in the literature (Wilcox, 2006).

As for the modeling of the near-wall region, in the COMSOL simulations we have adopted the *logarithmic wall-functions*, assuming that the computational domain begins at a certain distance, which depends on the mesh size, from the real wall. Instead, for FLUENT calculations, the *enhanced wall treatment* approach has been chosen.

Great effort was spent in setting up the mesh elements/cells size, particularly at walls and interfaces, by means of a mesh sensitivity analysis that is not reported here for brevity. It must be noted that, even for the simple circular-pipe geometry herein adopted as validation framework, the accuracy of numerical results depends on the fluid properties, on the meshing strategy and on the turbulence model, as clearly demonstrated by analogous studies performed for other fluids in the same geometry (Cheng and Tak, 2006; Yang et al., 2007).

Concerning the numerical strategy, the *segregated algorithm* has been used in both codes. A complete description of the fluid flow modeling and of the different available options is given in the FLUENT and COMSOL user's guides (COMSOL, 2007; FLUENT, 2005).

### 6.2.2 Laminar flow

The solution of the boundary-value problem defined by Eqs. (6.1), (6.2), and (6.3) was achieved by Poppendiek (1954) in the case of laminar flow, considering that the eddy diffusivity is null in laminar regime and the fluid velocity attains a parabolic profile along the pipe radius once the hydrodynamic pattern is established. The solution is given by Eq. (6.4):

$$\frac{T(r)-T_C}{q'''r_0^2/2\lambda}=\frac{2F-1}{2}\left(\frac{r}{r_0}\right)^2-\frac{F}{4}\left(\frac{r}{r_0}\right)^4 \tag{6.4}$$

where $T_C$ is the center-line temperature and $F=1-(2q''_W/q'''r_0)$, namely {1 − fraction of heat generated within moving fluid that is transferred at wall} (El-Wakil, 1978).

The dimensionless radial temperature profile given by Eq. (6.4) is plotted in Fig. 6.1 for several values of the function $F$, and is compared with the CFD simulation results obtained by means of COMSOL and FLUENT. As can be noticed, both numerical solutions are practically superimposed on the analytic one.

### 6.2.3 Turbulent flow

For the case of turbulent flow, the boundary-value problem defined by Eqs. (6.1), (6.2), and (6.3) can be separated into the following two simpler boundary-value problems, whose solutions can be superimposed to yield the solution of the "original problem":

1. A problem representing a flow-system with a volume-heat source, but with no wall-heat flux.
2. A problem representing a flow-system without a volume-heat source, but with a uniform wall-heat flux.

The solution for the first problem (1) was found by Poppendiek (1954) with the following procedure. At first, the radial heat flux profile is calculated assuming that the velocity profile may be satisfactorily represented by two regions (a laminar

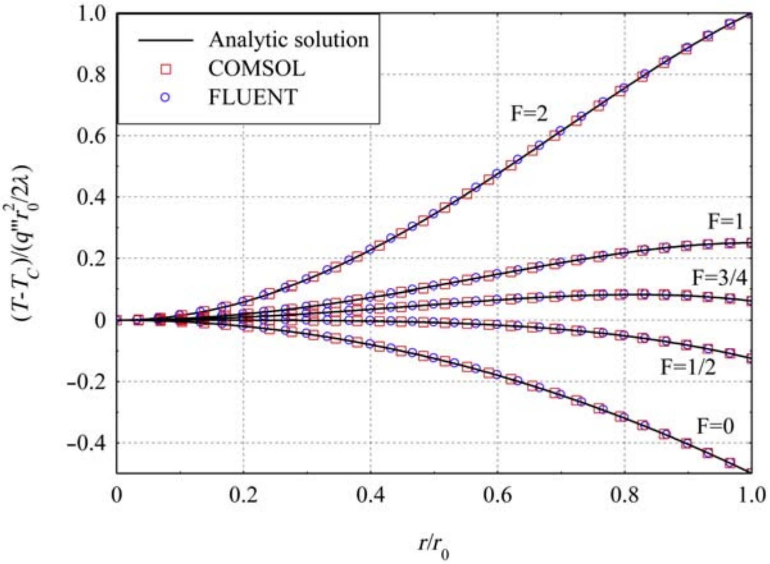

**Figure 6.1** Comparison between the different evaluations of the dimensionless radial temperature profile in a pipe with laminar flow.

layer and a turbulent core with the so-called "venerable" one-seventh power law for the velocity; see Nikuradse, 1950; De Chant, 2005). Therefore, the radial heat flux is replaced with simple monomials and polynomials, and is integrated layer by layer (laminar sublayer, buffer layer, outer turbulent layer, and inner turbulent layer) to find the radial temperature profile. The dimensionless radial temperature profile turns out to be a function of both Reynolds (*Re*) and Prandtl (*Pr*) numbers (Martinelli, 1947; Poppendiek, 1954).

The solution for the second problem (2) was originally found by Martinelli (1947) assuming three layers (laminar sublayer, buffer layer, turbulent layer) for the calculation of both the velocity and the temperature profiles. It is worth mentioning that in the buffer and turbulent layer Martinelli preferred a logarithmic law for the velocity based on experimental data (i.e., the so-called generalized velocity profile). In the present work, we follow an alternative analytic solution based on the same approach of Poppendiek, briefly described above for the problem (1), adopting the one-seventh power law for the velocity and the same four layers of Poppendiek for the radial temperature. The comparison between the Martinelli and the present work approaches is shown in Fig. 6.2 in terms of the temperature difference with respect to the center-line pipe temperature as a function of the dimensionless distance $n$ from the pipe wall ($n \equiv 1-r/r_0$). The two approaches substantially agree with little differences at lower Reynolds numbers and in the center of the pipe.

The temperature profile of the "original problem" can be easily achieved by superimposing the temperature profiles of the problems (1) and (2). In Fig. 6.3, results of the CFD analyses for the "original problem" are compared with the

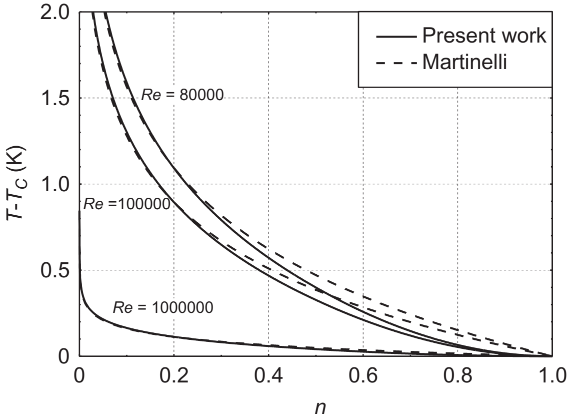

**Figure 6.2** Comparison between the different evaluations of the radial temperature profiles in a pipe with turbulent flow for several Reynolds numbers and $Pr = 1$ − problem (2).

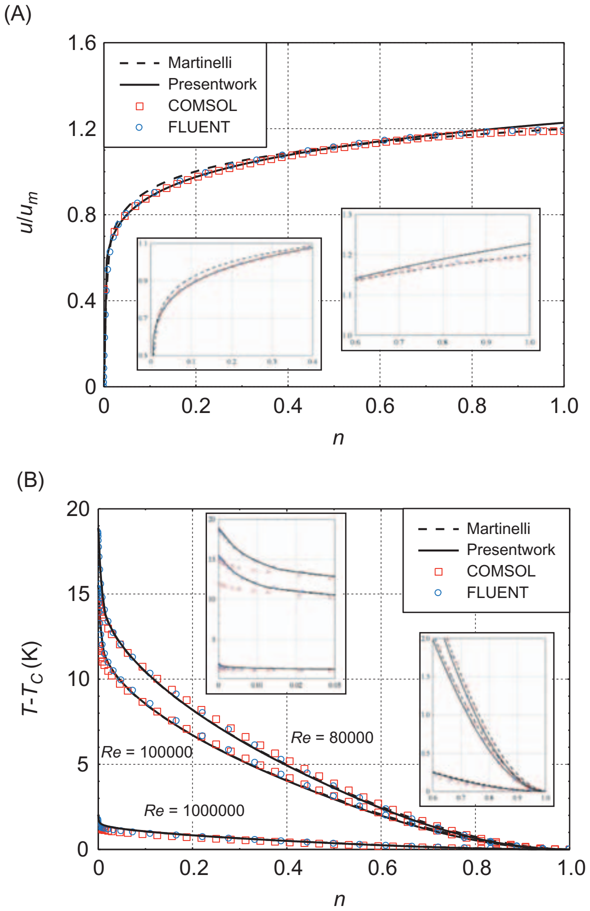

**Figure 6.3** Comparison between the different evaluations of (A) the dimensionless velocity profile, and (B) of the radial temperature profile in a pipe with turbulent flow for several Reynolds numbers and $Pr = 1$ − "original problem" = (1) + (2).

analytical ones achievable following the Martinelli and the present work approaches for the problem (2).

The numerical results in terms of velocity (Fig. 6.3A) and temperature (Fig. 6.3B) profiles follow very well those provided by both analytic approaches, which are very close to each other.

As for the velocity, numerical results provided by both codes are in good agreement, whereas the analytical profiles show some little differences due to the modeling assumptions (i.e., logarithmic and one-seventh laws).

As far as the temperature is concerned, it must be pointed out that a more accurate agreement can be found by means of FLUENT in the near-wall region thanks to the *enhanced wall treatment* approach of the boundary layer.

## 6.3 Heat transfer and pressure losses

It is specific to graphite-moderated MSRs that, even if the energy from nuclear fissions is predominantly released directly in the fuel, the graphite channels are heated-up by the gamma and neutron radiation and the presence of this heat source causes that in most cases the direction of radial temperature gradient is from the fuel to the graphite. In other words, the liquid fuel practically cools down the graphite in steady-state operation (Křepel et al., 2005).

The investigation of the heat exchange properties between molten salt and graphite is performed with reference to an axial-symmetric geometry representing a typical MSR core channel, idealized as a circular-pipe with circulating molten salt that is surrounded by a hollow cylinder of graphite.

By coupling the analytic approach described in Section 6.2 for modeling the fully developed flow of molten salt inside the pipe with the heat conduction problem for the graphite, it is possible to find the radial temperature profile in the channel (graphite + molten salt). The previous solutions (1) and (2) can be used for the molten salt, while for the graphite the following radial profile is obtained solving the 1-D heat conduction equation between the inner ($R_i$) and the outer ($R_o$) radii of graphite:

$$T(r) = \frac{q'''_g}{2\lambda_g}\left(\frac{R_i^2 - r^2}{2} + R_o^2 \ln\left(\frac{r}{R_i}\right)\right) + T_W \tag{6.5}$$

where $q'''_g$ and $\lambda_g$ are the volume-heat source and the thermal conductivity of the graphite, and $T_w$ is the interface molten salt-graphite temperature. The heat flux at the interface, $q''_W$, is given by Eq. (6.6):

$$q''_W = -q'''_g(R_o^2 - R_i^2)/2R_i \tag{6.6}$$

To calculate the wall temperature $T_W$, it is necessary to solve first the heat transfer problem in the molten salt applying as boundary condition the wall heat flux

**Table 6.1** **Main reference data of the analyzed MSR channel**

| Symbols/quantities | Molten salt | Graphite |
|---|---|---|
| $c_P$, specific heat capacity $[\mathrm{J \cdot kg^{-1} \cdot K^{-1}}]$ | 1357 | 1760 |
| $D_h$, channel hydraulic diameter [m] | 0.16 | – |
| $H$, channel length [m] | 4.8 | 4.8 |
| $Pr$, Prandtl number [–] | 11 | – |
| q‴, volume-heat source $[\mathrm{W \cdot m^{-3}}]$ | $1.3 \cdot 10^8$ | $3.4 \cdot 10^6$ |
| $R_i$, interface radius [m] | 0.08 | 0.08 |
| $R_o$, outer radius [m] | – | 0.12 |
| $T_{in}$, channel inlet temperature [K] | 900 | – |
| $\eta$, dynamic viscosity $[\mathrm{kg \cdot m^{-1} \cdot s^{-1}}]$ | 0.01 | – |
| $\lambda$, thermal conductivity $[\mathrm{W \cdot m^{-1} \cdot K^{-1}}]$ | 1.23 | 31.2 |
| $\rho$, density $[\mathrm{kg \cdot m^{-3}}]$ | 3330 | 1843 |

given by Eq. (6.6) and imposing the value of the volume-heat source in the molten salt ($q'''_s$) as well as in the graphite ($q'''_g$). In the next analyses, a ratio $q'''_g/q'''_s$ of about of 3% is adopted (Mandin et al., 2005).

Once the radial temperature profile is known, it is possible to calculate analytically the Nusselt number as $Nu = (D_h/\lambda) \cdot q''_W/(T_W - T_b)$, and consequently the heat transfer coefficient between the molten salt and the graphite as $h = Nu \cdot \lambda/D_h$, where $T_b$ and $D_h$ are the bulk (or mixed-mean) temperature of the molten salt and the channel hydraulic diameter, respectively.

It must be pointed out that in the case of heat source within the fluid, the Nusselt number is not only a function of Reynolds and Prandtl numbers, but also of the ratio between the heat source and the wall heat flux (Poppendiek, 1954; Fiorina et al., 2014).

Two different cases are considered for the CFD analyses: (I) no volume-heat source within the molten salt; and (II) molten salt with volume-heat source. The first case (whose results are shown for both the laminar and the turbulent flow) is important not only for the above statement about the Nusselt number but also because heat transfer properties of molten salt are of interest for its usage in the intermediate-heat exchanger (Mandin et al., 2005). The second case is more representative of a MSR core channel, and the respective results are shown for brevity only in turbulent flow, which is expected to occur during reactor operating conditions. For what concerns molten salt and graphite properties, MSR design specifications and the volume-heat sources, we refer to Mandin et al. (2005), while the most important data are summarized in Table 6.1.

### *6.3.1 Laminar flow*

A Reynolds number $Re = 80$ is chosen for the present analysis, referring to the case with no volume-heat source within the molten salt. In Fig. 6.4, the local Nusselt number achieved by the CFD simulations (considering a length of 15 m in order to

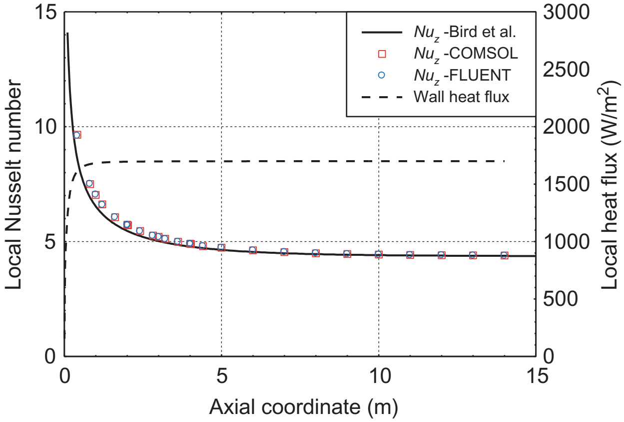

**Figure 6.4** Comparison between the different evaluations of the local Nusselt number in the MSR channel with laminar flow.

**Table 6.2 Comparison between analytic and numerical calculations of the local *Nu* and friction pressure losses in the MSR channel with laminar (fully developed) flow**

| | Analytic | COMSOL | Err (%) | FLUENT | Err (%) |
|---|---|---|---|---|---|
| Local *Nu* ($z$ = 13 m), [−] | 4.364 | 4.393 | 0.7 | 4.389 | 0.6 |
| Pressure losses ($z$ = H), [Pa] | $9.00 \cdot 10^{-2}$ | $8.99 \cdot 10^{-2}$ | 0.1 | $8.97 \cdot 10^{-2}$ | 0.3 |

reach fully developed flow conditions) is compared with the following correlation given by Bird et al. (1960), which is valid for thermally developing flow with constant wall heat flux:

$$Nu_z = \begin{cases} 1.302(z^*)^{-1/3} - 1.0 & \text{for} \quad z^* \leq 5 \cdot 10^{-5} \\ 1.302(z^*)^{-1/3} - 0.5 & \text{for} \quad 5 \cdot 10^{-5} \leq z^* \leq 1.5 \cdot 10^{-3} \\ 4.364 + 8.68\left(10^3 \cdot z^*\right)^{-0.56} \cdot \exp(-41 \cdot z^*) & \text{for} \quad z^* \geq 1.5 \cdot 10^{-3} \end{cases} \tag{6.7}$$

where $z^* = z/(Re \cdot Pr \cdot D_h)$. COMSOL and FLUENT codes supply the same results, which are in very good agreement with the correlation given by Bird et al. as well as with the analytical evaluation of the local Nusselt number (see also Table 6.2). The friction pressure losses are numerically evaluated considering a parabolic profile of the inlet velocity, and are compared in Table 6.2 with the classical Darcy formula for the friction coefficient $f$ in the Hagen-Poiseuille flow (i.e., $f = 64/Re$). As can be noticed, a very good agreement exists.

### 6.3.2 Turbulent flow

A Reynolds number $Re = 8 \cdot 10^4$ is chosen for the turbulent flow. In the present subsection, the effect of the *standard k-ω turbulence model* is also investigated, and results are compared to the analytic solution and those obtained with the *standard k-ε model* for both the considered cases (I) and (II). For the numerical simulations, COMSOL and FLUENT codes have been adopted. Radial temperature profiles are shown in Fig. 6.5, while the Nusselt number and the friction pressure losses calculations are given in Tables 6.3 and 6.4, respectively.

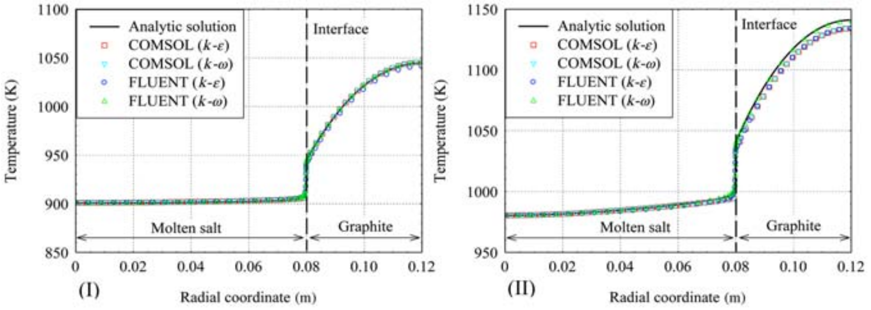

**Figure 6.5** Comparison between the different evaluations of the temperature profile in the MSR channel with turbulent flow ($z = 4.4$ m): (I) without, and (II) with volume-heat source.

**Table 6.3** **Nu comparison with the analytic solution in the MSR channel (turbulent flow)**

| **Local *Nu* (*z* = 4.4 m)** | **Case (I)** | **Err (%)** | **Case (II)** | **Err (%)** |
|---|---|---|---|---|
| Analytic solution | 523 | – | 418 | – |
| Dittus-Boelter correlation | 502 | 4.0 | 502 | 20 |
| COMSOL *k-ε* | 512 | 2.1 | 474 | 13 |
| COMSOL *k-ω* | 517 | 1.2 | 472 | 13 |
| FLUENT *k-ε* | 584 | 12 | 469 | 12 |
| FLUENT *k-ω* | 526 | 0.7 | 422 | 1.1 |

**Table 6.4** **Pressure losses comparison with the McAdams correlation in the MSR channel for the turbulent flow ($z = H$)**

| **Friction pressure losses** | **[Pa]** | **Err (%)** |
|---|---|---|
| McAdams correlation | 2163 | – |
| COMSOL *k-ε* | 2021 | 6.6 |
| COMSOL *k-ω* | 2036 | 5.9 |
| FLUENT *k-ε* | 2332 | 7.8 |
| FLUENT *k-ω* | 2193 | 1.4 |

As a result, there is good agreement of the numerical evaluations of both the Nusselt number and the temperature profiles with those obtained analytically. The well-known Dittus-Boelter correlation can be used for molten salt (El-Wakil, 1978; Mandin et al., 2005) giving a reasonable result in the case of no heat source with a discrepancy of 4% in comparison with the analytic solution, but it should be used carefully in the presence of a heat source within the fluid because it does not take into account the dependence of heat transfer on the ratio between wall heat flux and volume-heat source. As a consequence, the heat transfer coefficient could be excessively overestimated (see Table 6.3). This last issue has been the subject of several works (e.g., Di Marcello et al., 2010; Luzzi et al., 2010, 2012a; Fiorina et al., 2014), to which the reader is referred. Here, we just retrieve from Fiorina et al. (2014) an example concerning the core channels of the Molten Salt Breeder Reactor (Robertson, 1971). As can be noticed in Fig. 6.6, traditional correlations (Dittus and Boelter, 1930; Sieder and Tate, 1936; Gnielinski, 1976; Bin et al., 2009; Yu-ting et al., 2009) predict a higher Nusselt number compared to the correlation proposed by Di Marcello et al. (2010) that takes into account the volume-heat source in the molten salt. This leads to an underestimation of the graphite temperature, whose importance depends also on the channel diameter and the strength of heat source in the fuel.

A good agreement can be found between the numerical evaluations of the pressure losses and the well-known McAdams correlation (see Table 6.4).

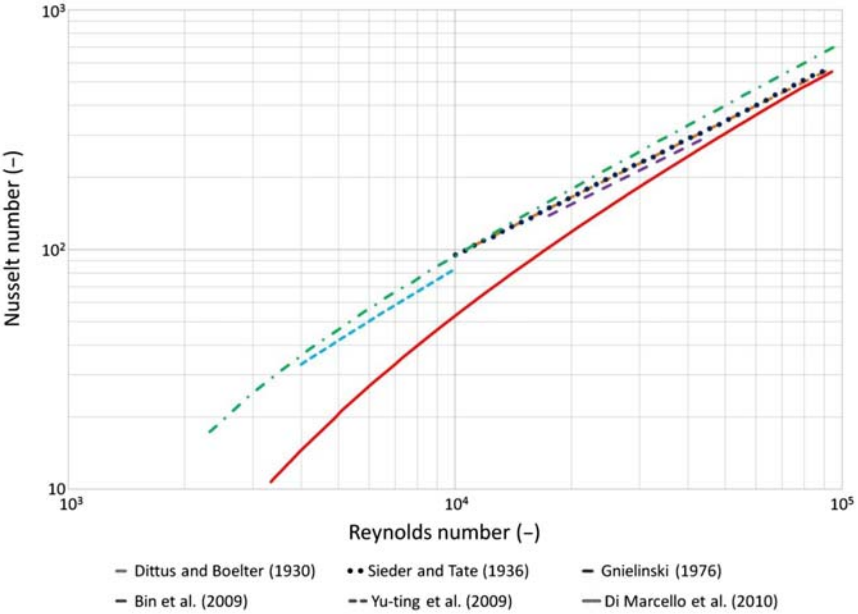

**Figure 6.6** Nusselt number in the core channels of the Molten Salt Breeder Reactor.

As a general comment on the analyses presented in this section, we can observe that the numerical results provided by COMSOL and FLUENT codes are close to each other in terms of temperature profiles, Nusselt number, and pressure losses. Some differences have been found, which are related to the choice of different turbulence models, but it is not the aim of this chapter to enter into such details. Moreover, the influence of the volume-heat source on the heat transfer properties may be relevant at low Reynolds numbers, and needs to be carefully taken into account.

## 6.4 Effects of internal heat generation on natural circulation stability

Analytical, numerical, and experimental studies on the stability and transient behavior of single-phase natural circulation loops (NCLs) have been performed in recent years by several authors. An overview can be found in Misale (2014). However, all these works performed the analysis of NCLs with localized hot and cold heat sinks, mainly focusing on the influence of the loop geometry on natural circulation instabilities, while the instance of an internal and distributed power source inside the system has been little investigated. In this regard, the first studies have been conducted by Pini et al. (2014), Ruiz et al. (2015), Pini et al. (2016), and Cammi et al. (2016b). Referring the reader to these two studies for a detailed description of the methods developed for the stability analysis, as well as of the main modeling assumptions adopted, hereafter the main results are summarized. They are expressed in terms of dimensionless stability maps, which are a compact way to describe the dynamic behavior of a given system.

Reference is made to the two vertical loop configurations with constant diameter $D$ shown in Fig. 6.7 that can be characterized by large instability regions, namely the HHHC (horizontal heater—horizontal cooler) and the VHHC (vertical heater—horizontal cooler) loops.

Their geometrical features (Vijayan et al., 2007) are given in Table 6.5. A single cooling section (called *cooler*) is considered, and is modeled as a constant wall temperature heat exchanger, while two heat sources can be taken into account. The first is a localized external heater (called *heater*), and is treated as a localized heat flux (LHF) source, $q''$. The second represents the heat generation inside the fluid (e.g., the circulating fuel in MSRs), and is modeled as a homogeneous distributed volumetric source, $q'''$. The fluid flow is considered one-dimensional along the curvilinear coordinate $s$ (adopted to describe the position inside the loop), and it is assumed that the same flow regime (laminar, laminar turbulent transition, or fully turbulent) exists in the whole loop.

For comprehension of the stability maps, which are obtained by perturbing the system equilibrium, the following steady-state quantities are to be defined: the

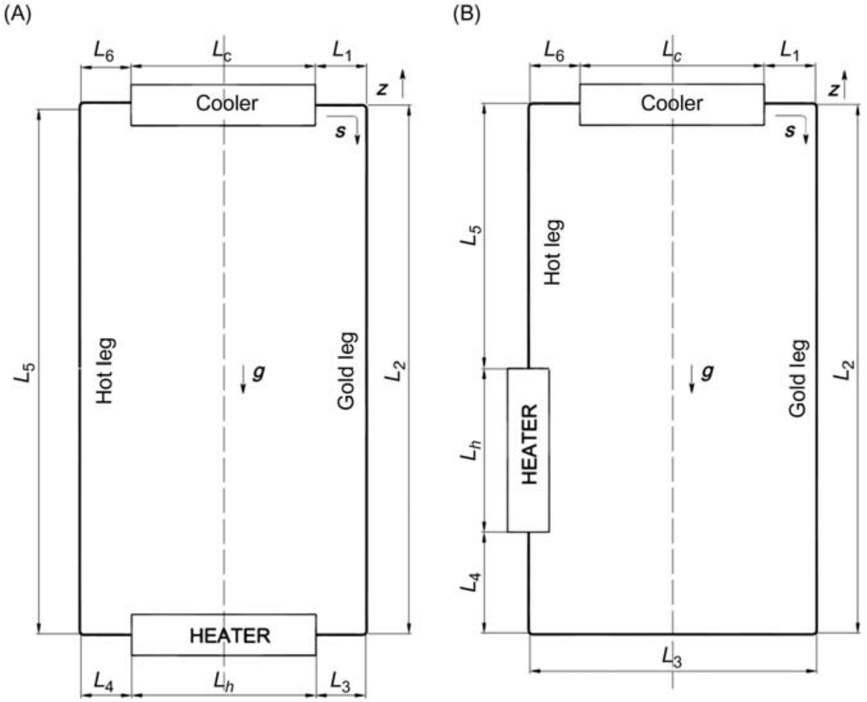

**Figure 6.7** Rectangular loop configurations: (A) horizontal heater–horizontal cooler; (B) vertical heater–horizontal cooler (not to scale).

**Table 6.5** **Dimensions (in meters) of the HHHC and VHHC loops**

| **Loop** | $L_1$ | $L_2$ | $L_3$ | $L_4$ | $L_5$ | $L_6$ | $L_c$ | $L_h$ | $L_t$ | $D$ |
|---|---|---|---|---|---|---|---|---|---|---|
| HHHC | 0.31 | 2.20 | 0.40 | 0.40 | 2.20 | 0.31 | 0.80 | 0.62 | 7.24 | 0.0269 |
| VHHC | 0.31 | 2.20 | 1.42 | 0.35 | 1.12 | 0.31 | 0.80 | 0.73 | 7.24 | 0.0269 |

temperature variation due to the external heat flux in the heater section ($\Delta T_{q''}$), and the temperature variation of the fluid induced by the internal generation outside the cooler ($\Delta T_{q'''}$):

$$\Delta T_{q''} = \frac{q''(P/A)}{G_0 C_p} L_h \tag{6.8}$$

$$\Delta T_{q'''} = \frac{q'''}{G_0 C_p} (L_t - L_c) \tag{6.9}$$

where $G_0$ is the mass flux, $C_p$ is the fluid reference specific heat (taken at the cooler entrance), $P$ and $A$ are the perimeter and the cross-section area of the pipes, respectively, $L_h$ is the heater length, $L_c$ is the cooler length, and $L_t$ is the total length of the loop. At this point, it is also possible to define the total temperature variation outside the cooler ($\Delta T_{tot}$), the ratio $\alpha$ between $\Delta T_{q''}$ and $\Delta T_{tot}$, and the modified Stanton number ($St_{m0}$):

$$\Delta T_{tot} = \Delta T_{q''} + \Delta T_{q'''} \tag{6.10}$$

$$\alpha = \frac{\Delta T_{q''}}{\Delta T_{tot}} (0 \le \alpha \le 1) \tag{6.11}$$

$$St_{m0} = 4St_0 \frac{L_t}{D} = 4\frac{Nu_0}{Re_0 Pr_0}\frac{L_t}{D} = \frac{h_0 \left(P/A\right)}{G_0 C_p} L_t \tag{6.12}$$

where $St_0$ is the Stanton number, $Nu_0$ the Nusselt number, $Re_0$ the Reynolds number, $Pr_0$ the Prandtl number, $h_0$ is the convective heat transfer coefficient, and the subscript 0 indicates steady-state values. The $\alpha$ ratio can assume all values between 0 and 1. For $\alpha = 1$, there is only the localized external heat source (*conventional* natural circulation). For $\alpha = 0$, only a homogeneously distributed IHG is present in the system. An example of steady-state distribution, both for $\alpha = 1$ and $\alpha = 0$, is shown in Fig. 6.8. This parameter has a great influence on the NCL dynamic behavior, because a variation of $\alpha$ directly implies a change in the ratio between the heat produced by the LHF in the heater and the distributed IHG. When $\alpha$ is changed, the same system can experience stable or unstable natural circulation flow regimes. Actually, as will be shown, the stability maps strongly depend on $\alpha$.

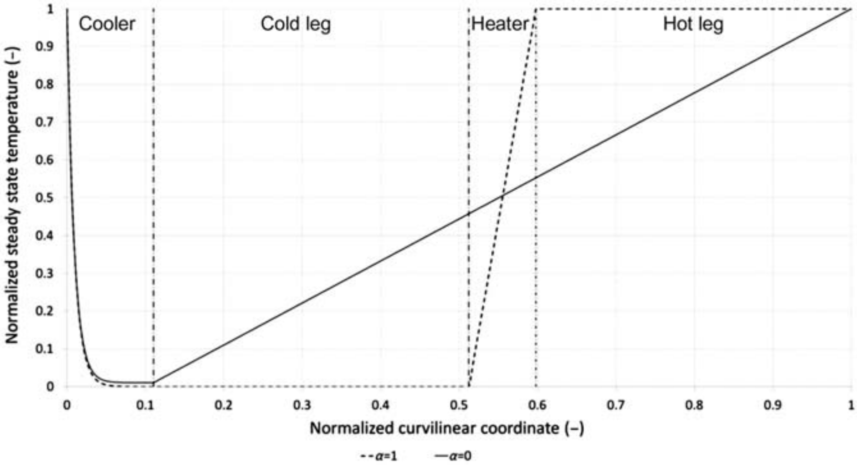

**Figure 6.8** HHHC loop: steady-state temperature field for $\alpha = 0$ (internal generation only) and $\alpha = 1$ (conventional natural circulation).

Another important parameter, generally not considered in the literature, but affecting the dynamic behavior of the system as well, is herein denoted $B$. It reads:

$$B = \frac{G_0}{h_0}\left(\frac{\partial h}{\partial G}\right)_0 \tag{6.13}$$

The parameter $B$ has been evaluated in Pini et al. (2016), to which we refer for details, and has the trend shown in Fig. 6.9 for different values of the Prandtl number. It represents the variation of convective heat transfer coefficient due to mass flux perturbations. If $B$ is equal to zero, this relation is not taken into account, and the heat transfer coefficient $h$ is treated as a fixed parameter at the steady state value ($h_0$), by neglecting its dependence on the mass flow rate (and hence on the Reynolds number).

Given the above definitions of the $\alpha$ and $B$ parameters, we can now summarize some significant results in terms of stability maps for the two considered loop configurations. Natural circulation may occur at different flow regimes, from the laminar to the turbulent, depending on the thermal power given to the system. The steady-state condition is reached when a dynamic equilibrium is established between the buoyancy and the frictional effects. This equilibrium can be stable or unstable. In the last case, the instabilities can lead to large pulsations in the fluid

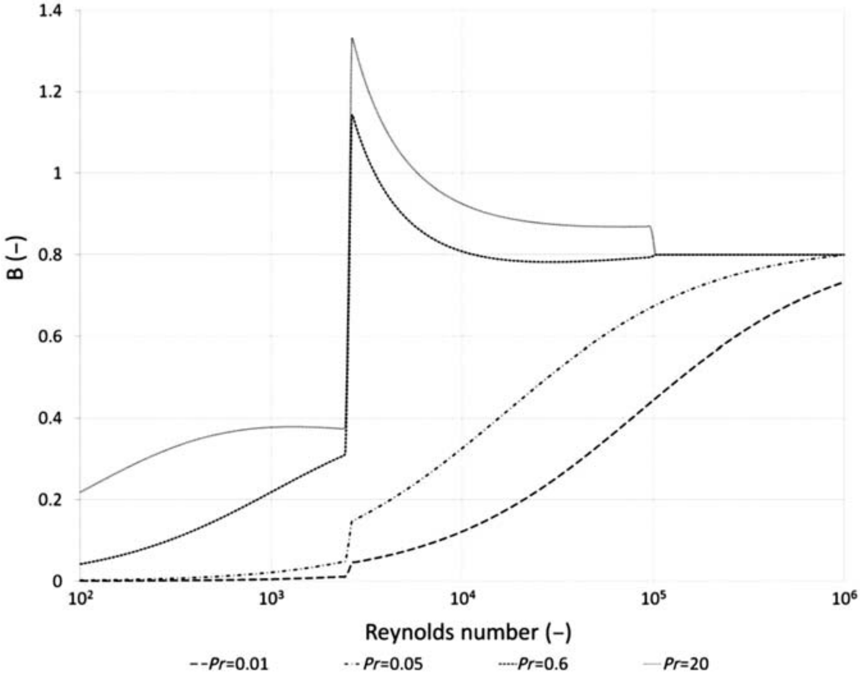

**Figure 6.9** Trend of $B$ with respect to the Reynolds and the Prandtl numbers.

flow rate and to unwanted behavior of the system. For a given loop configuration and a given value of $\alpha$, in a $Re$ versus $St_m$ diagram, the geometrical locus of the points for which the mass flux remains constant (after the perturbation of the steady state) sets a boundary separating the couples ($Re_0$, $St_{m0}$) for which the equilibrium is asymptotically stable from those for which the equilibrium is unstable. This is the definition of the stability map.

As already mentioned, IHG can significantly modify the dynamic behavior of natural convection loops. Fig. 6.10 shows the stability maps of the HHHC and VHHC systems for $B = 0$ (fixed heat transfer coefficient), from $\alpha = 1$ (only localized external heating) to $\alpha = 0$ (only IHG). As can be noticed, the unstable regime increases when IHG is present.

The HHHC loop configuration represents a very critical situation since, for any value of $\alpha$, it always remains a symmetric system (see Fig. 6.7A), and therefore the fluid does not have any preferable flowing direction. When $B \neq 0$ (see Fig. 6.11A), the heat exchange varies with the mass flux perturbation and induces a strong stabilization. This effect is larger in the range of Reynolds numbers for which the value of $B$ is higher (see Fig. 6.9). Moreover, the stabilization becomes stronger as the fraction of the power given by the internal generation increases (from $\alpha = 1$ to $\alpha = 0$). Since the influence of the volumetric heat generation is small, the effect of $B$ is able to reverse the stability behavior of the system for laminar-turbulent transition and fully turbulent zones (where $B$ is bigger compared to the laminar zone, as Fig. 6.9 shows). Hence, the system is more stable for $\alpha = 0$ than for $\alpha = 1$ when $Re > 2500$.

The behavior of the VHHC configuration is completely different with respect to the previous case. As a matter of fact, when the power is given by the localized heater ($\alpha = 1$), the flow has a preferred direction for its motion, that is the clockwise one (see Fig. 6.7B). On the contrary, as $\alpha$ becomes zero, the loop progressively acquires a symmetric configuration and hence the system becomes more unstable. The destabilization induced by the IHG is so marked (see Fig. 6.10B) that

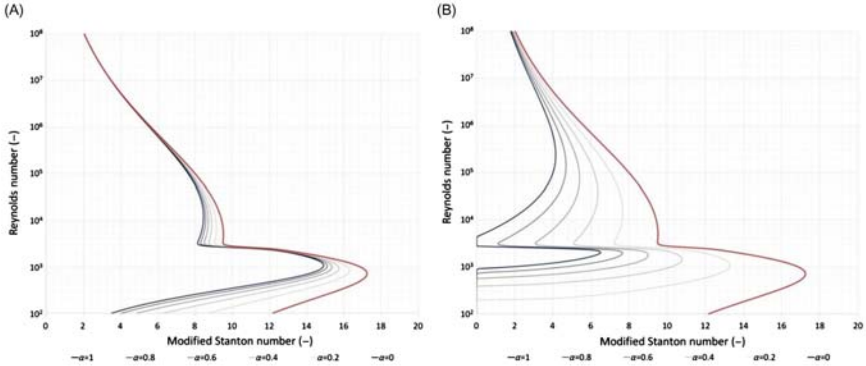

**Figure 6.10** Stability maps of HHHC (A) and VHHC (B) loops for various IHG levels. The effect of heat exchange is neglected ($B = 0$). Stable and unstable regions are on the right and on the left of the curves, respectively.

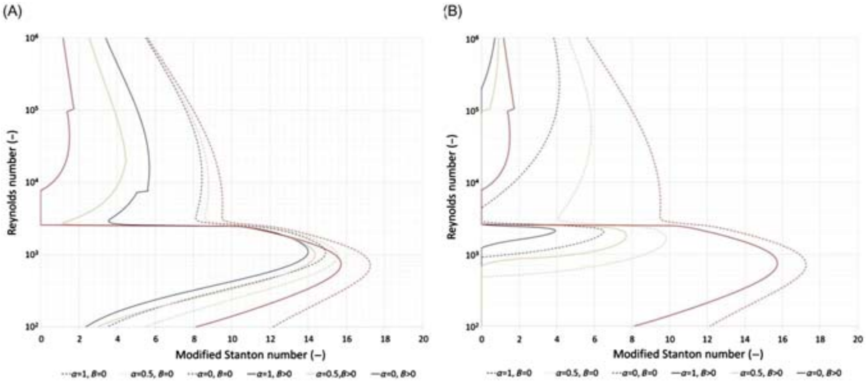

**Figure 6.11** Stability maps of HHHC (A) and VHHC (B) loops with ($B \neq 0$) and without ($B = 0$) the effect of heat exchange, for different IHG levels. Stable and unstable regions are on the right and on the left of the curves, respectively.

the case of $\alpha = 0$ remains the most unstable also considering the heat exchange effect (see Fig. 6.11B).

Fig. 6.11 clearly shows that the overall effect of the $B$ parameter is that of stabilizing the system dynamics. This can be explained as follows. If the mass flux oscillations increase, the convective heat transfer in the cooler is enhanced. Since the power given to the system is constant, when the heat exchange increases, the mean temperature difference between hot and cold legs of the loop becomes smaller. The final consequence of this mechanism is the weakening of the buoyancy force, which is induced by the density variation caused by the nonuniform temperature field.

To summarize, it has been found that IHG combined with heat exchange effect can induce a stabilization or a destabilization of the system dynamics depending on its action on the loop symmetry. For the HHHC loop, which presents a perfect axial symmetry for every value of $\alpha$, IHG together with the heat transfer phenomena induces a stabilization. On the other hand, for the VHHC loop, which does not have any symmetry for $\alpha = 1$, IHG combined with the heat exchange effect causes a destabilization because it increases the symmetry of the loop. By considering the two effects in a separate way, the heat exchange ($B \neq 0$) acts on the system oscillations with a negative feedback, whose influence increases as the fluid IHG becomes larger. On the contrary, the volumetric power source destabilizes the system.

We believe that it is fundamental to validate the predictions of the presented stability maps with experimental data. To this purpose, the DYNASTY testing facility (currently under construction at the Politecnico di Milano) can give a fundamental support (Cammi et al., 2016a), also providing useful information on some effects that were not discussed in this work, such as nonuniform power generation, cross-stream temperature gradients effects, and nonuniformity of the fluid parameters. The acquired knowledge will constitute the background necessary for understanding how the decay heat distributed along the primary circuit of an MSR can modify the dynamics of natural circulation, potentially leading to dangerous behavior of the reactor. Such an occurrence needs to be carefully avoided through an appropriate design based on the outcomes of the planned investigations. In other words, the study of the dynamic behavior of natural circulation with IHG is important in order to achieve high levels of intrinsic safety, which is one of the pillars of the Generation IV International Forum.

## 6.5 Conclusions

In this chapter, a preliminary approach to thermo-hydraulics of a typical (graphite-moderated) MSR channel has been presented, by assuming that the neutronic problem is decoupled from fluid dynamics and referring to a simple axial-symmetric geometry. Some relevant aspects of this system, featured by a heat source within the fuel/coolant molten salt, have been analyzed. In particular, a validation framework has been proposed in order to test different computer codes. In the presented analyses, we have adopted COMSOL and FLUENT, whose numerical results in terms of temperature profiles and pressure losses turned out to be very close to each other, and substantially in good agreement with the analytical solutions and data given by empirical correlations. However, more detailed analyses are required in the case of more complex and design-oriented geometries, taking into account the effects concerning the geometry itself, the influence of the volume-heat source on the heat transfer, and the choice of both the mesh structure and the turbulence model. For this purpose, the strong coupling between neutronics and thermo-hydraulics, which is a specific and intrinsic feature of liquid-fueled MSRs, needs to be considered as well.

The presented results on the natural circulation stability, although preliminary, have clearly shown that the behavior in the presence of IHG is characterized by a particular dynamics. Actually, system equilibria that are asymptotically stable for NCLs with conventional LHF can become unstable when IHG is present. The stability maps have proved that IHG, when it dominates the localized external heat source, can modify the shape and area of the stability regions. These findings contribute to the development of the natural circulation modeling, introducing physical phenomena previously neglected, and suggest that IHG effects should be taken into account when designing convective loops with internally heated fluids. As far as future developments are concerned, the influence of the thermal properties of the pipe walls are currently under investigation at Politecnico di Milano, and loop configurations featured by significant 3-D effects and with different positions of the localized heater and of the cooling section will be considered as well.

## Acknowledgments

We gratefully acknowledge financial support from Politecnico di Milano (FARB Project, Grant no. DDM2RIST06) for the construction of the DYNASTY testing facility.

# Abbreviations

| | |
|---|---|
| **CFD** | Computational fluid dynamics |
| **DYNASTY** | DYnamics of NAtural circulation for molten SalT internallY heated |
| **HHHC** | Horizontal heater–horizontal cooler |
| **IHG** | Internal heat generation |
| **LHF** | Localized heat flux |
| **MSR** | Molten salt reactor |
| **NCL** | Natural circulation loop |
| **VHHC** | Vertical heater–horizontal cooler |
| **1-D** | One-dimensional |
| **2-D** | Two-dimensional |
| **3-D** | Three-dimensional |

# References

Bin, L., Yu-ting, W., Chong-fang, M., Meng, Y., Hang, G., 2009. Turbulent convective heat transfer with molten salt in a circular pipe. International Communications in Heat and Mass Transfer. 36, 912–916.

Bird, R.B., Stewart, W.E., Lightfoot, E.N., 1960. Transport Phenomena. Wiley, New York, USA.

Cammi, A., Cauzzi, M.T., Luzzi, L., Pini, A. 2016a. DYNASTY: An experimental loop for the study of natural circulation with internally heated fluids. In: Proceedings of the 12th International Conference on Heat Transfer, Fluid Mechanics and Thermodynamics, 11–13 July 2016, Malaga, Spain, pp. 1159–1164.

Cammi, A., Luzzi, L., Pini, A., 2016b. The Influence of the wall thermal inertia over a single-phase natural convection loop with internally heated fluids. Chem. Eng. Sci. 153, 411–433.

Cheng, X., Tak, N., 2006. Investigation on turbulent heat transfer to lead-bismuth eutectic flows in circular tubes for nuclear applications. Nucl. Eng. Des. 236 (4), 385–393.

COMSOL, 2007. COMSOL Multiphysics® 3.4 User's Guide, COMSOL Inc., 2007.

De Chant, L.J., 2005. The venerable 1/7th power law turbulent velocity profile: a classical nonlinear boundary value problem solution and its relationship to stochastic processes. Appl. Math. Comput. 161, 463–474.

Di Marcello, V., Cammi, A., Luzzi, L., 2008. Analysis of thermal-hydraulic behaviour of the molten salt nuclear fuel. In: Proceedings of the International Conference Nuclear Energy for New Europe 2008, 7–11 September 2008, Portorož, Slovenia, pp. 301.1–301.10.

Di Marcello, V., Cammi, A., Luzzi, L., 2010. A generalized approach to heat transfer in pipe flow with internal heat generation. Chem. Eng. Sci. 65, 1301–1310.

Dittus, F.W., Boelter, L.M.K., 1930. Heat Transfer in Automobile Radiators of the Tubular Type, 2. University of California publications in Engineering, Berkeley, CA, pp. 443–461.

El-Wakil, M.M., 1978. Nuclear Heat Transport. American Nuclear Society, USA.

Fiorina, C., Cammi, A., Luzzi, L., Mikityuk, K., Ninokata, H., Ricotti, M.E., 2014. Thermal-hydraulics of internally heated molten salts and application to the Molten Salt Fast Reactor. J. Phys. 501, 012030, _1–10.

FLUENT, 2005. FLUENT® 6.2 User's Guide, Fluent Inc., 2005.

GIF, 2002. A technology roadmap for generation IV nuclear energy systems. US DOE Nuclear Energy Research Advisory Committee and the Generation IV International Forum, Technical Report GIF-002-00.

GIF, 2014. Technology roadmap update for generation IV. Nuclear energy systems. Technical Report, Available from: <https://www.gen-4.org/gif/jcms/c_74060/annual-report-2014>.

Gnielinski, V., 1976. New equations for heat and mass transfer in turbulent pipe and channel flow. Int. Chem. Eng. 16 (2), 359−367.

IRSN, 2015. Review of generation IV nuclear energy systems. Institut de Radioprotection et de Sûreté Nucléaire. Available from: <http://www.irsn.fr/EN/newsroom/News/Documents/IRSN_Report-GenIV_04-2015.pdf>.

Křepel, J., Grundmann, U., Rohde, U., Weiss, F.P., 2005. DYN1D-MSR dynamics code for Molten Salt Reactors. Ann. Nucl. Energy. 32, 1799−1824.

Křepel, J., Hombourger, B., Fiorina, C., Mikityuk, K., Rohde, U., Kliem, S., et al., 2014. Fuel cycle advantages and dynamics features of liquid fueled MSR. Ann. Nucl. Energy. 64, 380−397.

LeBlanc, D., 2010. Molten salt reactors: a new beginning for an old idea. Nucl. Eng. Des. 240 (6), 1644−1656.

Luzzi, L., Cammi, A., Di Marcello, V., Fiorina, C., 2010. An approach for the modelling and the analysis of the MSR thermo-hydrodynamic behaviour. Chem. Eng. Sci. 65 (16), 4873−4883.

Luzzi, L., Aufiero, M., Cammi, A., Fiorina, C., 2012a. Thermo-Hydrodynamics of Internally Heated Molten Salts for Innovative Nuclear Reactors. InTech, Rijeka, Croatia, pp. 119−142.

Luzzi, L., Di Marcello, V., Cammi, A., 2012b. Multi-Physics Approach to the Modeling and Analysis of Molten Salt Reactors. Nova Science Publishers, Inc, New York, pp. 1−140.

Mandin, P., Belachgar, H., Nuttin, A., Picard, G., 2005. Hydrothermal modelling for the molten salt reactor design optimisation. In: Proceedings of the 11th International Topical Meeting on Nuclear Reactor Thermal-Hydraulics (NURETH-11), 2−6 October 2005, Avignon, France, pp. 227.1−227.13.

Martinelli, R.C., 1947. Heat transfer to molten metals. Trans. ASME. 69, 947−959.

Misale, M., 2014. Overview on single-phase natural circulation loops. In: Proceedings of International Conference on Advances in Mechanical & Automation Engineering, 7−8 June, Rome, Italy.

Nikuradse, J., 1950. Laws of Flow in Rough Pipes. NACA Technical Memorandum 1292, Washington, DC.

Pini, A., Cammi, A., Luzzi, L., Ruiz, D.E., 2014. Linear and nonlinear analysis of the dynamic behaviour of natural circulation with internally heated fluids. In: Proceedings of NUTHOS-10, Paper NUTHOS10-1074, 14−18 December 2014, Okinawa, Japan.

Pini, A., Cammi, A., Luzzi, L., 2016. Analytical and numerical investigation of the heat exchange effect on the dynamic behaviour of natural circulation with internally heated fluids. Chem. Eng. Sci. 145, 108−125.

Poppendiek, H.F., 1954. Forced-convection heat transfer in pipes with volume-heat sources within the fluids. Chem. Eng. Prog. Symp. Ser. 50 (11), 93−104.

Robertson, R.C., 1971. Conceptual design study of a single-fluid molten-salt breeder reactor. Technical Report, ORNL-4541.

Ruiz, D.E., Cammi, A., Luzzi, L., 2015. Dynamic stability of natural circulation loops for single phase fluids with internal heat generation. Chem. Eng. Sci. 126, 573−583.

Serp, J., Allibert, M., Benes, O., Delpech, S., Feynberg, O., Ghetta, V., et al., 2014. The molten salt reactor (MSR) in generation IV: overview and perspectives. Prog. Nucl. Energy. 77, 308−319.

Sieder, E.N., Tate, G.E., 1936. Heat transfer and pressure drop of liquids in tubes. Ind. Eng. Chem. 28 (12), 1429−1435.

Wilcox, D.C., 2006. Turbulence Modeling for CFD. DCW Industries, Inc., La Cañada, CA.

Vijayan, P.K., Sharma, A.K., Saha, D., 2007. Steady state and stability characteristics of single- phase natural circulation in a rectangular loop with different heater and cooler orientations. Exp. Ther. Fluid Sci. 31, 925−945.

Yang, J., Oka, Y., Ishiwatari, Y., Liu, J., Yoo, J., 2007. Numerical investigation of heat transfer in upward flows of supercritical water in circular tubes and tight fuel rod bundles. Nucl. Eng. Des. 237 (4), 420−430.

Yu-ting, W., Bin, L., Chong-fang, M., Meng, Y., Hang, G., 2009. Convective heat transfer in the laminar-turbulent transition region with molten salt in a circular tube. Exp. Ther. Fluid Sci. 33, 1128−1132.

# Materials

# 7

*Ritsuo Yoshioka*[1], *Motoyasu Kinoshita*[2] *and Ian Scott*[3]
[1]International Thorium Molten-Salt Forum (ITMSF), Yokohama, Japan, [2]The University of Tokyo, Tokyo, Japan, [3]Moltex Energy, London, United Kingdom

## Chapter Outline

## 7.1 Molten salt

Molten salt is a liquid, which is in general a melted chemical compound of acid and alkali at high temperature. As is shown in Fig. 7.1, it is transparent and looks like water, but it does not contain water. There are thousands of molten salts, because they are combinations of acid and alkali, and besides that, some acid/alkali/oxides can be molten salts. For more basic understanding on molten salt thermodynamics in a molten salt reactor (MSR), Benes and Konings (2013) is recommended.

As is explained in Chapter 11.1, Development of molten salt reactor at Oak Ridge National Laboratory (ORNL), they selected molten salt fuel, because it is chemically stable and inert; it can be used at very low pressure owing to its very high boiling temperature and very low vapor pressure; and it can dissolve most nuclear materials such as uranium (U) and thorium (Th). Since most molten salts have high melting temperature, if leakage of molten salt occurs, it will freeze and not release radioactive materials (Briant and Weinberg, 1957).

Among many molten salts, ORNL finally proposed an eutectic mixture of lithium fluoride and beryllium fluoride called "FLiBe" ($LiF-BeF_2$), with fertile Th and fissile U or plutonium (Pu) dissolved as molten fluoride salts ($ThF_4$, $UF_4$, $PuF_3$).

**Molten Salt Reactors and Thorium Energy. DOI: http://dx.doi.org/10.1016/B978-0-08-101126-3.00007-5**

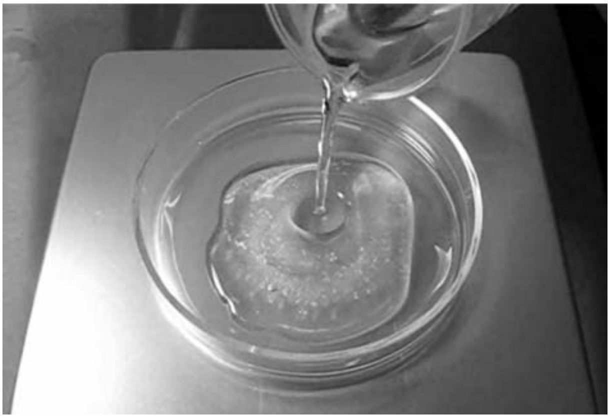

**Figure 7.1** Example of molten salt.
Chloride salt, courtesy of T. Goto.

This liquid serves as a fuel element, as a heat transfer medium, and as a fuel processing medium. Each of these functions is described below.

**1.** Molten salt as a liquid fuel element

In MSR fissionable isotopes, fertile isotopes, most fission products (FPs), and heavy elements reside as ionic elements dissolved in molten salt. When fission reactions occur in the core, molten salt is heated and it circulates through pumps, heat exchangers, and then returns back to the core. Fission reactions occur mainly in the core for thermal neutron spectrum MSR, because the reactor can keep criticality only when a neutron moderator, such as graphite, is present.

For solid fuel reactors, there is a mechanical limitation due to radiation damage on fuel pellets and cladding tubes, internal pressure due to accumulated gaseous FPs, fuel pellet swelling, oxidation of cladding tube, and so on. Also, there is another limitation due to depletion of fissile material. Due to these effects, periodic replacement of fuels is required for solid fuel reactors.

In molten salt fuel, however, there is no radiation damage, because it is an ionic liquid and not significantly affected by neutron or gamma irradiation. It is easy to adjust molten salt composition by adding molten salt containing fissile U/Pu or fertile Th in order to maintain an optimum fuel composition.

An important advantage of liquid fuel is that radioactive gases produced as FP can be removed from liquid fuel. In solid fuels, radioactive gases such as xenon ($^{133}$Xe/$^{135}$Xe/$^{137}$Xe/$^{138}$Xe) and krypton ($^{85}$Kr/$^{87}$Kr/$^{88}$Kr/$^{89}$Kr) are accumulated within cladding tubes, and they are released in severe accident conditions, such as the Fukushima accident.

Among these nuclides, $^{135}$Xe has a very large neutron absorption cross-section, and it deteriorates neutron economy during normal operation. For this reason, additional shutdown reactivity is required to override xenon reactivity change in a light water reactor (LWR), because $^{135}$Xe decays with a half-life of 9 hours. Also, the xenon oscillation issue must be considered for pressurized water reactors (PWR) (Iodine Pit Issue, 2015).

But, in liquid fuels, these gases are insoluble in molten salt. Therefore, they can be removed from molten salt, and captured by a charcoal filter system, then stored for enough decay periods. Removal of $^{135}$Xe makes load-following capability easier, and also removes the above xenon oscillation issue. In order to accelerate removal of radioactive gases, a helium (He) gas bubble injection system was proposed in the Molten salt breeder reactor (MSBR) design, and this system collects radioactive gases efficiently (Gabbard, 1972).

Molten salt can dissolve fissile and fertile materials. It is chemically stable and inert, and especially it can be used at very low pressure owing to its very high boiling temperature and very low vapor pressure. Normal operating pressure for an MSR is 0.5 MPascal (5 atm.), which is very low compared with 15 MPa (about 150 atm.) for a PWR. In addition, this low pressure returns back to 0.1 MPa (1 atm.) atmosphere pressure, when the molten salt pump stops. This low pressure reduces the danger of reactor vessel breakage or pipe breakage due to high pressure, such as in the LWR case. Higher temperature brings higher thermal efficiency of the plant. Outlet temperature of MSR is typically as high as 700°C, compared with 330°C in the PWR case. Liquid fuel design does not need fuel manufacturing such as a solid fuel case. These features make reactor design simple and economical.

ORNL chose a fuel salt based on $^{7}$LiF-BeF$_2$ (FLiBe), and NaBF$_4$-NaF as a secondary coolant. The properties of these molten salts are summarized in an ORNL report (Cantor, 1968). Some of them, compared with other molten salts and liquid Na (sodium), are shown in Table 7.1.

Molten fluoride salts are intrinsically noncorrosive to constituent elements in containment alloys, primarily because of greater thermodynamic stability of molten fluoride salt constituents as compared with fluorides of transition metals (Sohal et al., 2010). Compatibility to structure materials is discussed later.

As is shown in this table, FLiBe has an appropriate melting temperature, good viscosity, and a very high boiling temperature of 1430°C (Ingersoll et al., 2005).

FLiBe has a low neutron absorption cross-section, but natural Li will probably be enriched to $>99.9\%$ $^{7}$Li, because natural Li includes 7.42% of $^{6}$Li, which has a large neutron absorption cross-section and generates tritium. The $^{6}$Li is desired for fusion reactor blankets.

The Be in FLiBe is chemically toxic. In reactors, the fuel salt is radioactive and is enclosed within the primary loop. If there were a leak, it would freeze (solidify) to glassy material below its melting temperature. Therefore, there would be almost no release of Be or radioactive materials in an accidental situation.

### 2. Molten salt as heat transfer medium

Thermo-physical properties of molten FLiBe in Table 7.1 indicate that FLiBe has superior characteristics as a heat transfer medium. Such excellent characteristics are based on

Table 7.1 **Thermo-physical properties of molten salts and sodium (at c. 500°C) (Furukawa et al., 2005)**

| | **$NaNO_3$-$KNO_3$-$NaNO_2$ [HTS]** | **$NaBF_4$-NaF** | **$Li_2CO_3$-$Na_2CO_3$-$K_2CO_3$** | **LiF-NaF-KF [FLiNaK]** | **LiF-$BeF_2$ [FLiBe]** | **Na** |
|---|---|---|---|---|---|---|
| Chemical composition (mol%) | 7-44-49 | 92-8 | 41-36-23 | 46.5-11.5-42 | 66-34 | – |
| Melting temperature (°C) | 142 | 384 | 399 | 454 | 459 | 98 |
| Volumetric heat capacity: $C$ (J/m$^3$K) $\times 10^{-6}$ | 2.79 | 2.82 | 3.49 | 4.01 | 4.80 | 1.05 |
| Density: $d$ (kg/m$^3$) $\times 10^3$ | 1.79 | 1.87 | 2.02 | 2.17 | 2.05 | 0.83 |
| Thermal conductivity: $h$ (W/mK) | 0.59 | 0.35 | 0.55 | 1.2 | 1.00 | 66. |
| Kinematic viscosity: $k$ (m$^2$/s) $\times 10^6$ | 2.26 | 0.8 | 11.8 | 4.2 | 7.44 | 0.29 |
| Heat-transfer capability $(C/k)^{0.4} h^{0.6} \times 10^{-3}$ | 49.7 | 55.7 | 25.2 | 69.4 | 52.8 | 1.264 |
| Heat-transfer per unit pump-power: $C^3/d \times 10^{-15}$ | 12.1 | 12.1 | 21 | 29.4 | 53.8 | 1.39 |

1. Low pressure;
2. High boiling temperature;
3. High heat capacity (due to small ions);
4. Appropriate viscosity;
5. Suitable Prandtl number.

The Prandtl number of FLiBe is 10–20 in temperature range of 700–500°C, which is much higher than that of liquid Na (Pr = 0.004), and it means that FLiBe is a relatively adiabatic liquid. This fact mitigates a thermal shock during quick, inadvertent temperature changes. Also, the heat-transfer per unit pumping power has the highest value for FLiBe of all the materials in Table 7.1.

3. Molten salt as fuel reprocessing medium

Today, most spent fuel reprocessing is a hydrometallurgical process called PUREX (Plutonium and Uranium Recovery by EXtraction). This process uses organic solvent extraction from aqueous solutions, which result from dissolution of spent fuel. On the other hand, recent reprocessing, which does not use water or organic liquids, is called pyro-reprocessing or dry-reprocessing. In this process, solvents are molten salts such as LiCl-KCl, and molten metals such as cadmium or bismuth are used. Since this process does not use water or organic liquids, there is less danger of a criticality accident. In aqueous systems, concentration of fissile materials must be diluted in order to avoid a criticality accident, because they contain hydrogen or carbon, which is a good neutron moderator and could cause criticality. Therefore, a dry-reprocessing plant can be more compact than a PUREX plant.

For MSRs there are two cases.

- On-line reprocessing as for the MSBR;
- Off-site reprocessing like the Denatured Molten Salt Reactor (DMSR) or MSR-FUJI concept.

In any case the reprocessing medium is FLiBe, which is the same as MSR fuel salt.

Dry-reprocessing technology for molten salt fuel was proposed and developed during the MSBR development in the 1970 s at ORNL. They proposed on-line fuel reprocessing of fuel salt. This system consists of two parts:

- Removal of uranium (U) and protactinium (Pa) from fuel salt and reintroduction of U to fuel salt;
- Removal of rare-earth FPs from fuel salt (Alexander et al., 1959).

For off-site reprocessing, the above concept can also be applied. The FREGAT technology, which was developed *by Czech and in* Russia, is applying a fluoride volatility process based on separation of U and Pu in the form of volatile fluoride from FPs, the majority of which are nonvolatile fluorides. This process was originally developed to reprocess fast breeder reactor (FBR) spent fuels, but it can also be applied to LWR fuels (Uhlir et al., 2002; Uhlir and Marecek, 2009). A recent study was compiled with other technologies in an IAEA report (IAEA, 2010). Reprocessing of MSR fuels is described in detail in Chapter 8, Chemical processing of liquid fuel.

In summary, molten salts, especially FLiBe, have many excellent features, such as a low neutron absorption cross-section (if $^6$Li is removed), no radiation damage, large heat capacity, low vapor pressure, single-phase liquid, appropriate melting temperature, high boiling temperature, chemical inertness, good compatibility with structural material, compatibility with graphite, high solubility for U, Pu, and Th fluorides and FPs, no solubility for gaseous FPs such as Xe and Kr, and very limited radioactivity release in accidents.

## 7.2 Solid fuels with molten salt coolants

In a solid fuel reactor the allowable fuel burnup and lifetime are limited by:

- Fuel pellet swelling;
- Internal pressure from gaseous FPs;
- Clad thermal stress, creep, and corrosion;
- Clad radiation damage;
- Depletion of fissile material.

Therefore, periodic replacement of fuels is required.

Solid fuels used with molten salt coolants are similar to those used with water-cooled reactors, but the clad must be compatible with molten salts at high temperatures. This type of fuel is described in Chapter 13, Solid fuel, salt-cooled reactors.

## 7.3 Thorium fuel cycle

The thorium fuel cycle has unique features compared with the current uranium-plutonium fuel cycle:

1. More abundant resources;
2. Small production of plutonium and minor actinides;
3. Possibly better proliferation resistance (see Chapter 10, Non-proliferation and safeguards aspects of the MSR fuel cycle);
4. Can be a breeder with thermal neutrons.

MSRs are the most appropriate reactors for the thorium fuel cycle, because breeding (self-sustaining fuel supply) is possible even in thermal neutron spectrum MSRs with thorium fuel. The combination of MSRs and the thorium fuel cycle was developed at ORNL in the 1960s.

Thorium is a fuel *source* material (fertile material), from which $^{233}$U fuel is made by neutron absorption, so we speak of a "thorium fuel cycle," rather than "thorium fuel." Advantages of thorium fuel and of liquid fuels are discussed in Chapter 1, Introduction.

The properties of thorium, its minerals, abundance, and estimated resources are described in Chapter 9, Environment, waste, and resources.

Since thorium is not fissile, we need an initial MSR fuel load containing fissile material ($^{233}$U produced elsewhere, $^{235}$U, or $^{239}$Pu). The initial fissile material may be from low enriched uranium (LEU), from LWR spent fuel, from an accelerator-driven system (see Chapter 15: Accelerator driven systems), or from a fusion−fission hybrid (see Chapter 16: Fusion-fission hybrids). Proliferation resistance issues of the thorium fuel cycle are discussed in Chapter 10, Non-proliferation and safeguards aspects of the MSR fuel cycle.

## 7.4 Moderators

Fission reaction cross-sections are highest at low energies, and neutrons emitted by fission must undergo many collisions with materials to slow down from MeV energies to thermal energies ($\sim$ 0.025 eV). For example, the average number of collisions required to slow down in various media is shown in Table 7.2.

Besides the neutron slowing down, neutron absorption must be considered. For example, deuterium ($^2$H, or D) absorbs neutrons much less than ordinary hydrogen ($^1$H), so that the moderating efficiency of $D_2O$ is better than that of $H_2O$. Therefore, as a figure of merit of moderator, a moderating ratio (MR) is defined, which is slowing down power divided by absorption cross-section

**Table 7.2** **Average number of collisions for slowing down, and moderating ratio**

| Material | A | N | Moderating ratio |
|---|---|---|---|
| Hydrogen | 1 | 18 | |
| $H_2O$ | | 19 | 71 |
| $ZrH_2$ | | | 27 |
| Deuterium | 2 | 24 | |
| $D_2O$ | | 34 | 5670 |
| Lithium-7 | 7 | 67 | 11 |
| $^7LiF$ | | | 21 |
| Beryllium | 9 | 84 | 164 |
| BeO | | 101 | 217 |
| $BeF_2$ | | | 86 |
| Carbon | 12 | 110 | 191 |
| Oxygen | 16 | 145 | |

"N" is an average number of collisions required to slow down from 1 MeV to 0.025 eV versus atomic mass "A." Moderating ratio ($\xi\Sigma_s/\Sigma_a$) is referred from Lundy et al. (1960), except $H_2O$ and $D_2O$ from Duderstadt and Hamilton (1967).

$$MR = \xi\Sigma_s/\Sigma_a \tag{7.1}$$

where $\xi$ is the average change of the logarithm of the neutron energy per collision. As a potential moderator for MSR, ORNL investigated about 150 materials that could be used at high temperature (Lundy et al., 1960). They concluded that beryllium and carbon (graphite) have the highest MR among 150 candidates. Some are shown in Table 7.2, along with that of water and heavy water. Water was not considered as moderator in the above ORNL study, because it requires very high pressures at high temperatures, as in water-cooled reactors (see Section 11.1).

### 7.4.1 Graphite

Graphite is an important component in a thermal neutron spectrum MSR core, serving as a neutron moderator and reflector. Since graphite is irradiated and is in contact with the fuel salt, there are several requirements.

1. Prevention of fuel–graphite interactions

   If fuel salt penetrates into graphite, fission reactions cause additional radiation damage to graphite. But, since molten salt does not wet graphite, this can be easily prevented by manufacturing a pore-diameter of graphite less than $1 \times 10^{-6}$ m, owing to the surface tension of molten salt.

2. Prevention of Xe and Kr absorption by graphite

   FP $^{135}Xe$ has a large neutron absorption cross-section, which hurts the neutron economy of the core. It should be allowed to bubble out of the molten salt, instead of being trapped in the graphite. We could seal the graphite surface with cladding of pyro-carbon, SiC, or metal. This could be augmented by using an He-bubble injection system to extract the Xe and Kr efficiently from the molten salt.

**3.** Irradiation stability

When graphite is irradiated, it shows shrinkage at first, and then volume expansion (swelling) begins. $E > 50$ keV was proposed as $3 \times 1022$ neutrons/cm$^2$, where the volume returns back to an initial value, as shown in Fig. 7.2 (Rosenthal, 1972). This value can be applied to a thermal neutron spectrum MSR. (Fast-spectrum MSRs would use very little or no graphite.) This radiation limit may require periodic replacement of graphite components, which could be in various removable shapes, such as plates, rods, or balls.

**4.** Heat removal from the graphite

Since graphite is heated by gamma energy and by the neutron slowing down, its heat must be evaluated. Although its heat is several percent of the heat in fuel salt, its heat would affect the thermal-hydraulic design of the MSR and the irradiation stability of graphite.

When graphite is irradiated, it shows shrinkage at first, and then volume expansion (swelling) begins. In the MSBR design, a fluence limit of fast neutrons ($E > 50$ keV) was proposed as $3 \times 10^{22}$ neutrons/cm$^2$, where the AXF (Industrial grade graphite from Poco Graphite Inc.) volume returns back to an initial value, as shown in Fig. 7.2 (Rosenthal, 1972). This value can be applied to a thermal neutron spectrum MSR. (Fast spectrum MSRs would use very little or no graphite.) This radiation limit may require periodic replacement of graphite components, which could be in various removable shapes, such as plates, rods, or balls.

## 7.4.2 Beryllium

Beryllium (Be) is an excellent neutron moderator and reflector. It can serve as “neutron multipliers” through (n,2n) reactions by incident fast neutrons. Fig. 7.3 shows the cross-section for (n,2n) reactions in Be.

On the other hand, Be is toxic, generates helium through (n,α) reactions by fast neutrons, and has resource limitations. As a moderator or reflector of reactors, Be-

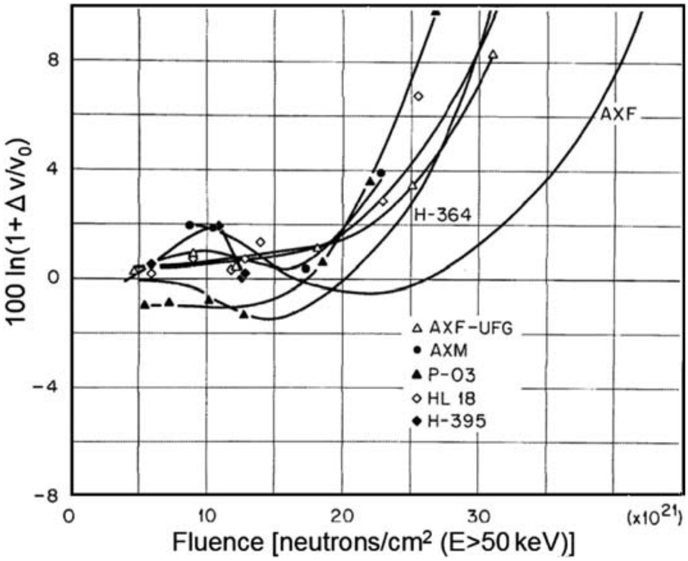

**Figure 7.2** Volume changes for monolithic graphite irradiated at 715°C (Rosenthal, 1972).

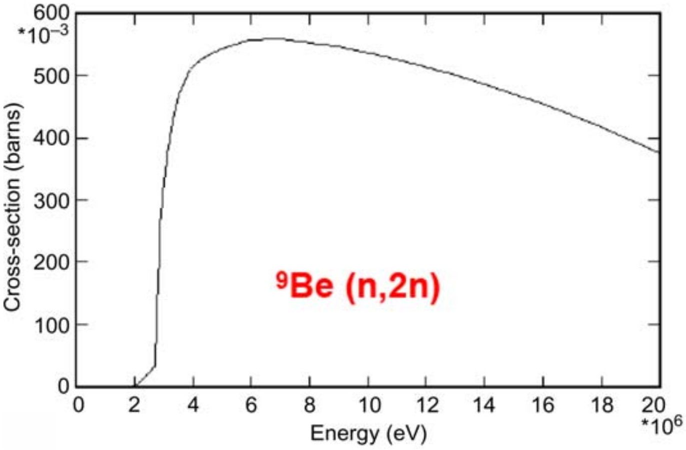

**Figure 7.3** Cross-sections for (n,2 n) reactions in Be vs neutron energy. 1 barn = $10^{-28}$ $m^2$. Courtesy of U. Fischer, Karlsruhe Institute of Technology.

oxide (BeO) is used. Ceramic BeO can be handled safely, and was used in the Aircraft Reactor Experiment (ARE) at ORNL (see Section 11.1). $Be_{12}Ti$ and $Be_{12}V$ are being studied for fusion reactor blankets.

### 7.4.3 Lithium

Natural lithium (Li) is composed of two isotopes; 7.42% $^6$Li and 92.6% $^7$Li. Since $^6$Li has a large absorption cross-section (about 940 barns for thermal neutrons) and generates tritium and helium, natural lithium is not appropriate as a moderator. Also, metallic Li has a low melting temperature, and $^7Li_2O$ or other compounds were candidates as solid moderators (Lundy et al., 1960).

As described below, $^7$LiF is used as a typical component of fuel salt in MSR. But, $^7$Li has a small capture cross-section for fast neutrons and it also produces some tritium.

Tritium is a beta-emitter with a half-life of 12.4 years, average energy 6 keV, maximum energy 18 keV. For safety reasons the tritium inventory in MSRs should be minimized. Fig. 7.4 shows the tritium production cross-sections of $^6$Li and $^7$Li vs. neutron energy. Additional cross-section data are available in BNL-325 (Garber and Kinsey, 1976).

In order to avoid thermal neutron capture in $^6$Li, MSRs could enrich $^7$Li by removal of $^6$Li. (In fusion reactor designs the opposite is true: It is desirable to maximize tritium breeding by using more $^6$Li and less $^7$Li.)

Lithium may be enriched by several processes:

- *Column exchange (Colex)*—LiH counter-flows through an amalgam of Li/Hg. Li-6 tends to stay in the Hg and migrate towards the bottom of the column, and the Li-7 tends to go with the LiH towards at the top. The bottom part is electrolyzed to separate the slightly enriched Li-6 and the top part is electrolyzed to separate the Li-7 fraction, in multiple

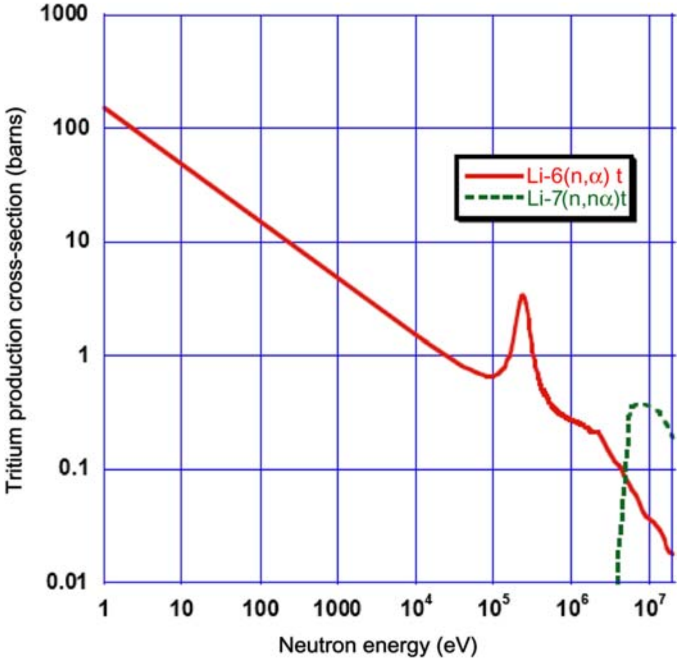

**Figure 7.4** Cross-sections for tritium production in $^6$Li and $^7$Li vs. neutron energy. Here (n,α) means that the lithium absorbs a neutron and the reaction releases an alpha particle, and (n,nα) means that both an alpha and a neutron are released.
Courtesy of U. Fischer, Karlsruhe Institute of Technology.

stages. Western countries do not use this method, in order to avoid toxic Hg contamination.

- *Vacuum distillation*—Lithium is heated to about 550°C in a vacuum. Lithium vapor is collected on a cold surface. Li-6 atoms have greater mobility and are collected preferentially. A multistage process would be used.
- *Atomic vapor laser isotope separation (AVLIS)*—A laser can be tuned to selectively ionize Li-6 or Li-7, which can then be separated by an electric field.
- *Crown ether method*—A water-insoluble solvent containing crown ethers is added to an aqueous mixture of LiCl. After the crown ethers distribute in the two solvent layers and form complexes, the Li-6 can be found preferentially in the solvent phase, with a separation factor per stage about 1.042 for Benzo15-crown5 (Ault et al., 2012).

"A predicted cost for 90% enriched Li-6 is about $2500/kg (2013 $), and the JASON report (2011) cited $1500/kg. In 2010, the estimated price for Chinese enriched Li-7 was $15,000/kg for 99.99% enrichment level. Since prices for 99.92% enriched lithium were not found, the price was estimated to be roughly in the $10,000/kg range (taken from the higher enrichment prices)" (Ault et al., 2012).

## 7.5 Structural materials

### 7.5.1 Requirements for good structural materials

Some requirements for good structural materials are:

- High-temperature operation for long durations;
- Adequate strength at elevated temperature;
- Corrosion resistance;
- Weldability;
- Low activation for waste disposal;
- Creep resistance;
- Good ductility after irradiation;
- Fatigue resistance;
- Minimal tritium retention;
- Established.

Most of these requirements apply to any nuclear use of metal alloys, however the requirement which is especially challenging for MSRs is corrosion.

This is because corrosion in molten salts is a fundamentally different process from that in conventional applications, and most of the methods to control corrosion developed over previous centuries are of limited value.

Corrosion of steel is an oxidative process, accelerated by contact with water. Corrosion-resistant steels (stainless steels) achieve their resistance by the formation of a stable oxide layer, often chromium oxide, on the surface of the steel. This layer acts as a barrier preventing the underlying alloy making contact with the oxygen and water in the environment. This is kinetic stabilization. The corrosion reaction still proceeds, but much more slowly. Stainless steel, exposed to oxygen for long enough or at a high enough temperature will still corrode.

Unfortunately, in molten salts this mechanism fails. Molten salts readily dissolve oxide layers from stainless steel, leaving the metal fully exposed to the molten salt. If the molten salt has the innate tendency to react with the metals in the alloy (chromium usually being the most reactive metal) then a rapid oxidation of the chromium to chromium chloride or fluoride will take place at the surface. This is evidenced as a rapid initial corrosion, which often progresses more rapidly along the grain boundaries of the alloy causing pitting and microcracking.

As the chromium is extracted, it leaves behind a chromium-depleted alloy which corrodes less easily so that over time corrosion slows down. Eventually, continued corrosion is limited by the diffusion of chromium through the alloy to the chromium-depleted surface layers. While normally a slow process, at high temperatures diffusion of metal atoms becomes more rapid. Of particular concern in nuclear applications is that intense radiation, gamma and neutron, will accelerate this metal diffusion process.

This last fact is a most challenging one for development of alloys for use in MSRs as it means that corrosion testing outside of the reactor environment can be quite misleading, giving erroneous measures of corrosion rates. Development of new alloys, or testing of existing alloys, can therefore by very slow and expensive.

There are in principle two approaches to prevent corrosion in MSRs. These are to change the alloy used, or to change the molten salt itself. These approaches are summarized in the following sections.

### 7.5.2 Development of corrosion resistant alloys

Two approaches are used in the development of corrosion-resistant alloys.

The first is to minimize the content of chromium or other reactive metals in the alloy. This usually involves the use of high nickel content "superalloys." The archetypal superalloy was Hastelloy N which is discussed in some depth below. The low chromium content is advantageous in two ways, it means that extraction of the chromium causes less physical damage to the alloy and it reduces the rate of dissolution of the chromium because the chromium has a lower thermodynamic activity, being present at a lower concentration in solid solution in the alloy.

The second approach is to change the properties of the alloy so that diffusion of chromium atoms is slowed. Typically this involves addition of refractory metals such as molybdenum to the alloy, giving it a higher softening temperature. Hastelloy N also incorporated this approach.

While substantial progress has been made in development of superior alloys, this approach can only slow down corrosion. Demonstration of long life under reactor conditions is very challenging indeed and would add years or decades to the development time for any MSR using such materials.

### 7.5.3 Reduction of the corrosive potential of molten salts

The lack of "passivating" oxide layers with molten salts makes the chemistry of the corrosion reaction rather simple. For any salt composition in contact with a chromium-containing alloy, there will be an equilibrium concentration of oxidized chromium (chloride or fluoride) in the salt such that no more chromium is extracted from the alloy. If it were that simple, then preventing corrosion would simply require the addition of enough chromium salt to the molten salt. Unfortunately, the equilibrium concentration of the chromium salt is temperature-dependent, so that chromium will be continually extracted from hot alloy surfaces and deposited at cooler ones.

To prevent corrosion therefore, the chemistry of the molten salt must be adjusted so that it has very little potential to dissolve chromium at any temperature. It is generally considered that an equilibrium chromium content of the molten salt of less than 1 ppm will result in corrosion being substantially absent.

The relevant chemical adjustment is of the redox potential of the salt. If the salt is made sufficiently reducing then chromium metal will be more stable than chromium chloride or fluoride and corrosion will not take place. This simple procedure was in fact tested as part of the ORNL Molten Salt Reactor Experiment in the 1960s where the introduction of a highly reactive sacrificial metal (beryllium) into the molten salt prevented corrosion of standard stainless steel.

This would suggest that corrosion control in MSRs should be very easily achieved. Unfortunately, it is not as simple as that.

Making the salt reducing by contacting it with a reactive metal does stop reaction of the chromium in the alloy. However, that reaction is replaced by corrosion of the reactive metal. That is a problem, because the same phenomenon of oxidation of the reactive metal at high temperatures but reduction back to metal at low temperatures takes place. The result is that the sacrificial metal migrates around the reactor, depositing in cooler regions such as heat exchangers. If the sacrificial metal is in electrical contact with other metals then this process is even more serious. One approach to mitigate this effect is to create a special low-temperature region of the molten salt system where the sacrificial metal is allowed to contact the salt. This approach has been adopted in the FHR reactor where it is hoped it will permit use of standard stainless steel in the reactor construction (Andreades et al., 2014). The use of sacrificial metals to stabilize molten salts which are in static, unpumped, systems where migration of the sacrificial metal is of no consequence is discussed in Chapter 21, Stable salt fast reactor.

An alternative way to make the salt strongly reducing is to add a reducing material to the salt which is itself soluble. In uranium fluoride-fueled reactors this material can be uranium trifluoride added together with uranium tetrafluoride but the approach is limited in value due to the higher melting point of uranium trifluoride and its lower solubility in most molten salts.

Another potentially generally useful approach is to take advantage of the fact that zirconium has two stable fluorides, $ZrF_2$ and $ZrF_4$. The addition of small amounts of $ZrF_2$ to molten salts, particularly those containing $ZrF_4$, is an effective inhibitor of corrosion, permitting standard stainless steels to be used. Details of this approach are also given in Chapter 21, Stable salt fast reactor. Other reducing salt couples, such as the divalent and trivalent halides of transition metals (Y, Sm, V), have also been proposed (Sridharan and Allen, 2013).

Making the molten salt strongly reducing is not, however, a panacea. It does have other, sometimes undesirable, effects.

Graphite is generally seen as unreactive to molten salts. This is however not true when the salt is strongly reducing. The formation of carbides is unavoidable in such systems. Where graphite moderator is used in the reactor and is directly exposed to the molten salt it is necessary to find a potentially very narrow window of molten salt chemistry where the salt is not too corrosive to the metal and not too reactive with the graphite. Validation that this balance has been achieved is a challenging experimental prospect as experiments under reactor radiation conditions will be necessary.

A similar problem occurs where uranium fluoride is used in the salt. If the salt is made strongly reducing, the uranium can be reduced to the metallic form. Again, a balance of not reducing the uranium too much while still reducing corrosion sufficiently must be found. This latter problem can be overcome by using chloride salts of uranium, which are more stable to reduction, but this approach is generally only applicable to fast neutron reactors due to the strong thermal neutron absorption of chlorine.

The discussion of molten salt chemistry and corrosion given above is necessarily brief. Much more detailed discussion is available in Sridharan and Allen (2013).

### 7.5.4 Hastelloy N and other Nickel-based superalloys

One of the most important achievements in the MSR development is the invention of INOR-8 by Inouye et al. (1958). The INOR-8 is an abbreviation of the eighth candidate of the superalloy by the International Nickel company for Oak Ridge (Roche, 2015), and its development story is described in McCoy (1969). This nickel-based superalloy was later tradenamed as Hastelloy N by the Haynes International Inc. The nominal composition of Hastelloy N is Ni-Mo-Cr-Fe-others (71-16-7-5-1 wt%), as is shown in Table 7.3.

Hastelloy N was used in the MSRE reactor vessel, pipes, pumps, heat exchangers, and all metal components facing its fluoride salt, and it showed a good performance. Current information on Hastelloy N is shown in the supplier's website (Haynes International Inc, 2002). Fig. 7.5 shows a photo of a sample plate.

Hastelloy N shows excellent compatibility with fluoride salts, containing LiF, $BeF_2$, $ThF_4$, and $UF_4$, because these fluorides are thermodynamically stable toward Hastelloy N. That is, these fluorides are much more stable than the structural metal fluorides ($NiF_2$, $BeF_2$, and $CrF_2$) (Rosenthal, 1972).

Among the above alloy constituents, chromium (Cr) is less noble and most reactive. Therefore, a Cr-depleted zone was observed on the surface exposed to MSRE fuel salt for 22,000 hours at 650°C, but the depth of degraded zone did not propagate any more than 0.2 mil (5 μm) (Rosenthal, 1972).

After the operation of the MSRE was ended, its Hastelloy N was investigated, and the standard Hastelloy N showed an intergranular attack, where grain boundaries were degraded due to the existence of FP tellurium (Te), although not deeply penetrating. Based on the parametric study on niobium (Nb) addition to the original Hastelloy N, modified Hastelloy N was developed in order to solve this issue, where Mo, Fe, and Si are reduced, and Nb (1%−2%) is added. Fig. 7.6 shows the

**Table 7.3 Chemical composition of Hastelloy N (weight %) (Haynes International Inc, 2002; Engel et al., 1979)**

| Element | Hastelloy N (Haynes)[a] | Hastelloy N (ORNL spec.) | Modified Hastelloy N (with Nb) | Modified alloy (with Ti) |
|---|---|---|---|---|
| Nickel | 71 | Base | Base | Base |
| Molybdenum | 16 | 15−18 | 11−13 | 11−13 |
| Chromium | 7 | 6−8 | 6−8 | 6−8 |
| Iron | <5 | <5 | <0.1 | <0.1 |
| Manganese | <1 | <1 | 0.15−0.25 | 0.15−0.25 |
| Silicon | <1 | <1 | <0.1 | <0.1 |
| Phosphorus | <0.8 | <0.015 | <0.01 | <0.01 |
| Sulfur | | <0.02 | <0.01 | <0.01 |
| Boron | | <0.01 | <0.001 | <0.001 |
| Niobium | | – | 1−2 | – |
| Titanium | | – | – | <2 |

[a] Other contents: Carbon < 0.08, Co < 0.20, Cu < 0.35, W < 0.50, [Al+Ti] < 0.35.

**Figure 7.5** Hastelloy N plate.
Courtesy of MMC Superalloy.

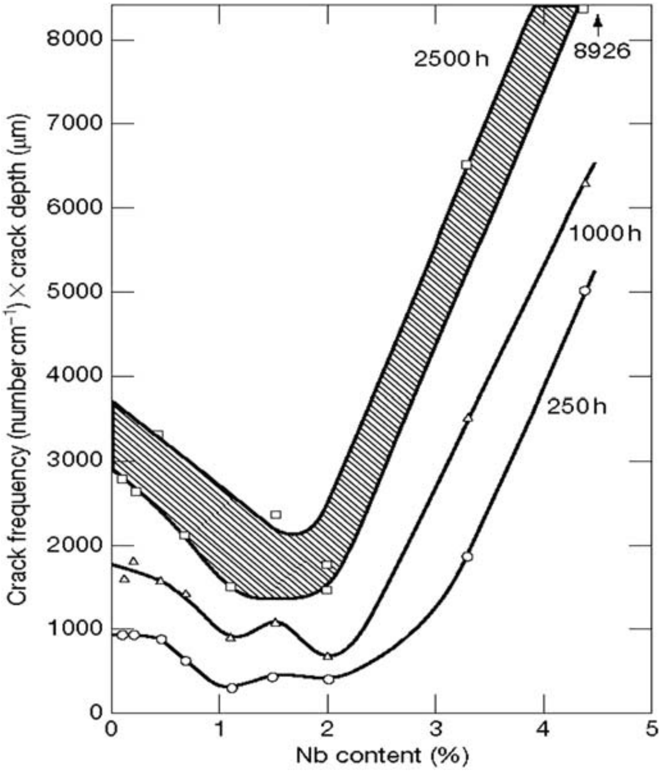

**Figure 7.6** Severity of cracking in Te-containing environments (Engel et al., 1979).

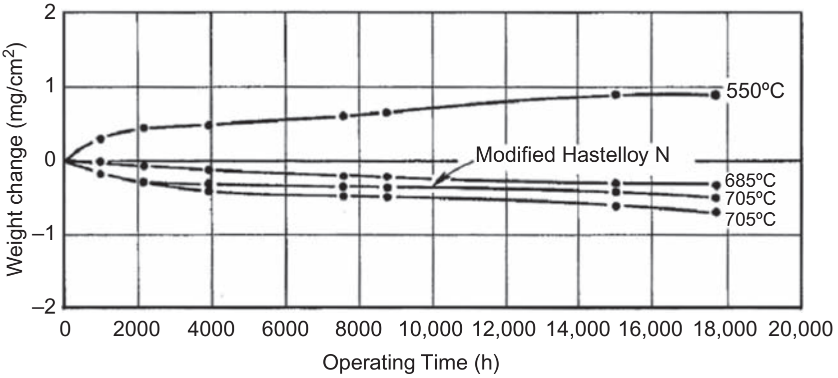

**Figure 7.7** Weight change versus time for Hastelloy N specimens exposed to fuel salt in thermal-convection loop (Rosenthal, 1973).

severity of cracking when the samples are exposed to Te-containing environments for up to 2500 hours at 700°C. A typical composition of modified Hastelloy N is Ni-Mo-Cr-Fe-Nb-others (79-12-7-0.1-1-1 wt%), as shown in Table 7.3 (Engel et al., 1979).

Advanced corrosion tests simulating nonisothermal dynamic conditions were performed in thermal and forced convection test loops. The weight change of standard and modified Hastelloy N was measured for over 22,000 hours exposure to MSBR fuel salt at a maximum 704°C, with temperature difference of 170°C. The corrosion specimens in the hot legs resulted in weight loss and weight gain in the cold legs. The estimated corrosion rate of Hastelloy N was 0.5 μm/y, and modified Hastelloy N exhibited better corrosion resistance. Fig. 7.7 shows these results for both Hastelloy N and modified Hastelloy N specimens (Rosenthal, 1973).

Besides the proposal of modified Hastelloy N, another solution was developed to control the reduction−oxidation (redox) potential by controlling the $U^{4+}/U^{3+}$ ratio. The MSRE experience suggests that Te is possibly converted to innocuous telluride (CrTe) by the reaction:

$$CrF_2 + Te + 2UF_3 \rightarrow 2UF_4 + CrTe.$$

An equilibrium of this reaction can be controlled by varying the $U^{4+}/U^{3+}$ ratio, that is, the redox potential can be controlled by adding metallic Be for reduction or $NiF_2$ for oxidization. It was observed that this Te attack becomes very small at a $U^{4+}/U^{3+}$ ratio less than 60, as is shown in Fig. 7.8 (Keiser, 1977). Therefore, this redox potential should be kept within the region of stable Te compound ($U^{4+}/U^{3+} < 60$) and above that of U-carbide deposition on graphite ($U^{4+}/U^{3+} > 6$).

After longtime irradiation, radiation damage such as embrittlement by helium (alpha particle), is caused by the following two-step reaction in nickel and by (n,α) reaction in boron contaminants.

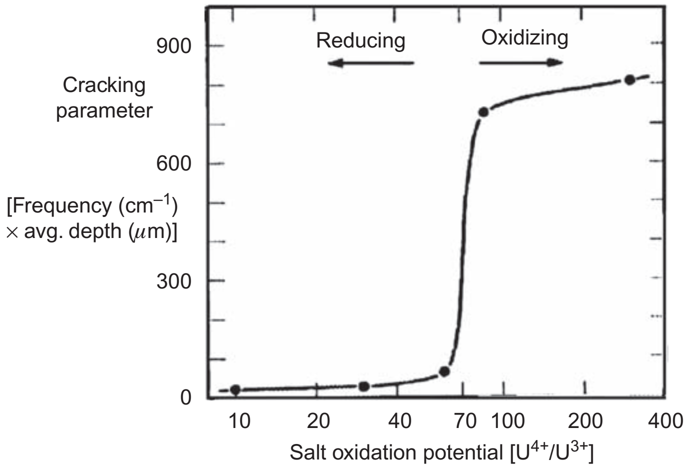

**Figure 7.8** Cracking behavior of Hastelloy N, exposed 260 h at 700°C to MSBR fuel salt containing $CrTe_{1.266}$ (Keiser, 1977).

$^{58}Ni\ (n,\gamma)\ ^{59}Ni \rightarrow\ ^{59}Ni\ (n,\alpha)\ ^{56}Fe$
$^{10}B\ (n,\alpha)\ ^{7}Li$

In the MSBR design, an anticipated service lifetime was 30 years, and the most highly irradiated portion of the reactor vessel would be exposed to a fast-neutron ($E > 0.1$ MeV) fluence of less than $1 \times 10^{21}$ neutrons/cm$^2$ and a thermal neutron fluence of about $5 \times 10^{22}$ neutrons/cm$^2$. Since the irradiation effect on Hastelloy N is small below these values (Keiser, 1977), these values can be considered as a conservative design limit for thermal neutron spectrum MSR.

In the 1970s, another modified Hastelloy N was proposed, where titanium (Ti) was added instead of niobium (Nb). At that time, it was found that the carbide precipitate that normally occurs in Hastelloy N could be modified to obtain resistance to the embrittlement by helium. Then, it was confirmed that 2% Ti contributed to the formation of a fine carbide precipitate and the alloy showed good resistance to embrittlement by helium. However, adding Ti did not show resistance against Te attack, and this alloy was abandoned (Engel et al., 1979).

The ASME Boiler and Pressure Vessel Code must be followed in order to use modified Hastelloy N in commercial reactors, and many property data, such as tensile data, ductility data, creep data, and so on, must be provided.

Besides the Hastelloy N development, Russia is developing alternative alloys for MSR. Under similar test conditions their new alloy showed a maximum corrosion rate of $6 \times 10^{-6}$ m/y, and no trace of Te attack. One alloy is named HN80MTY, which includes 1% aluminum (Al) and 1% Ti, instead of Nb in modified Hastelloy N (Ignatiev et al., 2012, 2013).

For more basic understanding of metal corrosion in molten salt, Sridharan and Allen (2013) is recommended.

## 7.6 Conclusions

This chapter first describes molten salt, which is most specific to MSR. Molten salt serves as a fuel element, as a heat transfer medium, and a as fuel processing medium. The thermo-physical properties of molten fluoride salts, such as LiF-$BeF_2$ (FLiBe), LiF-NaF-KF (FLiNaK), and others, are illustrated.

As for solid fuels with molten salt coolants, details of these are given in Chapter 13, Solid fuel, salt-cooled reactors.

Also, the thorium fuel cycle is briefly described, and details are given primarily in Chapter 9, Environment, waste, and resources, where the properties of thorium, its minerals, abundance, and estimated resources are detailed.

Possible moderators for thermal neutron spectrum MSR have been investigated in ORNL, and graphite was selected as the most appropriate moderator. Its compatibility with molten salts, irradiation stability, and other topics are described here. Some other moderators such as beryllium (Be) and lithium (Li) are also briefly introduced, because these elements are included, if LiF or $BeF_2$ is used in the MSR. The enrichment issue of natural Li to $_7$Li is also discussed.

The final topic on materials is the structural metal for MSR. Since its integrity in high-temperature molten salt under neutron irradiation circumstances is of the highest concern, a nickel-based superalloy, Hastelloy N, has been investigated, and is believed to be a feasible material. Some other candidates are also under investigation.

## References

Alexander, L.G., et al., 1959. Nuclear characteristics of spherical homogeneous two-region Molten-fluoride-salt reactors. ORNL-2751.

Andreades et al., 2014. Technical description of the “Mark 1” Pebble-Bed Fluoride-Salt-Cooled High-Temperature Reactor (PB-FHR) power plant. UCBTH-14-002.

Ault, Tim, et al., 2012. Lithium isotope enrichment: feasible domestic enrichment alternatives, Report UCBTH-12-005.

Benes, O., Konings, R.J.M., 2013. Thermodynamic calculations of Molten-salt reactor fuel systems. Chapter 4. In: Lantelme, F., Groult, H. (Eds.), Molten Salts Chemistry: From Lab to Applications. Elsevier Inc., USA.

Briant, R.C., Weinberg, A.M., 1957. Molten fluorides as power reactor fuels. Nucl. Sci. Eng. 2, 797–803.

Cantor, S. (1968). Physical properties of molten salt reactor fuel, coolant, and flush salts. ORNL-TM-2316.

Duderstadt, J.J., Hamilton, L.J., 1967. Nuclear Reactor Analysis. John Wiley & Sons, New York.

Engel, J.R., et al., 1979. Development status and potential program for development of proliferation resistance molten salt reactor. ORNL-TM-6415.

Furukawa, K., Numata, H., Kato, Y., Mitachi, K., Yoshioka, R., Furuhashi, A., et al., 2005. New primary energy source by thorium molten-salt reactor technology. Electrochemistry. 73, 552–563.

Gabbard, C.H., 1972. Development of a venturi type bubble generator for use in the molten-salt reactor xenon removal system. ORNL-TM-4122.

Garber, D.I, Kinsey, R.R, 1976. Neutron cross sections, volume II, curves, Brookhaven National Laboratory Report. *BNL 325*, Third Edition.

Haynes International Inc, 2002. HASTELLOY® N alloy. <https://www.haynesintl.com/pdf/h2052.pdf>

IAEA, 2010. Assessment of partitioning processes for transmutation of actinides. IAEA-TECDOC-1648.

Ignatiev, V., et al., 2012. Chapter 5.10-material performance in molten salts.. Comprehensive Nuclear Materials. Elsevier, Oxford.

Ignatiev, V., et al., 2013. Alloys compatibility in molten salt fluorides. J. Nucl. Mater. 441 (1-3), 592–603.

Ingersoll, D.T., Parma, E.J., Forsberg, C.W., Renier, J.P., 2005. Core Physics Characteristics and Issues for the Advanced High Temperature Reactor. ARWIF-2005. Oak Ridge, TN.

Inouye, H., Manly, W.D., Roche, T.K., 1958. Nickel-base Alloy. US-patent-2,921,850.

Iodine Pit Issue, 2015. <http://en.wikipedia.org/wiki/Iodine_pit>.

Keiser, J.R., 1977. Status of tellurium – Hastelloy N studies in molten fluoride salts. ORNL-TM-6002.

Lundy, T.S., et al. (1960) An evaluation of solid moderating materials. ORNL-2891.

McCoy, H.E., 1969. The INOR-8 Story. ORNL Rev. 3 (2), 35–49.

Roche, T.K., 2015. Personal communication.

Rosenthal, M.W., 1972. Development status of molten-salt breeder reactors. ORNL-4812.

Rosenthal, M.W., 1973. Molten-salt reactor program: semiannual progress report for period ending August 31, 1972. ORNL-4832.

Sohal, M.S., Ebner, M.A., Sabharwall, P., Sharpe, P., 2010. Engineering database of liquid salt thermo-physical and thermo-chemical properties. INL/EXT-10-18297.

Sridharan, K., Allen, T.R., 2013. Chapter-12-Corrosion in molten salts. In: Lantelme, F., Groult, H. (Eds.), Molten Salts Chemistry: From Lab to Applications. Elsevier Inc., USA.

Uhlir, J., Hron, M., Priman, V., Frejtic, Z., 2002. Current status of Czech R&D program in partitioning and transmutation. OECD/NEA meeting.

Uhlir, J., Marecek, M., 2009. Fluoride volatility method for reprocessing of LWR and FR fuels. J. Fluorine Chem. 130, 89–93.

# Chemical processing of liquid fuel

# 8

*Jan Uhlíř*
Research Centre Řež, Husinec - Řež, Czech Republic

## Chapter Outline

## 8.1 Introduction

The molten salt reactor (MSR) is classified as a nonclassical reactor system due to a specific character of its fuel, which is liquid—constituted by a molten fluoride salt mixture circulating between the reactor core and a heat exchanger. The fissile and fertile material are dissolved in a carrier molten salt, which concurrently plays the role of a heat-transferring agent (www.gen-4.org/gif/jcms/c_9359/msr). The liquid character of the MSR fuel exhibits several specific characteristics to this reactor type, which can be assessed both as advantages and also as complicated technical problems. Because the typical MSR features only a small reserve of reactivity, the MSR system needs a frequent supply of nuclear fuel which can be realized via its connection with the fuel processing/reprocessing unit. The "on-line" reprocessing of circulating fuel is necessary within a long run not only to keep the reactor in operation by clearing away some neutron poisoning elements, but this principle also allows very effective extraction of freshly constituted fissile material or its precursors. This technology is unique among the nuclear reactor systems and enables to operate MSR within the thorium−uranium fuel cycle in so economic and effective conditions, which are unattainable by any other reactor type with solid nuclear fuels.

The technology of chemical processing of liquid fuel for MSR can be divided into the processing of fresh liquid fuel and the reprocessing of the used fuel just circulated inside the fuel circuit of the reactor system. The final part of fuel processing technology should be also placed in the reactor site and tightly attached to the "on-line" reprocessing, because the refilling of the fresh fuel into the reactor has to

**Molten Salt Reactors and Thorium Energy. DOI: http://dx.doi.org/10.1016/B978-0-08-101126-3.00008-7**

be carried out in connection with the removal of the burned-out fuel and fission products from the primary fuel circuit. (Grimes, 1970; Uhlir, 2007).

There are some top-rated principles applicable in chemistry and chemical technology that should be also implemented in the decision-making, including what technologies should be chosen as preferable ones. Some of these principles applicable for the MSR chemical technology are the following:

- It will be most advisable to keep one chemical form (fluorides) of fuel for the entire fuel stream system in developing a compact fuel cycle of the liquid fuel reactor system.
- This principle results in a fundamental requirement on the choice of separation (partitioning) methods, which could be applied in the reactor fuel processing and especially in the "on-line" fuel reprocessing.

Based on these principles predominantly fluoride pyrochemical and/or pyrometallurgical procedures appear in the foreground of interest (Uhlir, 2007).

## 8.2 Processing of fresh liquid fuel for MSR

As mentioned above, typical MSR, as originally developed in ORNL or proposed by the Generation Four International Forum, uses molten salt fuel based on the carrier molten fluoride salt (usually the eutectic mixture of $^{7}LiF-BeF_2$) in which the uranium tetrafluoride $UF_4$ and thorium tetrafluoride $ThF_4$ are dissolved (Benedict et al., 1981). The design of the MSR core implicates the basic constitution of the fuel salt. When in the case of single-fluid (one-fluid) core design of MSR, the fuel salt contains both uranium and thorium fluorides together dissolved in the carrier salt, the double-fluid (two-fluid) core design of MSR requires the processing of two salts: the fuel salt, which contains dissolved fissile material only (e.g., uranium U-233 or U-235 in the form of $UF_4$) and the fertile salt in which the fertile material —thorium ($ThF_4$)—is dissolved.

Processing of uranium tetrafluoride and thorium tetrafluoride are widely known processes in the nuclear industry (Benedict et al., 1981). Processing of uranium tetrafluoride was mastered on a huge engineering scale for the uranium enrichment process, where the uranium tetrafluoride is an intermediate product in the uranium hexafluoride production. The similar technology can be used for the production of uranium tetrafluoride for MSR fuel. The technology is based on the hydrofluorination reaction which converts uranium dioxide $UO_2$ to $UF_4$.

$$UO_2 + 4HF = UF_4 + 2H_2O$$

The reaction is exothermically realized at about 500°C. The hydrofluorinating agent is anhydrous hydrogen fluoride (HF). In laboratory- or small-scale conditions, the reaction can be realized on the chemical boat in a heated reactor, but in industrial conditions, the series of fluidized-bed reactor is used.

Processing of thorium tetrafluoride was also well mastered in nuclear technology as it is the intermediate product in the production of thorium metal. The oxygen-free thorium tetrafluoride can be prepared by the hydrofluorination of thorium dioxide by anhydrous HF.

$$ThO_2 + 4HF = ThF_4 + 2H_2O$$

The reaction is exothermic and is usually realized at temperatures between 500−600°C. In this way, thorium dioxide can be completely converted to thorium tetrafluoride with practically no traces of residual oxygen.

Both chemical processes and chemical techniques described above can be used for the production of $UF_4$ and $ThF_4$ for the final preparation of liquid fuel for MSR. The final step in the production of fresh liquid MSR fuel is an individual or joint dissolution of $UF_4$ and $ThF_4$ in the carrier salt (typically $^7LiF-BeF_2$ eutectics). LiF and $BeF_2$ are common chemical products, but the lithium fluoride for use in MSR has to be prepared from pure isotope Li-7 to minimize tritium generation from Li-6. There are known enrichment technologies for the separation of lithium isotopes (Li-6 and Li-7) based either on LiOH/Li-Hg amalgam extraction technology (industrially used COLEX process) or atomic vapor laser isotope separation (AVLIS), which is still under development (Report UCBTH-12-005, 2012). Beryllium bifluoride $BeF_2$ is industrially available as an intermediate product of the beryllium metal production.

## 8.3 Reprocessing technology of MSR fuel

As mentioned above, the long run of MSR is possible only if the chemical composition of the MSR fuel is kept in an acceptable range in which the chain reaction can be safely controlled by control rods and the content of neutron poisons does not spoil the neutron economy. This requirement can be met only by the connection of the fuel circuit of the MSR system with the fuel reprocessing unit, where the fuel is cleaned up—fission products (neutron poisons) and bred materials are removed from the fuel circuit and new fuel and fertile material are supplied. On-line reprocessing containing the chemical separation processes is the method to meet these requirements. The general spirit of MSR on-line reprocessing is to keep the reactor in steady-state conditions by continuously cleaning-up the primary (fuel) circuit salt. It means that some part of the salt circulating in the primary circuit is piped to the reprocessing unit, where the fission products are extracted and then moved to waste, whereas the separated actinides are dissolved again in the carrier salt and returned back into the primary circuit. As there is always the same concentration of fission products in the primary circuit, the removal of these elements in the reprocessing unit need not be absolute, however no actinides may be moved into the waste stream. The scheme of a reprocessing principle is shown in Fig. 8.1.

The only exception is the removal of gaseous fission product elements, such as xenon and krypton. Xenon is the most important neutron poison among the fission products and its poisoning effect represents about 98 fission product capture rate

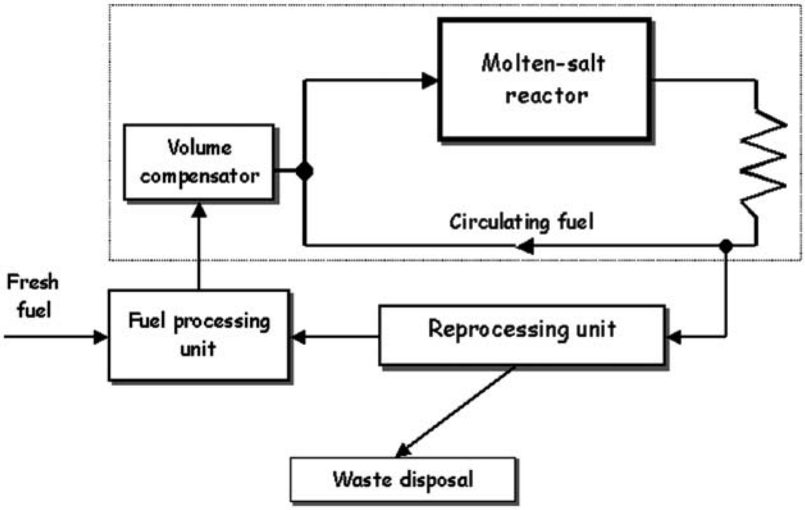

**Figure 8.1** Scheme of MSR fuel reprocessing principle.

(Štika, 2012). Therefore, the removal of gaseous fission products has to be realized permanently, completely, and immediately, directly inside the fuel circuit.

If the MSR system is designed as a thorium-breeder, the separation of protactinium can play a significant role. Protactinium Pa-233 is a precursor of desirable U-233 and it originates by β-decay from Th-233. The problem is that Pa-233 has a big cross-section for thermal neutrons and a relatively long half-life (about 27 days). Therefore the prompt extraction of protactinium from the fuel circuit is important for the maximized breeding of U-233, because it minimizes the undesirable formation of Pa-234.

A simplified scheme of the MSR operating in the thorium–uranium fuel cycle is shown in Fig. 8.2.

Chemical separation processes applicable within the MSR fuel cycle technology have to be in good accordance with the chemical nature of the molten fluoride fuel and with the requirement for virtually immediate fuel processing after leaving the reactor core. The separation processes must often work at the high temperatures, often over 500°C, and must be highly radiation-resistant. There are only few pyrochemical separation methods that meet these requirements (Grimes, 1970; Uhlir, 2007). Most were developed in the 1950s, 1960s, and 1970s, often for the MSR program investigated in Oak Ridge National Laboratory. The objective of the investigation at the end of the 1960s and the beginning of the 1970s was the development of a fuel processing technology devoted to the concept of the 1000 MWe molten salt breeder reactor (MSBR) working in the thorium–uranium fuel cycle. After the Generation Four International Forum was chartered in 2001, the investigation of selected pyrochemical methods suitable for MSR fuel cycle was restored. Existing and proposed technological development of the MSR fuel cycle comes extensively from the original investigations.

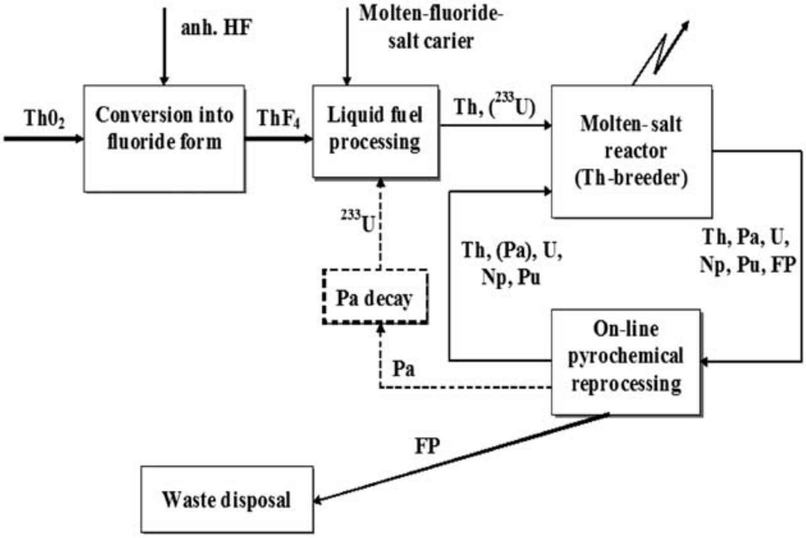

**Figure 8.2** Scheme of fuel cycle of MSR Th-breeder.

The main chemical separation processes applicable within the reprocessing technology of the liquid molten salt fuel are:

- Gas extraction process also known as “helium bubbling;”
- Fused salt volatilization;
- Molten salt/liquid metal reductive extraction;
- Electrochemical separation techniques from molten fluoride salt;
- Vacuum distillation of molten salt.

The processes mentioned above can serve both the removal of the actinides from the liquid molten salt fuel and the carrier salt clean-up from fission products (neutron poisons). Whereas the original MSR design was based on the thermal spectrum reactor working in the thorium−uranium fuel cycle (MSBR program developed by Oak Ridge National Laboratory), present MSR design considers also the fast spectrum MSR (Molten Salt Fast Reactor [MSFR] proposed mainly by French Centre National de la Recherche Scientifique [CNRS]) and Russian National Research Centre “Kurchatov Institute” (Rosenthal et al., 1970, 1971; Ignatiev et al., 2014). Although this difference partially affects the amount, constitution, and reprocessing rate of circulating MSR fuel, the main technological separation processes are similar for both—thermal and fast MSR concepts.

## 8.4 Gas extraction process

The principle of the gas extraction process—sparging the molten salt with inert gas (He)—is based on the application of a scientific principle of Henry’s Law. The solubility of dissolved gas (Xe, Kr) in a molten salt is proportional to the partial pressure of that gas in the atmosphere. If a new inert gas (He) is introduced in the molten salt, the difference in partial pressure causes the dissolved gas (Xe, Kr) to leave the molten salt. The efficiency of sparging is influenced by many factors such as bubble size, temperature, gas pressure, etc.

The gas extraction process, also known as the "helium bubbling method," was successfully used and verified during the Molten Salt Reactor Experiment (MSRE) 1965−1969. As the MSRE was operated only as an experimental reactor, the complete reprocessing of its fuel was not necessary, except for removal of the main neutron poisons—xenon (Xe)-135 and Kr-85. The gas extraction process (helium bubbling) emerged to be a suitable and effective method (Rosenthal et al., 1971). Noble gases have very low solubility in the fuel salt ($LiF-BeF_2-UF_4$), which makes it possible to strip them from the salt and reduce the poisoning effect of Xe-135. The removal was provided by sparging the salt with helium, which was then passed through charcoal traps in an off-gas clean-up system. The contact for noble gases (xenon and krypton) removal was produced by spraying of salt through the cover gas (helium) and into the pool of salt in the fuel pump bowl. The schematic view of the pump with helium sparging system is shown in Fig. 8.3.

At the end of the MSRE program, helium was temporarily replaced by argon, which has a much lower solubility in the fuel salt. Experiments at lower power showed substantial differences in the amounts of gas in the core with argon and with helium. At low pump speeds, the small amount of helium drawn into the pump suction could almost completely dissolve in the salt before reaching the core. A similar amount of argon at the pump suction meant more bubbles in the salt going through

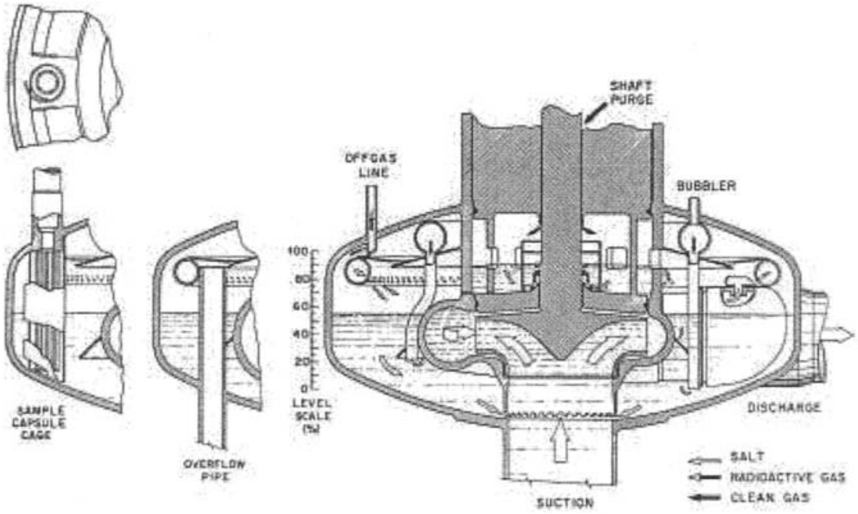

**Figure 8.3** Vertical section of fuel pump with helium sparging system.
*Source*: Courtesy of ORNL, US-DOE.

the core because less was dissolved. When the reactor was operated at the power with argon cover gas, the xenon poisoning at high void fractions was about the same as it was with helium, but the xenon poisoning was higher with argon when only small amounts of gas circulated with the salt. The difference between argon and helium is due almost entirely to the difference in solubility of these gases.

Xenon and krypton stayed with the purge stream (helium or argon) to the charcoal beds, where adsorption delayed their passage long enough for practically all the radionuclides, except krypton-85, to decay. The daughters of Xe and Kr deposited on surfaces contacting the gas stream, in quantities readily detectable by gamma-spectrometry and heat production. Through the end of the MSRE operation, however, temperatures in charcoal showed no evidence of any decrease in adsorptive capacity due to accumulation of these daughters (Rosenthal et al., 1971; Scott and Eatherly, 1970). The flowsheet of the MSRE fuel off-gas system is shown in Fig. 8.4.

Present investigation of the gas extraction process is carried out mainly in France by CNRS Grenoble. The effort is a part of the existing CNRS program devoted to the MSFR technology development (Merle-Lucotte, 2013).

Verification of the gas extraction process during MSRE projects was generally fully successful. Xenon gas—the main neutron poisoning element—was continuously removed from the fuel salt circuit during the reactor run. The extraction capacity was designed to enable an average xenon processing time of about 20 seconds. A similar xenon processing time was designed for MSBR system.

However xenon and krypton are not the only fission products that can be removed by gas extraction from the MSR fuel salt. As the MSR working temperatures are in the range of 650–750°C, there are some other elements, which tend to leave the salt. The group of noble metals like niobium, molybdenum, ruthenium, antimony, and tellurium did not form stable fluorides in the normal environment in the MSRE. The bulk of the fission product elements (lanthanides) form stable and soluble fluorides and remained with the fuel salt.

Noble metals were partially removed in the noble gases stripping system and accompanied xenon and krypton in the purge stream. They settled as radioactive dust everywhere on the surface of pipes, filters, and other parts of the off-gas system. Other portions of the noble metals that did not leave the primary circuit deposited on the surface of the primary circuit structural materials—Hastelloy N and graphite. The typical noble metals processing time designed for MSBR was similar to that of xenon, at about 20–50 seconds (Rosenthal et al., 1971).

## 8.5 Fused salt volatilization

The method called fused salt volatilization is based on the chemical reaction of fluorine gas with elements dissolved in fluoride molten carrier. Some elements originally dissolved in the salt form volatile fluorides, which tend to leave the salt. Fused salt volatilization was successfully applied during the MSRE program, when this process was used for uranium removal from the fuel circuit ($LiF-BeF_2$ was the

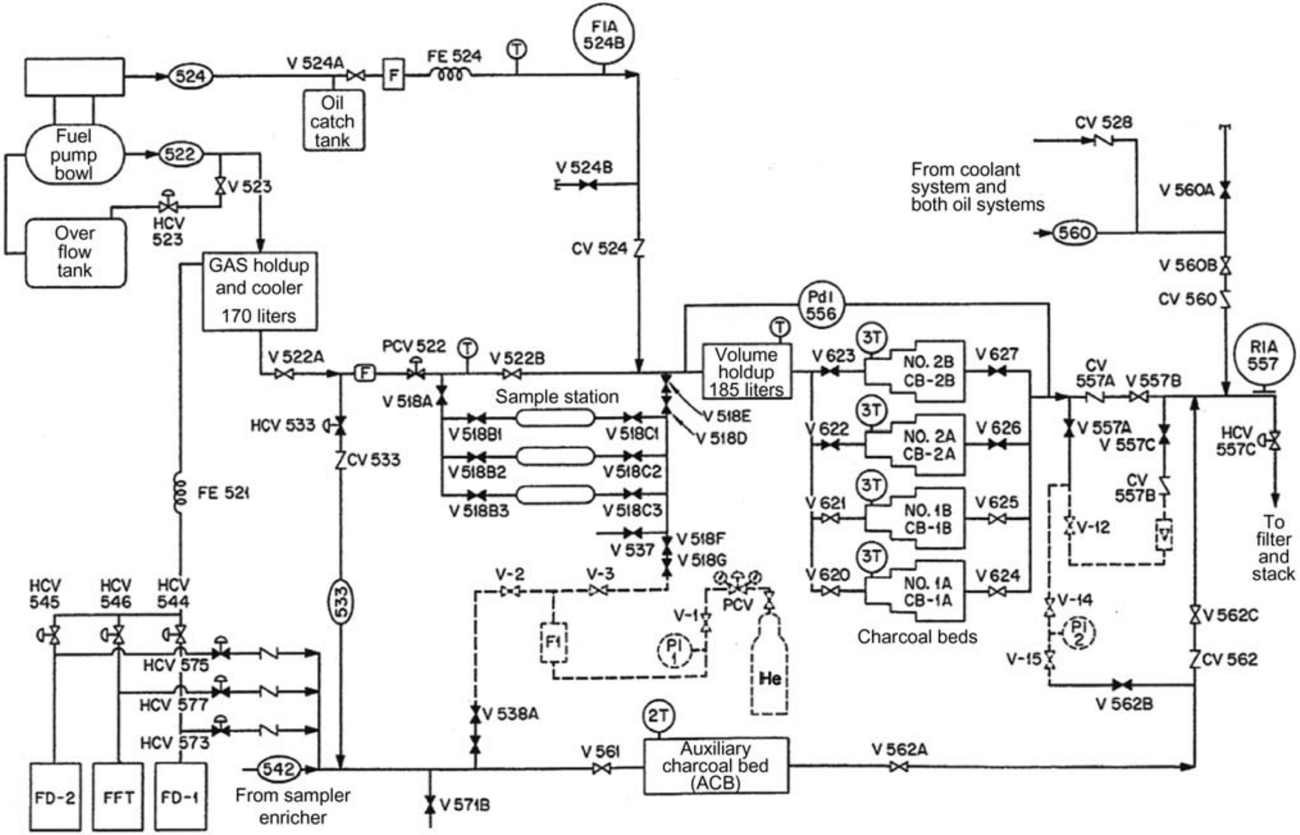

**Figure 8.4** Simplified flowsheet of MSRE fuel off-gas system.
*Source*: Courtesy of ORNL, US-DOE.

carrier salt). Uranium was recovered from the fuel salt as uranium hexafluorides ($UF_6$) by sparging the salt with fluorine gas. Oak Ridge National Laboratory realized this technology in the US in 1968. The goal of the extraction of uranium was the change of original U-235 for U-233. Carrier molten fluoride salt, in which uranium was dissolved, was $LiF-BeF_2$ melt. Uranium was recovered from the carrier salt as uranium hexafluoride by sparging the salt with fluorine gas. This fluorine gas bubbling through the salt containing uranium in the form of dissolved $UF_4$ produces a formation of $UF_6$ on the gas−liquid phase interface. The rate of fluorination reaction is high enough at the temperature range of 500−600°C. That's why it would lead one to expect the mass transfer of uranium compounds in the liquid phase to be the limiting stage of the process.

Special equipment for continual fluorination of the salt was designed by ORNL in 1960s (ORNL report No. 3936, 1966). The crucial part of the equipment was the continuous fluorination reactor with frozen wall for corrosion protection (Fig. 8.5). The main structural material of the fluorinator was pure nickel.

The carrier molten salt containing dissolved UF4 flowed into the top of the fluorination reactor and was contacted by a countercurrent stream of fluorine gas, which stripped out the uranium in the form of volatile UF6 according to the following reaction

$$UF_4 + F_2 \rightarrow UF_6$$

The working temperatures were in the range of 500−550°C; the reactor walls coolant was NaK. The off-gas containing uranium hexafluoride, fluorine gas, and volatile fluorides of some fission products (here mainly $CrF_4$ and $CrF_5$) passed through sorption column with NaF pellets heated to 400°C for removal of chromium fluorides. UF6 was then trapped at the same sorbent at 100°C. Similar technology was under development in ORNL during ensuing MSBR program at the beginning of the 1970s aimed mainly to design an on-line reprocessing scheme for molten salt reactors working under a $^{232}Th-^{233}U$ fuel cycle (ORNL report No. 5018, 1974).

A fused salt volatilization process was under development in ORNL also during the first period of preparation of the MSBR project. A close-coupled facility for processing (reprocessing) the fuel and fertile streams of the MSBR was understood to be an integral part of the reactor system. (Initially, the MSBR was designed with two separate circuits: fuel-stream and fertile-stream.) The preliminary design of the MSBR fuel and fertile stream processing is shown in Fig. 8.6.

Fig. 8.6 shows that only four major operations were proposed to accomplish the fuel stream processing: fluorination, sorption of $UF_6$, vacuum distillation, and salt reconstitution. After 36 hours of cooling time, the fuel processing should have begun by molten salt fluorination. Some fission products like Ru, Tc, Nb, Cs, Mo, and Te form also volatile fluorides and accompany the $UF_6$. Therefore the gas stream leaving the fluorinator passes through a sorption system composed of temperature-controlled beds of NaF and $MgF_2$ pellets. The first section of the NaF bed is held at about 400°C and sorbs most of the fission products, the second section of the bed is held at about 100°C and sorbs technetium, part of the molybdenum, and allows the remaining fission products to pass. Upon heating from 100°C

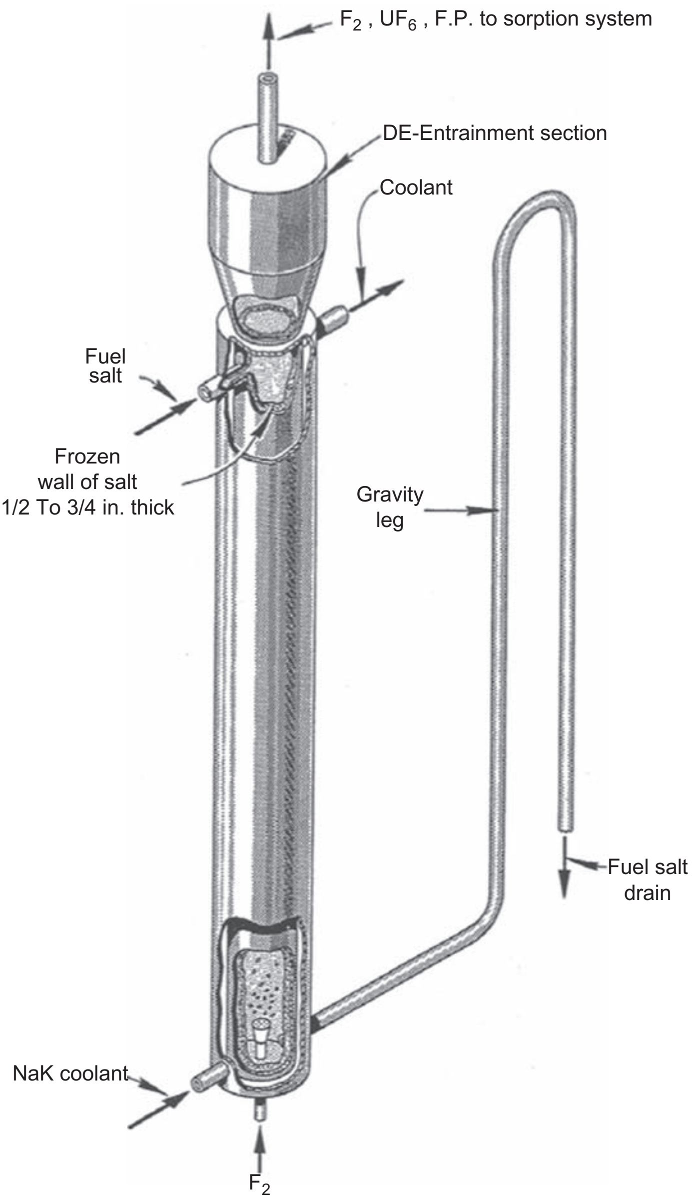

**Figure 8.5** Fused salt fluorination reactor.
*Source*: Courtesy of ORNL, US-DOE.

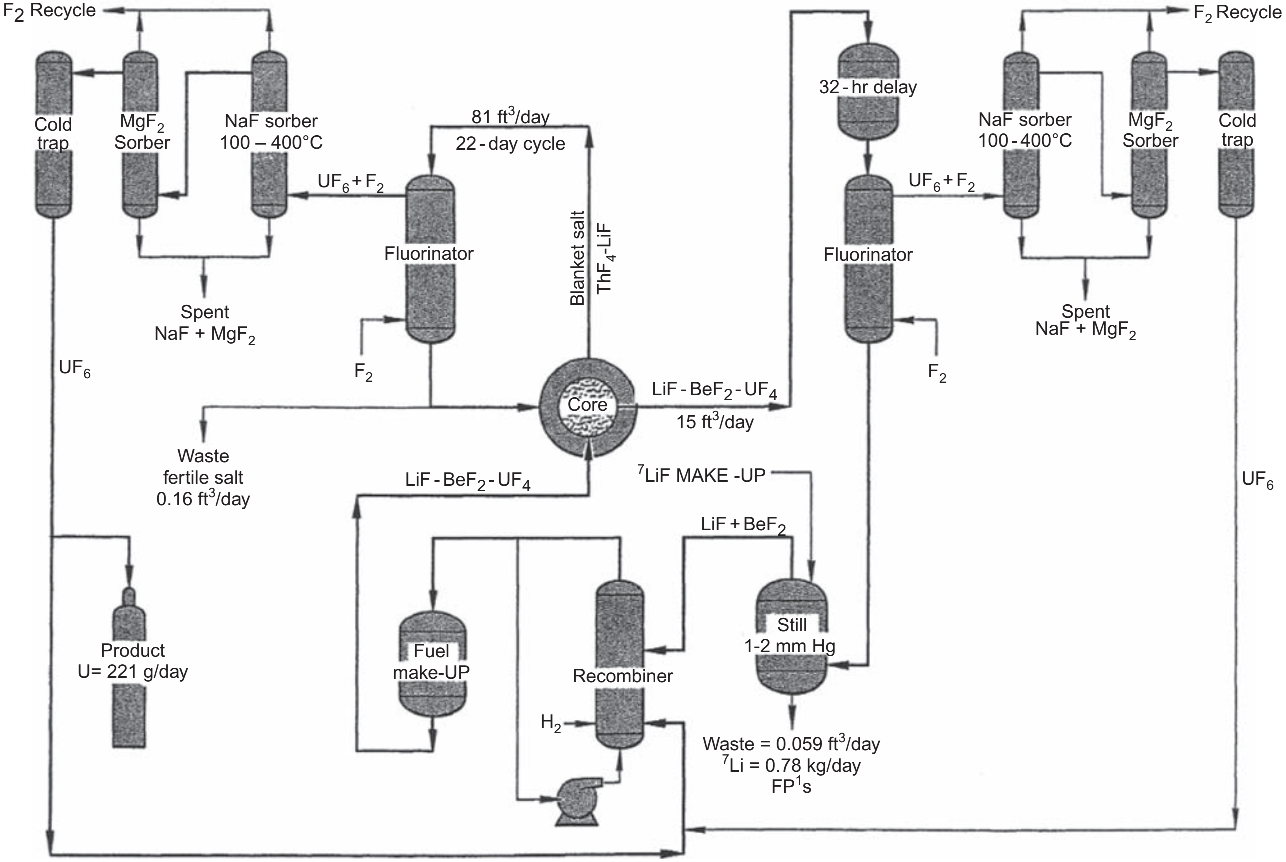

**Figure 8.6** Initial design of MSBR fuel and fertile stream processing.
*Source*: Courtesy of ORNL, US-DOE.

to 400°C, the second section of the sorber releases molybdenum, technetium, and $UF_6$, this passes through $MgF_2$ for retention of technetium while allowing $UF_6$ to pass. Uranium hexafluorides are then frozen in cold traps and retained for recycling to the reactor (Rosenthal et al., 1971).

At present, there is no running experimental development program of the fused salt volatilization technique, but nearly all of the MSR fuel cycle flowsheets proposed by several institutions under the frame of the Generation IV program include this method. Here, the fused salt volatilization is often proposed to be used, not only for uranium removal, but also for extraction of plutonium (in the form of $PuF_6$) and neptunium (in the form of $NpF_6$) (Delpech et al., 2009). However, it is necessary to take into account that whereas the formation of volatile $UF_6$ goes relatively easy and quantitatively, because the stable form of uranium is hexavalent, the preferable form of plutonium is tetravalent and therefore the formation of $PuF_6$ is more difficult and plutonium hexafluoride tends to decompose to $PuF_4$ and $F_2$ (Fischer et al., 1962).

## 8.6 Molten salt/liquid metal extraction

Molten salt/liquid metal reductive extraction is proposed as a separation method widely used for the MSR fuel salt clean-up. The technique was investigated by ORNL both for protactinium removal from the fuel salt and for the extraction of lanthanides (rare-earth elements) which represents the main group of fission products. The main principles of the technology were based on selective molten-salt/liquid metal reductive extraction into liquid bismuth in multistage countercurrent extraction system (Rosenthal et al., 1971).

The principle of the extraction into bismuth is based on the property of bismuth, which is a low-melting (271°C) metal that is essentially immiscible with molten halide mixtures, which include fluorides, chlorides, and bromides. Bismuth has a negligible vapor pressure in the temperature of interest, 500–700°C and the solubilities of metals such as lithium, thorium, uranium, protactinium, and the rare earths are adequate for processing application.

Reductive extraction reactions between materials in molten salt and liquid metal phases can be represented by the general reaction

$MX_n + nLi(Bi) \leftrightarrow M(Bi) + nLiX$,in which a metal halide $MX_n$ in the salt reacts with lithium from the bismuth phase to produce M in the bismuth phase and the respective lithium halide in the salt phase. The oxidation state of M in the salt is $n+$, and X represents fluorine, chlorine, or bromine.

Distribution data were obtained in ORNL for a number of materials between bismuth and fuel MSBR salt (72% LiF, 16% $BeF_2$, 12% $ThF_4$) at 640°C (Ferris et al., 1969). The data indicate that protactinium, as well as uranium and zirconium, can be easily extracted from the salt stream containing $ThF_4$. However, the separation factors of rare earth elements/thorium are close to unity (from 1.2 to 3.5), which indicates that selective extraction of the rare earth elements (lanthanides) from a molten fluoride salt containing thorium tetrafluoride is either difficult or nearly impossible. Therefore, another extraction system between the liquid bismuth and the molten lithium chloride was chosen as the most promising. Here, the separation of both divalent rare-earth elements and trivalent rare-earth elements from thorium is possible. The distribution coefficients for these materials are strongly affected by the concentration of lithium in the bismuth phase, and the best method for removing these materials from the LiCl appears to be extraction into bismuth containing lithium at a concentration of 0.05 to 0.5 mole fraction. A simplified flowsheet for the rare-earth removal system is shown in Fig. 8.7.

As mentioned above, the molten salt/liquid metal reductive extraction was proposed by ORNL also for the protactinium separation (Rosenthal et al., 1971). Protactinium, which exists in the fuel salt as $PaF_4$, can be relatively easily reduced by lithium and extracted into liquid bismuth. In order to avoid the use of large quantities of reductant, removal of uranium from the salt by fluoride volatilization was situated before the protactinium separation.

After removal of uranium by conversion of $UF_4$ to volatile $UF_6$, protactinium is extracted in the first instance into liquid bismuth and consequently converted by hydrofluorination to fluoride salt, wherefrom the $^{233}UF_6$ is extracted by fluorination after the protactinium decay. (The radioactive half-life of $^{232}Pa$ is about 27 days.) A schematic flowsheet of protactinium isolation is shown in Fig. 8.8.

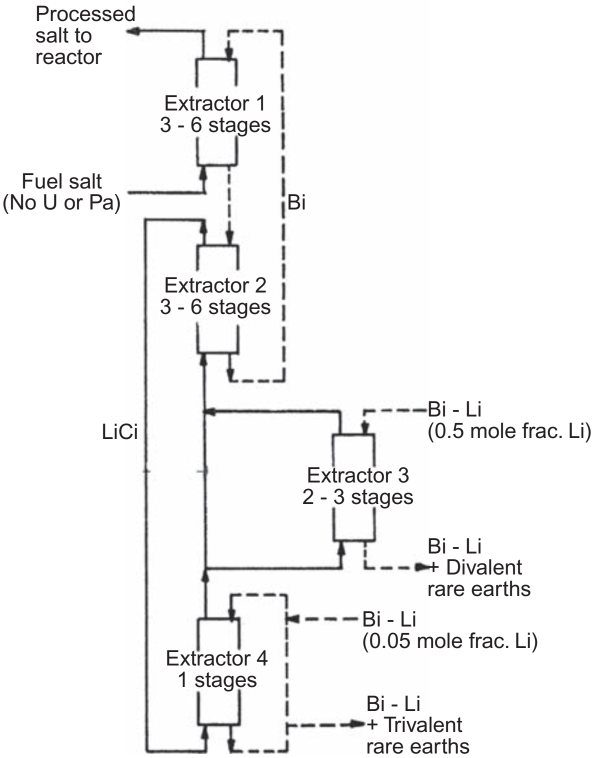

**Figure 8.7** Flowsheet of rare-earths removal system for MSBR.
*Source*: Courtesy of ORNL, US-DOE.

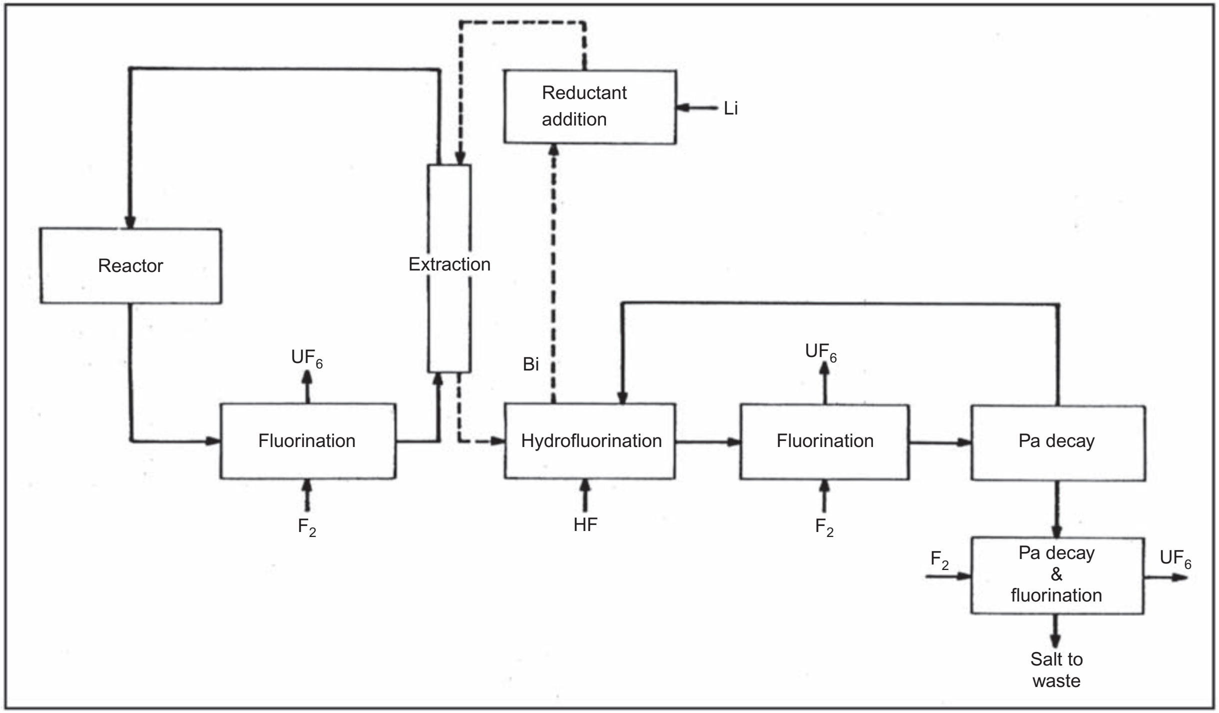

**Figure 8.8** Flowsheet for protactinium separation from MSBR by fluorination and reductive extraction.
*Source*: Courtesy of ORNL, US-DOE.

At present, with the exception of limited French and Russian activities (Delpech, 2013; Zagnitko and Ignatiev, 2013), there is no intensive experimental development program on molten salt/liquid metal reductive extraction for the uranium, protactinium, thorium, and fission products separation into liquid bismuth from fission products in an $LiF-BeF_2$ fluoride molten salt.

## 8.7 Electrochemical separation processes

The effort to use the electrochemical separation processes for reprocessing of MSR fuel containing thorium is relatively new, connected with the MSR development under the Generation Four International Forum. The main arguments for this effort were facts that the development of electro-separation processes made remarkable progress from the 1960s, when MSR reprocessing was under study in ORNL; and that the molten salt/liquid metal reductive extraction studied in the MSBR project showed some difficulties in the separation of thorium from rare earth elements.

The theoretical as well as experimental investigation of the electrochemical separation processes applicable within the MSR thorium fuel reprocessing have been studied mainly by the Nuclear Research Institute Řež (UJV) in the Czech Republic and at the Université Paul Sabatier in Toulouse in France (Uhlíř et al., 2012; Chamelot et al., 2010). The main objective of electrochemical separation research has been to determine the separation possibilities of the selected actinides (uranium, thorium) and fission products (lanthanides) in selected fluoride melt carriers.

Although the typical reference MSR fuel composition ($^7LiF-BeF_2-ThF_4-UF_4$) was already done by reactor physicists, it was clear that the melts based on $LiF-BeF_2$ will not be applicable for all electrochemical separation steps, because of the limited electrochemical stability of $BeF_2$. Therefore the first step was the choice of fluoride melts suitable for electrochemical separations. The chosen melt should meet some basic characteristics—low melting point, high solubility of studied compounds, high electrochemical stability, and appropriate physical properties (electrical conductivity, viscosity, etc.). Unfortunately no melt fulfilling all the requirements was found. Therefore three candidate melts were selected for further electrochemical separation studies: eutectic mixture of LiF-NaF-KF (acronym FLINAK, m.p. 454°C, however limited electrochemical stability), mixture of $LiF\text{-}BeF_2$ (acronym FLIBE, m.p. of chosen composition 456°C, however limited electrochemical stability), and eutectic mixture of $LiF\text{-}CaF_2$ (m.p. 766°C, good electrochemical stability). Electrochemical stability of the carrier melt is defined by the electrochemical window. It is a voltage range in which the carrier melt is neither oxidized nor reduced.

The cyclic voltammetry method was used for studying the basic electrochemical properties of actinides and fission products dissolved in selected fluoride melt media. A special reference electrode based on the $Ni/Ni^{2+}$ red-ox couple was developed to provide reproducible electrochemical measurements in molten fluoride salts (Bronstein and Manning, 1972; Straka et al., 2010).

**Table 8.1** Evaluated red-ox potentials [V]

| Red-ox couple | LiF-NaF-KF | LiF-CaF2 | LiF-BeF$_2$ |
|---|---|---|---|
| | Ref. Ni/Ni$^{2+}$ In FLINAK | Ref. Ni/Ni$^{2+}$ in LiF-CaF$_2$ | Ref. Ni/Ni$^{2+}$ in LiF-BeF$_2$ |
| $U^{3+}/U^0$ | −1.75 | −1.90 | −1.4 |
| $U^{4+}/U^{3+}$ | −1.20 | −1.40 | |
| $U^{5+}/U^{4+}$ | +0.40 | – | |
| $U^{6+}/U^{5+}$ | +1.40 | – | |
| $Th^{x+}/Th^0$ | ~ −2.00 | −1.70 | Out of window |
| $Th^{4+}/Th^{x+}$ | −0.70 | – | |
| $Nd^{2+}/Nd^0$ | < −2.05 | −2.00 | Out of window |
| $Nd^{3+}/Nd^{2+}$ | ~ −1.00 | Not detected | |
| $Gd^{2+}/Gd^0$ | < −2.05 | −2.10 | Out of window |
| $Gd^{3+}/Gd^{2+}$ | ~ −1.00 | Not detected | |
| $Eu^{3+}/Eu^{x+}$ | ~ −0.75 | Not detected | |
| $Eu^{x+}/Eu^0$ | −1.95 | < −2.30 | |
| $Zr^{4+}/Zr^{x+}$ | −1.50 | – | |
| $Zr^{x+}/Zr^0$ | −1.80 | – | |
| $Sr^{2+}/Sr^0$ | < −2.05 | – | |
| $La^{3+}/La^0$ | < −2.05 | – | Out of window |
| $Pr^{3+}/Pr^0$ | < −2.05 | – | Out of window |
| $Sm^{2+}/Sm^0$ | −0.8 | – | – |
| $Sm^{3+}/Sm^{2+}$ | Out of window | – | – |

The selected red-ox potentials evaluated by UJV for uranium, thorium, and selected fission products in individual carrier molten salts are listed in Table 8.1 (Uhlíř et al., 2012).

Results obtained from the measurements can be interpreted in the following way:

- In FLIBE melt, there is a good possibility for electrochemical separation of uranium, and the electrochemical removal of uranium can eventually replace the fused salt volatilization. Although the electrochemical studies of protactinium have not been realized yet, based on the thermodynamical properties of $PaF_4$, there is a presumption that also protactinium could be separated from this melt.
- In FLINAK melt, only uranium can be directly separated.
- In LiF-CaF$_2$ melt, uranium, thorium, and most fission products (lanthanides) can be electrochemically separated.

## 8.8 Vacuum distillation

The technology of vacuum distillation was also judged by ORNL for clean-up of the MSR fuel carrier salt (LiF−BeF$_2$) fission products. Originally this process, led at

1200°C, was proposed also for rare earth elements, and later on for the separation of those elements, which cannot be extracted from salt by reductive extraction due to their high thermodynamical stability. It is typical for alkaline fluorides and alkaline earth fluorides like CsF, RbF, $SrF_2$, $BaF_2$. However the cost of the technology, the length of time required, and the need to process total volume of the fuel salt caused this technology to almost be abandoned (Carter et al., 1968; Bauman et al., 1977).

## 8.9 MSR reprocessing flowsheets

The separation techniques discussed above have allowed the design of several schemes of MSR on-line reprocessing. The original conceptual flowsheets were proposed by ORNL for MSBR system with $LiF{-}BeF_2{-}ThF_4{-}UF_4$ composition. The flowsheet intended for single-fluid MSR design is shown in Fig. 8.9 (Rosenthal et al., 1971).

The present flowsheets of the Gen IV activities originate from this MSBR scheme, but they include some changes in MSR fuel composition and progress in electrochemical separation techniques. A conceptual flowsheet of MSFR isobreeder reprocessing proposed by CNRS is shown in Fig. 8.10 (Laplace et al., 2011; NEA Report on Thorium, 2015) and the MSR on-line reprocessing flowsheet based on the broader use of electrochemical separation processes proposed by the Nuclear Research Institute Řež (UJV) is drafted in Fig. 8.11 (Uhlíř et al., 2012).

As is evident, the MSR core is now often proposed to be designed as a double-fluid (two-fluid) system with separated channels of fissile and fertile salt. This design is often motivated by the wish to maximize the breeding factor of the MSR system. Concerning the corresponding fuel cycle, the main difference between the one-fluid and two-fluid systems comes from the fact, that in the case of the two-fluid system the requirements for reprocessing of fissile-fluid and fertile-fluid circuits are quite different. As the speed of fissile-fluid reprocessing is determined mainly by the requirement to keep the concentration of fission products at the acceptable level allowing the operation of the reactor, the extraction of $^{233}Pa$ from the fertile-fluid circuit has to be as fast as possible, because the speed of protactinium separation has a direct impact on the breeding factor of the system. The reason for the prompt separation of protactinium is to eliminate the nuclear reaction of $^{233}Pa(n,\gamma) \rightarrow {}^{234}Pa$, which leads to the undesirable $^{234}U$ production.

As the partitioning technology used for the reprocessing of the fissile-fluid circuit could be similar to those proposed for the one-fluid system (evidently without the protactinium and thorium separation), the partitioning technology of the fertile-fluid circuit could be significantly simplified. The supposed conceptual on-line reprocessing flowsheets of fissile-fluid and fertile-fluid MSR circuits proposed by the Nuclear Research Institute Řež (UJV) are shown in Figs. 8.12 and 8.13.

Chemical processing techniques are also discussed in Chapter 11, Liquid fuel, thermal neutron spectrum reactors.

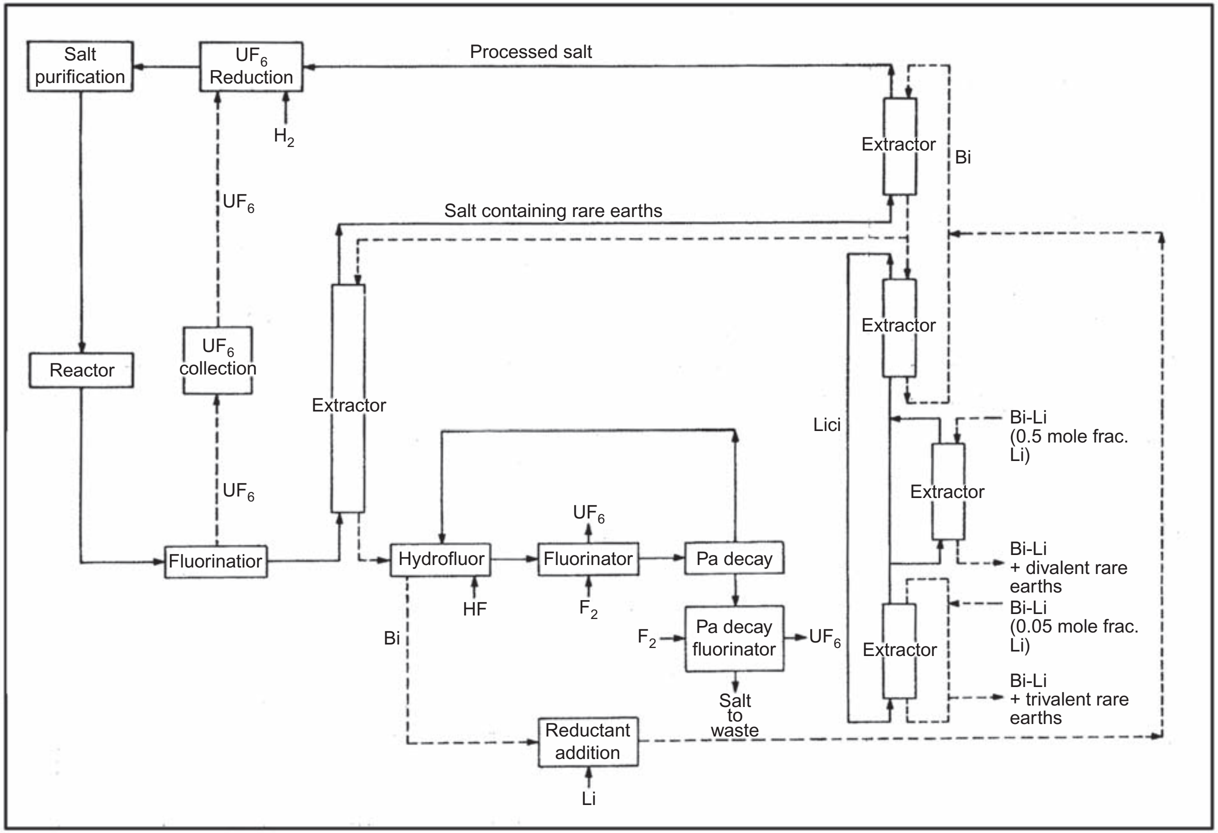

**Figure 8.9** Th-breeder flowsheet proposed by ORNL for MSBR.
*Source*: Courtesy of ORNL, US-DOE.

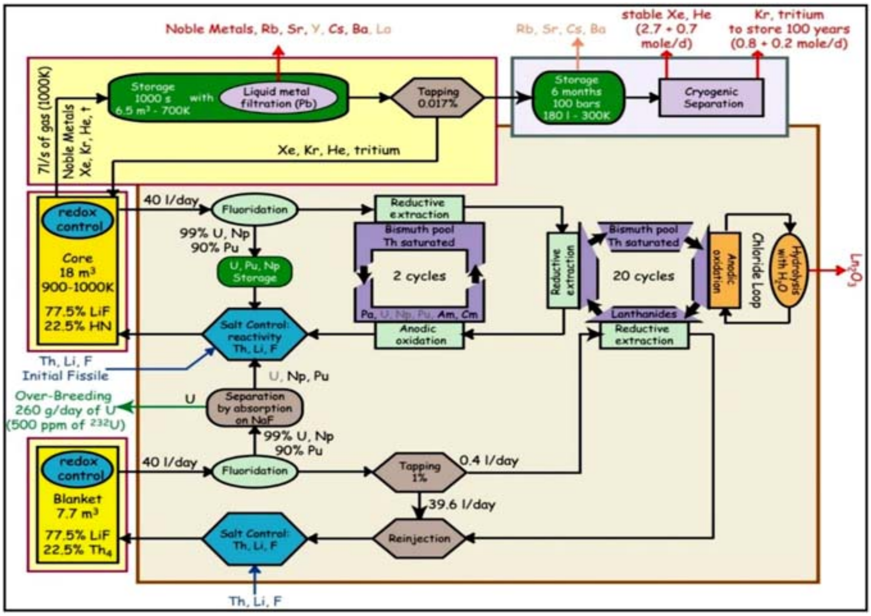

**Figure 8.10** Detailed flowsheet of double-fluid MSFR fissile and fertile salt reprocessing. *Source*: Courtesy of CNRS.

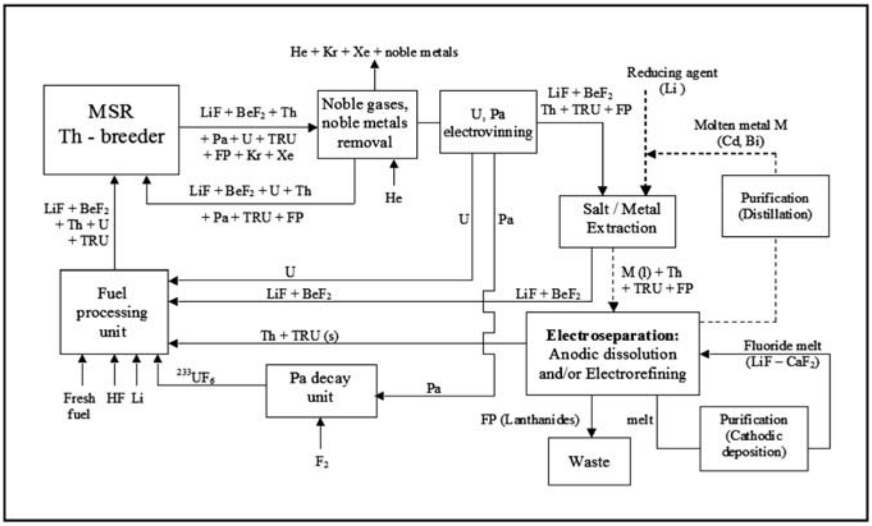

**Figure 8.11** Conceptual flowsheet of the single-fluid MSR on-line reprocessing technology. *TRU*, transuranium elements; *FP*, fission products.
*Source*: UJV.

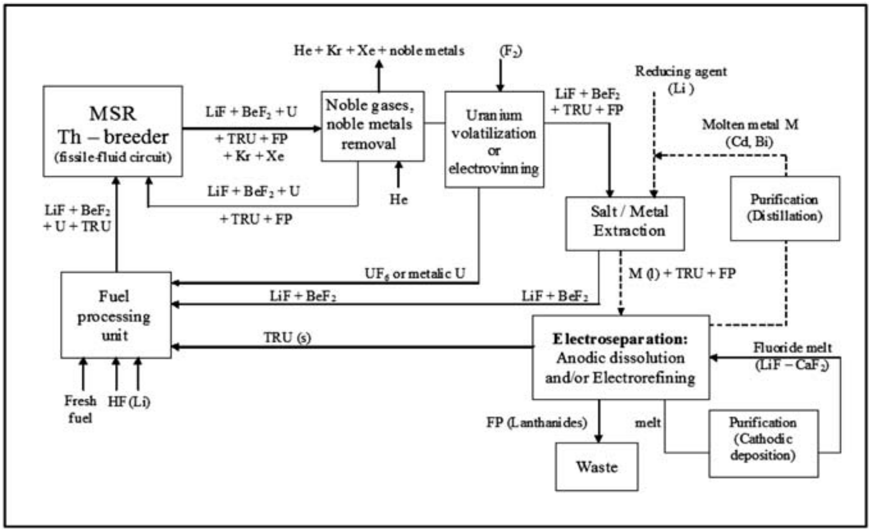

**Figure 8.12** Conceptual flowsheet of fissile circuit of double-fluid MSR on-line reprocessing technology.
*Source*: UJV.

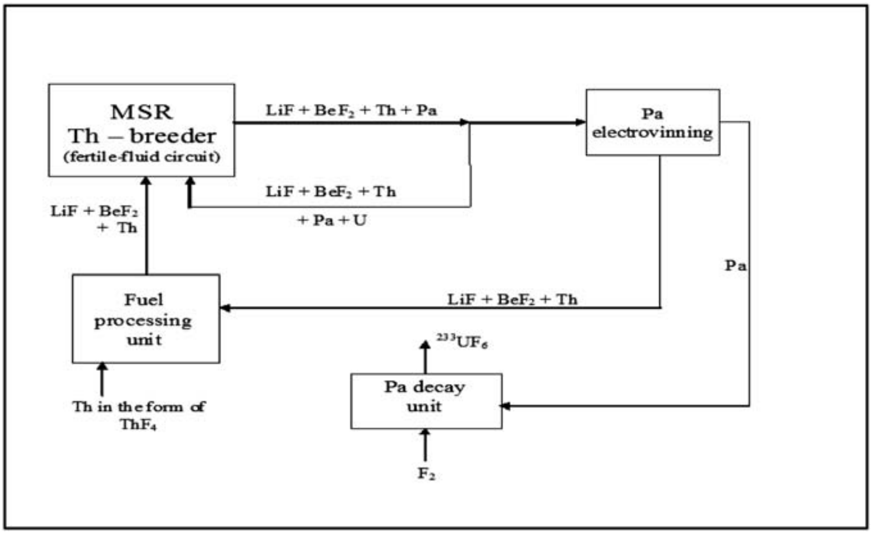

**Figure 8.13** Conceptual flowsheet of fertile circuit of double-fluid MSR on-line reprocessing technology.
*Source*: UJV.

## 8.10 Conclusions

On-line reprocessing of MSR fuel means that the MSR fuel cycle technology is strongly linked with the MSR physics, with the design of the reactor core, and with the chemistry of the reactor core. The fission reaction in the MSR core is not chemically neutral. It is a chemically oxidative process, which must then be chemically compensated in the fuel circuit to maintain slightly reductive conditions (red-ox potential) to protect the main structural material (nickel alloys) against corrosion (see Chapter 7: Materials). A direct link between MSR physics and on-line reprocessing chemistry is also extremely strong for MSRs operating as thorium-breeders. The fission power level affects the on-line reprocessing capacity; and the reprocessing rate affects the fissile material concentration. The rate of protactinium removal affects the reactor system breeding factor, and the rate of fission product extraction affects the neutron economy and the required fissile material concentration. To achieve good neutron economy, satisfactory breeding performance, and acceptable operational economy, reprocessing technology must be optimized.

Chemical processing of liquid fuel includes technologies with various technology readiness levels. Whereas some of them, like processing of fresh liquid fuel, are well mastered and adequately verified, some other technologies still represent a scientific and engineering challenge. The biggest is a full verification of on-line reprocessing technology as a whole. Although the problem was studied intensively at ORNL and significant progress was achieved, the termination of the MSBR project in the 1970s prevented the ORNL team from completing the development and verification. Nowadays interest in MSR systems and recent progress in new partitioning techniques (such as electroseparation), which were not studied during the MSBR project, inspire optimism that the on-line reprocessing technology can be also mastered in the foreseeable future. Additional chemical processes are discussed in Chapter 12, Fast spectrum, liquid fueled reactors.

## References

Bauman, H.F., Grimes, W.R., Engel, J.R., Ott, H.C., deBoisblanc, D.R., 1977. Molten-salt reactor concepts with reduced potential for proliferation of special nuclear materials, ORAU-IEA-77-13.

Benedict, M., Pigford, T.H., Levi, H.W., 1981. Nuclear Chemical Engineering. McGraw-Hill Book Company, New York.

Bronstein, H.R., Manning, D.L., 1972. Lanthanum trifluorides as a membrane in a reference electrode for use in certain molten fluorides. J. Electrochem. Soc. 119 (2), 125.

Carter, W.L., Lindauer, R.B., McNeese, L.E., 1968.Design on an engineering-scale, vacuum distillation experiment for molten-salt reactor fuel, ORNL TM-2213.

Chamelot, P., Massot, L., Cassayre, L., Taxil, P., 2010. Electrochemical behaviour of thorium(IV) in molten LiF-$CaF_2$ medium on inert and reactive electrodes. Electrochem. Acta. 55 (16), 4758.

Delpech, S., 2013. Possible routes for pyrochemical separations: focus on the reductive extraction in fluoride media. Pure Appl. Chem. 85, 71.

Delpech, S., Merle-Lucotte, E., Heuer, D., et al., 2009. Reactor physics and reprocessing scheme for innovative molten salt reactor system. J. Fluorine Chem. 130, 11.

Ferris, L.M., Mailen, J.C., Smith, J.J., 1969. Molten salt reactor program semiannual progress report, ORNL-4396.

Fischer, J., Trevorrow, L.E., Vogel, G.J., Shinn, W.A., 1962. Plutonium hexafluoride thermal decomposition rates. Ind. Eng. Chem. Process Des. Dev. 1 (1), 47.

Grimes, W.R., 1970. Molten-salt reactor chemistry. Nucl. Appl. Technol. 8, 137.

Ignatiev, V., Feynberg, O., Lizin, A., et al., 2014. Molten salt actinide recycler and transforming system without and with Th-U support: Fuel cycle flexibility and key material properties. Ann. Nucl. Energy. 64, 408.

Laplace, A., Vigier, J.F., Plet, T., Renard, C., Abraham, F., Slim, C., Delpech, S., Picard, G., 2011. Elaboration de solutions solides d’oxydes d’actinides et de lanthanides en milieu sels fondus: application à un nouveau procédé de refabrication du combustible par voie pyrochimique, Brevet déposé le 26/09/2011, n FR 11/58572.

Merle-Lucotte, E., 2013. Introduction to the physics of Molten Salt Fast Reactor, Proceeding of the Thorium Energy Conference, Geneva, Switzerland, 27−31 October 2013.

NEA Report on Thorium, 2015. OECD-NEA.

ORNL report No. 3936 (1966), Molten-Salt Reactor Program Semiannual Progress Report for Period Ending February 28, 1966, Oak Ridge, TN.

ORNL report No. 5018 (1974), Program Plant for Development of Molten-Salt Breeder Reactors, Oak, Ridge, TN.

Rosenthal, M.W., Kasten, P.R., Briggs, R.B., 1970. Molten-salt reactors−History, status, and potential. Nucl. Appl. Technol. 8, 107.

Rosenthal, M.W., Haubenreich, P.N., McCoy, H.E., McNeese, L.E., 1971. Recent proggress in molten-salt reactor experiment. Atom. Energy Rev. 9 (3).

Report UCBTH-12-005 (2012), Lithium Isotope Enrichment: Feasible Domestic Enrichment Alternatives, University of California, Berkeley, CA.

Scott, D., Eatherly, W.P., 1970. Graphite and xenon behaviour and their influence on molten salt reactor design. Nucl. Appl. Technol. 8, 179.

M. Štika, Analysis of the fuel cycle of Molten Salt Reactor system with thorium fuel and single-fluid and double-fluid reactor core design, M.S. Thesis, Czech Technical University Prague, 2012.

Straka, M., Korenko, M., Lisý, F., 2010. Electrochemistry of uranium in LiF-$BeF_2$ melt. J. Radioanal.Nucl. Chem. 284 (1), 245.

Uhlir, J., 2007. Chemistry and technology of Molten Salt Reactors - history and perspectives. J. Nucl. Mater. 360, 6.

Uhlíř, J., Straka, M., Szatmáry, L., 2012. Development of pyroprocessing technology for thorium-fuelled molten salt reactor, Proceeding of the ICAPP’12, Chicago, USA, 24-28 June 2012.

Zagnitko, A., Ignatiev, V., 2013. Equilibrium distribution of lanthanum, neodymium and thorium between fluoride salt melts and liquid bismuth. Russ. J. Phys. Chem. A. 86 (4), 611.

www.gen-4.org/gif/jcms/c_9359/msr

# Environment, waste, and resources

# 9

*Ritsuo Yoshioka*[1], *Motoyasu Kinoshita*[1,2], *Lars Jorgensen*[3] *and*
*Magdi Ragheb*[4]
[1]International Thorium Molten-Salt Forum, Yokohama, Japan, [2]The University of Tokyo, Tokyo, Japan, [3]ThorCon Energy, Stevenson, WA, United States, [4]University of Illinois at Urbana-Champaign, Champaign, IL, United States

## Chapter Outline

## 9.1 Decay heat in the thorium cycle

### *9.1.1 Introduction*

Decay heat is an important safety parameter of the nuclear fuel, especially shortly after reactor shutdown in a molten salt reactor (MSR). The MSR fuel salt flows by gravity to a drain tank in some accidental conditions, and its decay heat must be evaluated. Decay heat is also important for a long-term storage of spent fuels.

**Molten Salt Reactors and Thorium Energy. DOI: http://dx.doi.org/10.1016/B978-0-08-101126-3.00009-9**

Decay heat, caused by the decay of actinides and fission products (FPs), mainly depends on the fuel, which may contain isotopes of Th, U, and Pu as oxides, fluorides, chlorides, or metal.

The decay heat calculation is well-established for $UO_2$ and mixed oxide (MOX) fuel, but reliable papers on decay heat for thorium cores are limited. Therefore, this section provides the necessary information on decay heat evaluation for thorium fuel, compared with $UO_2$ fuel.

Heating from fissions caused by delayed neutrons disappears in several minutes, and this heating process is handled in the kinetic equations for accident analysis, so it is ignored here.

After unique features of MSR decay heat are first discussed, decay heat from thorium pressurized water reactor (PWR) fuel is compared with decay heat from conventional $UO_2$ PWR fuel.

### *9.1.2 Unique features of MSR decay heat*

One of the most unique features in MSR on decay heat is that the gaseous FPs such as krypton (Kr) and xenon (Xe) are removed from the fuel salt, because these FPs are inert gases and can be removed from a liquid molten fuel salt by a gas removal system. Then, some of the fuel salt decay heat can be reduced. On the other hand, these removed FPs will cause additional heat generation at a radioactive gas treatment system.

Typical decay heat generation by FP gas is as follows. The fission yield of $^{233}U$ (number of generated FP atoms per 100 $^{233}U$ fissions) for $^{88}Kr$ is 3.8, that is 3.8% fission yield. Since the half-life of $^{88}Kr$ is 2.8 hours with 2.9 MeV energy emission, its decay causes significant decay heat. Some Kr nuclides have a very short half-life, and they cannot be removed by an FP gas removal system. Meanwhile, some of Kr nuclides have a very long half-life or even are stable, and their contribution to decay heat is small or nothing. Here, fission yield data are based on England (1993), and decay data such as half-life and energy are based on Korea Atomic Energy Research Institute (2015).

The fission yield of $^{135}Xe$ is only 1.2%, but its parent nuclide $^{135}I$ (iodine) has a fission yield of 3.3% and a half-life of 6.6 hours. This $^{135}I$, which is circulating within fuel salt, decays to gaseous $^{135}Xe$. $^{135}Xe$ is transmuted both by neutron capture to stable $^{136}Xe$ and by beta decay to $^{135}Cs$ with a half-life of 9.1 hours and 1.2 MeV energy emission. However, most $^{135}Xe$ is removed from molten salt by an FP gas removal system before being transmuted.

Thus some of Kr and Xe can be removed by an FP gas removal system, but some of Kr and Xe cannot be removed. Also, the efficiency of an FP gas removal system affects the result. The decay heat from Kr and Xe is about 10% of the total decay heat by all nuclides. In a conservative safety analysis, the effect of FP gas removal may be disregarded, which gives a larger decay heat estimate.

The second concern on MSR decay heat may be the generation of gaseous tritium. Neutron absorption in $^{6}Li$ and $^{7}Li$, which are components of some fuel salts, such as LiF-$BeF_2$ ("FLiBe") generate tritium (T, or $^{3}H$). Since tritium is a beta-emitter (average energy only 6 keV) with a half-life of 12.3 years, its decay heat is negligible, but it is hazardous if ingested into the body. The generation rate of

**Table 9.1** **Generation rate of tritium for 1000 MWe MSBR (Robertson, 1971)**

| Reaction | T generation (Curie/day) |
|---|---|
| Ternary fission | 31 |
| $^{6}$Li(n,α)T | 1210 |
| $^{7}$Li(n,αn)T | 1170 |
| $^{19}$F(n,$^{17}$F)T | 9 |
| Total | 2420 |

tritium in a 1000 MWe Molten Salt Breeder Reactor (MSBR) with 99.995% enriched $^{7}$Li in one day is shown in Table 9.1. Here, 1 curie equals to $3.7 \times 10^{10}$ becquerel. ORNL proposed several countermeasures, which would reduce the release rate of tritium to the environment down to 1/100−1/1000th of the generation rate (Robertson, 1971).

In this table, the initial 6Li decreases with years by neutron absorption, but $^{6}$Li is newly generated by fast neutron absorption to 9Be, that is $^{9}$Be(n,α)$^{6}$He reaction and further beta-decay to $^{6}$Li. The last feature on MSR decay heat is the behavior of so-called "noble metals" (elements 41−52, insoluble in the fuel salt) in the MSBR design (Robertson, 1971). They are Nb (niobium), Mo (molybdenum), Tc (technetium), Ru (ruthenium), Rh (rhodium), Pd (palladium), Ag (silver), Cd (cadmium), In (indium), Sn (tin), Sb (antimony), and Te (tellurium). These FPs would deposit on metal and graphite surfaces or move to a gas removal system, where some decay heat is generated even after fuel salt is drained to a drain tank.

In this section online reprocessing is not assumed, but if it is adopted, decay heat within the fuel salt must be evaluated for the online reprocessing facility. Decay heat issues and design for the MSBR are provided in an ORNL report (Robertson, 1971).

### 9.1.3 Calculation method

In this section, decay heat for PWR thorium fuel is compared with conventional PWR $UO_2$ fuel, and ORIGEN2 code is used to calculate decay heat (Croff, 1980).

There are several cross-section libraries for different fuels in ORIGEN2, and their effects were studied in Yoshioka et al. (2014) and IAEA (to be published). The following two cores were assumed, with a rated power density of 39.2 MW/T.

1. U-PWR-core: 4%$^{235}$U+96%$^{238}$U.
2. Th-PWR-core: 4%$^{233}$U+96%$^{232}$Th

Since the output of decay heat in ORIGEN2 is "Watt/ton-HeavyMetal"(in general, "ton-HeavyMetal" is defined as a total weight of U/Pu/Th in fresh fuel), decay heat was divided by a rated power density in order to derive "% fraction."

Therefore, if "Watt/ton" value is required for discharged fuel, it can be derived by multiplying a rated power density (=39.2) to the following figures.

Also, if "Watt/ton" value is required for 1 GW (GWe or GWt) operation in a year, its conversion process is described at 9.2.4.

Fuel was burned up to 45 GWd/t, and then decay was calculated from 1 second to 1 million years.

### 9.1.4 Components of decay heat

First of all, the same $UO_2$ library was used for the above two cores. This comparison may show the basic difference between uranium (or $^{235}$U) and thorium (or $^{233}$U) on FP and actinide generation. One unique feature for Th-core is that there is a peak at 0.1 million years, which is explained later.

Components of decay heat are shown in Fig. 9.1 for the U-core, and Fig. 9.2 for the Th-core. Both figures show that decay heat by FP is dominant up to 100 years, but it fades out after 100 years. After that, decay heat by actinides becomes dominant.

There is some difference on decay heat between U-core and Th-core at a short time range. Of course, there is some difference on fission yield between $^{233}$U and $^{235}$U, and this may cause the decay heat difference. In order to investigate the cause of this difference, the top 10 contributions, when the reactor is shut down, are shown in Table 9.2. It is not clear what nuclide is dominant for each core.

The cause of the unique feature of a peak at 0.1 million years for Th-core is studied below. The decay heat contribution from each actinide is shown in Fig. 9.3. Here, these nuclides are generated from the decay of $^{233}$U, which has a half-life of 159,200 years. The daughter nuclides generated from the decay of $^{233}$U are:

> $^{233}$U (Half-life: 159,200 years) > $^{229}$Th (7340 y) > $^{225}$Ra (14.9 d) > $^{225}$Ac (10.0 d) > $^{221}$Fr (14.9 m) > $^{217}$At (32.3 ms) > $^{213}$Bi (45.59 m) > $^{213}$Po (4.2 μs) > $^{209}$Pb (3.253 h) > $^{209}$Bi (stable).

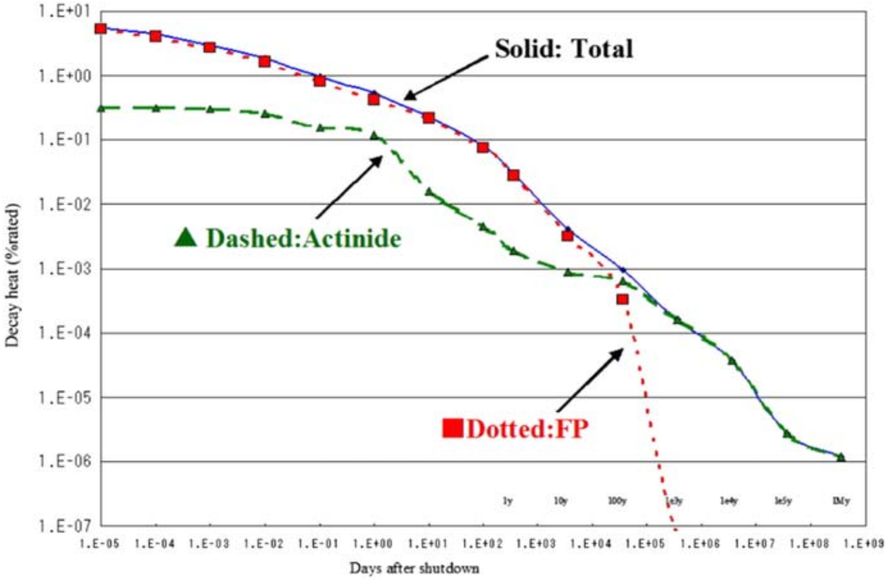

**Figure 9.1** Component of decay heat (U-core).

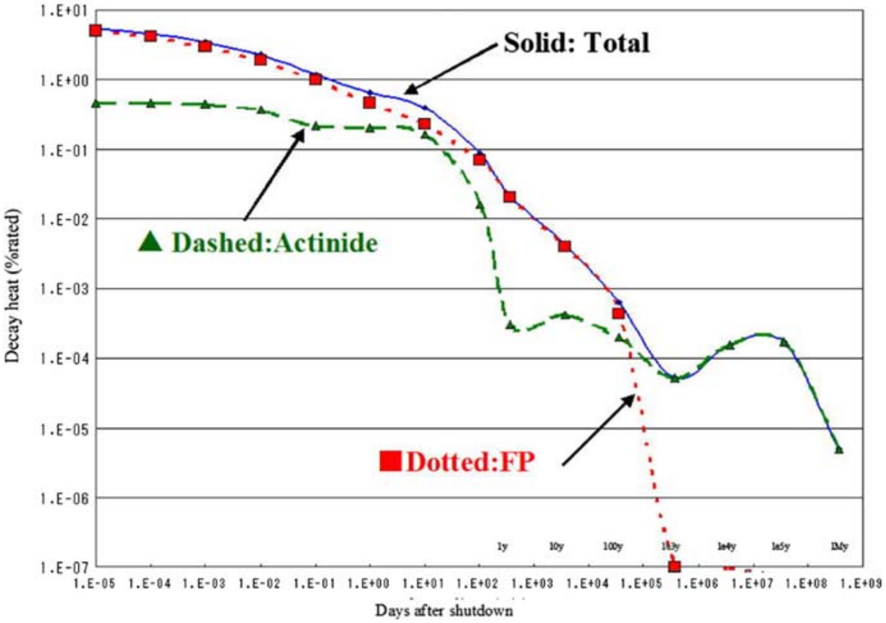

**Figure 9.2** Component of decay heat (Th-core).

**Table 9.2** Decay heat of top 10 FPs (% rated)

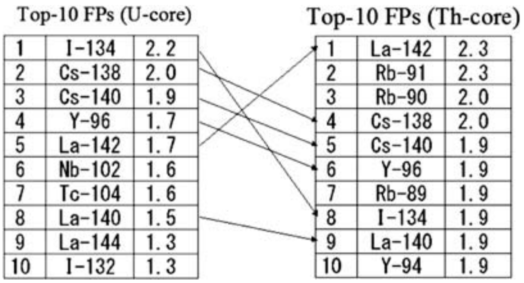

Top-10 FPs (U-core)

| | | |
|---|---|---|
| 1 | I-134 | 2.2 |
| 2 | Cs-138 | 2.0 |
| 3 | Cs-140 | 1.9 |
| 4 | Y-96 | 1.7 |
| 5 | La-142 | 1.7 |
| 6 | Nb-102 | 1.6 |
| 7 | Tc-104 | 1.6 |
| 8 | La-140 | 1.5 |
| 9 | La-144 | 1.3 |
| 10 | I-132 | 1.3 |

Top-10 FPs (Th-core)

| | | |
|---|---|---|
| 1 | La-142 | 2.3 |
| 2 | Rb-91 | 2.3 |
| 3 | Rb-90 | 2.0 |
| 4 | Cs-138 | 2.0 |
| 5 | Cs-140 | 1.9 |
| 6 | Y-96 | 1.9 |
| 7 | Rb-89 | 1.9 |
| 8 | I-134 | 1.9 |
| 9 | La-140 | 1.9 |
| 10 | Y-94 | 1.9 |

Then, radioactivity shows a peak, which is known as "transient equilibrium" in the theory of radiation chemistry ("Transient equilibrium", 2015).

As for MSR, $^{233}U$ in spent fuel is recovered by online reprocessing or by off-site reprocessing, because it is a fissile material and can be used as new fuel (see Section 9.2.4). Under this scenario, this peak does not appear.

### 9.1.5 Other influences on decay heat calculation

Since there are several libraries in ORIGEN2, its effect was studied. ORIGEN2 provides a Th-core library (213-library), which was verified as reasonable by the

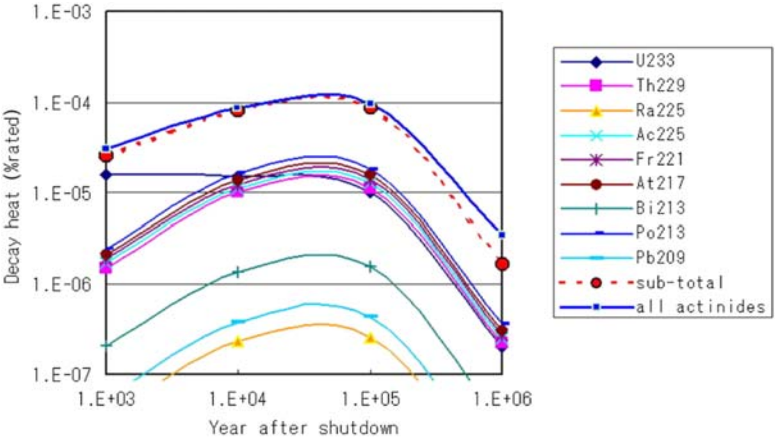

**Figure 9.3** Component of decay heat at its peak (Th-core).

authors (Yoshioka et al., 2014; IAEA (to be published)). The differences between different libraries are less than 10%–30%.

In general, higher burnup requires higher fissile content in the initial fuel. Therefore, influence by $^{233}$U content was studied. The initial $^{233}$U content was assumed as 2% artificially, and compared with a referenced 4% case. The result shows that the influence is negligible, because $^{232}$Th is converted to $^{233}$U, and its fission is dominant (Yoshioka et al., 2014; IAEA, to be published).

The effect of different burnups was also studied. In general, more actinides are accumulated at higher burnup, and it causes larger decay heat. This effect was studied for different burnups for the corresponding enriched U-core and Th-core (Yoshioka et al., 2014; IAEA, to be published). Since most FPs are short-lived, decay heat does not depend on burnup at short time range. But, for the timespan between 1 year to 1 million years, decay heat is almost proportional to discharge burnup.

### 9.1.6 Verification of decay heat calculation

As for verification of ORIGEN2, there is only one experimental measurement on decay heat, which provides the decay heat data up to $10^5$ s (about 1 day) after $2 \times 10^4$ s irradiation of pure $^{233}$U and $^{235}$U (Yarnell et al., 1978). That is, only FP contribution can be verified. It is verified that ORIGEN2 agrees very well to the measurement for $^{233}$U and $^{235}$U (Yoshioka et al., 2014; IAEA, to be published).

In order to verify the above results by a different approach, the most recent calculations are referred to, where recent nuclear cross-section libraries are used (Fleming et al., 2015). The ORIGEN2 result shows good agreement with recent nuclear cross-section libraries in the above short time range.

There are few papers for decay heat of Th-cycle by governmental organizations. Only one paper by Brookhaven National Laboratory was found, where burnup and decay are calculated by a unit-cell code for PWR fuel (Todosow et al., 2010).

Based on this paper, its general tendency is similar to the above ORIGEN2 result (IAEA, to be published).

### 9.1.7 *Final results*

The result for the U-core was obtained using ORIGEN2-U219-library for 50 GWd/t PWR fuel, which is close to the U204-library for 33 GWd/t PWR. For the Th-core, the Th-213 library was used.

The decay heat of the Th-core is 10% larger than that of U-core up to 100 days. One unique behavior is a peak at 0.1 million years for Th-core, as is shown in Fig. 9.4. The Th-core decay heat is 10% larger than that of U-core up to one day, which is important for accident analysis, as is shown in Fig. 9.5.

### 9.1.8 *Summary*

1. Decay heat is evaluated for U-core and Th-core of PWR, using the ORIGEN2 code.
2. Decay heat of Th-core is 10% larger than U-core after shutdown to one day, which is important for accident analysis.
3. After 100 years, decay heat of Th-core is smaller.
4. Between 10,000–100,000 years, there is a peak on Th-core, which is caused by $^{233}$U and its daughters.
5. As for MSR, if $^{233}$U in spent fuel is recovered by online reprocessing or by off-site reprocessing, the above peak does not appear.

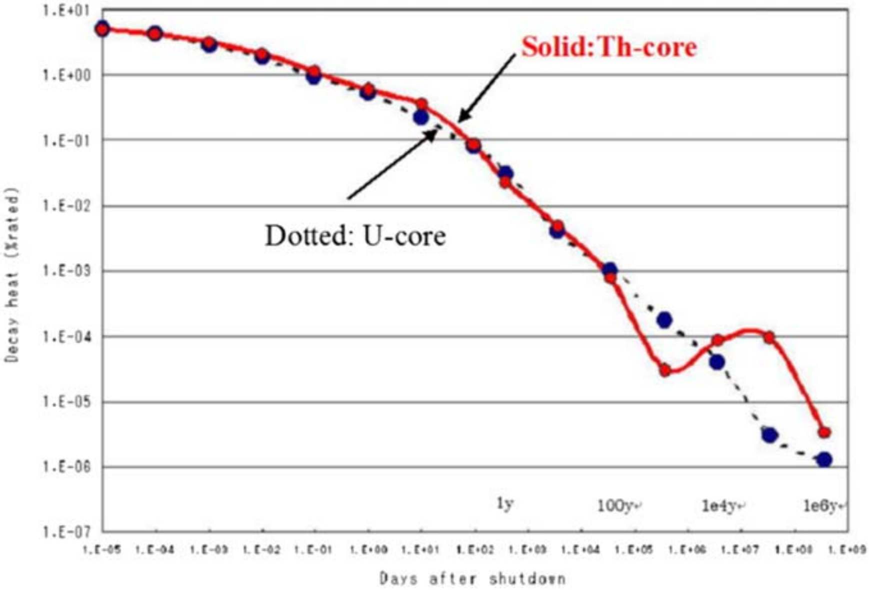

**Figure 9.4** Decay heat for U-fuel and Th-fuel (long range).

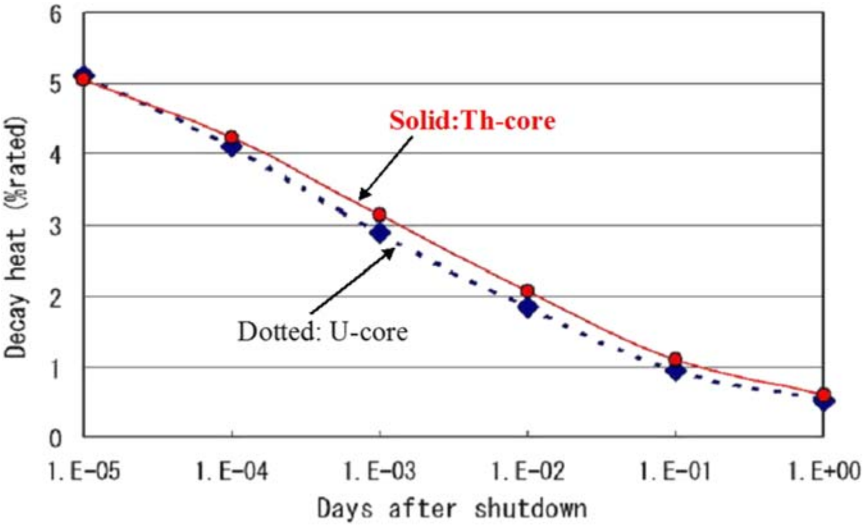

**Figure 9.5** Decay heat for Th-fuel and U-fuel (short range in linear scale).

## 9.2 Radiotoxicity in the thorium cycle

### 9.2.1 Introduction

Radiotoxicity is an important parameter in fuel cycle consideration, wherever spent fuel is stored. Since radiotoxicity is caused by the decay of actinides and FPs, it mainly depends on the fuel type, which is expected to be thorium (Th) in a MSR. Of course, either MOX fuel ($PuO_2$-$UO_2$) or LEU (low enriched uranium) fuel can be used in MSRs, as in light water reactors (LWRs).

A radiotoxicity calculation is established for $UO_2$ and MOX fuel, but reliable papers on radiotoxicity for thorium core are very limited. Therefore, this section provides the necessary information on radiotoxicity evaluation for mainly thorium fuel, compared with that of $UO_2$ fuel. Radiotoxicity for MOX fuel is also shown just as information.

### 9.2.2 Calculation method

In this section, radiotoxicity for PWR thorium fuel is compared with conventional PWR $UO_2$ fuel, and ORIGEN2 code is used to calculate radiotoxicity (Croff, 1980). The following core and libraries were selected, with a rated power density of 39.2 MW/T. Fuel was burnt up to 45 GWd/t, and then radiotoxicity was calculated from 1 year to 1 million years.

1. U-PWR-core: 4%$^{235}$U + 96%$^{238}$U. U219-library;
2. Th-PWR-core: 4%$^{233}$U + 96%$^{232}$Th. Th213-library.

ORIGEN2 provides radioactivity in "Ci/tHM (Curie/ton-HeavyMetal)" (in general, "ton-HeavyMetal" is defined as a total weight of U/Pu/Th in fresh fuel), which must be converted to "Becquerel (Bq)/tHM" (1 Ci $= 3.7 \times 10^{10}$ Bq). Radioactivity was calculated by ORIGEN2, and then converted to radiotoxicity in Sieverts (Sv). Normally, the unit of radiotoxicity is Sv/tHM, but it can be defined as Sv/gram-HM or Sv/assembly. If radiotoxicity for spent fuel per 1 GW (GWe or GWt) operation in a year is required, its conversion process is described in Section 9.2.4. In most of this section, Sv/tHM is used.

Radiotoxicity considers the type of radiation, its energy, and influence on human body as a DCF (dose conversion factor). Since DCF is not included in ORIGEN2, it must be found from appropriate references. Thus, radiotoxicity of spent fuel is calculated by the following formula:

Radiotoxicity [Sv/tHM] = Radioactivity [Bq/tHM] × DCF [Sv/Bq]

Most DCF data are shown in ICRP (1995) and Nishihara (2010), and DCF of some nuclides, which are not provided in these references, are supplemented in Clement (2012) and Kawai et al. (2002).

Since alpha particles cannot penetrate the skin, those emitted by actinides cause significant damage only after ingestion by eating/drinking or after inhalation by breathing. The ICRP (International Commission on Radiological Protection) provides different DCFs for these two cases (ICRP, 1995). For example, DCF for ingestion of $^{239}$Pu is $2.5 \times 10^{-7}$ Sv/Bq, but DCF for inhalation of small particles ($\sim 5$ μm) of $^{239}$Pu is $3.2 \times 10^{-5}$ Sv/Bq, about two orders of magnitude higher. But, in general, radiotoxicity is discussed based on an ingestion scenario, because inhalation is incredible for spent fuel. Of course, if radiotoxicity is discussed on reactor accident situations, then an inhalation scenario must be also considered.

The "ingestion hazard," which is computed by ORIGEN2, is the amount of water ($m^3$) needed to dilute the 1 ton of spent fuel in order to reduce potential intake of ingestion below the threshold for the general public. However there is no description for this calculation process in the ORIGEN2 manual, so this method is not used here.

### 9.2.3 Radiotoxicity comparison between U-core and Th-core in PWR

A radiotoxicity comparison between U-core and Th-core in PWR is shown in Fig. 9.6. Radiotoxicity of Th-core is 10%–90% lower than that of U-core up to 1000 years, but after 10,000 years it becomes higher, and there is a peak around 0.1 million years (IAEA, to be published; Yoshioka et al., 2015). These curves are similar to those of decay heat.

For the U-core the major contributor of long-term radiotoxicity (10,000–100,000 years) is $^{239}$Pu, and its contribution is almost half of the total radiotoxicity. The U-core generates much plutonium, while the Th-core does not. But, there is another contribution from $^{229}$Th in the Th-core. That is, the major long-term contributor (10,000–100,000 years) for the Th-core is $^{229}$Th, which is a daughter of $^{233}$U (half-life of 159,200 years). The $^{229}$Th portion is almost half of the total radiotoxicity.

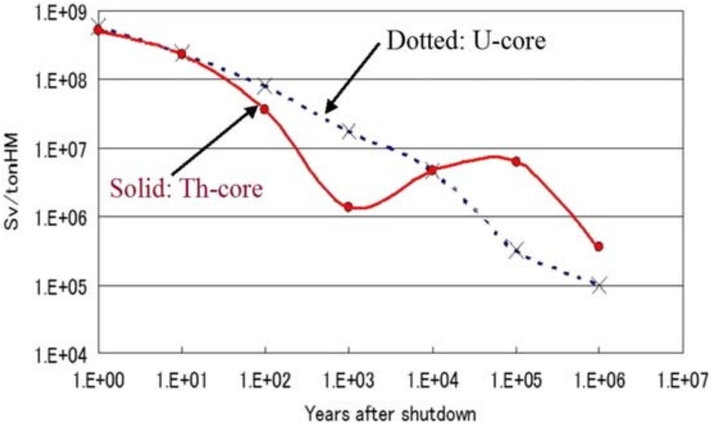

**Figure 9.6** Radiotoxicity for U-core and Th-core (IAEA, to be published; Yoshioka et al., 2015).

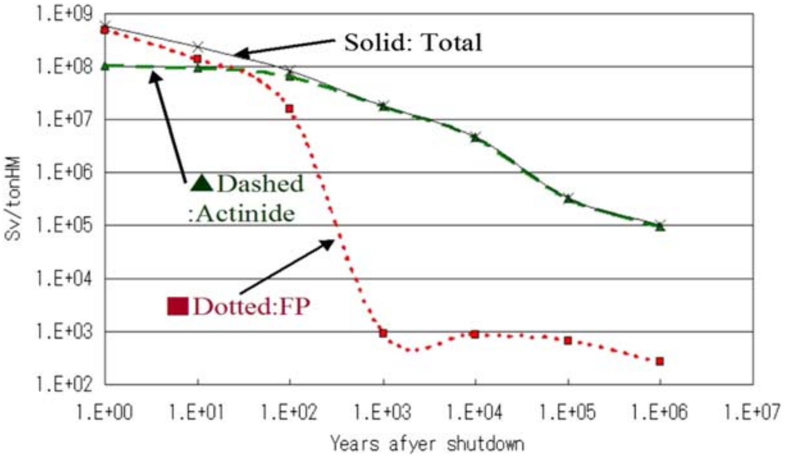

**Figure 9.7** Component of radiotoxicity for U-core (IAEA, to be published; Yoshioka et al., 2015).

There are few preceding papers for radiotoxicity of the Th-cycle by governmental organizations. Only one paper by BNFL (UK) was found (Hesketh, 2005), which provides similar results to the above ORIGEN2 result.

The components of radioactivity are shown in Fig. 9.7 for the U-core, and in Fig. 9.8 for the Th-core. Radioactivity by FPs is dominant up to 100 years, but it decreases rapidly after 100 years. After that, radioactivity by actinides becomes dominant.

If partitioning (separation of spent fuel actinides and FPs) is performed and all actinides are recycled and transmuted in MSRs, in other reactors, or in accelerator-driven systems (ADS), then total radiotoxicity decreases to that of FPs, which is nearly that of natural $^{238}$U or $^{232}$Th.

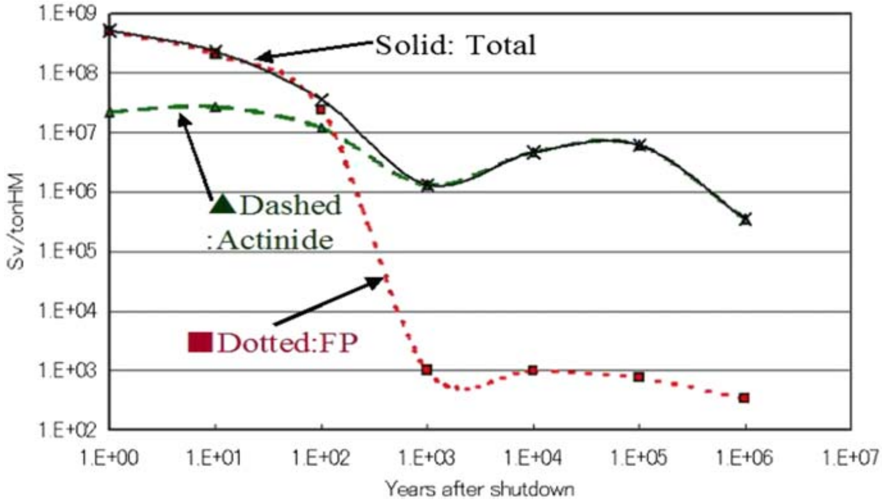

**Figure 9.8** Component of radiotoxicity for Th-core (IAEA, to be published; Yoshioka et al., 2015).

The cause of the peak at 0.1 million years for Th-core is mainly from the contributions by $^{233}$U and its daughters. In addition to $^{233}$U and its daughters, $^{234}$U and its daughters also contribute to this peak. $^{234}$U is generated from the neutron absorption of $^{233}$U, and it has a very long half-life of 245,500 years. These chains cause the peak, which is known as "transient equilibrium" in the theory of radiation chemistry ("Transient equilibrium", 2015).

Fig. 9.9 shows four different curves. The top curve is the total radiotoxicity, and the difference between top curve and the second curve shows the contribution from $^{233}$U and its daughters. The difference between the second curve and the third curve shows the contribution from $^{234}$U and its daughters. However, there is still a small peak around 10,000 years for the third curve. This small peak is caused by the decay of $^{231}$Pa, which has a relatively long half-life of 32,760 years. $^{231}$Pa and its daughters cause a small peak, which is known as "transient equilibrium." In the reactor using thorium fuel, $^{232}$Th absorbs a high-energy neutron or gamma, and generates $^{231}$Th by (n,2n) or ($\gamma$,n) reaction. And the following long decay chain starts as $^{231}$Th (Half-life: 25.52 h) > $^{231}$Pa (32,760 y) > $^{227}$Ac (21.773 y) > $^{227}$Th (18.72 d) > $^{223}$Ra (11.435 d) > $^{219}$Rn (3.96 s) > $^{215}$Po (1.781 ms) > $^{211}$Pb (36.1 min) > $^{211}$Bi (2.14 min) > $^{207}$Tl (4.77 min) > $^{207}$Pb (stable).

The above results suggest that if the uranium in spent thorium fuel is removed, for example, by fluorination technology, then the radiotoxicity can be greatly reduced. If Th and its daughters are also separated and recycled, then radiotoxicity can be further reduced.

Based on radiolysis results from MSRE, removal of uranium is a mandatory step for safe and long-term disposal of spent MSR fuel (US-DOE, 1997). Fluorination is a well-established technology used at an industrial scale as part of the conversion process from uranium ore to fuel.

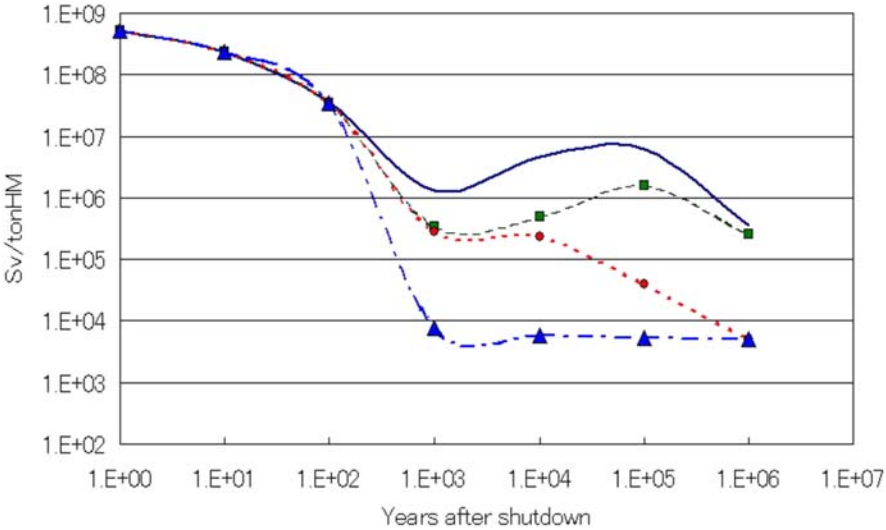

**Figure 9.9** Radiotoxicity for Th-core (IAEA, to be published) (Solid: Total; ■Dashed: Total-$^{233}$Uetc; ●Dotted: Total-$^{233}$Uetc-$^{234}$Uetc; ▲Break: Total-$^{233}$Uetc-$^{234}$Uetc-$^{231}$Pa, etc.).

### 9.2.4 *Effect of online reprocessing for MSR*

ORNL proposed an online reprocessing system in order to improve the breeding ratio, where most actinides could be recycled and transmuted in the MSR, and radiotoxicity could be decreased. Since the actual simulation of online reprocessing is difficult, the authors performed an alternative evaluation.

First of all, radiotoxicity by actinides is compared between $UO_2$ spent fuel and thorium fuel for PWR, and the result is shown in Fig. 9.10, where reprocessing is not adopted for either case. As is shown in this figure, actinide radiotoxicity for thorium fuel is lower than $UO_2$ fuel up to 10,000 years, and after that, thorium fuel radiotoxicity becomes higher.

MSR with Th-fuel is claimed to have lower radiotoxicity than conventional $UO_2$-PWR (David, 2007). Fig. 9.11 compares actinide radiotoxicity of spent U-fuel without reprocessing and Th-core assuming recycling with 100% transmutation efficiency, based on the above assumptions.

In order to compare the preceding paper, the data are shown in units of Sv/GWt/year, that is this figure shows the actinide radiotoxicity of 1-year operation for 1 GW(thermal) plant.

The conversion procedure is as follows.

Using the above RT (radiotoxicity in units of Sv/ton-HM) for 45,000 MWd/t fuel, and assuming 3000 MWt and 1000 MWe plant for 365 days operation with 100% load factor, annually discharged fuel weight (WT) is calculated by the following formula.

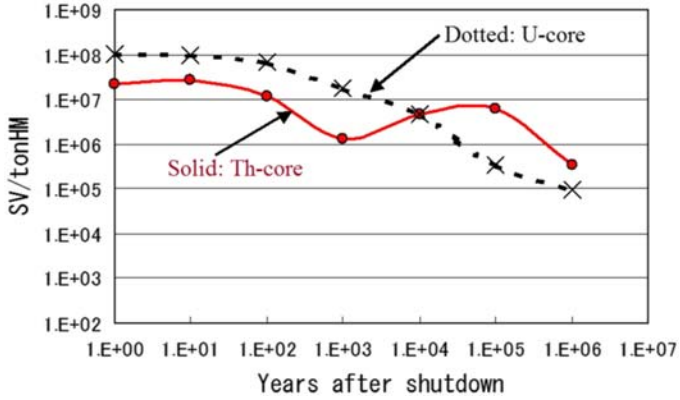

**Figure 9.10** Radiotoxicity by actinides of spent fuel (dotted line: $UO_2$ fuel; solid line: thorium fuel).

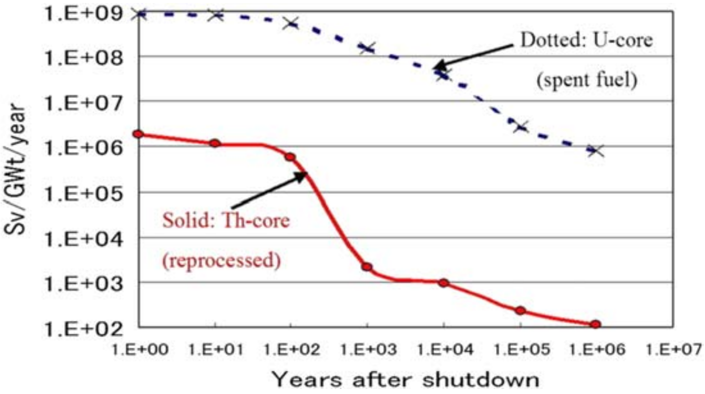

**Figure 9.11** Radiotoxicity by actinides (FP radiotoxicity not shown) (dotted line: $UO_2$ spent fuel; solid line: thorium fuel with actinide reprocessing).

$$\begin{aligned} WT &= [3000\ \text{MWt}] \times [365\ \text{days}] \times 1.0(100\%\ \text{load factor})/[45\ \text{GWd/t}] \\ &= 24.3\ \text{ton/year} \end{aligned}$$

If radiotoxicity per 1 GW(electric)-year is required, the above RT must be multiplied by 24.3, that is:

$$\text{Radiotoxicity per 1 GW(electric)-year} = WT \times RT = 24.3 \times RT.$$

And, if radiotoxicity per 1 GW(thermal)-year is required, the above RT must be multiplied by 24.3/3(GWe) = 8.1. That is;

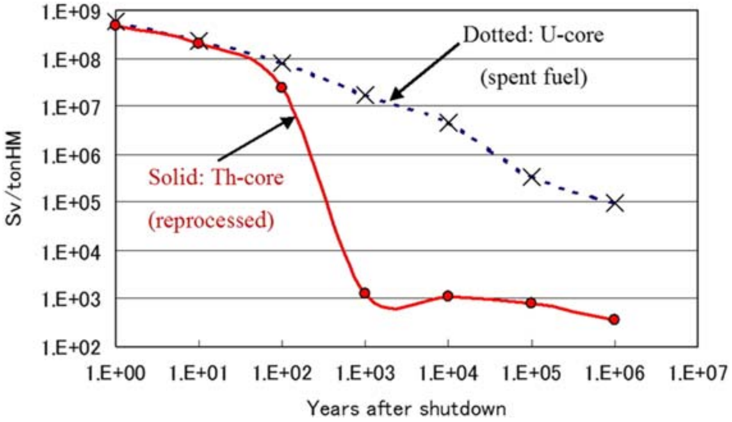

**Figure 9.12** Total radiotoxicity (including FP) (dotted line: $UO_2$ spent fuel; solid line: thorium fuel with reprocessing).

$$\text{Radiotoxicity per 1 GW(thermal)-year} = \text{WT}/3.0 \times \text{RT} = 8.1 \times \text{RT}$$

is used for conversion in Fig. 9.11.

Radiotoxicity by FPs is dominant up to 100 years, and the above effect appears after several hundred years. The result is shown in Fig. 9.12, assuming 100% separation and recycling for Th-core. In actual reprocessing, separation efficiency is not 100%, and also recycled U and Th will generate new daughter nuclides in other MSR or in ADS, and, as a result, reduction of radiotoxicity is less effective than shown here.

### 9.2.5 Radiotoxicity for PWR MOX fuel

Radiotoxicity for PWR MOX fuel is evaluated based on an ORIGEN2 calculation. Here, 7.50% Pu-total content is assumed for MOX fuel corresponding to 45 GWd/t discharge burnup. For simplicity, Pu is mixed with 100% $^{238}U$. Each Pu nuclide fraction (Pu vector) before burnup is based on the ORIGEN2 calculation for the 4.0% enriched PWR $UO_2$ fuel at 45 GWd/t, after 7 years decay by cooling and reprocessing.

Radiotoxicity of MOX fuel is shown in Fig. 9.13 with the $UO_2$ fuel result. The radiotoxicity of MOX fuel is almost 4–5 times higher than that of $UO_2$ fuel from 10 years to 1 million years. This is mainly because MOX fuel contains four times more Pu than $UO_2$ fuel at 45 GWd/t, and therefore, Pu and its daughter nuclides contribute largely to radiotoxicity at a long time range. Another factor is contribution from $^{242}Cm$ and $^{244}Cm$. For example, although the amount of $^{242}Cm$ is small, its half-life is very short at 162.8 days, and its radiotoxicity is large at 1–10 years.

The component of radiotoxicity for MOX fuel is shown in Fig. 9.14. General trends of FPs and actinides are similar to $UO_2$ fuel case, but, as is described above, actinide contribution is large from 1 year to 1 million years range.

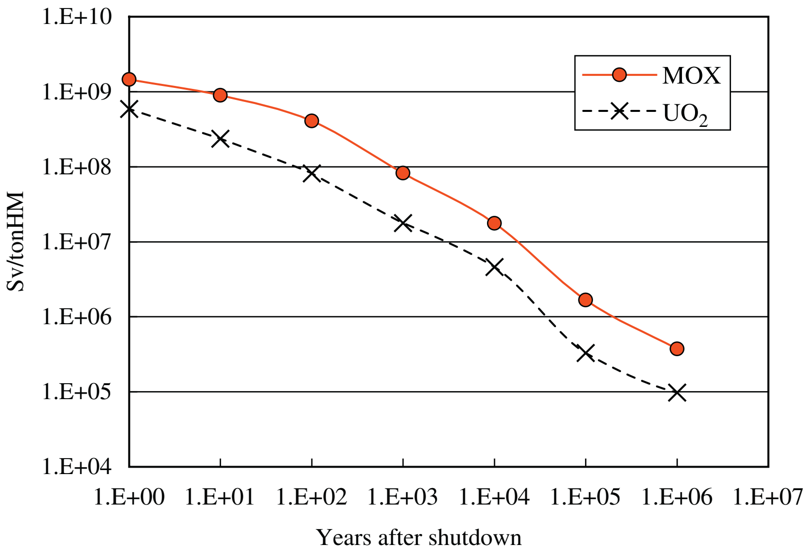

**Figure 9.13** Radiotoxicity for MOX fuel and $UO_2$ fuel (Sv/tonHM).

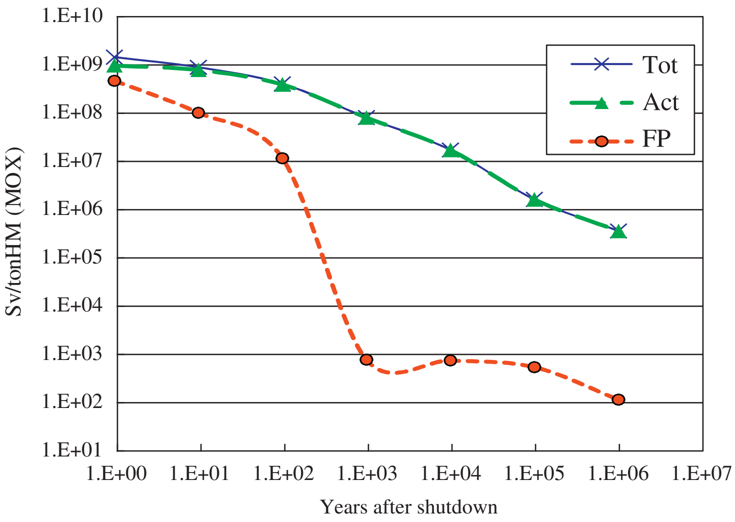

**Figure 9.14** Component of radiotoxicity for MOX fuel (Sv/tonHM).

## 9.2.6 Summary

1. Radiotoxicity was evaluated for spent fuels of U-core and Th-core of PWR, using ORIGEN2 and DCF.
2. Radiotoxicity of Th-core is 10−90% lower than that of U-core up to 1000 years, but after 10,000 years Th-core becomes higher, and there is a peak around 0.1 million years. These curves are similar to those of decay heat.

3. Radiotoxicity of MOX fuel is 4−5 times higher than that of $UO_2$ fuel from 10 to 1 million years.
4. If reprocessing is applied for MSR and most actinides such as U, Th, and their daughters are separated and recycled, then radiotoxicity after several hundred years can be greatly reduced.

## 9.3 Nuclear waste from ThorCon type reactors

ThorCon reactors are described in Chapter 19, ThorCon reactor. After a few hundred years, almost all the penetrating gamma radiation will be gone. The remaining radiotoxicity is almost all alpha emission, which must be ingested or inhaled in order to do harm. Most of the alpha emitters are chemically bound, such as in oxides and fluoride salts, so they are not easily dispersed into the environment.

A 1 GWe ThorCon will return 20 tons/year of used fuel salt to the recycling facility. The first step is to separate the uranium from the fuel salt via fluoride volatility, as in the enrichment step. That will remove about 1.5 tons of 9% LEU from the waste stream. This uranium can be used as part of the initial fuel charge for other ThorCons, or it could be re-enriched. Either way it will be returned to the plants. (See also Chapter 8: Chemical processing of liquid fuel, on chemical processing.)

In the re-enrichment case, we will have about 1000 kg (52 L) of depleted uranium. The depleted uranium will contain some residual $^{232}U$, $^{233}U$, and $^{234}U$ (25 ppm, 4%, and 0.7% respectively prior to enrichment) that will impact the radiotoxicity profile and needs to be considered when planning disposal. The next step will be vacuum distillation to recover the salt and thorium, which removes over 80% of the volume. The recovered salt will be returned to the reactors, leaving about 7 tons of ash. Thorium has little economic value and is not a significant waste issue to the impetus for thoroughly removing thorium from the waste stream. This ash will be mostly residual $ThF_4$ but will contain 103 kg of transuranics and 789 kg of FPs. The volume of this ash will be about 1.1 $m^3$ per GWe-year of power, which will be stored in dry casks. (Technological progress may later make it economic or socially required to separate out the transuranics for recycle back to the reactors.) The transuranics and thorium can be completely recycled to the limits of extraction efficiencies.

The remaining FPs can be stored in dry casks for 500 years, when they will have decayed to near background levels. (A coal plant produces about 100,000 times more solid waste per GWe-y than a ThorCon power plant.) There will also be some ancillary waste streams:

- Krypton and xenon stored in 100 L cylinders ~ 90 kg/GWe-y (may be sold).

  Xenon is nonradioactive after 4 months decay time. By the time the cylinders leave the power station only mildly radioactive krypton-85 remains. Krypton-85 is frequently used as a tracer gas.
- Graphite mixed with FPs ~ 250 kg/GWe-y;
- Metal from primary heat exchanger/pump impeller ~ 10,000 kg/GWe-y.

With experience, we should eventually be able to recycle most of the contaminated primary loop material (Devanney et al., 2015).

Inventories of FPs are also discussed in Chapter 11, Liquid fuel, thermal neutron spectrum reactors.

## 9.4 Resource utilization

This section discusses thorium and helium resource issues relative to MSRs.

### 9.4.1 Thorium

#### 9.4.1.1 Properties and resources

Thorium can be the basis of a valuable $^{232}$Th-$^{233}$U nuclear fuel cycle, possessing more attractive characteristics compared with the present $^{238}$U-$^{239}$Pu fuel cycle (see Chapters 1: Introduction and 7: Materials).

Thorium (Th), named after Thor, the Scandinavian god of thunder, occurs in nature in a single isotope: $^{232}$Th. Its large abundance can make it valuable for future electrical energy generation with supplies exceeding both coal and uranium combined.

Since natural thorium does not contain fissile materials, such as $^{233}$U, some fissile material ($^{233}$U, $^{235}$U, $^{239}$Pu) must be added to start up a thorium MSR. This could come from several sources, including an (ADS; Chapter 15: Accelerator driven systems), dismantled weapons Pu, spent LWR fuel, and fusion−fission hybrids (Chapter 13: Solid fuel, salt-cooled reactors).

In a thorium-fueled reactor, fertile material $^{232}$Th is converted to fissile material $^{233}$U by the following neutron absorption reaction:

$^{232}$Th (n,$\gamma$) $^{233}$Th ($\beta^-$: 22.3 m half-life) $^{233}$Pa ($\beta^-$: 27 d half-life) $^{233}$U.

Fig. 9.15 shows simplified burnup chains in the thorium cycle.

Repeating successive neutron absorptions, $^{233}$U is converted to $^{234}$U, $^{235}$U, $^{236}$U, $^{237}$Np, $^{238}$Pu, and finally to $^{239}$Pu. Since this is a long process, production of Pu is

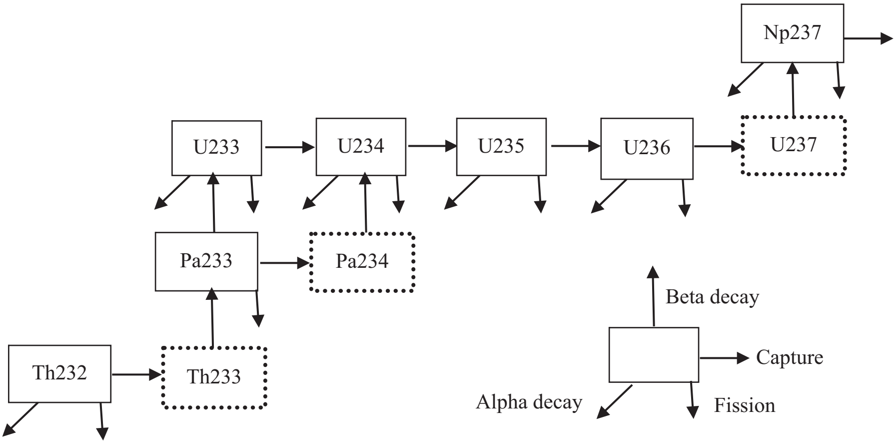

**Figure 9.15** Thorium cycle burnup chain (dotted nuclide has a short half-life, and may be assumed as decay only).

very small compared with the U fuel cycle. This small production of Pu makes the Th-fueled reactor a nuclear weapon proliferation-resistant technology. Also, production of long-lived minor actinides (MA) such as curium (Cm) and americium (Am) are very small, because these isotopes are mostly produced by neutron absorption of Pu isotopes.

As for other long-lived MA in U fuel, neptunium ($^{237}$Np) is produced mainly by the decay of $^{237}$U, which comes mainly from two times neutron absorption to $^{235}$U. As for Th+$^{233}$U fuel, a small amount of $^{237}$Np is produced, because $^{237}$U is produced by four times neutron absorption in $^{233}$U.

The thorium radioactive decay chain leads to stable lead isotopes with a half-life of $1.4 \times 10^{10}$ years for $^{232}$Th. Its decay contributes to the internal heat generation in the Earth.

Radon (Rn) is one of the causes of lung cancer, because of its radioactivity. Radon is gaseous at room temperature. The most well-known nuclide is $^{222}$Rn, which is the sixth decay product of $^{238}$U, and another isotope is $^{220}$Rn (sometimes called as thoron), which is the fifth decay product of $^{232}$Th. Both nuclides are emitted from the earth and from some house construction materials. So, they may be inhaled by humans, mostly in homes.

Metallic thorium can be produced by:

1. Reduction of $ThO_2$ using calcium or magnesium;
2. Electrolysis of anhydrous thorium chloride in a fused mixture of Na and K chlorides;
3. Calcium reduction of $ThCl_4$ mixed with anhydrous zinc chloride;
4. Reduction of $ThCl_4$ by an alkali metal.

Thorium is the second member of the actinides series in the periodic table of the elements. When pure, it is soft and ductile, can be cold-rolled and drawn. It is a silvery white metal retaining its luster in air for several months. If contaminated by the oxide, it tarnishes in air into a gray then black color.

Thorium oxide has the highest melting temperature of all the oxides at 3300°C. Just a few other elements and compounds have a higher melting point, such as tungsten and tantalum carbide. Water attacks it slowly, and acids do not attack it, except for hydrochloric acid.

Thorium in powder form is pyrophoric and can burn in air with a bright white light. In portable gas lights the Welsbach mantle is prepared with $ThO_2$ with 1% cerium oxide and other ingredients (Fig. 9.16).

As an alloying element in magnesium, it gives high strength and creep resistance at high temperatures. Tungsten wire and electrodes used in electrical and electronic equipment such as electron guns in X-ray tubes or video screens are coated with Th due to its low work function and associated high electron emission. Its oxide is used to control the grain size of tungsten used in light bulbs and in high-temperature laboratory crucibles. Glasses for lenses in cameras and scientific instruments are doped with Th to give them a high refractive index and low dispersion of light. In the petroleum industry it is used as a catalyst in the conversion of ammonia to nitric acid, in oil cracking, and in the production of sulfuric acid.

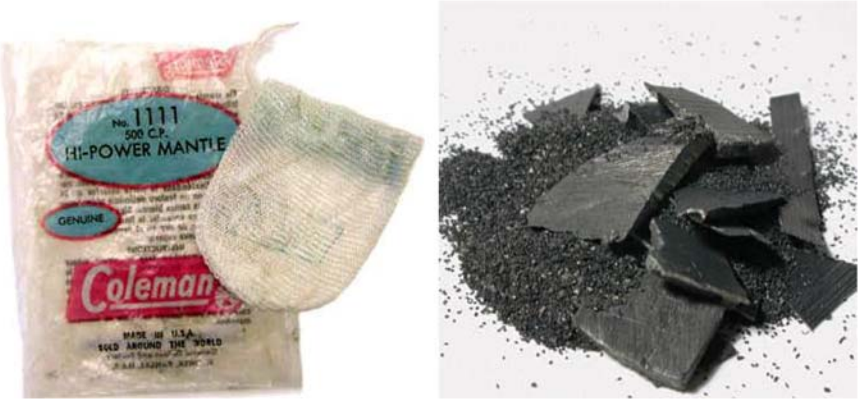

**Figure 9.16** Thorium dioxide with 1% cerium oxide-impregnated fabric, Welsbach incandescent gas mantles (left) and $ThO_2$ flakes (right). Yttrium compounds now substitute for Th in some mantles.

**Table 9.3** **Major thorium ore compositions**

| Ore | Composition |
|---|---|
| Thorite | $(Th,U)SiO_4$ |
| Thorianite | $(ThO_2 + UO_2)$ |
| Thorogummite | $Th(SiO_4)_{1-x}(OH)_{4x}$ |
| Monazite | $(Ce,La,Y,Th)PO_4$ |
| Brocktite | $(Ca,Th,Ce)(PO_4)H_2O$ |
| Xenotime | $(Y,Th)PO_4$ |
| Euxenite | $(Y,Ca,Ce,U,Th)(Nb,Ta,Ti)_2O_6$ |
| Basnäsite | $(Ce,La,Dy)F.CO_2$ |
| Iron ore | Fe + rare earths + Th apatite |

### 9.4.1.2 Thorium minerals

Thorium occurs in several minerals (Hedrick, 2009; Van Gosen et al., 2009).

Table 9.3 shows compositions of some Th ores.

*Monazite* $(Ce,La,Y,Th)PO_4$, is a rare earth-thorium phosphate with 5–5.5 hardness. Its Th content is 3%–22% with 14% rare earth elements and yttrium. It occurs as a yellowish, reddish-brown to brown, with shades of green, nearly white, yellowish brown, and yellow ore (Fig. 9.17). This is the primary source of the world's thorium production. Until World War II, thorium was extracted from monazite as a primary product for use in products such as camping lamp mantles. Since World War II, monazite has been primarily mined for its rare earth elements content. Thorium was extracted in small amounts and mainly discarded as waste.

*Thorite* $(Th,U)SiO_4$ is a thorium-uranium silicate with a 4.5 hardness with yellow, yellow-brown, red-brown, green, and orange to black colors. It shares a 22%

**Figure 9.17** Monazite (left) and thorium-salt [$Th(NO_3)_4$] (right).

**Table 9.4 Spectroscopic analysis showing the common occurrence of Th and rare earth elements in thorogummite (Vickers, 1956)**

| Element | Thorogummite, ($Th(SiO4)_{1-x}$ $(OH)_{4x}$) Syenite complex, Wausau, Wisconsin (Vickers, 1956) (%) |
|---|---|
| Th | >10 |
| Fe | 5−10 |
| Si | 2−5 |
| Al, Ca, Mg, Y | 1−2 |
| Ti | 0.5−1.0 |
| Mn, Na, Ce, Dy, Er, Gd, La, Sm | 0.2−0.5 |
| Nd, Yb | 0.1−0.2 |
| Cu, Nb, Pb, V | 0.05−0.1 |
| Ba, Co, Sc | 0.01−0.02 |
| Be | 0.002−0.005 |
| U | 2.5 |

Th and a 22% U content. This ore has been used as a source of uranium, particularly the uranium-rich uranothorite, and orangite; an orange-colored calcium-rich thorite variety.

The joint occurrence of Th and the rare earth elements in some ores such as monazite and thorogummite ($Th(SiO4)_{1-x}$ $(OH)_{4x}$), a variant of thorite containing hydroxyl, is shown in Table 9.4.

It occurs as nodules 0.5−1.0 in. in diameter in residual soil and weathered bedrock and appears associated with hematite, an iron oxide (Kennedy, 2009). Many

**Table 9.5** **Chemical composition of some rare earth ores with Th and U occurrence**

| Ore | Chemical composition |
|---|---|
| Allanite | $(Ca,Ce,Th)_2(Al,Fe,Mg)_3Si_3O_{12}(OH)$ |
| Monazite | $(Ce,La,Pr,Nd,Th,Y)PO_4$ |
| Parisite | $2(Ce,La,Di,Th)OF.CaO.3CO_3$ |
| Polymignite | $(Ca,Fe,Y,Th)(Nb,Ti,Ta,Zr)O_4$ |
| Euxenite | $(Y,Ca,Er,La,Ce,U,Th)(Nb,Ta,Ti)_2O_6$ |
| Cheralite | $(Ca,Ce,Th)(P,Si)O_4$ |
| Samarskite | $(Y,Er,Ce,U,Ca,Fe,Pb,Th)(Nb,Ta,Ti,Sn)_2O_6$ |
| Thorogummite | $(Th(SiO4)_{1-x}\ (OH)_{4x})$ |
| Davidite | $(La,Ce)(Y,U,Fe^{+2})(Ti,Fe^{+3})_{20}(O,OH)_{38}$ |
| Fergusonite | $(Y,Er,Ce,Fe)(Nb,Ta,Ti)O_4$ |
| Loparite | $(Ce,Na,Ca)(Ti,Nb)O_3$ |
| Bastnäsite | $(Ce,La,Di)F.CO_2$ |

**Figure 9.18** Black sand monazite layers in beach sand at Chennai, India.
*Source*: Photo: Mark A. Wilson.

rare earth ores contain Th (Table 9.5). In mining circles, Th and U are considered as "contaminants" favoring the mining of ores with low Th and U content.

Concentrated deposits occur as vein deposits, and disseminated deposits occur as massive carbonatite stocks, alkaline intrusions, and black sand placer or alluvial stream and beach deposits. Carbonatites are rare carbonate igneous rocks formed by magmatic or metasomatic processes. Most of these are composed of 50% or higher carbonate minerals such as calcite, dolomite, and ankerite. They occur near alkaline igneous rocks.

Figs. 9.18, 9.19, and 9.20 show examples of thorium minerals.

**Figure 9.19** Black sands monazite ore on Brazilian beaches are ascribed unsubstantiated medicinal radiation curative properties.

**Figure 9.20** Thorite (Th, U) $SiO_4$, a thorium–uranium silicate.

The alkaline igneous rocks, also referred to as alkali rocks, have formed from magmas and fluids so enriched in alkali elements that Na- and K-bearing minerals form components of the rocks in larger proportion than usual igneous rocks. They are characterized by feldspathoid minerals and/or alkali pyroxenes and amphiboles (Gosen et al., 2009).

### 9.4.1.3 Thorium abundance

Thorium is about four times more abundant than uranium in the Earth's crust and presents a more abundant long-term fuel resource (Table 9.6).

The thorium mass in the Earth's crust is estimated at 120 trillion tons. It can be extracted from granite rocks and from phosphate rock deposits, rare earths, tin ores, coal, and uranium mine tailings. Its occurrence is associated with the rare earth elements as well as yttrium and scandium, which are acquiring heightened interest in their use in renewable energy technologies. The tantalite [(Fe, Mn) $Ta_2O_6$], columbite (niobite) [(Fe, Mn) $Nb_2O_6$], and columbite-tantalite (coltan) ores, used to manufacture tantalum capacitors in consumer electronics, also contain thorium.

It has even been suggested that thorium could be extracted from the ash of coal power plants. A 1000 MWe coal power plant generates about 13 tons of thorium per year in its ash. Each ton of thorium can in turn generate 1 000 MWe of power in a well optimized thorium reactor. Thus, the ash from a coal power plant could conceptually fuel 13 thorium plants of its own power.

The calcium sulfate or phospho-gypsum resulting as a waste from phosphorites or phosphate rock processing into phosphate fertilizer contains substantial amounts of unextracted thorium and uranium.

Uranium mines with brannerite ores generated millions of tons of surface tailings containing thoria and rare earths.

**Table 9.6 Relative abundances of some elements in the Earth's crust**

| Element | Symbol | Abundance (g/ton) |
|---|---|---|
| Lead | Pb | 16 |
| Gallium | Ga | 15 |
| Thorium | Th | 10 |
| Samarium | Sm | 7 |
| Gadolinium | Gd | 6 |
| Praseodymium | Pr | 6 |
| Boron | B | 3 |
| Bromine | Br | 3 |
| Uranium | U | 2.5 |
| Beryllium | Be | 2 |
| Tin | Sn | 1.5 |
| Tungsten | W | 1 |
| Molybdenum | Mo | 1 |
| Mercury | Hg | 0.2 |
| Silver | Ag | 0.1 |
| Platinum | Pt | 0.005 |
| Gold | Au | 0.02 |

### 9.4.1.4 Thorium resources

Many countries have substantial thorium resources (Table 9.7).

There are also Th resources on the moon (Fig. 9.21).

Table 9.8 and Fig. 9.22 show the distribution of thorium reserves in the United States.

A large part is located on properties held by Thorium Energy Inc. at Lemhi Pass in Montana and Idaho (Fig. 9.23).

## 9.4.2 Helium resource

Helium (He) is relevant to MSR, because it may be used in a closed Brayton cycle. Small amounts are used in the He bubbling system to remove gaseous FPs (several $m^3$ for 1 GWe-MSBR).

Soon after He mining was developed at the turn of the 20th century, the USA established a National Helium Reserve in 1925. During the Second World War, helium was strategically important because of its use in military airships.

**Table 9.7** Estimated global thorium resources (Hedrick, 2009)

| Country | ThO$_2$ reserves (metric tonnes) USGS estimate 2010 (Hedrick, 2009) | ThO$_2$ reserves (metric tonnes) NEA estimate (WNA, 2009)[a] | Mined amounts 2007 (metric tonnes)[b] | OECD, NEA, and IAEA Red Book, 2011 (metric tonnes)[b] |
|---|---|---|---|---|
| USA | 440,000 | 400,000 | –[c] | 434,000 |
| Australia | 300,000 | 489,000 | – | 521,000 |
| Turkey | | 344,000 | | 744,000 |
| India | 290,000 | 319,000 | 5000 | 846,000 |
| Venezuela | | 300,000 | | 300.000 |
| Canada | 100,000 | 44,000 | – | 172,000 |
| South Africa | 35,000 | 18,000 | – | 148,000 |
| Brazil | 16,000 | 302,000 | 1173 | 606,000 |
| Norway | | 132,000 | | 320,000 |
| Egypt | | 100,000 | | 380,000 |
| Russia | | 75,000 | | 155,000 |
| Greenland | | 54,000 | | 86,000 |
| Canada | | 44,000 | | 172,000 |
| Malaysia | 4500 | | 800 | |
| China | | | | 100,000 |
| Finland | | | | 60,000 |
| Sweden | | | | 50,000 |
| Kazakhstan | | | | 50,000 |
| Other countries | 90,000 | 33,000 | – | 413,000 |
| Total | 1,300,000 | 2,610,000 | 6970 | 5,385,000 |

[a] Reasonably assured and inferred resources available at up to $80/kg Th.

[b] Average Th content of 6%–8%.

[c] Last mined in 1994.

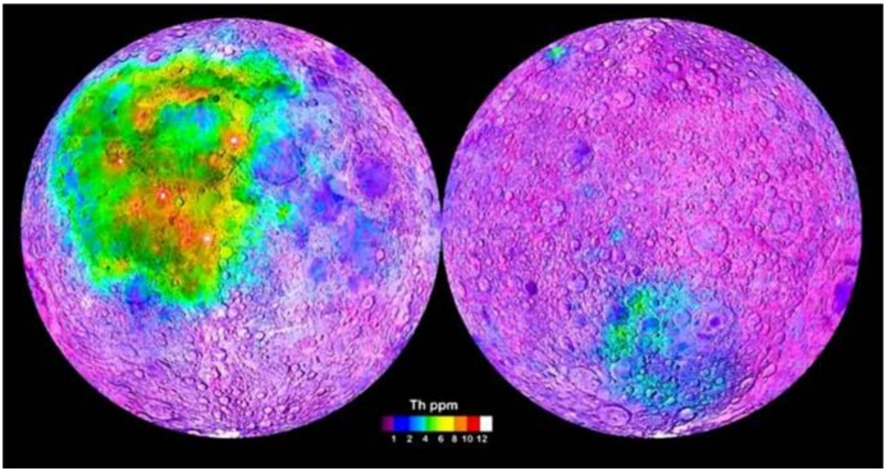

**Figure 9.21** Thorium resources on the moon. Thorium possesses electromagnetic properties allowing its identification from space.
*Source*: NASA.

**Table 9.8 Locations of USA major $ThO_2$ proven reserves (Gosen et al., 2009)**

| Deposit type | Mining district | Location | $ThO_2$ reserves (metric tonnes) |
|---|---|---|---|
| Vein deposits | Lehmi Pass district | Montana-Idaho | 64,000 |
| | Wet Mountain area | Colorado | 58,200 |
| | Hall Mountain | Idaho | 4150 |
| | Iron Hill | Colorado | 1700 (thorium veins), 690 (carbonatite dikes) |
| | Diamond Creek | Idaho | – |
| | Bear Lodge Mountains | Wyoming | – |
| | Monroe Canyon | Utah | – |
| | Mountain Pass district | California | – |
| | Quartzite district | Arizona | – |
| | Cottonwood area | Arizona | – |
| | Gold Hill district | New Mexico | – |
| | Capitan Mountain | New Mexico | – |
| | Laughlin Peak | New Mexico | – |
| | Wausau, Marathon County | Wisconsin | – |
| | Bokan Mountain | Alaska | – |
| Massive carbonatite stocks | Iron Hill | Colorado | 28,200 |
| | Mountain Pass | California | 8850 |
| Black sand placer, alluvial deposits | Stream deposits | North, South Carolina | 4800 |
| | Stream placers | Idaho | 9130 |
| | Beach placers | Florida–Georgia | 14700 |
| Alkaline intrusions | Bear lodge mountains | Wyoming | – |
| | Hicks dome | Illinois | – |

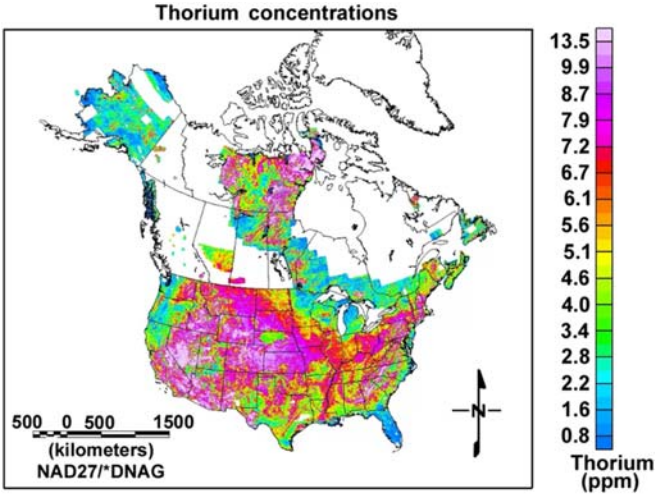

**Figure 9.22** Thorium distribution in the North American continent.
*Source*: USAGS.

**Figure 9.23** Lehmi Pass is a part of Beaverhead Mountains along the continental divide on the Montana–Idaho border, USA. Its thorium veins also contain rare earth elements, particularly neodymium.

When the Cold War came along, helium became even more important because of its uses in the purging of rocket fuel in intercontinental ballistic missiles. The national reserve was established in the porous rock of a disused natural gas field 30 miles north of Amarillo, which soon became known as the helium capital of the world.

A billion $m^3$, or about half of the world's reserves are stored in this cluster of mines, pipes, and vats that extend underground for more than 200 miles from Amarillo to Kansas.

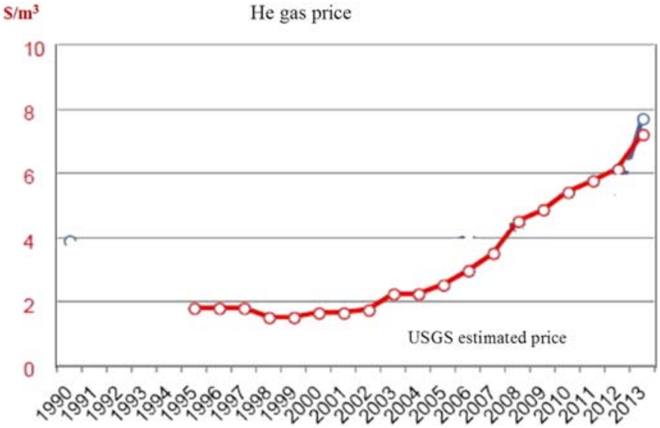

**Figure 9.24** Helium gas price versus year (Ministry of Economy, Trade and Industry, 2014).

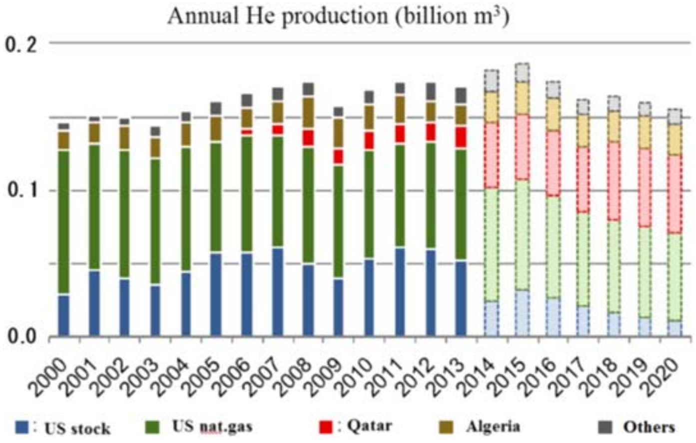

**Figure 9.25** Annual helium production versus year (Ministry of Economy, Trade and Industry, 2014).

In 1996, the United States passed the Helium Privatization Act which directed that this reserve should be sold by 2015 at a price that would substantially pay off the federal government's original investment in building up the reserve.

At the current rate of consumption, US stock at the Cliffside site will be empty within several years, and the Earth may be helium-free by the end of the 21st century. Based on this speculation, the price of helium has more than doubled over the 2003–2013 period (Fig. 9.24).

As is described above, a discount sale by the US stock is ending, but it does not mean to exhaust the He resource on the Earth. Production of He is continuing at natural gas plants, and its recent trend is shown in Fig. 9.25. In a short time range, production will be slightly decreasing, meanwhile demand may increase, and then a shortage may occur. In order to see what will happen in the long-term, reserves on the Earth must be known.

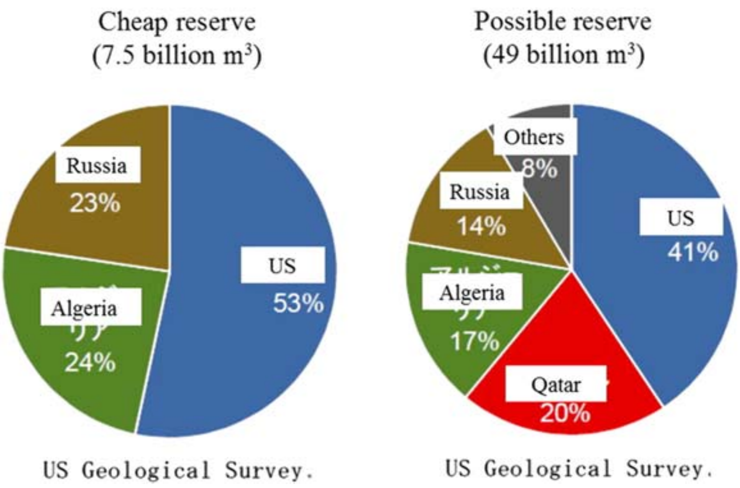

**Figure 9.26** Distribution of helium reserves (Ministry of Economy, Trade and Industry, 2014).

Both cheap reserves of He and technically possible reserves of He are shown in Fig. 9.26. It suggests that cheap He will be exhausted within 50 years, but the Earth has 300 years of He resources, if current production and demand continue.

## 9.5 Summary

In this chapter, decay heat and radiotoxicity for PWR thorium fuel cycle are compared with the conventional PWR uranium fuel cycle, using ORIGEN2 code. Both decay heat and radiotoxicity have some difference, but, in general, the difference is not large except around 0.1 million years.

If reprocessing is applied for MSR and most actinides such as U, Th, and their daughters are separated and recycled, then both decay heat and radiotoxicity after several hundred years can be greatly reduced.

A rough estimate for a ThorCon type molten salt reactor was shown. Thorium is abundant and is a byproduct of rare earth mining, but its radioactivity restricts its handling in the United States. The United States no longer conserves helium, in spite of the growing need for superconducting wires, motors, and magnets.

## References

Clement, C.h., 2012. Compendium of dose coefficients based on ICRP publication 60. ICRP Publication 119.

Croff, A.G., 1980. A users manual for the ORIGEN2 computer code. ORNL/TM-7175.

David, S., 2007. Revisiting the Thorium-Uranium nuclear fuel cycle. Europhys. News. 38 (2), 24–27.

Devanney J., et al., 2015. ThorCon™, The Do-able molten salt reactor, 2015 Martingale, Inc. <http://thorconpower.com/docs/domsr.pdf>.

England, T.R., 1993. Evaluation and compilation of fission product yields. LA-UR-94-3106.

Fleming, M., et al., 2015. Validation of FISPACT-II, decay heat and inventory predictions for fission events, CCFE-R(15)28.

Hedrick, J.B., 2009. Thorium in the United States. 1st Thorium Energy Alliance Conference, The Future Thorium Energy Economy. Kellog Conference Center, Gallaudet University, Washington, DC.

Hesketh, K., 2005. Radiotoxicity of Thorium fuel cycles in PWRs. ARWIF-2005.

IAEA (to be published in 2017) Specification for Improved Nuclear Fuel Cycle Simulation System: NFCSS-2. IAEA- TECDOC-xxxx.

ICRP, 1995. Age-dependent doses to members of the public from intake of radionuclides. ICRP Publication 72.

Kawai, K., et al., 2002. Dose coefficients for radionuclides produced in high energy proton accelerator facilities: coefficients for radionuclides not listed in ICRP publications. JAERI-Data/Code 2002-013.

Kennedy, Jim, 2009. Critical and strategic failure in rare earth resources, A national defense and industrial policy failure. 1st Thorium Energy Alliance Conference, The Future Thorium Energy Economy. Kellog Conference Center, Gallaudet University, Washington, DC.

Korea Atomic Energy Research Institute, 2015. Nuclide table. <http://atom.kaeri.re.kr/ton/>.

Ministry of Economy, Trade and Industry, 2014. Research report on Natural Gas, which contains Helium (in Japanese).

Nishihara, K., 2010. Data for estimating potential radiotoxicity of spent nuclear fuel. JAEA-Data/Code2010-012. (Data are identical to ICRP (1995). Document is written in Japanese, but English Excel file can be downloaded; <http://nsec.jaea.go.jp/ndre/ndre3/trans/DataRadiotoxicity.xls>).

Robertson, R.C., 1971. Conceptual design study of a single-fluid molten-salt breeder reactor. ORNL-4541.

Todosow, M., et al., 2010. Thorium based fuel cycle options for PWRs. ICAPP-2010.

"Transient equilibrium", 2015. <http://en.wikipedia.org/wiki/Transient_equilibrium>.

US-DOE, 1997. Evaluation of the U.S. department of energy's alternatives for the removal and disposition of molten salt reactor experiment fluoride salts. ISBN: 0-309-59010-8. <http://www.nap.edu/catalog/5538.html>.

Van Gosen, B.S., Gillerman, V.S., Armbrustmacher, T.J., 2009. Thoriun resources of the United States-Energy resources for the future? Circular 1336, USA Geological Survey, USGS, Reston, VA.

Vickers R.C., 1956. Airborne and ground reconnaissance of part of the syenite complex near Wausau, Wisconsin, contributions to the economic geology, USGS, Geological Survey Bulletin 1042-B.

WNA, World Nuclear Association, 2009. Thorium. <http://www.world-nuclear.org/info/inf62.html>.

Yarnell, J.L., et al., 1978. Calorimetric fission product decay heat measurements for $^{239}$Pu, $^{233}$U, and $^{235}$U (for thermal neutron irradiation). NUREG/CR-0349, LA-7452-MS.

Yoshioka, R., Kinoshita, M., Takaki, N., Yoshida, T., 2014. Decay heat evaluation for thorium fuel in PWR (in Japanese). Transaction of AESJ-2014 meeting. Tokyo, Japan.

Yoshioka, R., Kinoshita, M., Takaki, N., Yoshida, T., 2015. Radiotoxicity evaluation for spent thorium fuel in PWR (in Japanese). Transaction of AESJ-2015 meeting, Hitachi, Japan.

# Nonproliferation and safeguards aspects of the MSR fuel cycle

# 10

*Sophie Grape and Carl Hellesen*
Uppsala University, Uppsala, Sweden

## Chapter Outline

In this chapter we introduce the reader to the concepts of nonproliferation: safeguards and security. We briefly discuss identified threats to the peaceful nuclear fuel cycle as well as possible targets, and describe the existing nuclear safeguards system. We also discuss the advantages and disadvantages of the molten salt reactor (MSR) fuel cycle in terms of nonproliferation and compare it to that of the light-water reactor fuel cycle, which is widely implemented today.

## 10.1 Introduction to nonproliferation and nuclear safeguards

An important nonproliferation treaty is the Treaty on the Non-Proliferation of Nuclear Weapons (NPT), signed by a vast majority of the world's states. Its success stems from the fact that a very large fraction of the world's states have signed it,

**Molten Salt Reactors and Thorium Energy. DOI: http://dx.doi.org/10.1016/B978-0-08-101126-3.00010-5**

and that it has been an efficient way to slow down the nuclear arms race. This treaty specifies the duties and responsibilities associated with the peaceful use of nuclear power technology in an effort to stop the spread of nuclear weapons. In order to assure that states honor their international obligations, and in order to detect any misuse of nuclear material or technology, a set of technical measures referred to as *safeguards* are applied. As defined by the International Atomic Energy Agency (IAEA),

> . . . the objective of safeguards is the timely detection of diversion of significant quantities of *nuclear material* from peaceful nuclear activities to the manufacture of nuclear weapons or of other nuclear explosive devices or for purposes unknown, and deterrence of such diversion by the risk of early detection *(IAEA, 1972, p. 9)*

The timely detection in practice means that detection times for possible diversion should be shorter than the time required to transform the diverted material to a form in which it may be used in a nuclear explosive devices (NEDs). The significant quantity is the approximate amount of nuclear material for which the possibility of manufacturing a NED cannot be excluded. The safeguards aim to verify the completeness and correctness of declarations on nuclear material and activities. Hence, the nonproliferation of nuclear weapons is strongly connected to the existing nuclear activities and the nuclear safeguards applied to them.

In this part of the book we will elaborate on nonproliferation aspects of the MSR with respect to nuclear weapons technology, the nonproliferation threat, and nuclear safeguards, before discussing the advantages and disadvantages of MSRs.

## 10.2 The proliferation threat

We consider in this chapter the target for a possible nuclear proliferator to be nuclear material for the manufacture of one or several NEDs. However, we point out that in addition to the nuclear material itself, the actors must also be able to manufacture the weapon in order to acquire the NED. Depending on the type and amount of nuclear material, a different set of knowledge, financial resources, facilities, etc. may be required.

There are a number of actors who may be considered to pose a threat. We have chosen to mention two types of threats: that of a state and that of an independent actor, such as a terrorist group.

A *state* could, openly or covertly, decide to proceed on the path of acquiring material for nuclear weapons in noncompliance with the NPT. In the open scenario, a state could declare that it will withdraw from the NPT, as the Democratic People's Republic of Korea (DPRK) did in 2003. Alternatively, states could decide not to sign the NPT and develop and test NEDs on their own, as India did in 1974 and Pakistan in 1998. In the covert scenario, a state could construct clandestine facilities or have covert nuclear weapons programs, as was discovered in Iraq in the

1990s (UN, 1997; IAEA, 2003) and in Iran in 2002 (The IAEA Board of Governors, 2011). Finally, an *independent actor* would rather try to attack or manipulate parts of the fuel cycle, or covertly introduce new activities without the knowledge of the host state.

Depending on who the proliferator is, the threat looks different. One often distinguishes between state and nonstate actors (NSA) and the line between the two is not always clear. Examples of NSA could be different types of national or international groups such as corporations, private sector entities, terrorist groups, nongovernmental bodies, etc. Different proliferators have different resources and different concerns.

## 10.3 Attractiveness of nuclear materials

The basic principle of a nuclear explosive is rather simple. The starting configuration is a subcritical assembly of one or several pieces of a nuclear material that can sustain a fast neutron chain reaction. The nuclear material is quickly assembled to an overcritical configuration. A precisely timed neutron source initiates a supercritical chain reaction, which stops when the assembly becomes subcritical again. There are a number of different nuclear materials that can be used in a NED.

For example, in International Atomic Energy Agency(2011) the two uranium isotopes U-233 and U-235 as well as plutonium are listed. Uranium enriched to more than 20% U-235 (Bathke et al., 2012) is graded as high-enriched uranium (HEU). This limit corresponds roughly to the lowest enrichment of U-235 that is capable of sustaining a fast neutron chain reaction, which is a prerequisite for a NED. However, higher enrichments will result in a considerably lower critical mass, which is beneficial for nuclear weapons design. In Bathke (2010), an enrichment above 80% U-235 is mentioned as a generic definition of weapons-grade uranium. In principle, any composition of plutonium can sustain a fast neutron chain reaction and is therefore weapons usable. But as will be explained later, the isotope Pu-239 is the most suitable for weapons design, and a plutonium mix containing at least 93% of Pu-239 is considered weapons-grade plutonium (WGPu). Some basic properties of U-233, HEU, as well as WGPu of relevance to nonproliferation are given in Table 10.1.

**Table 10.1 Comparison of reflected critical mass, decay heat, and spontaneous fission rate for U-233, highly enriched uranium, and weapons-grade plutonium**

| | $M_{\text{crit}}$ (kg) | $P_{\text{DH}}$ (W kg$^{-1}$) | $S_{\text{f}}$ (s$^{-1}$ kg$^{-1}$) |
|---|---|---|---|
| U-233 | 8.4 | 0.3 | 0.5 |
| HEU (94% U-235) | 21 | $10^{-4}$ | 0.6 |
| WGPu (94% Pu239) | 7.5 | 2.4 | $2.5 \cdot 10^{4}$ |

To understand what makes a nuclear material attractive or unattractive, we consider three properties that complicate the design of a nuclear explosive: the dose rate a person would receive when handling the material, the heat generation of the material, and its spontaneous neutron generation.

When the attractiveness is discussed, it should be pointed out that even if some materials are less attractive than others, there are no "safe" materials that meet the above-mentioned criterion on sustaining a fast neutron chain reaction. Any isotopic composition that can sustain a fast neutron chain reaction can in principle be used as raw material for a nuclear explosive; in this regard, there is no *proliferation-proof* fuel cycle. On the other hand, it is generally considered that a fuel cycle that minimizes the attractiveness of the materials as much as possible is more *proliferation-resistant* than others and should be encouraged (Bathke et al., 2012).

### 10.3.1 Heat generation

The heat generation originates from the fact that all weapons-usable isotopes are unstable and produce heat in connection to radioactive decay. The heat generation is determined from the half-life of the isotopes in the material as well as their decay types. Typically, an alpha decay releases more energy, and hence more heat, than beta decays. The exact isotopic composition of the material is therefore important.

For example, HEU has a negligible heat generation while a critical mass of WGPu has a heat generation of about 14 W (Table 10.1). The heat from WGPu mainly originates from the beta decay of Pu-239 and Pu-240 and is enough to make it feel hot upon touching. It is however not enough to considerably complicate the design of a weapon. On the other hand, reactor-grade plutonium (RGPu) typically found in spent light-water reactor (LWR) fuel will have a few percent of Pu-238, which has a relatively strong heat production due to its alpha decay (half-life 88 years). This can result in a heat production of around 100−200 W for a critical mass. Even if it is still usable as a weapons material, the heat generation introduces some complications in the design of a weapon. Plutonium from high-burnup LWR fuel can therefore be considered more proliferation-resistant than HEU and WGPu. For U-233, the heat generation is about one-tenth of that for WGPu (Table 10.1), which makes heat a nonissue in nuclear weapons design.

### 10.3.2 Spontaneous neutron generation

Neutrons are released from spontaneous fission events in the weapons material. If such a neutron is generated during the implosion phase of an NED, but before it has reached optimum reactivity, a chain reaction can be initiated prematurely. Some nuclear weapon designs are sensitive to preinitiation, and the use of materials with a comparatively strong neutron generation, such as reactor-grade plutonium, can substantially degrade the yield of such designs (DOE, 1997). Therefore, for an unadvanced proliferator, preinitiation is an issue if a high and reliable yield is desired. However, it should be mentioned in this context that even if preinitiation occurs at the worst possible moment, when the material first reaches prompt criticality, the explosive yield of a relatively simple first-generation device will still be of the order of one or a few thousand tons of TNT equivalent. This is still a significant yield and far greater than any conventional weapon ever manufactured.

### 10.3.3 Radiation

The radiation from a nuclear material will also impose a proliferation barrier. If the material is strongly radioactive, the weapon would need to be manufactured in remotely controlled hot-cells. For an unskilled proliferator, like a terrorist group, such facilities are less likely to be available. For this reason, the IAEA has considered materials that would give a dose rate of 100 rem/h to a person handling them as self-protecting (Doyle, 2008). After receiving a dose of 300 rem, or 100 rem/h for 3 hours, there is a 50% probability of survival.

However, a terrorist organization or a totalitarian state might be less concerned about the health of the weapons manufacturers. In the example considered above, the time to death is about 1 month (ORNL, 2005), which means that the dose rate is not high enough to prevent a dedicated proliferator from acquiring a working NED. The dose rate must be significantly higher than 100 rem/h to consider the material as self-protecting. In Bathke et al. (2012) a level of 1000 rem/h is considered enough to achieve a significant increase in the proliferation resistance of the material.

None of the fissile materials discussed above (U-233, HEU, and WGPu) has any significant radiation, and they can all be handled with minimal radiation protection. However, when U-233 is produced via neutron capture in Th-232, a small amount of U-232 is also produced. U-232 is an isotope that first decays to Th-228 and eventually to Tl-208, which in 36% of the decays emits a very energetic gamma ray at 2.6 MeV. This gamma emission makes handling of material contaminated with U-232 very difficult. The high-energy of the gamma ray also makes shielding more difficult compared with materials that emit gamma rays with lower energies. Due to the relatively long half-life of Th-228 (1.91 years), the dose from U-232 initially increases with time. The strong radiation from the decay of U-232 is positive from a nonproliferation point of view, but unwanted by operators of MSRs, since the consequence is that the material needs to be handled remotely in hot-cells. To reach a significant level of self-protection, several percent of U-232 is needed (Moir, 2010). The amount of U-232 in the fuel depends strongly on the exact type of reactor, but in a simulation of a thorium-fueled molten salt breeder reactor (MSBR) (Vanderhaegen and Janssens-Maenhout, 2010), a level of about 60 ppm U-232 was reached after 2.5 years of full-power operation. This is several orders of magnitude lower than what is required for the material to be considered as self-protecting.

## 10.4 Nuclear safeguards

In order to address the nuclear threat and prevent the spread of nuclear weapons, the nuclear safeguards system was created. It was founded in the late 1950s as a response to the manufacture and testing of nuclear weapons by several states, with the establishment of the IAEA and Euratom. The safeguards system comprises all parts of the nuclear fuel cycle, i.e., all activities and facilities ranging from mining the ore to the reprocessing or storage of spent nuclear fuel. In order to ensure the full compliance of states to treaties regulating the nonproliferation of nuclear weapons technologies, the IAEA together with other inspecting authorities take a number of measures. For example, they verify documentation provided by operators, inspect facilities, measure material samples, conduct surveillance, and perform export control. The materials of interest are mainly special nuclear material (SNM), which means plutonium, uranium-233, or uranium enriched in the isotopes uranium-233 or uranium-235.

The basis for all nuclear safeguards activities is the NPT, with 191 state parties. In this treaty, a distinction is made between nonnuclear weapons states (NNWS) and nuclear weapons states (NWS)—originally corresponding to the UK, France, the US, the Soviet Union, and China—concerning their obligations. This distinction remains today, with a consequence being that NWS are not expected to provide the same transparency to inspecting authorities as NNWS. In addition to the NPT, the *Additional Protocol* (AP), which further strengthens international safeguards, has entered into force in many states. Also, the focus has, since the late 1990s, been to the implement *Integrated Safeguards*, which describes efforts to reach an optimal combination of all safeguards measures available to the IAEA, in order to achieve maximum effectiveness and efficiency within the available resources.

With an increasing number of nuclear facilities and the foreseen introduction of innovative fuel cycles, the IAEA has taken a step in the direction of more effective and efficient implementation of IAEA safeguards (Nackaerts, 2010; IAEA, 2015). The IAEA is, among other things, promoting *Safeguards-By-Design* (or SBD) (IAEA, 2013), which should be seen as an approach whereby international safeguards are fully integrated into the design process of a nuclear facility—from initial planning through design, construction, operation, and decommissioning (IAEA, 2009). The IAEA has actively supported efforts relating to nuclear safeguards applications to innovative fuel cycles via the INPRO project (INPRO, 2015) and the Generation IV International Forum (GIF, 2015) with the development of, for example, assessment methodologies for proliferation resistance. In parallel, the IAEA is working together with member states to define both an SBD framework and a process that provides sufficient guidance for operators of nuclear fuel cycle facilities to implement SBD. This should include, e.g., the development of basic principles and design features, definition of roles and responsibilities, and guidance documents (IAEA, 2013).

Since no commercial MSR has ever been operated, there is no answer to what a safeguards system for such a reactor type would look like. However, we can expect that it will have to be at least as effective as that of today's nuclear energy systems. In this chapter, we will therefore compare the fundamentals of the MSR fuel cycle with that of the LWR and identify the most sensitive parts in the two. The way the sensitive parts of the LWR fuel cycle are handled today can provide a guideline to what the safeguards implementation of an MSR fuel cycle would look like. The following three subsections are devoted to describing the LWR and MSR fuel cycles from a safeguards perspective: we briefly describe the respective fuel cycles and identify the parts which are most sensitive from a nonproliferation point-of-view.

### 10.4.1 Safeguarding the LWR fuel cycle

Nuclear safeguards are applied to the complete fuel cycle and not only to the reactors. A simplified description of the standard LWR fuel cycle is shown in Fig. 10.1. The natural uranium that is mined is a rather weak proliferation threat. It is not possible to design a nuclear weapon from its isotopic composition, and it cannot be used as fuel in a light-water reactor. In the enrichment process, the concentration of the fissile isotope U235 is raised to about 4%. Although this material is also not usable in a weapon, the enrichment process can easily be modified to produce HEU with more than 80% U235. In fact about 80% of the work needed to raise the enrichment to 80% is already done when LEU is produced. The enrichment facilities are therefore highly sensitive from a nonproliferation perspective and need to be meticulously safeguarded. A further complication here is that the material is not handled in discrete units, like fuel assemblies, but rather as continuous material flows. This makes it easier to continuously divert a small stream of sensitive material.

During the remainder of the standard LWR fuel cycle, i.e., without reprocessing, the nonproliferation risks are less pronounced. The low-enriched uranium that leaves the enrichment plant can be used as fuel in an LWR, but the U-235 concentration is too low to be used in an NED. When the fuel is taken out of the core, it typically contains about 1% of reactor-grade plutonium. As was discussed above, this is not the preferred material for an NED, but is nevertheless usable. It will however need an additional reprocessing step where the plutonium is separated from the other actinides as well as the fission products.

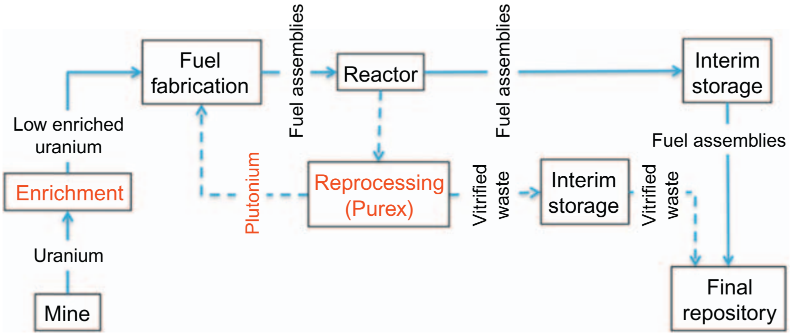

**Figure 10.1** Simplified overview of the fuel cycle for the light-water reactor. Steps that are particularly sensitive in a nonproliferation perspective are marked in red.

Further, the material is contained in well-defined fuel assemblies, typically about 4 m high, which makes the safeguards process simpler since remotely handled cameras can be used to guarantee the continuity of knowledge. For this reason, diverting small quantities of sensitive material is very difficult.

Also, when the spent fuel is taken out of the reactor it is highly radioactive and cannot be handled directly, even if health concerns are not an issue. Typically, the spent fuel assemblies are handled submerged in storage pools, and transportation of one or more assemblies from the reactor sites is done in large and heavy transport casks. This is a slow process, which significantly simplifies the safeguarding of the operations. Safeguards personnel are typically only needed on-site when the reactor is refueled or when fuel is moved.

In the case of CANada Deuterium Uranium (CANDU) reactors with online refueling, a number of solutions have been identified and deemed sufficient for nuclear safeguards purposes. These include frequent (and costly) inspections (Leaver, 2009), the use of extrinsic as well as intrinsic proliferation barriers (Whitlock and Lee, 2009), and continuous cooperation with the IAEA to ensure satisfactory solutions in the development of new reactor concepts (Ellacott et al., 2010).

Some countries operate light-water reactors with a semiclosed fuel cycle in which plutonium is separated from the fuel and reused in the reactors in the form of Mixed oxide fuel (MOX) fuel. The flow is illustrated in Fig. 10.1 as dashed lines. The reprocessing of spent fuel may be a controversial activity from a nuclear safeguards point of view since sensitive nuclear materials in the form of uranium and plutonium are separated from other actinides as well as the fission products. Not only is weapons-usable material separated, the self-protecting radiation barrier that the fission products provided is also lost, and the well-defined fuel assemblies are replaced with a more continuous material flow where a slow diversion of small quantities is made easier. This opens up for a gradual accumulation of significant quantities of weapons material.

Partly for these reasons, civilian reprocessing has mainly been carried out in NWS. One exception is Japan, which has a reprocessing plant (Rokkasho) with a capacity of 800 tons of uranium per year (Japan Nuclear Fuel Limited, 2015). The safeguarding of the Rokkasho plant is extensive and includes, among other things, an IAEA-operated on-site laboratory that samples every step of the process (Duhamel et al., 2004). The onsite laboratory is permanently staffed with IAEA personnel. Further, the Plutonium Uranium Redox EXtraction (PUREX) process itself is also a modified variant in which pure plutonium is not separated, but a mixture of uranium and plutonium. This reduces the attractiveness of the separated material somewhat.

### 10.4.2 Safeguarding the MSR fuel cycle

When comparing the safeguards of the MSR fuel cycle with that of today’s conventional reactors we have chosen the traditional MSBR fuel cycle as a reference. It should be stressed that a number of alternative MSR fuel cycles have been suggested. Some of these do not include any reprocessing of spent fuel. This makes them less problematic from a safeguards point of view compared to fuel cycles with extensive reprocessing. One such example is the Integral Molten Salt Reactor (IMSR) presented in Chapter 18, Integral molten salt reactor.

However, the MSBR fuel cycle is the only one with, at least partial, operational experience. In the Molten Salt Reactor Experiment (MSRE) the graphite-moderated core was tested (Rosenthal et al.,1972; Haubenreich and Engel, 1970), but the breeding of fissile material was made in other reactors. Even if the analysis presented here is focused on the MSBR fuel cycle, many of the conclusions are still valid for the other proposed fuel cycles. From a safeguards perspective, it can be noted that recent research activities have focused to a larger extent on the transuranic waste-burning capabilities of the MSRs; for example the MOSART design in Russia (Ignatiev et al., 2007) as well as the thorium molten salt reactor, which combines a high fissile concentration with a partial blanket (Merle-Lucotte et al., 2007).

A simplification of the MSBR fuel cycle is schematically shown in Fig. 10.2. Excluded from this figure is the start-up fissile material for the fuel cycle. This is typically proposed to be uranium enriched to 20%, or plutonium from LWR spent nuclear fuel. It can be noted that both of these materials are also of significant safeguards interest, as discussed in Section 10.4.1.

The natural resource in the MSR fuel cycle, here thorium, is not considered to be a significant proliferation threat by itself. This is in common with the LWR fuel cycle. In fact, natural thorium contains no fissile isotopes at all. A reprocessing step is perceived in which fission products are separated, and the bred fissile fuel is returned to the reactor. In the MSBR fuel cycle, a conversion ratio of 1 is envisaged, and for this reason, no enrichment is needed. Also, in contrast to the LWR fuel cycle, refueling and reprocessing of an MSR are performed on-line with the

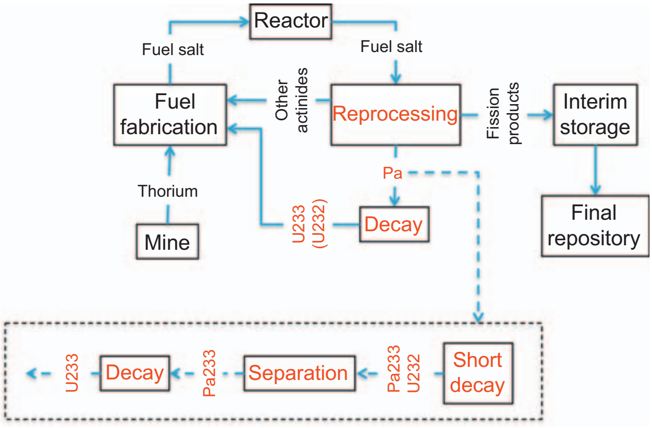

**Figure 10.2** Simplified overview of a proposed fuel cycle for the molten salt breeder reactor.

fuel in liquid form. There are therefore no well-defined fuel assemblies as in the LWR fuel cycle.

In the case of the MSBR (McNeese et al., 1974), the reprocessing takes place in three steps in areas outside the reactor. In the first step, uranium is separated from the salt via a fluorination process. In the second step, protactinium, fission products, and rare-earth metals are removed. The protactinium stream is then directed to a decay tank where it decays to uranium. In the third step, UF6 is reduced to UF4. This keeps the Pa-231 concentration in the fuel salt low, and hence reduces also the U-232 levels. The decay tank outside the reactor is needed to enhance the breeding capability of the reactor. If the protactinium were allowed to circulate in the reactor core, parasitic neutron absorption in Pa-233 would result in the production of fertile U-234 instead of the fissile U-233.

The uranium that is obtained in the decay tank is mainly composed of U-233, which is a weapons material as discussed above. However, since both Pa-233 (which decays to U-233) and Pa-232 (which decays to U-232) are separated together, the resulting uranium stream will always contain a fraction of highly gamma-radiating U-232. This is beneficial from a nonproliferation point of view as the resulting uranium stream will build up a radioactive proliferation barrier. The high-energy gamma radiation will also be difficult to shield, and the signature in the gamma emission makes any diversion possible to detect by gamma monitors.

Nevertheless, it is possible to modify the MSR fuel cycle to produce almost pure U-233. This is illustrated in Fig. 10.2 as dashed lines in the bottom of the figure. Pa-232 has a half-life of only 1.3 days, in contrast to 27 days for Pa-233. If the Pa stream from the reprocessing stage is first allowed to decay in a short intermediate decay step, most of the Pa-232 will have decayed to U-232, while only a small fraction of Pa-233 has decayed to U-233. For example, after 2 weeks more than 99.9% of the Pa-232 has decayed to U-232 while only 30% of the Pa-233 has decayed to U-233. If the resulting Pa/U mix is separated in a clandestine facility, almost pure Pa-233 can be obtained which will then decay to almost pure U-233 in a second decay step. For safeguards purposes, this points to the importance of accurate salt composition and materials flow monitoring.

Although we are here mainly considering the reprocessing for the MSBR, it can be pointed out that other MSR concepts foresee varying degrees of reprocessing and that different reprocessing options have been (and are) considered. For example, in the proposed reprocessing for the future MSR (GIF, 2011), uranium, minor actinides (neptunium, plutonium, americium, and curium), and protactinium are removed from the fuel salt and sent back to the core using a fluorination process and an extraction loop.

In the present Non-Proliferation Treaty, there are no formal barriers for any country to deploy reprocessing technologies. However, the safeguards requirements for such facilities will probably be extensive. The Rokkasho reprocessing plant discussed above could likely serve as a guideline to what would be required in a non-nuclear weapons country (Johnson and Lockwood, 2011). The material streams in an MSR reprocessing stage must be strictly safeguarded to guarantee that no illicit activities take place covertly, and depending on the implementation of the reprocessing, the degree of proliferation resistance of the fuel cycle varies.

## 10.5 Nonproliferation advantages and disadvantages with MSRs

In order to summarize the nonproliferation advantages and disadvantages with MSRs, we first clarify objective differences to LWRs and then proceed with details on their interpretation and nonproliferation implications.

### *10.5.1 Fundamental differences between MSRs and LWRs*

The operational experience of MSRs is today very limited, which makes it difficult to draw conclusions on the full range of implementations that are possible. The Aircraft Reactor Experiment operated in 1954, and the MSRE was in operation between 1965 and 1969.

#### *10.5.1.1 The fuel cycle*

Starting with a comparison of the steps involved in the LWR and MSR fuel cycles, a number of substantial differences can be identified. The largest difference is that the LWR fuel cycle is an *open cycle* (or partly closed, considering reprocessing and MOX fuel fabrication), while the MSR fuel cycle is typically fully *closed* and relies on complete fuel reprocessing. There are also substantial differences between the materials in the fuel cycles. In the LWR cycle, enrichment and reprocessing activities handle *bulk material* while the part from fuel fabrication and onwards handles *items* (fuel elements). In the MSR cycle, all materials are in bulk form at all times.

Also, the extent and types of reprocessing differ between the fuel cycles. Typically, the MSR fuel cycle relies to a much higher degree on reprocessing than the LWR fuel cycle. Furthermore, MSRs foresee online reprocessing, which is currently not done in any nonnuclear weapons state. It should also be noted that the LWR fuel cycle employs an *aqueous* reprocessing technique (such as PUREX), while the MSR fuel cycle is likely to employ fluoride volatilization (removal of uranium from the fuel salt before further processing for fission products), molten salt/liquid metal extraction techniques, and *pyroprocessing*. There are fundamental differences between these types of reprocessing technologies, which in turn have implications for the design of the safeguards system (Uhlir et al., 2007; Durst et al., 2007; Li et al., 2011).

#### *10.5.1.2 The reactor*

A difference that is not clearly seen from the comparison of the fuel cycles concerns the reactors themselves. The majority of today's commercial reactors—except CANDU reactors currently used in Canada, India, and the Republic of Korea—are shut down for revision and refueling. It is physically not possible to access the fuel inside the reactor while it is in operation. This simplifies the verification of the nuclear material to periods when the fuel is accessible. On the other hand, MSRs rely on online refueling, which makes it possible to access fuel also during reactor operations. Further, while CANDU reactors are refueled online with natural uranium, MSRs are refueled with reprocessed fissile material.

#### *10.5.1.3 The fuel*

MSR fuels have characteristics that differ from fuels that are used in the LWR fuel cycle and are based on the use of mainly U-235 as fuel material. One aspect of this is the liquid fuel, which is very different from the fuel assemblies that are part of a conventional LWR core. For fuel assemblies residing in the storage pool outside the reactor, a remotely controlled surveillance camera is typically used to guarantee that no tampering of the fuel has occurred. No sensitive materials can be diverted as long as no movements of the fuel assemblies are detected. With liquid fuels, more advanced monitoring systems are required to ensure that no sensitive materials have been diverted.

Another aspect is the material itself, which is primarily not based on the use of U-235, but rather on U-233/Th-232 of very high quality, or alternatively plutonium. Depending on the choice of reprocessing technique, the fuel salt is treated in different ways and goes through a number of separation steps (online and offline) with the remaining fuel being sent back to the core (although the thorium recycling technology is currently only under development). Some, but not all, MSR designs also include a fertile blanket where new fuel is bred, and occasionally fractions of the fertile salt may also be reprocessed and then sent back to the core.

In the one-fluid design MSRE campaign, uranium-235 tetrafluoride (UF4) enriched to 33% was dissolved in molten lithium, beryllium, and zirconium fluorides ($LiF\text{-}BeF_2\text{-}ZrF_4\text{-}UF_4$). Later campaigns used also U-233 in the fuel salt. The graphite = moderated MSBR was also a single-fluid design, employing (in the reference case) $LiF\text{-}BeF_2\text{-}ThF_4\text{-}UF_4$ as fuel salt with U-233 or U-235 enriched to around 72% (Engel et al., 1978). Chloride fuel salts have also been proposed, but lack operational experience to draw upon.

### **10.5.2 Nonproliferation aspects of MSRs**

There are several nonproliferation aspects that are often brought forward in the discussions of MSR concepts. This section will discuss some of these advantages and disadvantages.

A selection of advantages of the MSR concept with respect to nonproliferation are:

- No need for enrichment facilities during routine operation (in the case of the breeder fuel cycle);
- A smaller fissile inventory in the core;
- A strong gamma radiation, which makes the fuel material more unattractive for proliferators; and
- A collocated reprocessing, which reduces the transportation of SNM offsite.

MSRs utilizing the thorium fuel cycle are designed to make use of actinide recycling and a closed Th/U fuel cycle, thereby removing the need for uranium enrichment facilities, which are sensitive from a nonproliferation point of view. Note that this is true for the equilibrium fuel cycle only. During the start-up phase of a MSR fuel cycle, fissile material must be added externally.

The fissile inventory in an MSR core can be smaller than that of an LWR. Because the fissile isotopes in an MSR are not contained in conventional fuel rods with limitations on the total power density, the power density can be increased, which in turn implies a smaller fissile amount per unit power produced.

In addition, the online removal of xenon eliminates the need for reactivity excess early in the fuel cycle in order to compensate for the reactivity decrease with increased burnup. Furthermore, the continuous removal of neutron-absorbing fission products has the consequence that the loading of fissile material is lower in an MSR than an LWR. Given the strong *gamma radiation*, the MSR fuel needs to be handled in a hot cell, which facilitates the application of C/S (containment and surveillance). (GIF, 2011).

Operational efficiency would require the collocation of the reactor(s) with the reprocessing facilities, unlike in the LWR fuel cycle where standalone reprocessing facilities can receive used fuel shipped from multiple states. Transportation of nuclear materials is typically considered a vulnerability and of great interest to safeguards and security.

Finally, it can be pointed out that thorium-fueled MSRs produce small amounts of plutonium compared to uranium-fueled reactors, but on the other hand they produce large amounts of U-233, which is an excellent weapons material, as discussed in Section 10.3. Fast (nonmoderated) MSRs also allow for improved burning of plutonium and other transuranic wastes. This is an advantage for all fast reactor fuel cycles when compared with the LWR fuel cycle, which typically generates a net production of plutonium. The burning of transuranic waste, such as plutonium, could reduce the future risks with so-called plutonium mines associated with geological repositories (Grape et al., 2014). However, a quantitative comparison between the plutonium-burning capabilities of different fast reactor concepts is beyond the scope of this chapter.

Identified disadvantages of the MSR with regards to nonproliferation are:

- A fuel inventory residing outside the core, which increases the total fissile inventory;
- The use of liquid fuel, as opposed to fuel assemblies, which makes it more difficult to account for all material;
- An online reprocessing, which makes the fuel material more accessible and hence easier to manipulate;
- An online reprocessing with fission product removal, which lowers the proliferation barrier;
- The produced U-233 is of weapons quality and equivalent to plutonium.

Due to the smaller fissile inventory inside the core, some fuel needs to reside outside the MSR core. This increases the fissile inventory, thus compensating for the lower fissile inventory inside the core (GIF, 2011). The use of liquid fuel instead of fuel rods in fuel assemblies also removes the possibility for item counting and ID-verification. With liquid fuels, the concepts of burnup and irradiation cycles are meaningless, which in practice means that it is not possible to track or verify a "specific fuel item," as is done today for LWRs. This makes inventory taking and material accountancy more difficult since materials change form and composition and are distributed over several locations (pipes, tanks, etc.). Furthermore, the liquid fuel allows for a high accessibility of the nuclear material in the salt because of the online reprocessing/refueling mechanism (Vanderhaegen and Janssens-Maenhout, 2010). This could mean that it becomes challenging to detect low-quantity diversions, which in total amount to one or several significant quantities.

Also, in liquid fuels, gaseous fission products come off continuously with a purification process such as liquid extraction, which is much easier for an MSR than for solid fuel, since the dissolution and fuel refabrication steps are avoided (MacPherson, 1985). However, the process of removing fission products further lowers the radiation barrier of the fuel and hence makes it less difficult to handle. The removal of fission products from the fuel also makes these more easily accessible for the construction of a radiological dispersive device ("dirty bomb").

## 10.6 Means of improving MSR fuel cycle proliferation resistance

Nonproliferation aspects of the MSR often concern U-232 contamination and the presence of weapons-quality U-233. To increase the proliferation resistance, it is often advantageous to have materials that are difficult to handle. At the same time, such materials are also difficult to handle for civil operators and will likely increase the costs of the electricity production.

In this section we elaborate on these isotopes and also on the reprocessing associated with the operation of MSRs.

### *10.6.1 Denaturation*

In the case that U-232 and its intense gamma radiation is not considered sufficient to deter proliferators, it has been suggested that the uranium could be denatured with U-238 (Engel et al., 1980; Gat and Engel, 2000). This does however not solve all problems. Primarily, the issues with protactinium separation and subsequent U-233 production still remain. In addition, denaturing with U-238 also introduces plutonium to the used fuel.

Denaturing MSR fuel with fertile U-238, leaving the uranium unfit for weapons use, was early on concluded inferior to the pure thorium fuel cycle. The use of U-238 leads to a poorer performance, increased plutonium production, as well as production of other transuranic elements that need to be recovered during processing for fission products (Rosenthal et al.,1969). The proposed denatured molten salt reactor (DMSR) has a lower concentration of fissile uranium, but as a consequence it is also associated with larger long-lived transuranic inventory and lower breeding ratio (Engel et al., 1980). This in turn lowers the economic interest to employ this type of reactor. In order to maximize the breeding ratio, protactinium must be removed quickly, which in turn results in a pure Pa-233 stream which decays to a pure U-233 stream unless this stream is denatured by other uranium isotopes.

In order to avoid the U-233 problem altogether, MSRs can also be operated with uranium fuel enriched to just below 20% (Gat and Engel, 2000). There have also been proposals for nonbreeding MSRs without any fuel reprocessing (Alexander et al., 1965). The molten salt converter reactor (MSCR) converts, but does not breed, fuel unless chemical processing equipment is added. A study at ORNL has shown that such a reactor, using thorium and 20% enriched uranium, could be operated for 30 years with only a gas purge system removing gases that naturally come off and with no fuel reprocessing. However, there is a need to periodically add more 20% enriched uranium (MacPherson, 1985).

In Chapter 18, Integral molten salt reactor, a nonbreeding MSR design, the IMSR, operating with low-enriched uranium is also described. This reactor design does not include any type of reprocessing and the nonproliferation weaknesses related to reprocessing are therefore greatly reduced. However, all such options involving enriched uranium imply the continued use of uranium enrichment facilities, which are one of the most sensitive parts of the LWR fuel cycle from a nonproliferation perspective.

### 10.6.2 Physical protection

It has been suggested that a way to remedy the shortcoming of the MSR with respect to nonproliferation could be to integrate physical protection with nuclear safeguards. According to the IAEA Convention on physical protection of nuclear material, this includes measures to protect the nuclear material (or the containers and facilities in which they are stored) against unlawful taking and use (IAEA, 1979). This could be part of a solution to a problem where the nonproliferation threat is a nonstate actor (Uhlir, 2014).

### 10.6.3 Options for MSR fuel salt reprocessing

The MSR concept with online refueling relies on (continuous) separation of waste products and fuel material. The actual details of the reprocessing are difficult to specify once and for all because different MSR concepts foresee a varying degree of reprocessing. Depending on the implementation of the reprocessing, the degree of proliferation resistance varies. Suggested fuel reprocessing for MSRs vary from:

1. Removal of only gases and volatiles (as foreseen for the MSRE), to
2. A 10-day reprocessing cycle for the MSBR, and
3. Even shorter processing periods for complete online reprocessing.

1. Reprocessing in MSRE (Haubenreich and Engel, 1970): Reprocessing for the purpose of removing oxide contamination from the salt, and to recover the uranium from the salt at the end of the experiment. Reprocessing after shutdown for the MSRE was foreseen to

consist of on-site separation of uranium from the fuel salt via a fluoride volatility process, with subsequent substitution of U-233.

2. Reprocessing in MSBR (McNeese et al., 1974): The reprocessing of MSBR builds on three steps where direct online reprocessing takes place with separation of U and Pa in areas outside the reactor. There are three main steps: the first is the separation of uranium from the salt via a fluorination process, the second is the removal of protactinium, fission products and rare-earth metals, and lastly the hydro-reduction of UF6 to UF4. This keeps the Pa-231 concentration in the fuel salt low, and hence reduces also the U-232 levels.
3. Simplified schematic molten salt processing (Gat and Dodds, 1993): In the first step noble gases, other gases, and volatiles are removed (this step is the same for all MSRs in order to avoid unstable operation). In the second step, the fluoride volatility process, uranium hexafluoride is quantitatively removed, reduced to tetrafluoride, and then returned to the reactor with the entire inventory being processed in 3 days. The salt containing the fission products, the U-233 precursor protactinium and possibly other fissile isotopes, then continues to the third stage where they are separated and the salt (free of fission products) is returned to the reactor. Protactinium and any plutonium that may be present due to either breeding or because it was used as initial fissile material, is removed first. Plutonium will then be returned to the core while protactinium may be held up to convert to uranium prior to return to the core. If actinides are present or other long-lived elements are present, they may be separated out and fed back to the reactor for transmutation. Note: As the MSRE switched from uranium-235 fuel to uranium-233 fuel, the entire inventory (218 kg uranium) was processed in 4 days by the fluoride volatility process (MacPherson, 1985).
4. Reprocessing in MSFR (GIF, 2011): The purpose of the reprocessing unit is to separate lanthanides (elements with atomic numbers between 57 and 71). First, however, uranium, minor actinides (neptunium, plutonium, americium, and curium) and protactinium are removed from the fuel salt and sent back to the core using a fluorination process and an extraction loop. A modification of the extraction loop could lead to Pa-233 recovery, which decays into U-233. However, this uranium would still contain other uranium isotopes, and it would be mixed with minor actinides. This points to the importance of accurate salt composition monitoring, which is necessary for both operational and safeguards purposes.

Frequent reprocessing may be argued to enhance safety, but it leads at the same time to more manipulations and accessibility of the fuel. Since the reprocessing for future commercial MSRs is not well determined at this stage, neither are the future waste streams that need to be handled.

## 10.7 Summary and conclusion

From a nonproliferation point of view, there are advantages and disadvantages with the MSR concept. Any new reactor concept and fuel cycle always poses a challenge for nuclear safeguards to develop and implement an effective and efficient approach. It is not only the reactor that is subject to nuclear safeguards, but its entire associated fuel cycle. For this reason it is crucial to assess strengths as well as weaknesses early on in the process, preferably at the design stage, in order to facilitate the licensing procedure.

The MSR concept poses challenges to the existing nuclear safeguards system, as it contains many features that are not present in the standard light-water reactor fuel cycle, for which most of the currently implemented nuclear safeguards activities were designed. The use of liquid fuels instead of fuel assemblies, online refueling of fissile material instead of well-specified irradiation cycles, and fuel reprocessing will pose challenges to the safeguards system. The level of reprocessing for future commercial MSRs is not determined at this stage, and neither are the anticipated waste streams that need to be handled. How a safeguards system for a future MSR would be designed can therefore not be answered today. One can however, at a minimum, expect the safeguards to monitor in detail the material balance of U, Pu, and other actinides (Johnson and Lockwood, 2011).

In conclusion, comparing the MSR fuel cycle with that of today's commercial reactors, sensitive parts can be identified. Even if the MSR fuel cycle differs considerably from today's fuel cycles, many steps in the MSR fuel cycle have similar counterparts, e.g., the reprocessing of spent LWR fuel as well as the operation of CANDU reactors. For these systems, satisfactory safeguards implementations have been arranged.

The level of proliferation resistance that can be achieved depends on what proliferation threat one considers and what the implemented fuel cycle looks like. If the threat is a nonstate organization, such as a terrorist group, the MSR fuel cycle can potentially be designed to be very unattractive for theft and diversion. However, if one considers the threat to be the host state, it could be rather straightforward to modify the fuel cycle to produce materials with very high weapons quality. To prevent a host state from covertly diverting such material, options are for inspecting authorities to have a permanent presence at the reactor site, to use remote and unattended monitoring, or to have a very high inspection frequency.

## References

Alexander, L.G., et al., 1965. Molten Salt Converter Reactor—Design Study and Cost Estimates for a 1000 MWe station. Oak Ridge National Laboratory, Oak Ridge, TN, ORNLTM-1060 [Online], Available from: <http://moltensalt.org/references/static/downloads/pdf/ORNL-TM-1060.pdf> (accessed 28.01.16.).

Bathke, C.G., et al., 2012. The attractiveness of materials in advanced nuclear fuel cycles for various proliferation and theft scenarios. Nucl. Technol. 179, 5–30.

Ellacott, T., Casterton, J., Kent, M., 2010. Safeguards-by-design: The Canadian Experience, In: The proceedings of the IAEA International Safeguards Symposium 2010—Preparing for Future Verification Challenges, Vienna, Austria [Online], Available from: <https://www.iaea.org/safeguards/symposium/2010/Documents/PapersRepository/219.pdf> (accessed 28.01.16.).

DOE, 1997. Nonproliferation and Arms Control Assessment of Weapons-Usable Fissile Material Storage and Excess Plutonium Disposition Alternatives, DOE/NN-0007, U.S. Department of Energy.

Doyle, J., 2008. Nuclear Safeguards, Security, and Nonproliferation Achieving Security with Technology and Policy. *Elsevier*, Oxford.

Duhamel, G., et al., 2004. 7th International Conference on Facility Operations–Safeguards Interface, February 29–March 5, 2004, Charleston, SC, on CD-ROM, Linda Rose, Oak Ridge National Laboratory, Oak Ridge, TN.

Durst, P.C., et al., 2007. Advanced Safeguards Approaches for new TRU fuel fabrication Facilities, PNNL-17151. Pacific North Western National Lab, Richland, WA [Online], Available from: <http://www.pnl.gov/main/publications/external/technical_reports/PNNL-17151.pdf> (accessed 25.02.16.).

Engel, J.R., et al., 1978. Molten-Salt Reactors for Efficient Nuclear Fuel Utilization Without Plutonium Separation, ORNL/TM-6413. Oak Ridge National Laboratory, Oak Ridge, TN.

Engel, J.R., et al., 1980. Conceptual design of a denatured molten salt reactor with once-through fueling, ORNLTM-7207 [Online], Available from: <http://web.ornl.gov/info/reports/1980/3445603575931.pdf> (accessed 28.01.16.).

Gat, U., Dodds, H.L., 1993. The source term and waste optimization of molten salt reactors with processing. In: Paper presented at the GLOBAL'93, 12-17 September, 1993 Seattle, Wa [Online], Available from: <http://www.iaea.org/inis/collection/NCLCollectionStore/_Public/25/011/25011404.pdf> (accessed 28.01.16.).

Gat, U., Engel, J.R., 2000. Non-proliferation attributes of molten salt reactors. Nucl. Eng. Des. 201 (2–3), 327–334.

Generation IV International Forum. 2011. Proliferation resistance and physical protection of the six generation IV nuclear energy systems. GIF/PRPPWG/2011/002, [Online], Available from: <https://www.gen-4.org/gif/upload/docs/application/pdf/2013-09/gif_prppwg_ssc_report_final.pdf> (accessed 28.01.16.).

GIF, 2015. Generation IV International Forum. Available from: <http://www.gen-4.org/> (accessed 28.01.16.).

Grape, S., et al., 2014. New perspectives on nuclear power—Generation IV nuclear energy systems to strengthen nuclear non-proliferation and support nuclear disarmament. Energy Policy. 73 (C), 815–819.

Haubenreich, P.N., Engel, J.R., 1970. Experience with the molten salt reactor experiment. Nucl. Technol. 8 (2), 118–136.

IAEA, 1972. International Atomic Energy Agency Information Circular 153 (INFCIRC/153), paragraph 28, 1972, [Online], Available from: <https://www.iaea.org/publications/documents/infcircs?field_infcirc_number_value=153&field_infcirc_date_value[value][date]> (accessed 28.01.16.).

International Atomic Energy Agency Convention on the Physical Protection of Nuclear Material, 1979. [Online], Available from: <https://www.iaea.org/publications/documents/conventions/convention-physical-protection-nuclear-material> (accessed 28.01.16.).

IAEA, 2003. International Atomic Energy Agency factsheet, Copyright 2003-2004, Iraq Nuclear File: Key Findings, [Online], Available from: <https://www.iaea.org/OurWork/SV/Invo/factsheet.html>.

International Atomic Energy Agency SGCP-CCA, 2009. Facility design and plant operation features that facilitate the implementation of IAEA safeguards, Report IAEA-STR-360.

The IAEA Board of Governors, 2011. Implementation of the NPT Safeguards Agreement and relevant provisions of Security Council resolutions in the Islamic Republic of Iran, GOV /2011/65.

International Atomic Energy Agency, 2011. Nuclear security recommendations on physical protection of nuclear material and nuclear facilities (INFCIRC/225/REVISION 5), IAEA Nuclear Security Series No. 13.

International Atomic Energy Agency, 2013. International safeguards in nuclear facility design and construction, IAEA Nuclear Energy Series. No. NP-T-2.8.

IAEA, 2015. Report by the IAEA director general 2015, strengthening the effectiveness and improving the efficiency of agency safeguards, GC(59)/18.

Ignatiev, V., et al., 2007. Progress in development of Li, Be, Na/F molten salt actinide recycler and transmuter concept, In: Proceedings of ICAPP 2007.

INPRO, 2015. International Atomic Energy Agency International Project on Innovative Nuclear Reactors and Fuel Cycles (INPRO), [Online], Available from: <www.iaea.org/INPRO> (accessed 28.01.16.).

Japan Nuclear Fuel Limited, 2015. Japan Nuclear Fuel Limited, [Online], Available from: <http://www.jnfl.co.jp/english/> (accessed 28.01.16.).

Johnson, S., Lockwood, D., 2011. Safeguarding the plutonium fuel cycle. In: Proceedings of the ESARDA Workshop−Future Directions for Nuclear Safeguards and Verification, Aix-en-Provence, 16−20 October 2011.

Leaver, R., 2009. Nuclear Safeguards: Some Canadian Questions About Australiean Policy. Nautilus Institute, Australia [Online], Available from: <http://nautilus.org/wp-content/uploads/2012/01/Leaver.pdf> (accessed 28.01.16.).

Li, S., Zarucki, R., Pellechi, M., 2011.The emerging safeguards challenges of pyroprocessing technology. In: The proceedings of GLOBAL 2011, Makuhari, Japan, December 11−16, 2011, Paper No. 508867.

MacPherson, H.G., 1985. The molten salt reactor adventure. Nucl. Sci. Eng. 90 (4), 374−380.

McNeese, L.E. et al., 1974. Program plan for development of molten-salt breeder reactors. Report ORNL-5018, [Online], Available from: <http://www.iaea.org/inis/collection/NCLCollectionStore/_Public/06/188/6188059.pdf> (accessed 28.01.16.).

Merle-Lucotte, E., et al., 2007. Optimized transition from the reactors of second and third generation to the Thorium Molten Salt Reactor. In: Proceedings of ICAPP 2007.

Moir, R., 2010.U232 Nonproliferation Features, Vallecitos Molten Salt Research Report No. 2. LLNL-TR-438648.

Nackaerts, H., 2010. Available in the opening statements of the proceedings from the IAEA International Safeguards Symposium 2010−Preparing for Future Verification Challenges, Vienna, Austria.

ORNL, 2005. C.W. Coates et al. Radiation Effects on Personnel Performance Capability and a Summary of Dose Levels for Spent Research Reactor Fuels.

Uhlir, J., et al., 2007. Development of fluoride reprocessing technologies devoted to molten-salt reactor systems. In: Proceedings of GLOBAL 2007, Boise, USA, September 9−13, 2007.

Uhlir, J., 2014. MSR on-line reprocessing technology and nonproliferation aspects. Trans. Am. Nucl. Soc. 110, 409−411.

United Nations Security Council, 1997. Fourth Consolidated report of the Director General of the International Atomic Energy Agency under paragraph 16 of Security Council Resolution 1051 (1996) S/1997/779, [Online], Available from: <https://www.iaea.org/OurWork/SV/Invo/reports/s_1997_779.pdf> (accessed 28.01.16.).

Vanderhaegen, M., Janssens-Maenhout, G., 2010. Considerations on safety and proliferation-resistant aspects for the MSBR design. Nucl. Energy Des. 240 (3), 482−488.

Whitlock, J.J., Lee, A.G., 2009. CANDU: setting the standard for proliferation resistance of generation III and III+ reactors. In: Proceedings of the International Conference on Opportunities and Challenges for Water Cooled Reactors in the 21st Century, Vienna, Austria. IAEA-CN-164-5P07, [Online], Available from: <http://www-pub.iaea.org/MTCD/publications/PDF/P1500_CD_Web/htm/pdf/poster/5P07_J.%20Whitlock.pdf> (accessed 28.01.16.).

# Liquid fuel, thermal neutron spectrum reactors

# 11

*Ritsuo Yoshioka*[1] *and Motoyasu Kinoshita*[1,2]
[1]International Thorium Molten-Salt Forum, Yokohama, Japan, [2]The University of Tokyo, Tokyo, Japan

## Chapter Outline

**Molten Salt Reactors and Thorium Energy. DOI: http://dx.doi.org/10.1016/B978-0-08-101126-3.00011-7**

## 11.1 Development of molten salt reactor at ORNL

In this section, the development history of the molten salt reactor (MSR) at Oak Ridge National Laboratory (ORNL) is described. The starting point of MSR at ORNL and their various designs including the final one are explained sequentially.

### *11.1.1 Liquid fuel reactor, from water to molten salt*

At the end of World War II, after ORNL had provided atomic bomb technology, they started the discussion on future nuclear plants. Its history is described in the autobiography of Alvin Weinberg, who was a director of ORNL for 18 years from 1955 until 1973 and a development leader of MSR (Weinberg, 1994).

They discussed many ideas at "the New Pile Committee," which was composed of Enrico Fermi, Eugene Wigner (both Novel prize winners), Leo Szilard (coinventor of the reactor with Fermi), and many other scientists, such as Alvin Weinberg. One of the ideas was a fast breeder reactor (FBR) utilizing plutonium generation from $^{238}U$ by Fermi and Szilard, and another was a thermal breeder reactor utilizing $^{233}U$ generation from thorium by Wigner. Especially, Wigner provided a prospect that the reactor should be a "chemical engineering device" using liquid fuel because of its simplicity, and not a "mechanical engineering device" using solid fuel (Weinberg, 1997). Wigner and Weinberg had proposed a liquid fuel reactor in 1945, where aqueous heavy water is circulating with $^{233}U$-Th fuel (Wigner et al., 1945).

It is not well known that Alvin Weinberg was an inventor of the light-water reactor (LWR), but actually he submitted a paper on the LWR concept in 1946 (Weinberg, 1946), and later he issued several patent applications. Soon after, this concept was applied to nuclear submarines, and later to power-generating plants worldwide as pressurized water reactors (PWR).

Although Weinberg was an inventor of the LWR, he recognized the dangers of the LWR. Actually, he wrote a huge textbook on reactor theory in 1958 (Weinberg and Wigner, 1958), and he commented as follows: "When a fuel element is overheated (due to loss of cooling), it fails and the entire system is contaminated by radioactivity, and then repair becomes extremely difficult." This is exactly what happened at the Fukushima accident in 2011, where we were forced to see his prophecy become real 50 years later.

After Wigner left ORNL, Weinberg realized this concept as the Homogeneous Reactor Experiment (HRE) by using light water instead of heavy water, and it generated 150 KW electricity in 1953 (Rosenthal, 2009; Lane, 1958). As is described later, the most unique feature of the MSR is the circulating liquid fuel concept, and in this HRE development stage, ORNL established this concept, although it utilized water and not molten salt. The concept of the HRE and its core are shown in Figs. 11.1 and 11.2.

The principal advantages of aqueous fuel systems were considered as: (1) high power density; (2) high burnup fuel; (3) continuous fissile recovery; (4) simple fuel preparation and reprocessing; (5) continuous addition/removal of fuel; (6) high neutron economy; (7) simple control system; and (8) wide range of core size.

On the other hand, disadvantages of the aqueous fuel system would be: (1) corrosion/erosion of equipment; (2) radiation-induced corrosion; (3) external circulation of fuel solution; (4) nuclear safety; (5) limited uranium concentration; (6) limited operating temperature; and (7) explosive decomposition product (Lane, 1958).

In parallel with the HRE development, ORNL was investigating a nuclear application to aircraft jet engines, which was also a request by the US Air Force in 1948. At that time, an Intercontinental ballistic missile (ICBM) was not developed, and a long-time flying bomber aircraft was considered as necessary. Since they needed as high as 870°C temperature for jet engines, water could not be adopted as the coolant.

At first, R. Briant and his team studied a reactor concept using liquid sodium as coolant with solid fuel rods and moderator made of beryllium oxide, which had been proposed by General Electric for nuclear submarines. However, they considered that solid fuel rods would not retain their integrity at such severe heat condition, and abandoned this concept (Weinberg, 1994).

They soon reached a design concept of liquid fuel reactor using molten salt instead of water and solid fuel, because molten salt is chemically stable and inert, and especially it can be used at very low pressure owing to its very high boiling temperature. Since salt is a chemical compound of acid and alkali, there are thousands of molten salts. (In chemistry, molten salt is defined as an ionic liquid normally at high-temperature. Therefore, any compounds, which become positive ion

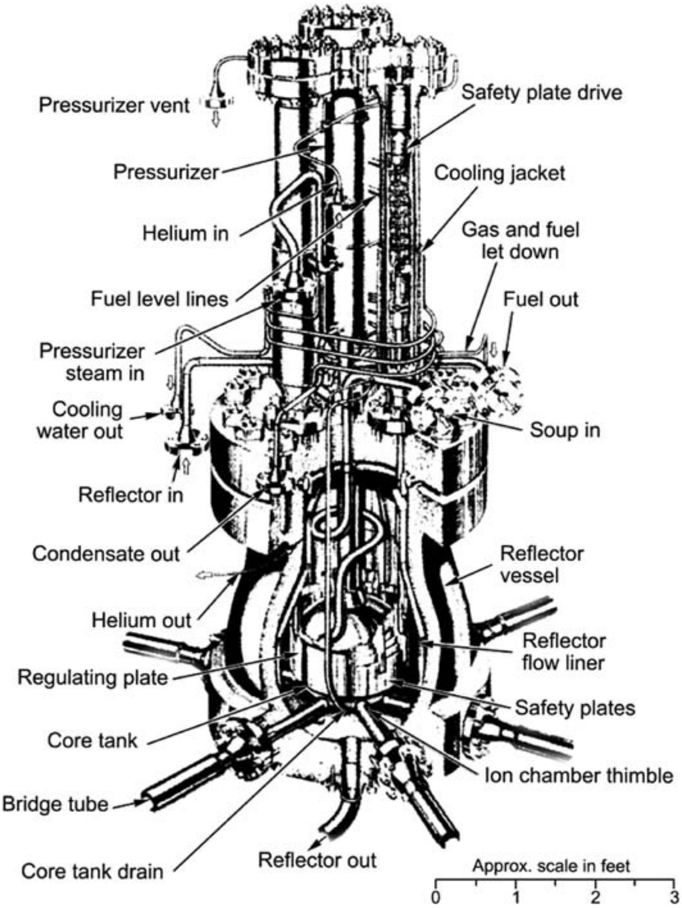

**Figure 11.1** HRE concept (Rosenthal, 2009).

and negative ion at melted condition, can be defined as molten salt. Actually, ORNL investigated sodium hydroxide (NaOH), which is a strong alkali, as a candidate for fuel salt (Weinberg, 1994). (One more remark in chemistry is melting and dissolving is different. For example, table salt (NaCl) becomes molten salt by heating without water. Dissolving NaCl is just putting it in water. That is, molten salt does not contain water, and it brings unique features.) They soon chose molten fluoride, owing to the suggestion by R. Briant and other chemists (Weinberg, 1994; Briant and Weinberg, 1957). After that, they found a nickel-based alloy that is corrosion-resistant in molten fluoride, which was later named Hastelloy N.

The MSR development history is well described in the summary paper by M. Rosenthal, who was a deputy director of ORNL in the 1970s (Rosenthal et al., 1970), besides Weinberg's biography (Weinberg, 1994), and H. MacPherson's paper (MacPherson, 1985).

**Figure 11.2** Core of HRE (Rosenthal, 2009).

The first MSR for aircraft engines, which was named the Aircraft Reactor Experiment (ARE), achieved criticality in 1954. Here, "criticality" means that the ARE attained continuous fission reactions. The ARE applied molten fuel salt of NaF-$ZrF_4$-$UF_4$ (53-41-6 in mol%), which was circulating within fuel tubes, as is shown in Fig. 11.3, and adopted a BeO (beryllium oxide) moderator as is shown in Fig. 11.4. The ARE achieved maximum temperature of 880°C and 2.5 MW thermal output during its 9 days' operation. Although the ARE never flew on an aircraft, it showed the MSR's capability to provide high heat to aircraft jet engines (Bettis et al., 1957; MacPherson, 1958).

As is shown in Fig. 11.3, the heat of fuel salt is cooled by helium gas at the heat exchangers (HXs). Meanwhile, the heat at BeO moderator is cooled by the molten sodium, and all systems including fuel tubes are made of Inconel. A somewhat strange design of fuel tubes has an interesting background. (The fuel tube of the ARE looks strange, like a crawling snake. Bettis explains its background in his paper (Bettis et al., 1957). The BeO moderator blocks have been already manufactured for the solid fuel ($UO_2$ in a tube) using molten sodium (Na) as a coolant. That is, a solid-fuel-pin, BeO-moderated, sodium-cooled reactor had been considered at first. But, this reactor concept was abandoned, and an alternative design of fuel tubes containing stagnant molten salt was considered. But again, this concept was abandoned, and finally, a circulating molten salt fuel tube design was adopted.)

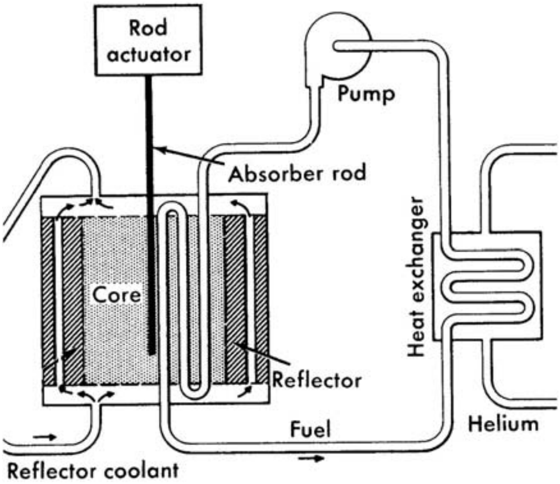

**Figure 11.3** Flow diagram of ARE (Bettis et al., 1957).

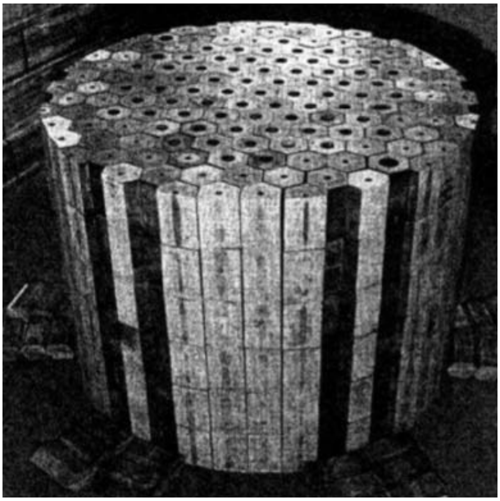

**Figure 11.4** BeO moderator of ARE (Bettis et al., 1957).

Besides its high heat capability, the ARE provided two other important achievements for the MSR. One was that it showed a sufficiently negative reactivity coefficient with temperature, and another was that most of the xenon (Xe) gas was removed from the molten salt. Since Xe is a neutron-absorbing material generated by nuclear fissions, this result showed an important advantage of the MSR.

In parallel with the ARE development, another MSR for aircraft engines was developed, which was named the Pratt and Whitney Aircraft Reactor (PWAR-1) (Scott et al., 1958). The PWAR-1 was a reflector-moderated reactor, and its core was composed of fuel salt within a Hastelloy X core shell surrounded by a cylindrical beryllium reflector as the moderator, as is shown in Figs. 11.5 and 11.6. Fuel salt is a ternary salt of NaF-ZrF$_4$-$^{235}$UF $_4$. The PWAR-1 was essentially a zero-power reactor, and its operating temperature was maintained at 677°C by external heaters. Therefore, its purpose was to acquire reactor physics data for the MSR concept, and a criticality experiment was performed in 1957.

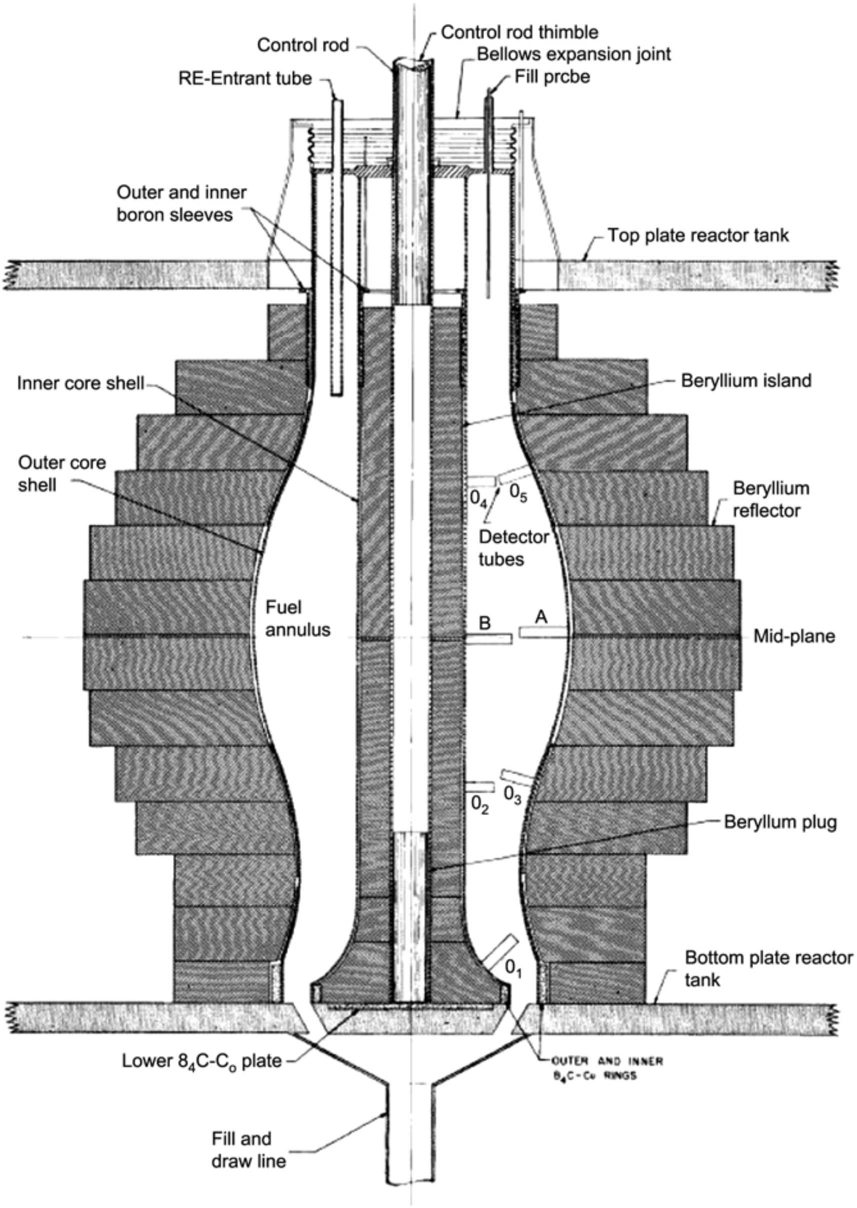

**Figure 11.5** Cross-section of PWAR-1 core (Scott et al., 1958).

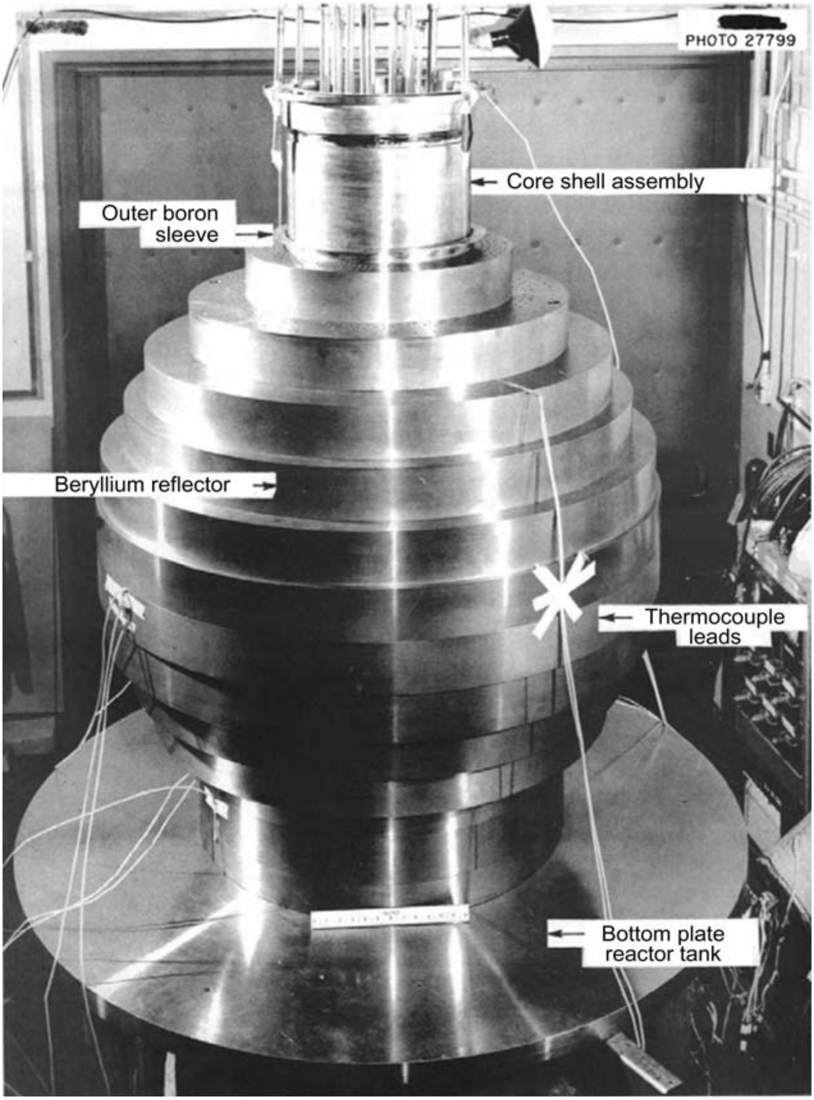

**Figure 11.6** PWAR-1 core shell (Scott et al., 1958).

Since this book is focusing on MSRs, nonMSRs for jet engines, such as Heat Transfer Reactor Experiments (HTRE) in the 1950s designed by General Electric, are not described here. The history of the Aircraft Nuclear Propulsion (ANP) program can be found elsewhere.

At the same time as the PWAR-1 construction, a successive program called the Aircraft Reactor Test (ART) was started in 1955 at ORNL (Cottrell et al., 1955; Fraas et al., 1956). The ART was designed to provide 60 MWt heat, which would be enough for actual aircraft engines. The ART applies the BeO reflector-moderated design similar to the PWAR-1, in order to protect the aircraft crew from its radiation, as shown in Fig. 11.7. One more innovative point is that it adopts in-vessel molten salt pumps and HXs, and HX is cooled by the molten NaK. Although almost all other MSR designs in ORNL adopted out-vessel pumps and HX, the ART could accommodate pumps and HX owing to its small reactor size. The ART was principally design

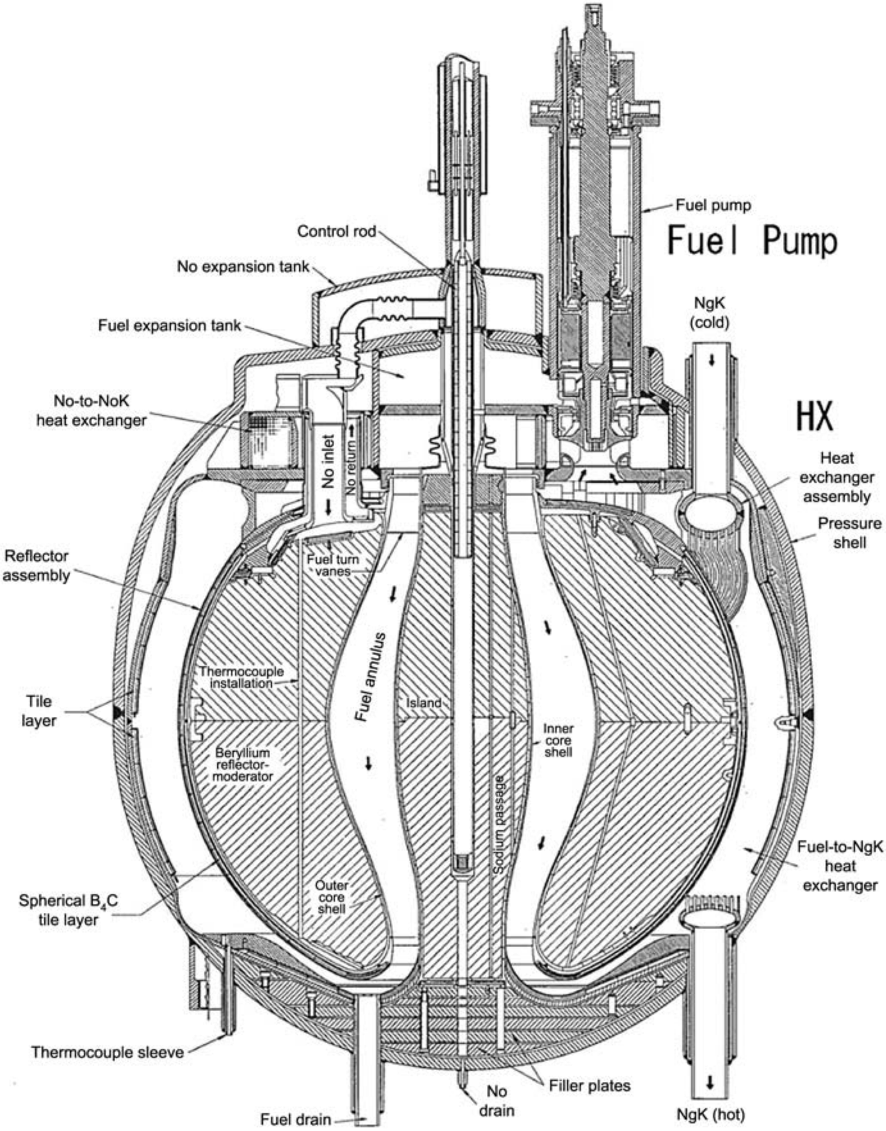

**Figure 11.7** Cross-section of ART core (Cottrell et al., 1955).

work, and was not actually constructed. However, some mockups and components were manufactured, as shown in Fig. 11.8. And some building modifications were made which were later adopted and remodified for the MSRE.

After the success of the ARE, the PWAR-1, and the ART, design of an experimental MSR for land-based power plants was started in 1960, and it was constructed as the Molten Salt Reactor Experiment (MSRE), as is shown in Figs. 11.9 and 11.10. The MSRE showed extremely successful operation from 1965–69 at ORNL. Its success is summarized in a 1970 paper (Haubenreich and Engel, 1970). The MSRE had a single region core with a graphite moderator as shown in Fig. 11.8, and an Hastelloy N vessel and pipes. They achieved 8 MW thermal output with molten fuel salt of $^7$LiF-BeF$_2$-ZrF$_4$-UF$_4$ or $^7$LiF-BeF$_2$-ZrF$_4$-PuF$_3$ at 650°C. Here, natural lithium (Li) was enriched to $^7$Li, in order to reduce neutron absorption by $^6$Li.

The reason why the MSRE did not contain thorium fluoride (ThF$_4$) is explained as follows (Haubenreich and Engel, 1970). Since a commercial-type MSR was expected to be a two-fluid breeder design, that is a fuel region containing fissile material and a surrounding or interlaced blanket region containing thorium, they designed the MSRE in order to simulate this fissile fuel salt region. The history or reason for selecting a two-fluid design is described in Section 11.1.4.

As is shown in Fig. 11.11, fuel salt is circulated by the molten salt pump, and its heat is removed to the secondary salt through the HX. And finally, its heat is released to the air, using radiators.

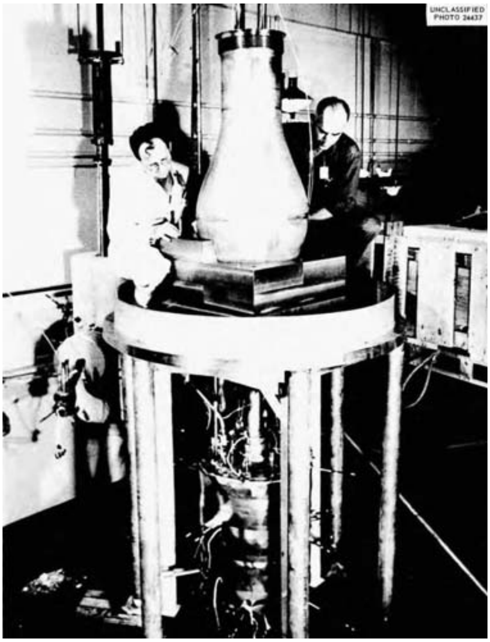

**Figure 11.8** ART mockup (Fraas et al., 1956).

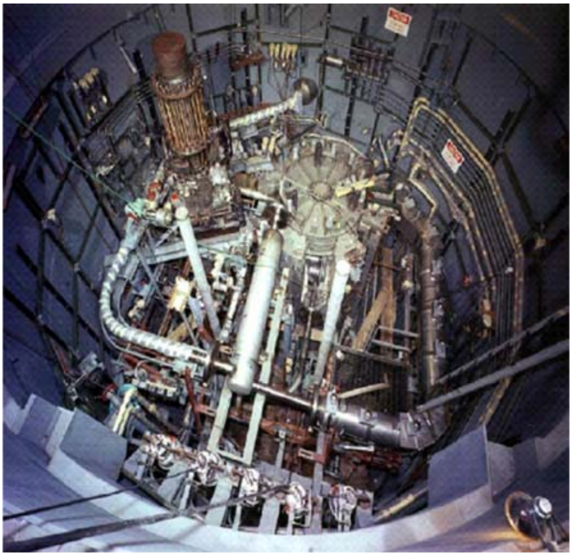

**Figure 11.9** MSRE upper zone (Rosenthal, 2009).

**Figure 11.10** MSRE graphite core (Rosenthal, 2009).

The purpose of the MSRE was to demonstrate key features of a molten salt power reactor, although a steam-generator (SG) and a turbine/generator were not provided. They achieved many unique features, such as stability of fuel salt, integrity for Hastelloy N and graphite, and removing capability of gaseous radioactive fission product (FP) such as xenon and krypton from fuel salt. One more unique

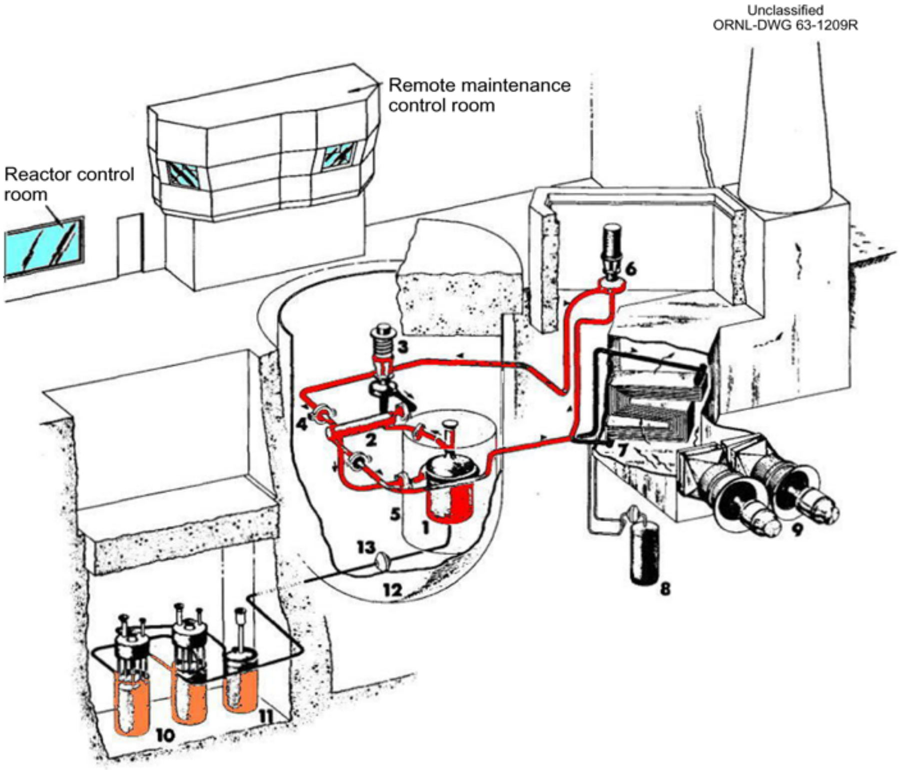

**Figure 11.11** MSRE flow diagram (Rosenthal, 2009). (1) Reactor vessel, (2) heat exchanger, (3) fuel pump, (4) freeze flange, (5) thermal shield, (6) coolant pump, (7) radiator, (8) coolant drain tank, (9) fans, (10) fuel drain tanks, (11) flush tank, (12) containment vessel, (13) freeze valve.

achievement was operation by $^{233}$U. Fig. 11.12 shows a snapshot of the day of its first operation by $^{233}$U at the MSRE control room.

### 11.1.2 Selection of thermal neutron spectrum

From the very beginning of reactor development, it was known that a fission reaction is easier to achieve with thermal neutrons than fast neutrons. As is shown in Fig. 11.13, fission cross-sections of $^{233}$U/$^{235}$U/$^{239}$Pu are almost 100 times higher for thermal neutrons. This fact means that a thermal spectrum reactor requires less fissile material, which was not abundant at that time.

Since fission neutrons are fast neutrons, the moderator is required in order to slow down these fast neutrons. Fortunately, there are good moderator materials, such as water (either light water or heavy water), graphite, and beryllium, which are naturally abundant, except heavy water.

**Figure 11.12** MSRE began operation with $^{233}$U in 1968. (Left to right: A. Weinberg [standing], A. Krakoviak, R. Stoughton, G. Seaborg [pointing, Chairman of US-AEC, Nobel prize winner who discovered $^{233}$U], and J. Engel.) (Weinberg, 1994; Rosenthal, 2009).

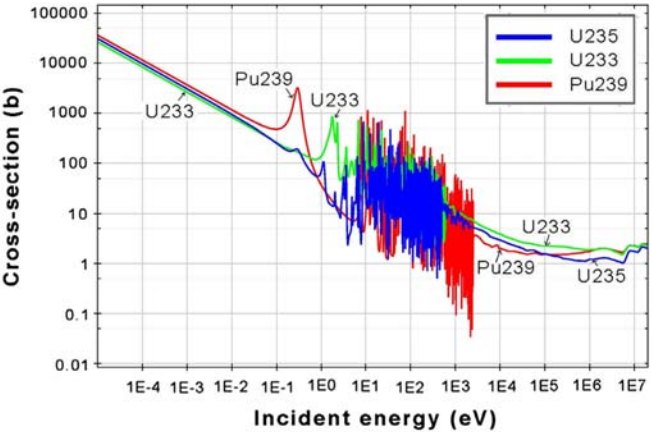

**Figure 11.13** Fission cross-sections of $^{233}$U/$^{235}$U/$^{235}$Pu (van Rooijen, 2015).

Therefore, it was natural that they adopted a thermal spectrum reactor as a faster and easier one in order to start the nuclear power plant age.

As is described at first, the development of nuclear power plants was based on the assumption in the late 1940s that uranium was scarce on the globe and breeding was one of the highest-priority targets. Actually, this was one of the strong incentives to propose the thorium cycle, because thorium is 3—4 times more abundant than uranium.

Here, a certain reactor physics parameter is explained, which is called the reproduction factor "$\eta$." This parameter $\eta$ is defined as the number of neutrons produced per neutron absorbed in the fissile nuclide. Then, breeding is possible only if $\eta$ is larger than 2.0. As is shown in Fig. 11.14, when $^{233}$U causes a fission, it produces two or more neutrons. One neutron is required for the continuous chain reaction. Another neutron can be absorbed by the fertile nuclide such as $^{232}$Th, which decays to $^{233}$U. (Actual decay chains for both Th cycle and U/Pu cycle are shown in Section 11.1.4.) Therefore, if $\eta$ is larger than 2.0, then more $^{233}$U is produced than consumed $^{233}$U, that is, breeding becomes possible. But, exactly speaking, some neutrons are absorbed by core internal materials, and also lost to the outside of the reactor. Therefore, $\eta$ must be a little bit larger than 2.0 for actual breeding.

Energy dependence of $\eta$ for $^{233}$U/$^{235}$U/$^{239}$Pu is shown in Fig. 11.15. It is shown that in general $\eta$ is higher at a fast neutron energy, and especially $\eta$ of $^{239}$Pu is the highest of all. One more finding in this figure is that $\eta$ of $^{233}$U is as high for thermal neutrons as fast neutrons. And this suggests that breeding is possible for $^{233}$U-Th MSR with thermal neutron spectrum.

## 11.1.3 Molten salt fast-spectrum reactor (MSFR)

The molten salt fast-spectrum reactor (MSFR) is described in Chapter 12, Fast spectrum, liquid fueled reactors but a brief summary of the MSFR study in ORNL is given here (Bulmer et al., 1956; Alexander, 1963).

In the mid-1950s, a fast-spectrum breeding MSR producing 700 MW of heat was designed, utilizing plutonium as the fissile fuel in a mixture of chloride salt, that is $MgCl_2$-NaCl-[$^{239}PuCl_3$-$^{238}UCl_3$] (33-50-17 in mol%) circulating the core region. The reason for selection of chloride is because it has considerably less moderating power than fluoride, and then a higher breeding performance would be achieved.

One more feature in this MSFR is that chlorine (Cl) is enriched to nearly pure $^{37}$Cl. There are two nuclides in natural chlorine, that is $^{35}$Cl (76%) and $^{37}$Cl (24%).

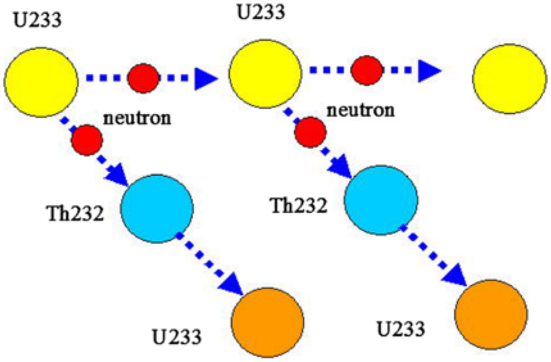

**Figure 11.14** Breeding scheme for $^{233}$U/Th cycle.

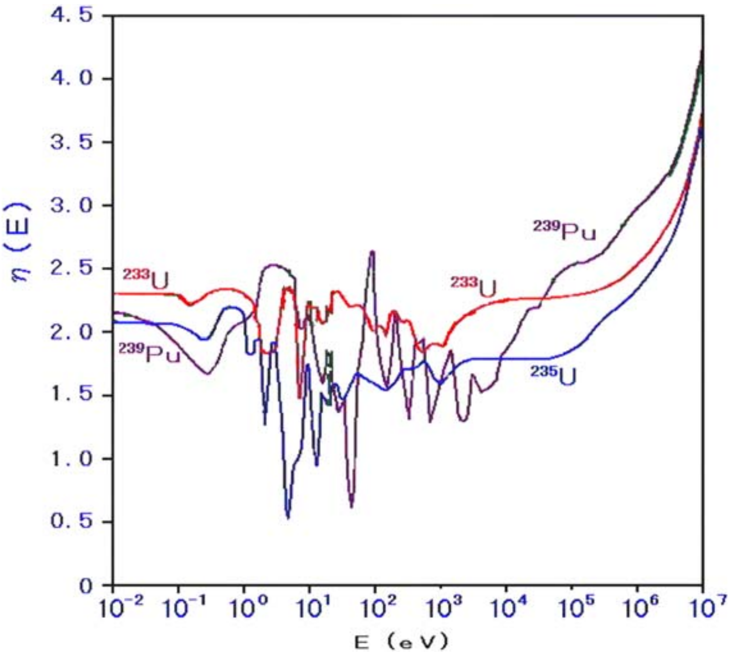

**Figure 11.15** Reproduction factor ($\eta$) for $^{233}$U/$^{235}$U/$^{239}$Pu (Duderstadt and Hamilton, 1967). Reproduction factor ($\eta$) is defined as follows; $\eta = (\nu\sigma f)/\sigma a$. Therefore, $\eta$ can be calculated using open data of cross-sections, for example; http://www.oecd-nea.org/janis/.

Since $^{35}$Cl has a 10 times larger absorption cross-section than $^{37}$Cl, if natural chlorine is used, breeding performance becomes worse. Of course, if breeding performance for Pu-fueled MSFR is high enough, this might be acceptable. But, besides this issue, ORNL people had a concern that the generated $^{36}$Cl has a very long half-life of 0.3 million years with a high-energy beta-ray emission. In order to avoid a future radioactive waste issue, they proposed to use enriched $^{37}$Cl, instead of natural chlorine. Regardless of chlorine enrichment, a small amount of residual $^{35}$Cl and a very small cross-section for ($n$,2$n$) reaction in $^{37}$Cl would generate $^{36}$Cl (Okumura, 2013). (The ($n$,$\gamma$) cross-section of $^{35}$Cl is 10.4 mb (milli-barn), and 5.9 mb for ($n$,$p$) reaction in a typical FBR core. On the other hand, ($n$,$\gamma$) cross-section of $^{37}$Cl is 1.7 mb, and thus, chlorine enrichment to $^{37}$Cl improves neutron economy. Of course, 100% enrichment is impossible, and residual $^{35}$Cl generates radioactive $^{36}$Cl by neutron capture reaction. Meanwhile, $^{37}$Cl has a very small cross-section of 0.01 mb for ($n$,2$n$) reaction, and some radioactive $^{36}$Cl would be generated, based on ORIGEN2 FBR library. But, recent nuclear libraries (http://www.oecd-nea.org/janis/) do not provide cross-section of ($n$,2$n$) reaction in $^{37}$Cl, and this path must be confirmed in the future.)

In this MSFR concept, the fertile material in a blanket is $UO_2$ powder in sodium paste, as is shown in Fig. 11.16. That is, this concept was intended to apply a U-Pu cycle, the same as FBR. After this study, there were some other studies on MSFR,

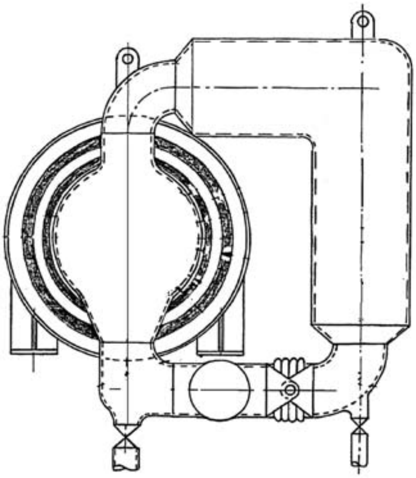

**Figure 11.16** Molten salt fast reactor (MSFR) concept (Bulmer et al., 1956).

but ORNL's main focus was thermal-spectrum MSR. More recently, several fast-spectrum MSR concepts are being proposed for actinide burners using fluoride salt as a part of the Generation-IV program (Serp et al., 2014), and they are described in Chapter 12, Fast spectrum, liquid fueled reactors.

### 11.1.4 Two-fluid MSR

As was explained at first, breeding was one of the highest-priority goals for the MSR, and they proposed a two-fluid design at the end of the 1950s (Alexander et al., 1959). Although MSFR could achieve higher breeding performance, ORNL's main focus was thermal-spectrum MSR, which could be realized earlier.

As is shown in Fig. 11.17, its core region contains fissile material such as $^{233}$U for power generation. Meanwhile, a surrounding blanket region contains thorium, which is converted to fissile $^{233}$U by neutron absorption. This concept is similar to an FBR concept, but the MSR is a liquid fuel reactor, and core region salt and blanket region salt are each circulated by molten salt pumps.

There were two other reasons to adopt a two-fluid concept for the MSR:

1. The online reprocessing was also proposed in order to increase breeding capability for the MSR. But, at that time, it was considered that removing FP from thorium-containing salt would be difficult. Therefore, it was convenient that a core region did not contain thorium.
2. Thorium is converted to $^{233}$U through protactinium (Pa) by the following neutron absorption reaction:
   $^{232}$Th($n$,$\gamma$) →$^{233}$Th(decay with 22.3 minutes half-life) →$^{233}$Pa(decay with 27.0 day half-life) →$^{233}$U.

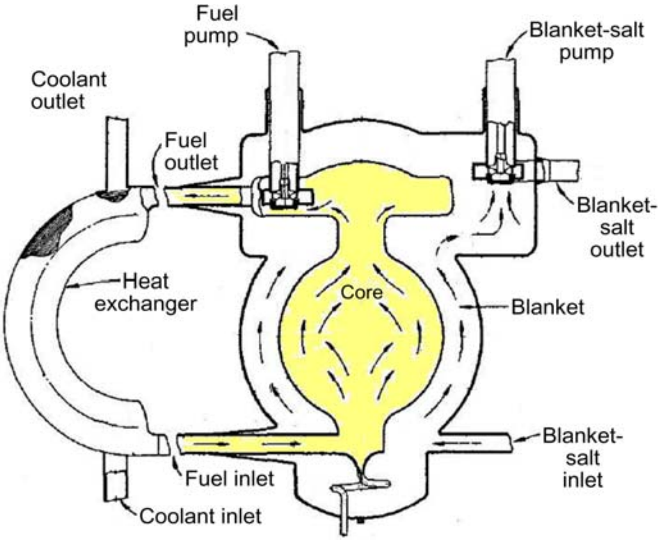

**Figure 11.17** Two-fluid MSR concept (Alexander et al., 1959).

Since the decay of $^{233}$Th is rapid, the number $N_{pa}$ of $^{233}$Pa atoms varies approximately as:

$$dN_{pa}/dt \approx N_{th}\,\sigma_{th}\,\phi - N_{pa}\,\sigma_{pa}\,\phi - \lambda_{pa}\,N_{pa}$$

where $\sigma_{th}$ and $\sigma_{pa}$ are the neutron absorption cross-sections in thorium and protactinium, resectively, $\phi$ is the neutron flux, and $\lambda_{pa}$ is the protactinium decay constant. If $^{233}$Pa absorbs a neutron before it decays to $^{233}$U, breeding performance becomes worse.

In a two-fluid design as shown in Fig. 11.17, its blanket is large and the neutron flux there is low. Thus, neutron absorption to $^{233}$Pa can be minimized, and rapid processing to remove Pa and allow it to decay to $^{233}$U is not required (LeBlanc, 2010).

If we breed $^{239}$Pu from $^{238}$U, the reaction chain is:

$^{238}$U($n$,$\gamma$)→$^{239}$U(decay with 23.4 minutes half-life) →$^{239}$Np(decay with 2.36 day half-life) →$^{239}$Pu.

Since the half-life of $^{239}$Np is short, it can be assumed that $^{238}$U goes to $^{239}$Pu directly, in contrast to the slow decay of $^{233}$Pa to $^{233}$U.

The breeding ratio (BR) is the number of fissile atoms generated per fissile atom consumed.

The doubling time, $t_2$, is the time required to produce enough new fissile material to start another reactor, given by

$$t_2 = N_o W/P(\mathrm{BR} - 1)$$

where $N_o$ is the initial numer of fissile atoms, W is the energy released per fission ($3.2 \times 10^{-11}$ J), and $P$ is the reactor thermal power (Watts). For example, if $N_o = 2.6 \times 10^{27}$ atoms (1000 kg fissile material), BR = 1.2, and $P = 1\ \mathrm{GW_{th}}$, then $t_2 = 4.2 \times 10^8$ seconds = 13 years.

For one case the BR was evaluated as 1.07 with Pa removal (online processing), and BR without Pa removal was 1.05 (Briggs, 1967). For this case the doubling time was 17 years with Pa removal and 26 years without Pa removal. This difference was important for the designers at that time, because their target was to achieve better performance than that of the FBR.

As is explained in Fig. 11.14, at least 50% of the neutrons must be leaked from the core region and absorbed in the blanket region, in order to achieve breeding for a two-fluid MSR.

In the FBR a mean free path (average flight length) of a fast neutron is long, because it has a high speed, and the absorption cross-section is small. The concentration of fissile material is high in the core region, and neutrons cannot be fully absorbed by the fertile material there, so a fertile blanket is desirable.

In contrast to the FBR, the MSR core neutrons have shorter mean free paths, because it is a thermal neutron spectrum reactor with high absorption cross-sections. Therefore, in order to achieve high leakage ($\geq$50%) of neutrons from the core, its size must be small enough. For example, in a graphite-moderated MSR, 50% leakage will be expected only if the radius of the core sphere is smaller than 60 cm. (Based on the one-group reactor theory, leakage fraction (LF) is defined as $1/(1 + M^2B^2)$. Here, migration length ($M$, which is an index similar to a mean free path) is assumed as 20 cm in a graphite-moderated core, and $B^2$ is defined as $(\pi/R)^2$ for sphere geometry. If $R = 60$ cm, then LF = 0.5, that is, 50% leakage will be expected from core region to blanket region.) This size is too small for a large power reactor, and therefore, a spherical design concept shown in Fig. 11.17 is impractical for a large power reactor with a thermal spectrum.

Based on this consideration, ORNL proposed an alternative two-fluid MSR in the late 1960s, which applied an interlaced blanket concept. This is a very unique concept, as is shown in Fig. 11.18 (Robertson, 1970). Since the mean free path of neutrons in thermal spectrum MSR is small, it is necessary to design the blanket region as close as possible to the core region. This interlaced blanket concept would use graphite tubes, which are used to circulate fuel salt, within the blanket salt tank.

The reason why they selected graphite tubes is explained as follows. At that time, the most promising metal for high-temperature use in molten salt was a nickel-based alloy, and then Hastelloy N was developed in ORNL and used in the MSRE. But, nickel causes helium embrittlement due to $(n, \alpha)$ reactions at high neutron fluence. That is, Hastelloy N could not be used as fuel tubes, which would suffer high neutron irradiation. Also, nuclides in nickel-based alloy absorb neutrons, and breeding performance becomes worse. Because of these facts, graphite was selected for the fuel tubes.

This interlaced design was possible on a drawing, but actual manufacturing, maintenance, and irradiation integrity of hundreds of graphite tubes were considered impractical, so this interlaced design was abandoned.

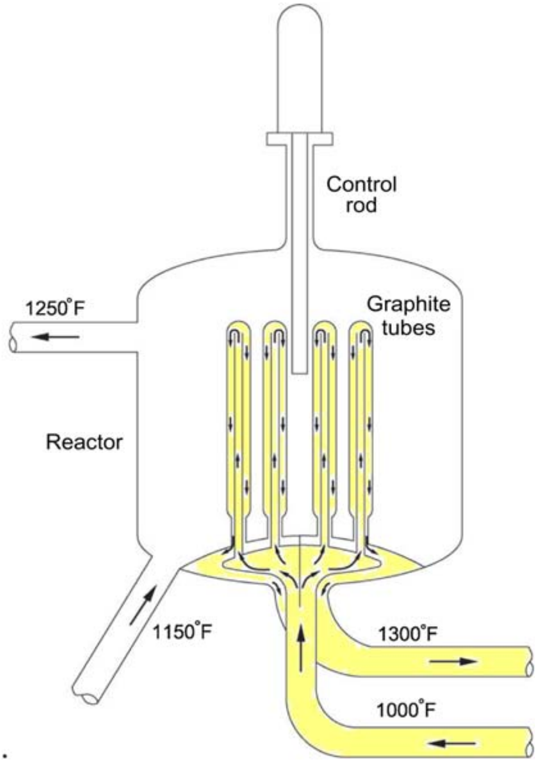

**Figure 11.18** Two-fluid MSR with interlaced blanket (LeBlanc, 2010; Robertson, 1970).

### 11.1.5 MSBR, large-sized single-fluid molten salt breeder reactor

Based on the above 20 years' study, ORNL finally switched from two-fluid MSR to single-fluid MSR, and proposed a single-fluid design for a large-sized power plant as the molten salt breeder reactor (MSBR), and issued a conceptual design report in 1971 (Robertson, 1971), although the MSBR was not constructed.

As was explained above, there were two assumptions leading to a two-fluid MSR, especially for a graphite-moderated MSR. (1) Online reprocessing is impractical with thorium fluoride, so a core region should not contain thorium. (2) Neutron leakage from a core region must be collected by blanket. But, these assumptions were changed as follows:

1. Chemical processing technology was greatly improved, which is a liquid–liquid reductive extraction process for removing Pa and U from molten fluoride salts. This technique is to exchange Th and Li dissolved in molten bismuth for the constituents to be removed from the salt. Thus, a single-fluid MSR becomes feasible with thorium-containing salt; $^7$LiF-BeF$_2$-UF$_4$-ThF$_4$. The base binary salt (LiF-BeF$_2$) is called FLiBe.

   Online chemical processing recovers U and Pa from the fuel salt and removes FPs, as is shown in Fig. 11.19 (Rosenthal et al., 1970; Grimes, 1967).

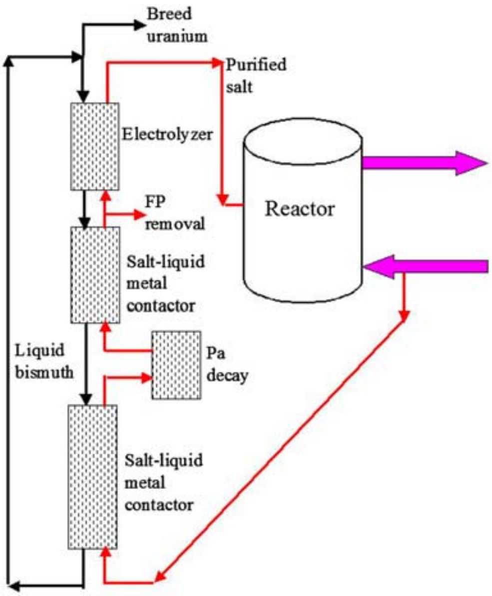

**Figure 11.19** Online chemical processing plant in MSBR (Rosenthal et al., 1970).

2. The core design was greatly improved by allocating a kind of blanket region at the outer part of the core, both using the same fuel salt, as is shown in Fig. 11.20. In this concept, the inner core region has a smaller volume fraction (13%) of fuel salt and a larger volume fraction (87%) of graphite moderator, which enhances neutron moderation and increases the reactivity. Meanwhile the outer region has a larger volume fraction (37%) of fuel salt, and a smaller volume fraction (63%) of graphite, which enhances more conversion from Th to $^{233}$U. Although lower neutron moderation decreases reactivity in the periphery, it reduces neutron leakage from the core and improves breeding performance (Rosenthal et al., 1970). Then, this concept is called a single-fluid two-region MSBR, or just the MSBR hereafter.

The effect of changing fuel salt volume fraction is as follows. Using the same nuclear design code as explained in the next Section 11.2, and assuming the unit cell model, K-infinity is calculated for different radii of fuel salt path, by the present authors. The core 13% fuel salt volume fraction corresponds to 3.5 cm radius, and 37% fraction to 6.0 cm radius. Fig. 11.21 shows that higher fuel salt volume fraction decreases K-infinity or reactivity.

The effect of changing fuel salt volume fraction on neutron spectrum is shown in Fig. 11.22. The inner core of the MSBR has a high peak at thermal neutron energy, and the outer core has a small peak there. As is explained in Section 11.2, MSR-FUJI has a 36% fuel salt volume fraction in average, and its neutron spectrum is close to the outer core of the MSBR.

The MSBR was designed to produce a large electric output of 1000 MWe, and its major design parameters are shown in Table 11.1.

The MSBR flow diagram is shown in Fig. 11.23, although a freeze valve and a drain tank are not shown. The reactor vessel, pipes, and pumps are made of Hastelloy

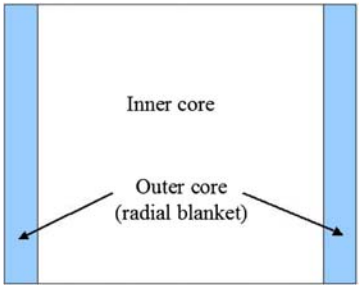

**Figure 11.20** Vertical cross-section of MSBR core.

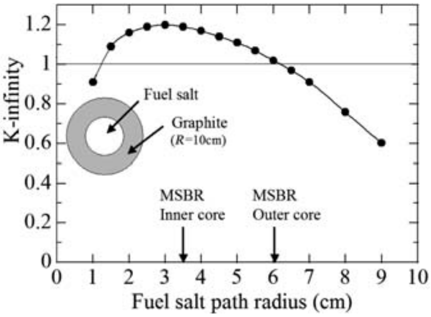

**Figure 11.21** K-infinity versus fuel salt path radius (graphite radius = 10 cm).

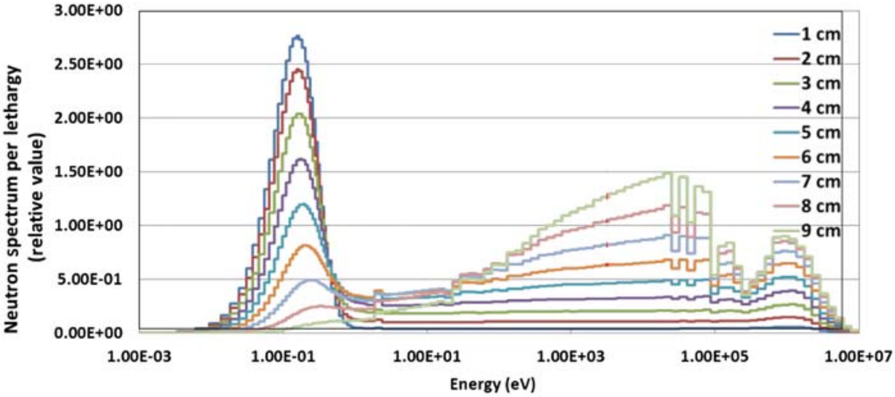

**Figure 11.22** Neutron spectrum for different fuel salt path radius (graphite radius = 10 cm).

**Table 11.1** Design parameters of MSBR (Robertson, 1971)

| | |
|---|---|
| Electric output | 1000 MWe |
| Thermal output | 2250 MWt |
| Thermal efficiency | 44.4% |
| Reactor vessel, diameter/height | 6.8 m/6.1 m |
| Inner core, radius/height | 2.2 m/4.0 m |
| Fuel volume fraction | 13 vol% |
| Outer core, radius/height | 2.6 m/4.0 m |
| Fuel volume fraction | 37 vol% |
| Reflector thickness (radial) | 0.8 m |
| Breeding ratio | 1.06 |
| Doubling time (80% load factor) | 22 years |
| Power density (within core) | 22 $MW/m^3$ |
| Fuel salt composition (mol%) | $^7LiF-BeF_2-ThF_4-UF_4$<br>71.7-16-12-0.3 |
| Fuel salt volume (in reactor vessel) | 30.4 $m^3$ |
| Fuel salt volume (in primary loop) | 48.7 $m^3$ |
| $^{233}U$ weight (in primary loop) | 1.50 t |
| Th weight (in primary loop) | 68.1 t |
| Graphite weight (in reactor vessel) | 304 t |

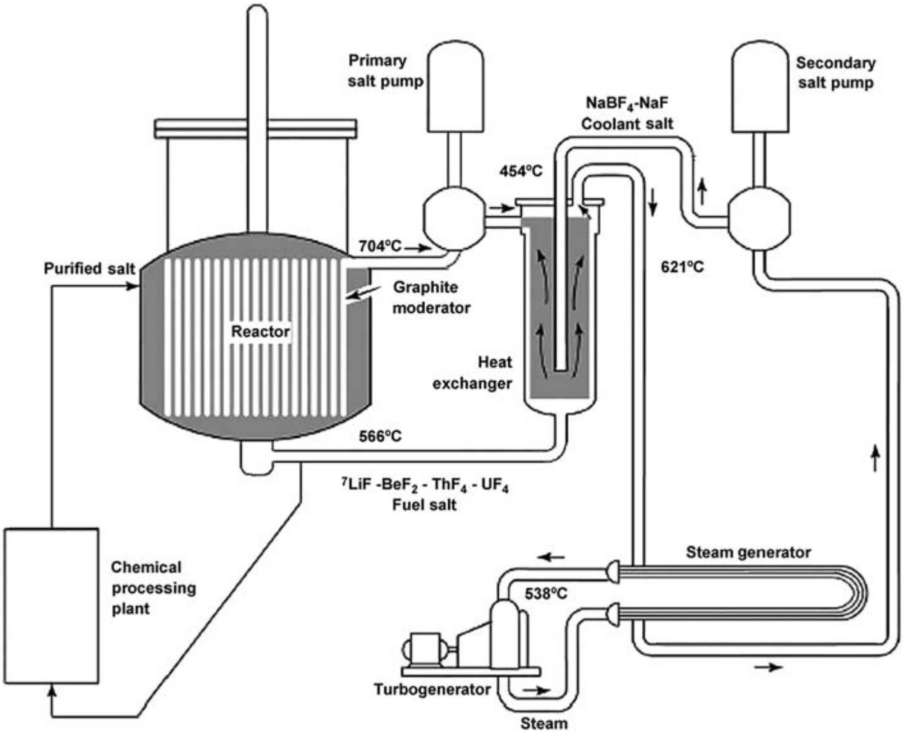

**Figure 11.23** Flow diagram of single-fluid two-region MSBR (Rosenthal et al., 1970; LeBlanc, 2010).

N. There is a graphite moderator within a reactor vessel. Fuel salt flows upwards from a primary pump and then goes to HXs to transfer the heat to secondary coolant salt. The heat of secondary salt is transferred to the steam through a supercritical steam generator. Although this figure shows only one loop, the actual MSBR design had four loops. Then, its steam goes to a turbine/generator to produce electricity. Due to a limitation of irradiation growth, the graphite moderator is replaced every 4 years. Fuel salt is $^7$LiF-BeF$_2$-ThF$_4$-UF$_4$, and secondary salt is NaBF$_4$-NaF.

The sectional elevation of the reactor vessel is shown in Fig. 11.24. Its core is composed of graphite moderator rods and surrounding graphite reflectors. The MSBR applies a single-fluid design, but its core has two regions as described before.

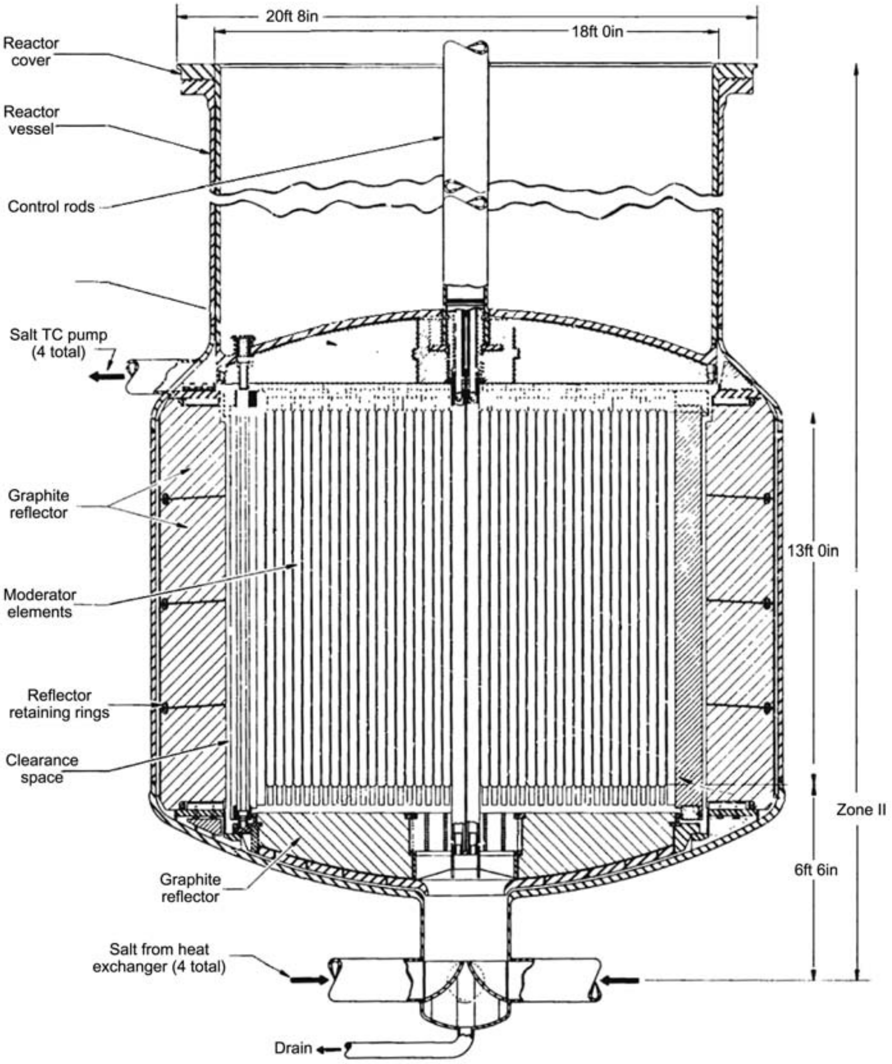

**Figure 11.24** Vertical cross-section of MSBR reactor vessel (Robertson, 1971).

Fuel salt enters from the bottom and flows upward within the flow path in graphite rods. The original design of a graphite rod by ORNL is square-shaped, as is shown in Fig. 11.25. In order to calculate the accurate temperature coefficient, this unique shape has to be considered. (As is shown in Fig. 11.19, fuel salt flows both in the center round path and the peripheral rectangular path, which is a groove of the graphite rod. In order to calculate an accurate Doppler coefficient and a temperature coefficient, this layout has to be considered, because these coefficients depend strongly on resonance absorption, which occurs mostly at the surface of the fuel path. This is called a surface effect as Weinberg described in his textbook (p. 683 of Weinberg and Wigner, 1958)).

Radial power distribution is shown in Fig. 11.26, which is a result of the two-region design.

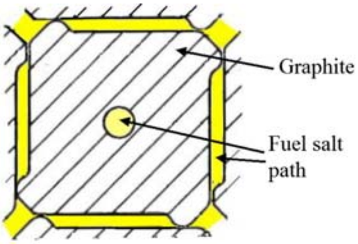

Figure 11.25 MSBR graphite rod (Robertson, 1971).

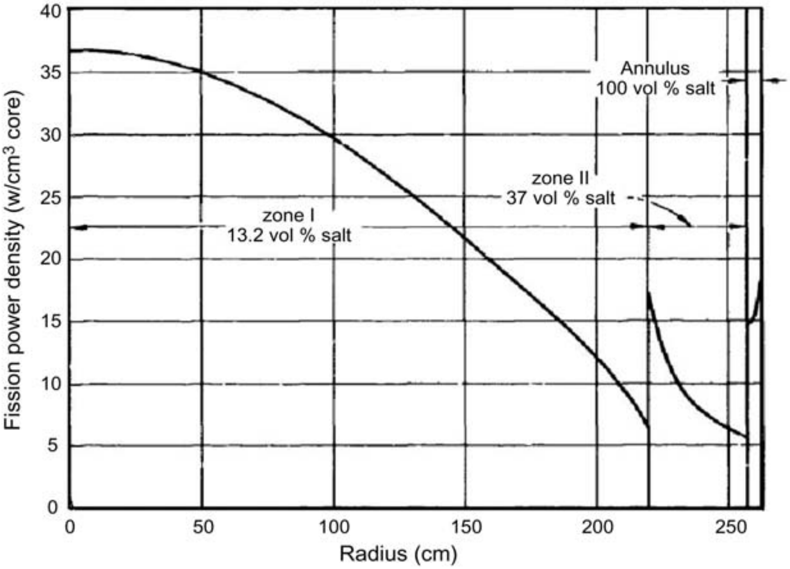

Figure 11.26 MSBR radial power distribution (Robertson, 1971).

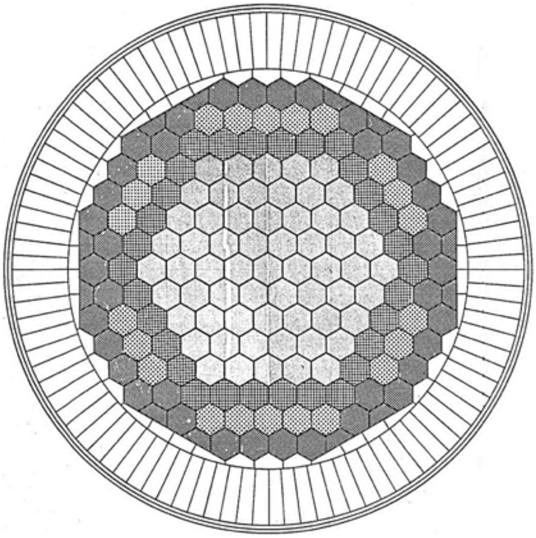

**Figure 11.27** Horizontal layout of Ebasco-MSBR (EBASCO Services Inc., 1972).

After the conceptual design for the MSBR at ORNL, another study was headed by Ebasco Services, Inc. with utilities, and they issued a long report in 1972 (EBASCO Services Inc., 1972). They adopted a hexagonal graphite assembly as a moderator. Each assembly is composed of multiple graphite slabs, and its horizontal core layout is shown in Fig. 11.27.

### *11.1.6 Denatured molten salt reactor (DMSR)*

After ORNL issued the MSBR design report, all essential works were terminated, except the study on denatured molten salt reactor (DMSR) in the late 1970s (Engel et al., 1980).

In 1977, when President Jimmy Carter started his administration, he issued a National Energy Program, which deferred the commercial reprocessing of spent fuels indefinitely, and deferred the Clinch River FBR project indefinitely. This policy change was based on the nuclear explosion test by India in 1974, where reprocessed plutonium from spent fuels was used.

The Program also said that the breeder program would redirect efforts toward evaluation of alternate breeders, fuels, and advanced converter reactors with an emphasis on nonproliferation and safety concerns. Since the MSBR was considered to have proliferation resistance, ORNL investigated the possibility to enhance it more. Thus, the DMSR study was started.

The DMSR is based on the plant design of the MSBR, but there are several modifications as follows, in order to achieve a “30 Year Once Through” reactor.

One big difference from MSBR is to start from low-enriched uranium (LEU) with thorium. Here, LEU means less than 20% $^{235}$U enriched uranium. (LEU is defined as uranium which contains less than 20% $^{235}U$. As for uranium containing $^{233}U$ (LEU-233), it is proposed to be defined as uranium less than the weighted average of 20% $^{235}U$ and/or 12% $^{233}U$. See the details in Forsberg (1998).) And, $^{233}U$ which is generated from thorium is diluted with $^{238}U$, that is *denatured*.

A second difference is to *reduce* the function of online reprocessing, that is, to limit its function only to remove gaseous FP and noble metals.

A third difference is to confine all fuel salt within the reactor containment for the *30-year* operation period to allow the accumulation of all other FPs.

Each of these design changes *decreases breeding* performance, and annual addition of LEU is required. Thus, DMSR is not a breeder reactor, but a converter reactor.

A fourth improvement is to allow 30-year usage of a *graphite* moderator, while the MSBR was designed to replace the graphite moderator every 4 years. This improvement is owing to the lower power density and the flattened neutron flux distribution, as is shown in Fig. 11.28.

Of course, this lower power density needs a larger reactor vessel, which is almost four times larger volume than the MSBR, and then, the reactor containment and reactor building (RB) would become larger.

The fuel salt is $^7LiF\text{-}BeF_2\text{-}AcF_4$ (74.0-16.5-9.5 in mol%, $Ac = U + Th$), and 1000 MWe DMSR would start from 17 tons of LEU (20% $^{235}U$, that is 3.5 tons of $^{235}U$) along with 110 tons of thorium. Annual makeup fissile material is LEU, and uranium always remains in the denatured state.

Its chemical processing system is very much simplified for removal only of gaseous FPs and noble metals. Therefore, most other FPs stay in fuel salt for the

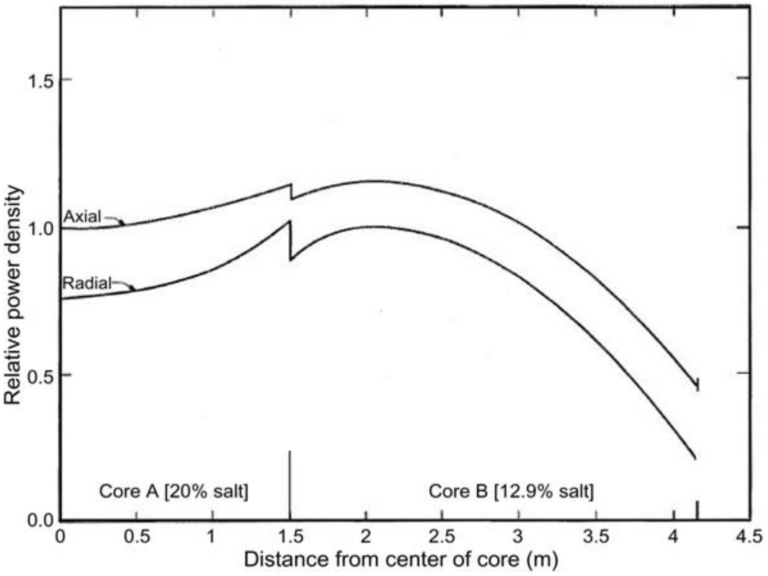

**Figure 11.28** DMSR radial/axial power distribution (Engel et al., 1980).

30-year operation period. Also, no fuel reprocessing means no removal and hold up of $^{233}$Pa, which was proposed for the MSBR design. But its penalty is small enough to achieve satisfactory converter performance, because of its lower neutron flux.

One concern may be the production of plutonium (Pu) from $^{238}$U. The total amount of Pu at the end of operation is 0.7 tons, but its fissile fraction is 45%, and the rest (55%) is $^{238}$Pu, $^{240}$Pu, and $^{242}$Pu, any of which emits many neutrons by spontaneous fissions. This result would contribute to proliferation resistance, because of difficult manufacturing and easy detection of nuclear weapons.

### 11.1.7 Termination of MSR development at ORNL

Regardless of the above significant achievements, the development plan of the MSR was canceled in the 1970s. As for the reasons, Alvin Weinberg later described in his biography (Weinberg, 1994), and also his deputy director H. MacPherson explained (MacPherson, 1985).

1. The LWR and U-Pu cycle had already started, and the Na-FBR program acquired large funding and participants.
2. Compared with this trend, the MSR with Th cycle was too late, and participants were limited to ORNL.
3. Since the MSR was a different concept from a solid fuel reactor, supporting voices were weak.
4. Besides these points, Weinberg stated that the U-Pu cycle was preferred, because it was closer to a nuclear weapon.

Regardless of these historic results, Weinberg predicted in his biography that his proposal would be revived in the future.

### 11.1.8 Summary

As is described above, the MSR development has been initiated by the prospect of genius scientists, and has been performed by innovative scientists and engineers at ORNL. They constructed three experimental MSRs, and one of them (the MSRE) provided excellent operation experience. After a wide variety of investigations on different concepts, they finally proposed the 1000 MWe MSBR design as future power plants.

It is clear that this development was led strongly by Alvin Weinberg. As is shown in his books, he recognized the danger of LWRs and of the U-Pu cycle. Therefore, as is explained in the next section, he visited many countries as an evangelist of the MSR. For example, in 1991, he visited Japan to meet E. Nishibori and K. Furukawa (Fig. 11.29). He also visited Hiroshima and Nagasaki. Meanwhile, he contributed to building a bell for peace and international friendship at the city park of Oak Ridge in 1996, as is shown in Fig. 11.30.

We would like to express our respects and appreciation to them, especially to Weinberg.

**Figure 11.29** Weinberg and Furukawa (1996).

**Figure 11.30** Peace and international friendship bell at Oak Ridge
*Photo by M. Kinoshita.*

## 11.2 Current MSR designs after ORNL (FUJI)

Most ORNL reports including the reference list are available at the following website (2015): http://energyfromthorium.com/pdf/.

### 11.2.1 Introduction

After MSR development had been terminated at ORNL in the 1970s, several countries were inspired by their achievement and continued their work. Since the details for current activities will be described in a separate section of this book, major activities just after ORNL work are shortly introduced at first.

France investigated the feasibility of a graphite-moderated MSR within CEA (French Atomic Energy Commission) and an electric utility, starting from the mid-1970s until 2000 (Vergnes et al., 2000) (As for the early stage, it is based on private communication with A. Lecocq (ex-CEA scientist)).

In the 1980s, the former Czechoslovakia and Soviet Union jointly developed a reprocessing technology, which applied molten salt and was named “FREGAT” by Russian Scientists (Uhlir, 1998; Furukawa et al., 2010). This technology is based on a fluorination flame reactor technology used in France to produce $UF_6$ gas for uranium enrichment from uranium oxide.

The United Kingdom investigated MSFR instead of graphite-moderated MSR within the UK Atomic Energy Authority in the 1970s (UK Atomic Energy Authority, 1974).

China disclosed very recently that it constructed a zero-powered experimental reactor using unmelted fuel salt at Shanghai as early as 1971 (Xu, 2012).

Kazuo Furukawa and his group in Japan have been investigating graphite-moderated MSR “FUJI” and related accelerator technology since the 1980s (Furukawa et al., 2008, 2010; Yoshioka, 2013). FUJI is mostly based on MSBR designs with some improvements. This section shows their design results, such as detailed design result of FUJI-U3, brief summary of FUJI-Pu, transmutation capability of minor actinides (MA), super-FUJI of 1000 MWe, a pilot plant mini-FUJI. Another achievement on accelerator molten-salt breeder (AMSB) is described in Chapter 15 (Accelerator Driven Systems).

### 11.2.2 Concept of FUJI-U3 (using $^{233}U$ as fissile)

The conceptual design of FUJI was started in the 1980s (Furukawa et al., 1986) based on the ORNL’s MSBR studies, and its latest design is shown in Mitachi et al. (2007, 2008).

FUJI is size-flexible from 100 MWe to 1000 MWe. However, a typical value is 100−200 MWe, in order to deploy widely around the world. The latest design, FUJI-U3, is 200 MWe with a thermal output of 450 MWt. This means a thermal efficiency of about 44% owing to its high exit temperature, compared with the LWR case of 33%.

A schematic diagram of the MSR-FUJI is shown in Fig. 11.31. A reactor vessel and pipes are made of Hastelloy N. There is a graphite moderator within a reactor vessel. Fuel salt flows upwards by primary pumps, and then goes to HXs to transfer the heat to secondary coolant salt. The heat of secondary salt is transferred to the steam through a supercritical steam generator, and then to a turbine/generator to produce electricity. Based on an optimized core design, the graphite moderator does not require replacement during a reactors’ lifetime of 30 years.

The fuel salt for FUJI-U3 is $^7LiF\text{-}BeF_2\text{-}ThF_4\text{-}UF_4$ (71.76-16.0-12.0-0.24 mol%). Although fuel salt is based on $^7LiF\text{-}BeF_2$ (FLiBe), secondary salt is selected as $NaBF_4\text{-}NaF$ (92-8 mol%), the same as the MSBR design, because of cost performance. Properties of FLiBe and $NaBF_4\text{-}NaF$ are shown in Chapter 7, Materials. Both salts have good compatibility with Hastelloy N.

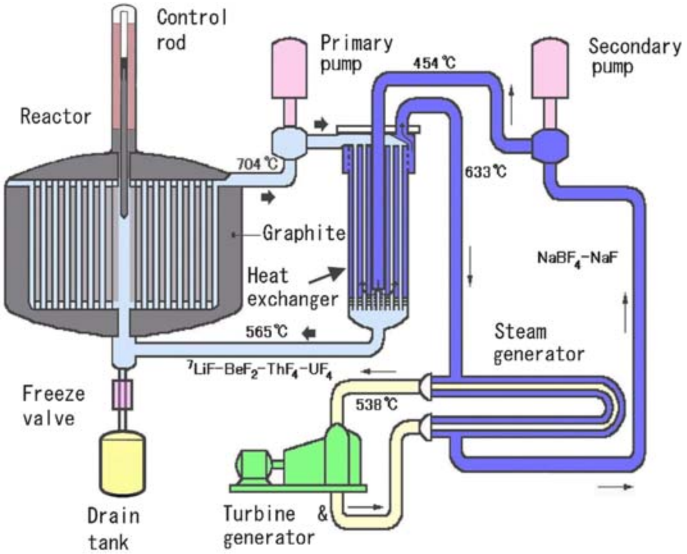

**Figure 11.31** Schematic diagram of the MSR-FUJI (one loop is shown).

A vertical cross-section of the primary system of FUJI is shown in Fig. 11.32. If fuel salt is overheated, fuel salt goes down to a drain tank, which is located below the reactor, through a freeze valve. Since there is no graphite moderator in a drain tank, there is no danger of a recriticality accident. Also, in the case of a pipe break, leaked fuel salt is collected in an emergency drain tank, which is also located below the reactor.

Continuous chemical processing of fuel salt is not performed in FUJI, but radioactive Xe, Kr, and T (tritium) are continuously removed from the reactor not only to improve the conversion ratio (CR; ratio of discharged fissile amount to loaded fissile amount), but also to prevent their release in a pipe break accident.

A bird's-eye view of FUJI is shown in Fig. 11.33. This reactor design has a three-level containment safety, as was proposed in the MSBR design (Robertson, 1971). The first level is a reactor vessel and pipes made of Hastelloy N. The second level is a high-temperature containment (HTC) composed of three layers, which contains a reactor vessel, pipes, and HXs. The third level is a reactor building (RB) composed of two layers.

### *11.2.3 Design conditions*

The electric power of FUJI-U3 is 200 MWe, and the thermal power is 450 MW(th), which implies a thermal efficiency of 44.4%. The fuel salt is initially composed of mixed fluoride of $ThF_4$ (12 mol%), $BeF_2$ (16 mol%), and LiF + $^{233}UF_4$ (72 mol%). Here, Li is enriched lithium corresponding to $^7$Li (99.995 mol%), and the relative proportion between LiF and $^{233}UF_4$ is a variable in this design.

The graphite moderator is used without being replaced for the 30 years of the reactor lifetime. Since FUJI-U3 is a small reactor, load-following operation is assumed according to the electric power demand. Assuming 100% power during

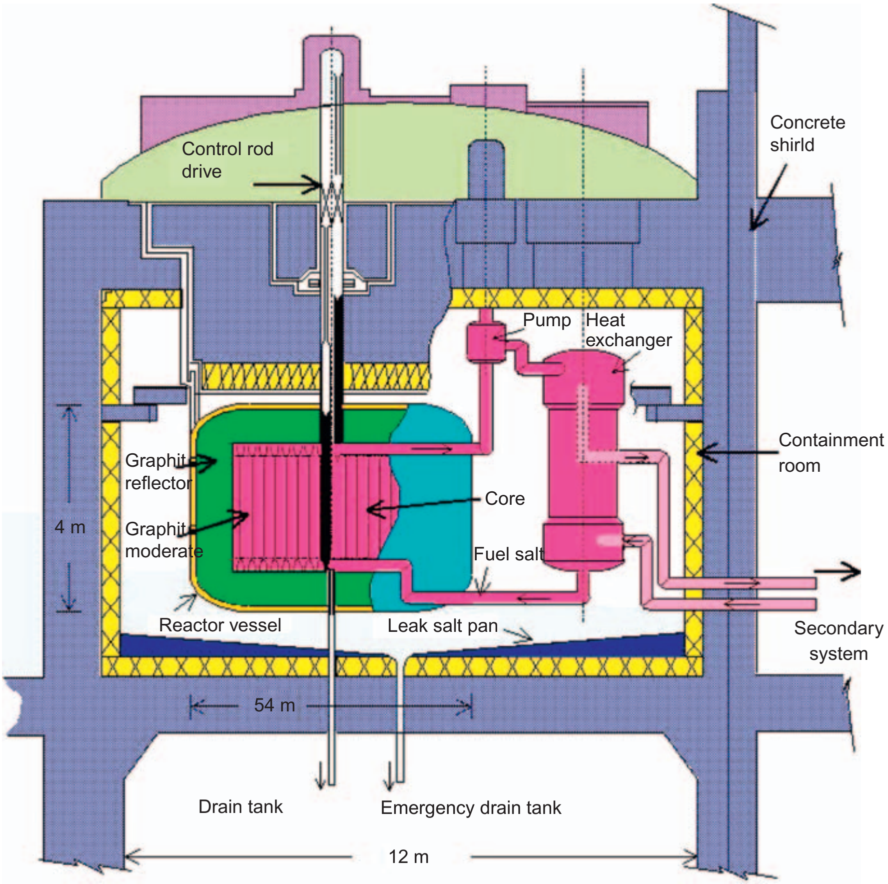

**Figure 11.32** Vertical cross-section of primary system of the MSR-FUJI.

14 hours of operation in the daytime, 50% power during 8 hours of operation in the nighttime, and a linear change in between, the average load factor is 81%. Further, assuming 12 months of operation and 1 month of downtime, the average load factor amounts to 75%. Therefore, the average load factor in this study is assumed to be 75%. The above-mentioned 30 years operation period is based on the assumption that the core internals are enclosed in the reactor vessel that is not opened during the period. If a longer operation period is required, this vessel may be replaced along with the core internals such as the graphite moderator.

Assuming 30 years operation with a 75% load factor, the irradiation limit of the graphite moderator equals $4.2 \times 10^{13}\,\text{cm}^{-2}\,\text{s}^{-1}$ for the fast neutron flux of energy higher than 52 keV. Furthermore, the irradiation limit of the vessel, which is made of Hastelloy N (Ni-based alloy with Mo/Cr/Nb/Si), is $1.4 \times 10^{11}\,\text{cm}^{-2}\,\text{s}^{-1}$ for the fast neutron flux of energy higher than 0.8 MeV, and $7.1 \times 10^{12}\,\text{cm}^{-2}\,\text{s}^{-1}$ for the thermal neutron flux of energy lower than 1.0 eV. These limits are based on the MSBR design (Robertson, 1971). These limits are slightly old, and may be revised due to recent improvements in the manufacturing technology.

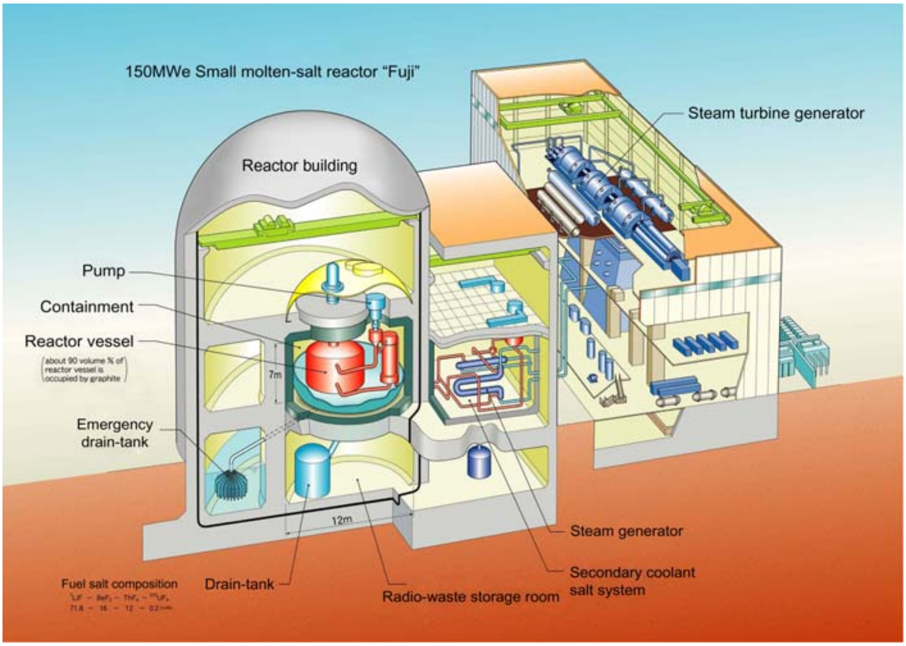

**Figure 11.33** Bird's-eye view of the MSR-FUJI.

When $^{232}$Th captures a neutron, $^{232}$Th is transmuted to $^{233}$Pa (protactinium-233), which decays to $^{233}$U with 27 days half-life. In the actual burnup calculation, full-power operation is assumed, but, in the actual FUJI operation, there is an above-mentioned 1-month shutdown time, and almost half of $^{233}$Pa in the core decays to $^{233}$U in this down time. Since the reactivity-loss due to Pa is about 0.5% delta-K, it means that about 0.25% delta-K higher reactivity is added due to this effect, and this will improve neutron economy a little. However, after the reactor is started again, the core soon reaches equilibrium condition, and the Pa content reaches the previous equilibrium value. Therefore, this Pa effect is neglected in the calculation.

### 11.2.4 Calculation procedure for criticality

The criticality of FUJI-U3 is calculated using the nuclear analysis code SRAC95 (Okumura et al., 1996). At first, a collision probability routine PIJ (Tsuchihashi et al., 1979) is applied with 107 energy groups for the unit fuel cell model, which is shown in Fig. 11.34. Nuclear cross-sections of the 107 groups are compressed into 30 groups, which are composed of 24 fast neutron groups and six thermal neutron groups. Finally, a diffusion calculation by the CITATION (Fowler et al., 1971) routine is performed using the cross-sections of the above-mentioned 30 groups. In the two-dimensional RZ (Radial direction and Z-axis)diffusion calculation, the core is divided into 65 radial regions and 32 axial zones. In these calculations, JENDL-3.2 (Nakagawa et al., 1995) is used as a nuclear data library.

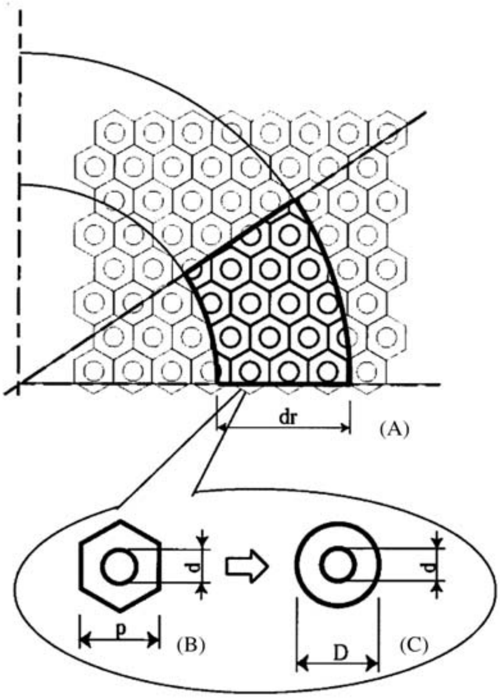

**Figure 11.34** Fuel-cell model of FUJI-U3. (A) is the layout of graphite moderator in a quarter core. (B) is the hexagonal unit cell of graphite moderator and fuel salt path. (C) is the cylindrical cell model in the calculation.

In the fuel cell calculation, the temperature of the fuel cell, composed of the fuel salt and a graphite moderator, is assumed to be 900 K, which is the mean value between the core inlet and outlet temperatures. With regard to the RZ calculation for the core, the temperature of the entire core is also assumed to be 900 K. The effect of the axial temperature distribution has been evaluated in a separate report (Yamamoto et al., 2004). According to this report, the actual temperature is higher in the upper part of the core than in the lower part, and this causes a slightly lower neutron flux at the upper part of the core due to a decrease in reactivity. However, the influence of the assumption of a constant temperature on the neutron flux is small, that is, approximately 2%–3% difference. Therefore, a constant temperature is assumed for the entire core in this calculation.

As shown in Fig. 11.34, the FUJI core is composed of graphite moderator and fuel salt. In this study, hexagonal graphite ($p = 0.19$ m) is modeled as a cylindrical element ($D = 0.20$ m), and the flow hole in the graphite is designed to be cylindrical ($d$ = variable), where this flow hole acts as a passage for the flow of the fuel salt. The lower part of this figure shows the fuel cell model considered in this calculation.

For the calculation of criticality, the size of the reactor core and the graphite reflector are varied. The volume fraction of the fuel salt in each region (Fr) is varied by changing the flow hole diameter ($= d$) of graphite. With regard to the fuel salt, the total percentage concentration of (LiF + $^{233}UF_4$) is fixed as 72 mol%, while the $^{233}UF_4$ concentration is varied in order to achieve criticality.

The eigenvalue calculation is performed using SRAC95, and in this calculation, the neutron effective multiplication factor ($K_{eff}$), fuel conversion ratio (CR), temperature coefficient of the reactivity, and neutron flux distribution ($\phi$) are calculated. The obtained value of the neutron flux distribution is compared with the irradiation limit, and if it does not meet the design criteria, the above core parameters are varied until all design conditions are met.

The calculation procedure discussed above is shown in Fig. 11.35, where both the criticality calculation (discussed in this section) and the burnup calculation (discussed in the next section) are described.

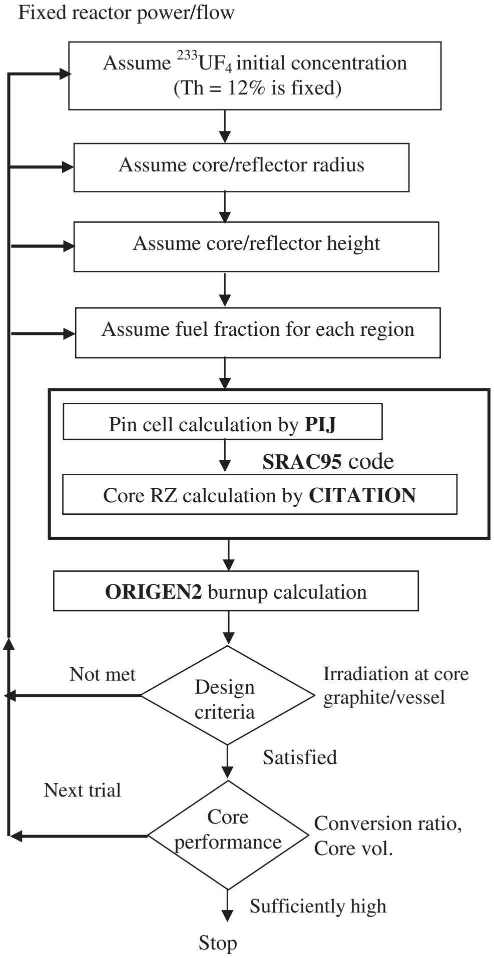

**Figure 11.35** Calculation procedure for FUJI-U3.

### 11.2.5 Criticality property and main results

Fig. 11.36 shows the quarter portion of the RZ cylindrical core configuration with dimensions and the volume fractions (Fr) of the fuel salt in each region.

As described in the discussion on design conditions, the fast neutron fluence is limited in the graphite of the core; hence, it is important to reduce the fast neutron flux at the center of the core. In this study, the core is designed to have three regions. This three-region concept is explained as follows.

First of all, let us consider the two-region core. In order to reduce the peak neutron flux, it is necessary to reduce K-infinity ($K_{\mathrm{inf}}$) in the center region of the core, and to increase the $K_{\mathrm{inf}}$ at the outer region. But, increasing $K_{\mathrm{inf}}$ at the outer region causes more neutron leakage, and then, the CR becomes worse. Since our targets are both to flatten the neutron flux and to achieve high CR, the above two-region core cannot satisfy these conflicting targets.

Therefore, the third region is introduced at the peripheral of the core, where $K_{\mathrm{inf}}$ is lowest among the whole core, in order to reduce the neutron leakage from the peripheral of the core.

In the above concept, changing $K_{\mathrm{inf}}$ is achieved by changing the fuel volume fraction in the graphite. Fig. 11.37 shows the relation between $K_{\mathrm{inf}}$ and the graphite/$^{233}$U (G/U) atom density ratio. In this fuel cell calculation, the concentration of $^{233}UF_4$ is fixed at 0.24 mol%, which corresponds to that at the beginning of the cycle condition. The hatched region corresponds to the range for the core design of FUJI-U3, which is designed at the undermoderated region (left side of the curve). Since the center region of the core in FUJI-U3 has a higher fuel fraction and a lower graphite fraction, which means it has a lower G/U ratio, $K_{\mathrm{inf}}$ in this region becomes lower than that in the outer region. This effect causes the flattening of the neutron flux.

Based on the above concept, 2 million cases were investigated using the nuclear analysis code SRAC95, and the final case was proposed as the optimized three-region core, as is shown in Fig. 11.36.

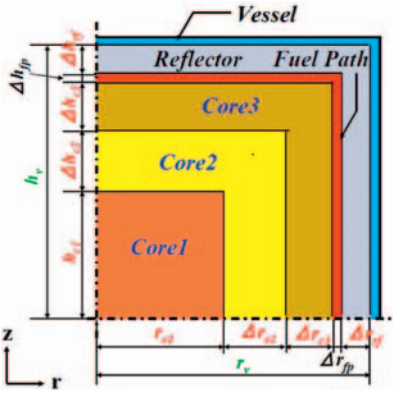

| | Core 1 | Core 2 | Core 3 |
|---|---|---|---|
| $r$ or $\Delta r$ (m) | 1.16 | 0.80 | 0.40 |
| $h$ or $\Delta h$ (m) | 1.23 | 0.70 | 0.40 |
| Fuel volume fraction (Fr) | 0.39 | 0.27 | 0.45 |

**Figure 11.36** Core configuration of FUJI-U3 (vertical section).

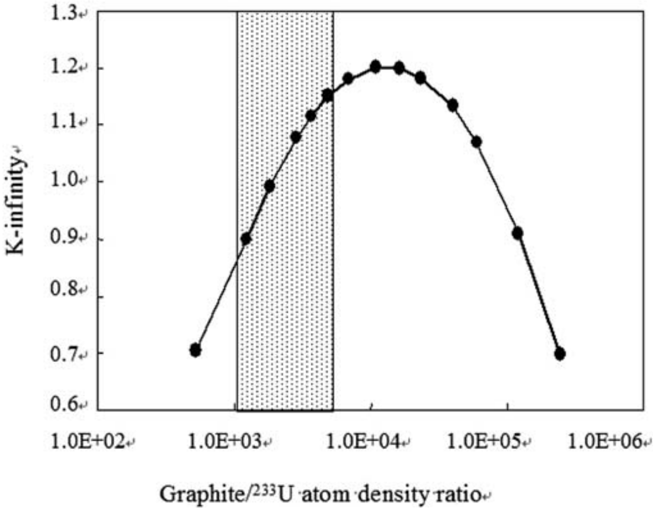

**Figure 11.37** K-infinity versus graphite/$^{233}$U atom density ratio (Mitachi et al., 2007) ($^{233}UF_4$ = 0.24 mol%).

The region located closest to the center is Core 1, and it has a fuel fraction of 39 vol%. Core 2 and Core 3 have fuel fractions of 27 vol% and 45 vol%, respectively. The core diameter is 4.72 m, and its height is 4.66 m, then the power density in the core region is 5.5 MW/m$^3$; on the other hand, the MSBR was designed with a power density of 22 MW/m$^3$ (Robertson, 1971). There is a fuel path between Core 3 and the graphite reflector; further, there are fuel ducts at the bottom and top of the core. The width of fuel path or duct is 0.04 m. The thicknesses of the radial and axial graphite reflectors are both 0.30 m. The entire core is enclosed in a reactor vessel made of Hastelloy N, which has a thickness of 0.05 m with an inner diameter of 5.40 m and a height of 5.34 m.

Table 11.2 shows the design parameters of FUJI-U3 for a capacity of 200 MWe. In the criticality calculation, the effective multiplication factor ($K_{eff}$) is maintained close to unity, actually about 1.01.

Since SRAC95 is a static nuclear code, delayed neutron behavior is not considered. The delayed neutron fraction of FUJI-U3 is as small as 0.21%, because of a smaller value of $^{233}$U than $^{235}$U. Since about 15% of fuel inventory exists out of core, 15% of delayed neutron is lost out of core. Therefore, 0.03% delta-K ($= 0.21\% \times 0.15$) must be subtracted from the above-calculated $K_{eff}$ by SRAC95. But this value is very small, and it does not affect design results.

The mean CR is 1.01, and the temperature coefficient of reactivity is $-2.7 \times 10^{-5}$ 1/K in average.

Figs. 11.38 and 11.39 show the FUJI-U3 radial and axial distribution of the fast neutron flux with energy higher than 52 keV at the center of the core, compared with the previous designs of FUJI-II (Furukawa et al., 1986) and FUJI-12 (Mitachi et al., 2000). These are the flux distributions at the beginning of operation. In these

**Table 11.2** **Design parameters of FUJI-U3 (Mitachi et al., 2008)**

| | |
|---|---|
| Electric output | 200 MWe |
| Thermal output | 450 MW(th) |
| Thermal efficiency | 44.4% |
| **Reactor vessel** | |
| Diameter/height (inner) | 5.40 m/5.34 m |
| Thickness | 0.05 m |
| **Core** | |
| Diameter/height | 4.72 m/4.66 m |
| Fuel volume fraction (av.) | 36 vol.% (see Fig. 11.36) |
| **Fuel path/duct** | |
| Width | 0.04 m |
| Fuel volume fraction | 90 vol% |
| **Reflector** | |
| Thickness | 0.30 m |
| Fuel volume fraction | 0.5 vol% |
| Power density within core | 5.5 MW/m$^3$ |
| Multiplication factor | c. 1.01 |
| Conversion ratio (av.) | 1.01 |
| Temperature coefficient (av) | $-2.7 \times 10^{-5}$ 1/K |
| **Maximum neutron flux** | |
| Graphite ($>$52 keV) | $4.1 \times 10^{13}$ cm$^{-2}$ s$^{-1}$ |
| Vessel ($>$0.8 MeV) | $1.4 \times 10^{11}$ cm$^{-2}$ s$^{-1}$ |
| ($<$1.0 eV) | $2.5 \times 10^{12}$ cm$^{-2}$ s$^{-1}$ |
| **Fuel salt** | |
| Composition | LiF-BeF$_2$-ThF$_4$-UF$_4$ |
| mol% | 71.76-16.0-12.0-0.24[a] |
| Volume in reactor | 33.6 m$^3$ |
| Volume in primary loop | 38.8 m$^3$ |
| Flow rate | 0.711 m$^3$/s |
| Temperature; in/out | 565°C/704°C |
| **Inventory in primary loop** | |
| $^{233}$U | 1.133 t[a] |
| Th | 56.4 t[a] |
| Graphite | 163.1 t |

[a] Initial condition.

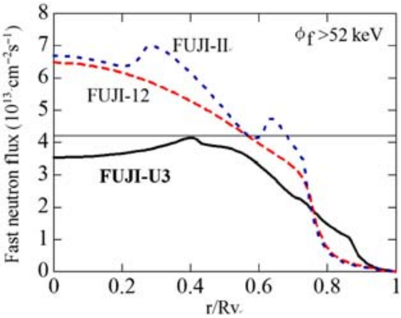

**Figure 11.38** Radial distribution of fast neutron flux (Mitachi et al., 2008).

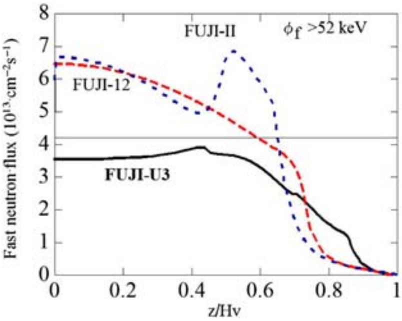

**Figure 11.39** Axial distribution of fast neutron flux (Mitachi et al., 2008).

figures, the x-axis is normalized to 1.0 for each vessel outer radius ($R_V$) or each vessel half-height ($H_V$) of the different designs.

Since the three-region core design is applied to FUJI-U3, the maximum value of the fast neutron flux is fairly reduced compared with the previous FUJI-II and FUJI-12 design results. Since the fast neutron flux of FUJI-U3 is below the irradiation limit, which is specified to be $4.2 \times 10^{13}\ \mathrm{cm}^{-2}\,\mathrm{s}^{-1}$ in the design condition section, FUJI-U3 can be operated for 30 years without replacing the graphite moderator.

Figs. 11.40 and 11.41 show the radial and axial distribution of the thermal neutron flux with energy lower than 1.0 eV at the center of the core. The thermal neutron flux is also flattened due to the three-region core design of FUJI-U3. Compared with FUJI-II, FUJI-U3 has a lower graphite fraction at the center of the core, and then, thermal neutron flux becomes lower there and is flattened. This brings flatter heat generation throughout the core.

### 11.2.6 Computational procedure for burnup characteristics

The burnup characteristics are calculated using the nuclear analysis code SRAC95 with JENDL-3.2 cross-section library and the burnup/decay analysis code

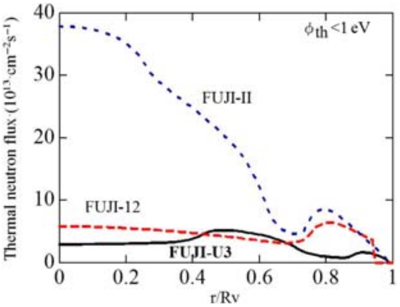

**Figure 11.40** Radial distribution of thermal neutron flux (Mitachi et al., 2008).

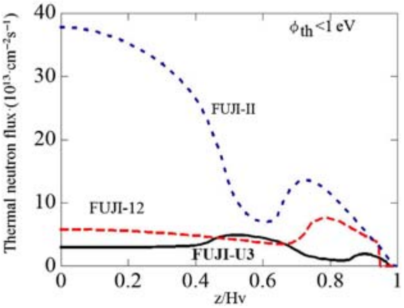

**Figure 11.41** Axial distribution of thermal neutron flux (Mitachi et al., 2008).

ORIGEN2 (Croff et al., 1980). Since ORIGEN2 requires one-group cross-sections, it is necessary to reduce the number of energy groups for the cross-sections of SRAC95. Using 107-group cross-sections and neutron flux of SRAC95 for each region of FUJI-U3, one-group cross-sections are obtained for 211 nuclides (70 actinides and 141 FPs). These 211 nuclides are selected because they have larger total cross-sections and more importance among the 1297 nuclides in the core. For the other 1086 nuclides having smaller total cross-sections, the ORIGEN2 cross-section library for PWR is used. A total of 1297 nuclides are considered in this burnup calculation.

In the burnup calculation, the continuous removal of FP gas from the fuel salt is assumed through the gas removal system, as was proposed for the MSBR. These gaseous FPs are Kr, Xe, H, T, Ne, Ar, and Rn. The removal speed in the system is estimated to be 1.4% per minute of gaseous FPs in the fuel salt. And, in the actual calculation, it is assumed that 99.9% of gaseous FP is removed and the residual 0.1% remains in the core at the $K_{\mathrm{eff}}$ calculation point of every 40-day interval. Since Xe reactivity loss is about 1.6% delta-K, which is dominant among gaseous FPs, the above 0.1% residual effect is negligibly small.

$K_{\mathrm{eff}}$ is calculated every 40 days, and it is maintained at approximately 1.01 by feeding the new fuel salt. This makeup fuel for replenishment is composed of the mixture of LiF (73 mol%) and $^{233}UF_4$ (27 mol%), according to a proposal for the

MSBR. LiF is added to the mixture to achieve a low melting point. In this makeup fuel, the recovered U is used at first, and this U is obtained from the chemical processing of the fuel salt, which is described later. If the amount of this recovered U is not enough, then new $^{233}U$ is used as an additional makeup fuel.

The fuel salt composition in the core changes with the burnup. The composition is examined every 40–200 days, and Li, Be, Th, and F are then added, if necessary. As a result, the chemical composition of the fuel salt is maintained close to that of the initial core. At this makeup time when Li/Be/Th/F are added, the one-group cross-sections are also updated to those of the chemical composition of the new fuel salt. In the makeup fuel, Li is supplied in the form of LiF, Be in the form of $BeF_2$ or metallic Be, and F as $F_2$ in the gaseous form. Furthermore, Th is supplied in a mixture of LiF (71 mol%) and $ThF_4$ (29 mol%), according to a proposal for the MSBR.

### 11.2.7 Chemical processing of fuel salt

The FPs are accumulated in the fuel salt during the operation of the FUJI, and their precipitation or extraction occurs when the concentration of the FPs is too high after a long-time operation. Therefore, it is necessary to process the fuel salt chemically before such a situation occurs. In this study, it is assumed that the chemical processing of the fuel salt is performed every 2000 EFPD (effective full-power days), which corresponds to a 7.5-year interval with a 75% load factor. The details of the chemical processing are described in the MSBR report (Robertson, 1971).

In this study, it is assumed that 100% of the actinides and FPs are removed from the discharged fuel salt. The reactivity loss due to all FPs is about 5% delta-K, and if a 95% removal is assumed, it will result in a small penalty of 0.25% delta-K in the above calculation.

In the chemical processing, LiF, $BeF_2$, $ThF_4$, and $UF_4$ are recovered and purified from the discharged salt and are reused as fresh fuel salt. Moreover, the remainder is used as a makeup fuel. Since Th decreases with burnup, it is added. On the other hand, a small amount of U is removed in order to decrease $K_{eff}$, because the removal of FPs increases $K_{eff}$ just after the chemical processing. Since $^{233}Pa$ decays to $^{233}U$ with a half-life of 27 days, all the $PaF_4$ is recovered after the chemical processing and reused as a potential fissile material of fuel salts.

### 11.2.8 Power control options for FUJI

There are several options for the power control of the MSR-FUJI. These options can be also used for a small change of burnup behavior. Although the reactivity decrease by fuel burnup is small in the MSR-FUJI, compensation for fuel burnup can be performed by the fuel salt concentration adjustment system.

1. Control rod made of neutron-absorbing material

   Current LWR licensing requires control rods in order to shutdown the reactor, which are made of neutron-absorbing material, such as Ag-In-Cd for PWR, and $B_4C$ or hafnium (Hf) for Boiling water reactor (BWR). The MSBR report does not show the design of this type, but these control rods can be used not only to shutdown the MSR, but also to control the power of the reactor.

2. Graphite control rod

   A graphite control rod concept has been proposed for the MSBR (Robertson, 1971). When the graphite rod is inserted into the core, it enhances neutron moderation, and causes a small positive reactivity. Although the addition of reactivity is small (about 0.2% delta-K/rod), it is enough for power control.

3. Flow control technology

   When the core flow is increased, it causes a small positive reactivity, because of negative temperature coefficient. Then, this method is applicable to FUJI as shown by the colleagues of the authors (Ishihara et al., 2007a). This technology is the same as the power control system in current BWRs, where the core flow is changed by a pump speed. Some of the results are shown in Section 11.5. The advantage of this option is that there is no depletion of control rods by the neutron irradiation in the core.

4. Temperature control technology

   Recently, colleagues of the authors proposed another control method for the MSR, which is to change the temperature of fuel salt by changing the turbine/generator output (Yamamoto et al., 2006b). Its principle is the same as the power control system in current PWRs, and feasible for the MSR too.

### 11.2.9 Burnup behavior of reactor characteristics

Fig. 11.42 shows the time behavior of $K_{eff}$ and CR. The x-axis shows EFPD, and 8213 EFPD corresponds to 30 years of operation with a load factor of 75%.

FUJI-U3 is designed to maintain criticality mainly by the makeup of $^{233}UF_4$ fuel salt every 40 days (30 EFPD) for the 30-year operation.

Since the decrease in reactivity within 40 days is about 0.2% delta-K, this small change can be regulated either by the movement of the graphite rod, or by the adjustment of the core flow, or by the change of the temperature of fuel salt by changing the turbine/generator output.

The mean value of the CR throughout the lifetime for the above-mentioned case is 1.01. Meanwhile the CR of old FUJI-12 value was 0.92, showing the effectiveness of FUJI-U3's three-region concept.

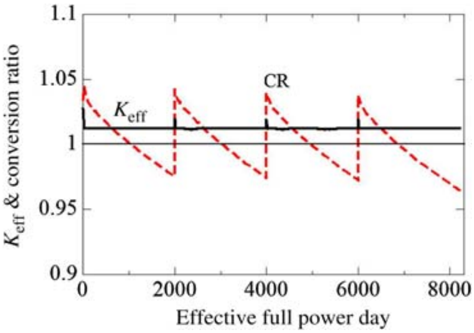

**Figure 11.42** Time behavior of $K_{eff}$ and conversion ratio (Mitachi et al., 2008).

**Table 11.3 Time behavior of FUJI-U3 characteristics (Mitachi et al., 2008)**

| Operation period (EFPD) | $K_{\mathrm{eff}}$ | CR | $\alpha_{\mathrm{T}}$ [1/K] ($\times 10^{-5}$) | $\phi_{\mathrm{G}}$ ($\mathrm{cm}^{-2}\,\mathrm{s}^{-1}$) >52 keV ($\times 10^{13}$) | $\phi_{\mathrm{V}}$ | |
|---|---|---|---|---|---|---|
| | | | | | ($\mathrm{cm}^{-2}\mathrm{s}^{-1}$) | |
| | | | | | > 0.8 MeV | < 1.0 eV |
| | | | | | ($\times 10^{11}$) | ($\times 10^{12}$) |
| 0 | 1.027 | 1.034 | −3.10 | 4.10 | 1.34 | 2.46 |
| 2000 | 1.012 | 0.975 | −2.39 | 4.12 | 1.40 | 2.33 |
| 2001 | 1.019 | 1.042 | −2.97 | 4.10 | 1.36 | 2.42 |
| 4000 | 1.012 | 0.974 | −2.43 | 4.10 | 1.41 | 2.30 |
| 4001 | 1.019 | 1.040 | −3.00 | 4.09 | 1.36 | 2.38 |
| 6000 | 1.012 | 0.972 | −2.47 | 4.09 | 1.41 | 2.27 |
| 6001 | 1.018 | 1.038 | −3.03 | 4.08 | 1.37 | 2.36 |
| 8213 | 1.012 | 0.965 | −2.50 | 4.07 | 1.42 | 2.24 |

Table 11.3 shows the change in the reactor characteristic parameters when FUJI-U3 is operated for 30 years. In this table, it is assumed that chemical processing is performed between the dates of 2000 and 2001, and so on. $K_{\mathrm{eff}}$ is kept about 1.01, except at the starting point. The maximum neutron flux ($\phi_{\mathrm{G}}$) of energy higher than 52 keV in the graphite moderator is $4.1 \times 10^{13}\,\mathrm{cm}^{-2}\,\mathrm{s}^{-1}$, which is restricted by neutron radiation damage. The maximum neutron flux $\phi_{\mathrm{V}}$ on the inner wall of the vessel is $1.4 \times 10^{11}\,\mathrm{cm}^{-2}\,\mathrm{s}^{-1}$ for the fast neutron flux with energy higher than 0.8 MeV, and $2.5 \times 10^{12}\,\mathrm{cm}^{-2}\,\mathrm{s}^{-1}$ for the thermal neutron flux with energy lower than 1.0 eV. Both values are below the irradiation limit of this study, and the FUJI-U3 design satisfies the design condition for the neutron irradiation of 30 years operation. As a future study, borated graphite can be used to reduce the neutron flux at the vessel.

The temperature coefficient of reactivity ($\alpha_{\mathrm{T}}$) is $-2.7 \times 10^{-5}$ 1/K on average, and this temperature coefficient is sufficient for stable control.

### 11.2.10 Material balance of actinides

Table 11.4 shows the material balance of actinides such as U/Th/Pu and MA in FUJI-U3. This table shows the calculated results for the initial inventory, reload fuel, and total feed for 30 years' operation. The final remaining amount of actinides and their net production are the values after 30 years' operation. In this table, "Initial inventory" is the weight of Th and U-fissile at the beginning of the FUJI-U3 operation, and "Net feed" is the weight of charged Th and U-fissile after startup and up to the closing of the reactor, which is 30 years later. "Total demand" is the sum of "Initial inventory" and "Net feed." "Final remaining amount" is the weight of the actinides at the closing of the reactor. Finally, "Net production" is the difference

**Table 11.4** Material balance of FUJI-U3 for a 30-year operation (Mitachi et al., 2008)

| | Th(t) | U-fissile (t) | Pu (kg) | MA (kg) |
|---|---|---|---|---|
| Initial inventory | 56.4 | 1.133 | – | – |
| Net feed | 5.2 | 0.426 | – | – |
| Total demand | 61.6 | 1.559 | – | – |
| Final remaining amount | 57.5 | 1.584 | 0.70 | 4.55[a] |
| Net production | −4.1 | 0.025 | 0.70 | 4.55[a] |

[a] Np = 3.16 kg, Pa (except $^{233}$Pa) = 1.39 kg, Am = 0.2 g, Cm = 0.02 g.

**Table 11.5** Fission products in fuel salt of the core at 30 years (Mitachi et al., 2008)

| | | |
|---|---|---|
| Gaseous fission products | g | 178 |
| **Liquid fission products** | | |
| Third valence metal | mol% | 0.11 |
| | kg | 323 |
| Other metal, except third valence | mol% | 0.16 |
| | kg | 364 |
| Solid (precipitated) fission products | kg | 158 |

between "Final remaining amount" and "Total demand." The negative value for the net production implies consumption. In the column of "Final remaining amount" of this table, $^{233}$Pa is added to U-fissile, because $^{233}$Pa decays to $^{233}$U with a half-life of 27 days.

As shown in this table, the net production of Pu is 0.70 kg and that of MA (mostly Np) is 4.55 kg. Therefore, it is confirmed that there is very little production of Pu and MA, and it shows the benefits of the Th cycle.

## 11.2.11 Fission products

Table 11.5 shows the amount of FP, which is accumulated in FUJI-U3 at the point of 30 years. These FPs are classified into gaseous FP, liquid FP, and solid FP.

Since the gas solubility of the fuel salt is sufficiently low, the FP gas is easily and continuously removed from the fuel salt by the He gas bubbling system. As shown in this table, the residual gaseous FP mass is only 178 g.

The concentration of the third valence FP must be less than 1 mol%, considering the solubility of the FP in the fuel salt, as is evaluated in the MSBR report (Robertson, 1971). As is shown in this table, the maximum concentration of the third valence FP is 0.11 mol%. Therefore, precipitation does not occur for the third valence liquid FP.

The concentration of other metals, except third valence FP, is 0.16 mol%. Since this concentration is less than 1 mol%, it is considered that there is no chemical influence on the graphite and the vessel, as is evaluated in the MSBR report (Robertson, 1971).

As for the solid FP, the total amount is 158 kg, and they are Mo/Ru/Tc and so on. Most of them are removed by the filter system, which is equipped in the primary loop; subsequently, there will be little precipitation of the solid FP on the wall of the primary loop. However, this should be confirmed in the future.

Based on the above consideration, the operation of FUJI-U3 will not face serious problems for FP accumulation.

### 11.2.12 Fuel requirement and actinides for a 1 GWe plant

In order to compare the MSR performance with a 1 GWe BWR (Hida and Yoshioka, 1992), the above-mentioned FUJI-U3 results are multiplied by 5 (1000 MWe/200 MWe = 5). The fuel requirement and the amount of Pu/MA are shown in Table 11.6. In this comparison, it is assumed that the BWR uses uranium oxide as the fuel and has an operation period of 25.9 years with an 87% load factor. This means that the operation period is 22.5 EFPY (effective full-power years) for both reactors.

The initial fissile ($^{233}U$) amount for FUJI-U3 is extrapolated to be 5.7 t for a capacity of 1-Gwe, and that ($^{235}U$) for the BWR is 3.9 t.

The amount of fissile material fed as a reload fuel is 2.1 t of $^{233}U$. This value is 10% of the BWR amount of 20.7 t of $^{235}U$.

The total requirement of fissile material for the entire operation period is 7.8 t of $^{233}U$. This value is 32% of the BWR amount of 24.6 t of $^{235}U$. One of the big

**Table 11.6** **Production of U/Pu/MA in a 1 GWe reactor (Mitachi et al., 2008)**

| | **Extrapolated from FUJI-U3** | **BWR** |
|---|---|---|
| Output power (GWe) | 1.0 | 1.0 |
| Reactor operation time (year) | 30.0 | 25.9 |
| Load factor | 0.75 | 0.87 |
| Initial inventory of U-fissile (t) | 5.7 | 3.9 |
| Net feed of U-fissile (t) | 2.1 | 20.7 |
| U-fissile total demand (t) | 7.8 | 24.6 |
| Final remaining U-fissile (t) | 7.9 | – |
| **Net production in reactor life** | | |
| U-fissile (t) | 0.1 | −17.7 |
| Pu-total (kg) | 3.5 | 5080 |
| Minor actinides (kg) | 23 | 543 |

benefits of FUJI-U3 is that since CR is almost 1.0, the same amount of fissile is discharged at the end of FUJI operation, and this fissile (7.9 t) can be used to the next FUJI.

FUJI-U3 produces 3.5 kg of Pu for a 30-year operation period, whereas BWR produces 5080 kg for the same period. This implies that Pu production in FUJI-U3 is only 0.1% of that in BWR.

The production of MA, which are long-lived nuclear wastes, is 23 kg, whereas BWR produces 543 kg for the same period. This implies that MA production in FUJI-U3 is 4% of that in BWR.

### 11.2.13 FUJI-Pu (using Pu as initial fissile)

At the initial stage of the Th cycle, MSR needs fissile material for initial start-up, because natural Th does not contain $^{233}$U. One proposal is to utilize plutonium (Pu) from LWR spent fuel, Therefore, Pu burner version: FUJI-Pu was studied (Mitachi and Furukawa, 1995). FUJI-Pu can be applied to incinerate recovered Pu from LWR spent fuels and convert Th to $^{233}$U.

In this study, 100 MW (electric) and 250 MW (thermal) output are assumed, and the initial fuel composition is $^7$LiF-BeF$_2$-ThF$_4$-PuF$_3$ (71.8-16.0-12.0-0.25 mol%). As is shown in Fig. 11.43 and Table 11.7, FUJI-Pu can consume 244 kg of Pu-fissile, and produce 112 kg of U-fissile for 900 days full-power operation.

If these values can be extrapolated to 1 GWe plant in 365 EFPD with 100% power operation, these values can be multiplied by 4.06 (= 1000 MWe/100 MWe × 365 days/900 days). Then, FUJI-Pu of 1 GWe can consume fissile Pu of 991 kg for each 365 EFPD, and can generate fissile U of 455 kg for that period.

### 11.2.14 Transmutation of minor actinides by the MSR-FUJI

As is shown above, production of MA in the MSR-FUJI is very small. Since these MAs have certain absorption cross-sections for thermal neutrons, MAs from LWR

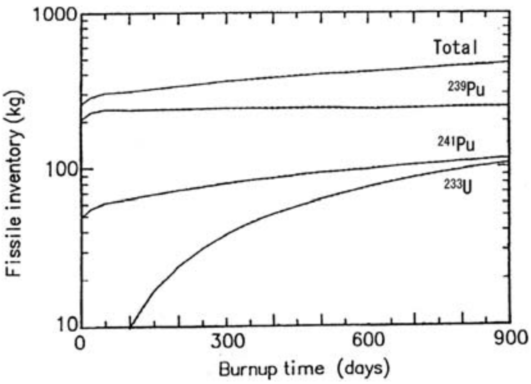

**Figure 11.43** Fissile inventory of FUJI-Pu for 900 EFPD (Mitachi and Furukawa, 1995).

**Table 11.7** **Material balance for FUJI-Pu (Mitachi and Furukawa, 1995)**

| | Initial weight | Feed up to 900 EFPD | Residual at 900 EFPD | Net generation |
|---|---|---|---|---|
| Fissile Pu (kg) | 254 | 350 | 360 | −244 |
| Fissile U + $^{233}$Pa (kg) | 0 | 0 | 112 | 112 |
| Th weight (ton) | 17.4 | 0.13 | 17.4 | −0.1 |
| Conversion ratio | – | – | 0.61 | – |

Negative value means consumption

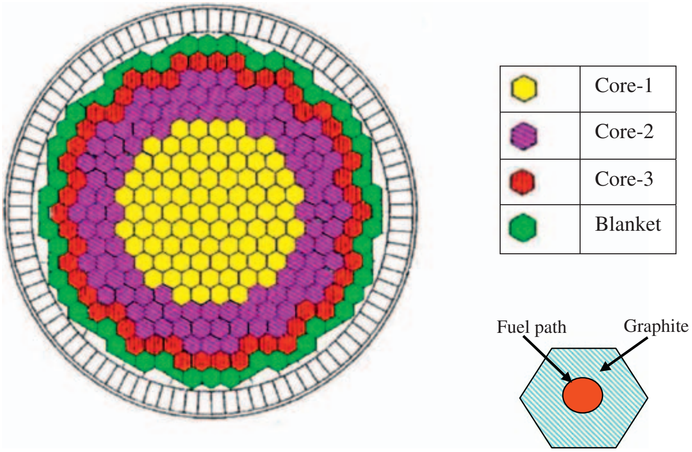

**Figure 11.44** Horizontal core layout of super-FUJI (Mitachi et al., 1994).

spent fuel can be efficiently transmuted to stable or shorter lifetime elements. A preliminary study was performed on 1000 MWe (2250 MWt) FUJI case. Assuming totally loaded MA of 5940 kg, it is calculated that 85% of MA is transmuted for 30 years' operation. This means 170 kg MA is consumed yearly (Osaka et al., 1995).

### 11.2.15 super-FUJI (large-sized plant)

FUJI was originally designed as a relatively small-sized plant, because it is aimed to deploy widely in the world. But, large-sized plant, such as 1000 MWe are also possible, such as the 1000 MWe MSBR by ORNL. Since the MSR does not need a high-pressure vessel, it will be easier to design a large-sized plant, of course, large-sized equipment, such as molten salt pump or graphite, have to be developed.

A preliminary design was performed as "super-FUJI," assuming 1000 MW (electric) and 2272 MW (thermal) output (Mitachi et al., 1994). As is shown in Fig. 11.44, the core is composed of graphite rods of hexagonal shape, and the fuel salt passes through center holes of each graphite rods. Each graphite fraction can be optimized by changing a fuel path diameter, and the average graphite fraction is 0.87, the same as MSBR. An initial fuel composition is $^{7}LiF\text{-}BeF_2\text{-}ThF_4\text{-}^{233}UF_4$ (71.8-16.0-12.0-0.2 mol%), and an initial $^{233}UF_4$ inventory is 1.5 ton. This is a somewhat old design, but fissile inventory is minimized owing to a higher graphite fraction and softer neutron spectrum. An initial CR is 0.98, and lifetime average CR will be lower than this value. In general, a large-sized plant has better neutron economy, and CR can be improved. But, an initial fissile inventory and CR are in a trade-off relationship in most cases.

### 11.2.16 mini-FUJI (pilot plant)

Almost all reactor engineering was established at ORNL for the MSRE and the MSBR design. But, it was 40–50 years ago, and the technology has to be rebuilt by a pilot plant "mini-FUJI" (Furukawa et al., 2010). Two major items were not demonstrated in the MSRE.

1. Use of Th in fuel salt;
2. Development of a SG, because the heat in secondary salt of the MSRE was released to the open air. SG development experience for the FBR can be applied.

Table 11.8 shows basic design parameters for FUJI-U3 in the previous section, mini-FUJI, and the MSRE (Robertson, 1965). Fig. 11.45 shows a horizontal cross-section and vertical cross-section of mini-FUJI.

**Table 11.8 Design parameters of three MSRs (FUJI-U3, mini-FUJI, and MSRE)**

| | **FUJI-U3 (Mitachi et al., 2008)** | **mini-FUJI (Furukawa et al., 2010)** | **MSRE (Robertson, 1965)** |
|---|---|---|---|
| Electric output (MWe) | 200 | 7 | – |
| Thermal output (MWt) | 450 | 17 | 8 |
| Thermal efficiency (%) | 44 | 41 | – |
| Graphite fraction (vol%) | 55–73 | 70 | 77 |
| Fuel conversion ratio | 1.01 | 0.6 | – |
| $^{233}U$ inventory (kg) | 1133 | 27 | 32 |
| $^{232}Th$ (ton) | 56 | 0.65 | – |
| Fuel salt | $^{7}LiF\text{-}BeF_2\text{-}ThF_4\text{-}UF_4$ | $^{7}LiF\text{-}BeF_2\text{-}ThF_4\text{-}UF_4$ | $^{7}LiF\text{-}BeF_2\text{-}ZrF_4\text{-}UF_4$ |
| Secondary salt | $NaBF_4\text{-}NaF$ | $NaBF_4\text{-}NaF$ | $LiF\text{-}BeF_2$ |
| Total fuel salt volume ($m^3$) | 39 | 4.5 | 2.1 |
| Core flow rate ($m^3$/min) | 43 | 1.6 | 4.5 |
| Temperature in-out (°C) | 565–704 | 565–704 | 632–654 |
| Graphite inventory (ton) | 163 | 8.8 | 3.7 |

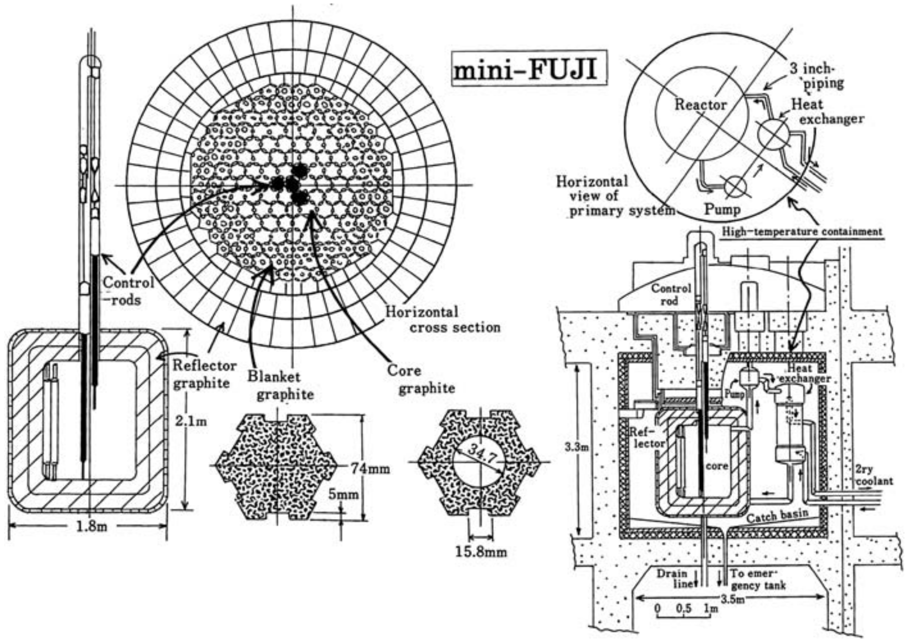

**Figure 11.45** Mini-FUJI cross-sections (Furukawa et al., 2010).

### 11.2.17 Summary of FUJI design results

A small MSR FUJI-U3 with a three-region core design achieved the optimum combination among flattening and leakage of neutron flux. The core performance of the reactor is obtained by calculations performed using the reactor analysis code SRAC95 and the burnup analysis code ORIGEN2. The main results obtained are as follows.

1. It is possible to operate the reactor with an electric power of 200 MWe (thermal power output of 450 MW(th), 44.4% thermal efficiency) together with a load factor of 75% for 30 years without replacing the graphite moderator.
2. With regard to the average CR, a high value of 1.01 is achieved without online reprocessing, and it is almost self-sustaining. Also, the residual fissile at the end of the reactor life can be used to the next FUJI.

For comparison with a 1-GWe BWR, the results of FUJI-U3 for a 30-year operation period are scaled to those of a 1-GWe capacity.

3. The $^{233}$U requirement for FUJI-U3 is 7.8 t, and this value is 32% of the BWR. At the end of FUJI-U3 operation, 7.9 t of fissile is discharged, and this fissile can be used to the next FUJI.
4. FUJI-U3 produces 3.5 kg of Pu for a 30-year operation period, whereas BWR produces 5080 kg for the same period. This implies that Pu production in FUJI-U3 is only 0.1% of that in BWR.
5. The production of MA, which are long-lived nuclear wastes, is 23 kg, whereas BWR produces 543 kg for the same period. This implies that MA production in FUJI-U3 is 4% of that in BWR.

Besides FUJI-U3 design, a brief summary of FUJI-Pu is shown, which can consume fissile Pu of 991 kg for each 365 EFPD, and can generate fissile U of 455 kg for that period, if FUJI-Pu can be extrapolated to 1 GWe plant. Also, transmutation capability of MA in 1000 MWe FUJI is investigated, and it is shown that 170 kg MA is consumed yearly. As for the flexibility of plant size, a conceptual design of super-FUJI of 1000 MWe is shown. Finally, a concept of pilot plant mini-FUJI is described.

## 11.3 Safety concepts of the MSR

### 11.3.1 Introduction

The MSR has very high safety, because of the following unique features, including practically no possibility of a severe accident (Furukawa et al., 2007).

1. Its primary loop and a secondary loop are operated at a very low *pressure* (about 0.5 MPa), which essentially eliminates accidents such as system rupture due to high pressure.
2. The molten salt is chemically *inert*, that is, it does not react violently with air or water, and is not flammable. The corrosion of Hastelloy N can be minimized by the appropriate chemical control and maintenance of the molten salt.
3. Pressure increase in a primary loop is incredible, because *boiling* temperature of the fuel salt is very high (about 1400°C) compared with the operating temperature (about 700°C).
4. Since there is *no water* within a containment, there is no possibility of high pressure by *steam* generation, and no possibility of *hydrogen* explosion, at any accidental conditions.
5. The fuel salt is drained to a *drain* tank through a freeze valve, if required. In case of a rupture in the primary loop, the spilled fuel salt is drained to an emergency drain tank without passing a freeze valve.
6. The fuel salt can keep criticality only where graphite exists in an appropriate fraction. In an accident, the fuel salt, which is drained to a drain tank, cannot cause a *recriticality* accident.

   (As for the MSR without graphite moderator, this drain tank is appropriately designed to prevent recriticality.)
7. The MSR has a large negative *reactivity coefficient* of a fuel salt temperature that can suppress an abnormal change of the reactor power. Although a temperature coefficient of graphite is positive, it does not affect the safety, because the heat capacity of graphite is large enough.
8. Since *gaseous* FPs can be removed by separating from the fuel salt, the danger due to the release of radioactivity from the core at accidental conditions can be minimized.
9. Since fuel composition can be adjusted when necessary, an *excess reactivity* and a reactivity margin to be compensated by control rods are small. Therefore, reactivity requirements for control rods are also small.
10. The *delayed neutron* fraction of $^{233}$U is lower than that of $^{235}$U and some delayed neutrons are generated outside the core. However, safe control of the reactor is possible because of a large negative reactivity coefficient with fuel salt temperature, and small reactivity insertion.
11. Since there is no airflow and no heat source within a core when fuel salt is drained at an accidental condition, graphite *fire* does not occur.

## 11.3.2 *Safety concepts of the MSR*

In the current LWR licensing, there are two major guidelines for safety. One is used as a guide for safety design of the reactor at a conceptual design stage, which is called "General Design Criteria (GDC)." And another is used for accident analysis, which defines the events to be studied in licensing and provides the criteria of the analyzed results. Both guidelines have not been issued for the MSR. As for the former one, GDC for FHR (fluoride salt-cooled high-temperature reactor) is now being established in the framework of the American Nuclear Society (Flanagan, 2012; ANS 20.1 working group, 2014). Based on its results, the GDC for the MSR is being proposed by the authors, and is described in Section 11.6. As for the latter one on accident analysis, it is proposed by the authors, and is described in Section 11.4 (Yoshioka et al., 2014; Yoshioka and Kinoshita, 2014).

The following safety concept of the MSR should be reinvestigated after these two guidelines are issued. Also, PRA/PSA (Probabilistic Risk Assessment/Probabilistic Safety Assessment) is required at a detailed design stage, when numerical data for risk evaluation become available.

The safety concept of the MSR in this section is based on the 150 MWe Fuji design shown in Fig. 11.46, which is a typical thermal neutron spectrum MSR without online reprocessing, as was explained in Section 11.2. If online reprocessing is applied, or if other designs are applied, then its safety must be redefined and described.

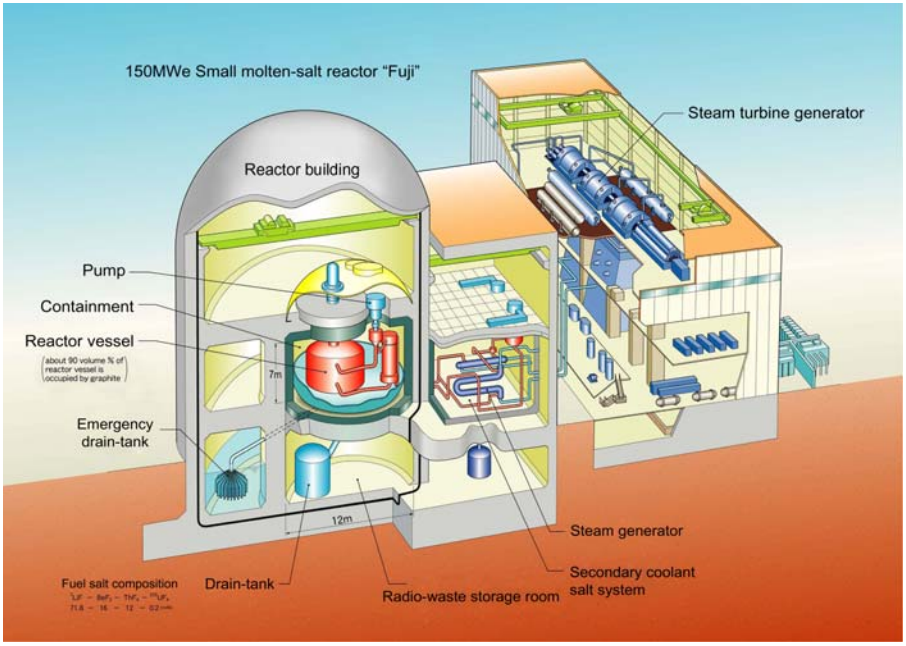

Figure 11.46 Bird's-eye view of the MSR (see Section 11.2).

The safety functions, which the MSR must be equipped with, are essentially the same as those for LWR. In any nuclear facilities, it is most important to prevent or to minimize the release of radioactive materials into the environment. In order to achieve this objective, the following three safety functions are required, the same as LWR, which are shutdown function, cooling function, and containment function.

1. Shutdown function

   This function is to stop (shutdown) nuclear fission and to terminate the fission energy generation at any time so as not to damage the core. As for the shutdown function of the MSR, there are three different diverse systems. The first is a high-speed shutdown system (scram system) by a small number of control rods, and the second shutdown system is a fuel salt passive drain system. The above two systems satisfy current licensing criteria. But in the MSR, the third shutdown system by fuel salt concentration adjustment would be applicable as a backup system, for example, adding thorium as neutron-absorbing material, although its effect is slow.
2. Cooling function

   This function is to remove the decay heat continuously even after the accident, and to keep the integrity of the fuel or the primary loop by providing enough cooling. As for the emergency core cooling system (ECCS), which is required in order to make-up the cooling water for LWR, it is not required for the MSR. In case of loss of all cooling functions such as station blackout (SBO), the fuel salt is drained to the drain tank. This drain tank is passively cooled without electricity by the decay heat removal system.
3. Containment function

   This function is to control or minimize the influence on the environment by the radioactive materials in case of a large accident. The MSR has three levels for containment safety, as was proposed in MSBR design at ORNL. The first level is a reactor vessel and pipes made of Hastelloy N. The second level is a HTC composed of three layers, which contains a reactor vessel, pipes, and HXs. The third level is a RB composed of two layers. Therefore, in total six layers are designed for the MSR.

As was explained in previous sections, gaseous FPs are continuously removed from the fuel salt, and the release of radioactivity is minimized before an accidental situation. Also, danger by steam generation or hydrogen gas generation is excluded in the MSR. These features would strengthen the containment function.

Besides the above three safety functions, the concept of the “defense in depth” principle is adopted to assure the higher safety of the facility. High safety is achieved by taking this concept at five different levels to the design. Each level, objective, and essential means are summarized in Table 11.9, based on the IAEA’s definition (IAEA, 1996).

The concept of the “defense in depth” principle in the MSR should be the same as for LWRs, and it is not described further here.

### *11.3.3 Safety analysis of the MSR*

In the current LWR licensing, all abnormal events are categorized into three types, which are abnormal operating transients (AOT), design basis accidents (DBA), and severe accidents (SA) which are beyond DBA.

Table 11.9 **Levels of "defense in depth" (IAEA, 1996)**

| Level | Objective | Essential means |
|---|---|---|
| Level 1 | Prevention of abnormal operation and failures | Conservative design and high quality in construction and operation |
| Level 2 | Control of abnormal operation and detection of failures | Control, limiting and protection systems and other surveillance features |
| Level 3 | Control of accidents within the design basis | Engineered safety features and accident procedures |
| Level 4 | Control of severe plant conditions, including prevention of accident progression and mitigation of the consequences of severe accidents | Complementary measures and accident management |
| Level 5 | Mitigation of radiological consequences of significant releases of radioactive materials | Off-site emergency response |

In order to investigate a wide range of safety on the MSR, all possible accidental scenarios must be considered. Their details are described in Section 11.4, but its conclusion is briefly described below.

At first, the following two types of accidental scenarios are considered. The first is the external cause accident, which is initiated by external events, such as earthquake, tsunami, flood, wind, fire, turbine missiles, terrorism, and so on. Another is the internal cause accident, which is caused by internal events, such as overpressure, overheating, and other mechanical failures of the primary loop boundary. The external cause accidents are generic to any reactors, and are not described here. The internal cause accidents are subcategorized as below.

1. Power increase accident or RIA (reactivity initiated accident), for example, control rod ejection accident.
2. Flow decrease accident, for example, fuel salt pump stopping accident.
3. Fuel salt leak accident, for example, rupture of primary loop pipes.
4. Other accidents, mostly MSR-specific, such as molten salt freeze accident.

Preliminary evaluations for the MSR major accidents (AOT and DBA) are shown in Section 11.4, and it is shown that there will be no release of radioactive materials into the environment even in DBAs, except the failure accident of an off-gas system.

As for the following three accidents, which were previously considered "beyond DBA," they are now included in the DBA. This is because these accidents are considered more probable than before, and some of them have actually occurred.

1. SBO is caused by a loss of external electric sources and failures of emergency diesel generators, and its occurrence has been believed incredible. However, SBO has occurred in several nuclear plants, and SBO provision was issued by the US-NRC (2010) (Also, check the latest information at US-NRC web-site, such as "10CFR50.63: Loss of All Alternating Current Power".), to be included in DBA.

2. Anticipated transients without scram (ATWS) is a transient event at a reactor without insertion of control rods for shutdown. This provision was issued and applied as ATWS rules by the US-NRC (2014b).
3. Aircraft impact assessment is now required by the US-NRC (2014a), for newly licensed nuclear plants in USA, after the 9/11 aircraft attack in 2001.

As for the consideration on SA in the MSR, there will be no release of radioactive materials into the environment in DBAs. And as a result, SA such as simultaneous loss of cooling function and containment function is incredible, except the external cause accident by terrorism or missiles. Of course, since SA assumes any possible accidental situation of the reactor, its possibility and source term issue at the release of radioactive material into the environment should be re-evaluated in a detailed design stage. The source term issue is described again in Section 11.4.

### 11.3.4 MSR safety against fukushima-type accidents

It was studied whether the MSR is still safe against a Fukushima-type accident, which was a SA that occurred on March 11 2011, and the study conclusion is referred as follows (Yoshioka, 2013).

1. The MSR is safe in case of loss of all electricity and/or loss of all core cooling, because natural circulation cooling is possible. In addition, fuel salt is drained to a drain tank if required.
2. The drain tank is equipped with a cooling system that does not need electricity.
3. There is no fuel damage or fuel melt-down, owing to its intrinsic feature of molten salt.
4. There is no danger of high pressure in the reactor vessel or containment, because there is no overpressure possibility due to vaporization of molten salt or water.
5. There is no danger of hydrogen explosion, because there is no water or zirconium within the containment.
6. Spent fuel salt is drained to a spent fuel tank, which is cooled the same as a drain tank.
7. Seismic design and countermeasures for tsunami are required, as for an LWR.
8. Even in a worst-case scenario, gaseous FPs are not released, because they are already removed in normal operation. Other FPs stay within fuel salt, and solidify to glassy material below melting temperature.

### 11.3.5 Summary

The basic safety concept of the MSR and a summary of the analysis are described here. Based on the preliminary evaluations for the MSR major accidents (AOT and DBA), as is shown in Section 11.4, there will be no release of radioactive materials into the environment, except for failure of the off-gas system. Therefore, the MSR can be designed to have superior safety.

## 11.4 Safety criteria of the MSR

### 11.4.1 Introduction

Possible accidents for MSR have been investigated, and several calculations were made for the experimental reactor MSRE (Haubenreich and Engel, 1962; Beall et al., 1964). However, those studies were 50 years ago, and they may not be applicable from the standpoint of the recent licensing approach for LWRs. Since then, safety criteria or guidelines have not been defined for MSR accident analysis.

In the current LWR licensing, there are two major guidelines. One is used as a guide for safety design of the reactor at a conceptual stage (Nuclear Safety Commission of Japan, 1990a), which is called GDC. And another is used for accident analysis (Nuclear Safety Commission of Japan, 1990b), which defines the events to be studied in licensing and provides the criteria for analyzing the results.

In this section, the authors describe several candidates for MSR safety criteria, and show one proposal, which is based on temperature limitations of the component material: Hastelloy N.

### 11.4.2 Definition of "accident"

In the current LWR licensing, all abnormal events are categorized into three types, which are AOT, DBA, and SA which are beyond DBA, as is shown in Fig. 11.47 and Table 11.10. In this section, the authors include all three types as "accidents," because their definitions for LWR may not be applicable to the MSR, and also may be changed depending on different safety designs. Therefore, each accident shown in Section 11.5.3 (Accident to be considered) must be categorized to AOT or DBA or SA at a later stage, depending on its severity, probability, and safety design.

### 11.4.3 Safety criteria for the MSR

Since there are no safety criteria for the MSR, the authors started from safety criteria for LWR, and propose the possible criteria for AOT. Safety criteria for DBA, SA, and normal operation are future discussions.

#### Safety criteria for abnormal operating transients (AOT)

As for LWR, the objective of safety criteria for AOT is to keep re-startup capability of the reactor after AOT occurs. Therefore, in order to keep fuel integrity, heat flux index such as DNBR (departure from nucleate boiling) or MCPR (minimum critical

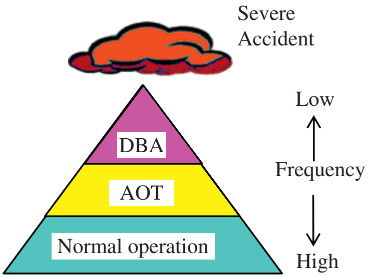

**Figure 11.47** Classification of reactor status.

**Table 11.10** Classification of reactor status and definition

| | |
|---|---|
| Severe accident (SA) | Events beyond DBAs, which will cause core melt-down for LWR and/or large release of radioactivity |
| Design basis accident (DBA) | Events beyond AOTs, which will cause LWR fuel failure. Initiated by two equipment malfunctions or two operator errors, or a combination of each |
| Abnormal operating transient (AOT) | Anticipated events to occur once or more during a plant service lifetime. Initiated by a single equipment malfunction or a single operator error |
| Normal operation | Reactor startup, operation at power, and shutdown |

power ratio) shall not violate the limit, fuel cladding tube shall not mechanically fail, and fuel enthalpy shall be less than the limit. Also, in order to keep primary system integrity, reactor system pressure shall be less than the limit.

Since the fuel of MSR is molten salt, mechanical fuel failure is impossible. Then, the above criteria for fuel integrity cannot be applied directly. Also, since molten salt has high boiling temperature and low vapor pressure, a boiling accident would be incredible. Therefore, pressure criteria for primary system integrity are not appropriate to apply.

Therefore, appropriate criteria for primary loop boundary should be considered. Of course, the reactor vessel of MSR must satisfy the provision of the ASME code (ASME Boiler and Pressure Vessel Code) such as ductility, brittleness, fatigue failure, or stress corrosion cracking, and so on, but these are mostly for steady state and for long-term design conditions.

There are two candidates for safety criteria as follows. The first is the maximum allowable design stress. In the MSBR design report, they defined the maximum allowable design stress as 250 kg/cm$^2$ at 704°C for Hastelloy N (Robertson, 1971). This value is generally derived from the (ultimate) tensile strength of the material by dividing a safety factor, for example 10 or more, but the above source document does not show the deriving process.

The maximum allowable design stress of Hastelloy N is shown in Fig. 11.48, but there is no information beyond 704°C (Robertson, 1971). The author's aim is not to apply this value directly, but to estimate the temperature limitation. If this curve is extrapolated beyond that point, limiting temperature may be somewhere between 900 and 1000°C. However, these limiting temperatures are applicable for long-term operation. Therefore, these criteria may be conservative for a short-time event such as AOT.

One more possible candidate is the (ultimate) tensile strength of Hastelloy N. Since a reactor vessel for MSR is not a "pressure vessel" and pressurization transient is incredible, loss of strength of the material could be limiting. In general, the tensile strength is used as the ultimate strength of metals. Based on the existing data for the tensile strength as is shown in Fig. 11.49, if it is extrapolated, the maximum allowable temperature could be somewhere between 900 and 1000°C (Haynes International Inc., 2002). For other Hastelloys such as Hastelloy B/Hastelloy

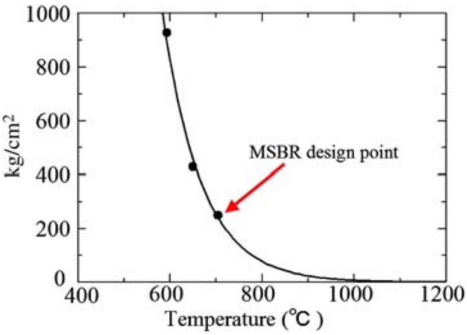

**Figure 11.48** Maximum allowable stress of Hastelloy N (Robertson, 1971).

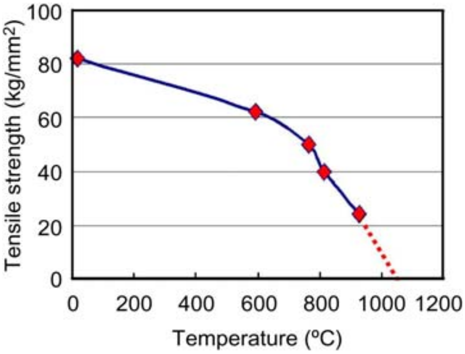

**Figure 11.49** Tensile strength of Hastelloy N (Haynes International Inc., 2002).

C/Hastelloy X, the maximum allowable temperatures are similar (Taihei Techno Service, 2015).

As is described above, the author's aim is not to apply the tensile strength directly, but to estimate the temperature limitation. Apart from this attempt, the tensile strength is about 5300 kg/cm$^2$ at 704°C based on this figure, and this means that the safety factor for maximum allowable design stress for MSBR is about 21 (= 5300/250).

Based on the above consideration, the limiting temperature may be somewhere between 900 and 1000°C. In order to decide the limiting point, the author's group proposes to apply the same concept of safety criteria for LWR fuel cladding tube to reactor vessel and piping of MSR. That is, current LWR licensing requires that the plastic strain of fuel cladding tube shall be less than 1% to prevent mechanical failure of the fuel cladding tube. Assuming MSR's vessel temperature is identical to fuel salt, the allowable fuel salt temperature should be less than the temperature that causes a plastic strain of 1% during 1 hour for primary loop boundary under the design load. Here, the maximum duration is conservatively chosen to be 1 hour, which is long enough to shutdown the reactor and take corrective actions. This is

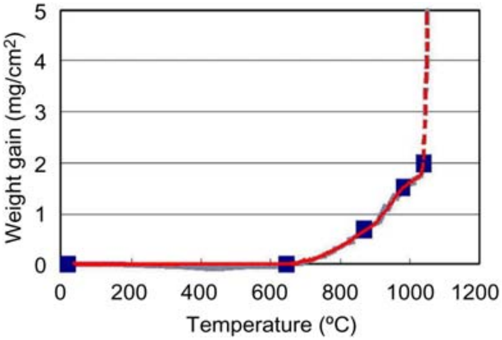

**Figure 11.50** Oxidation resistance (weight gains at 1000 h) for Hastelloy N (Haynes International Inc., 2002).

similar to the fuel rod cladding tube criteria of LWRs, although time endurance is not defined in LWR.

Using a Larson-Miller plot of Hastelloy N (Haubenreich and Engel, 1962; Haynes International Inc., 2002), the limiting temperatures can be estimated. For example, 930°C for outlet and 790°C for inlet fuel salt in the MSBR reactor vessel (Shimazu, 1978b). Violating this fuel temperature criteria, fuel salt must be drained to a drain tank quickly. The drain tank of MSR can confine radioactivity, thus no radiation release will occur.

Of course, LWR fuels are discharged after 4−5 years even if AOT occurs, and they do not experience second AOT. On the other hand, reactor vessel and piping of MSR are used for several decades. This issue must be discussed in the future.

Another possible candidate may be oxidation criteria. The ASME pressure vessel standard requires the allowable oxidation, if it occurs. The report of the Hastelloy N manufacturer says that about 1000°C may be the limit, as is shown in Fig. 11.50 (Haynes International Inc., 2002). But, since the primary loop of MSR is enclosed with an inert gas such as nitrogen gas within the containment, oxidation will be very minor. Therefore, the oxidation criterion is not applicable.

## *Safety criteria for design basis accidents (DBAs) and other events*

As for LWR, the objective of safety criteria for DBAs is to prevent the occurrence of a large release of radioactivity from the reactor, even if fuel failure occurs and radioactivity is released outside the fuel cladding tube. In order to prevent this situation, it is required that the reactor is not damaged severely, the reactor maintains coolable geometry, fuel enthalpy is lower than the limit, pressure of primary loop boundary is lower than the limit, pressure of containment boundary is lower than the limit, and radiation risk to the public is not severe.

Based on the possible scenarios for MSR accidents, it is incredible that any DBAs will cause large radioactivity release. Therefore, safety criteria for DBAs should be investigated in the future.

Regarding the safety criteria for SA, which are beyond DBA, there is no global standard at this time. Also, SA is more incredible for the MSR than DBA. Therefore, this issue should be also discussed in the future.

As for the limit for normal operation, criteria are defined for LWR, in order to prevent the violation of AOT criteria even if AOT occurs. The MSR may also need similar criteria, for example, criteria for maximum outlet temperature of fuel salt at normal operation in order to satisfy the AOT criteria even if AOT occurs. This issue should be also discussed in the future.

### *11.4.4 Summary*

Regarding the safety criteria for MSR accident analysis, based on the allowable stress and tensile strength of Hastelloy N, temperatures between 900 and 1000°C will be applicable for long-time limitation of the fuel salt. But, for short-time events such as AOT, the author's group proposes to limit the fuel salt temperature based on the plastic strain of 1% during 1 hour for primary loop boundary under design load.

Safety criteria against DBA, SA beyond DBA, and normal operation should be discussed in the future.

## 11.5 MSR accident analysis

### *11.5.1 Introduction*

In order to perform MSR accident analyses and to establish guidelines for them, we have to investigate all possible accidents. This study is also required to prepare a preliminary safety analysis report (PSAR). In this section, the authors describe the philosophy for MSR accident analysis, and show 40 possible accidents based on the philosophy with some numerical results.

### *11.5.2 Classification of accidents*

The objective of accident analysis is to prevent or mitigate radioactivity release in case of accidents, which may affect human health. In the MSR, this is caused by rupture or break of the primary loop boundary, which is composed of a reactor vessel, pipes, pumps, HXs, and so on. Either external or internal accidents may cause such a break.

#### *External cause accidents*

External cause accidents are initiated by external events, such as earthquake, tsunami, flood, wind, fire, turbine missiles, terrorism, and so on. In addition to these accidents, there are other standard accidents such as turbine trip accident, generator trip accident (load rejection accident), loss of external electric source accident, which are caused by initiating events outside the RB but affect the reactor. These ten types accidents are generic ones, and not discussed here.

### Internal cause accidents

Internal cause accidents are caused by internal events, such as overpressure, overheat, and other mechanical failures of the primary loop boundary. These are discussed in Section 11.5.3.

Of course, even if the above accidents occur, it does not mean release of radioactivity to outside the reactor. Based on the defense-in-depth principle, there are additional containments and the RB, which prevent or mitigate radioactivity release, and therefore, these systems are sometimes called "mitigation system" (MS) in current LWR licensing. MS includes containment, RB, control-rod scram system, ECCS, and so on. Meanwhile, a primary loop boundary such as a reactor vessel is called a "prevention system" (PS), whose failure initiates the accident.

## 11.5.3 Accident to be considered

The above internal cause accidents are categorized into the following four types (Table 11.11), which must be evaluated or analyzed in the framework of safety guidelines.

Regarding accidental causes such as overpressure or overheating, they are caused by power increase accident (Section 11.5.3.1) or flow decrease accident (Section 11.5.3.2), because temperature rise or enthalpy rise is proportional to power and inversely proportional to flow. In the MSR, vapor pressure is very low, and overpressure accidents are incredible with one exception, which is a SG break accident described in Section 11.5.3.4. Besides these two accidents, fuel salt leak accident (Section 11.5.3.3) may be caused by other mechanical failures of the primary loop boundary. Therefore, the above three types of accidents must be considered. Of course, some of the second and the third types ofaccidents may cause a reactivity increase as a

**Table 11.11** Accident category

| | | | |
|---|---|---|---|
| External cause accidents | | Accidents by external causes, such as earthquake, tsunami, etc. | 10 cases |
| Internal cause accidents | 11.5.3.1 | Power increase accident or RIA (reactivity initiated accident)<br>For example, control rod ejection accident | 11 |
| | 11.5.3.2 | Flow decrease accident<br>For example, fuel salt pump stopping accident | 6 |
| | 11.5.3.3 | Fuel salt leak accident<br>For example, rupture of primary loop pipes | 1 |
| | 11.5.3.4 | Other accidents<br>Mostly MSR specific. For example, molten salt freeze accident | 12 |

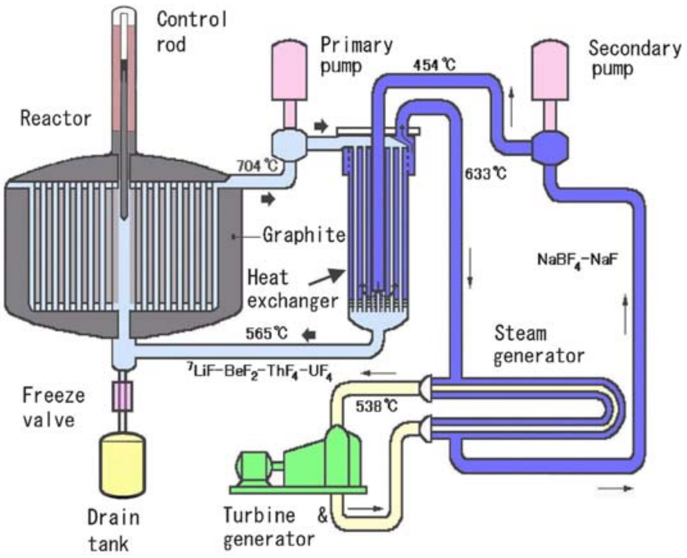

**Figure 11.51** Presumed concept for MSR accident analysis (loops are redundant) (copied from Fig. 11.31).

result. Meanwhile, the first accident type is usually called a reactivity initiated accident (RIA), because it is initiated by the insertion of positive reactivity at first.

Besides these three categories, the fourth category, named "other accidents" (Section 11.5.3.4) is considered. These accidents are mostly specific to the MSR. In some cases, this category is just a cause of the above three accidents, and then these accidents may be recategorized in the future.

In this section, the following typical MSR concept is assumed as is shown in Fig. 11.51, which was originally proposed by ORNL for MSBR design (Robertson, 1971), applying graphite moderator, single-fluid design, with gaseous FP removal system. One big improvement from the original design by the authors is removal of online reprocessing equipment, in order to simplify the reactor (Furukawa et al., 2008; Yoshioka, 2013).

### *11.5.3.1 Power increase accident or RIA (Reactivity Initiated Accident)*

#### 11.5.3.1.1 Control rod withdrawal/ejection accident

This is a most typical RIA. If we adopt a control rod made of neutron-absorbing material, and when this control rod is inserted in operation and is withdrawn or ejected by some equipment failure or operator error, then an RIA occurs. If we adopt a control rod made of graphite, which was proposed for the MSBR (Robertson, 1971), insertion of graphite control rod increases more neutron moderation and it may cause an RIA. Owing to a large negative reactivity coefficient of fuel salt temperature, power excursion terminates, even if control rod scram function fails. Meanwhile, a reactivity coefficient of graphite temperature is slightly positive, but this does not cause any problem, because heat transfer to graphite is slow. RIA was analyzed for the MSBR as shown in Fig. 11.52 (Shimazu, 1978b), and for small-sized MSR: FUJI case (Suzuki and Shimazu, 2008).

Although delayed neutron fraction ($\beta$) of $^{233}$U is smaller than $^{235}$U, this does not affect dynamic behavior of the MSR. In order to confirm this, the authors show one-point kinetic equations using an adiabatic model without core cooling (Ishimori, 1973).

$$\frac{dn}{dt} = \frac{\rho - \beta}{\ell} n + \lambda \cdot C$$

$$\frac{dc}{dt} = \frac{\beta}{\ell} n - \lambda \cdot C$$

Captions are identical to typical kinetic equations.

$\rho = \rho_0 - |\alpha| \cdot (\theta - \theta_0)$ $\alpha$: temperature reactivity coefficient, $\rho_0$: inserted reactivity

Relation between temperature ($\theta$) and core thermal power ($P$) is described as follows.

$$\frac{d\theta}{dt} = \frac{P}{C_P} \quad C_p\text{: Heat capacity, } P \propto \Sigma_f \, \phi \propto n$$

For prompt critical situation in a short time, concentration of delayed neutron precursor "C" does not change and can be assumed as constant. Then, the above equation can be solved as follows, and its behavior is shown in Fig. 11.53.

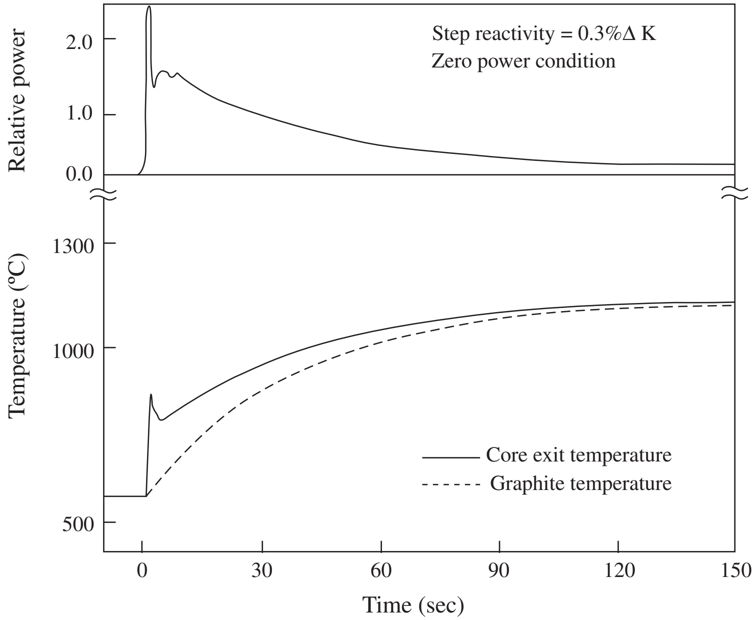

**Figure 11.52** Typical RIA (reactivity initiated accident) (Shimazu, 1978b).

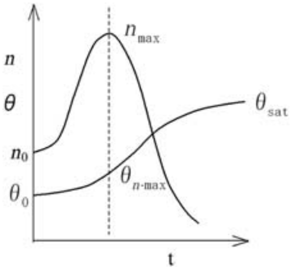

**Figure 11.53** Number of neutrons and temperature after step reactivity insertion (Ishimori, 1973).

$$n_{\max} = n_0 + \frac{C_P \cdot \rho_0^2}{2|\alpha| \cdot \ell}$$

$$\theta_{n\,\max} = \theta_0 + \frac{2\rho_0}{|\alpha|}$$

$$\theta_{\mathrm{sat}} = \theta_0 + \frac{\rho_0 + \sqrt{\rho_0^2 + 2\ell \cdot |\alpha| \cdot n_0 / C_P}}{|\alpha|}$$

It is clear that delayed neutron fraction does not affect the maximum neutron flux nor maximum fuel salt temperature. On the other hand, the MSR has a longer prompt neutron lifetime than LWR, and this fact mitigates the maximum neutron flux.

### 11.5.3.1.2 Cold-loop startup accident

Since the reactivity coefficient of fuel salt temperature is negative, if fuel salt pump is inadvertently restarted from stand-by condition, and cold fuel salt is injected into the core, then positive reactivity is inserted. However, the lowest possible temperature of fuel salt is the melting temperature, and the consequence is limited.

### 11.5.3.1.3 Secondary salt flow increase accident

If secondary salt flow increases, then fuel salt is more cooled than before and positive reactivity is inserted.

### 11.5.3.1.4 Secondary salt temperature decrease accident

If secondary salt flow decreases, then fuel salt is more cooled than before and positive reactivity is inserted.

If secondary salt temperature decreases, same situation as above occurs.

### 11.5.3.1.5 Fuel salt flow increase accident

If fuel salt flow is increased, then a core temperature is decreased, and then the reactor power is increased due to negative temperature coefficient. However, the reactor power is stabilized to a certain value, which is called a "consistent power level," as is shown in Fig. 11.54 (Ishihara et al., 2007b).

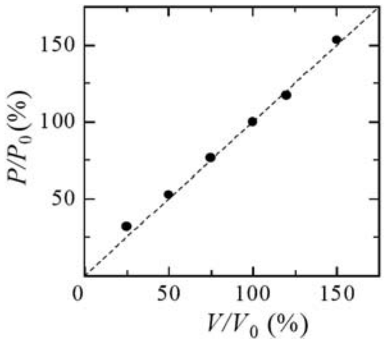

**Figure 11.54** Reactor power versus fuel salt flow (Ishihara et al., 2007b).

#### 11.5.3.1.6 Fuel salt filling accident

When fuel salt is filled from a drain tank to the core without any safety protection systems, a criticality accident may occur. Since an accident consequence depends on safety design, therefore its design must be described.

#### 11.5.3.1.7 Excessive fissile addition or fertile removal accident

MSR is equipped with a system that can adjust fuel salt composition. If excessive fissile material is injected into fuel salt, positive reactivity is inserted. Removal of thorium salt, which is a neutron absorber, causes the same result. Therefore, the safety design must be described.

#### 11.5.3.1.8 Depressurization accident

MSR has a slightly positive void reactivity coefficient of fuel salt, and a small amount of He bubbles circulate within the primary loops in order to remove gaseous FPs (Xe/Kr/T) from fuel salt. Therefore, if depressurization occurs, bubbles become larger and positive reactivity is inserted, as is shown in Fig. 11.55 (Suzuki and Shimazu, 2006). Depressurization may be caused by break of primary loop boundary, stopping of pumps, and so on, because in normal operation, fuel salt pumps give about 0.5 MPa (Mega Pascal) pressure to the primary loop. Malfunction in a He-bubble injection system may cause a similar result.

#### 11.5.3.1.9 Fissile precipitation accident

Fissile material such as uranium (U) has high solubility in fuel salt. However, if U precipitates and this U deposit is suddenly injected into the core, then positive reactivity is inserted. The cause of this accident may be invasion of moisture or oxygen in fuel salt.

#### 11.5.3.1.10 Graphite loss accident

If graphite breaks and flows out from the core, increased volume of fuel salt may causes positive reactivity insertion. However, as is explained above, graphite control rod insertion causes positive reactivity by increasing neutron moderation. Therefore, loss of graphite will insert negative reactivity.

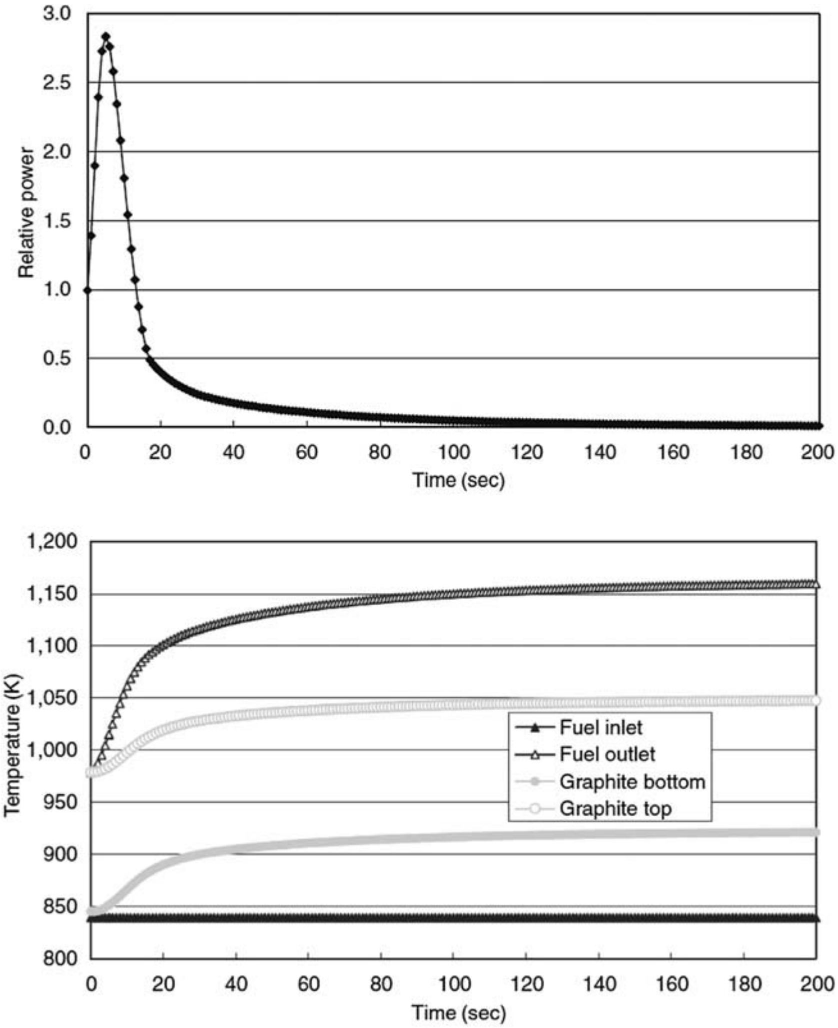

**Figure 11.55** Depressurization accident (Suzuki and Shimazu, 2006).

#### 11.5.3.1.11 Fissile penetration to graphite accident

If uranium (U) penetrates to the surface of graphite, and if this U is suddenly released into fuel salt, then positive reactivity may be inserted.

### *11.5.3.2 Flow decrease accident*

#### 11.5.3.2.1 Pump trip accident

If all fuel salt pumps trip (stop), heat removal function is lost. (In LWR licensing, one pump trip is categorized to AOT, and if all pumps trip it is categorized to DBA.) Then, fuel salt temperature increases. Also, delayed neutrons increase in the core

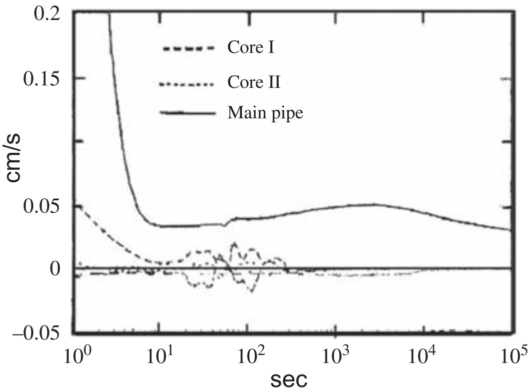

**Figure 11.56** Fuel salt flow under natural circulation in the MSR (Mitachi et al., 1998).

when salt circulation stops, and it causes the same effect as positive reactivity insertion. This is because normally some of the delayed neutrons are lost out of the core; for example, about 10% for FUJI-U3 case, and about 40% for MSBR design case. However, owing to the negative reactivity coefficient, its consequence is not as severe as pump seizure accident as is described below. In this pump trip accident case, control rods are inserted and nuclear fissions stop. In this situation, since pump has a free rotation, natural circulation is expected, as is shown in Fig. 11.56 (Mitachi et al., 1998). Installing a small motor (pony motor driven by battery, if possible) to the fuel salt pump is effective, as is demonstrated in the Japanese FBR "Monju."

#### 11.5.3.2.2 Pump seizure accident

If the pump shaft is stuck, a more severe situation than the above pump trip accident occurs. Because fuel salt flow becomes almost zero in a short time, and core-cooling function is lost, the fuel salt temperature increases. Therefore, numerical evaluation is required. Based on the preliminary evaluation for all fuel salt pumps seizure accident, even if control rods are not scrammed, maximum fuel salt temperature reaches about 900°C after 300 seconds, as is shown in Fig. 11.57 (Shimazu, 1978a). In the actual case that control rods are scrammed, the consequence will be milder than this result. If this happens in all fuel salt pumps, the fuel salt must be drained to a drain tank.

#### 11.5.3.2.3 Flow blockage accident

If blockage occurs anywhere in the primary loops, fuel salt flow stops. The consequence is similar to a pump trip/seizure accident. Total mechanical blockage is incredible, and in the case that 20 flow channels are blocked among totally 100 flow channels, the result is shown in Fig. 11.58 (Yamamoto et al., 2005). Another possible cause may be fuel salt freeze accident, which is discussed later.

#### 11.5.3.2.4 Loss of secondary salt cooling accident

If a secondary salt pump trips or pump seizure occurs, the fuel salt is not cooled, and then the fuel salt temperature increases. In some severe cases, the fuel salt must

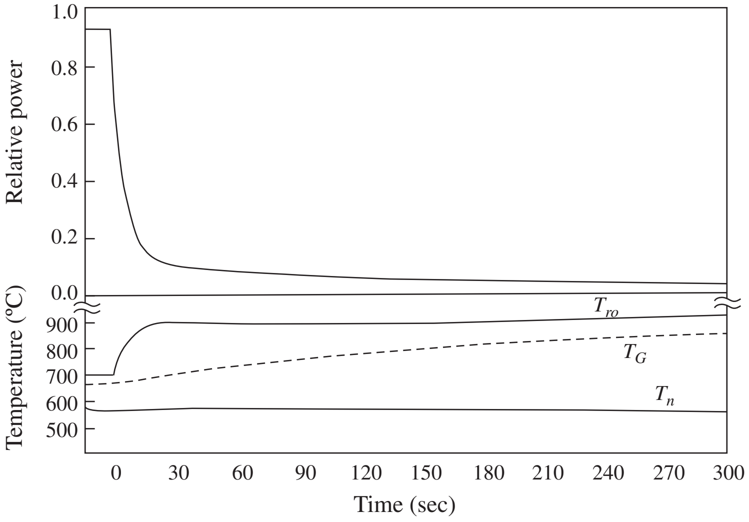

**Figure 11.57** Pump seizure accident in MSBR (Shimazu, 1978a).

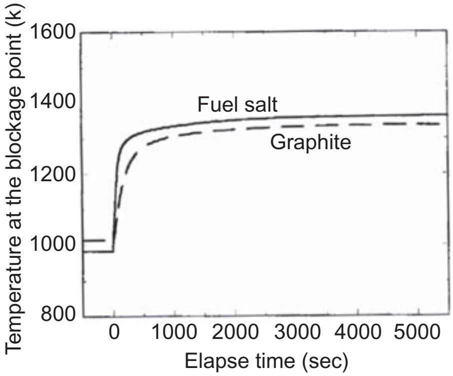

**Figure 11.58** Flow blockage accident in the MSR (Yamamoto et al., 2005).

be drained to a drain tank. Loss of secondary salt cooling will occur in other scenarios, such as rupture or break of the secondary salt loop, or SG loop failure, and then the same situation will occur.

### 11.5.3.2.5 Loss of decay heat cooling accident (in core)

After the reactor is shut down, the fuel salt must be cooled, because it has decay heat. This function is required in any cases, as long as the fuel salt stays in the core. Therefore, an appropriate decay heat cooling system must be equipped, unless fuel salt is not drained. As is shown in Fig. 11.56, the natural circulation can be utilized for this purpose.

#### 11.5.3.2.6 Loss of decay heat cooling accident (in drain tank)

If fuel salt is drained to a drain tank, the fuel salt must be cooled there. Therefore, cooling function must be provided for a drain tank. The MSBR proposed a passive cooling system for the drain tank (Robertson, 1971).

### *11.5.3.3 Fuel salt leak accident*

#### 11.5.3.3.1 Primary loop break accident

If rupture or break of primary loop boundary such as vessel, pipes, pumps, HXs occurs for some reason, then the integrity of the primary loop boundary is lost, and the fuel salt will leak out. Of course, leaked salt is caught by a catch-pan, and collected in a drain tank or an emergency drain tank without passing a freeze valve, as is shown in Fig. 11.59 (Robertson, 1971). Regarding the rupture of the HX, mixing of the fuel salt and secondary salt must be evaluated. The causes of these accidents may be a manufacturing flaw, excessive increase of boundary temperature, pressure increase by sudden boiling, corrosion, thermal stress cycling, and so on.

### *11.5.3.4 Other accidents*

#### 11.5.3.4.1 Steam-generator break accident

As is described at first, the vapor pressure of the molten salt is very low, and an overpressure accident is incredible. The only one exception is a SG break accident. The MSR uses a supercritical SG, and its pressure is about 25 MPa, and higher than

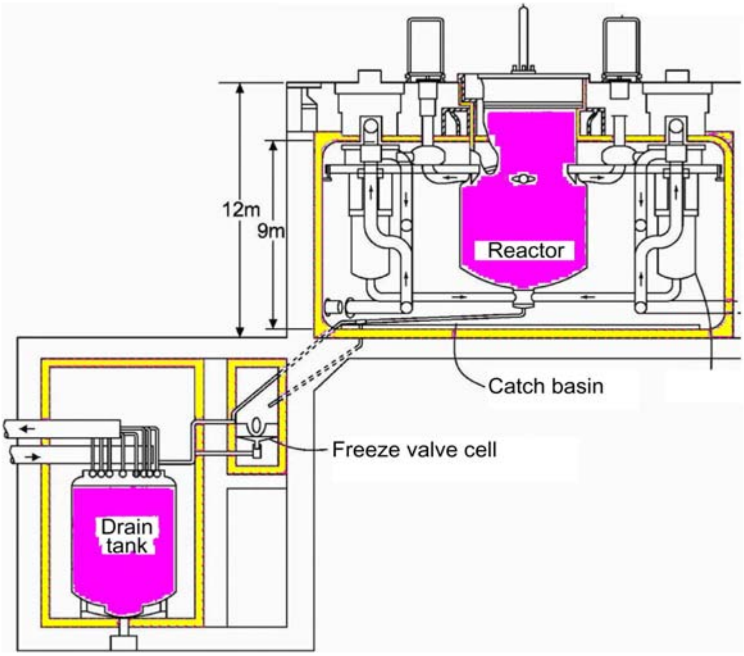

**Figure 11.59** Freeze valve and drain tank in MSBR (Robertson, 1971).

the LWR case of about 7 MPa. If the SG breaks, this high-pressure steam is injected into the secondary loop. In order to avoid the propagation to the primary loop, appropriate protection systems must be equipped, such as an isolation valve or rupture disc.

#### 11.5.3.4.2 Recriticality accident in drain tank

Since there is no graphite as a neutron moderator in a drain tank, a recriticality accident is incredible. A possible cause may be isolation or precipitation of fissile material.

#### 11.5.3.4.3 Fuel salt freeze accident

The volume of frozen fuel salt (at 20°C) is about 15% lower than that of molten fuel salt (at 600°C), mostly due to the thermal expansion property of fuel salt. For example, the formula for the density of typical fuel salt is [3.628 g/cc − 0.00066 × Temp (°C)] (Cantor, 1968). Therefore, even if freezing occurs, it does not cause pipe break. Also, since the primary loop is within the HTC (see Figs. 11.59 and 11.62), which is heated higher than freezing temperature of fuel salt, fuel salt freezing is incredible to occur. Of course, malfunction of the heating system at HTC is to be considered, although this event will be gradual.

The most probable scenario is fuel salt freezing at the HX, because the inlet temperature of secondary salt (c. 450°C) is lower than the freezing temperature of the fuel salt (c. 500°C). If one of the fuel salt pumps stops but the secondary salt pump does not stop, then fuel salt is overcooled, and starts freezing at the HX (a kind of "overcool" accident). This situation is similar to the above flow blockage accident.

In some cases, the fuel salt must be drained to a drain tank. However, opening the freeze valve may take 5−10 minutes, if there is no heater to hasten melting of fuel salt at the freeze valve. Therefore, faster mechanical valve or rupture disc may be required. Salt freezing may occur at the drain tank, as is shown in Fig. 11.60 (Williams, 1999).

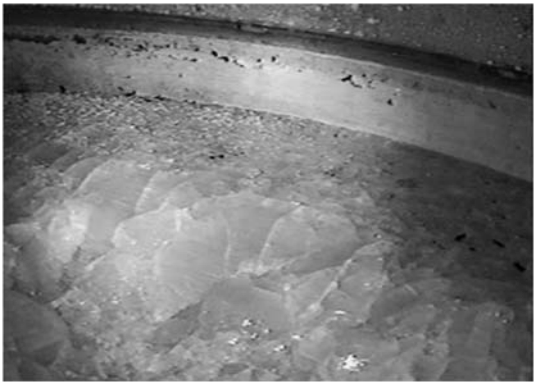

**Figure 11.60** Frozen salt (FLiBe in the MSRE tank) (Williams, 1999).

#### 11.5.3.4.4 Secondary salt freeze accident

An accident similar to the fuel salt freeze accident (see above) may occur in the secondary loop. If the reactor is shut down and its power decreases, but the SG does not stop, then secondary salt is overcooled and will freeze (a kind of "overcool" accident). The actual consequence must be evaluated, and in some severe cases fuel salt must be drained to a drain tank.

#### 11.5.3.4.5 Remelt accident

The volume of molten fuel salt (at 600°C) is about 15% higher than that of a solid one (at 20°C), mostly due to thermal expansion of fuel salt (Cantor, 1968). Therefore, careful remelting is required to avoid unexpected pressure/stress increase in pipes or in tanks. This may happen on secondary salt loops too. Therefore, safety design must be described in the safety report for licensing.

#### 11.5.3.4.6 Freeze valve failure accident

Opening the freeze valve is just to switch off a valve cooling system. Therefore, the failure probability of the freeze valve is very low, but it is not zero. Since the freeze valve is the last countermeasure to keep the integrity of primary loop boundary, some verification is required, and/or faster mechanical valve or rupture disc may be required.

#### 11.5.3.4.7 Graphite fire accident

It is incredible that graphite fire occurs in the MSR. Because reactor-grade graphite has a high density it does not burn without continuous external heat. In the MSR, there is no heat source near the graphite, after the fuel salt is transferred to a drain/ emergency tank. Also, there is no oxygen within the reactor vessel and containment, because it is filled with inert gas.

#### 11.5.3.4.8 Wigner effect accident

Another cause of graphite fire is known as the Wigner effect, which was discovered by Eugene P. Wigner (the first research director of ORNL), and the Windscale fire accident occurred in 1957 (Windscale fire, 2015). However, the Wigner effect occurs only at low-temperature operation ($< 200°C$), and the MSR operates at higher temperature ($> 500°C$) than this effect. Therefore, there is no possibility of a Windscale-type fire.

#### 11.5.3.4.9 Off-gas system failure accident

Gaseous fission products (FP) such as xenon/krypton/tritium, as shown in Table 11.12 (Robertson, 1971), are removed from fuel salt and collected in normal operation of the MSR. Therefore, it must be confirmed which FPs will be collected by the FP gas removal system, and these FPs must be confined in secure tanks for sufficient decay periods.

#### 11.5.3.4.10 Reactor oscillation accident

Safety guidelines require that the reactor can be operated with enough stability, because reactor oscillation may occur even if the reactivity coefficient is negative.

**Table 11.12** Gaseous FPs to be considered (Robertson, 1971)

| Nuclides | Half-life of decay |
|---|---|
| $^{3}H$ | 12 years |
| $^{133}Xe$ | 5.3 days |
| $^{135}Xe$ | 9.1 h |
| $^{137}Xe$ | 4.2 min |
| $^{138}Xe$ | 17 min |
| $^{85}Kr$ | 11 years |
| $^{87}Kr$ | 1.3 h |
| $^{88}Kr$ | 2.8 h |
| $^{89}Kr$ | 3.2 min |

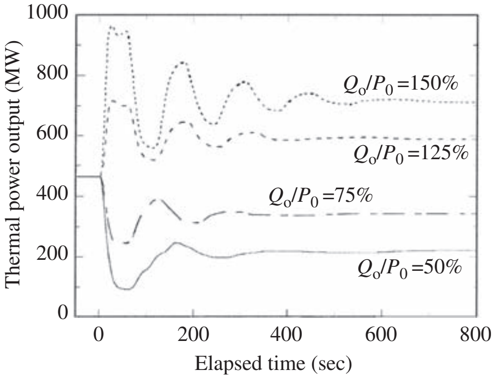

**Figure 11.61** Reactor power behavior for core flow change (Yamamoto et al., 2006a).

One example is xenon oscillations in a PWR (Iodine Pit Issue, 2015), and another is flow instability in a BWR (US-NRC, 1988).

Gaseous FPs such as Xe/Kr are always removed from the core in the MSR, and xenon oscillations do not occur.

A preliminary study on MSR controllability, which is shown in Fig. 11.61, suggests that the core can be stabilized within several minutes, when reactor power is changed by core flow from 100% to 50/75/125/150% (Yamamoto et al., 2006a). However, wider analysis must be performed based on reactor control design.

#### 11.5.3.4.11 Fuel salt or beryllium release accident

Any radioactive isotopes in fuel salt are toxic to human health, and also beryllium (Be) in fuel salt has chemical toxicity. As was explained above (primary loop break accident), if there is a leak of fuel salt, it is collected in a drain tank, and finally it freezes (solidifies) to a glassy material. In any case, the fuel salt will be confined within the containment. Therefore, release of radioactive elements of fuel salt or Be to outside of the RB is incredible, but it must be confirmed.

#### 11.5.3.4.12 Rupture of containment accident

MSR has three-level containment safety, as proposed in the MSBR design and shown in Fig. 11.62 (Furukawa et al., 2008; Yoshioka, 2013).

1. The first level is a reactor vessel and pipes made of Hastelloy N.
2. The second level is a HTC composed of three layers, which contains a reactor vessel, pipes, and HXs.
3. The third level is a RB composed of two layers.

In any of the above accidents, HTC and RB prevent or mitigate radioactivity release. Based on the above scenarios, loss of HTC/RB integrity is incredible, but possible damages on HTC/RB must be evaluated in each accident analysis. As is explained in Section 11.5.2, HTC and RB are identified as a part of the MS, whose failure does not initiate an accident, but its mitigation capability must be evaluated.

#### 11.5.3.4.13 Source term issue

The source term issue is considered to be not required in the MSR at this moment because of the following reason.

Based on the NRC definition, "source term" is "Types and amounts of radioactive or hazardous material released to the environment following an accident." In order to evaluate the source term, it is necessary to assume in the accident scenarios how the radioactive materials in nuclear fuel are discharged to outside of the reactor. For example, types of radioactive materials if they are gas or solid, or liquid, initiating events of accidents, effectiveness of defense barriers, MSs, and so on, must be assumed. In LWRs, some amount of radioactive material is discharged to the environment in DBAs, and large amounts of radioactive materials are discharged in SA (Soffer et al., 1995).

In the MSR, there will be no release of radioactive materials to the environment in DBAs, except the failure accident of an off-gas system. Based on the above

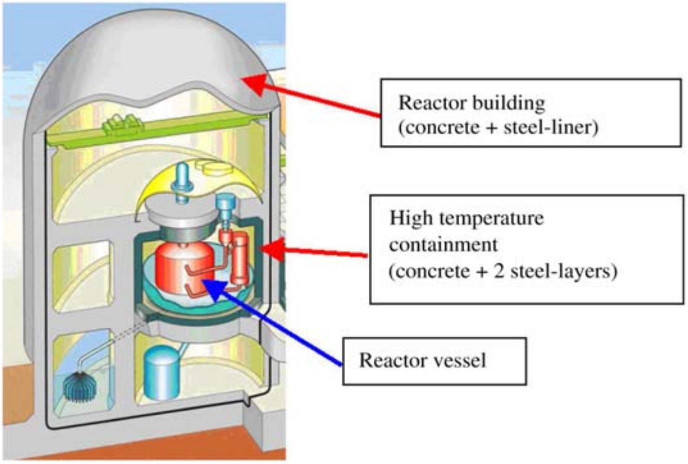

**Figure 11.62** Containment function of the MSR (part of Fig. 11.32).

preliminary evaluations for internal cause accidents such as a pipe break accident, rupture of containment is incredible to occur, and hence there will be no release of radioactive material to the environment in DBAs.

As for the "station blackout" (loss of all AC electric power), passive cooling system, which does not need electricity, is proposed for drain tank cooling (Robertson, 1971; Ishiguro et al., 2014).

As a result, simultaneous loss of cooling function and containment function will not occur in the MSR, except by severe external causes. In current LWR licensing, these external cause accidents by terrorism or missiles are categorized as SA, and the only requirement as DBA is the aircraft attack consideration (see Item 92 of Section 11.6). Since this section describes only AOT and DBA and does not refer SA, it is not required to include the source term issue in DBA for the MSR.

Although the source term issue is not required at this moment, a preliminary prospect on simultaneous loss of both the cooling function and the containment function is discussed in this section, because unfortunately this happened at the Fukushima accident in 2011.

In the MSR, since gaseous FPs such as Xe and Kr are always removed from the fuel salt, instantaneous release of radioactive materials will not occur even with simultaneous failure of reactor vessels/pipes and containment. In this scenario, the fuel salt is liquid, and most of the radioactive materials will stay within the fuel salt in ionic form, but their behavior must be confirmed. Some of them, such as iodine and cesium, which were dominant source terms at the Fukushima accident, are described in the ORNL report (Haubenreich and Engel, 1962). After decay heat decreases, fuel salt solidifies and all radioactive materials will be confined.

In this section, online reprocessing is not adopted, but if it is included in the design, the above discussion must include its safety, as is discussed in Gat et al. (1993).

### 11.5.4 Summary

In order to perform the MSR accident analysis and to establish guidelines for this analysis, the authors showed 40 possible accidents for the MSR. They were classified as external cause accidents and internal cause accidents. We investigated the internal ones and categorized them into four types: power excursion accident, flow decrease accident, fuel salt leak accident, and other accidents mostly specific to the MSR. Each accident was described briefly with some numerical results. In several accidental scenarios, fuel salt must be transferred to a drain tank, and this system assures high safety of the MSR. However, its consequence depends on the freeze valve function, because its operation is slow, and this means that some verification is required. Also, some other accidents need quantitative evaluation. As for the source term issue, it is not required to be included at the moment, but a preliminary prospect for future study was discussed.

These results may be varied for different designs, and should be improved depending on the progress of design. Also, PRA is required at the detail design stage (US-NRC, 2014c).

After completion of these evaluations it can be concluded that the MSR has superior safety, and that the MSR has an intrinsic safety (Yoshioka et al., 2014).

## 11.6 General design criteria for MSR design

This GDC document is a draft of safety guidelines for MSR design, and it is not authorized yet. This GDC is based on the current GDC draft for FHR, which is modified from the GDC for LWR. The GDC for FHR is now being established in the framework of the American Nuclear Society (Flanagan, 2012; ANS 20.1 working group, 2014). We are proposing the following GDC for MSR, but these provisions will be revised in the future. Especially the *italic* part of the following provisions are modified or added by the authors for the MSR or for recent licensing requirements/movements. MSR safety shall be designed based on the following provisions, where "shall" means mandatory requirement by the licensing authority, and "should" means recommendations and voluntary for licensing applicants.

### *11.6.1 Overall requirements*

#### *1. Quality standards and records*

Structures, systems, and components (SSCs) important to safety shall be designed, fabricated, erected, and tested to quality standards commensurate with the importance of the safety functions to be performed. Where generally recognized codes and standards are used, they shall be identified and evaluated to determine their applicability, adequacy, and sufficiency and shall be supplemented or modified as necessary to assure a quality product in keeping with the required safety function. A quality assurance program shall be established and implemented in order to provide adequate assurance that these SSCs will satisfactorily perform their safety functions. Appropriate records of the design, fabrication, erection, and testing of SSCs important to safety shall be maintained by or under the control of the nuclear power unit licensee throughout the life of the unit.

#### *2. Design bases for protection against natural phenomena*

SSCs important to safety shall be designed to withstand the effects of natural phenomena such as earthquakes, tornadoes, hurricanes, fires, floods, tsunami, and seiches without loss of capability to perform their safety functions. The design bases for these SSCs shall reflect: (1) Appropriate consideration of the most severe of the natural phenomena that have been historically reported for the site and surrounding area, with sufficient margin for the limited accuracy, quantity, and period of time in which the historical data have been accumulated, (2) appropriate combinations of the effects of normal and accident conditions with the effects of the natural phenomena and (3) the importance of the safety functions to be performed.

*As for the earthquake, the maximum earthquake shall be estimated not only by historic data but also by possible future prediction. Tsunami shall be evaluated based on these evaluations.*

### 3. Fire protection

SSCs important to safety shall be designed and located to minimize, consistent with other safety requirements, the probability and effect of fires and explosions. Noncombustible and heat-resistant materials shall be used wherever practical throughout the unit, particularly in locations such as the containment and control room. Fire detection and fighting systems of appropriate capacity and capability shall be provided and designed to minimize the adverse effects of fires on SSCs important to safety. Firefighting systems shall be designed to assure that their rupture or inadvertent operation does not significantly impair the safety capability of these SSCs.

*If graphite is used in the reactor, protection against graphite fire shall be considered.*

### 4. Environmental and dynamic effects design bases

SSCs important to safety shall be designed to accommodate the effects of and to be compatible with the environmental conditions associated with normal operation, maintenance, testing, and postulated accidents. These SSCs shall be appropriately protected against dynamic effects, including the effects of missiles, pipe whipping, and discharging fluids, that may result from equipment failures and from events and conditions outside the nuclear power unit. However, dynamic effects associated with postulated pipe ruptures in nuclear power units may be excluded from the design basis when analyses reviewed and approved by the NRC demonstrate that the probability of fluid system piping rupture is extremely low under conditions consistent with the design basis for the piping.

### 5. Sharing of structures, systems, and components

SSCs important to safety shall not be shared among nuclear power units unless it can be shown that such sharing will not significantly impair their ability to perform their safety functions, including, in the event of an accident in one unit, an orderly shutdown and cooldown of the remaining units.

## 11.6.2 Protection by multiple fission product barriers

### 10. Reactor design

The reactor core and associated coolant, control, and protection systems shall be designed with appropriate margin to assure that specified acceptable fuel design limits are not exceeded during any condition of normal operation, and in anticipated operational occurrences (AOOs).

*The above acceptable fuel design limits shall be determined as the limits, below which fuel failure does not occur. In this process, statistical evaluation can be used.*

*The reactor core shall maintain both shutdown capability and coolable geometry, during normal operation, AOOs, and DBAs.*

## 11. Reactor inherent protection

The reactor core and associated systems that contribute to reactivity feedback shall be designed so that *in any operating range* the net effect of the prompt inherent nuclear feedback characteristics tends to compensate for a rapid increase in reactivity.

## 12. Suppression of reactor power oscillations

The reactor core and associated coolant, control, and protection systems shall be designed to assure that power oscillations which can result in conditions exceeding specified acceptable fuel design limits are not possible or can be reliably and readily detected and suppressed.

## 13. Instrumentation and control

Instrumentation shall be provided to monitor variables and systems over their anticipated ranges for normal operation, for AOOs, and for accident conditions as appropriate to assure adequate safety, including those variables and systems that can affect the fission process, the integrity of the reactor core, the reactor coolant pressure boundary, and the containment and its associated systems. Appropriate controls shall be provided to maintain these variables and systems within prescribed operating ranges.

## 14. Reactor primary coolant boundary

The reactor primary coolant boundary shall be designed, fabricated, erected, and tested so as to have an extremely low probability of abnormal leakage, of rapidly propagating failure, and of gross rupture.

*In addition, if the reactor is equipped with a drain tank connecting to reactor coolant, then the drain tank and connecting pipes shall be regarded as reactor coolant boundary.*

## 15. Reactor primary coolant system design

The reactor primary coolant system and associated auxiliary, control, and protection systems shall be designed with sufficient margin to assure that the design conditions of the reactor primary coolant boundary are not exceeded during any condition of normal operation, including AOOs.

## 16. Containment design

*No. 16 is not used, because containment design is described at No. 50—55 in detail.*

## *17. Electric power systems*

An onsite electric power system and an offsite electric power system shall be provided, if required, to permit functioning of safety-related SSCs. The nuclear safety function for each system (assuming the other system is not functioning) shall be to provide sufficient capacity and capability to assure that (1) specified acceptable fuel design limits and design conditions of the reactor coolant boundary are not exceeded as a result of AOOs and (2) the core is cooled and containment integrity and other safety-related vital functions are maintained in the event of postulated accidents.

If onsite electric power supplies, including the batteries, and the onsite electric distribution system, are required to permit functioning of safety-related SSCs, they shall have sufficient independence, redundancy, and testability to perform their nuclear safety functions assuming a single failure.

If electric power from the transmission network to the onsite electric distribution system is required to permit functioning of safety-related SSCs, it shall be supplied by two physically independent circuits (not necessarily on separate rights of way) designed and located so as to minimize to the extent practical the likelihood of their simultaneous failure under operating and postulated accident and environmental conditions. A switchyard common to both circuits is acceptable. Each of these circuits shall be designed to be available in sufficient time following a loss of all onsite alternating current power supplies and the other offsite electric power circuit, to assure that specified acceptable fuel design limits and design conditions of the reactor coolant boundary are not exceeded, and that other safety-related functions are maintained.

Provisions shall be included to minimize the probability of losing electric power from any of the remaining supplies as a result of, or coincident with, the loss of power generated by the nuclear power unit, the loss of power from the transmission network, or the loss of power from the onsite electric power supplies.

## *18. Inspection and testing of electric power systems*

Electric power systems important to safety shall be designed to permit appropriate periodic inspection and testing of important areas and features, such as wiring, insulation, connections, and switchboards, to assess the continuity of the systems and the condition of their components. The systems shall be designed with a capability to test periodically (1) the operability and functional performance of the components of the systems, such as onsite power sources, relays, switches, and buses, and (2) the operability of the systems as a whole and, under conditions as close to design as practical, the full operation sequence that brings the systems into operation, including operation of applicable portions of the protection system, and the transfer of power among systems.

## *19. Control room*

A control room shall be provided from which actions can be taken to operate the nuclear power unit safely under normal conditions and to maintain it in a safe condition under accident conditions. Adequate radiation protection shall be provided to permit access and occupancy of the control room under accident conditions without personnel receiving radiation exposures in excess of 5 rem total effective dose equivalent (TEDE), for the duration of the accident.

Adequate habitability measures shall be provided to permit access and occupancy of the control room during normal operations and under accident conditions.

Equipment at appropriate locations outside the control room shall be provided (1) with a design capability for prompt hot shutdown of the reactor, including necessary instrumentation and controls to maintain the unit in a safe condition during *hot shutdown*, and (2) with a potential capability for subsequent *cold shutdown* of the reactor through the use of suitable procedures.

*Cold shutdown and hot shutdown shall be defined, if molten salt is used.*

## 11.6.3 Protection and reactivity control systems

### 20. Protection system functions

The protection system shall be designed (1) to initiate automatically the operation of appropriate systems including the reactivity control systems, to assure that specified acceptable fuel design limits are not exceeded as a result of AOOs and (2) to sense accident conditions and to initiate the operation of systems and components important to safety.

### 21. Protection system reliability and testability

The protection system shall be designed for high functional reliability and inservice testability commensurate with the safety functions to be performed. Redundancy and independence designed into the protection system shall be sufficient to assure that (1) no single failure results in loss of the protection function and (2) removal from service of any component or channel does not result in loss of the required minimum redundancy unless the acceptable reliability of operation of the protection system can be otherwise demonstrated. The protection system shall be designed to permit periodic testing of its functioning when the reactor is in operation, including a capability to test channels independently to determine failures and losses of redundancy that may have occurred.

### 22. Protection system independence

The protection system shall be designed to assure that the effects of natural phenomena, and of normal operating, maintenance, testing, and postulated accident conditions on redundant channels do not result in loss of the protection function, or shall be demonstrated to be acceptable on some other defined basis. Design techniques, such as functional diversity or diversity in component design and principles of operation, shall be used to the extent practical to prevent loss of the protection function.

## *23. Protection system failure modes*

The protection system shall be designed to fail into a safe state or into a state demonstrated to be acceptable on some other defined basis if conditions such as disconnection of the system, loss of energy (e.g., electric power, instrument air), or postulated adverse environments (e.g., extreme heat or cold, fire, pressure, steam, water, and radiation) are experienced.

## *24. Separation of protection and control systems*

The protection system shall be separated from control systems to the extent that failure of any single control system component or channel, or failure or removal from service of any single protection system component or channel which is common to the control and protection systems leaves intact a system satisfying all reliability, redundancy, and independence requirements of the protection system. Interconnection of the protection and control systems shall be limited so as to assure that safety is not significantly impaired.

## *25. Protection system requirements for reactivity control malfunctions*

The protection system shall be designed to assure that specified acceptable fuel design limits are not exceeded *for the initiating event of single active component failure or of single operator error*, such as accidental withdrawal (not ejection or dropout) of control rods.

## *26. Reactivity control redundancy and capability*

Two independent reactivity control systems of different design principles shall be provided. One of the systems shall use control rods, preferably including a positive means for inserting the rods, and shall be capable of reliably controlling reactivity changes to assure that under conditions of normal operation, including AOOs, and with appropriate margin *for single control rod stuck or for single malfunction of grouped control rods*, specified acceptable fuel design limits are not exceeded. A second reactivity control system shall be capable of reliably controlling the rate of reactivity changes resulting from planned, normal power changes (including xenon burnout) to assure acceptable fuel design limits are not exceeded. One of the systems shall be capable of holding the reactor core subcritical under *cold conditions*.

*Cold condition shall be defined, if molten salt is used.*

## *27. Combined reactivity control systems capability*

The reactivity control systems shall be designed to have a combined capability *with emergency cooling system or RHR system* of reliably controlling reactivity changes to assure that under postulated accident conditions and with appropriate margin for stuck rods the capability to cool the core is maintained.

## *28. Reactivity limits*

The reactivity control systems shall be designed with appropriate limits on the potential amount and rate of reactivity increase to assure that the effects of postulated reactivity accidents can neither (1) result in damage to the reactor primary coolant boundary greater than limited local yielding nor (2) sufficiently disturb the core, its support structures, or other reactor vessel internals to impair significantly the capability to cool the core. These postulated reactivity accidents shall include consideration of *control rod ejection (unless prevented by positive means)*, changes in reactor coolant temperature, and changes in power/flow rates.

## *29. Protection against anticipated operational occurrences*

The protection and reactivity control systems shall be designed to assure an extremely high probability of accomplishing their safety functions in the event of AOOs.

## *11.6.4 Fluid systems*

## *30. Quality of reactor primary coolant boundary*

Components which are part of the reactor primary coolant boundary shall be designed, fabricated, erected, and tested to the highest quality standards practical. Means shall be provided for detecting and, to the extent practical, identifying the location of the source of reactor coolant leakage.

## *31. Fracture prevention of reactor primary coolant boundary*

The reactor primary coolant boundary shall be designed with sufficient margin to assure that when stressed under operating, maintenance, testing, and postulated accident conditions (1) the boundary behaves in a nonbrittle manner and (2) the probability of rapidly propagating fracture is minimized. The design shall reflect consideration of service temperatures, service degradation of material properties, creep, fatigue, stress rupture, and other conditions of the boundary material under operating, maintenance, testing, and postulated accident conditions and the uncertainties in determining (1) material properties, (2) the effects of irradiation on material properties, (3) residual, steady state and transient stresses, and (4) size of flaws.

## *32. Inspection reactor primary coolant boundary*

Components which are part of the reactor primary coolant boundary shall be designed to permit (1) periodic inspection and testing of important areas and features to assess their structural and leaktight integrity, and (2) an appropriate material surveillance program for the reactor vessel.

### 33. Reactor primary coolant inventory maintenance

A system to maintain reactor coolant inventory for protection against small breaks in the reactor primary coolant boundary shall be provided as necessary to assure that specified acceptable fuel design limits are not exceeded as a result of reactor inventory loss due to leakage from the reactor primary coolant boundary and rupture of small piping or other small components which are part of the boundary.

*If the reactor is equipped with a guard vessel, it shall be confirmed that the primary coolant inventory is maintained after a primary boundary break.*

### 34. Residual heat removal

A system to remove residual heat shall be provided. The system safety function shall be to transfer FP decay heat and other residual heat from the reactor core to an ultimate heat sink at a rate such that specified acceptable fuel design limits and the design conditions of the reactor primary coolant boundary are not exceeded under all plant shutdown conditions following normal operation, including AOOs, and to provide continuous effective core cooling during postulated accidents.

Suitable redundancy in components and features, and suitable interconnections, leak detection, and isolation capabilities shall be provided to assure that the system safety function can be accomplished, assuming a single failure.

### 35. Emergency core cooling

Emergency core cooling is not applicable to the MSR. the MSR design criterion for core cooling under accident conditions is contained in Criterion 34.

### 36. Inspection of residual heat removal system

The residual heat removal system shall be designed to permit appropriate periodic inspection of important components, such as HXs and piping, to assure the integrity and capability of the system.

### 37. Testing of residual heat removal system

The residual heat removal system shall be designed to permit appropriate periodic functional testing to assure (1) the structural integrity of its components, (2) the operability and performance of the system components, and (3) the operability of the system as a whole and, under conditions as close to design as practical, the performance of the full operational sequence that brings the system into operation, including operation of associated systems and interfaces with an ultimate heat sink.

### 38. Containment heat removal

A system to remove heat from the reactor containment shall be provided as necessary to maintain the containment pressure and temperature within acceptable limits following postulated accidents.

Suitable redundancy in components and features, and suitable interconnections, leak detection, isolation, and containment capabilities shall be provided to assure that the system safety function can be accomplished, assuming a single failure.

### *39. Inspection of containment heat removal system*

The containment heat removal system shall be designed to permit appropriate periodic inspection of important components, such as piping to assure the integrity and capability of the system.

### *40. Testing of containment heat removal system*

The containment heat removal system shall be designed to permit appropriate periodic functional testing to assure (1) the structural integrity of its components, (2) the operability and performance of the system components, and (3) the operability of the system as a whole, and under conditions as close to the design as practical, the performance of the full operational sequence that brings the system into operation, including operation of associated systems.

### *41. Containment atmosphere cleanup*

Systems to control FPs, hydrogen, oxygen, and other substances which may be released into the reactor containment shall be provided as necessary to reduce, consistent with the functioning of other associated systems, the concentration and quality of FPs released to the environment following postulated accidents, and to control the concentration of hydrogen or oxygen and other substances in the containment atmosphere following postulated accidents to assure that containment integrity is maintained.

Each system shall have suitable redundancy in components and features, and suitable interconnections, leak detection, isolation, and containment capabilities to assure that its safety function can be accomplished, assuming a single failure.

### *42. Inspection of containment atmosphere cleanup systems*

The containment atmosphere cleanup systems shall be designed to permit appropriate periodic inspection of important components, such as filter frames, ducts, and piping to assure the integrity and capability of the systems.

### *43. Testing of containment atmosphere cleanup systems*

The containment atmosphere cleanup systems shall be designed to permit appropriate periodic functional testing to assure (1) the structural integrity of its components, (2) the operability and performance of the system components, and (3) the operability of the systems as a whole and, under conditions as close to design as practical, the performance of the full operational sequence that brings the systems into operation, including the operation of associated systems.

### 44. Structural and equipment cooling

In addition to the heat rejection capability of the residual heat removal system, systems to transfer heat from SSCs important to safety, to an ultimate heat sink shall be provided, as necessary to transfer the combined heat load of these SSCs under normal operating and accident conditions.

Suitable redundancy in components and features, and suitable interconnections, leak detection, and isolation capabilities shall be provided to assure that each system safety function can be accomplished, assuming a single failure.

### 45. Inspection of structural and equipment cooling systems

The structural and equipment cooling systems shall be designed to permit appropriate periodic inspection of important components, such as HXs and piping, to assure the integrity and capability of the systems.

### 46. Testing of structural and equipment cooling systems

The structural and equipment cooling systems shall be designed to permit appropriate periodic functional testing to assure (1) the structural integrity of their components, (2) the operability and the performance of the system components, and (3) the operability of the systems as a whole and, under conditions as close to design as practical, the performance of the full operational sequences that bring the systems into operation for reactor shutdown and postulated accidents, including operation of associated systems.

## 11.6.5 Reactor containment

### 50. Containment structure design basis

The reactor containment structure, including access openings, penetrations, and the containment heat removal system shall be designed so that the containment structure and its internal compartments can accommodate, without exceeding the design leakage rate and with sufficient margin, the calculated pressure and temperature conditions resulting from postulated accidents. This margin shall reflect consideration of (1) the effects of potential energy sources which have not been included in the determination of the peak conditions, (2) the limited experience and experimental data available for defining accident phenomena and containment responses, and (3) the conservatism of the calculational model and input parameters.

### 51. Fracture prevention of containment boundary

The boundary of the reactor containment structure shall be designed with sufficient margin to assure that under operating, maintenance, testing, and postulated accident conditions (1) its materials behave in a nonbrittle manner and (2) the probability of rapidly propagating fracture is minimized. The design shall reflect consideration of service temperatures and other conditions of the containment boundary materials during operation, maintenance, testing, and postulated accident conditions, and the uncertainties in determining (1) material properties, (2) residual, steady state, and transient stresses, and (3) size of flaws.

## 52. Capability for containment leakage rate testing

The reactor containment structure and other equipment which may be subjected to containment test conditions shall be designed so that periodic integrated leakage rate testing can be conducted at containment design pressure.

## 53. Provisions for containment testing and inspection

The reactor containment structure shall be designed to permit (1) appropriate periodic inspection of all important areas, such as penetrations, (2) an appropriate surveillance program, and (3) periodic testing at containment design pressure of the leaktightness of penetrations which have resilient seals and expansion bellows.

## 54. Piping systems penetrating containment

Piping systems penetrating the primary reactor containment structure shall be provided with leak detection, isolation, and containment capabilities having redundancy, reliability, and performance capabilities necessary to perform the containment safety function and which reflect the importance to safety of preventing radioactivity releases from containment through these piping systems. When isolation valves are required, piping systems shall be designed with a capability to test periodically the operability of the isolation valves and associated apparatus and to determine if valve leakage is within acceptable limits.

## 55. Reactor primary coolant boundary penetrating containment

Each line that is part of the reactor primary coolant boundary and that penetrates the primary reactor containment structure shall be provided with containment isolation valves as follows, unless it can be demonstrated that the containment isolation provisions for a specific class of lines, such as instrument lines, are acceptable on some other defined basis:

1. One locked closed isolation valve inside and one locked closed isolation valve outside containment; or
2. One automatic isolation valve inside and one locked closed isolation valve outside containment; or
3. One locked closed isolation valve inside and one automatic isolation valve outside containment. A simple check valve may not be used as the automatic isolation valve outside containment; or
4. One automatic isolation valve inside and one automatic isolation valve outside containment. A simple check valve may not be used as the automatic isolation valve outside containment.

Isolation valves outside containment shall be located as close to containment as practical and upon loss of actuating power, automatic isolation valves shall be designed to take the position that provide greater safety.

Other appropriate requirements to minimize the probability or consequences of an accidental rupture of these lines or of lines connected to them shall be provided as necessary to assure adequate safety. Determination of the appropriateness of these requirements, such as higher quality in design, fabrication, and testing, additional provisions for inservice inspection, protection against more severe natural phenomena, and additional isolation valves and containment, shall include consideration of the population density, use characteristics, and physical characteristics of the site environs.

*The isolation valve for large-sized pipe, which penetrates containment boundary, shall be equipped, in order to protect the leak of reactor coolant to the outside of containment, for example at the steam generator break accident.*

## 56. Primary containment isolation

Each line that connects directly to the containment atmosphere and penetrates the primary reactor containment structure shall be provided with containment isolation valves as follows, unless it can be demonstrated that the containment isolation provisions for a specific class of lines, such as instrument lines, are acceptable on some other defined basis:

1. One locked closed isolation valve inside and one locked closed isolation valve outside containment; or
2. One automatic isolation valve inside and one locked closed isolation valve outside containment; or
3. One locked closed isolation valve inside and one automatic isolation valve outside containment. A simple check valve may not be used as the automatic isolation valve outside containment; or
4. One automatic isolation valve inside and one automatic isolation valve outside containment. A simple check valve may not be used as the automatic isolation valve outside containment.

Isolation valves outside containment shall be located as close to the containment as practical and upon loss of actuating power, automatic isolation valves shall be designed to take the position that provides greater safety.

## 57. Closed system isolation valves

Each line that penetrates the primary reactor containment structure and is neither part of the reactor primary coolant boundary nor connected directly to the containment atmosphere shall have at least one containment isolation valve unless it can be demonstrated that the containment safety function can be met without an isolation valve and assuming failure of a single active component. The isolation valve, if required, shall be either automatic, or locked closed, or capable of remote manual operation. This valve shall be outside containment and located as close to the containment as practical. A simple check valve may not be used as the automatic isolation valve.

### *11.6.6 Fuel and radioactivity control*

#### *60. Control of releases of radioactive materials to the environment*

The nuclear power unit design shall include means to control suitably the release of radioactive materials in gaseous and liquid effluents and to handle radioactive solid wastes produced during normal reactor operation, including AOOs. Sufficient holdup capacity shall be provided for retention of gaseous and liquid effluents containing radioactive materials, particularly where unfavorable site environmental conditions can be expected to impose unusual operational limitations upon the release of such effluents to the environment.

#### *61. Fuel storage and handling and radioactivity control*

The fuel storage and handling, radioactive waste, and other systems which may contain radioactivity shall be designed to assure adequate safety under normal and postulated accident conditions. These systems shall be designed (1) with a capability to permit appropriate periodic inspection and testing of components important to safety, (2) with suitable shielding for radiation protection, (3) with appropriate containment, confinement, and filtering systems, (4) with a residual heat removal capability having reliability and testability that reflects the importance to safety of decay heat and other residual heat removal, and (5) to prevent significant reduction in fuel storage cooling under accident conditions.

#### *62. Prevention of criticality in fuel storage and handling*

Criticality in the fuel storage and handling system shall be prevented by physical systems or processes, preferably by use of geometrically safe configurations, *even if single component failure or single operator error occurs.*

#### *63. Monitoring fuel and waste storage*

Appropriate systems shall be provided in fuel storage and radioactive waste systems and associated handling areas (1) to detect conditions that may result in loss of residual heat removal capability and excessive radiation levels and (2) to initiate appropriate safety actions.

#### *64. Monitoring of radioactivity releases*

Means shall be provided for monitoring the reactor containment atmosphere, spaces containing components for primary coolant salt and cover gas cleanup and processing, effluent discharge paths, and the plant environs for radioactivity that may be released from normal operations, including AOOs, and from postulated accidents.

## *11.6.7 Salt systems and control*

### *70. Intermediate coolant systems*

If an intermediate coolant system is provided, the intermediate coolant shall be compatible with primary coolant salt (fluoride or chloride) if it is separated from the primary coolant by a single passive barrier. Where a single barrier separates the reactor primary coolant from the intermediate coolant, a pressure differential shall be maintained such that any leakage would flow from the intermediate coolant system to the reactor primary coolant system unless other provisions can be shown to be acceptable. The intermediate coolant boundary shall be designed to permit inspection and surveillance in areas where leakage can affect the safety functions of systems, structures, and components.

### *71. Reactor coolant and cover gas purity control*

*No. 71 is not used at current LWR licensing.*

### *72. Salt heating systems*

Heating systems shall be provided as necessary for systems and components important to safety, which contain or could be required to contain salt. These heating systems and their controls shall be appropriately designed to assure that the temperature distribution and rate of change of temperature in systems and components containing salt are maintained within design limits *assuming single component failure or single operator error.*

### *73. Salt receiving, storage, and processing systems*

Salt receiving, storage, and processing systems shall be designed to ensure that the safety function of systems and components important to safety is not compromised.

The receiving, storage, and processing systems shall be designed with appropriate containment, confinement, and filtering systems, and with a capability to permit appropriate periodic inspection and testing.

### *74. Salt leakage detection*

A means to detect salt leakage shall be provided as necessary to assure that the safety functions of SSCs important to safety are maintained.

### *75. Protection against salt freezing* and remelting

SSCs important to safety containing salt shall be designed, fabricated, and tested so as not to lose their structural integrity in the event of salt freezing, *and remelting*.

### 11.6.8 Other design requirements

#### 80. Aging management

The facility design shall consider the effects of aging on the performance structures and equipment important to safety. This may include provisions for inspection, testing, maintenance, replacement, condition monitoring, or sufficient allowance in the design for age-related degradation (e.g., corrosion, thermal fatigue, thermal striping, or flow-induced vibration) to ensure that the integrity of structures and equipment performance remains consistent with the assumptions in the safety analysis.

#### 81. Human factors

A Human Factors Engineering (HFE) program shall be developed and implemented for the duration of the plant life. To ensure adequate quality of the HFE products, the program should plan the HFE effort, develop HFE requirements, and integrate key expertise, accepted state-of-the-art HFE principles, lessons learned from practical experience, and accepted validation and verification procedures and testing. The HFE program should ensure that (1) the role of personnel and automation is well defined and supports plant reliability and safety performance requirements; (2) the requirements for human task performance are clearly specified; (3) the numbers of staff, their functions, and qualifications are adequate to fulfill the role of personnel; (4) the working environments (i.e., control rooms and local workstations), user interfaces (i.e., alarms, displays, controls, procedures, and other task aids), and personnel training meet task performance requirements and are designed to be consistent with human cognitive and physiological characteristics, and (5) the safety of the facility is not adversely affected by human interaction with key design features.

#### 82. Physical security/safeguards

Physical protection of the facility against malicious acts shall be considered in the design. Protection of the facility shall be accomplished by design, as much as practical, with safety and security being considered in an integrated fashion such that design and operational decisions are made in consideration of the impact each has on the other.

Design considerations shall include:

- Use of designs and layouts with proper attention to defense-in-depth principles to minimize the likelihood and consequences of malicious acts;
- Designing the layout of safety-related buildings and equipment to facilitate controlling access;
- Providing multiple layers of protection such that physical protection is not dependent upon a single design, operational, or physical security measure;
- Providing and locating (e.g., separation) redundant safety equipment such that malicious acts cannot prevent the accomplishment of key safety functions; and
- Providing barriers with sufficient structural integrity to withstand a range of external threats.

### 83. Emergency access

All areas of the plant facility that require operator actions shall be accessible and equipped with emergency lighting that will function in case of loss of the normal power supply and the emergency power supply. Access and evacuation routes will be clearly marked.

### 84. Fuel failure detection

*No. 84 is not used in current LWR licensing.*

## 11.6.9 Additional design basis accidents

### 90. Station blackout (SBO)

Consideration shall be given to the effect of station blackout on plant environment (e.g., cell temperatures), and to providing adequate instrumentation to monitor plant status for this event.

For station blackout, either (1) a means to maintain containment pressure and temperature shall be provided or (2) measures to mitigate loss of the system safety function shall be provided. An acceptable means to prevent loss of the containment safety function is to assure that containment design leakage rate is not exceeded in the event of a station blackout of a specified duration. This may be demonstrated by analyses showing that additional heat removal is not required. Consideration shall be given to providing adequate instrumentation to monitor plant status for this event.

*As for the duration of station blackout, it shall be 72 hours.*

### 91. ATWS

For ATWS, an acceptably high reliability reactivity control system or inherent reactivity feedback sufficient such that ATWS accidents do not result in excessive vessel creep shall be provided. Adequate instrumentation to monitor all critical plant variables during ATWS events shall be provided.

### 92. Aircraft impact

The design shall incorporate features and capabilities to ensure that in the event of the impact of a large commercial aircraft, that the reactor core remains cooled and that used fuel cooling is maintained.

### 93. Severe accidents

*Severe accident is becoming a mandatory requirement.*

Diverse and redundant active systems and/or passive design features should be provided to prevent accidents from escalating into SA with extensive core damage and/or significant FP release into the environment.

Countermeasures or features should be incorporated in the plant design to mitigate the accident severity in the event of the disability or failure of the plant safety systems. Consideration shall be given in the containment design for the provision of features to mitigate the consequences of SA in order to limit the release of radioactive material to the environment.

The reactor should also be designed to prevent large early release of radioactive material into the environment as a result of earthquakes, tornadoes, hurricanes, floods, fires, tsunami, and seiches, whose severity and occurrence frequencies are technically and historically nonnegligible but beyond the design basis.

### 11.6.10 Several definitions

**Anticipated Operational Occurrences (AOOs):**

*The events, which are initiated by single active component failure or single operator error, and are expected to occur at least once in the plant lifecycle.*

**Anticipated Transient Without Scram (ATWS):**

*ATWS is one of the "worst case" accidents, consideration of which frequently motivates the NRC to take regulatory action. Such an accident could happen if the scram system fails to work during an anticipated transient.*

**Beyond Design-Basis Accidents (B-DBA):**

*B-DBA is used as a technical way to discuss accident sequences that are possible but were not fully considered in the design process because they were judged to be too unlikely.*

**Design Basis Accidents (DBA):**

Postulated accidents that a nuclear facility must be designed and built to withstand without loss of the SSCs necessary to assure public health and safety. DBAs are used to establish performance requirements of safety-related SSCs.

**Station Blackout (SBO):**

*SBO means the complete loss of alternating current (AC) electric power to the essential and nonessential switchgear buses in a nuclear power plant.*

**Severe Accident:**

*A type of accident that may challenge safety systems at a level much higher than expected.*

### 11.6.11 Conclusion

MSR safety shall be designed based on the above GDC. This GDC is based on the current GDC draft for a FHR, which is modified from the GDC for LWR. The above GDC is a draft of safety guidelines for the MSR design proposed by the authors, and will be revised in the future.

## References

Alexander, L.G., 1963. Molten-salt fast reactors. *ANL-6792*.

Alexander, L.G., et al., 1959. Nuclear characteristics of spherical homogeneous two-region molten-fluoride-salt reactors. *ORNL-2751*.

ANS 20.1 working group, 2014. Nuclear safety criteria and design process for fluoride salt-cooled high-temperature reactor nuclear power plants. ANS 20.1 draft (to be published).

Beall, S.E., et al., 1964. MSRE design and operations report part-V, Reactor safety analysis report. *ORNL-TM-732*.

Bettis, E.S., et al., 1957. The aircraft reactor experiment - design and construction. Nucl. Sci. Eng. 2, 804–825.

Briant, R.C., Weinberg, A.M., 1957. Molten fluorides as power reactor fuels. Nucl. Sci. Eng. 2, 797–803.

Briggs, R.B., 1967. Summary of the objectives, the design, and a program of development of molten-salt breeder reactors (Table-17, right column). *ORNL-TM-1851*.

Bulmer, J.J., et al., 1956. Fused salt fast breeder. *ORNL-CF-56-8-20*.

Cantor, S., 1968. Physical properties of molten salt reactor fuel, coolant, and flush salts. *ORNL-TM-2316*.

Cottrell, W.B., et al., 1955. Aircraft reactor test, hazards summary Report. *ORNL-1835*.

Croff, A.G., et al., 1980. A user's manual for the ORIGEN-2 computer code. *ORNL-TM7175*.

Duderstadt, J.J., Hamilton, L.J., 1967. Nuclear Reactor Analysis. John Wiley & Sons.

EBASCO Services Inc., 1972. 1,000MWe molten salt breeder reactor conceptual design study. *TID-26156*.

Engel, J.R., et al., 1980. Conceptual design of a denatured molten salt reactor with once-through fueling. *ORNL-TM-7207*.

Flanagan, G.F., 2012. FHR generic design criteria. *ORNL/TM-2012/226*.

Forsberg, C.W., 1998. Definition of Weapons-usable Uranium-233. *ORNL/TM-13517*.

Fowler, T.B., et al., 1971. Nuclear reactor analysis code: CITATION. *ORNL-2496 Rev.2*.

Fraas, A.P., et al., 1956. Design report on the aircrft reactor test. *ORNL-2095*.

Furukawa, K., Minami, K., Oosawa, T., Ohta, M., Nakamura, N., Mitachi, K., et al., 1986. Design Study of Small Molten-Salt Fission Power Station Suitable for Coupling with Accelerator Molten-Salt Breeder. 4th ICENES, Madrid.

Furukawa, K., et al., 2007. Molten salt reactor for sustainable nuclear power—MSR FUJI. IAEA-TECDOC-1536 (Status of small reactor designs without on-site refueling), pp. 821–856.

Furukawa, K., Arakawa, K., Erbay, L.B., Ito, Y., Kato, Y., Kiyavitskaya, H., et al., 2008. A road map for the realization of global-scale thorium breeding fuel cycle by single molten-fluoride flow. Energy Convers. Manage. 49, 1832–1847.

Furukawa, K., Greaves, E.D., Erbay, L.B., Hron, M., Kato, Y., 2010. New sustainable secure nuclear industry based on thorium molten-salt nuclear energy synergetics. Chapter-17. Nuclear Power. InTech Publishing, Rijeka, Croatia.

Gat, U., et al., 1993. The source term and waste optimization of molten salt reactors with processing. Available from: <http://www.iaea.org/inis/collection/NCLCollectionStore/_Public/25/011/25011404.pdf>.

Grimes, W.R., 1967. Chemical research and development for molten-salt breeder reactors. *ORNL-TM-1853*.

Haubenreich, P.N., Engel, J.R., 1962. Safety calculations for MSRE. *ORNL-TM-251*.

Haubenreich, P.N., Engel, J.R., 1970. Experience with the molten-salt reactor experiment. Nucl. Appl. Technol. 8, 118–136.

Haynes International Inc., 2002. HASTELLOY® N alloy. <https://www.haynesintl.com/pdf/h2052.pdf>.

Hida, K., Yoshioka, R., 1992. Transmutation of minor actinides in boiling water reactors, In: Proceedings of ANP'92, 1, 3.1-1.

IAEA, 1996. Defence in depth in nuclear safety, INSAG-10.

Iodine Pit Issue, 2015. <http://en.wikipedia.org/wiki/Iodine_pit>.

Ishiguro, T., van Rooijen, W.F.G., Shimazu, Y., et al., 2014. Design of a passive residual heat removal system for the FUJI-233Um molten salt reactor system. Ann. Nucl. Energy. 64, 398–407.

Ishihara, A., Yamamoto, T., Mitachi, K., 2007a. A study of power control of three-region core molten salt reactor (in Japanese). In: *Transaction of Japan Atomic Energy Society of Japan*, D-01.

Ishihara, A., Yamamoto, T., Mitachi, K., 2007b. Study for power control of three-core molten salt reactor by fuel salt flow control (in Japanese). In: Transaction of Japan Atomic Energy Society of Japan.

Ishimori, T., 1973. Reactor Physics (in Japanese). Baifukan press, Tokyo, p. 183.

Lane, J.A., 1958. Fluid Fuel Reactors, Part 1: Aqueous Homogeneous Reactors. Addison-Wesley, Reading, MA.

LeBlanc, D., 2010. Molten salt reactors: a new beginning for an old idea. Nucl. Eng. Des. 240, 1644–1656.

MacPherson, H.G., 1958. Fluid Fuel Reactors, Part 2: Molten Salt Reactors. Addison-Wesley, Reading, MA.

MacPherson, H.G., 1985. The molten salt reactor adventure. Nucl. Sci. Eng. 90, 374–380.

Mitachi, K., Furukawa, K., 1995. Neutronic examination on plutonium transmutation by a small molten-salt fission power station. IAEA-TECDOC-840, pp. 183–195.

Mitachi, K., Yamana, Y., Suzuki, T., Furukawa, K., Yoshioka, R., 1994. A conceptual design of 1 GWe molten salt reactor (in Japanese). In: 4th Power Energy Symposium.

Mitachi, K., et al., 1998. Natural circulation in MSR under Decay Heat (in Japanese). In: Heat Transfer Symposium, Nagoya, Japan.

Mitachi, K., Okabayashi, D., Suzuki, T., Yoshioka, R., 2000. Re-estimation of nuclear characteristics of a small molten salt power reactor. (FUJI-12, in Japanese). J. Atom. Energy Soc. Jpn. 42 (9), 98–104.

Mitachi, K., Yamamoto, T., Yoshioka, R., 2007. Self-sustaining core design for 200 MWe molten-salt reactor with thorium-uranium fuel: FUJI-U3. In: TU2007 at Beijing, China.

Mitachi, K., Yamamoto, T., Yoshioka, R., Sugimoto, T., 2008. Characteristics of thorium molten-salt reactor with self-sustainability (in Japanese). J. Atom. Energy Soc. Jpn. 7 (2), 127–133.

Nakagawa, T., et al., 1995. Japanese evaluated nuclear data library version 3 revision-2, JENDL-3.2. J. Nucl. Sci. Technol. 32, 1259–1271.

Nuclear Safety Commission of Japan, 1990a. Regulatory guide for reviewing safety design of light water nuclear power reactor facilities. NSCRG: L-DS-I.0.

Nuclear Safety Commission of Japan, 1990b. Regulatory guide for reviewing safety assessment of light water nuclear power reactor facilities. NSCRG: L-SE-I.0.

Okumura, K., 2013. A set of ORIGEN2 cross section libraries based on JENDL-4.0: ORLIBJ40. *JAEA-Data/Code2012-032*.

Okumura, K., Kaneko, K., Tsuchihashi, K., 1996. The SRAC95: general neutronic calculation code system. *JAERI-Data/Code 96-015*.

Osaka, M., Misawa, T., Mitachi, K., 1995. Study on TRU transmutation using thorium-fuelled molten salt reactor (in Japanese). In: Transaction of Atomic Energy Society of Japan, C-54.

Robertson, R.C., 1965. MSRE design and operation report, Part-1, description of reactor design. *ORNL-TM-728*.

Robertson, R.C., 1970. Two-fluid molten salt breeder reactor, Status of 1968. *ORNL-4528*.

Robertson, R.C., 1971. Conceptual design study of a single-fluid molten-salt breeder reactor. *ORNL-4541*.

Rosenthal, M.W., 2009. An account of Oak Ridge National Laboratory's thirteen nuclear reactors. *ORNL/TM-2009/181*.

Rosenthal, M.W., Kasten, P.R., Briggs, R.B., 1970. Molten-salt reactors - history, status and potential. Nucl. Appl. Technol. 8, 107−117.

Scott, D., et al., 1958. A zero power reflector-moderated reactor experiment at elevated temperature. *ORNL-2536*.

Serp, J., et al., 2014. The molten salt reactor (MSR) in generation IV: overview and perspectives. Prog. Nucl. Energy. 77, 308−319.

Shimazu, Y., 1978a. Locked rotor accident analysis in a molten salt breeder reactor. Nucl. Sci. Technol. 15 (12), 935−940.

Shimazu, Y., 1978b. Nuclear safety analysis of a molten salt breeder reactor. Nucl. Sci. Technol. 15 (7), 514−522.

Soffer, L., et al., 1995. Accident source terms for light-water nuclear power plants. NUREG-1465 (1995).

Suzuki, N., Shimazu, Y., 2006. Preliminary safety analysis on depressurization accident without scram of a molten salt reactor. Nucl. Sci. Technol. 43 (7), 720−730.

Suzuki, N., Shimazu, Y., 2008. Reactivity-initiated-accident analysis without scram of a molten salt reactor. Nucl. Sci. Technol. 45 (6), 575−581.

Taihei Techno Service, 2015. Data on several hastelloys (in Japanese). <http://www.taihei-s.com/products/products14>.

Tsuchihashi, K., et al., 1979. A fortran program for the lattice cell analysis by collision probability method. JAERI-1259.

Uhlir, J., 1998. An experience on dry nuclear fuel reprocessing in the Czech Republic. In: Fifth OECD/NEA P and T Information Exchange Meeting. Mol, Belgium.

UK Atomic Energy Authority, 1974. An assessment of a 2500 MWe molten chloride salt fast reactor. *AEEW-R956*.

US-NRC, 1988. Lasalle unit 2 loss of recirculation pumps with power oscillation event. Information Notice No. 88-39.

US-NRC, 2010. Standard review plan 8.4, station blackout. NUREG-0800.

US-NRC, 2014a. Aircraft impact assessment. 10CFR50.150.

US-NRC, 2014b. Requirements for reduction of risk from anticipated transients without scram events. 10CFR50.62.

US-NRC, 2014c. 10 CFR part 52 - licenses, certifications, and approvals for nuclear power plants.

van Rooijen, W.F.G., 2015. Fission cross sections by JENDL-4.0. <http://iriaxp.iri.tudelft.nl/∼rooijen/spectra_en.html>.

Vergnes, J. et al., 2000. The AMSTER concept (Actinide Molten Salt TransmutER). In: Physor 2000 Conference, Pittsburgh, PA, USA.

Weinberg, A.M., 1946. High-pressure water as a heat transfer medium in nuclear power plants. *ORNL report MonP-93*.

Weinberg, A.M., 1994. The First Nuclear Era: The Life and Times of a Technological Fixer. AIP Press, New York.

Weinberg, A.M., 1997. The proto-history of the molten salt system. J. Accel. Plasma Res. 2 (1), 23−26.

Weinberg, A.M., Wigner, E.P., 1958. Physical Theory of Neutron Chain Reactors. University of Chicago Press, Chicago.

Wigner, E.P., Young, G., Weinberg, A.M., 1945. Preliminary calculations on a breeder with circulating fuel. *MUC-EPW-134*.

Williams, D.F., 1999. Molten salt fuel cycle requirements for ADTT applications. ADTTA-99.

Windscale fire, 2015. <http://en.wikipedia.org/wiki/Windscale_fire>.

Xu, H., 2012. TMSR (thorium molten salt reactors) project in China. In: ThEC12 Conference Shanghai, China.

Yamamoto, T., Mitachi, K., Suzuki, T., 2004. Steady state analysis of molten-salt reactor in consideration of the effect of fuel-salt flow. In: Proceedings of ICONE12, 49077.

Yamamoto, T., Mitachi, K., et al., 2005. Transient response of flow blockage accident in small molten salt reactor (in Japanese). In: Transaction of Japan Mechanical Society.

Yamamoto, T., Mitachi, K., et al., 2006a. Reactor controllability of 3-region-core molten salt reactor. In: ICONE-14, Miami, FL, USA.

Yamamoto, T., Mitachi, K., Nishio, M., 2006b. Reactor controllability of 3-region core molten salt reactor. In: Proceedings of ICONE14, 89440.

Yoshioka, R., 2013. Nuclear energy based on thorium molten salt, Chapter-23 of the book. In: Lantelme, F., Groult, H. (Eds.), Molten Salts Chemistry: From Lab to Applications. Elsevier Inc., USA.

Yoshioka, R. Kinoshita, M., 2014. Safety criteria and guidelines for MSR accident analysis. In: GIF-MSR-pSSC, Shanghai, China.

Yoshioka, R., Mitachi, K., Shimazu, Y., Kinoshita, M., 2014. Safety criteria and guidelines for MSR accident analysis. In: PHYSOR-2014, Kyoto, Japan.

# Fast-spectrum, liquid-fueled reactors

# 12

A.A. Lizin[1], S.V. Tomilin[1], Leonid I. Ponomarev[2], Yu S. Fedorov[3] and
Yasuo Hirose[4]
[1]State Research Centre—Research Institute of Atomic Reactors, Dimitrovgrad, Russia,
[2]A.A. Bochvar High-Technology Scientific Research Institute for Inorganic Materials,
Moscow, Russia,
[3]Petersburg State Technological Institute (Technical University), St. Petersburg, Russia,
[4]Retired, the former Institute of Research and Innovation, Kashiwa, Chiba-ken, Japan

## Chapter Outline

Four concepts of the fast molten salt reactor are known today. Two of them use Th—U fuel and carrier salts LiF—$BeF_2$ and LiF—NaF—$BeF_2$ (over 10 years' development); the others use U—Pu fuel and carrier salts LiF—NaF—KF (3 years' development) and NaF—KF (1 year). The fast neutron spectrum MSR has definite advantages in comparison with thermal MSR, especially for long-lived nuclear waste incineration and nuclear breeding. To realize these advantages extended research programs are needed, including neutronics and thermo-hydraulic calculations, physics and chemistry of molten salts, development of a closed nuclear fuel cycle, new construction materials

**Molten Salt Reactors and Thorium Energy. DOI: http://dx.doi.org/10.1016/B978-0-08-101126-3.00012-9**

resistant to corrosion, and fast neutron radiation, etc. The advantages of the fast MSRs are so important that these efforts are worthwhile.

## 12.1 Carrier salt for the fast molten-salt reactor

### 12.1.1 Introduction

The choice of the carrier salt for MSR was the subject of the many research studies since the MSRE experience (the last one is the program ALISIA, Benes et al., 2009). The molten fluorides of the alkaline and the alkaline-earth elements (Li, Be, Na, K, etc.) are usually used as the carrier salts. They should meet the numerous requirements:

- Low melting temperature;
- Low neutron absorption;
- Low corrosive activity;
- High heat capacity and conductivity;
- Low viscosity;
- Low cost and toxicity;
- High solubility of the actinide and lanthanide fluorides.

The last property is necessary for MSRs with fast neutron spectrum

### 12.1.2 Physical properties of the fluoride carrier salts

The properties of the most commonly known fluoride salts are presented in Table 12.1. All these properties are important, because the fuel compositions are used not only as nuclear fuel, but also as the heat transfer agent at the same time. Because the MSR operating temperature range is limited to 550–700°C, the salts with melting temperature $T_m < 550°C$ only are included in Table 12.1. The characteristics of the usual heat transfer agents ($H_2O$, Na, Pb, Pb-Bi) are presented for the comparison.

### 12.1.3 The solubility of the actinide and lanthanide fluorides in the fluoride molten salts

The solubility of the actinide and lanthanide fluorides in the fluoride salts is the key point in the carrier salt choice for the fast molten salt reactor. The MSR fuel composition (FC) consists of the carrier salt, the fissile and raw actinide fluorides, the minor actinide and fission product fluorides, etc. To provide the fast neutron spectrum, the FC should contain ~20 at.% of the heavy elements (Merle-Lucotte, 2013). Several fluoride carrier salts have high solubility of $ThF_4$ and $UF_4$ ($LiF-BeF_2$, $LiF-NaF-BeF_2$, etc.) and they can be used not only both in thermal reactors with Th–U fuel cycle like MSRE/MSBR (Haubenrich Engel, 1970; Merk and Konheiser, 2014) and fast/intermediate neutron spectrum (Holcomb et al., 2011, Merle-Lucotte et al., 2013, Ignatiev et al., 2012b). However, until recently the $PuF_3$ solubility in all the known salts did not exceed 6 mol% (Table 12.2).

**Table 12.1** Carrier fluoride salts characteristics at 700°C (Ponomarev et al., 2013)

| Composition (mol%) | $T_m$ (°C) | Mol. mass (g/mol) | Density (g/cm$^3$) | Heat capacity (J/g K) | Heat conductivity [W/(m K)] | Viscosity (m$^2$/s) | Vapor pressure at 900°C, mm/Hg | Neutron absorption with respect to graphite | Moderating efficient with respect to graphite |
|---|---|---|---|---|---|---|---|---|---|
| 67 LiF–33 BeF$_2$ | 460 | 33 | 1.94 | 2.42 | 1.00 | 5.6 | 1.2 | 8[a] | 60[b] |
| 15 LiF–58 NaF–27 BeF$_2$ | 479 | 41.0 | 2.12 | 2.09 | 0.83 | 2.7 | 1.7 | 20 | 22 |
| 46.5 LiF–11.5 NaF–42 KF | 454 | 41.3 | 2.02 | 1.88 | 0.92 | 2.9 | 0.7 | 4[a] | 0.4[a] |
| 26 LiF–37 NaF–37 ZrF$_4$ | 436 | 84.2 | 2.79 | 1.26 | 0.53 | 6.9 | ~5 | 20 | 13 |
| 57 NaF–43 BeF$_2$ | 340 | 44.1 | 0.72 | 2.18 | 0.87 | 7.0 | 1.4 | 28 | 15 |
| 59.5 NaF–40.5 ZrF$_4$ | 500 | 92.7 | 3.14 | 1.17 | 0.49 | 5.1 | 5.0 | 24 | 10 |
| Na (450°C) | 98 | 23 | 0.844 | 1.27 | 71.2 | 0.23 | 10.7 | 36 | 0.34 |
| Pb (450°C) | 328 | 207.2 | 10.52 | 0.15 | 17.1 | 0.15 | 10.6 | 29 | 0.15 |
| Pb-Bi (450°C) | 125 | 208.2 | 10.15 | 0.15 | 14.2 | 0.11 | | 63 | 1.13 |
| $H_2O$ (300°C) | 0 | 18 | 0.72 | 5.6 | 0.54 | 0.09 | 10.3 | 16 | 55 |

[a] Fast neutron spectrum.
[b] Thermal neutron spectrum.

**Table 12.2** $PuF_3$ solubility in the molten fluoride salts, mol%

| Composition (mol%) | $T_m$ (°C) | Temperature (°C) | | | | References |
|---|---|---|---|---|---|---|
| | | 550 | 600 | 650 | 700 | |
| 67 LiF–33 $BeF_2$ | 460 | 0.31 | 0.45 | 0.88 | – | Barton et al. (1958a) |
| 67 LiF–33 $BeF_2$ | 460 | 0.23[a] | 0.66[b] | 0.72[c] | – | Mailen et al. (1971) |
| 71.3 LiF–28.7 $BeF_2$ | – | 0.57 | 0.82 | 1.35 | – | Barton et al. (1960) |
| 68.1 LiF–31.9 $BeF_2$ | – | 0.32 | 0.53 | 0.82 | – | |
| 63 LiF–37 $BeF_2$ | – | 0.27 | 0.41 | 0.68 | – | Barton et al. (1960), Barton (1960) |
| 56.3 LiF–43.7 $BeF_2$ | – | 0.30 | 0.46 | 0.83 | – | Barton et al. (1960) |
| 51.7 LiF–48.3 $BeF_2$ | – | 0.38 | 0.60 | 0.92 | – | |
| 66.7 LiF–33.3 $BeF_2$ | 460 | 0.39[d] | 0.58 | 0.83 | – | |
| 66.7 LiF–33.3 $BeF_2$ | 460 | 0.36[d] | 0.52[b] | 0.84 | – | Ignatiev et al. (2003) |
| 17.5 LiF–56.5 NaF–26 $BeF_2$ | 505 | 1.56 | 1.56 | 2.80 | – | Barton et al. (1960) |
| 60.1 LiF–2.1 NaF–37.8 $BeF_2$ | – | 0.28 | 0.42 | 0.73 | | |
| 15 LiF–58 NaF–27 $BeF_2$ | 480 | 1.33 | 1.94 | 2.89 | – | Ignatiev et al. (2006) |
| 17 LiF–58 NaF–25 $BeF_2$ | 500 | 1.94 | 3.00 | 4 | – | |
| 63.4 NaF–36.6 $BeF_2$ | – | 0.29 | 0.46 | 0.84 | – | Barton et al. (1960) |
| 49.7 NaF–50.3 $BeF_2$ | – | 0.22 | 0.34 | 0.52 | – | |
| 57.0 NaF–43.0 $BeF_2$ | – | – | 0.25 | 0.42 | 0.68 | |
| 80 LiF–20 $ThF_4$ | | | 4.0 | 5.2 | – | Sood et al. (1975) |
| 78 LiF–22 $ThF_4$ | – | – | 3.98 | 5.02 | 5.88 | Ignatiev et al. (2012a,b) |
| 72 LiF–16 $BeF_2$–12 $ThF_4$ | – | 1.17 | 1.78 | 2.57 | 3.46 | Bamberger et al. (1970) |
| 75 LiF–20 $BeF_2$–5 $ThF_4$ | – | – | 2.88 | – | 4.75 | Iyer et al. (1973b) |
| 75 LiF–5 $BeF_2$–20 $ThF_4$ | – | – | 3.16 | 3.98 | 4.89 | Ignatiev et al. (2012a,b) |
| 75 LiF–5 $BeF_2$–20 $ThF_4$ | | | 3.4 | 4.0 | 4.9 | Ignatiev et al. (2014) |
| 70 LiF–10 $BeF_2$–20 $UF_4$ | – | 1.27 | 1.70 | 2.48 | – | Thoma (1959) |
| 65 LiF–30 $BeF_2$–5 $ZrF_4$ | 450 | 0.10 | 0.15[b] | – | 0.19 | Naumov et al. (1996) |
| 63 LiF–30 $BeF_2$–7 $ZrF_4$ | 450 | 0.12 | 0.17[b] | – | 0.26 | |

[a] At 525°C.
[b] At 625°C.
[c] At 675°C.
[d] At 575°C.

Recently it was found that in the eutectic 46.5LiF−11.5NaF−42.0KF (FLiNaK) the solubility of $UF_4$, $PuF_3$, and $AmF_3$ reaches ~45, ~30, and ~40 mol% respectively at 700°C (Lizin et al., 2013a,b; Volozhin et al., 2013). This observation opens the way for the development of the fast molten salt reactor with U−Pu fuel cycle (Degtyarev and Ponomarev, 2012; Degtyarev et al., 2015) as well as the effective Am incinerator (Degtyarev et al., 2013).

### *12.1.3.1 Molten salts based on LiF and NaF*

According to the fusion diagram of LiF−$PuF_3$ the $PuF_3$ solubility in LiF may be estimated as 20−40 mol% within the temperature range of 750−1000°C. In NaF−$PuF_3$ melts similar estimations give the solubility value of 25−40 mol% in the temperature range 730−850°C (Barton et al., 1960). The addition of $BeF_2$ into LiF suppress the $PuF_3$ solubility almost by an order of magnitude: in LiF−$BeF_2$ the $PuF_3$ solubility in the temperature range of 500−700°C varies from 0.1 to 1.0 mol % (Barton, 1960). The addition of $ZrF_4$ into NaF produces the effect similar in magnitude (Ponomarev et al., 2013).

The addition of $ThF_4$ into LiF also decreases the $PuF_3$ solubility (in comparison with pure LiF) but less than the addition of $BeF_2$. For example, in the molten salt 80LiF−20$ThF_4$ the $PuF_3$ solubility varies from 4 to 10 mol% within the temperature range of 600−800°C. The addition of $UF_4$ has much the same effect on the $PuF_3$ solubility as in case of $ThF_4$ addition (Barton et al., 1960).

### *12.1.3.2 Salt system LiF−$BeF_2$*

The $PuF_3$ solubility in the most studied system, LiF−$BeF_2$ varies from 0.2 to 1.4 mol% within the temperature range of 500−700°C depending on the salt composition (Barton et al., 1958a).

The compositions in which LiF is partially replaced with NaF are similar to the LiF−$BeF_2$ physical and chemical properties, but in this case the tritium generation in (n,α)-reaction on the $^6Li$ is suppressed and the $PuF_3$ solubility increases about threefold. The important advantage of LiF−$BeF_2$ melts with different content of LiF and $BeF_2$ components is the high solubility of $UF_4$ and $ThF_4$ which are the main fissile ($^{233}U$) and raw ($^{232}Th$) materials in the Th−U fuel cycle. The early measurements (Thoma, 1959) and later theoretical estimations (Van der Meer et al., 2006; Benes and Konings, 2009) based on the fusion diagrams of LiF−$BeF_2$−$AnF_4$ confirm that the solubility of $UF_4$ and $ThF_4$ is 20−30 mol% at the fuel composition temperature 500−700°C and the pressure of saturated vapors does not exceed 10 Pa (Rosenthal et al., 1972). The high solubility of $UF_4$ and $ThF_4$ creates the good preconditions for using LiF−$BeF_2$ salt in the thermal reactors with Th−U fuel and in the fast breeder reactors (Merle-Lucotte, 2013).

It has been shown (Barton and Strehlow, 1958; Barton et al., 1958b) that the addition of $CeF_3$ into eutectic 67LiF−33$BeF_2$ decreases significantly the solubility of $PuF_3$: the larger the fraction of $CeF_3$ entered into the system, the more $PuF_3$ solubility is decreased. The addition of $ThF_4$ increases the $PuF_3$ solubility up to

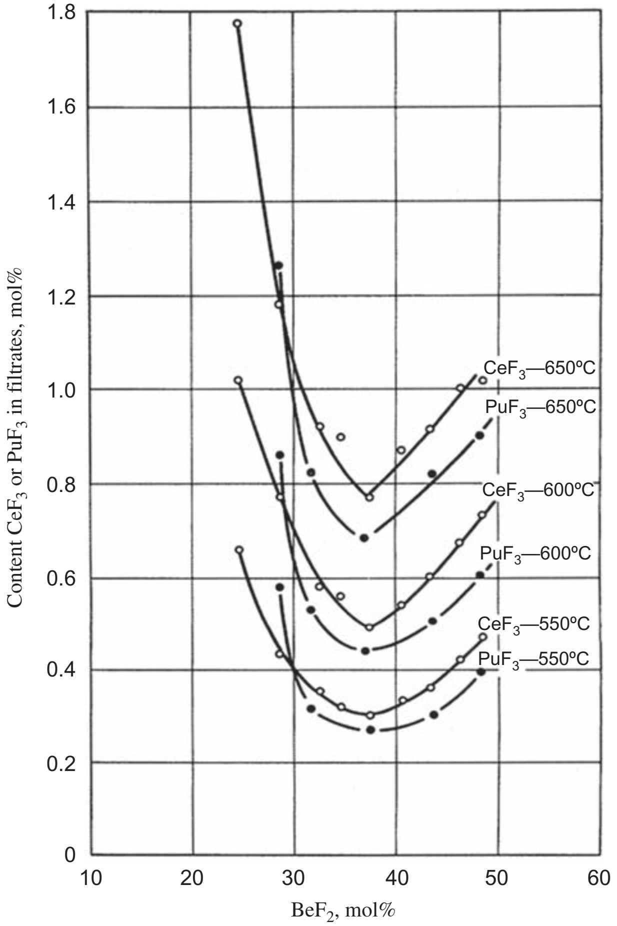

**Figure 12.1** Comparative graphs of $CeF_3$ and $PuF_3$ solubility in molten LiF–$BeF_2$ vs content of $BeF_2$ (Ward et al., 1959; Barton et al., 1960).

5–6 mol%. The temperature dependencies of the $PuF_3$ molar solubility S are described by liner function $\log S = A + B/T$ (Ignatiev et al., 2003).

The $CeF_3$ solubility as the chemical analog of $PuF_3$ solubility $S$ is described by many authors (Barton et al., 1970; Iyer et al., 1973a; Naumov et al., 1996). It has been established that the solubilities of $CeF_3$ and $PuF_3$, are very similar and differ ~14% (Fig. 12.1)

### 12.1.3.3 Salt system LiF–$BeF_2$–$ThF_4$

The influence of $ThF_4$ addition into LiF–$BeF_2$ on the $CeF_3$ solubility was studied by Barton et al. (1970). In Fig. 12.2 and Table 12.3 the temperature dependencies

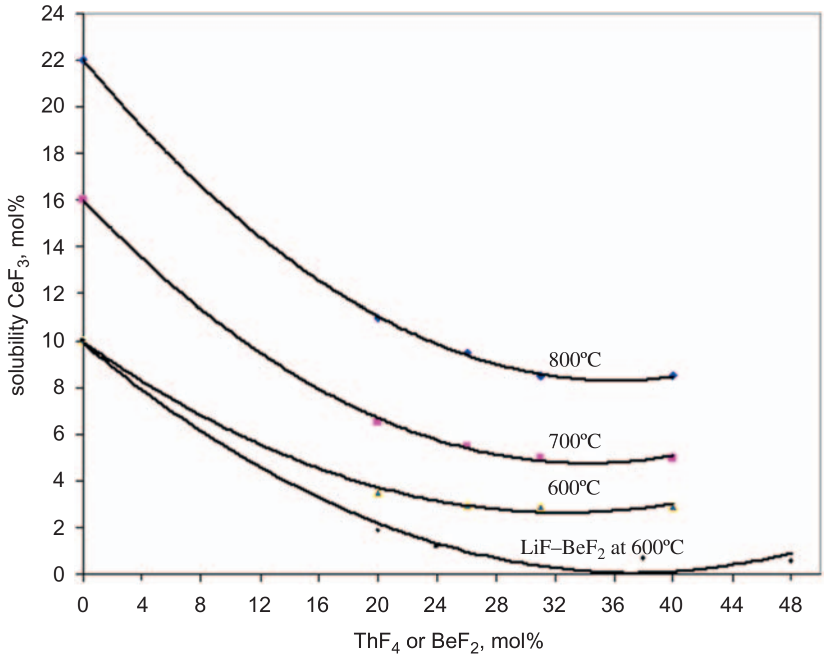

**Figure 12.2** $CeF_3$ solubility in $LiF-ThF_4$ and $LiF-BeF_2$ depending on melt composition (Barton et al., 1970).

**Table 12.3** **$CeF_3$ solubility in salts $LiF-BeF_2-ThF_4$ (Barton et al., 1970)**

| Mixture no. | Salt composition (mol%) | | | $CeF_3$ solubility (mol%) | |
|---|---|---|---|---|---|
| | LiF | $BeF_2$ | $ThF_4$ | 600°C | 800°C |
| 1 | 72 | 16 | 12 | 1.62(3) | 5.28(11) |
| 2 | 73 | 0 | 27 | 2.65(5) | 8.90(18) |
| 3 | 72.7 | 4.8 | 22.5 | 2.24(5) | 8.25(17) |
| 4 | 68 | 20 | 12 | 1.45(3) | 5.78(12) |
| 5 | 72.3 | 11.0 | 16.7 | 2.10(4) | 5.93(12) |
| 6 | 67.8 | 25.2 | 7.0 | 1.06(2) | 4.92(10) |
| 7 | 58 | 30 | 12 | 1.13(2) | 4.43(10) |
| 8 | 75 | 17.9 | 7.1 | 1.52(3) | 6.59(13) |
| 9 | 58.4 | 20.0 | 21.6 | 1.90(4) | 6.50(14) |
| 10 | 67 | 0 | 33 | 2.54(5) | 7.91(17) |
| 11 | 80 | 0 | 20 | 3.30(7) | 10.07(21) |
| 12 | 60 | 0 | 40 | 2.77(6) | 7.00(14) |
| 13 | 66.7 | 33.3 | 0 | 0.60 | 3.7 |
| 14 | 72.7 | 27.3 | 0 | 0.95 | 5.7 |

*Note*: Errors in the last significant digits are given in brackets.

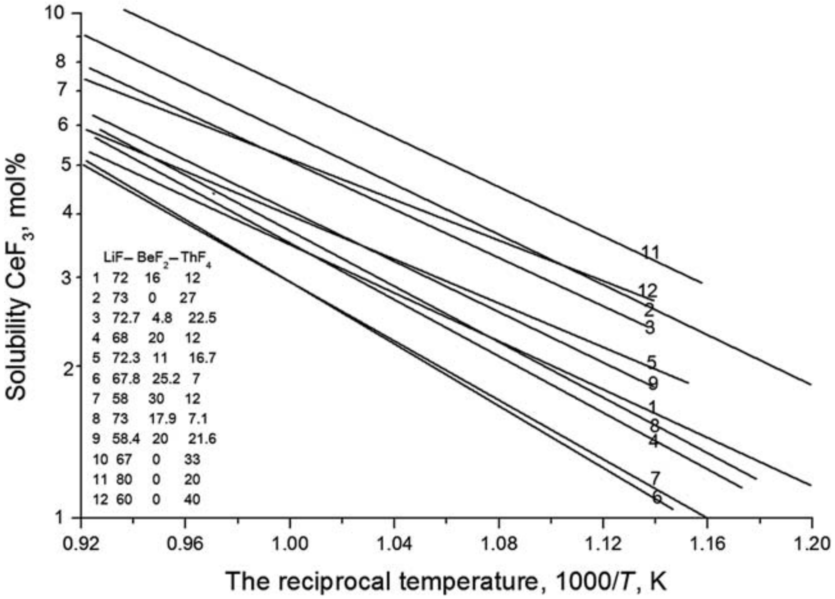

**Figure 12.3** Dependencies of $CeF_3$ solubility in molten $LiF-ThF_4$ and $LiF-BeF_2-ThF_4$ on reciprocal temperature (Barton et al., 1970).

of the $CeF_3$ solubility are presented. The total or partial replacement of $BeF_2$ with $ThF_4$ increases the $CeF_3$ solubility by 30%–90%.

The temperature dependencies of the molar solubility $S$ (Fig. 12.3) within the range of 600–800°C are well described by linear functions $\log S = A + B/T$. Later work (Iyer et al., 1973a) demonstrates a good correlation with these results.

### 12.1.3.4 Salt System $LiF-BeF_2-ZrF_4$

The $CeF_3$ solubility in $65LiF-30BeF_2-5ZrF_4$ at 550–625–700°C is equal 1.01, 1.98, and 3.04 mol%, respectively (Naumov et al., 1996).

The solubility of the other lanthanide fluorides (Table 12.4) is also studied in the salt $65LiF-30BeF_2-5ZrF_4$ which was proposed as the solvent for ADTT plant (Naumov et al., 1996).

The solubility data for $LnF_3$, (Ln = Y, Sm, Ce, La) in the salts $62.8LiF-36.4BeF_2-0.8UF_4$ and $50NaF-46ZrF_4-4UF_4$ (Barton et al., 1960) are presented in Table 12.5.

The influence of the lanthanide atomic number on the lanthanide fluoride solubility has been demonstrated with the salt $62.8LiF-36.4BeF_2-0.8UF_4$ (Barton and Strehlow, 1958) where the solubility is increased by a series of $LaF_3 < CeF_3 < SmF_3$, i.e., it is increased with growing nuclear charge and decreasing ionic radius.

**Table 12.4** **Solubility of the lanthanide fluorides in salt system $65LiF-30BeF_2-5ZrF_4$ (Naumov et al., 1996)**

| Compound | Temperature ($T$,°C) | Solubility ($S$, mol%) | Solubility-temperature equation |
|---|---|---|---|
| $LaF_3$ | 550 | 0.52(5) | $\log S = 2.05 - 3984/T \pm 0.06$ |
| | 625 | 1.60(16) | |
| | 700 | 2.72(25) | |
| $CeF_3$ | 550 | 1.01(10) | $\log S = 0.46 - 2605/T \pm 0.04$ |
| | 625 | 1.98(18) | |
| | 700 | 3.04(28) | |
| $NdF_3$ | 550 | 0.68(7) | $\log S = 5.48 - 7042/T \pm 0.02$ |
| | 625 | 1.62(16) | |
| | 700 | 3.75(32) | |
| $CeF_4$ | 550 | 0.62(6) | $\log S = 1.36 - 3406/T \pm 0.03$ |
| | 625 | 1.10(10) | |
| | 700 | 2.50(22) | |

**Table 12.5** **Solubility of the lanthanide fluorides (Barton et al., 1960)**

| Salt system | Temperature (°C) | $LnF_3$ | Solubility (mol%) |
|---|---|---|---|
| $50NaF-46ZrF_4-4UF_4$ | 550–750 | $YF_3$ | 2.8–7.0 |
| | | $SmF_3$ | 2.4–4.0 |
| | | $CeF_3$ | 2.0–3.5 |
| | | $LaF_3$ | 1.9–3.0 |
| $62.8LiF-36.4BeF_2-0.8UF_4$ | 500–650 | $SmF_3$ | 0.4–2.0 |
| | | $CeF_3$ | 0.2–1.0 |
| | | $LaF_3$ | 0.2–0.8 |

### 12.1.3.5 Salt system $NaF-ZrF_4$

In Table 12.6 the solubility of the different fluorides in $NaF-ZrF_4$ are presented (Mel'nik et al., 2003) and $52.5NaF-47.5ZrF_4$ (Thoma et al., 1968; Naumov et al., 1996)

The salt $52NaF-48ZrF_4$ is comparable or slightly higher in the fluoride solubility as $LiF-BeF_2$ but less toxic and corrosive, but its disadvantage is a high volatility of $ZrF_4$ vapors that results in formation of zirconium tetrafluoride deposit in MSR communications (Souček et al., 2005).

### 12.1.3.6 Salt system $LiF-ThF_4-UF_4$

The $CeF_3$ and $PuF_3$ solubility at their joint presence in the melts $78LiF-7ThF_4-15UF_4$ and $72.5LiF-7ThF_4-20.5UF_4$ within the temperature range of 600–750°C are presented in Tables 12.7 and 12.8. These compositions meet the

**Table 12.6 Actinide and lanthanide fluorides solubility in 52NaF−48ZrF$_4$**

| *T* (°C) | Solubility (mol%) | | | | | | | |
|---|---|---|---|---|---|---|---|---|
| | Thoma (1968) | | Naumov et al. (1996) | | | Mel'nik et al. (2003) | | |
| | LaF$_3$ | PrF$_3$ | UF$_4$ | ThF$_4$ | CeF$_3$ | NpF$_4$ | PuF$_3$ | AmF$_3$ |
| 550 | 1.1 | 0.2 | 9.8 | 0.2 | 0.9 | 5.8 | 2.0 | 1.15 |
| 600 | 1.1 | 0.3 | 14.8 | 2.8 | 1.4 | – | – | – |
| 650 | 1.7 | 0.4 | 17.1 | 4.1 | 1.9 | – | – | – |
| 700 | 2.1 | 0.6 | 25.1 | 5.9 | 2.1 | | | |
| 750 | 2.7 | 0.6 | 29.4 | 7.3 | 2.5 | 12.3 | 3.2 | 1.20 |

**Table 12.7 Solubility of PuF$_3$ and CeF$_3$ in 78LiF−7ThF$_4$−15UF$_4$ (Lizin et al., 2015a)**

| Temperature (°C) | PuF$_3$ solubility (mol%) | CeF$_3$ solubility (mol%) |
|---|---|---|
| 600 | 1.48 ± 0.07 | 4.6 ± 0.2 |
| 650 | 5.8 ± 0.3 | 6.3 ± 0.3 |
| 700 | 9.9 ± 0.5 | 8.5 ± 0.4 |
| 750 | 10.9 ± 0.6 | 8.9 ± 0.4 |

**Table 12.8 Solubility of PuF$_3$ and CeF$_3$ in 72.5LiF−7ThF$_4$−20.5UF$_4$ (Lizin et al., 2015a)**

| Temperature (°C) | PuF$_3$ solubility (mol%) | CeF$_3$ solubility (mol%) |
|---|---|---|
| 600 | 0.36 ± 0.02 | 2.6 ± 0.1 |
| 650 | 4.6 ± 0.2 | 4.4 ± 0.2 |
| 700 | 8.6 ± 0.4 | 6.4 ± 0.2 |
| 750 | 9.6 ± 0.5 | 6.8 ± 0.3 |

special requirements imposed to fuel salt of MSR launch load with cavity-type reactor core (Ignatiev et al., 2014) where the fraction of heavy metal tetrafluorides is essential (22 and 27.5 mol%, respectively).

The joint solubility of CeF$_3$ and PuF$_3$ increases with temperature and decreases with increasing UF$_4$ and ThF$_4$. Similar behavior is observed at the PuF$_3$ solubility in LiF−ThF$_4$ with the same fraction (22−27 mol%) of thorium tetrafluoride (Ignatiev et al., 2014).

### *12.1.3.7 Salt system LiF−NaF−BeF$_2$*

The solubility of PuF$_3$ in molten salts LiF−NF−BeF$_2$ of different compositions is presented in Table 12.9 (Ignatiev et al., 2006).

**Table 12.9** Solubility of $PuF_3$ in LiF–NaF–KF

| Content (mol%) | Temperature (°C) | | | | | |
|---|---|---|---|---|---|---|
| | 525 | 550 | 575 | 600 | 625 | 650 |
| $15LiF-58NaF-27BeF_2$ | – | 1.33 | 1.66 | 1.94 | 2.48 | 2.89 |
| $17LiF-58NaF-25BeF_2$ | 1.58 | 1.94 | 2.48 | 3.0 | 3.84 | – |

**Table 12.10** Solubility (mol%) of $ThF_4$, $UF_4$ (Lizin et al., 2013b) and $AmF_3$ (Lizin et al., 2013a) in the eutectic 46.5LiF–11.5NaF–42.0KF

| *T* (°C) | $ThF_4$ | $UF_4$ | $AmF_3$ |
|---|---|---|---|
| 550 | 23.2 | 15.3 | 18.0 |
| 600 | 27.9 | 24.6 | 31.7 |
| 650 | 32.8 | 34.8 | 34.0 |
| 700 | 41.4 | 44.7 | 43.4 |

### *12.1.3.8 Salt system 46.5 LiF–11.5 NaF–42.0 KF (FLiNaK)*

The fusion diagram of LiF–NaF–KF system was obtained first by Bergmann and Dergunov (1941). This system has the single eutectic 0.465LiF–0.115 NaF–0.420KF (FLiNaK) with the melting temperature $T_m = 454°C$ (Janz et al., 1974). The later experimental works confirmed these results (Williams et al., 2006).

The eutectic salt composition 46.5LiF–11.5NaF–42.0KF mol% (FLiNaK) was considered earlier as perspective coolant for the fast nuclear reactors (Williams et al., 2006) and the hybrid fusion–fission systems. The theoretical estimations (Benes and Konings, 2008) and experiments (Lizin et al., 2013a,b; Volozhin et al., 2013) have demonstrated also the extremely high solubility of $PuF_3$, $UF_4$, $ThF_4$, and $AmF_3$ as well as the lanthanide fluorides (Ponomarev et al., 2013). These measurements attracted the special attention to this salt.

The data on the solubility of $UF_4$, $ThF_4$, and $AmF_3$ in FLiNaK are presented in Table 12.10.

PuF3 and AmF3 solubility have been studied using the isothermal saturation (Lizin et al., 2013a,b) and local γ-spectrometry (Volozhin et al., 2013) methods (Tables 12.11 and 12.12). The $AmF_3$ solubility is even higher than the $PuF_3$ solubility.

The $PuF_3$ solubility is presented in Table 12.11. The values measured by two groups coincided in the range 600–700°C within the experiment errors (~10%) and close to the theoretical estimates (Benes and Konings, 2008).

It is well known (Barton et al., 1970) that $CeF_3$ solubility in various salts is similar to $PuF_3$ solubility. The measurements of $CeF_3$ solubility in FLiNaK confirm this survey (Table 12.12).

Table 12.11 $PuF_3$ solubility (mol%) in FLiNaK

| Temperature (°C) | $PuF_3$ (Lizin et al., 2013a) | $PuF_3$ (Volozhin et al., 2013) |
|---|---|---|
| 550 | 6.2(0.6) | 7.5(1.0) |
| 600 | 11.3(1.1) | 12.8(1.7) |
| 650 | 21.5(2.1) | 21.2(2.7) |
| 700 | 33.1(3.3) | 30.7(4.0) |

Table 12.12 $CeF_3$ solubility in FLiNaK

| Temperature(°C) | $CeF_3$ (Volozhin et al., 2013) | $CeF_3$ (Lizin et al., 2013a) |
|---|---|---|
| 550 | 12.9 | – |
| 600 | 16.6 | 21.6 |
| 650 | 23.7 | – |
| 700 | 29.2 | 31.9 |

Joint solubility of $PuF_3$ and $UF_4$ in FLiNaK, important for the fast MSR operation, was measured by Lizin et al. (2015b).

It is evident from Table 12.13 that the joint presence of $UF_4$ and $PuF_3$ in FLiNaK results in essential decreasing of their individual solubility: at 600°C the individual solubility of $PuF_3$ and $UF_4$ is 11.1 and 24.6 mol%, respectively, but their joint solubility is only 2.9 and 3.5 mol%. The total solubility of $PuF_3$ and $UF_4$ in the mixture is comparable with the individual $PuF_3$ and $UF_4$ solubility and this difference decreases with increasing temperature.

The measured solubility of $LaF_3$, $NdF_3$, $CeF_3$, and $PrF_3$ in FLiNaK are presented in Table 12.14. These results are important for the organization of the MSR closed fuel cycle and the MSR fuel composition feeding and cleaning.

Particularly, such a high solubility of the lanthanide fluorides in the fuel composition facilitates can increase in the intervals between the fuel cleaning operations from the neutron poisons.

The high $PuF_3$ and $UF_4$ solubility in FLiNaK open at first the way for the development of the fast MSR and U–Pu fuel cycle (Ponomarev et al., 2013; Degtyarev et al., 2015).

### 12.1.4 The other essential fluoride molten-salt properties

The main physical, chemical, and nuclear characteristics of the most commonly known fluoride molten salts are presented in Table 12.1. The fluoride molten salts have satisfactory heat capacity and conductivity as well as viscosity to effectively remove the heat at operating temperatures (500–800°C) in a wide range of salt compositions (McNeese et al., 1974, Khokhlov et al., 2009). The thermal properties of these melts provide the high efficiency of the heat removal even in the case of

## Table 12.13 Joint solubility of $PuF_3$ and $UF_4$ in FLiNaK

| Temperature (°C) | Individual solubility (mol%) (Lizin et al., 2013a,b) | | Joint solubility (mol%) (Lizin et al., 2015b) | | |
|---|---|---|---|---|---|
| | $PuF_3$ | $UF_4$ | $PuF_3$ | $UF_4$ | $PuF_3 + UF_4$ |
| 550 | 6.1 ± 0.6 | 15.3 ± 0.8 | 1.2 ± 0.1 | 1.8 ± 0.1 | 3.0 |
| 600 | 11.1 ± 1.1 | 24.6 ± 1.2 | 2.9 ± 0.3 | 3.5 ± 0.5 | 6.4 |
| 650 | 21.3 ± 2.1 | 34.8 ± 1.7 | 13.2 ± 1.6 | 11.0 ± 1.6 | 24.2 |
| 700 | 32.8 ± 3.3 | 44.7 ± 2.2 | 19.1 ± 2.3 | 17.3 ± 2.6 | 36.4 |
| 750 | – | – | 21.0 ± 2.5 | 19.0 ± 2.8 | 40.0 |
| 800 | – | – | 22.5 ± 2.7 | 20.0 ± 3.0 | 42.5 |

## Table 12.14 Solubility (*S*, mol%) of the lanthanide fluorides in molten salt FLiNaK

| *T* (°C) | Ponomarev et al. (2013) | | Lizin et al. (2013a) | Volozhin et al. (2013) |
|---|---|---|---|---|
| | $LaF_3$ | $PrF_3$ | $NdF_3$ | $CeF_3$ |
| 550 | 1.9 | – | 13.3 | 12.9 |
| 600 | 8.9 | 8.7 | 22.0 | 16.6 |
| 650 | 12.6 | 10.4 | 27.8 | 23.7 |
| 700 | 20.8 | 13.7 | 36.8 | 29.2 |

the natural circulation: the factor of the "salt-wall" heat transfer is close to that of water, although the coefficient of the salt heat conductivity is ~100 times less than that of sodium. The molten fluorides differ in high radiation resistance and relatively low corrosion activity in relation to graphite and some metal alloys.

The most studied MSR fuel composition is the salt $67LiF-33BeF_2$ (99.995% $^7Li$) with the fissile ($^{233}U$) and raw ($^{232}Th$) isotope fluorides dissolved. The very important advantage of $LiF-BeF_2$ melt is the high solubility of $UF_4$ and $ThF_4$ (~20 mol% at ~600°C) and the saturated vapor pressure ~ 10 Pa at 700°C (Rosenthal et al., 1972).

The accumulation of fission products in MSR fuel compositions up to concentration of 1–2 mol% does not change significantly their physical and chemical properties and does not result in their sedimentation. These fuel compositions are acceptable as the base for MSR with Th–U cycle, including fast MSR.

The fast MSR with U–Pu cycle needs the high $UF_4$ and $PuF_3$ solubility but they also meet a series of other requirements imposed on its physical and chemical properties: density, heat capacity and heat conductivity, corrosive activity, etc.

#### 12.1.4.1 Viscosity

The viscosity of the molten mixtures of lithium, sodium, potassium, beryllium, aluminum, thorium, and uranium fluorides was studied experimentally in many works (Cantor, 1968; Haubenreich and Engel, 1970; Janz et al., 1974; Desyatnik et al., 1979; Smirnov et al., 1974; Desyatnik et al., 1981; Ignatiev et al., 2012a,b; Merzlyakov et al., 2014). The method of the torsion vibration damping of the cylindrical crucible filled with the studied melt was used (Haubenrich and Engel, 1970; Ignatiev et al., 2012a,b). The comparison of the experimental and estimated data at different temperatures is given in Table 12.15.

Data on the FLiNaK dynamic viscosity are given in Table 12.15. The recent viscosity data (Merzlyakov et al., 2014) are within the values published earlier by other authors (Janz et al., 1974; Hoffman and Jones 1955; Vriesema 1979). Fig. 12.4 presents temperature dependence of dynamic viscosity for 46.5LiF–11.5NaF–42 KF salt system. The addition of 5 and 10 mol% of $CeF_3$ decreases the FLiNaK viscosity with the temperature descent (Merzlyakov et al., 2011, Merzlyakov et al. 2014).

#### 12.1.4.2 Corrosion of the construction materials

Since the time of the MSRE project several alloys have been tested for corrosive properties in contact with molten fluoride salts and fission products (Rosenthal et al., 1972; McNeese et al., 1974; Olson et al., 2009; Ignatiev et al., 2012a,b, 2014). These data demonstrate that the corrosion rate of the constructional materials depends on the salt composition, impurities (especially Te, $NiF_2$, $FeF_2$, $H_2O$, the metal oxides, and sulfates), operation temperature, and melt flow rate, and especially Red-Ox potential of the fuel composition.

Recently it has been proposed (Olson et al., 2009; Ignatiev et al., 2012a,b, 2014) that the nickel alloys with high heat resistance and high-temperature strength for the MSR fuel composition at temperature up to 800°C. The nickel–molybdenum alloys niobium-doped ХН80М-ВЛ, aluminum-doped ХН80МТЮ, tungsten-doped ХН80МТВ (Ignatiev et al., 2012a,b,2014), and the special nickel–tungsten alloy EM-721 (Olson et al., 2009) have been studied.

FLiNaK corrosive activity have been studied by Olson et al. (2009). It was established that Hastelloy-N and the alloys with high content of nickel and low content of chromium, in particular Ni-203, are the most appropriate construction materials within the temperature range up to 700°C.

### 12.1.5 Conclusion

The salt compositions based on the alkaline element (Li, Na, K) fluorides have all the necessary properties for the reliable molten salt reactor operation. Currently available information on the molten salt properties allows us to make some recommendations for the choice of the carrier salt for the fast MSR of different types. The high solubility of the actinide and lanthanide fluorides in FLiNaK combined with its other physical and chemical characteristics allows us to consider it as

**Table 12.15** Dynamic viscosity of Li, Na, Be, K, Th, F molten salts

| Composition (mol%) | Measurement range (°C) | Dynamic viscosity (mPa/s) | | | Source |
|---|---|---|---|---|---|
| | | 600 | 700 | 800 | |
| 46.5LiF–11.5NaF–42 KF | 503–703 | 4.2 | 2.48 | – | Janz et al. (1974) |
| | – | 6.04 | 3.44 | 2.17 | Hoffman, Jones (1955) |
| | – | 5.28 | 3.54 | 2.56 | Vriesema (1979) |
| | 500–800 | 4.75 | 2.91 | 1.95 | Klimenkov et al. (1983) |
| | 454–871 | 5.40 | 3.48 | 2.48 | Merzlyakov et al. (2014) |
| 46.5LiF–11.5NaF–42 KF | 454–871 | 2.65 | 1.76 | 1.30 | Merzlyakov et al. (2014) |
| (46.5LiF–11.5NaF–42KF) +5CeF$_3$ | 488–886 | 2.56 | 2.05 | 1.70 | |
| (46.5LiF–11.5NaF–42KF) +10CeF$_3$ | 551–875 | 2.70 | 1.91 | 1.44 | |
| 15LiF–58NaF–27 BeF$_2$ | 490–790 | 3.65 | 2.91 | 2.14 | Merzlyakov et al. (2014) |
| (15LiF–58NaF–27BeF$_2$) +1CeF$_3$ | 469–797 | 3.07 | 2.35 | 2.00 | |
| 70LiF– 30BeF$_2$ | 630–936 | – | 2.66 | 1.90 | Desyatnik et al. (1979) |
| 80LiF–20BeF$_2$ | 758–945 | – | – | 1.24 | |
| 72LiF–20BeF$_2$– 8ThF$_4$ | 709–1023 | – | – | 1.45 | |
| 81LiF–10BeF$_2$–9ThF$_4$ | 783–1038 | – | – | 1.35 | Janz et al. (1974) |
| 63LiF–30BeF$_2$–7ThF$_4$ | 698–1044 | – | 2.09 | 1.68 | |
| 70.1LiF–23.9BeF$_2$–6ThF$_4$ | 527–627 | 3.68 | – | – | |
| 71LiF–16BeF$_2$–12ThF$_4$–1UF$_4$ | 730–1060 | – | – | 1.52 | Merzlyakov et al. (2011) |
| 75LiF–20BeF$_2$–5ThF$_4$ | 651–885 | – | 2.49 | 1.83 | Haubenreich and Engel (1970) |
| 70LiF–30ThF$_4$ | 637–989 | – | 1.94 | 1.48 | Desyatnik et al. (1979) |
| 80LiF–20ThF$_4$ | 723–997 | – | – | 1.37 | |
| 80LiF–20UF$_4$ | 723–997 | – | – | 0.81 | |
| 80LiF–20UF$_4$ | 600–800 | 3.90 | 2.18 | 1.37 | Janz et al. (1974) |
| 78LiF–22ThF$_4$ | Estimation | 2.30 | 1.64 | 1.31 | Benes (2009) |
| 78LiF–22ThF$_4$ | Estimation | – | 1.40 | 1.11 | Benes and Konings (2009) |
| 78LiF–22ThF$_4$ | 625–846 | – | 2.46 | 1.73 | Merzlyakov et al. (2011) |
| 75LiF–20ThF$_4$–5BeF$_2$ | Estimate | 2.21 | 1.74 | 1.37 | Benes (2009) |
| 72LiF–18ThF$_4$–10BeF$_2$ | 730–1060 | – | – | 1.37 | Desyatnik et al. (1979) |
| 71LiF–27ThF$_4$–2BeF$_2$ | 593–805 | 2.94 | 2.04 | 1.52 | Merzlyakov et al. (2011) |
| 75LiF–5BeF$_2$–20ThF$_4$ | 578–820 | 2.81 | 2.25 | 1.88 | Merzlyakov et al. (2011) |
| (75LiF–5BeF$_2$–20ThF$_4$) +3CeF$_3$ | 693–842 | – | 2.27 | 1.94 | |

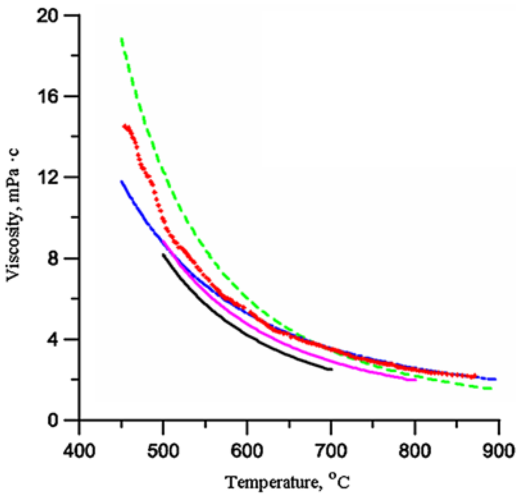

**Figure 12.4** Temperature dependence of dynamic viscosity for 46.5LiF-11.5NaF—42 KF melt, according to the data of ♦(Merzlyakov), ——— (Janz), - - - - - (Hoffman), —·—·- (Vriesema), and ——— (Klimenkov).

the prospective one for the fast MSR with U—Pu fuel cycle (Degtyarev and Ponomarev, 2012; Degtyarev et al., 2015). It can be used as well for MSR-burner of minor actinides with a fast neutron spectrum (Degtyarev et al., 2013).

One more candidate carrier salt 50.4NaF—21.6KF—28.0$UF_4$ was pointed out by Hirose et al. (2015). The big advantage of this salt is the absence of Li and Be in its composition, but it is not yet known if the $PuF_3$ solubility in this salt is high enough to meet the requirements necessary for the equilibrium mode reactor operation.

It is important to study this salt as a possible carrier salt for the fast molten salt reactor with U—Pu fuel cycle.

## 12.2 U—Pu fast MSR based on FLiNaK

### 12.2.1 Introduction

The first molten salt rector (MSR) was created in Los Alamos in 1944 and has been used as the neutron source (Segre, 1970). However, the first successful experience with MSR was achieved in Oak Ridge, USA, with the experimental reactor MSRE (Haubenrich and Engel, 1970) which used the eutectics 2LiF—$BeF_2$ (FLiBe) as the carrier salt and was in operation during almost 5 years (1965—69) (MacPherson, 1985).

In this experiment "the theorem of existence" has been proved: MSR can work and be maintained. This is a very important conclusion because MSR has many well-known preferences in comparison with the solid fuel reactors (negative void and temperature coefficients, low reactivity excess, no burning limits, no fuel elements, simpler closed fuel cycle, etc.).

From the early beginning MSR was oriented for Th—U fuel cycle with thermal neutron spectrum and $^{232}$Th and $^{233}$U as the row and fission isotopes, respectively. But in the following years the nuclear community came to the conclusion that it was impossible to solve the key problems of the nuclear power with thermal reactors only: the resource problem, problem of the nuclear waste incineration, of the nuclear fuel cycle closing, etc. In the last decade the MSR concept was revived (Le Blanc, 2010), particularly there have appeared projects of the molten salt fast reactors (MSFR) (Holcomb et al., 2011), especially on the base of the carrier salts LiF—UF$_4$ (Merle-Lucotte, 2011, 2013), chloride salts (Mourogov et al., 2006) and reactors with intermediate neutron spectrum based on LiF—NaF—BeF$_2$ (Ignatiev et al., 2007a,b).

The European programs (ALISIA, 2009) and (EVOL, 2012, 2013, 2015) were developed for the choice of the appropriate carrier salts, development of the MSFR design and its nuclear fuel cycle (Delpech et al., 2009). Particularly it was shown that the fuel cycle of MSFR can be essentially simplified: due to the small $n\gamma$-cross-sections of lanthanides irradiated by fast neutrons. Because of that the fuel composition cleaning can be performed only once in 30 years or even at the end of the total period of MSFR operation (Matheu et al., 2009).

The main goals of these projects are minor actinide incineration and $^{233}$U production in thorium blanket, but these attempts do not look promising due to the pure neutron balance of Th—U cycle of MSFR in comparison with U—Pu (Table 12.16).

The thorium MSFR can provide the fuel breeding but with a very long doubling time (~40 years) due to the small neutron excess at the $^{233}$U fission. The neutron excess in the U—Pu fuel cycle is much higher but the solubility of PuF$_3$ in almost all fluoride salts is very low even at 700°C: ~1 mol% in 2LiF—BeF$_2$ (Barton, 1960), ~3 mol% in LiF—NaF—BeF$_2$ (Ignatiev et al., 2006)). Such a small concentration of heavy elements in the carrier salt prevents the opportunity to create the fast reactor with U—Pu fuel cycle.

**Table 12.16 Neutron balance for the thermal and fast neutron spectra ($\nu$ is the multiplicity of the fission neutrons; $\alpha = \sigma_c/\sigma_f$; $\eta = \nu/(1 + \alpha)$; $\delta = \eta - 1$ is the neutron excess)**

| | **Thermal spectrum** | | | | **Fast spectrum**[a] | | | |
|---|---|---|---|---|---|---|---|---|
| | $\nu$ | $\alpha$ | $\eta$ | $\delta$ | $\nu$ | $\alpha$ | $\eta$ | $\delta$ |
| $^{235}$U | 2.43 | 0.167 | 2.07 | 1.07 | 2.67 | 0.09 | 2.38 | 1.38 |
| $^{238}$U | – | – | – | – | 2.64 | 5.9[b] | 0.45 | −0.55 |
| $^{239}$Pu | 2.88 | 0.358 | 2.12 | 1.12 | 3.18 | 0.025 | 3.10 | 2.10 |
| $^{232}$Th | – | – | – | – | 2.41 | 12.5[b] | 0.18 | −0.82 |
| $^{233}$U | 2.49 | 0.085 | 2.29 | 1.29 | 2.67 | 0.041 | 2.56 | 1.56 |

[a] Averaged over the neutron fission spectrum of $^{235}$U.
[b] Taking into account the neutron inelastic scattering on $^{238}$U and $^{232}$Th.

The situation was changed in the last 3 years when it was experimentally established that in the eutectic 46.5LiF−11.5NaF−42.0KF (FLiNaK) the solubility of $PuF_3$ is equal ~30 mol% (Lizin et al., 2013a; Volozhin et al., 2013). This observation opens the way for the development of fast MSR with U−Pu fuel (U−Pu FMSR) (Degtyarev and Ponomarev, 2012; Degtyarev et al., 2015).

### 12.2.2 Carrier salt for U−Pu FMSR

The eutectic 46.5LiF−11.5NaF−42.0KF mol%(FLiNaK) is well known and it was considered several times as the coolant for high-temperature reactors (Forsberg, 2006; Williams et al., 2006, 2016) and hybrid fusion−fission systems (LIFE, 2008). Its fusion diagram is presented in Fig. 12.5 (Bergman and Dergunov, 1941) with the melting temperature $T_m = 454°C$. The comparison of the FLiBe and FLiNaK properties is presented in Table 12.17.

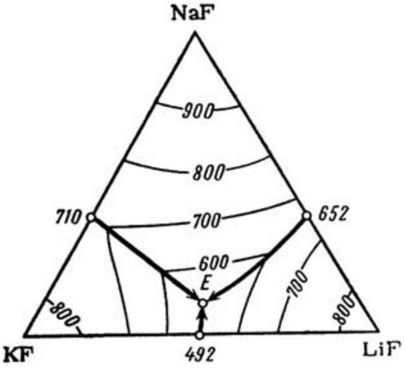

**Figure 12.5** Fusion diagrams of LiF−NaF−KF.

**Table 12.17** **Physical properties of FLiBe and FLiNaK**

| Carrier salt (mol%) | LiF−$BeF_2$ (67−33) | LiF−NaF−KF (46,5−11,5−42) |
|---|---|---|
| Mol. mass (g/mol) | 33 | 41.3 |
| Density $\rho$ ($g/cm^3$) | 1.94 | 2.02 |
| Melt. temp. $T_m$ (°C) | 460 | 454 |
| Heat capacity $qC_p$ (J/g K) | 2.42 | 1.88 |
| Thermal conduct. (W/m K) | 1.00 | 0.92 |
| Visc. $C_P$ ($m^2/c$) | 5.6 | 6.9 |
| Vapor press. at 900°C (mmHg) | 1.2 | 0.7 |
| Capture relat. to carbon | 8[a] | 4[b] |
| Moderation relat. to carbon | 60[a] | 0.4[b] |

[a] Thermal neutron spectrum.
[b] Fast spectrum.

It is evident that all the thermophysical properties of both salts are very similar in contrary to nuclear ones and the actinide solubility (Table 12.18, Fig. 12.6).

The individual solubilities of $PuF_3$ and $UF_4$ at their joint presence in the fuel composition FLiNaK$-UF_4-PuF_3$ are presented in Fig. 12.7. It is evident that at the joint presence of $UF_4$ and $PuF_3$ the individual solubilities are suppressed but the total concentration of $PuF_3$ and $UF_4$ ($\sim$25 mol% at 650°C) is high enough to keep the fast neutron spectrum.

The high lanthanide fluoride solubility is also important because it allows us to lengthen the intervals between the fuel composition adjustment (Fig. 12.8).

**Table 12.18 Solubility (mol%) of $PuF_3$ and $UF_4$ in FLiBe and FLiNaK as a function of temperature**

| Fluoride | Salt\Temp. (°C) | 550 | 600 | 650 | 700 | References |
|---|---|---|---|---|---|---|
| $PuF_3$ | FLiBe | 0.31 | 0.45 | 0.84 | – | Barton (1960) |
| | FLiNaK | 6.8 | 12.7 | 21.2 | 31.1 | Lisin et al. (2013a), Volozhin et al. (2013) |
| $UF_4$ | | 15.3 | 24.6 | 34.8 | 44.7 | Lisin et al. (2013b) |

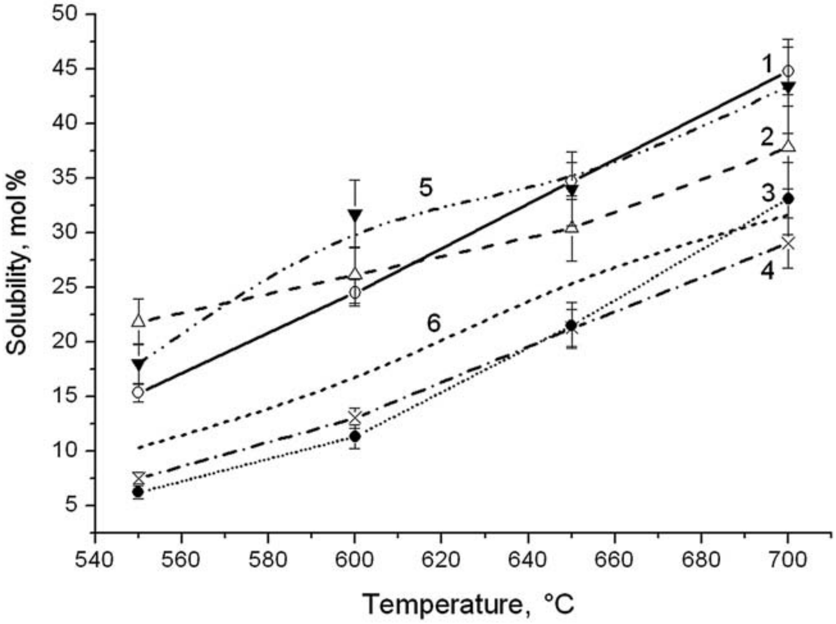

**Figure 12.6** Solubility of the actinide fluorides in FLiNaK: 1—$UF_4$ (Lizin et al., 2013b); 2—$ThF_4$ (Lizin et al., 2013b), 3—$PuF_3$ (Lizin et al., 2013a), 4—$PuF_3$ (Volozhin et al., 2013), 5—$AmF_3$ (Lizin et al., 2013a), 6—$PuF_3$ (Benes and Konings, 2008).

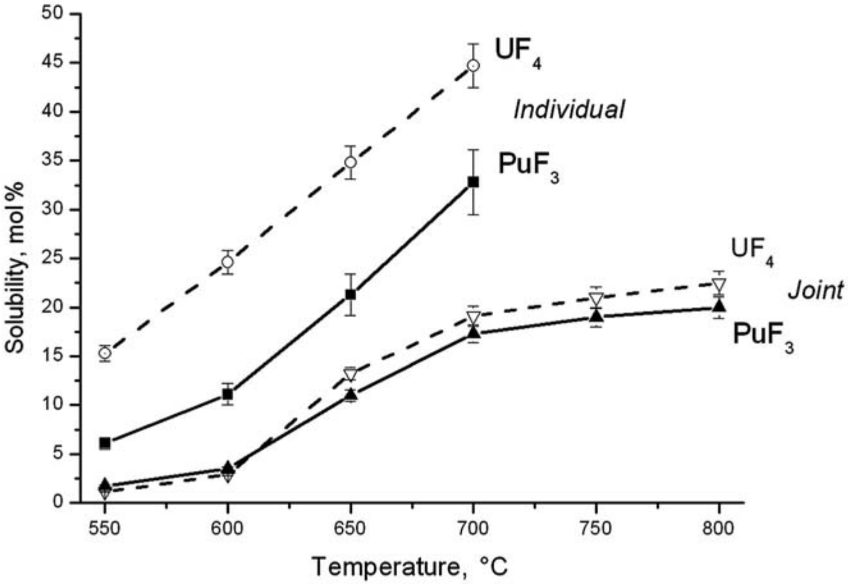

**Figure 12.7** Individual solubilities of $PuF_3$ and $UF_4$ in FLiNaK and their joint solubilities in the fuel composition FLiNaK$-$$UF_4$$-$$PuF_3$. (Lizin et al., 2015b).

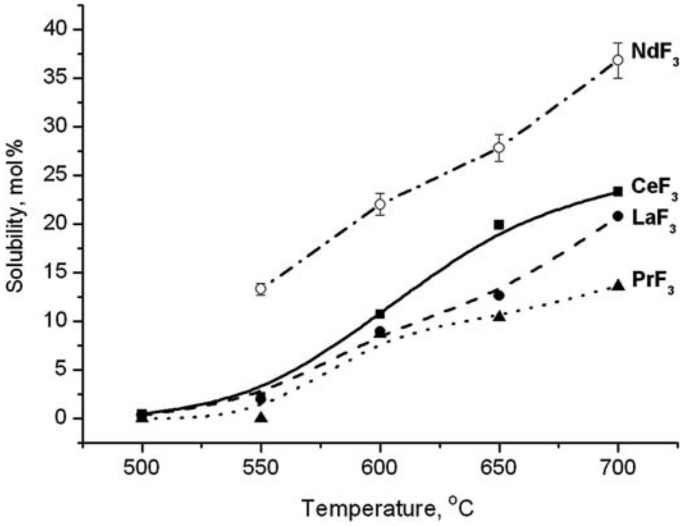

**Figure 12.8** Solubility of the lanthanide fluorides in FLiNaK: 1—$NdF_3$ (Lizin et al., 2013a, b); 2—$CeF_3$ (Lizin et al., 2013a; Volozhin et al., 2013); 3—$LaF_3$ (Ponomarev et al., 2013); 4—$PrF_3$ (Ponomarev et al., 2013).

### 12.2.3 Neutron physics of U–Pu FMSR

The conceptual schema of U–Pu FMSR used for the core neutronics calculations is presented in Fig. 12.9.

The results of these calculations are presented in Table 12.19. In the equilibrium mode of the reactor operation only $^{238}U$ is used and the reactor does not need

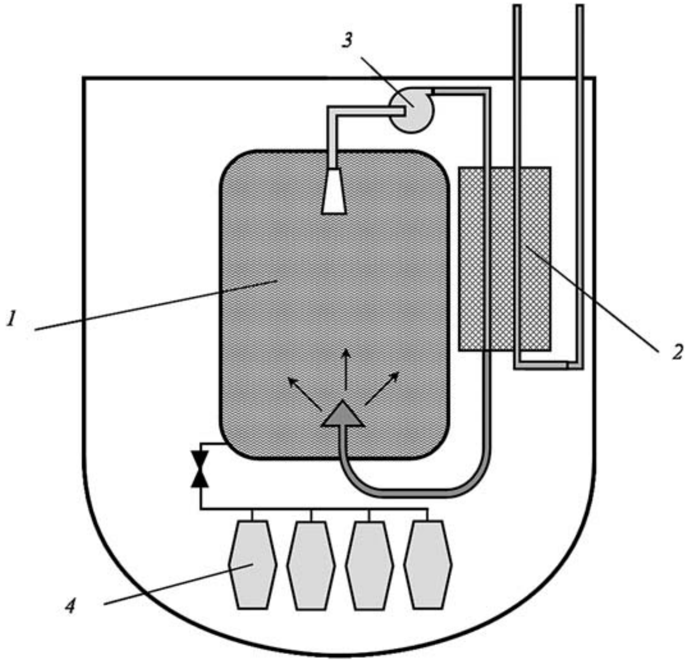

**Figure 12.9** The conceptual schema of FMSR: 1—core, 2—heat exchanger, 3—pump, 4—emergency vessels.

**Table 12.19 Main parameters of U–Pu FMSR in the equilibrium mode (Degtyarev et al., 2015)**

| | |
|---|---|
| Power (MWth) | 3200 |
| Volume ($m^3$) | 21.2 |
| Specific power ($W/cm^3$) | 150 |
| Average neutron flux ($cm^{-2}\ s^{-1}$) | $\sim 10^{15}$ |
| Initial fuel loading (U/Pu/Am, Cm, tons) | 68.5/15/– |
| Equilibrium fuel (U/Pu/Am, Cm, tons) | 68.6/20.9/1.4 |
| $UF_4/PuF_3$ equilibrium concentration (mol%) | 21/7 |
| Pu/Am, Cm equilibrium concentration (mol%) | 7.0/0.5 |
| $k_{ef}$ in equilibrium state | 1.008 |
| $k_\infty$ | 1.044 |
| Fraction of the delayed neutrons (β%) | 0.34 |
| Void coefficient, $dk_{ef}/(d\rho/\rho)$ | $-0.06$ |
| Temperature coefficient, $[dk_{ef}/d\rho/\rho]\cdot[d\rho/\rho/dT]$ (1/K) | $-2.4\cdot10^{-5}$ |

in-feeding by fissile nuclei $^{235}$U and $^{239}$Pu. If the reactor starts with $^{235}$U as a fuel the equilibrium mode is achieved in ~20 years (Fig. 12.10).

The neutron spectrum of U–Pu FMSR is presented in Fig. 12.11, in comparison with the neutron spectrum of the fast reactor BN-1200. The deep gap in the U–Pu FMSR spectrum is explained by the resonance in the elastic cross-section of the neutron scattering on the F nuclei.

In Table 12.20 the comparison of the U–Pu FMSR and fast lead-cooled reactor parameters is presented. It is interesting that the principal characteristics of both reactors are quite similar: the specific power, reactor volume, and average fuel density.

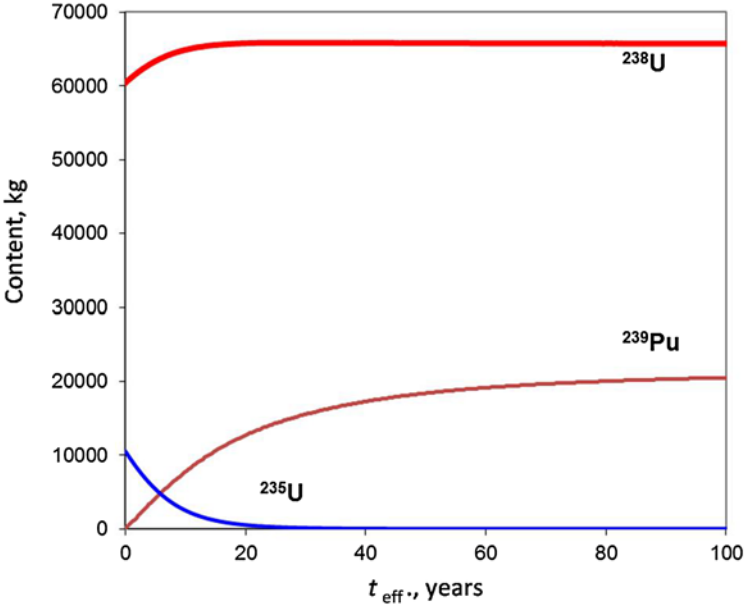

**Figure 12.10** Transition of U–Pu FMSR to the equilibrium mode.

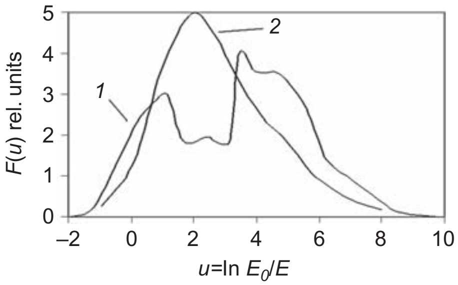

**Figure 12.11** The neutron spectra of FMSR (1) and fast reactor (2) as a function of lethargy $u = \ln E_0/E$, $E_0 = 2$ MeV.

Table 12.20 **Comparison of the U–Pu FMSR and BREST-1200 parameters**

| | U–Pu FMSR | BREST-1200 |
|---|---|---|
| Reactor power $W_b$ (MWth) | 3200 | 2800 |
| Full loading U/Pu (tons) | 68.6/21 (equilibrium) | 60/5.7 |
| Specific power (W/cm$^3$) | 150 | 143 |
| Reactor volume (m$^3$) | 21.2 | 19.5 |
| Effective fuel density (g/cm$^3$) | 3.1 | 3.4 |

### 12.2.4 U–Pu FMSR nuclear fuel cycle

In the framework of the MSRE project the studies of the fuel salt composition processing have been initiated. The first processing diagram (ORNL, 1966) was based on the volatility of $UF_6$ and vacuum distillation, as well as on the extraction recovery process (ORNL, 1969) of the molten fluorides mixture on the liquid metal (for instance, Bi). These works are ongoing. Currently, a new technology is being considered combining three main processes: volatility of fluorides (U, Pu, and Np), recovery extraction of minor actinides from molten salt into liquid metal, and the anodic oxidation with precipitation of lanthanide oxides (Uhlir and Marecek, 2005; Delpech et al., 2009). The technology developed is based on two processes: salt/metal extraction and electric separation (Uhlir et al., 2007). The simplified processing of FLiNaK salt composition, i.e., removal of the rare earth elements directly from the electrochemical cell based on the liquid metal extraction is also under study (Long et al., 2013).

All these nonaqueous technologies have not been used in industrial nuclear power for various reasons, and only one spent nuclear fuel (SNF) reprocessing technology based on the Purex process has been implemented on an industrial scale and is still being developed. The prototype of the third generation plant, which combines both nonaqueous and hydrometallurgy extraction processes is under development (Gavrilov et al., 2015). This approach has proven to be extremely effective and can help to solve one of the principal problems of the SNF radiochemical processing: to avoid the liquid radioactive waste releases.

#### 12.2.4.1 FMSR fuel cycle process diagram

The process diagram of the U–Pu FMSR closed nuclear fuel cycle should include the following key elements:

- Removal of the gaseous and volatile fission products;
- Recovery and recycling of fissionable nuclides;
- Isolation of the rare earth elements and other fission products;
- Partitioning and transmutation of the transplutonium actinide elements;
- Regeneration of the carrier salt and fuel composition adjustment;
- Immobilization and disposal of the fission products.

**Table 12.21** **Initial loading and equilibrium fuel composition of U−Pu FMSR (at.%)**

| Element | U-235 Initial loading | Pu initial loading | Equilibrium concentration | | |
|---|---|---|---|---|---|
| F | 64.47 | 63.80 | 63.78 | Am (total) | 0.10 |
| $^{7}$Li | 12.39 | 12.26 | 11.85 | $^{241}$Am | 0.060 |
| K | 11.19 | 11.07 | 10.71 | $^{242m}$Am | 0.003 |
| Na | 3.06 | 3.03 | 2.93 | $^{243}$Am | 0.037 |
| U (total) | 8.89 | 7.91 | 7.65 | Zr | 0.09 |
| $^{234}$U | – | – | 0.008 | Nd | 0.08 |
| $^{235}$U | 1.32 | – | 0.002 | Ce | 0.06 |
| $^{238}$U | 7.57 | 7.91 | 7.631 | Cm (total) | 0.06 |
| Pu (total) | – | 1.936 | 2.41 | $^{244}$Cm | 0.034 |
| $^{238}$Pu | – | 0.032 | 0.053 | $^{245}$Cm | 0.011 |
| $^{239}$Pu | – | 1.264 | 1.112 | Sr | 0.05 |
| $^{240}$Pu | – | 0.463 | 0.963 | Cs | 0.04 |
| $^{241}$Pu | – | 0.069 | 0.149 | Pr | 0.03 |
| $^{242}$Pu | – | 0.108 | 0.133 | Sm | 0.02 |
| $^{237}$Np | – | – | 0.01 | La | 0.02 |
| Ba | – | – | 0.12 | $^{231}$Np | 0.01 |
| Total | 100 | 100 | – | | 100 |

The first and the last operations have been thoroughly studied, however the problem of the minor actinides disposal remains pending. This section is mainly focused on the recovery and recycling of the fissile isotopes (including Am), as well as their separation from fission products. To process the irradiated FLiNaK-based fuel composition it is reasonable to consider the combined technology consisting of the nonaqueous part (separation of actinides and rare earth elements) and Purex process of the fissile element eliminations.

Usually, in order to use the Purex process in the fuel cycle the spent fuel must be first stored for about 3−5 years, which is sufficient to reduce the background radiation by approximately $10^3$ times and to lower the temperature allowing use of the water extraction methods. The equilibrium concentration of elements in the spent FMSR fuel to be processed is similar to the elements concentration in the spent MOX fuel of fast reactors, excluding the primary salt elements (Table 12.21).

During the MSRE project the experiment was performed to eliminate U, Th, and Ce from the hot spent fuel based on LiF-NaF salt at a temperature of 750°C, by the precipitation with CaO (ORNL, 1959). In this case, actinides and Ce precipitate in the form of oxides, and $CaF_2$ remains in the melted salt (Fig. 12.12).

However, the primary composition salt in this case is changed from LiF-NaF to LiF−NaF−$CaF_2$, and cannot be reused.

For Li−NaF−KF carrier salt it is suggested to use sodium oxide for the actinide and rare earth element precipitation from the fuel composition. The scheme and results of the preliminary experiments of the U and Nd precipitation from the fluoride mixture using $Na_2O$ at 650°C are presented in Fig. 12.13 and Table 12.22

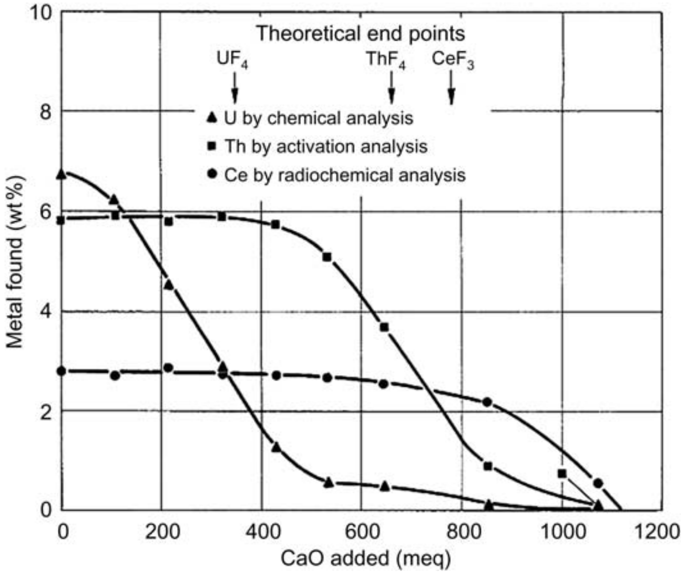

**Figure 12.12** Precipitation of U, Th, and Ce oxides from the fuel composition based on LiF−NaF (60−40 mol%) using CaO at 750°C (ORNL, 1959).

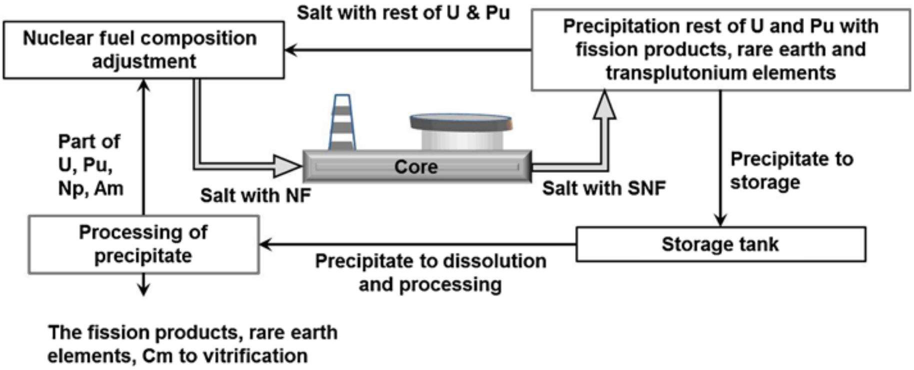

**Figure 12.13** Conceptual diagram for U−Pu FMSR closed fuel cycle with U and Pu recirculation by the fractional precipitation from the fuel composition (Ponomarev et al., 2016).

(Ponomarev et al., 2015, 2016). The precipitation allegedly takes place in accordance with the following chemical reactions:

$$UF_4 + 2\,Na_2O \rightarrow UO_2 + 4\,NaF;$$

$$2\,NdF_3 + 3\,Na_2O \rightarrow Nd_2O_3 + 6\,NaF.$$

Table 12.22 **Coprecipitation of U and Nd from LiF–NaF–KF**

| **Element** | **Ref. in FLiNaK (mol%)** | **$Na_2O$ stoichiometry to total amount of metals (%)** | | |
|---|---|---|---|---|
| | | **80 precipitation** | **200 precipitation** | **800 precipitation** |
| U | 1.57 | 45 | 84 | 72 |
| Nd | 2.06 | 85 | 97 | 97 |

The oxides are separated from the carrier salt by filtration, dissolution in the 3 mol/l nitric acid and uranium extraction using 30% TBF in dodecane. After scrubbing, U is re-extracted using a weak solution of nitric acid and, upon denitration, it changes into $UF_4$ that comes back to the fuel composition with the predefined concentration.

In the case of the U and Nd coprecipitation with stoichiometric $Na_2O$ stress, Nd precipitation is approximately twice as efficient as that of U (Table 12.22). In this case a new diagram can be developed for FLiNaK-based FMSR fuel cycle closing. It consists of the periodic removal of the significant part of the lanthanide elements and returning most of the uranium into the reactor.

The behavior of Pu under such conditions requires a special study, but the level of its precipitation is expected to reside between the indices of uranium and lanthanide elements. The fuel composition essentially cleared out of the lanthanides is returned into the reactor after its adjustment (Fig. 12.13); and the nonprecipitated lanthanides with the part of U and Pu are directed to storage and after cooling the rest of U and Pu are separated and returned into the reactor.

This diagram provides for Pu amount minimization outside the reactor, as well as for the use of the well-known water extraction technology of the fuel composition processing.

One more improvement of the fuel cycle closing diagram is the possibility to avoid the fission products, removing them from the fuel composition throughout the total reactor service life (Matieu et al., 2009). This is possible due to the small lanthanide cross-sections of fast neutron capture. The combination of this diagram with the capabilities of the fractional precipitation of the lanthanide oxides may provide additional benefits.

The fuel cycle closing diagram of the spent fuel (Fig. 12.14) has certain benefits in comparison with VVER and fast reactors ones:

- No need for the fuel rods production from the high active spent fuel;
- Lack of transportation, breakdown of the spent fuel assemblies and other mechanical procedures;
- Reduction by about threefold of the waste disposal mass due to the lack of the fuel assembly metal parts.

#### 12.2.4.2 *Economic Evaluation*

Due to the lack of fuel assembly manufacture, simplification of fuel composition processing, elimination of the high-level activity fuel rods cladding and fuel

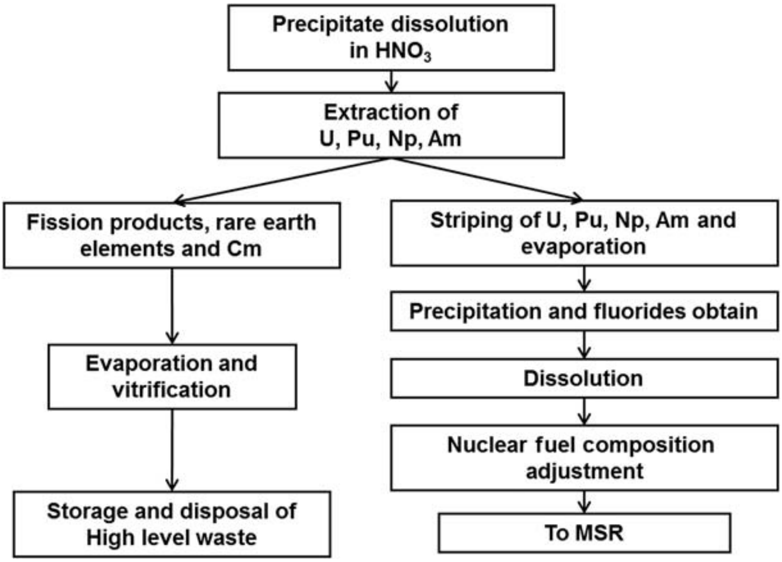

**Figure 12.14** Diagram for U–Pu FMSR spent fuel processing after storage.

assembly parts, the cost of the FMSR spent fuel handling is essentially reduced. The economic evaluations based on the IAEA methods (OECD, 2013) indicate that the cost of FMSR spent fuel handling operations is approximately fourfold lower than the cost of the fuel cycle of solid fuel reactors.

The high-level radioactive waste disposal is determined as follows: 1 part of Class 1 RW + 3 parts of Class 2 RW. The cost of Class 1 RW disposal is twice as high as that of Class 2 RW. Accordingly, the cost of Class 1 RW disposal is USD 600, and that of Class 2 RW is USD 400.

According to OECD (2013) the cost (USD/1 tonne SNF) of SNF handling for fast neutron reactors of BN-1000 type is equal 1000 + 2000 + 1000 = 4000 USD (processing + manufacture + disposal, Class 1 + 2 RW).

For FMSR: 500 + 600 = 1100 USD (processing + disposal Class 1 RW).

Therefore, the SNF handling cost for FMSR should be several times lower than that of the fast BN and VVER (PWR) reactors, which is equal to 1500 to 2000 USD, respectively, depending on the nuclear fuel cycle type (open or closed; OECD, 2013).

### 12.2.5 Conclusion

In the last 3 years it has been demonstrated that it is possible to create the fast molten salt reactor with U–Pu fuel cycle based on FLiNaK. This reactor can operate in the equilibrium mode using $^{238}U$ only. Its fuel cycle is simpler and cheaper than the fast reactor with solid fuel elements. For the realization of these advantages it is necessary to provide a complex scientific and technological study of the U–Pu FMSR concept, similar to the MSRE and MSBR. It is also essential to study other candidates for the FMSR carrier salts, e.g., NaF–KF–$UF_4$ (Hirose et al., 2015).

## 12.3 Feasibility of the U—Pu fast-spectrum molten-salt reactors using (Li, Na, K)F—$UF_4$—$TRUF_3$ fuel salts

### 12.3.1 Introduction

The author has proposed a concept of a U—Pu fast molten salt reactor using the NaF—KF—$UF_4$ solvent to dissolve an indefinite amount of $TRUF_3$. This reactor system including an on-line chemical processing was designated as the molten-salt fast breeder reactor (MSFBR) (Hirose et al., 2015). There was also innovative intention to confirm the feasibility of the fuel salt free from any issues associated with $^7$Li, such as tritium control, chemical process complexity, and economic pressure. The engineering feasibility of the MSFBR is studied by evaluating the amounts of fissile material to be fed and to be discharged, which depend upon the initial U charge and the fuel salt clean-up interval (Hirose et al., 2016; Hirose Y., 2017).

The viability of the concept requires a high solubility of actinide fluorides in common alkali fluoride liquid eutectic mixtures and a good understanding of phase stability during cooling until complete solidification.

The author is optimistic that fuel salts could be formulated by neutral compounds of alkali—actinide fluoride without concerning uncertain solubility issues. This goal is supported by the fact that alkali fluoride components such as LiF, NaF, and KF modify their acidic counterparts such as $UF_4$ and $PuF_3$ to form neutral compounds with lower melting points.

The present work intends to clarify the possibility if the U—Pu fast-spectrum molten-salt reactors with predictable freezing behavior can be feasible by using selected mixtures of alkali fluoride—$UF_4$ eutectic and alkali fluoride—$TRUF_3$ eutectic to make reasonable breeding, relying on the phase relationships provided experimentally or theoretically.

### 12.3.2 Preliminary survey and study

#### 12.3.2.1 Alkali fluorides eutectic mixtures

Extensive phase-diagram studies, in which the relationship illustrating the variation of compositions along with the liquidus temperature of mixtures have been defined, for alkali fluorides (LiF, NaF, and KF) eutectic systems containing $UF_4$ have done by ORNL (Tohma, 1959; Barton et al., 1958a,b, 1961a,b) as listed in Table 12.23 and those containing $PuF_3$ have been done thermodynamically (Benes et al., 2008, 2009) as listed in Table 12.24.

The binary and ternary phase diagrams of alkali fluoride mixtures containing $UF_4$ and those containing $PuF_3$ are shown in Figs. 12.15 and 12.16.

#### 12.3.2.2 Physical properties of alkali fluoride salt mixtures as fuel matrices

Since most molten salt reactors considered during the early stages of the MSR project in ORNL were thermal or epithermal, the fluorides of lithium, sodium,

**Table 12.23** Alkali fluoride eutectic mixtures containing $UF_4$

| Composition | Molecular ratio | Eutectic temperature (°C) |
|---|---|---|
| $LiF-UF_4$ | 0.730–0.270 | 490 |
| $NaF-UF_4$ | 0.785–0.215 | 735 |
| | 0.720–0.280 | 623 |
| | 0.440–0.560 | 680 |
| $KF-UF_4$ | 0.850–0.150 | 618 |
| | 0.615–0.385 | 740 |
| | 0.460–0.540 | 735 |
| $LiF-NaF-UF_4$ | 0.600–0.210–0.190 | 480 |
| | 0.350–0.370–0.280 | 480 |
| | 0.435–0.243–0.322 | 445 |
| | 0.245–0.290–0.465 | 602 |
| $LiF-KF-UF_4$ | 0.331–0.589–0.080 | 470 |
| | 0.267–0.476–0.257 | 500 |
| $NaF-KF-UF_4$ | 0.293–0.622–0.085 | 650 |
| | 0.504–0.216–0.280 | 490 |
| | 0.355–0.120–0.520 | 650 |

**Table 12.24** Alkali fluoride eutectic mixtures containing $PuF_3$

| Composition | Molecular ratio | Eutectic temperature (°C) |
|---|---|---|
| $LiF-PuF_3$ | 0.798–0.212 | 745 |
| $NaF-PuF_3$ | 0.779–0.221 | 726 |
| $KF-PuF_3$ | 0.651–0.349 | 619 |
| $LiF-UF_4-PuF_3$ | 0.733–0.257–0.010 | 484 |
| $LiF-NaF-PuF_3$ | 0.429–0.472–0.099 | 604 |
| | 0.611–0.167–0.222 | 685 |
| $LiF-KF-PuF_3$ | 0.431–0.522–0.047 | 476 |
| | 0.341–0.471–0.188 | 513 |
| $NaF-KF-PuF_3$ | 0.285–0.528–0.187 | 567 |
| | 0.053–0.607–0.340 | 605 |

beryllium, and zirconium have been given the most serious attention for reactor use. However, some alkali fluoride mixtures including potassium with $UF_4$ were also investigated.

The originally acquired data (Grimes et al., 1960, Hill et all., 1967, Hara and Ogino, 1989) of physical properties such as melting point, density, viscosity, and heat capacity of alkali fluorides containing $UF_4$ were compiled (Janz, 1967) and are shown in Table 12.25.

Of all the properties, the density of fuel salt is immediately required information to perform reactor physics calculations. The density of a molten salt mixture is customarily obtained from a weighted average of molecular volume of components; however it has been recognized that the results might be significantly erroneous

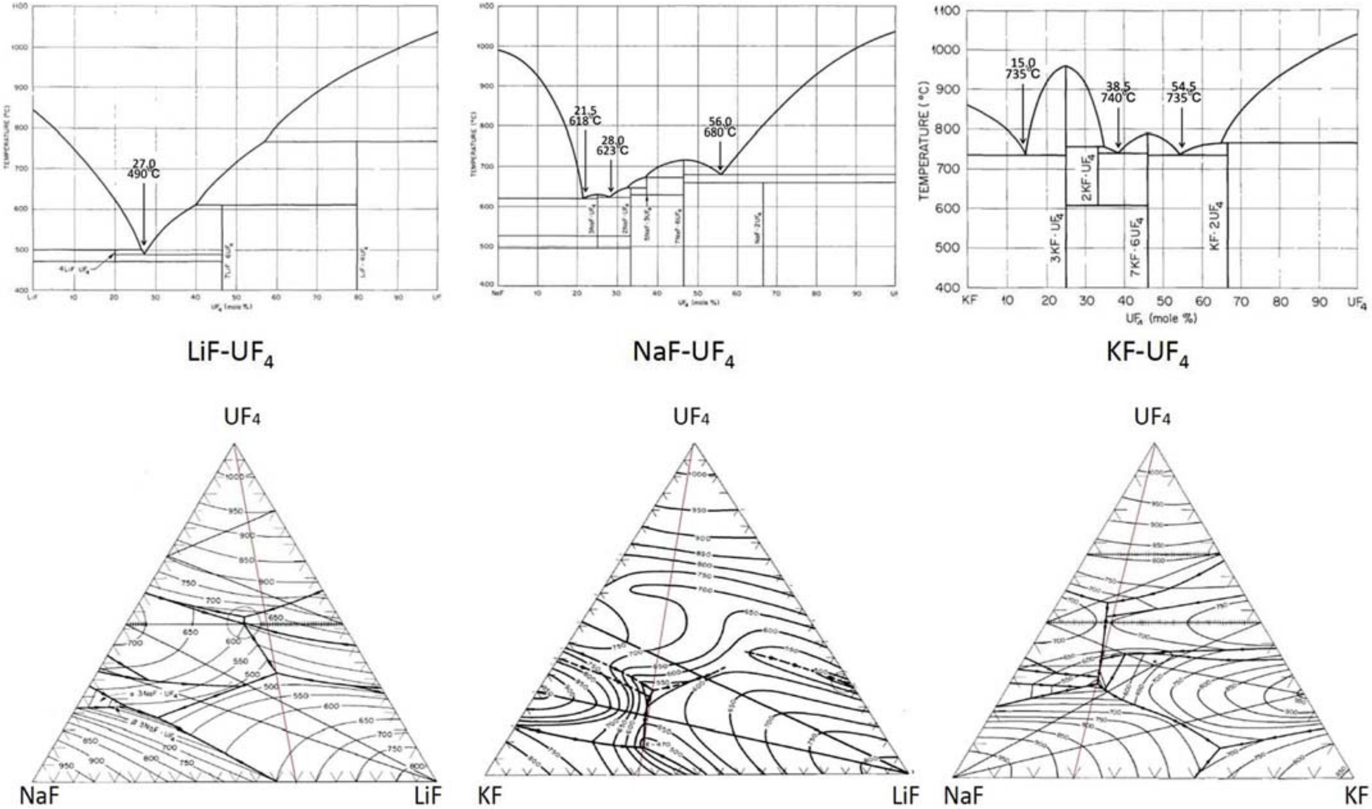

Eutectic T=445°C
0.435LiF-0.243NaF-0.322UF4

Eutectic T=500°C
0.267LiF-0.476KF-0.257UF4

Eutectic T=490°C
0.504NaF-0.216KF-0.280UF4

**Figure 12.15** Phase diagrams of selected alkali fluoride ternary eutectic mixtures containing UF$_4$ (Tohma, 1959).

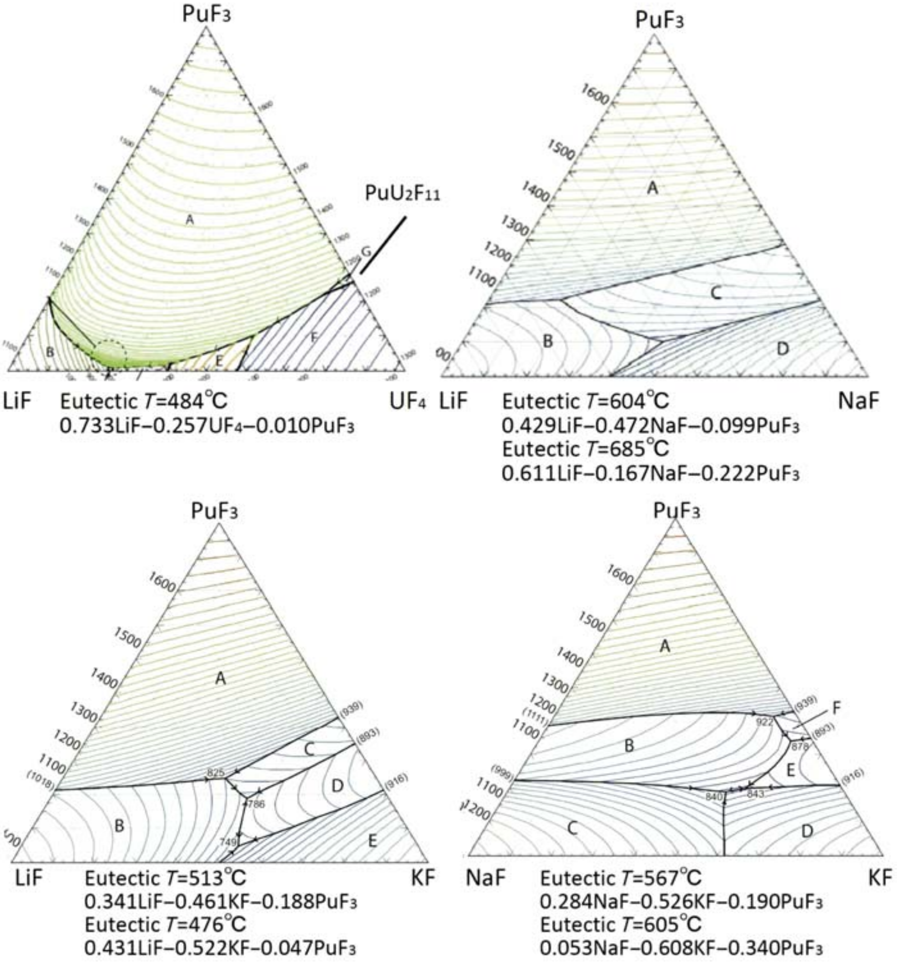

**Figure 12.16** Phase diagrams of selected alkali fluoride ternary eutectic mixtures containing $PuF_3$ (Benes et al., 2008).

without pertinent information about the respective components. There were not so many available density data of alkali fluorides containing $UF_4$ as listed in Table 12.25. However, it seems that all listed mixtures are approximately expressed by an identical second-order function for a very wide concentration range of $UF_4$, i.e., 0–45 mol% as shown in Fig. 12.17. The averaged temperature coefficients were reported as 0.0008/°C in the range of 0–4 mol% of $UF_4$, however as 0.0011/°C in the range higher than 22 mol%.

Based upon the density data for pure $UF_4$, $UF_3$, $PuF_4$, and $PuF_3$, i.e., 6.72, 8.97, 7.0, and 9.32 $g/cm^3$, respectively (Benedict et al., 1981a), it is observed that the densities of uranium trifluoride and plutonium trifluoride are four and three times higher than those of tetrafluorides, respectively, and plutonium fluorides are 1.04

**Table 12.25** **Available physical properties for liquid alkali fluorides containing $UF_4$**

| Composition (mol%) | | | | MP | Liquid density | Liquid viscosity | Heat capacity | Thermal conductivity |
|---|---|---|---|---|---|---|---|---|
| Li | Na | K | U | (°C) | (g/cc) ($T$: °C) | (cp) | (Cal/g deg) | (W/m K) |
| | 60.0 | 40.0 | | 710 | $2.40 - 0.00060\,T$ | — | — | — |
| 60.0 | 40.0 | | | 652 | $2.42 - 0.00055\,T$ | 4.66 (600°C) | 0.5803 (700°C) | — |
| 50.0 | | 50.0 | | 492 | $2.46 - 0.00068\,T$ | 4.75 (600°C) | 0.4400 (700°C) | — |
| 46.5 | 11.5 | 42.0 | | 454 | $2.53 - 0.00073\,T$ | 4.75 (600°C) | 0.45 (700°C) | 4.53 |
| 72.5 | | | 27.5 | 490 | $6.11 - 0.00127\,T$ | 12.1 (700°C) | — | — |
| | 66.7 | | 33.3 | 623 | $5.51 - 0.00130\,T$[a] | 16.27[a] (600°C) | 0.21 (700°C) | — |
| | 50.0 | | 50.0 | 680 | $6.16 - 0.00107\,T$ | — | — | — |
| | | 45.0 | 55.0 | 735 | $6.07 - 0.00115\,T$ | — | — | — |
| 38.4 | 57.6 | | 4.0 | 645 | $2.95 - 0.0077\,T$ | 3.5 (700°C) | 0.53[a] (700°C) | — |
| 33.0 | 45.0 | | 22.0 | 506 | $4.50 - 0.00101\,T$ | — | 0.26 (700°C) | — |
| 48.0 | | 48.0 | 4.0 | 560 | $2.75 - 0.00073\,T$ | 3.2 (700°C) | 0.382 (700°C) | — |
| | 48.2 | 26.8 | 25.0 | 558 | $4.54 - 0.00110\,T$ | 9.8 (700°C) | 0.23 (700°C) | — |
| | 46.5 | 26.0 | 27.5 | 530 | $4.70 - 0.00115\,T$ | 17.31 (600°C) | 0.23[a] (700 °C) | 0.87 |
| | 50.0 | 20.0 | 30.0 | 575 | $4.78 - 0.00104\,T$ | 10.0 (700°C) | 0.22 (700 °C) | — |
| | 35.0 | 20.0 | 45.0 | 708 | $5.60 - 0.00116\,T$ | — | — | — |
| 44.5 | 10.9 | 43.5 | 1.1 | 452 | $2.65 - 0.00090\,T$[a] | 4.61[a] (600°C) | 0.44[a] (700°C) | 4.00 |
| 45.3 | 11.2 | 41.0 | 2.5 | 490 | $2.67 - 0.00072\,T$ | 5.10[a] (600°C) | 0.38 (700°C) | — |
| 44.7 | 11.0 | 40.3 | 4.0 | 560 | $2.80 - 0.00074\,T$ | 5.35 (600°C) | 0.41 (700°C) | — |

[a] Explicitly indicated as experimental values (Janz, 1967).

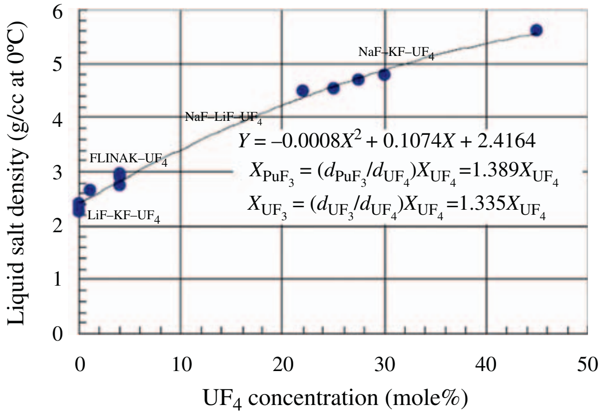

**Figure 12.17** Density of alkali fluorides containing UF$_4$ (Hirose et al., 2015).

times higher than those of uranium fluorides. Thus it is hypothetically assumed that PuF$_3$ can be substituted by 1.389 molecules of UF$_4$ in the sense of density effect and UF$_3$ by 1.335 molecules of UF$_4$.

This procedure can give the density of 4.23 g/cm$^3$ for FLiNaK—UF$_4$—PuF$_3$ (74—23—5 mol%), that of 4.61 g/cm$^3$ for NaF—KF—UF$_4$—PuF$_3$ (42—23.5—27.5—7.0 mol%), and that of 4.65 g/cm$^3$ for NaF—KF—UF$_4$—UF$_3$—PuF$_3$ (42—23.5—25—2.5—7.0 mol%) all at 627°C. This procedure was a breakthrough in the study; however, it should be experimentally verified later.

### 12.3.2.3 Chemical implication of Pu fissioning

It had been traditionally understood by ORNL (Thoma, 1968) that during UF$_4$ fissioning, the net oxidation state of fission products was less than four and yet four fluorine atoms were released, leaving a somewhat oxidizing event per fission, meanwhile, in the case of PuF$_3$, it was expected to produce a slightly reducing event per fission.

Meanwhile, it was suggested that the fission of PuF$_3$ should produce some free fluorine per fission in the proposed TRU burning MSR concept based on the fission product yield data of $^{239}$Pu in thermal neutron spectrum and adapted the same assumption of chemical behavior made during the MSBR conceptual design (Hirose et al., 2001).

The author is more confident in giving free fluorine production by fast neutron $^{239}$PuF$_3$ fission based upon relevant data obtained in an LMFBR (Benedict et al., 1981b) and compared with the data for the MSBR (Baes, 1974) shown in Table 12.26.

It takes a different approach (Shimazu et al., 2015) to certify the new Red-Ox potential control paradigm by computation based on the ENDF/B-VII 238 groups nuclear data, TRITON evaluation module, ORIGEN-S, and compiled by OPUS module of the SCALE6.1 (ORNL, 2011), and elucidated that the free fluorine yield

## Table 12.26 Comparison of free fluorine production between MSBR and LMFBR

| Fission products | Valency of FPs in molten fluorides | $^{233}UF_4$ fission in SBR | | $^{239}Puf_3$ fission in MFBR | |
|---|---|---|---|---|---|
| | | Yield/ fission[a] | Combined F/fission | Yield/ fission[b] | Combined F/fission |
| Br, I | −1 | 0.015 | −0.015 | 0.0236 | −0.0238 |
| Kr, Xe | 0 | 0.606 | 0.000 | 0.2410 | 0.0000 |
| Rb,Cs | +1 | 0.004 | 0.004 | 0.2072 | 0.2072 |
| Sr, Ba | +2 | 0.072 | 0.144 | 0.1046 | 0.2344 |
| Y, RE | +3 | 0.538 | 1.644 | 0.4848 | 1.4616 |
| Zr | +4 | 0.318 | 1.272 | 0.1998 | 0.7988 |
| Nb, Mo, Tc | 0 | 0.274 | 0.000 | 0.3076 | 0.0000 |
| Ru, Rh, Pd, Ag, Cd, Te | 0 | 0.126 | 0.000 | 0.4312 | 0.0000 |
| Total FP Yield | | 1.953 | | 2.0000 | |
| Total combined F/fission | | | 3.049 | | 2.6462 |
| Excess F/fission | | | 0.951 | | 0.3538 |

[a] Baes (1974).
[b] 37,000 MWD/t in LMFBR after 150 days cooling (Benedict et al., 1981b).

## Table 12.27 Free fluorine production rates

| Fissionable materials | mole-F/fission | | mole-F/MWt-y | |
|---|---|---|---|---|
| | Fast | Thermal | Fast | Thermal |
| $^{233}UF_4$ | 0.65 | 0.8 | 1.13 | 1.14 |
| $^{235}UF_4$ | 0.8 | 0.8 | 1.35 | 1.36 |
| $^{239}PuF_3$ | 0.6 | 0.6 | 1.02 | 1.09 |

value for $^{233}UF_4$, $^{235}UF_4$, and $^{239}PuF_3$ per unit power output under both thermal neutron (MSRE) and fast neutron (MSFBR) environment as shown in Table 12.27 and Fig. 12.18.

New free fluorine yield for $^{235}UF_4$ is identical to the classic experience, but that for $^{239}PuF_3$ is substantially larger than the previously estimated value, based on LMFBR yield data (Benedict et al., 1981b).

The study of molten LiF–BeF$_2$–ThF$_4$ (75–5–20 mol%) salt mixture fueled by 2 mol% of UF$_4$ with additives of Cr$_3$Te$_4$, using 250-hour tests with exposure of

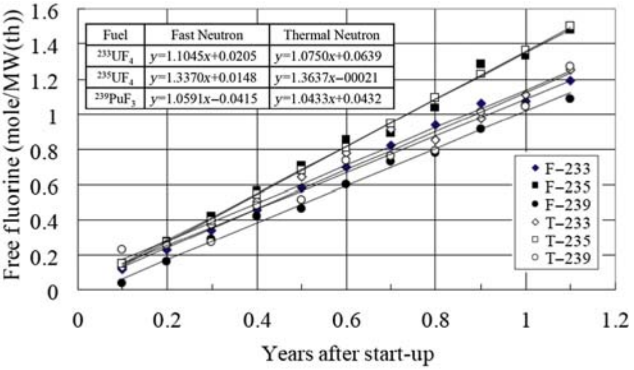

**Figure 12.18** Build-up of free fluorine along with burnup.

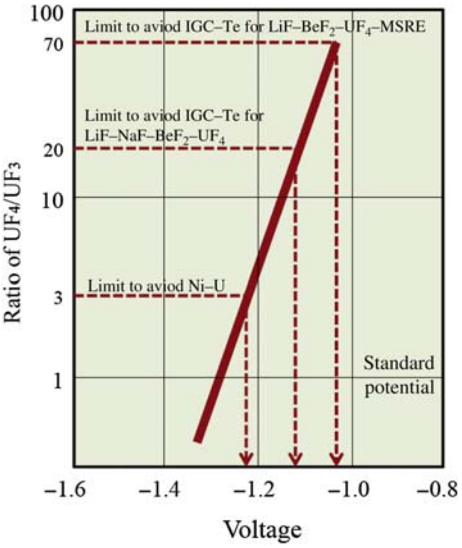

**Figure 12.19** Dependence of the Red-Ox potential on the $UF_4/UF_3$ ratio in fluoride salt.

nickel-based alloys specimens under mechanical loading at 700−750°C, found that there were no traces of tellurium intergranular cracking on specimens in the fuel salt with [U(IV)]/[U(III)] ratio from 0.7 to 20 and no nickel−uranium intermetallic film on the specimens with fuel salts characterized by a ratio larger than 3 (Ignatiev et al., 2012a,b), as shown by the acceptable Red-Ox voltage range in Fig. 12.19 (Williams et al., 2002). Alkali fluoride−$UF_4$ as well as alkali fluoride−$PuF_3$ might be Lewis neutral (Toth et al., 1994), however it would be reasonable to take the [U (IV)]/[U(III)] ratio as 20.

### *12.3.2.4 Chemical implication of fission product lanthanides*

#### 12.3.2.4.1 Molar yield of fission product lanthanides

The molar yield of fission product lanthanides was elucidated from the same calculation (Shimazu et al., 2015) for the free fluorine yield of $^{239}PuF_3$ per unit power output under fast neutron fission based on the ENDF/B-VII 238 group as shown in Table 12.28.

### *12.3.2.5 Operational characteristics of the MSFBR*

The engineering feasibility of the MSFBR feeding with TRU by evaluating control characteristics is mainly associated with the amount of fissile material to be fed and to be discharged which depend on the initial U charge and the fuel salt clean-up interval (Hirose et al., 2016).

#### 12.3.2.5.1 Reactor physical properties

Physical calculations were made taking originally proposed configurations of the reactor (core height/radius ratio: 1.85, core volume: 21.2 $m^3$, primary circuit volume: 31.8 $m^3$) and the definition of the terms, such as the power output (3.2 GWth) and the effective density of fuel salt (3.1 $g/cm^3$) were the same as the reference (Ponomarev, 2013), but other factors, such as the actinides isotopic composition (Ando et al., 1999), neutron leakage (with 30-cm steel reflector), the fuel temperature (627°C), the fuel salt density, and the salt clean-up and make-up condition, etc., were discretely specified to give a verified number of heavy element masses and concentrations in the fuel salt to give designated criticality from the start-up to the final state (40 years), using the SRAC2006 standard nuclear analytical code with PIJ-BURN routine (Okumura et al., 2007) based upon JENDLE3.3 (Shibata et al., 2002), which has been a traditional practice applied on the thermal neutron molten salt reactors such as the FUJI series (Mitachi et al., 2008).

The pertinent results of physical calculation using recovered uranium instead of $^{238}U$ are shown in Tables 12.29 and 12.30. The experimental data are classified according to the mass of initial U charge, the TRU source, and the interval of chemical cleaning (300 efpd or 1500 efpd).

**Table 12.28** **Molar yield of fission product elements**

| Fission products | Mole rate to total FP | Mole rate to TRU[a] |
|---|---|---|
| Rare gases | 0.1691 | 0.0417 |
| Halogens | 0.0153 | 0.0038 |
| Transient metals | 0.1641 | 0.0405 |
| Alc./Alc. earth metals | 0.2368 | 0.0584 |
| Lanthanides | 0.2794 | 0.0689 |
| Zirconium | 0.1353 | 0.0334 |
| Total | 1.0000 | 0.2466 |

[a] TRU inventory: (20.92 tons) 87,167 moles (Shimazu et al., 2015).

**Table 12.29** Reactor physics calculations to NaF−KF−$UF_4$−$TRUF_3$ fuel salt (1)

| Fuel salt | Element | Inventory at start (tons) | Peak supply (tons/y) | Total supply (tons) | Total feed (tons) | Inventory at equilibrium (tons) | Surplus (tons) |
|---|---|---|---|---|---|---|---|
| U:61 ton | U | 61.437 | 1.052 | 42.072 | 103.509 | 60.915 | 0.1790 |
| 300 efpd | TRU | 17.086 | 0.741 | 2.555 | 19.641 | 20.039 | 0.0589 |
| U:66 ton | U | 66.528 | 1.196 | 47.834 | 114.361 | 65.910 | 4.4689 |
| 300 efpd | TRU | 17.757 | 0.616 | 1.768 | 19.525 | 20.039 | 1.3587 |
| U:71 ton | U | 71.465 | 1.366 | 54.634 | 126.096 | 70.909 | 9.7312 |
| 300 efpd | TRU | 18.351 | 0.593 | 1.316 | 20.394 | 20.258 | 2.7800 |
| U:71 ton | U | 71.465 | 1.075 | 43.006 | 114.468 | 70.912 | 0.8003 |
| 1500 efpd | TRU | 18.351 | 0.655 | 3.702 | 22.053 | 22.620 | 0.2553 |

**Table 12.30** Reactor physics calculations to NaF−KF−$UF_4$−$TRUF_3$ fuel salt (2)

| Fuel salt | Years from start | Na | K | $^{235}U$ | U | TRU[a] | Pu | MA | Temp. [b] coeff. of reactivity | Neutron leak rate |
|---|---|---|---|---|---|---|---|---|---|---|
| | | (mole rate) | | (mole rate) | (mole rate) | | (mole rate) | | | |
| U:61 ton | 0 | 0.451 | 0.252 | 0.00186 | 0.233 | 0.0643 | 0.0574 | 0.0069 | − 4.4E − 05 | 0.050 |
| 300 efpd | 40 | 0.447 | 0.250 | 0.00034 | 0.229 | 0.0747 | 0.0696 | 0.0051 | − 4.0E − 05 | 0.048 |
| U:66 ton | 0 | 0.432 | 0.242 | 0.00206 | 0.258 | 0.0648 | 0.0610 | 0.0074 | − 4.2E − 05 | 0.048 |
| 300 efpd | 40 | 0.429 | 0.240 | 0.00034 | 0.254 | 0.0774 | 0.0724 | 0.0050 | − 4.0E − 05 | 0.046 |
| U:71 ton | 0 | 0.413 | 0.231 | 0.00227 | 0.284 | 0.0724 | 0.0646 | 0.0078 | − 4.0E − 05 | 0.046 |
| 300 efpd | 40 | 0.410 | 0.229 | 0.00041 | 0.280 | 0.0803 | 0.0754 | 0.0049 | − 3.9E − 05 | 0.045 |
| U:71ton | 0 | 0.413 | 0.231 | 0.00227 | 0.294 | 0.0724 | 0.0646 | 0.0078 | − 4.0E − 05 | 0.046 |
| 1500 efpd | 40 | 0.407 | 0.227 | 0.00044 | 0.278 | 0.0879 | 0.0819 | 0.0060 | − 3.3E − 05 | 0.041 |

[a] TRU from BWR−UOX−45GWd/t-U (Ando et al. 1999), Np/Pu/Am/Cm = 5.19/89.22/4.90/0.69 (wt%) Pu-238/239/240/241/242 = 2.80/51.77/25.98/11.07/8.38 (wt%).

[b] Temperature coefficient of reactivity: The coefficient of reactivity within 20°C of temperature deviation is defined as a sum of the Doppler effect and the temperature effect and expressed by the following relationship, where *K* is effective reactivity coefficient, *ρ* is density and *T* is temperature as expressed in the following formulae: $\left(\frac{\partial K}{\partial T}\right)_\rho + \rho\left(\frac{\partial K}{\partial \rho}\right)_T \times \frac{1}{\rho}\left(\frac{\partial \rho}{\partial T}\right)$

### 12.3.2.5.2 Initial U charge

The initial uranium inventory dominates linearly the initial critical fissile mass, the breeding gain, and inversely the total supplement charge as shown in Fig. 12.20 (Hirose et al., 2016). The effect of initial U charge on feed/breed balance is evaluated in three cases in which fuel salt cleaning started after 300 effective full power days (efpd) with an interval of 300 efpd. The larger initial charge of U represents a larger amount of initial fissile inventory but a smaller amount of supplement; however, the peak annual supplement is less dependent on the initial U charge. A total 61.4 tons of initial charge of U is the lowest threshold limit to make breeding

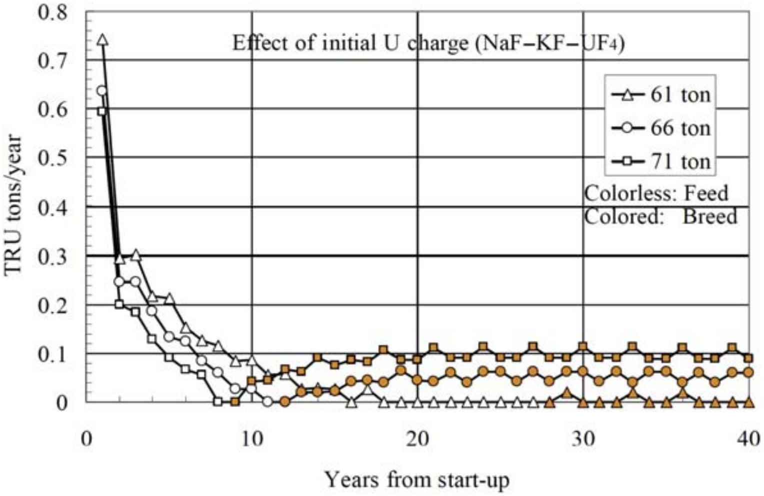

**Figure 12.20** Effect of initial U charge on feed/breed balance.

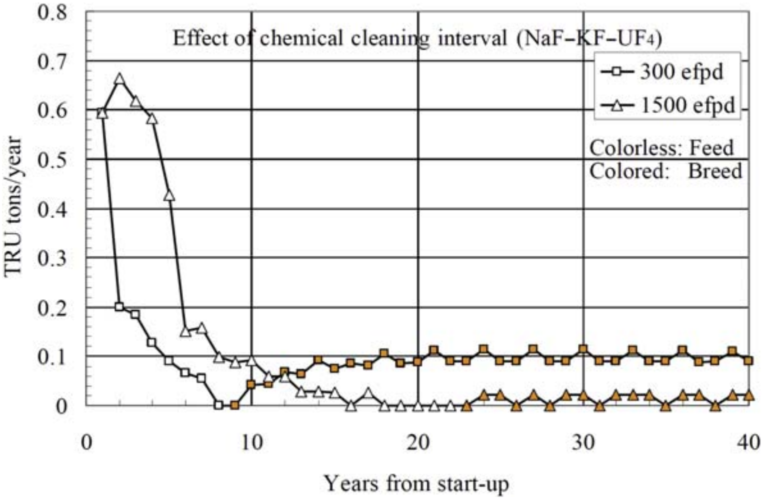

**Figure 12.21** Effect of chemical cleaning interval on feed/breed balance.

breakeven possible, while 71.5 tons of U can provide as much as 100 kg TRU of annual breeding; however, it has the highest threshold limit by U content acceptable by the fuel salt.

### 12.3.2.5.3 Fuel salt cleaning interval

Three hundred efpd and 1500 efpd fuel salt cleaning intervals are evaluated with the same charge of the fuel salt composition, as shown in Fig. 12.21 (Hirose et al., 2016). No chemical cleaning but only making up of actinides was made during the designated initial interval. This guarantees sufficient build-up of fission products in the fuel salt all the way from the start-up to equilibrium.

The longer interval represents a larger amount of fissile material initial supplement ($0.73t$ to $3.53t$), but the peak annual supplement is nearly irrespective to the cleaning interval ($0.59t$ to $0.66t$). From the standpoint of reactor operation control, the peak make-up value (not the total fissile supplement) determines the cost relative to throughput of the chemical process.

The operation of an MSFBR with 300 efpd of fuel salt cleaning interval can provide good breeding (100 kg-TRU/year), while that with 1500 efpd barely provides a sustaining operation with appreciable breeding (10 kg-TRU/year) at equilibrium. Intervals longer than 1500 efpd should not be acceptable, due to build-up of neutron-absorbing fission products.

### *12.3.2.6 Chemical processing in the MSFBR*

#### 12.3.2.6.1 Oxide selective precipitation process

The chemical processing in the MSFBR should efficiently remove fuel materials from the fission products, but not necessarily efficiently remove fission products that become neutron poisons, if it were operated with thermal neutrons.

To perform this perpetual mission, a processing interval of 1500 efpd is sufficiently long, and provides a small throughput. The on-line chemical processing facility with remote handling of radioactive isotopes would be the most expensive part of the plant. The cost would depend upon the process complexity, material compatibility, process wastes, and capacity.

In the very early stage of the MSR Program at ORNL, experimental studies on selective precipitation of oxides were carried out, because it might be a suitable scheme for the reprocessing of molten salt reactor fuels. It was abandoned after discovery of the reductive extraction and metal-transfer process associated with the $UF_6$ volatile process, which, though complex and material-incompatible, involved handling only liquids and gases. The fluoride volatile process of $UF_6$ had been perceived as the most practical since successful operation in MSRE. However, the fact that metallic Zr scrap addition should be followed, a prolonged $H_2$ sparge to remove metallic corrosion products (Ni, Fe, Cr) caused by $F_2$ treatment was sometimes overlooked.

The initial selective oxide precipitation experiment chose LiF−KF (50−50 mol%) as a matrix, and estimated the concentration of the particular metal ion remaining in solution in the presence of some 25% excess precipitating agents (usually CaO) and it was concluded that $UO_2$ would precipitate almost completely (liquid phase $< 0.0008$ wt%) before any $Ce_2O_3$ precipitates as shown in Table 12.31 and Fig. 12.22 (Shaffer, 1958).

It was envisioned to apply the oxidation process to the DMSR fuel. They could treat the melt with a strong oxidant to convert $UF_3$ to $UF_4$, $PaF_4$ to $PaF_5$, and $PuF_3$ to $PuF_4$. Precipitating the insoluble oxides was achieved using water vapor diluted in helium. The oxides $UO_2$, $Pa_2O_5$, $PuO_2$, $CeO_2$, probably $NpO_2$, and possibly $AmO_2$ and $CmO_2$ should be obtained. The oxides are recovered by decantation and

**Table 12.31** **Oxide selective precipitation experiment**

| Metal ion | Precipitating phase | Metal found (wt%) |
|---|---|---|
| Zr | $ZrO_2$ | <0.0008 |
| U | $UO_2$ | <0.0008 |
| Ce | $Ce_2O_3$ | <0.0085 |
| Be | BeO | <0.01 |
| Ba | Soluble | >6.5 |

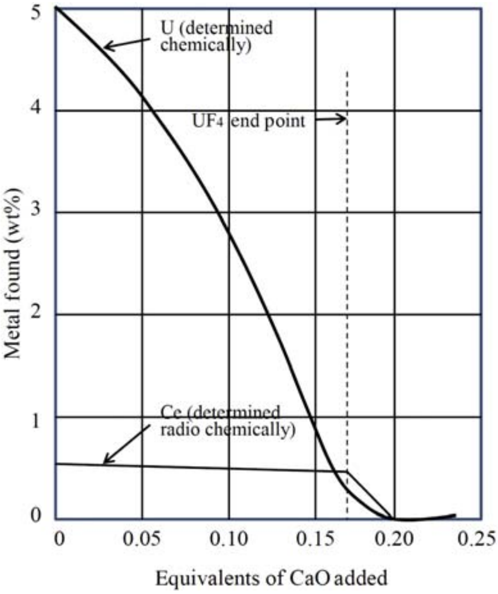

**Figure 12.22** Reaction of $UF_4$ and $CeF_3$ with CaO in LiF−KF.

filtration. The oxides are hydrofluorinated into the purified melt of $LiF-BeF_2-ThF_4$ and the melt reduced with $H_2$ and fuel reconstituted with the desired $UF_3/UF_4$ ratio (Engel et al., 1980).

It was also suggested (Ignatiev et al., 2007a,b) that the oxide precipitation process could be a possible option compared to the reductive extraction process or electrochemical process, because of ultimate simplicity and more acceptable corrosion of material (pure Ni), referring to a successful attempt by a Russian scientist (Gorbunov et al., 1976), which was made to precipitate mixed uranium, plutonium, minor actinides, and rare earths from LiF−NaF molten salt solution by fluor-oxide exchange with other oxides (for example, CaO, $Al_2O_3$) at temperatures of 700−800°C. The following order of precipitation was found in the system: U−Pu−Am−Ln−Ca. Essentially all U and TRU were recovered from the molten salt till to a residual concentration $5 \times 10^{-4}\%$, when 5–10 mol% of rare earths was still concentrated in solution.

### 12.3.2.6.2 Fuel salt clean-up process

Basing upon the survey, it is concluded that the application of the selective oxide precipitation process with alkali or alkali-earth metal oxides ($K_2O_2$; melt at 490°C and CaO; solid) as the oxidizer can be feasible under special selectivity cautions to the MSFBR technology relying on NaF and KF as major components of the fuel matrix, as shown in Fig. 12.23 (Hirose et al., 2016).

If it can reduce TRU concentration to $5 \times 10^{-4}$ mol% in liquid phase from 8 mol %, the available loss rate will be $6.25 \times 10^{-5}$. This loss rate is substantially lower than $10^{-3}$ of the target to be achieved by the pyro-processes currently under development.

It should be taken into account that melting temperature increases during actinide removal treatment. Using $K_2O_2$ as a precipitator can modify the Na/K ratio to give a eutectic mixture of 710°C. Fluorine freed from $UO_2$ precipitation would react with $TRUF_3$ to oxidize them into $TRUF_4$ which can be eventually precipitated as $TRUO_2$. Succeeding use of CaO as a precipitator up to ca. 20 mol% may give stable ternary eutectic at ca. 700°C of the waste salt after the eutectic has been achieved.

The on-line chemical processing flowsheet applicable to the cleaning interval of 1500 efpd is shown in Fig. 12.24 (Hirose et al., 2016), in which He sparge process to purge gaseous fission products as well as noble and seminoble metal fission products, electro reductive removing zirconium developed for the MSRE remediation (Peretz, 1996) are incorporated. It is noteworthy that the process is facilitated to eliminate solid handling but performed by liquid phase handling only. Up to 10% of fission product lanthanides would be allowed to leak into the fuel salt stream after processing.

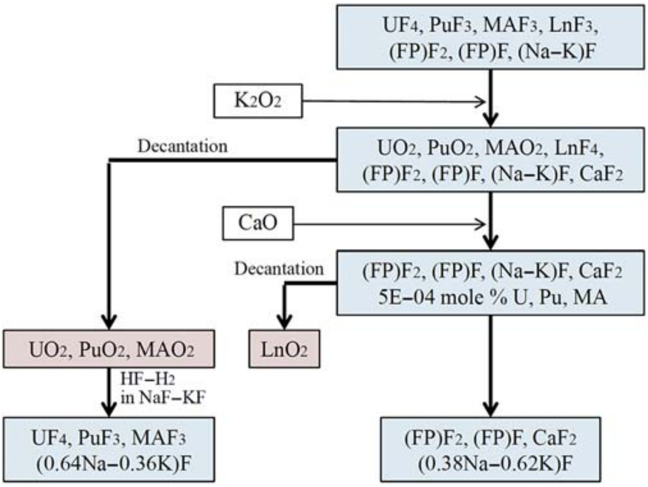

**Figure 12.23** Oxide selective precipitation process flowsheet.

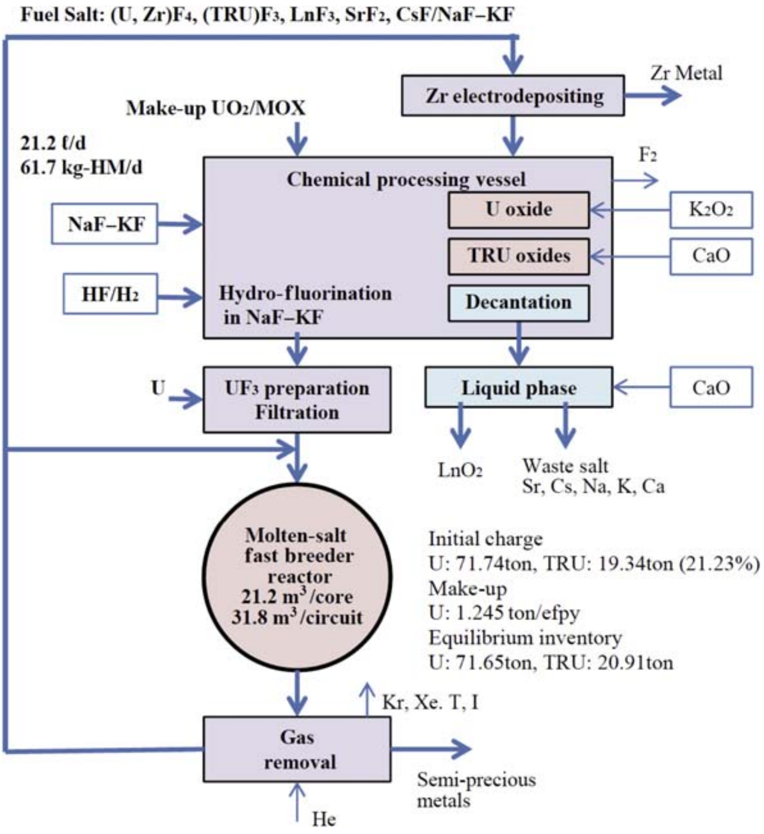

**Figure 12.24** On-line chemical processing in the MSFBR.

### 12.3.2.6.3 Actinide make-up

Flexibility of the fuel charge–discharge for the molten salt reactor has been often perceived as the prominent advantageous feature associated with the operation. However, the only way used to charge the MSR with fuel during MSRE operation was to use an initial charge of $0.73LiF–0.27UF_4$ eutectic (490°C) solution, and to use make-up of $UF_4$ solid in a 1.5 kg-U batch. Meanwhile Pu make-up was done as $PuF_3$ powder in 30 g-Pu batch dissolved into the fuel salt at 654°C within 3 hours (Grimes, 1970). Introducing a $0.805LiF–0.195PuF_3$ eutectic mixture (743°C) into the fuel salt circuit might be possible (Thoma, 1968), however it will be questionable because of high eutectic temperature compared with the reactor operating temperature.

The oxide precipitation process incorporated with the hydrofluorination process makes feasible the use of mixed solid compounds as make-up materials. A typical 3.2 GWt MSFBR requires 21.2% U–TRU mixed compound of 90 tons for the initial charge and 3.41 kg-U/efpd (1245 kg-U/efpy) of make-up in the equilibrium state, compared with the 47.8 kg-U/efpd of projected throughput of the chemical processing.

The MSFBR requires several tons of TRU supplement until reaching equilibrium. This system is capable to make-up 0.92 kg-TRU/efpd (336 kg-TRU/efpy), if the same U—TRU mixed compound as the initial charge is applied.

However, the peak TRU supplement during the initial stage of operation, for example, is 661 kg-TRU/efpy, while U make-up is 1.088*t*. This means that up to 37.8% U—TRU mixed compound should be temporally required in these occasions.

Excess actinides should be removed from the system not as the separated components, but simply as the fuel salt. The annual loss of TRU due to fuel salt chemical cleaning is 6 kg basing upon 1500 efpd of interval and 0.1% of nominal loss rate for 22.6 tons-TRU inventory. This can be accounted for in the equilibrium phase indefinitely because the accumulated TRU surplus is typically 266 kg for 20 years.

#### 12.3.2.6.4 Red-Ox potential control

The nuclear reaction in the MSFBR does not transform LiF into HF, but does transform $UF_4$ into $TRUF_3$, and fission of $TRUF_3$ into fission products. The annual free fluorine production of 3.2 GWt MSFBR at the equilibrium is 1308 moles from the transmutation of $UF_4$ and 3258 moles from the fission of $TRUF_3$ according to the chemical processing scheme shown in Fig. 12.24. The annual consumption of $UF_3$ is 4566 moles (1087 kg-U). This can be compensated by dissolution of 1522 moles-uranium metal (362 kg) in the fuel salt containing $UF_4$ as a part of annual U make-up (1245 kg-U), though hydrofluorination is also available in a side stream.

## *12.3.3 U—Pu fast-spectrum molten-salt reactors*

The possibility of fluoride molten salt fuel for a U/Pu breeder reactor is investigated not by dissolving actinide fluorides in a solvent, but by producing a well-established alkali fluoride eutectic mixture containing $UF_4$ and a theoretically assessed alkali fluoride eutectic mixture containing $PuF_3$. The alkali fluorides, such as LiF, NaF, and KF, modify their acidic counterparts such as $UF_4$ and $PuF_3$ to form neutral compounds with certainly lower melting points. The candidates are specific combinations of fertile salt and fissile salt with a higher heavy metal concentration and a lower eutectic temperature.

### *12.3.3.1 Feasibility of the U—Pu fast-spectrum molten-salt reactors*

#### 12.3.3.1.1 Alkali fluoride—actinide fluoride mixtures

According to the classic design principle of molten salt reactors, the fuel salt should compose a eutectic mixture and all components of the fuel salt should congruously solidify at the eutectic point.

The fast neutron fluoride molten salt reactor fuel is feasible if the liquidus temperature (i.e., nothing but liquid is stable higher than that) is kept at least 50°C lower than the reactor core inlet temperature. A fuel salt should be qualified by the

**Table 12.32 Candidates of combination by fertile salt and fissile salt**

| | Fertile salt (eutectic temp.) | Fissile salt (eutectic temp.) |
|---|---|---|
| Case I | $0.730LiF-0.270UF_4$ (490°C) | $0.788LiF-0.212PuF_3$ (745°C) |
| Case II | $0.435LiF-0.243NaF-0.322UF_4$ (445°C) | $0.611LiF-0.167NaF-0.222PuF_3$ (685°C) |
| Case III | $0.435LiF-0.243NaF-0.322UF_4$ (445°C) | $0.341LiF-0.461KF-0.188PuF_3$ (513°C) |
| Case IV | $0.267LiF-0.476KF-0.257UF_4$ (500°C) | $0.053NaF-0.608KF-0.340PuF_3$ (605°C) |
| Case V | $0.504NaF-0.216KF-0.280UF_4$ (490°C) | $0.053NaF-0.608KF-0.340PuF_3$ (605°C) |
| Case VI | $0.504NaF-0.216KF-0.280UF_4$ (490°C) | $0.053NaF-0.608KF-0.340TRUF_3$ (605°C) |

highest freezing temperature, at which any deposition of solid phase starts, as the phase change is incongruous in nature in this case. However, freezing behavior should be observed until the final solidification in order to perform any engineering as well as safety evaluations. Candidates of combination by fissile salt and fertile salt are selected from eutectic compounds based upon higher heavy element concentration and lower melting point as listed in Table 12.32.

#### 12.3.3.1.2 Fuel salt constitution procedure

A fuel salt is constituted by use of a smaller portion of the fissile salt containing $PuF_3$ to satisfy neutronic requirements and by use of the balance of the fertile salt appropriately enriched with $UF_4$ to satisfy neutronic requirements, taking into account dilution by mixing with the fissile salt.

The fundamental scheme of the procedure to constitute a fuel salt and to identify freezing points is illustrated in Fig. 12.25 (Hirose, 2017). In this case, the fuel salt of $0.349NaF-0.289KF-0.281UF_4-0.081PuF_3$ (liquidus at 605°C) is constituted by adding 23.8 mol% of $0.053NaF-0.607KF-0.340PuF_3$ (eutectic at 605°C) to 76.2 mol% of $0.442NaF-0.189KF-0.369UF_4$ (liquidus at 590°C). In this fuel salt, the fissile salt completely freezes at 605°C, meanwhile the fertile salt starts to freeze at 590°C and completely solidifies at 490°C during cooling.

Any supplement or make-up of heavy elements is principally carried out using U–Pu mixed compounds; however adjustment of alkali fluoride composition might be done, if required.

#### 12.3.3.1.3 Neutronic behavior of fuel salts

The reactor physics calculations are made using the same process as described in Section 12.3.2.5.1. The results of calculation are summarized in Tables 12.33, 12.34, and Fig. 12.26.

It was revealed from the overall results that an appreciable breeding gain could be realized after a certain number of years from the start-up in the use of alkali

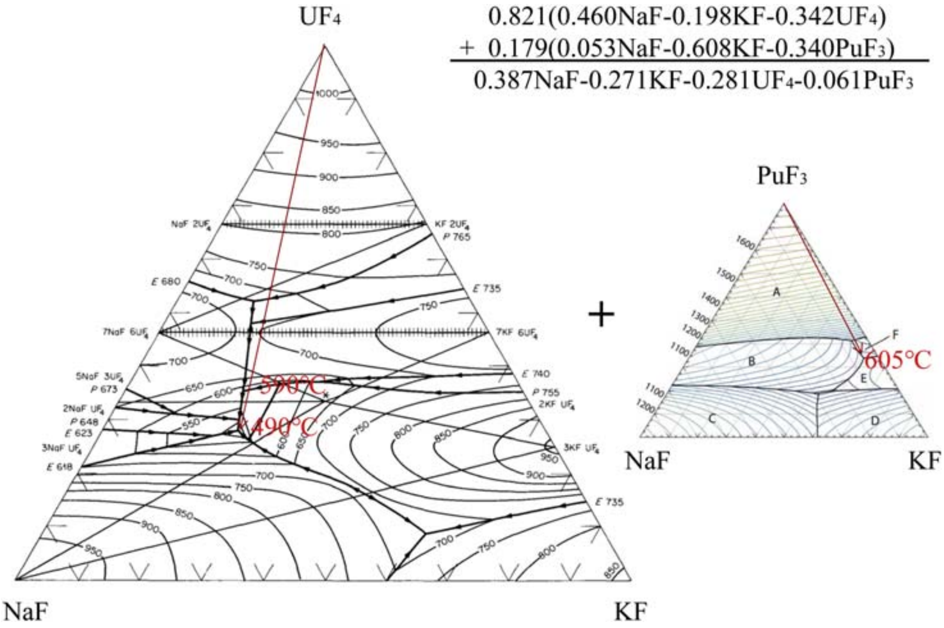

**Figure 12.25** Scheme of procedure to constitute a fuel salt and to identify freezing points.

**Table 12.33 Reactor physics calculations to alkali fluoride–$UF_4$–$PuF_3$ (1)**

| Fuel salt combination | Element | Inventory at start (tons) | Peak supply (tons/y) | Supply (tons) | Total feed (tons) | Inventory at equilibrium (tons) | Breeding (tons) |
|---|---|---|---|---|---|---|---|
| LiF–$UF_4$–$PuF_3$ | U | 71.60 | 1.331 | 53.24 | 124.85 | 70.91 | 6.836 |
| | Pu | 15.51 | 0.68 | 2.241 | 17.755 | 19.71 | 1.906 |
| | MA | 0.000 | | 0.000 | 0.000 | 1.243 | 0.114 |
| (LiF–NaF)–$UF_4$–$PuF_3$ | U | 71.43 | 1.356 | 54.23 | 125.66 | 70.91 | 7.469 |
| | Pu | 15.25 | 0.69 | 2.125 | 17.373 | 19.41 | 2.044 |
| | MA | 0.000 | | 0.000 | 0.000 | 1.208 | 0.120 |
| (LiF–KF)–$UF_4$–$PuF_3$ | U | 70.80 | 1.159 | 46.36 | 117.16 | 70.92 | 1.561 |
| | Pu | 16.40 | 0.75 | 3.117 | 19.516 | 20.48 | 0.451 |
| | MA | 0.000 | | 0.000 | 0.000 | 1.337 | 0.029 |
| (LiF–NaF–KF)–$UF_4$–$PuF_3$ | U | 71.49 | 1.175 | 50.01 | 121.49 | 71.31 | 4.183 |
| | Pu | 15.96 | 0.72 | 2.630 | 18.59 | 20.02 | 1.178 |
| | MA | 0.000 | | 0.000 | 0.000 | 1.303 | 0.073 |
| (NaF–KF)–$UF_4$–$PuF_3$ | U | 71.58 | 1.269 | 50.74 | 122.32 | 71.65 | 4.559 |
| | Pu | 15.73 | 0.66 | 2.59 | 18.32 | 19.93 | 1.268 |
| | MA | 0.00 | | 0.00 | 0.00 | 1.26 | 0.077 |
| (NaF–KF)–$UF_4$–$TRUF_3$ | U | 71.74 | 1.368 | 54.52 | 126.26 | 71.65 | 9.697 |
| | Pu | 17.26 | 0.63 | 1.36 | 18.54 | 19.61 | 2.654 |
| | MA | 2.08 | 0.08 | 0.16 | 2.24 | 1.30 | 0.198 |

**Table 12.34** Reactor physics calculations to alkali fluoride−$UF_4$−$PuF_3$ (2)

| Fuel salt | Years from start | Li[a] | Na | K | U | Pu | MA | Keff | Density (g/cc) | Temp. coeff. of reactivity | Neutron leak rate |
|---|---|---|---|---|---|---|---|---|---|---|---|
| | | (mole rate) | | | (mole rate) | | | | | | |
| LiF−$UF_4$−$PuF_3$ | 0 | 0.711 | | | 0.238 | 0.051 | 0.000 | 1.009 | 4.282 | −5.5E − 0.5 | 0.051 |
| | 40 | 0.700 | | | 0.232 | 0.064 | 0.004 | 1.007 | 4.381 | −4.3E − 05 | 0.048 |
| (LiF−NaF)−$UF_4$−$PuF_3$ | 0 | 0.474 | 0.223 | | 0.250 | 0.053 | 0.000 | 1.010 | 4.365 | −5.4E − 05 | 0.048 |
| | 40 | 0.460 | 0.226 | | 0.244 | 0.066 | 0.004 | 1.007 | 4.464 | −4.3E − 05 | 0.043 |
| (LiF−KF)−$UF_4$−$Pu_3$ | 0 | 0.248 | | 0.411 | 0.277 | 0.064 | 0.000 | 1.010 | 4.583 | −4.9E − 05 | 0.056 |
| | 40 | 0.245 | | 0.400 | 0.272 | 0.078 | 0.005 | 1.007 | 4.684 | −3.8E − 05 | 0.050 |
| (LiF−NaF−KF)−$U_4$−$PuF_3$ | 0 | 0.378 | 0.145 | 0.148 | 0.270 | 0.060 | 0.000 | 1.013 | 4.469 | −5.0E − 05 | 0.051 |
| | 40 | 0.351 | 0.112 | 0.194 | 0.264 | 0.074 | 0.005 | 1.010 | 4.567 | −3.9E − 05 | 0.045 |
| (NaF−KF)−$UF_4$−$PuF_3$ | 0 | | 0.387 | 0.271 | 0.281 | 0.061 | 0.000 | 1.010 | 4.532 | −4.8E − 05 | 0.049 |
| | 40 | | 0.354 | 0.290 | 0.275 | 0.076 | 0.005 | 1.007 | 4.633 | −3.8E − 05 | 0.043 |
| (NaF−KF)−$UF_4$−$TRUF_3$ | 0 | | 0.357 | 0.284 | 0.283 | 0.068 | 0.008 | 1.010 | 4.635 | −3.9E − 05 | 0.046 |
| | 40 | | 0.349 | 0.289 | 0.281 | 0.076 | 0.005 | 1.007 | 4.661 | −3.8E − 05 | 0.044 |

[a] 99.995% enriched Li-7.

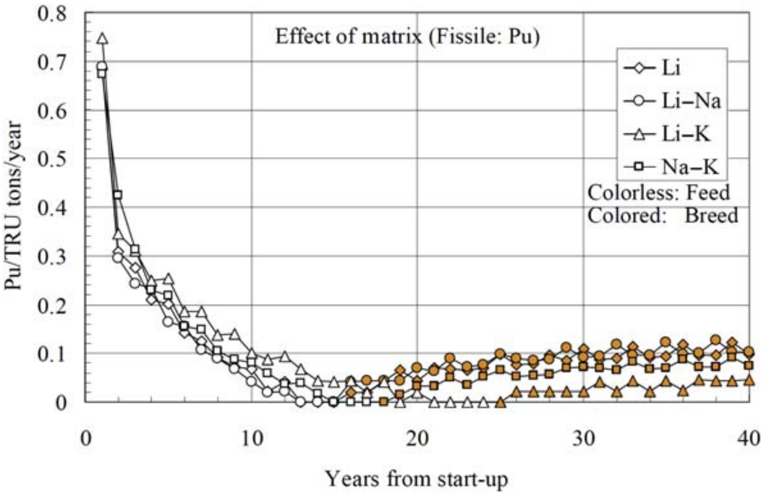

**Figure 12.26** Feed/breed balance according to selection of alkali fluorides–$UF_4$–$PuF_3$ (Hirose, 2017).

fluorides–$UF_4$–$PuF_3$ under the U initial inventory of 70.8–71.6 tons (24–28 mol%) and Pu initial inventory of 15.1–16.4 tons (5.1–6.4 mol%), provided that 2.1–3.1 tons of Pu were supplemented in certain patterns after the start-up. At equilibrium U does not increase from start-up but TRU increases to 20.6–21.8 tons (7.1–8.3 mol%).

Absence of potassium in the alkali fluoride salts such as LiF and LiF–NaF is evidently favorable to the neutronic performance, and consequently to the feed and breed performance, evaluated by smaller need of fissile supplement, shorter period of zero-breeding, and larger breeding gain than the potassium-containing salt. The breeding performance appeared to be quantitatively suppressed according to the level of potassium content.

The calculation for NaF–KF–$UF_4$–$TRUF_3$ instead of NaF–KF–$UF_4$–$PuF_3$ revealed the highest breeding with the lowest supplementary feeding backed up by higher initial feed so far in cases investigated as shown in Fig. 12.27. This, plus the fact that the Pu/MA molar ratio of TRU in the equilibrium inventory is almost the same as in the initial charge, mean that the U–Pu fast-spectrum reactor can accept and favorably manage all trans-uranium elements without elaborate partitioning.

### 12.3.3.1.4 Freezing behavior of fuel salt

The freezing temperature of the fuel salts principally depends upon the highest eutectic temperature of all the systems. The higher eutectic concentration of fissile salts is the principal factor to be concerned with the fissile salt, if there are options (Benes et al., 2008). The freezing temperature of the fertile salt depends upon mainly $UF_4$ concentration at the fixed molar ratios of alkali fluorides in the experimentally derived classic ternary phase diagrams.

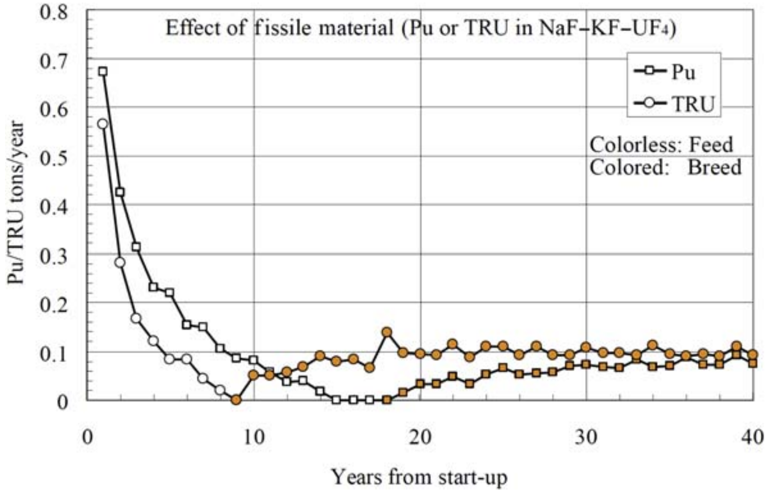

**Figure 12.27** Feed/breed balance compared between NaF–KF–$UF_4$–$PuF_3$ and NaF–KF–$UF_4$–$TRU_3$ (Hirose, 2017).

The constituents of fuel salts, freezing temperatures of individual fertile salts and fissile salts, and the highest solid-depositing temperatures of the fuel salts at the start-up and at equilibrium are shown in Table 12.35.

The eutectic temperature of fissile salts is always higher than that of fertile salts as shown in Table 12.32. However, in principle the eutectic temperature of the fissile salt dominates the highest liquidus temperature (i.e., solid-depositing) temperature in a fuel salt, there is a possibility to initiate $UF_4$ deposition above that temperature when the $PuF_3$ concentration is not high enough and a higher $UF_4$ concentration required, as in the case of LiF–KF–$PuF_3$, for example.

It is noteworthy that the LiF–NaF–KF–$UF_4$–$PuF_3$ system can provide the lowest freezing temperature at 513°C among studied cases if the concentration of $UF_4$ is kept lower than 25 mol% by decreasing the initial U inventory and that of $PuF_3$ is lower than 6 mol%.

The freezing of NaF–KF–$UF_4$–$PuF_3$ fuel salt is dictated by the eutectic point of fissile salt (605°C) to give eutectic freezing of NaF–KF–$PuF_3$ almost irrespective to the concentration of $UF_4$. This temperature is substantially higher than that of the classic fuel salts for thermal neutron molten salt reactors (500°C) based upon the Hastelloy-N, however it is not so different from that of the revised MSFR (594°C) (EVOL, 2015) or a chloride molten-salt reactor (REBUS-3700) (600°C) (Mourogov et al., 2006).

### 12.3.3.2 System optimization

#### 12.3.3.2.1 Effect of $UF_3$ and lanthanide trifluorides on freezing behavior

Burnup of a solid fuel is in proportion to the core replacement interval, however that of a molten salt fuel depends on the on-line chemical processing interval. In an

## Table 12.35 Constitution of fuel salt and associated freezing behavior

| **Fuel salt (Li, Na, K)F–$UF_4$–$PuF_3$** | | | | | | **Fertile salt (Li, Na, K)–$UF_4$** | | | | | | **Fissile salt (Li, Na, K) F–$PuF_3$** | | | | | |
|---|---|---|---|---|---|---|---|---|---|---|---|---|---|---|---|---|---|
| **Composition (mol%)** | | | | | **Liq.* (°C)** | **Mol %** | **Composition (mol%)** | | | | **Liq.* (°C)** | **Mol %** | **Composition (mol%)** | | | | **Liq.* (°C)** |
| **LiF** | **NaF** | **KF** | **$UF_4$** | **$PuF_3$** | | | **LiF** | **NaF** | **KF** | **$UF_4$** | | | **LiF** | **NaF** | **KF** | **$PuF_3$** | |
| **LiF–$UF_4$–$PuF_3$** | | | | | | | | | | | | | | | | | |
| 71.1 | | – | 23.8 | 5.1 | 745 | 75.7 | 68.6 | – | – | 31.4 | 540 | 24.3 | 79.8 | – | – | 21.2 | 745 |
| 70.0 | – | – | 23.2 | 6.8 | 745 | 67.6 | 65.7 | – | – | 34.3 | 540 | 32.4 | 79.8 | – | – | 21.2 | 745 |
| **LiF–NaF–$UF_4$–$PuF_3$** | | | | | | | | | | | | | | | | | |
| 47.4 | 22.3 | – | 25.0 | 5.3 | 685 | 76.1 | 43.1 | 24.0 | – | 32.9 | 445 | 23.9 | 61.1 | 16.7 | – | 22.2 | 685 |
| 46.0 | 22.6 | – | 24.4 | 7.0 | 685 | 68.5 | 39.0 | 25.3 | – | 35.7 | 500 | 31.5 | 61.1 | 16.7 | – | 22.2 | 685 |
| **LiF–KF–$UF_4$–$PUF_3$** | | | | | | | | | | | | | | | | | |
| 24.8 | – | 41.1 | 27.7 | 6.4 | 720 | 66.0 | 19.9 | – | 38.4 | 41.7 | 720 | 34.0 | 34.1 | – | 46.1 | 18.8 | 513 |
| 24.5 | – | 40.0 | 27.2 | 8.3 | 720 | 55.9 | 16.8 | – | 34.7 | 48.5 | 720 | 44.1 | 34.1 | – | 46.1 | 18.8 | 513 |
| **LiF–NaF–KF–$UF_4$–$PUF_3$** | | | | | | | | | | | | | | | | | |
| 37.8 | 14.5 | 14.7 | 27.0 | 6.0 | 560 | 68.1 | 39.3 | 21.2 | – | 39.5 | 560 | 31.9 | 34.1 | – | 46.1 | 18.8 | 513 |
| 35.1 | 11.2 | 19.4 | 26.4 | 7.9 | 620 | 58.0 | 35.6 | 19.2 | – | 45.2 | 620 | 42.0 | 34.1 | – | 46.1 | 18.8 | 513 |
| **NaF–KF–$UF_4$–$PuF_3$** | | | | | | | | | | | | | | | | | |
| – | 38.7 | 27.1 | 28.1 | 6.1 | 605 | 82.1 | – | 46.0 | 19.7 | 34.2 | 570 | 17.9 | – | 5.3 | 60.7 | 34.0 | 605 |
| – | 35.4 | 29.0 | 27.5 | 8.1 | 605 | 76.2 | – | 44.8 | 19.2 | 36.1 | 580 | 23.8 | – | 5.3 | 60.7 | 34.0 | 605 |
| **NaF–KF–$UF_4$–$TRUF_3$** | | | | | | | | | | | | | | | | | |
| – | 35.7 | 28.4 | 28.3 | 7.6 | 605 | 77.6 | – | 44.5 | 19.1 | 36.4 | 580 | 22.4 | – | 5.3 | 60.7 | 34.0 | 605 |
| – | 34.9 | 28.9 | 28.1 | 8.1 | 605 | 76.2 | – | 44.2 | 18.9 | 36.9 | 590 | 23.8 | – | 5.3 | 60.7 | 34.0 | 605 |

liq.*: The highest liquidus temperature (Tohma, 1959; Benes et al., 2008).

MSFBR with 3.2 GWt output, the chemical processing interval of 1500 efpd represents 52,000 MWd/t-HM. This burnup is the upper limit due to neutron absorption by building up of fission products.

Meanwhile, it has been thermodynamically suggested that trifluorides of fission product lanthanides behave like $PuF_3$ and minor actinide fluorides in the phase relationship, and that they would interfere with the freezing behavior. A system of 3.2 GWt output produces 6000 moles of fission product lanthanide trifluorides within 1500 efpy (Table 12.28). This corresponds to 6.9% of $TRUF_3$ assuming that the inventory is 20.9 tons-TRU (87,100 moles).

It was also perceived that $UF_3$ substitutes dissolved $PuF_3$ as it forms a solid solution with $PuF_3$ during freezing (Ward et al., 1959). The phase diagram of the alkali fluoride−$UF_3$ system might be assumed to be the same as the $PuF_3$ system, though experimental verification should be required.

If the U(IV)/U(III) ratio in the system is fixed at 20 as a Red-Ox buffer medium, 71.4 tons-U (300,000 moles) of the total U inventory should consist of 285,700 moles of $UF_4$ and 14,300 moles of $UF_3$. The concentration of $UF_3$ is 1.33 mol% when that of $PuF_3$ is 8.10 mol%. The total inventory of trifluoride, including $UF_3$, is kept to a burnup level 1.164 times that of $PuF_3$. Meanwhile, the $UF_4$ inventory is reduced to 0.952 by chemical reduction to $UF_3$.

Calculations are based upon appropriate phase diagrams to evaluate the effect of reduction of $UF_4$ to $UF_3$ and build-up of fission product lanthanide trifluorides in the case of NaF−KF−$0.281UF_4$−$0.081PuF_3$ fuel salt according to the chemical processing interval for two cases of fissile salt arrangement; (1) 0.053NaF−0.607KF−$0.340PuF_3$ (eutectic at 605°C), (2) 0.052NaF−0.599KF−$0.349PuF_3$ (liquidus at 610°C) as shown in Table 12.36 (Hirose, 2017).

It is found that the $UF_4$ reduction to $UF_3$ does not have significant effects, irrespective of the fissile salt, while the build-up of lanthanide trifluorides can be overcome by using the fissile salt with a liquidus temperature of 610°C, instead of the salt with a eutectic temperature of 605°C.

Even if all $UF_3$ were produced intentionally at the start-up or oxidized incidentally to $UF_4$ at 1500 efpd of the chemical processing interval, the highest fuel salt liquidus temperature does not exceed 610°C by using the fissile salt.

#### 12.3.3.2.2 Validity of criteria

Although it is conservatively assumed in this study that the phase relationship of fertile salt and that of fissile salt would be independent in a mixture, some additional amount of $PuF_3$ may dissolve in alkali fluoride−$UF_4$ fertile salts at the eutectic temperature. It has been thermodynamically suggested that 0.74LiF−$0.26UF_4$ could dissolve $PuF_3$ as high as 1.0 mol% at the eutectic point of 484°C (Capelli et al., 2015), nevertheless further experimental verification is required.

The feasibility and characteristics of the fast neutron U−Pu molten salt reactor are evaluated, based upon concentrations of actinide fluorides derived from the phase diagrams. The molar concentration of actinide fluorides in a fuel salt are calculated, based upon the molar composition and estimated density of a fuel salt at designated actinide inventories. The calculated molar concentration value of

## Table 12.36 Effect of $UF_3$ and fission product trifluoride build-up on constitution of $NaF-KF-UF_4-TRUF_3$ fuel salts

| Chemical processing interval (efpd) | UF3 mol % | Fuel salt $(NAF-KF)-UF_4-TRUF_3$ | | | | | Fertile salt $(NaF-KF)-UF_4$ | | | | | Fissile salt $(NaF-KF)-TRUF_3$ | | | | |
|---|---|---|---|---|---|---|---|---|---|---|---|---|---|---|---|---|
| | | Composition (mol%) | | | | Liq.[a] (°C) | Mol % | Composition (mol%) | | | Liq.[a] (°C) | Mol % | Composition (mol%) | | | Liq.[a] (°C) |
| | | NaF | KF | $UF_4$ | $XF_3$[b] | | | NaF | KF | $UF_4$ | | | NaF | KF | $XF_3$[b] | |
| 0 | 0 | 34.62 | 28.88 | 28.10 | 8.10 | 605 | 76.18 | 44.18 | 18.94 | 36.88 | 590 | 23.82 | 5.3 | 60.7 | 34.0 | 605 |
| 0 | 1.33 | 33.33 | 30.49 | 26.75 | 9.43 | | 72.26 | 44.09 | 18.89 | 37.02 | 600 | 27.74 | | | | |
| 300 | | 33.12 | 30.59 | 26.75 | 9.54 | | 71.94 | 43.97 | 18.85 | 37.18 | 600 | 28.06 | | | | |
| 600 | | 32.91 | 30.69 | 26.75 | 9.65 | | 71.62 | 43.86 | 18.80 | 37.34 | 605 | 28.38 | | | | |
| 900 | | 32.68 | 30.80 | 26.75 | 9.77 | 610 | 71.26 | 43.73 | 18.74 | 37.53 | 610 | 28.74 | | | | |
| 1200 | | 32.47 | 30.90 | 26.75 | 9.88 | 620 | 70.94 | 43.00 | 18.69 | 37.71 | 620 | 29.06 | | | | |
| 1500 | | 32.26 | 31.00 | 26.75 | 9.99 | 625 | 70.62 | 43.48 | 18.64 | 37.88 | 625 | 29.38 | | | | |
| 1500 | 0 | 33.85 | 29.39 | 28.10 | 8.66 | 620 | 74.53 | 43.62 | 18.70 | 37.68 | 620 | 25.47 | | | | |
| 0 | 0 | 35.29 | 28.51 | 28.10 | 8.10 | 610 | 76.79 | 44.39 | 19.02 | 36.59 | 580 | 23.21 | 5.2 | 59.9 | 34.9 | 610 |
| 0 | 1.33 | 33.76 | 30.06 | 26.75 | 9.43 | | 72.98 | 44.34 | 19.00 | 36.66 | 590 | 27.02 | | | | |
| 300 | | 33.56 | 30.15 | 26.75 | 9.54 | | 72.66 | 44.23 | 18.96 | 36.81 | 590 | 27.34 | | | | |
| 600 | | 33.36 | 30.24 | 26.75 | 9.65 | | 72.35 | 44.12 | 18.91 | 36.97 | 590 | 27.65 | | | | |
| 900 | | 33.14 | 30.35 | 26.75 | 9.77 | | 72.01 | 44.00 | 18.86 | 37.14 | 600 | 27.99 | | | | |
| 1200 | | 32.93 | 30.44 | 26.75 | 9.88 | | 71.69 | 43.88 | 18.81 | 37.31 | 605 | 28.31 | | | | |
| 1500 | | 32.72 | 39.54 | 26.75 | 9.99 | | 71.38 | 43.76 | 18.76 | 37.48 | 610 | 28.62 | | | | |
| 1500 | 0 | 34.25 | 28.99 | 28.10 | 8.66 | | 75.19 | 43.84 | 18.79 | 37.37 | 605 | 2481 | | | | |

liq.[a]: The highest liquidus temperature (Tohma, 1959; Benes et al., 2008).

$XF_3$[b]: represents $UF_3 + LnF_3$ if any.

actinide fluorides is inversely proportional to the density of fuel salt. The algorism to obtain the density of fuel salt should be standardized, if physical calculations are to be compared between respective organizations.

#### 12.3.3.2.3 Reiterate calculations

The alkali fluoride compositions in fuel salts presented in Table 12.36 represented the specific NaF/KF molar ratio to give the highest liquidus temperature, but they have not been generalized for reactor physical calculations. Reiterated calculations of reactor physical assessments by applying chemically elucidated NaF/KF molar ratios are required in the next step.

The system under investigation has not yet been optimized in various factors such as power output, system size, power density, operating temperature, etc. Any reiterated calculations would be appreciated.

### 12.3.4 Conclusions

The MSFBR concept that excludes lithium, provides us with not only acceptable performances in nuclear physics, but also a simplified process in chemical engineering, with enormous potential benefit for nuclear fission energy, not relying on existing fuel cycle infrastructure, with ultimate safety, cleanliness, and simplicity, even though complete optimization has not yet been made.

The viability of the proposed concept is not due to any sophisticated theories or mechanisms, but to a high concentration of heavy metal fluorides in common alkali fluoride eutectic mixtures as liquid phases.

The present study confirms the feasibility to eliminate uncertainties about solubility, using a discreet compound of the fertile salt and the fissile salt, for which phase relationships have been elucidated experimentally or thermodynamically. The favorable features of the MSFBR should not be almost tarnished by the new fuel constitution paradigm. Freezing behaviors of fuel salts are analyzed as a collateral outcome. The disadvantage of the required hotter core inlet temperature might be outweighed by the advantage of a lithium-free operation.

## Acknowledgments

I sincerely acknowledge Prof. Dr. Koshi Mitachi and Prof. Dr. Yoichiro Shimazu for their voluntary dedication to the entire physical calculations in this work. This work would not have been done without the inspiration and assistance given by ORNL scientists for over a decade. I would like to dedicate this paper to the late Prof. Dr. Yoichi Takashima, the former director of the Kashiwa Research Center of the Institute of Research and Innovation for his guidance to initiate the research work associated with MSR technology.

# References

ALISIA—Assessment of Liquid Salts for Innovative Applications (2009) Review Report on Liquid Salts for Various Applications. [pdf] Available at <http://cordis.europa.eu/pub/fp6-euratom/docs/alisia-deliverable-d50-v4_en.pdf>.

Ando, R., et al. (1999) Evaluation of Nuclide Composition in LWR Spent Fuels. JAERI-Research 99-004.

Baes Jr., C.F., 1974. The chemistry and thermodynamics of molten salt reactor fuels. J. Nucl. Mater. 51, 149–162.

Bamberger C.E., Ross R.G., Baes C.F.Jr. (1970) The instability of PuOF and Solubility of Pu (III) in MSBR Solvent Salt. Molten Salt Reactor Program Semiannual Progress Report for Period Ending August 31, 1970, ORNL-4622, Oak Ridge National Laboratory. <http://web.ornl.gov/info/reports/1971/ 3445605157923.pdf>.

Barton, C.J., 1960. Solubility of plutonium-trifluoride in fused alkali fluoride beryllium fluoride mixtures. J. Phys. Chem. 64 (3), 306–312.

Barton C.J., Strehlow R.A. (1958) Solubility of $PuF_3$. Molten-Salt reactor Program, Quarterly Progress Report for Period Ending June 30, 1958. ORNL-2551, Oak Ridge National Laboratory. <http://issuu.com/e_generation/docs/ornl-2551/1 >.

Barton C.J., Strehlow R.A. (1959) Solubility of $PuF_3$ in Alkali Fluoride-Beryllium Fluoride Mixtures. Molten Salt Reactor Program, Quarterly Progress Report for Period Ending October 31, 1958, ORNL-2626, Oak Ridge National Laboratory. < http://web.ornl.gov/info/reports/1959/ 3445603613267.pdf>.

Barton C.J., Grimes W.R., Strehlow R.A. (1958a) Solubility and Stability of $PuF_3$ in Fused Alkali Fluoride-Beryllium Fluoride Mixtures. ORNL-2530, Oak Ridge National Laboratory. <http://web.ornl.gov/info/reports/1958/ 3445603612650.pdf>.

Barton, C.J., et al., 1958b. Phase equilibria in the alkali fluoride–uranium tetrafluoride fused salt systems: 1. The systems $LiF-UF_4$ and $NaF-UF_4$,. J. Am. Ceram. Soc. 41, 63–69.

Barton C.J., Friedman H.A., Insley H. et al. (1960) High-Temperature Phase Equilibrium Studies. Reactor Chemistry Division. Annual Progress Report, ORNL-2931, Oak Ridge National Laboratory. <http://web.ornl.gov/info/reports /1960/3445603614845.pdf>.

Barton, C.J., 1960b. Solubility of plutonium - trifluoride in fused alkali fluoride beryllium fluoride mixtures. J. Phys. Chem. 64 (3), 306–312.

Barton, C.J., et al., 1961a. Phase equilibria in the systems $NaF-PuF_3$ and $NaF-CeF_3$. J. Inorg. Nucl. Chem. 20, 45–49.

Barton, C.J., et al., 1961b. Phase relations in the system $LiF-PuF_3$. J. Inorg. Nucl. Chem. 18, 143–149.

Barton, C.J., Bredig, M.A., Gilpatrick, L.O., Fredericksen, J.A., 1970. Solubility of cerium trifluoride in molten mixtures of lithium, beryllium, and thorium fluorides. Inorg. Chem. 9 (2), 307–310.

Benedict, M., et al., 1981a. Nuclear Chemical Engineering. 2nd ed. McGraw-Hill Book Co., New York, USA, pp. 225, 435.

Benedict, M., et al., 1981b. Nuclear Chemical Engineering. 2nd ed. McGraw-Hill Book Co., New York, USA, p. p. 389.

Benes, O. (2009) Thermodynamics of Molten Salts for Nuclear Applications. JRC-ITU-TN-2008/40, Thesis approved and released February 2009.

Benes, O., Konings, R., 2008. Actinide burner fuel: potential compositions based on the thermodynamic evaluation of $MF-PuF_3$ ($M = Li$, Na, K, Rb, Cs) and $LaF_3-PuF_3$ systems. J. Nucl. Mater. 377 (3), 449–457.

Benes, O., Konings, R.J.M., 2009. Thermodynamic properties and phase diagrams of fluoride salts for nuclear applications. J. Fluor. Chem. 130, 22–25.

Benes, O., et al., 2008. Actinide burner fuel: potential compositions based on the thermodynamic evaluation of $MF-PuF_3$ (M = Li, Na, K, Rb, Cs) and $LaF_3-PuF_3$ systems. J. Nucl. Mater. 377, 449–457.

Benes O., Cabet C., Delpech S., Hosnedl P., Ignatiev V., Konings R., et al. (2009) Assessment of Liquid Salts for Innovative Applications (ALISIA), Deliverable (D-50). Review Report <ftp://ftp.cordis.europa.eu/pub/fp6-euratom/docs/alisia-deliverable-d50-v4_en.pdf>.

Bergman, G., Dergunov, T.P., 1941. Fusion diagram of LiF–KF–NaF. C. R. Acad. Sci. USSR. 31, 753–754.

Cantor S., (Ed.) (1968) Physical Properties of Molten Salt Reactor Fuel, Coolant and Flash Salts. Report ORNL-TM-2316, Oak Ridge National Laboratory, TN. <http://moltensalt.org/references/static/downloads/pdf/ORNL-TM-2316.pdf>.

Capelli, E., et al., 2015. Thermodynamic assessment of the $LiF-ThF_4-PuF_3-UF_4$ system. J. Nucl. Mater. 462, 34–53.

Degtyarev, A.M., Ponomarev, L.I., 2012. LiF–NaF–KF molten salt reactor with a fast neutron spectrum. At. Energy. 112 (6), 451–453.

Degtyarev, A.M., Kolyaskin, O.E., Myasnikov, A.A., Ponomarev, L.I., Karmanov, F.I., Seregin, M.B., et al., 2013. Molten salt subcritical transplutonium actinide incinerator. At. Energy. 114 (4), 225–232.

Degtyarev, A., Mysnikov, A., Ponomarev, L., 2015. Molten salt fast reactor with U–Pu fuel cycle. Prog. Nucl. Energy. 82, 33–36.

Delpech, S., Merle-Lucotte, E., Heuer, D., Allibert, M., Ghetta, V., Le-Brun, C., et al., 2009. Reactor physics and reprocessing scheme for innovative molten salt reactor system. J. Fluor. Chem. 130, 11–17.

Desyatnik, V., Nechaev, V., Chervinsky, J., 1981. The viscosity of the molten mixtures of beryllium fluoride with fluoride of sodium and lithium. Russ. J. Appl. Chem. 54 (10), 2310–2312.

Desyatnik V.N., Kurbatov N.N., Raspopin S.P. et al. (1979) Study of Physicochemical and Thermophysical Properties of Molten Fluoride Salts of Lithium, Sodium, Beryllium, Uranium and Thorium. UPI Report, Inv. No. 78027681, Sverdlovsk, p. 189.

Engel, J. R., et al. (1979) Develop Status and Potential Program for Development of Proliferation-Resistant Molten Salt Reactors. ORNL-TM-6415.

Engel, J. R., et al. (1980) Conceptual Design Characteristics of a Denatured Molten Salt Reactor with Once-Through Fueling. ORNL/TM-7207.

EVOL—Evaluation and Viability of Liquid Fuel Fast Reactor Systems (2012) <http://www.li2c.upmc.fr>.

EVOL (Project no. 249696). Final Report. <http://cordis.europa.eu/docs/results/249/249696/final1-final-report-f.pdf>, 2013.

EVOL (2015) (Project no. 249696). Final Report, <http://cordis.europa.eu/docs/results/249/249696/final1-final-report-f.pdf#search = %27EVOL%28Project + no.249696%29Final + Report%27 >.

Fiorina, C., Aufieroa, M., Cammia, A., Franceschinib, F., Krepelc, J., Luzzia, L., et al., 2013. Investigations of MSFR core physics and fuel cycle characteristics. Prog. Nucl. Energy. 68, 153–168.

Forsberg C.W., (2006) Developments in Molten Salt and Liquid_Salt_Cooled Reactors. In: Proceedings of ICAPP'06, Reno, NV USA, June 4–8, 2006, Paper 6292.

Gavrilov P., Merkulov I., Kryukov O., Khaperskaya A.V., Ivanov K.V., Fedorov Yu.S., et al. (2015) Experimental-demonstration centre as a key element of creation of an integrated centre for NPP spent fuel reprocessing at MCC. In: Proceedings of the International Conference, Global 2015, September 20–24, Paris, France, Paper No. 5078, pp. 1513–1517.

Gorbunov, V.F., et al., 1976. Experimental studies on interaction of plutonium, uranium and rare earth fluorides with some metal oxides in molten fluoride mixtures. Radiochimija. 17, 109–224.

Grimes, W.R., 1970. Molten-salt reactor chemistry. Nucl. Appl. Technol. 8, 137–155.

Grimes, W.R., et al. (1958) Chemical aspects of molten fluoride salt reactor fuels. In: Fluid Fuel Reactors. Addison-Wesley Pub. Co, Reading, Mass., pp. 569–591 (Chapter 12).

Grimes, W.R., et al., 1960. In: Tipton, C.R. (Ed.), Reactor Handbook, Vol. I. Wiley (Interscience), New York (Chapter 17).

Hara, Sh, Ogino, K., 1989. The densities and the surface tensions of fluoride melts. ISIJ Int. 29 (6), 477–485.

Haubenrich, P.N., Engel, J.R., 1970. Experience with the molten salt reactor experiment. Nucl. Appl. and Technol. 8 (2), 118–136.

Heuer, D., Merle-Lucotte, E., Alibert, M., Brovchenko, M., Ghetta, V., Rubiolo, P., 2014. Towards the thorium fuel cycle with molten salt fast reactors. Ann. Nucl. Energy. 64, 421–429.

Hill, D.J., Cantor, S., Ward, W.T., 1967. Molar volumes in the LiF–$ThF_4$ system. J. Inorg. Nucl. Chem. 29 (1), 241–243.

Hirose, Y., et al. (2001) The concept of fuel cycle integrated molten salt reactor for transmuting Pu + MA from spent LWR fuels. In: Proceedings of Global 01, Paris, France, September 10–12, 2001.

Hirose, Y., et al. (2015) Feasibility of molten salt fast reactor for emerging national tasks. In: Proceedings of 2015 ANS International High-Level Radioactive Waste Management, Charleston, SC, April 12–16, 2015, pp. 608–617.

Hirose, Y., et al. (2016) Operation control of molten salt U-Pu fast breeder reactors. Proc. ICAPP 2016, San Francisco, CA, April 17–20, p.785–795, 2016.

Hirose, Y., (2017) Feasibility of using (Li, Na, K)F-UF4-TRUF3 fuels for U-Pu fast-spectrum molten-salt reactors. Proc. ICAPP 2017, Fukui/Kyoto, Japan, April 25-28, 17107, 2017.

Hoffman H., Jones L. (1955) Fused Salt Heat Transfer. Part II: Forced Convection Heat Transfer in Circular Tubes Containing NaF–KF–LiF Eutectic. Oak Ridge National Laboratory, Report ORNL-1977.

Holcomb D.E., Flanagan G.F., Patton B.W., Gehin J.C., Howard R.L., Harrison T.J. (2011) Fast Spectrum Molten Salt Reactor Options. ORNL/TM-2011/105. [pdf] Available at <http://info.ornl.gov/sites/publications/files/Pub29596.pdf>.

IAEA (2004) Implications of Partitioning and Transmutation in Radioactive Waste Management. Technical Reports Series No. 435.

Ignatiev V., Merzlyakov A., Gorbunov V., Afonichkin V., Khokhlov V., Salyulev A., et al. (2003) Physical and chemical properties of molten salt reactor fuel salts. In: Proceedings of ICAPP'03 Conference, Cordoba Spain, May 4–7, 2003.

Ignatiev, V.V., Merzlyakov, V.A., Subbotin, V.G., Panov, A.V., 2006. Experimental investigation of the physical properties of salt melts containing sodium and lithium fluorides and beryllium difluoride. At. Energy. 101 (5), 822–829.

Ignatiev, V., et al. (2007a) Fuels and Fission Products Clean Up for Molten Salt Reactor of the Incinerator Type. ISTC Task #1606.

Ignatiev V., Feinberg O., Gnidoi A., Merzlyakov V., Smirnov A., Surenkov A. (2007b) Progress in development of Li, Be, Na/F molten salt actinide recycler & transmuter, In: Proceedings of ICAPP-2007, May 13–18, Nice, France.

Ignatiev, V.V., Feynberg, O.S., Zagnitko, A.V., Merzlyakov, A.V., Surenkov, A.I., Panov, A. V., et al., 2012a. Molten salt reactors: new possibilities, problems and solutions. At. Energy. 112 (3), 157−165.

Ignatiev, V., et al. (2012b) Progress in development of MOSART concept with Th support. In: Proceedings of ICAPP 2012, Chicago, June 24−28, 2012, p. 12394.

Ignatiev, V., Feynberg, O., Gnidoi, I., Merzlyakov, A., Surenkov, V., Uglov, A., et al., 2014. Molten salt actinide recycler and transforming system without and with Th−U support: fuel cycle flexibility and key materials properties. Ann. Nucl. Energy. 64, 408−420.

Iyer P.N., Prasad R., Vaidya V.N., Roy K.N., Nag K., Singh Z., et al. (1973a) Molten salt chemistry—Part II. Solubility of $CeF_3$ in molten $LiF-BeF_2-ThF_4$ mixture. BARC-671. Bhabha Atomic Research Centre.

Iyer P.N., Prasad R., Vaidya V.N., Roy K.N., Singh Z., Sood D.D., et al. (1973b) Molten salt chemistry—Part III. Solubility of $PuF_3$ in molten mixtures $LiF-BeF_2-ThF_4$ and $LiF-ThF_4$. BARC-676. Bhabha Atomic Research Centre.

Janz, G.J., 1967. Molten Salt Handbook. Academic Press, New York, USA, pp. 479−488.

Janz, G.J., Gardner, G.L., Krebs, U., Tomkins, R.P.T., 1974. Molten Salts: Vol. 4, Part 1, Fluorides and mixtures, electrical conductance, density, viscosity, and surface tension data. J. Phys. Chem. Ref. Data. 3 (1), 1−116.

Khokhlov, V., Ignatiev, V., Afonichkin, V., 2009. Evaluating physical properties of molten salt reactor fluoride compositions. J. Fluor. Chem. 130 (1), 30−37.

Klimenkov A.A., Kurbatov N.N., Raspopin S.P., Cervinsky Yu. (1983) The density and surface tension of the molten thorium and lithium fluorides. In: Proceedings of the Universities, Non-Ferrous Metallurgy, vol. 1, pp. 129−131.

Le Blanc, D., 2010. Molten Salt Reactors: a new beginning for an old idea. Nucl. Eng. Des. 240, 1644−1656.

Lizin, A.A., Tomilin, S.V., Gnevashov, O.E., Gazizov, A.G., Osipenko, A.G., Kormilitsin, M.V., et al., 2013a. $PuF_3$, $AmF_3$, $CeF_3$, $NdF_3$ solubility in LiF−NaF−KF melt. At. Energy. 115 (1), 11−17.

Lizin, A.A., Tomilin, S.V., Gnevashov, O.E., Gazizov, A.G., Osipenko, A.G., Kormilitsin, M.V., et al., 2013b. $UF_4$ and $ThF_4$ solubility in LiF−NaF−KF melt. At. Energy. 115 (1), 22−25.

Lizin, A.A., Tomilin, S.V., Ignat'ev, V.V., 2015a. Joint solubility of $CeF_3$ and $PuF_3$ in ternary melts of lithium, thorium and uranium fluorides. Radiochemistry. 57 (1), 32−37.

Lizin, A.A., Tomilin, S.V., Naumov, S.V., Ignatiev, V.V., Nezgovorov, N.Yu, Baranov, A. Yu, 2015b. The study of joint solubility of $UF_4$ and $PuF_3$ in molten fluorides of lithium, sodium and potassium. Radiochemistry. 57 (5), 425−429.

Long D., Huang W., Feng J., Lifang T., Qingnuan L. (2013) Study on the electrochemical extraction of rare earth elements from FLiNaK. In: Proceedings of the International Conference, Global 2013, Salt Lake City, Utah, pp. 413−418.

Luzzi L., Aufiero M., Cammi A. and Fiorina, C. (2012). Thermo-hydrodynamics of internally heated molten salts for innovative nuclear reactors. In: Zheng, Jin-Hai (Ed.) Hydrodynamics—Theory and Model. InTech Europe (Chapter 6), DOI: 10572/2114, [pdf]. Available at: <http://cdn.intechopen.com/pdfs-wm/31454.pdf>.

Mac Pherson, H.G., 1985. The molten salt reactor adventure. Nucl. Sci. Eng. 90, 374−380.

Mailen, J.C., Smith, F.J., Ferris, L.M., 1971. Solubility of $PuF_3$ in molten $2LiF-BeF_2$. J. Chem. Eng. Data. 16 (1), 68−69.

Matieu, L., Heuer, D., Merle-Lucotte, E., Brissot, R., Le Brun, C., Liatard, E., et al., 2009. Possible configurations for the thorium molten salt reactor and advantages of the fast non-moderated version. Nucl. Sci. Eng. 161, 78−89.

McNeese L.E. and Staff for MSR Programm (1974), Program Plan for Development of Molten Salt Breeder Reactors. ORNL-5018, Oak Ridge National Laboratory. <http://www.energyfromthorium.com/pdf/ORNL-5018.pdf >, December.

Mel'nik M.I., Bychkov A.V., Kormilitsyn M.V., Ponomarev L.I. (2003), Cascade subcritical molten-salt reactor (CSMSR) for RW transmutation. The study on solubility of $PuF_3$, $NpF_4$, $AmF_3$ in molten fluorides. In: Proceedings of GLOBAL—2003 International Conference, New Orleans, USA, 16−20 November, 2003, pp. 2218−2221.

Merk, B., Konheiser, J., 2014. Neutron shielding studies on an advanced molten salt fast reactor design. Ann. Nucl. Energy. 64, 441−448.

Merle-Lucotte E. (2011) Thorium fuel cycle with the molten salt fast reactor. In: Proceedings of ICAPP 2011, Nice, France, May 2−5, No. 11190.

Merle-Lucotte E. (2013) Introduction to the physics of MSFR. In: Thorium Energy Conference (ThEC13). CERN, Geneva. Available at <http://indico.cern.ch/getFile.py/access?contribId = 368< sessionId = 98<resId = 18< materialId = slides&confId = 222140>.

Merle-Lucotte E., Heuer D., Allibert M. et al. (2013), Recommendations for a demonstrator of molten salt fast reactor. In: Proceedings of Interenational Conference on Fast Reactors and Related Fuel Cycles Safe Technologies and Sustainable scenarios FR13, Paris, 2013, Paper P147.

Merzlyakov, A., Ignatiev, V., Abalin, S., 2011. Viscosity of molten lithium, thorium and beryllium fluoride mixtures. J. Nucl. Mater. 419, 361−365.

Merzlyakov, A., Ignatiev, V., Abalin, S., 2014. Viscosity of LiF−NaF−KF eutectic and effect of cerium trifluoride and uranium tetrafluoride additions. Nucl. Eng. Des. 278, 268−273.

Mitachi, K., et al., 2008. Characteristics of thorium molten-salt reactor with self-sustainability. J. AESJ. 7 (2), 127−133 (in Japanese).

Mourogov, A., et al., 2006. Potentialities of the fast spectrum molten salt reactor concept: REBUS-3700. Energy Convers. Manag. 47, 2761−2771, Elsevier Science Direct.

National Nuclear Laboratory UK (2012) Comparison of Thorium and Uranium Fuel Cycles. Report NNL (11)11593, Issue 5, pp. 1−31.

Naumov V.S., Bychkov A.V., Tomilin S.V., Chistyakov, M.V., Kormilitzyn M.V., Smolensky V.V., et al. (1996) Interaction of actinide and rare-earth element fluorides with molten fluoride salt and possibility of their separation for ADTT fuel reprocessing. In: Proceedings of 2nd International Conference on ADTTA, Kalmar, Sweden, June 1996, pp. 1144−1155.

OECD/NEA, Report, No. 7061 (2013), Nuclear Energy Agency. The Economics of the Back End of the Nuclear Fuel Cycle. [pdf] Available at: <http://www.oecd-nea.org/ndd/pubs/2013/7061-ebenfc.pdf>.

Okumura, K., et al. (2007) SRAC2006: A Comprehensive Neutronics Calculation Code System. JAERI-Data/Code2007-004.

Olson, L., Ambrosek, J., Sridharan, K., Anderson, M., Allen, T., 2009. Materials corrosion in molten LiF−NaF−KF salt. J. Flour. Chem. 130 (1), 67−73.

ORNL (2011) A Comprehensive Modeling and Simulation Suite for Nuclear Safety Analysis and Design, Version 6.1. ORNL/TM-2005/39, June.

ORNL-2799 (1959) Report, Oak Ridge National Laboratory. Molten Salt Reactor Program. Quarterly Progress Report for Period Ending, July 31, p. 99.

ORNL-3936 (1966) Report, Oak Ridge National Laboratory. Molten Salt Reactor Program, p. 216.

ORNL-4449 (1969) Report, Oak Ridge National Laboratory. Molten Salt Reactor Program. p. 252.

Peretz, J. F. (1996) Identification and Evaluation of Alternatives for the Disposition of Fluoride Fuel and Flush Salts from the MSRE at ORNL. ORNL-ER-380.

Ponomarev, L. I. (2013) Molten salt fast reactor based on LiF–NaF–KF. In: Proceedings of INES-4, Tokyo, November 6–8, 2013, p. A12-1.

Ponomarev, L.I., Seregin, M.B., Parshin, A.P., Mel'nikov, S.A., Mikhalichenko, A.A., Zagorets, L.P., et al., 2013. Fuel salt for the molten-salt reactor. At. Energy. 115 (1), 5–10.

Ponomarev L.I., et al. (2015) U–Pu fast molten salt reactor and its fuel cycle. In: Proceedings of GLOBAL-2015, September 20–24, 2015, Paris, France, Paper 5336.

Ponomarev, L.I., Fedorov, Yu.S., Miroslavov, A.A., Degtyarev, A.M., 2016. U–Pu fuel cycle of the fast molten salt reactor. At. Energiya.

Rosenthal M.W., Haubenreich P.N., Briggs R.B. (1972) Molten Salts Reactor Program. The Development Status of Molten Salt Breeder Reactors. ORNL-4812, Oak Ridge National Laboratory. <http://www.energyfromthorium.com/ pdf/ORNL-4812.pdf>.

Segre, E., 1970. Enrico Fermi, Physicist. University of Chicago Press, Chicago and London.

Shaffer, J. H. (1958) Chemical Reactions of Oxides with Fluorides in LiF-KF. ORNL-2474, pp. 99–101.

Shibata, K., et al., 2002. Japanese evaluated nuclear data library version 3 revision 3: JENDL-3.3. J. Nucl. Sci. Technol. 39, 1125.

Shimazu, Y., et al. (2015) Evaluation of red-ox environment in fluoride molten salt reactors based on ENDF-VII. In: Proceedings of AESJ 2015 Autumn Meeting, Shizuoka, Japan, September 10–12,2015, p. B-20.

Smirnov, M.V., Stepanov, V.P., Khokhlov, V.A., Antonov, A.A., 1974. Density and surface tension of alkali halides and their binary mixtures. Russ. J. Phys. Chem. 78 (2), 467–469.

Sood, D.D., Iyer, P.N., Prasad, R., et al., 1975. Plutonium trifluoride as a fuel for molten salt reactors- solubility studies. Nucl. Technol. 27, 411–415.

Souček P., Chuchvalcova-Bimova K., Lisy F., Tulackova R. (2005) Development of electrochemical separation methods from molten fluoride salt media. In: Proceedings of Global 2005, Japan, 2005, 9–13 October, Paper 062.

Thoma R.E. (1959) Phase Diagrams of Nuclear Reactor Materials. ORNL-2548, Oak Ridge National Laboratory. <http://www.osti.gov/scitech/ servlets/purl/4234144>.

Thoma R.E. (1968) Chemical Feasibility of Fueling Molten Salt Reactors with $PuF_3$. Report ORNL TM-2256, Oak Ridge National Laboratory. <http://moltensalt.org/references/static/downloads/pdf/ORNL-TM-2256.pdf >.

Thoma, R.E., Insley, H., Friedman, H.A., Hebert, G.M., 1968. Equilibrium phase diagram of the lithium fluoride–berillium fluoride–zirconium fluoride system. J.Nucl. Mater. 27 (2), 166–180.

Toth, L. M., et al. (1994) Molten fluoride fuel salt chemistry. In: AIP Conference Proceedings, vol. 346, International Conference on ADTTA, Las Vegas, NV, July 1994, pp. 617–619.

Uhlir J., Marecek M. (2005) R&D of pyrochemical reprocessing technologies dedicated to MSR fuel cycle. In: Proceedings of International Conference, Global 2005, Tsukuba (Japan), Paper No. 282.

Uhlir J., Marecek M., Tulackova R., Chuchvalcova-Bimova K. (2007) Development of fluoride reprocessing technologies devoted to molten salt reactor systems. In: Proceedings of International Conference, Global 2007, Boise, Idaho, pp. 1490–1496.

Van der Meer, J., Konings, R.J.M., Oonk, H.A.J., 2006. Thermodynamic assessment of the $LiF–BeF_2–ThF_4–UF_4$ system. J. Nucl. Mater. 357, 48–57.

Volozhin, M.V., Zakirov, R.Ya, Mushnikov, P.N., Subbotin, V.G., Sannikov, I.V., Naumov, S.P., 2013. $CeF_3$, $PuF_3$ solubility in LiF–NaF–KF melt. At. Energy. 115 (1), 18–21.

Vriesema, A., 1979. Aspects of Molten Fluorides as Heat Transfer Agents for Power Generation. Delft University of Technology, Delft, The Netherlands Report, WTHD, p. 112.

Ward W.T., Strehlow R.A., Grimes W.R., Watson G.M. (1959) Solubility Relations Among Rare Earth Fluorides in Selected Molten Fluorides Solvents. Report ORNL-2749, Oak Ridge National Laboratory. <http://web.ornl.gov/info/reports /1959/3445603613882.pdf>.

Williams, D. F., (2016) Additional Physical Property Measurements and Assessment of Salt Compositions Proposed for the Intermediate Heat Transfer Loop. ORNL/GEN4/LTR-06-033, September 30.

Williams, D. F., et al. (2002) REDOX Control of MSR Fuel. GEDEON-PRACTIS Workshop, Cadarache, France, June 19–20.

Williams D.F., Toth L.M., Clarno K.T. (2006) Assessment of Candidate Molten Salt Coolants for the Advanced High-Temperature Reactor (AHTR). ORNL/TM-2006/12, Oak Ridge National Laboratory, Oak Ridge, Tennessee. <http://web.ornl.gov/~webworks/cppr/y2006/rpt/124584.pdf>.

# Solid fuel, salt-cooled reactors

# 13

*Raluca Scarlat*[1] *and Charalampos Andreades*[2]
[1]University of Madison-Wisconsin, Madison, WI, United States,
[2]University of California, Berkeley, CA, United States

## Chapter Outline

## 13.1 Introduction: definition of the FHR concept

Solid-fuel salt-cooled reactors are a class of thermal-spectrum nuclear reactors that use fuel-free fluoride-salts as the primary coolant, solid fuel elements, graphite

**Molten Salt Reactors and Thorium Energy. DOI: http://dx.doi.org/10.1016/B978-0-08-101126-3.00013-0**

moderator, stainless steel (SS) alloys for the structural components, and operating at nearly atmospheric pressures. In the United States, where the concept initiated, these reactors are termed fluoride-salt cooled high-temperature reactors (FHRs). In China, they are called thorium molten salt reactors—solid fuel (TMSR-SF; Chapter 17: Thorium molten salt reactor nuclear energy system (TMSR)).

FHRs combine technologies and system architectures originally developed for MSRs, gas-cooled reactors, and liquid-metal-cooled reactors. Since the 1970s, high-temperature, gas-cooled reactor (HTGR) technology has been studied because of the potential advantages of delivering heat at substantially higher temperatures than are achievable with light-water reactors (LWRs). The advantages of higher temperatures include increased efficiency for power conversion; reduced waste heat generation, reduced cooling water, and thus increased siting flexibility; and the capability to provide cogeneration and process heat services. It has proven challenging, however, to develop helium-cooled reactor designs with passive decay heat removal capability that can compete economically with conventional LWRs.

Research on salt-cooled, high-temperature reactors was initiated in 2002 with studies of a liquid salt very high-temperature reactor (LS-VHTR) aimed at achieving high core outlet temperatures (950–1000°C), derived from the work at Oak Ridge National Laboratory (ORNL) in the 1960s and 1970s (Forsberg et al., 2003). The LS-VHTR was essentially a modified helium-cooled VHTR, using liquid salt as the primary coolant, which operated at near atmospheric pressure and substantially greater power density (two to six times higher) than helium-cooled reactors (Ingersoll and Clarno, 2005; Clarno and Gehin, 2006; Casino, 2006). FHR core power densities are in the range of 10–30 MW/m$^3$; gas-cooled reactor core power densities are 4.8 MW/m$^3$ for the 400 MWth pebble bed modular helium reactor (PBMR), and 6.6 MW/m$^3$ for the 600 MWth gas turbine (GT) modular helium reactor (Gas Turbine-Modular Helium Reactor, 1996; Matzer and Wallace, 2005). While substantially higher than these HTGRs, FHR core power densities are lower than for PWRs (105 MW/m$^3$) and SFRs (321 MW/m$^3$). Based upon the metric of primary system volume, given by the specific reactor vessel power (MWe/m$^3$), FHR reactor vessels are much more compact than PBMRs and Super-Power Reactor Innovative Small Module (S-PRISM), and less compact than PWR reactor vessels.

As comparisons like these were made, researchers also quickly recognized that liquid salt coolants could achieve the same average primary coolant temperature with a significantly lower maximum outlet coolant temperature compared to helium-cooled reactors. Because thermal efficiency depends primarily on average coolant temperature, rather than peak temperature, the LS-VHTR concept evolved into the advanced high-temperature reactor (AHTR), and then the FHR.

The goal of FHRs is to provide an energy technology with a short commercialization timeline, with significant safety advantages compared to advanced light-water nuclear reactors currently under construction, and at costs that are competitive with natural gas. The current development efforts are exclusively for reactors with inlet core temperatures of 600°C, and an outlet core temperature of 700°C. The upper temperature limit imposed on the core outlet temperature stems from the use of

American Society of Mechanical Engineers code-certified structural materials, i.e., ferritic steels, for the primary pressure boundary (Ingersoll et al., 2004; Forsberg et al., 2012; Forsberg et al., 2013; Sabharwall et al., 2013; Peterson and Zhao, 2006; Fei et al., 2008), whose modulus of elasticity sees a rapid decrease past 704°C. On the opposing end, the 600°C inlet core temperature is selected based on the power conversion efficiency. More specifically, the compressor exit temperatures of modern industrial-scale GT compressor with pressure ratios of 15.5−23 range between 350 and 580°C as depicted in Fig. 13.1 (Andreades, 2015; Andreades et al., 2014a).

Future designs may use better materials, yielding higher operational temperatures, and thus more efficient power conversion cycles, or a broader market for high-temperature process heat applications. The current development efforts are focused on a short deployment timeline, and thus aim at taking advantage as much as possible of off-the-shelf equipment, and already demonstrated technology.

The nominal salt is FLiBe, which has the most favorable neutronic, heat transfer, and physicochemical properties among all fluoride salt mixtures studied to date. However, other fluoride-salt mixtures continue to be explored. The two main drivers for considering alternatives to FLiBe are:

1. To avoid beryllium-containing melts, because beryllium has high respiratory toxicity, its inhaled particulates leading to lung disease similar to that from asbestos;
2. To avoid lithium and beryllium, both of which transmute to tritium under neutron irradiation.

Neither of these issues lead to a scientific roadblock, but they present engineering challenges, with consequences on economics and public opinion.

As part of the effort to commercialize HTGRs, a wide experience base with manufacturing and performance of coated-particle fuel has been established in the United States, United Kingdom, Germany, France, China, Russia, Japan, South Africa, and the Republic of Korea (Greene et al., 2010). The FHR also uses coated-particle fuel, and relies on much of the experience base with HTGR fuel. The fuel form

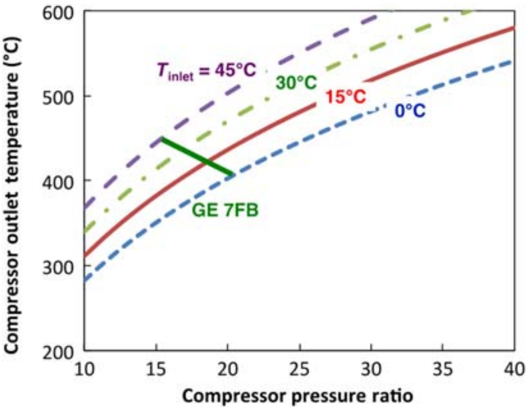

**Figure 13.1** Compressor air outlet temperature as a function of inlet temperature and compression ratio, for a modern, large, high-efficiency (89.4%) axial compressor.

studied thus far is TRISO fuel (tri-isotopic ceramic-encapsulated particle fuel). TRISO fuel particles are triple-coated spherical particles of uranium fuel, less than one millimeter in diameter. A uranium center is coated by a layer of carbon, which is then coated by silicon carbide, with an outer shell of carbon. In effect, this gives each tiny particle its own primary containment system. The particles are then fabricated into fuel pebbles. This pebble design enables a substantial increase in power density while maintaining relatively low peak fuel particle temperature. The higher power density of the fuel pebbles will imply a higher inventory of short-lived fission products; however, irradiation experiments at two US national laboratories (Idaho National and Oak Ridge National Laboratories) found that TRISO particles retain fission products even at temperatures of 1800°C, several hundred degrees above design operating temperatures and 200°C above postulated design basis accident conditions (Petti, 2014). This margin provides a strong case for safe performance of the fuel.

The FHR can be coupled to a number of different power conversion systems, among them Nuclear Air-Brayton Combined Cycle (NACC), Supercitical Carbon Dioxide (S-$CO_2$) Brayton cycle, Helium Brayton cycle, or conventional Rankine steam cycle (Chapter 2: Electricity production). Steam cycles are the most mature and commercially available technology, and offer the nearest path solution; however steam cycles are limited in terms of operational flexibility and restrict FHR to be base-load power plants. NACCs are of a medium-term development timescale due to the widespread availability of heavy industrial GTs, and modifications to the machines can be made to accommodate external heating of air (Andreades, 2015; Andreades et al., 2014a,b). The novel aspect of NACCs is their ability to simultaneously burn natural gas or other combustible fuels at very high efficiency and high ramp rates, thus providing flexible capacity to the integrated electric grid. This is particularly important and pertinent to electric grids with high renewable penetration and intermittency issues. Finally, the S-$CO_2$ Brayton cycle is the most compact configuration thus providing a reduced footprint for the FHR. Additionally, the S-$CO_2$ cycle can have an efficiency ranging from 40 to 50%, depending on configuration. S-$CO_2$ cycles however are the least mature technology and have the longest development roadmap.

We will now delve into specific designs being investigated at various universities and research institutions, followed by their inherent and passive safety features, unique phenomenology to FHRs, and finally their safety analysis and licensing approaches.

## 13.2 FHR designs: pool versus loop, fuel element shape, power

The most recent conceptual designs classified as FHR technologies include the Pebble Bed FHR (PB-FHR) at UCB (Scarlat and Peterson, 2014; Krumwiede et al., 2013), the Small Modular AHTR (SmAHTR) at ORNL (Greene et al., 2010), the large central-station AHTR at ORNL (Holcomb et al., 2011; Hong et al., 2014; Varma et al., 2012), and the solid fuel thorium molten salt reactor (SF-TMSR) at the Shanghai Institute of Applied Physics (SINAP) in China. Table 13.1

Table 13.1 **Comparison of design parameters for PB-FHR, AHTR, and other advanced reactors (Greene et al., 2010; Andreades et al., 2014)**

| | Mk1 PB-FHR | ORNL 2012 AHTR | ORNL 2010 SmAHTR | Westing-house four-loop PWR | PBMR | S-PRISM |
|---|---|---|---|---|---|---|
| Reactor thermal power (MWt) | 236 | 3400 | 125 | 3411 | 400 | 1000 |
| Reactor electrical power (MWe) | 100 | 1530 | 50 + | 1092 | 175 | 380 |
| Fuel enrichment [a] | 19.90% | 9.00% | 19.75% | 4.50% | 9.60% | 8.93% |
| Fuel discharge burn up (MWt-d/kg) | 180 | 71 | – | 48 | 92 | 106 |
| Fuel full-power residence time in core (year) | 1.38 | 1.00 | 4.19 | 3.15 | 2.50 | 7.59 |
| Power conversion efficiency | 42.4% | 45.0% | 40.0% | 32.0% | 43.8% | 38.0% |
| Core power density (MW/m$^3$) | 22.7 | 12.9 | 9.4 | 105.2 | 4.8 | 321.1 |
| Fuel average surface heat flux (MW/m$^2$) | 0.189 | 0.285 | 0.630 | 0.637 | 0.080 | 1.13 |
| Fuel specific surface area (area/volume) (1/m) | 120 | 45 | – | 165 | 60 | 285 |
| Reactor vessel diameter (m) | 3.5 | 10.5 | 3.5 | 6.0 | 6.2 | 9.0 |
| Reactor vessel height (m) | 12.0 | 19.1 | 9 | 13.6 | 24.0 | 20.0 |
| Reactor vessel specific power (MWe/m$^3$) | 0.866 | 0.925 | 0.578 | 2.839 | 0.242 | 0.299 |
| Start-up fissile inventory (kg-U235/MWe) [b] | 0.79 | 0.62 | 7.14 | 2.02 | 1.30 | 6.15 |
| EOC Cs-137 inventory in core (g/MWe)[c] | 30.8 | 26.1 | – | 104.8 | 53.8 | 269.5 |
| EOC Cs-137 inventory in core (Ci/MWe)[c] | 2672 | 2260 | – | 9083 | 4667 | 23,359 |
| Spent fuel dry storage density (MWe-d/m$^3$) | 4855 | 2120 | – | 15,413 | 1922 | – |
| Natural uranium (MWe-d/kg-NU)[d] | 1.56 | 1.47 | – | 1.46 | 1.73 | – |
| Separative work (MWe-d/kg-SWU)[d] | 1.98 | 2.08 | – | 2.43 | 2.42 | – |

[a] For S-PRISM, effective enrichment is the beginning of sycle weight fraction of fissile Pu in fuel.

[b] Assume start-up U-235 enrichment is 60% of equilibrium enrichment; for S-PRISM startup uses fissile Pu.

[c] End of cycle (EOC) life value (fixed fuel) or equilibrium value (pebble fuel).

[d] Assumes a uranium tails assay of 0.003.

summarizes other key design parameters for some, plus a conventional Generation II Westinghouse four-loop pressurized water reactor (AISC Specification, 2014), a helium-cooled PBMR (Nuclear Energy Institute, 2009), and the S-PRISM sodium fast reactor (International Atomic Energy Agency, 2006).

### 13.2.1 PB-FHR—UC Berkeley

The University of California, Berkeley, released a preconceptual design for a small modular 236 MWth randomly packed pebble-bed FHR in 2014 (Andreades et al., 2016). The Mk1 FHR, as it was named, uses a NACC based upon a modified General Electric 7FB GT, designed to produce 100 MWe of base-load electricity when operated with only nuclear heat, and to increase this power output to 242 MWe using gas cofiring for peak electricity generation. Due to the high thermal efficiency of the NACC system, the steam-bottoming condenser of the Mk1 PB-FHR requires only 40% of the cooling water supply that is required for a conventional LWR, for each MWh of base-load generation. As with conventional natural-gas combined cycles (NGCC), this makes the efficiency penalty of using dry cooling with air-cooled condensers much smaller, enabling economic operation in regions where water is scarce.

A new value proposition for NACC arises from additional revenues earned by providing flexible grid support services to handle the ever-increasing demand for dispatchable peak power, in addition to traditional base-load electrical power generation. Under base-load operation NACC power conversion has lower fuel costs than NGCC, and under peaking operation it has higher efficiency in converting natural gas to electricity than NGCC, so NACC plants will always be dispatched before conventional NGCC plants (Andreades, 2015; Andreades and Per, 2016; Andreades et al., 2014a,b).

The reference configuration for the Mk1 site uses 12 Mk1 units, as shown in Fig. 13.2, capable of producing 1200 MWe of base load electricity, and ramping to a peak power output of 2900 MWe.

PB-FHR fuel pebbles are 3.0 cm in dimeter. The annular core design has a removable graphite central reflector and an outer graphite reflector pebble layer to protect the outer fixed reflector. The Mk1 is also capable of online refueling. The Mk1 reactor vessel is depicted in Fig. 13.3. Four Mk1 pebbles can provide electricity for a full year for an average US household, which in 2011 consumed 11.3 MWe-h. These four small pebbles are far less than the 8.1 tons of anthracite coal, or 17 tons of lignite coal, needed to produce the same amount of electricity using a coal power plant.

The Mk1 does not use an intermediate coolant loop and instead directly heats the power conversion fluid. It eliminates the conventional reactor guard vessel used in sodium fast reactors and instead uses a refractory reactor cavity liner system. Full passive decay heat removal is utilized. All components for the Mk1 design are rail-transportable.

### 13.2.2 SmAHTR—ORNL

SmAHTR is a 125-MWth cartridge-core, integral-primary-system FHR that uses fixed plate-type fuel. The ORNL 2012 AHTR is a large 3400-MWth fixed plate

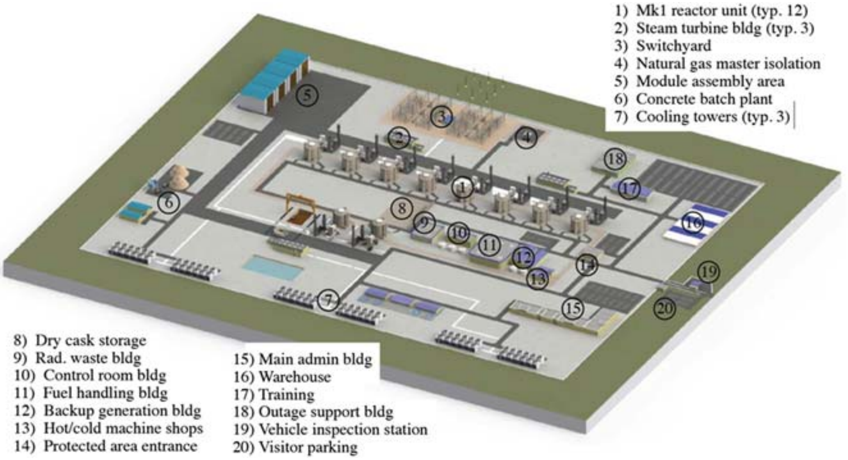

**Figure 13.2** Reference site arrangement for a 12-unit PB-FHR plant (Andreades).

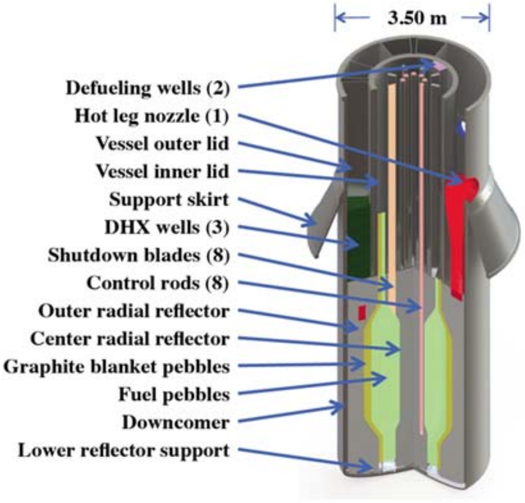

**Figure 13.3** The Mk1 PB-FHR reactor vessel (Andreades).

fuel variant of the FHR. This 2012 AHTR design implements novel designs for fuel and refueling, and demonstrates a practical application of supercritical steam for power conversion based upon extensive experience in fossil power plants. Other potential power conversion systems that could be coupled to the SmAHTR include S-$CO_2$ or multi-reheat Helium Brayton cycles. The SmAHTR reactor vessel is 3.5 m in diameter, and as such is transportable by tractor-trailor to its deployment location. Fig. 13.4 depicts the SmAHTR being transported on a tractor-trailer.

The SmAHTR design takes advantage of the existing safety philosophy of several small modular reactors (SMRs). The reactor employs passive decay-heat

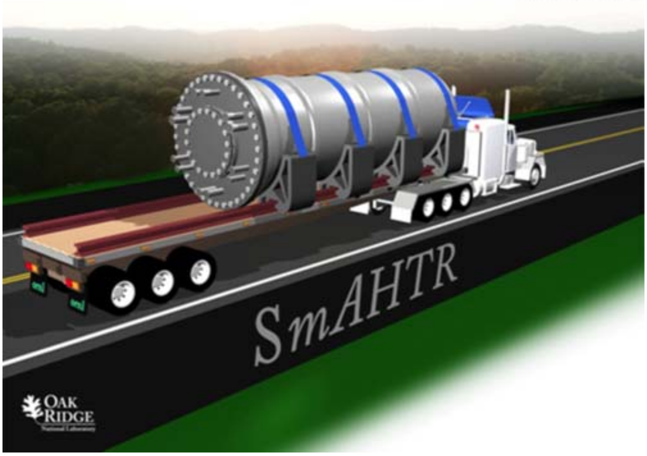
ORNL 2011-G00113/chj

**Figure 13.4** SmAHTR reactor vessel can be transported via tractor-trailer (Greene et al., 2010).

removal systems relying on natural convection, and the core is designed with large negative reactivity feedback coefficients. The core and all primary components are contained in the reactor vessel (integral design). This design eliminates the large break loss-of-coolant accident scenario. Only intermediate-loop piping carrying nonradioactive coolant penetrates the vessel. The passive decay-heat removal design eliminates the reliance on off-site power (which is needed in remote locations) and the need for safety-related emergency on-site AC power. The reactor can be seen as having several barriers to fission product release in the case of an accident: coated particle fuel, the graphite moderator, the reactor vessel/guard vessel, and the containment.

The SmAHTR concept has been developed with three potential operating modes and applications in mind: (1) process heat production; (2) electricity production; and (3) a combined cogeneration mode in which both electricity and process heat are produced.

### *13.2.3 AHTR—ORNL*

The AHTR is a design concept for a central station type (1500 $\mathrm{MW_e}$/3400 $\mathrm{MW_{th}}$) FHR that was as of 2016 under development by ORNL for the US Department of Energy, Office of Nuclear Energy's Advanced Reactor Concepts program. FHRs, by definition, feature low-pressure liquid fluoride salt cooling, coated-particle fuel, a high-temperature power cycle, and fully passive decay heat rejection.

The reactor vessel has an exterior diameter of 10.48 m, a height of 17.7 m, and a core height of 5.5 m, with 25 cm of reflector above and below with plate-type fuel. A row of replaceable graphite reflector prismatic blocks surrounds the core radially. The reactor confinement is not required to withstand high pressures since there is

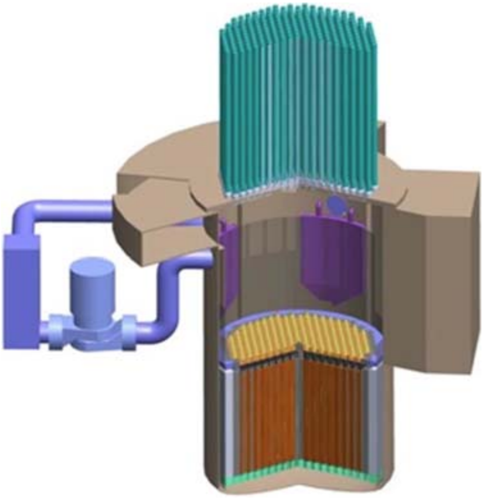

**Figure 13.5** Current AHTR core, reactor vessel, and nearby structures (Holcomb et al., 2011).

no source of stored energy in the reactor, in contrast to LWRs. A three-loop intermediate coolant system separates the primary coolant from the power conversion working fluid, while also reducing the inventory of primary coolant. The AHTR uses an advanced supercritical steam Rankine cycle, due to its high efficiency and technological maturity relative to other power cycles. It uses a dual powertrain to reduce the steam generator sizing and the possibility of losing 100% of the primary heatsink. Decay heat is removed by three direct reactor auxiliary cooling systems (DRACS) modular decay heat removal loops. Fig. 13.5 depicts the current AHTR core, reactor vessel, and nearby structures. In orange are the fuel elements; in teal are the control rods and associated drive mechanisms; in violet are the DRACS; in light violet are the primary coolant pump, primary-to-intermediate heat exchanger, and primary coolant loop piping.

The AHTR is a combination of a pool and loop-type reactor design, avoiding an integral setup to improve maintainability and servicing and reduce complication of reactor internal design. Plate-type fuel in a hexagonal lattice is used to reduce primary coolant pressure losses flowing the core, especially during loss of forced coolant accidents. The fuel is UCO-coated particles enriched to 19.75% U-235, with a refueling interval of 2 years. All components of the overall thermal feedback are negative or very near zero for all design variants considered, providing a large overall negative thermal reactivity feedback.

The intermediate salt KF-$ZrF_4$ was chosen in part because it does not contain lithium or beryllium. It is relatively nontoxic, and any leaks into the primary coolant will not dilute the enrichment of the lithium, which would make such leaks prohibitively expensive to rectify. The salt has a melting temperature near 400°C, so the intermediate system, like the primary system, must be heated.

A preconceptual design report series, along with an update, provide further detail of the overall AHTR design and economics (Holcomb et al., 2011a, b; 2012).

### 13.2.4 FHTR—MIT

The fluoride-salt-cooled high-temperature test reactor (FHTR) is a test reactor design that will enable development and demonstration of a commercial FHR, currently being studied at MIT, and details for its goals, requirements, ownership, design, and licensing are laid out in a full report (Forsberg et al., 2014). A test reactor is required to demonstrate technical viability, provide data required for design and licensing of a precommercial demonstration plant, provide operational and maintenance experience, and provide a test bed for alternative fuels, fluoride salt coolants, and other systems.

An FHTR would be a government owned Class I-A reactor to allow for operational and design flexibility, and to provide a demonstration, since development is beyond the timeframe of private investment.

Most likely funding options come from a joint partnership with China to jointly develop a small FHTR in China, or from a US-led international consortium to reduce the financial risks for each partner, and also to widen the support from international partners.

Some of the main design features of an FHTR are:

- *Core design*. The reactor core has driver fuel and a flux trap in the center experimental hole to enable high thermal fluxes for fuel tests. The fuel blocks can be assembled in a variety of configurations to meet experimental needs.
- *Fuel assembly*. The fuel assembly is a prismatic block similar to that used in the Ft. St. Vrain HTGR. This is a proven HTGR fuel that allows three-dimensional variations in enrichment and particle packing fractions to meet neutron flux design goals. The assembly design, termed fFuel inside radial moderator, places fuel compacts and cooling channels inside a region of solid graphite moderator. The solid graphite regions introduce spatial self-shielding of the fuel resonances, increasing the resonance escape probability of the neutrons born in fission, which in turn increases core reactivity. It also implies that the smaller test positions inside a single assembly have a relatively hard neutron flux for accelerated materials testing.
- *Coolant salt*. The FHTR is designed to operate with four different coolant salts from $^7$Li2BeF4 (FLiBe) to NaF-ZrF4 coolant salt. The NaF-ZrF4 has the lowest cost but poorest neutronic and thermal hydraulic behavior. FLiBe has the best neutronic and thermal hydraulic behavior but is more costly because of the need to enrich $^7$Li. The expectation is that the FHTR over its operational lifetime would operate on four different salts as part of its test program.

Fig. 13.6 shows a top-down view of an FHTR core and inner/outer radial reflectors, alongside a standard fuel assembly.

### 13.2.5 TMSR-SF—CAS

The SF-TMSR is the solid fuel variant of the molten salt reactor program at SINAP. A 2-MWth test reactor, with capability for expansion to 10 MWth, is

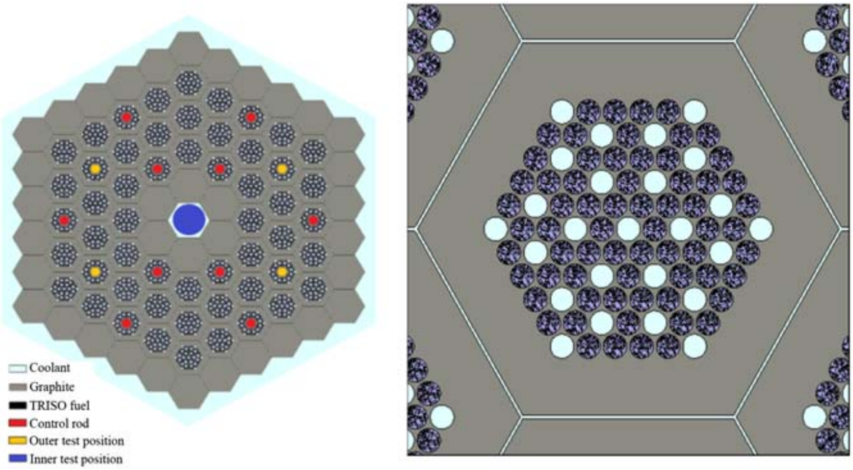

**Figure 13.6** Top-down view of FHTR core and inner/outer radial reflectors, and a standard fuel assembly (Forsberg et al., 2014).

currently under development and will be built in Da Feng city, 250 km from Shanghai. The test reactor has fixed ordered lattice pebble fuel (Chapter 17: Thorium molten salt reactor nuclear energy system (TMSR)).

## 13.3 Plant-level features

Generation IV reactors all have a combination of novel features, such as modular construction, rail transportability, and seismic isolation techniques, that are not present in current Generation II reactor designs and started to first appear on some Generation III and III + reactor designs.

The trend to modularization was adopted by the Westinghouse AP1000, in which factory prefabricated modules, consisting of steel plates and additional structural elements such as tie rods and stiffening elements, which are delivered to the site, assembled into larger, crane-liftable modules, which are then installed and filled with concrete. This type of construction technique is different to the traditional stick-build, in which all construction work is performed on-site from the ground up. The purpose of modular construction is to cut down on construction time and cost by transferring part of the construction process to a factory setting in which highly repetitive tasks can be automated or performed in a controlled environment. By the time the order book reaches “nth-of-a-kind,” where tooling and supply chains are in place, quality issues are ironed out, and vendors and contractors are far along the assembly and construction learning curve. Modular construction thus lends itself better to SMRs, similar to the Mk1 PB-FHR and SmAHTR described above, rather than larger gigawatt-class reactors simply because there are more identical modules to produce per unit of power output.

This then leads to the next novel feature of SMRs—rail transportability. The Mk1 PB-FHR is designed so that all components—including the reactor vessel, GT, and building structural submodules—can be transported by rail, enabling modular construction. The design constraint of rail transport limits the width of components (laid down to be horizontal) to 3.6 m; this result constrains the Mk1 reactor vessel size and thermal power to a value that matches well to the largest rail-shippable GTs now commercially available. Similarly, both the SmAHTR and AHTR are designed for modular construction, with large components being shipped in smaller rail-shippable modules and welded on-site or at a local workshop. Rail transportability has less of a siting restriction than with barge shipment.

Finally, seismic base isolation is being explored for all FHR variants. Seismic base isolation uses specialized structural elements to substantially decouple the substructure from the superstructure of the building and the severity of seismic ground motions. Bellows in the intermediate loop of the AHTR and the air ducts of the Mk1 PB-FHR will also accommodate some lateral ground motion and thermal expansion.

### 13.3.1 Less developed designs, and longer-term features

Alternative fuel types and coolant selections have been proposed, but much less design work has been done to date with these alternative choices. Clad fuel can be an alternative to ceramic encapsulated fuel. The current LWR program on accident-tolerant fuel could yield cladding concepts that are compatible with molten fluoride salts—such as SiC cladding, or stainless-steel alloys that are sufficiently stable in fluoride salts. The interest in exploring other fuel types is to increase the power density by using a fuel form that allows for higher heavy-metal loading.

Alternative coolant choices have been explored that do not breed tritium, and that eliminate beryllium. The downside of moving away from beryllium and lithium salts is a fuel utilization penalty, and a design challenge to ensure that the core has a negative temperature reactivity coefficient. There might also be a slight penalty on the thermal-hydraulic performance of fluoride-salt mixtures other than FLiBe, an increase in vapor pressure, and a change in the corrosion behavior of metal alloys and ceramics.

Lastly, the current upper temperature limit of operation is bounded by currently available structural materials that are compatible with fluoride salts: SS 316 and Hastelloy N. Should the code case for these materials be extended to allow operation above 700°C, and transients above 800°C, then FHRs could operate at higher power conversion efficiency. Composite and ceramic structural materials are also under development, and under testing for compatibility with molten fluoride salts. These could extend the temperature limit to over 800°C.

Very small reactor concepts, in the range of 10 MWe, for deployment to remote mining sites or military operations may opt to use one of these alternative features, accepting higher fuel and capital costs for a reactor that is easier to transport and operate.

### 13.3.2 Inherent safety features and passive safety systems

The nuclear industry's strong safety record can be further enhanced by inherent safety features of FHR design and by passive safety features in Generation IV reactors.

The coolant should prevent fuel overheating and transport heat to the energy conversion system. FHRs use FLiBe coolant because it has attractive properties compared to water, helium, sodium, and other coolants. FLiBe operates at nearly atmospheric pressure. It has a high volumetric heat capacity (the product of density and specific heat capacity)—higher than that of water—and can transfer more heat with a smaller coolant inventory than water. Thermal transients are very slow, allowing the operators hours or days to respond to transients that may otherwise take minutes or hours to unfold in a water-cooled reactor. The large graphite inventory in FHRs also has large thermal inertia, thus behaving as temporary heat sinks during thermal transients, and leading to very slowly evolving transients.

FLiBe is also highly chemically nonreactive with most fission products of concern and has a high boiling point, making it a good radioisotope barrier. Most fission products are soluble in the salt over a broad temperature range, which includes normal operating temperature and accident temperatures. Only a few fission products, once in contact with the fluoride salt, remain in a chemical form that is gaseous, namely xenon, krypton, and possibly tritium (depending on the chemical state of the salt, tritium can convert to tritium fluoride, which would have a higher solubility in the salt than molecular tritium).

In gas-cooled reactors that use the same fuel type as FHRs, air ingress at high temperatures can lead to graphite oxidation by air, which is an exothermic reaction. Molten fluoride salt covering the graphitic fuel and the graphite blocks, topped by an inert cover gas, serves as a barrier for air ingress.

Coolant inventory is ensured through inherent features in the mechanical design of the primary circuit. The reactor vessel is designed with penetrations only at the top of the core. All instrumentation and control rods feed through the upper lid of the core. The lowest elevation penetrations on the reactor vessel are for the cold leg and the hot leg feeding the external heat exchangers. In the event of a break in the primary coolant circuit outside the core, the coolant surface remains above the in-core decay heat removal heat exchangers, and above all graphite blocks. In the event of a break in the reactor vessel, salt will leak in the narrow space between the reactor vessel, and a steel-lined reactor cavity. The volume of this space is designed to be small enough such that the fault level of the coolant in the core will still be sufficient to ensure coverage of the graphitic fuel spheres, and of the graphite blocks.

The coolant in FHRs is not pressurized, so there is no source of stored (explosive) energy. Lacking coolant volatility, high pressure, and any source of chemical stored energy, FHRs cannot generate significant pressure inside their containment, except by the small pressure changes due to cooling gases in the reactor cavity. The pressure is controlled by a cover gas handling system inside the low-leakage containment boundary, which has a much larger total volume than the volume of gas inside the reactor cavity.

The FHR fuel has a high temperature margin to failure, and the TRISO fuel particles have multiple barriers for radioisotope retention: the fuel kernel retains actinides, the silicon carbide layer retains fission products, and the inner pyrocarbon layer retains gaseous fission products. The subsequent barrier to release of radionuclides is the coolant.

FLiBe is transparent in its liquid phase, which allows for easy visual inspection, as opposed to liquid metals, which are opaque at operating temperatures.

The Mk1 FHR uses eight cylindrical buoyancy-driven control rods to maintain constant power during normal operation. The rods are weighted to be neutrally buoyant in FLiBe at 615°C and contain natural boron carbide and are clad with either 316SS or CFRC. Any transient that raises the temperature of the coolant in the channel above the 615°C neutral buoyancy value causes the rod to insert passively and thus provide thermal negative reactivity to reduce or maintain stable power. This is in addition to the strong negative reactivity feedback of the coolant and fuel. Under off-nominal or accident conditions crucifix reserve shutdown blades are gravity-driven directly into the pebble core to shut down the reactor.

Fluoride-salt coolants have very effective natural circulation heat transfer. Salt density differences due to temperature differences between a heat source (the core), and an elevated heat sink (heat exchanger at higher elevation) induce a natural circulation flow, which is used to remove decay heat from the core without the need of active pumping or external power. Several natural circulation loops are designed within the FHR system to provide redundant means of decay heat removal. The natural circulation decay heat removal system activates itself passively, if a loss of forced circulation (LOFC) occurs. The Mk1 FHR is also equipped with a forced circulation loop for decay heat removal.

Fluoride salts also have the inherent feature of establishing buoyancy-driven natural convection paths, driven by local temperature gradients. This makes salt-cooled systems resilient to the formation of local hotspots or coldspots. For example, this feature in a pebble bed core drives self-mixing. In a decay heat-scenario, coolant gradients that would be $\sim$ 50°C without buoyant mixing drop to a few degrees Celsius. This protects the fuel from high peak temperatures, and it also protects the outlet mixing plenum from thermal gradients due to nonisothermal flow. If the coolant leaked into the space between the reactor vessel and the reactor cavity, natural convection paths will self-establish to transport heat from the core to the walls of the reactor cavity. The steel-lined reactor cavity is passively and actively cooled.

Initial scoping studies showed that under severe transients average fuel temperatures remain below 800°C. Anticipated transients without SCRAM, which rely on temperature reactivity feedback to shutdown and on natural circulation for decay heat removal, will not reach temperatures sufficient to cause fuel failure or damage to metallic structures in the PB-FHR primary system (Andreades). *It is a unique characteristic of FHRs that there are no postulated severe accident transients that can lead to core damage or fuel failure.* This characteristic of FHRs is enabled by inherent features of the solid-fuel coolant combination, and the design passive safety systems that rely on the advantageous physical properties of the coolant.

*Inherent safety features include:*

- High thermal inertia leads to slowly evolving thermal transients;
- Resilience to hotspots and coldspots due to natural convection;
- No stored chemical energy (i.e., no exothermic reactions);
- No stored mechanical energy (i.e., no high pressure, and large margin to coolant-boiling);
- Coolant serves as a barrier to radioisotope release, having high solubility for fission products and very low vapor pressure ($< 20$ Pa at 700°C);
- Transparent coolant allows for optical inspection (unlike liquid metal coolants);
- Negative temperature reactivity coefficient;
- Negative coolant voiding reactivity coefficient.

*Passive safety systems that are also passively activated include:*

- Natural circulation cooling to air as the ultimate heat sink;
- Buoyancy-driven shut-down rods.

## 13.4 Phenomenology unique to FHRs

FHRs exhibit different thermal hydraulic, neutronic, and structural mechanics phenomena compared to conventional reactors, and to more extensively studied advanced nuclear reactor concepts. They use a novel combination of fuel, coolant, and materials: graphite-matrix, coated-particle fuel; fluoride salt coolant; graphite moderator materials; and high-temperature metallic structural materials. A detailed discussion of key thermal hydraulic, neutronic, material phenomenology unique to FHRs can be found in Zweibaum et al. (2014).

## 13.5 Thermal-hydraulics

Thermal hydraulic phenomenology unique to FHRs include the use of a high Prandtl number coolant, potential for freezing during overcooling transients, bypass flow due to swelling or contraction of graphite blocks in the core, radiative heat transfer due to high operating temperatures, and establishment of effective natural circulation for passive decay heat removal.

A major part of modeling efforts for FHRs so far has been scaled experiments using the principles of similitude, maintaining certain nondimensional parameters of interest between the scaled and prototypical systems. Water and heat transfer oils can be used as liquid salt simulant fluids and they provide the tremendous advantage of low-distortion thermal-hydraulic experiments at significantly lower temperatures, reduced size, and reduced thermal power input. The cost is also reduced compared to constructing facilities at prototypical operating conditions. The primary experimental facilities devoted to this effort are currently at the University of California Berkeley, the University of New Mexico, Ohio State University (OSU), and the University of Wisconsin-Madison. Other experimental facilities are found at ORNL and the SINAP, the two major research institutions developing molten salt reactor technology for FHRs.

### 13.5.1 University of California, Berkeley (UCB) facilities

UCB has constructed experiments to research key thermal hydraulic phenomenology of FHRs using separate and integral effects test facilities. For safety and licensing purposes for PB-FHRs, it is important to accurately model the heat transfer coefficient between fuel pebbles and the FLiBe coolant in order to better estimate temperatures in a PB-FHR core. UCB has been performing scaled pebble-bed heat transfer experiments using simulant oils that match key nondimensional parameters for FLiBe. Using temperatures throughout a scaled pebble-bed test section along with other experimental parameters, the interfacial heat transfer coefficient can be extracted as a function of position within the bed and time. The scaled pebble-bed test section is shown in Fig. 13.7. Experimental heat transfer coefficients for this scenario have also been derived using experimental data outside the Mk1 PB-FHR's characteristic conditions. There is significant disagreement between the established correlations and the experimental ones, proving that it is important to perform tests and develop new correlations in the appropriate Re and Pr range.

UCB designed the first iteration of the compact integral effects test (CIET) facility (CIET 1.0) to reproduce the response of FHRs under forced and natural circulation operation. CIET 1.0 provides validation data to confirm the predicted

**Figure 13.7** Pebble-bed test section for heat transfer coefficient measurement experiments (Andreades).

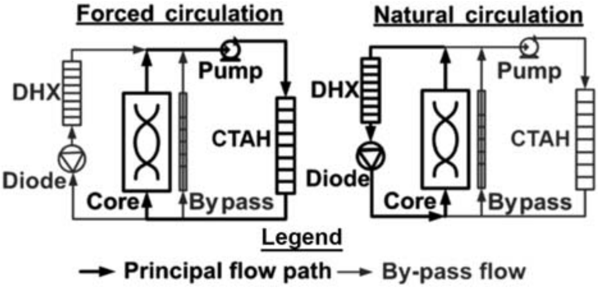

**Figure 13.8** FHR primary coolant flow paths for forced and natural circulation operation.

performance of the DRACS in FHRs. The facility has two coupled flow circuits: the primary coolant flow circuit, which replicates the main and bypass flow paths shown in Fig. 13.8, and the DRACS circuit. The two flow circuits exchange heat through the DRACS heat exchanger (DHX). The facility uses Dowtherm A as a simulant fluid for FLiBe, at reduced geometric and power scales. Test loops for CIET 1.0 were fabricated from thin-walled (schedule 10) 304 SS pipe and butt-welded fittings to minimize the mass and thermal inertia. The favorable power scaling with oil (10 kW into oil being equivalent to 625 kW into FLiBe), along with the simplicity of the construction for low-temperature operation, compared to the complexity and safety requirements for tests with the prototypical salts and other prototypical reactor coolants, were a key element enabling the CIET 1.0 facility to be constructed at lower cost than previous IETs for other reactor classes.

Because the designs of FHR commercial prototype reactors will evolve, inherent distortions will exist between the CIET 1.0 facility and future FHR commercial prototype reactors. For a transient response, such distortions may arise from unmatched coolant residence times between future FHRs and CIET 1.0 subsystems, as well as the use of reduced flow area SS piping with unscaled thermal inertia in CIET 1.0. CIET 1.0 was based on the earlier design of a 900-MWth channel-type pebble-bed advanced high-temperature reactor (PB-AHTR), and the preconceptual design of a 236-MWth Mk1 PB-FHR was completed after scaling and design of CIET 1.0 were already finalized; but elevations of the main heat sources and sinks in CIET 1.0 and the Mk1 PB-FHR design reveal a reasonable agreement between the scaled model and prototype. Therefore, CIET 1.0 will provide useful validation data for integral transient behavior of a generic set of FHRs. Given the low cost of the CIET facility, final code validation for a future commercial prototype plant would likely include construction of a new CIET-type loop scaled to closely match the prototypical design. All instrumentation, as well as the computer-controlled power supply and VFDs are integrated through the LabVIEW software and manually or automatically controlled from a central computer station. Fig. 13.9 shows the computer-aided design rendering of the CIET 1.0 loop and the actual facility.

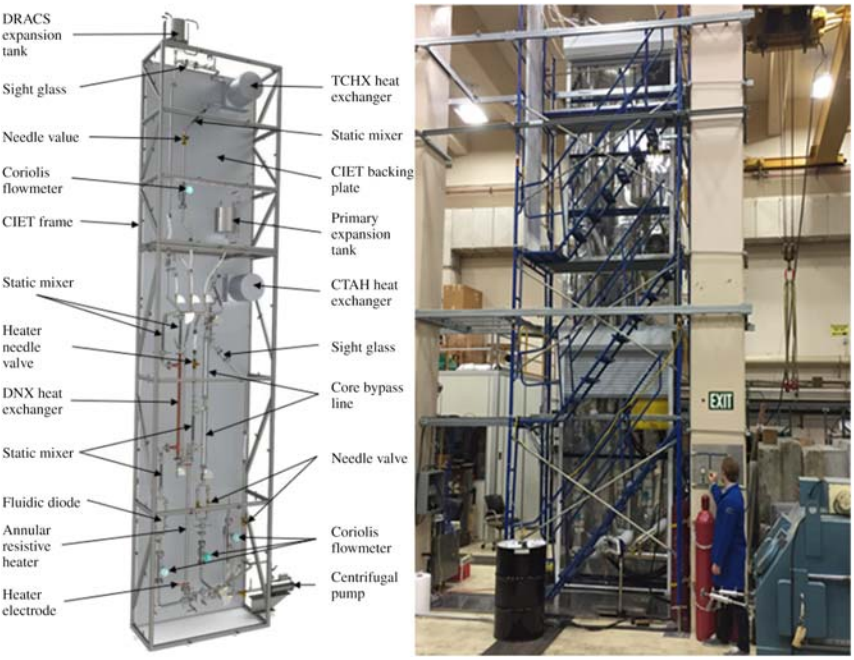

**Figure 13.9** 3-D rendering and photograph of CIET 1.0.

Between 2011 and 2014, CIET 1.0 was designed, fabricated, filled with Dowtherm A oil, and operated. Isothermal pressure drop tests were completed, with extensive pressure data collection to determine friction losses in the system. CIET-specific friction loss correlations were compared with handbook values, and empirically measured values were implemented in the system codes that are to be validated by CIET data. The project then entered a phase of heated tests, from parasitic heat loss tests to more complex feedback control tests and natural circulation experiments. In parallel, UCB has been developing thermal hydraulic models to predict FHR steady-state characteristics and transient response for a set of reference licensing basis events (LBEs). The general strategy is to rely on existing general-purpose thermal hydraulic codes with a significant V&V basis for design and licensing by the US Nuclear Regulatory Commission (NRC), such as RELAP5. Validation data will include steady-state forced and coupled natural circulation data in the primary loop and the DRACS loop, and thermal transients data (e.g., startup, shutdown, LOFC with scram, and loss of heat sink (LOHS) with scram) (Zweibaum et al., 2015).

### 13.5.2 University of New Mexico (UNM) facilities

Due to the high volumetric heat capacity of fluoride salts, FHR heat exchangers commonly operate in the transition and laminar flow regimes where heat transfer

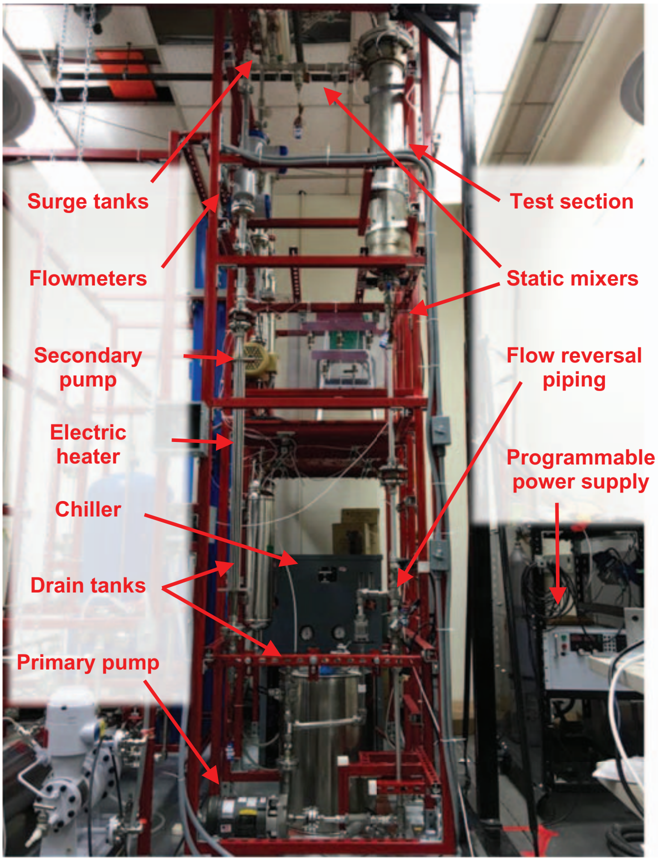

**Figure 13.10** UNM heat transfer loop.

coefficients can depend strongly on Reynolds number (Re) and potentially on Grashof number (Gr). Several reduced-scale experiments investigating heat exchanger phenomenology for FHRs are currently underway at UNM. A multiflow regime heat transfer loop, shown in Fig. 13.10, has been constructed for use with Dowtherm A to collect data and validate current heat transfer correlations (or develop new, when necessary) for several promising heat exchanger concepts. In parallel, a simple water loop investigating hydrodynamics was constructed and has been testing directional heat exchanger concepts for the DHX, which have the potential to help minimize parasitic heat losses during normal operation of the plant and enhance heat extraction during accidents.

The heat transfer loop was initially designed to test bayonet-style heat exchangers, which are inserted into the FHR coolant pool from the top and feature both the secondary (tube-side) feeder and outlet tubes attached to the top of the heat exchanger. Validation data will be collected for two conventional bayonet-style configurations: plain tubes and twisted tubes. Twisted tubes are a particularly promising technology to the development of the FHR due to their enhanced heat transfer and their self-supporting design, which eliminates the need for baffles and reduces hotspots and tube vibration.

The loop will be able to match shell-side Re and Pr for the primary-to-DHX, and have the capability to test a range of Gr, and by extension, Rayleigh (Ra) and Richardson (Ri) numbers, owing to the flexibility of the temperature conditions. The same plain and twisted tube bayonet heat exchangers will also be tested in a novel directionally enhanced shell concept. Because the DRACS is passive and always operating, heat is perpetually being removed from the primary coolant through the DHX. These parasitic heat losses lower the effective reactor outlet temperature during normal operation, reducing the efficiency of the FHR. The hydrodynamics of a directional DHX have been empirically investigated using a simple water loop with promising initial results. The design will be further optimized with computational fluid dynamics, and the resulting shell design will be implemented in the heat transfer loop and tested with the plain and twisted tube bundles.

Finally, the loop will be configured to test a double-wall twisted-tube heat exchanger. Due to the relatively large quantity of tritium generated in FHRs and the high operating temperature (which accelerates tritium transport), the use of double-wall heat exchangers with an intermediate fluid, such as lithium, to capture the tritium is under consideration. By using a twisted outer tube, it is possible to take advantage of the higher shell-side heat transfer coefficients and more uniform shell-side flow while also enhancing heat transfer to the intermediate fluid flowing in the annulus. Two configurations will be tested at UNM: a double-wall exchanger with inner plain tube/outer plain tube and a double-wall exchanger with inner plain tube/outer twisted tube to determine the heat transfer enhancement possible with the twisted-tube version (Zweibaum et al., 2015).

### 13.5.3 Ohio state facilities

A high-temperature DRACS test facility (HTDF) that is being constructed at The OSU is shown in Fig. 13.11 (in red), along with the low-temperature DRACS test facility (LTDF) that is currently in operation (Fig. 13.11 in gray). Both the HTDF and LTDF are scaled down from a 200-kW prototypic DRACS design for a pebble bed reactor design by following a rigorous scaling analysis. The HTDF employs FLiNaK and KF-ZrF4 as the primary and secondary coolants, respectively. With the HTDF, the DRACS capability of removing decay heat under prototypic reactor conditions can be evaluated.

The HTDF will be fully instrumented with gauge pressure transmitters to monitor the cover gas pressure in all the salt tanks, capacitance level sensors to monitor the tank salt levels, and thermocouples (N-type) to measure/monitor the salt temperatures along the loop, and in the tanks. High-temperature clamp-on ultrasonic flow meters from Flexim will measure the flow rates. ORNL will use the same

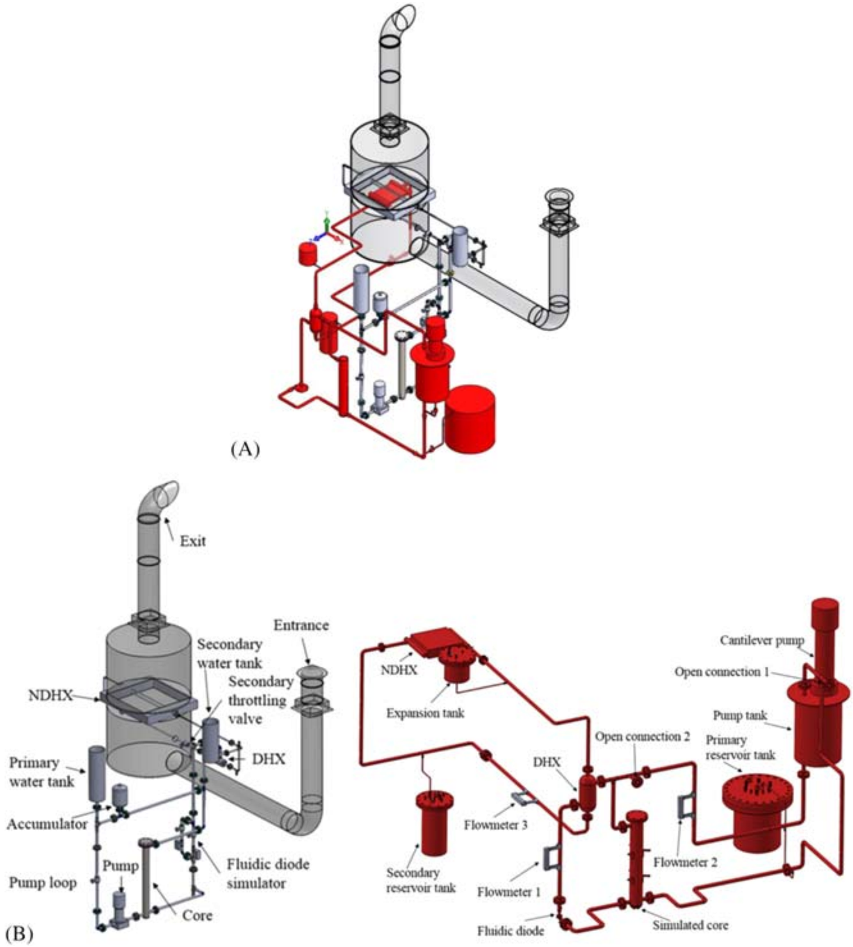

**Figure 13.11** (A) Combined HTDF and LTDF OSU DRACS test facilities. (B) LTDF (left) and HTDF (right) OSUE DRACS test facilities.

type flow meters at temperatures up to 700°C. For the differential pressure measurement, in-house designs utilize commercial differential pressure transmitters, which will require accurate control of the salt–Ar interface in the pressure-sensing lines.

The LTDF uses water as both the primary and secondary coolants. The LTDF is intended to examine the couplings among the natural circulation/convection loops, to provide OSU experience before building the HTDF. A vertical inline recirculation pump in the loop simulates the intermediate heat transfer loop, enabling experimental study of the pump trip process.

**Figure 13.12** ORNL liquid salt test loop.

### 13.5.4 Oak Ridge National Laboratory (ORNL)

The Liquid salt test loop facility at ORNL supports the development of the fluoride-salt-cooled high-temperature reactor concept. It can operate at up to 700°C and incorporates a centrifugal pump to circulate FliNaK salt through a removable test section. Inductive heating heats the test section, facilitating heat transfer testing. An air-cooled heat exchanger removes the added heat. Loop infrastructure includes a pressure control system, a trace heating system, and instrumentation to measure salt flow, temperatures, and pressures around the loop.

The goals of this facility (shown in Fig. 13.12) include providing operational knowledge and equipment to test high-temperature salt systems, developing a non-intrusive inductive heating technique for thermal/fluid experimentation, measuring heat transfer characteristics in a molten salt-cooled pebble bed, and demonstrating the use of silicon carbide as a structural material for molten salt systems (Lv et al., 2015).

ORNL, the location of the MSRE project, can provide legacy data for verification of experimental data and validation of computer models.

### 13.5.5 Shanghai institute of applied physics (SINAP)

The TMSR-SF1 is an experimental test reactor designed to enable the development of the Chinese Academy of Sciences' Thorium Molten Salt Reactor (TMSR) solid fuel molten salt reactor (also referred to as an FHR). The purpose of this test reactor is to verify the feasibility and safety of the solid fuel molten salt reactor concept, and to enable the subsequent design and licensing of a demonstration commercial reactor design by providing a comprehensive experimental platform. The TMSR-SF1 adopts a conservative design approach, where reactor safety is the primary consideration in the design, taking into account the basic research capabilities.

SINAP has designed and built several test loops to support their development process. The three principal loops at SINAP are the HTS Test Loop, FLiNaK Test Loop, and FLiBe Test Loop. The purpose of these loops includes experience with the experimental method, design, and construction of molten salt loops; thermal hydraulics of molten salt; the development of equipment to operate and measure the salt loop properties; and the exploration of chemistry issues for molten salts that include fluoride and beryllium.

The TMSR-SF0 is an electrically heated simulator for solid fuel molten salt reactors. Its primary functions are:

- To provide data and experience to support TMSR-SF1 licensing;
- To provide practical experience for TMSR-SF1 design, start up, operation, and maintenance;
- To verify TMSR-SF1 thermal-hydraulic design, safety programs, and other technical problem solutions;
- To test SF1 equipment;
- To simulate SF1 start up, operation, accident conditions, and maintenance.

TMSR-SF0 will also provide experimental evidence for verification and validation for solid fuel molten salt reactor thermal hydraulics and safety analysis codes.

Based on the above considerations, the TMSR-SF0 is designed as a full-scale, 1:1 geometrically scaled simulator for the TMSR-SF1. The key materials, technologies, and equipment used in the SF0 have the same design with SF1, and the plant layout is also basically the same. The main differences between the SF0 and SF1 are that SF0 graphite fuel pebbles are not loaded with nuclear fuel, the coolant is heated by electrical heating elements with a total power greater than 1 MW. The electrical heating is currently expected to use heating rods installed in channels in the graphite reflector. In addition, FLiNaK is used as the primary salt instead of FLiBe to avoid the safety issues of beryllium. Taking into account the needs of thermal-hydraulic experiments and the low radiation levels, the SF0 core and loop have more instrumentation. In addition, the loop has a flow control valve and shut-off valves to facilitate experiments. For long-term development considerations, SF0 will include pebble fuel recirculation test equipment.

### 13.5.6 Pebble dynamics and fuel handling

One FHR option is annular graphite pebbles with embedded TRISO fuel, as in the UCB Mk1 FHR preconceptual design. The X-Ray Pebble Recirculation Experiment (X-PREX) at UCB seeks to demonstrate the viability of pebble fuel handling and reactivity control for FHRs. The research results should clarify understanding of pebble motion in helium-cooled reactors and of low-velocity granular flows. Pebble fuels enable on-line refueling, operation with low excess reactivity, simpler reactivity control, and improved fuel utilization. If fixed fuel designs are used, the power density of salt-cooled reactors is limited to 10 MW/m$^3$ to obtain adequate duration between refuelings, but pebble fuels allow power densities in the range of 20–30 MW/m$^3$, much higher than the typical modular helium reactor 5 MW/m$^3$. Pebble fuels also permit radial zoning in annular cores, use of thorium or graphite pebble blankets to reduce neutron fluences to outer radial reflectors, and increase of total power.

The X-PREX facility uses novel digital X-ray tomography methods to track both the translational and rotational motion of spherical pebbles, which provides unique experimental results that can be used to validate discrete element method (DEM) simulations of pebble motion. The validation effort supported by the X-PREX facility provides a means to build confidence in analysis of pebble bed configuration and residence time distributions that impact the neutronics, thermal hydraulics, and safety analysis of pebble bed reactor cores.

Fig. 13.13 provides a view of the facility. Further information can be obtained from Laufer and Buster (2015).

**Figure 13.13** View of the X-ray pebble recirculation experiment (X-PREX) facility at UC Berkeley.

## 13.6 Chemistry and corrosion control

Compatibility and chemical control of nonuranium-bearing salts with structural materials is a key issue. There have been some primary corrosion experiments under static and dynamic conditions, but standardization of data sharing is needed for accurate comparison of materials and salts. Metallic structural materials, such as Hastelloy-N, are not yet code-qualified under the ASME Boiler and Pressure Vessel Code. High-temperature phenomenology, such as long-term creep deformation, is important. Compatibility of carbon and ceramic composite materials with fluoride salts also needs investigation (Chapter 7, Materials and Chapter 8, Chemical processing of liquid fuel).

## 13.7 Neutronics

In FHRs, the fuel is lumped in tiny TRISO particles that are dispersed in a graphite matrix of fuel pebbles or plates. A spherical fuel element is shown in Fig. 13.14. FHR cores present unique challenges for both deterministic and Monte Carlo approaches, due to the double heterogeneity (fuel elements in coolant, and TRISO particles within a fuel element).

Double heterogeneity makes it difficult to model and requires methods different from those used for a typical LWR fuel. Monte Carlo codes, such as MCNP and Serpent, can model the particles and pebbles explicitly without distortion introduced by any homogenization processes. Combined with DEMs, fuel kernel locations can be modeled as randomly distributed as they are manufactured. But various studies

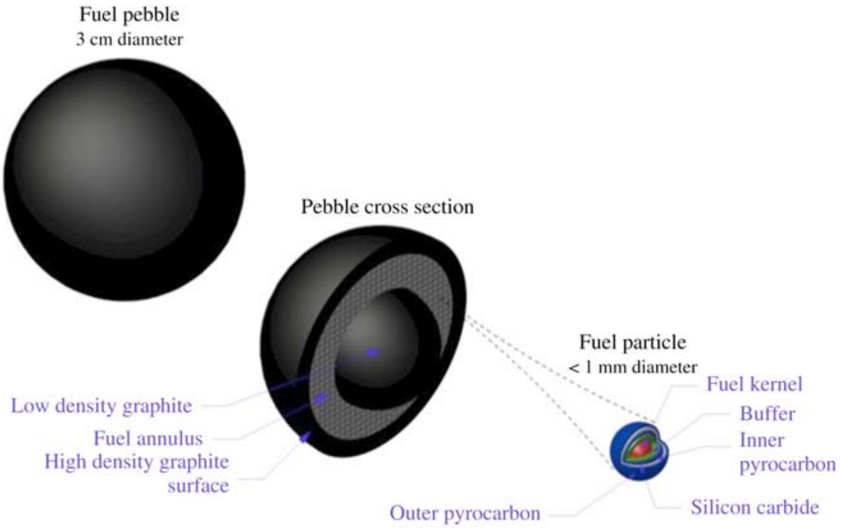

**Figure 13.14** A UC Berkeley-designed Mark I PB-FHR fuel pebble element.

show that models with ordered structure such as simple cubic, body-centered cubic, or face-centered cubic, give accurate results as long as the moderator to fuel ratio is preserved. The stochastic nature of Monte Carlo neutron transport method provides great flexibility in modeling complex geometries. However, an explicit full-core simulation can be computationally challenging and sometimes prohibitive to achieve accurate statistics. Deterministic codes need the effective homogenized cross-sections because a simple volume-weighted homogenization would underestimate the resonance self-shielding effect. In order to treat this effect correctly, various cross-section homogenization methods have been developed for media containing randomly and uniformly dispersed particles.

## 13.8 Tritium management

Tritium (3 H or T) is produced as a neutron activation product of the FLiBe primary coolant. Neutron reactions with $^{6}$Li and $^{7}$Li produce tritium, and neutron reactions with $^{9}$Be produce $^{6}$Li. The dominant source of tritium production is $^{6}$Li, with only small contributions from $^{7}$Li. The natural isotopic abundance of $^{6}$Li is 7.5%, and for FHR operation, it is reduced to hundreds or tens of ppm, by isotopic enrichment. Lithium isotopic enrichment reduces tritium production, and also improves the neutronic performance of the coolant, and hence fuel utilization. Therefore, the FHR coolant is most correctly denoted as 2 $^{7}$LiF-BeF$_2$. $^{9}$Be is the only stable isotope of Be, and the beryllium natural isotopic composition is 100% $^{9}$Be.

Tritium production rates in the FHR primary coolant, and production rates in primary coolants of other types of reactors are:

FHR → 2,000,000 Ci/year/GWe = 5500 Ci/day/GWe = 200 g T/year/GWe → from $^{6}$Li, $^{7}$Li, and $^{9}$Be in the coolant (at steady state 4 ppm $^{6}$Li, and 60% power conversion efficiency) (Cao, Gerczak, Kelleher, & Zheng, 2013; Fratoni & Greenspan, 2011; Young, Wu, & Scarlat, 2015);
PWR → 20,000 Ci/year/GWe = 50 Ci/day/GWe = 2 g T/year/GWe → from $^{6}$Li, $^{7}$Li, $^{10}$B, and $^{11}$B in the primary coolant water, used form chemistry control and chemical shim (Weaver, Harward, & Peterson, 1969);
BWR → 0.1 Ci/year/GWe = 0.3 mCi/day/GWe = 0.01 mg T/year/GWe → from $^{2}$H in the primary coolant (Weaver et al., 1969);
CANDU → 1,400,000 Ci/year/GWe = 3,800 Ci/day/GWe = 150 g T/year/GWe → from $^{2}$H in the heavy water moderator (*Management of Waste Containing Tritium and Carbon-*14, 2004);
HTGR → HTGR → 5000 Ci/year/GWe = 14 Ci/day/GWe = 0.5 g T/year/GWe → from $^{3}$He in the coolant, and $^{6}$Li and $^{7}$Li in the graphite moderators (*Management of Waste Containing Tritium and Carbon-*14, 2004)

Another interesting point of reference for the tritium production rate of FHRs is to consider that tritium could be used as fuel for a D-T fusion reaction. Given that the energy yield is 17.6 MeV for the D-T fusion reaction, and assuming a 50% power conversion efficiency, the tritium production rate from 1 GWe of FHR-produced electricity would supply the fuel for about 10 MWe to be produced by a D-T fusion reactor. Finally, it is worthwhile to note that natural sources of tritium production on

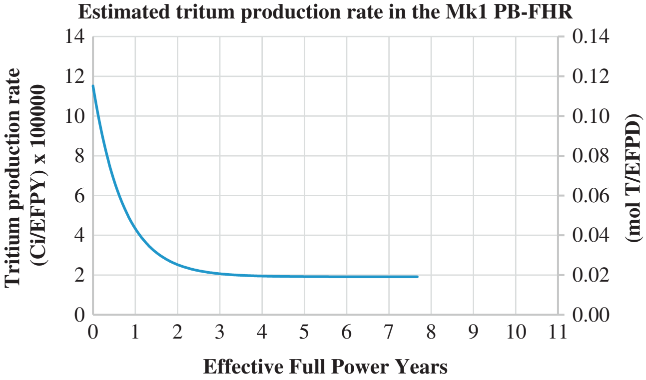

**Figure 13.15** Estimated tritium production rate in the Mk1 PB-FHR core, as a function of effective full-power years of operation (EFPY), starting with 0.005% $^6$Li enrichment. *Source*: Adapted from on neutronic calculations for the 900 $MW_{th}$ PB-FHR. Forsberg, C., Peterson, P.F., Pickard, P. 2003. Molten-salt-cooled advanced high-temperature reactor for production of hydrogen and electricity. Nuclear Technol. 144(3), 289-302.

Earth are estimated at 4–8 MCi/year, so 1 GWe from FHR plants would produce one half to one quarter of the natural global tritium production rate (Jacobs, 1968).

NRC and EPA established regulatory limits for tritium concentration in air and water effluents (0.1 pCi/L for air, 1 μCi/L for water), but they do not specify cumulative tritium emission limits (Forsberg et al., 2003; Sabharwall et al., 2013). In the absence of regulatory guidance on cumulative tritium emissions from power plants, the design goal of the FHR is to limit the tritium emissions to the emission rates of a PWR. In the United States the PWR emissions rates are reported by the NRC to be 700 Ci/year/GWe as liquid effluents (equivalent to 0.024 mol T/yr/GWe) (Forsberg et al., 2003), so the design goal is to recover 99.9% of the tritium produced in an FHR (Casino, 2006).

In the first few years of operation with fresh salt, the tritium production will be higher due to a higher fraction of $^6$Li. How much higher will depend on the initial isotopic enrichments of Li in FLiBe, which is an expensive process, and therefore a question of economic optimization, depending on the effectiveness and availability of the tritium management systems that will be implemented in the FHR. At startup, an initial $^6$Li percentage of 0.005% corresponds to a tritium production rate of 0.11 mol/EFPD (Peterson and Zhao, 2006). As the initial $^6$Li is consumed, its consumption rate eventually equilibrates with its production rate from $^9$Be to a $^6$Li isotopic composition of 4 ppm (Fei et al., 2008), and the tritium production rate reaches a steady-state value at 0.023 mol T/EFPD (Casino, 2006). The time to reach steady-state tritium production is a function of the total inventory, in-core and out of core, of primary coolant, and for Mark 1 FHR, it is on the order of 2 years of full-power operation. The tritium production rate against time for the Mk1 design is shown in Fig. 13.15. This figure was modified from a figure in FHR (2013) to account for the power density and salt inventory differences between the 236 $MW_{th}$ Mk1 design and the 900 $MW_{th}$ PB-FHR design; the Mk1 design has an active core power density of 23 $MW/m^3$, and primary salt inventory of 47 $m^3$ (Casino, 2006).

The initial chemical form of tritium in FLiBe is TF, as it is produced by transmutation of Li, which is present in the FLiBe in the chemical form of LiF. TF cannot permeate metal barriers easily, but at high temperature $T_2$ and HT easily permeate metallic heat exchangers, escaping from the primary coolant circuit to the power conversion cycle (Krumwiede et al., 2013). The redox control system in the salt prevents corrosion of structural steels by TF and leads to the formation of $T_2$ (Scarlat and Peterson, 2014), but, at FHR temperatures, $T_2$ is highly permeable through metal heat exchangers (Scarlat and Peterson, 2014). The chemical equilibrium ratio between $T_2$ and TF will be set by the redox potential of the salt, which is maintained by the chemical control system at a value that prevents the metallic alloys and the graphite from corrosion; most of the tritium is expected to be in the form of $T_2$, with a nonzero concentration of TF also present. The chemical form of tritium also depends on the amount of $H_2$ in the FHR system. With $H_2$ in the system, HT will be selectively produced, instead of $T_2$. However, based on the current status of the FHR design, it is not expected that appreciable quantities of $H_2$ will be in an FHR system.

### 13.8.1 *Tritium sinks*

The sources and sinks for tritium in the primary coolant loop of an FHR are shown in Fig. 13.16. Under FHR operating temperatures, the hydrogen isotopes have low solubility in fluoride salt and high permeability through metallic alloys. Therefore, the tritium concentration in the salt needs to be kept low to limit tritium release through the salt-to-air metallic heat exchangers to the power conversion cycle and eventual tritium release to the atmosphere. Tritium has low solubility in FLiBe salt and it can rapidly diffuse through metals at high temperature (Greene et al., 2010; Malinauskas and Richardson, 1974). Tritium permeation barriers are being considered to reduce tritium permeation through coiled-tube air heater (CTAH) tubes (Casino, 2006). Without permeation barriers, tritium transport through the CTAH is a mass-convection limited process (Krumwiede et al., 2013; Holcomb et al., 2011).

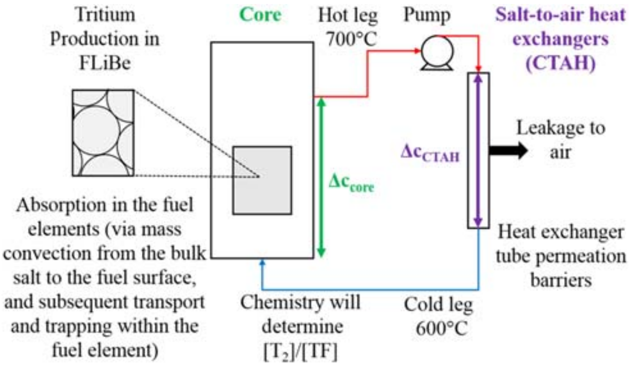

**Figure 13.16** Tritium sources and sinks in the FHR primary coolant loop.

Effective tritium permeation barriers will increase the tolerable concentration of tritium in the salt, while still meeting the target air emission rates of tritium through the CTAH. A high target concentration of tritium in the salt makes it easier to design tritium sinks and separation systems to clean up the salt upstream of the heat exchangers.

Several types of tritium sinks have been proposed for the primary system: solid getters, permeators, gas spargers, and vacuum disengagers. Solid getters are high surface-area solid materials that have high affinity and trapping capability for tritium at high temperatures. Graphite is one such material that is under investigation because it is known to chemically trap tritium, at small concentrations, at high temperatures. The fuel elements of FHR consist of a graphite matrix, which is being evaluated for its effectiveness to absorb tritium from the salt; other graphite types are being evaluated for ex-core absorption of tritium from the salt. Permeators are high surface area systems that extract the tritium from the salt by permeation through a metal; they would need to be designed to compete in mass transport effectiveness with CTAH. They can be standalone systems, or integrated with CTAH, in double-walled heat exchangers with an intermediate sweep gas. Gas spargers rely on generating a high mass-exchange surface area between a sweep gas and the salt; there is ongoing research on the optimization of bubble generation in the salt, and on ultrasonically enhanced mass transfer in gas−liquid tritium separators. Vacuum disengagers spray small droplets of molten salt into a vacuum chamber, where the tritium desorbs and is pumped away (Dolan et al., 1992).

### 13.8.2 Tritium mass transport in the primary coolant circuit

Without permeation barriers, tritium transport through the CTAH is a mass-convection limited process (Krumwiede et al., 2013; Holcomb et al., 2011). Because heat generation in FHRs occurs in solid fuel, rather than in the primary salt, FHRs have much larger graphite surface areas than the MSRE and MSRs in general. To achieve the FHR tritium recovery goal of 99.9%, the permeation barrier system in the primary heat exchangers must reduce tritium releases through the primary heat exchanger tubes by a factor of 200, or a factor of 100 considering additional graphite surface area provided in the primary heat exchanger hot manifold pipe annular cartridges. Experimental studies and additional analysis to determine whether the necessary mass transfer resistance can be achieved are needed, to select a specific coating method and to determine whether the Mk1 PB-FHR tritium control system is capable of achieving its tritium control target. Further work to study this question will be important to perform as the FHR design is refined.

### 13.8.3 Tritium absorption in the fuel elements

Upstream of the metallic heat exchangers, a large surface area of removable graphite components is in contact with the primary coolant: fuel pebbles, graphite pebbles, and inner reflectors. Because heat generation in FHRs occurs in solid fuel, rather than in the primary salt, FHRs have much larger graphite surface areas than MSRs in general. For comparison, the surface area of salt-to-air heat exchangers is $\sim 10{,}000\ \mathrm{m}^2$, and that of the removable graphite components is $\sim 2000\ \mathrm{m}^2$ (Andreades et al., 2016). If graphite exhibits appropriate tritium retention characteristics, tritium can be recovered by taking advantage of the removable graphite components that are part of the reactor core. Therefore it is important to characterize the diffusion and chemical trapping kinetics of hydrogen on graphite material at high temperatures (600−800°C), low tritium partial pressures at the graphite surface (a few to tens of Pa), and low tritium loading in the graphite materials (a few ppm).

In order to evaluate the effectiveness of the fuel elements as a tritium sink, we need to know the maximum hydrogen absorption capacity of the graphite fuel elements, and the mass transport rate from the salt into the graphite. Neither of them is well characterized. Posing the question backwards, we can calculate a desired T/C loading at the end of the fuel life.

Assuming a tritium absorption rate in the fuel elements and graphite reflector pebbles equals the tritium generation rate and the residence time of a fuel element in the core, and the parameters given in Table 13.2, we calculate the tritium concentration in the fuel element to be 2 μg T/g C. If the fuel elements and graphite reflector pebbles are recirculated through the core several times before discharge at 1.4 effective full-power years, and there is a tritium removal step before reintroduction to the core, then this estimated tritium per carbon loading could be lower by a factor of a few.

Saturation conditions of tritium in graphite vary greatly by experimental condition, but a reasonable estimate is on the order of tens of wppm T/C. Data on tritium saturation in nuclear graphite are available from MSRE (Forsberg et al., 2014; Zweibaum et al., 2014), fusion reactors (Zweibaum et al., 2015; Lv et al., 2015; Laufer and Buster, 2015; Malinauskas and Richardson, 1974), gas-cooled reactors in the UK (Adams, 1994; UC Berkeley Thermal Hydraulics Laboratory, 2013), and the very high-temperature reactor (VHTR) (Nie et al., 2013) research activities. A review of this literature is presented here and experimental values are summarized in Table 13.3. It should be noted that experimental results vary greatly for the type of graphite and appear to be strongly dependent on porosity (Forsberg et al., 2014). This data do indicate that the 2 wppm tritium loading at fuel discharge might be achievable, and the graphite fuel elements remain a candidate for the primary tritium sink in the FHR system.

We cannot quantify the mass transport resistance due to diffusion within the fuel element because fundamental work for the characterization of tritium diffusion and trapping within the graphite matrix is lacking. However we can estimate the mass transfer resistance due to convection from the bulk of the coolant to the surface of the fuel elements. We perform here calculations for a pebble bed. Using the same assumptions as above, we calculate the bulk concentration of tritium in the salt that would be necessary to drive mass convection to the surface of the pebbles to be $(2)10^{-6}$ mol/m$^3$; using a Henry's law solubility coefficient of $(5)10^{-5}$ mol/L-atm, this concentration corresponds to 4 Pa $T_2$ in the cover gas. This is the minimum bulk

**Table 13.2** Perfect sink calculation input and outputs based on Mk1 PB-FHR design (Andreades et al., 2016)

| Inputs | | | Inputs | | |
|---|---|---|---|---|---|
| **Parameter** | **Value** | **Units** | **Parameter** | **Value** | **Units** |
| Salt average temperature | 650 | °C | Carbon molecular weight | 12 | g/mol |
| Reynolds number | 500 | – | Tritium molecular weight | 3 | g/mol |
| Schmidt number (ν/D) | 1.76E + 14 | – | Graphite density | 1.745E + 06 | g/$m^3$ |
| Diffusivity (tritium in FLiBe) (Krumwiede et al., 2013) | 3.91E-09 | $m^2$/s | Pebble life | 1.4 | year |
| Pebble diameter | 0.03 | M | FLiBe inventory (primary system) | 46.82 | $m^3$ |
| Salt viscosity | 6.78E-03 | kg/(m × s) | Outputs | | |
| Salt density | 1.96E + 03 | kg/$m^3$ | Mass transfer coefficient | 3.34E-01 | m/s |
| Steady-state tritium production rate | 2.66E-07 | mol T/s | Bulk salt concentration at steady state | 4.09E-10 | mol T/$m^3$ |
| Startup tritium production rate | 1.28E-06 | mol T/s | Bulk salt concentration at startup | 1.97E-09 | mol T/$m^3$ |
| Number of graphite reflector and fuel pebbles in the core | 688,000 | – | Graphite saturation at steady state | 2.08 | μg T/g C |
| Pebble surface area | 1945 | $m^2$ | Graphite saturation at startup | 9.99 | μg T/g C |

concentration of tritium in the salt that will drive tritium to the surface of the pebbles at a rate that balances generation in the coolant. To this, the additional mass transport resistance due to diffusion of tritium into the graphite will need to be added; we do not know yet which one of these transport resistances is dominant.

Even though the hydrogen isotope transport mechanism in nuclear graphite has not been fully understood, and the graphite matrix has not been investigated yet,

Table 13.3 **Summary of hydrogen/tritium saturation in graphite by exposure to a gas**

| **Retention** | **Redmond (Malinauskas and Richardson, 1974)** | **Kanashenko (Laufer and Buster, 2015)** | **Atsumi (Lv et al., 2015)** | **Strehlow (Forsberg et al., 2014)** | **Compere (Zweibaum et al., 2014)** |
|---|---|---|---|---|---|
| Hydrogen isotope pressure (Pa) | 133–101,325 | 2500–90,000 | 10,000 | 0.14 | MSRE salt |
| Temperature (°C) | 900–1500 | 700–1200 | 750–1050 | 750 | 650 |
| Graphite type | TSP | TSP | IG-430U | POCO | CGB |
| Saturation (wppm) | 2.5–17.5 | 12.5–55 | 15–20 | 0.24–3.4 | 0.025–5 |

there are some experimental results for nuclear-grade graphite. The main tritium transport mechanism in graphite is expected to be Knudsen diffusion in open pores, which is characterized by molecular diffusion through the interconnected pores in graphite (Forsberg et al., 2003). Intragranular bulk diffusion within the graphite grains is also possible. Lastly, interstitial diffusion within the graphite crystallites is possible, but unlikely to dominate (Petti, 2014). Table 13.4 summarizes the available data for overall bulk diffusion of hydrogen in nuclear graphite at high temperature.

Most of the data summarized above are for unirradiated graphite material. There are two neutron irradiation effects that are expected to affect tritium transport in graphite. (1) The intragranular diffusion coefficient initially decreases with small damage levels, and then increases past approximately 0.2 dpa in isotropic graphites (IG-110U, IG-430U) (Lv et al., 2015). This behavior is attributed to the saturation of trapping sites and either a decrease in crystallite size or newly introduced pathways from microcracks (Lv et al., 2015). (2) Tritium retention in trapping sites increases (Lv et al., 2015; Laufer and Buster, 2015). Kanashenko et al. (1996) reported that irradiation above 1 dpa causes an increase in Trap 1 and 2 sites to 1500 and 5000 appm (Laufer and Buster, 2015). Atsumi found that the amount of hydrogen retained increases by a factor of about 100, where the intragranular diffusion and retention in Trap 1 sites significantly increases with irradiation as shown in Figs. 13.17 and 13.18 (Lv et al., 2015).

Further studies of the ability of the graphite matrix fuel elements to serve as an effective in situ tritium sink need to investigate (1) limits on the tritium retention capability of the graphite matrix, (2) transport and trapping mechanisms into the graphite matrix, (3) better characterization of mass convection in the salt at the prototypical conditions in the core, (4) the role of the salt–graphite interface and the

**Table 13.4** **Summary of diffusion coefficient correlations from experiment (Forsberg et al., 2003; Ingersoll and Clarno, 2005; Ingersoll et al., 2004; Sabharwall et al., 2013)**

| Isotope | Diffusion coefficient | @700°C | Unit | Researcher | Treatment |
|---|---|---|---|---|---|
| (pore)$D_2$ | 1800exp(−1.21(kJ/mol)/RT) | 5.71e-4 | $cm^2/s$ | H. Atsumi (1988)[1] | Unirradiated |
| (bulk)$D_2$ | 1.69exp(−251(kJ/mol)/RT) | 5.60e-14 | $cm^2/s$ | H. Atsumi (1988)[1] | Unirradiated |
| $H_2$ | 3.3e-10exp(1.3 eV/kT) | 3.30e-10 | $cm^2/s$ | H. Atsumi (2002)[2] | Unirradiated |
| $H_2$ | 8.95e-10exp(−1.99 eV/kT) | 8.95e-10 | $cm^2/s$ | H. Atsumi (2011)[3] | Unirradiated |
| $H_2$ | 8.26e-10exp(−1.92 eV/kT) | 8.26e-10 | $cm^2/s$ | H. Atsumi (2011)[3] | Irradiated[4] |
| $T_2$ | 3.32e2exp(−98,400 cal/RT) | 2.57e-20 | $cm^2/s$ | R.A. Causey (1979)[5] | Irradiated |
| $D_2$ | 2.0e-6exp(−0.1 eV/kT) | 2.00e-6 | $1 \times 10^6$ | DIFFUE code[6] | – |

1. Deuterium pressure is 60 kPa, the sample is high-density (1.90 g/$cm^3$) isotropic graphite; pore diffusion means molecular diffusion in pores, while bulk diffusion means trapping and detrapping process inside filler grain;
2. "Crystallite boundary diffusion coefficient" which trapped effect are neglected. Didn't mention pressure, assume to be around 10−20 kPa;
3. Sample IG-430, hydrogen pressure, 10 kPa, temperature range is 790−1050°C;
4. Neutron fluence: 5.0e9 n/$m^2$ (> 1 MeV);
5. The sample is pyrolytic graphite and tritium pressure is not specified. Neutron fluence: 1.0e14 n/$m^2$;
6. The sample is Papyex graphite, low-density graphite (1.1 g/$cm^3$); deuterium pressure is 0.66 Pa,temperature range is 50−700°C (Forsberg et al., 2012).

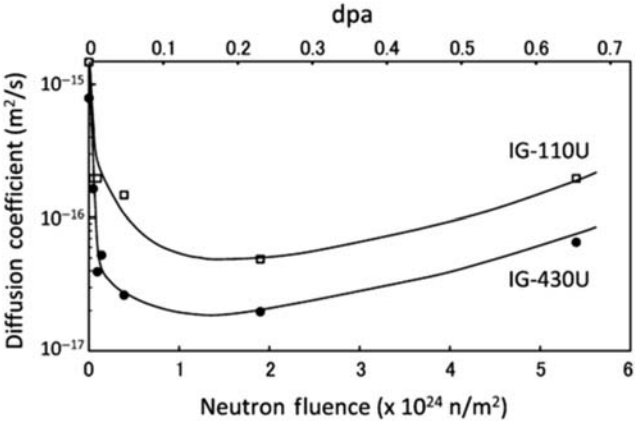

**Figure 13.17** Granular diffusion coefficients with graphite damage (Lv et al., 2015).

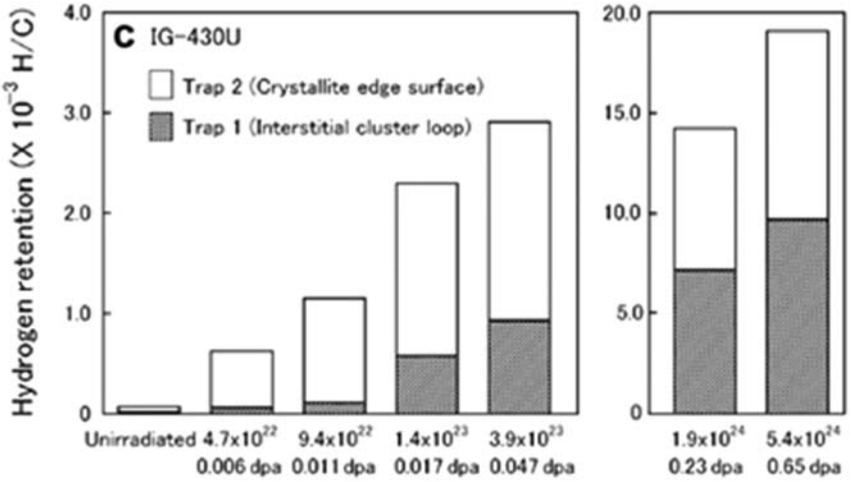

**Figure 13.18** Hydrogen retention with graphite damage (Zweibaum et al., 2015).

role of other species that may be present at the interface, such as corrosion products and metallic impurities, and (5) the effect of neutron irradiation on all of the above.

## 13.9 Safety analysis and licensing strategy

Performing a safety analysis and developing a licensing strategy for the FHR is a key step in the commercialization path. A primary focus is identifying high-level functional requirements of major FHR systems, structures, and components (SSCs); and how to identify a range of LBEs that should be considered in design and in the developments of modeling tools and supporting experiments, including a discussion of lessons from the Fukushima Daiichi accident for severe external beyond design basis events (BDBEs).

### 13.9.1 Safety design criteria, strategies, subordinate goals

Four white papers issued after the four FHR expert workshops held in 2012 outline the novel aspects of FHR technology and propose a technology development path. The initial drafts of the white papers were prepared before the respective workshops by graduate students and postdoctoral scholars, and the comments of the experts attending the workshops were subsequently integrated. The experts who attended the workshops represent industry, academia, and national laboratories.

For FHR design and safety analysis, six high-level safety design criteria (SDC) based on earlier work by the NGNP and PBMR projects provide an appropriate framework to guide the design of safety-relevant FHR SSCs: SDC 1—Maintain control of radionuclides; SDC 2—Control heat generation (reactivity); SDC 3—

Control heat removal and addition; SDC 4—Control primary coolant inventory; SDC 5—Maintain core and reactor vessel geometry; SDC 6—Maintain reactor building structural integrity.

The NRC has extensive experience reviewing liquid metal reactor (LMR) technology. Publications such as the NRC preliminary safety evaluation report of the S-PRISM design are highly useful in identifying technical gaps in key FHR technologies that are shared with the LMR (Adams, 1994). Additionally, the American Nuclear Society (ANS) has created a safety standard for FHRs, ANS 20.1, which will provide the basis to develop consensus-based FHR-specific general design criteria, to be used in licensing reviews.

### 13.9.2 Licensing experience from liquid metal and gas-cooled reactors

One of the key elements on the development and deployment path of any advanced reactor, and thus also the FHR, is the licensing by the host country's nuclear regulator. The nuclear regulator focuses on the safety of the plant personnel, the general public, and the environment. There have been advanced reactor designs that have undergone review by the US NRC, such as LMRs and PBMRs that have significant overlaps with the FHR and can provide guidance in the licensing approach and process, but also demonstrate gaps that need addressing.

For the FHR, a system decomposition scheme, presenting key constituents and material selection options, and identifying functional requirements for key subsystems, fits within an overall framework to guide the design and licensing efforts. A set of six design criteria are proposed as the top level safety requirements for FHRs, and defense-in-depth strategies for meeting each of the requirements are suggested. Likewise, the white paper proposes an initial set of LBEs and system operating states to be used in developing safety systems designs and models for FHRs. This information can be found in extensive detail in a UCB white paper discussing the topic (UC Berkeley Thermal Hydraulics Laboratory, 2013).

FHR fuel is similar in nature to the one used by the NGNP. An NGNP fuel qualification white paper provides a detailed review of the current regulatory basis for licensing coated-particle fuels in cladding USNRC regulatory, policy statements, guidance documents, and licensing precedents from earlier US HTGRs; summarizes existing understanding, date and analysis methods regarding coated-particle fuel performance; reviews fuel designs and resulting fuel service conditions and performance requirements; and recommends an approach for qualification of NGNP fuel. These existing NGNP capabilities are important to the development of similar coated-particle fuels for FHR. A major benefit of the high particle powers used in FHRs, and of continuous fuel circulation, for pebble fuel, is that the fuel reaches full discharge burnup rapidly, typically in around 1 year for FHR pebble fuels. Therefore, the time to develop, test, and qualify new fuels for FHRs has the potential to be much shorter that for typical reactors, whose fuel reaches full discharge burnup in 4–6 years.

In terms of structural materials, there are three categories: metallic structure and components, ceramic structures and components, and building structures. For chemistry and corrosion control simplicity, a single metallic alloy should be selected for all metallic materials contacting the coolant salt. Building structures will be made of steel-plate/concrete composites, similar to the AP-1000 LWR, several of which are currently under construction (Nie et al., 2013; Varma et al., 2014).

### 13.9.3 Severe accidents source term

Existing risk-informed approaches for identifying anticipated operational occurrences and design basis events can be readily informed event categories, the LBE selection process must develop a set of plausible initiating events based on a combination of informed judgment and a hierarchical system decomposition to develop failure modes for major reactor systems. Subsequently, the conceptual design-phase probabilistic risk assessment (PRA) suggested for FHRs would categorize events based on the anticipated frequency using assigned, rather than observed, system reliability requirements. The assigned frequencies translate to functional requirements for the subsystem performance; functional requirements are instrumental in guiding future design development, and documenting the assumptions on which the current analysis is based.

The approach to identifying BDBEs and assessing the ability of an FHR to respond to and mitigate consequences of BDBEs requires further development, particularly because the high thermal margins of FHR fuel suggest that these reactors can be designed to have a very robust and effective response to BDBEs even when they result in extensive plant damage. The possible elimination of offsite consequences appears to be unique to the combination of fuel and coolant in FHRs and merits consideration. A set of bounding event categories that should be evaluated for specific FHR designs is listed below:

1. Unprotected overpower events;
2. Station blackout;
3. Protected LOHS with additional failure of safety-related heat removal system;
4. Unprotected LOHS;
5. Protected LOFC with additional failure of safety-related heat removal system;
6. Unprotected LOFC;
7. Large loss of primary coolant (e.g., vessel rupture);
8. Severe overcooling transient;
9. Flow blockage (fixed fuel design only);
10. Failure of hold-down structures;
11. Severe external events.

## 13.10 Summary

FHRs are a Generation IV fluoride salt-cooled, solid-fueled, high-temperature reactor class currently under development in the United States and China, by both research institutions and universities. The concept of an FHR was generated by trying to integrate advantages of other reactor classes (low pressure, high temperature, high efficiency) while eliminating some of their drawbacks (huge containment domes, low efficiencies). Fixed fuel and pebble fuel, SMRs, and gigawatt reactors are being studied.

FHRs feature both inherent and engineered safety features. The primary coolant brings inherent features. FLiBe has a high volumetric heat capacity, leading to high thermal inertia and slowly evolving thermal transients. FLiBe is at near atmospheric pressure, and thus has no stored chemical energy (no exothermic reactions) and no mechanical energy (no high pressure, and large margin to coolant-boiling). FLiBe is transparent and allows for optical inspection (unlike liquid metal coolants).

FHRs are designed using defense in depth. FHRs are designed to have both negative temperature and coolant voiding reactivity coefficients. TRISO fuel has two barriers against fission product release. FLiBe serves as a barrier to radioisotope release, having high solubility for fission products and very low vapor pressure ($<20$ Pa at 700°C). Natural circulation cooling to air as the ultimate heat sink provides a means for passive decay heat removal. Finally, buoyancy-driven control-down rods are employed to moderate power.

Several experimental facilities have been constructed and are under fabrication to study phenomenology unique to FHRs. Natural circulation loops using simulant fluids, natural circulation loops at prototypical conditions, salt purification techniques, in core irradiation experiments of salts and structural components are all taking place at several research institutions to study phenomenology applicable to FHRs.

Performing a safety analysis and developing a licensing strategy for the FHR is a key step in the commercialization path. A primary focus is identifying high-level functional requirements of major FHR SSCs; and identifying a range of LBEs that should be considered in design and in the developments of modeling tools and supporting experiments, including a discussion of lessons from the Fukushima Daiichi accident for severe external BDBE.

FHRs are a promising reactor technology for the needs of a future electrical grid with highly fluctuating solar and wind power. FHRs might also serve as a stepping stone to liquid fuel molten salt reactors, helping to understand phenomenology and engineering issues prior to having fuel and associated fission products present in the primary coolant.

## References

Adams, S., 1994. "Preacpplication safety evaluation report for the power reactor innovative small module (PRISM) liquid-metal reactor," NUREG-1368, B-4, Washington, DC.

AISC Specification for Safety-Related Steel Structures for Nuclear Facilities, ANSI/AISC N690-12, draft issued for public comment, 2014.

Andreades, C., 2015. Dissertation: Nuclear Air-Brayton Combined Cycle Power Conversion Design, Physical Performance Estimation and Economic Assessment. University of California, Berkeley, CA.

Andreades, C., 2016. Charalampos, and Per Peterson. Nuclear air brayton combined cycle and Mark 1 pebble bed fluoride-salt-cooled high-temperature reactor economic performance in a regulated electricity market. Nucl. Eng. Des..

Andreades, C., Cisneros, A., Choi, J., Chong, A., Fratoni, M., Hong, S., et al., 2016. Design summary of the Mark I pebble-bed, fluoride-salt-cooled, high-temperature reactor commercial plant. Nucl. Technol. 195 (3), 223–238.

Andreades, C., Cisneros, A.T., Choi, J.K., Chong, A.Y.K., Krumwiede, D.L., Huddar, L.R., et al., 2014. , September 30 .Technical Description of the 'Mark 1' Pebble-Bed Fluoride-Salt-Cooled High-Temperature Reactor (PB-FHR) Power Plant. Department of Nuclear Engineering, U.C, Berkeley

Andreades, C., Lindsay, D., Peterson, P., 2014a. Reheat air-brayton combined cycle (RACC) power conversion design and performance under off-nominal conditions. J. Eng. Gas Turbines Power. 136 (6).

Andreades, C., Scarlat, R., Dempsey, L., Peterson, P., 2014b. Reheat air-brayton combined cycle (RACC) power conversion design and performance under nominal ambient conditions. J. Eng. Gas Turbines Power. 136 (7).

Cao, G., Gerczak, T., Kelleher, B., & Zheng, G. (2013). Fluoride-Salt-Cooled, High-Temperature Reactor (FHR) Materials, Fuels and Components White Paper (No. UCBTH-12-003). Madison, Wisconsin.

Casino, W. Jr., 2006. "Investigation of an alternative fuel form for the liquid salt cooled very high temperature reactor (LS-VHTR)," In: *International Congress on Advances in Nuclear Power Plants 2006*, Reno, NV.

Clarno, K., Gehin, J., 2006. "Physics analysis of the LS-VHTR: salt coolant and fuel block design," In: *PHYSOR-2006, ANS Topical Meeting on Reactor Physics*, Vancouver, BC.

Dolan, T.J., Longhurst, G.R., Garcia-Otero, E., 1992. A vacuum disengager for tritium removal from HYLIFE-II reactor FLiBe. Fusion Technol. 21, 1949–1954.

Fei, T., Ogata, D. et-al., 2008. "A modular pebble-bed advanced high temperature reactor," University of California, Berkeley, NE-170 Senior Design Project, Berkeley, CA.

Forsberg, C., Hu, L., Peterson, P., Sridharan, K., 2013. "Fluoride-salt-cooled high-temperature reactors (FHRs) for baseload and peak electricity, grid stabilization, and process heat." Massachussetts Institute of Technology, MIT-ANP-TR-147, Cambridge, MA.

Fluoride-Salt-Cooled High Temperature Reactor (FHR). Materials, Fuels and Components White Paper. University of California - Berkeley, UCBTH-12-003, (2013).

Fratoni, M., Greenspan, E., 2011. Neutronic feasibility assessment of liquid salt – cooled pebble bed reactors. Nucl. Sci. Eng.1–22.

Forsberg, C., Hu, L.-W., Peterson, P.F., Allen, T., 2012. "Luoride-Salt-Cooled High-Temperature Reactors (Fhrs) for Power and Process Heat," Massachusetts Institute of Technology MIT-ANP-TR-157, Cambridge, MA.

Forsberg, C., Hu, L.-W., Richard, J., Tomatoski, R., Forget, B., Stempien, J., et al., 2014. "Fluoride-salt-cooled high-temperature test reactor (FHTR): goals, options, ownership, requirements, design, licensing, and support facilities." Center For Advanced Nuclear Energy Systems, Cambridge, MA (MIT-ANP-TR-154).

Forsberg, C., Peterson, P.F., Pickard, P., 2003. Molten-salt-cooled advanced high-temperature reactor for production of hydrogen and electricity. Nuclear Technol. 144 (3), 289–302.

Frequently Asked Questions About Liquid Radioactive Releases. Nuclear Regulation commission. [Online]. Available: http://www.nrc.gov/reactors/operating/opsexperience/tritium/faqs.html#normal.

Gas Turbine-Modular Helium Reactor (GT-MHR) 1996. Conceptual Design Description Report. General Atomics 7658, San Diego, CA.

Greene, S., Gehin, J., Holcomb, D., et al., 2010. "Pre-conceptual design of a Fluoride-salt-cooled small modular advanced high-temperature reactor (SmAHTR)." Oak Ridge National Laboratory (ORNL/TM-2010/199), Oak Ridge, TN.

Holcomb, D., Ilas, D., Qualls, A., Peretz, F., Varma, V., Bradley, E., et al., 2012. "Current status of the advanced high temperature reactor." In: *Proceedings of ICAPP '12*, Chicago, Jun 24–28.

Holcomb, D., Ilas, D., Varma, V., Cisneros, A., Kelly, R., Gehin, J., 2011a. "Core and refueling studies for the advanced high temperature reactor." Oak Ridge National Laboratory (ORNL/TM-2011/365, Oak Ridge, TN.

Holcomb, D., Peretz, F., Qualls, A., 2011b. "Advanced high temperature reactor systems and economic analysis," oak ridge national laboratory (ORNL/TM-2011/364), Oak Ridge, TN.

Hong, S., Kazama, D., Nguyen, H.D., Root J., 2014. "NE-170 Physical arrangement and structural design for the Mk1 PB-FHR reactor building," Department of Nuclear Engineering, U.C. Berkeley, Report UCBTH-14-003.

Ingersoll, D., Clarno, K., 2005. "Status of physics and safety analyses for the liquid-salt-cooled very high-temperature reactor (LS-VHTR)." Oak Ridge National Laboratory, ORNL/TM-2005/218, Oak Ridge, TN.

Ingersoll, D., Forsberg, C., Ott, L., Williams, D., Renier, J., Wilson, D., et al., 2004. "Status of preconceptual design of the advanced high-temperature reactor (AHTR)." Oak Ridge National Laboratory ORNL/TM-2004/104, Oak Ridge, TN.

International Atomic Energy Agency, 2006. "Characterization, treatment and conditioning of radioactive graphite from decommissioning of nuclear reactors." IAEATECDOC-1521, p. 40.

Jacobs, D.G. (1968). Sources of Tritium and Its Behavior Upon Release to the Environment (No. TID-24635). ORNL Nuclear Safety Information Center Health Physics Division.

Kanashenko, S.L., Gorodetsky, A.E., Chernikov, V.N., Markin, A.V., Zakharov, A.P., Doyle, et al., 1996. Hydrogen adsorption on and solubility in graphites. J. Nucl. Mater. 233, 1207–1212.

Krumwiede, D., Scarlat, R., et-al., 2013. "Three-dimensional modeling of the pebble-bed fluoride-salt-cooled, high-temperature reactor (PB-FHR) commercial plant design." In: *Proceedings of the American Nuclear Society Winter Meeting*, Washington, DC.

Laufer, M., Buster, G., 2015. X-Ray Pebble Recirculation Experiment (X-PREX) Design and Initial Experimental Results. University of California, Berkeley, CA.

Lv, Q., Lin, H.C., Kim, I.H., Sun, X., Christensen, R.N., Blue, T.E., et al., 2015. DRACS thermal performance evaluation for FHR. Ann. Nucl. Energy. 77, 115–128.

Malinauskas, A., Richardson, D., 1974. Solubilities of hydrogen, deuterium, and helium in molten Li2BeF4. Ind. Eng. Chem., Fundam. 13 (3), 242–245.

Management of Waste Containing Tritium and Carbon-14. (2004). Technical Reports Series (Vol. 421). Retrieved from: < http://www-pub.iaea.org/MTCD/Publications/PDF/TRS421_web.pdf >.

Matzer, D., Wallace, E., 2005. PBMR moves forward with higher power and horizontal turbine. Model Power Systems. 25 (1), 11–15.

Nie, J.-G., Hu, H.-S., Fan, J.-S., Tao, M.-X., Li, S.-Y., Liu, F.-J., 2013. "Experimental study on seismic behavior of high-strength concrete filled double-steel-plate composite walls,". J. Constr. Steel Res. 88, 206–219.

Nuclear Energy Institute, Methodology for performing aircraft impact assessments for new plant designs, NEI 07-13 REV. 07 Public Version, May 2009.

Ohashi, H., Sherman, S.R., 2007. Tritium Movement and Accumulation in the NGNP System Interface and Hydrogen Plant, Idaho National Laboratory, INL/EXT-07-12746, (2007).

Peterson, P., Zhao, H., 2006. "A flexible base-line design for the advanced high-temperature reactor utilizing metallic reactor internals (AHTR-MI)." In: *International Congress on Advances in Nuclear Power Plants*, Reno, NV.

Petti D., 2014. "Results from the DOE advanced gas reactor fuel development and qualification program." Idaho National Laboratory, Idaho Falls, ID (INL/CON-14-31456.

Sabharwall, P., Bragg-Sitton, S., Stoots, C., 2013. Challenges in the development of high temperature reactors. Energy Convers. Manage. 74, 574–581.

Scarlat, R., Peterson, P., 2014. The current status of fluoride salt cooled high temperature reactor (FHR) technology and its overlap with HIF target chamber concepts. Nucl. Instrum. Methods Phys. Res. Sect. A. 733, 57–64.

UC Berkeley Thermal Hydraulics Laboratory, 2013. "Fluoride-salt-cooled, high-temperature reactor (FHR) subsystems definition, functional requirement definition, and licensing basis event (LBE) identification white paper." UCBTH-12-001, Berkeley, CA.

Varma, A.H., Malushte, S.R., Sener, K.C., Lai, Z., 2014. "Steel-plate composite (SC) walls for safety related nuclear facilities: Design for in-plane forces and out-of-plane moments,". Nucl. Eng. Des. 269, 240–249.

Varma, V.K., Holcomb, D.E., Peretz, F.J., Bradley, E.C., Ilas, D., Qualls, A.L., et al., 2012. AHTR mechanical, structural, and neutronic preconceptual design. ORNL/TM-2012/320. ORNL, Oak Ridge, TN.

Weaver, C.L., Harward, E.D., Peterson, H.T., 1969. Tritium in the environment from nuclear power plants. Public Health Rep. 84 (4), 363–371.

Young, M., Wu, H., & Scarlat, R. (2015). Characterization of Tritium Transport in the Flibe-Graphite System, for In- Situ Tritium Absorption by the Fuel Elements of the Fluoride-Salt-Cooled High-Temperature Reactor (FHR). In NURETH-16, Chicago, IL, August 30-September 4, 2015 (4972–4986).

Zweibaum, N., Cao, G., Cisneros, A., Kellher, B., Laufer, M., Scarlat, R., et al., 2014. Phenomenology, methods and experimental program for fluoride-salt-cooled, high-temperature reactors (FHR). Prog. Nucl. Energy. 77, 390–405.

Zweibaum, N., Huddar, L., Hughes, J.T., Laufer, M.R., Blandford, E.D., Scarlat, R.O., et al., 2015. "Role and status of scaled experiments in the development of fluoride-salt-cooled, high-temperature reactors." In: *International Congress on Advances in Nuclear Power Plants*, Nice, France.

# Static liquid fuel reactors

# 14

*Ian Scott*
Moltex Energy, London, United Kingdom

## Chapter Outline

## 14.1 Pumped versus static fuel molten salt reactor

Molten salt-fueled nuclear reactors were first conceived of in the United States in the aftermath of the Manhattan project as part of a program to develop a nuclear-powered strategic bomber. The first design concept considered was a simple one. Instead of putting solid uranium metal or oxide fuel into metal tubes to form fuel pins, as in conventional reactors, the project team proposed putting molten salt fuel into the tubes (Briant, 1950).

This concept survived less than a year. It was known that molten salts had low thermal conductivity and simple calculations showed that conduction alone could only transfer sufficient heat out of the molten salt fuel if the tube diameters were kept below 2 mm. This was seen as quite impractical, leading to the concept being abandoned.

Although it was well known, even in 1950, that conduction was far less important to heat transfer in fluids than convection, the impact of convective heat flow

**Molten Salt Reactors and Thorium Energy. DOI: http://dx.doi.org/10.1016/B978-0-08-101126-3.00014-2**

on heat transfer out of the molten fuel was never considered. Two factors were probably behind this omission.

Firstly, the techniques of computational fluid dynamics had not been invented. That happened in the 1970s. There was no way short of building physical models to work out how much of an impact convective heat transfer might have. Secondly, and perhaps decisively, the project was aimed at producing an aircraft engine which would inevitably be subject to strongly varying "g" forces which would make convection very unreliable.

The project team accordingly adopted a different strategy whereby the molten fuel salt was rapidly pumped around a circuit between a reaction chamber, where it achieved criticality, and a heat exchanger where the heat produced was removed. The rapid flow of the fuel salt resulted in turbulent mixing which provided effective heat transfer independent of gravity and convection. This design was the basis for both the Aircraft Reactor Experiment and Molten Salt Reactor Experiment (MSRE), which were both successfully operated, as described in Chapters 1, Introduction and 11, Liquid fuel, thermal neutron spectrum reactors.

That same design principle has been embedded in every conceptual design for molten salt reactors devised in the last half century. The original decision to ignore convection as a heat transfer mechanism, which was entirely valid for an aircraft engine, was never reconsidered in the context of ground-based nuclear reactors, where convection would be a highly reliable process.

In 2013 we re-examined the contribution of convective heat transfer in molten salt nuclear fuel using computational fluid dynamics codes and established that fuel rods containing molten salt fuel could operate at similar power densities as conventional solid fuel rods. This chapter summarizes those findings and explores the potential that the discovery unlocks for new, much simpler, safer, and cheaper molten salt-fueled reactors.

## 14.2 Potential advantages of static fueled reactors

"Conventional" pumped fuel salt reactors require relatively complex engineering which can be eliminated in static fueled reactors. This is summarized below.

### *14.2.1 Pumps and valves*

Pumps and valves capable of handling hot molten salts are practical, though challenging from a materials point of view. The major challenge for pumps however is reliability and maintenance. The fuel salt passing through the pump is extremely radioactive. The decay heat level is about 7% of the full power level so for a reactor operating at a typical power level of 200 kW/L of fuel salt, there is about 14 kW of decay heat per liter, of which a substantial fraction is in the form of gamma radiation. No human entry into the reactor area containing the pipework carrying the fuel salt will be possible. The fuel salt is also a relatively intense neutron emitter. Approximately 0.4% of neutrons produced during fission are "delayed" and a significant portion of those neutrons will be emitted in the piping system outside the reactor core and will activate the metals forming that pipework. Therefore, even if residual fuel salt is flushed from the pipework with "clean" molten salt, human handling of the pipework will probably not be permitted—and an entire extra plumbing and clean up system for the "clean" salt would be required.

The upshot is that regulators would be likely to require an entirely remotely operated system to remove and replace any component of the fuel salt circuit. That system itself would be required to have an extremely high level of reliability since it would not be possible to carry out maintenance on those parts of the system within the reactor radiation field.

Static fuel salt systems entirely eliminate these challenges as set out in detail below.

### 14.2.2 Fuel salt leaks

Regulators would assume that any fluid circulation system could at some point leak. Leakage of fuel salt would be an extremely hazardous event due to its very high radioactivity. The oft-repeated claim that leaks would simple freeze does not stand up to even a cursory examination. A fluid generating heat at about 14 kW per liter will not freeze. Even after 24 hours the decay heat will still be 1 kW per liter. There is instead a high probability that leaked fuel salt forming a layer more than about 1 mm thick on concrete would actually evaporate, spreading the radioactive products to condense on every surface they reach.

Accordingly, designers would need to provide a data-supported safety case showing that the frequency of leaks over the entire life of the reactor would be essentially zero. Producing data to support such a safety case would be challenging, given the lack of experience in pumped molten salt systems.

Static fuel systems are inherently much less prone to leaks since the fuel salt is held under no pressure in simple tubes. In the extremely unlikely event of a leak, the leaked fuel salt would mix with the coolant salt outside the tube, contaminating it but safely containing and diluting the leaked fuel salt while retaining it within the reactor vessel.

### 14.2.3 Heat exchangers

High-efficiency heat exchangers are essential in pumped molten salt reactors to minimize the fuel salt volume outside the core and hence the delayed neutron fraction lost to the core. That requires thin-walled heat exchangers and the materials challenges of achieving such thin walls are considerable, given the known corrosion potential of molten salts. Heat exchanger failure could result in serious contamination of the secondary coolant circuit and systems to prevent this would be required. The heat exchangers would become radioactive due to contamination by the fuel salt and due to neutron activation of their structural materials. Replacement or maintenance of the heat exchangers would be subject to the same challenges as for the pumps and valves.

The primary heat exchanger in a static fueled system is the fuel tube. It experiences low flow rates on both sides and no pressure differences. Tube walls do not have to be extremely thin since heat transfer is not limited by heat conduction through the wall (see Section 14.3). Most importantly, the fuel tubes are consumable items in such a reactor and therefore do not have to be certified for lifetimes in excess of the refueling frequency.

### 14.2.4 Drain systems

Pumped fuel salt reactors have, at any one time, about half of their fuel in the core. With a heat production in the core of about 200 kW/L of fuel the rate of fuel circulation to the heat exchangers has to be very rapid. The EVOL reactor, for example, circulates its entire 18 $m^3$ fuel volume every 4 seconds (Heuer et al., 2014). In the event of pump failure, the core is rapidly rendered subcritical either by control rods or by thermal expansion of the fuel salt. Decay heat is still being produced however at an initial rate of 7% which corresponds to a temperature rise of about 12°C per second. Very rapid and completely reliable systems to drain the fuel salt into a configuration where it is both subcritical and effectively cooled are therefore essential.

It is commonly said that passive "freeze valves" permit this but a robust case to prove the speed and reliability of any such system would be required—the 10–30 minute thaw time achieved for freeze valves in the MSRE (Briggs, 1965) would be unlikely to be adequate for a full-scale reactor. Failure of the drain system would be a major incident, resulting in rapid overheating of the fuel salt to the point where its containment would fail. Systems to ensure safe drainage of fuel salt released from any point in the fuel salt circuit into a cooled passively safe and subcritical location would be essential.

The system furthermore must allow the drained fuel salt to be pumped back into the reactor, a further level of plumbing complexity.

In a static fuel salt system, no drain system is required. Fuel salt in the fuel tubes is continuously cooled by the reactor coolant which can continue circulating by natural convection in the event of pump failure and reactor Safety Control Rods Activation Method (SCRAM).

### 14.2.5 Noble metal filtration system

A substantial fraction of fission products are noble or seminoble metals which are insoluble in the salt. These metals precipitate on surfaces with which they are in contact. In a pumped system it is essential that such metals are removed before they can deposit in vulnerable locations within the fuel circuit—pumps, valves, and narrow channels in heat exchangers would be particularly dangerous places for the metals to accumulate.

Two systems have been proposed to do this in conventional pumped molten salt reactors.

First is sparging of the fuel salt with helium which causes much of the noble metals to accumulate at the surfaces as foams. These foams then have to be removed, separated into solid, liquid, and gas components and the gas and solid components removed from the reactor for disposal while the liquid is returned to the reactor.

Second is continuous filtration of the fuel salt through metal filters where the noble metals deposit. The highly radioactive filters must be replaced periodically, using remote operation as their location will not be accessible to humans.

In a static fuel salt system, the noble metals can be simply allowed to deposit on the inner walls of the tubes where they will cause no problems.

### 14.2.6 Gas handling system

Fission produces relatively large amounts of radioactive gases, primarily the noble gases xenon and krypton but also volatile zirconium salts and iodine compounds. These gases must be removed from the fuel as it circulates. Many reactor designs remove the gases by sparging the fuel with a continuous stream of helium. This is highly effective at removing volatile species but requires both a system to defoam the resulting gas stream and a system to manage the radioactive gas stream and radioactive solids stream. In the MSRE a large fraction of the very hazardous fission product iodine was never accounted for and may have been vented with the off-gas stream (Compere et al., 1975).

Static fueled reactors can simply permit fission gases to vent from the fuel tubes into the coolant salt. If the fuel salt chemistry and redox state is properly controlled, these vented gases are radiologically benign and require no special collection or treatment (see Section 14.5).

### 14.2.7 Chemistry control and refueling

The chemical composition of fuel salt evolves during use. Production of gases and noble metals has been covered above. The other major changes are the production of neutron-absorbing fission products, the depletion of fissile isotopes. and the net release of halogen from fission of actinide halides. The first two result in reductions in core reactivity, the last results in extreme corrosion of metals.

Most molten salt reactor designs incorporate a relatively complex chemical engineering system to continually process the fuel, adjusting the redox potential, removing fission products, and adding additional fissile materials. None of these chemical engineering systems has been developed to the functioning prototype stage.

In a static fueled reactor such a processing system is impractical, but the challenges of the evolution of the fuel must still be met. This is achieved as follows.

Loss of reactivity is countered exactly as in conventional solid-fueled reactors by replacement of spent fuel assemblies with fresh ones.

Net halogen release is countered by including a sacrificial metal inside the fuel tube which scavenges any excess halogen and maintains the fuel salt in a strongly reducing state. Details of this are given in Section 14.4.

### 14.2.8 Summary

It is clear from the analyses above that static fueled molten salt reactors have the potential to be intrinsically safer, simpler, and therefore cheaper and easier to achieve regulatory approval than pumped fuel salt systems.

The remainder of this chapter analyses whether these theoretical advantages are in fact achievable and then suggests reactor designs leveraging these advantages. We start with the fundamental question of whether effective heat transfer from static fuel in tubes does in fact take place.

## 14.3 Convective heat transfer in molten fuel salt

The majority of molten salt reactor designs use salt mixtures based on LiF in order to achieve low melting points. This carries a substantial penalty. Lithium has to be isotopically purified to be substantially free of the $^6$Li isotope because that isotope has a very high neutron capture cross-section and will poison the reactor. There is no commercial source of pure $^7$Li and the process used in the United States to separate lithium isotopes for the H bomb project left the site so badly contaminated with 100–200 tonnes of mercury that it is today a "superfund" site.

Even more critical is that, even after isotopic purification, lithium salts generate substantial tritium on neutron irradiation. Tritium in molten salts readily diffuses through metals (Mays et al., 1977) making an effective tritium removal system essential in any reactor utilizing lithium salts. This adds cost and complexity and creates a volatile radiological hazard in the reactor complex.

Accordingly, the fuel salt selected for computation fluid dynamics calculations was a chloride salt mixture of 40% $UCl_3$/60% NaCl. The physical properties of this fuel salt mixture are given in Table 14.1, which also summarizes the other system properties. The vertical variation in heat production in the tube was derived from MonteCarl N Particle (MCNP) calculations on a model reactor core comprising an

**Table 14.1 Parameters used in CFD analysis of fuel tube heat transfer**

| | |
|---|---|
| Fuel salt composition | 60 mol% NaCl, 20 mol% $PuCl_3$, 20 mol% $UCl_3$ |
| Coolant salt composition | 42 mol% $ZrF_4$, 10 mol% NaF, 48 mol% KF |
| Fuel salt melting point/boiling point | 730 K/1837 K |
| Coolant salt melting point | 658 K |
| Fuel salt density | $4.1690-9.014\times10^{-4}\times T$ (temp in K) kg/L |
| Coolant salt density | 2.77 kg/L |
| Fuel salt viscosity | $\text{Log}_{10}$ viscosity (cP) $= -1.2675 + 1704/T$ |
| Coolant salt viscosity | $0.17\times10^{-6}$ m$^2$/s |
| Thermal conductivity fuel salt | 0.5 W/m/K |
| Thermal conductivity coolant salt | 0.7 W/m/K |
| Specific heat capacity fuel salt | 510–700 J/kg/K over temperature range 500–1500°C |
| Specific heat capacity coolant salt | 1050 J/kg/K |
| Coolant flow velocity | 4 m/s |
| Tube material | Molybdenum 0.5 mm thickness |

array of fuel tubes, which was carried out by Olga Negri under the guidance of Prof. Tim Abram, both of Manchester University (UK).

The analysis was undertaken using ANSYS CFD tools (V15.0): Design Modeler for geometry preparation; ANSYS Meshing; and ANSYS Fluent for preprocessing and solving. Some quantitative results were obtained directly from Fluent; others from expressions calculated in ANSYS CFD-Post (the postprocessing tool), which was also employed to generate all contour and streamline plots. This work was carried out by Simon Leefe and Peter Jackson-Laver of Wilde Analysis Ltd, a professional Computational Fluid Dynamics (CFD) consultancy.

Fig. 14.1 shows the relationship between the maximum temperature reached in the hottest part of the fuel salt at different average power levels and with different diameters of fuel tube. Fig. 14.2 shows the relationship between maximum fuel salt temperature, maximum fuel tube wall temperature, and maximum coolant salt temperature for 10 mm diameter tubes at varying power levels.

Two key conclusions can be drawn from these simulations.

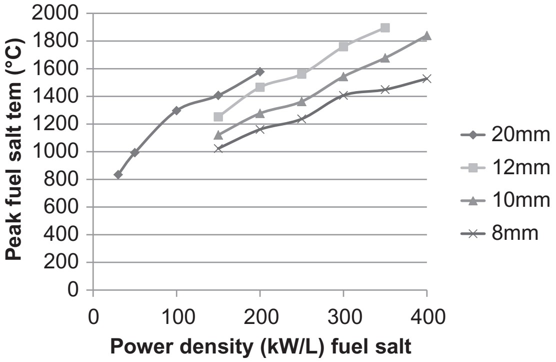

**Figure 14.1** Peak fuel salt temperature in tubes of different diameters.

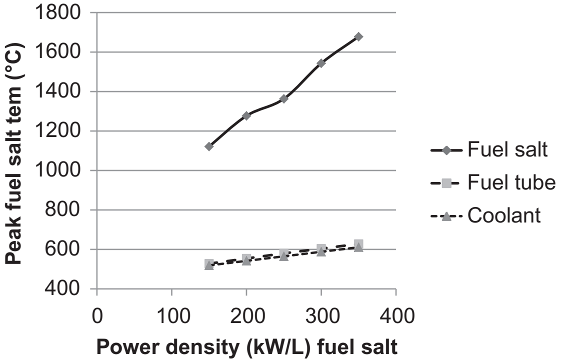

**Figure 14.2** Relationship of peak fuel salt, fuel tube and coolant temperatures.

Firstly, that it is possible to achieve power densities over 200 kW/L, higher than those in a Pressurized Water Reactor (PWR) core ($\sim$100 kW/L) while keeping the fuel salt comfortably below its boiling point.

Secondly, that even with peak fuel salt temperatures approaching boiling point, the fuel tube wall experiences temperatures only marginally higher than those of the coolant salt. The reason for this is that the heat transfer process from the fuel salt to the tube wall is many times less effective than that from the fuel tube wall to the more rapidly moving coolant salt. This latter finding has a substantial impact on the range of materials that can be considered for the fuel tubes, as is considered in the next section.

## 14.4 Fuel tube materials

Conventional wisdom in molten salt reactor designs is that special, corrosion-resistant, alloys such as Hastelloy N are required to contain the fuel salt. In the static fuel salt system this challenge had the potential to be compounded by the high peak temperatures in the fuel salt, which are higher than temperatures generally considered for molten salt reactors.

As set out in the previous section, the high peak temperature of the fuel salt is no more relevant than is the high temperature at the center of conventional solid uranium oxide fuel pellets. That high temperature does not lead to high temperatures for the tube containing the fuel. Accordingly, from a temperature perspective it is not necessary to use refractory materials such as molybdenum or ceramics for the tubes. Standard steels would be quite adequate.

Corrosion of the tube material by the molten fuel salt is a more difficult challenge. Experience from the MSRE showed that the major corrosion mechanism was leaching of chromium from the alloy (Williams et al., 2006). Hastelloy N, a relatively low-chromium alloy, was developed to minimize this effect—though corrosion still occurred leading to questions over long-term use.

Corrosion by molten salt fuel is driven by a number of factors. Probably the most critical is that the mechanism by which metals typically become resistant to corrosion (formation of passivating oxide or other layers) does not operate in molten salts because they effectively dissolve such layers. Corrosion is thus essentially thermodynamically driven. If the thermodynamics of the system permit a component of the alloy to dissolve in the molten salt then it will do so. Corrosion rates then become controlled by how fast the susceptible metal can migrate to the exposed surface of the alloy. Formation of cracks and pits greatly facilitates this process with particularly rapid corrosion occurring at alloy grain boundaries.

There are multiple potential sources of corrosion in the molten salt:

- The intrinsic corrosion due to the pure salt;
- Additional complexity due to fission products, especially tellurium, which will react with metals in the alloy causing embrittlement;
- Net release of halogen from the actinide halide salt due to fission products having a lower average valency than the actinide;

- Contamination of the fuel salt with oxygen from oxides or traces of air or water;
- For chloride fuel salt, formation of sulfur as a chlorine neutron activation product.

Fortunately, all of these factors can be simultaneously analyzed using modern thermodynamic software which, via Gibbs free energy minimization, calculates the equilibrium composition of any mixture of elements or compounds. Outotek HSC Chemistry v7 was used in the current studies. Such thermodynamic analysis provides a "worst-case" corrosion picture representing the state when sufficient time has elapsed for the system to reach equilibrium. A result showing that corrosion can happen thermodynamically does not necessarily mean that corrosion will actually happen fast enough to be a problem. However, a result showing that corrosion cannot happen thermodynamically can be relied on.

Fig. 14.3 shows the thermodynamic equilibrium level of $CrCl_2$ in a simulated fuel salt consisting of 60 mol% NaCl and 40 mol% $UCl_3$ in which 5 mol% of the uranium has fissioned releasing 10 mol% fission products and 15 mol% chlorine. This salt is in contact with a metal phase containing elements (treated as an ideal solid solution) in the proportions of Hastelloy N or stainless steel Nimonic PE16, which is a widely used structural steel in nuclear reactor cores. PE16 has an exceptionally low swelling behavior in high neutron fluxes, which makes it ideal for use in the fuel tube (Special Metals, 2004).

There is clearly potential for substantial dissolution of chromium, even from Hastelloy N. This is primarily a consequence of the net release of chlorine during fission which renders the fuel salt strongly oxidizing. In conventional, pumped, molten salt reactors there has to be provision for continuous online monitoring of the redox state of the fuel salt with frequent chemical adjustments to maintain a constant redox state. That is clearly not possible with the thousands of fuel tubes that would be in a full-scale static molten salt reactor.

Fig. 14.3 also shows, however, the equilibrium level of $CrCl_2$ in a Hastelloy N or stainless steel fuel tube that contains a source of zirconium metal, as a coating on the inside or as an inserted component. The presence of the zirconium drives the redox potential to a strongly reducing state and reduces the chromium dissolution from both alloys to less than 10 ppb—a level at which corrosion would be

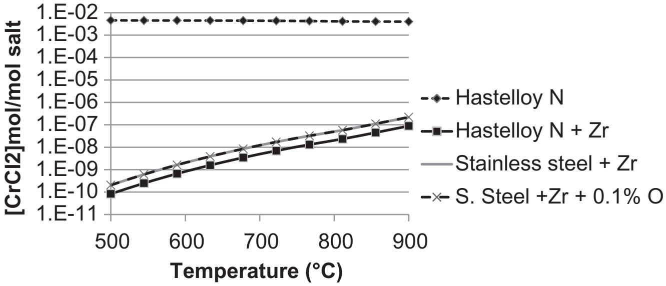

**Figure 14.3** Corrosion potential for fuel salt in contact with Nimonic PE16.

undetectable. Addition of 0.1% oxygen to this system makes no difference whatsoever to the concentration of $CrCl_2$—the oxygen is quantitatively converted to $ZrO_2$.

Thus an entirely passive redox control system is easily incorporated into the fuel tube. Note that a continuous film of zirconium is not required. This is not zirconium shielding the surface from attack, it is zirconium controlling the fuel salt chemical state.

The sacrificial zirconium has other significant benefits. Fig. 14.4 shows the fate of tellurium fission product and sulfur from neutron activation of $^{35}Cl$ in the presence of zirconium. Tellurium is quantitatively trapped as zirconium telluride. Thus tellurium embrittlement of the steel alloys is prevented. Sulfur reacts primarily with actinide and lanthanides forming sulfides. Notably, reaction of sulfur with the metals of the alloy tubes is essentially prevented, avoiding the danger of sulfur-driven corrosion of the tubes.

Control of fuel salt redox state by use of sacrificial reactive metals is by no means a new idea. In common life, galvanizing steel with zinc is a similar process. Protecting alloys from corrosion by contacting Lithium Beryllium Fluoride salt (FLIBE) salt with beryllium metal was tested successfully in the MSRE (Keiser, 1977).

Use of this very simple technique in conventional pumped, fluoride-based molten salt reactors is however probably not practical. Similar thermodynamic calculations have been carried out for such fuel salts. Graphite has a strong potential to react to form zirconium carbide, while uranium fluorides are reduced to uranium metal. Even if a different, less reducing, sacrificial metal was used to avoid this problem, migration of the sacrificial metal from hot to cool regions of the pumped circuit, or, worse, galvanic transfer of the sacrificial metal, would risk fouling pumps, valves, and narrow passages in heat exchangers. It must be emphasized that a thermodynamic driver for a reaction taking place does not prove that it will happen rapidly enough to be a problem—however substantial experimental data under

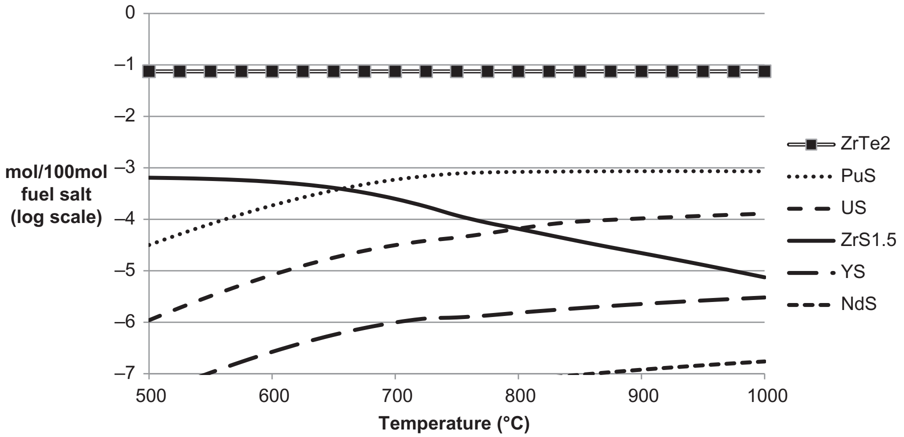

**Figure 14.4** Scavenging of tellurium and sulphur by sacrificial zirconium.

the precise conditions of the reactor would be required to prove that kinetic stabilization effects were sufficient to prevent the reaction. Producing these data would be arduous and costly, especially since it is predicted theoretically and demonstrated practically that ionizing radiation affects the reaction rates. Where the reaction can be shown to be thermodynamically nonfavored, then concerns over corrosion or other reactions are easily allayed.

The use of static molten salt fuel, in conjunction with sacrificial metals, thus eliminates the need for active management of fuel salt chemistry, which is essential in pumped molten salt reactors and which adds significant complexity to their design, regulatory approval, and operation. It also permits the use of standard stainless steels such as PE16 with their extensive databases of function under reactor conditions, thereby avoiding the need for complex, expensive, and time-consuming nuclear certification for alloys which are not currently used in nuclear applications (which include Hastelloy N).

Fuel salt is, of course, not the only molten salt for which resistant materials are required. The coolant salt also contacts the outer surfaces of the fuel tubes as well as many other reactor components. Permanently contacting the coolant salt with a sacrificial metal would have similarly beneficial corrosion benefits as for the fuel salt. However, migration and deposition of the sacrificial metal would be a significant problem and would be expected to lead to deposition on the coolest surfaces which would be in the heat exchanger. While that problem is probably not insuperable and ideas to overcome it are proposed for the Fluoride-salt-cooled High-temperature Reactor (FHR) concept, (Andreades et al., 2014), use of a $ZrF_4$-based coolant allows it to be side-stepped.

Zirconium forms two principal stable fluorides, difluoride and tetrafluoride. Addition of small amounts of $ZrF_2$ to the salt reduces its corrosion potential dramatically, as shown in Fig. 14.5, which shows the equilibrium chromium fluoride concentration for pure coolant salt (42% $ZrF_4$/10% NaF/48% KF), the same salt contaminated with 0.1% oxygen and the contaminated salt containing 2% $ZrF_2$. Dissolved chromium concentration of less than 1 ppm guarantees virtually undetectable corrosion. This would allow standard stainless steels to be used throughout the reactor vessel.

## 14.5 Fission products and gases

Perhaps the defining advantage of molten salt fuel over solid fuels is the form that fission products take. Fission products are inevitable products in nuclear reactors but the chemical form they take matters a great deal to the risks associated with such reactors. This was dramatically shown at Chernobyl where a large fraction of the core iodine, cesium, and tellurium was released, largely in airborne form, which spread for thousands of miles, while a far smaller fraction of other nonvolatile fission products and actinides were released mostly as larger particles concentrated around the reactor area (NEA Committee in Radiation Protection and Health, 1995).

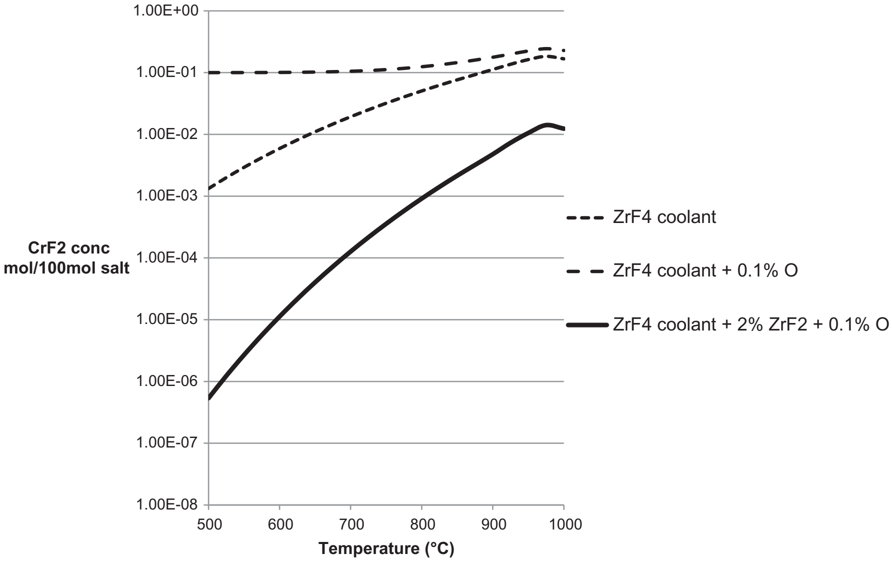

**Figure 14.5** Stabilisation of coolant salt with the ZrF2/ZrF4 redox buffer.

In any molten salt fuel, cesium is present not as the element (as it predominantly is in solid fuels) but as cesium chloride or fluoride. Cesium metal has a boiling point of just 670°C and is highly reactive with air, forming oxide fumes. Cesium halides are chemically stable and have boiling points above 1250°C and are diluted in the bulk molten salt where their vapor pressure is greatly reduced until temperatures are even higher than this. From the perspective of cesium, any molten salt fuel is thus far safer than a solid fuel under core damage conditions.

The form of iodine and tellurium in molten salt reactors can be less favorable. While sodium iodide has a high boiling point, like the cesium salts, iodine can form volatile species in molten salts of which the most important are the tellurium iodides. Molten salt reactors where the fuel salt is constantly sparged with helium pass much of the iodine and tellurium out in the waste helium stream where it must be trapped and disposed of. This creates a hazard during normal operation greater than the hazard in sealed solid fuel rods, though in an accident scenario the fact that much of the iodine and tellurium have been removed from the reactor core could be an advantage.

In static molten salt fuel tubes there are three options for managing gaseous fission products. Sparging each tube with helium is not practical, therefore the noble gas fission products will simply bubble out of the fuel salt when they reach saturating concentrations, which takes about 20 minutes at typical fission rates. This gas stream could be:

- Allowed to accumulate in the sealed tube, though high pressures would then be created, increasing the risk of tube rupture and fuel salt leakage;
- Vented through a tubing system to a central collection and treatment facility, though such a system would be complex and cumbersome;

- Allowed to vent from the fuel tube directly into the coolant salt and hence to the gas space in the reactor.

The last option has major attractions in terms of simplicity. It is not an original idea for nuclear fuel rods, fuel rods used in the early days of the Dounreay Experimental Fast Reactor used such vented tubes (Keilholst and Battle, 1969) but the solid fuel pellets released volatile cesium and iodine into the coolant (molten sodium) creating a safety and disposal hazard.

To establish whether such a vented tube system would be safe and practical in static molten salt-fueled reactors, thermodynamic equilibrium calculations were carried out on a model partly burned molten salt fuel similar to that described in Section 14.3, with a focus on the composition of the gas phase present in the system. An illustration of the fuel tube and gas venting apparatus is shown in Fig. 14.6. The top of the tube is closed with a "diving bell" assembly which allows gas to escape but prevents coolant entering the fuel tube. There is a gas space in the

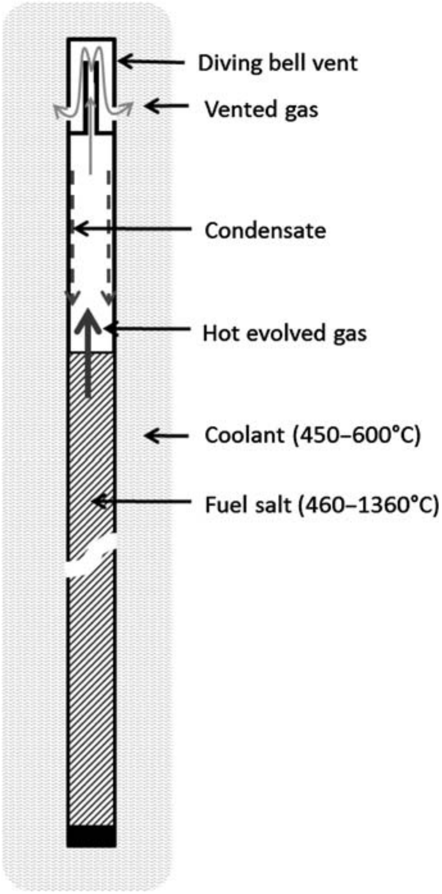

**Figure 14.6** Vented molten salt fuel tube.

tube above the hot fuel salt where the tube walls are cooled to the temperature of the coolant, about 600°C. Calculating the gas phase composition is therefore a two-stage process.

First the composition of the gas actually released from the hot fuel salt is calculated. This gas rises in the form of bubbles formed in the fuel salt, primarily from the noble gases, xenon and krypton. The temperature selected to define the composition of this gas was 1020°C. This is a pessimistic (high) temperature estimate since the noble gases have lower solubility at lower temperatures in molten salts (Grimes and McDuffie, 1960) and will therefore form bubbles in the cooler regions of the fuel salt. The high temperature and the assumption that the volatile fission products in the molten salt fully equilibrate with the gas bubbles both represent very conservative assumptions that will overestimate the amount of volatile fission products in the gas.

The second stage is to allow this hot gas to condense on the cooler walls of the fuel tube. The mean residence time of the gas in this space is many days (see below) so full equilibration of the gas with the cooler tube wall is expected. This final gas phase is what is vented from the "diving bell" gas venting system.

Fig. 14.7 shows the composition of the gas evolved from the fuel salt and its composition after condensing at 600°C. The fuel salt was in contact with sacrificial zirconium in this simulation. Without the sacrificial zirconium there were high levels of tellurium iodide and uranium tetrachloride in the gas phase, showing that the sacrificial zirconium has very positive effects on the vapor produced from the fuel salt in addition to its other benefits.

The gas stream from the fuel salt thus contains principally the noble gases with substantial amounts of $ZrCl_4$ and only traces of other compounds. Of particular importance is the very low level of iodine compounds, representing just 0.001% of the total produced.

The substantial amounts of $ZrCl_4$ in the gas stream will contain radioactive isotopes of zirconium since, although much of the zirconium comes from the

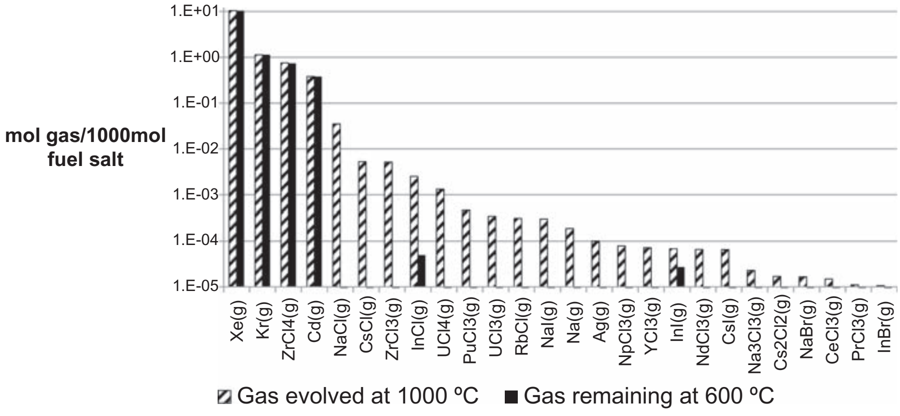

**Figure 14.7** Gas evolved from vented fuel tubes.

sacrificial metal, some is formed as fission products. The preferred molten coolant salt contains $ZrF_4$ and KF (see below) which undergo neutron activation while passing through the reactor core. The $ZrCl_4$ will readily dissolve in this coolant and the additional radioactivity created in the coolant salt makes minimal difference to the safety or disposal route for used coolant salt, given that it already contains radioactive zirconium and chlorine (from activation of K) isotopes.

This leaves just the fate of the xenon and krypton to be considered. Both contain radioactive isotopes and will not dissolve significantly in the coolant salt, instead accumulating in the gas space within the reactor. Noble gases have rather low radiological hazard levels since they readily disperse and are rapidly eliminated from the human body even if inhaled. Indeed, $^{85}$Kr, which is the main radioactive gas remaining in spent conventional nuclear fuel, is routinely discharged to the atmosphere during fuel reprocessing operations. However, xenon isotopes can decay to far more hazardous cesium isotopes and it is therefore a legitimate concern that such cesium isotopes should not escape from the fuel tube indirectly via the xenon precursor.

The fuel tube (see Fig. 14.6) can be considered to contain three separate reservoirs of gas—that dissolved in the fuel salt, that in the gas space above the fuel salt, and that in the diving bell apparatus. Flow between these reservoirs is essentially unidirectional, even allowing for diffusion in gases, due to the very small surface area of the fuel salt in contact with the first gas space and the narrow long tube separating the first gas space from the diving bell gas space. These gas spaces can individually be considered to be well mixed since the mean time spent by gas in each space before passing on is relatively long.

Flow of radioactive xenon and krypton through this series of gas spaces can therefore be calculated based on the gas flow rate, the volume of the three gas spaces, and the half-life of the isotope. The results are shown in Table 14.2. Significant amounts of $^{133}$Xe, decaying to nonradioactive $^{133}$Cs, just 0.2% of $^{135}$Xe, decaying to the very mildly radioactive $^{135}$Cs, and virtually none of the $^{137}$Xe decaying to the dangerous isotope $^{137}$Cs are released from the fuel tube. The only significant volatile hazard associated with the gases is therefore that of the noble gases themselves. It is likely that it will be acceptable to allow those gasses to be accumulated and decay within the reactor containment.

**Table 14.2** **Release of radioactive Xenon isotopes from vented fuel tubes**

| Xe isotope | Isotope half-life (h) | % emerging from fuel salt | % emerging from main tube | % emerging from diving bell | Overall % released |
|---|---|---|---|---|---|
| 133 | 125.94 | 99.55193 | 39.42738 | 72.25031 | 28.3588 |
| 135 | 9.14 | 93.41306 | 4.682505 | 16.423 | 0.7184 |
| 137 | 0.063333 | 8.948511 | 0.033793 | 0.135036 | 4.08E-06 |
| 138 | 0.233333 | 26.58122 | 0.124362 | 0.495598 | 1.64E-04 |

## 14.6 Static molten salt-fueled reactor options

Many reactor designs can be created utilizing the concept of static molten salt fuel. Simple core designs with fuel tube assemblies immersed in coolant salt provide a fast-spectrum reactor. Incorporation of moderating materials such as graphite or zirconium hydride into the fuel assemblies or into the reactor core would allow thermal or epithermal reactors to be designed. Use of a coolant salt based on thorium salts would allow efficient breeding of fissile material from fast or thermal versions of the reactor.

Small modular versions of the reactor are also feasible, with the possibility of entirely eliminating moving parts from the reactor tank by using a tall geometry allowing natural convection of the coolant salt and/or achieving entirely passive decay heat removal by natural air convection, greatly facilitated by the high operating temperatures of molten salt reactors.

Operation at lower power densities ($\sim 150$ kW/L) where the average fuel salt temperature during operation is within the acceptable range of coolant salt temperatures ($<850°C$) would allow control of reactivity of the core to be achieved merely by the temperature of the coolant with maximum coolant design temperature corresponding to a core being safely subcritical. That would permit passive load following operation of a small modular reactor without any active intervention with reactivity control devices.

The ability of such a reactor core to tolerate substantial power density differences across the core would also open up the possibility of a long-life reactor core requiring no refueling and relying solely on the consumption of burnable poisons to maintain its reactivity as fuel was consumed.

Static molten salt-fueled reactors should therefore be seen as an entirely new class of reactors. All of the reactor types described in Chapters 11, Liquid fuel, thermal neutron spectrum reactors and 12, Fast spectrum, liquid fueled reactors have equivalents based on static fuel salt, as indeed do most reactors designed for solid fuels. The family of static salt-fueled reactors currently under development by Moltex Energy have been named the Stable Salt Reactors, with the term “stable” reflecting both the stability of the reactor core and the stability of the nonvolatile fission products.

Fast spectrum, thermal spectrum and thorium breeding Stable Salt Reactors are now under development but the most advanced of these designs is a fast-spectrum plutonium/higher actinide burning reactor, the Stable Salt Fast Reactor, which is described in greater detail in Chapter 21, Stable salt fast reactor. This utilizes a chloride-based fuel salt and a zirconium fluoride-based coolant salt and is the basis for much of the quantitative analysis in this chapter.

Thermal spectrum versions of the Stable Salt Reactor do however bring their own unique set of challenges which are summarized in the following section.

## 14.7 Thermal spectrum static molten salt reactors

Thermal neutron spectrum reactors could in principle use a similar fuel and coolant salt system as that for the fast reactor. However, to avoid neutron poisoning by chlorine-35 the chloride salts would have to be produced using isotopically purified chlorine-37, which is not currently commercially available. The alternative is to use fluoride salt fuel as well as coolant.

Use of fluoride salts instead of chloride salts as fuel brings two challenges.

First is their higher melting point. Eutectic mixtures of $UF_3$/$UF_4$/NaF have melting points in the range 623−660°C depending on the redox state of the uranium fluoride. This would require a coolant with a minimum temperature of about 620°C, which is comfortably within the range for $ZrF_4$/NaF mixtures. Core output temperatures of 700−750°C would then be required, which is just within the long-term operating temperatures of stainless steels. Temperatures could, however, be reduced by addition of RbF to the fuel salt which forms eutectics in the region of 535°C, providing a substantial temperature margin.

The second challenge relates to the thermodynamic instability of $UF_3$, which undergoes disproportionation to uranium metal at higher temperatures. Pure $UF_3$ cannot therefore be used as fuel and a redox state maintaining the $UF_3$/$UF_4$ ratio in the salt at less than 1:1 is essential to avoid this. That makes use of sacrificial zirconium metal not possible and a less reactive sacrificial metal must be used. Chromium is in many ways the optimum choice, at equilibrium it maintains a $UF_3$ fraction below 0.25 as net fluorine release during fission takes place.

Sacrificial chromium is, inevitably, less effective at preventing alloyed chromium leaching from the structural metal than is zirconium. The thermodynamics can nonetheless be made unfavorable for corrosion by two approaches. First is use of pure chromium as sacrificial metal. Chromium in this state has a thermodynamic activity roughly four times greater than alloyed chromium and will therefore be preferentially attacked. Second is to place the sacrificial chromium as an insert in the fuel tube rather than as a coating on the tube. Because temperatures in the fuel salt are very much higher than the tube wall temperatures (see Fig. 14.2), the sacrificial chromium will be at a much higher temperature than the wall and will accordingly be substantially more reactive.

The consequence of these two factors is that there will be a net transfer of chromium from the sacrificial chromium to all areas of the inner wall of the fuel tube, thus effectively preventing corrosion.

There are also unique challenges for the coolant salt from operating in a thermal spectrum. In the fast-spectrum reactor, the coolant salt contains $ZrF_4$ from which hafnium has not been removed. This has only a marginal effect on the core reactivity but makes the coolant a highly effective neutron shield. This allows a small reactor size without exposing critical components, such as heat exchangers and the tank wall, to high neutron flux.

In order to avoid using very large coolant pools (as are used for sodium-cooled reactors) the coolant must be made neutron-absorbing. This can be achieved by allowing tightly controlled levels of hafnium to remain in the zirconium salt. Alternatively, the coolant can be based on $ThF_4$ which provides both an excellent neutron shield and a uranium-233 breeding blanket—though at the expense of contaminating the coolant salt with low levels of fission products produced by relatively rare fast-neutron fissions of the thorium.

## 14.8 Fuel cycle for stable salt reactors

General discussions of the fuel cycles for molten salt reactors are covered elsewhere in this book. There are however certain specific and very positive aspects of the fuel cycle as required for Stable Salt Reactors and related static fueled reactor concepts.

The key to these positive aspects is that static molten salt fuel can tolerate quite high concentrations of contaminating materials, in particular the lanthanides. This is due to the similarity of melting point and hence miscibility of the lanthanide and actinide trihalides.

This fuel salt formulation flexibility would thus allow, for example, a fuel salt containing 60% NaCl and 40% of a mixture of $PuCl_3$, $UCl_3$, and mixed lanthanide trichlorides in the approximate ratio of 2:1:1. Pyroprocessing of spent nuclear fuel achieving such modest separations has already been demonstrated (Lee et al., 2011). It is indeed plausible that a separation of spent nuclear fuel achieving purities of that level with virtually complete retention of higher actinides, like americium and curium, in the fuel could be achieved. This would result in an actinide-free fission product waste stream, which would decay to a lower radioactivity than the original uranium ore after just 300 years.

The main barriers to use of reprocessed fuel on a large scale in the nuclear industry are the high costs of reprocessing to produce fuel of a purity compatible with the use in ceramic or metal fuel forms, the high cost of precision manufacture of solid fuels like Mixed Oxide fuel (MOX), and the reluctance to utilize a reprocessing method that inevitably produces weapons-usable fissile material at some point in the process. A simple pyro-processing system would avoid all three of those concerns and could therefore be at the heart of a massive expansion of nuclear energy use.

## 14.9 Global mix of static fueled molten salt reactors

The various Intergovernmental Panel on Climate Change (IPCC) reports strongly suggest that unless the world substantially decarbonizes its energy economy by mid-century there is real potential for very adverse climate consequences. China and India will represent the largest new carbon emitters. While Europe and to a lesser extent the United States can economically tolerate higher energy prices to achieve carbon reduction, poor nations would measure the consequence of higher energy prices in human lives. A technological breakthrough making nuclear energy cheaper than fossil fuels is the only realistic prospect of derailing the burgeoning fossil fuel burning bandwagon.

Many cost estimates for novel nuclear reactors exist in the literature, promising lower capital cost. They are of highly variable credibility and often ignore the unavoidable fact that engineering work in the nuclear industry inevitably costs more than in other industries. The Stable Salt Fast Reactor has been developed to a sufficiently detailed design stage that a credible, initial, rough order of magnitude cost estimate could be produced. This project was carried out independently of the reactor designers by a well-established nuclear engineering consultancy, Atkins Ltd. This estimate was for an “nth of a kind” reactor but was for a single 1 $GW_e$

power plant. No attempt was made to estimate the economies of scale available from an increase to 2–3 $GW_e$ which is the planned size for other UK power stations. Even at those large scales, overnight costs for those generation III reactors are stated as ~£5000 per $kW_e$.

The estimated "most likely" overnight capital cost for the nuclear island of a Stable Salt Reactor (comprising reactor building, emergency diesel generator buildings, control building, interim fuel storage building, and interim waste storage building) was £718 per $kW_e$. The costs are expressed in UK pounds because the cost basis was for UK construction—arguably the most expensive nuclear construction costs in the world. The conventional island cost was £696 per $kW_e$. Monte Carlo probability analysis indicated a 90% probability of the combined cost being less than £1756 per $kW_e$. While some other site-specific costs must be added to this figure for a full plant overnight capital cost, the Stable Salt Reactor is credibly substantially cheaper than conventional nuclear and has clear potential to be able to generate power more cheaply than coal since it has a similar capital cost and lower fuel cost.

This economic advantage could drive a massive increase in deployment of nuclear energy. Moving from a world where 10% of electricity comes from nuclear to one where most electricity is nuclear and nuclear is expanding in process heat applications carries significant challenges. Three factors in particular must be considered:

- Sustainability of the fuel supply;
- Increased weapons proliferation risk;
- Management of hazardous waste.

A family of two designs of static fueled molten salt reactors might provide a promising solution to these challenges. The first design is a global workhorse reactor which would be a thermal spectrum thorium breeder. This design is less advanced than the Stable Salt Fast Reactor, but the basic principles have been established. It is a high-temperature reactor (coolant output at 750°C), using as coolant a eutectic mixture of 78:22 $NaF/ThF_4$ melting at 618°C, though addition of RbF or KF to reduce the melting point may be desirable. Moderation is by steel-clad graphite constructed as the inner core of rectangular fuel assemblies.

The fuel salt is a mixture of $UF_3/UF_4/RbF/NaF$ with a melting point in the region of 600°C. It is maintained in a suitable redox state using sacrificial chromium metal inserts in each fuel tube.

$^{233}U$ is bred from thorium in the coolant salt which also acts as the breeding blanket. There is a layer of molten bismuth alloyed with depleted uranium and thorium in the bottom of the tank which removes bred uranium (and protactinium) from the coolant salt by reductive extraction, as demonstrated at Oak Ridge National Laboratory (Shaffer, 1971). The presence of depleted uranium in this layer ensures that isotopically pure $^{233}U$ is never produced. This eliminates a serious proliferation risk, since (contrary to many claims) $^{233}U$ is quite capable of being used for weapons purposes (Forsberg et al., 1998). The location of the bismuth layer, protected from the core neutron flux by the coolant layer, ensures that fission of the bred uranium and parasitic neutron capture by $^{233}Pa$ are avoided. The bismuth layer is periodically removed for processing and replaced with fresh alloy when the "enrichment" of the $^{233}U$ has reached the desired level of ~5%.

This reactor design produces a spent fuel stream containing plutonium and higher actinides, due to the presence of $^{238}$U in the fuel. This is where the second reactor is required. It is the Stable Salt Fast Reactor described in Chapter 21, Stable salt fast reactor, which will consume the plutonium and higher actinides, removing them as proliferation risks and reducing the hazardous life of the resulting waste from tens of thousands of years to mere hundreds of years. Perhaps one of these fast reactors would be required for every 10 thermal spectrum reactors.

Together these two static molten salt-fueled reactors can provide essentially unlimited power, at low cost, with minimum proliferation risk, and with actinide-free spent fuel waste.

## References

Andreades, C.H., et al., 2014. UCBTH-14-002 Technical Description of the Mark 1 Pebble Bed Fluoride Salt Cooled High Temperature Reactor Power Plant. US Department of Energy, Berkeley, CA.

Briant, R.C., 1950. ORNL 919 Aircraft Nuclear Propulsion Projecjt Quaterly Progress Report. Oak Ridge National Laboratory, Oak Ridge, TN.

Briggs, R.B., 1965. ORNL-3872 Molten Salt Reactor Program Semiannual Progress Report. Oak Ridge National Laboratoty, Oak Ridge, TN.

Compere, E.L., et al., 1975. ORNL 4865 Fission Product Behaviour in the Molten Salt Reactor Experiment. Oak Ridge National Laboratory, Oak Ridge, TN.

Forsberg, G., Hopper, C., Richter, J., Vaantine, H., 1998. ORNL/TM-13517 Definition of Weapons Usable Uranium-233. Oak Ridge National Laboratory, Oak Ridge, TN.

Grimes, W.R., McDuffie, H.F., 1960. ORNL 2931 Reactor Chemistry Division Annual Progress Report. Oak Ridge National Laboratory, Oak Ridge, TN.

Heuer, D., et al., 2014. Towards the thorium fuel cycle with molten salt fast reactors. Ann. Nucl. Energy 64, 421–429.

Keilholst, G.W., Battle, G.C., 1969. ORNL NSIC 37 Fission Product Release and Transport in Liquid Metal Fast Breeder Reactors. Oak Ridge National Laboratory, Oak Ridge, TN.

Keiser, J.R., 1977. ORNL/TM 5783 Compatibility Studies of Potential Molten Salt Breeder Reactor Materials in Molten Fluoride Salts. Oak Ridge National Laboratory, Oak Ridge, TN.

Lee, H., et al., 2011. Pyroprocessing technology developement at KAERI. Nucl. Eng. Technol. 43, 317–328.

Mays, G.T., Smith, A.N., Engel, J.R., 1977. ORNL/TM 5759 Distribution and Behaviour or Tritium in the Coolant Salt Technology Facility. Oak Ridge National Laboratory, Oak Ridge, TN.

NEA Committee on Radiation Protection and Health, 1995. Chernobyl Ten Years On. OECD Nuclear Energy Agency, Paris.

Shaffer, J.H., 1971. Method for separating uranium, protactinium and rare earth fission products from spent molten fluoride salt reactor fuel. USA, Patent No. 3577225.

Special Metals, 2004. Nimonoc Alloy PE16-Publication SMC-102. Special Metals Corporation, New Harford, NY.

Williams, D.F., Toth, L.M., Clarno, K.T., 2006. ORNL/TM 2006/12 Assessment of Candidate Molten Salt Coolants for the Advanced High Temperature Reactor. Oak Ridge National Laboratory, Oak Ridge, TN.

# Accelerator-driven systems

# 15

*Ritsuo Yoshioka*[1], *Kazuro Furukawa*[2], *Motoyasu Kinoshita*[3],
*Alexey M. Degtyarev*[4], *Andrey A. Myasnikov*[4], *Laszlo Sajo-Bohus*[5] *and*
*Eduardo D. Greaves*[5]
[1]International Thorium Molten-Salt Forum (ITMSF), Yokohama, Japan, [2]High Energy Accelerator Research Organization, ITMSF, Tsukuba, Japan, [3]The University of Tokyo, ITMSF, Tokyo, Japan, [4]NRC "Kurchatov Institute", Moscow, Russia, [5]Simón Bolívar University, Caracas, Venezuela

## Chapter Outline

## 15.1 Introduction to accelerator-driven systems (ADS)

Usually ADS (accelerator-driven systems or accelerator-driven subcritical reactors) are not categorized as a fission reactor, because ADS are operated under subcritical conditions, and a self-sustaining chain reaction does not occur in ADS. However, in order to deploy molten salt reactor (MSR) widely around the world, a large amount of fissile material is required, and ADS would be a solution to meet this requirement. Also, ADS are widely studied for various applications besides fissile production. Therefore, ADS are introduced briefly here.

ADS utilize a high-intensity proton accelerator with an energy of about 1 GeV, directed to a spallation target. Usually, this target is made of solid metals such as Pb/W/U/Th. The injected protons cause a spallation reaction, which emits a few tens of neutrons per incident proton to the surrounding blanket region. Then, these neutrons can be used for fissile production or minor actinide (MA) incineration. Since produced fissile materials cause fission reactions, the heat can be recovered to generate electricity. Fig. 15.1 shows a concept of ADS. In some cases, there may

**Molten Salt Reactors and Thorium Energy. DOI: http://dx.doi.org/10.1016/B978-0-08-101126-3.00015-4**

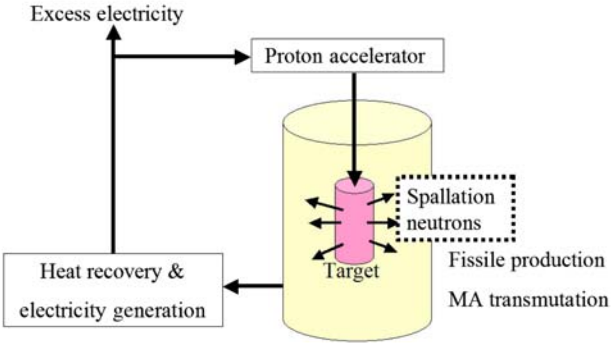

**Figure 15.1** Concept of accelerator-driven systems (ADS).

be excess electricity, but it depends on the design. Development activity in each country is described in IAEA (2015).

Its basic concept was originally proposed by a Canadian scientist, W. B., Lewis in 1952 (Lewis, 1952), and an integrated concept can be found in A. Harms' book in 1982 (Harms and Heindler, 1982). If the above target and blanket are a molten salt of thorium (Th), then the above two-region concept can be simplified. $^{232}$Th in the core can be converted by spallation neutrons to fissile $^{233}$U, which will be utilized for other reactors. K. Furukawa provided a numerical study and proposed this concept as accelerator molten salt breeder (AMSB) in 1981 (Furukawa et al., 1981).

## 15.2 Accelerator Molten Salt Breeder (AMSB)

AMSB is composed of the following three parts:

1. 1 GeV × 200−300 mA proton accelerator;
2. Single-fluid molten fluoride target system; and
3. Heat transfer and electric power recovery system.

A diagram of this system is shown in Fig. 15.2. The size of the target salt bath is 4.5 m in diameter and 7 m in depth. A Hastelloy N vessel is protected by a graphite reflector. The salt flows into the top of the bath, forming a vortex of about 1 m in depth. The proton beam is injected in an off-centered position, hitting near the bottom of the vortex to minimize neutron leakage and to improve generated heat dispersion. This target molten salt system is subcritical and is not affected by radiation, unlike solid targets. This makes heat removal easier, and does not need target shuffling. The beam injection port will be designed by an improved gas-curtain technology. A high-energy proton accelerator will utilize multibeam funneling. Spallation neutrons transmute Th to $^{233}$U, and also cause fissions in the target.

Target salt is $^{7}$LiF-BeF$_2$-ThF$_4$-$^{233}$UF$_4$ in equilibrium condition. Since there is no fissile $^{233}$U in this salt at the start-up stage, one idea is to add PuF$_3$ as an initial

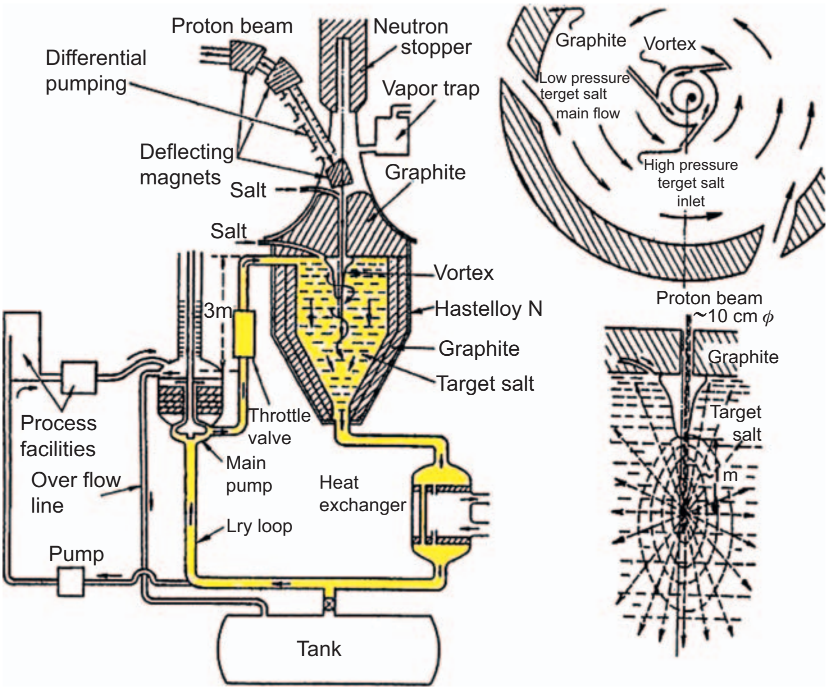

**Figure 15.2** Schematic diagram of accelerator molten salt breeder (AMSB) (Furukawa et al., 2008).

fissile in the same way as FUJI-Pu, that is AMSB-Pu (Furukawa et al., 2008; Yoshioka, 2013).

Assuming 32% efficiency of proton accelerator, 940 MWe is required to operate the accelerator of proton beam of 1 GeV × 300 mA. This electricity is recovered by fission energy in the target salt. Assuming $K_{\mathrm{eff}} = 0.67$ (effective multiplication factor) of the target salt, and 36 neutrons for each spallation reaction by a proton, 2140 MWt is generated, that is 940 MWe is generated based on 44% thermal efficiency of the power recovery system. Here, $K_{\mathrm{eff}} = 0.67$ means that multiplication by fission is 2 $(=K_{\mathrm{eff}}/(1 - K_{\mathrm{eff}}))$, and one neutron is used to convert Th to $^{233}$U and another neutron is used for fission reaction. Also, since the conversion ratio (CR) of target salt is high and close to 1.0, consumption of $^{233}$U by fission is almost compensated for by the chain reaction.

In this AMSB design, a relatively large accelerator with a current of 300 mA beam is assumed. As far as the energy balance, this size can be smaller. But, at the initial start-up stage of AMSB, there is no fissile, and fissile material ($^{233}$U) is mainly generated by spallation reaction. If the accelerator is small, for example 30 mA with $K_{\mathrm{eff}} = 0.90$, then it will take a long time to build-up the fissile material to achieve this high $K_{\mathrm{eff}}$. Therefore, a large accelerator with a current of 300 mA beam is required to achieve an equilibrium condition as soon as possible.

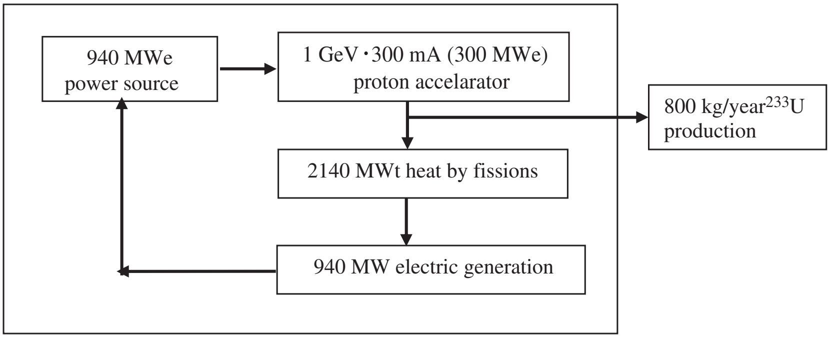

**Figure 15.3** Energy balance of AMSB (Furukawa et al., 1981).

Once the equilibrium condition is achieved, an annual net production of $^{233}U$ is about 800 kg/year, assuming 80% load factor of this AMSB. As is shown in Section 11.2, one 1000 MWe super-FUJI requires 1.5 tons of initial $^{233}U$, and this fissile amount will be supplied by 1 year operation of two AMSBs. The energy balance of AMSB is shown in Fig. 15.3 (Furukawa et al., 1981).

As a future integrated system, K. Furukawa proposed the Thorium Molten Salt Nuclear Energy Synergetic System (THORIMS-NES), which is a combination of MSR fission power reactors and AMSB for production of fissile $^{233}U$. In between these two facilities, a fuel chemical processing facility is placed, as shown in Fig. 15.4 (Furukawa et al., 2008; Yoshioka, 2013).

THORIMS-NES has the following three unique features:

1. Using Th instead of U as fertile element, that is Th cycle instead of U-Pu cycle;
2. Using liquid fuel (molten fluoride salt fuel) instead of solid fuel;
3. Separation of electric power station (MSR-FUJI) and fissile breeding facility (AMSB).

The total system is simply integrated by a single phase of molten fluorides based on LiF-$BeF_2$ solvent, after doing some make-up in each component facility. Each regional center for chemical processing and fissile production will accommodate 4–40 AMSBs, two chemical processing plants, and one radio-waste processing plant. It is planned that several tens of centers will be built in different locations around the world.

## 15.3 Fast subcritical MSR for MA incineration

The essential problem of the closing nuclear fuel cycle (CNFC) is the high radioactivity of the spent fuel (SF), particularly the long-lived radioactive waste and especially the MA, which are represented mainly by Am and in relatively less quantity by higher actinides (Cm and others).

According to basic conceptions of MA utilization they have to be safely buried or according to a more decisive approach they have to be transmuted, i.e., converted

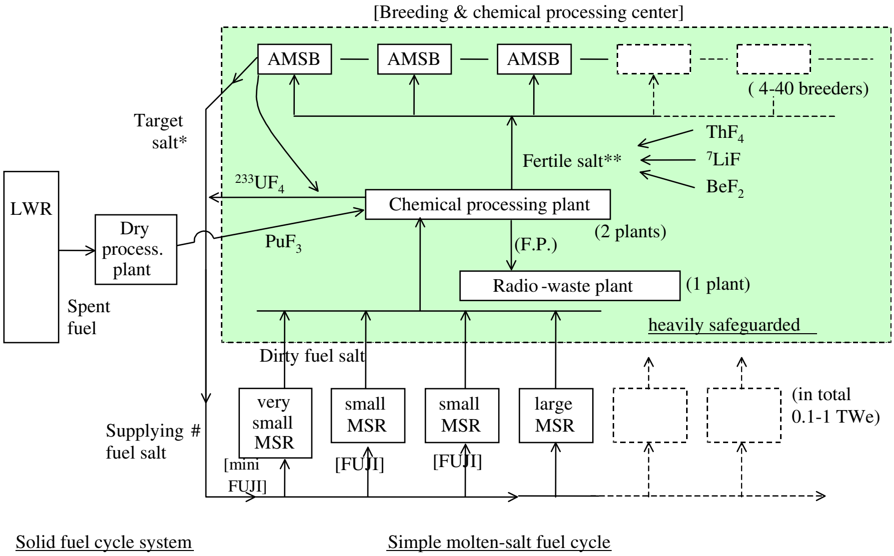

(*)$^{7}LiF$-$BeF_2$-$ThF_4$ - $^{233}UF_4$ (**)$^{7}LiF$-$BeF_2$-$ThF_4$ (#)target salt* + additive $^{233}UF_4$

**Figure 15.4** Thorium Molten Salt Nuclear Energy Synergetic System (THORIMS-NES) (regional center for chemical processing and fissile production) (Furukawa et al., 2008).

to relatively short-lived fission products and thus eliminated from the Earth's ecosystem. The main stream of the MA transmutation is to burn them out together with recycled fuel of Pu, Np, and U probably due to the lack of effective technology for the MA elimination from SF.

Another promising way, which is known as the double-strata approach (OMEGA project) (Takizuka, 1997), consists of CNFC separation into two subcycles: the first (basic) is for the fast reactor fresh fuel fabrication free of MA and the second (supporting) is MA incineration in specialized reactors. The principal important advantage of such a strategy is the possibility of relatively independent optimization of each cycle, including choice of a reactor and its operating mode.

The 1-year MA production from a 1 GWe nuclear power plant (Pressurized Water Reactor (PWR) or Russian pressurized water reactor (VVER)) is $\sim 3.5$ kg of Am and $\sim 0.9$ kg of Cm. After 30 years of storing this amount grows up to $\sim 30$ kg of Am and $\sim 0.2$ kg of Cm due to $^{241}Pu \rightarrow {}^{241}Am$ decay, i.e., every year the amount of Am increases by $\sim 2\%$ and the amount of Cm is reduced by $\sim 5\%$.

The nuclear power of 500 GWe planned for the middle of the 21st century will result in annual production of about $\sim 1.7$ t of Am and $\sim 0.5$ t of Cm. In addition, Am and Cm isotopes produced by existing nuclear power should be eliminated from the SF storages and transmuted (today's amount are $\sim 2.5 \times 10^5$ t) (IAEA-TECDOC, 2008). Both MA inventories should be transmuted with a reasonable rate, i.e., at least faster than the rate of their production.

Presently the total amount of Am and Cm in the world SF storages can be estimated as ~250 t of Am and ~2 t of Cm and every year it increases by ~5 t Am and reduces by ~0.1 t Cm. To eliminate this amount of MA in ~50 years it is necessary to burn them out at a rate of ~10 t/year.

The conception of the specialized reactor for MA burning is a subject of current discussion (Bultman, 1995; NEA Nuclear Science Committee, 2000). The MSR is considered highly as a proposal for this purpose. It has some advantages over solid fuel reactors. The first is the absence of the need for fuel element fabrication with subsequent recycling of extremely toxic wastes. The second is the lack of limitations on the fuel burn-up that, in the case of solid fuel, leads to fuel element swelling.

One of the most common advantages of this reactor type is the principal impossibility of severe accidents with reactor power run-up since the void and temperature coefficients are negative and the reactor is operated with minimum reactivity margin.

There is an operational experience of the experimental MSR of 7.6 MW power (MSRE, ORNL, USA; 1964–69) (McPherson, 1985; Haubenrich and Engel, 1970). Furthermore, MSR is also included in the Generation IV program (Serp et al., 2013) and national programs in Japan, China, Korea, and India. These circumstances indicate that the prospects of MSR, considered from the standpoint of technical implementation, are a possibility in the foreseeable future possessing competitiveness with traditional solid-fuel reactors. Note that most of these listed projects, as well as MSRE, are based on Th-U fuel cycle with fuel salt (FS) 2LiF-$BeF_2$ and thermal neutron spectrum.

By now it is clearly recognized that the fast-neutron spectrum is preferred for the reactor-burner (IAEA-TECDOC, 2008). In this case the fission process in the neutron absorption reaction contributes to the direct transmutation of MA into fission fragments, and at the same time allows to minimize the involvement of the ignition material in the form of Pu or odd uranium isotopes $^{233}U$ or $^{235}U$.

Attempts to achieve a fast neutron spectrum by the use of chloride salts have been unsuccessful due to their high corrosiveness. Fluoride salts, unlike chloride salts, have a satisfactory compatibility with construction materials. But to achieve a fast neutron spectrum, concentration of actinides in fluoride salts should be at least about 10 at.% (~10 mol.% of $PuF_3$ and $UF_4$ or ~50 wt.% of fissile elements) (Merle-Lucotte et al., 2004, 2006). Such solubility values are many times higher than solubility limits of $PuF_3$ which have become recently known (Ponomarev et al., 2013). The situation has radically changed in recent years due to conducted experiments with eutectic 46.5% LiF-11.5% NaF-42% KF (FLiNaK), as is shown in Fig. 15.5. In accordance with some theoretical estimations (Benes and Konings, 2008) the solubility of actinides 10 mol% was experimentally confirmed (Lizin et al., 2013a,b; Volozhin et al., 2013), which provides a reasonably fast neutron spectrum. An extremely high solubility of $AmF_3$ should be especially noted.

These new findings open the prospect for development of the molten salt reactor-burner with a fast neutron spectrum (MSR-B) based on FLiNaK for actinide transmutation.

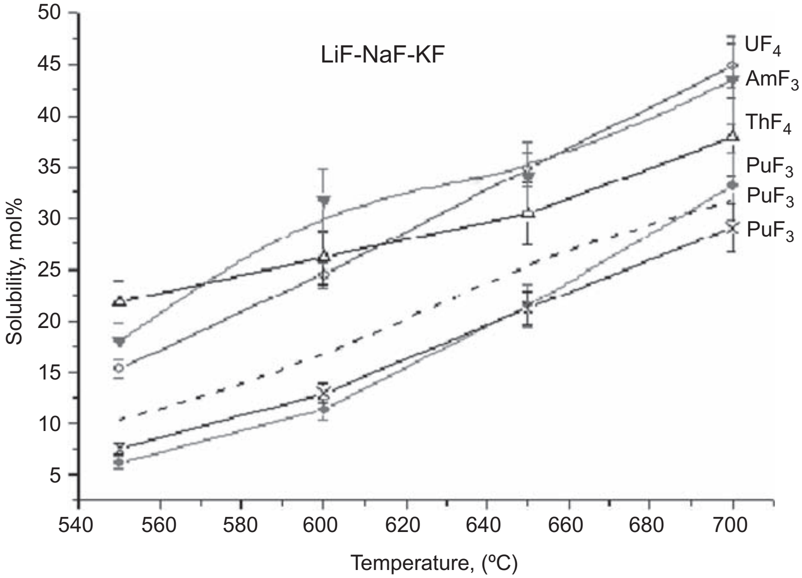

**Figure 15.5** Solubility of the actinide fluorides in FLiNaK: UF$_4$, AmF$_3$, ThF$_4$, and PuF$_3$ (Lizin et al., 2013a,b), PuF$_3$ (*dashed line*;Benes and Konings, 2008); PuF$_3$ (*crosses*; Volozhin et al., 2013).

MA and actinides formed from them during the burning process are characterized by a low yield of delayed neutrons β: $^{241}$Am—0.14%, $^{245}$Cm—0.18% $^{239}$Pu—0.22%, $^{238}$Pu—0.14%. In this regard, from the point of view of reactor operating and behavior in accidents related to the introduction of positive reactivity, MSR-B is inferior to reactors on U-Pu fuel. This is especially important for high-performance reactor-burners operated only on MA or with a minimum feeding of fissile isotopes ($^{235}$U and $^{239}$Pu). Besides that, FS circulation leads to reduction of effective delayed neutron fraction β (Weinberg and Wigner, 1959). The known method to compensate reduction of β is to convert reactor to subcritical mode with an external neutron source (Vasil'kov et al., 1970; Carminati et al., 1993). Such an approach is used in considered conceptions for reactor stabilization. A reactor with subcritical reactivity $\Delta k$, under otherwise equal conditions, is not inferior to the critical reactor with $\beta \approx \Delta k$ with respect to reactor power inertia.

## 15.4 Main characteristics of the subcritical MSR-B

Properties in the light of the aforesaid considerations are combined in the concept of a subcritical MSR-B based on the salt LiF-NaF-KF for the MA transmutation:

- The reactor is operated in subcritical mode and it is developed under the scheme: accelerator, target, blanket;

- Primary neutrons are generated in the target, and afterwards they are multiplied in the blanket;
- Blanket is a molten salt homogeneous reactor with carrier salt FLiNaK, which provides a fast neutron spectrum.

The integration of these properties in one reactor system defines a new concept. The conceptual scheme of subcritical MSR-B and its general layout are presented in Figs. 15.6 and 15.7.

The target node consists of the proton beam tube and the neutron production target. According to the traditional approach for such systems, the target is located in the center of the reactor. It is surrounded by a subcritical molten salt blanket where neutrons that escape from the target produce additional fission neutrons and the incineration of the transplutonium elements takes place. Outside of the transmutation zone there is the first circulation circuit that includes pumps and heat

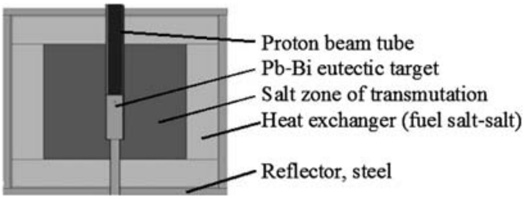

**Figure 15.6** Scheme of subcritical MSR-B.

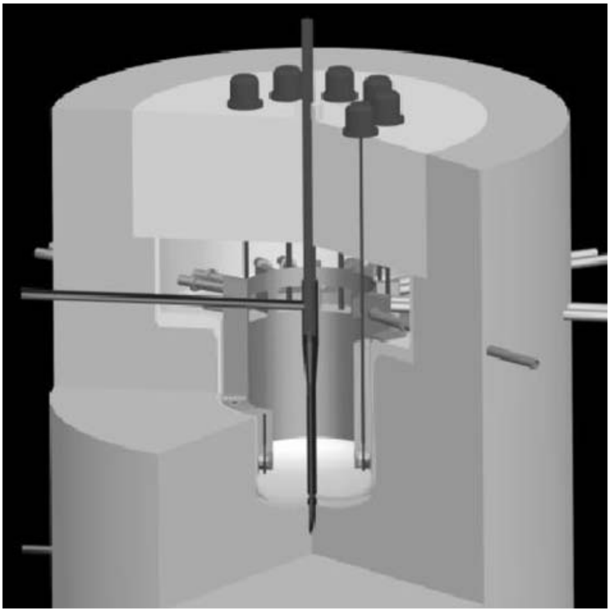

**Figure 15.7** General layout of subcritical MSR-B.

exchangers. The LiF-NaF-KF salt is used in the first and second circulation circuits. The whole system is surrounded by a steel reflector. Not shown in the figures is reactor equipment including cleanup and fuel feeding systems.

With regard to this reactor scheme, neutron and thermal calculations have been carried out with the aim to substantiate the principal structural parameters of the reactor and its physical properties. The initial data on the following parameters have been taken:

1. Subcriticality $\Delta k = 0.01$ and 0.03. At higher subcriticality $\Delta k = 0.03$, the reactor is comparable to the storages of the SF with regard to nuclear safety. At $\Delta k = 0.01$ the reactor is equivalent to a critical reactor with $\beta \sim 1\%$ with regard to inertness of transition processes. This can be simply demonstrated on the one-point reactor model (Bell and Glasstone, 1970). In this approximation the neutron kinetic equation with one group of delay neutron is written as:

   $$\Lambda \frac{dP(t)}{dt} = (\rho - \beta)P(t) + \int_0^\infty d\tau \beta \lambda \exp(-\lambda \tau)P(t - \tau) = (\rho - \beta)P(t) + q_d(t),$$

   where the standard notations are used and $P(t)$ is reactor power.

   As the utmost case of the subcritical reactor on prompt neutrons ($\beta = 0$) with reactivity $\rho_s \approx \rho_0 + \rho_p$, where $\rho_0 \approx -\Delta k$ (reactivity in the operation reactor mode) and $\rho_p$ (reactivity perturbation), the kinetic equation is written as:

   $$\Lambda \frac{dP(t)}{dt} \approx (\rho_p - \Delta k)P(t) + q_{\text{out}},$$

   where $q_{\text{out}}$ defines the outer neutron source that is assumed to be constant.

   In the steady state $P(t) = P_0$, $q_d(t) = q_{d0} = \beta P_0$, $q_{\text{out}} \approx \Delta k P_0$ and if both reactors have equal power and $\Delta k \approx \beta$, then $q_{\text{out}} \approx q_{d0}$. Thus, the equations differ mainly in the fact that in the transient mode term $q_d(t)$ in a critical reactor with delay follows the change of its power, and in the subcritical reactor a similar term $q_{\text{out}}$ remains constant. It is clear that when disturbed reactivity $\rho_p$ is inserted in a subcritical reactor with $\Delta k \approx \beta$, reactor power varies more inertially than in a critical reactor with the same reactivity $\rho = \rho_p$. It should be noted that the small subcriticality additionally requires its reliable online monitoring, which can be implemented, for example, using reactor noise (Degtyarev et al., 2013a,b).
2. At the proton energy $E_a = 1$ GeV and proton accelerator current $I_a = 3$ or 10 mA, the power of the accelerator is $W_a = 3$ or 10 MW, respectively. Such accelerator parameters are assumed to be achieved in the foreseeable future. Three MSR-B conceptions were examined: one for power $W_b = 1650$ MWth, and two for the power $W_b = 495$ MWth.

As a target material the liquid lead-bismuth eutectic is used. Several high-energy particle transport codes, such as Fluctuating Kascade Monte Carlo Code (FLUKA), Monte Carlo N-Particle Transport Code (MCNP/MCNPX), Multipurpose Hadron Transport Code (SHIELD), Calculation Code for the Transport of Charged Particles and Neutrons (CASCADE/INPE), etc. might be used for calculation of the thermal and neutron characteristics of the target neutron production and molten salt blanket. The description of the spallation interaction of protons with the target nuclei and the transport of secondary particles in the target of the MSR-B was done with the

CASCADE/INPE code (Barashenkov et al., 1999). According to the research result, the target height was determined as 60 cm, and the diameter as 14–26 cm (depending on the power of the proton accelerator). The input temperature of the Pb-Bi eutectics in the target is 320°C, its maximal flow speed is 2.5 m/s, the maximum target temperature is 620°C, the maximum energy release is ~270 kW/L. The neutron spectrum produced by the Pb-Bi target is presented in Fig. 15.8, its total intensity at the 10 MW proton beam power is $\sim 1.3 \times 10^{18}$ n/s. The neutron multiplicity per one proton with energy $E_a = 1$ GeV was found to be at the level of 20 n/p, which is in accordance with the experimental results (Yurevich et al., 2006).

Neutron calculations to evaluate MSR transmutation zone parameters were carried out using the MCNP-4B (MCNP, 1997) and ORIGEN2.1 (1996) codes in a full-scale model. MCNP calculations are performed with a neutron cross-section library based on ENDF/B-VI (Cross Section Evaluation Working Group, 1991).

In the MSR-B blanket, molten salt of 0.465% LiF − 0.115% NaF − 0.42% KF is used with 14 mol% of heavy metal (HM) contamination. Such concentrations are significantly below the solubility limits (~30 mol% for $PuF_3$ and ~40 mol.% for $AmF_3$) in the operating temperature range ~ 650–700°C (Fig. 15.5).

The size of transmutation zone and feeding composition is determined in order to provide the target value of reactor subcriticality $\Delta k$ in a steady state mode, when the fuel composition (FC) is stabilized. The ratio *H*/*R* (height/radius) is assumed to be equal to 1.85, which is optimal for the reactor without a reflector. The internal cavity volume of the transmutation zone is varied in agreement with the size of the target node.

The composition of the loading fuel is formed on the basis of transuranium components of PWR SF cooled for 30 years, that is given in Table 15.1.

Pu is assumed as an ignition material for the starting FC and, if necessary, for reactor feeding. A possible alternative can be enriched uranium. However, taking into account the value of U for conventional nuclear power reactors, the purpose of a reactor incinerator to work with a highly radioactive fuel, and the peculiarity of transmutation processes in a reactor, the choice in favor of Pu looks more natural.

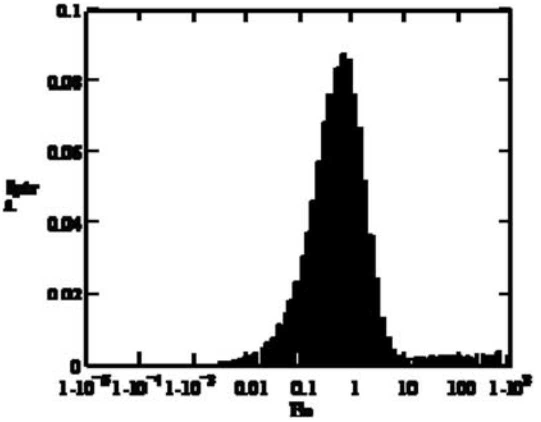

**Figure 15.8** Neutron spectrum from Pb-Bi target.

**Table 15.1** **Composition of transuranic elements in the VVER spent fuel after 30 years' cooling normalized by the sum of all the transuranic elements**

| Nuclide | Nuclide concentration | Element concentration |
|---|---|---|
| $^{237}Np$<br>$^{239}Np$ | 5.19E-02<br>8.29E-09 | 5.19E-02 |
| $^{236}Pu$<br>$^{238}Pu$<br>$^{239}Pu$<br>$^{240}Pu$<br>$^{241}Pu$<br>$^{242}Pu$ | 1.41E-10<br>1.44E-02<br>5.47E-01<br>2.00E-01<br>3.01E-02<br>4.66E-02 | 8.39E-01 |
| $^{241}Am$<br>$^{242m}Am$<br>$^{243}Am$ | 9.85E-02<br>7.08E-05<br>9.48E-03 | 1.08E-01 |
| $^{242}Cm$<br>$^{243}Cm$<br>$^{244}Cm$<br>$^{245}Cm$<br>$^{246}Cm$<br>$^{247}Cm$<br>$^{248}Cm$ | 1.84E-07<br>1.46E-05<br>9.18E-04<br>1.78E-04<br>1.48E-05<br>1.59E-07<br>1.21E-08 | 1.13E-03 |
| $^{249}Bk$<br>$^{250}Bk$ | 6.79E-21<br>2.66E-25 | 6.79E-21 |
| $^{249}Cf$<br>$^{250}Cf$<br>$^{251}Cf$<br>$^{252}Cf$ | 1.46E-10<br>9.50E-12<br>2.71E-11<br>4.03E-15 | 1.83E-10 |
| Total | 1.00 | 1.00 |

Initial FS composition is a solution of $PuF_3$ (7 mol%) and $AmF_3$ (7 mol%) in FLiNaK. Nuclide composition of each element of the fuel fraction is given in Table 15.2. The density of the FS at 700°C is 3.18 g/cm$^3$, and the content of actinides is 1.28 g/cm$^3$ (Table 15.2).

Fuel burn-up calculations were carried out in relation to the irradiation conditions in the transmutation zone. Primary neutron generation power in the target was obtained from calculation results of the spallation interaction of protons in the target. The feeding rate ensures constant mass of actinides in the reactor. MA and Pu feeding fractions are formed on the base of the irradiated FS. FS cleanup systems are also taken into account in the calculation.

The main geometric parameters of reactors are presented in Table 15.3.

Table 15.2 **Initial fuel salt composition (in units of $10^{24}$ 1/cm$^3$)**

| **Nuclide** | **Nuclide concentration** |
|---|---|
| $^{23}$Na | 2.764E-03 |
| $^{39}$K | 9.240E-03 |
| $^{41}$K | 6.635E-04 |
| $^{7}$Li | 1.036E-02 |
| $^{19}$F | 3.270E-02 |
| $^{237}$Np | 5.193E-04 |
| $^{239}$Np | 8.304E-11 |
| $^{236}$Pu | 2.707E-13 |
| $^{238}$Pu | 2.764E-05 |
| $^{239}$Pu | 1.052E-03 |
| $^{240}$Pu | 3.852E-04 |
| $^{241}$Pu | 5.776E-05 |
| $^{242}$Pu | 8.957E-05 |
| $^{241}$Am | 9.860E-04 |
| $^{242m}$Am | 7.086E-07 |
| $^{243}$Am | 9.491E-05 |
| $^{242}$Cm | 1.846E-09 |
| $^{243}$Cm | 1.462E-07 |
| $^{244}$Cm | 9.189E-06 |
| $^{245}$Cm | 1.778E-06 |
| $^{246}$Cm | 1.484E-07 |
| $^{247}$Cm | 1.596E-09 |
| $^{248}$Cm | 1.214E-10 |
| $^{249}$Bk | 6.796E-23 |
| $^{249}$Cf | 1.460E-12 |
| $^{250}$Cf | 9.517E-14 |
| $^{251}$Cf | 2.716E-13 |

Table 15.3 **Main geometrical parameters of the subcritical MSR-B**

| **Parameter** | **Characteristics** | | | **Notes** |
|---|---|---|---|---|
| Power (MWth) | 1650 | 495 | 495 | |
| Accelerator power (MW) | 10 | 3 | 9 | |
| Subcriticality ($\Delta k$) | 0.01 | 0.01 | 0.03 | |
| Inner/outer radius of the proton beam tube (cm) | 11.3/11.8 | 6.2/6.5 | 11.3/11.8 | Vacuum inside the tube |
| Large/small radius of the target (cm) | 13.2/6.0 | 7.2/3.3 | 13.2/6.0 | Material of the target 55.5% Bi + 44.5%Pb |
| Thickness of the target tube (cm) | 0.35 | 0.2 | 0.35 | Material of the tube: steel |
| Height of the fuel salt zone (cm) | 174 | 116 | 118 | |
| Outer radius of the fuel salt zone (cm) | 94 | 63 | 64 | |
| Thickness of the primary coolant zone (cm) | 41 | 28 | 27 | |
| Thickness of the steel reflector (cm) | | 10 | | |

The main physical and operation parameters of MSR-B in the equilibrium state are shown in Table 15.4. This shows the equilibrium state with constant FC. As a consequence, the rate of fuel injection into the reactor equals the rate of fuel burnup (i.e., its transmutation to the fission products).

According to the results obtained MAs can be burned in a reactor with 1650 MWth power without plutonium feeding (except for the initial loading). For reactors with less power, plutonium feeding is needed to compensate for neutron leakage that is higher in a smaller reactor (Table 15.5).

The possibility to burn MA alone or with a relatively moderate Pu feeding is determined crucially by the high concentration of nuclides. At higher heavy nuclear concentrations the neutron spectrum is close to the spectrum of fast reactors that intensifies fission of actinides (see Figs. 15.9 and 15.10).

The dip in the neutron spectrum of MSR-B in the 30−200 keV energy range is due to elastic neutron scattering resonances of $^{19}$F and describes their impact in the smoothed form. Secondary neutron yields for the most important actinides in

**Table 15.4** Main equilibrium parameters of subcritical MSR-B

| Reactor power (MWth) | 31650 | 495 | |
|---|---|---|---|
| Accelerator power (MW) | 10 | 3 | 9 |
| Subcriticality | 0.01 | 0.01 | 0.03 |
| Neutron spectrum | Fast | | |
| Averaged neutron flux (n/cm$^2$s) | $2.2 \times 10^{15}$ | $2.1 \times 10^{15}$ | |
| Radius/height of the core (m) | 0.94/1.74 | 0.63/1.16 | 0.64/1.18 |
| Volume of FS in the core (m$^3$) | 4.7 | 1.4 | |
| Volume of FS out of the core (m$^3$) | 3.3 | 1.0 | |
| Volume of FS in the reprocessing unit (m$^3$) | 0.2 | 0.06 | |
| Total volume of FS in the reactor (m$^3$) | 8.3 | 2.5 | |
| FS volume in the heat exchanger (m$^3$) | 3.0 | 0.6 | |
| Average speed of FS in the core (m/s) | 3.1 | 2.1 | |
| HM concentration in the FS (mol.%) | 14 | | |
| U/Np/Pu/MA (tons) | 0.05/0.01/ 5.26/5.39 | 0.014/0.003/ 2.03/1.16 | 0.014/0.003/ 2.01/1.19 |
| Total HM loading Q (tons) | 10.7 | 3.2 | |
| Pu/MA ratio in the reactor loading | 0.975 | 1.75 | 1.69 |
| Pu fraction in the feeding $\varepsilon$ = Pu/MA | 0 | 0.59 | 0.54 |
| Rate of MA burning (MA feeding), $q_{MA}$ (kg/year) | 520 | 98 | 101 |
| Normalized MA burning rate (kg/year GWth) | 315 | 200 | 206 |
| Transmutation time $\tau_{in} = Q/q_{MA}$ (years) | ~20 | ~30 | |

**Table 15.5** Feeding fuel composition for full and reduced power

| Nuclide | Feeding fuel composition (kg/ton HM) | |
|---|---|---|
| | 1650 MWth | 495 MWth[a] |
| $^{238}$Pu | – | 6.3 |
| $^{239}$Pu | – | 241.0 |
| $^{240}$Pu | – | 88.6 |
| $^{241}$Pu | – | 13.3 |
| $^{242}$Pu | – | 20.8 |
| $^{241}$Am | 901.4 | 567.9 |
| $^{242m}$Am | 0.66 | 0.42 |
| $^{243}$Am | 87.49 | 55.1 |
| $^{243}$Cm | 0.14 | 0.087 |
| $^{244}$Cm | 8.51 | 5.36 |
| $^{245}$Cm | 1.66 | 1.046 |
| $^{246}$Cm | 0.14 | 0.087 |
| Total | 1000 | 1000 |

[a] Due to similarity of reactors with 495 MWth power here and further data are provided for reactor with accelerator power 3 MW and subcriticality 0.01.

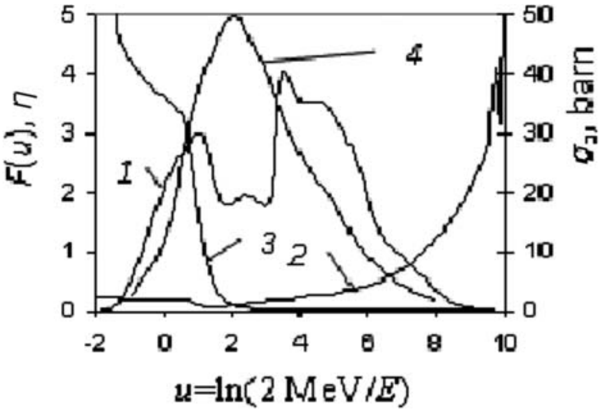

**Figure 15.9** Neutron characteristics of $^{241}$Am in the neutron spectrum MSR-B. (1) neutron spectrum $F(u)$ (relative units), (2) neutron absorption cross-sections $\sigma_a$, (3) neutron yield $\eta$ per one absorption act versus lethargy u for $^{241}$Am; (4) neutron spectrum of the fast reactor.

dependence of the spectrum are given in Table 15.6. Comparison of MSR-B is carried out with an intermediate spectrum reactor incinerator (Degtyarev et al., 2006) and a model system with a fast spectrum.

The reactor considered occupies an intermediate position, somewhat shifted to a reactor with a fast spectrum. The greatest sensitivity to the spectrum is observed for

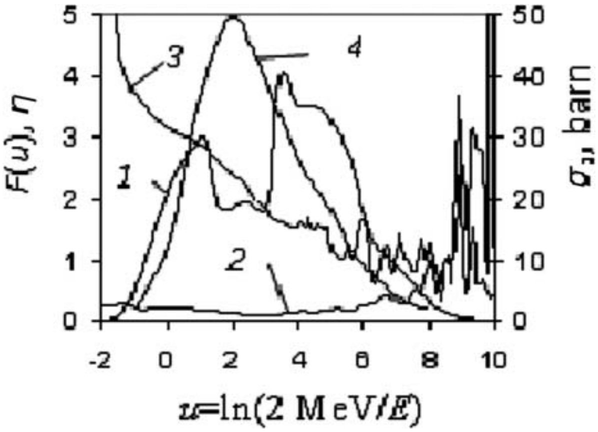

**Figure 15.10** Neutron characteristics of $^{239}$Pu in the neutron spectrum MSR-B. (1) neutron spectrum $F(u)$ (relative units), (2) absorption neutron cross-sections $\sigma_a$, (3) neutrons released η per one absorption act versus lethargy u for $^{239}$Pu; (4) neutron spectrum of the fast reactor.

**Table 15.6 Secondary neutron yield $\eta$ per neutron absorption for different reactor neutron spectra**

| Nuclide | Considered reactor with fast neutron spectrum ($W_b$ = 1650 MWth) | Reactor with fast neutron spectrum Pb-Bi (MA 3%, Pu 0.97%) | MSR with intermediate spectrum (Degtyarev et al., 2006) |
|---|---|---|---|
| $^{238}$Pu | **1.682** | **2.049** | 0.991 |
| $^{239}$Pu | **2.131** | **2.531** | **1.767** |
| $^{240}$Pu | **1.165** | **1.581** | 0.340 |
| $^{241}$Pu | **2.474** | **2.594** | **2.356** |
| $^{242}$Pu | **1.036** | **1.449** | 0.313 |
| $^{241}$Am | 0.459 | 0.618 | 0.127 |
| $^{242m}$Am | **2.857** | **3.115** | **2.821** |
| $^{243}$Am | 0.403 | 0.517 | 0.106 |
| $^{243}$Cm | **3.132** | **3.283** | **2.991** |
| $^{244}$Cm | **1.148** | **1.545** | 0.399 |
| $^{245}$Cm | **3.245** | **3.270** | **3.205** |

The values above 1 are given in bold font.

nuclei with an even number of neutrons which are characterized by a threshold fission. The majority of such nuclei in the reactor considered produce neutrons in excess quantity, in contrast to the reactor with an intermediate neutron spectrum.

Note that burning of MA without involvement of the fissile material also can be realized in a reactor with a fast neutron spectrum on the basis of the LiF-BeF$_2$ salt.

However, to provide the fast neutron spectrum the feeding of such reactors must include $^{232}$Th, which thereby dilutes MA as a fuel (Ignatiev et al., 2012a,b, 2014).

As already mentioned above, two reactor models with power 495 MWth do not have significant differences in physical parameters, including the composition of the feeding, despite the significant difference in subcriticality and neutron balance. This is explained by increased neutron leakage in the model with subcriticality 0.03 caused by the increase of the size of the target node.

FC in a steady state significantly differs from the initial loading. In particular, the proportion of curium increases 10–20 times and achieves about 1/10th of the total mass of actinides (Table 15.7).

The share of $^{239}$Pu is reduced in plutonium fraction and $^{238}$Pu becomes predominant, which even in the absence of plutonium in the fuel feeding is formed from $^{241}$Am decay chain with two relatively short-lived intermediate nuclides

**Table 15.7** Initial and equilibrium HM loading of MSR-B

| Nuclide | Initial loading for $W_b$ = 1650 MWth (kg)[a] | Equilibrium loading (kg) | |
|---|---|---|---|
| | | $W_b$ = 1650 MWth | $W_b$ = 495 MWth |
| $^{234}$U | – | 43.8 | 12.0 |
| $^{235}$U | – | 5.2 | 1.3 |
| $^{236}$U | – | 1.1 | 0.4 |
| $^{237}$Np | 1689.9 | 10.0 | 2.8 |
| $^{238}$Pu | 90.3 | 2239.4 | 481.6 |
| $^{239}$Pu | 3452.6 | 784.3 | 432.9 |
| $^{240}$Pu | 1269.6 | 833.3 | 628.7 |
| $^{241}$Pu | 191.1 | 138.7 | 103.5 |
| $^{242}$Pu | 297.7 | 1268.1 | 384.3 |
| $^{241}$Am | 3263.3 | 3063.4 | 655.5 |
| $^{242}$Am | – | 1.3 | 0.2 |
| $^{242m}$Am | 2.4 | 153.5 | 32.8 |
| $^{243}$Am | 316.7 | 714.2 | 178.8 |
| $^{244}$Am | – | 0.2 | – |
| $^{242}$Cm | 0.0 | 258.4 | 37.5 |
| $^{243}$Cm | 0.5 | 34.8 | 5.0 |
| $^{244}$Cm | 30.8 | 749.8 | 165.3 |
| $^{245}$Cm | 6.0 | 231.3 | 51.0 |
| $^{246}$Cm | 0.5 | 145.5 | 28.8 |
| $^{247}$Cm | 0.0 | 20.3 | 4.0 |
| $^{248}$Cm | 0.0 | 11.7 | 1.8 |
| Total | 10611.4 | 10708.3 | 3208.2 |

[a] For the reactor power of 495 MWth the presented initial loading should be multiplied by a factor of 0.3.

$$^{241}\mathrm{Am}(n,\gamma) \rightarrow {}^{242}\mathrm{Am} \underset{16\ \mathrm{h}}{\overset{\beta}{\rightarrow}} {}^{242}\mathrm{Cm} \underset{163\ \mathrm{d}}{\overset{\beta}{\rightarrow}} {}^{238}\mathrm{Pu}.$$

The essential fraction ($\sim$30%) of $^{241}$Am transmutations takes place via this chain with fission of $^{238}$Pu. Note that in a thermal neutron spectrum the burning of $^{241}$Am nucleus in the same scheme would require an additional neutron to convert $^{238}$Pu to $^{239}$Pu due to the low probability of $^{238}$Pu fission.

Table 15.7 shows a large reduction of $^{237}$Np, and this suggests that $^{237}$Np captures a neutron to $^{238}$Np, and decays to $^{238}$Pu with half-life of 2.1 days. But, $\mathbf{^{237}}$Np may have little significance in terms of radioactivity, and this path is not described here.

Neutron balance in the reactor is characterized by a relatively small share of absorption in the structural elements $<2\%$ and the neutron leakage $<2\%$ in 1650 MWth reactor and $<5\%$ in a reactor of 495 MWth power. Nonproductive neutron losses in the FC, which includes the absorption on the elements of the carrier salt, fission products, as well as on uranium and neptunium, do not exceed 8%. The largest contribution to the neutron absorption belongs to $^{241}$Am and to the generation of secondary fission neutrons—$^{238}$Pu (in the 1650 MWth reactor) and $^{239}$Pu (in the 495 MWth reactor). Some characteristics of MSR-B are presented in Table 15.8.)

**Table 15.8** **The neutron balance of FC for MSR-B with power $W_b$ = 1650 MWth per one absorbed neutron**

| Nucleus | Absorption | Fission | Neutron generation |
|---|---|---|---|
| $^{6}$Li | 0.00001 | – | – |
| $^{7}$Li | 0.00007 | – | – |
| $^{19}$F | 0.0142 | – | – |
| $^{23}$Na | 0.00125 | – | – |
| $^{39}$K | 0.0473 | – | – |
| $^{41}$K | 0.00510 | – | – |
| $^{238}$Pu | 0.197 | 0.109 | 0.331 |
| $^{239}$Pu | 0.0873 | 0.0630 | 0.186 |
| $^{240}$Pu | 0.0387 | 0.0148 | 0.0450 |
| $^{241}$Pu | 0.0203 | 0.0170 | 0.0504 |
| $^{242}$Pu | 0.0478 | 0.0160 | 0.0495 |
| $^{241}$Am | 0.331 | 0.0433 | 0.152 |
| $^{242m}$Am | 0.0267 | 0.0232 | 0.0764 |
| $^{243}$Am | 0.0672 | 0.00760 | 0.0271 |
| $^{244}$Cm | 0.0483 | 0.0147 | 0.0555 |
| $^{245}$Cm | 0.0341 | 0.0303 | 0.111 |
| Fission product | 0.0108 | – | – |
| Total | 0.977 | 0.340 | 1.084 |

Slow changes of criticality due to fuel burnup in MSR are compensated mainly by feeding that facilitates the control and protection system (CPS). However, in the case of MSR-B 1650 MWth with MA feeding such a control is unstable, leading to an increase in the imbalance of material compositions and criticality even for small deviations (Degtyarev et al., 2012). It is explained by sign-changing reactivity introduced by MA during their transmutation. Immediately on entering the reactor MA, whose composition is dominated by $^{241}$Am, introduce negative reactivity. But later the impact of MA changes sign due to their partial transition in plutonium fraction (mainly $^{238}$Pu). Therefore, for example, if excess criticality is suppressed by introducing an additional amount of MA, then over time it leads to an increase in the initial criticality perturbation. Reactivity control based on using plutonium fraction is devoid of this shortcoming. In this case the plutonium portion is drawn from or returned to the core, depending on the criticality imbalance. This regulation does not mean, of course, attraction of additional plutonium, because plutonium produced in the reactor core is used. In the steady state of reactor operation stable makeup can also be organized on the basis of monitoring of the actual imbalance of nuclide concentration.

The inlet temperature of the FS in the blanket is equal to 650°C and outlet temperature is about 700°C. The speed of the FS flow is 3.1 m/s and 2.1 m/s for the reactor of power 1650 MWth and 495 MWth, respectively. The average energy release is ~350 kW/L in both cases. The molten salt flow speed in the heat exchangers is 5 m/s (Gulevich et al., 2008, 2009).

High power density (~ 300 W/cm$^3$), a high-energy neutron spectrum, the presence of the target node in the central region of the reactor, and the integrated layout of the reactor are favorable for efficient burnup of transplutonium elements. On the other hand, the same features lead to high levels of radiation damage of the reactor main structural elements, and thus it severely limits its life, which can be estimated from 1–5 years.

## 15.5 Low-energy linear accelerator-driven subcritical assembly

### 15.5.1 Introduction and scope

Several radiotherapy linear accelerators have been installed in Venezuela, and as they get older they are replaced by new ones. Several replaced equipments are available for new physics research applications, since LINAC devices are reliable machines (Barrera et al., 2015). One such application is the employment of accelerators as drivers for subcritical thorium-uranium fuel assemblies as proposed by Rubbia et al. (1993), Sajo-Bohus et al. (2015b), and Bermudez et al. (2016). Here we suggest taking advantage of bremsstrahlung produced energetic photons (5.5–25 MeV) which early experimental data by Castillo et al. (2014) showed neutron production even in the energy window of the Pygmy Dipole Resonance reaction (PDR). Therefore photons in the Giant Dipole Resonance (GDR) region, where most medical LINACs are actively operated, could be employed with effectiveness to induce neutrons by ($\gamma$, *n*), ($\gamma$, *fis*), and (*e*, *e'n*) reactions in the W-target. They could serve as neutron sources to increase a subcritical reactor's $k_{\mathrm{eff}}$. Photons, photoneutrons $n_{\mathrm{ph}}$, or fission neutrons $\nu$, absorbed by Th/U fluid fuel could generate energy with a non-negligible rate, depending mainly on the beam intensity. The advantage is that, for a given subcritical assembly, several LINACs could supply energetic neutrons using tungsten as target or other elements that have relatively large reaction cross-sections. This suggests the feasibility of a photodriven MSR (PD MSR) that could be employed for energy generation (Sajo-Bohus et al., 2015a). Another suggestion is to employ such a PD MSR subcritical assembly to reduce radiotoxicity of nuclear waste (e.g., minor actinides) including medical radioisotopes such as the radio toxic $^{99}$Tc (byproduct of the decay of $^{99\mathrm{m}}$Tc widely used in medical diagnostic applications). A further suggestion is to employ LINACs to produce new radioisotopes for medical theranostic (therapy and diagnostic) applications. In fact, high linear energy transfer (LET) radiation, such as is given by alpha particles, is advisable for radioimmunotherapy, e.g., $^{223}$Ra, to reduce metastatic bone tumor or to be employed for hormone-refractory prostate cancer. Other radioisotopes could be produced such as $^{225}$Ac, $^{211}$At, $^{212}$Pb/ $^{212}$Bi, $^{213}$Bi, $^{226}$Th, and $^{227}$Th for neoplasia (DOE, 2015).

Our study is oriented to determine fission rates and neutron production rates employing nuclear track detector (NTM) methodology with poly-allyl-diglicol-carbonate (PADC) passive detectors since these cope with the required sensitivity for neutron field measurements (Pálfalvi et al., 2001; Espinosa et al., 2015). The latent track formed during charged particle absorption is enlarged by appropriate development and analyzed. Results yield conveniently the efficiency of neutron production and their applicability as an external neutron source for a subcritical assembly.

### 15.5.2 Theory

At relatively low photon energy ($\sim$10–20 MeV), a value near or above the nucleon mean binding energy ($\sim$8 MeV), reactions are induced by GDR in the simulated target fuel, the reaction cross-section for the Th-U mixture increases with the photon energy around 10–15 MeV, and then drops rapidly. Due to collective oscillation in the heavy nuclei, a neutron breaks free during photonuclear ($\gamma$, *n*) and ($\gamma$, *2n*), electronuclear (*e, e'n*) or ($\gamma$, *pn*) reactions including ($\gamma$, *fis*). The reaction total cross-section may be expressed as the sum of cross-sections $\sigma_i$ for a set of possible ($\gamma$, *i*) reactions,

$$\sigma_{\mathrm{tot}}(\gamma,\ n) = \sum_i \sigma_i(\gamma,\ i) \tag{15.1}$$

in which $\Sigma_i\ \sigma_i\ (\gamma,\ i) = \sigma\ (\gamma,\ n) + 2\sigma\ (\gamma,\ 2n) + \nu\ \sigma\ (\gamma,\ fis)$ and $\nu$ is the neutron multiplicity which for actinides fission is around 2.2. The neutron yield $Y(k)$ per incident photon and energy group $k$, for target and PADC-detector-($C_{12}H_{18}O_7$) elements, assuming a parallel beam of photons, is given by

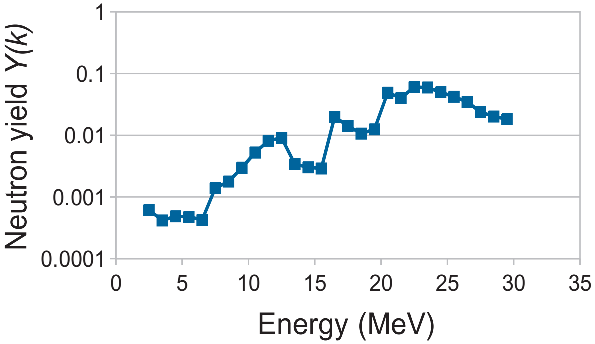

**Figure 15.11** Photoneutron yields calculated for passive detectors.
Adapted from Allen and Chaudhri (1988).

$$Y(k) = f_1(k)t\Sigma_j \rho_j \sigma_j(k) \tag{15.2}$$

where $\rho_j$ is the atomic density, $\sigma_j(k)$ is the cross-section for ($\gamma$, $n$) reaction of the j-th isotope and $t$ is the target thickness. The factor $f_1(k)$ takes into account photon attenuation when relatively thick target material is considered. The photoneutron yields calculated by Allen and Chaudhri (1988) are given in Fig. 15.11 for passive detectors.

Relevant processes other than direct neutron induced fission are shown in the following scheme:

$U_{nat}$ = 99.3% ($^{238}$U) + 0.7% ($^{235}$U); $Th_{nat}$ is assumed pure $^{232}$Th.
$^{238}U + \gamma \rightarrow {}^{236}U + 2n + \gamma \rightarrow {}^{235}U + n \rightarrow$ fission fragments ($A_1$, $A_2$)
$^{238}U + \gamma \rightarrow {}^{237}U + n + \gamma \rightarrow {}^{236}U + n + \gamma \rightarrow {}^{235}U + n \rightarrow$ fission fragments ($A_1$, $A_2$)
$^{238}U + \gamma \rightarrow {}^{237}U + n \rightarrow {}^{237}Np + \beta^- + \gamma \rightarrow {}^{235}Np + 2n + e \rightarrow {}^{235}U \rightarrow$ fission fragments ($A_1$, $A_2$)
$^{232}Th + \gamma \rightarrow {}^{231}Th + n$; $^{232}Th + \gamma \rightarrow$ fission fragments ($A_1$, $A_2$)

The photofission reaction cross-section for both isotopes $^{232}$Th and $^{238}$U are very similar as shown in Fig. 15.12.

The number of delayed neutron number $\nu_d$ per energy in the interval 9–17 MeV is almost the same (Van Lawe et al., 2006) so that the simulation for FC is less complicated.

### 15.5.3 Experimental procedure

Experiments were carried out with a radiotherapy machine (LINAC Varian 2100 accelerator at the La Trinidad, GURVE-Clinic, Caracas, Venezuela), operated at 18 MV for 66 minutes with 400 Monitor Unit (or MU) and at a rate of 600 MU for target irradiation. Detectors employed were combinations of different or mixed elements as given in Table 15.9 assembled into simulated fuel samples.

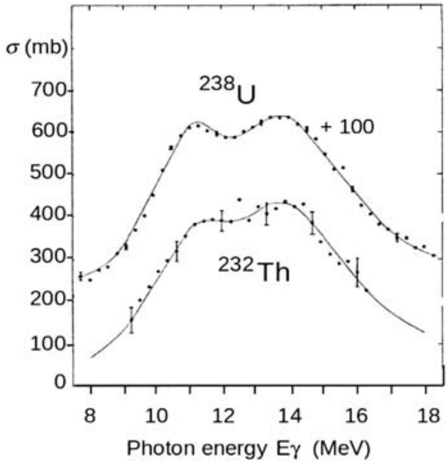

**Figure 15.12** Comparison between two isotopes photofission cross-section to show similarities.
Adapted from Caldwell et al. (1980).

**Table 15.9** Set of assembled simulated fuel samples

| Assembled target compound |
|---|
| $^{238}$U (99.7%) + $^{235}$U (0.7%) + ($C_{12}H_{18}O_7$) |
| $^{238}$U (99.7%) + $^{235}$U (0.7%) + $^{10}$B (20%) + $^{11}$B(80%) + ($C_{12}H_{18}O_7$) |
| $^{238}$U (99.7%) + $^{235}$U (0.7%) + $^{232}$Th + $^{10}$B (20%) + $^{11}$B(80%) + ($C_{12}H_{18}O_7$) |
| $^{232}$Th + $^{10}$B (20%) + $^{11}$B(80%) + ($C_{12}H_{18}O_7$) |

The additive $B_{nat}$ ($^{10}$B (20%) + $^{11}$B(80%)) is used as a boric acid compound.

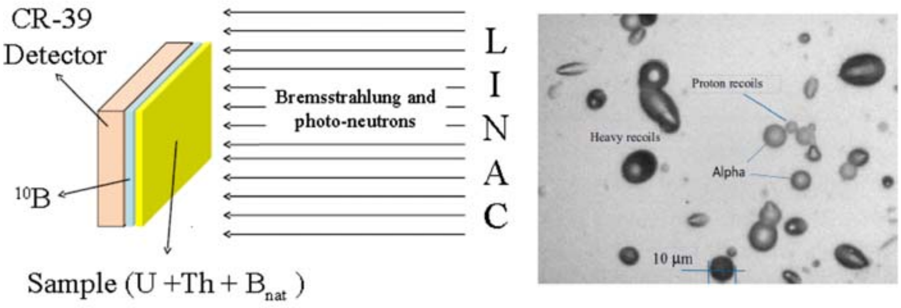

**Figure 15.13** Left: Geometry of the detector, $^{10}$B and target sample. Right: Micrograph of the etched tracks.

The set of sample detectors were employed in a sandwiched configuration of fertile/fissile material and $B_{nat}$ as shown in Fig. 15.13. The latter is included in the target material Th as $Th(NO_3)_4 \cdot 4H_2O$ and U as $UO_2(NO_3)_2 \cdot 6H_2O$ because it is expected that through the reaction ($\alpha$, $n$), more neutrons will be available to increase the neutron source strength (i.e., neutron economy).

The alpha spectrum of $^{232}$Th is mainly composed of two most important groups: 5.4210 MeV (71%) and 5.3385 MeV (28%). To observe neutron fluence for the assembled fuel-detector configurations, the passive detectors were covered by a thin $^{10}$B layer; so that nuclear tracks would be related only to neutrons coming from the target and counted through their alpha and proton fingerprint. When absorbing energetic charged particles, the detecting material registers a damaged region creating a so-called latent nuclear track. This track is then visualized by chemical development and microscopic examination. The PADC material was selected for its efficient recording properties for alpha particles and proton recoils, when these have impinging energy above the threshold values of 200 and 500 keV, respectively. Details of the assembled fuel samples (targets) are given in Table 15.9 and Fig. 15.13.

It is expected that energetic photons absorbed by the target compound release prompt and delayed neutrons. Additionally, natural boron ($B_{nat}$) absorbing alpha particles (from $^{232}$Th, $U_{nat}$) as mentioned, increase the neutron economy. All these neutrons to some extent will be detected by the PADC enhanced sensitivity due to the cover of boron-10 neutron-to-alpha particle converter (as it has a relatively high reaction cross-section of 3838 b for thermal neutron capture) and often is employed in neutron counting (Pino et al., 2014). Since the reaction cross-section values increases with the Fermi law (1/v), 3 cm thick paraffin is also used as moderator to enhance the material-detecting property. Passive detecting PADC material from Tastrack was available for this study supplied by the manufacturer (TASL, Track Analysis System Ltd, Napier House, Meadow Grove, Bristol BS11 9PJ, UK). We already mentioned the requirement for chemical treatment, the nuclear track methodology requires a solution 6N, NaOH at 70°C for 4–6 hours to make visible the latent track under a light transmission microscope. On completion detectors were analyzed employing a semiautomatic system following a well-established protocol (Pálfalvi and Sajó-Bohus, 2015). The system provides etched track density and size distribution in the form of an area histogram, from which fuel neutron production is determined.

### 15.5.4 Results and discussion

Results for detectors in Table 15.10 indicate that track densities, i.e., the number of neutrons, are comparable but their track size distributions are very different. This is explained by the target assembly efficiency to generate neutrons, which in fact depends on the fuel isotopic or whole target composition. In the first case with sample composition of Th + $B_{nat}$ the neutron production was 15% less in respect to U + $B_{nat}$; that is explained by the track density observed in relation to the ($\alpha$, $n$) reaction induced in $B_{nat}$. We have also studied the FC Th + $U_{nat}$ + $B_{nat}$. Analyzing

**Table 15.10** **Values employed to predict reaction rate per gamma flux unit expected in the nuclear track detectors**

| | Reaction | $\Sigma(\sigma \times \Phi)$ | Mass (g) +/− 0.1 mg | Number of nuclei | Detector number | Reaction rate in the detector (1/s) |
|---|---|---|---|---|---|---|
| $^{232}$Th | $(\gamma, fis)$ | 0.03673 | 0.2895 | $7.33 \times 10^{20}$ | 67 | $2.7 \times 10^{-5}$ |
| | | | 1.2464 | $3.15 \times 10^{21}$ | 70 | $1.2 \times 10^{-4}$ |
| | | | 0.8245 | $2.09 \times 10^{21}$ | 68 | $7.7 \times 10^{-5}$ |
| | | | 1.4520 | $3.67 \times 10^{21}$ | 71 | $1.3 \times 10^{-4}$ |
| | | | 1.8016 | $4.56 \times 10^{21}$ | 69 | $1.7 \times 10^{-4}$ |
| $U_{nat}$ | $(\gamma, fis)$ | 0.43959 | 0.7927 | $2.06 \times 10^{21}$ | 70 | $9.0 \times 10^{-4}$ |
| | | | 0.2937 | $7.62 \times 10^{20}$ | 68 | $3.4 \times 10^{-4}$ |
| | | | 1.2355 | $3.21 \times 10^{21}$ | 71 | $1.4 \times 10^{-3}$ |
| | | | 0.0522 | $1.35 \times 10^{20}$ | 66 | $6.0 \times 10^{-5}$ |
| | | | 0.5560 | $1.44 \times 10^{21}$ | 69 | $6.3 \times 10^{-4}$ |

the track density a larger number of low-energy neutrons were observed, confirming that uranium offers higher photofission neutrons. The study proves the usefulness of NTD sandwiched with natural or enriched to 98% boron by $^{10}$B and Th or U compounds, to study in a simple and economical way the photonuclear reactions produced by low-energy radiotherapy accelerators.

## 15.6 Conclusions

The concept of ADS is introduced briefly at first, and a typical application of an AMSB for fissile production is proposed, where molten salt is used as a proton beam target and blanket for fissile production. Assuming 80% load factor in AMSB, an annual net production rate of $^{233}$U is about 800 kg/year, which can be used to start one 1-GWe FUJI-MSR every 2 years.

Another application of MA incineration is described. The presented conception of the subcritical MSR-B is restricted only by the physical aspects of the MA-transmutation problem. It does not discuss the technological, economical, safety, etc. problems which require much more serious considerations in the framework of chosen strategy of the nuclear power development and its closing. In case all these problems can be overcome about 10 such reactor-burners would be enough to clean all the SF storages from MA in 50 years. The same number of $\sim$10 reactor-burners is enough to arrange the special cycle for the MA transmutation in CNFC of the nuclear power of about 200 GWe by fast reactor (FR) among total nuclear power generation of 500 GWe. The transmutation time, $\tau_{in}$, necessary for the burning of the equilibrium loading, $Q$, is short enough to fulfill this task during the reactor lifetime.

The reactor concept is based on a high dissolving ability of the actinide fluorides in the salt FLiNaK, which has recently been demonstrated in a series of pioneering experiments. Due to this phenomenon fast neutron spectrum is formed in the reactor, eliminating the need for additional feeding by fissile isotopes. In this case the fuel is transplutonium elements themselves.

This discovered ability of salt LiF-NaF-KF opens promising prospects for the creation of molten salt reactors not only for MA transmutation but for other purposes, similar to traditional solid-fuel reactors with a fast neutron spectrum.

Conclusions on low-energy linear ADS are as follows. Measurements carried out in a low-energy accelerator used for clinical applications with the employment of passive NTMs shows the production of neutrons in the accelerator tungsten target and the production of neutrons in thorium and uranium targets. These results demonstrate in principle the feasibility of the use of these accelerators for photodriven subcritical assemblies. Finally, in this study we demonstrate that the employments of passive NTMs are effective and economical means to ascertain fission rates and neutron production rates.

## Acknowledgments

The passive detectors supplied by Tasl (Bristol, U.K) are acknowledged as well as the LINAC accelerator time provided by Dr. J. E. Davila, and irradiation given by Lic. E. Salcedo; special thanks for the support given by the GURVE-Radiotherapy Clinic at Centro Medico Docente La Trinidad, Caracas, Venezuela. We also thank Dr Takashi Kamei for critical reading of and suggestions to the manuscript.

## References

Allen, P.D., Chaudhri, M.A., 1988. Photoneutron production in tissue during high energy bremsstrahlung radiotherapy. Phys. Med. Biol. 33 (9), 1017.

Barashenkov, V.S., Konobeyev, A.Yu, Korovin, Yu.A., Sosnin, V.N., 1999. Software package “CASCADE/INPE”. At. Energy 87 (4), 283.

Barrera, M.T., Barros, H., Pino, F., Dávila, J.E., Sajo-Bohus, L., 2015. Thermal and epithermal neutron fluence rate gradient measurements by PADC detectors in LINAC radiotherapy treatments-field. In: AIP Conf. Proc. 1671, 030002 (2015); <http://dx.doi.org/10.1063/1.4927191>.

Bell, G.I., Glasstone, S., 1970. Nuclear Reactor Theory. Van Nostrand Reinhold Inc, New York.

Benes, O., Konings, R., 2008. Actinide burner fuel: potential compositions based on thermodynamics evaluation of MF-PuF3 (M-Li, Na, K, Rb, Cs) and $LaF_3$-$PuF_3$ systems. J. Nucl. Mater. 377 (3), 449–457.

Bermudez, J., Pino, F., Greaves, E.D., Sajo-Bohus, L., 2016. Thorium target design for a AD-MSR. Thorium Energy for the World Book part VI, 289–295. <http://dx.doi.org/10.1007/978-3-319-26542-1_42> Print ISBN 978-3-319-26540-7 Online ISBN 978-3-319-26542-1 Publisher Springer International Publishing <http://thoriumenergyconference.org/Program>.

Bultman, J.H., 1995. Actinide Transmutation in Nuclear Reactors, Thesis Delft University of Technology.

NEA Nuclear Science Committee, 2000. Calculation of Different Transmutation Concepts. An International Benchmark Exercise.

Caldwell, J.T., Dowdy, E.J., Berman, B.L., Alvarez, R.A., Meyer, P., 1980. Giant resonance for the actinide nuclei: photoneutron and photofission cross sections for $^{235}U$, $^{236}U$, $^{238}U$ and $^{232}Th$. Phys. Rev. C. 21 (4), 1215−1231.

Carminati, F., Klapisch, R., Revol, J.P., Rubbia, C., Revol, J.P.C. 1993. An energy amplifier for cleaner and inexhaustible nuclear energy production driven by a particle beam accelerator, CERN/AT/93-47(ET).

Castillo, R., Dávila, J.E., Sajo-Bohus, L., 2014. Estimate of photoneutrons generated by 6−18 MV X-ray beams for radiotherapy techniques. X Latin American Symposium on Nuclear Physics and Applications (X LASNPA), 1−6 December 2013, Montevideo, Uruguay Proceeding of Science, PoS(X LASNPA) 067. <http://pos.sissa.it/archive/conferences/194/060/X%20LASNPA_067pdf>.

Cross Section Evaluation Working Group, 1991. ENDF/B VI Summary Documentation BNL-NCS-17541 (ENDF-201).

Degtyarev, A.M., Kalugin, A.K., Kolyaskin, O.E., et al., 2006. Cascade subcritical molten salt rector for transplutonium actinide inciniration. At. Energy 101 (2), 116−125.

Degtyarev, A.M., Myasnikov, A.A., Trofimova, T.E., 2012. Fuel composition stabilization in a subcritical liquid-salt transplutonium burner reactor. At. Energy 111 (6), 381−388.

Degtyarev, A.M., Myasnikov, A.A., Saltykova, O.N., et al., 2013a. Statistical control k(eff) for subcritical fused-salt transplutonium burner reactor. At. Energy 113 (4), 227−235.

Degtyarev, A.M., Karmanov, F.I., Myasnikov, A.A., et al., 2013b. Noise lag effect in transients of a subcritical molten salt transplutonium incinerator. At. Energy 114 (3), 149−156.

DOE, 2015. Meeting. Isotope needs and capturing opportunities for the future: the 2015 long range plan for the DOE-NP isotope program. NSAC Isotopes Subcommittee July 20.

Espinosa, G., Golzarri, J.I., Raya-Arredondo, R., Cruz-Galindo, S., Sajo-Bohus, L., 2015. Neutron detection of the Triga Mark III reactor, using nuclear track methodology. In: AIP Conf. Proc. 1671, 020005; <http://dx.doi.org/10.1063/1.4927182>.

Furukawa, K., Tsukada, K., Nakahara, Y., 1981. Single-fluid-type accelerator molten-salt breeder concept. J. Nucl. Sci. Technol. 18 (1), 79−81.

Furukawa, K., Arakawa, K., Erbay, L.B., Ito, Y., Kato, Y., Kiyavitskaya, H., et al., 2008. A road map for the realization of global-scale thorium breeding fuel cycle by single molten-fluoride flow. Energy Convers. Manage. 49, 1832−1847.

Gulevich, A., Kalugin, A., Ponomarev, L., et al., 2008. Comparative study of ADS for minor actinides transmutation. Prog. Nucl. Energy 50 (2−6), 359−362.

Gulevich A., Kalugin A., Ponomarev L., et al., 2009. Comparative study of ADS for minor actinides transmutation. In: Proc. GLOBAL-2009. Paris, 6−11 September 2009, pp. 1843−1846.

Harms, A.A., Heindler, M., 1982. Nuclear Energy Synergetics - An Introduction to Conceptual Models of Integrated Nuclear Energy Systems. Plenum Press, New York.

IAEA, 2015. Status of accelerator driven systems research and technology development. TECDOC-1766.

Ignatiev, V., Feynberg, O., Surenkov, A., et al., 2012a. Progress in development of MOSART concept with Th support. In: International Congress on Advances in Nuclear Power Plants 2012, ICAPP 2012, 2, pp. 943−952.

Ignatiev, V., Feinberg, O., Zagnitko, A., et al., 2012b. Molten-salt reactors: new possibilities, problems and solutions. At. Energy 112 (3), 157−165.

Ignatiev, V., Feinberg, O., Zagnitko, A., et al., 2014. Molten salt actinide recycler & transforming system without and with Th-U support: fuel cycle flexibility and key material properties. Ann. Nucl. Energy 64, 408−420, Special Issue on MSR and FHR.

Lewis, W.B., 1952 The Significance of the yield of neutrons from heavy elements excited to high energies. AECL-968.

Lizin, A.A., Tomilin, S.V., Gnevashov, O.E., Gazizov, R.K., Osipenko, A.G., Kormilitsyn, M.V., et al., 2013a. Solubility of $PuF_3$, $AmF_3$, $CeF_3$ and $NdF_3$ in the molten salt LiF−NaF−KF. At. Energy 115 (1), 11−16.

Lizin, A.A., Tomilin, S.V., Gnevashov, O.E., Gazizov, R.K., Osipenko, A.G., Kormilitsyn, M.V., et al., 2013b. $UF_4$ and $ThF_4$ solubility in molten salt LiF−NaF−KF. At. Energy 115 (1), 20−22.

MCNP, 1997. A general Monte Carlo *N*−Particle Transport Code. Version 4B. LA-12625-M.

McPherson, H.G., 1985. The molten salt reactor adventure. Nucl. Sci. Eng. 90, 374−380.

Haubenrich, P., Engel, J., 1970. Experience with the molten-salt reactor experiment. Nucl. Appl. Technol. 8, 118−136.

Merle-Lucotte, E., Mathieu, L., Heuer, D., 2004. Molten salt reactors and possible scenarios for future nuclear power deployment. In: American Nuclear Society (Ed.), Proceedings of the Physor 2004 Conference, The Physics of Fuel Cycles and Advanced Nuclear Systems: Global Developments, pp. 1−12.

Merle-Lucotte, E., Heuer, D., Le Brun, C., 2006. Fast thorium molten salt reactors started with plutonium. In: Proceedings of the International Congress on Advances in Nuclear Power Plants (ICAPP), Reno, USA.

ORIGEN 2.1, 1996. Isotope generation and depletion code. ORNL, CCC-371.

Pálfalvi, J., Sajó-Bohus, L., 2015. Cosmic Radiation Detection by Solid State Nuclear Track Detector Technique. Solid State Phenom. 238, 16−54, Trans Tech Publications, Switzerland, http://dx.doi.org/10.4028/www.scientific.net/SSP.238.16.

Pálfalvi, J.K., Sajó-Bohus, L., Balaskó, M., Balásházy, I., 2001. Neutron field mapping and dosimetry by CR-39 for radiography and other applications. Radiat. Meas. 34 (1−6), 471−475.

Pino, F., Stevanato, L., Cester, D., Nebbia, G., Sajo-Bohus, L., Viesti, G., 2014. Detecting fast and thermal neutrons with the boron loaded liquid, EJ-339A. Appl. Radiat. Isot. 92, 6−11.

Ponomarev, L.I., Seregin, M.B., Parshin, A.P., Mel'nikov, S.A., Mikhalichenko, A.A., Zagorets, L.P., et al., 2013. Fuel salt for the molten salt reactor. At. Energy. 115 (1), 6−11.

Rubbia, C., Rubio, J.A., Buono, S., 1993. Nuclear energy production driven by a particle beam accelerator, CERN/AT/93-47 (ET).

Sajo-Bohus, L., Vega-Carrillo, H.V., Virk, H.S., 2015a. SSNTD technique in photoneutron applications. Solid State Phenom. 239, 180−214, Trans Tech Publications, Switzerland, http://dx.doi.org/10.4028/www.scientific.net/SSP.239.180.

Sajo-Bohus, L., Greaves, E.D., Davila, J.E., Barros, H., Pino, F., Barrera, M.T., et al., 2015b. Th and U fuel photofission study by NTD for AD-MSR subcritical assembly. In: AIP Conf. Proc. 1671, 020009. <http://dx.doi.org/10.1063/1>.

Serp, J., Allibert, M., Beneš, O., Delpech, S., 2013. The molten salt reactor in generation IV: overview and perspectives. Prog. Nucl. Energy 77, 308−319.

Spent fuel reprocessing options, 2008. IAEA-TECDOC-1587.

Takizuka, T., 1997. JAERI and PNC - OMEGA project (Japan), IAEA-TECDOC-985.

Van Lawe, C., David, J.C., Doré, D., Giacri-Mauborgne, M.L., Ridikas, D., Laborie, J.M., et al., 2006. Photofission of 232Th and 238U with Bremsstrahlung Photons below

20 MeV: Measurements and Model Predictions of Delayed Neutron Yields and Spectra. Electronic Version from a server July 2006. (accessed june 2016). <http://inspirehep.net/record/736301?ln = en>.

Vasil'kov, V.G., Gol'danskii, V.I., Dzhelepov, V.P., Dmitrievskii, V.P., 1970. The electronuclear method of generating *Neutrons* and producing fissionable materials. At. Energy 29 (3), 151–158.

Volozhin, N.V., Zakirov, R.Ya, Mushnikov, P.N., et al., 2013. Solubility of cerium and plutonium threefluorides in the molten salt LiF–NaF–KF. At. Energy 115 (1), 17–19.

Weinberg, A.M., Wigner, E.P., 1959. The Physical Theory of Neutron Chain Reactors. The University of Chicago Press, Chicago.

Yoshioka, R., 2013. Nuclear energy based on thorium molten salt, Chapter-23. In: Lantelme, F., Groult, H. (Eds.), Molten Salts Chemistry: From Lab to Applications. Elsevier Inc., USA.

Yurevich, V.I., Yakovlev, R.M., Vassilkov, R.G., et al., 2006. Production and multiplication of neutrons in lead targets induced by protons above 1 GeV. Nucl. Instr. Meth. A562, 747–749.

# Fusion–fission hybrids

## 16

*Evgeny P. Velikhov*
Kurchatov Institute, Moscow, Russia

### Chapter Outline

## 16.1 Energy needs

World economic development correlates clearly with increasing energy consumption. At present, world consumption is almost 13 billion tons of oil equivalent annually. Taking into account continuing population growth of about 1.5% and world economic growth of about 3%–4% annually, primary energy consumption increases about 1% annually. Use of fossil fuels, such as oil, natural gas, and coal, is increasing. The ecological problems of greenhouse gas and pollution emission occur together with the use of fossil fuels. The recent Congress on climate problems in Paris has confirmed this once more. The world is showing concern over the growth of average temperature on the planet. It needs to stimulate actions to limit temperature growth within 2°C of the preindustrial era value (~1900). Just these facts, along with natural resource limitations and the high cost of developing new deposits are enough to require new energy sources. Technologies with high-energy potential and minimal negative environment impact are nuclear fission energy and thermonuclear energy.

The desire to develop energy technologies is not only an attractive direction that responds to global interests, but also an opportunity to create high environmental quality energy sources. Such growth may change industrial, social, and economic structure by developing human potential for living well in the high-technology world. It can provide sustainable development and long-term prosperity, and the dominant role of fossil fuels will diminish.

At present the growth of the world economy is predominantly in developing countries. By the end of the 21st century consumption per capita will gradually tend towards equality. The population of developing countries is about five times more than that of developed countries, and present consumption per capita is 4–5 times less than that of developed countries. Levelling of primary energy

**Molten Salt Reactors and Thorium Energy. DOI: http://dx.doi.org/10.1016/B978-0-08-101126-3.00016-6**

consumption per capita can be expected under the influence of globalization processes. This means that primary energy consumptions will increase at least 3–5 times by the end of the 21st century, even accounting for significant energy conservation measures. Different forecasts of almost all analytical centers of the world (Intergovernmental Panel on Climate Change, International Energy Agency, etc.) estimated growth of world energy consumption by 2100 confirm this prediction.

It is clear that such scales of energy consumption, regardless of primary energy source, will lead to an unacceptably profound influence on the Earth's atmosphere and climate. Taking into account population growth, energy consumption growth, and ecological problems, the development of new energy sources is one of the most important tasks of our current civilization. The odds-on favorite is nuclear energy, which provides great potential for reliable power and environmental quality. The resource base of nuclear energy at acceptable prices (16 Mton U-235) is equal to 120 billion tons of oil, and it is not enough for long-term large-scale industry operation. Nearly unlimited resources can be attained with a closed fuel cycle using U-238 and Th-232 to breed Pu-239 and U-233, which can be hundreds of times more plentiful than U-235, which is currently used. The resources of U-238 and Th-232 are enough to last for thousands of years. These technological innovations should be realized in a way to minimize radioactive pollution of the environment.

## 16.2 Fast breeder reactors

Traditionally a part of the nuclear community thinks that large-scale nuclear energy development is connected with fast reactor development and the uranium–plutonium fuel cycle. This scenario means that in the long-term perspective the system will include mostly fast reactors, with very few thermal reactors. Let BR be the breeding ratio in a fast reactor. Each nucleus of Pu-239 fissioned in the fast reactor will be converted $BR > 1$ of new Pu-239 from U-238. One new fissile nucleus must be returned back to the reactor for its further operation. Thus, there will remain BR-1 nuclei to use in thermal reactors. Burning these new nuclei in thermal reactor energy (BR-1)*200 MeV will be generated, and in a fast reactor to produce these nuclei energy of 200 MeV was generated. Consequently, in the nuclear energy system the ratio of thermal reactors to fast reactors will be (BR-1). Using present fast reactor designs, $BR \leq 1.2$, the fraction of thermal reactors cannot exceed 20%. In practice, fast reactors are more expensive than thermal reactors, and their operation must be stable, base-load power without unscheduled shutdowns.

Of course, such development of nuclear energy is possible, but only if it is optimal and uncontested. Meanwhile, only thermal reactors are constructed worldwide and fast reactor deployment is delayed until the middle of the century, when nuclear energy will be more expensive, if it all possible.

There is one more serious troublesome aspect to fast reactors. To use newly developed fissile isotopes, spent fuel must be reprocessed as soon as possible, much faster than present reprocessing of spent fuel from light-water reactors (LWRs).

At present fuel is reprocessed after 5−7 years of service, when burnup is ~ 4%. Keeping fuel out of the closed fuel cycle a long time leads to a long delay of a large amount of plutonium, which will adversely affect the reactor deployment rate. For this reason, we usually focus on fuel staying out of recycling not longer than 3 years, and burnup ~ 10%. Such recycling technology, with the required safety guarantee, is not yet accomplished. If fuel is recycled after a short decay, then its activity will be very high, and this obviously increases the risk of pollution and significantly raises the price of the process.

## 16.3 Fusion−fission hybrids

Taking into account the difficulties of nuclear energy development based on fast breeder reactors, it is worthwhile to consider other ways of development that can provide abundant fuel for large-scale nuclear energy deployment. It would also be beneficial to reduce the associated radioactive waste disposal burden.

The most attractive perspective is to generate energy in thermonuclear fusion reactors. Fusion is an almost ideal system, but construction of an economically attractive fusion power plant may be delayed until the distant future.

Near-term fusion reactors with lower energy gain can be used to breed fissile fuel by placing U or Th in the blanket, called a fusion−fission hybrid. The blanket breeds fissile isotopes and produces additional power from fission reactions. The thermonuclear reactor in this case is a neutron source for the blanket reactions. Such a hybrid system is like a typical fission reactor with an external neutron source, and it is a self-sufficient energy system. An uncontrolled supercritical chain reaction can be prevented by keeping the neutron multiplication factor well below unity.

In nuclear fission reactors the greatest danger is fuel rods' loss of cooling. Residual energy release fission product decay was dominant in the most serious emergencies, such as the Three Mile Island, Chernobyl, and Fukushima accidents. During loss of cooling fuel heating happens fast. The temperature of spent fuel and construction materials increases, and the clad may fail, releasing radioactivity. Thus, considering these safety issues, it is difficult to find strong arguments in favor of putting a fission blanket around a fusion reactor. The main advantage of low radioactive waste is lost.

An alternative strategy is to minimize fission in the blanket while maximizing fissile breeding, called a "fission-suppressed" blanket. The bred fissile isotopes are quickly removed from the blanket and processed to provide fuel for satellite fission reactors. A special fuel composition facilitates rapid removal and processing.

## 16.4 Thorium fuel cycle

Neutrons from the core of the thermonuclear reactor are used as a high-intensity external neutron source. To remove the disadvantages associated with fission in the hybrid blanket, a special fuel composition using molten salt including thorium halides is used. This facilitates continuous processing of a side stream of blanket salt for removal of accumulated fissile isotopes and fission products.

A molten salt hybrid reactor can clean the salt continuously, so the fission product content can be kept low, with half as much leakage of radioactivity per gram of coolant than other means of fissile fuel breeding. Thorium irradiated by neutrons breeds U-233 by the following reaction chain:

Th-232 + n→Th-233 (β-, 22,3 min) →Pa-233 (β-, 27 days) →U-233,

In the thorium fuel cycle the energy lost in production of one U-233 nucleus is about 25 MeV, much less than the 43 MeV lost in generating one Pu-239 nucleus in the U-Pu fuel cycle. The fast fission cross-section of Th-232 is only about half that of U-238, so the thorium fuel cycle generates fewer fission products in the blanket.

Using Pu-239 as a fissile isotope in thermal reactors is not desirable. Plutonium has quite a large capture cross-section in thermal energy range, which leads to neutron production decreasing to 1.8 neutrons per capture in comparison with U-235, which produces about 2.05 neutrons per capture. This affects fuel breeding in the thermal reactor, which will decrease approximately for 0.2 units. For VVER (Vodo-Vodyanoi Energetichesky Reaktors or Water-Water Power Reactors) reactors using U-235 BR $\sim$ 0.6, so switching to Pu-239 makes BR $\sim$ 0.4. And then to provide new fuel for this reactor, larger fissile isotope provision will be required.

Quite the contrary, using U-233 in thermal reactors is highly desirable. In a thermal spectrum the breeding ability of 233-U is better than 235-U by 0.2 units, and BR $\sim$ 0.8. Only about 20% of the annual fissile fuel needs must be supplied externally.

Approximately 1 ton of 235-U annually burns in 1 GWt reactor, and the quantity of 233-U or 239-Pu will be approximately the same. If BR = 0.8 provides 800 kg annually, the external system should provide just 200 kg of 233-U to sustain the fuel cycle.

## 16.5 Nuclear energy system

A fusion neutron source power of 1 GWt annually could breed about 3000 kg of new fissile isotope. I.V. Kurchatov made the same assessment on new fuel accumulation in the blanket of a thermonuclear reactor long ago. Under this assessment, one thermonuclear reactor is able to provide fuel to more than 15 thermal reactors. Thus, only about 7% of the power system needs to be fusion power. Replacement of fast reactors by fusion reactors for fissile fuel production has a number of advantages.

First, it will not be necessary to replace thermal reactors and their pervasive infrastructure with fast reactors. The system with fusion−fission hybrids supporting thermal reactors can become more viable than fast breeder reactors.

Second, potential radiation leakage during spent fuel recycling will be reduced. Used fuel with high burnup is very hot, and it needs to cool for several years before reprocessing, but fast reactor irradiated fuel is supposed to be recycled after 1 or 2 years to extract bred Pu-239. During chemical reprocessing all fission products and actinides will be released from the fuel pins, and it will take extensive precautions to prevent their escape. Fission products must be extracted and disposed of, and fissile isotopes must be cleared of chemically similar minor actinides and lanthanides.

Continuous reprocessing of the molten salt composition minimizes the radiation released. The removal of fission products reduces the energy released in the blanket. During loss of cooling the blanket integrity is significantly easier to preserve, preventing uncontrolled leakage of radioactive isotopes.

Another important question is the use of heterogeneous fuel assemblies in nuclear cores: one set of fuel rods with fertile isotopes, and one set with concentrated fissile isotopes. Most of the fissions occur in the fissile rods, so the energy release and fission products will be concentrated there. In modern VVER reactors the fuel burnup of 235-U is about 80% and this value can be increased to about 90%. In the future there will be no need to recycle these rods, and they will be buried with highly active fission products. Only fuel rods with fertile isotopes should be recycled to extract bred U-233 and Pu-239. Energy release in these rods will be approximately a factor of 10 lower than in rods with fissile isotopes. Consequently, the radioactivity released during their recycling will be a tenth of total activity.

Fusion–fission hybrid reactors to breed fissile fuels can be developed quickly. In the initial stage the fusion neutron source is not required to have a high Q value (ratio of fusion energy to input energy) for the fuel production to become economically feasible. The fusion neutron source can be gradually improved towards a pure fusion power plant. Radiation loads on the first wall of the fusion reactor will be high, and its maintenance can be time-consuming.

The concept presented here does not exclude fast reactors. If their cost and quality will be more attractive than thermal reactors, then there are no limitations of their development.

The main advantages of a closed fuel cycle using fusion–fission hybrid reactors and the thorium-U-233 fuel cycle are as follows:

1. There are no rigid requirements about the ratio of fast reactors to thermal reactors in a nuclear energy system with a closed fuel cycle.
2. There are no rigid requirements on the speed of spent fuel reprocessing.
3. One possible mode uses direct burial of spent fuel with high burnup ($> 90\%$).
4. The total radioactivity from spent fuel during its reprocessing will be at least a factor of 10 less than in the scenario of fast reactor development.
5. The present nuclear system oriented to thermal reactors is consistent with the hybrid scenario, and thermal reactors can evolve to use the thorium fuel cycle.
6. Fast reactors will develop according to their cost and quality relative to thermal reactors.

## 16.6 Actinide incineration

“The hybrid blanket can be kept subcritical at all times, in contrast to a fast fission reactor, where reactivity control is a safety issue. The harder neutron spectra from a

14 MeV neutron source means that more neutrons will cause fission, destroying the actinides (desirable), and fewer will be captured, producing higher atomic number transuranics (undesirable). Actinide wastes could be processed out of spent fuel and then be put in a fusion blanket in suitable form for incineration (fissioning). The revenues would come from both electrical power sales and waste disposal." (Moir and Manheimer, 2014).

Cheng (2005) has studied a blanket design that incinerates separated transuranics from used LWR fuel. In the "hard spectra" case there is only molten salt with the dissolved actinides; and in the "soft spectra" case 50% of the volume is taken up by beryllium that multiplies and moderates the neutrons. Chemical attack of the beryllium by the molten salt would be prevented by separate zones or by cladding.

Table 16.1 shows the results when steady state is achieved. $F$ = number of atoms fissioned per 14 MeV neutron incident on the blanket; $k_{\text{eff}}$ = effective neutron multiplier.

The low $k_{\text{eff}}$ values would keep the blanket far below criticality. One hybrid reactor could incinerate about 1 tonne of actinides per year.

The molten salt could generate copious energy while incinerating weapons materials and nuclear "waste." Only about 5% as much repository space would be needed, compared with LWRs (Moses et al., 2009).

**Table 16.1** **Neutron sources and sinks for molten salt example (Cheng, 2005)**

| **Average burn, soft spectra, $M = 13$, $F = 0.83$, $k_{\text{eff}} = 0.6$** | | | |
|---|---|---|---|
| **Sources** | | **Sinks** | |
| D-T | 1 | $(n,\gamma)$ | 1.08 |
| $(n,f)$ | 2.16 | $(n,f)$ | 0.83 |
| $(n,2n$ etc.) | 0.2 | $^{6}\text{Li}(n,\alpha)\text{T}$ | 1.1 |
| | | Captures | 0.3 |
| | | Leakage | 0.05 |
| Total | 3.36 | Total | 3.36 |
| **Hard spectra, $M = 8.6$, $F = 0.51$, $k_{\text{eff}} = 0.56$** | | | |
| **Sources** | | **Sinks** | |
| D-T | 1 | $(n,\gamma)$ | 0.57 |
| $(n,f)$ | 1.33 | $(n,f)$ | 0.51 |
| $(n,2n$ etc.) | 0.2 | $^{6}\text{Li}(n,\alpha)\text{T}$ | 1.1 |
| | | Captures | 0.3 |
| | | Leakage | 0.05 |
| Total | 2.53 | Total | 2.53 |

## 16.7 Molten salt hybrid tokamak

Russia is developing Molten Salt Hybrid Tokamak (MSHT) reactors to eliminate five vital risks:

1. *Severe accidents* could be eliminated by keeping the fusion reactor blanket subcritical; by removing fission products continuously from the circulating molten salt; and by avoiding mechanical energy sources (high pressure) and chemical energy sources (Zr, Na, H).
2. *Theft* of weapons-grade fissile materials could be prevented by using only self-protected fuel and by ceasing isotopic enrichment.
3. Risks of transuranium *wastes* and long-lived fission products can be avoided by using nonenriched uranium; by separating fission products from used fuel; by incineration of actinides in reactors instead of separating them; and by partial transmutation of highly toxic long-lived fission products in MSHT.
4. Vital risks of *investment* loss can be reduced, shortening construction time by using factory-made precision modules, simpler reactor safety methods (such as passive safety), and cheaper fuel inventories.
5. The vital risk of rapid exhaustion of *fuel resources* would be eliminated by deployment of MSHT. Fuel self-supply and the growth of nuclear power plant parks would be facilitated by positive breeding gain of fissile materials. Such a nuclear power could start almost "from zero level" when the first fuel inventory of a Vital Risk Free Reactor would be available.

Deployment of MSHT power plants could eliminate all five vital risks and facilitate a renaissance of the nuclear industry (Velikhov, 2012).

## References

Cheng, E.T., 2005. Performance characteristics of actinide-burning fusion power plants. Fusion Sci. Technol. 47, 1219−1223.

Moir, R.W., Manheimer, W., 2014. Fusion-fission hybrids. In: Dolan, T.J. (Ed.), Magnetic Fusion Technology, Chapter 14. Springer, London.

Moses, E.I., et al., 2009. A sustainable nuclear fuel cycle based on laser inertial fusion energy. Fusion Sci. Technol. 56, 548−565.

Velikhov, E.P., 2012. Future Development of Nuclear Power and Role of Fusion Neutron Source−Green Nuclear Power. NRC Kurchatov Institute, Moscow, downloaded from ITER Newsline #248, 03 December 2012.

# Thorium molten salt reactor nuclear energy system (TMSR)

# 17

*Zhimin Dai*
Shanghai Institute of Applied Physics (SINAP), Shanghai, China

## Chapter Outline

## 17.1 Introduction

Fissionable nuclear fuel can be divided into two categories, i.e., uranium-based and thorium-based. Currently, fuels of the entire nuclear power industry are all uranium-based. Because of the rapid growth of energy demand, together with the abundant global reserves of thorium, the utilization of thorium-based fuel has become increasingly prominent.

The thorium molten salt reactor (TMSR) nuclear energy system is designed for thorium-based nuclear energy utilization and hybrid nuclear energy application based on the liquid-fueled thorium molten salt reactor (TMSR-LF) and solid-fueled thorium salt reactor (TMSR-SF) in coming 20 years.

The TMSR-LF, in which the fuel is dissolved within the salt, is designed for thorium-based nuclear energy utilization with online refueling and online/offline reprocessing capability. The TMSR-SF, which uses the TRISO-type nuclear fuel, is optimized for a high-temperature-based hybrid nuclear energy application.

As Fig. 17.1 shows, TMSR has characteristics and applications including thorium energy utilization, hydrogen production, water-free cooling, and small modular design. Moreover, TMSR has advantages in economics, safety, sustainability, and nonproliferation. Commercialized TMSR is very feasible under current technology conditions.

**Molten Salt Reactors and Thorium Energy. DOI: http://dx.doi.org/10.1016/B978-0-08-101126-3.00017-8**

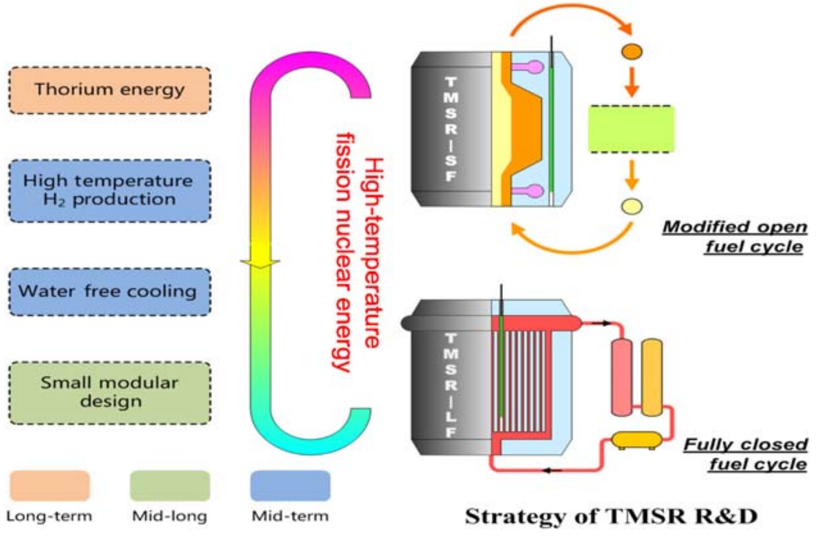

**Figure 17.1** Purpose and scope of TMSR.

**Table 17.1 The main features of TMSR-LF (single unit)**

| | |
|---|---|
| Electrical capacity (MWe) | 168 |
| Thermal capacity (MWt) | 395 |
| Inlet/outlet temperatures of primary loop | 600/700°C |
| Fuel salt (salt of primary loop) | LiF-BeF$_2$-UF$_4$-ThF$_4$ |
| Salt of second loop | FNaBe |
| Moderator | Graphite |
| Structural material | Nickel-based alloy or surface-treated stainless steel |
| Main vessel size (D × H) (m) | 5.2 × 6.0 |
| Processing for fuel cycle | Online degassing (Xe, He, T), offline removing solid fission products |
| Residual heat removal | Passive residual heat removal system |
| Generator system | Open air Brayton cycle and Rankine cycle |

## 17.2 TMSR-LF

TMSR-LF is a small modular liquid-fueled thorium molten salt reactor with electrical power of 168 MWe. Its main features are listed in Table 17.1. Mature technologies adopted in its design promote feasibility facilitate rapid deployment and construction in the near future.

### 17.2.1 *Design overview of TMSR-LF*

TMSR-LF is designed with electrical power of 168 MWe for a single unit. It can be scaled up for different power requirements, i.e., one unit, two units, six units

(GWe level). It consists of three loops, which are the primary loop with fuel salt, a second loop for radioactivity isolation, and a third loop for energy utilization.

LiF-BeF$_2$-UF$_4$-ThF$_4$ is used as fuel salt and also carrier salt of the primary loop of TMSR-LF, in which the abundance of Li-7 is 99.995% and the abundance of U-235 is 19.75%, and FNaBe is taken as salt of the second loop.

The inlet temperature and outlet temperature of the TMSR-LF primary loop are 600°C and 700°C, respectively. Due to its high temperature output, the open air Brayton cycle and Rankine cycle combined system is used for TMSR-LF power generation, and the thermoelectric conversion efficiency could be more than 45%.

An online refueling system is designed for TMSR-LF. The excess reactivity can be kept at a low level because of online refueling. An online off-gas system is also design for TMSR-LF, which can remove gaseous fission products online, including Xe, He, and T. Thus, the neutron efficiency can be improved, while the requirements of the reactivity control system can be reduced.

A passive residual heat removal system is designed to remove the heat during accidents at the TMSR-LF. A passive fuel salt discharging system with a freezing valve is designed to shut down and remove heat in extreme accidents.

The plant of TMSR-LF is separated into a nuclear island, a conventional island, and a service region. The nuclear island is placed underground to improve safety. The conventional island is located close to the nuclear island and the cooling towers are located close to the turbine-generators to minimize the heat transfer distances. The buildings of potential auxiliary applications, such as hydrogen production and seawater desalination, are also located in the conventional island. The administration building, the plant services building, and the training buildings are located in the service region and near the entrance of the plant. The layout of TMSR-LF nuclear island and reactor body is shown in Fig. 17.2.

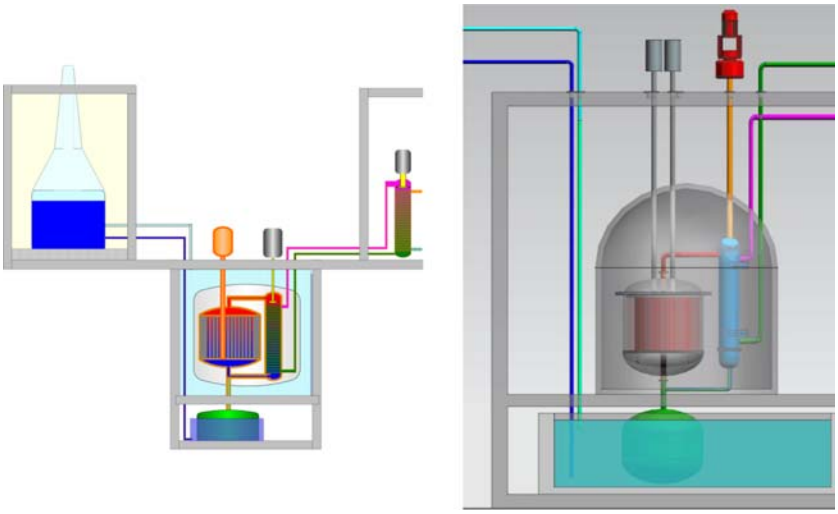

**Figure 17.2** Layout of TMSR-LF nuclear island and reactor body.

TMSR-LF adopts a modular design, in which the lifetime of the reactor body module is about 5 years. Installation and replacement of each module is simple, and it is easy to maintain. As shown in Fig. 17.2, the reactor vessel and primary circuit (pump and the main heat exchanger) are both located inside a steel containment, which is a safety barrier. Also, the gas layer between the containment and reactor vessel can be used for tritium removal.

### 17.2.2 Safety features of TMSR-LF

Compared to the third-generation reactors, TMSR-LF meets high level safety standards, including intrinsic safety and the ability to contain radioactivity.

TMSR-LF is intrinsically safe, which is shown in the following aspects. It operates at near atmospheric pressure, so the reactor vessel and the loops used in TMSR-LF need only low-pressure resistance. The fuel salt has higher boiling temperature (as high as 1400°C) and higher volumetric heat capacity compared to other typical coolants. Therefore, the fuel salt can absorb large amounts of heat in accidents, which will slow the progression of accidents. It is operated with negative coolant temperature reactivity coefficient, and low excessive reactivity due to the online refueling.

The safety system of TMSR-LF includes: passive residual heat removal system to cool the reactor core during an emergency, and a passive system to discharge the fuel salt to the drain tank at high temperature, which would shut down the reactor directly.

TMSR-LF has a good ability for radioactivity retention. Some accidents can be avoided, such as large break loss of coolant accident (LBLOCA), etc. Most radioactive nuclides, such as Cs-137, I-131, and Sr-90, are soluble in the salt which prevents the leaking of radioactivity to the environment. The reactor vessel and containment are used to prevent radioactivity leakage. Underground construction is adopted to prevent leaking of radioactivity, resist natural disasters, and terrorist attacks.

### 17.2.3 Advanced Th-U fuel cycle based on TMSR-LF

The Th-U fuel cycle has several advantages compared to the U-Pu fuel cycle:

1. The thermal capture cross-section of Th-232 (7.4 barns) is about three times higher than U-238 (2.7 barns) while that of U-233 (45.76 barns) is much smaller than that of Pu-239 (268 barns). It means that U-233 has higher production and lower consumption compared with Pu-239 in thermal reactors. With the effective fission neutron number higher than 2 in the whole spectrum region, U-233 can be bred in both thermal and fast reactors. In addition, the long-lived minor actinide (MA) resulting from fission is much lower in the Th-U fuel cycle compared with the U-Pu fuel cycle. Therefore, U-233 has better neutron economy than Pu-239 in the thermal neutron energy region and the Th-U fuel cycle is the only one that can breed in thermal reactors with significantly reduced fissile inventory.
2. There is a benefit from the very low actinide production; the Th-U fuel cycle is also very attractive in fast reactors compared with the U-Pu fuel cycle, which breeds too much MA. In fast reactors, compared with Pu-239 the $\eta$ (the number of fission neutrons produced per

absorption) of U-233 is lower, so the breeding ratio of Th-U is lower than in the U-Pu cycle. However, Th-U fuel cycle is the best choice for trans-uranium (TRU) incineration in fast reactors. The breeding of U-233 and TRU incineration can be achieved in the same reactor simultaneously.

3. As one of the six Gen-IV reactor candidates the liquid-fueled thorium molten salt reactor (MSR-LF) is a class of liquid fuel reactors, in which nuclear fuel is dissolved in molten fluoride used as the primary coolant. Pyro-reprocessing can be applied in the MSR-LF system to separate isotopes simultaneously, so that online reprocessing and breeding of nuclear fuel can be achieved. Such a scenario is particularly suitable for the use of thorium fuel.

TMSR-LF is the optimal choice for the Th-U fuel cycle. The goal of TMSR-LF is to improve thorium resource utilization, minimize nuclear waste, promote nuclear nonproliferationn and finally realize a fully closed Th-U fuel cycle. The advanced Th-U fuel cycle system consists of a molten salt reactor, online degassing (Xe, He, T), an online/offline fuel processing system, and a fuel salt preparation and reconstruction system.

Continuously removing gaseous FPs and online refueling are implemented. After several years' operation, the whole core fuel salt is discharged, offline U&Th recycling is made for the discharged fuel salt, and finally the recycled fuel salt is reloaded to core for operation. In the processing, FP&MA are kept for interim storage and only U&Th are recycled.

1. In the first phase this fuel cycle uses LEU + Th as fuel loading, and then it gradually transforms to the Th cycle. In the future, the system would use U-233 + Th as standard fuel.
2. In the second phase online gaseous FP extraction and online U extraction and reinjection will be adopted for continuously recycling of U and enhancing the fuel utilization ratio. At the same time, offline batch processing and recycling residual U and Th will also be implemented. In the processing FP & MA are also kept for interim storage.
3. In the third phase, the fully closed fuel cycle will use online gaseous FP extraction, online U extraction and reinjection as in the second step above. However, offline TRU separation and reinjection are implemented in this step. In this processing, all heavy elements are recycled, and only FPs and a small amount of U and MA loss need geologic disposal. The fully closed fuel cycle can have three different recycle optional modes: burners, breeders, and break-even.

## 17.3 TMSR-SF

TMSR-SF is a small modular solid-fueled thorium molten salt reactor with electrical power of 168 MWe, with the main features as listed in Table 17.2. Mature technologies adopted in its design promote feasibility, which facilitates rapid deployment and construction in the near future.

### *17.3.1 Design overview of TMSR-SF*

The TMSR-SF is a small modular fluoride salt-cooled high-temperature reactor (FHR) with electrical power of 168 MWe. TRISO fuel particles, like those of

Table 17.2 **The main features of TMSR-SF (single unit)**

| | |
|---|---|
| Electrical capacity (MWe) | 168 |
| Thermal capacity (MWt) | 395 |
| Inlet/outlet temperatures of primary loop | 600/700°C |
| Salt of primary loop | LiF-BeF2 |
| Salt of second loop | FNaBe |
| Moderator | Graphite |
| Structural material | Nickel-based alloy or surface-treated stainless steel |
| Main vessel size (D × H) (m) | 3.8 × 12 |
| Residual heat removal | Passive residual heat removal system |
| Generator system | Open air Brayton cycle and Rankine cycle |

a high-temperature gas-cooled reactor, cooled by molten salt, with a passive natural circulation heat removal system can achieve high-temperature output and inherent safety under near-ambient pressure. The reactor adopts a simplified modular design, online refueling strategy, and water-free cooling to expand its applications in different conditions.

The major nuclear heat supply system of TMSR-SF consists of a pebble-bed core, reactor internals, a reactivity control system, a fuel handling system, a coolant system, and a passive decay heat removal system. During normal operation, energy is produced by fuel pebbles in core, then transferred to the primary loop and secondary salt loop using forced circulation. Salt-air heat exchangers are employed to translate nuclear heat to an open air Brayton cycle system and Rankine cycle. A fully passive residual heat removal system is utilized for emergency conditions.

The active core region of TMSR-SF is constructed with graphite internals enclosing a top cone, a bottom cone and a middle cylindrical zone. The reactor core size is finely optimized to match transportation demand by railway and highway for the modular design. The active region is 250-cm diameter and 420-cm-equivalent height. The graphite reflector is a cylinder with 350-cm outer-diameter and 650-cm height. An online fuel handing system is employed to achieve high discharge burnup, high loading factor, and automated fuel management. Discharge fuel burnup is about 180 GWd/tonHM.

The TMSR-SF fuel pebbles are 30-mm diameter, spherical fuel elements with tristructural isotropic (TRISO)-coated particles dispersed in the graphite matrix. Each pebble contains about 2400 microfuel particles with 500-μm uranium kernels (19.75% enriched uranium). When the core is full it contains about 870,000 fuel pebbles randomly packed in the core. A fuel handling system circulates the pebbles, performing six functions:

1. Pebble loading and discharge;
2. Pebble purification;
3. Pebble monitoring;
4. Pebble transfer;

5. Pebble storage;
6. Pebble replenishment.

A mechanical system combined with effects of buoyancy and pebble gravity is used to implement fuel pebble loading and discharge.

Reactivity control is achieved by using control rods (the first shutdown system) and shutdown blades system (the second shutdown system). The control rods system consists of 12 rectangle rods, which move vertically in the SiC plate cut channels to control the reactivity during normal operation. The control blades system consists of eight shutdown blades, which insert directly through the upper-center graphite reflector into the pebble bed during emergency shutdown. The rods and blades contain natural (unenriched) boron carbide and are clad with nickel-based alloy. Reactivity control systems can provide sufficient shutdown to shut down the reactor and maintain subcritical conditions.

The reactor vessel defines the pressure boundary of the primary coolant. The reactor vessel houses the graphite structures, core barrel, control rods, fuel pebble loading/unloading devices, and so on. Because of the near-ambient operating pressure the reactor vessel can be much thinner than for high-pressure reactors.

The reactor coolant system consists of two branches, each having a primary loop coupled to a secondary loop by an intermediate heat exchanger. This redundancy provides a high level of safety when one branch encounters an accident. In each branch, there are two pumps, one salt/salt heat exchanger and one salt/air heat exchanger. The secondary loop is used to isolate the primary loop from the high-pressure air loop, also as a radioactivity isolation loop. The two primary loops are designed with compact layouts for safety considerations.

There are salt/air heat exchangers in both secondary loops, which transfer heat from salt in the secondary loops to the compressed air coming from the power conversion unit (PCU). Both of the coolants in the salt/air heat exchanger flow under forced circulation. The salt/air heat exchangers are spirally fluted tube-shell type exchangers that ensure enhanced heat convection. Under normal operation, the heat exchanger system also has the capability to deal with the great pressure difference between the salt side and the air side.

TMSR-SF uses an open air Brayton and steam Rankine combined cycle, in which the thermoelectric conversion efficiency could be more than 45%. The PCU include compressor, turbines, generators, residual heat recovery units, etc. The air used in the Brayton cycle should be purified primarily. Hot, compressed air flowing from a salt-air heat exchanger drives turbines to produce electricity. Residual heat in air after the air Brayton cycle will be collected to drive the steam Rankine combined cycle (Fig. 17.3).

## 17.3.2 Safety features of TMSR-SF

The inherent safety, passive and active safety systems are combined to achieve a high level of safety in TMSR-SF. Inherent safety characteristics include near-ambient pressure, low excess reactivity, passive residual heat removal

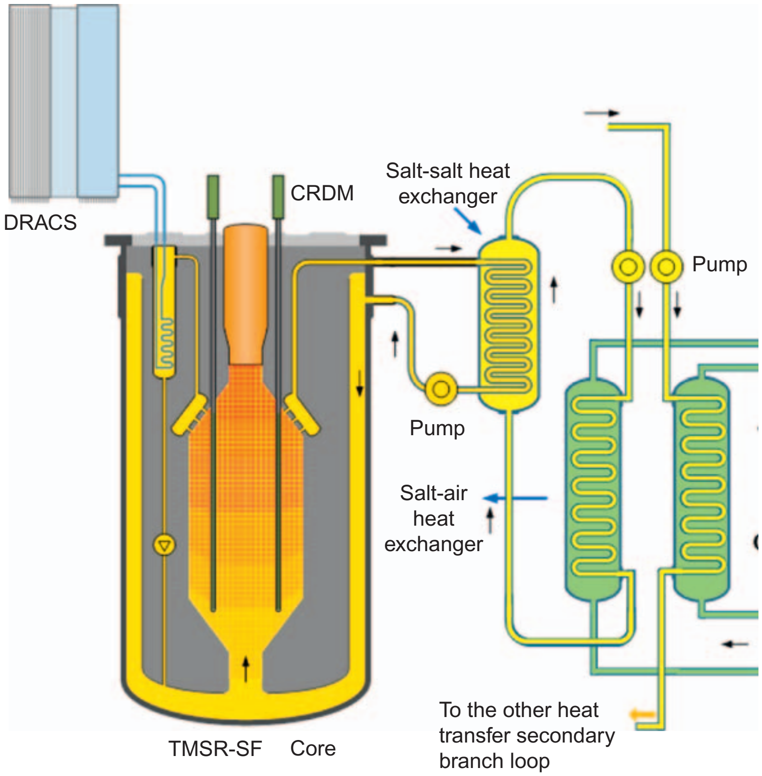

**Figure 17.3** TMSR-SF with air Brayton and steam Rankine combined cycle.

systems, a large margin of fuel temperature, large thermal capacity, negative coolant temperature reactivity coefficient, and radioactive nuclide retention by salt. The emergency safety system consists of two dependent reactor shutdown systems and a passive decay heat removal system. A confinement building is employed to prevent radioactivity diffusion as the last barrier. These inherent safety characteristics and safety system will greatly increase the safety level and alleviate accident consequences.

Under accident conditions (such as loss of forced convection circulation accident), a fully passive residual heat removal system based on natural circulation of molten salt and air will be put into operation and discharge the residual heat into the atmosphere. It consists of four independent trains. The rated discharge heat is designed to be 2% of total power. After safe shutdown, the decay heat of the reactor will be exported into the environment through a pool reactor auxiliary cooling system (PRACS), a direct reactor auxiliary cooling system (DRACS), and a natural convection cooling tower.

TMSR-SF contains two sets of shutdown systems including eight rods and 12 blades to reach safe shutdown during accidents. The two shutdown systems use different driving mechanisms, which will automatically go down in accidents.

The confinement system is designed to isolate the radioactive fission products under design basis accidents, and to restrict and retard the radiation leakage under severe accidents. The TRISO particles can maintain a quite large temperature margin from the design limitation of 1600°C, resulting in no massive release of radiation. Because of near-ambient pressure in the primary loop, there will be no large break accident. The molten salt bears an extremely high boiling point (1430°C), so coolant leakage in break accident will not follow a similar pattern in Pressurized water reactor (PWR) with instant jet flow and flashing phenomenon leading to catastrophic pressure rise inside the confinement. In contrast to conventional PWR, molten salt coolant has a large degree of retention on some of the important radioactive elements, such as CS-137, I-131, and Sr-90, etc.

With online pebble fuel circulation, TMSR-SF is operated with small excessive reactivity during normal operation. The reactivity induced by loading or unloading one pebble is small and would not affect the operation of the reactor. The high heat capacity of the coolant and graphite can minimize coolant temperature fluctuation and allow operators enough time to intervene before the occurrence of accidents.

### *17.3.3 Multipurpose utilization of nuclear energy based on TMSR-SF*

The TMSR-SF has outstanding suitability for the comprehensive utilization of nuclear power, based on hydrogen production. TMSR-SF is a multipurpose clean energy supplier designed for electricity production, hydrogen or methyl alcohol production, steam supply, heat delivering, seawater desalination, etc. TMSR-SF, based on modularized design and waterless cooling, is suitable for a variety of areas, such as remote areas, seaside, arid areas, hilly areas, mineral areas, and underground holes. Fig 17.4 shows different multipurpose applications of TMSR-SF.

In TMSR, the multipurpose utilization of nuclear energy includes two fields. On the one hand, nonelectric applications of nuclear energy could present sustainable solutions for many energy challenges that current and future generations will have to face. There is growing interest around the world in using molten salt reactor nuclear energy systems for such applications as nuclear hydrogen production, district heating, various industrial applications, seawater desalination, and chemical or fuel production (see Chapter 3: Chemical fundamentals and other applications).

On the other hand, many technologies, such as molten salt material preparation and purification, molten salt loops, and instruments for molten salt reactors have been developed. All these technologies can be applied in thermal energy utilization fields, including concentrated solar power, thermal storage in grid, and waste heat recovery.

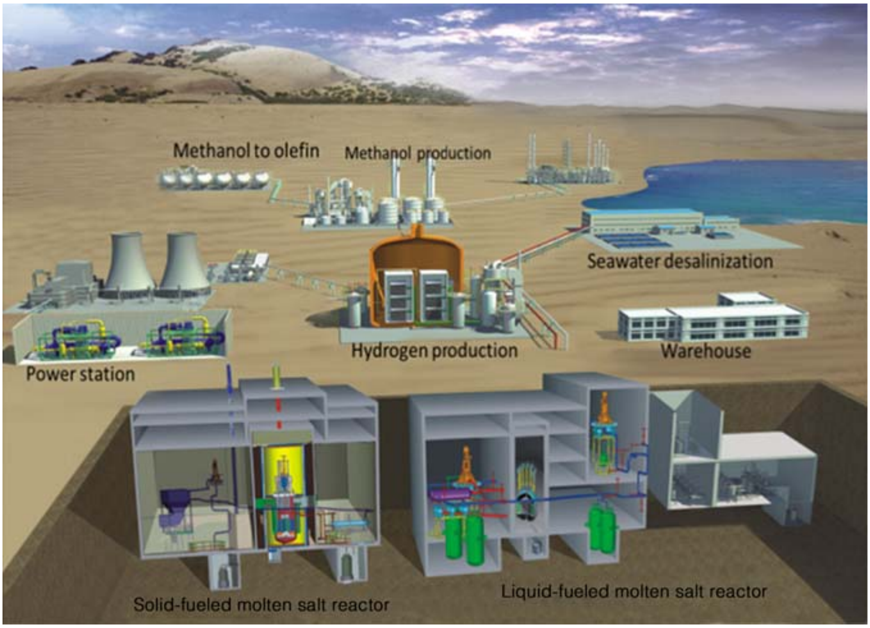

**Figure 17.4** TMSR nuclear energy park with multiutilization based on TMSR-SF.

## 17.4 Summary

The TMSR nuclear energy system has been designed for thorium-based nuclear energy utilization and hybrid nuclear energy application, based on a liquid-fueled thorium molten salt reactor (TMSR-LF) and a solid-fueled thorium molten salt reactor (TMSR-SF).

# Integral molten salt reactor

# 18

*David LeBlanc and Cyril Rodenburg*
Terrestrial Energy, Inc., Oakville, ON, Canada

**Chapter Outline**

## 18.1 Introduction

Fig. 18.1 shows the 400 $MW_{th}$ Integral Molten Salt Reactor (IMSR400).

The IMSR400 is a small modular molten salt-fueled reactor. It features a completely sealed reactor vessel with integrated pumps, heat exchangers, and shutdown rods. This vessel, called the IMSR core-unit, is replaced completely as a single unit at the end of its useful service life (nominally 7 years). This allows factory production levels of quality control and economy, while avoiding any need to open and service the reactor vessel at the power plant site. The heat transfer paths are shown in Fig. 18.2.

The IMSR uses molten fluoride salt, a highly stable, inert liquid with robust coolant properties and high intrinsic radionuclide retention properties, for its primary fuel salt. A secondary, coolant salt loop, also using a fluoride salt (but without fuel), transfers heat away from the primary heat exchangers integrated inside the core-unit. As shown in Fig. 18.2, the coolant salt loop, in turn, transfers its heat load to a solar salt loop, which is pumped out of the nuclear island to a separate building where it either heats steam generators that generate superheated steam for power generation or is used for process heat applications.

The design is based heavily on the intensive molten salt reactor (MSR) project of Oak Ridge National Laboratory (ORNL) in the 1950s–70s. In this project,

**Molten Salt Reactors and Thorium Energy. DOI: http://dx.doi.org/10.1016/B978-0-08-101126-3.00018-X**

**Figure 18.1** Cutaway view of the IMSR400.

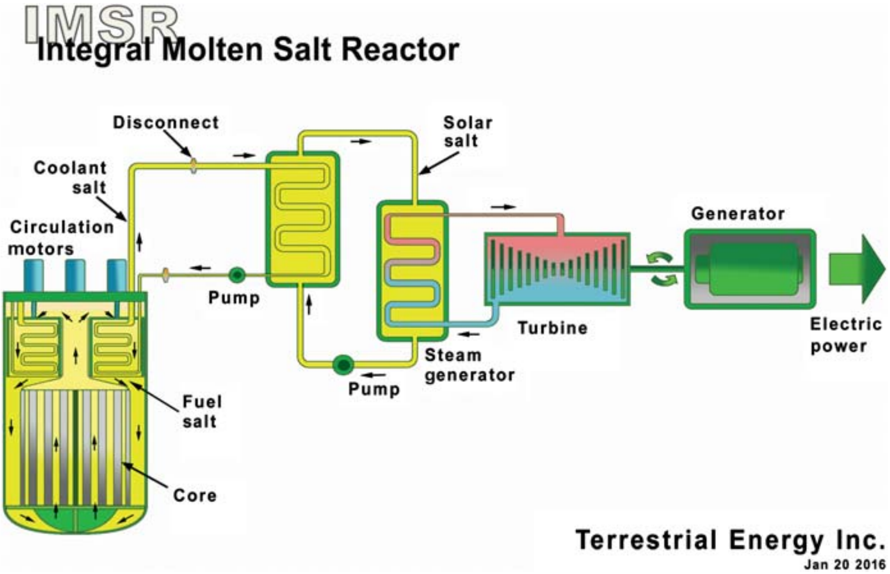

**Figure 18.2** IMSR400 main heat transport paths for power generation.

extensive R&D was done and MSR materials and equipment were developed. This included such items as suitable graphite to act as neutron moderator, drain tanks for the salts, and hot cells for housing the equipment, pumps, and heat exchangers. The ORNL program culminated in the construction and successful operation of the Molten Salt Reactor Experiment (MSRE). The MSRE employed a molten fluoride fuel salt, which was also the primary coolant. This fuel—coolant mixture was circulated between a critical graphite-moderated core and external heat exchangers. The IMSR is essentially a reconfigured, scaled-up version of the MSRE. This minimizes required research and development (R&D). The IMSR has also been influenced by a more recent ORNL design, the small modular advanced high-temperature reactor (SmAHTR) which was to use solid fuel with fluoride salt coolant, but had an "integral" architecture where all primary pumps, heat exchangers, and control rods are integrated inside the sealed reactor vessel.

The safety philosophy behind the IMSR is to produce a nuclear power plant with generation IV reactor levels of safety. For ultimate safety, there is no dependence on operator intervention, powered mechanical components, coolant injection or their support systems, such as electricity supply or instrument air in dealing with upset conditions. This is achieved through a combination of design features:

- The inert, stable properties of the salt;
- An inherently stable nuclear core;
- Fully passive backup core and containment cooling systems;
- An integral reactor architecture.

## 18.2 Description of nuclear systems

Fig. 18.3 shows one of the core-units.

The IMSR is an integral nuclear reactor design. This means that the reactor core, pumps, heat exchangers, and control rods are all mounted inside a single vessel, which is referred to as the IMSR core-unit. This core-unit is manufactured in a controlled factory environment and then brought to the reactor power plant site where, following final assembly, it is lowered into a surrounding guard (containment) vessel which itself sits in a below-grade reactor silo. There, the core-unit is connected to secondary piping, which contains a nonradioactive coolant salt. For optimal safety and containment, this coolant salt is used as an inert, low-pressure intermediate loop between the critical reactor circuit and the steam power generation circuit. The steam circuit powers a conventional, off-the-shelf industrial steam turbine for power generation and/or industrial steam production, depending on the required application. Alternatively, some or all of the hot molten salt may be sent directly to a process heat application.

Since it is a liquid fuel reactor, there are no fuel elements in the reactor core. The fuel may consist of low-enriched uranium fluoride, plutonium fluoride, thorium fluoride, or any mixture of these. The first of a kind IMSR400, however, will utilize a once-through, low-enriched uranium fuel cycle as this is the simplest option. This

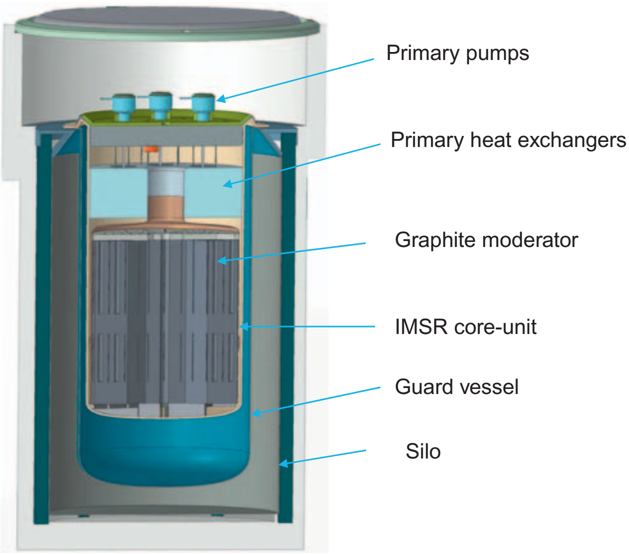

**Figure 18.3** Core-unit and guard vessel in one of the two reactor silos.

fuel salt is diluted with coolant salt, consisting of fluorides such as sodium fluoride, beryllium fluoride, and/or lithium fluoride. This mixture constitutes both fuel and primary coolant. The fuel–coolant mixture is pumped between a critical, graphite-moderated (thermal spectrum) core, and then through the integral heat exchangers to transfer its heat to the secondary, coolant salt loop (Fig. 18.2). The secondary loop consists of bare diluent salts (without fuel salt added), that in turn transfer its heat to a third salt loop. This third loop improves safety by adding another barrier between the radioactive primary inventory and the steam turbine. It uses a "solar salt" (nitrate salt), for its lower melting point (to avoid steam generator freezing) and compatibility with steam (in the event of a leak). Finally, the third loop steam generator produces steam for process heat or to power a steam turbine–generator set.

This fuel is separately brought to the power plant site as a solid, where it is melted and added to the IMSR core-unit. This allows the IMSR to operate with online fueling. Additionally, and unlike solid-fuel reactors, there is no need to remove a proportion of old fuel during makeup fueling. All of the fuel stays inside the closed IMSR core-unit during the entire power operations period of the core-unit. The volume of small amounts of additional "makeup" fuel salt is simply accommodated in the upper gas plenum. Unlike other power reactor systems, the IMSR core-unit needs never be opened at the power plant site, either during start-up fueling or during refueling. After ~7 years of power operation, the core-unit is shut down and after a cool-down period, the used fuel charge is pumped out to robust holding tanks located inside the containment. The spent, empty core-unit is then allowed to cool down for several more years, at which point its radioactivity has diminished sufficiently to permit its safe removal from its containment silo. The IMSR400 is a single unit plant, however two core-unit silos are used, to allow

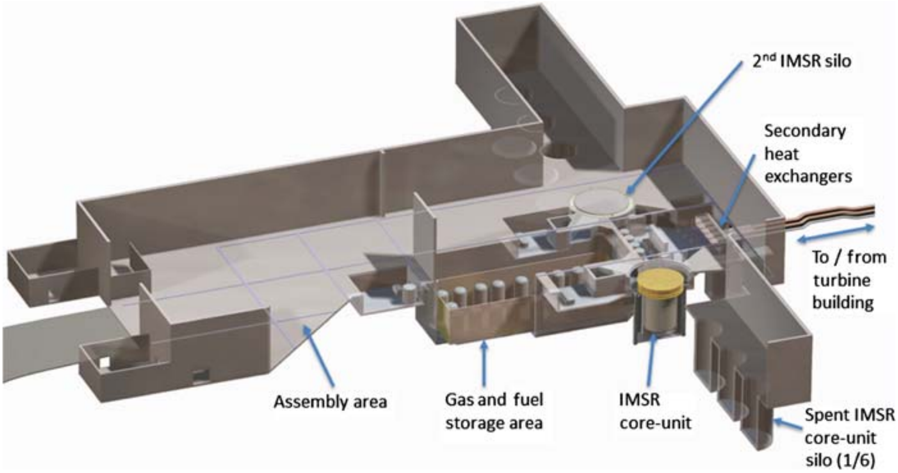

**Figure 18.4** Cut-away view into the reactor auxiliary building.

switch-loading of the silos: this allows a long period of cool-down for the spent silo, while another is connected by switching over the secondary, coolant salt lines to the new unit. After this long cool-down period, the spent, empty core-unit is then moved into a long-term storage silo where it can stay for an extended period. Beyond this period the core-unit can be shipped to a central facility, to be recycled or prepared for geological sequestration. Similarly the separately stored spent fuel charge can also be shipped to a central facility to recover the fuel or for conversion to a form for sequestration. This sealed, integral reactor architecture and once-through, "burner" fuel cycle mode allows the actual power plant site to always operate in a clean, simple environment without risk of facility contamination.

Fig. 18.4 shows the layout of the reactor auxiliary building.

## 18.3 Description of safety concept

All nuclear power reactors must fulfill three fundamental safety requirements:

- The chain reaction must be controlled;
- Sufficient cooling must be provided to transfer heat out of the reactor core;
- The radioactive materials must be contained inside the plant.

The basic design approach to safety in the IMSR is to achieve an inherent, walk-away safe nuclear plant. No operator action, electricity, or externally powered mechanical components are needed to assure the most basic safety functions:

- *Control*: failure of control systems or reactivity insertion events only leads to reactor stabilization at a slightly higher temperature.
- *Cool*: inherent heat sinks are available initially to absorb transient and decay heat, with heat losses providing long-term cooling for both core and containment.

- *Contain*: the fluoride salts are chemically stable, bind radioactive fission products to the salt, and have extremely high boiling points. Multiple engineered barriers are provided as backup to this inherent containment. Partial entrenchment of the reactor, combined with thick concrete and steel shielding, provides resistance to external events such as earthquakes, explosions, and aircraft crash.

An important part of the IMSR safety philosophy is to start by removing drivers that push radioactive material into the environment. Specifically, the reactor always operates at low pressure due to the inert, low-volatile fuel−coolant mixture and the absence of water or steam in the reactor. As the materials employed in the reactor system and even the interfacing systems, are all chemically compatible with each other, there is no potential for adverse chemical reactions such as fuel cladding hydrogen production or sodium reactions with air or water. This approach completely eliminates stored energy, both physical and chemical, from the reactor system. The IMSR further augments this high level of inherent, physics-based safety with its integrated, pipeless, failsafe systems architecture. The result is a simple and robust system with inherent safety.

In light-water reactors (LWRs) the safety concept is dependent on providing sufficient coolant flow to the solid fuel assemblies at all times. This must occur at high pressure. During loss of coolant accidents (LOCA) such as pipe leaks or breaks, reliable depressurization is required, followed by low-pressure coolant injection. These systems require various mechanical, electrical/control systems, instrumentation/sensing, instrument air, and other support systems to operate reliably.

The IMSR does not depend on depressurizing the reactor or bringing coolant to the reactor. All required control and heat sink functions are already present where they are needed—in and directly around the IMSR core-unit. As such the IMSR completely eliminates any dependence on support systems, valves, pumps, and operator actions. This is the case in both the short term and the long term. To make this possible, IMSR designers have combined MSR technology with integral reactor design and a unique cooling system.

Reactor criticality control is assured through a negative temperature feedback made possible by molten salt fuel. This negative temperature feedback assures reactor safety on overheating, even with loss of all control systems. Molten salt fuel does not degrade by heat or radiation, so there are effectively no reactor power limits to the fuel.

The unique cooling system is based on heat capacity and heat loss—which are immutable. Heat capacity is due to the thermal mass of the fuel salt, vessel metal, and graphite. Heat loss occurs as the reactor vessel is not insulated. Short-term cooling is provided by the low power density core-unit, and the internal natural circulation capability of the fluoride fuel salt, resulting in a large capacity to absorb transient and decay heat generation. Longer-term cooling is provided by heat loss from the uninsulated reactor vessel which itself is enveloped by a guard vessel. This guard vessel is a closed vessel that envelops the core-unit, providing containment and cooling through its vessel wall. Overheating of the core-unit will cause the core-unit to heat up and increase heat loss from the core-unit, in turn increasing heat transfer, via thermal radiation, to the guard vessel. The guard vessel in turn is surrounded by a robust air-cooling jacket. This cooling jacket will provide long-term cooling. The cooling jacket operates at atmospheric pressure so will continue to cool in the event of a leak or damage to the jacket.

The guard vessel containment is provided as an additional hermetic barrier in the extremely unlikely event that the integral core-unit itself would experience major failures. Without sources of pressure in the core-unit or in the containment itself, the containment is never challenged by pressure. Overheating of the containment is precluded by the balance of heat losses and heat generation even if the core-unit would fail. The containment itself is covered by thick horizontal steel radiation shield plates at the top. These plates also provide protection against extreme external events such as aircraft crash or explosion pressure waves, and provide an additional heat sink in any overheating scenario.

Fig. 18.5 shows the core heat removal system.

The IMSR has a highly attractive seismic profile due to its compact, integral (pipeless) primary system. In addition, the below-grade silo housing the core-unit, and low profile buildings, result in a very low center of gravity. Apart from the reactor system and buildings themselves, earthquakes can often threaten support systems such as main power, backup power, battery power, instrumentation and control systems, emergency coolant injection lines, or pneumatic and hydraulic systems. As the IMSR does not rely on any of these support systems, or even the cooling jacket, for ultimate safety, the IMSR's safety is inherently insensitive to earthquakes.

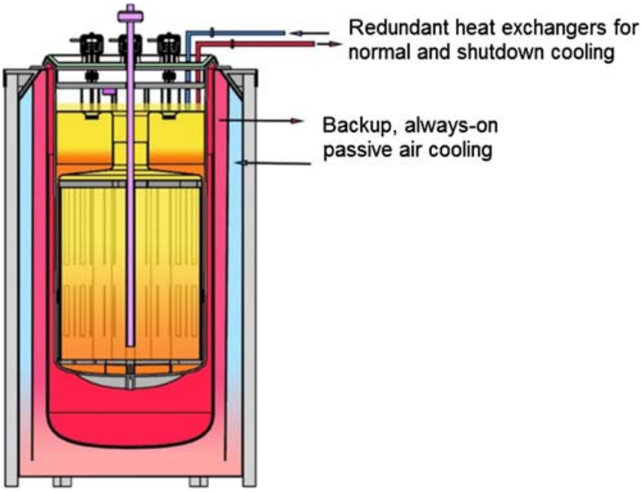

**Figure 18.5** The core-unit loses heat to an enveloping guard vessel, which in turn loses heat to a passive air-cooling jacket. This provides backup cooling in the unlikely event all of the redundant normal heat exchangers are unavailable for any reason.

The IMSR system is a high-temperature reactor system whose key safety systems are designed for extreme normal and emergency temperature profiles. No support systems are required for safe shutdown. As a result of these features, the design is inherently insensitive to fires.

As explained above, ultimate safety is provided by inherent and fail-safe features. Nevertheless, with a view of further improving the robustness of the design, to improve the reliability, and as investment protection, a considerable amount of defense-in-depth is built into the systems. For the control function, redundant, shutdown rods are also integrated into the IMSR core-unit. These shutdown rods will shut down the reactor upon loss of forced circulation and will also insert upon loss of power. Another backup is provided in the form of meltable cans, filled with a liquid neutron-absorbing material that will shut down the reactor on overheating. A complete loss of flow is however itself unlikely, as redundant primary pumps are used for circulating the fuel salt, so that the system can continue to operate at full power with any single pump failed or tripped, and slightly derated operation is possible with any two pumps failed or tripped. Similarly, to drive the pumps, conventional backup engine-driven power is available upon loss of main power. For containment, in addition to the inherently stable salt properties that act as physical and chemical containment, the integrated reactor architecture maximizes the integrity of the primary reactor system, the core-unit. This makes leaks very unlikely. Should any leaks occur, a conventional, leak-tight containment is also provided. Overpressure failure is not a plausible event due to the very high boiling points of the salts and to a lack of pressurization sources inside the core-unit and even in interfacing systems. Overheating failure of the core-unit is precluded by the use of high-quality, high-temperature capable materials in conjunction with the inherent heat loss to the surrounding passive cooling jacket.

## 18.4 Proliferation defenses

The IMSR has intrinsic, design, and procedural features that resist proliferation of fissile materials for weapons production:

1. *Fuel cycle*: The IMSR core-unit itself is fueled with low-enriched uranium on a once-through fuel cycle without fuel processing. There is no need for highly enriched uranium, and, with no fuel processing on-site, there is no possibility of separating fissile materials from the bulk of fuel salt. In addition, the high burnup and lack of online fuel removal from the IMSR core-unit results in extremely poor isotopic quality in the spent fuel inventory. In a MSR such as the IMSR, fuel and coolant are intrinsically mixed. Removal of any significant amount of fuel therefore entails the removal of much larger volumes of coolant salt. Any future fuel processing would be done in a secure, centralized facility.
2. *Systems design*: The plant engineering does not allow the removal of significant quantities of fuel salt to small, and thus mobile, shielded containers during normal operation. Fuel is added to the core-unit, fuel salt need not be removed during the 7-year cycle. Minor transfers for chemistry monitoring and control, or for final spent fuel salt transfer to large shielded holding tanks will be completely human-inaccessible due to the high-temperature

and radiation levels. Any future transfer of spent fuel salt for sequestration or processing will involve time-consuming protocols under full supervision. Such off-site transfers would entail full self-protection due to activity levels of contained fission products.

3. *Procedural controls*: The IMSR will comply with all IAEA proliferation safeguards, procedural controls, monitoring, and other requirements.

## 18.5 Safety and security (physical protection)

The IMSR is a MSR, having a highly radioactive primary fuel−coolant loop. In addition, the high operating temperature means special shielded, insulated cells and systems will be employed. These features make the reactor design highly inaccessible to potential sabotage or terrorist attack. The IMSR also employs the integral architecture, which produces a compact, robust, and fully sealed primary core-heat exchanger unit. Another design feature that protects against external threats is the provision of a hardened below-grade silo as the holding cell for the core-unit. Such hardening and below-grade construction provides superior protection against external events. The core-unit itself is provided with additional layers of protection: a sealed guard vessel surrounding the bottom and sides of the core-unit, and a steel containment plate at the top. This containment head plate is made of very thick steel primarily for radiation shielding, which also makes for a high-strength, ductile external-events shield capable of stopping the impact of a large commercial aircraft crash or explosive devices. Because the IMSR does not rely on any support systems, any attack on such support systems does not impede any of the three primary safety functions—control, cooling, and containment—of the IMSR.

## 18.6 Description of turbine−generator systems

The turbine−generator system does not serve any safety-related mission and is not needed for ultimate safe shutdown of the IMSR core-unit. Therefore, the IMSR will employ a standard, off-the-shelf, industrial-grade superheated steam turbine plant. The use of a standard turbine avoids the necessity of having to develop a new turbine and control system for the IMSR, and allows the highly flexible and reliable industrial-grade steam turbines to be used, that can be sourced from a variety of major suppliers. These steam turbines are highly flexible, being capable of high degrees of bleed off steam for cogeneration/industrial heat purposes, whilst also being capable of operating as condensing (power-generating) turbine-only if required. This affords the IMSR access to many industrial power and heat markets such as steam-assisted gravity drainage (SAGD), chemicals production, paper and pulp production, desalination, etc. In fact, these turbines, powered by fossil fuel boilers, are widely used already in many such industries today. The turbine−generator is a simple and compact, high-speed, skid-mounted design. A gearbox couples the high-speed turbine to a lower-speed, 1500−1800 RPM electrical generator.

## 18.7 Electrical and I&C systems

The IMSR does not depend on electrical or even I&C systems for ultimate safety. For operability and investment protection, a few additional requirements do exist, such as freeze protection, as the fluoride salts have high freezing points. The normal plant operations systems provide this protection, in the form of pump trips, electrical (trace) heating, and thermocouple sensors. As with the steam turbine–generator, this type of equipment is available off-the-shelf from many suppliers. The pumps are the primary control units, as passive, flow-driven control rods are utilized. This links the trip and protection logic to the pump rather than to a control rod drive and logic system. The result is a simple and easy to control system where the only real variable to control actively is the pump speed (trace heating is typically kept in automatic mode for normal operations). For example, to rapidly shut down the reactor, no control rod drives, drive power, hydraulic supply, or other support systems are needed; instead the pumps are simply tripped. The simplicity of this approach and the lack of dependence on any electrical systems also means that cybersecurity is easy to address.

As the IMSR does not depend on the electrical systems for ultimate safety, the design of a detailed plant electrical and control room system is eased. However, as with the steam turbine–generator, standard, off-the-shelf industrial equipment is expected to be used due to the generic nature of the requirements.

## 18.8 Spent fuel and waste management

The IMSR utilizes nuclear fuel with far greater efficiency than LWRs. There are three basic factors that improve the fuel utilization of the IMSR compared to LWRs:

1. The thermal-to-electrical efficiency is high: despite the modest size, the IMSR400 features higher plant electrical efficiency than LWRs. Depending on heat sink conditions and balance-of-plant arrangement, the IMSR400 generates 185–192 MWe from 400 MWth, resulting in a net efficiency of some 46%–48%.
2. The fuel burnup is high: rather than removing fuel from the reactor, new fuel is simply added to the total fuel charge forming the reactor core. The high burnup and retention of fuel inside the core results in improved plutonium and minor actinide burning capability.
3. Without fuel cladding, internal metallic structures or $H_2O$, and with the IMSR design permitting the passive exit of xenon from the core, there are far fewer parasitic neutron captures.

An additional advantage of the design is that its spent liquid fuel inventory is much easier to recycle than solid fuel elements, making it more attractive to recycle the fuel. As the fuel does not degrade, it can potentially be recycled many times. If fuel recycling is employed, Terrestrial Energy envisages this to occur in a central fuel recycling center, servicing many IMSR power plants.

The design also makes efficient use of engineering and construction materials. This is mostly due to the low operating pressure and lack of stored energy in the salts, eliminating the need for massive pressure vessels, pipe restraints, and containment buildings. High pressures are confined to the steam turbine plant, which is a very compact, standard industrial-grade unit. The salts also have high volumetric heat capacity resulting in compact heat exchangers, pumps, and other heat transport equipment. The result is very compact equipment and small buildings.

The IMSR features a fully sealed unit, avoiding the need to open the reactor vessel during operation. This feature greatly reduces expected dose rates to personnel, and avoids the generation of large amounts of contaminated drainage water and disposables.

## 18.9 Plant layout

The IMSR core-unit is housed in a below-grade silo. This forms the heart of the IMSR system. Surrounding the core-unit are the guard vessel cooling jacket, and at the top, a removable steel containment head plate. All these components are located below-grade as well. Above the containment head, shield plates cover the core-unit for radiation shielding. An idle silo is provided next to the active silo, so that this silo can be loaded with a new core-unit while facilitating cool down of a spent core-unit. These two silos make up the main components of the reactor building. After draining the spent core-unit followed by a cool-down period, the empty spent module is then lifted out and stored in long-term storage silos in an area adjacent to the reactor building. Inlets and outlets are provided for the (nonradioactive) coolant salt lines coming into and out of the core-unit, which transfer the heat to steam generators and reheaters. The coolant salt lines are located inside the reactor building. The steam and reheat steam are utilized in a conventional, off-the-shelf turbine−generator system located in an adjacent building (Fig. 18.6).

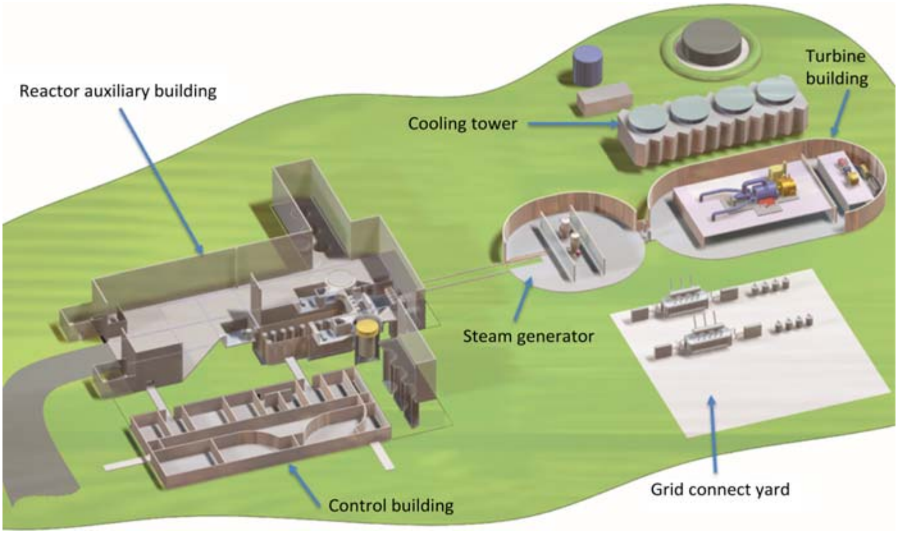

**Figure 18.6** IMSR400 plant layout.

## 18.10 Plant performance

The IMSR plant is designed to accommodate various load users, from baseload to load-following. Featuring a simple modular and replaceable core-unit, very high reliability ratings are targeted. The core-unit has only a few moving parts (pumps) and these are redundantly fitted. Even premature replacement of a faulty module only mildly affects reliability and levelized cost. The use of an idling silo greatly increases plant capacity factor, as long cool-down times (for radiation dose reduction) are possible without plant downtime.

The IMSR has been specifically designed for factory fabrication. Nuclear components are small and road-transportable. The IMSR core-unit is designed for a short service lifetime, which allows dedicated factory lines to produce the units semiautomatically, similar to aircraft jet engine production lines, for example.

The IMSR reactor building has a low profile and low mass, allowing rapid construction. The reactor building is a simple lightweight industrial building as it does not serve any major safety-related function—these are all provided by dedicated, robust, fail-safe systems.

Being a MSR, the IMSR has low fuel reload costs; fuel fabrication costs are zero, only extensive purification of the salts is required which, being bulk chemical processing, has a much lower cost than traditional high-precision fuel fabrication with all its quality and process control costs. Fuel recycling costs are also much lower with molten salt fuels, as costly fuel deconstruction and reconstruction steps are avoided and also because simple, compact, low waste volume creating distillation and fluorination processes can be utilized. This makes it likely that spent IMSR fuel will be recycled.

## 18.11 Development status of technologies relevant to the NPP

The IMSR is a simplified burner-type MSR. All of the basic technology has been proven during the operation of the MSRE at Oak Ridge National Laboratories. The MSRE was a fully functional burner-type MSR. Heat exchangers, pumps, suitable graphites, fuel salts and purification steps, off-gas systems, fuel addition mechanisms, as well as alloys of construction were all successfully developed. The IMSR builds on this rich experimental evidence to assure a high degree of technological maturity. The IMSR utilizes an off-the-shelf industrial-grade steam turbine−generator. Molten salt heated steam generators are also proven technology, with recent and very successful experience in advanced, large-scale, salt-cooled concentrated solar power (CSP) projects. Similarly water-cooled silo liners have been successfully employed in many nuclear reactor systems. Other technologies, such as tritium capture and management, are also proven technologies in the nuclear industry with a wide and current experience base in LWRs and high-temperature reactors. There are only a few components that have not been used before, such as the air-cooling jacket. These components are technologically simple and their proper function will be verified in large-scale non-nuclear testing.

## 18.12 Deployment status and planned schedule

This phase of work involves the support of a growing number of universities, third-party laboratories, and industrial partners. In addition, the Canadian nuclear regulator, the Canadian Nuclear Safety Commission (CNSC), at the request of Terrestrial Energy Inc. (TEI), has started Phase 1 of a prelicensing Vendor Design Review of the IMSR. This is an assessment of a nuclear power plant design based on a vendor's reactor technology. The assessment is completed by the CNSC, at the request of the vendor. The word "prelicensing" signifies that a design review is undertaken prior to the submission of a license application to the CNSC by an applicant seeking to build and operate a new nuclear power plant. This review does not certify a reactor design or involve the issuance of a license under the *Nuclear Safety and Control Act*, and it is not required as part of the licensing process for a new nuclear power plant.

The basic engineering phase will be followed by the construction and start-up of a first full-scale commercial IMSR NNP at a site in Canada after securing all necessary operating licenses from the CNSC (and licenses from other authorities), a process that can be completed by early in the 2020s.

## Further reading

Oak Ridge Denatured Molten Salt Reactor work, <http://web.ornl.gov/info/reports/1980/3445603575931.pdfd>.

Presentation by Terrestrial Energy CTO David Leblanc, <http://www.janleenkloosterman.nl/reports/kivi_leblanc_20150417.pdf>.

Terrestrial Energy website, <www.terrestrialenergy.com>.

World Nuclear article on Molten Salt Reactors, <http://www.world-nuclear.org/info/Current-and-Future-Generation/Molten-Salt-Reactors/>.

## Appendix: Summarized technical data

| *General plant data* | | |
|---|---|---|
| Reactor thermal output | 400 | MWth |
| Power plant output, gross | 194–202 | MWe |
| Power plant output, net | 185–192 | MWe |
| Power plant efficiency, net | 46–48 | % |
| Mode of operation | Baseload and load follow | |
| Plant design life | 60 | Years |

| | | |
|---|---|---|
| Plant availability target | 90 | % |
| Seismic design, SSE | ~0.3 (tbd in detailed design phase) | g |
| Primary coolant material | Fluoride fuel salt (proprietary mixture) | |
| Secondary coolant material | Fluoride coolant salt | |
| Moderator material | Graphite | |
| Thermodynamic cycle | Rankine (superheated) | |
| Type of cycle | Indirect | |
| Nonelectric application | District heating, hydrogen production, liquid fuel production, Industrial cogeneration, ammonia production, mineral resource extraction, petrochemical refining | |
| *Safety goals* | | |
| Core damage frequency | Tbd (inherent safety) | /RY |
| Large early-release frequency | 0 (no large volatile source term present) | /RY |
| Occupational radiation exposure | <1 | Person-Sv/RY |
| Operator action time | No operator recovery needed | hours |
| *Steam supply system* | | |
| Main steam flow rate (full power) | 148.5 | kg/s |
| Reheat steam flow rate (full power) | 137.2 | |
| Steam pressure/temperature | 19/585 (max) | MPa(a)/°C |
| Feedwater flow rate at nominal conditions | 148.5 | kg/s |
| Feedwater temperature | 240–280 | °C |
| *Reactor coolant system* | | |
| Primary coolant flow rate | 5400 | kg/s |
| Reactor operating pressure | <0.4 (hydrostatic) | MPa(a) |
| Core coolant inlet temperature | 625–660 | °C |
| Core coolant outlet temperature | 670–700 | °C |
| Mean temperature rise across core | 75 | °C |
| *Reactor core* | | |
| Active core height | 4 | m |
| Equivalent core diameter | 3.4 | m |
| Average linear heat rate | N/A—liquid fuel | kW/m |
| Average fuel power density | Depends on fuel mixture | kW/kgU |
| Average core power density | 11–15 | $MW/m^3$ |
| Fuel material | $UF_4$ in diluent fluorides (proprietary mixtures) | |
| Cladding tube material | | |

| | | |
|---|---|---|
| | No cladding employed—fluid fuel reactor | |
| Outer diameter of fuel rods | N/A—liquid fuel | mm |
| Rod array of a fuel assembly | N/A—liquid fuel | |
| Number of fuel assemblies | N/A—liquid fuel | |
| Enrichment of reload fuel at equilibrium core | 2%–3% for start-up, 5%–19% makeup fuel | Wt% |
| Fuel cycle length | 84 | months |
| Average discharge burnup of fuel | 26–29 | MWd/kg |
| Burnable absorber (strategy/material) | None—online fueling | |
| Control rod absorber material | N/A—no control rods | |
| Shutdown rod absorber material | Gadolinium oxide | |
| Soluble neutron absorber | None—online fuel makeup | |
| *Reactor pressure vessel* | | |
| Inner diameter of cylindrical shell | 3500 | mm |
| Wall thickness of cylindrical shell | 50 | mm |
| Total height, inside | 7000 | mm |
| Base material | SS316H or Alloy N | |
| Design pressure/temperature | 0.5/700 | MPa(a)/°C |
| Transport weight | 170 | t |
| *Reactor coolant pump* | | |
| Type | Vertical, single-stage, overhung, propeller pump | |
| Number | 6 | |
| Head at rated conditions | 1.5 | bar |
| Flow at rated conditions | 0.27 | $m^3$/s/pump |
| Pump speed | Variable speed drive | rpm |
| *Pressurizer (if applicable)* | | |
| Total volume | – (low pressure) | $m^3$ |
| Steam volume: full power/zero power | – (low pressure) | $m^3$ |
| Heating power of heater rods | – (low pressure) | kW |
| *Primary containment* | | |
| Type | Metal, dry, low pressure | |
| Overall form (spherical/cylindrical) | Cylindrical silos and rectangular shielded vault | |
| Dimensions (diameter/height) | 4/9 | m |
| Design pressure/temperature | Atmospheric | kPa(a)/°C |
| Design leakage rate | 0.5 | Vol%/day |

| | | |
|---|---|---|
| Is secondary containment provided? | Yes (reactor building) | |
| *Residual heat removal systems* | | |
| Active/passive systems | Active (pumps) with passive (heat loss) backup | |
| *Safety injection systems* | | |
| Active/passive systems | No injection required (low-pressure passive pool-type design) | |
| *Turbine* | | |
| Type of turbines | Superheat steam Rankine | |
| Number of turbine sections per unit (e.g., HP/MP/LP) | Dual casing (1/0/1) | |
| Turbine speed | Up to 12,000, geared to 1500−1800 rpm generator | rpm |
| HP turbine inlet pressure/temperature | 19/585 (max) | MPa(a)/°C |

# ThorCon reactor

# 19

*Lars Jorgensen*
ThorCon Energy, Stevenson, WA, United States

## Chapter Outline

## 19.1 Need for deployment

As of June, 2013, a total of 1199 coal plants were planned for construction worldwide, with a nameplate capacity of 1401 GWe. Each year these 1200 coal power plants will require 5 billion tons of coal, will emit 12 billion tons of $CO_2$ into the environment, and will kill at least 400,000 people. The world needs clean energy to avoid these deaths, environmental pollution, and waste of resources. Molten salt reactors (MSRs) could help alleviate the situation if they could be deployed successfully (Devanney et al., 2017, 2016, 2015).

Any new power plant should satisfy the goals of the utility companies that build and operate them, and should be acceptable to the public (Chapter 1: Introduction). Here we will illustrate one design that is aimed at fast deployment based on modular, factory construction, noting that this book does not endorse any particular MSR company or design.

## 19.2 Modular power plant

"ThorCon" is a molten salt nuclear reactor with liquid fuel, which can be moved around with a pump, and passively drained in the event of a casualty. It operates at 3 bar, about the same pressure as a garden hose.

**Molten Salt Reactors and Thorium Energy. DOI: http://dx.doi.org/10.1016/B978-0-08-101126-3.00019-1**

The reactor uses normal piping thicknesses and easily automated, steel-plate construction. The entire nuclear portion of the plant is underground as shown in Fig. 19.1.

The decay heat cooling towers are on the far left. The underground nuclear island is under the yellow rectangular hatches, served by gantry cranes. The turbo-generator halls are the large buildings at the center, and the switchyard is on the right. The main cooling towers, if required, would be to the right of the switchyard.

The cranes allow periodic replacement of all critical components including the reactors and fuel salt. The reactors and fuel salt are transported by a special-purpose ship shown in the background.

Fig. 19.2 is a cutaway view of the underground structure.

The reactor is divided into 250-MWe power modules. The drawing shows two such modules. Each module contains two replaceable reactors in sealed cans (red) in silos. At any given time, one of the cans of each module is producing power, and the other can is in cooldown mode. Every 4 years the can that has been cooling is

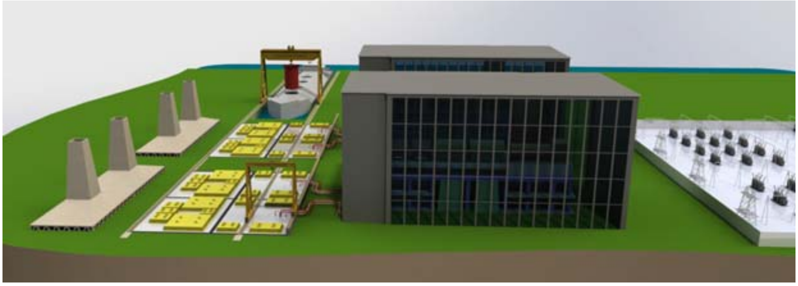

**Figure 19.1** Conceptual drawing of 1 GWe ThorCon power plant (Devanney et al., 2017, 2016, 2015).

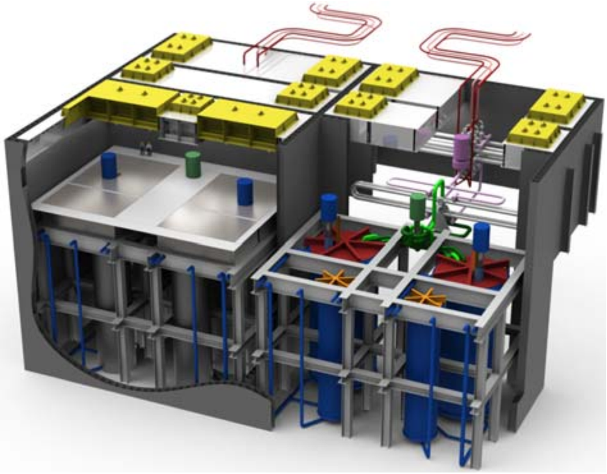

**Figure 19.2** Cutaway view of a two-module silo hall (Devanney et al., 2017, 2016, 2015).

removed and replaced with a new can, which is then filled with fuel salt. The can that has been operating goes into cooldown mode.

Each can contains a pot containing liquid fuel, a pump, and a primary heat exchanger (PHX), with a fuel salt drain tank underneath (Fig. 19.3).

The pot contains graphite moderator and fuel salt (mixture of NaF, $BeF_2$, $UF_4$, $ThF_4$). The pump pushes just under 3000 kg/s of hot liquid fuel (red pipe, 704°C) downward through the PHX, from where it returns into the pot bottom (green pipe, 564°C). The pot gage pressure is 3 bar. The high outlet temperature facilitates an overall plant efficiency of 45%, and a net electrical output per can of 250 MWe. Each can is 11.6 m high, 7.3 m diameter, and weighs about 400 tons. The pump impeller is the only major moving part in the can.

A membrane wall (blue) around the can and drain tank comprises water-filled vertical steel tubes connected by strips of steel plate welded to the tubes and connected by top and bottom circular headers (Fig. 19.3). The can and fuel drain tank are cooled by radiation to the membrane wall. Steam from the top header flows by natural convection up to a condenser and decay heat cooling tower (Fig. 19.1), and the cool condensed water returns to the bottom header. This cooling process is totally passive, requiring no operator intervention or outside power.

Each can is located in a silo, as shown in Fig. 19.4. The top of the silo is 14 m underground (under the yellow hatches of Fig. 19.2).

The heat engine uses four coolant loops to isolate the steam turbine from any radioactive materials:

1. The primary loop inside the can.
2. The secondary salt loop (dashed green line, mixture of NaF and $BeF_2$).

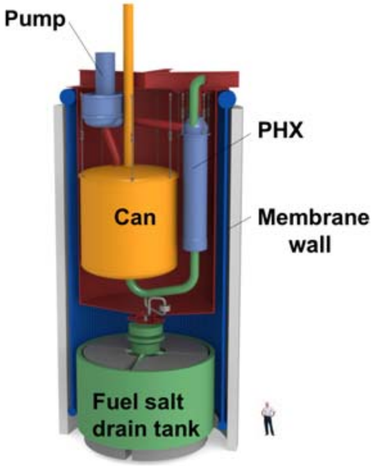

**Figure 19.3** Cutaway view of fuel salt drain tank (green) below the can (yellow), pump (blue), PHX (blue), and fuse valve (gray), surrounded by the membrane wall (blue) (Devanney et al., 2017, 2016, 2015) (1.7 m man added for perspective).

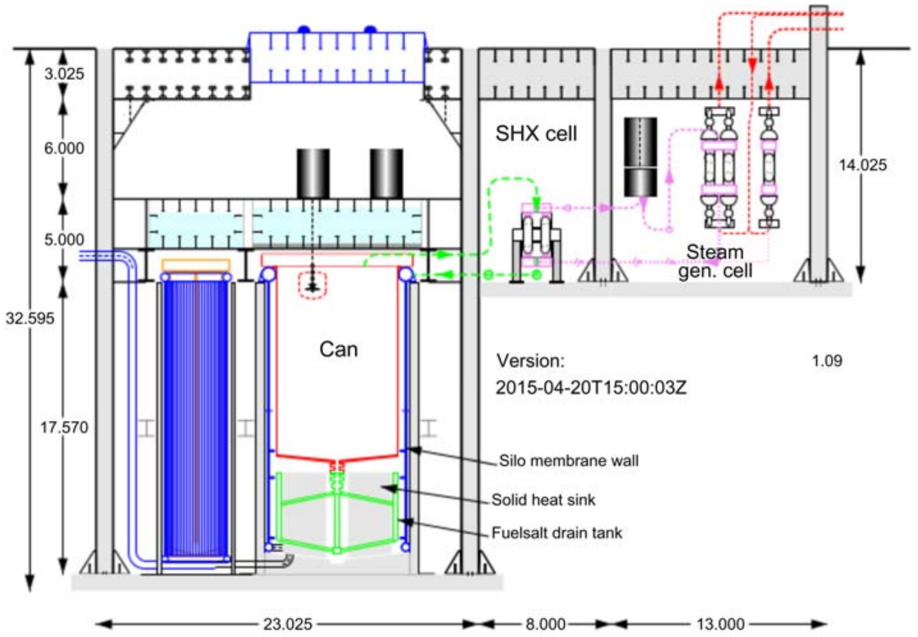

**Figure 19.4** Cross-section of a silo hall (Devanney et al., 2017, 2016, 2015).

3. The tertiary "solar salt" loop (pink, mixture of $NaNO_3$ and $KNO_3$).
4. The supercritical steam loop.

Hot secondary salt (dashed green line) is pumped from the PHX to a secondary heat exchanger (SHX) where it transfers its heat to the solar salt (pink), which transfers its heat to the supercritical steam loop (red), which drives the steam turbine to generate 250 MWe electrical power, using the same steam cycle as a modern coal power plant. The solar salt loop captures any tritium that has made it to the secondary loop.

## 19.3 Safety features

This reactor design has the following safety features.

### *19.3.1 Passive, unavoidable shutdown and cooling*

The reactor has a negative temperature coefficient of reactivity, which prevents overheating. At normal operating temperatures, the fuel salt in the fuse valve is frozen. If the fuel salt becomes too hot, the plug will thaw, and the fuel salt will drain to the fuel drain tank. Since the drain tank has no graphite moderator, fission will stop quickly, and only fission product decay heat will be generated. This draining is totally passive, and not preventable by operator actions. (Operator error exacerbated the Three Mile Island accident.)

If the fuel drains, the peak fuel salt temperature 3 hours later would be 960°C, 470°C below its boiling point. The cooling pool contains a 72-day supply of water. Safety is ensured without any operator actions, and there is nothing the operators can do to prevent the draining and cooling. The salt would remain molten for over 100 days, facilitating restart.

### 19.3.2 Radioactivity release resistance

Four coolant loops isolate the steam turbine from hazardous and radioactive materials. The reactor is 15 m underground, with four gas-tight barriers between the fuel salt and the atmosphere, and it operates near atmospheric pressure. In the event of a primary loop rupture there is no dispersal energy and no phase change. The spilled fuel merely flows to the drain tank where it is passively cooled. The most troublesome fission products (including $^{131}$I, $^{90}$Sr, and $^{137}$Cs) are chemically bound to the salt, ending up in the drain tank. Even if all four barriers were somehow breached, few of these salt seekers would disperse.

### 19.3.3 Separate spent fuel storage not required

The reactor uses an 8-year fuel salt processing cycle, after which the used salt is allowed to cool down in the nonoperating can for 4 years, eliminating the need for a separate, vulnerable spent fuel storage facility.

## 19.4 Maintenance

No complex MSR repairs are attempted on site. Everything in the nuclear island except the building itself is replaceable with little or no interruption in power output.

Fission product accumulation requires changing the fuel salt after 8 years operation and 4 years cooling, when the decay heat will be down to 80 kW (0.25% of the original). The cooled cans are shipped in a special canship to a recycling facility, where they are disassembled, cleaned, inspected, and worn parts replaced. The fuel salt going both ways will be unattractive as weapons material. The uranium will be fully denatured and, after the initial load, contain enough Th-232, U-232, Pu-238, Pu-240, and Pu-242 to make a weapon infeasible for all but the most advanced weapons states.

The recycled cans would be disassembled and fully inspected, so incipient problems would be caught before they can turn into casualties. Decommissioning would simply consist of pulling out all the replaceable parts.

## 19.5 MSR vs. coal

Since MSR plants operate at low pressure, they can be much smaller than both coal plants and light-water reactors. For a 1-GWe plant the ThorCon MSR would need 85,000 $m^3$ concrete and 36,000 metric tons steel; while a coal power plant would require 178,000 $m^3$ concrete and 109,000 metric tons steel. The MSR would require an extra 100 M$ of nuclear specialty items (graphite, SS316, Haynes 230 alloy, lead, and excavation). The estimated overnight cost of a coal plant is 1400−2000 $/kWe, while that of the MSR is about 1200 $/kW (Devanney et al., 2017, 2016, 2015).

Fission reactors require kilograms of fuel per day, while coal plants require thousands of tons fuel per day. According to one analysis the fuel cost of a 1-GWe coal plant would be about 2.3 cents/kWh, while the fuel cost of an MSR would be about 0.53 cents/kWh. So the MSR would have cost advantages relative to coal in both capital cost and fuel cost (Devanney et al., 2017, 2016, 2015).

Nuclear waste from MSR power plants is discussed in Chapter 9: Environment, Waste, and Resources. About 1 $m^3$ of dry cask storage would be needed for each GWe-year of power produced.

## 19.6 Construction speed

Rapid construction is facilitated by the following features.

### *19.6.1 No new technology is required*

The reactor is a straightforward scale-up of the Molten Salt Reactor Experiment (MSRE), which ran successfully for 4 years at the Oak Ridge National Laboratory. A full-scale 250-MWe prototype can be operating within 4 years, then subjected to all the failures and problems that the designers claim the plant can handle. As soon as the prototype passes these tests, commercial production could begin in year 7.

### *19.6.2 Historical examples*

There are several historical examples of rapid nuclear reactor deployment.

Between April 1942 and October 1944 the first 250-MW *Hanford plutonium production reactor* was designed and built, under the leadership of Eugene Wigner.

After March 1950, Captain Hyman Rickover decided to build the *Nautilus*, a full-scale prototype, which was operational in less than 6 years, instead of using cautious intermediate steps.

In 1959−60 the American Locomotive Company (ALC) designed and built the 10-MWt PM-2A nuclear power plant at *Camp Century*, just 800 miles from the North Pole, in 16 months. The plant comprised 27 blocks, which were shipped to Thule, sledded 150 miles north, and erected in 78 days. When Camp Century was shut down in 1964 the PM-2A was simply disassembled and returned to the USA.

### 19.6.3 Shipyard quality and productivity

The 500,000-ton Hellespont Metropolis supertanker (Fig. 19.5) was built in less than 1 year and cost 89 M$.

A good shipyard needs about 5 man-hours to cut, weld, coat, and erect a ton of hull steel by using block construction. Subassemblies are produced on a panel line, and combined into fully coated blocks with piping, wiring, and HVAC preinstalled. Then the blocks, weighing up to 600 tons, are dropped into place in an immense building dock.

Block construction facilitates excellent quality control via extensive inspection and testing at the block level. Defects can be caught early and corrected more easily than after erection. The MSR silo hall can employ concrete-filled, steel-plate sandwich-like walls, which results in a strong, air-tight, ductile building. A 1-GWe MSR requires about 18,000 tons of flat plate steel for the nuclear island, and a factory panel line could produce these blocks using less than 2 man-hours per ton of

**Figure 19.5** The 500,000-ton Hellespont Metropolis (Devanney et al., 2017, 2016, 2015).

steel. The other components could also be manufactured on an assembly line and delivered to the site as fully outfitted and pretested blocks. Each power module would require 31 blocks. Upon arrival at the site, the blocks would be dropped into place. The wall and roof blocks would be welded together using the automatic hull welding machines from a shipyard. The wall cells would then be filled with concrete. Almost no form work would be required. The MSR blocks, up to 23 m wide and 40 m long, could be barged up most major rivers, such as the St. Lawrence River.

Regulation should be based on rigorous physical testing of a full-scale prototype, including all design basis casualties. One schedule proposed for rapid deployment is:

> Year 1. Complete design, prepare specifications for yard and other vendors. Get quotes, negotiate prefission, full-scale prototype contracts. Conduct subsystem tests.
>
> Year 2. Build prefission prototype; do subsystem tests; prepare detailed design/specifications of fission prototype.
>
> Year 3. Prefission tests. Confirm thermohydraulics, stresses at operating temperature, exercise safety, instrumentation, and replacement systems. Raise Phase 2 capital. Make long lead time contracts for fission prototype. Obtain approval for zero power fission testing.
>
> Year 4. Convert prefission module to fission. Install turbine-generator. Start build of second Module.
>
> Year 5. Ramp up Module 1 to full power in a step-wise fashion over the year. Complete build of second module.
>
> Year 6. Long-run tests on one module; prototype self-supporting from power sales. Casualty testing on other module. Start accepting orders.

Once a design has passed all these tests, it can be replicated efficiently, up to 50 GWe per year (Devanney et al., 2017, 2016, 2015).

The ThorCon type MSR competes economically with coal – the dominate source for electricity in the world. A ThorCon type of MSR could be built and deployed rapidly because no new research or technology is required, all the materials are available, factory quality control can be used, shipyard production speed can be achieved, the steam cycle is already deployed, cans and components can be replaced, and there is no delay for scale-up. The main barrier to rapid civilian deployment in the USA is regulatory delays, so initial deployment may be done elsewhere.

## Reference

Devanney, J., et al., 2017. 2016, 2015. ThorCon™, The Do-able Molten Salt Reactor, © 2017, 2016, 2015. Martingale, Inc, < http://thorconpower.com/docs/domsr.pdf >, < http://thorconpower.com/library/documents >.

# Safety assessment of the molten salt fast reactor (SAMOFAR)

# 20

*Jan L. Kloosterman and On behalf of the SAMOFAR consortium*
Delft University of Technology, Delft, The Netherlands

## Chapter Outline

The SAMOFAR project (Safety Assessment of the Molten Salt Fast Reactor) is one of the major Research and Innovation projects in the Horizon 2020 Euratom research program. The grand objective of the project is to deliver a paradigm shift in nuclear safety and nuclear waste management to make nuclear energy truly safe and sustainable. To this end, we have developed a new type of nuclear reactor, the molten salt fast reactor (MSFR), whose key safety features will be demonstrated in the SAMOFAR project.

The MSFR is the only nuclear reactor that can efficiently consume thorium and process existing plutonium stock piles as well. The fuel is dissolved in a molten fluoride salt that simultaneously serves as a coolant, avoiding many of the safety issues of existing nuclear power plants. By using thorium, the production of plutonium and other long-lived nuclear waste is reduced by a factor of 1000 or more. This would reduce the required storage time of nuclear waste to just a few centuries. Furthermore, thorium is abundantly present and can serve global electricity production for tens of thousands of years.

## 20.1 Objectives of the project

The grand objective of SAMOFAR is to prove the innovative safety concepts of the MSFR by advanced experimental and numerical techniques, to deliver a breakthrough in nuclear safety and optimal waste management, and to create a consortium of stakeholders containing Technical Support Organisations (TSO) and industry to advance with the MSFR up to the demonstration phase of this technology. Besides the research efforts in SAMOFAR, the consortium tightly connects with other large projects in China, Russia, and the United States to exchange information, and to coordinate and share resources.

**Molten Salt Reactors and Thorium Energy. DOI: http://dx.doi.org/10.1016/B978-0-08-101126-3.00020-8**

The grand objectives will be achieved via the following specific subobjectives:

1. To deliver the experimental proof of concept of the unique safety features of the MSFR;
2. To provide a safety assessment of the MSFR for both the reactor and the chemical plant;
3. To update the conceptual design of the MSFR with all the improvements and recommendations from afore-mentioned studies incorporated;
4. To deliver a roadmap for further exploitation of the project results by creating momentum among key stakeholders that can validate and demonstrate the MSFR beyond SAMOFAR.

## 20.2 The concept of the molten salt fast reactor

The MSFR is a further development of the graphite-moderated molten salt breeder reactor originally designed at the Oak Ridge National Laboratory (ORNL) in the 1960s, and is the current reference design studied within the Generation-IV International Forum. It consists of a cylindrical vessel with diameter and height of 2.25 m made of a nickel-based alloy filled with a liquid fuel salt under ambient pressure at operating temperature of 750°C. The fuel salt, 18 $m^3$ total in the primary circuit, is pumped upward through the central core zone and downward through the heat exchangers located circumferentially around the core. In between, a container filled with a blanket salt containing thorium surrounds the core to increase the breeding gain. A schematic view of the primary circuit is shown in Fig. 20.1.

The reactor is designed with a fast neutron spectrum, and it can be operated in the full range from breeder to burner reactor. This flexibility is facilitated by the fact that the fuel salt composition can easily be adapted during reactor operation

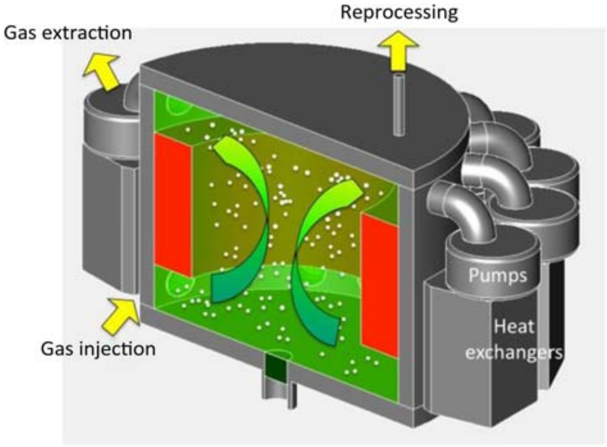

**Figure 20.1** Schematic layout of the MSFR core. The central region (*green*) is the core surrounded by the annular breeding blanket (*red*). The heat exchangers are located circumferentially around the vessel.

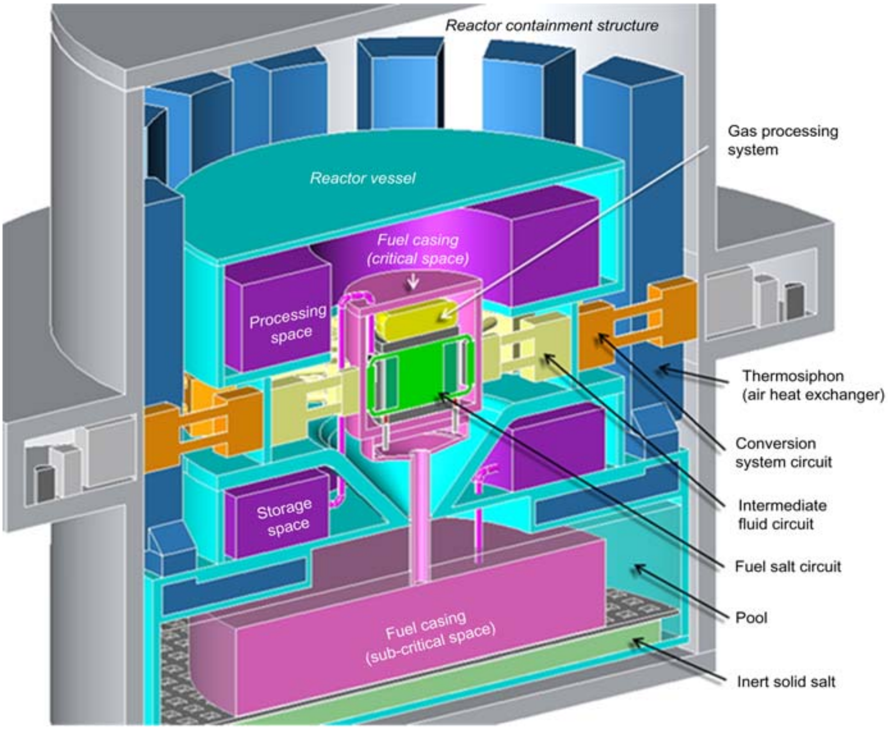

**Figure 20.2** Schematic layout of the MSFR, showing the location of the systems for cleaning and draining of the fuel salt, and the three containment barriers (*pink*, *yellow*, *gray*).

without manufacturing of solid fuel elements. During reactor operation a fraction of the salt is continuously diverted to an ex-core salt clean-up unit to extract lanthanides and actinides. A more detailed view of the whole MSFR plant layout is shown in Fig. 20.2.

The fast neutron spectrum relaxes the requirements for this process enormously. While in a thermal molten salt breeder reactor, the salt should be cleaned at a processing rate of about 4 $m^3$/day, this is only 40 L/day in a fast reactor. The salt clean-up process is a unique feature of the MSFR and contains two major steps. First, the gaseous and nonsoluble fission products like the noble metals are removed from the primary circuit by gas bubbling near the pumps. In a second step the uranium, actinides, and some fission product can be separated by pyro-chemical techniques (fluorination and reductive extraction) in the ex-core chemical plant.

The use of a liquid fuel salt under ambient pressure offers unique assets not present in other reactor types, based on the following mechanisms:

- *Thermal expansion of the fuel salt.* The first mechanism to limit any reactivity excursion is to let the fuel salt expand upon heating, which gives a strong negative void and temperature reactivity feedback everywhere in the core. This is in addition to the nuclear Doppler effect. The resulting temperature feedback coefficient is around −5 pcm/K.

- *Natural circulation of the fuel salt.* The first mechanism to remove the decay heat from the fuel salt is to let it circulate in the primary vessel through the heat exchangers, even if the pumps are not operating. This is facilitated by the facts that the fuel salt has a high heat capacity and a large temperature margin to boiling ($\approx$2000 K).
- *Draining of the fuel salt.* The second mechanism to remove the decay heat from the fuel salt is to let the salt drain in passively cooled tanks underneath the reactor core. The connection between the primary vessel and the drain tanks is sealed with a freeze plug that will melt upon overheating, e.g., when the external power fails. This mechanism also brings the fuel salt in a safe deep subcritical state.
- *Cleaning the fuel salt.* The third principle to facilitate the decay heat removal from the fuel salt is to reduce the decay heat production by continuously cleaning the fuel salt by helium bubbling and by the chemical separation processes mentioned before. This reduces the decay heat in the salt by approximately 35%.
- *High solubility of fission products in the salt.* Most fission products dissolve in the fuel and are strongly bonded, which may virtually eliminate the source term in the reactor core of volatile fission products like cesium and iodine.

All these mechanisms lead to a robust safety approach of the MSFR, which will be validated and quantified in SAMOFAR by advanced experimental and numerical simulation tools.

## 20.3 Main research themes

In SAMOFAR, the following experimental research is carried out.

First, the reliability of the *freeze plug* concept and the mechanism to drain the fuel salt in fail-safe storage tanks underneath the reactor core will be validated experimentally. This requires experimental setups with molten salts at high temperatures.

Second, the *natural circulation* dynamics of the fuel salt will be investigated. Because the decay heat is produced homogeneously in the salt, the natural circulation dynamics may be different from those in solid-fuel reactors.

Third, the safety-related *salt properties* like viscosity, heat capacity, melting and solidification behavior, need accurate experimental determination. This will be done in advanced experiments with actinide-containing salts at high temperature ($\approx$600°C).

Fourth, the synthesis of the fuel salt will be developed, as well as the *extraction* of the lanthanides and actinides from the fuel salt by reductive methods.

Finally, the *interaction* between the salt and materials and coatings will be experimentally investigated and demonstrated.

Besides this extensive experimental work, the integral safety assessment of the reactor including the drain tanks and the processing unit will be carried out with a newly developed method, and control strategies will be identified and simulated for all kind of operation modes, such as start-up, shut-down, and load-follow operation. An extensive risk assessment will lead to a complete set of transient scenarios that will be evaluated by leading-edge multiphysics software specially developed for this purpose. All these analyses will be done for the complete system including all components in contact with the fuel salt.

## 20.4 The SAMOFAR consortium

The SAMOFAR consortium comprises the 11 partners shown in Table 20.1. Because the MSFR is a reactor design with safety features that need to be moved from low to high technology readiness, a major part of the work program is fundamental of nature. This part is mainly executed by universities and research laboratories, like Centre National de la Recherche Scientifique (CNRS), Joint Research Centre (JRC), Consorzio Interuniversitario per la Ricerca Technologica Nucleare (CIRTEN), Technical University-Delft (TU-Delft), and Paul Scherrer Institute (PSI), thereby exploiting each other's unique expertise and infrastructure. CNRS is a French research institute with many branches and with strong expertise on the MSFR reactor design and integral safety assessment and on experimental research with molten salts, both in the field of physics (loop experiments) and chemistry (chemical separation processes). Joint Research Center-Institute for Transuranic Elements (JRC-ITU) is leading in Europe with fundamental experimental research on molten salt thermo-dynamics and chemistry. It has an excellent infrastructure to investigate actinide-containing molten salts. CIRTEN has a strong reputation in experimental thermal-hydraulics and loop-dynamics as well as in numerical reactor design. TU-Delft is an expert in fundamental experimental thermal-hydraulics and computational reactor physics. PSI is the leading Swiss institute on nuclear research with broad expertise, and with unique contributions to various work packages, like the structural mechanics effects of some transients. Centro de Investigacion y de Estudios Avanzados del Instituto Politecnico Nacional (CINVESTAV) is the

**Table 20.1** Organizations participating in the SAMOFAR project

| Number | Organization name | Country |
|---|---|---|
| 1 | Technische Universiteit Delft (TU-Delft) | The Netherlands |
| 2 | Centre National de la Recherche Scientifique (CNRS) | France |
| 3 | JRC—Joint Research Centre—European Commission (JRC) | Germany |
| 4 | Consorzio Interuniversitario Nazionale per la Ricerca Tecnologica Nucleare (CIRTEN) | Italy |
| 5 | Institut de Radioprotection et de Sûreté Nucléaire (IRSN) | France |
| 6 | Centro de Investigacion y de Estudios Avanzados del Instituto Politecnico Nacional (CINVESTAV) | Mexico |
| 7 | AREVA NP SAS (AREVA) | France |
| 8 | Commissariat a l'Energie Atomique et aux Energies Alternatives (CEA) | France |
| 9 | Electricité de France S.A. (EDF) | France |
| 10 | Paul Scherrer Institute (PSI) | Switzerland |
| 11 | Karlsruher Institut für Technologie (KIT) | Germany |

Mexican research institute with materials expertise. All academic partners also strongly contribute to the education and training part of SAMOFAR.

Besides the work of a fundamental nature, the input of TSOs, industry, and utilities is indispensable for their experience in reactor design and safety assessment, for the implementation of industrial standards, and for the exploitation of results. Institut de Radioprotection et de Sûreté Nucléaire (IRSN) is the leading French TSO contributing strongly to the design of the integral safety assessment method. AREVA, Europe's largest nuclear industry, will contribute their huge experience on the reactor design, safety assessment, and industrial standards. Karlsruher Institut für Technologie (KIT) and Electricité de France (EDF) will contribute with the industrially adopted safety assessment code SIMMER for transient analyses of fuel drainage and subsequent cooling. Commissariat a l'Energie Atomique et aux Energies Alternatives (CEA) has many multidisciplinary experts who will contribute with the complex multidisciplinary design of the chemical plant, combining chemical, nuclear, radiological, and other industrial process technologies. The combined approach of the academic and industrial partners ensures the uptake of fundamental results into the industrial design processes and standards needed for the successful exploitation of the results.

# Stable salt fast reactor

## 21

*Ian Scott*
Moltex Energy, London, United Kingdom

### Chapter Outline

## 21.1 Design principles

The fundamental principles of using static (unpumped) molten salt fuel in fuel tubes and fuel assemblies very similar to those used with uranium oxide pellet fuel are set out in Chapter 14, Static liquid fuel reactors. In this chapter, one particular design of such a reactor is described. It is a fast spectrum reactor designed for consumption of stocks of plutonium and higher actinides from spent nuclear fuel.

The design principles that have been followed are to:

1. Achieve intrinsic safety wherever that is possible;
2. Achieve passive safety when intrinsic safety is not achievable;
3. Minimize complexity, both to minimize cost but also to reduce the number of interacting systems that inevitably create unexpected fault scenarios.

The resulting design bears a degree of similarity to modern pool-type designs for sodium-cooled fast reactors, but differs in a number of key aspects. It is far smaller; it contains no highly chemically reactive materials; its coolant has a much higher volumetric heat capacity allowing much lower pumping speeds; and it is modular in construction, allowing a wide range of reactor sizes to be constructed from standard modules.

And, of course, it has the defining and overwhelming advantage of molten salt fuel of a very small volatile radioactive source term. Accepting design principle 1 (intrinsic safety whenever possible) would make choice of any other fuel system incompatible with the ALARP principle.

**Molten Salt Reactors and Thorium Energy. DOI: http://dx.doi.org/10.1016/B978-0-08-101126-3.00021-X**

The small size and intrinsic safety make this reactor much less costly to build, and probably to operate, than modern sodium fast reactors and pressurized water reactors. Chapter 14, Static liquid fuel reactors described the capital cost estimation carried out for an earlier design of stable salt fast reactor based on typical UK onsite construction. The design described in this chapter is a derivative of that design, but modified to allow substantial factory-based modular construction, use of standard parts for reactors of different sizes, and use of standard nuclear certified steels, rather than more exotic superalloy materials. It is therefore anticipated that this design will have a yet lower overnight capital cost and, due to its short onsite construction schedule, a substantially lower total capital cost.

## 21.2 Design outline

The basic unit of the reactor core is the fuel assembly. One is illustrated in Fig. 21.1.

Each assembly contains a square 18 × 21 hexagonal close-packed array of 10 mm diameter fuel tubes with 1 mm helical wire wrap filled to a height of 1600 mm with fuel salt. The tubes have diving bell gas vents at the top to allow fission gasses to escape as described in Chapter 14, Static liquid fuel reactors. The assembly is clad with stainless steel and has a spike at the base which contains a filter apparatus and through which the bottom of the assembly is positively located into the diagrid bottom support.

The region of the assembly above the fuel tubes is a lattice structure that is narrower than the main part of the assembly, allowing space for instrument thimbles

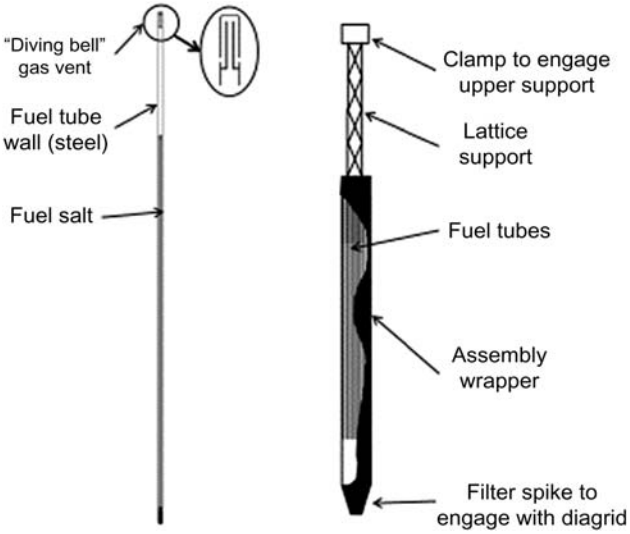

Figure 21.1 Single fuel tube and fuel tube assembly.

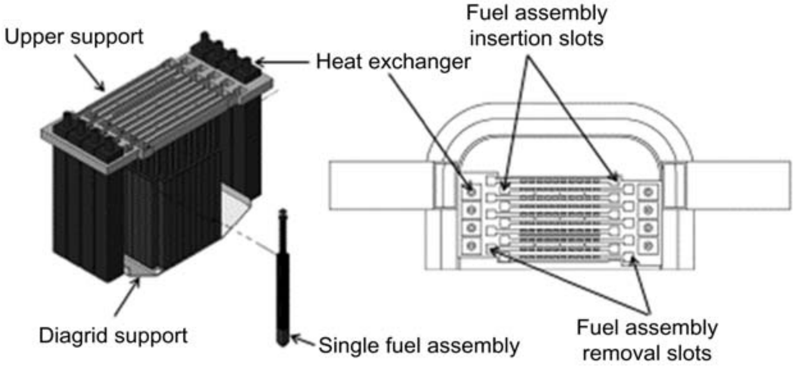

**Figure 21.2** View of reactor module—3D and top view.

to be inserted between the fuel assemblies. At the top the assembly has a spring-loaded apparatus that positively locates the assembly into the upper support grid, while permitting the springs to be compressed to disengage the assembly from the upper support grid. When this is done, the assembly can be raised to disengage the bottom spike from the diagrid, moved laterally along the channel in the upper support grid and then securely reengaged in the bottom diagrid and upper support grid.

An unusual design feature of the reactor is that its core is rectangular in shape. This is relatively neutronically inefficient compared to a cylindrical core but enables substantial simplification of the movement of fuel assemblies and permits the core to be extended essentially indefinitely in its long dimension simply by adding additional modules. This compromise is driven by design principle number 3 above.

Fig. 21.2 shows an illustration of a reactor module. Each module contains 10 rows of 10 fuel assemblies, upper support grid, lower diagrid, heat exchangers, pumps, control assemblies, and instrumentation. Each module has a thermal output of 375 MW. Two or more of these modules are assembled side by side into a rectangular reactor tank (single modules are theoretically possible but suffer from more significant "end effects" where power output is lower).

The modules (without fuel assemblies) are preassembled into the stainless steel tank and delivered to the construction site as single road-transportable components. They are placed in concrete- and steel-lined pits below grade level.

The upper part of the reactor consists of an argon containment dome, incorporating two crane type systems, a low load device designed to move fuel assemblies within the reactor core, and a high load device designed to raise and lower fuel assemblies into the coolant and to replace entire modules should that be necessary.

## 21.3 Fuel salt

The fuel salt is a close to eutectic mixture of 60 mol% NaCl with 40% mixed uranium, plutonium, and lanthanide trichlorides. Initial fuel for the reactor is

**Table 21.1** Composition and properties of the fuel salt

| | |
|---|---|
| Composition (mol%) | 60% NaCl, 20% $PuCl_3$/20% ($UCl_3$/$LnCl_3$) |
| Melting point | 730 K |
| Boiling point | ~1837 K |
| Density | $4.1690-9.014\times10^{-4}\ g\cdot ml^{-1}\cdot K^{-1}$ |
| Viscosity of the fuel salt | $\log_{10}(\eta[cP]) = -1.2675 + \frac{1704}{T[K]}$ |
| Thermal conductivity | $0.5\ W\cdot m^{-1}\cdot K^{-1}$ |
| Specific heat capacity | Rises from $520\ J\cdot kg^{-1}\cdot K^{-1}$ at M · Pt to 670 at B · Pt |

expected to come from stocks of pure $PuO_2$ from Plutonium uranium redox extraction (PUREX) reprocessed conventional spent nuclear fuel, mixed with pure depleted uranium trichloride. The acceptability of substantial lanthanide contamination of the Stable salt reactor (SSR) fuel will make significantly lower cost reprocessing of spent uranium oxide fuel possible when the existing stocks of pure plutonium have been consumed.

The properties of this salt are given in Table 21.1. Being a trichloride, it is much more thermodynamically stable than the corresponding fluoride salts. It can therefore be maintained in a strongly reducing state by contact with sacrificial nuclear-grade zirconium metal added as a coating on, or an insert within, the fuel tube. As a result the fuel tube can be made from standard nuclear certified steel. Since the reactor is fast spectrum, the tubes will be exposed to very high neutron flux and suffer high damage (dpa) levels, estimated at 100–200 dpa over the tube life. Highly neutron damage tolerant steels such as HT9 would therefore be used for the tubes. See Chapter 14, Static liquid fuel reactors for further details.

Gas produced during fission bubbles out from the fuel salt at a rate of approximately 0.5 mL per day per tube. This gas is primarily noble gases of longer half-lives and cadmium (see Chapter 14: Static liquid fuel reactors). The gas enters the argon containment dome and the cadmium metal and other traces of condensable volatile species are collected in a cold (~10°C) trap incorporated in the argon circulation and cooling system. Accumulated noble gases undergo significant further decay inside the containment and are released to atmosphere at intervals through operation of the airlock which discharges argon from the containment to atmosphere through the hot air decay heat removal stacks (see below).

The average power density in the fuel salt is 150 kW/L which allows a very generous margin for salt temperature below the salt boiling point. Power peaking to double this level for substantial periods would not exceed the safe operating conditions for the fuel tube.

## 21.4 Primary coolant salt

The coolant salt in the reactor tank is composed of 42 mol% $ZrF_4$/48 mol% KF/10% NaF. Its properties are given in Table 21.2. The zirconium is not nuclear-grade and

**Table 21.2** Composition and properties of the coolant salt

| | |
|---|---|
| Composition (mol%) | 48% KF, 10% NaF, 40% $ZrF_4$/2% $ZrF_2$ |
| Density | $2770\ \text{kg} \cdot \text{m}^{-3}$ |
| Specific heat capacity | $1050\ \text{J} \cdot \text{kg}^{-1} \cdot \text{K}^{-1}$ |
| Kinematic viscosity | $1.7 \times 10^{-6}\ \text{m}^2 \cdot \text{s}^{-1}$ |
| Thermal conductivity | $0.7\ \text{W} \cdot \text{m}^{-1} \cdot \text{K}^{-1}$ |
| Inlet temperature | 450–460°C |

still contains ~2% hafnium. This has a minimal effect on core reactivity but makes the coolant salt a highly effective neutron shield. The 1 m of coolant reduces neutron flux by four orders of magnitude.

The coolant also contains 1 mol% zirconium metal (which dissolves forming 2 mol% $ZrF_2$). This reduces its redox potential to a level making it virtually noncorrosive to standard steels. The reactor tank, support structures, and heat exchangers can therefore be constructed from standard 316L stainless steel.

The coolant salt is circulated through the reactor core by pumps attached to the heat exchangers in each module. Flow rates are modest, approximately 1 m/s with a resulting low requirement for pump power. The primary coolant salt becomes radiaoactive due to absorption of neutrons, short-term activation ($<1$ day) is dominated by activation products of Na while longer-term Zr dominates. In the very long term (10 years), $^{36}Cl$ formed by activation of K dominates and is the critical factor in disposal of the coolant salt during decommissioning (Williams et al., 2006).

## 21.5 Secondary heat transfer loop and steam island

The radioactivity of the primary coolant salt makes use of a secondary heat transfer loop necessary to avoid potential for high-pressure steam interaction with radioactive salt in heat exchangers. The secondary circuit uses the same salt as the primary coolant, maintained at a small positive pressure relative to the primary coolant to prevent radioactive material entering the secondary loop in the extremely unlikely event of a leak in a heat exchanger tube. The heat exchanger is of the twisted tube/shell type with the secondary coolant salt in the tubes. The tube sheets are located above the lid section of the heat exchanger so that any leaks at that point are visible and do not allow mixing of the primary and secondary coolants.

The secondary coolant passes to a steam-generating heat exchanger of the tube/shell type where the high-pressure steam is contained within the tubes. Backup heating is not required for the salt in the tank, however the salt-containing structures outside the primary salt pool are insulated and have electrical heating elements to maintain temperatures above the coolant salt freezing points during shutdown periods.

The steam system is of standard construction. The outlet temperature of the secondary coolant salt is high enough to operate a supercritical steam cycle, however the choice of that vs. a superheated steam cycle will be essentially economic.

## 21.6 Fuel management and refueling

In conventional light-water reactors, refueling is a major undertaking involving shutting the reactor down for several weeks, flooding the reactor containment with water and removing and replacing about one-third of the fuel assemblies. The remaining assemblies are shuffled to make the "new" core as efficient as possible. Each shuffling involves lifting an assembly entirely out of the core, moving it to its new position and reinserting it into the core. This process requires large, complex mechanisms.

The stable salt fast reactor uses a radically simpler and faster procedure, enabled by operation at atmospheric pressure, absence of chemically highly reactive fluids, and with fuel assemblies compatible with a wide range of power levels and temperatures. The simplicity evolves from the fundamentally superior physics of the reactor.

The fuel assemblies in the core are arranged in rows of 10 aligned along linear support structures. Refueling involves three simple stages.

- A spent fuel assembly is lifted from its anchoring point at one end of the row and moved laterally, still immersed in the coolant salt, to a storage location at the extreme end of the row. It remains there for 3–6 months until its decay heat has fallen to the level where it can be lifted from the coolant, allowed to freeze, and then moved into dry cask storage.
- The remaining fuel assemblies on that row are migrated one step across the core, in each case involving only a few cm lifting and a short lateral movement. Alternate rows migrate in opposite directions across the core.
- A fresh fuel assembly is moved from its temporary storage location at the opposite extreme edge of the row to the vacant position in the core.

This process can take place with the reactor at full power or with power reduced to $\sim 10\%$ of full power or with the reactor shut down. The advantage of doing it at low power is a simplification of the process to restore it to full power.

The refueling process is carried out every 3 months on each fourth row of assemblies so assemblies spend 5 years in the core. The time required is consistent with an overnight shutdown period. Removal of cooled spent fuel assemblies and insertion of fresh assemblies into the temporary storage locations takes place with the reactor at full power during the period between refuelings. The period between refuelings is relatively short, and the reactor is able to maintain full power, despite reduced core reactivity due to fissile burnup, through small variations in primary coolant flow rate. No reactivity shim or control rod systems are required to control reactivity under normal conditions.

Fresh fuel assemblies for an upcoming refueling are delivered as single consignments and immediately loaded into the temporary storage locations in the reactor tank. Fresh fuel stores are therefore not required. Spent fuel is transferred to dry casks or to transport containers and either placed in air-cooled storage or sent for reprocessing.

## 21.7 Neutronics and reactivity control

The unusual geometry of the reactor core leads to a power distribution across the core which is also atypical. Fig. 21.3 shows the results of MonteCarl N Particle

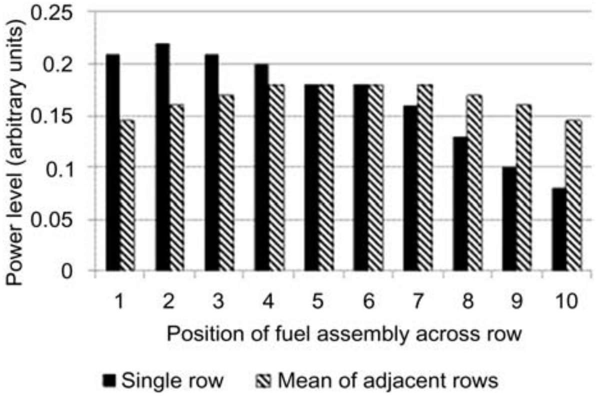

**Figure 21.3** MCNP analysis of power distribution across a row of fuel assemblies.

neutronics code (MCNP) neutronic analysis on a core where fresh fuel was introduced at one end of each row with a range of reactor-grade plutonium concentrations from 16% in the central rows to 22% in the peripheral rows and then underwent a 66% burnup as the fuel assembly traversed the core.

The figure shows that power output from an assembly falls by about 64% as the fissile isotopes are consumed but that averaged over adjacent rows of fuel assemblies an approximately uniform power distribution is achieved. The burnup of fissile isotopes is approximately 60%.

This burnup is readily achieved both neutronically and chemically and represents a burnup of ~500 GWd/tonne, a level which has only been dreamed of for solid fueled reactors and which is only possible due to the chemical and (most importantly) physical stability of the liquid fuel.

The temperature coefficient of reactivity of the fuel is a critical factor in reactor safety. It is a measure of how much the nuclear reactivity of the reactor falls as it heats up. A negative coefficient means that if reactor power increases, it heats up and the power then falls. It is self-regulating. No reactor would be approved today without a negative temperature coefficient. The temperature coefficient for the stable salt fast reactor fuel is −10 pcm/K, a negative value around 5−10 times greater than solid fueled reactors. The high negative coefficient is driven by the relatively large thermal expansion of the liquid fuel as it heats. This has an obvious safety advantage but also is vital in allowing the reactor to run between refueling episodes without having initial excess reactivity that has to be "held down" by control rods or neutron poisons. The small reductions in reactivity that occur as fuel is burned merely lead to a very small reduction in average fuel temperature which compensates for the fuel burnup. In a solid fueled reactor, the fall in temperature necessary would be 5−10 times higher and would severely impact on power output.

Control rods and other reactivity control systems are not therefore required during operation of the reactor. However, they are provided in the form of narrow control blades which can be inserted between the rows of fuel assemblies. These allow shutdown of the reactor when that is desired and have the usual fail-safe properties of shutdown systems in all reactors.

## 21.8 Decay heat removal

Even when shut down, all reactors continue producing heat from decay of radioactive fission products. Failure to remove that heat will lead to any reactor core heating up continually until the dreaded "melt down" happens. Molten salt fueled reactors may be immune from melt down (they are already molten) but uncontrolled heating of the fuel salt would still be a serious accident—though without the long-distance catastrophic release of gaseous radioactivity that happens with solid fuels.

Emergency heat removal systems that will prevent this happening under all circumstances are now sought for all new reactor designs. Systems requiring active pumping of water can fail, as happened at Fukushima. The very best designs of heat removal system do not require power, do not require operator intervention, and will continue to operate forever with no reservoirs of coolant that could be depleted.

The stable salt fast reactor has such a cooling system. As shown in Fig. 21.4 the reactor tank fits into a double-walled outer vessel.

Cold air is drawn into the outer space of this double wall, passes down, and then enters the inner space at the bottom of the reactor. It then heats up, rises, and is released to the atmosphere through tall chimneys which provide the draught that drives the air flow with no need for pumps.

Such entirely passive heat loss systems have been conceived before, but they have been found to only work with reactors that are either very low power, or which have huge vessels providing a large surface area for heat loss. The stable salt fast reactor is neither of these. It is a high power and very compact reactor.

What makes passive decay heat loss possible in the stable salt reactor is its high operating temperature. Convective heat loss to flowing air is roughly proportional to the temperature T of the vessel. Heat emission by infrared rays, however, is proportional to $T^4$! A mechanism which is barely relevant at Pressurized water reactor (PWR) temperatures becomes dominant at molten salt reactor temperatures.

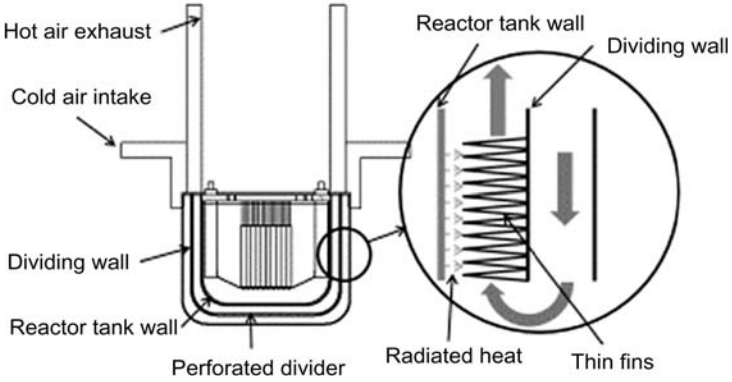

**Figure 21.4** Passive decay heat removal system.

Radiative heat loss from the reactor tank would be pointless, however, unless there was a mechanism to then remove that heat, otherwise the concrete pit in which the reactor sits would just get hotter and hotter. The mechanism used is to fit a large number of thin "fins" to the divider separating the incoming cold and outgoing hot air. The radiated heat is absorbed by the fins which provide a huge surface area for convective heat transfer to the flowing air. This is illustrated in Fig. 21.4.

This mechanism differs fundamentally from the conventional approach of adding fins to the tank itself. Doing this does increase the area for convective heat loss, but because the heat must be transmitted along the fins by conduction, the fins usually have to be relatively short and thick. Thin fins that receive their heat by radiation allow far greater efficiency of heat loss because far greater areas are practical.

## 21.9 Waste and spent fuel management

The fast-spectrum SSR is designed as a plutonium/higher actinide burner. It can be operated on a once-through basis with the substantially burned fuel stored until decay heat production is reduced to the level allowing for disposal in a geologically stable repository.

However, while that process would reduce the amount of long-lived actinide waste from thermal reactors by a factor of about three, the true value of the fast-spectrum SSR is in completely closing the fuel cycle so that long-lived actinide-containing waste is no longer produced.

Spent fuel from the reactor would therefore be reprocessed. Being already in a salt form this is far simpler than is the case for oxide fuel. The spent salt fuel is melted and reprocessed directly by electrolysis. This produces four streams of product:

- A metallic waste form containing the fuel tube metal plus deposited noble metal fission products, including technetium;
- A pure uranium metal fraction which can be stored for future use in breeder reactors;
- An impure uranium/plutonium/higher actinide/lanthanide fraction which is usable as fuel for the SSR with no further purification;
- A mix of actinide free fission products for storage and useful applications or disposal.

Both the metallic waste and fission product waste decay to a level no more radioactive than the original uranium ore after approximately 300 years. They can therefore be stored without the need for a repository that is stable over geological time periods. They could in fact be a source of valuable elements after the 300-year period.

The key feature of the SSR that makes this very desirable process possible is its ability to use fuel that is of very low purity, with the primary fissile fuel (plutonium) contaminated with as much as 50% of uranium and lanthanides. No solid fuel could tolerate such a low purity because the physical properties of the fuel would suffer. Molten salts of course suffer from no such limitation.

## 21.10 Breeding potential

Fast reactors are traditionally seen as routes to breeding new nuclear fuel from fertile isotopes, especially for the high breeding potential of plutonium in the fast neutron spectrum. The reactor described in this chapter is not a net breeder. Breeding of new nuclear fuel is not the economic imperative today that it was expected to be in the 1960s when it was thought that uranium was a very limited resource. Today it is known that uranium is more plentiful and the low contribution to nuclear costs represented by uranium ore means that a large increase in uranium cost would not be an economic problem. At such higher costs, very large reserves of low-grade uranium ore become economically viable, possibly even including sea water. There is therefore no imperative for a breeding program.

Nonetheless, the fast-spectrum SSR is readily converted to a breeding configuration simply by replacing the zirconium fluoride-based coolant with a thorium fluoride-based coolant. This configuration will breed uranium-233 in the coolant which can be readily extracted into molten bismuth using methods established half a century ago. It is actually a mixed breeder, with plutonium-239 being bred from uranium-238 in the fuel salt and uranium-233 from thorium in the coolant salt. At some point, increased uranium costs will make this option economically advantageous—that point will come sooner if the world successfully expands its use of nuclear energy far faster than seems likely today with our focus on economically marginal light-water reactors.

## 21.11 Conclusions

The fast-spectrum stable salt reactor has an enormous economic advantage over other fast reactor designs, due to its far superior intrinsic safety. It can be both highly profitable at electricity prices lower than those achievable by fossil fuels and simultaneously can clean up the long-lived radioactive waste from current and future generation of light-water reactors. It will form a critical part of the massively expanded global nuclear power generation system that is needed if the world is to truly decarbonize its power production.

# Transatomic Power

# 22

*Sean Robertson, Stephen Smith, Mark Massie and Leslie Dewan*
Transatomic Power Corporation, Cambridge, MA, United States

## Chapter Outline

## 22.1 Introduction

In many respects, nuclear energy is an ideal alternative to fossil fuels—it is a well-characterized technology that can generate a large baseload supply of carbon-free electricity at minimal operating cost. However, the nuclear power industry has historically been hampered in part by concerns about nuclear waste production. To address this concern, multiple advanced reactor technologies feature innovative designs that are capable of achieving higher fuel utilization and thus producing significantly less long-lived actinide waste than conventional reactor designs. One of these technologies, the molten salt reactor (MSR), was first developed at the Oak Ridge National Laboratory in the 1950s and 1960s, and is a reactor design that utilizes liquid fuel.

Transatomic Power's (TAP's) previous publicly released technical white paper described how to adapt this design with a new moderator and fuel salt to attain criticality using low-enriched uranium (LEU) fuel (Transatomic Power Corporation, 2014). This report provides additional detail about the reactor physics and

**Molten Salt Reactors and Thorium Energy. DOI: http://dx.doi.org/10.1016/B978-0-08-101126-3.00022-1**

operational characteristics of such a design. TAP's goal in developing this reactor is to reduce reactor waste production by increasing fuel burnup (Burnup, also known as fuel utilization, is defined as the thermal energy extracted per unit mass of heavy metal, typically given in units of GWd/MTHM, where MTHM stands for metric tons of heavy metal [Alain, 2009].). To achieve this goal, the design incorporates a new method of moderator rod operation that minimizes excess reactivity in the core, allowing for considerably higher-burnup than LWRs and decreased waste production (Reactivity, $\rho$, is defined by the equation, $\rho = \frac{k_{\text{eff}} - 1}{k_{\text{eff}}}$, in which $k_{\text{eff}}$ is the reactor's effective multiplication factor, the ratio of neutron populations from one neutron life cycle to the next.).

## 22.2 Fuel utilization in liquid-fueled reactors

The typical definition of fuel burnup is given by the following equation:

$$Bu = \frac{P \cdot t}{m_I}$$

in which $Bu$ is the burnup, $P$ is the reactor's thermal power, $t$ is the fuel residence time, and $m_I$ is the initial actinide loading in the reactor.

In liquid-fueled reactors, it is necessary to modify this equation to take into account the additional mass of actinides, $m_a$, added to the reactor over the course of operation:

$$Bu = \frac{P \cdot t}{m_I + m_a}$$

Nuclear fuel burnup is a key parameter for measuring the efficiency of the nuclear fuel cycle. A higher-burnup fuel cycle decreases waste production, and thus potentially reduces long-term waste storage costs and environmental impact. Increasing burnup is equivalent to increasing the amount of time that a reactor maintains criticality with a given amount of fuel, which is typically accomplished by having either a large initial loading of fissile material, or a high conversion of fertile to fissile nuclei in the reactor (Cochran and Tsoulfanidis, 1999) (This conversion is quantified by a parameter known as the *conversion ratio*, which is defined as the ratio of the fissile material production rate to the fissile material consumption rate.). The main factors limiting fuel burnup in LWRs are structural damage and trapping of fission products in the solid fuel pellets. Over the course of operation, fission product buildup within the rods can reduce the fuel pellets' thermal conductivity, thereby increasing the rod's centerline temperature and decreasing the margin to the fuel's melting point. Increased fuel temperature and radiation-induced damage can lead to swelling in the fuel pellets, which in turn can cause the fuel pellets to impinge on the cladding and, in extreme cases, lead to cladding failure. Buildup of fission products within the fuel rods also reduces the system's reactivity over time, because of several isotopes' high neutron absorption cross-sections.

## 22.3 Fission product removal and reactor fuel utilization

In contrast to solid fuel, liquid fuel has numerous advantages that allow for increased fuel burnup. Liquid fuel has no long-range structure to be damaged, does not experience significant volumetric swelling, and avoids fission product poisoning through continuous fission product removal. To measure quantitatively the effect of fission product removal in molten salt systems, two depletion calculations on otherwise identical models were run using the neutronics software Serpent 2.26 (Leppänen, 2007) (Depletion calculations are computer simulations that model burnup over the course of the reactor's life.). The results of the simulation can be seen in Fig. 22.1, with additional parameters given in Appendix A.

Although fission product removal increases the maximum burnup by more than 27% (44.5 GWd/MTHM compared to 34.8 GWd/MTHM), the final value still falls short of yielding significant improvements when compared to current LWR limits (45 GWd/MTHM). To increase this value further, it is possible to take advantage of

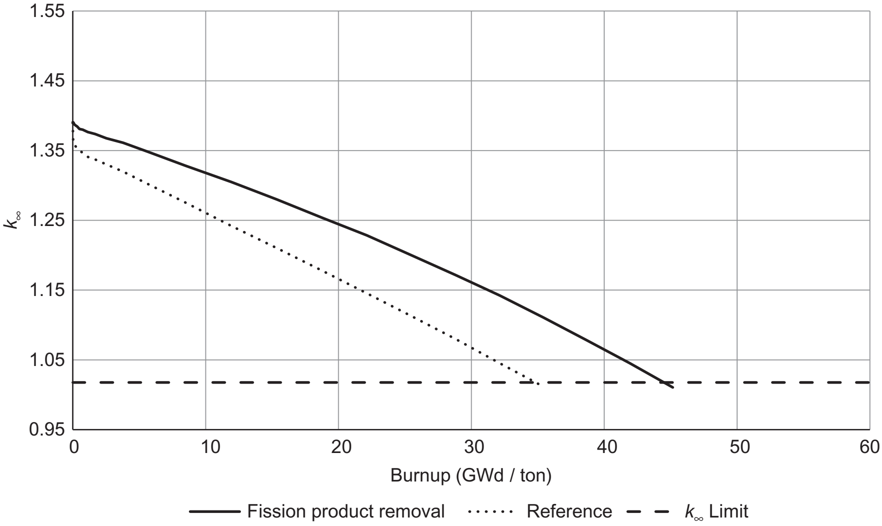

**Figure 22.1** The infinite multiplication factor, $k_\infty$, as a function of burnup, illustrating the effects of fission product removal on two otherwise identical systems. The dashed line for a $k_\infty$ of 1.018 indicates the point at which the reactor can no longer sustain the fission chain reaction when taking into account radial and axial leakage.

another aspect of liquid-fueled reactors: the ability to easily vary their geometry, by inserting or removing moderator rods in the reactor core.

## 22.4 A new take on reactivity control

In order to account for the loss of fissile material over the course of operation, solid-fueled nuclear reactors use core configurations and fuel compositions that result in excess positive reactivity at the beginning of life (BOL). During normal operation, excess reactivity is accounted for using control rods and soluble absorbers—the additional neutrons are captured, and the reactor can be operated safely.

The concept of "reactivity swing" (the variation in reactivity in a reactor over the course of a given fuel loading) is shown graphically in Fig. 22.2. A reactor with a large reactivity swing is inherently inefficient, as neutrons that could have otherwise been used for fission and conversion in the fuel are effectively wasted in the absorbers and control rods. An ideal reactor therefore has minimal reactivity swing, and can use its neutron population with the greatest efficiency during operation.

The neutron balance in a reactor is a function of both geometry and core material composition. In solid-fueled reactors, geometry is largely fixed, and control is achieved through modifications in the composition—insertion and removal of neutron-absorbing material. Liquid-fueled reactors, however, make it possible to control reactivity by altering the core's geometry, thereby largely eliminating

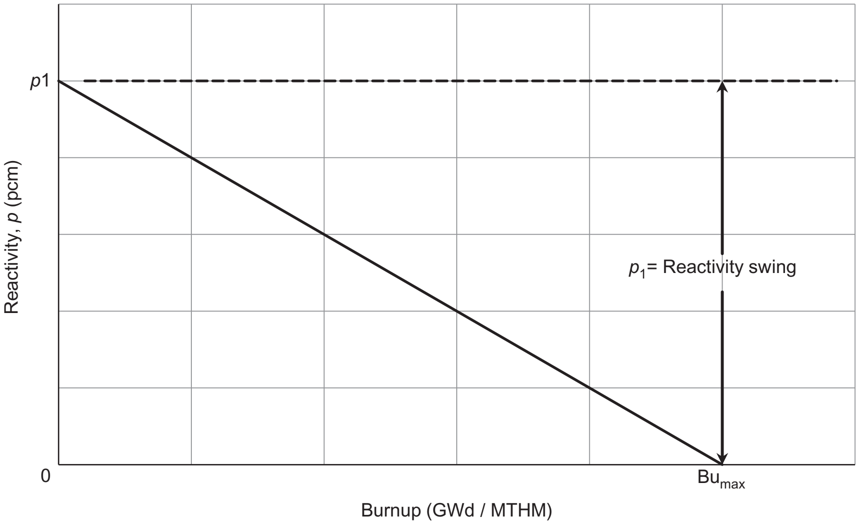

**Figure 22.2** A graphical depiction of reactivity swing, adapted from Cochran and Tsoulfanidis (1999). As fissile material is consumed throughout the course of operation, the extent to which positive reactivity exists in the core diminishes, up until the point at which criticality ($\rho = 0$) is no longer achievable (maximum burnup).

reactivity swing in the system. Specifically, it is possible to readily vary the salt volume fraction (SVF; the percentage of the core volume occupied by fuel salt) in an MSR core by inserting or removing moderator rods. In order to illustrate the effect of changing SVF in the core, a scoping study consisting of multiple steady-state pin cell calculations was performed in Serpent 2.26.

Varying the levels of $^{235}$U enrichment (1%–5%) and modifying SVF through the simulation of different-sized moderator rods makes it possible to estimate the evolution of the fuel with time. Fig. 22.3 shows a plot of infinite multiplication factor as a function of SVF for these multiple enrichment levels. The graph shows that as fissile material concentration in the reactor decreases, the reactor can either maintain criticality:

1. By beginning with a large amount of excess reactivity and a constant SVF, as in a stationary moderator rod configuration, or,
2. By decreasing SVF, as in a moveable moderator rod configuration.

Although exact operational progression cannot be derived from this graph, since the simulations do not take into account the generation of transuranic isotopes over the course of life, the general relationships among fissile concentration, multiplication factor, and SVF can be inferred.

From this trend, it can be seen that it is possible to control the system's reactivity by adjusting the reactor's SVF. Such an adjustment can thus be used to eliminate reactivity swing, thereby increasing the reactor's neutron utilization efficiency and

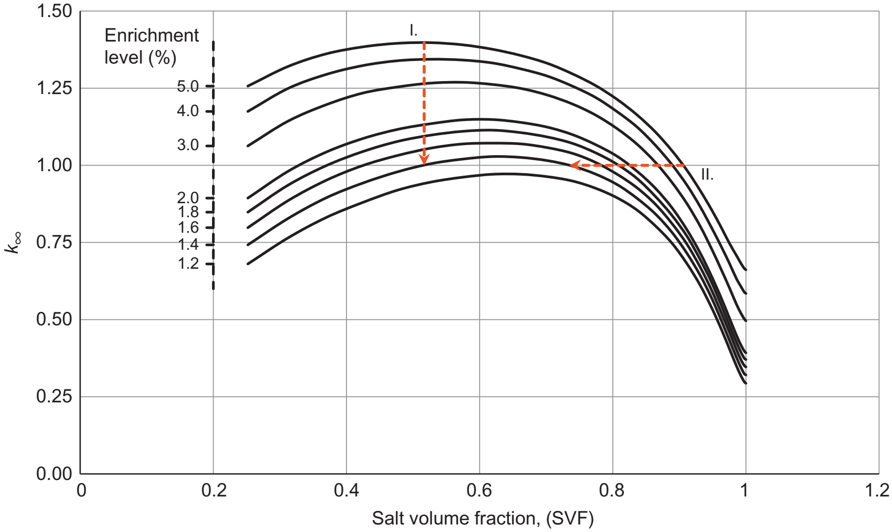

**Figure 22.3** The infinite multiplication factor as a function of SVF and $^{235}$U enrichment. The expected operational progression of both a stationary rod configuration (I, vertical) and moveable rod configuration (II, horizontal) have been presented through the use of red dashed lines. Additional simulation details are given in Appendix A.

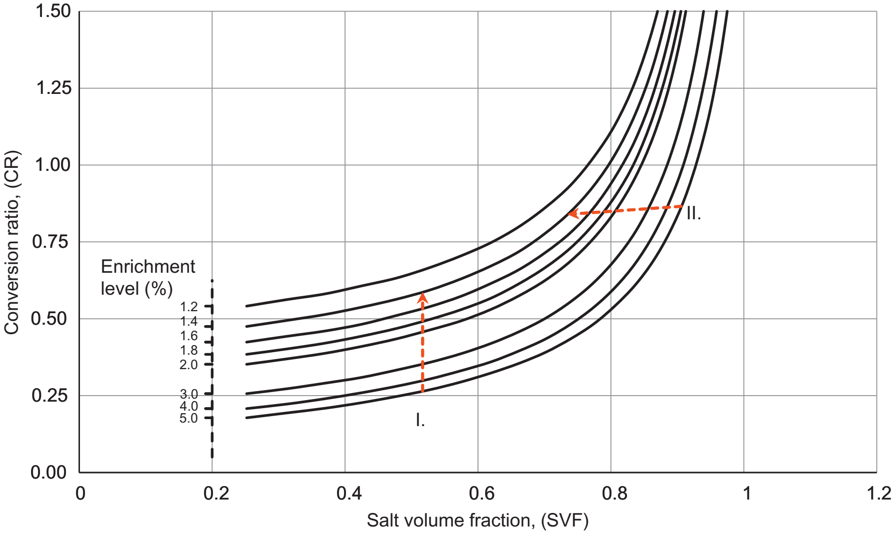

**Figure 22.4** Conversion ratio as a function of SVF and $^{235}$U enrichment. SVF was modified by changing the moderator rod radius. The expected operational progression of both a stationary rod configuration (I, vertical) and moveable rod configuration (II, horizontal) have been presented through the use of red dashed lines.

conversion ratio. Fig. 22.4 illustrates this effect through a plot of conversion ratio as function of enrichment and SVF. The graph demonstrates that as fissile material concentration decreases, moving from higher to lower SVF does, in fact, produce a higher conversion ratio over the course of life (2) than does a stationary rod configuration (1).

In practice, SVF will be varied by inserting fixed-sized moderator rods via the bottom of the reactor vessel (for safety considerations), in a manner analogous to moving the control rods in a boiling water reactor, as shown in Fig. 22.5. The reactor therefore does not require control rods beyond a single shutdown rod for safety. As an additional shutdown mechanism, moderator rod removal may also act as a means of bringing the reactor into a subcritical state.

## 22.5 Depletion calculations with movable moderator rods

The scoping calculations make it possible to infer the influence of SVF on burnup and reactivity control in an MSR. Following this initial scoping, assembly-level depletion calculations were used to simulate the system evolution over time to a higher degree of accuracy. In these simulations, SVF was adjusted to minimize excess reactivity. The model employs continual fission product removal and a fuel addition method that maintains constant actinide concentration following each time

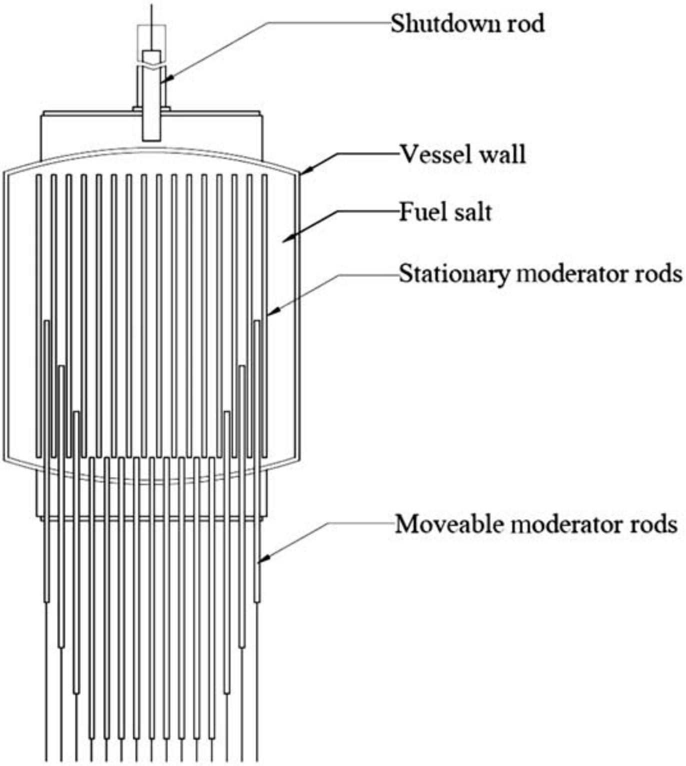

**Figure 22.5** A conceptual depiction of a reactor core design that uses movable moderator rods for reactivity control. The gap between the moderated region and the reactor vessel wall contains unmoderated fuel salt that acts as both a reflector and fertile nuclei conversion zone.

step (In an operating MSR, it is necessary to add additional actinide fuel to the system so that the fuel salt can remain at its eutectic composition. Additionally, further details on fission product removal are included in Appendix A.). The initial actinide loading is comprised of 5% LEU, with two different feed compositions being used for comparison: one consisting of 5% LEU, and the other consisting of 50 GWd/MTHM SNF.

Fig. 22.6 shows the change in SVF in the TAP reactor as a function of burnup for both feed compositions. At the BOL, a high SVF is used to harden the spectrum and convert the maximum amount of fertile material while the fissile content is still high (Also note that at the beginning of life, leakage in the system is approximately 4.3%, dropping to 1.8% by the end of life. Leakage considerations are described in more detail in Appendix B.). As shown in Fig. 22.7, as fissile concentration begins to drop additional moderator rods are inserted in order to maintain criticality, leading to a decrease in SVF and subsequently conversion ratio (Fig. 22.8).

As the final mass of feed in these simulations is small in comparison to the initial actinide load, the small difference between the two fuel cycles is caused by the

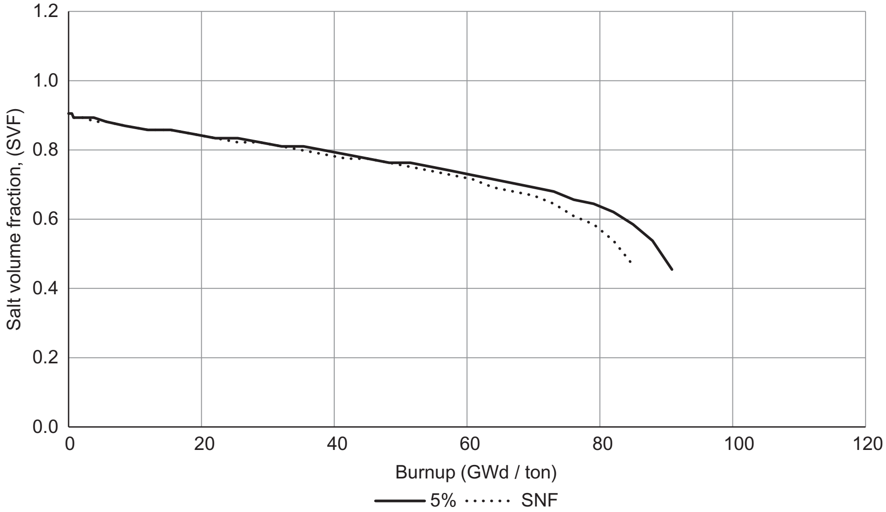

**Figure 22.6** The change in SVF as a function of burnup in the TAP reactor for a 5% enriched initial fuel load. The legend refers to the two analyzed feed compositions: 5% enriched and SNF. Additional calculation details are given in Appendix A.

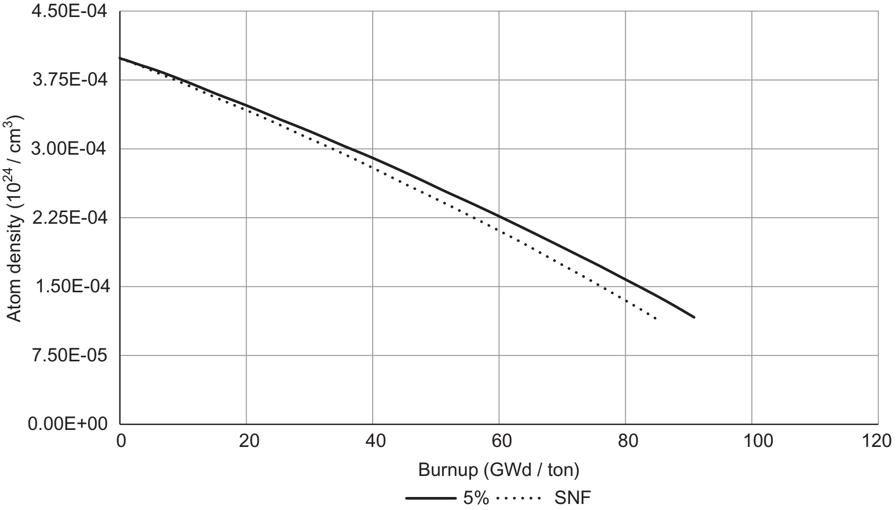

**Figure 22.7** Fissile atom density as a function of burnup for the representative TAP reactor operation. The legend refers to the two analyzed feed compositions: 5% enriched and SNF. The data represent a summation of the $^{235}$U, $^{239}$Pu, and $^{241}$Pu atom densities, with their respective individual trends being given in Appendix C.

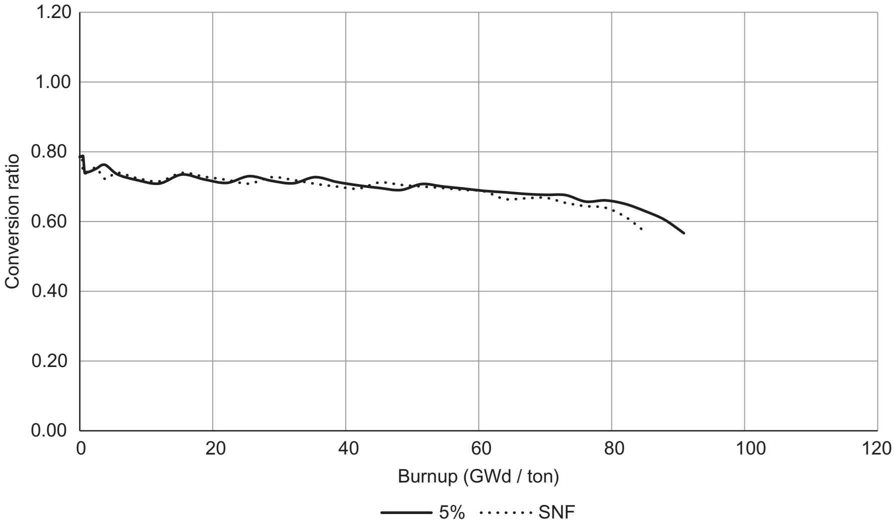

**Figure 22.8** Conversion ratio as a function of burnup for the representative TAP reactor operation. The legend refers to the two analyzed feed compositions: 5% enriched and SNF. Additional calculation details are given in Appendix A.

slight difference in feed composition. Specifically, the fissile concentration of the feed material has a direct influence on conversion ratio, as it can be thought of as an additional fissile production term. Eq. (22.1) illustrates this effect by presenting an effective conversion ratio ($CR_{\mathrm{eff}}$), defined as the system's conversion ratio ($CR$) plus the fissile concentration of the feed ($F_{\mathrm{Feed}}$).

$$CR_{\mathrm{eff}} = CR + F_{\mathrm{Feed}} \tag{22.1}$$

## 22.6 Waste reduction

Addressing nuclear energy's major challenge of long-lived waste disposal requires two substantial steps, as the industry must both reduce the rate at which waste is produced and find a long-term solution for the world's nuclear waste stockpiles. The TAP MSR's unique reactor design makes significant strides by maximizing burnup to reduce the waste production rate, and in doing so limiting the requirement of future repositories.

As shown in Fig. 22.9, fuel burnup and waste production exhibit an inverse power relationship, meaning that the effect of increased burnup on waste production depends highly on the reference position. With 100% fuel utilization being equivalent to 909 GWd/MTHM and current LWR achieving burnups on the order of 45 GWd/MTHM, it is clear that there remains substantial room for improvement.

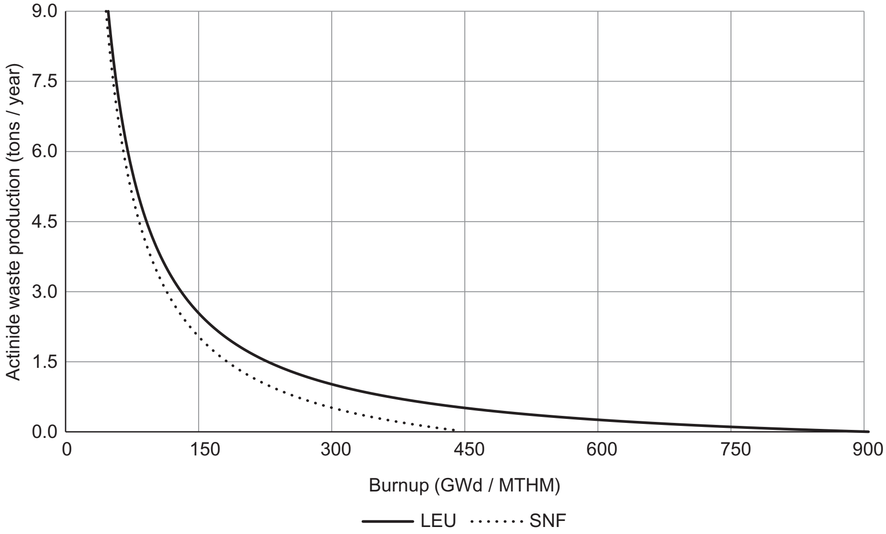

**Figure 22.9** Annual actinide waste production as a function of burnup, normalized to a 1250 MWth power level. The legend indicates feed compositions of low-enriched uranium (LEU) and SNF.

To fully explore TAP's goal of maximizing burnup in the TAP MSR, in addition to the fuel cycle cases discussed above, an identical depletion calculation was run for a fuel cycle in line with the enrichment levels proposed by other advanced reactor developers: a 10% enriched initial fuel load with a 20% enriched feed. Fig. 22.10 compares the results of this calculation and those discussed previously in terms of the TAP MSR's improvement over current LWR technology.

As shown in Fig. 22.10, higher enrichments lead to higher burnups, and therefore less waste, due to their ability to maintain criticality for longer periods of time. At the highest LEU enrichment levels, this ability results in an 83% reduction in annual waste production below that of LWRs. Even under the current industry fuel cycle regime of a 5% enriched initial load with a 5% feed, the TAP MSR reduces annual waste production by approximately 53%.

Further details on the calculations used to determine the TAP MSR's fuel cycle profile can be found in Appendix A.

## 22.7 Conclusion

The TAP MSR design takes advantage of its liquid fuel to allow for more than twice the fuel utilization of LWRs, leading to an approximately 53% reduction in waste when using 5% enriched uranium, the maximum enrichment readily available in the current supply chain. Using higher enrichments, up to the 20% LEU limit, this reduction reaches 83%. These accomplishments represent major leaps forward,

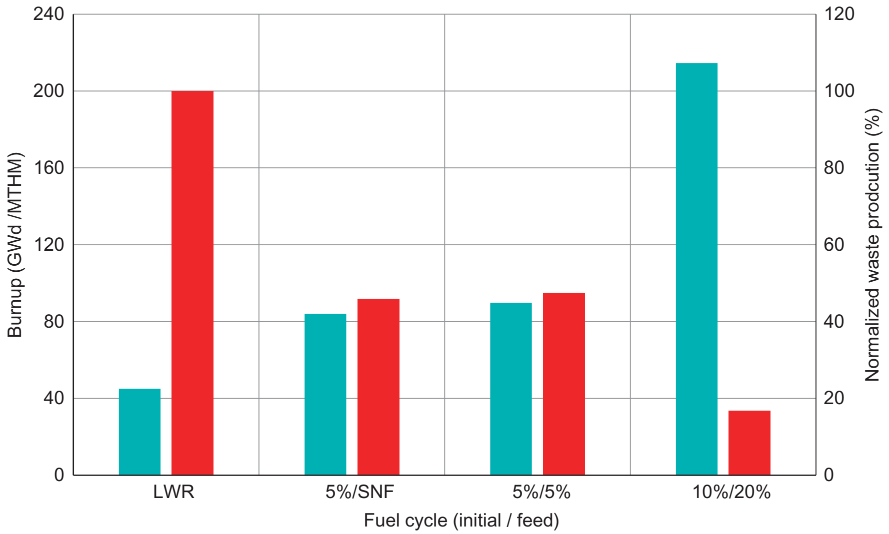

**Figure 22.10** Burnup (left) and normalized waste production (right) for the examined fuel cycles, normalized to a 1250 MWth power level.

inverting commonly held beliefs about the nature of nuclear technology, and enabling nuclear energy to be a viable source of carbon-free baseload power.

## 22.8 Appendix A: calculation details

All data presented in this report were generated using the Monte Carlo neutronics software Serpent 2.26.

### *22.8.1 Geometry*

The geometry modeled throughout the report is a three-dimensional, 3 cm pitch, 7 × 7 rod assembly, as depicted in Fig. A.1. The $ZrH_{1.66}$ moderator rod radius is 1.25 cm, and the rod insertion order used in the simulations is illustrated by the number located in the center of each rod, with 1 indicating the first rod inserted and 49 the last. It should be noted that 4 and 5 cm-pitch models produce similar results, and may be chosen moving forward to limit the total number of rods in the reactor.

### *22.8.2 Materials*

A summary of the material compositions used throughout the simulations is given in Table A.1. Calculations using graphite cladding were also performed and show similar results. For simplicity, only one fuel example (5% LEU) is presented in Table A.1.

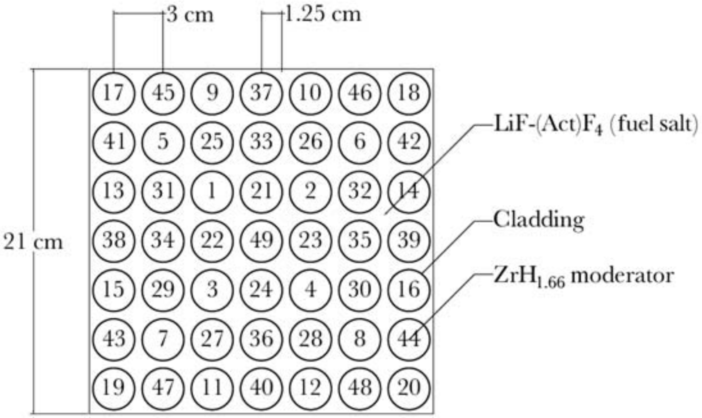

**Figure A.1** Radial cross-section of the assembly simulated in Serpent 2.26. The numbers located in the center of each rod indicate the insertion order used throughout the report, with 1 indicating the first rod inserted and 49 the last.

**Table A.1** **A summary of material compositions and densities used in the simulations referenced throughout the report**

| Fuel salt (5.01 g/$cm^3$) | | Silicon carbide (3.21 g/$cm^3$) | | Zirconium hydride (5.66 g/$cm^3$) | |
|---|---|---|---|---|---|
| **Isotope** | **Weight fraction** | **Isotope** | **Weight fraction** | **Isotope** | **Weight fraction** |
| $^{235}U$ | 3.1100E-02 | $^{12}C$ | 2.9936E-01 | $^{90}Zr$ | 4.9793E-01 |
| $^{238}U$ | 5.9090E-01 | $^{28}Si$ | 6.4365E-01 | $^{91}Zr$ | 1.0980E-01 |
| $^{7}Li$ | 4.8358E-02 | $^{29}Si$ | 3.3866E-02 | $^{92}Zr$ | 1.6967E-01 |
| $^{6}Li$ | 2.4180E-06 | $^{30}Si$ | 2.3120E-02 | $^{94}Zr$ | 1.7569E-01 |
| $^{19}F$ | 3.2964E-01 | | | $^{96}Zr$ | 2.8908E-02 |
| | | | | $^{1}H$ | 1.8007E-02 |
| | | | | $^{2}H$ | 4.1389E-06 |

The weight fractions listed are relative to the individual materials and are not representative of the system as a whole.

## 22.8.3 Boundary conditions

In order for the model to better represent the core configuration, the simulations invoked reflective boundary conditions, allowing for simulation of an infinite array of the defined assembly (Fig. A.1). Leakage considerations as a result of this infinite lattice are discussed further in Appendix B.

## 22.8.4 Cross-section libraries

All cross-sections used in the calculations were obtained through the evaluated nuclear data file database ENDF-VII.1. Scattering kernels for zirconium hydride are

**Table A.2** **The fission product removal rates implemented in the depletion calculations discussed previously**

| Element | Removal rate (atoms/second) | Element | Removal rate (atoms/second) | Element | Removal rate (atoms/second) |
|---|---|---|---|---|---|
| H | 5.00E-2 | Br | 1.93E-7 | Sn | 5.79E-8 |
| Ca | 3.37E-9 | Kr | 5.00E-2 | Sb | 5.00E-2 |
| Sc | 3.37E-9 | Rb | 3.37E-9 | Te | 5.00E-2 |
| Ti | 3.37E-9 | Sr | 3.37E-9 | I | 1.93E-7 |
| V | 3.37E-9 | Y | 2.31E-7 | Xe | 5.00E-2 |
| Cr | 3.37E-9 | Zr | 5.79E-8 | Cs | 3.37E-9 |
| Mn | 3.37E-9 | Nb | 5.00E-2 | Ba | 3.37E-9 |
| Fe | 3.37E-9 | Mo | 5.00E-2 | La | 2.31E-7 |
| Co | 3.37E-9 | Tc | 5.00E-2 | Ce | 2.31E-7 |
| Ni | 3.37E-9 | Ru | 5.00E-2 | Pr | 2.31E-7 |
| Cu | 3.37E-9 | Rh | 5.00E-2 | Nd | 2.31E-7 |
| Zn | 3.37E-9 | Pd | 5.00E-2 | Pm | 2.31E-7 |
| Ga | 3.37E-9 | Ag | 5.00E-2 | Sm | 2.31E-7 |
| Ge | 3.37E-9 | Cd | 5.79E-8 | Eu | 2.31E-7 |
| As | 3.37E-9 | In | 5.79E-8 | Gd | 2.31E-7 |
| Se | 5.00E-2 | | | | |

not provided by default in Serpent 2.26, and therefore additional data from MonteCarl N Particle neutronics code (MCNP) were converted into the appropriate format.

### 22.8.5 Neutron population

All assembly-level calculations discussed were modeled using a simulated population of 10,000 neutrons per cycle, for 30 inactive and 300 active cycles. The statistical error associated with this level of convergence is on the order of ±0.0006 and 0.0004 for the analogue and implicit $k_\infty$ values of each time step, respectively.

### 22.8.6 Fission product removal

The fission product removal rates used in the simulations can be seen in Table A.2.

### 22.8.7 Time step

In depletion calculations for systems out of equilibrium, it is important to ensure that the initial time steps are short enough to properly simulate the initial evolution of the different actinide vectors. As a result, exponential progression in the size of the steps, as shown in Eq. (A.1), is common practice, with the current simulations beginning with an initial step of 0.1 days ($\Delta t_I$), increasing by a factor of 1.5 for each subsequent step ($n$).

$$\Delta t = \Delta t_I \cdot 1.5^{n-1} \tag{A.1}$$

Over the course of operation, fuel addition and SVF continually disrupt this aforementioned equilibrium, and it is therefore also important to limit the size of the maximum allowable time step. For all results discussed previously, 6 months was chosen as the maximum step limit ($\Delta t_{\max}$), with an even more accurate estimation into the final burnup values coming through the use of a Richardson extrapolation Eq. (A.2).

$$Bu = \frac{4Bu(\Delta t_{max}) - Bu(2\Delta t_{max})}{3} \tag{A.2}$$

By running a second depletion calculation with a maximum time step of 12 months ($2\Delta t_{\max}$) and extrapolating in combination with the previous 6-month results, the uncertainty associated with the final burnup values is drastically reduced.

## 22.9 Appendix B: leakage considerations

In order to limit excess reactivity and achieve a high conversion ratio at the BOL, the initial SVF must be very high, on the order of 0.9 for a 5% initial load. As a result, the neutron spectrum at the BOL is hardened compared to that of the end of life (EOL), as shown in Fig. B.1.

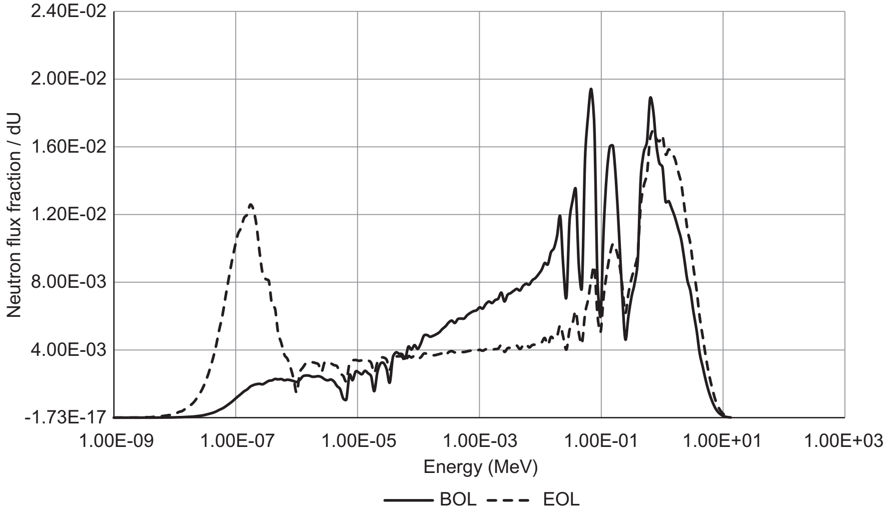

**Figure B.1** Normalized neutron flux per lethargy as a function of energy at the beginning of life (BOL) and end of life (EOL). The spectra were taken from the depletion results of the 5% LEU initial load/5% feed fuel cycle trial.

To accurately model such a spectrum, unresolved resonance probability tables were included in the calculations for several significant isotopes: $^{235}$U, $^{238}$U, $^{238}$Pu, $^{239}$Pu $^{240}$Pu, $^{241}$Pu, and $^{242}$Pu. The omission of other actinides in this consideration is not expected to introduce significant error, as their low concentrations over the course of operation minimize their overall influence.

As the leakage rate of the hardened spectrum is expected to be higher than that of the more thermal spectrum at the EOL, $k_\infty$ limits over the course of a depletion calculation must reflect this evolution. Fig. B.2 shows the estimated $k_\infty$ trend as a function of the number of rods inserted in an assembly, with leakage considerations, both radially and axially, being obtained by comparing the $k_\infty$ of the infinite assembly to that of a representative three-dimensional core, as shown in Fig. B.3.

Acting as a complement to Figs. B.2, B.4 and B.5 show the radial flux profile of the reactor at the BOL for a 5% enriched initial actinide load, and the Shannon entropy as a function of the number of inactive cycles, respectively. Shannon entropy is used as a metric to verify that the source distribution has converged prior to the start of active simulation cycles.

## 22.10 Appendix C: isotopic evolution

In stationary rod configurations, the conversion ratio is expected to increase over time as a result of the evolving plutonium vector: plutonium's fissile

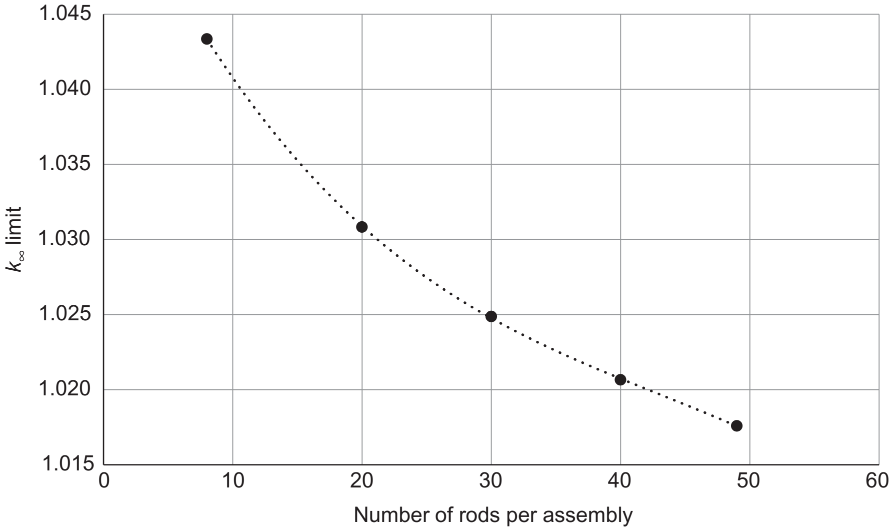

**Figure B.2** Assembly level $k_\infty$ limit as a function of the number of rods inserted. Assemblies are comprised of a 7 × 7 array of $ZrH_{1.66}$ moderator rods.

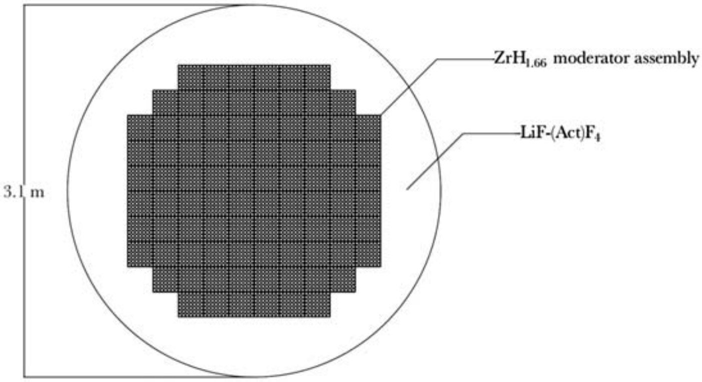

**Figure B.3** A radial cross-section of the EOL full core model used in the leakage calculations.

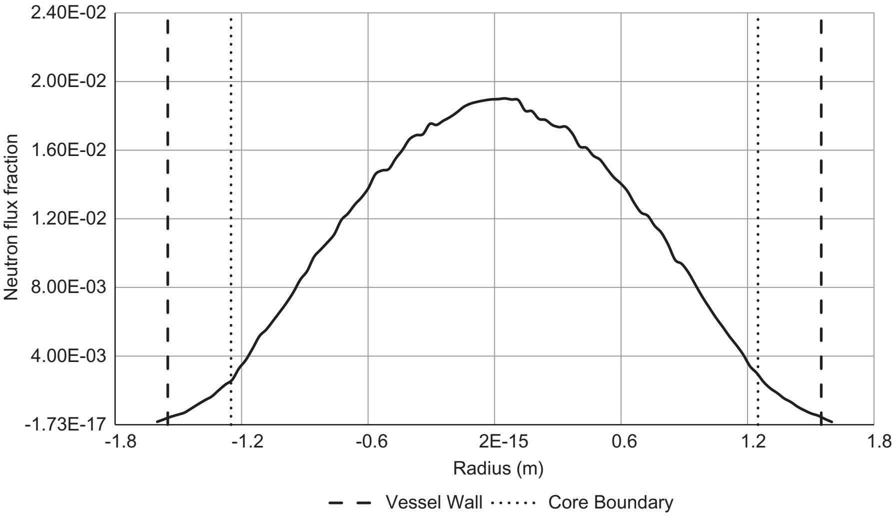

**Figure B.4** Full core radial flux profile for a 5% enriched initial actinide load.

isotopes (e.g., $^{239}$Pu and $^{241}$Pu) produce both more neutrons, and greater energy per fission than that of $^{235}$U, as well as $^{240}$Pu possesses a significantly higher capture cross-section at lower energies ($<10^{-5}$ MeV) than that of $^{238}$U. In a movable rod method, this effect is outweighed by increased moderation, producing a thermalized spectrum at the EOL (see Fig. B.1), which is unfavorable for conversion.

Fig. C.1 shows the evolution of some of the primary fissile and fertile isotopes as a result of this changing neutron spectrum.

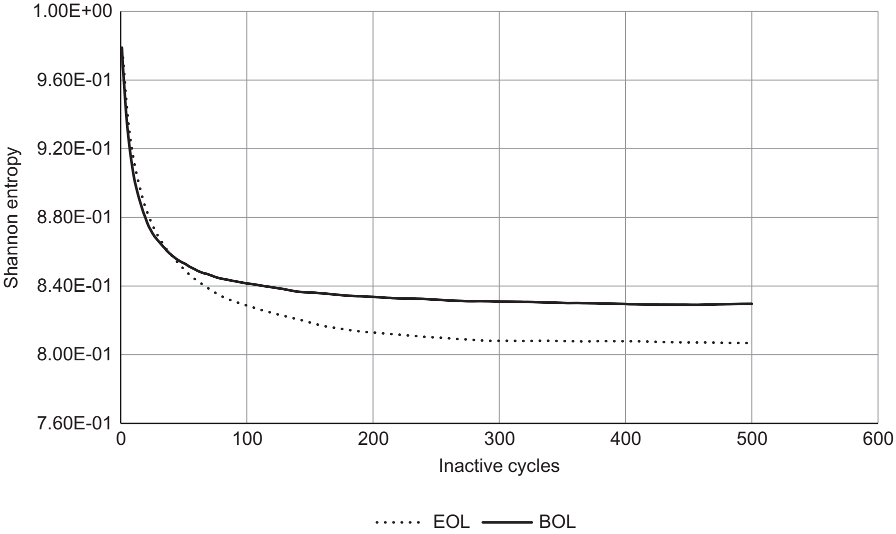

**Figure B.5** Shannon entropy as a function of the number of inactive cycles for the full core leakage calculations.

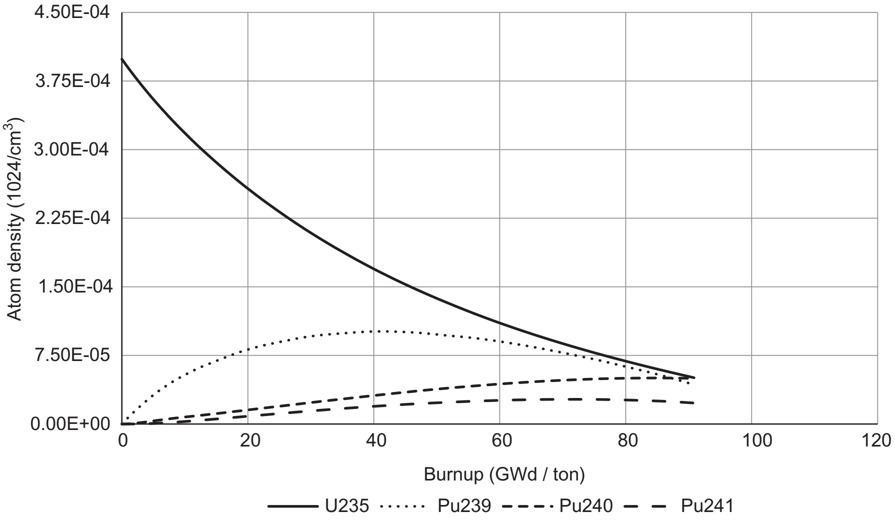

**Figure C.1** The evolution of several primary fissile and fertile isotopes for the 5% initial load / 5% feed depletion simulation.

The effect of the movable rods is most visible upon examination of the sharp decrease in $^{239}$Pu. After roughly 30 GWd/MTHM, $^{239}$Pu surpasses $^{235}$U as the primary contributor to fission in the core, as shown in Table C.1. In addition to this larger consumption rate, $^{238}$U capture can also be seen to drastically decrease over the course of life, as shown in Table C.2, reducing the production rate of $^{239}$Pu.

**Table C.1** Relative fission rate fraction for the three primary fissile isotopes as a function of burnup

| | Burnup (GWd/MTHM) | | | | | | |
|---|---|---|---|---|---|---|---|
| **Isotope** | **0** | **15** | **30** | **45** | **60** | **75** | **90** |
| $^{235}$U | 0.93 | 0.56 | 0.42 | 0.31 | 0.24 | 0.20 | 0.18 |
| $^{239}$Pu | 0.00 | 0.33 | 0.43 | 0.50 | 0.52 | 0.52 | 0.50 |
| $^{241}$Pu | 0.00 | 0.03 | 0.06 | 0.11 | 0.15 | 0.19 | 0.25 |

The remaining fraction is a combination of $^{238}$U fast fission and higher actinides.

**Table C.2** Relative capture rate as a function of burnup for $^{238}$U

| | Burnup (GWd/MTHM) | | | | | | |
|---|---|---|---|---|---|---|---|
| **Isotope** | **0** | **15** | **30** | **45** | **60** | **75** | **90** |
| $^{238}$U | 1 | 0.89 | 0.81 | 0.76 | 0.71 | 0.63 | 0.50 |

The data are normalized to the $^{238}$U capture rate at the beginning of life.

## References

Alain, H., 2009. Applied Reactor Physics. Presses Internationales Polytechnique, Montreal, Quebec.

Cochran, R.G., Tsoulfanidis, N., 1999. In-core fuel management. The Nuclear Fuel Cycle: Analysis and Management. American Nuclear Society, La Grange Park, IL, pp. 165–205.

Leppänen, 2007. Development of a new monte carlo reactor physics code, D.Sc., Helsinki University of Technology, Helsinki, Finland.

Transatomic Power Corporation, 2014. Transatomic technical white paper.

# Copenhagen Atomics waste burner

# 23

*Thomas J. Pedersen*
Copenhagen Atomics, Denmark

## Chapter Outline

Copenhagen Atomics (CA) is working on a thorium molten salt reactor (MSR), configured as a waste burner and placed in an airtight 13-m (40-ft) shipping container. The goals are

1. To develop a MSR that is able to start on plutonium from *spent nuclear fuel* (SNF).
2. To show that it is plausible that these reactors can be manufactured at *low cost* on an assembly line and decommissioned and recycled on another assembly line.
3. To help develop systems that can *convert* SNF from fuel rods into a molten salt fuel for our reactor design.

We aim to create partnerships with other companies, countries, and researchers that want to achieve some of the same objectives. Copenhagen Atomics' primary strengths currently lie in chemistry, measurement technology, and control systems. We will start from here and build our competences and partnerships where it makes most sense. The structure of our project resembles that of an open-source project more than one of a large organization with a fully funded project and a fixed delivery date. Our mindset towards collaboration, openness, and sharing also resembles that of an open-source project more than the typical corporate nuclear industry

**Molten Salt Reactors and Thorium Energy. DOI: http://dx.doi.org/10.1016/B978-0-08-101126-3.00023-3**

project. The long-term goal is to be able to start more than one thorium breeder MSR every day.

## 23.1 Reactor design choices

The best way to explain the design choices behind the CA Waste Burner is to understand what it would take to power more than two-thirds of the entire global population with energy at 200 GJ per capita per year ($\approx 10^{20}$ J/year). Clearly, it would be possible to mine enough thorium to do so at low cost, thus the main problem is to get enough fissile material (U233, U235, and Pu239) to start these thorium reactors. Only the last two will be available in significant quantities within the next 2−3 decades. U235 is obtained through enrichment of natural U, and Pu239 is obtained from recycling SNF or old bomb material. Both enrichment of uranium and recycling of plutonium are large political problems, because these techniques can also be used for nuclear weapons. Therefore, it has been agreed internationally that these technologies and the access to U and Th source materials must be guarded with high security. The USA and the international atomic energy agency (IAEA) have been trying to limit the number of countries globally with access to enrichment and plutonium recycling, but all the weapon states have this technology.

Even if plutonium recycling and uranium enrichment were not political problems, it would still be highly unlikely that we humans would be able to produce two-thirds or even 10% of global energy ($10^{20}$ J/year) from any nuclear technology before 2050 (www.theng.dk/simulation/breederfactor), unless we built some type of breeder reactor. Research has shown that it may be possible to build thermal neutron spectrum solid fuel thorium breeder reactors. However, the same research shows that the breeding ratio would be very close to 1, with a doubling time of many decades. Thus, it is clear that if nuclear energy is ever going to play a significant role in global energy, then we must use (thermal or fast spectrum) liquid fuel MSRs or fast spectrum solid fuel reactors. Nearly 20 fast spectrum solid fuel reactors have been developed since the 1950s, and none of these has become a commercial reactor. Thus, liquid fuel molten salt reactors are the best route to follow.

It is very important to depart from the mindset of today's nuclear industry, where it often takes more than 10 years to incorporate small changes to the current light-water reactor technology. We must find a way to build MSRs with a rapid technology improvement cycle. The oak ridge national laboratory-molten salt reactor experiment (ORNL-MSRE) and physics capability show that it would be possible to power the entire world with thorium MSRs, but political and funding issues are large roadblocks. We concluded that a small modular reactor is likely to create the least political problems and funding issues, while facilitating rapid technology improvement cycles. However, we must be able to demonstrate to the public that MSRs are safe and that the waste problem can be solved.

This book lists a number of different reactor designs, each of which advocates different combinations of fuel mix and neutron spectrum (see Table 23.1).

Table 23.1 **Overview of thorium MSR configurations and fuel choices**

| **MSR types** | **Moderator:** | **Startup fuel** | |
|---|---|---|---|
| | | **U235 + U238** | **Pu239 + Th232** |
| Fast spectrum | None | U235F | P239F |
| Thermal spectrum | Graphite | U235G | P239G |
| | Heavy water | U235HW | P239HW |

Here we will only list a few of the main reasons why CA has chosen P239HW for our reactor design.

We favor *thermal* reactors over fast reactors for two reasons:

1. The major limiting factor to how fast the world can deploy thorium MSRs as the primary energy source is the amount of fissile fuel available in the world to start up these reactors. The thermal fission cross-section is over 100 times larger than the fast spectrum cross-section, so much more fissile inventory is needed to start up a fast reactor vs. a thermal reactor of the same power rating.
2. Because the fissile fuel density of fast reactors is much higher than that of thermal reactors they could go supercritical if a moderator (such as water or graphite) entered the salt. To circumvent this danger requires extra safety systems, which may be complex, risky, and expensive.

We favor *heavy water* over graphite as a moderator two reasons:

1. Heavy water captures fewer neutrons than graphite, facilitating a better neutron economy and breeding ratio. This makes it easier to solve problems related to reactor design and waste reduction. In the very long term (30 years) we expect that the breeding ratio of the CA Waste Burner, running on pure U233 after 10 generations, will reach a breeder ratio of 1.1. By that time we will have burned most of the Pu239 from SNF in the world.
2. Until now, no one has been able to propose a way to decommission, or even better to recycle, the radioactive graphite moderator after use. Thus, until the problem of graphite decommissioning has been solved, we believe heavy water is an economic and ecologically better choice, with less R&D risk.

CA favors *Pu239* over U235 as the startup fuel because:

1. The cost of enriched uranium may increase, which add risk to the choice of this fuel cycle. Enrichment is also directly related to proliferation issues, and therefore may cause additional risk associated with changing political and public opinion. Finally, the U235 fuel cycle results in large mining operations and waste.
2. The U235 fuel cycle eventually produces more long-lived actinides than the plutonium–thorium fuel cycle. Thus since CA want to make waste burners that minimize the amount of SNF in the world the logical choice is to use the plutonium–thorium fuel cycle (Pu239 startup and Thorium breeding).

## 23.2 Mechanical design choices

CA believes it is paramount to have fast technology cycles and good breeding potential, and has therefore chosen to focus on a MSR design which can be made small, while still having a fairly good breeding ratio. CA believes that a 13-m (40-ft) shipping container unit size (see Fig. 23.1) gives the best tradeoff between performance and small size for easy transport, recycling, and fast technology cycles.

Fig. 23.2 shows the plant arrangement. The reactor and the blanket are placed underground (Fig. 23.3) and any such units can be placed next to each other inside the reactor building dome to increase power and reliability. The thorium in the blanket will capture leaking neutrons and ensure that the neutron and gamma radiations on the outside of the blanket are very small. After several years the blanket can be processed and a mix of Th232–U233 can be used in a new reactor.

The CA Waste Burner uses the primary fuel salt as the heat transport medium. Thus the flow rate of salt through the core is dictated by the reactor power output, the heat capacity of the fuel salt, and the temperature drop of the primary heat exchanger. Flow rates above 100 L/s are expected.

Simulations by CA show that it may be possible to remove between 25% and 50% of the fission products from the fuel salt (https://youtu.be/sDMFONiFAaI), if it is fed through a vacuum aerosol directly after exiting the reactor core. This aerosol chamber is placed between the reactor core and the primary heat exchanger as shown in Fig. 23.2.

Helium is used as the cover gas everywhere inside the waste burner, which is sealed airtight after the fuel salt has been loaded. Helium is used to improve the fission product removal in the vacuum aerosol, and to separate the fission products from the helium flow gas a helium purification membrane is used. All these systems are located inside the waste burner container.

The CA Waste Burner does not require a freeze plug, the dump tank is integrated in the primary fuel salt loop. If power is lost, the salt will drain to the dump tank where passive cooling is available when the liquid level rises above a certain point. Passive cooling is achieved via long pipes drilled into the surrounding dirt at an angle > 5° above horizontal and filled with oil (see Fig. 23.3). Passive convection in the pipes removes the decay heat efficiently. Other decay heat removal systems with contact to outside air or water streams carry the risk of attack on an easy single point of failure by terrorists or other adversaries. If required by regulators our

**Figure 23.1** Illustration of the CA Waste Burner concept fitting into a 40-ft. container.

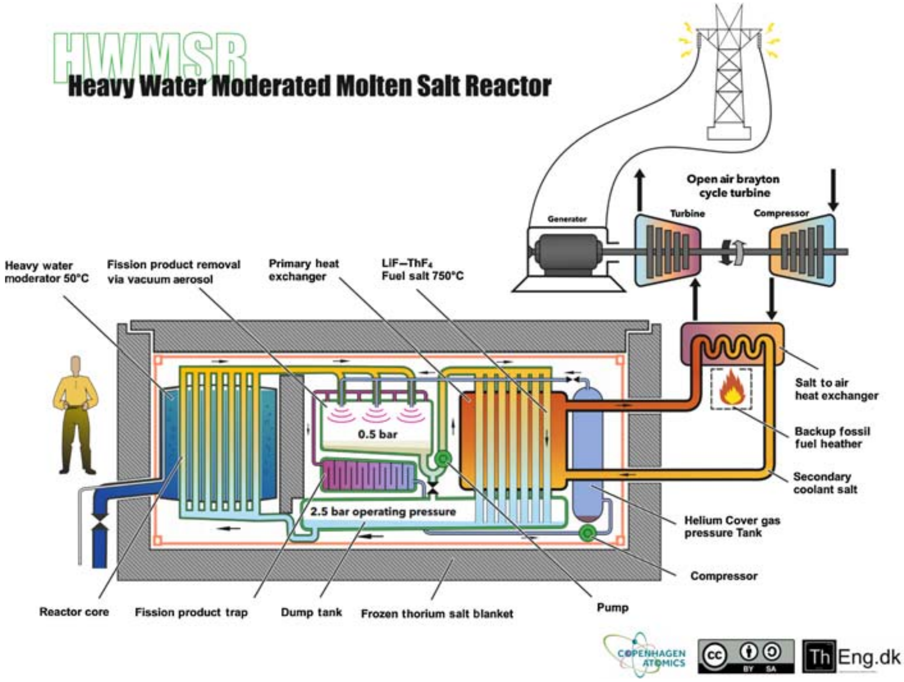

**Figure 23.2** Schematic of the CA Waste Burner.

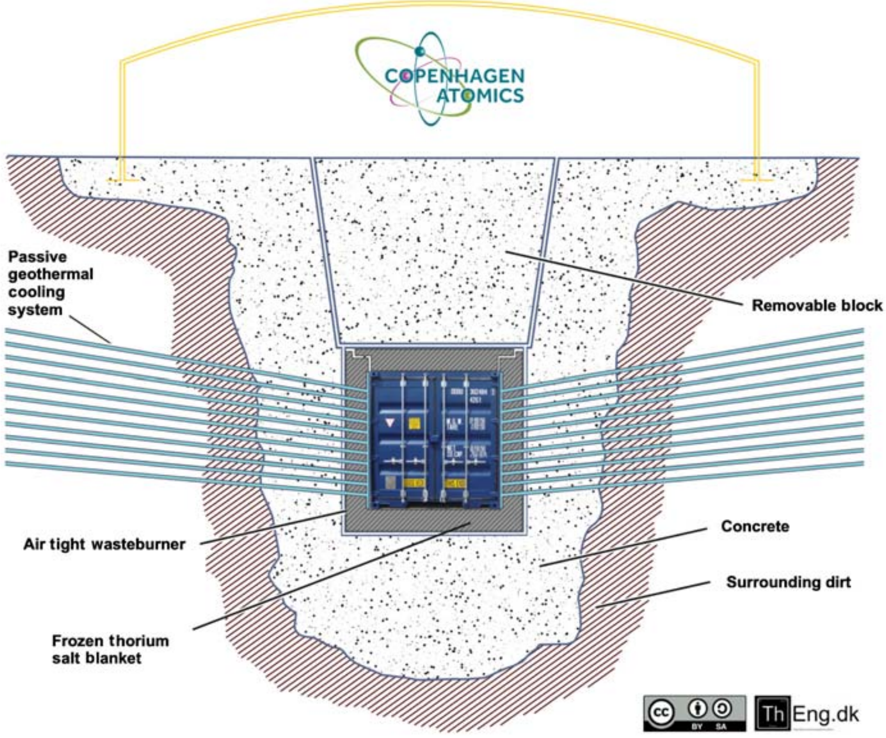

**Figure 23.3** CA Waste Burner underground with decay heat removal pipes.

passive underground decay heat removal system can be supplemented by one of the traditional decay heat removal systems.

Control rods are known to capture precious neutrons and to make it difficult to control power output of the reactor at low power. In the CA design the heavy water tank is configured such that 95% of the water can be dumped in less than 2 seconds. Thus, this can operate as a very efficient power control mechanism and allow the reactor to run at very low power output. The heavy water moderator will only absorb $\approx$ 1% of the reactor core heat, therefore the water will be circulated and cooled outside the waste burner container. Hydrogen recombiners are also located outside the waste burner container.

## 23.3 Recycling of spent nuclear fuel

A flame reactor (see Fig. 23.4) is an instrument that is less than 1 m high and 0.3 m in diameter. It mixes a powder or a liquid with a $F_2$ gas at the top and this creates a very exothermic chemical reaction that often results in a visible flame, hence the name.

$F_2$ reacts very willingly with any uranium in the input mix and creates $UF_6$, which is a gas. $F_2$ may also react with other elements in the input stream. These different elements can usually be separated from $UF_6$ very efficiently through simple distillation. This makes the flame reactor a very efficient and low-cost method of separating uranium from the fuel salt or from a spent fuel pellet granulate. Because

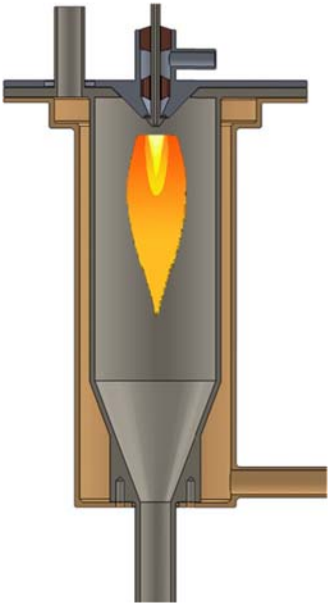

**Figure 23.4** Illustration of a flame reactor.

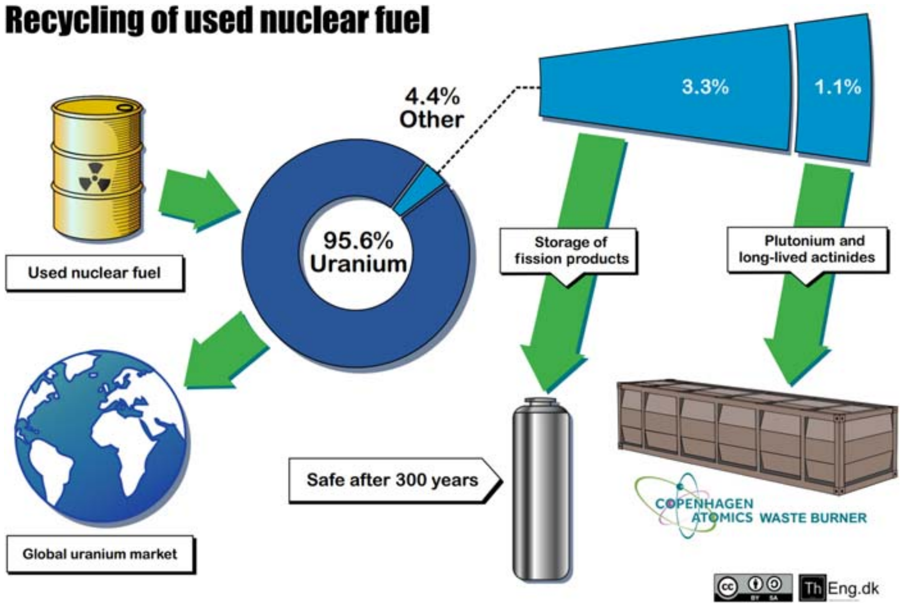

**Figure 23.5** Illustration of the used nuclear fuel recycling scheme.

more than 95% of SNF is uranium, this is a great way to separate the uranium from all the rest, which is mainly fission products and higher actinides.

UF and PuF species have different boiling points, they can be separated through distillation. When the stream becomes relatively pure laser separation can be used go to very high purity.

In a waste burner we want to feed all the higher actinides and plutonium into the waste burner and burn them to become fission products or to transmute them into something that can fission either in the waste burner or in an accelerator-driven system. Some of these higher actinides capture neutrons, which is one of the reasons we need to have a very good neutron economy in this MSR design.

The Pu239 in the spent fuel is especially valuable because it is ideal for starting thermal MSRs. The pure uranium extracted from the SNF via the flame reactor is similar in composition to the uranium extracted from mining, and it can be sold on the global uranium market, as illustrated in Fig. 23.5. The extracted uranium is expected to have a $10^{-5}-10^{-7}$ contamination factor.

## 23.4 Molten salt reactor research

*Nozzle spraying*, an alternative to the traditional helium bubbling method, relies on evaporation of noble gases and boiling of volatile fission product compounds. Some fission products decay through multiple elements that are either noble gases or volatile compounds. Salt droplets in a gas increase the surface area to volume ratio, thereby significantly improving the fission product extraction relative to helium bubbling. This research, carried out by members from CA, in cooperation with partners from the MIMOSA consortium. It includes both a theoretical study and numerical simulations to determine and compare the efficiency of the nozzle spraying method in comparison with traditional helium bubbling.

The objectives of the CA research are:

1. Theoretical models for diffusion and evaporation of volatile fission product fluoride species from spherical droplets of varying diameters.
2. Literature review and experimental determination of boiling points, diffusion constants, and vapor pressures of fuel components.
3. Numerical estimation of aerosolized salt advection out of the spraying chamber and means of separating aerosolized salt from the flow stream.
4. Numerical estimation of the evaporation of fission products, fuel components, and actinide fluoride species with nozzle spraying, at a given ambient pressure and temperature.

The numerical simulations will be coupled with experimental data from two techniques: low-pressure evaporation of volatile fluoride species at high temperature using a pipe furnace, with different pressures and flow gasses. A nozzle spraying loop under construction at CA will be used to determine nozzle spraying droplet size under various conditions of temperature, flow rate, and pressure. Both experiments will be carried out with LiF−ThF4 salts. The nozzle spraying technology was presented at ThEC2015 (www.youtube.com/watch?v=md90-FaEw7w). Similarly, a molten salt droplet spray was designed earlier for tritium extraction from fusion reactor (Dolan et al., 1992).

*Laser-induced breakdown spectroscopy* (LIBS) is a measurement technology that may be very well suited for molten salt reactors, reprocessing plants, and control of fuel salts storage and transport. LIBS is considered a nondestructive technique—less than 1 nanogram of material is consumed during a typical test. Tests can be repeated several times per second. Laser pulses generate a high-temperature microplasma on the surface of the sample, and the emitted light is analyzed by a spectrometer, which facilitates remote in situ chemical composition analysis of molten salts. CA staff have done LIBS analysis of lithium/fluoride, thorium/uranium salt samples and confirmed the ability to measure isotopes of Li6, Li7, U235, U238, etc. Calibration of the LIBS equipment, part of the MIMOSA project, will measure relative quantities of radioactive isotopes in irradiated fuel salt, to prepare for use at the in-pile-loop at the Petten reactor in the Netherlands. LIBS ability to measure ppm level salt components, such as corrosion materials and fission products, may be validated here.

If the above experiments turn out favorably, the IAEA and other nuclear authorities may adopt LIBS as one of the technologies for safety and control of salts containing fissile isotopes, for storage, transport, and online control of reactor systems. The LIBS measurement technology will also be incorporated in the nozzle spraying loops in Copenhagen.

By combining several technologies, we can measure accurately how much of each isotope is in the frozen or molten salt or in the gases. This allows us to control the redox potential of the salt accurately and to know the exact burnup, corrosion, and radioactivity of the materials at any time during radioactive decay. Having accurate measurements will allow us to build a very accurate model of the physical processes in the reactor and help improve the safety, efficiency, and lifespan of the waste burner. For both LIBS and infrared, it is possible to transfer the light to instruments outside the waste burner container via optical fibers, in order to avoid sensitive electronics inside the high-radiation zone.

## 23.5 "Prime minister safety"

It is often mentioned that MSRs should be built such that they are "prime minister safe." This refers to a design philosophy where no human, regardless of authority level, would be able to prevent the reactor from shutting down when needed. The CA Waste Burner has a set of systems governed by the laws of physics that cannot be overruled by humans, and which will cause the reactor to shut down safely if something goes wrong. As a second level of safety, a large number of the measurement values such as temperature, pressure, vibrations, and isotopic composition are combined into a measurement vector. This vector is continuously recorded similar to the black box recorders in airplanes, and the values are recorded off site.

If this measurement vector is found outside a well-defined boundary of safe operation then the reactor is automatically shut down by the computer system. This well-defined boundary of safe operation will be hardcoded by CA in agreement with the approval authority and cannot be changed by operators without entering a new reactor design approval process.

This means that operators are not required to watch for alarms and act in accordance. The CA Waste Burner must be able to automatically shut down before any human can react to an alarm and choose what to do. If human action were ever required for operation, other than during startup procedures, then we would consider it a design failure, and recommend that all reactors of that design should be shut down until the problem was corrected.

## References

Dolan, T.J., Longhurst, G.R., Garcia-Otero, E., 1992. A vacuum disengager for tritium removal from HYLIFE-II reactor Flibe. Fusion Technol. 21, 1949–1954.

< www.youtube.com/watch?v=md90-FaEw7w>.

# Molten salt thermal wasteburner

# 24

*Troels Schønfeldt and Esben Klinkby*
Seaborg Technologies, Copenhagen, Denmark

## Chapter Outline

## 24.1 Introduction

The Seaborg Technologies' Molten Salt Thermal Wasteburner (MSTW) is a thermal spectrum, single salt, molten salt reactor, operated on a combination of spent nuclear fuel (SNF) and thorium (Fig. 24.1). It is envisioned to produce 115 MW(e) with a two-stage turbine, from 270 MW(th). The core outlet temperature is 700°C, but it can go as high as 900°C for special uses, such as hydrogen production. The MSTW is designed around inherent safety features; no active measures are required to control the reactor under abnormal circumstances.

The fully modularized MSTW is suitable for mass production. As a module reaches the end of its lifecycle, it will be extracted and returned for recycling in a central production facility after it has cooled down. The reactor core, including the graphite-based moderator, is projected to have a lifecycle of 7 years, while the power plant will operate on the same batch of SNF for the 60-year facility lifetime.

The MSTW is in the early design phase, and Seaborg Technologies (ST) is focused primarily on neutronics, radiative transfer, computational fluid dynamics (CFD), and the physics of the design. The reactor will be located in an underground cave (Fig. 24.2).

The MSTW is designed for electricity production, district heating/cooling, sea water desalination, etc. Due to the high outlet temperature it is well suited for

**Molten Salt Reactors and Thorium Energy. DOI: http://dx.doi.org/10.1016/B978-0-08-101126-3.00024-5**

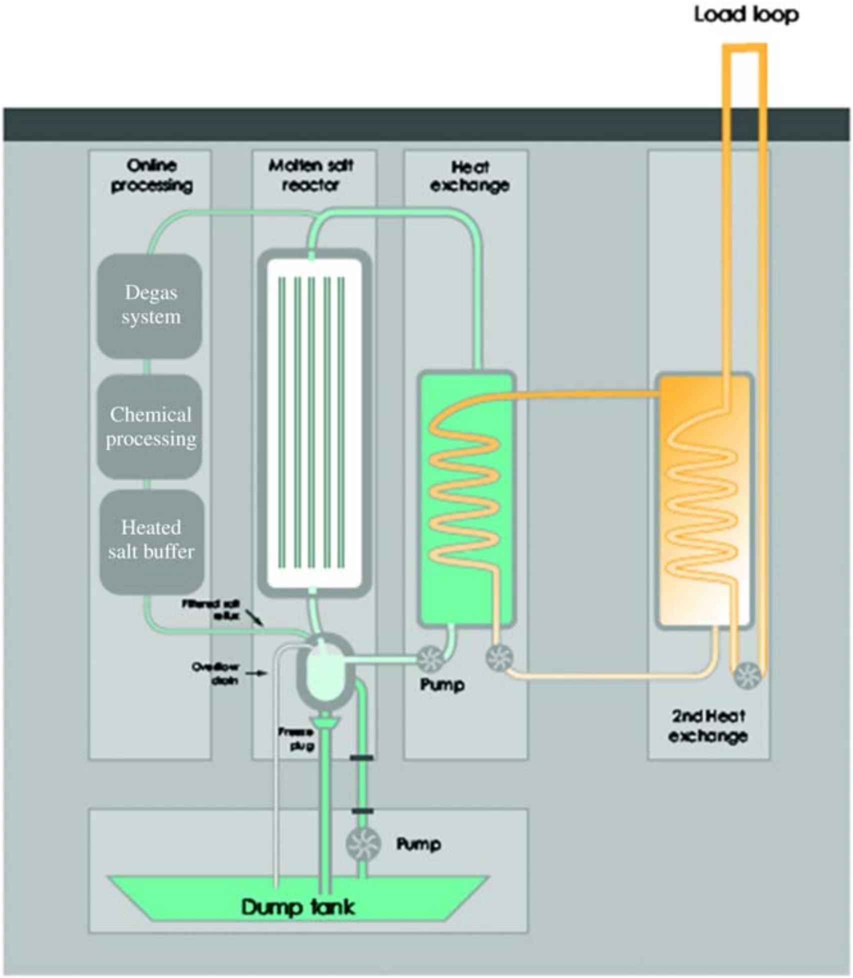

**Figure 24.1** The molten salt thermal wasteburner reactor.

synthetic fuel production, as well as industrial process heat applications. Its high burnup and the fact that it is fueled directly with SNF make it a good option for SNF stockpile reduction. However, as shown in Table 24.1, it can, without modification, operate on a wide array of different fuels.

## 24.2 Design overview

### 24.2.1 Design philosophy

The MSTW was originally designed to address the three main concerns that resulted in the Danish ban on nuclear power in 1985, namely safety, waste, and

**Figure 24.2** Early model of the underground cave, showing the dome with the reactor inside.

**Table 24.1 The thorium fraction to be added in order to arrive at an initial $k_{\mathrm{eff}} = 1.0005$ for a variety of different types of initial fissile material**

| | Processed waste | 4.5% $^{235}$U | 19.99% $^{235}$U | 93% $^{235}$U | 100% $^{239}$Pu |
|---|---|---|---|---|---|
| $^{232}$Th fraction | 86.7% | 6.9% | 73.3% | 93.9% | 97.6% |

proliferation. As the design has been developed and matured, these three concepts together have been the essential philosophy around which the other features have been planned and implemented.

*Safety*: The system is placed in an optimized configuration, whereby any perturbation to such a system—from operator mistakes to major earthquakes—will move the system away from the optimum and thus result in an automatic power reduction and, if the situation is not alleviated, eventually reactor shutdown.

*Waste*: By combining SNF with thorium, the production of transuranic elements (TRU) is lower than the rate at which they are created. The net reduction is roughly five tonnes TRU over the 60-year plant lifetime. Fig. 24.3 shows the thorium fuel cycle.

*Nonproliferation*: To ensure high proliferation-resistance the MSTW is designed to be a single salt reactor wherein the chemical reprocessing system is incapable of extracting specific actinides. Furthermore, no actinide element will have an isotopic composition usable for nuclear weapons at any point in the fuel cycle.

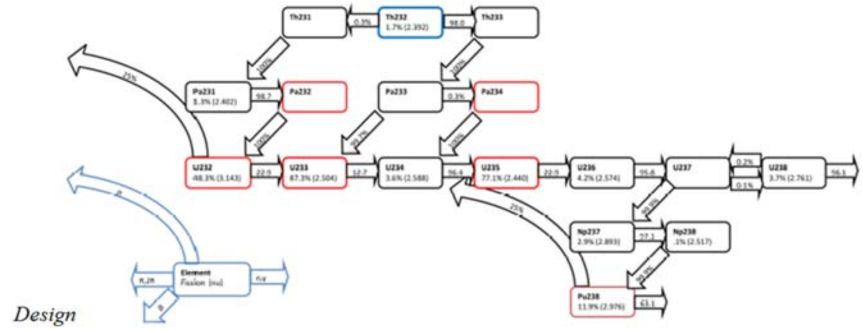

**Figure 24.3** Thorium fuel cycle, showing reaction probabilities as observed in the MSTW.

### 24.2.2 Power conversion unit

The MSTW utilizes a coolant salt-based core-integrated primary heat exchanger system. The coolant salt acts as heat storage and flows through the primary side of the steam generator, which transfers heat to a secondary salt circuit. A secondary heat exchanger then transfers the heat to a tertiary circuit that delivers steam at 550°C to the single- or two-stage turbines (Rankine cycle). The coolant salt and heat exchanger system also serves as core shielding and neutron reflector.

### 24.2.3 Reactor core

The MSTW core is a graphite-based compound-moderator thermal reactor core (Fig. 24.4). The core is slightly overmoderated to ensure negative void and temperature reactivity coefficients. The graphite is coated with a metal, and corrosion is reduced by regularly circulating the fluoride salt through a fluoride burner and by adding a reducing anode to the fuel salt. The reactor operates at 12 kW per liter core volume, with a peak power density of 250 kW per liter fuel near the core center.

Swelling and corrosion of the graphite moderator is expected to be the limiting factor for the lifetime of the core module.

The reactor core will passively shut down if overheated (negative thermal coefficient); therefore, loss of coolant accidents (LOCAs) will result in the reactor automatically powering down. In the case of a continued inability to cool the core, the fuel will eventually drain itself through a freeze plug to a passively cooled dump tank.

### 24.2.4 Fuel characteristics

The fuel salt is currently an eutectic sodium—actinide fluoride salt mixture, but sodium—rubidium—actinide or sodium—zirconium—actinide fluoride salts are being considered to reduce the actinide fraction in the salt, which will decrease the power density in the fuel salt and reduce pumping power requirements. As shown in Table 24.1, the design is highly flexible in terms of fuel. Initially an actinide fuel mixture of 93% thorium, and 7% preprocessed SNF (3.5% uranium [1.1% enrichment] and 3.5% reactor-grade plutonium) is foreseen, but over time the plutonium quality decreases, and so only SNF is added, and the thorium fraction decreases.

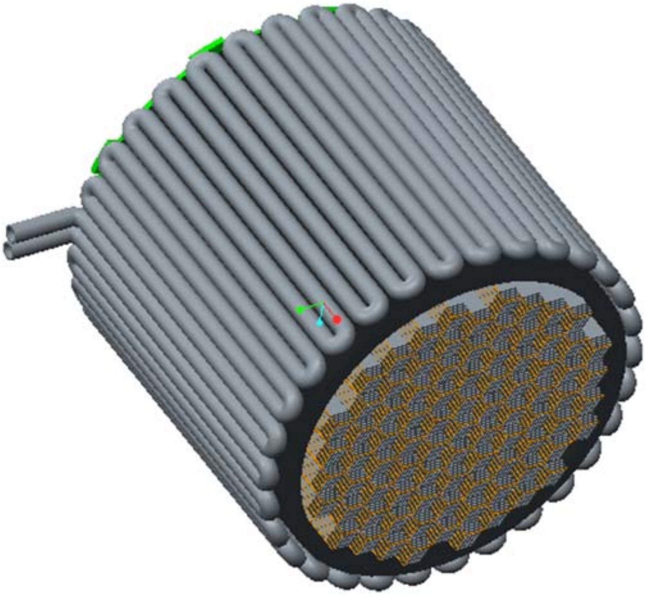

**Figure 24.4** Bottom view of the inner reactor core.

**Major technical parameters**

| Parameter | Value |
|---|---|
| Technology developer | Seaborg Technologies |
| Country of origin | Denmark |
| Reactor type | Molten Salt Reactor |
| Electrical capacity (MW(e)) | 100 (one-stage turbine) or 115 (two-stage turbine) |
| Thermal capacity (MW(th)) | 270 |
| Expected capacity factor (%) | 97.5% |
| Design life (years) | 7 years components, 60 years plant life |
| Plant footprint ($m^2$) | 20,000 |
| Coolant/moderator | Graphite-based |
| Primary circulation | Forced circulation |
| System pressure (MPa) | 0.1 (subatmospheric) |
| Core inlet/exit temperatures (°C) | 600/700—or 700/900 in the high-temperature configuration |
| Main reactivity control mechanism | Negative temperature coefficient; graphite control rods |
| RPV height (m) | 5 |
| RPV diameter (m) | 4 |
| RPV or module weight (metric ton) | 158 (including fuel and coolant) |
| Configuration of reactor coolant system | Integrated |
| Power conversion process | Rankine cycle |
| Process heat capabilities (high/low T) | Different configurations possible (850°C/550°C) |

**Major technical parameters**

| Parameter | Value |
|---|---|
| Passive safety features | Many: negative temp. coef.; freeze plug; overflow sys, etc. |
| Active safety features | Redundant, but, SCRAM and borofluoride injection installed |
| Fuel salt | Sodium−actinide fluoride (93% Th, 3.5% U 3.5% Pu) |
| Moderator height (m) | 2.9 |
| Number of moderator assemblies | 91 |
| Fuel enrichment (%) | Preprocessed SNF (U 1.1% fissile, Pu 69% fissile) |
| Fuel burnup (GWd/ton) | 250 (U and Pu—negligible Th cycle burning) |
| Fuel cycle (months) | 720 |
| Approach to engineered safety systems | Passive |
| Emergency safety systems | Inherent—passive |
| Residual heat removal system | Radiative (core), conduction (dump tank) |
| Refueling outage (days) | NA (60 day module exchange, every 7 years) |
| Distinguishing features | Thermal spectrum wasteburner; integrated heat-exchangers;<br>power production controlled by coolant pump speed |
| Modules per plant | One or more |
| Target construction duration (months) | 36 |
| Design status | Conceptual (mainly neutronics benchmarks done) |

### 24.2.5 Reactivity control

As shown in Fig. 24.5, the reactor has a strongly negative temperature coefficient, which ensures a saturation temperature level of the core. For this reason the power can be reduced by reducing cooling pump speed, or vice versa. The online refueling slowly feeds fresh SNF into the salt (see Fig. 24.6), for continuous operation. Daily adjustment of saturation temperature level is achieved using a series of graphite fine-tuning rods, which can be inserted or extracted from the reactor. Using these rods, the reactor can be maintained critical at its operational temperature for up to 2 months, without any addition of fresh SNF.

A Safety Control Rods Activation Method (SCRAM) system exists for the operators' convenience, in additon to a redundant borofluoride injection system.

### 24.2.6 Reactor pressure vessel and internals

The reactor operates below atmospheric pressure above the fluid surface. The core, chemical unit, dump tank, and other critical components are planned to be contained in an airtight dome, able to withstand significant pressure, both from internal and external events.

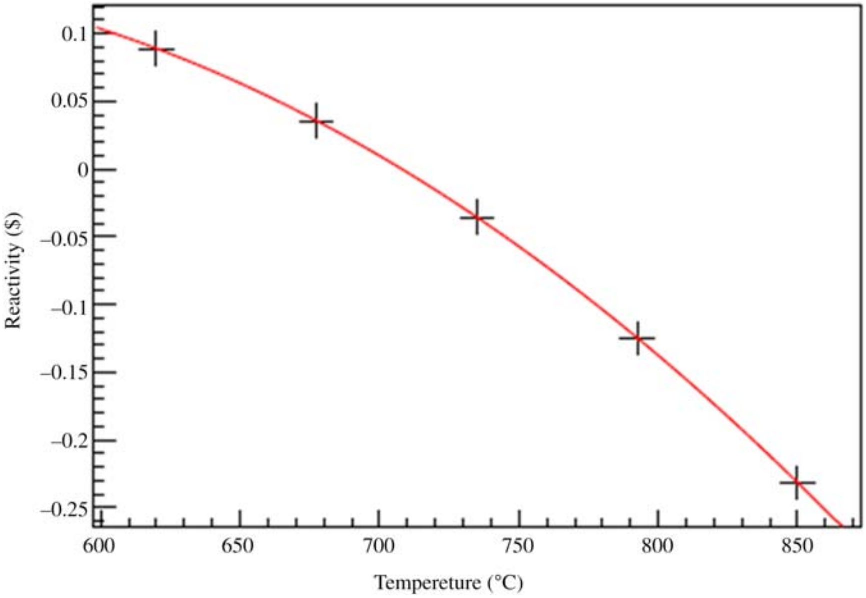

**Figure 24.5** Reactivity as a function of inlet temperature. The salt density decreases by 4.8% as the temperature increases from 620°C to 850°C, causing the reactivity to decrease.

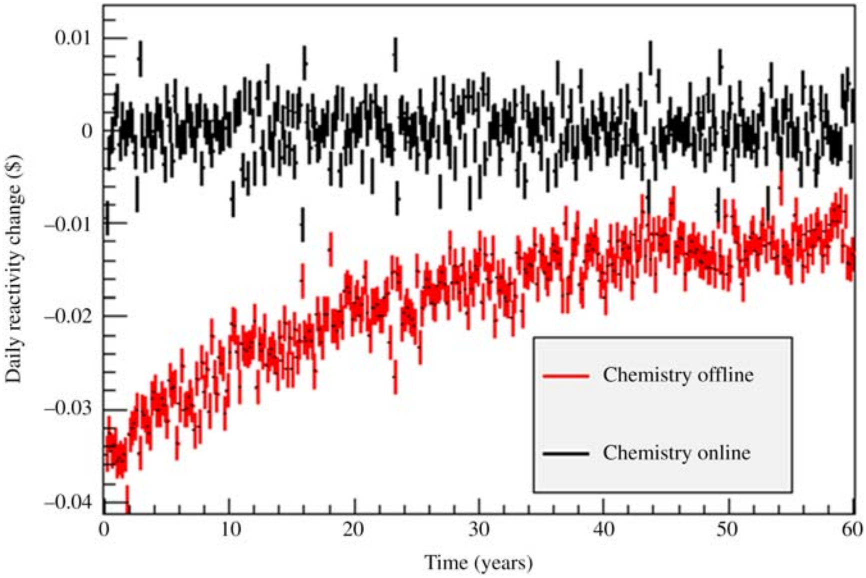

**Figure 24.6** Simulation of reactivity control using the chemical system. Note the migration towards a closed fuel cycle (*red* graph $=>$ 0) over the lifetime of the reactor.

## 24.3 Safety and operation

In the MSTW safety is guaranteed by physics rather than engineering. The reactor relies on natural convection, radiative heat transfer, and gravity for safety. The neutronics of the reactor is designed to be under optimal conditions. Any unexpected change to the system will result in a move away from the optimum, and thus a power reduction or shutdown of the reactor. All active safety systems are redundant.

### 24.3.1 Emergency core cooling system and decay heat removal system

In case of LOCA the core will heat up and the strong negative temperature coefficient will reduce reactivity and terminate power production without any operator interference. After shut down the core will heat up from residual heating, and passive cooling will be ensured through natural convection and radiative heat transfer for a substantial time. However, if main cooling is not restored, the reactor fuel will eventually drain itself (actively or passively) by melting a salt freeze plug. In the drain tank the fuel will solidify and is cooled by conduction to an underground heat sink.

### 24.3.2 Containment system

With the exception of noble gases, noble metals, and cadmium, fission products are nonvolatile in a fluoride salt. Note that this includes the hazardous cesium and iodine. The MSTW is designed so that temperatures which risk structural damage are physically unreachable for a number of reasons, including the negative temperature coefficient and the balancing of residual heating and radiative heat transfer. As such, no internally initialized accident events will lead to radioactive contamination of the biosphere. Moreover, the noble gases and other similarly volatile fission products created in the salt are continuously extracted, handled, and vitrified, and are therefore never present in significant amounts in the fluid. For this reason, the source term, even during extreme disasters, will be small and will pose a minimal off-site risk.

Despite the inherent safety, the reactor is designed with three barriers, where no irradiated component, coolant, or fuel leaves the outer two barriers (dome and reactor building—see Fig. 24.2) at point. This way licensing is anticipated by adhering to well-known and accepted safety standards.

### 24.3.3 Plant safety and operational performances

The neutronic optimum design philosophy provides excellent transient behavior and inherent safety features, and the plant has good load-following capabilities. The heat storage in the coolant salt and the automatic saturation temperature of the reactor enable power production to be cycled as fast as the steam generators can be switched on and off. Furthermore, due to the removal of noble gases, and the relatively large fuel inventory, the reactor will not experience issues with xenon poisoning during shutdown or power reduction.

### 24.3.4 Instrumentation and control systems

The MSTW will have a series of control and monitoring features. Control will be based on a series of fine-tuning moderator rods placed near the edge of the reactor core, so that an ejection event will reduce reactivity (loss of reflector). The reactivity span of these rods will be such that the reactor core saturation temperature can be adjusted within 200°C, and such that critical temperatures are not reachable through intentional or unintentional operator failures.

## 24.4 Plant arrangement

The plant design is not yet finalized. However, all irradiated components are contained in an approximately 8 m deep and 12 m wide underground area, covered with 2 m of concrete during operation (Fig. 24.2). The turbine building, control room, and module handling area are placed above ground, above and around the underground area. Since the overground components have no shielding requirements, distinguishing architectural designs will be used where applicable to consolidate the Seaborg trademark.

The plant is envisioned to have two operators, plus maintenance personnel for turbines and other plant components. During module substitution, a team from the central manufacturing site will be dispatched to the site.

## 24.5 Design and licensing status

ST is currently focused on advanced multiphysics, neutronics, and early engineering details. The facility is planned as a green-field concept; decommissioning considerations feature heavily in the design process; and most component parts are recyclable. Licensing considerations are included in the design process, and a plan has been drafted, although it is not yet of prime importance.

## 24.6 Plant economics

The design is at a conceptual stage and the details of the plant economics are yet to be assessed. It is our belief that the redundancy of all active systems will result in significant cost reductions, through fewer engineering requirements and general simplicity. Also, the centralized manufacturing and recycling of modules are expected to benefit plant economics. Lastly, the short lifecycle of modules will heavily reduce requirements of materials and engineering. This is expected to significantly reduce the overnight cost, but will come at the expense of a increased operating costs. Current trends in the nuclear industry suggest that postponing a large fraction of the capital costs will be favorable from an economical point-of-view.

# Dual-fluid reactor

# 25

*Armin Huke*[1], *Götz Ruprecht*[1], *Daniel Weißbach*[1],
*Konrad Czerski*[1,2], *Stephan Gottlieb*[1], *Ahmed Hussein*[1,3] *and*
*Fabian Herrmann*[1]
[1]Institute for Solid-State Nuclear Physics, Berlin, Germany, [2]University of Szczecin, Szczecin, Poland, [3]University of Northern British Columbia, Prince George, BC, Canada

## Chapter Outline

## 25.1 The dual-fluid technology

The dual-fluid reactor (DFR) (Huke et al., 2013, 2014, 2015; Wang et al., 2015; Wang, 2016) is a complete redesign of a nuclear power reactor, employing mature technologies—among these many from areas other than nuclear technology—thus resulting in a system which can be swiftly implemented as a straightforward engineering project without further fundamental research. The resulting design remedies the primary fault of deployed nuclear power plants (NPPs) of Generation I–III as well as most of Generation IV and similar concepts and projects: the insufficient economic competitiveness towards fossil fuel-fired power plants (particularly coal), which is the chief reason why NPPs have such low market penetration among worldwide power production. The ratio of reaction enthalpies between nuclear fission and carbon/hydrogen atom combustion amounts to eight orders of magnitude. The NPP's low utilization of its potential is especially dissatisfying. The DFR technology exploits this potential to a much higher degree and is capable of surpassing the energy efficiency of fossil-fired power plants by two orders of magnitude with

**Molten Salt Reactors and Thorium Energy. DOI: http://dx.doi.org/10.1016/B978-0-08-101126-3.00025-7**

profound impact on national economies (Lambert, 2014). Since the DFR is also a VHTR, operating at 1000°C, its high efficiency would facilitate, contrary to the Generation IV VHTR concepts, the synthesis of automotive fuels with an economic edge in competition with fossil fuels.

The basic idea of the dual-fluid principle is a liquid-fueled fast reactor with separation of the coolant from the fuel loop (see Fig. 25.1). The nuclear chain reaction takes place in an arrangement of tubes through which the liquid fuel cycles and which is set within a stream of pure molten lead (not an eutectic), the cooling liquid. This goes beyond MSR concepts where both functions, cooling and fuel supply, must be provided by the same medium. What at first sight seems like a simple invention has massive implications and resolves the former clash between high power density, which is a sine qua non for a powerful economy, and inherent passive safety, rendering expensive and failure-prone active safety systems superfluous. It combines the positive properties of the lead-cooled fast reactor (LFR), i.e., high heat transportation capability and low activation of the coolant, with the advantages of liquid fuel (as is used in an MSR), i.e., online reprocessing and passive safety via melting fuses. This efficiency enhancement is further sustained by the internal liquid fuel cycle with partitioning and transmutation, thus enabling the consumption of today's LWR waste, thorium, natural and depleted uranium (see Section 25.2). The economic advantages of liquid fuel, shedding the costly nuclear fuel element cycle infrastructure, are also shared by the MSR, rendering the MSR the only reactor concept with improved economics among Generation IV. In order to simplify pyroprocessing and enable very high power density, the dual-fluid

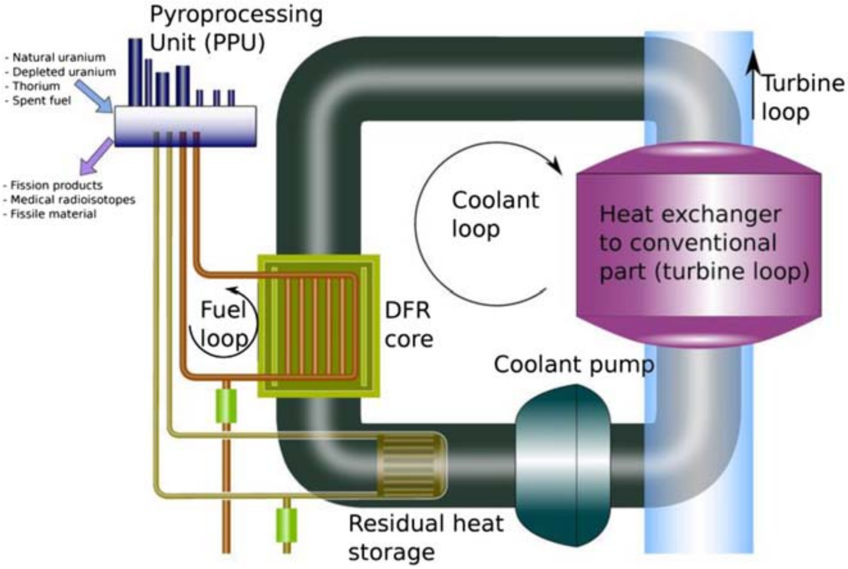

**Figure 25.1** Dual-fluid principle: Fuel loop and coolant loop. The main safety feature are the melting fuses (green cylinders).

principle goes a step further than usual MSR designs though, by employing undiluted actinide trichloride salts such as $UCl_3$ in the DFR/s (see below), without a carrier salt.

There are two variants of the DFR currently under development:

- *DFR/s with molten salt fuel* already boasts a number of advantages in respect to the "usual" MSR concepts. Thanks to the dual-fluid principle, heat can be removed from the core much more efficiently, making it possible to use pure undiluted actinide chloride salts. This results in a very compact core, allowing for the economical use of expensive, highly corrosion-resistant materials, which allow a very high operating temperature of 1000°C.
- *DFR/m with molten metal fuel* further increases power density and the hardness of the neutron spectrum. Due to much higher heat conduction and actinide atomic density of the metallic fuel (consisting of eutectics with more than 70 atomic% actinides), several improvements of the reactor construction could be additionally made, considerably enhancing its economics. Tentative simulations indicate conversion ratios approaching two (when included, most actinides with even neutron number become burnable, e.g., $^{234}U$, $^{240}Pu$) as a consequence of the hardened neutron spectrum.

Neutron simulations (Wang et al., 2015; Wang, 2016) show that the DFR has a deeply negative fuel temperature coefficient which makes the DFR self-regulating with no need for any mechanical parts in the core. Moreover, the DFR can satisfy all the goals of Gen IV (Generation IV), as defined by the Generation Four International Forum (GIF), in one system: sustainability, nonproliferation, physical protection, economics, safety, waste management, and high temperature heat energy for process chemistry.

Even compared to other fast-fission reactors, the DFR's neutron spectrum is extremely hard, making it highly efficient both as a transuranium incinerator and as a thorium breeder. As for all fast-fission reactors, during DFR operation no waste stream of unwanted actinides (e.g., minor actinides or Pu) is produced, thus the search for geological repositories becomes irrelevant.

## 25.2 Fuel cycle: the pyroprocessing unit

The fuel is recycled online within the containment in the pyrochemical processing unit (PPU). The PPU can be directly fed with irradiated fuel from current LWRs—the material only needs to be transformed from oxides to chlorides, which could be done on-site. Thus, the complex PUREX process becomes obsolete and the handling of used fuel is simplified enormously. The DFR unites partitioning and transmutation (P&T) in one plant.

The lower boiling points of the chloride salts allow for partitioning by fractional distillation/rectification, a very straightforward reprocessing technology compared to MSRs. This industrial technology is well-established in chemical plants, petroleum refineries, gas and liquid air processing, and can easily be adapted to the partitioning of the fuel salt using similar distillation columns. Indeed, a process operating under similar conditions has already seen large-scale industrial application since the 1930s: the Kroll process for production of titantium group metals.

For the metal fuel variant, DFR/m, a further chlorination and reduction process needs to be inserted before and after the PPU. Volatile and noble metal fission products are processed in a prestage, analogous to the MSR. The considerably lower total volume of the undiluted actinide fuel salt reduces the size of the processing facility accordingly and thus also presents a safety improvement. Since outside of the reactor core neutronics do not need to be taken into account, there is a much wider choice of suitable structural materials. Any refractory material or combinations thereof can be considered. The heat generation of fission products is not an obstacle but an asset, since it supports evaporation of the fuel.

Partitioning by the PPU optimizes nuclear waste management in an economical manner. The low volume of the fuel inventory as well as the shedding of the fuel element cycle along with aqueous PUREX-type reprocessing and its accompanying production of considerable volumes of medium-level radioactive waste from radiolytically destroyed auxiliary chemicals mark substantial progress. The DFR is an adiabatic reactor, meaning that only fissionable material must be provided to the plant, without any transports to an off-site fuel cycle infrastructure being required.

## 25.3 Applications

Possible applications are shown in Fig. 25.2. Even though they are possible for every high-temperature reactor system, the low production costs enabled by the DFR give them a pronounced economic advantage. Not only can electricity be generated with very high efficiency, but the synthesis chain also becomes viable for

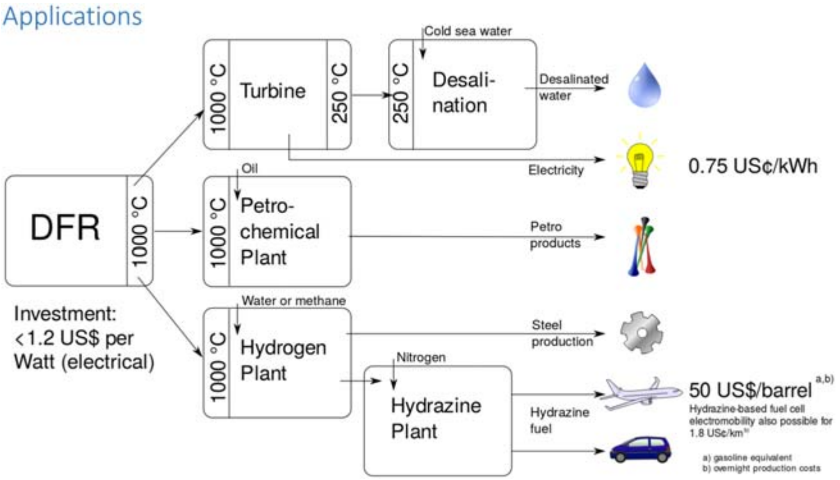

**Figure 25.2** Applications of the dual-fluid reactor.

inexpensive chemical products such as ammonia and hydrazine for vehicles or petrochemical compounds. Additionally, large-scale desalination of seawater would be possible.

## 25.4 Electricity production

For electricity generation, the heat energy needs to be transduced from the liquid metal, a medium with very high heat transport capacity, to a working medium with considerably lower capacity suitable for turbines. Without further research and development, the most cost-effective state-of-the-art technology is the supercritical water ($scH_2O$) cycle. Another near-future possibility are supercritical carbon dioxide ($scCO_2$) turbines (Dostal, 2004; Wright et al., 2010; US Department of Energy, 2013), resulting in more compact machine components with a slightly higher thermal efficiency and significantly reduced corrosion rates [e.g., using industrial INCONEL MA 754 nickel-base alloy (Oh et al., 2004)], but pressures approximately equal to $scH_2O$ turbines.

## 25.5 Synthetic fuels

The operating temperature of 1000°C enables highly efficient production of hydrogen from water through combined electrolysis and thermolysis. This method, the HOT ELLY process, was developed for the high-temperature reactor at the Jülich Research Center in Germany. Alternatively, the sulfur-iodine cycle could produce hydrogen at a temperature of only $>830°C$.

Due to the low energy density of hydrogen gas, it may be more useful to bind the hydrogen in fluid chemical compounds that are easy to handle. These synthetic fuels are also known as XtL-fuels, meaning *conversion of substance X to liquid*. The relevant industrial-scale synthesis processes are well-developed and used commercially—mainly for chemical engineering in primary production. Synthesized fuels made from fossil fuels are wasteful compared to petroleum products.

The situation changes when nuclear thermal energy is utilized. Combined with the previously generated hydrogen, it allows hydrogenation of coal via the Bergius process, through which synthetic benzine or diesel could be formed (CtL-fuel: *coal to liquid*). Instead of hydrogen, the Fischer-Tropsch process may employ syngas.

## 25.6 Hydrazine for combustion and fuel cells

In order to avoid the exploitation of coal—because it is not available or the generation of carbon dioxide is undesirable—atmospheric nitrogen may be used instead of carbon. Here, the synthetic fuel of choice would be hydrazine ($N_2H_4$), a liquid fuel with properties similar to benzine (including toxicity). Hydrazine has been used as a rocket propellant for 80 years. Produced by nuclear energy, it becomes an affordable alternative to petroleum products for use in transport. As liquid fuel, it may be combusted in piston engines of vehicles and in turbines of aircraft with only minor modifications similar to those for other alternative fuels, mostly affecting the quantities of injected fuel and the ignition points. Hydrazine combustion is a very clean process creating water and nitrogen. Thus, hydrazine may be considered an NtL-fuel: *nitrogen to liquid*.

Hydrazine fuel cells may be produced at a lower price and be operated more efficiently than hydrogen fuel cells, as power density and the level of efficiency are significantly higher, and no rare, expensive metals such as platinum are needed for their production. In the past, hydrazine fuel cells have already been used successfully in spacecraft.

## 25.7 Silane

Silanes are the silicon homologs to carbon-based alkanes, which present an StL (silicon to liquid) synhetic fuel option. Starting with heptasilane ($Si_7H_{16}$), they are stable, easy to handle and possess very high energy densities. At combustion temperatures above 1400°C, where silane burns exothermically with oxygen to water and with nitrogen to silicon nitride ($Si_3N_4$), consuming 99% of atmospheric intake, it is perfectly suitable for hypersonic ramjets or scramjets. Modified Wankel engines in vehicles could also handle the dusty combustion products.

## 25.8 Other applications

### 25.8.1 Radiotomic chemical production

The short-lived fission product storage may be designed in an alternative fashion in order to utilize the intense radiation for radiotomic induction of chemical reactions requiring high doses (kGy/s) (Stannet and Stahel, 1971). Examples are production of nitrogen oxides ($NO_{(2)}$), ozone ($O_3$), hydrocyanic acid (HCN), and carbon monoxide (CO). Nitrogen oxide and ozone can be obtained by irradiation of compressed air. Hydrocyanic acid originates from methane and nitrogen. Carbon monoxide results from radiative dissociation of carbon dioxide. In the chemical industry, such processes are already in use, though with radionuclide gamma sources and considerably lower yield. The application of reactors for radiotomic chemical synthesis has been investigated in the past. When the exploration of innovative reactor concepts was abandoned, this research was also stopped. The topic is comprehensively covered in a review article (Stannet and Stahel, 1971). The short-lived fission product storage of the DFR reference plant with its own thermal power of $\sim$30 MW may produce $10^{4-5}$ tons/year of chemicals. It is also possible to design a special reactor core in order to utilize its much higher radiation intensity for chemical synthesis.

### 25.8.2 Medical isotope production

The radiotracer $^{99m}$Tc is a prime example of a medical application that would not be possible without a nuclear reactor. The search for an alternative during the worldwide molybdenum crisis in 2009/2010 failed due to the high neutron flux required for the production of the $^{99m}$Tc precursor $^{99}$Mo (A Supply and Demand Update of the Molybdenum-99 Market, 2012). Cost-effective production of $^{99}$Mo in commercial reactors seems to be impossible, as this would necessitate near-daily fuel element cycling coupled with high-throughput reprocessing, which would be extremely uneconomic and pose proliferation risks, so research reactors are mainly used. An expensive separation process follows, and due to the short half-life of $^{99}$Mo of only 3 days, a sophisticated logistic chain to finally deliver the technetium generators to hospitals is required. One single DFR produces several times the world demand—around 300 g per year, corresponding to 700,000 6 day Curies or the amount created by a 3 $GW_{th}$ DFR in approximately 1 day, and, more importantly, already provides it in separated form, as volatile fission products as well as inert (with respect to chlorine) metals including molybdenum are removed from the salt by noble gas bubbling; the metals will accumulate on the bubble surfaces. From this concentrated inert metal mixture, the molybdenum can be fairly easily extracted, so that complete on-site medical-clean production of the technetium generators becomes feasible, simplifying the logistics of delivery to hospitals. This could lead to a cost implosion for the $^{99m}$Tc radiotracer and therefore a surge in applications.

## 25.9 Structural materials

The high operating temperature requires very stable and corrosion-resistant materials in the reactor core. For a solid-fueled reactor, this would be problematic, as the amount of structural material for solid reactors is high with respect to the nominal power and the cladding cannot be reused upon fuel exchange. In contrast, the DFR core is very compact, requiring only small amounts that remain in the core for a long time while the liquid fuel is constantly exchanged (10 times lower structural material consumption). This allows for the utilization of substances that are difficult to manufacture. Several suitable refractory alloys and industrial ceramics have been known for decades, but their fabrication was too difficult and therefore uneconomical. The situation has changed in recent decades. Today, these materials can be tooled to versatile shapes in mass production, using advanced sintering and forging/joining techniques.

Silicon carbide (SiC), which is known for its low neutron capture cross-section, has been selected for the DFR/s core. Most of all dense CVD-like SiC is very resistant against lead corrosion at over 1000°C, even when lithium is added (Pb-17Li), while pure Li would dissolve SiC at 500°C (Pint et al., 2005). Regarding molten salt corrosion, much less data are available for SiC. It has been tested with NaCl which has an enthalpy (Taube and Ligou, 1974) similar to $UCl_3$ and showed good resistance at up to 900°C (Rigaud, 2011), even though it was a much less corrosion-resistant variant (reaction-bonded SiC with Si excess). In comparison, the corrosion resistance of CVD-SiC has been shown to be far greater (Olson, 2009). Below 1200°C, this material also displays high irradiation resistance, whereas SiC/SiC fiber pieces are less durable, although the newest generation of these composites seems to be more robust (Katoh et al., 2007). Microcrystalline damage caused by the high neutron flux and thermal stress will be automatically healed at these high temperatures (annealing in metals). Ceramics are even more resilient at elevated temperatures. Most likely SiC is also suitable for the DFR/m though insufficient data for interaction with the liquid euctetic fuel are available. A suitable alternative is ZrC-20mass%TiC with low penalty, due to the outstanding neutron economy of the DFR/m.

## 25.10 Energy return on investment

Energy return on investment is probably the most important factor characterizing the economical efficiency of an energy source. It is defined as the ratio of the total electricity output of a power plant during its lifetime to the expended exergy for construction, fuel supply expense, maintenance, and decommissioning (Ayres et al., 1998; Weißbach et al., 2013), also called *energy invested* or *cumulative energy demand* (CED).

Calculation of the EROI requires a full life cycle assessment (LCA) in order to determine the correct CED. For a typical 1400 $MW_e$ PWR, a major part of the CED is needed for the enrichment of uranium. A newly built PWR with mostly centrifuge enrichment has an EROI of 75−105, with complete LASER enrichment up to 115 (Weißbach et al., 2013), more than four times greater than the EROI of fossil power plants—but it also shows the limits of PWRs and Generation III(+ + ) technology in general. Another important factor contributing to the low EROI is the expenses for the fuel element infrastructure industry. The utilization of fuel elements also requires elaborate multiple-redundancy active and passive safety systems in order to counteract the risk of core meltdown, further reducing the EROI in effect.

Table 25.1 describes the CED for the DFR/s NPP, leading to an EROI of 2000 which is 25 times higher than that of today's PWR technique (Weißbach et al., 2013).

The large EROI gain of the DFR mainly results from two aspects: The shedding of costly external fuel processing infrastructure (improvement of more than a factor of three) and the far greater compactness and simplicity compared to a light-water reactor (another factor of six). Additional minor improvements arise from lower maintenance and much less fuel consumption as well as significantly smaller disposal needs. The higher per-mass efforts for the refractory parts are far outweighed by the extreme reduction of material amounts needed for construction (several 1000 metric tons of nickel alloys and highly alloyed steels in a light-water reactor versus

**Table 25.1** **Input energy amounts of the DFR**

| Item | Units (or total amount in 1000 kg) | Energy inventory in TJ/(1000 kg) | Total inventory in TJ |
|---|---|---|---|
| Concrete containment for reactor, fission products, and turbine building | 21,000 | 0.0014 | 30 |
| High-performance refractory metals and ceramics (PPU and core) | 60 | 0.5 | 30 |
| High-temperature isolation material for PPU and core | 100 | 0.1 | 10 |
| Initial load, isotopically purified $^{37}$Cl + fuel | 25 + 60 | 2.5/0.4 | 50 + 25 |
| Refractory metals and ceramics for the heat exchanger | 180 | 0.5 | 90 |
| Isolation and structural materials, heat exchanger | 300 | 0.1 | 30 |
| Untreated, low-alloyed metal for fission product encapsulation | 3000 | 0.033 | 100 |
| Structural materials (steel) for nonnuclear part | 1000 | 0.02 | 20 |
| Lead coolant | 1200 | 0.036 | 45 |
| Turbines with generators | 3 | 40 | 120 |
| Mechanical engineering parts | | | 150 |
| Cooling tower (special concrete) | 20000 | 0.003 | 60 |
| Refueling, 1200 kg/a actinides over 50 years | ~60 | 0.4 | ~25 |
| $^{37}$Cl loss compensation | 2 | 2.5 | 5 |
| Maintenance, high-performance refractories + isolation for one new core | 30 + 50 | 0.5/0.1 | 20 |
| Maintenance, 50% of other reactor parts, refractories + isolation | 90 + 175 | 0.5/0.1 | 62.5 |
| Maintenance, 50% of mechanical engineering and turbines | | | 135 |
| Maintenance electricity, 2 MW over 20 days/a and heating, 50*0.2 TJ | | | 182.5 |
| **Sum** | | | **1190** |
| **Output over 50 years lifetime, ~1500 MW net, ~8300 full-load hours** | | | **2,250,000** |

The ratio leads to the EROI of amost 2000. Since some materials (especially refractory metals) must be investigated and modified for use in the DFR, their energy inventory must be estimated. Furthermore, the maintenance for the nuclear part is also unknown, causing the same uncertainties
Bold: The sum of all inputs and the total electricity output

Table 25.2 **DFR technical data**

| | **DFR/s (hexag.)** | **DFR/m (hexag.)** |
|---|---|---|
| Fission zone D × H (m) | 2.8 × 2.8 | 2.5 × 2.5 |
| Outer/inner tube diameter (mm) | 18/15 | 22/18 |
| Pitch-to-diameter ratio | 1.25 | 1.25 |
| Mean linear power density (W/cm) | 900 | 1800 |
| Melting point/boiling point of fuel (K) | 1100/1950 | 1080/ > 3500 |
| Mean temperatures fuel inlet/outlet (K) | 1270/1540 | 1330/1600 |
| Temperatures coolant inlet/outlet (K) | 1030/1300 | 1000/1270 |
| Conversion ratio U-Pu/Th-U cycle at start | > 1.2/1.1 | 1.7/1.1 |
| \forall {$^{234}$U, $^{240}$Pu, $^{242}$Pu} $k_{\text{inf}} > 1$ & (resp. CR) | False (1.2/1.1) | True (2.1/1.3) |
| $^{238}$U fast fission/all fission | 6% | 20% |
| Fission zone volume without reflector (m$^3$) (fuel fraction) | 17.5 (39%) | 12.3 (39%) |
| Fuel processing, coarse/complete (kg/a) | 400,000/12 × 28,000 | 0/4 × 65,000 |
| Fresh fuel/coolant + reflector reactivity coefficients (pcm/K) | −8 to −40/ < +0.25 | −5/~0 |
| Inner core pressure at nominal power, fuel/coolant (MPa) | <0.2/<0.5 | 0.1/<0.5 |
| Fuel/coolant velocity (m/s) | 1.2/3.6 | 0(.06)/3.7 |

a few 100 metric tons of refractories for the DFR). Likewise, a DFR/m NPP exceeds this figure significantly, approaching 5000.

The very compact design lowers the construction energy demand almost to the level of CCGT plants on a per-watt basis, and the fuel-related energy demands are tiny compared to light-water reactors due to their efficient usage. Further optimizing the design and extracting the fuel at basic crust concentrations (~10 ppm for thorium) leads to a domination of the fuel-related input, showing that the DFR exhausts the potential of nuclear fission to a large extent. Indeed, mining fissionable material at the crust's mean concentration limits the EROI of nuclear power to 10,000 (neglecting the plant's CED), concurrently extending the range of fission fuel to ~1 Ga, thus turning fission power by definition into a "renewable energy source," since it will last until the further evolution of the Sun renders the Earth inhospitable to life (Table 25.2).

## 25.11 Key properties of the DFR (3 GW$_{\text{th}}$, 1.5 GW$_{\text{el}}$)

- DFR/s (liquid salt fuel variant)
- Undiluted Act.-Cl3 salt, density (3500−4500) kg/m$^3$
- 20.5/18.3/15 HMmass-% reactor-Pu/$^{235}$U/$^{233}$U
- *Blanket*: cylindrical, thickness 1 m, height 5.5 m (100 m$^3$)

## Table 25.3 Reactor type comparison

| **Property** | **DFR/s** | **DFR/m** | **SFR** | **MSR** | **TP-1** | **LFR** | **HT-GCR** | **LWR** |
|---|---|---|---|---|---|---|---|---|
| Neutron spectrum | Fast | Very fast | Fast | Epithermal to fast | Fast | Very fast | Epithermal to fast | Thermal |
| Neutron excess (fraction of fissions) after self-sustaining breeding[a] Pu-U (**U-Th**) | >0.2 (**0.1**) | 0.7 (**0.2**) | 0.1–0.3 (**0**) | 0.15–0.2 (**0.07**) | 0 (**0**) | 0.3–0.5 (**0.1–0.2**) | 0–0.2 (**0**) | <0 (no self-sustaining breeding) |
| Fission inventory doubling time (a)[a] | 13 | <8 | 10–20 | 15–20 | Not applicable | 10 | 30 to infinity | Not applicable |
| Waste storage time, PUREX (a),[b] long-lived fission product transmutation | 300, yes | 300, yes | ~10,000, very limited | 300, yes | >100,000,[c] no | ~10,000, limited | ~10,000, limited | several 10,000/100,000 (w/o reprocessing), no |
| Waste storage time, electro refinement (a),[b] long-lived fission product transmutation | 300, yes | 300, yes | 300, very limited | 300, yes | >100,000,[c] no | 300, limited | 300, limited | Several 10,000/100,000 (w/o reprocessing), no |
| "Useful" isotope production (e.g., nuclear medicine) | Yes, very good | Yes, very good | Uneconomical | Yes, good | None | Limited | Uneconomical | Very uneconomical in commercial LWRs, low neutron economy |
| Average burnup between discharges[d] | >99% (internal online-reprocessing) | >99% (internal online-reprocessing) | 10–15% with shuffling | >99% (complicated internal online/offline reprocessing) | Up to 25% with much shuffling/venting | 15–20% with shuffling (Pb-Bi) | Up to 20% with shuffling (fast spectrum) | <1% (6 % of reactor uranium) |
| Primary coolant | Lead | Lead | Sodium | Fluoride or chloride salts | Sodium | Lead-bismuth (Pb-Bi) | Noble gas (He) | Water |

(*Continued*)

## Table 25.3 (Continued)

| **Property** | **DFR/s** | **DFR/m** | **SFR** | **MSR** | **TP-1** | **LFR** | **HT-GCR** | **LWR** |
|---|---|---|---|---|---|---|---|---|
| Power density of core + all heat exchangers before turbine (MW$_{th}$/m$^3$) | 150 | 250 | 40–50 (Kalimer-600) | ca. 50–100 | Far less than 50 (only a part of core is critical) | 140 (BREST-1200) | 1–several 10s | <30 |
| Natural uranium consumption (mining, t/GWa), PUREX for solid fuel | 0.75 | 0.75 | 1.5 | >0.9 | 6[c] for once-through breed/burn | 1.3 | 1.2 | w/o PUREX 50–100/150 |
| External infrastructure[e] | None | None | All | None | All, reduced capacities | All, reduced capacities | All, increased capacities | All (without reprocessing) |
| Proliferation resistance Pu-U (**U-Th**) | Very high (**high**, partial Pa extraction necessary) | Extreme, no blanket (**very high**, Pa extraction unnecessary) | Medium (breeding zone) to high (**medium to high**) | Very high (**high, lower than DFR because Pa has to be separated**) | Medium (breeding zone) to high (**medium to high**) | Medium (breeding zone) to high (**medium to high**) | Medium to high (**medium to high**) | Medium (**medium**) |
| Mechanical control efforts | None (only coolant flux control) | None (only coolant flux control) | Control rods/fuel element shuffling | Few control elements if fuel processed offline | Control rods/fuel element shuffling | Control rods/less fuel element shuffling | Control rods/much fuel element shuffling | Control rods/fuel element shuffling |
| Power excursion countermeasures/ criticality reserves | Inherent, strong negative fuel coefficient/ very low | Inherent, prompt negative fuel coefficient/ very low | Inherent if special fuel rod designs used/ high | Inherent, negative fuel coefficient/ low | Inherent, strongly depending on fuel composition/very high | Inherent depending on reflector geometry/ very high | Inherent, medium negative void coefficient/high | Inherent, medium negative void coefficient/ high |
| Coolant loss countermeasures | Inherent (melt plug for liquid core) | Inherent (melt plug for liquid core) | Armored pool, low-pressure liquid coolant | Inherent (melt plug for liquid core) | Armored pool, low-pressure liquid coolant | Armored pool, low-pressure liquid coolant | Core meltdown to be managed | Core meltdown possible, can be managed then |
| Electricity cutoff countermeasures | Inherent (melt plug) and passive cooling, natural coolant circulation | Inherent (melt plug) and passive cooling, natural coolant circulation | Active pool cooling | Inherent (melt plug) and passive cooling | Active pool cooling | Active pool cooling, natural coolant circulation | No passive cooling possible, core meltdown countermeasures | Core meltdown possible/ redundant on-site supply |

| | | | | | | | | |
|---|---|---|---|---|---|---|---|---|
| Time limit to restore active cooling | ∞ | ∞ | 1 day | ∞ | 1 day | 1 day | Several minutes | 3 days |
| Coolant contamination countermeasures/activity of primary coolant | No (freeze-out)/extremely weak | No (freeze-out)/extremely weak | Secondary coolant loop/high | Secondary coolant loop/very high | Secondary coolant loop/high | No (freeze-out)/very weak | Very weak/high-temperature resistant and dense materials | Medium to high |
| Inventory volatility due to incidental events | Medium (some gaseous salts) | Medium (some volatile FPs) | Medium (activated coolant with some volatile fission products) | Medium (some gaseous salts) | Elevated (activated coolant with some volatile fission products, separated fission products) | Low | Medium to low, depending on fuel element design | Medium |
| Fire fight/explosion countermeasures (burnables?) | No (no) | No (no) | Complex containment (high) | No (no) | Complex containment (high) | No (no) | Medium to low (fast pressure drop) | Complex (fast pressure drop, hydrogen explosion) |
| Pressure in nuclear part | Low | Low | Slightly increased | Low | Slightly increased | Low | High | Very high |
| Plant complexity | Very compact/relatively low | Very compact/relatively low | Relativey high (Na) | Relatively compact and relatively low | Very high (Na, fuel pin design) | Medium | Medium to very large, very high to medium complexity | Large, very high complexity |
| Electric efficiency | 60% | 60% | Up to 45% | Up to 50% | Up to 45% | Up to 50% | Up to 60% | Up to 36% |
| Chemistry process heat, especially hydrogen production | Yes (1300K) | Yes (1350K) | No (800K) | Yes with significantly increased efforts (1100K) | No (850K) | Yes with significantly increased efforts (1100K) | Yes (1250K) | No |

[a] Depends on fuel reprocessing frequency (eleminating neutron poisons), especially for the TP-1. The higher the residence time (burnup) between the fuel reprocessings, the lower/higher the neutron excess (transmutation ability)/the doubling time.

[b] Time until waste radiotoxicity falls below the same amount of natural uranium.

[c] If TP-1 fuel is reprocessed, fuel consumption is reduced to 1.5 t/GWa and waste storage time to 300 years, resulting in higher overall costs.

[d] Calculated fraction of mined natural uranium.

[e] Fuel fabrication, reprocessing, partitioning, geological disposal.

- Structural material: pure high-density SiC, 3210 kg/m$^3$.
- DFR/m (liquid metal fuel variant)
- HM fraction >80% U/Pu or >70% Th/U, density 16500/9500 kg/m$^3$
- 9.0/9.5/9.5 mass-% reactor-Pu/$^{235}$U/$^{233}$U content of actinides
- *No blanket*: thicker reflector (Pb coolant) 0.5 m
- Structural material: ZrC-20mass%TiC, 6100 kg/m$^3$.

## 25.12 Comparison with other reactor types

Table 25.3 shows the DFR in comparison with other reactor types. We restricted the table to fast fission systems and the LWR.

One major characteristic of a nuclear reactor with regard to sustainable fuel usage and waste production is its neutron economy expressed by the neutron excess. The DFR and especially the metal fuel variant has the highest possible excess which allows for multiple transmutation applications, reduced inventory doubling times, and thus improves the utilization of the difficult thorium cycle significantly. Apart from the LWR, only SFR operating experience has been gathered, indicating that the electricity production costs for a Superphénix-like SFR are twice that of a PWR (Nifenecker et al., 2003). Power density, system complexity, and necessity of an external infrastructure contribute to the overall expenditures. Therefore, the GCR and TP-1 would probably be more expensive than the SFR. The LFR is comparable to an LWR, although somewhat better. Only the MSR can considerably outperform an LWR, thus it is the most viable concept of Generation IV. The DFR exploits the advantages of liquid fuels to the fullest, widely opening up the power plant market for nuclear.

## References

A Supply and Demand Update of the Molybdenum-99 Market, August 2012. NEA. <http://www.oecd-nea.org/med-radio/docs/2012-supply-demand.pdf>.

Ayres, R.U., Leslie, W.A., Martinás, K., 1998. Exergy, waste accounting, and life-cycle analysis. Energy. 23, 355, http://dx.doi.org/10.1016/S0360-5442(97)00076-5.

Dostal, V., 2004. A supercritical carbon dioxide cycle for next generation nuclear reactors, PhD thesis. Massachusetts Institute of Technology. Dept. of Nuclear Engineering, http://dspace.mit.edu/handle/1721.1/17746.

Generation IV Forum Website: Generation IV Goals.

Huke, A., Ruprecht, G., Weißbach, D., Gottlieb, S., Hussein, A., Czerski, K., March 4–7 2013. The Dual Fluid Reactor - a new concept for a highly effective fast reactor. The International Atomic Energy Agency IAEA "Fast Reactors and related Fuel Cycles" (FR13) conference in Paris.

Huke, A., Ruprecht, G., Weißbach, D., Gottlieb, S., Hussein, A., Czerski, K., August 24–28 2014. The Dual Fluid Reactor - A New Concept For A Highly Effective Fast Reactor. The 19th Pacific Basin Nuclear Conference (PBNC 2014) Vancouver, British Columbia, Canada.

Huke, A., Ruprecht, G., Weißbach, D., Gottlieb, S., Hussein, A., Czerski, K., 2015. The dual fluid reactor - a novel concept for a fast nuclear reactor of high efficiency. Ann. Nucl. Energy. 80, 225–235.

Katoh, Y., Wilson, D.F., Forsberg, C.W., 2007. Assessment of Silicon Carbide Composites for Advanced Salt-Cooled Reactors. Oak Ridge National Laboratory, USA, http://dx.doi.org/10.2172/982717.

Nifenecker, H., Meplan, O., David, S., 2003. Accelerator Driven Subcritical Reactors. Institute of Physics Publishing Ltd, Bristol, Philadelphia.

Oh, C., Lillo, T., Windes, W., Totemeier, T., Moore, R., October 2004. Development of a supercritical carbon dioxide brayton cycle: improving pbr efficiency and testing material compatibility. Project Number: 02-190, Nuclear Energy Research Initiative, Report, Idaho National Engineering and Environmental Laboratory. <http://www.inl.gov/technicalpublications/Documents/2906955.pdf>.

Olson, L.C., 2009. Materials Corrosion in Molten LiF-NaF-KF Eutectic Salt, dissertation. University of Wisconsin-Madison, http://allen.neep.wisc.edu/docs/dissertation-olson-luke.pdf.

Pint, B.A., Moser, J.L., Tortorelli, P.F., 2005. Investigation of Pb-Li Compatibility for the Dual Coolant Test Blanket Module. Oak Ridge National Laboratory, USA, http://web.ornl.gov/sci/physical_sciences_directorate/mst/fusionreactor/pdf/dec2005/7_MHD%20INSULATORS/Pint2.pdf.

Rigaud, M., 2011. Corrosion of refractories and ceramics. In: Winston Revie, R. (Ed.), Département de Génie Physique et de Génie des Matériaux, Ecole Polytechnique, Montréal, Québec, Canada, Uhlig's Corrosion Handbook, Third Edition John Wiley & Sons, Inc, pp. 387–398.

Stannet, V.T., Stahel, E.P., 1971. Large scale radiation-induced chemical processing. Annu. Rev. Nucl. Sci. Vol. 21, 397–416, http://dx.doi.org/10.1146/annurev.ns.21.120171.002145.

Taube, M., Ligou, J., 1974. Molten plutonium chloride fast breeder reactor cooled by molten uranium chloride, Annals of Nuclear Science and Engineering, Vol. 1. Pergamon Press, pp. 277–281., http://moltensalt.org/references/static/downloads/pdf/ANE_MCFBR.pdf.

Lambert, J., et al., 2014. Energy, EROI and quality of life. Energy Policy 64, 153–167. http://dx.doi.org/10.1016/j.enpol.2013.07.001.

US Department of Energy, April 2013. Development of a "10-MW Supercritical-CO2 Turbine" (SunShot CSP R&D 2012 Program), Report. <http://energy.gov/eere/sunshot/project-profile-10-megawatt-supercritical-carbon-dioxide-turbine>.

Wang, X, 2016. PhD thesis. Technische Universität München, Department of Mechanical Engineering, Nuclear Engineering.

Wang, X., Macian-Juan, R., Seidl, M., May 03–06 2015. Preliminary analysis of basic reactor physics of the dual fluid reactor concept. Proceeding (Track 6, ID 15270) of *International Congress on Advances in Nuclear Power Plants* ICAPP 2015, Nice (France).

Weißbach, D., Ruprecht, G., Huke, A., Czerski, K., Gottlieb, S., Hussein, A., 2013. Energy intensities, EROIs (energy returned on invested), and energy payback times of electricity generating power plants. Energy. 52, 210, http://dx.doi.org/10.1016/j.energy.2013.01.029.

Wright, S.A., Radel, R.F., Vernon, M.E., Rochau, G.E., Pickard, P.S., September 2010. Operation and analysis of a supercritical $CO_2$ Brayton Cycle", Report, Sandia National Laboratories, <http://prod.sandia.gov/techlib/access-control.cgi/2010/100171.pdf>.

This page intentionally left blank

# Worldwide activities

# 26

## Chapter Outline

**Molten Salt Reactors and Thorium Energy. DOI: http://dx.doi.org/10.1016/B978-0-08-101126-3.00026-9**

---

# 26.1 Australia

*Lyndon Edwards*
Australian Nuclear Science and Technology Organisation (ANSTO), Sydney, Australia

Australia has been a major supplier of nuclear fuel cycle materials since the 1950s and on current estimates (Uranium, 2014; <www.ansto.gov.au/AboutANSTO/OPAL>) has over 30% of the world's easily accessible uranium resources and over

10% of the world's easily accessible thorium. Much of the thorium resources in Australia are in the rare earth-thorium phosphate mineral, monazite, within heavy mineral sand deposits, which are mined for their ilmenite, rutile, leucoxene, and zircon contents, where the thorium remains in the tailings which are usually returned to the mine site and dispersed to reduce the radiation hazard. The mineral resource extraction industry in Australia is globally competitive. If the market for thorium does become viable, then Australia would be one of the top three thorium producers, as is the case for uranium.

The Australian Nuclear Science and Technology Organisation (ANSTO) and its predecessor, the Australian Atomic Energy Commission (AAEC), have a long history of research on the development and sustainment of nuclear reactors. Although there have been proposals and initiatives to introduce nuclear power in Australia in the past, none has ever progressed to construction or operation of a nuclear power plant, for both political and economic reasons.

In recent times, in conjunction with the Argentinian firm, INVAP, ANSTO has designed, developed, constructed and now operates what is arguably the most modern research reactor in the world. The OPAL multipurpose reactor provides state-of-the-art facilities for neutron diffraction, radiopharmaceutical production, and materials irradiation (<www.world-nuclear-news.org/RS-IAEA-chief-witnesses-progress-of-Australian-medicine-plant-08081601.html>).

ANSTO's current nuclear power-related research concentrates on nuclear materials engineering in their widest context, including fundamental radiation damage research, nuclear component manufacturing, component and system structural assessment, and component life in high-temperature nuclear environments. Australia also has a long and distinguished history of innovation in waste conditioning and is the world leader in the use of Synroc, an Australian invention. ANSTO is currently constructing the world's first operational intermediate-level waste (ILW) conditioning plant, based on Australian Synroc technology as part of its expansion of its production of the radiopharmaceutical $Mo^{99}$ (<www.ansto.gov.au/BusinessServices/ANMProject/index.htm>; <www.science.gov.au/international/CollaborativeOpportunities/ACSRF/jointResearch/Pages/ANSTO-SINAP.aspx>).

In 2012, the Institute of Materials Engineering (IME), whose capabilities and expertise now form ANSTO's nuclear materials platform (the ANSTO's Nuclear Fuel Research Group), was the recipient of a grant from the Australia-China Science Research Fund to form a Joint Research Centre (JRC) with the Shanghai Institute of Applied Physics (SINAP), to conduct fundamental studies of the performance of materials in molten salt environments (<www.science.gov.au/international/CollaborativeOpportunities/ACSRF/jointResearch/Pages/ANSTO-SINAP.aspx>; <www.ansto.gov.au/ResearchHub/IME/Projects/SINAP/>). The ANSTO/SINAP Joint Materials Research Centre has focused on MSR-relevant research on the high-temperature properties (He et al., 2015; Li et al., 2015; Shrestha et al., 2016), radiation effects (De Los Reyes et al., 2014, 2016; Reichardt et al., 2015), and the corrosion behavior of relevant nickel alloys and graphite materials (Reichardt et al., 2015; Zhu et al., 2015).

Following unanimous approval by the Generation IV International Forum (GIF) members, Australia became the 14th member of the Forum on June 22, 2016. The

GIF Charter was signed by CEO Dr Adrian (Adi) Paterson of the ANSTO (<www.gen-4.org/gif/jcms/c_71564/australia-joins-the-generation-iv-international-forum>; <www.world-nuclear-news.org/NP-Australia-joins-fourth-generation-reactor-forum-0305165.html>). Australia's intention is to contribute research on the very high temperature reactor (VHTR) and the molten salt reactor (MSR) systems. Australia also proposes to participate in the VHTR Material (MAT) Project Arrangement and the Risk and Safety Working Group. It is thus expected that Australia will continue research into MSRs and in particular the materials challenges of MSRs for the foreseeable future.

## References

De Los Reyes, M., Edwards, L., Kirk, M.A., Bhattacharyya, D., Lu, K.T., Lumpkin, G.R., 2014. Microstructural evolution of an ion irradiated Ni-Mo-Cr-Fe alloy at elevated temperatures. Mater. Trans. 55, 428–433.

De Los Reyes, M., Voskoboinikov, R., Kirk, M.A., Huang, H., Lumpkin, G., Bhattacharyya, D., 2016. Defect evolution in a Ni-Mo-Cr-Fe alloy subjected to high-dose Kr ion irradiation at elevated temperature. J. Nucl. Mater. 474, 155–162.

He, Z.T., Gao, L.N., Qi, W., Zhang, B.L., Wang, X., Song, J.L., et al., 2015. Molten FLiNaK salt infiltration into degassed nuclear graphite under inert gas pressure. Carbon. 84, 511–518.

Li, J., Shrestha, S.L., Long, Y., Li, Z.J., Zhou, X.T., 2016. The formation of eutectic phases and hot cracks in one Ni-Mo-Cr superalloy. Mater. Des. 93, 324–333.

Reichardt, A., Ionescu, M., Davis, J., Edwards, L., Harrison, R.P., Hosemann, P., et al., 2015. In-situ micro tensile testing of He+ 2 ion irradiated and implanted single crystal nickel film. Acta Mater. 100, 147–154.

Shrestha, S.L., Bhattacharyya, D., Yuan, G., Li, Z.J., Budzakoska-Testone, E., De Los Reyes, M., et al., 2016. Creep resistance and material degradation of a candidate Ni–Mo–Cr corrosion resistant alloy. Mater. Sci. Eng. A. 674, 64–75.

Uranium, 2014. Resources, Production and Demand: A Joint Report by the OECD Nuclear Energy Agency and the International Atomic Energy Agency English, 504 pages, published: 09/09/14 NEA#7209 Volume of the series: Nuclear Development. Available from: <www.oecd-nea.org/ndd/pubs/2014/7209-uranium-2014.pdf>.

<www.ansto.gov.au/AboutANSTO/OPAL>.

<www.ansto.gov.au/BusinessServices/ANMProject/index.htm>.

<www.ansto.gov.au/ResearchHub/IME/Projects/SINAP/>.

<www.gen-4.org/gif/jcms/c_71564/australia-joins-the-generation-iv-international-forum>.

<www.science.gov.au/international/CollaborativeOpportunities/ACSRF/jointResearch/Pages/ANSTO-SINAP.aspx>.

<www.world-nuclear-news.org/NP-Australia-joins-fourth-generation-reactor-forum-0305165.html>.

<www.world-nuclear-news.org/RS-IAEA-chief-witnesses-progress-of-Australian-medicine-plant-08081601.html>.

Zhu, H., Holmes, R., Hanley, T., Davis, J., Short, K., Edwards, L., 2015. High temperature corrosion of helium ion-irradiated Ni-based alloy in fluoride molten salt. Corros. Sci. 921, 1–6.

## 26.2 Canada

*David LeBlanc and Cyril Rodenburg*
Terrestrial Energy, Inc., Oakville, ON, Canada

MSR activities in Canada are concentrated in the Integral Molten Salt Reactor (IMSR), which is a uranium-fueled, graphite-moderated, fluoride chemistry, thermal spectrum molten salt reactor system designed by Terrestrial Energy Incorporated. It is described in Chapter 18, Integral molten salt reactor.

Website: www.terrestrialenergy.com

## 26.3 Czech Republic

*Jan Uhlíř*
Research Centre Řež, Husinec - Řež, Czech Republic

The technology of nuclear reactor systems with liquid molten salt fuel has been investigated in the Czech Republic since 1999. The original effort came from the national partitioning and transmutation concept based on the subcritical accelerator-driven system for the incineration of transuranium elements with liquid fluoride fuel and fluoride pyrochemical partitioning fuel cycle technology. After 2005, the original R&D intentions were gradually converted to a classical molten salt reactor technology and to the thorium–uranium fuel cycle. Arguments for this decision were presented by a group of prominent Czech nuclear scientists. These arguments were based on the fact that the Czech Republic should support the development of a technology that can minimize the environmental impact of nuclear power, save natural resources and has a potential to be deployed also in non-superpower countries, whereas fast reactors, which need highly enriched uranium or a high plutonium content, will represent the future of nuclear power for superpowers.

The theoretical and experimental development of MSR and liquid thorium fuel technology have been realized by a national consortium of institutions and companies originally led by the Nuclear Research Institute Řež.

After the first R&D activities in 2000–03, devoted mainly to the subcritical molten salt system for incineration of transuranium elements, since 2004 the main R&D effort has been focused on critical MSR systems; and since 2005 the thorium–uranium fuel cycle technology has also been under intensive study.

The Ministry of Industry and Trade of the Czech Republic supported two important R&D projects devoted to the MSR system and thorium–uranium fuel cycle. The first, which was opened in 2004, was called “Nuclear system SPHINX with molten fluoride salts based liquid nuclear fuel,” the second, opened in 2006, was “Fluoride reprocessing of GEN IV reactor fuels.” The investigations were based on experience obtained by the US Oak Ridge National Laboratory during the Molten-Salt Reactor Experiment project in the 1960s (Rosenthal et al., 1971) and also from the exchange of scientific information with the French EDF team on the AMSTER project in 2000 (Vergnes et al., 2000).

The SPHINX project was devoted to the broad spectrum of the MSR technology covering theoretical and experimental activities in MSR physics, fuel salt and fuel cycle chemistry, molten salt thermohydraulics, structural material development, and testing of apparatuses for molten fluoride salt media. The project was carried out by a consortium of institutions and companies led by the Nuclear Research Institute Řež in cooperation with ŠKODA JS (ŠKODA—Nuclear Machinery), Nuclear Physics Institute of the Academy of Sciences of the Czech Republic, Faculty of Nuclear Sciences and Physical Engineering of the Czech Technical University in Prague, and Energovyzkum Ltd. Brno, and later also with the Research Centre Řež and COMTES FHT. The main aims of the project were to contribute to the knowledge of MSR reactor physics, core design and safety, structural material development, MSR fuel cycle technology; to verify experimentally selected important areas of MSR technology; and to contribute to the solution of existing bottlenecks. Research work under the SPHINX project was divided into following work packages:

- WP1—MSR core and primary circuit;
- WP2—MSR fuel cycle technology;
- WP3—Experimental MSR core and its control system;
- WP4—Secondary circuit and its components;
- WP5—Structural materials for MSR technology;
- WP6—System study of MSR-SPHINX;
- WP7—Experimental program SR-0.

The second project "Fluoride reprocessing" was devoted to the experimental development of two fluoride partitioning technologies, specifically to the fluoride volatility method and to electrochemical separation processes from fluoride molten salt media. As the fluoride volatility method can be used for oxide fuels from fast reactors, the investigation of electrochemical separation processes has been exclusively devoted to the thorium−uranium fuel cycle of the molten salt reactor system. The work within this project also covered the experimental verification of fresh liquid molten salt fuel processing—a technology of $ThF_4$ and $UF_4$ preparation from $ThO_2$ and $UO_2$, respectively, and final processing of MSR fuel salts LiF-$BeF_2$-$ThF_4$ and LiF-$BeF_2$-$UF_4$. Other objectives of the MSR fuel cycle investigation were system studies focused on the material balance calculations and a conceptual flow-sheet design of MSR on-line reprocessing. Both one-fluid (single-fluid) and two-fluid (double-fluid) systems of MSR core design were investigated, and conceptual flow-sheets were designed for both design systems. Finally, the project also covered the nonproliferation and physical protection aspects of Th-U MSR fuel cycle technology.

Although the MSR design and operation were already verified by ORNL in the 1960s, the on-line reprocessing was never fully realized and still represents a crucial problem of MSR technology, which must be solved before MSRs can be deployed in the future. The "Fluoride reprocessing" project was solved by the Nuclear Research Institute Řež.

The main achievements of both projects were:

- Challenging reactor physics experiments with inserted molten salt zones were realized in LR-0 and LVR-15 and VR-1 reactors at the Nuclear Research Institute Řež, the Research Centre Řež, and the Czech Technical University.
- Computer codes for calculation of neutronic characteristics of the MSR system and for calculation of the composition evolution during the burnout of liquid fuel were developed.
- In the fluorine chemistry laboratory of the Nuclear Research Institute Řež, handling with beryllium-containing molten salts was mastered, fresh thorium and uranium molten salt fuel processing for MSR systems was verified in semipilot conditions, and the basic studies of electrochemical separation of actinides (Th, U) from fission products were realized. These electrochemical studies were devoted to MSR on-line reprocessing development.
- MSR fuel cycle mass balance calculations and conceptual flow-sheets of on-line reprocessing were designed.
- A special nickel alloy called MONICR, resistant to molten fluoride salt media, was developed by ŠKODA JS and COMTES FHT companies. Irradiation and corrosion tests of the MONICR alloy and metallographic studies were performed and experimental production of sheets, tubes, and rods was realized.
- Basic design and theoretical and experimental development of impellers and valves for molten fluoride salts and “salt/salt” and “salt/air” heat exchangers were realized by Energovýzkum Ltd.
- The Faculty of Nuclear Sciences and Physical Engineering of the Czech Technical University in Prague opened new facultative topics “Liquid nuclear fuels” and “MSR system technology” for regular and PhD students.

The LR-0 reactor, operated by the Research Centre Řež, has proved to be extremely suitable equipment for measurement of molten salt neutronics. The measurements were realized in molten salt zones inserted in the central part of the reactor core. The standard VVER fuel served as the neutron driver (Fig. 26.3.1). Basic critical parameters (the critical height of the moderator, the moderator level coefficient) were determined for each arrangement using the approved methodology of the initial critical experiments for the LR-0 reactor. These, along with a description of the fuel quantity, enrichment, and filling material, represent the fundamental data needed to determine the effects of the filling on the physical properties of the core, and serve as the input for calculations and benchmark comparisons. The initial critical experiments were followed by measurements of neutron flux and reaction rate to determine the characteristics of the neutron and photon field using the following methods. The increase in reactivity was determined by differences in the critical moderator level with and without the salt (Hron and Matal, 2008; Frýbort and Vočka, 2009).

The theoretical and experimental investigations of MSR fuel cycle technology at the Nuclear Research Institute Řež have been focused mainly on the electrochemical separation processes in fluoride media suitable for utilization within the MSR on-line reprocessing technology. The main objective of experimental activities on electrochemical separation technology has been to survey the separation possibilities of the selected actinides (uranium, thorium) and fission products (lanthanides) in selected fluoride melt carriers. The cyclic voltammetry method was used to study the basic electrochemical properties.

The first step was the choice of fluoride melts suitable for electrochemical separations. The melt should meet some basic characteristics—low melting point, high solubility, high electrochemical stability, and appropriate physical properties

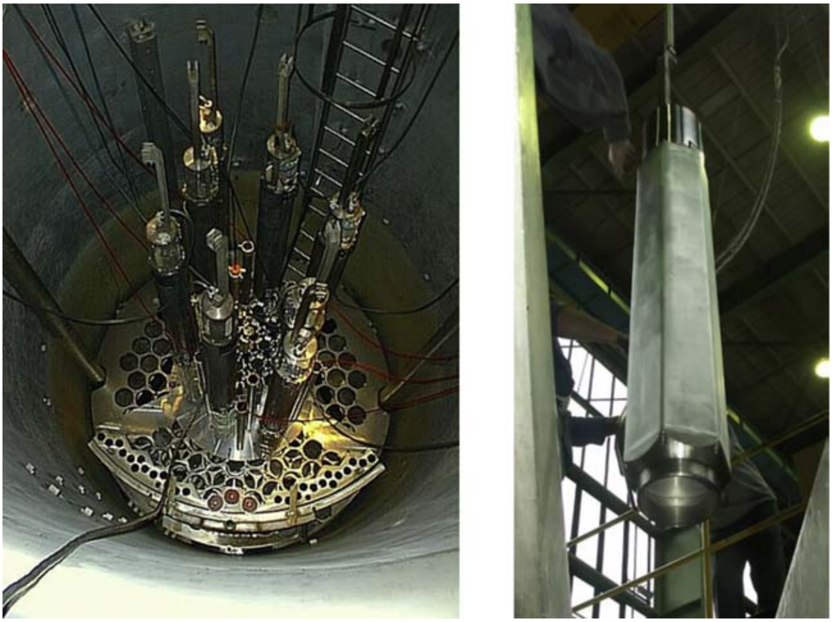

**Figure 26.3.1** View into the LR-0 reactor core with inserted salt zone and the manipulation with the salt zone before the insertion into reactor core.

(electrical conductivity, viscosity, etc.). A special reference electrode based on the Ni/Ni$^{2+}$ red-ox couple was developed to provide reproducible electrochemical measurements in fluoride melts (Straka et al., 2009, 2011) and to facilitate the on-line reprocessing flow-sheet design (Uhlíř et al., 2012a).

Results obtained from the measurements were interpreted in the following way:

- In FLIBE melt, there is a good possibility for electrochemical separation of uranium. Although the electrochemical studies of protactinium have not been realized yet, based on the thermodynamical properties of $PaF_4$, there is a presumption that protactinium could be separated from this melt as well.
- In FLINAK and in LiF-$CaF_2$ melts, both uranium and thorium and most of the fission products (lanthanides) can be electrochemically separated.

The national projects described above were successfully finalized in 2009 (SPHINX) and 2012 (fluoride reprocessing) (Hron et al., 2009; Uhlíř et al., 2012b). The main goals were achieved in both projects, and the obtained knowledge and experience created a good basis for international collaboration of Czech companies in further collaborative R&D projects of MSR technology. In 2012, the Ministry of Industry and Trade of the Czech Republic and US Department of Energy concluded a Memorandum of Understanding focused on the collaborative investigation of the fluoride-salt-cooled high-temperature reactor (FHR) and molten salt reactor technologies. Current Czech activities in this field cover mainly the areas of:

- Experimental reactor physics of FHR and MSR;
- Measurement of new neutronic data of coolant and fuel salts;

- Structural materials proposed for FHR and MSR technology;
- Further development of nickel alloys for molten fluoride salt technologies;
- MSR core chemistry;
- FHR coolant salt purification and control;
- Mastering selected techniques for MSR on-line reprocessing.

These activities are supported by the Ministry of Industry and Trade.

Czech activity in R&D of MSR technology has also enabled individual Czech research teams to participate in several international projects devoted to MSR technology (MOST, ALISIA, and EVOL projects of the 5th, 6th, and 7th Framework Programme of EC-EURATOM, selected CRP projects of IAEA and studies of OECD-NEA). Czech representatives also participate in the work of the Provisional System Steering Committee of MSR System of the Generation Four International Forum under the membership of the EURATOM team.

## References

Frýbort, J., Vočka, R., 2009. Neutronic analysis of two-fluid molten salt reactor. In: Proc. ICAPP 2009, Tokyo, Japan, May 10–14, 2009.

Hron, M., Matal, O., 2008. R&D program in the frame of the MSR-SPHINX actinide burner concept development. In: Proc. ARWIF 2008, Fukui, Japan, February 20–22, 2008.

Hron, M., et al., 2009. Jaderný transmutační systém SPHINX s kapalným jaderným palivem na bázi roztavených fluoridů (Nuclear system SPHINX with molten fluoride salts based liquid nuclear fuel). Final report MPO ČR FT-TA/055, ÚJV Řež (in Czech).

Rosenthal, M.W., Haubenreich, P.N., McCoy, F.E., McNeese, L.E., 1971. Recent progress in molten-salt reactor development. Atom. Energy Rev. 9 (3), 601–650.

Straka, M., Chuchvalcová Bímová, K., Korenko, M., Lisý, F., 2009. Development of electrochemical separation methods in molten fluoride salts FLINAK and FLIBE. In: Proc. GLOBAL 2009, Paris, France, September 6–11, 2009.

Straka, M., Korenko, M., Szatmáry, L., 2011. Electrochemistry of praseodymium in LiF-$CaF_2$. J. Radioanal. Nucl. Chem. 289 (2), 591.

Uhlíř, J., Straka, M., Szatmáry, L., 2012a. Development of pyroprocessing technology for thorium-fuelled molten salt reactor. In: Proc. ICAPP 2012, Chicago, IL, June 24–28, 2012.

Uhlíř, J., et al., 2012b. Fluoridové přepracování paliva reaktorů 4. generace (Fluoride reprocessing of GEN IV reactor fuels). Final report MPO ČR 2A-1TP1/030, ÚJV Řež (in Czech).

Vergnes, J., et al., 2000. The AMSTER concept (Actinide Molten Salt TransmutER). In: PHYSOR 2000 Conference, Pittsburgh, PA, May 2000.

# 26.4 China

*Zhimin Dai*
Shanghai Institute of Applied Physics (SINAP), Shanghai, China

China is involved with the TMSR (see Chapter 17: Thorium molten salt reactor nuclear energy system (TMSR)).

# 26.5 Denmark

*Thomas J. Pedersen*
Technical University of Denmark, Copenhagen, Denmark

Along with other European countries, Denmark from the mid-1950s engaged in the development of peaceful applications of nuclear energy. In 1956 the Atomic Energy Commission, later the Risø National Laboratory, was established with three nuclear reactors, becoming a large Danish research center for nuclear technologies. With Niels Bohr as one of its founding fathers, R&D at the Risø National Laboratory took a broader perspective than nuclear energy only, and resources were allocated to other technologies, including isotope production, materials studies, and (later) renewable energy and environmental research. The DR3 reactor, a 10-MW heavy water reactor was for many years a major research facility in Europe, used as a neutron source for materials investigations, for medical isotope production, and for doping semiconductors for the electrical power industry.

During the 1970s the public attitude to atomic energy shifted, and the larger Danish utilities lost interest in building nuclear power plants. Instead, the energy supply was based on imported oil and coal, later supplemented by natural gas production from the North Sea. In 1985, the Danish Parliament decided not to include nuclear power in Danish energy planning. Today, Denmark is self-sufficient in primary energy supply, due to the large domestic production of oil, natural gas, and wind energy. A goal is to discontinue the use of fossil fuels entirely by 2050.

As a consequence of the nuclear power production ban, public funding for R&D related to nuclear energy also diminished. The last of the three nuclear reactors at Risø was closed in 2000 and the state-owned company Danish Decommissioning was established to take responsibility for the nuclear facilities at Risø and for the radioactive waste in Denmark. In 2007, Risø National Laboratory became part of the Technical University of Denmark (DTU). Meanwhile, nuclear technologies R&D at DTU shifted towards other fields of research, including radiation physics, dosimetry, radioecology, and the production of medical isotopes.

In 2015, Denmark saw the dawn of two small start-ups aimed at developing molten salt reactor (MSR) technologies: *Copenhagen Atomics* and *Seaborg Technologies.*

## 26.5.1 Copenhagen Atomics

*Thomas Jam Pedersen, Chairman of the Board, Copenhagen Atomics*

Copenhagen Atomics (CA) is a startup company developing a heavy water moderated molten salt reactor design (HWMSR), which improves neutron economy and recycling economy significantly over typical thermal MSR designs that rely on graphite moderators. The goal is to develop this into a breeder reactor, which can be manufactured on an assembly line. CA is based on an open-source philosophy, where publishing results and collaboration with other teams are encouraged. In such collaborations CA strengths are primarily related to measurement technology, chemical processing, and control systems. In collaboration with other European players CA is currently developing equipment for measuring isotopic compositions down to ppm levels in fluoride and chloride salts up to 900°C in a sealed reactor environment. CA also has a salt loop experiment where they test fission product removal from molten salts. A shareholder company of CA (Th Engineering) is developing an operating system for MSRs, which will be licensed for free to research and demonstration reactors. CA also hosts monthly meeting sessions on thorium MSR in Copenhagen (see Chapter 23: Copenhagen atomics waste burner).

### 26.5.2 Seaborg Technologies ApS

*Troels Schönfeldt, CEO, Seaborg Technologies*

Seaborg Technologies is a startup company founded by particle, nuclear, and neutron physicists, with roots at CERN, European Spallation Sources (ESS), and the Center of Nuclear Technologies at DTU. Today, Seaborg consists of 15 people with backgrounds in physics, chemistry, engineering, and business. Seaborg's main field of expertise is neutronics. The team combines conventional simulation, modeling, and analysis tools used in particle, spallation, and reactor physics to derive new results. With its own conceptual MSR design Seaborg uses its new software suite to venture into uncharted territory, developing new experience and intellectual property. Seaborg deploys their unique knowledge and tools through their design and neutronics consultancy services; and they have delivered key neutronic results for other MSR developers (see Chapter 24: Molten salt thermal wasteburner).

## 26.6 France

*Michel Allibert[1], Daniel Heuer[3], Axel Laureau[3], Elsa Merle[3],*
*Mariya Brovchenko[2] and Sylvie Delpech[3]*
[1]Centre national de la recherche scientifique, Paris, France, [2]Institut de Radioprotection et de Sûreté Nucléaire, France, [3]Centre national de la recherche scientifique, Paris, France

Since the ORNL experiments and projects on MSR, studies on this kind of reactor were resumed in the 1980s in Japan with the Thorims-NES (Furukawa et al., 1990) then the FUJI-AMSB projects (Furukawa et al., 2005), as well as in France with studies on the MSBR by EDF and CEA at the same time. In the 1990s, the concept was taken up again with a view to incinerating nuclear wastes in subcritical reactors such as the TIER-1 project (Bowman, 1998), proposed by C. Bowman to transmute the plutonium of pressurized water reactors, the CEA TASSE project (Berthou, 2000), and the EDF AMSTER project (Lecarpentier, 2001).

The French National Center for Scientific Research (CNRS) has been involved in molten salt reactor studies since 1997. It re-evaluated the Oak-Ridge National Laboratory Molten Salt Breeder Reactor project (Whatley et al., 1970) using a probabilistic neutron code (MCNP) and an in-house evolution code for materials (REM), both being coupled (Nuttin et al., 2005). To solve the issues of the MSBR project (positive void coefficient, molten salt reprocessing, and graphite management), an innovative concept called the molten salt fast reactor or MSFR (Merle-Lucotte et al., 2008, 2009b, 2011, 2012, 2013; Mathieu et al., 2009; Brovchenko et al., 2014a; Rouch et al., 2014; Allibert et al., 2015) has been proposed. This concept results from extensive parametric studies in which various core arrangements, reprocessing performances, and salt compositions were investigated with a view to the deployment of a thorium-based reactor fleet on a worldwide scale. Systematic studies of MSRs have been undertaken at LPSC/IN2P3/CNRS in Grenoble to optimize an MSR in the framework of the deployment of a Gen IV concept, first regarding neutronics and then including reactor physics, thermal hydraulics, chemistry, materials, and safety. This led to the concept of an MSFR that has been recognized as a long-term alternative to solid-fueled fast neutron systems with unique potential (excellent safety coefficients, smaller fissile inventory, no need for criticality reserve, simplified fuel cycle, etc.) and has thus been officially selected for further studies by the Generation IV International Forum as of 2008 (GIF, 2008; Renault et al., 2009; Boussier et al., 2012; Serp et al., 2014).

This research has been supported by several French interdisciplinary programs involving public laboratories (CNRS, IRSN, CEA) and private companies (AREVA: EDF): the former PACEN and present NEEDS national programs, as well as local support in Grenoble (TSF from Carnot Energy Institute, CLEF from Grenoble Institute of Technology), or direct industry support from Rhodia/Solvay and AREVA (PhD theses) or material issues solved by Aubert&Duval.

Euratom provided important support by promoting international collaborations on various aspects of MSRs. One can cite the following Euratom's projects: MOST (2001/2004), ALISIA (2007/2008), EVOL (2011/2013, coupled to MARS Rosatom's project), SAMOFAR (2015/2019) as having significant contributions from France.

Some aspects of fuel processing were studied by CNRS at IPNO (Delpech et al., 2009) and LPSC showing that the impact of fuel processing on neutronics is low, allowing parallel studies on chemical and neutronic issues (Doligez, 2010). Safety studies led by CNRS have also been undertaken (Brovchenko, 2013; Brovchenko et al., 2013, 2014b; Wang et al., 2014) in collaboration with IRSN and AREVA to ascertain the high safety level of the concept and to find a suitable safety analysis procedure for this new type of reactor (GIF methodology ISAM, and risk analysis) in the frame of the EVOL then SAMOFAR projects (Chapter 20: Safety assessment of the molten salt fast reactor (SAMOFAR)). A new approach of transient calculations, coupling neutronics and thermal-hydraulics and based on the "transient fission matrix" (TFM) innovative neutronic model has been achieved (Laureau, 2015; Laureau et al., 2015a). This showed the excellent capability of load following of the MSFR in a very large power range and strong resilience of the reactor to perturbations (Laureau, 2015; Laureau et al., 2015b). Currently, a system code (plant simulator) is under development at LPSC in the framework of the SAMOFAR European project.

Regarding the first demonstration steps of the MSFR concept, an experimental 50-L salt loop called the FFFER project was built at LPSC using FLiNaK at 650°C flowing at about 1 m/s in a circuit with a centrifuge pump, a bubble injection system, and a cyclone to separate bubbles from the salt. A cold plug valve and an ultrasonic velocity measurement were also tested on this loop.

## Acknowledgments

The authors wish to thank the NEEDS (Nucléaire: Energie, Environnement, Déchets, Société) French Interdisciplinary program and the IN2P3 department of the National Centre for Scientific Research (CNRS), Grenoble Institute of Technology, and the European programs EVOL (FP7) for their support.

## References

Allibert, M., Aufiero, M., Brovchenko, M., Delpech, S., Ghetta, V., Heuer, D., et al., 2015. Molten salt fast reactors. Handbook of Generation IV Nuclear Reactors, Woodhead Publishing Series in Energy. Woodhead Publishing, Duxford, UK.

Boussier, H., et al., 2012. The molten salt reactor in generation IV: overview and perspectives. In: Proceedings of the Generation-4 International Forum Symposium, San Diego, CA.

Brovchenko, M., 2013. Etudes préliminaires de sûreté du réacteur à sels fondus MSFR, PhD Thesis (in French). Grenoble Institute of Technology, France.

Brovchenko, M., Heuer, D., Merle-Lucotte, E., Allibert, M., Ghetta, V., Laureau, A., et al., 2013. Design-related studies for the preliminary safety assessment of the molten salt fast reactor. Nucl. Sci. Eng. 175, 329−339.

Brovchenko, M., Merle-Lucotte, E., Rouch, H., Alcaro, F., Allibert, M., Aufiero, M., et al., 2014a. Optimization of the pre-conceptual design of the MSFR. In: Work-Package WP2, Deliverable D2.2, EVOL (Evaluation and Viability of Liquid Fuel Fast Reactor System) European FP7 Project, Contract number: 249696.

Brovchenko, M., Heuer, D., Huffer, E., Merle-Lucotte, E., Allibert, M., Feynberg, O., et al., 2014b. Safety approach of a fast liquid fuel system. In: Work-Package WP2, Deliverable D2.5, EVOL (Evaluation and Viability of Liquid Fuel Fast Reactor System) European FP7 project, Contract number: 249696.

Delpech, S., Merle-Lucotte, E., Heuer, D., et al., 2009. Reactor physics and reprocessing scheme for innovative molten salt reactor system. J. Fluorine Chem. 130 (1), 11−17.

Doligez, X., 2010. Influence du retraitement physico-chimique du sel combustible sur le comportement du MSFR et sur le dimensionnement de son unité de retraitement, PhD Thesis. Grenoble Institute of Technology, France.

Furukawa, K., Lecocq, A., Kato, Y., Mitachi, K., 1990. Thorium molten-salt nuclear energy synergetics. J. Nucl. Sci. Technol. 27 (12), 1157−1178.

Furukawa, K., Numata, H., Kato, Y., Mitachi, K., Yoshioka, R., Furuhashi, A., et al., 2005. New primary energy source by thorium molten-salt reactor technology. Electrochemistry. 73 (8), 552−563.

GIF (Generation IV International Forum), 2008. Annual report 2008, pp. 36−41. <http://www.gen-4.org/PDFs/GIF_2008_Annual_Report.pdf>.

Heuer, D., Merle-Lucotte, E., Allibert, M., Brovchenko, M., Ghetta, V., Rubiolo, P., 2014. Towards the thorium fuel cycle with molten salt fast reactors. Ann. Nucl. Energy. 64, 421−429.

Laureau, A., 2015. Développement de modèles neutroniques pour le couplage thermohydraulique du MSFR et le calcul de paramètres cinétiques effectifs, PhD Thesis. Université Grenoble Alpes, France.

Laureau, A., Aufiero, M., Rubiolo, P., Merle-Lucotte, E., Heuer, D., 2015a. Transient Fission Matrix: kinetic calculation and kinetic parameters βeff and Λeff calculation. Ann. Nucl. Energy. 85, 1035−1044.

Laureau, A., Aufiero, M., Rubiolo, P., Merle-Lucotte, E., Heuer, D., 2015b. Coupled neutronics and thermal-hydraulics transient calculations based on a fission matrix approach: application to the molten salt fast reactor. Proceedings of the Joint International Conference on Mathematics and Computation (M&C), Supercomputing in Nuclear Applications (SNA) and the Monte Carlo (MC) Method, Nashville, TN. American Nuclear Society, LaGrange Park, IL, pp. 1−12.

Lecarpentier, D., 2001. Le concept AMSTER, aspects physiques et sûreté, Ph.D. Thesis. Conservatoire National des Arts et Métiers, France.

Mathieu, L., Heuer, D., Merle-Lucotte, E., et al., 2009. Possible configurations for the thorium molten salt reactor and advantages of the fast non-moderated version. Nucl. Sci. Eng. 161, 78−89.

Merle-Lucotte, E., Heuer, D., et al., 2009a. Minimizing the fissile inventory of the molten salt fast reactor. In: Proceedings of the Advances in Nuclear Fuel Management IV (ANFM 2009), Hilton Head Island, SC.

Merle-Lucotte, E., Heuer, D., et al., 2009b. Optimizing the burning efficiency and the deployment capacities of the molten salt fast reactor. In: Proceedings of the International Conference Global 2009—The Nuclear Fuel Cycle: Sustainable Options & Industrial Perspectives, Paper 9149, Paris, France.

Merle-Lucotte, E., Heuer, D., Allibert, M., Brovchenko, M., Capellan, N, Ghetta, V., 2011. Launching the thorium cycle with molten salt fast reactor. In: Proceedings of ICAPP 2011, May, paper 11190, Nice, France.

Merle-Lucotte, E., Heuer, D. et al., 2012. Preliminary design assessments of the molten salt fast reactor. In: Proceedings of the European Nuclear Conference ENC2012, paper A0053, Manchester, UK.

Merle-Lucotte, E., Heuer, D., Allibert, M., Brovchenko, M., Ghetta, V., Laureau, A., et al., 2013. Recommendations for a demonstrator of molten salt fast reactor. In: Proceedings of the International Conference on Fast Reactors and Related Fuel Cycles: Safe Technologies and Sustainable Scenarios (FR13), Paris, France.

Nuttin, A., Heuer, D., et al., 2005. Potential of thorium molten salt reactors. Prog. Nucl. Energy. 46, 77−99.

Renault, C., Delpech, S., Merle-Lucotte, E., Konings, R., Hron, M., Ignatiev, V., 2009. The molten salt reactor: R&D status and perspectives in Europe. In: Proceedings of the FISA2009: 7th European Commission Conference on EURATOM Research and Training in Reactor Systems, Prague, Tchéquie.

Rouch, H., Geoffroy, O., Rubiolo, P., Laureau, A., Brovchenko, B., Heuer, D., et al., 2014. Preliminary thermal-hydraulic core design of the molten salt fast reactor (MSFR). Ann. Nucl. Energy. 64, 449–456.

Serp, J., Allibert, M., Beneš, O., Delpech, S., Feynberg, O., Ghetta, V., et al., 2014. The molten salt reactor (MSR) in generation IV: overview and perspectives. Prog. Nucl. Energy. 77, 308–319.

Wang, S., Rineiski, A., Li, R., Brovchenko, M., Merle-Lucotte, E., Heuer, D., et al., 2014. Safety analysis: transient calculations, EVOL (evaluation and viability of liquid fuel fast reactor system) European FP7 project, Contract number: 249696.

Whatley, M.E., McNeese, L.E., Carter, W.L., Ferris, L.M., Nicholson, E.L., 1970. Engineering development of the MSBR fuel recycle. Nucl. Appl. Technol. 8, 170–178.

## Many MSFR references may be found on the LPSC website:

<http://lpsc.in2p3.fr/index.php/en/groupes-de-physique/enjeux-societaux/physique-des-reacteurs/systemes-et-scenarios/rsf-reacteurs-a-sels-fondus/lang-fr-msfr-bibliographie-lang-lang-en-msfr-bibliography-lang>.

# 26.7 Germany

*Andrei Rineiski*
Karlsruhe Institute of Technology, Germany

Molten salt reactors (MSRs) were studied during early phases of reactor development in Germany. A fast neutron spectrum reactor concept without graphite in the core, MOSEL, was proposed in Germany at Jülich and studied in cooperation with US partners (Kasten et al., 1965; Gat, 1967). The MOSEL reactor with a fast neutron spectrum was developed primarily for the Th-U fuel cycle, with a fissile liquid fuel for the core and a fertile one for the blanket. The core was fueled with uranium fluoride dissolved in a carrier salt. The latter salt was a mixture of beryllium- and alkali-metal-fluorides.

The core contained nickel-alloy structures, such as tubes or plates. Within these structures the fuel was circulated primarily for the purposes of fuel mixing, addition, and removal. The blanket fluid was thorium fluoride dissolved in the same carrier salt.

In Kasten et al. (1965) the blanket fluid was also employed for cooling the core. In Gat (1967) liquid lead was alternatively considered for cooling the MOSEL core; the coolant was allowed to come into direct contact with the liquid fuel while passing through the core. This option was proposed to enhance heat transfer from the fuel to the lead coolant and under assumption that the lead coolant is easily separated from the fuel when it leaves the core.

In the 1970s and 1980s major nuclear activities in Germany were on alternatives to MSR reactor types. Later, some interest in MSRs reappeared, in particular, due to proposals to use these reactors for nuclear waste burning. These activities were integrated in EURATOM FP projects, to which German Institutions contributed. Different MSR systems were also studied with the participation of German institutions within an IAEA project on options for nuclear waste incineration (Maschek et al., 2009). In particular, safety-related reactor physics parameters, transmutation potential, and transient behavior in different kinds of MSRs, including those with fertile and without fertile components in the fuel, were evaluated for the latter IAEA project. More recently, MSRs were considered as an option in the German study on partitioning and transmutation (Renn, 2014).

Since early 2000, several EURATOM projects have been organized on MSR studies, namely the MOST, ALISIA, EVOL, and SAMOFAR projects. The latter project is running from 2015 to 2019. Major nuclear German institutions, in particular the Research Centers of Dresden-Rossendorf, Jülich, and Karlsruhe, have been involved in these EU projects. Only the Karlsruhe Institute of Technology is currently contributing to the SAMOFAR project. The European Institute for Transuranic Elements, actively contributing to all EU activities on MSRs, is also located at Karlsruhe.

In Jülich, the major effort in the past EURATOM projects was done on fuel chemistry and reprocessing, while at Karlsruhe and Dresden, the activities were mainly on the development and application of coupled fluid-dynamics and neutronics models for simulating core behavior under nominal and transient conditions and for fuel cycle analyses. Initially, both fluoride and chloride salts were considered, but soon the efforts were concentrated on fluorides in the MOST and the following projects.

The initially studied systems in the MOST project contained graphite in the core for neutron moderation, similar to the MSRE reactor. In these systems with a thermal neutron spectrum, the fuel flows through graphite channels in the core.

Information on MSRE experiments was used to validate new computation models developed for MSRs, including the effects of circulation of delayed neutron precursors on transient core behavior and neutron balance. For later EURATOM projects, including SAMOFAR, mainly fast neutron spectrum MSRs were under investigation. The fast systems were introduced in order to improve safety-related neutronics parameters, in particular reactivity coefficients, while keeping the MSR breeding potential. The fast spectrum system systems are also considered preferable for nuclear waste burning. The reason is that the probability of fission—after a neutron interacts with a nucleus of transuranic fuel—is higher at higher energies.

In Dresden a coupled code developed earlier for LWR reactor transient analyses, DYN3D, was extended for MSR applications (Krepel et al., 2007). The neutron transport solver in DYN3D is based on the diffusion approximation, initially developed for HEX-Z geometry and more recently extended to XYZ in space and to SP3 in angle approximation. The employed cross-section library contains cross-sections for a reference set of reactor parameters, such as fuel temperature. These cross-sections are computed in advance by a cell code and interpolated during the calculations. The fluid-dynamics part of the code for simulating fuel behavior in the core is based on a multichannel approach and is well suited for thermal spectrum MSR analyses: the fuel flow is essentially one dimensional in the graphite channels in the core.

For the fast neutron spectrum cores without graphite, studies in Dresden were mainly done on irradiation of structure materials surrounding the core (Merk et al., 2014) and on the fast spectrum MSR potential for nuclear waste management.

For fast spectrum MSRs, studied in EVOL and SAMOFAR, the fluid pattern in the reactor core can be rather complex because the core is essentially a large tank, in which regions with stagnant flow may appear. Special design efforts were made to exclude the possibility for formation of these reasons, in which the temperature can be rather high. At Karlsruhe this was done by introducing a special flow distribution plate below the core for flow profiling. A more recent approach proposed by other EVOL partners was to modify the shape of the core/blanket boundary.

At KIT a safety code, SIMMER, was extended for MSR simulations in order to support the MSR design and safety studies. This code was and is being developed by JAEA of Japan, in cooperation with CEA of France, KIT of Germany, and other partners, initially for analyses of severe accidents in sodium fast reactors (Tobita et al., 2002). The code framework is rather general. It was extended in early 2000s for accelerator-driven systems (ADSs) and other reactor types at KIT. For neutron transport calculations, 2D RZ and 3D XYZ Sn method-based models are used in SIMMER-III, 2D version, and SIMMER-IV, 3D version, respectively. The cross-sections employed in neutron transport calculations are generated by the SIMMER code while employing multigroup libraries with f-factors. The spatial kinetics model is based on the quasistatic method. The neutronics part of the code was extended first (Rineiski et al., 2005) and checked for an MSRE experimental model, where the transient flow can be described in a rather simple manner. The effect of neutron precursor movement was taken into account via an additional source-like term. This integrally negative source-like term was introduced in the spatial and point-kinetics parts of the code similarly to what was done earlier to take into account the external neutron source in ADSs. Unlike ADSs, for which the reactivity at nominal conditions is negative and the source term is positive, the reactivity at nominal conditions for MSRs in SIMMER is positive, that is compensated by the "negative" source-like term appeared due to decay of part of the delayed neutron precursors outside of the core. The SIMMER fluid-dynamics part is based on a multiphase, multiple velocity field approach and includes models for phase transfers of reactor materials, such as melting/freezing, vaporization/condensation, etc. Flexible equations of states (EOSs) are used to describe the reactor material properties.

For making possible coupled neutronics and fluid-dynamics/thermal-hydraulics MSR calculations with SIMMER in the general case, the fluid dynamics part was extended further; in particular, a new turbulence model was introduced and new EOSs for several fluoride salts were included in SIMMER at KIT (Wang et al., 2006).

Due to a very general SIMMER code framework, its application takes a lot of computing time. For transient MSR analyses, to which simplified calculation models are applicable, a faster running coupled code with a two-phase computational fluid dynamics model is also being developed at KIT (Guo et al., 2016).

Recently a new MSR concept, a so-called dual-fluid reactor, was proposed by a research group from Berlin, both for energy production and waste management. The reactor employs a chloride salt as fuel that flows inside metallic structures, which are cooled by liquid lead (http://dual-fluid-reaktor.de/; see also Chapter 24: Molten salt thermal wasteburner). This activity is running in parallel to the above-mentioned EU projects focusing on fluoride salts.

## References

Gat, U., 1967. Cooling concepts for a compact MOSEL (molten salt) reactor. Nucl. Eng. Des. 5, 113−122.

Guo, L., et al., 2016. Further development of COUPLE code taking account of gas-liquid interfacial motion. In: Int. Conf. NUTHOS-11, Gyeongju, Korea, October 9−13, 2016.

Kasten, P.R., et al., 1965. Design concepts for the core structure of a MOSEL (molten salt experimental) reactor. Nucl. Struct. Eng. 2, 224−232.

Krepel, J., et al., 2007. DYN3D-MSR spatial dynamics code for molten salt reactors. Ann. Nucl. Energy. 34 (6), 449−462.

Maschek, W., et al., 2009. Advanced Reactor Technology Options for Utilization and Transmutation of Actinides in Spent Nuclear Fuel, IAEA-Tecdoc 1626. IAEA, Vienna.

Merk, B., et al., 2014. Neutron shielding studies on an advanced molten salt fast reactor design. Ann. Nucl. Energy. 64, 441−448.

Renn, O. (Hrsg.), 2014. Partitionierung und Transmutation. Forschung−Entwicklung−Gesellschaftliche, Implikationen (acatech STUDIE). München, Herbert Utz Verlag.

Rineiski, A., et al., 2005. Kinetics and cross-section developments for analyses of reactor transmutation concepts with SIMMER. In: Proc. Int. Conf., M&C 2005, Avignon, France, September 12−15, 2005.

Tobita, Y., et al., 2002. The development of SIMMER-III, an advanced computer program for LMFR safety analysis. In: Proceedings of the IAEA/NEA Technical Meeting on Use of Computational Fluid Dynamics (CFD) Codes for Safety Analysis of Reactor Systems Including Containment, Pisa, Italy, November 11−14, 2002.

Wang, S., et al., 2006. Molten salt related extensions of the SIMMER-III code and its application for a burner reactor. Nucl. Eng. Des. 236 (14), 1580−1588.

# 26.8 India

*P.K. Vijayan, I.V. Dulera, A. Rama Rao and R.K. Sinha*
Bhabha Atomic Research Centre, Mumbai, Maharashtra, India

## 26.8.1 Introduction to the Indian MSR Program

India is pursuing the design of two molten salt reactors. The first is the Indian Molten Salt Breeder Reactor (IMSBR), which is expected to be a self-sustaining thorium-based molten salt-fueled reactor, attractive for the third stage of the Indian nuclear power program. The other concept is the molten salt-cooled high-temperature reactor, named the Innovative High Temperature Reactor (IHTR) with nuclear hydrogen production by splitting water as the main objective. Both concepts could be used for high-efficiency electricity generation. One of the important design goals for IHTR is to achieve a maximum coolant temperature of 1273K and this is based on a pebble bed fuel concept with molten salt as the coolant. R&D activities for these reactors are being pursued in India and are covered briefly in this section.

## 26.8.2 Background to the Indian nuclear power program and the relevance of MSBRs

India's unique, sequential three-stage nuclear power program (http://dae.nic.in/writereaddata/publ/saga/vol2/pdf2/Chapter-01.pdf) is aimed at the optimum utilization of India's nuclear resource profile of modest uranium and abundant thorium. The three stages are natural uranium-fueled pressurized heavy water reactors (PHWRs) in the first stage, plutonium-fueled fast breeder reactors (FBRs), including metallic fueled ones, in the second stage, and $^{233}$U-fueled systems in the third stage. The spent fuel of one stage is reprocessed to produce fuel for the next stage, multiplying the energy potential of the fuel many-fold and at the same time reducing the quantity of waste. HTRs based on the $^{233}$U-Th cycle are also contemplated during this stage for nuclear hydrogen production by splitting water. The closed fuel cycle thus provides an ideal solution for satisfying the energy needs of a large country like India in a sustainable manner, securing its energy freedom in the long term. A schematic of the Indian three-stage nuclear power program is shown in Fig. 26.8.1.

As mentioned earlier, the third stage of the Indian nuclear power program envisages the use of thorium as a fertile material with $^{233}$U, which would be obtained from the operation of $^{239}$Pu-Th-based fast reactors in the later part of the second stage. A candidate reactor concept, which holds promise for this stage, is the molten salt-fueled reactor, which has the potential to provide significant breeding ratios so as to maintain long-term sustainability. India is carrying out fundamental studies so

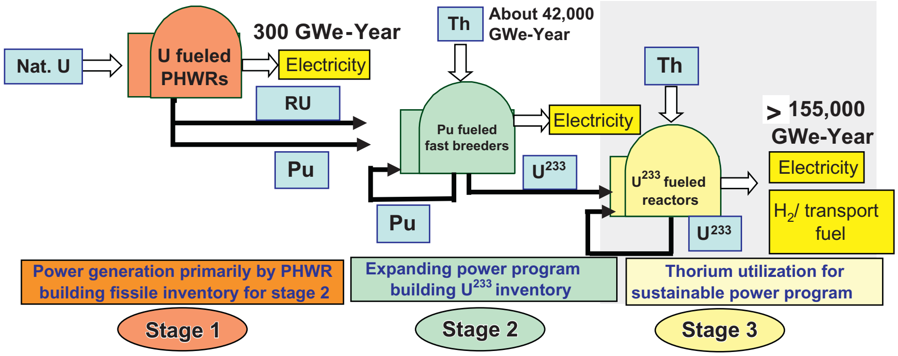

**Figure 26.8.1** Three stages of the Indian nuclear power program.

as to arrive at a conceptual design of the IMSBR. Currently, various design options and possibilities are being studied from the point of view of reactor physics and thermal hydraulic design. In parallel, studies on salt preparation, salt characterization, salt purification, thermal hydraulics, component and instrumentation development, material development, and corrosion behavior of various molten salts are also being carried out. The large-scale deployment of thorium-based reactors is likely to take place in the second half of the 21st century, and it is planned to master all the technologies much before large-scale deployment stage. The developed technologies would be demonstrated by setting-up prototype small power reactors with the aim of optimizing the design for the larger reactors.

### 26.8.2.1 Molten salt breeder reactor program in India

India has one of the largest reserves of thorium in the world. The Atomic Minerals Directorate for Exploration and Research (AMD), a constituent unit of Department of Atomic Energy (DAE), India, has so far established 11.93 million tonnes of monazite (thorium-bearing mineral) in India, which in situ contains about 1.07 million tonnes of thorium oxide. In view of this, the third stage of the Indian nuclear power program is based on extensive use of $^{233}$U-fueled reactors with thorium as the fertile material. Efficient utilization of domestic thorium resources is one of the primary aims of the third stage of the program. To maintain or expand the scale of the program in the third stage in a sustainable manner, it is essential that the reactor systems (i.e., the reactor and its associated fuel cycle facilities) should have a breeding ratio of at least unity, after considering material losses. Hence the majority of the reactor systems in the third stage, especially for electricity production, are expected to be breeders operating on a $^{233}$U-Th fuel cycle.

While, it is possible to breed $^{233}$U from thorium in reactors of conventional design (i.e., with solid fuel rod bundles), thorium, if used in conventional reactors, suffers from one disadvantage. In the thorium fuel cycle, $^{233}$Pa is an intermediate isotope in the nuclear reaction chain (Fig. 26.8.2), which results in conversion of $^{232}$Th to $^{233}$U. The conversion of $^{233}$Pa to $^{233}$U takes place by beta decay. However, in a reactor core $^{233}$Pa is always subjected to the presence of fission neutrons, which if absorbed, neither leads to the formation of $^{233}$U, nor to fission, and hence is a parasitic loss. This is unavoidable in the case of solid-fueled reactors, since the fuel pins need to be exposed to certain burnups before being extracted for reprocessing. This can be avoided if the fuel is in fluid form, so that the $^{233}$Pa is separated out as soon as it is produced, and allowed to decay to $^{233}$U out of core. A feasible way of doing this is the molten salt breeder reactor (MSBR). Therefore, the MSBR is being considered as an attractive option for large-scale deployment during the third stage of the Indian nuclear power program.

MSBR has fuel in the form of a continuously circulating molten salt, which contains the fissile and fertile elements, besides other salts, as its constituents. These are made to flow through heat exchangers, ultimately transferring the high-temperature heat for power production. In order to generate electricity with higher efficiency, R&D efforts have been initiated to develop supercritical $CO_2$-based Brayton cycle.

The critical configuration of the salt is achieved only when it enters the nuclear reactor core. When the salt is moved out of the core, criticality is not achieved and hence it does not undergo fission. Thus, if the salt is dumped into smaller dump tanks, subcriticality is automatically achieved and thus the reactor is safely shutdown. A crucial part for achieving reasonable breeding in such reactors is the need to reprocess the salt continuously. Depending on the design, the reprocessing can be configured to be in an online mode, or in an offline batch mode. In an online mode, the reprocessing plant is located with the reactor and continuously reprocesses the fuel salt. On the other hand in an offline mode, the reprocessing is done in a separate plant located nearby, with some portion of the fuel salt removed and the reprocessed salt added to the primary circuit periodically.

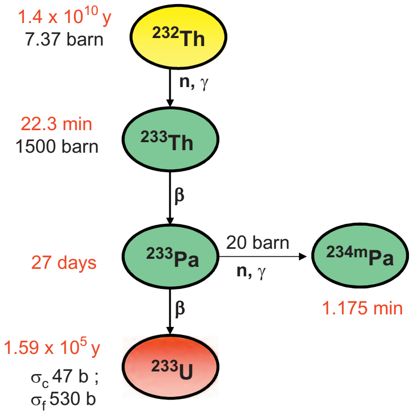

**Figure 26.8.2** Conversion chain of $^{232}$Th to $^{233}$U (Dulera et al., 2013).

Currently, studies for two conceptual designs of 850-MWe IMSBR (Dulera et al., 2013; Vijayan et al., 2015) are being carried out. One concept is based on a loop-type design and the other is based on a pool-type design. The major design parameters for both concepts have been worked out. In order to develop and demonstrate the involved technologies, before launching a large power reactor, it is proposed to develop a small power (5 MWth) technology demonstration reactor. As compared to other reactors, the use of fluid fuel allows for the removal of neutron-absorbing products at regular intervals, allowing for efficient utilization of nuclear materials. $^{233}$Pa removed is allowed to decay to $^{233}$U and re-introduced into the reactor.

### 26.8.2.2 Conceptual design of the IMSBR

In order to arrive at the conceptual design of IMSBR, some of the design guidelines which are being followed are as follows:

1. Self-sustaining in the $^{233}$U-Th cycle;
2. Minimization of fissile material inventory in the reactor;
3. Enhanced safety with inherent safety features as compared to current-generation reactors;
4. Avoiding the use of beryllium and beryllium-based salts to avoid chemical toxicity;
5. Minimization of waste generation and hence avoidance of the use of graphite;
6. Feasibility for inspection and replacement of components ensuring the long life of the reactor.

A schematic of IMSBR is shown in Fig. 26.8.3. Two different concepts for the 850-MWe IMSBR have been investigated. For both concepts thermal efficiency is aimed around 45%. The first design is a loop-in-tank concept, while the other is a pool-type concept. Because of the need to avoid graphite and beryllium, the reactor has been designed to operate primarily in the fast spectrum.

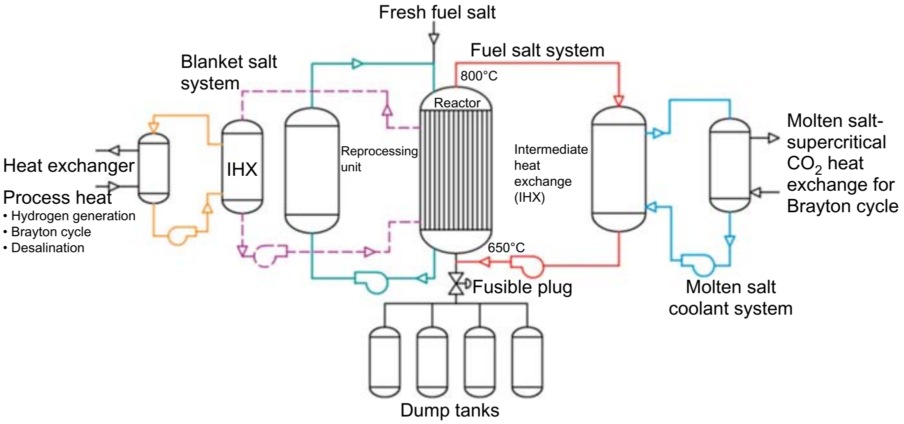

**Figure 26.8.3** Schematic of a large-power IMSBR.

In the loop-in-tank concept (Basak et al., 2015), the reactor vessel and all the highly active systems containing U, Th, fission products, and minor actinides are contained within a nickel-lined safety vessel such that no active material leaves the safety vessel. All potential active salt leakage scenarios are thus contained in the safety vessel. Additionally, all major components are accessible for carrying out in-service inspection (ISI). Such equipment would see only a gas environment. This arrangement is expected to facilitate easy replacement of the blanket vessel, if required.

The schematic of the reactor is shown in Fig. 26.8.4 and the salient features are listed in Table 26.8.1.

The pool-type concept (Borgohain et al., 2015) has the primary system contained in a vessel to prevent any leakage of highly active fuel salts. Natural circulation-based cooling of the reactor is found to be feasible, but need temperatures to be as high as around 1000°C. Forced circulation operation is possible at temperatures around 800°C. To mitigate the cost of a large vessel, a sacrificial frozen salt layer has been considered. The major design parameters of two variations of the pool-type concept are shown in Table 26.8.2. Schematics of the same are shown in Fig. 26.8.5.

The loop-in-tank-type and pool-type concepts (natural circulation) have been analyzed from the point of view of reactor physics design using a Monte Carlo code. The initial results are briefly outlined in the following section. In the preliminary analyses, no effect of circulation of fuel salt and reprocessing has been considered. Computer codes for carrying out detailed analysis are under development.

### 26.8.2.3 Reactor physics design of IMSBR concepts

In order to achieve a higher breeding ratio (BR), a fast neutron spectrum has been preferred for the above-mentioned concepts. The loop-type concept with forced circulation (Srivastava et al., 2015b) was found to be a viable option for meeting the criteria of relatively low initial fissile inventory ( ~ 3.2 t/GWe) and high initial BR ( ~ 1.1). The effect of voiding in fuel in loop-type MSRs shows that the void reactivity coefficient is negative at all voiding states, which become more negative at higher voiding. Reactor physics feasibility analysis of the pool-type concept with natural circulation, operating at a power of 850 MWe was also carried out as an alternative design option which also operates in the fast neutron spectrum. The initial fissile inventory, however, was found to be higher ( ~ 5.4 t/GWe) compared to the loop-type version for the same operating power, whereas the initial BR has been found to be around 1.1. This is shown in Table 26.8.3. Neutron spectra for loop- and pool-type concepts are shown in Figs. 26.8.6 and 26.8.7, respectively.

### 26.8.2.4 Key challenges for the design

Some of the major challenges for IMSBR, where R&D have been initiated include:

1. Development of closely coupled neutron transport and CFD codes with capability to account for online reprocessing.

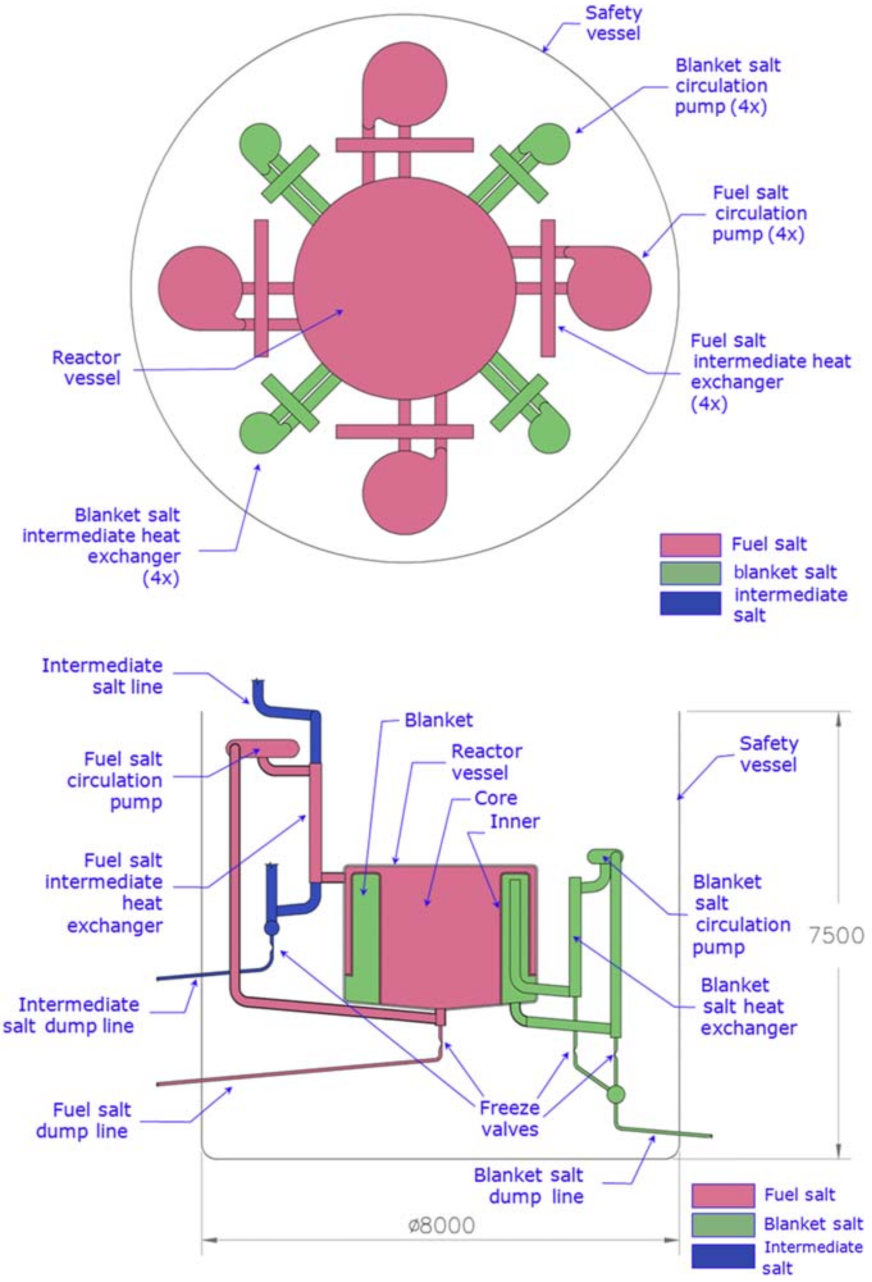

**Figure 26.8.4** Loop-in-tank concept of IMSBR.

**Table 26.8.1** **Loop-in-tank IMSBR—major proposed design parameters**

| | Attributes | Parameter |
|---|---|---|
| 1. | Power | 850 MWe |
| 2. | Thermal efficiency | >45% |
| 3. | Active core diameter/height | 2 m/2.05 m |
| 4. | Core inlet/outlet | 700/800°C |
| 5. | Fuel salt | $LiF-ThF_4-UF_4$ |
| 6. | Blanket salt | $LiF-ThF_4$ |
| 7. | Secondary salt | $LiF-KF-AlF_3$ |
| 8. | Flow rate (primary) | 10.9 t/s |
| 9. | Flow rate (secondary) | 6.3 t/s |
| 10. | Velocity (core) | 0.85 m/s |
| 11. | Fuel salt inventory (total) | 41.1 t (2.7 t of $^{233}U$) |
| 12. | Proposed power production system | Based on a supercritical $CO_2$ Brayton cycle |

**Table 26.8.2** **Pool-type IMSBR—major proposed design parameters**

| | Parameters | Option 1, natural circulation | Option 2, forced circulation |
|---|---|---|---|
| 1. | Power | 850 MWe | |
| 2. | Inlet/outlet temperature | 650/1000°C | 650/800°C |
| 3. | Power conversion efficiency | >45% | |
| 3. | Fuel salt/blanket salt | $LiF-ThF_4-UF_4/LiF-ThF_4$ | |
| 4. | Secondary/tertiary coolant | FLiNaK/supercritical $CO_2$ | |
| 5. | Total fuel salt inventory | 74.6 t (5.22 t of $^{233}U$) | 55 t (3.64 t of $^{233}U$) |
| 6. | Velocity in the core | 0.2 m/s | 0.77 m/s |
| 7. | Primary/secondary pump power | –/0.65 MW | 0.71 MW/0.65 MW |

**Figure 26.8.5** Pool-type concept of IMSBR, natural circulation version on the left and forced circulation version on the right.

**Table 26.8.3** **Results of initial reactor physics calculations**

| | $k_{\mathrm{eff}}$ | Initial breeding ratio considering fuel and blanket |
|---|---|---|
| Loop-in-tank | 1.0428 | 1.091 |
| Pool type (natural convection) | 1.0266 | 1.116 |

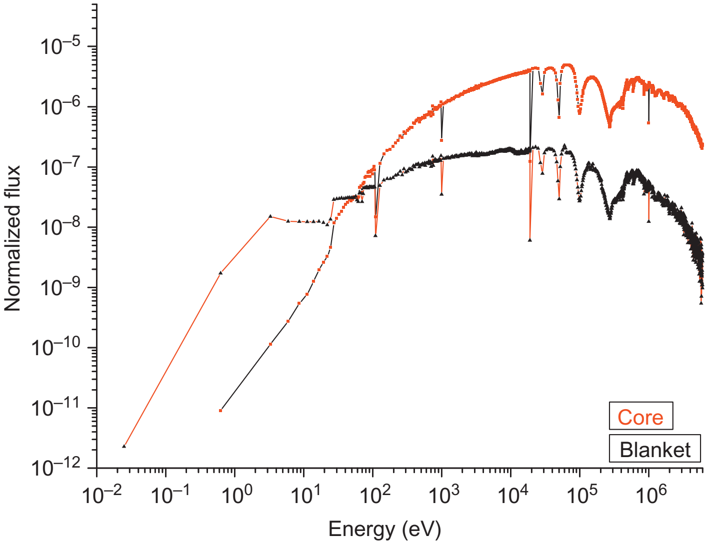

**Figure 26.8.6** Neutron spectrum in core and blanket of loop-type IMSBR.

2. Large-scale salt preparation and purification.
3. Physical property characterization for molten salts.
4. Metallic materials for use with molten salts at high temperatures and qualification to meet ASME Boiler and Pressure Vessel Code, Section III, Subsection—NH design rules.
5. Design rules for carbon−carbon composites for use in nuclear reactors.
6. Joining techniques for carbon−carbon composite to metallic materials.
7. Batch mode offline reprocessing, without requiring cooling of fuel salt.
8. Instrumentation for operation at high-temperature, high-radiation, molten salt environment.
9. Online chemistry control techniques.
10. Tritium capture.
11. Validation of computational chemistry methods in the context of MSBRs.
12. Supercritical $CO_2$-based Brayton cycle (SCBC) and components of the power system.
13. Reprocessing issues: The reprocessing in an MSBR is different from conventional reprocessing by PUREX or THOREX, in particular due to low concentrations of fission products. In addition, R&D efforts also need to be directed towards addressing issues of plate-out of noble metal fission products that do not dissolve as stable fluorides on heat

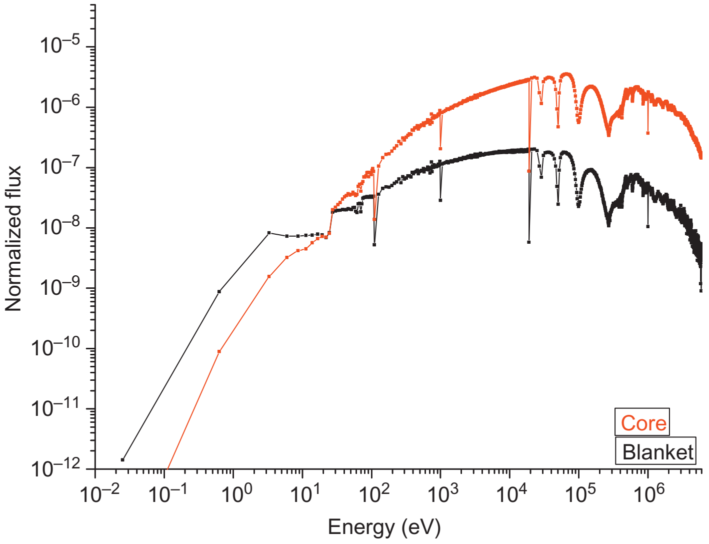

**Figure 26.8.7** Neutron spectrum in core and blanket—natural circulation pool-type IMBSR.

exchanger walls, development of a fluoride high-level waste form, and an integrated fuel recycle strategy.

### 26.8.2.5 Research & development to meet the challenges

India is carrying out R&D in most of the major areas. Some of the prominent areas are described in the following sections.

#### 26.8.2.5.1 Chemistry of inactive salts and their characterization

Lithium fluoride (LiF) is one of the most important salts for MSBRs. It can be prepared either by reacting LiOH with fluorine gas in a closed vessel or by neutralization of LiOH with concentrated HF acid. In India the latter method is employed to make LiF because of the ease of operation. First, the LiOH (3.6N) solution is purified for the removal of metal impurities by passing through a strong cation exchange resin column. The purified LiOH solution is then neutralized using 20% HF acid for the LiF production:

$$\mathrm{LiOH} + \mathrm{HF} \rightarrow \mathrm{LiF} + \mathrm{H_2O} \quad \Delta H^0 = -57.35\ \mathrm{kJ/mol}$$

The wetted parts of the reactor are lined with Teflon. The reaction is carried out in a well-ventilated plant with primary ventilation of gases being scrubbed before they are discharged. pH is monitored to ensure that the solution is alkaline near the end point of reaction. Once the neutralization is completed, the solution is filtered. The residue is washed with distilled water 3—4 times to remove the hydroxide

**Table 26.8.4** **Elemental and isotopic purity of LiF BDL**

| | |
|---|---|
| LiF | 99% |
| pH value | 7.0–7.5 |
| Calcium (Ca) | 0.0002% |
| Iron (Fe) | 0.00007 % |
| Chromium (Cr) | BDL |
| Cobalt (Co) | BDL |
| Copper (Cu) | BDL |
| Magnesium (Mg) | BDL |
| Nickel (Ni) | BDL |
| Lead (Pb) | BDL |
| Isotopic purity (Li-7) | 95% |

BDL, below detection limit.

impurities. The solid product formed is then dried in a vacuum oven. As high-purity LiOH is used for the preparation of LiF, no further purification is carried out. The product specification is given in Table 26.8.4.

### *26.8.2.5.2 Chemistry of active salts, their purification and characterization*

In India, uranium tetra-fluoride ($UF_4$) is prepared by a gas–solid reaction route (Satpati et al., 2006) called the hydrofluorination method reacting nuclear pure metal-grade uranium di-oxide ($UO_2$) with anhydrous hydrofluoric acid (HF) at 450°C in an inclined rotary tubular continuous reactor (Fig. 26.8.8). $UF_4$, also called green salt, is produced following a reversible exothermic reaction as:

$$UO_2 + 4HF \longleftrightarrow UF_4 + 2H_2O \quad \Delta H^0 = -43.2\ \mathrm{kcal} \tag{26.8.1}$$

The produced salt is subjected to an expulsion operation (vacuum heating) to remove adhered moisture and free acidity. Monitoring and controlling of critical process parameters are important for obtaining metal-grade $UF_4$. Specific design and administrative control mechanisms are in place for the handling of highly corrosive HF in both vapor and aqueous forms. Zero discharge of fluoride effluent has been adopted in the process cycle. The quality of the produced $UF_4$ is monitored for each batch of operation. In general, particle size distribution and morphology of the metal-grade salt is obtained as shown in Figs. 26.8.9 and 26.8.10, respectively. The facility for salt purification is shown in Fig. 26.8.11. The metal-grade salt is suitable for the production of uranium metal and other nuclear applications, such as fuel for molten salt reactor, etc. The $UF_4$ production process technology along with effluent handing scheme and required safety measures are well established in the Uranium Extraction Division (UED) of Bhabha Atomic Research Centre (BARC), India. Fluorination of thorium oxide by ammonium bifluoride (Mishra et al., 2015) has also been studied. Determination of eutectic composition and heat capacities of

**Figure 26.8.8** $UF_4$ powder production system.

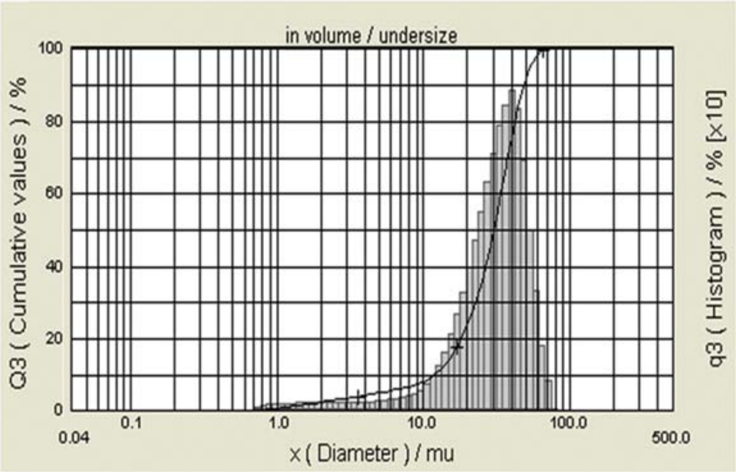

**Figure 26.8.9** Particle size distribution of $UF_4$ powder.

fuel salt (LiF-$ThF_4$-$UF_4$) and blanket salt (LiF-$ThF_4$) mixtures have also been carried out (Mukherjee and Awasthi, 2015). R&D on the preparation of pure $ThF_4$ and $LiF_4$, including development of equipment as well as estimation of solubility of $PuF_3$ in $LiF_4$-$BeF_2$-$ThF_4$, was carried out in BARC (Fig. 26.8.12) during 1970s (Sood et al., 1972) as part of a collaboration with ORNL.

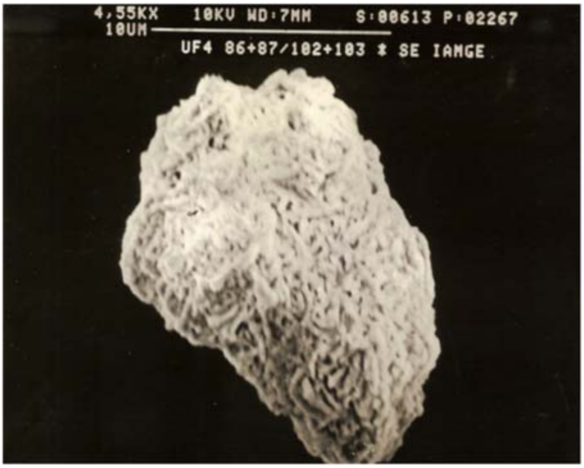

**Figure 26.8.10** Morphology of $UF_4$ powder.

**Figure 26.8.11** Facility for salt purification.

### 26.8.2.5.3 Engineering facilities for thermal hydraulics and corrosion studies

Currently, besides carrying out fundamental studies on various salts, the facility for natural circulation-based thermal hydraulic studies called MAFL (molten active fluoride salt loop), with an active blanket salt (using LiF-$ThF_4$) has been designed, manufactured, commissioned, and operated up to 700°C to verify the thermal hydraulics code (Srivastava et al., 2015a; Sarkar et al., 2015). This is a natural circulation loop for thermal-hydraulic studies having a design pressure and temperature of 5 kg/cm$^2$ and 850°C, respectively. The loop has been analyzed using OpenFOAM and stability calculations have been carried out using the LeBENC code. This loop is shown in Fig. 26.8.13. A similar facility for fuel salt (i.e., LiF-$ThF_4$-$UF_4$) is under fabrication.

**Figure 26.8.12** Work done in BARC on molten salts during the 1970s as part of a collaboration with ORNL.

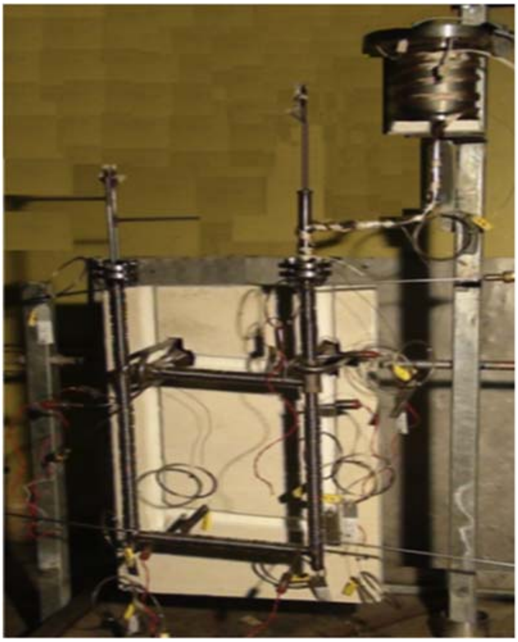

**Figure 26.8.13** MAFL—molten active fluoride salt loop.

### 26.8.2.5.4 *Materials for molten salts*

The development of structural materials with long-term compatibility with molten fluoride salts at high temperatures and under a high radiation environment is essential for long-term operation of molten salt reactors. From a thermodynamics point of view, nickel-based superalloys are the most suitable materials if moisture and other impurities, like sulfides, are not present in the salt. Thermodynamic considerations also dictate that the chromium content should be as low as possible. Hastelloy-N and its variants have been proposed worldwide. This material is covered under ASME-Boiler & Pressure Vessel Code; Section VIII Division-1, for use up to 750°C. Significant data generation efforts have been envisaged to generate the relevant data needed for design as per ASME-BPVC Section III Division-1 Subsection-NH for use in nuclear reactors at high temperatures. These include long-term creep testing, creep testing under multiaxial loadings, creep fatigue tests, statistical quantification of property variation, among others. Alternate alloys are also being investigated. Expertise developed in India for ODS alloys (for fast reactor fuel cladding) and Alloy 617M (for supercritical boilers) is expected to play a significant role in the development of super alloys for use in IMSBR. Alloys compatible with supercritical $CO_2$ as well as molten salts are also being developed.

### 26.8.2.5.5 *Reprocessing*

The foremost objective of the reprocessing system for Indian MBSR is removal of protactinium ${}^{91}Pa^{233}$ and its subsequent decay to ${}^{92}U^{233}$ (beta decay: 27 days half-life) and reintroduction of ${}^{92}U^{233}$ in fluoride form into reprocessed molten fuel salt. The second objective is conventional removal of fission products and other nuclear wastes. This would help in reducing the radio toxicity of waste and simultaneously open the scope for separating and using some of the isotopes like Cs and Sr for societal applications.

At the current stage, various technological options for reprocessing have been evaluated and feasibility has been established. The rate of reprocessing would be finalized, based on detailed reactor physics analysis. Since the current version of the IMSBR designs being pursued in India is fast reactors, it is possible to adopt a strategy for offline and batch mode reprocessing at intervals determined by reactor physics design. Offline reprocessing is considered to be the more robust and safe approach, as it decouples the reactor operation, and thus provides operational flexibility to the reprocessing facility. The major steps and alternative methods in reprocessing are being studied, so as to arrive at the flow-sheet for the process. Some of the methods being studied include Xe and Kr gas extraction by helium bubbling, fluoride volatilization processes, reductive metal extraction, and electrochemical processes.

Mass transfer-related studies and modeling for online helium bubbling are being pursued. Trapping and fixing of fission product gases in a permanent matrix is challenging as it needs He in a closed loop, online stripping, fixing in permanent matrix, its online management, active compressor, etc. For offline reprocessing of the salt, the uranium and the elements with high gaseous oxidation states such as Np, Pu for actinides and Nb, Ru, Te, I, Mo, Cr, and Tc for the fission products in the salt are proposed to be removed by fluorination. Various technological options to separate and recover the different elements are also being studied.

After the uranium and other high gaseous oxidation state elements are removed, the fuel salt is proposed to be purified by reductive metal extraction processes. Various technological options for this stage are also being studied. The actinides (Pu, Pa, Am, Cm) could be extracted by reductive extraction in a liquid metal solvent constituted of Bi with metallic thorium. The lanthanides can also be separated by a reductive extraction in a liquid Bi pool containing metallic thorium as the reductive reagent. In this case, the concentration of metallic thorium is kept higher than the concentration used for the actinide extraction, in order to sufficiently lower the potential to values which correspond to the reduction of the lanthanides dissolved in the molten salt. The back extraction of lanthanides from the Bi-Th bath is done by anodic oxidation in LiCl-KCl chloride medium at 500°C. A molten salt based liquid−liquid contactor operating in a hostile environment both with respect to temperature and material is a major challenge, and India is working on developing an effective and reliable contactor. It is felt that the electrochemical method has good potential to simplify the overall reprocessing scheme.

### *26.8.2.5.6 Equipment and sensors for molten salts*

Operation of IMSBR will require continuous monitoring of the molten salt environment, property evaluation, and other mechanical equipments. In addition to the high radiation environment, the molten salt provides a very aggressive media for the sensors. Some of the areas in which R&D has been initiated are:

1. Online measurement of oxide and sulfide content in molten salts, so as to prevent local criticality issues due to precipitation of oxyfluorides of uranium and thorium as well as nickel superalloy corrosion issues.
2. Online measurement of redox potential and development of dynamic reference electrodes for use in molten salt environments with thermal cycling resistance.
3. Instrumentation and sensors for high-temperature, molten halide salts, and high radiation:
   - **a.** Level sensors (e.g., ultrasonic, laser-based, conductivity-based, etc.)
   - **b.** Flow sensors (e.g., EM flowmeter, ultrasonic-based, etc.)
   - **c.** Pressure sensor (e.g., capacitance-based, Fabre-Perot-type, etc.)
   - **d.** Temperature sensors
4. Characterization techniques for thermophysical properties of molten salts:
   - **a.** Thermal conductivity (e.g., laser flash) (both solid and molten samples)
   - **b.** Viscosity: In-house development using novel techniques are being investigated
   - **c.** Vapor pressure and vapor phase composition, especially ensuring a vapor phase composition as close as possible to the liquid phase ensuring that the vapor condenses to a liquid state
   - **d.** Density and specific heat.
5. Equipment:
   - **a.** Molten salt pump
   - **b.** Printed circuit heat exchangers

- **c.** In-service inspection equipments
- **d.** Freeze valves
- **e.** Flanges for molten salt use.

#### *26.8.2.5.7 Future work*

For IMSBR, development of most of the technologies has either been initiated or is being initiated. In parallel, conceptual design of a 5 MWth is being worked out. In order to carry out technology development for various technologies related to salts, materials, components, power conversion systems, a molten salt breeder reactor development facility (MSBRDF) has been planned at the new BARC campus in the southern Indian city of Visakhapatnam. This is briefly explained in the next section.

#### *26.8.2.5.8 Molten salt breeder reactor development facility*

In order to carry out detailed R&D, facilities are under various stages of development. These facilities will be set-up at the new BARC campus, in the southern Indian city of Visakhapatnam. The following is a list of facilities proposed to be set-up there:

1. Fuel salt corrosion test loop cluster;
2. In salt mechanical testing facility—active salt;
3. Fuel salt pump and heat exchanger development and testing facilities (for loop-type and pool-type designs);
4. Active salt preparation and purification facility;
5. Active salt chemical analysis laboratory;
6. Active salt thermophysical properties evaluation laboratory;
7. Intermediate salt corrosion test loop cluster;
8. Freeze valve development and test facility;
9. Intermediate salt pump and heat exchanger development and test facilities (for loop-type and pool-type designs);
10. In salt mechanical testing facility—inactive salt;
11. Creep testing facility;
12. Inactive salt preparation and purification facility;
13. Argon purification facility;
14. Supercritical $CO_2$ Brayton cycle development test bed;
15. Machinery cooling water system;
16. Decontamination facility.

## 26.8.3 Introduction to IHTR and its relevance

For India, a high-temperature reactor development program is significant mainly for nonelectric applications. This requirement originated because of a need to develop an alternate energy carrier to substitute for fossil fuel for transport applications. Hydrogen is considered an alternate energy carrier. High-efficiency hydrogen production from water needs process heat at high temperatures or electricity, or both, depending upon the process of hydrogen production selected. High-temperature nuclear reactors have a large potential for sustainably supplying energy for these hydrogen production processes at the required high-temperature conditions. Although the development of relatively lower-temperature hydrogen production processes (e.g., copper-chlorine process) as well as high-temperature processes (e.g., sulfur-iodine process and high-temperature steam electrolysis) are being carried out in India, the decision for a more challenging goal of development of technologies for reactor systems capable of producing process heat at 1273K was taken. Therefore, under this program (Sinha et al., 2016) India is developing a small power compact high-temperature reactor (CHTR), which is a lead-bismuth eutectic (LBE)-cooled reactor, and a 600 MWth IHTR, both capable of producing process heat at 1273K. For the demonstration of IHTR technologies, a small power (20 MWth) version would be initially set-up before deployment of large power reactors. Design and R&D activities for IHTR are described in the following sections.

### 26.8.3.1 General description

BARC is carrying out the design of a 600 MWth reactor (Dulera and Sinha, 2008; Vijayan et al., 2013) for commercial hydrogen production. This is a pebble bed-based molten salt-cooled reactor. Pebbles consist of TRISO-coated particle fuel and the coolant is driven through natural circulation. The IHTR reactor core is a long right circular cylinder with annular core which consists of fuel pebbles and a molten salt coolant. Fig. 26.8.14 shows a schematic of a 600 MWth Innovative HTR. There

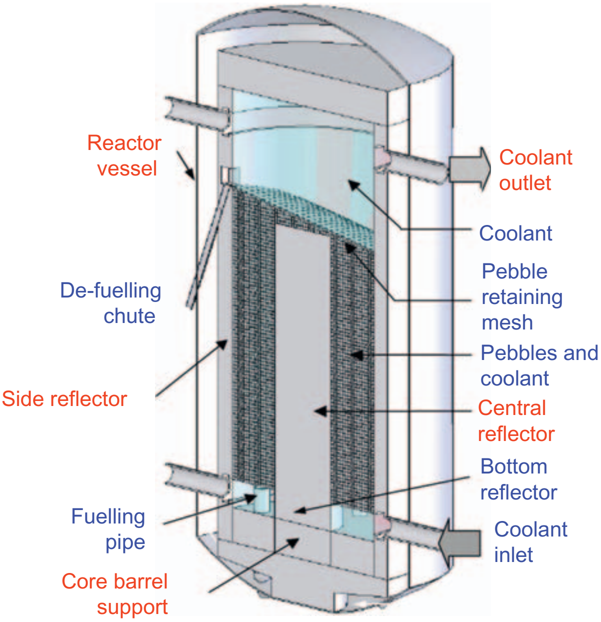

**Figure 26.8.14** Schematic of IHTR (Dulera et al., 2017).

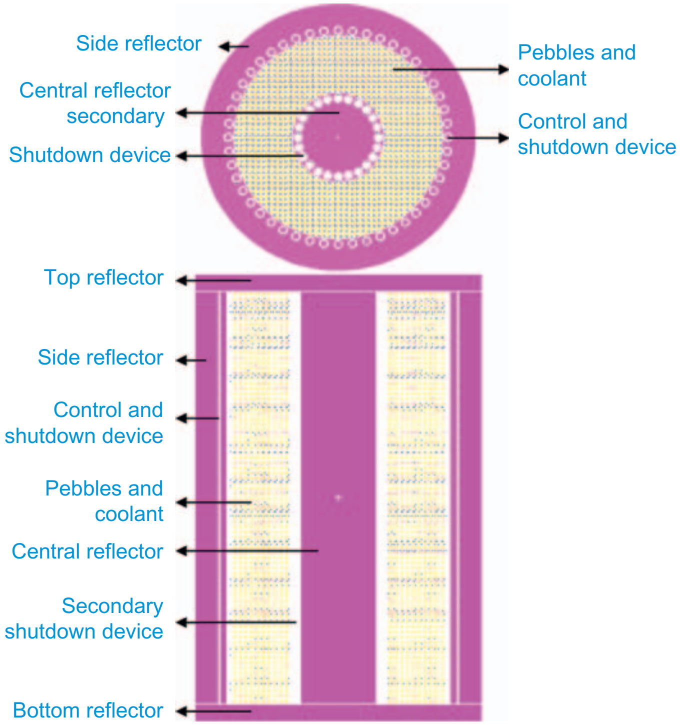

**Figure 26.8.15** Cross-sectional layout for IHTR (Dulera et al., 2017).

are graphite neutron reflectors in the center and on the top, bottom, and outside of this fuel annulus as shown in Fig. 26.8.15. Table 26.8.5 describes key characteristics of IHTR-600 MWth (Dulera et al., 2009). Vertical bores in the central and outer reflectors are provided for the reactivity control elements.

### 26.8.3.2 Reactor physics design and analysis

The IHTR-600 MWth has an elongated cylindrical core with an inner reflector of 2 m diameter followed by a 1.5 m wide reactor core and then another outer reflector of 0.5 m. The core height is 8 m with 60% of the annular core volume filled with pebbles and the remaining space occupied by the coolant. Reactor physics analysis has been carried out with molten salt FLiBe. The IHTR annular core consists of about 150,000 pebbles. The fuel pebbles consist of a fuel zone of 4.5 cm radius with a protective layer of 0.5 cm. Each pebble consists of 46.7 g total heavy element ($^{233}$U + $^{232}$Th) with 7.6% enrichment. Reactivity control and shutdown devices are located in the inner and outer reflectors. A smaller pebble-bed demonstration reactor called IHTR-20 MWth is also in the design stage (Singh et al., 2015b). This has a cylindrical region of 86.5 cm radius and 190 cm core height, accommodating about 24,000 fuel pebbles and FLiBe as coolant. Each of these 6 cm diameter fuel pebbles consists of about 51,440 TRISO fuel particles, thus

**Table 26.8.5** **IHTR parameters and objectives**

| Attributes | Properties |
|---|---|
| IHTR thermal power | 600 MWth |
| Objectives (optimized to hydrogen production) | Hydrogen: 80,000 $Nm^3/h$<br>Electricity: 18 MWe<br>Drinking water: 375 $m^3/h$ |
| Coolant outlet/inlet temperature | 1000°C/600°C |
| Side reflector thickness | 50 cm |
| Bottom and top reflector thickness | 30 cm |
| Outer diameter of central reflector | 200 cm |
| Outer diameter of core | 600 cm |
| Annular Core thickness | 150 cm |
| Active height of core | 800 cm |
| Equilibrium fuel enrichment | 7.6% $(^{232}Th + ^{233}U)O_2$ |
| Number of spheres in annular core | 151,200 |
| Average pebble packing fraction | 0.60 |

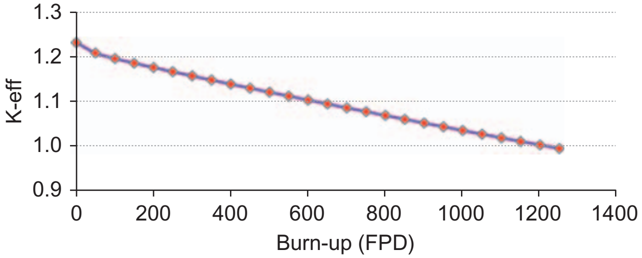

**Figure 26.8.16** Variation of $k_{eff}$ with burn-up of equilibrium fuel pebbles.

containing 27.8 g total heavy metal ($^{233}U + ^{232}Th$) with 6.5% enrichment. Fig. 26.8.16 presents variation of effective multiplication factor when core is loaded with equilibrium fuel pebbles. The maximum attainable burn-up corresponding to 1200 FPD (Singh et al., 2015a) is found to be about 86,000 MWd/t.

Studies have been carried out to design fuel pebbles for this low-power IHTR with maximum conversion of $^{232}Th$ to $^{233}U$ under the constraint of maintaining all the reactivity coefficients as negative. Variation of conversion ratio and reactivity coefficients with fuel depletion has also been studied.

### 26.8.3.3 Thermal hydraulic and material compatibility studies

A molten salt natural circulation loop (Srivastava et al., 2015), as shown in Fig. 26.8.17, has been set up to carry out thermal hydraulic studies of molten salts. Fig. 26.8.18 shows a comparison of analytical and experimental studies. In addition, an experimental facility to study corrosion behavior (Keny et al., 2015) of FLiNaK salt on the structural materials has also been set-up. Experiments on various materials have been initiated. This is shown in Fig. 26.8.19.

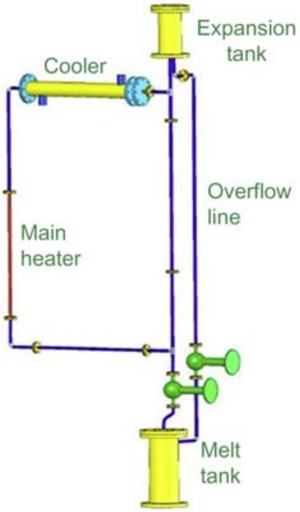

**Figure 26.8.17** Schematic of natural circulation loop for molten salt coolants (Dulera et al., 2017).

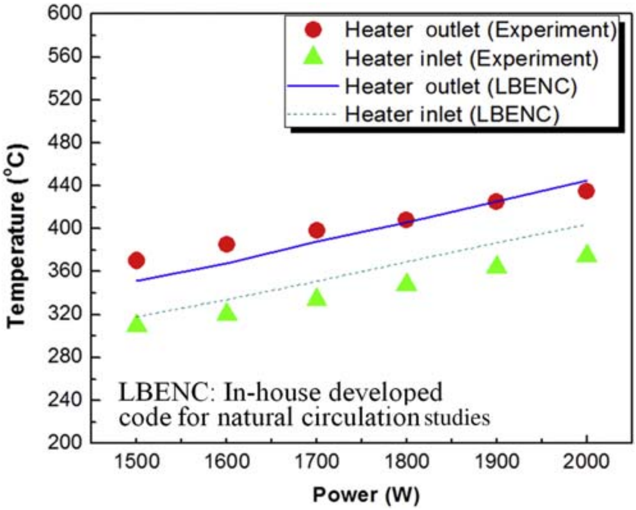

**Figure 26.8.18** Comparison of analytical and experimental results for steady-state heater inlet/outlet temperature at different powers (Dulera et al., 2017).

### 26.8.3.4 Key safety issues for the design

In addition to concerns common to electricity-producing nuclear reactors, hydrogen-producing nuclear reactors have additional challenges and safety-related issues, which would be addressed through analytical and experimental studies:

**Figure 26.8.19** Experimental facility for corrosion studies for molten salt coolants (Dulera et al., 2017).

1. Tritium production and permeation of hydrogen and tritium through walls of heat exchangers.
2. Contamination of the hydrogen production system by radionuclides in primary coolant.
3. Diffusion of hydrogen from the secondary to primary side.
4. Embrittlement issues of material with hydrogen.
5. Safety against potential explosion of hydrogen.

Design options with intermediate heat-exchangers, getters for hydrogen and tritium, providing coatings on tubes, and providing safe distance between nuclear and hydrogen plant are being considered.

### 26.8.3.5 Future work

Future activities involve the development of pebble-based fuel, pebble feeding and removal mechanism, thermal hydraulic studies for molten salts in pebble bed geometry, development of large graphite components, high-efficiency power conversion system, development of an intermediate heat exchanger, pump, instrumentation, and other components for the molten salt environment, and development of hydrogen production technologies.

### 26.8.3.6 Fuel development

A typical IHTR fuel consists of fuel pebbles made of TRISO-coated particle fuels with $^{233}$U-Th-based fuel. A schematic of a single pebble is shown in Fig. 26.8.20. Technology for fuel kernel manufacture has been long established in BARC by the

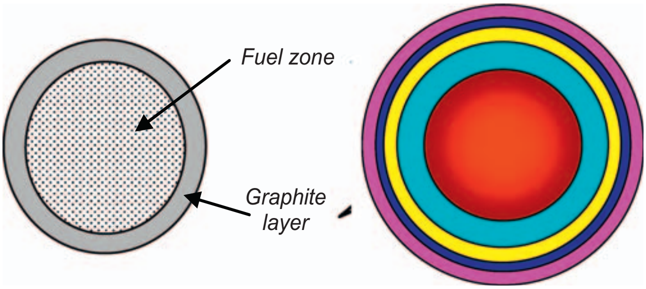

| | |
|---|---|
| 🟧 | ($^{233}$U+Th)$O_2$kernel (500 μm) diameter |
| 🟦 | Pyrolitic graphite (90 μm) thick |
| 🟨 | Inner dense carbon (30 μm) thick |
| 🟦 | Silicon carbide (30 μm) thick |
| 🟪 | Outer dense carbon (50 μm) thick |

**Figure 26.8.20** Schematic of a fuel pebble and single TRISO particle for IHTR.

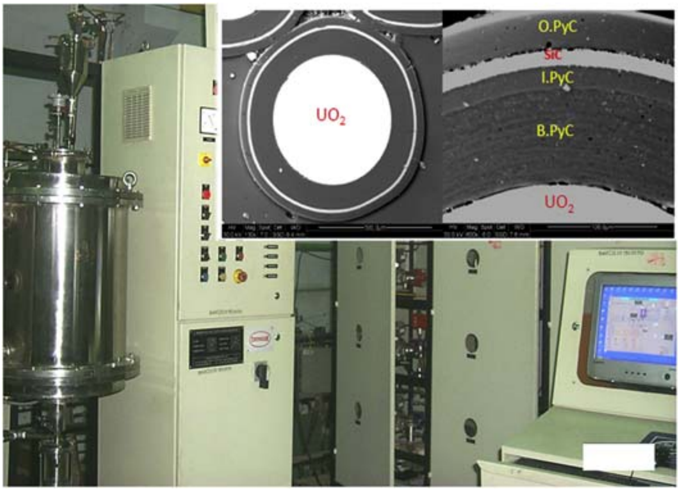

**Figure 26.8.21** Facility for coating TRISO-coated particle fuel.

sol-gel technique (Dulera and Vaze, 2009). The facility for coating TRISO-coated particle fuel and radiography of a typical particle is shown in Fig. 26.8.21. After developing the coating technology, coatings were successfully carried out on natural $UO_2$ (Sathiyamoorthy et al., 2009; Aggarwal et al., 2013; Mollick et al., 2014). Some of the coated particles are being irradiated in the fast breeder test reactor (FBTR) in IGCAR, Kalpakkam, India.

### 26.8.3.7 Materials development

CHTR core internal materials comprise nuclear-grade high-purity materials. These are high-density isotropic graphite (Dhami et al., 2006; Sinha and Dulera, 2010); for reflector blocks. Other metallic structural materials are based on Ni-based super alloys compatible to molten salt coolant and high temperatures. Graphite components are coated with oxidation-resistant coatings (Chakravarthy et al., 2013; Sure et al., 2015). These technologies have been successfully developed within BARC and sister organizations, such as Nuclear Fuel Complex (NFC) and Indira Gandhi Centre for Atomic Research (IGCAR).

### 26.8.3.8 Inherent safety features and passive heat removal systems

IHTR is being designed to have many features that make it inherently safe. Some of these features are: strong negative Doppler coefficient of the fuel, high thermal inertia of the all-ceramic core and low core power density, very large thermal margin between operating temperature and boiling point of molten salt, chemical inertness and negative reactivity effects of molten salt coolant, low-pressure natural circulation of coolant, etc. In addition, passive systems for reactor heat removal under normal and postulated accident conditions have been incorporated. This includes natural circulation of molten salt for reactor heat removal, passive shutdown systems, passive dissipation of decay heat, etc.

### 26.8.3.9 Key challenges for the design

The major challenges for the design, which are being met through sustained R&D efforts within India, include coatings on TRISO-coated particle fuel and their characterization, production of nuclear-grade high-density isotropic carbon-based materials and component manufacture, development of molten salt resistant structural material for high-temperature applications, oxidation-resistant coatings and their characterization, development of components and instrumentation for service in intimate contact with molten salt coolant at high temperatures, molten salt coolant technologies, etc.

## 26.8.4 R&D on high-efficiency power conversion system

High-efficiency supercritical $CO_2$ Brayton cycle (SCBC)-based power conversion systems are proposed to be used in many of the advanced reactors, including the Indian High Temperature Reactor (IHTR), and IMSBR (Kaushik et al., 2015). BARC has formulated a three-stage roadmap for the development of SCBC. The first stage is the development of a kW range SCBC for use in solar power plants as well as the CHTR. In the second stage it will be scaled up to MW range for application in solar plants as well as the 5 MWth molten salt demonstration reactor, under development, and the 20 MWth Demonstration IHTR. The third stage will be a scale up to large-power IMSBR. The optimized process parameters for Brayton cycle operating with 20 MWth IHTR and IMSBR are shown in Figs. 26.8.22 and 26.8.23, respectively. The cycle layout was modeled and analyzed to optimize the process parameters and efficiency. The scoping studies were carried out as per the parametric conditions, like compressor inlet pressure, pressure ratio, and turbine inlet temperature. The properties of S-$CO_2$ were taken by using different equation of state models, namely Lee—Kesler—Plocker (LKP) and Peng—Robinson models. As per the literature, the National Institute of Standards and Technology (NIST)

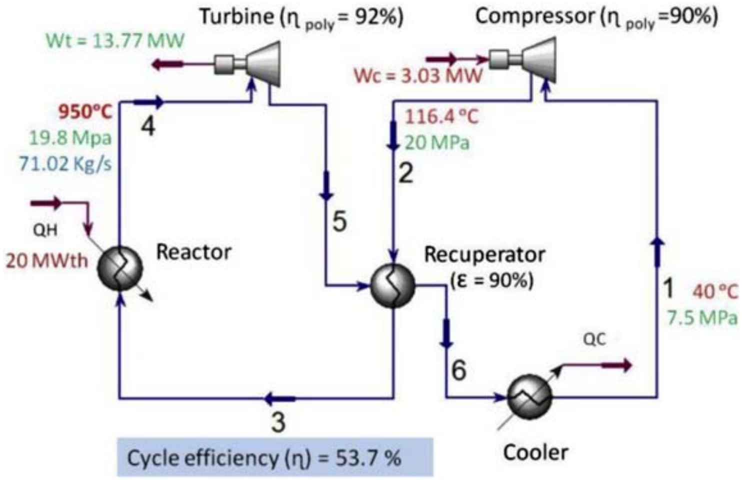

**Figure 26.8.22** Optimized process parameters for SCBC for 20 MWth IHTR at 1223K.

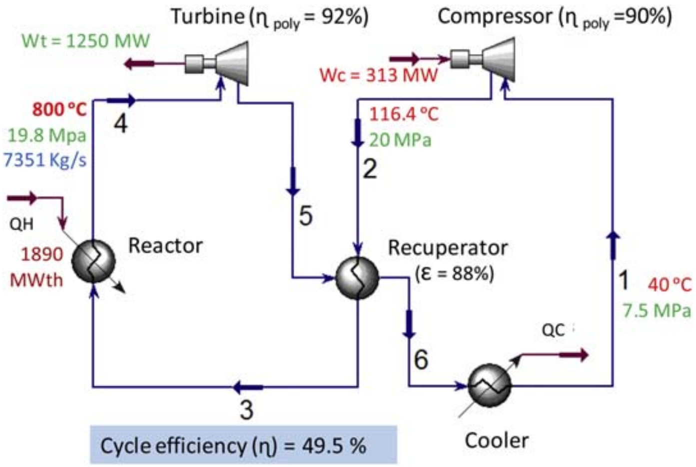

**Figure 26.8.23** Optimized process parameters for SCBC for IMSBR at 1073K.

property database is very accurate. The NIST database was compared with the LKP model and the properties were found to be coherent. Thus, for the current analysis, the NIST database was used for the S-$CO_2$ properties.

In parallel, technology development for critical components such as turbine, compressor, compact heat exchanger, etc. have been initiated. This includes the manufacture of miniature turbo-generator components and modules of a printed circuit heat exchanger (PCHE) being manufactured by Laser Additive Manufacturing (LAM). BARC has a great deal of experience in thermal hydraulics studies with supercritical $CO_2$ and supercritical water systems. A supercritical $CO_2$ loop was operated for generating heat transfer and stability data. The data were used for validation of the Nonlinear Stability Analysis Code (NOLSTA), which is an in-house developed code to predict the flow stability of supercritical fluids.

## 26.8.5 R&D on a high-efficiency hydrogen production system

BARC is developing thermochemical processes (Prasad and Dulera, 2009; Shriniwas Rao et al., 2015) as well as high-temperature steam electrolysis for hydrogen production by splitting water. The thermochemical processes use a sequence of thermally driven chemical reactions in which water and heat are the inputs, hydrogen and oxygen are the outputs, and the chemicals and reagents are recycled in a closed cycle. Two promising thermochemical processes representing high- and relatively lower-temperature regimes are the sulfur-iodine (S—I) and copper-chlorine (Cu—Cl) processes. Presently R&D in BARC is focused on the more challenging S—I process. Other options will also be considered before a large-scale deployment is planned so as to have an optimum mix of the technologies. The S—I process is a three-step process involving formation (Bunsen reaction) and decomposition of sulfuric acid ($H_2SO_4$) and hydriodic acid (HI). The decomposition reactions, being endothermic, need external heat. Inputs to the process are only water and heat and outputs are hydrogen and by-product oxygen. The process is operated in a closed loop, and other chemicals used such as sulfur and iodine are recycled back to the process. Apart from the feasibility of the process, efficiency, stability of close loop operation, safety, suitable materials, catalysts, and integration aspects with a HTR are the key challenges. BARC has carried out R&D on the basic reactions, development of catalysts for $H_2SO_4$, and HI decomposition. It has demonstrated a closed loop S—I process using glass/quartz as material for equipment and produced hydrogen at 30 L/h. India is the fifth country to achieve this feat. A metallic system for high-pressure operation is being set up for individual sections. In parallel, technologies for HTSE and other thermochemical process are also being developed.

### 26.8.6 Summary

Efficient utilization of thorium is the cornerstone of the Indian nuclear program. India has developed technologies for all the aspects of the thorium fuel cycle. An advanced heavy water reactor is being developed as a technology demonstrator for an industrial-scale thorium fuel cycle. India is also developing concepts of molten salt cooled high-temperature reactors dedicated for high-efficiency nuclear hydrogen production. Large-scale deployment of MSBRs is envisaged during the third stage of the Indian nuclear power program. Research and development have been initiated to achieve designs with enhanced levels of safety. In the long term, molten salt reactors offer sustainability to Indian energy needs.

## Acknowledgments

The authors gratefully acknowledge input provided by many scientists and engineers at Bhabha Atomic Research Centre. The list includes Dr. (Mrs.) S.B. Roy, Dr. K.T. Shenoy, Dr. P.D. Krishnani, Dr. (Mrs.) K. Umasankari, Mr. B.V. Shah, Dr. Anurag Gupta, Mr. S.K. Satpati, Mr. S. Chowdhury, Mr. A. Shriniwas Rao, Mr. A. Basak, Mr. A. Borgohain, Mr. I. Singh, Mr. A. Kaushik, and Mr. K.K. Panda.

## References

Aggarwal, S., Kumar, N., Suryanarayana, S., Bamankar, Y.R., Vittal Rao, T.V., Radhakrishna, J., et al., 2013. Preparation of UO2 microspheres for SGMP by internal gelation technique on 1 kg/day scale. In: XVIIth International Solgel Conference, Madrid, Spain, August 25−30, 2013.

Basak, A., Dulera, I.V., Vijayan, P.K., 2015. Conceptual design of loop-in-tank type Indian Molten Salt Breeder Reactor concept. In: International Thorium Energy Conference (ThEC15), Mumbai, India, October 12−15, 2015.

Borgohain, A., Srivstava, A.K., Gupta, A., Maheshwari, N.K., Krishnani, P.D., Vijayan, P.K., 2015. Conceptual design of a pool type molten salt breeder reactor. In: International Thorium Energy Conference (ThEC15), October 12−15, 2015.

Chakravarthy, Y., Bhandari, S., Vandana, Padmanabhan, P.V.A., Das, A.K., 2013. Plasma spray coating of yttrium oxide on graphite substrates for compatibility studies in molten metals. In: Proceedings of the Twenty Eighth National Symposium on Plasma Science and Technology: Fusion Science and Technology—Abstract Book, PLASMA, pp. 136−137.

Dhami, T.L., Mathur, R.B., Dakate, S.R., Aggarwal, R.K., Haldar, S.K., Sangal, A., et al., 2006. Development of special carbon materials for novel nuclear reactors. In: Bahl, O.P., Tripathi, V.S., Goyal, P. (Eds.), Indo Carbon 2006 Conference Proceedings. Shipra Publication, Delhi, India, pp. 242−254.

Dulera, I.V., Sinha, R.K., 2008. High temperature reactors. J. Nucl. Mater. 383, 183−188.

Dulera, I.V., Vaze, V.V., 2009. Fuel for high temperature reactors. IANCAS Bull. Adv. Nucl. Fuels. VIII (2), 2009, pp. 168−179.

Dulera, I.V., Vijayan, P.K., Sinha, R.K., 2013. Indian programme on molten salt cooled nuclear reactor. In: Conference on Molten Salts in Nuclear Technology, Bhabha Atomic Research Centre, Mumbai, January 9−11, 2013.

Dulera, I.V., Sinha, R.K., Saha, D., 2009. High temperature reactors. In: Proceedings of International Conference on Peaceful Uses of Nuclear Energy, New Delhi, 29 September to 01 October, 2009.

Dulera I.V., Sinha R.K., Rama Rao A. and Patel R.J., 2017. Under Publication. High temperature reactor technology development in India. Prog. Nucl. Energy.

<http://dae.nic.in/writereaddata/publ/saga/vol2/pdf2/Chapter-01.pdf>.

Kaushik, A., Dulera, I.V., Vijayan, P.K., 2015. Super-critical carbon dioxide based Brayton cycle for Indian high temperature reactors. In: International Thorium Energy Conference (ThEC15), October 12−15, 2015.

Keny, S.J., Gupta, V.K., Kumbhar, A.G., Rangarajan, S., Daitkar, M.R., Maheshwari, N.K., et al., 2015. Corrosion aspects of compatible alloys in molten salt (FLINAK) medium for Indian MSR program in the temperature range of 550−750°C using electrochemical techniques. In: Thorium Energy Conference 2015 (ThEC15), Mumbai, India, October, 2015.

Mishra, R., Phapale, S., Shirsat, A N., Kolay, S., Basu, M., 2015. Determination of eutectic composition and heat capacities of fuel salt (LiF-$ThF_4$-$UF_4$) and blanket salt (LiF-$ThF_4$) mixtures. In: International Thorium Energy Conference (ThEC15), October 12−15, 2015.

Mollick, P.K., Sathiyamoorthy, D., Rao, P.T., Venugopalan, R., Chakravartty, J.K., 2014. Process modeling and simulation to develop UO2-TRISO coated particle for Indian high temperature reactors. BARC Newsletter, Special Issue.

Mukherjee, A., Awasthi, A., 2015. Fluorination of thorium oxide by ammonium bifluoride. In: International Thorium Energy Conference (ThEC15), October 12−15, 2015.

Prasad, C.S.R., Dulera, I.V., 2009. Nuclear hydrogen production. In: Proceedings of International Conference on Peaceful Uses of Nuclear Energy, New Delhi, 29 September to 01 October, 2009.

Sarkar, T., Bhargavaa, P., Borgohain, A., Srivastava, A.K., Yadav, R.K.B., 2015. Radiation dose rate mapping of molten active fluoride salt loop at UED, BARC. In: Paper presented at Thorium Energy Conference (ThEC15), Mumbai, India.

Sathiyamoorthy, D., Rao, V.G., Rao, P.T., Mollick, P.K., 2009. Operational aspects of spouted bed for the quality control of TRISO coated particles. In: International Conference on Characterization and Quality Control of Nuclear Fuels (CQCNF).

Satpati, S.K., et al., 2006. Mathematical modeling of hydro fluorination of uranium dioxide in a rotary kiln. In: 18th International and 7th ISHMT-ASME Heat and Mass Transfer Conference, IIT Guwahati, January 4−6, 2006, pp. 2183−2190.

Shriniwas Rao, A., Sujeesh, S., Nafees Ahmed, V., Fani, H.Z., Tewari, P.K., Gantayet, L.M., 2015. Study of effect of high pressures and elevated temperatures on Bunsen reaction of Iodine-Sulfur thermo-chemical process. Int. J. Hydrogen Energy. 40, 5025−5033.

Singh, I., Gupta, A., Krishnani, P.D., 2015a. A dynamic analysis of circulating fuel reactor with zero dimensional modeling. In: Thorium Energy Conference 2015 (ThEC15), Mumbai, India, October, 2015.

Singh, I., Gupta, A., Krishnani, P.D., 2015b. Study on design of thorium based fuel pebble for IHTR-20 MWth. In: Thorium Energy Conference 2015 (ThEC15), Mumbai, India, October, 2015.

Sinha, R.K., Dulera, I.V., 2010. Carbon based materials: applications in high temperature nuclear reactors. In: First Asian Carbon Conference (FACC 2009), Indian Habitat

Center, New Delhi, India, November 25–27, 2009. Published by Indian Journal of Engineering and Material Sciences, Vol. 17, pp. 321–326, October, 2010.

Sinha, R.K., Chellapandi, P., Srinivasan, G., Dulera, I., Vijayan, P.K., Chande, S.K., 2016. Generation IV concepts: India. Handbook of Generation IV Nuclear Reactors. Woodhead Publishing, Duxford, UK.

Sood, D., Iyer, P., Prasad, R., Vaidya, V., Roy, K.N., Venugopal, V., et al., 1972. Chemical development work in molten salt breeder reactor concept. In: Tech. Rep. BARC-690, BARC.

Srivastava, A.K., Borgohain, A., Maheshwari, N.K., Vijayan, P.K., 2015a. Experimental studies on natural circulation in molten salt loops. In: International Thorium Energy Conference (ThEC15), Mumbai, India, October 12–15, 2015.

Srivastava, A.K., Gupta, A., Krishnani, P.D., 2015b. A simplified burnup calculation strategy with refueling in static molten salt reactor. In: International Thorium Energy Conference (ThEC15), Mumbai, India, October 12–15, 2015.

Sure, J., Thyagarajan, K., Mallika, C., Kamachi Mudali, U., 2015. Thermal-cycling behavior of plasma-sprayed partially stabilized zirconia coatings on high-density graphite substrate. J. Therm. Spray Technol. 24 (6), 925–937.

Vijayan, P.K., Kamble, M.T., Dulera, I.V., 2013. Nuclear reactors for the future. J. Sci. Cult. 79 (1–2), 17–22.

Vijayan, P.K., Basak, A., Dulera, I.V., Vaze, K.K., Basu, S., Sinha, R.K., 2015. Conceptual design of Indian molten salt breeder reactor. Pramana. 85, 539–554.

## 26.9 Indonesia

*Abdul Waris*
Bandung Institute of Technology, Bandung, Indonesia

Research activities on MSR in Indonesia are conducted by universities and by the national agency for nuclear energy. The two main university MSR research groups are:

1. Nuclear Physics and Biophysics Research Division, Department of Physics, Faculty of Mathematics and Natural Sciences, Bandung Institute of Technology (ITB);
2. Nuclear Engineering Program, Department of Engineering Physics (UGM).

A group of faculty members at ITB has been interested in MSR since 2010, especially the FUJI designs: FUJI-12, miniFUJI, FUJI-U1, and FUJI-U3 (Waris et al., 2010, 2012a, 2013, 2015; Aji andWaris, 2014; Aji et al., 2015). At first they were mainly focused on high-level nuclear waste (especially plutonium and minor actinides) utilization in MSR. However, they are now studying the safety aspects of MSRs. The FUJI designs are based on the ORNL MSBR design with several improvements. The staff at UGM is mostly concentrated on the fuel cycle and safety aspects of passive, compact molten salt reactors (PCMSRs) (Harto, 2015).

The National Nuclear Energy Regulatory Agency of Indonesia (BAPETEN) is preparing the National Regulation on Technology and Safety Aspects of MSR.

Regarding the thorium fuel cycle in solid fuel nuclear reactors, the group from ITB started research in 2007 (Waris et al., 2014, 2016; Subkhi et al., 2012, 2013, 2014, 2015, 2016; Trianti et al., 2015; Ariani et al., 2012; Permana et al., 2009a, 2009b, 2010, 2011; Ismail et al., 2009; Sidik et al., 2008a, 2008b; Waris, 2008; Waris et al., 2007a, 2007b, 2008, 2009, 2010, 2012b). The National Nuclear Energy Agency (BATAN) operates a research center for uranium and thorium extraction from uranium−thorium-bearing minerals.

# References

Aji, I.K., Waris, A., 2014. Preliminary study on weapon grade uranium utilization in molten salt reactor miniFUJI. AIP Conf. Proc. 1615, 57−60.

Aji, I.K., Waris, A., Permana, S., 2015. Analysis of fluid fuel flow to the neutron kinetics on molten salt reactor FUJI-12. The 5th International Conference on Mathematics and Natural Sciences 2014 (ICMNS 2014), 1677, 120012. AIP Publishing, New York.

Ariani, M., Su'ud, Z., Waris, A., Khairurrijal, Monado, F., Fahmi, F., Sekimoto, H., 2012. The feasibility study of small long-life gas cooled fast reactor with mixed natural Uranium/Thorium as fuel cycle input. AIP Conf. Proc. 1448, 59−64.

Harto, A.W., 2015. Sustainable criticality analysis of PCMSR fuel using thorium as sustainable fuel and low enriched uranium as starting fuel. Int. J. Nucl. Energy Sci. Technol. 9 (3), 224−237.

Ismail, Liem, P.H., Sidik, P., Takaki, N., Sekimoto, H., 2009. Symbiotic systems consisting of large-FBR and small water-cooled thorium reactors (WTR). Ann. Nucl. Energy. 33, 1076−1085.

Permana, S., Waris, A., Sekimoto, H., 2009a. Comparative analysis on breeding and void reactivity of light and heavy water-cooled reactor for different fuels. In: Proceedings of the 9th International Conference GLOBAL, Paris, September 6−11, 2009.

Permana, S., Takaki, N., Sekimoto, H., 2009b. Plutonium proliferation analysis on MA doped of actinides closed water-cooled thorium reactor. In: Proceedings of the 9th International Conference GLOBAL, Paris, September 6−11, 2009.

Permana, S., Sekimoto, H., Waris, A., Subhki, M.N., Ismail, 2010. Fuel breeding and core behavior analyses on in core fuel management of water cooled thorium reactors. The 4th Asian Physics Symposium (APS), Bandung-Indonesia 2010. AIP Conf. Proc. 1325, 229−232.

Permana, S., Takaki, N., Sekimoto, H., 2011. Breeding and void reactivity analysis on heavy metal closed-cycle water cooled thorium reactor. Ann. Nucl. Energy. 38, 337−347.

Sidik, P., Takaki, N., Sekimoto, H., 2008a. Power density effect on feasibility of water cooled thorium breeder reactor. Prog. Nucl. Energy. 50, 308−313.

Sidik, P., Takaki, N., Sekimoto, H., 2008b. Breeding capability and void reactivity performance of heavy water cooled thorium reactor. J. Nucl. Sci. Technol. 45 (7), 589−600.

Subkhi, M.N., Su'ud, Z., Waris, A., 2012. Design study of long-life PWR using thorium cycle. AIP Conf. Proc. 1448, 101−106.

Subkhi, M.N., Su'ud, Z., Waris, A., 2013. Neutronic design of small long-life PWR using thorium cycle. Adv. Mater. Res. 772, 524−529.

Subkhi, M.N., Su'ud, Z., Waris, A., Permana, S., 2014. Conceptual design study of small long-life PWR based on thorium cycle fuel. The 4th International Conference on Advances in Nuclear Science and Engineering 2013 (ICANSE 2013). AIP Conf. Proc. 1615, 61−64.

Subkhi, M.N., Suud, Z., Waris, A., Permana, S., 2015. Optimization of small long-life PWR based on thorium fuel. The 5th International Conference on Mathematics and Natural Sciences 2014 (ICMNS 2014), 1677, 120001. AIP Publishing, New York.

Subkhi, M.N., Su'ud, Z., Waris, A., Permana, S., 2016. Design concept of small long-life PWR using square and hexagonal thorium fuel. ARPN J. Eng. Appl. Sci. 11 (2), 830−832.

Trianti, N., Zaki, S., Arif, I., Permana, S., Riyana, E.S., 2015. Power flattening on design study of small long-life boiling water reactor (BWR) with tight lattice thorium nitride fuel. Appl. Mech. Mater. 751, 257−262.

Waris, A., 2008. Preliminary study on characteristics of equilibrium thorium fuel cycle of BWR. Indones. J. Phys. 19 (2), 47−49.

Waris, A., Kurniadi, R., Novitrian, Su'ud, Z., 2007a. High level waste confining in BWR with thorium fuel. In: Proceedings of the International Conference on Advances in Nuclear Science and Engineering 2007 (ICANSE 2007), Bandung, Indonesia, November 13−14, 2007.

Waris, A., Nawangsary, W., Pramuditya, S., 2007b. Scenario for thorium fuel cycle with free $^{233}$U in BWR. In: Proceedings of the International Conference on Advances in Nuclear Science and Engineering 2007 (ICANSE 2007), Bandung, Indonesia, November 13−14, 2007.

Waris, A., Kurniadi, R., Su'ud, Z., Mulyana, D., Perkasa, Y.S., 2008. Thorium fuel cycle scenario in PWR without U-233. In: Proceedings of the International Conference on Mathematics and Natural Sciences (ICMNS) 2008, Bandung, Indonesia, October 28−30, 2008.

Waris, A., Permana, S., Kurniadi, R., Su'ud, Z., Mulyana, D., 2009. TRU recycling in thorium fuel cycle of PWR with various moderator-to-fuel volume ratio. In: Proceeding of GLOBAL 2009, Paris, France, September 6−11, 2009.

Waris, A., Aji, I.K., Yulianti, Y., Shafii, M.A., Taufiq, I., Suud, Z., 2010. Comparative study on $^{233}$U and plutonium utilization in molten salt reactor. Indones. J. Phys. 21 (3), 77−81.

Waris, A., Permana, S., Kurniadi, R., Suud, Z., Sekimoto, H., 2010. Study on equilibrium characteristics of thorium-plutonium-minor actinides mixed oxide fuel in PWR. AIP Conf. Proc. 1244, 85−90.

Waris, A., Aji, I.K., Novitrian, Kurniadi, R., Su'ud, Z., 2012a. , Plutonium and minor actinides utilization in Thorium molten salt reactor. AIP Conf. Proc. 1448, 115−118.

Waris, A., Shafii, M.A., Pramuditya, S., Kurniadi, R., Novitrian, Su'ud, Z., 2012b. Effect of void-fraction on characteristics of several thorium fuel cycles in BWR. Energy Convers. Manage. 63, 11−16.

Waris, A., Richardina, V., Aji, I.K., Permana, S., Su'ud, Z., 2013. Preliminary study on plutonium and minor actinides utilization in thoriums-nes minifuji reactor. Energy Convers. Manage. 72, 27−32.

Waris, A., Pramudhitya, S., Perkasa, Y.S., Arif, I., 2014. Comparative studies on thorium fuel cycles of BWR with JENDL 3.2 and JEF 2.2 data libraries. Int. J. Nucl. Energy Sci. Technol. (IJNEST). 8 (1), 1−11.

Waris, A., Aji, I.K., Pramuditya, S., Permana, S., Su'ud, Z., 2015. Comparative studies on plutonium and minor actinides utilization in small molten salt reactors with various powers and core sizes. Energy Procedia. 71, 62−68.

Waris, A., Prastyo, P.A., Pramuditya, S., Irwanto, D., Sekimoto, H., 2016. Comparative studies on plutonium utilization in HTTR with helium and carbon dioxide gas coolants. Int. J. Hydrogen Energy. 41 (17), 6984−6989.

# 26.10 Italy

*Lelio Luzzi and Antonio Cammi*
Polytechnic University of Milan, Milan, Italy

## 26.10.1 R&D activities at Polito

The research group at Politecnico di Torino has been involved in all the EURATOM-supported Projects on MSRs (IABAT, MOST, ALISIA, EVOL) and in an IAEA Coordinated Research Project on transmutation (Maschek et al., 2008), which also considered such systems. The R&D activities were focused on basic reactor physics to handle the molten salt system specificities, with particular regard to the moving fuel feature (Lapenta and Ravetto, 2000). Delayed neutron precursors are also in motion, leading to a reduction of the importance of emitted neutrons. Moreover, some neutrons are emitted outside the core, thus they are unable to take part in the chain reaction. These phenomena lead to a reduction of the effectiveness of the delayed emissions. In this regard, criticality and time-dependent analyses were carried out by the Polito research group in a benchmark of dynamic simulation tools for molten salt reactors (Delpech et al., 2003), and taking into account also the interaction of thermal-hydraulics with neutronics (Dulla and Ravetto, 2007; Nicolino et al., 2008). Kinetic methods were extended to the specific circulating fuel configuration (e.g., adapting the DYNAMOSS code) (Dulla et al., 2008), some issues related to local perturbations introduced by fuel precipitates and gaseous bubbles were investigated (Dulla and Nicolino, 2008), and stochastic effects were considered as well (Dulla et al., 2014).

## 26.10.2 R&D activities at Polimi

The research group at Politecnico di Milano has been involved in the modeling and analysis of both thermal and fast-neutron spectrum MSR concepts, in the context of several collaborations with other research institutions (e.g., TU-Delft, PSI, CNRS-Grenoble, KIT, Westinghouse Electric Co., VTT Technical Research Centre of Finland). In both thermal and fast liquid-fueled MSRs, the molten salt simultaneously acts as fuel and coolant. This leads to a complex environment characterized by peculiar features, in comparison with solid-fueled reactors, i.e., the mentioned drift of delayed neutron precursors and the internal heat generation in a fluid. These aspects notably affect the system dynamic behavior and require dedicated tools (Luzzi et al., 2012a) to allow for the intrinsic coupling between neutronics and thermal fluid dynamics. Hereinafter, the main R&D activities carried out by the Polimi group are summarized.

In order to evaluate the effects of the fuel circulation on the system kinetics, simplified models (Cammi et al., 2011a) were preliminarily set up to allow for the decay of delayed neutron precursors in the out-of-core part of the primary circuit, and assessed against the experimental data available for the MSRE (Molten Salt Reactor Experiment). Later, analytic, deterministic, and Monte Carlo approaches (Aufiero et al., 2014a) were developed for calculating the effective delayed neutron fraction in the Molten Salt Fast Reactor (MSFR), which is the European fast reactor concept studied in the framework of both the EURATOM EVOL (http://cordis.europa.eu/project/rcn/97054_en.html; http://cordis.europa.eu/result/rcn/159411_en.html) and SAMOFAR (http://samofar.eu/) projects. As concerns the analysis of MSR dynamics, different numerical models were conceived for studying the core and system (primary/secondary circuits) behavior of thermal-neutron spectrum MSRs, based on lumped and one-dimensional approaches. In this framework, the approximations related to the adoption of simplified geometries were also investigated (Cammi et al., 2012). These models were adopted for stability analyses concerning both thermal and fast MSRs (Guerrieri et al., 2013), and for a preliminary control-oriented analysis focused on the MSFR (Guerrieri et al., 2014). As a further development in the direction of more accurate dynamic analyses, a multiphysics modeling (MPM) approach (Cammi et al., 2011b; Luzzi et al., 2012a) was developed to better reproduce the intrinsic coupling between neutronics and thermal-hydraulics. The adoption of this approach to the study of graphite-moderated MSRs allowed a preliminary assessment of the developed models on the basis of international benchmarks available for both the MSBR (Molten Salt Breeder Reactor) and the MSRE (e.g., in the framework of the MOST project), pointing out the main advantages offered by the multiphysics approach in comparison with the models available in literature for the MSRs. The MPM approach was also adopted for the MSFR transient analysis (Aufiero et al., 2014b; Fiorina et al., 2014b).

More recently, a geometric multiscale modeling strategy (Zanetti et al., 2015) for the analysis of MSR "plant dynamics" was developed at Polimi. It consists in the optimization of the MPM through the coupling between a multiphysics code (addressing the core modeling with a 3-D PDE-based approach) and a computational environment that adopts simplified 0-D ODE-based models for handling the boundary conditions and simulating the remaining part of the system (e.g., the cooling loop) with a different level of detail. The aim is to conjugate the accuracy of the MPM approach with acceptable computing power in order to analyze the overall plant dynamics.

With reference to the MSFR, the research group at Polimi also developed an extended version of the SERPENT-2 code to study fuel burn-up and core material evolution (Aufiero et al., 2013), and carried out an investigation into the fuel cycle and the long-term core physics performance (in terms of possible initial core loading, actinide burning capabilities, radio-toxicity generation, decay heat, and safety features), that also included a systematic comparison with solid-fueled fast reactors (Fiorina et al., 2013). This R&D activity was also the subject of the

IAEA CRP “Near Term and Promising Long Term Options for Deployment of Thorium Based Nuclear Energy,” (https://www.iaea.org/OurWork/ST/NE/NEFW/Technical-Areas/NFC/advanced-fuel-cycles-crp-thorium-2011.html), to which Polimi participated.

The thermal-hydraulic behavior of internally heated molten salts flowing in straight circular channels was analyzed using both analytic and numerical tools (Luzzi et al., 2012a, 2012b), with application to graphite-moderated MSRs and to the MSFR as well (see also Chapter 6: Thermal hydraulics of liquid-fueled MSRs). In this framework, a preliminary heat transfer correlation was proposed (Fiorina et al., 2014a). In particular, it has been shown that the effect of internal heat generation can be described by means of a corrective factor to be applied to traditional correlations (e.g., the Dittus−Boelter or Gnielinski correlations) for the Nusselt number. The corrective factor has been demonstrated to be lower than 1 in the case of inward wall heat flux, thus implying an overestimation of the heat transfer coefficient in the case that traditional correlations were used. In the case of outward wall heat flux, the correction factor is instead generally higher than 1. Finally, the developed correlation has been used to carry out a parametric investigation of the effect of decay heat on the out-of-core components of the MSFR. The volumetric power determines higher temperatures at the channel wall, but the effect is significant only in the case of large diameters and/or low velocities. This might be the case for the channels of the salt reprocessing system (Fiorina et al., 2014a).

As for the natural circulation dynamics with internal heat generation, linear and nonlinear analysis methods were developed to investigate the natural circulation features of internally heated fluids for MSR applications (Pini et al., 2014, 2016; Ruiz et al., 2015; Cammi et al., 2016b). These methods have constituted the basis for the design of a testing facility (DYNASTY), which is under construction at Polimi (Cammi et al., 2016a). DYNASTY will be aimed at: (1) the experimental investigation of the natural circulation dynamics in the presence of distributed heat generation, with a specific focus on the analysis of thermal-hydraulic instabilities (stability maps); (2) the experimental validation of the theoretical models and simulation tools developed to study the natural circulation capability of a loop with a homogeneously heated molten salt, useful for design optimization of the MSFR primary circuit. In Chapter 6, Thermal hydraulics of liquid-fueled MSRs (Section 6.4), the influence of the volumetric heat generation on the stability features of natural circulation is briefly presented, with reference to the stability maps of single-phase rectangular loops.

## References

Aufiero, M., Cammi, A., Fiorina, C., Leppänen, J., Luzzi, L., Ricotti, M.E., 2013. An extended version of the SERPENT-2 code to investigate fuel burn-up and core material evolution of the Molten Salt Fast Reactor. J. Nucl. Mater. 441 (1−3), 473−486.

Aufiero, M., Brovchenko, M., Cammi, A., Clifford, I., Geoffroy, O., Heuer, D., et al., 2014a. Calculating the effective delayed neutron fraction in the Molten Salt Fast Reactor: Analytical, deterministic and Monte Carlo approaches. Ann. Nucl. Energy. 65, 78–90.

Aufiero, M., Cammi, A., Geoffroy, O., Losa, M., Luzzi, L., Ricotti, M.E., et al., 2014b. Development of an OpenFOAM model for the Molten Salt Fast Reactor transient analysis. Chem. Eng. Sci. 111, 390–401.

Cammi, A., Di Marcello, V., Guerrieri, C., Luzzi, L., 2011a. Transfer function modeling of zero-power dynamics of circulating fuel reactors. J. Eng. Gas Turbines Power. 133 (5), 052916-1–052916-8.

Cammi, A., Di Marcello, V., Luzzi, L., Memoli, V., Ricotti, M.E., 2011b. A multi-physics modelling approach to the dynamics of molten salt reactors. Ann. Nucl. Energy. 38 (6), 1356–1372.

Cammi, A., Fiorina, C., Guerrieri, C., Luzzi, L., 2012. Dimensional effects in the modelling of MSR dynamics: moving on from simplified schemes of analysis to a multi-physics modelling approach. Nucl. Eng. Des. 246, 12–26.

Cammi, A., Cauzzi, M.T., Luzzi, L., Pini, A., 2016a. DYNASTY: an experimental loop for the study of natural circulation with internally heated fluids. In: Proceedings of the 12th International Conference on Heat Transfer, Fluid Mechanics and Thermodynamics, Malaga, Spain, July 11–13, 2016, pp. 1159–1164.

Cammi, A., Luzzi, L., Pini, A., 2016b. The influence of the wall thermal inertia over a single-phase natural convection loop with internally heated fluids. Chem. Eng. Sci. 153, 411–433.

Delpech, M., Dulla, S., Garzenne, C., Kophazi, J., Krepel, J., Lebrun, C., et al., 2003. Benchmark of dynamic simulation tools for molten salt reactors. In: Proceedings of GLOBAL 2003, New Orleans, LA, November 16–20, 2003, pp. 2182–2187.

Dulla, S., Nicolino, C., 2008. Dynamics of fluid fuel reactors in the presence of periodic perturbations. Sci. Technol. Nucl. Install. 2008, 816543-1–816543-11.

Dulla, S., Ravetto, P., 2007. Interaction between fluid-dynamic and neutronics phenomena in the physics of molten-salt systems. Nucl. Sci. Eng. 155 (3), 478–488.

Dulla, S., Mund, E.H., Ravetto, P., 2008. The quasi-static method revisited. Prog. Nucl. Energy. 50, 908–920.

Dulla, S., Prinja, A.K., Ravetto, P., 2014. Random effects on reactivity in molten salt reactors. Ann. Nucl. Energy. 64, 353–364.

Fiorina, C., Aufiero, M., Cammi, A., Franceschini, F., Krepel, J., Luzzi, L., et al., 2013. Investigation of the MSFR core physics and fuel cycle characteristics. Prog. Nucl. Energy. 68, 153–168.

Fiorina, C., Cammi, A., Luzzi, L., Mikityuk, K., Ninokata, H., Ricotti, M.E., 2014a. Thermal-hydraulics of internally heated molten salts and application to the Molten Salt Fast Reactor. J. Phys. Conf. Ser. 501, 012030-1–012030-10.

Fiorina, C., Lathouwers, D., Aufiero, M., Cammi, A., Guerrieri, C., Kloosterman, J.L., et al., 2014b. Modelling and analysis of the MSFR transient behavior. Ann. Nucl. Energy. 64, 485–498.

Guerrieri, C., Cammi, A., Luzzi, L., 2013. An approach to the MSR dynamics and stability analysis. Prog. Nucl. Energy. 67, 56–73.

Guerrieri, C., Cammi, A., Luzzi, L., 2014. A preliminary approach to the MSFR control issues. Ann. Nucl. Energy. 64, 472–484.

Lapenta, G., Ravetto, P., 2000. Basic reactor physics problems in fluid-fuel recirculated reactors. Kerntechnik. 65 (5–6), 250–253.

Luzzi, L., Di Marcello, V., Cammi, A., 2012a. Multi-Physics Approach to the Modeling and Analysis of Molten Salt Reactors. Nova Science Publishers, Inc., New York, pp. 1–140.

Luzzi, L., Aufiero, M., Cammi, A., Fiorina, C., 2012b. Thermo-hydrodynamics of internally heated molten salts for innovative nuclear reactors. In: Zheng, J. (Ed.), Hydrodynamics: Theory and Model. InTech, Rijeka, Croatia, pp. 119–142.

Maschek, W., Stanculescu, A., Arien, B., Bai, Y., Chabert, C., Chebeskov, A.A., et al., 2008. Report on intermediate results of the IAEA CRP on "Studies of advanced reactor technology options for effective incineration of radioactive wastes". Energy Convers. Manage. 49, 1810–1819.

Nicolino, C., Lapenta, G., Dulla, S., Ravetto, P., 2008. Coupled dynamics in the physics of molten salt reactors. Ann. Nucl. Energy. 35, 314–322.

Pini, A., Cammi, A., Luzzi, L., Ruiz, D.E., 2014. Linear and nonlinear analysis of the dynamic behaviour of natural circulation with internally heated fluids. In: Proceedings of NUTHOS-10, Paper NUTHOS10-1074, Okinawa, Japan, December 14–18, 2014.

Pini, A., Cammi, A., Luzzi, L., 2016. Analytical and numerical investigation of the heat exchange effect on the dynamic behaviour of natural circulation with internally heated fluids. Chem. Eng. Sci. 145, 108–125.

Ruiz, D.E., Cammi, A., Luzzi, L., 2015. Dynamic stability of natural circulation loops for single phase fluids with internal heat generation. Chem. Eng. Sci. 126, 573–583.

Zanetti, M., Cammi, A., Fiorina, C., Luzzi, L., 2015. A geometric multiscale modelling approach to the analysis of MSR plant dynamics. Prog. Nucl. Energy. 83, 82–98.

## 26.11 Japan

*Ritsuo Yoshioka*[1] *and Motoyasu Kinoshita*[1,2]
[1]International Thorium Molten-Salt Forum, Yokohama, Japan, [2]University of Tokyo, Tokyo, Japan

Based on the long and wide development of ORNL from the 1950s to the 1970s, Kazuo Furukawa and his group in Japan have been investigating graphite moderated MSR "FUJI" and related accelerator technology since the 1980s until the present day (Furukawa et al., 2008; Yoshioka, 2013). FUJI is mostly based on the MSBR design, with some improvements. His group has provided wide design results, such as detailed design results of FUJI-U3 for self-sustaining, FUJI-Pu for Pu start-up, transmutation capability of minor actinides, super-FUJI of 1000 MWe, and a pilot plant mini-FUJI, which are described in Chapter 11, Liquid fuel, thermal neutron spectrum reactors. In order to promote MSR development, Furukawa and his group established the International Thorium Molten-Salt Forum (ITMSF) (2008), and the Thorium Tech Solution Inc. (TTS) (2010).

ITMSF is a nonprofit organization, which is composed of researchers and engineers from 14 countries who are involved or interested in MSR and related thorium cycles. Until 2016, 20 seminars had been held in Japan (Japan Atomic Energy Committee) and in 2015, executives from China and the Czech Republic gave lectures on their MSR developments. The Japan Atomic Energy Committee (JAEC) issued a formal opinion paper in 2012, which mentioned candidates for future nuclear applications, including thorium utilization. ITMSF proposed its MSR to the JAEC in 2013 (Yoshioka and Kinoshita, 2013). ITMSF has been an observer member of the MSR group of the GIF (the Generation IV International Forum) since it started in 2005, and has participated in the discussions in recent years (Serp et al., 2014).

Under the Atomic Energy Society of Japan, a special committee was started as "Nuclear Application of Molten Salt." In this committee, experts, including several ITMSF members, discuss MSR, dry-reprocessing, fusion application, and so on. A working group within this committee is participating in the ANS20.1 committee, where the general design criteria (GDC) for the FHR (fluoride salt-cooled high-temperature reactor) are discussed (ANS 20.1 Working Group, 2014). Based on the discussions in the ANS20.1 committee, the GDC for the MSR is proposed in Chapter 11, Liquid fuel, thermal neutron spectrum reactors.

Meanwhile, TTS's final target is the commercialization of FUJI, which is based on developments including ITMSF. TTS is now working on molten salt technology in test reactors, such as the Halden Reactor in Norway. Irradiation experimentation will proceed in the near future.

Kyoto Neutronics is designing a small thorium MSR integrated with heat exchangers, named UNOMI (Universally Operable Molten-salt reactor Integrated) (Kamei, 2013).

The following are the basic studies related to MSR at Japanese universities or research laboratories.

1. Volatile FP release experiment in molten salts which is related to the MSR source term issue, at the University of Fukui (Yamawaki et al., 2015).
2. Corrosion study of Hastelloy N in molten salt, at the University of Fukui (Fukumoto et al., 2015).
3. Molten salt chemistry for nuclear systems, at the University of Tokyo (Terai et al., 2001).
4. Dry-reprocessing utilizing molten salt, at the Central Research Institute of Electric Power Industry (CRIEPI) (Koyama et al., 2012).
5. FLiNaK-loop experiment for fusion technology, at the National Institute for Fusion Science (NIFS) (Sagara et al., 2015).

In Japan, we will also continue our studies and activities, cooperating with worldwide researches and promoters, in the future.

## References

ANS 20.1 Working Group, 2014. Nuclear safety criteria and design process for fluoride salt-cooled high-temperature reactor nuclear power plants. ANS 20.1 draft (to be published).

Furukawa, K., et al., 2008. A road map for the realization of global-scale thorium breeding fuel cycle by single molten-fluoride flow. Energy Convers. Manage. 49, 1832–1847.

Fukumoto, K., et al., 2015. Corrosion behavior of Hastelloy-N alloys in molten salt fluoride in Ar gas or in air. J. Nucl. Sci. Technol. 52, 1323–1327.

International Thorium Molten-Salt Forum: ITMSF, 2008. <http://msr21.fc2web.com/english.htm>.

Kamei, T., 2013. Review of R&D of thorium molten-salt reactor. Nucl. Saf. Simul. 4 (2), 80–96.

Koyama, T., et al., 2012. Development of pyro-processing fuel cycle technology for closing actinide cycle. Procedia Chem. 7, 772–778.

Sagara, A., et al., 2015. First operation of the Flinak/LiPb twin loop Orosh$^2$i-2 with a 3T SC magnet. Fusion Sci. Technol. 68, 303–307.

Serp, J., et al., 2014. The molten salt reactor (MSR) in generation IV: overview and perspectives. Prog. Nucl. Energy. 77, 308–319.

Terai, T., et al., 2001. Tritium release from Li2BeF4 molten salt breeder under neutron irradiation at elevated temperature. Fusion Technol. 39, 768–772.

Thorium Tech Solution Inc.: TTS, 2010. <http://ttsinc.jp/indexenglish.html>.

Yamawaki, M., et al., 2015. Evaluation study of source term for severe accident analysis of molten salt reactors. J. Plasma Fusion. 11, 113–119.

Yoshioka, R., 2013. Nuclear energy based on thorium molten salt. In: Lantelme, F., Groult, H. (Eds.), Molten Salts Chemistry: From Lab to Applications. Elsevier Inc, San Diego, CA.

Yoshioka, R., Kinoshita M., 2013. Recent developments in molten salt reactor (in Japanese). Document No.2-2 at 17th Japan Atomic Energy Committee in 2013. <http://www.aec.go.jp/jicst/NC/iinkai/teirei/siryo2013/siryo17/siryo2-2.pdf>.

## 26.12 Korea

*Deokjung Lee and Yongjin Jeong*
Ulsan National Institute of Science and Technology, Ulsan, Republic of Korea

In Korea, Se Kee Oh and his group at Ajou University performed MSR research actively from 1998 to 2008, and UNIST (Ulsan National Institute of Science and Technology) started MSR research in 2002. Work on basic research has continued up to the present day.

Ajou University first set up a computer code system for MSR analysis, which consists of HELIOS (1998), AMDEC, and AMBIKIN2D (Lee, 2008; Lee and Oh, 2008). HELIOS is a commercially available code from Studsvik Scandpower Inc., and AMDEC and AMBIKIN2D are inhouse codes developed at Ajou University specifically for MSR analyses. HELIOS solves two-dimensional neutron/gamma transport problems and generates lattice parameters for the downstream diffusion calculations by AMBIKIN2D. AMBIKIN2D is a two-group, two-dimensional neutron kinetics code for MSR transient analysis, taking into account the flowing fuel-induced neutronics effects such as the reduction of effective delayed neutron fractions caused by the liquid fuel loop circulating through the outside loop of the core. It solves the R-Z time-dependent diffusion problems and calculates eigenvalues, fluxes, power shapes, and reaction rates of the core. AMDEC performs the fuel depletion calculations in multiregion fluid-fuel loop systems with continuous feeding and reconditioning processes. HELIOS provides AMDEC with spectrum weighted one-group cross-section sets, and AMDEC provides HELIOS with updated nuclide number densities. HELIOS also provides the AMBIKIN2D code with two-group macroscopic cross-section data. The code system was used for the design and analysis of Ajou University's unique MSR design, AMBIDEXTER.

Ajou University designed AMBIDEXTER-NEC (Advanced Molten-salt Break-even Inherently-safe Dual-function EXcellenTly-Ecological Reactor Nuclear Energy Complex), which encompasses a reactor core, primary pump, heat exchanger, power generator, chemical processing units, etc. (Oh et al., 1998, 2000a, 2000b, 2001, 2002). The design objective of the reactor is to burn DUPIC fuel (Ham et al., 2007; Oh et al., 2007) and to minimize minor actinide production while generating electric power. To achieve the objectives, the AMBIDEXTER reactor core consists of two parts: a blanket region and a seed region. The blanket region consists of only molten salt fuel (LiF-$BeF_2$-(Th,U,Pu)$F_4$) and the seed region consists of the molten salt fuel and graphite moderator channel. The blanket region has a very hard neutron spectrum like a fast reactor, and the seed region has a soft neutron spectrum like a pressurized water reactor (PWR). The seed region mainly burns molten-salt fuel, and the blanket region mainly burns minor actinides because of the neutron spectrum characteristics of each region. AMBIDEXTER was designed as a burner reactor which has a low conversion ratio, 0.298. Unfortunately, when Prof. Oh retired from Ajou University, the MSR research in Korea stopped until 2012, when UNIST started MSR research.

Deokjung Lee and his group at UNIST have been developing a code system for the simulation of online reprocessing and refueling, and depletion of a molten salt breeder reactor (MSBR) (Robertson, 1971). The MSBR was designed by ORNL (Oak Ridge National Laboratory) in the 1970s. The MSBR adopts molten-salt as a liquid fuel as well as coolant, and graphite material as a neutron moderator and reflector. The reactor core of the MSBR is divided into two zones with different fuel-to-graphite ratios. Zone-1 has a low fuel-to-graphite ratio and most fission reactions occur here, while zone-2 has a high fuel-to-graphite ratio and most breeding occurs here. UNIST investigated three different equilibrium composition search approaches for the MSBR using the nuclear reactor core analysis computer code system based on the MCNP6 Monte-Carlo code. (1) The first search method uses a representative average single unit cell for both zones. The single unit cell model uses volume-weighted average fuel and moderator compositions and sizes (Jeong et al., 2014a, 2014b, 2015a). (2) The second method uses two representative unit cells, one for each zone, which preserves the fuel-to-moderator ratio of each zone (Jeong et al., 2015a, 2015b). (3) The third method directly models the whole MSBR core. The code system was set up with the MCNP6 Monte-Carlo code, its depletion module CINDER90, and the Python scripting language (Park et al., 2015a–c). Python is used for implementing batchwise reprocessing and refueling. In the process of calculating the equilibrium fuel compositions, various parameters like the multiplication factor, breeding ratio, and number density can be obtained to analyze the MSBR. The MSBR whole core analysis is performed at the initial and equilibrium core conditions, for various reactor design parameters such as normalized neutron flux distribution, temperature coefficients, rod worth, and power distributions. The neutronics core characteristics were analyzed using the four-factor formula applied to the single-cell model, two-cell model, and the two zones of the whole core, separately.

UNIST plans to develop a new high-fidelity code system for MSR analysis including online reprocessing and refueling, and the modeling capability of the movement of liquid fuel and the delayed neutron precursors. Furthermore, it is planning to develop a new MSR core concept using the developed code system.

## References

Ham, T.K., Lee, Y.J., Seo, M.H., Oh, S.K., 2007. Ambidexter-dupic: an LWR-MSR symbiont operating on an effective and efficient fuel cycle. Proceedings of GLOBAL. American Nuclear Society, La Grange Park, IL.

HELIOS, 1998. "HELIOS methods" in program manual Rev 3. Program HELIOS-1.5, Studsvik-Scandpower.

Jeong, Y., Choi, S., Lee, D., 2014a. Molten salt breeder reactor analysis based on unit cell model. KNS Spring Meeting, Jeju Convention Center, May 28–30, 2014.

Jeong, Y., Choi, S., Lee, D., 2014b. Development of computer code packages for molten salt reactor core analysis. In: PHYSOR2014, Kyoto, Japan, September 28–October 3, 2014.

Jeong, Y., Park, J., Lee, H.C., Lee, D., 2015a. Equilibrium core design methods for molten salt breeder reactor based on two-cell model. J. Nucl. Sci. Tech. 53 (4). Available from: http://dx.doi.org/10.1080/00223131.2015.1062812.

Jeong, Y., Park, J., Lee, D., 2015b. Advanced equilibrium composition search method for molten salt breeder reactor based on two-cell model. In: 2015 ANS Annual Meeting, San Antonio, TX, June 7–11, 2015.

Lee, Y.J., October 2008. Development of the AMBIKIN2D code for the space-time neutronics in fluid fuel reactors. PhD Thesis, Department of Energy Engineering, Ajou University, pp. 23–30.

Lee, Y.J., Oh, S.K., 2008. Development and verification of AMBIKIN2D: a two dimensional kinetics code for fluid fuel reactors. J. Energy Eng. 17 (1).

Oh, S.K., Won, S.H., et al., 1998. Some analyses of reactivity characteristics and power distribution of the 250MWth AMBIDEXTER core. In: Proceeding of 1998 KEES Annual Conference, pp. 29–34.

Oh, S.K., et al., 2000a. AMBIDEXTER nuclear energy complex: a practicable approach for rekindling nuclear energy application. Nucl. Eng. Des. 2001 (207), 11–19.

Oh, S.K., et al., 2000b. Eligibility of the AMBIDEXTER nuclear energy complex for a generation IV nuclear power system. 15-th KAIF/KNS Annl. Conf. 1 (1), 347–354.

Oh, S.K., et al., 2001. An ultimate fission energy system option for the next generation—the AMBIDEXTER nuclear complex. In: IAEA Tech, Comm. Mtng. Utilization of Thorium Fuel; Option in Emerging Nuclear Energy, IAEA TECDOC-1319.

Oh, S.K., et al., 2002. Physics and safety features of the AMBIDEXTER nuclear energy complex. In: Proceedings of the PHYSOR 2002, ANS, Seoul, Korea, pp. 87–97.

Oh, S.K., Lee, Y.J., Ham, T.K., Seo, M.H., Kim, H.S., 2007. Designed and operational characteristics of the AMBIDEXTER-NEC with uranium-reduced DUPIC fuel material. ICAPP. 3, 1361–1367.

Park, J., Jeong, Y., Lee, H.C., Lee, D., 2015a. Whole core analysis of molten salt breeder reactor with online fuel reprocessing. Int. J. Energ. Res. Available from: http://dx.doi.org/10.1002/er.3371.

Park, J., Jeong, Y., Lee, D., 2015b. Whole core analysis of molten salt breeder reactor. In: Advances in Nuclear Fuel Management V, Hilton Head, SC, March 29–April 1, 2015.
Park, J., Jeong, Y., Lee, D., 2015c. Molten salt breeder reactor analysis methods. In: KNS Spring Meeting, Jeju Convention Center, May 6–8, 2015.
Robertson, R.C., 1971. Conceptual Design Study of a Single-Fluid Molten Salt Breeder Reactor. Oak Ridge National Laboratory, ORNL-4541, Oak Ridge, TN.

## 26.13 Netherlands

*Jan L. Kloosterman*
Delft University of Technology, Delft, The Netherlands

The Netherlands has a long tradition with homogeneous nuclear reactors, starting with the vision of Jan Went, the first professor of nuclear reactor physics at TU Delft and director at the KEMA research center in Arnhem, to develop a homogeneous reactor in Europe (Andriesse, 2000). In 1957, the KEMA opened a new nuclear laboratory for the development of the KEMA Suspension Test Reactor (KSTR); a reactor with small uranium–thorium–oxide fuel particles in a water flow pumped through the primary circuit. The particles were made by a newly developed sol-gel process that laid the foundation for the later manufacturing of the HTR TRISO particles in Germany (Kistemaker et al., 1988). They had a diameter of less than 10 μm, allowing the fission products to escape from the particles and to dissolve in the water coolant. By continuously (re)fueling and cleaning the coolant, a long-term uninterrupted operation was envisaged. At first instance the focus was on a zero power reactor which operated from 1957 till 1967. The construction of the 1 MW reactor started in 1963 and took 9 years to finish. In 1974, after having solved some unexpected issues with flow instabilities, the reactor became critical. Unfortunately, cracking and clustering of fuel particles and unexpected wear at the primary pumps caused the reactor to shut down in 1977. Meanwhile, another faculty member of TU Delft, Prof. D.G.H. Latzko worked in the 1960s on the use of molten salts as heat transfer fluids for power generation, resulting in the thesis by Dr. B. Vriesema (1969).

The interest in homogeneous reactors revived at TU Delft at the beginning of the 21st century as part of a research program on Generation-IV reactors. It was realized that breeding of new fuel and complete destruction of long-lived actinides could best be realized in a homogeneous reactor. Research on the thermal molten salt reactor started around 2005 and was focused on the thorough understanding of the Molten Salt Reactor Experiment (MSRE) behavior (Kophazi et al., 2009), and on improving the thermal molten salt breeder reactor (MSBR) design originally developed in the US (Nagy, 2012). Various alternatives were investigated among which were one-fluid, one-and-a-half fluid, and two-fluid reactor core designs. In addition, the chemical and physical properties of various fuel salts were studied, in close collaboration with the European Commission's Joint Research Centre in Karlsruhe (Capelli, 2016). Although the thermal MSR design clearly has a lot of potential to be explored and developed, research at TU Delft now focuses on the molten salt fast reactor (MSFR) design originally proposed by CNRS and adopted as the reference design for Generation-IV, which culminated in the SAMOFAR project within the HORIZON2020 European framework program (2014−20). The SAMOFAR project is described in Chapter 20, Safety assessment of the molten salt fast reactor (SAMOFAR).

In the framework of the government-supported research into $CO_2$-free energy supply, the Dutch NRG research and consultancy organization in cooperation with JRC-Karlsruhe is preparing an irradiation of samples of fissile and fertile material containing fluoride fuel salt in corrosion-resistant graphite crucibles to determine the stability of the fission products in the fuel salt during irradiation. The irradiations will take place in the Petten High Flux Reactor with a total neutron flux of around $10^{15}$ $cm^{-2}$ $s^{-1}$. Two campaigns with different irradiation times ranging up to 1 year will be carried out, during which the samples will be held at a constant temperature well above the melting point. The postirradiation experiments will be carried out at both NRG and JRC-Karlsruhe, and will include a detailed evaluation of the fission gas composition and distribution, as well as determination of the temperature above which the fission products become volatile. In parallel, cooperation between NRG and TU Delft will support the molten salt irradiation experiments by studying helium bubbling and fission product behavior. The irradiations are expected to start in 2016, and are part of a multiyear nuclear R&D program.

## References

Andriesse, C.D., 2000. De Republiek der Kerngeleerden, Beta text (in Dutch).

Capelli, E., 2016. Thermodynamic characterization of salt components for molten salt reactor fuel. PhD Thesis, TU Delft.

Kistemaker, J., Levensbericht, Went, J.J., 1988. Proceedings of the Royal Netherlands Academy of Arts and Sciences (KNAW), Amsterdam, pp. 200−203 (in Dutch).

Kophazi, J., Lathouwers, D., Kloosterman, J.L., 2009. Development of a three-dimensional time-dependent calculation scheme for molten salt reactors and validation of the measurement data of the molten salt reactor experiment. Nucl. Sci. Eng. 163, 118−131.

Nagy, K., 2012. Dynamics and fuel cycle analysis of a moderated molten salt reactor. PhD Thesis, TU Delft.

Vriesema, B., 1969. Aspects of molten salts as heat transfer agent for power generation. PhD Thesis, TU Delft.

# 26.14 Norway

*Elling Disen*
Norwegian Reactor facility at Halden, Norway

## 26.14.1 Thorium discovery in Norway

The element thorium (Th) was actually discovered in Norway in 1828. At that time Norway was in a union with Sweden after having been part of Denmark for some 400 years. Norway in the 19th century experienced a blossoming of science, literature, and Arctic discoveries that paved the way for full independence in 1905.

The mineral "thoritt" was discovered by Hans Morten Thrane Esmark on the tiny island of Løvøy in Telemark. He was the son of the geology assessor Jens Esmark at Kongsberg, where silver had been mined for centuries. Even though Hans had a passion for minerals he chose to become a priest and was sent to Brevik in Telemark. His duties in the parish meant crisscrossing circuits in the fjord archipelagos. The brown mineral "thoritt" was sent to his chemist friend Jöns Jakob Berzelius in Stockholm which was the intellectual capital of the union of kingdoms.

Berzelius undertook the then state-of-the-art examinations and concluded that "thoritt" had to be a newly discovered mineral and that it also contained a new element. Berzelius had long dreamt of naming a new element after the Norse God of Thunder, Thor; apparently the priest did not protest to its naming after a pagan god.

## 26.14.2 "Thorium fever"

Th has special geochemical properties and as a result Th minerals have ended up in pegmatites, a kind of geological dustbin from melting processes in the inner Earth. "Thoritt" nuggets the size of walnuts can be found along the fjordline of Telemark. From the 1880s a "klondyke" set in and the entire world production came from only this area. Th was sold for several hundred crowns per kilo, a fortune at the time, for use as glowing mantles in Auer lamps. People fought over claims but the bonanza came to a stop when Th was able to be extracted easily using spades and picks in the US, Brazil, and India before the turn of the century. Electric lights soon outcompeted the lamps and "Thoritt" chunks will probably never be of commercial interest again.

### 26.14.3 Telemark geology

Th has been identified at several locations in Telemark but Fen is the main area. Fen is a very unique formation; 600 million years old it seems to have been a plug sprung open during the creation of the Oslofjord, spewing up exotic minerals from deep down. Its twin is the Tanzanian volcano Ol Doinyo Lengai. “Thoritt” $ThSO_4$ is not the main mineral. “Rauhaugkitt” and “ankeritt” contain iron and carbonates. $ThO_2$ crystals are finely dissolved in the hard rock at concentrations of 0.2%–0.4%. Mining and refining are deemed too costly compared to monazite. However europium, cerium, neodymium, lanthanum and other rare Earth elements at around 1% could make profitable value chains in the current marketplace.

### 26.14.4 Commercial interest

The Germans initiated mining for niobium during the Second World War. The operation was closed down in 1965.

Helicopter gamma surveys were carried out in 2006 but Th reserves are hard to predict since gammas do not penetrate from that far down. Historically the estimate has been 170,000 tons Th, but the exact origin of this estimate cannot be pinned down. Some prospectors claim much higher quantities as well as higher local concentrations in smaller ores. A drilling campaign would cost in the hundreds of millions USD.

Th from Fen needs to be highly automated since radiation and radon levels are high. Tailings will be voluminous given low concentrations, and acidic waste after separations will need a repository sealed off from the drinking water supplies of the region.

### 26.14.5 Governmental investigation 2008

Heavy water production in Norway became globally known due to the commando raid during the Second World War and the subsequent Hollywood films. It is no secret that Norwegian heavy water was smuggled to Israel and to other nations as well. The revelations caused exports to stop in 1988.

Norway built a 25-MWth heavy-water boiler in Halden, Østfold in the 1950s. The test reactor is part the OECD framework on nuclear energy and has specialized in fuel characterization and irradiation testing. Norway also houses a smaller installation for the production of medical isotopes at Kjeller, north of the capital Oslo. The reactors were recently licensed until the end of 2020.

Prior to the Norwegian oil boom taking off in the 1980s a governmental committee recommended 12 reactors as a response to the oil crisis of the 1970s. The debate was more relevant in Sweden where 24 reactors were proposed and 12 were built.

Out of the blue came a photo in late 2006 of CERN's Carlo Rubbia posing with the leaders of the Progress Party. This liberal-conservative movement had become a force that no longer could be ignored by the traditional left–right split. The photo was widely circulated in the press and sparked off a dynamic that led to the Minister of Energy's request for an international assessment on the thorium resource.

### 26.14.6 Thorium report

The mandate of the Thorium Report of February 2008 was: "The Committee's work and the resulting Report shall establish a solid knowledge base concerning both opportunities and risks related to the use of thorium for long-term energy production. The work should be conducted as a study of the opportunities and possibilities (screening), based on a review of Norway's thorium resources and the status of key technologies." The Chairman was Mikko Kara, former CEO of Finnish VTT, a governmental R&D organization.

CERN had advocated the accelerator-driven system (ADS) to the French for over a decade without success. The company Thor Energy AS published press releases about building a Norwegian thorium reactor in cooperation with Atomic Energy of Canada Limited AECL. The report gained considerable interest from diverse concerned actors including energy companies and environmental lobby groups. Opinion polls showed that a large majority of citizens was favorable to the prospect of "clean" nuclear thorium energy from Norway as opposed to "dirty" uranium from abroad. The public opinion is still positive since the green lobby has lost its hegemony. The molten salt option received little attention and was authored by the French CNRS. However, the debate soon lost traction. In 2009 Sverre Hval with the Kjeller reactor penned a proposal to the National Research Council for a Norwegian molten salt R&D initiative that was dead on arrival.

### 26.14.7 Recent events

Then, in 2012, another report was taken by a collaborative foundation "Oslofjordfondet," a sign that the prospect still lingered among some academics at regional universities; powerful energy companies do not participate in the discussion of thorium. A small startup, 232 Thorwards AS, advocating molten salts met with the Conservative Party in 2009. Since 2013 Norway has had a Conservative–Progress Party coalition minority government that has a national "thorium R&D center" in the works but nothing has crystallized as of the time of this writing; crucial parliamentary support is needed from parties in the center of the political spectrum.

In hindsight, confusion reigned on comparative safety, resistance to proliferation, and waste footprints. ADS proponents and Thor Energy AS proclaimed vast improvements that were easily questioned by the green groups simply by referring to the historical record of thorium rods. It was also acknowledged that Telemark Thorium would not be competitive. Clear guidance on the important issues was not provided by the very small number of senior nuclear experts within the reactor staffs.

The political climate is improving under the new government. The country is eagerly debating what is to follow the oil era initiated in the 1980s. Politicians are looking for a new industry that can shoulder a national strategy when petroleum revenues decline. In the tradition of the Norwegian consensus culture Thor Energy AS invited all thorium proponents to sign a petition to the Minister of Energy for their rod technology in late 2013, but molten salt advocates from Thorium Electronuclear AB did not concede to the roll call. Thorium Electronucear AB advocates a denatured molten salt reactor (DMSR) commercial pilot.

Norway is particularly well positioned to launch a relevant initiative for molten salt reactors. The safety culture in the world leading oil industry, subsea heavy duty robotics, niche shipyards, high temperature aluminum ovens, and the Halden fuel irradiation facility, unique in northern Europe, all harbor key competences.

## 26.14.8 IThEO started in Sweden

Andreas Norlin in Stockholm, Sweden, initiated the International Thorium Energy Organization in 2009. With support from the UN Business Council yearly conferences have been organized in different regions of the world. IThEO advocates thorium energy in general and can be seen as a counterpart to John Kutch's Thorium Energy Alliance in the US.

## 26.14.9 Irradiation experiments at Halden R&D reactor

### *26.14.9.1 Th rods*

In April 2013 the technical weekly "Teknisk Ukeblad" reported that Thor Energy had inserted thorium rods in the flux of the Halden test reactor.

Thor Energy explains: "Thor Energy undertook to explore the operation of U-233/thorium oxide fuel in a Gen III+ reduced-moderation BWR (RBWR). This reactor platform should be well suited for achieving high U-233 conversion factors due to its epithermal neutron spectrum. It was designed by Hitachi Ltd and JAEA as a platform for flexible uranium–plutonium fuels in which high conversion or actinide destruction can be achieved. It is based on the ABWR architecture but has a shorter, flatter pancake-shaped core and a tight lattice to ensure sufficient fast neutron leakage and a negative void reactivity coefficient. The study undertaken by Thor Energy aimed to shed light on the characteristics of uranium that is multi-recycled in a RBWR and the extent to which U-233 breeding can be achieved while maintaining an acceptable cycle length and discharge burnup."

"Thorium−plutonium fuels can be designed according to two distinct objectives:

1. Maximizing the utilization—and hence incineration—of plutonium. This is done by operating the fuel in a core environment with high neutron-moderation (a high hydrogen-to-heavy-metal ratio).
2. Maximizing the cycle length for the reactor-fuel system. This is achieved by operating the fuel in a reduced-moderation core environment (lower hydrogen-to-heavy-metal ratio), resulting in higher production of 233U and hence a slower rate of fissile depletion in the fuel."

Another irradiation series is planned for 2015.

### 26.14.10 Molten salts

Thorium Electronuclear AB seeks finance to initiate irradiations aimed at the DMSR at the Halden facility. DMSR was the last design from the Oak Ridge National Laboratories after difficulties encountered during the two-fluid breeder concept. MSRE ran smoothly on highly enriched U235, U233, and "pills" of plutonium but the complete and irradiated chemistry has not been verified with thorium also added to the mix. The DMSR is a one-fluid once-through concept with low power density that allows for a 30-year graphite life. Eighty per cent of the energy produced originates from thorium. It starts up on 19.75% enriched U. The physical properties, thermal hydraulics, and corrosion mechanisms are not expected to change significantly from the MSRE. Details were not disclosed at the time of this writing.

## 26.15 Russia

*Leonid I. Ponomarev*
A.A. Bochvar High Technology Research Institute of Inorganic Materials, Moscow, Russia

MSR research in Russia has had a long tradition (since the 1970s). Several monographs have been published in this time (Blinkin and Novikov, 1978; Smirnov et al., 1979; Mourogov et al., 1983; Novikov et al., 1993, 1998; Alexeev and Zajtsev, 2014). The main centers of activity are:

- Kurchatov Institute (Moscow);
- Institute of Physics and Power Engineering (IPPE, Obninsk);
- Research Institute of Atomic Reactors (RIAR, Dimitrovgrad);
- Institute of Theoretical and Experimental Physics (ITEP, Moscow);

- A.A. Bochvar Institute of Inorganic Materials (VNIINM, Moscow);
- V.G. Khlopin Radium Institute (RI, St Petersburg);
- Leading Research Institute of Chemical Technology (VNIIKHT, Moscow);
- Research Institute of Technical Physics (VNIITP, Snezhinsk);
- Research Institute of Experimental Physics (VNIIEF, Sarov);
- Ural Institute of High Temperature Electrochemistry and Ural Polytechnic Institute (Ekaterinburg).

The main directions of MSR activity are:

- Physical and chemical properties of MSR materials;
- Subcritical MSR systems for minor actinide incineration;
- MSR with a Th-U fuel cycle;
- Fast MSR with a U-Pu fuel cycle.

Almost all these activities are devoted to the theoretical and experimental reasons for different modifications to the thorium MSR and its fuel cycle. In the last 3 years the concept of the fast MSR with U-Pu fuel has been developed.

## 26.15.1 Physics and chemistry of MSR materials

Molten salt properties (density, viscosity, thermal capacity and conductivity, etc.) have been studied in Russia for a long time. One of the first works was the determination of the fusion diagram of LiF-NaF-KF (Bergman and Dergunov, 1941). The essential contribution to this field was done by VNIINM (Gorbunov et al., 1976), Ural Polytechnic Institute (Smirnov et al., 1974; Desyatnik et al., 1979, 1981; Klimenkov et al., 1983), RIAR (Naumov et al., 1996), and especially by the “Kurchatov Institute” (Ignat’ev et al., 1984; Naumov et al., 1996; Ignatiev et al., 1999, 2003, 2006a, 2006b, 2008, 2013; Afonichkin et al., 2009; Khokhlov et al., 2009; Merzlyakov et al., 2011, 2014; Ignatiev and Surenkov, 2012, 2013; Alexeev et al., 1997, 1998, 2014).

Measurements of the solubility of the actinide and lanthanide fluorides in molten salts were performed recently at VNIIKHT (Seregin et al., 2011a, 2011b; Ponomarev et al., 2011, 2013), VNIITP (Volozhin et al., 2013), and RIAR (Lizin et al., 2013a, 2013b, 2015a, 2015b).

## 26.15.2 Subcritical MSR systems for minor actinide incineration

Due to the small fraction of the Am delayed neutrons ($ß \approx 0.14\%$) MSR burners of the minor actinides are considered mainly as subcritical ones. Many theoretical and experimental works have been performed in this respect (Dubovsky, 1959; Vasil’kov et al., 1970; Kolesov and Guzhovsky, 1994; Kolesov et al., 1995, 1997, 2002; Alekseev et al., 1995a, 1995b, 2015; Kolesov and Khoruzhii, 2000; Kiselev, 2001; Gerasimov and Kiselev, 2001; Mel'nik et al., 2003; ISTC Project#1486, 2004; Degtyarev et al., 2005, 2006, 2012, 2013a, 2013b, 2013c; Yurevich et al., 2006; Gulevich et al., 2008a, 2008b, 2013).

The accelerator power $W_a$ with proton energy $E_a \approx 1$ GeV and the blanket core power $W_b$ with subcriticality $\Delta k$ are connected by the relation (Degtyarev et al., 2005):

$$W_a \approx 0.7 \cdot \Delta k \cdot W_b$$

At $W_a = 10\,\text{MW}$ and $\Delta k = 0.05$ the blanket power is restricted up to $W_b \approx 300\,\text{MWth}$.

To enhance $W_b$ to $A \cdot W_b$ at fixed $W_a$ with amplification factor A, the cascade schema of the MSR burner was considered (Dubovsky, 1959; Kolesov and Guzhovsky, 1994; Kolesov et al., 1995, 1997, 2002; Alekseev et al., 1995a, 1995b; Kolesov and Khoruzhii, 2000; Mel'nik et al., 2003; ISTC Project#1486, 2004; Degtyarev et al., 2005, 2006). The experiment was performed at VNIIEF (Fig. 26.15.1) (Kolesov et al., 2002; ISTC Project#1486, 2004). The measured value $A = 2.0 \pm 0.1$ is in fair agreement with theoretical estimations.

The effective MSR burner of Am was considered on the base of eutectic LiF-NaF-KF in which the solubility of $AmF_3$ is $\sim 40$ mol% at 700°C (Lizin et al., 2013a). Such an MSR burner can incinerate $\sim 300$ kg Am/year · GWth using Am as fuel, without feeding by Pu and U-235 (Degtyarev et al., 2013b).

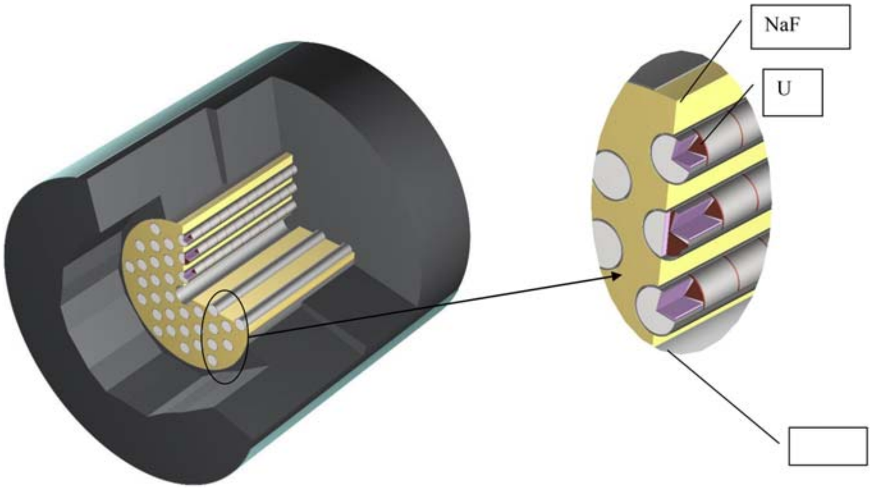

**Figure 26.15.1** Schema of the experiment: salt cylinder (320 kg of $NaF{-}ZrF_4$) with 220 tablets of U-235 (18.6 kg, 90% enrichment), in which the sphere of Np-237 (5 kg) is imbedded with the neutron source (Cf-252) inside.

## 26.15.3 Thorium-based reactor and its fuel cycle

The thorium fuel cycle was studied for many years in the Institute of Physics and Power Engineering (IPPE, Obninsk) and Moscow Engineering Physics Institute (MEPHI, Moscow) (Mourogov et al., 1983), as well as in the Institutes of the Russian Academy of Sciences (Suglobov et al., 2007). The most systematic consideration was performed in the Russian Research Center "Kurchatov Institute" (Ignatiev et al., 2007, 2008; ISTC Task #1606, 2007), especially in the framework of the "MOSART" conception, based on the salt LiF-NaF-$BeF_2$ (Ignatiev et al., 2012a, 2012b, 2014). This reactor has an intermediate neutron spectrum, and it is proposed as a minor actinides incinerator.

## 26.15.4 Fast MSR with U-Pu fuel cycle

The concept of the fast MSR based on chloride salt was considered in the work by Mourogov and Bokov (2006).

Until recently the fast MSR with U-Pu fuel based on the fluoride molten salts was not considered because the $PuF_3$ solubility in these salts does not exceed ~3 mol%. In the last 3 years the extremely high solubility of the actinide fluorides $PuF_3$, $UF_4$, and $AmF_3$ in the eutectic 46.5LiF–11.5NaF–42.0KF (FLiNaK) was established experimentally (~30, 45, and 40 mol%, respectively, at 700°C) (Lizin et al., 2013a, 2013b; Volozhin et al., 2013), as well as the lanthanide fluoride solubility (Seregin et al., 2011a, 2011b; Ponomarev et al., 2011, 2013). These observations at first opened the way for the development of the fast MSR with U-Pu fuel cycle, which can operate in the equilibrium mode (Degtyarev et al., 2015; Ponomarev and Fedorov, 2015; Ponomarev et al., 2016) (see also Chapter 12: Fast-spectrum, liquid-fueled reactors). The closed fuel cycle of such an MSR is simplified in comparison with that of the solid fuel reactors and its cost is essentially reduced (Ponomarev et al., 2016). The subcritical fast MSR burner of minor actinides based on FLiNaK can incinerate ~300 kg Am/year · GWth (Degtyarev et al., 2013b) (see Chapter 15: Accelerator-driven systems).

## References

Afonichkin, V.K., Bovet, A.L., Panov, A.V., Subbotin, V.G., Toropov, A.D., Zherebtsov, A.L., et al., 2009. Dynamic reference electrode for investigation of fluoride melts containing beryllium. I. Fluor. Chem. 130 (1), 83–88.

Alekseev, P.N., Ignatiev, V.V., Kolyaskin, O.E., Mostovoj, V.I., Men'shikov, L.I., Prusakov, V.N., et al., 1995a. Subcritical cascade liquid-salt reactor as an element of the fuel cycle. Atomic Energy. 79 (4), 651–659.

Alekseev, P.N., Ignatiev, V.V., Kolyaskin, O.E., Mostovoj, V.I., Men'shikov, L.I., Prusakov, V.N., et al., 1995b. Cascade subcritical enhanced-safety reactor. Atomic Energy. 79 (5), 733–742.

Alekseev, P.N., Ignatiev, V.V., Ponomarev-Stepnoi, N.N., Prusakov, V.N., Stukalov, V.A., Subbotin, S.A., 1998. Harmonization of fuel cycles for nuclear energy system with the use of molten-salt technology. Prog. Nucl. Energy. 32 (3–4), 341–348.

Alekseev, P.N., Balanin, A.L., Blandinsky, V.Yu, Dudnikov, A.A., Fomichenko, P.A., Nevinitsa, V.A., et al., 2015. Prospects of subcritical molten salt reactor for minor actinides incineration in closed fuel cycle. Kerntechnik. 80 (4), 389–393.

Alexeev, P.N., Ignatiev, V.V., Konakov, S.A., Menshikov, L.I., Ponomarev-Stephoj, N.N., Prusakov, V.N., et al., 1997. Harmonization of fuel cycles for nuclear energy system with the use of molten salt technology. Nucl. Eng. Des. 173 (1–3), 151–158.

Alexeev, P.N., Grishanin, E., Shimkevich, A., 2014. Elektromagnetical sensor for monitoring redox potential of molten salts. Key Eng. Mater. 605, 1–6.

Alexeev, S., Zajtsev, V.A., 2014. Thorium in Nuclear Power. Technosphera, Moscow (in Russian).

Bergman, G., Dergunov, T., 1941. Fusion diagram of LiF-KF-NaF. Comp. Rend. Acad. Sci. USSR. 31, 753–754.

Blinkin, V.L., Novikov, V.M., 1978. Molten Salt Reactors. Atomizdat, Moscow (in Russian).

Degtyarev, A.M., Ponomarev, L.I., 2012. LiF-NaF-KF Molten salt reactor with a fast neutron spectrum. Atomic Energy. 112 (6), 451–453.

Degtyarev, A.M., Kalugin, A.K., Ponomarev, L.I., 2005. Estimation of some characteristics of cascade subcritical molten sait. reactor (CSMSR): features and restrictions. Prog. Nucl. Energy. 47, 99–105.

Degtyarev, A.M., Kalugin, A.K., Kolyaskin, O.E., Myasnikov, A.A., Ponomarev, L.I., Karmanov, F.I., et al., 2006. Cascade subcritical liquid-salt reactor for burning transplutonium actinides. Atomic Energy. 101 (2), 569–577.

Degtyarev, A.M., Myasnikov, A.A., Trofimova, T.E, 2012. Fuel composition stabilization in a subcritical liquid-salt transplutonium burner reactor. Atomic Energy. 111 (6), 381–388.

Degtyarev, A.M., Karmanov, F.I., Myasnikov, A.A., 2013a. Noise lag effect in transients of a subcritical molten salt transplutonium incinerator. Atomnaya Energia. 114 (3), 149–156.

Degtyarev, A.M., Kolyaskin, O.E., Myasnikov, A.A., Ponomarev, L.I., Karmanov, F.I., Seregin, M.B., et al., 2013b. Molten-salt subcritical transplutonium actinide incinerator. Atomic Energy. 114 (4), 225–232.

Degtyarev, A.M., Myasnikov, A.A., Saltykova, O.N., 2013c. Statistical control $k_{eff}$ for subcritical fused salt transplutonium burner reactor. Atomic Energy. 113 (4), 227–235.

Degtyarev, A.M., Myasnikov, A., Ponomarev, L., 2015. Molten salt fast reactor with U-Pu fuel cycle. Prog. Nucl. Energy. 82, 33–36.

Desyatnik, V., Nechaev, V., Chervinsky, J., 1981. The viscosity of the molten mixtures of beryllium fluoride with fluoride of sodium and lithium. J. Appl. Chem. 54 (10), 2310–2312.

Desyatnik, V.N., Kurbatov, N.N., Raspopin, S.P., 1979. Study of Physicochemical and Thermophysical Properties of Molten Fluoride Salts of Lithium, Sodium, Beryllium, Uranium and Thorium. UPI Report, No. 78027681, Sverdlovsk 189, Russia.

Dubovsky, B.G., 1959. Section type reactor systems. Atomnaya Energia. 7 (5), 456–503.

Gerasimov, A.S., Kiselev, G.V., 2001. Scientific and technical problems of the electronuclear installation creation (Russian experience). Part. Nucl. 32 (1), 143–188.

Gorbunov, V.F., Novoselov, G.P., Ulanov, S.A., 1976. Study on interaction of plutonium, uranium and rare earth fluorides with some metal oxides in fluoric salt melts. Radiochimija. 17, 109−224.

Gulevich, A., Chekunov, V., Fokina, O., Komlev, O., Kukharchuk, O., Melnikov, C., et al., 2008a. Concept of electron accelerator-driven system based on subcrititical cascade reactor. Prog. Nucl. Energy. 5 (2−6), 347−352.

Gulevich, A., Kalugin, A., Ponomarev, L., Seliverstov, V., Seregin, M., 2008b. Comparative study of ADS for minor actinides transmutation. Prog. Nucl. Energy. 50 (2−6), 347−352.

Gulevich, A.V., Zemskov, E.A., Komlev, O.G., Ponomarev, L.I., 2013. Accelerator-blanket system as Np, Am, Cm incinerator in different NFC closure scenarios. Atomic Energy. 115 (3), 143−155.

Ignat'ev, V., Keronovskii, S., Surenkov, A.I., Shcherbanyuk, O., Manchkha, S., Smirnov, Y., 1984. Heat exchange during the flow of a melt of LiF-NaF-KF fluoride salts in a circular tube. Atomnaya Energia. 57 (2), 123.

Ignatiev, V., Surenkov, A., 2012. Material performance in molten salts. Comprehensive Nuclear Materials. Elsevier, Amsterdam, pp. 221−250.

Ignatiev, V., Surenkov, A., 2013. Alloys compatibility in molten salt fluorides: Kurchatov institute related experience. J. Nucl. Mater. 441 (1−4), 592−603.

Ignatiev, V., Merzlyakov, A., Gorbunov, V., 2003. Physical and chemical properties of molten salt reactor fuel salts. In: Proceedings of ICAPP'03 Conference, Cordoba Spain, May 4−7, 2003.

Ignatiev, V., Feinberg, O., Gnidoi, A., Merzlyakov, V., Smirnov, A., Surenkov, A., 2007. Progress in development of Li, Be, Na/F molten salt actinide recycler&transmuter. In: Proc. ICAPP-2007, May 13−18, Nice, France.

Ignatiev, V., Surenkov, A., Gnidoj, I., Fedulov, V., Uglov, V., Afonichkin, V., et al., 2008. Compatibility of selected Ni-based alloys in molten Li, Na, Be/F salts with $PuF_3$ and tellurium additions. Nucl. Technol. 164 (1), 130−142.

Ignatiev, V., Surenkov, A., Gnidoy, I., Kulakov, A., Uglov, V., Vasiliev, A., et al., 2013. Intergranular tellurium cracking of nickel-based alloys in molten Li, Be, Th, U/F salt mixture. J. Nucl. Mater. 440 (1−3), 243−249.

Ignatiev, V., Feinberg, O., Gnidoi, A., Merzlyakov, A., Surenkov, A., Uglov, V., et al., 2014. Molten salt actinide recycler & transforming system without and with Th-U support: fuel cycle flexibility and key material properties. Ann. Nucl. Energy, Special Issue on MSR and FHR. 64, 408−420.

Ignatiev, V.V., Konakov, S.A., Subbotin, S.A., Zakirov, R.Y., Grebenkin, K.F., 1999. Molten salt reactor technology for separation and transmutation. High Temp. Mater. Processes. 3 (1), 51−66.

Ignatiev, V.V., Merzlyakov, V.A., Subbotin, V.G., Panov, A.V., 2006a. Experimental investigation of the physical properties of salt melts containing sodium and lithium fluorides and beryllium difluoride. Atomic Energy. 101 (5), 822−829.

Ignatiev, V.V., Surenkov, A.I., Gnidoj, I.P., Fedulov, V.I., Uglov, V.S., Panov, A.B., et al., 2006b. Investigation of the corrosion resistance of the nickel-based alloys in fluoride melts. Atomic Energy. 101 (4), 730−738.

Ignatiev, V.V., Feynberg, O.S., Merzlyakov, V.A., 2008. Main experimental results of ISTC#1606 for recycling & transmutation in molten salt systems. In: Proceedings of the Int. Conf. Atalanta-2008, Montpellier, France, May 19−22.

Ignatiev, V., Feynberg, O., Surenkov, A., 2012a. Progress in development of MOSART concept with Th support, Int. Congress on Advances in Nuclear Power Plants, 2. ICAPP, Chicago, pp. 943−952. June 24−28, 2012.

Ignatiev, V.V., Feynberg, O.S., Zagnitko, A.V., Merzlyakov, A.V., Surenkov, A.I., Panov, A.V., et al., 2012b. Molten salt reactors, new possibilities, problems and solutions. Atomic Energy. 112 (3), 157−165.

ISTC Project#1486, 2004. Experimental and Theoretical Justification of the Cascade Scheme of the Subcritical Molten-Salt Reactor for Transmutation of Long-Lived Radioactive Wastes of the Nuclear Fuel Cycle. Final report.

ISTC Task #1606, 2007. Fuels and Fission Products Clean Up for Molten Salt Reactor of the Incinerator Type.

Khokhlov, V., Ignatiev, V., Afonichkin, V., 2009. Evaluating physical properties of molten salt reactor fluoride compositions. J. Fluor. Chem. 130 (1), 30−37.

Kiselev, G.V., 2001. Possibilities for improving electronuclear systems. Atomic Energy. 91 (1), 571−580.

Klimenkov, A.A., Kurbatov, N.N., Raspopin, S.P., Cervinsky, Yu, 1983. The density and surface tension of the molten thorium and lithium fluorides. Proc. Univ. Non-Ferrous Metall. 1, 129−131.

Kolesov, V.F., Guzhovsky, B.Ya, 1994. Increase of the efficiency of an electronuclear transmutator due to the multiple-section of the structure blanket. Atomic Energy. 76 (1), 67−71.

Kolesov, V.F., Khoruzhii, B.Kh, 2000. Neutron characteristics model of a cascade two-section blanket. Atomic Energy. 88 (5), 345−351.

Kolesov, V.F., Shtarev, S.K., Khoruzhij, B.Kh, Zhitnik, A.K., 1995. Efficiency of an electronuclear plant with a fused salt blanket and a neptunium breeding target. Atomic Energy. 79 (1), 450−455.

Kolesov, V.F., Shtarev, S.K., Khoruzhiy, V.Kh., 1997 Transmutation efficiency calculation in the blanket of melted salts with central neptunium target. In: Int. Conf. on Accelerator-Driven Transmutation Technologies and Applications, Las Vegas, 1994, AIP Conf. Proc. vol., 346, Woodburn, New York, pp. 569−574.

Kolesov, V.F., Zavyalov, N.V., Ivanin, I.A., Khoruzhii, B.Kh, Khokhlov, Yu.A., Punin, B.T., et al., 2002. Experimental investigation of models of a the cascade blanket in an electronuclear installation. Atomic Energy. 92 (1), 41−49.

Lizin, A.A., Tomilin, S.V., Gnevashov, O.E., Gazizov, R.K., Osipenko, A.G., Kormilitsin, M.V., et al., 2013a. $PuF_3$, $AmF_3$, $CeF_3$, and $NdF_3$ solubility in LiF-NaF-KF melt. Atomic Energy. 115 (1), 11−17.

Lizin, A.A., Tomilin, S.V., Gnevashov, O.E., Gazizov, R.K., Osipenko, A.G., Kormilitsyn, M.V., et al., 2013b. $UF_4$, $ThF_4$ solubility in LiF−NaF−KF melt. Atomic Energy. 115 (1), 22−25.

Lizin, A.A., Tomilin, S.V., Ignatiev, V.V., Osipenko, A.G., Kormilitsin, M.V., Nezgovorov, N.Yu, 2015a. Joint solubility $PuF_3$ and $CeF_3$ in the ternary melts of the lithium, thorium and uranium fluorides. Radiochemistry. 57 (1), 36−42.

Lizin, A.A., Tomilin, S.V., Naumov, V.S., Ignatiev, V.V., 2015b. Joint solubility of $PuF_3$ and $UF_4$ in a melt of the Li, Na and K fluorides. Radiochemistry. 57 (1), 498−503.

Mel'nik, M.I., Bychkov, A.V., Kormilitsyn, M.V., Ponomarev, L.I., 2003. Cascade subcritical molten-salt reactor (CSMSR) for RW transmutation. The study on solubility of $PuF_3$, $NpF_4$, $AmF_3$ in Molten Fluorides. In: Proc. GLOBAL - 2003 Intern. Conf., New Orleans, USA, 16-20 Nov. 2003, pp. 2218−2221.

Merzlyakov, A., Ignatiev, V., Abalin, S., 2011. Viscosity of molten lithium, thorium and beryllium fluoride mixtures. J. Nucl. Mater. 419, 361−365.

Merzlyakov, A., Ignatiev, V., Abalin, S., 2014. Viscosity of LiF−NaF−KF eutectic and effect of cerium three fluoride and uranium tetrafluoride additions. Nucl. Eng. Des. 278, 268−273.

Mourogov, A., Bokov, 2006. Potentialities of the fast spectrum molten salt reactor concept: REBUS-3700. Energy Convers. Manage. 47, 2761−2771.

Mourogov, V.M., Troyanov, M.F., Shmelev, A.N., 1983. Thorium Using in Nuclear Reactors. Energoatomizdat, Moscow (in Russian).

Naumov, V.S., Bychkov, A.V., Tomilin, S.V., 1996. Interaction of actinide and rare-earth element fluorides with molten fluoride salt and possibility of their separation for ADTT fuel reprocessing. In: Proc. of 2nd Int. Conf. ADTTA, Kalmar, Sweden, June 1996, pp. 1144−1155.

Novikov, V.M., Slesarev, I.S., Alexeev, P.N., 1993. Nuclear Reactors of the Heightened Safety. Energoatomizdat, Moscow (in Russian).

Novikov, V.M., Ignatiev, V.V., Fedulov, V.I., Cherednikov, V.N., 1998. Molten Salt Nuclear Power Installations. Perspectives and Problems. Energoatomizdat, Moscow (in Russian).

Ponomarev, L.I., Fedorov, Y.S., 2015. U-Pu fast molten salt reactor and its fuel cycle. In: Proc. GLOBAL-2015, Sept.20-24, 2015, Paris, France, paper 5336.

Ponomarev, L.I., Seregin, M.B., Michalichenko, A.A., Parshin, A.P., Zagorez, L.P., 2011. Validation of actinide fluoride simulators for studying solubility in fuel salt of molten-salt reactors. Atomic Energy. 112 (6), 417−422.

Ponomarev, L.I., Seregin, M.B., Parshin, A.P., Mel'nikov, S.A., Mihalichenko, A.A., Zagorec, L.P., et al., 2013. Fuel salt for the molten salt reactor. Atomnic Energy. 115 (1), 5−10.

Ponomarev, L.I., Fedorov, Y.S., Miroslavov, A.A., Degtyarev, A.M., 2016. U-Pu fuel cycle of the fast molten salt reactor. Atomic Energy. 121 (1), 51−54.

Seregin, M.B., Parshin, A.P. Kuznetsov, A.Yu, Ponomarev, L.I., Melnikov, S.A., Mikhalichenko, A.A., et al., 2011a. Solubility investigation of actinide tetrafluorides and lanthanide trifluorides in NaF-$ZrF_4$ and LiF-NaF-KF. In: GLOBAL-2011, Dec. 11−16, 2011, Makuhari, Japan, Proc. Paper No. 358885.

Seregin, M.B., Parshin, A.P., Kuznetsov, A.Yu, Ponomarev, L.I., Melnikov, S.A., Mikhalichenko, A.A., et al., 2011b. Solubility study of $UF_4$, $ThF_4$ and $CeF_3$ in the NaF-$ZrF_4$ melt. Radiochemistry. 53 (1), 69−72.

Smirnov, M., Khokhlov, V., Antonov, A., 1979. Viscosity of Molten Alkali Halides and their Binary Mixtures. Nauka, Moscow (in Russian).

Smirnov, M.V., Stepanov, V.P., Khokhlov, V.A., 1974. Density and surface tension of alkali halides and their binary mixtures. J. Phys. Chem. 78 (2), 467−469.

Suglobov, D.N., Yakovlev, R.M., Myasoedov, B.F., 2007. Thorium-uranium fuel cycle for heat and power engineering. Radiochemistry. 49 (5), 441−448.

Vasil'kov, V.G., Gol'danskii, V.I., Dzhelepov, V.P., Dmitrievskii, V.P., 1970. The electronuclear method of generating neutrons and producing fissionable materials. Atomnaya Energia. 29 (3), 151−158.

Volozhin, N.V., Zakirov, R.Ya, Mushnikov, P.N., Subbotin, V.G., Sannikov, I.V., Naumov, S.P., 2013. $CF_3$, $PuF_3$ solubility in LiF-NaF-KF melt. Atomic Energy. 115 (1), 18−21.

Yurevich, V.I., Yakovlev, R.M., Vassilkov, R.G., 2006. Production and multiplication of neutrons in lead targets induced by protons above 1 GeV. Nucl. Instrum. Methods. A562, 747−749.

# 26.16 South Africa

*Wayne Boyes*
Steenkampskraal Thorium Limited, Centurion, South Africa

## 26.16.1 Introduction

Steenkampskraal Thorium Limited (STL), is developing the HTMR-100 (High Temperature Modular Reactor) pebble bed reactor, a high-temperature gas-cooled reactor, graphite moderated, and cooled by forced helium flow. The existing design of the module is to produce high-quality steam which is coupled to a steam-turbine/generator system to produce 35 MW of electric power. The steam can be used in a wide range of cogeneration applications. The reactor is also suitable to provide direct high-temperature energy for process heat. The design of the reactor is based on proven technology and therefore no new basic technology development is needed. The size of the reactor and the fuel cycle were chosen to simplify the design and operation of the module and to facilitate the use of thorium. The approach to small intrinsic safe modular units ensures continuous production, easy road transportability, skid mounted subsystems, a wider range of manufacturers, fast construction, and an enhanced licensing process (Fig. 26.16.1).

## 26.16.2 Target applications

The HTMR-100 is capable of supplying electric power to any distribution grid and to standalone or isolated electricity users. It can be deployed as single modules or multimodule plants as well as for medium-temperature process heat applications. The HTMR-100 is a perfect fit for clients who want to progressively extend their generating capability. The unique safety characteristics make it possible to introduce and construct these plants in non-nuclear countries. First World countries that want to utilize their stock of plutonium for peaceful applications are also markets for HTMR-100 reactors.

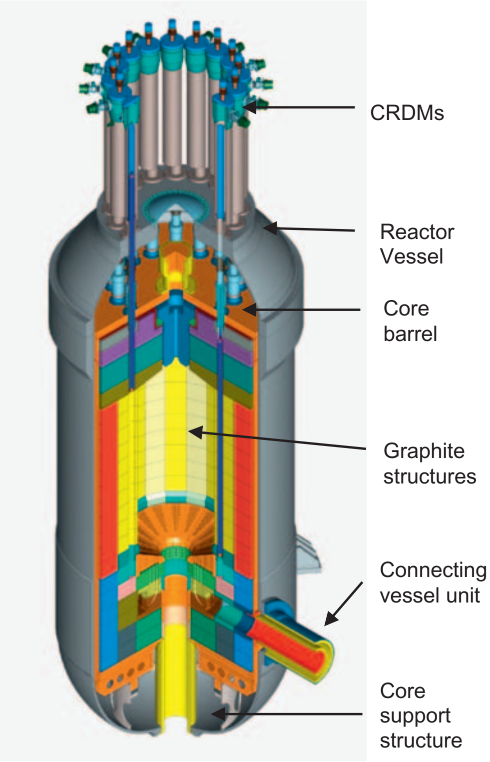

**Figure 26.16.1** Reactor configuration of the HTMR-100.
*Source*: Reproduced courtesy of STL.

## 26.16.3 Development milestones

| | |
|---|---|
| 2012 | Project started |
| 2017 | Preparation for prelicense application |
| 2018 | Conceptual design finished |

## 26.16.4 General design description

### *26.16.4.1 Design philosophy*

The reactor has good load-following characteristics which are needed for standalone (not grid-coupled) applications. The "once through then out" (OTTO) fueling scheme leads to a simple and cost-effective fuel management system. The relative low primary loop pressure requires a thinner-walled pressure vessel and thus an easier manufacturing process, resulting in a wider range of vessel manufacturers.

The HTMR-100 plant design caters for different site and client requirements. It allows flexibility in protection against external events and flexibility in multimodule configuration and power capacity.

### 26.16.4.2 Reactor core and power conversion unit

The reactor unit consists of a steel pressure vessel, a steel core barrel, graphite reflector blocks, neutron absorber rods, rod guide tubes, drive mechanisms, and in-vessel instrumentation. The vessel is designed for 4 MPa pressure.

The graphite structure allows for differential expansion and volumetric changes due to temperature and neutron fluence-induced distortion. This is done to keep the stresses low and minimize primary fluid bypass and leaks. The side, top, and bottom reflector material is nuclear grade graphite (Fig. 26.16.2).

**Major technical parameters**

| **Parameter** | **Value** |
|---|---|
| Technology developer | Steenkampskraal Thorium Limited (STL) |
| Country of origin | South Africa |
| Reactor type | High-temperature gas-cooled reactor (HTGR) |
| Electrical capacity (MWe) | 35 for single module, 140 for four-module plant |
| Thermal capacity (MWth) | 100 for single module |
| Expected availability factor | >95% |
| Design life (years) | 40 full-power years |
| Plant footprint ($m^2$) | 5000 (buildings only) |
| Coolant/moderator | Helium as coolant, graphite as moderator |
| Primary circulation | Forced He circulation |
| System pressure | 4 MPa |
| Main reactivity control mechanism | Absorber rods in the reflector |
| RPV height (m) | 15.3 |
| RPV diameter (m) | 5.9 on flange |
| Coolant temperature, core outlet (°C) | 750 |
| Coolant temperature, core inlet (°C) | 250 |
| Integral design | Yes |
| Power conversion process | Indirect Rankine cycle |
| High-temperature process heat | Yes |
| Low-temperature process heat | Yes |
| Cogeneration capability | Yes |
| Design configured for process heat applications | Yes |
| Passive safety features | Yes |
| Active safety features | Only residual heat removal backed up by passive systems |
| Fuel type | TRISO particles in pebbles: LEU, Th/LEU, Th/HEU, or Th/Pu |
| Fuel size | 60 mm diameter |
| Number of fuel units | ~150,000 pebbles; about 125 pebbles/day throughput |
| Fuel enrichment | Various—see fuel description |
| Fuel burnup (GWd/ton HM) | 80–90 |
| Fuel cycle | Continuous online fuel loading |
| Number of safety trains | No engineered safety train |

(*Continued*)

**(Continued)**

| **Major technical parameters** | |
|---|---|
| **Parameter** | **Value** |
| Emergency active safety functions | None required |
| Residual heat removal systems | Passive and active |
| Maintenance schedule (frequency and outage (days)) | Every 6 years/30 days, 12 years/50 days, mid-life 180 days |
| Distinguishing features | No core meltdown, modular design, reduced construction time, no active engineered safety systems, high-quality steam, reactor upgradable to very high temperature, spent fuel in highly acceptable form, minimal production of tritium, thus ideal for inland sites |
| Modules per plant | One or multiples of two modules |
| Estimated construction schedule (months) | 36 months, based on continuous manufacturing and construction |
| Seismic design | 0.3 g for generic site (0.5 g under consideration) |
| Core damage frequency | Slight damage with water ingress event with design base frequency $<10-4$ per year |
| Design status | Advanced concept phase |

The flow through the core is from top to bottom where the heated gas is collected in a hot plenum. From the plenum the hot gas flows through a connecting pipe to the steam generator. The power conversion system (PCS) uses a helical coil steam-generator unit supplying superheated steam to the turbine. The main system will be supplied as four skid-mounted units, namely the condenser, turbine, gearbox and electric generator. The turbine can be used in a back-pressure configuration or intermediate-temperature steam can be taken off for process heat applications.

### 26.16.4.3 Fuel characteristics and supply

The fuel elements (FE) for the HTMR-100 are 60 mm diameter spheres consisting of a spherical fuel zone of approximately 50 mm diameter, in which the TRISO-coated particles are randomly distributed in the graphitic matrix material. A fuel-free shell of graphite matrix of about 5 mm in thickness is then molded to the fuel zone. The fuel kernel and coatings serve as a fission product barrier in normal and accident operating conditions.

There are various types of fuel that will be used in the HTMR-100 reactor, ranging from LEU $UO_2$ to mixtures of Th/LEU, Th/HEU, and Th/Pu. The following options have already been studied and show to be viable

- LEU: <10% enrichment (7−10 g HM/sphere);
- Th/LEU: various options;
- 50% LEU by mass 20% enrichment, 50% Th (10−12 g HM/sphere);
- 25% LEU by mass 20% enrichment, 75% Th (16−20 g HM/sphere);

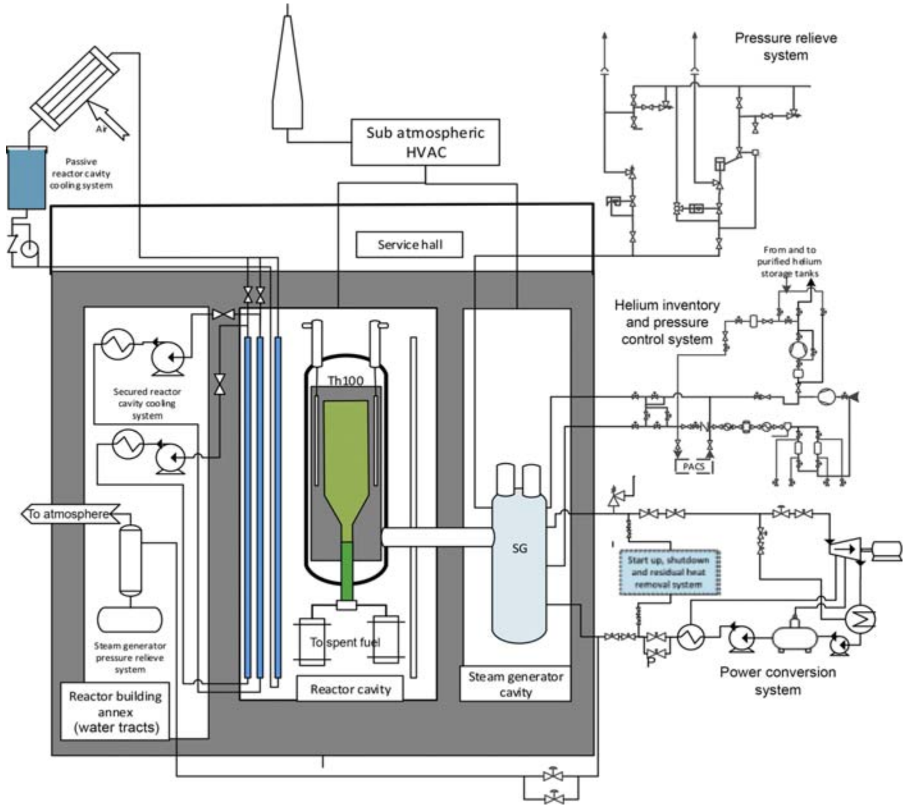

**Figure 26.16.2** Power conversion and main support systems.
*Source*: Reproduced courtesy of STL.

- Th/HEU, 10% HEU by mass 93% enrichment, 90% Th by mass (10−12 g HM/sphere);
- Th/Pu: 15% reactor grade Pu by mass (12 g HM/sphere).

A fuel qualification and test program will be conducted on the fuel prior to loading of the reactor.

The HTMR-100 operates on a much longer burn-up fuel cycle compared to conventional reactors. The nonproliferation characteristic of the OTTO cycle is the extended time the pebbles reside inside the core, making it more difficult to divert partially burnt fuel.

### 26.16.4.4 Fuel handling system

The fuel handling and storage system (FHSS) is a support system to the main power system of the HTMR-100.

A 6-month supply of fresh fuel is kept in the fresh fuel storage facility. New spherical fuel elements (fresh fuel) are loaded by the fuel-loading machine into a charge lock. The charge lock is purged, filled with clean helium, and pressurized to system pressure, before it is opened and fuel is gravity-fed into the core cavity. The charge lock has a physical capacity for approximately one full-power day's fuel sphere inventory.

Spent fuel is removed from the reactor pressure vessel (RPV) by means of two fuel-unloading machines (FUMs), connected to a single reactor defueling chute. Each FUM discharges spent fuel into a discharge lock. The discharge locks have sufficient capacity for a full-power day of spent fuel elements.

Spent fuel, damaged in such a manner that gravity conveyance is compromised, is mechanically separated inside the FUM and accumulated in a dedicated scrap canister, located inside the FUM.

Provision is made in the design of the FHSS for the temporary fitment of activity-measuring devices. These are to be used for the removal of the first core graphite spheres. Separate burn-up measuring devices can also be temporarily installed for core performance and calculational purposes when running fuel composition trials.

During decommissioning the FHSS extracts the last used fuel in the same manner as during normal operation (Fig. 26.16.3).

### 26.16.4.5 Reactivity control

Eighteen neutron absorber rods are provided in graphite sleeves inside the graphite side reflector blocks. The absorber rods can be operated independently as a group or as subgroups, as required by the reactor operating control system. A control rod consists of several rod absorber material segments, pinned together to form articulating

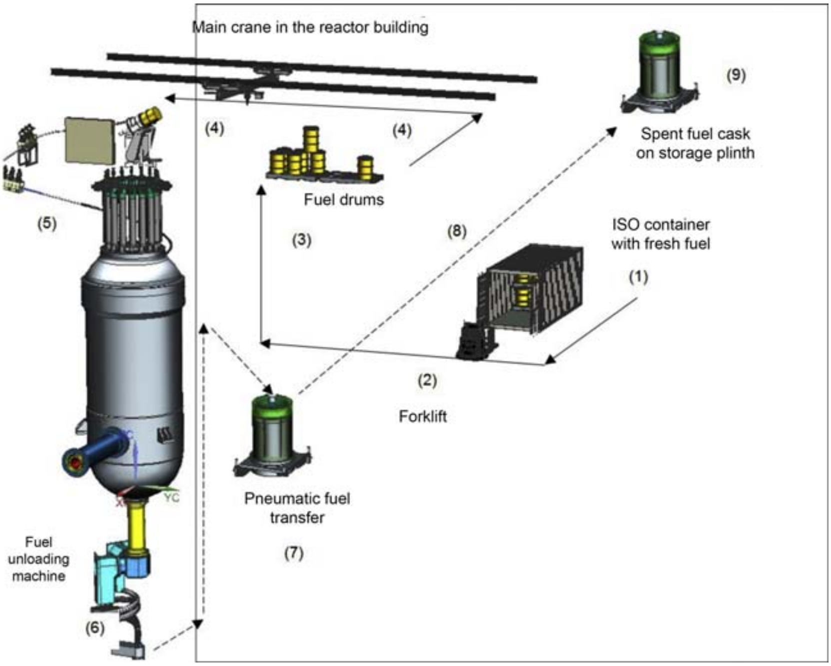

Figure 26.16.3 Fuel handling scheme.

joints. The segments consist of sintered B4C absorber material, sandwiched between an inner and an outer tube segment. The inner tube segment allows cooling helium gas to flow from the top down in the circular channels. Each rod is equipped with a position indicator which measures the position of the rod over its entire positioning range and with position indicators for the upper and lower limit positions.

### *26.16.4.6 Reactor pressure vessel and internals*

The RPV is constructed to the ASME III subsection NB code. It is comprised of two main components:

1. Reactor vessel body;
2. Vessel head which is bolted to the vessel body.

The reactor vessel body consists of several forged ring-components circumferentially welded together.

The core structures consist of the metallic parts and the graphite structures. The function of these internal structures is to provide stable core geometry, neutron reflection, cold and hot gas channeling, fuel element flow, shielding, thermal insulation, and support of the control and shutdown systems guide tubes and the neutron source. The functional design of the structural core internals is such that they are capable of withstanding the steady state and transient loadings during normal operation, anticipated operational occurrences, and design basis accidents.

The shape and structure of the inner side reflector wall and the 30 degrees angled core bottom permit uniform fuel element flow.

The loads borne by the ceramic internals are transferred to the steel core barrel and then to the RPV through metallic components, such as the lower support structure and the core barrel axial and radial supports.

All areas of the core internals are designed for the service life of the reactor. Access for ceramic structure inspections can be done through the fuel-loading channel and the reflector rod holes.

## 26.16.5 Plant safety features

### *26.16.5.1 Engineered safety system configuration and approach*

In principle the plant is designed to perform its safety functions without reliance on the automated plant control system, or the operator. The engineered safety system of the plant has no engineered safety systems in terms of active human or machine intervention to assure nuclear safety.

The low-power density, the large mass of the core structures, the slender core geometry, and the use of materials capable of withstanding high temperatures ensure complete passive residual heat removal capability without exceeding the design limits of components.

Provision for beyond-design basis conditions is made. Beyond-design basis scenarios include the nonfunctioning/noninsertion of all active control and shutdown systems. The reactor core characteristics, e.g., small excess reactivity and strong negative reactivity coefficient with temperature will shut down the reactor and maintain a condition where no damage to the fuel, core structures, and reactor vessel occurs.

Excessive reactivity increases during water or water vapor ingress (increasing moderation) is prevented by designing the reactor for limited heavy metal content of the fuel.

### 26.16.5.2 Reactor cooling philosophy

The reactor cavity cooling system (RCCS) removes heat radiated from the reactor towards the reactor cavity walls. It consists of welded membrane tubes arranged side-by-side on the inside of the reactor cavity wall. Water is circulated through the tubes to form a cold wall. The RCCS is a passive system and consists of three independent cooling trains and is designed for all postulated design basis conditions.

### 26.16.5.3 Containment function

The primary fission product barrier is the TRISO-coated fuel particles, which keep the fission products contained under all postulated events, even if the second barrier (the primary pressure vessel system) and the third barrier (the building filter system) collapse.

## 26.16.6 Plant safety and operational performances

The central consideration is the demand for high availability of process steam supply and/or electricity generation. To reduce or minimize the nuclear steam supply system (NSSS) daily or weekly load changes of the reactor, the preference is to change the ratio between steam supply and electricity supply. Excess steam and/or electricity can be utilized in the desalination plants to provide water as a sellable commodity earning additional revenue. This allows the plant to operate virtually continually at full power very close to the plant availability.

In order to maintain the plant safety and operational performance, specific areas are controlled for human occupation and protection.

## 26.16.7 Instrumentation and control systems

The automation system (ATS) comprises that group of safety and nonsafety C&I systems that provide automated protection, control, monitoring, and human–system interfaces. The following three specific systems in the HTMR-100 system structure define control and instrumentation:

1. *Plant control, data, and instrumentation system*: Provides overall plant control and monitoring. It includes architecture which combines C&I systems and the control room equipment.
2. *Equipment/investment protection system*: Reduce the risk of losing critical or expensive components by maintaining the plant within its normal and safe operating envelope.
3. *Protection system*: Initiates reactor SCRAM to protect against nuclear control failure or loss of primary coolant, etc.

The HTMR-100 ATS architecture implements modern digital C&I designs and equipment. The architecture of the overall automation system is based on redundancy, diversity, separation, and functional and physical independence. This concept includes four levels of defense-in-depth: (1) distributed control system or control system; (2) reactor protection system (RPS); (3) manual shutdown system; and (4) post-event information system.

## 26.16.8 Site and plant layout

The HTMR-100 is configured to simplify the construction of the various buildings and to ensure easy installation of the reactor, steam generator, and handling of spent fuel. The proposed plant layout aims to protect safety-important functions while simplifying operational and maintenance tasks. The plant layout allows for the addition of multiple reactors (and associated equipment) in a compact multimodule fashion.

### *26.16.8.1 Reactor building*

The reactor building contains the safety equipment that provides the necessary functions for the safe shutdown of the reactor under all design basis conditions. The reactor building is partially submerged below ground level such that the reactor and steam generator cavities are completely protected against postulated external threats. The depth can be further adapted to suit the geological conditions of the specific site to provide for the necessary level of seismic protection.

The reactor building, electrical building, and auxiliary buildings are connected by means of underground tunnels, providing protection for interlinked services and it also ensures that spent fuel is never brought above ground level. Provision is made for the storage of all spent fuel produced during the operating life of the plant. The reactor building is seismically designed to withstand a design basis earthquake (DBE) and together with the spent fuel storage bunker, is the only safety-related building structure of the HTMR-100 (Fig. 26.16.4).

### *26.16.8.2 Electrical building*

The electrical building houses the main control and computer rooms, primary and secondary plant security alarm rooms, and provides the primary access facilities for

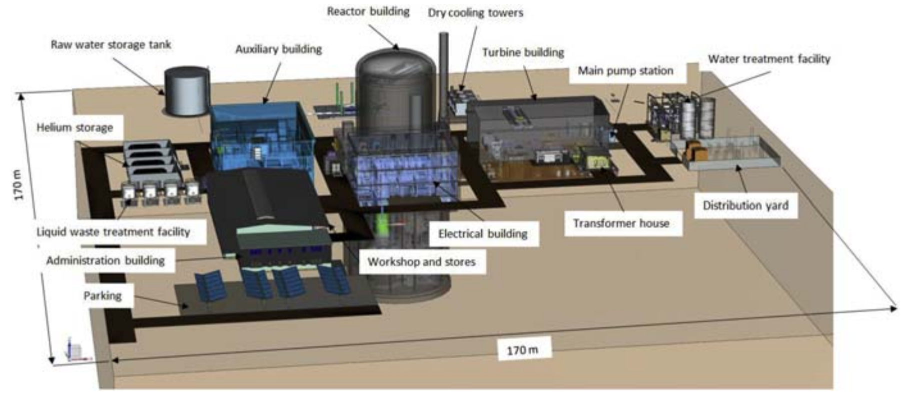

**Figure 26.16.4** HTMR-100 site and plant concept layout.
*Source*: Reproduced courtesy of STL.

the nuclear island and the energy conversion area. This center also provides space for activities associated with plant administration and security services. The plant control, data, and instrumentation system control/display panels and computers are housed in the control room.

### 26.16.8.3 Turbine generator building

The turbine generator building provides the foundation and housing for the PCS, including other support systems such as the compressed air, water sampling, HVAC, voltage distribution systems, permanent 11 kVAC and 400 VAC diesel generator sets, and steam safety valves.

### 26.16.8.4 Balance of plant

The balance of plant consists of the secondary systems and the tertiary systems.

The PCS has one set of isolation valves between itself and the NSSS. The PCS and its major subsystems are of non-nuclear safety class and thus conventional safety class and the product is of a high-quality industrial standard.

### 26.16.8.5 Electric power systems

The electrical power supply system (EPSS) for the single-module HTMR-100 plant supplies power to the plant safety and nonsafety equipment for normal plant operation, start-up, normal shutdown, as well as for accident mitigation and safe shutdown.

The EPSS provides the following voltage levels: 230 VAC, 400 VAC, 11 kVAC, 24/48 VDC, and 250 VDC. The primary voltage of the station feeder transformer is transmission grid dependent and thus site specific.

The majority of plant loads are powered from the main power supply system (MPSS), while all safety-related loads as well as nonsafety-related loads on the nuclear island (NI) portion of the EPSS are powered by the reactor power supply system (RPSS). The RPS and some nonsafety-related loads (i.e., primary blowers 1 and 2, etc.) are powered from the RPSS. A portion of the RPSS circuit (inside the reactor building) is categorized as safety-related (Class 1E).

### 26.16.9 Design and licensing status

Conceptual design is in an advanced stage. The core nucleonic, thermohydraulic, and heat transfer analyses are carried out to optimize the performance and verify the safety analysis. Nuclear regulator engagement is planned for 2017 with the aim of commencing the preassessment for licensing in order to reach design certification status at the end of the concept phase.

### 26.16.10 Plant economics

Since the HTMR-100 is mainly intended to service the needs of isolated geographical areas, it is not meant to compete economically with large (>1 GW) reactors connected to an existing national grid. The HTR SMR comes into its own right when the various combinations of electricity, process heat, and water desalination are considered and holds great promise for the long-term economics of users.

Preliminary capital and operating cost studies indicate that this flexibility of the HTMR-100 provides the most efficient energy to isolated communities and industries. It is well suited to deployment in developing countries with its affordability and Gen IV safety characteristics.

## 26.17 Sweden

*Imre Pázsit*
Chalmers University of Technology, Gothenburg, Sweden

### 26.17.1 Preliminaries

Research in advanced nuclear reactors (such as accelerator-driven systems (ADS) or Gen-IV reactors) has not been very intensive in Sweden. Before the Three Mile Island accident some aspects of fast reactor concepts were tested in critical assemblies at the national research center at Studsvik. After that accident, a national vote (referendum) was held on nuclear energy, which resulted in a recommendation of phasing out nuclear power in the long term. This had the consequence that in the continuation, education, and research into nuclear engineering only obtained funding from the industry (coordinated by the Swedish Centre for Nuclear Technology (SKC)), and the safety authority. For obvious reasons, the activity was restricted to the safety of the existing installations.

Research on ADS and transmutation was started at the Royal Institute of Technology (KTH) in Stockholm, with support from the Swedish Nuclear Fuel and Waste Management Co., as well as from the EU, in the early 1990s. About the same time, Chalmers (Göteborg) and Uppsala joined research on transmutation techniques and Chalmers also participated in FP 4, 5, and 7 projects on ADS.

Regarding Gen-IV systems, the main interest in Sweden lies in lead-cooled fast reactors. In 2009, in the midst of a short hopeful period in the pre-Fukushima era, the Swedish Research council financed a 3-year-long framework project called GENIUS, aimed at research in lead-cooled reactors. All three universities with nuclear engineering faculties (KTH, Uppsala, and Chalmers) participated in the project.

### 26.17.2 MSR kinetics, dynamics, and neutron noise

The Department of Nuclear Engineering at Chalmers University of Technology has long been carrying out research and development work on reactor dynamics and noise diagnostics in co-operation with the nuclear industry (the Ringhals power plant) and the safety authority (the Swedish Radiation Safety Authority). Research on the dynamics and neutron fluctuations in molten salt systems was started in 2008, partly as a PhD research project (Jonsson, 2012). Some of the work was performed with international co-operation, with a visiting professor from CEA Saclay, France. This research is described in Chapter 5, Kinetics, dynamics, and neutron noise in stationary MSRs, hence only a brief summary of the main findings is given here.

In this research, the kinetic behavior of molten salt systems was investigated in simple models, in which analytical or semianalytical solutions can be obtained. This facilitates the insight and understanding of the physics of such systems. A number of characteristics of MSR dynamics were identified and interpreted in comparison with traditional solid fuel systems. It was shown that due to the movement of the delayed neutron precursors, such systems become more tightly coupled from the neutron physics point of view, which manifests itself in their dynamic response. Due to the smaller effective fraction of delayed neutron precursors, the neutron fluctuations induced by perturbations in a critical core have a larger amplitude than in traditional reactors with solid fuel, hence neutron diagnostics might be an effective tool for monitoring and surveillance of such systems. It was also shown that application of the traditional point kinetic approximation, which assumes factorization between the space- and time-dependence, meets difficulties due to the fact that the propagating property of the delayed neutron precursors is in contradiction with factorization.

There was no Swedish technical participation in any of the European MSR projects, but the Division of Nuclear Engineering from Chalmers had a member in the stakeholders' committee of the 3-year-long FP7 Project on the Evaluation of the Viability Of Liquid fuel fast reactor system (EVOL), dedicated to the design of the molten salt fast reactor (MSFR) concept. The EVOL project run between 2011–2013. The Division was also invited to present their research at the CMSNT-2013 (Conference on Molten Salts in Nuclear Technology), January 9–11, 2013, Mumbai, India.

### 26.17.3 Nonproliferation and safeguard aspects of the MSR fuel cycle

Uppsala University has long had research and education activities within nonproliferation and nuclear safeguards of the fuel cycle, initially for light-water reactor systems. They have extended this activity also to the fuel cycle of advanced reactor systems, including molten salt reactors. This research is summarized in Chapter 10, Nonproliferation and safeguards aspects of the MSR fuel cycle. The work concerns the analysis of the whole fuel cycle of an MSR, and the attractiveness of the nuclear materials used; and the vulnerability of the fuel cycle is compared to the case of light-water reactors. As is demonstrated, the fuel cycle of the MSR contains a number of challenges, as compared to the already-existing and proven technologies, due to the differences and the lack of operating experience. There are both advantages (high-energy gamma radiation of one of the daughter nuclides, as well as low fuel inventory) and disadvantages (a continuous material stream, easier divertible compared to discrete fuel rods, on-line refueling and reprocessing, fuel residence outside the core, and finally the good suitability of U-233 for constructing simple gun-type bombs). The conclusion is that significant work remains to be done and experience to be gained to improve and secure the proliferation resistance of the MSR fuel cycle.

### 26.17.4 Thorium research

In 2006, the largest Swedish nuclear utility Vattenfall, together with the Norwegian privately owned company Thor Energy, initiated a feasibility study of various thorium systems. The focus was on reactor types that were either already on the market or perceived to be ready for commercialization within the next 10–15 years. Parts of the study were carried out by researchers within Vattenfall, some parts were carried out at Swedish universities, and some parts were subcontracted to researchers in other countries. The research performed at the Swedish universities included two MSc thesis projects involving neutronic simulations, one focusing on the nuclear design and evaluation of a BWR with four different variants of thorium-based fuel (Insulander Björk, 2008) and the other involving similar simulations but for a PWR (Liu, 2008). The feasibility study did not indicate any showstoppers for the use of thorium in any of the investigated systems. Based on the study, Vattenfall decided not to engage more with thorium fuel, whereas Thor Energy decided to proceed with irradiation testing of thorium-based oxide fuel with plutonium as a fissile component (Th-MOX). An irradiation test rig was loaded in the Halden research reactor in 2013, comprising Th-MOX pellets and also some uranium oxide fuel with thorium added as a minor component.

As a further consequence of the feasibility study, Thor Energy, with the support of the Norwegian Research Council, sponsored an industrial PhD project at the Division of Nuclear Engineering at Chalmers, which involved neutronic simulations of the usage of Th-MOX fuel in BWRs and PWRs, as well as analysis of the data from the test irradiation and related thermal-mechanical simulations of the fuel material (Insulander Björk, 2015). In parallel, another PhD project was performed at the Division of Nuclear Engineering at Chalmers, on the feasibility of using thorium in PWRs, funded by the Oskarshamn Power plant and Vattenfall (Lau, 2014). The origin of this project was that some sponsoring members of the Swedish Centre for Nuclear Technology expressed interest in knowing more about the thorium cycle and research in India in this respect. In this study, the main focus was the use of thorium as a minor component in uranium oxide fuel, which was proven to provide some benefits, in particular with regards to power-peaking factors.

This concept attracted the interest of Thor Energy, which was the reason why a fuel material typical for this application was included in the irradiation test rig in the Halden research reactor. Some simulations were also performed by Thor Energy on the neutronic merits of thorium as an additive to uranium oxide fuel in BWRs (Insulander Björk, 2015), and several different fuel materials typical for this application were loaded in a second test rig in 2015, together with other uranium-based fuel types with different additives for improving fuel performance.

## 26.17.5 The chemistry of the thorium cycle with a view to MSR

At the Department of Nuclear Chemistry at Chalmers the specialty has for a long time been the chemistry of the fuel cycle from mining to final repository, including separation for transmutation. In this context several processes based on aqueous reprocessing have been developed mainly for uranium- and uranium/plutonium-based fuels. One of the reasons for this is that the nuclear chemistry laboratory at Chalmers is one of very few in the world that can handle all chemical elements present in spent nuclear fuel in reasonable amounts. Thus, advanced fuels such as (Pu, Zr)N and minor actinide-bearing oxides can also be manufactured (the first pure PuN pellet in the world was made here in 2015).

For thorium fuels the fabrication is rather straightforward. The choice of starter nuclide is naturally pivotal for the choice of facility to work in. Today there are several choices for such a starter, e.g., $^{239}$Pu, $^{233}$U, or $^{235}$U. In the latter cases $(U,Th)O_2$ fuels have been prepared at Chalmers by the powder-mixing route. However, as the percentage of the starter increases or if the fuel is used for minor actinide burning, other production routes, e.g. the dust-free sol-gel may be used. This technique is also used in the Chalmers laboratories.

The recycling of thorium-based fuels is a major challenge, as is discussed in the literature. The conclusion is that for normal Th-based fuel the U and the Th will be recycled for further use, while the remaining elements will be vitrified. The separation process is rather simple and can be tested at Chalmers. However, the actual dissolution of the thorium fuel is not as simple, due to the very high stability of $ThO_2$ (which makes it ideal for direct storage without recycling). So far, the dominating suggested route has still been the $HF/HNO_3$-based THOREX dissolution. More novel methods exist but have not been tried industrially or in pilot plant scale.

In the case of the MSR, laboratories exist with the capability to develop processes based on the uranium and thorium fuel cycles. In essence this means that an MSR fuel simulate can be made mimicking any stage of the operational cycle. This salt can then be used for separation studies in batch processes. No equipment for continuous processes exists. In principle the methods that potentially can be used for MSR cycles are:

1. Physical methods with fractionated distillation or sublimation and crystallization as well as methods of liquid—liquid extraction and distribution in immiscible molten metals and molten salts;
2. Chemical methods such as cyclic oxidation and reduction methods using chemical and electrochemical processes.

Depending on fuel type, i.e., uranium- or thorium-based, these methods may be more or less suitable. However, for practical reasons, the preferred techniques at Chalmers would be electrochemical separation from the molten salt or molten salt/molten metal extractive separation. The present equipment is placed in a glove box with possibilities to control the main atmosphere as well as the oxygen potential, etc. This equipment is shown in Fig. 26.17.1.

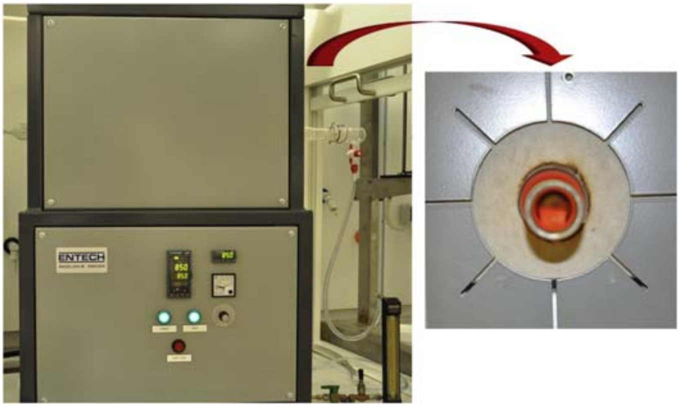

**Figure 26.17.1** The pyrochemical glove box at the nuclear chemistry laboratory at Chalmers.

## 26.17.6 Research into heat and mass transfer in molten salts

Extensive studies into natural convection in molten salt pools (Sehgal et al., 1998; Gubaidullin, 2002; Gubaidullin & Sehgal, 2002) have been completed at the Division of Nuclear Power Safety at the Royal Institute of Technology in Stockholm, with primary interest in severe accident research. A series of experiments employing eutectic and noneutectic salt mixtures in a $NaNO_3$-$KNO_3$ system were performed in the SIMECO facility (Fig. 26.17.2). Tests with stratified molten pools with two and three unmixable layers were carried out to study and develop heat transfer models for molten pools undergoing a miscibility gap. The heat-focusing effect of a metal layer atop of the molten salt pool was investigated experimentally.

Advanced numerical models were elaborated and tested, which enable quantitative analysis of a two-layer salt-stratified system in a wide range of flow regimes, including flow instabilities and turbulent effects. The turbulent characteristics inherent to the convection at Rayleigh numbers of interest were obtained by direct numerical simulation (DNS). The results were compared against experimental data. The underlying physics of the flow characteristics was explained, and the shortcomings of existing turbulence models were pointed out.

Currently the studies are extended to more refractory NaCl-$BaCl_2$ salt systems and pure aluminum or aluminum—silicon alloy unmixable layers. The research is conducted within the European research program Horizon-2020 in the framework of the IVMR project. Small-scale experiments on material compatibility and tests of different heating methods were performed (Fig. 26.17.3). A new large-scale SIMECO-2 facility is under construction to study both steady-state and transient behavior of molten salt pools. The experimental results and the numerical

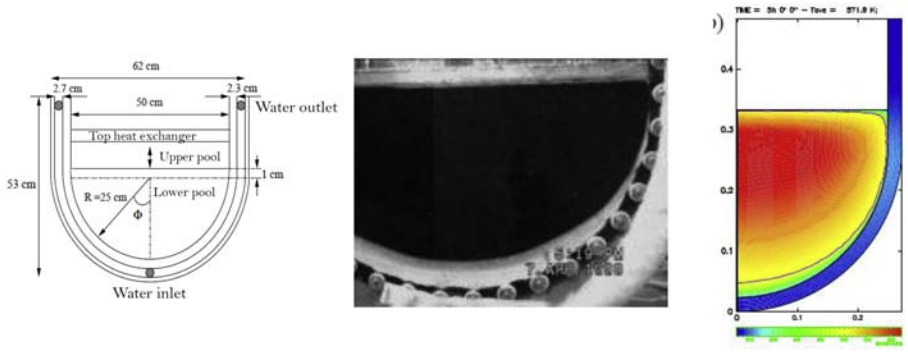

(A) (B) (C)

**Figure 26.17.2** Schematics of the test section of the SIMECO facility (A), view of the test section in an experiment with a single-layer molten pool of $NaNO_3$-$KNO_3$ (B), and temperature distribution computed with MVITA code developed at NPS/RIT by Bui (C).

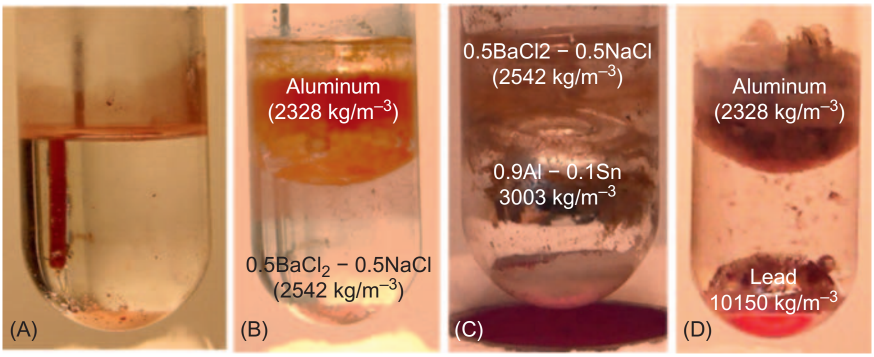

**Figure 26.17.3** Molten pool behavior of (NaCl-BaCl$_2$)/Al system: Single layer pool of NaCl-BaCl$_2$ (A), two-layered pools with top and bottom locations of metal (B, C), and three-layer pool (D).

simulation methods developed will also benefit the research in and construction of a wide spectrum of molten salt systems.

# References

Gubaidullin, A.A., 2002. Natural convection heat transfer in two-fluid stratified pools with internal heat sources. Doctoral Thesis, January 21, 2002.

Gubaidullin, A.A., Sehgal, B.R., 2002. An estimate of the crust thickness on the surface of a thermally convecting liquid-metal pool. Nucl. Technol. 138, 90–92.

Insulander Björk, K., 2008. Nuclear design of a thorium fueled light water reactor. MSc Thesis, CTH-NT-215. Winner of the national Polhem Prize for best M.Sc. thesis in 2009.

Insulander Björk, K., 2015. Thorium fuels for light water reactors. Steps towards commercialization. Ph.D. Thesis, Chalmers University of Technology. Co-winner of the national Sigward Eklund Prize for best Ph.D. thesis in 2015.

Jonsson, A., 2012. Neutronics in reactors with propagating perturbations. Ph.D. thesis, Chalmers University of Technology, CTH-NT-256.

Lau, C.W., 2014. Improved PWR core characteristics with thorium-containing fuel. Ph.D. Thesis, Chalmers University of Technology, CTH-NT-285. Co-winner of the national Sigward Eklund Prize for best Ph.D. thesis in 2015.

Liu, C., 2008. Design and neutronic evaluation of thorium fuel in pressurized water reactors. M.Sc. Thesis, Royal Institute of Technology, TRITA-FYS 2008:05.

Sehgal, B.R., et al., 1998. SIMECO experiments on in-vessel melt pool formation and heat transfer with and without a metallic layer. In: Proc. OECD/CSNI Workshop on “In-Vessel Core Debris Retention and Coolability”, Germany, p. 205.

# 26.18 Switzerland

*Jiří Křepel*[1], *Sergii Nichenko*[1], *Boris Hombourger*[1,2],
*Andreas Pautz*[1,2] *and Michael Prasser*[1,3]
[1]Paul Scherrer Institute (PSI), Villigen, Switzerland, [2]Laboratory for Reactor Physics and Systems Behaviour, EPFL Lausanne, Switzerland, [3]Laboratory of Nuclear Energy Systems, ETH Zürich, Switzerland

## 26.18.1 Introduction

Switzerland is a member of the Generation IV International Forum (GIF). In 2015, the GIF general framework agreement, as well as the Swiss participation in GIF, was extended for another 10 years. Switzerland, through its representative the Paul Scherrer Institut (PSI), was traditionally involved in high-temperature reactor (HTR) and gas-cooled fast reactor (GFR) research. However, participation in the GFR system was terminated and Switzerland joined the GIF MSR project on November 20, 2015.

The MSR-related research was launched at the Nuclear Energy and Safety (NES) division of PSI at the end of 2012. Nonetheless, there was historically already some research effort in the field of chloride salt-based MSRs at the predecessor of PSI, the Eidgenössisches Institut für Reaktorforschung (EIR), in the 1970s (Taube et al., 1978). The recent activities were initiated at the Laboratory for Reactor Physics and System Behaviour (LRS) and related mainly to the fuel cycle in thorium–uranium-fueled MSRs (Fiorina et al., 2013; Křepel et al., 2013). Later the development of two different approaches for MSR transient analysis was launched based on the coupled system code TRACE-PARCS (Kim, 2015; Zanetti et al., 2015) and OpenFOAM high-fidelity solver GeN-Foam (Fiorina et al., 2015, 2016; Fiorina and Mikityuk, 2015). Currently, four laboratories of NES are already partly involved in MSR research and, for instance, the chemical thermodynamic study of mixed fluoride salt systems with the PSI in-house code GEMS was launched. PSI is one of the SAMOFAR consortium members and it belongs to the research institutions working intensively on MSR development.

## 26.18.2 Motivation and main research areas

One of the NES missions is to maintain excellence in nuclear engineering and to provide an attractive working area for future generations of scientists and engineers. Innovative research projects represent an important asset to ensure successful recruiting of a highly motivated and efficient workforce in the coming years. Furthermore, the NES strategy calls for a new project at the department level that attempts to consolidate the research efforts of all NES labs towards a holistic consideration of safety of an innovative reactor concept, which led to the choice of MSR.

MSR has a potential for high resources utilization, low waste production, and risk reduction with the exclusion of severe accidents. It may fulfill the "low-waste, low-risk" requirement of the broad public towards a better acceptance of nuclear energy generation in the future. Furthermore, since MSR operates at low pressure and since both the safety approach and the fuel cycle may be potentially simplified, in the long term it may become cheaper than current or planned nuclear reactors.

The safety of MSR, as the key point and main interest of NES, cannot be evaluated without knowing the system design, fuel chemistry, salt thermal-hydraulics features, safety and fuel cycle approach, and the relevant material and chemical limits. Not all of these issues will be addressed at PSI; however, there are several NES competences related to thermal and fast solid fuel reactors which are planned to be extended to the MSR analysis. These activities can be grouped into four topical areas:

1. Core design and fuel cycle;
2. Fuel behavior at nominal and accidental conditions;
3. Transient behavior and decay heat removal system;
4. Safety, fuel stream, and relevant limits.

All these activities are interconnected and safety represents the central point of interest (see Fig. 26.18.1). At the same time, the structure is proposed so that there are research topics which can be independently studied within each of the groups.

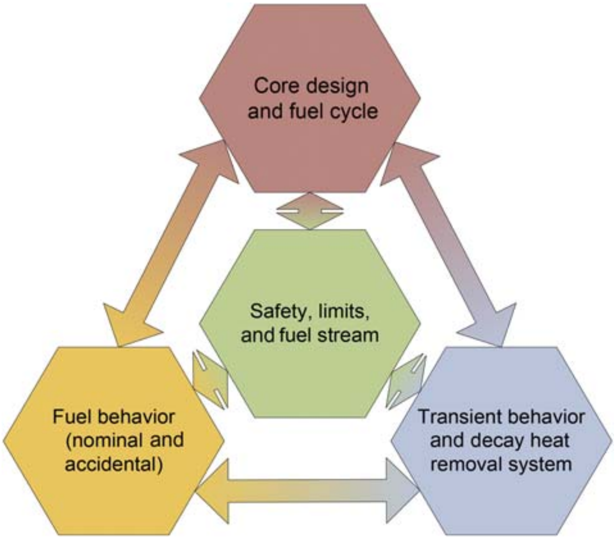

**Figure 26.18.1** Illustration of four research areas and their interdependency.

### 26.18.3 Related national and international projects

In 2012, PSI joined as an observer of the 4-year EU FP7 project on the Evaluation of the Viability Of Liquid fuel fast reactor system (EVOL), dedicated to the design of the molten salt fast reactor (MSFR) concept. Since 2015, the PSI has participated in the EVOL follow-up project. It is a 4-year Horizon 2020 project entitled Safety Assessment of the MOlten salt FAst Reactor (SAMOFAR) dedicated to innovative MSFR safety features. The contribution of PSI ranges from reactor physics to chemistry, as well as preliminary severe accident modeling and risk assessment.

In 2014, the Swiss National Science Foundation (SNF) financed a PhD study “Small Modular Molten Salt Reactor Designing for Low Waste Production” for a 3-year PhD project, which started in April 2014. SNF approved another 3-year PhD grant related to MSRs in 2015 with the title “Data Assimilation Methods for Reactor Physics Design and Safety Calculations of Molten Salt and High Temperature Reactor Cores.”

In May 2015 a 2-year research project dedicated to HTR and MSR “Feasibility and plausibility of innovative reactor concepts in a European electricity supply environment” was launched. It is financed by the Project and Study Fund of the Electricity Industry (PSEL) of the Association of Swiss Electricity Producers (VSE), Swiss electricity grid operators (swiss*electric*), and ETH Zurich.

For the chemistry of molten salts it is relevant that in 2008 PSI joined as a partner of the 4-year FP7 Project “Actinide recycling by SEParation and Transmutation” (ACSEPT). The project lasted until 2012 and in its framework the HERACLES database for the PSI in-house chemical thermodynamics modeling code GEMS was created. In 2013 PSI joined the 3-year FP7 follow-up project “Safety of ACtinide SEparation proceSSes” (SACSESS), which lasted until 2016. The PSI contribution focused on Mo and MgO behavior in LiCl-KCl salts and on the behavior of actinide fluorides in LiF-$AlF_3$ salts.

### 26.18.4 Core design and fuel cycle

The core design and fuel cycle-related activities at PSI focus on the identification of MSR designs appropriate for sustainable energy production and simultaneously limiting the waste production and granting high levels of safety. The work plan is based mainly on the SNF PhD study and the PSEL project. It is divided into two main phases. The initial and ongoing phase is a parametric study evaluating major design options such as salts, moderators, feed materials, fuel cycle, core layout, etc. The second phase objective is to identify a reactor design out of the choices from the parametric studies. It is foreseen to use criteria for selection such as: dimensions, materials lifetime, fissile inventory, etc. The main design criterion is, nonetheless, the neutron economy. Excellent neutron economy should enable both breeding of fissile fuel from fertile nuclides ($^{232}$Th or $^{238}$U) and reduction of legacy and own waste volume. The pivotal tool for related simulations is the PSI in-house equilibrium closed cycle routine EQL0D (Hombourger et al., 2015a, 2016). This is a MATLAB script coupled with the Monte-Carlo code SERPENT capable of

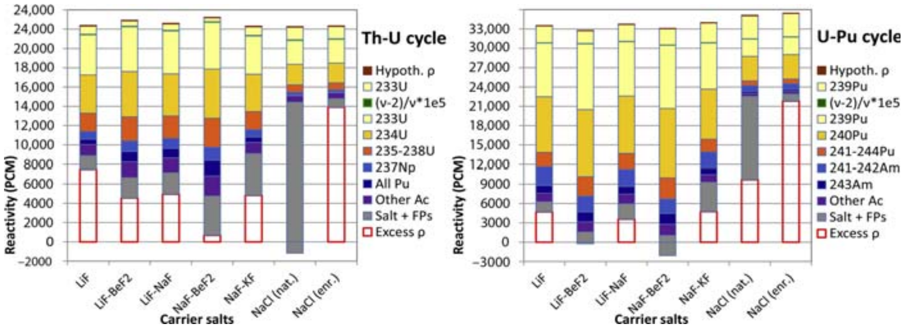

**Figure 26.18.2** Excess reactivity in infinite media for Th-U (left) and U-Pu (right) fuel cycles and selected carrier salts. The difference between excess and hypothetical reactivity (for zero parasitic capture) is isotope-wise breakdown into actual components of parasitic capture.

simulating continuous reprocessing; for instance, removal of gaseous fission products (FPs) from the MSR core.

The performance of fast spectrum MSR was evaluated for several selected carrier salt compositions including both fluoride and chloride salts: $^{7}LiF-BeF_2$, $^{7}LiF$, $^{7}LiF-NaF$, $NaF-BeF_2$, NaF-KF, NaCl, and $Na^{37}Cl$. The labels $^{7}Li$ and $^{37}Cl$ indicate assumption of isotopic enrichment. These carrier salts were mixed with the fuel salt to form an eutectic mixture with lowest melting point. Both U-Pu and Th-U fuel cycles were evaluated using EQL0D by means of the equilibrium closed cycle excess reactivity $\rho$ for infinite medium. To provide further insight major contributors to the parasitic neutron capture were identified (see Fig. 26.18.2).

The highest reactivity excess and so the best performance in both fuel cycles was provided by $Na^{37}Cl$ carrier salt. Its tremendous reactivity excess in the U-Pu cycle can even enable the use of a breed-and-burn fuel strategy (Hombourger et al., 2015b). The best performance from the fluoride carrier salts was $^{7}LiF$, the reference carrier salt of the SAMOFAR project. It was used for several fuel cycle studies. A parametric spectral study at equilibrium cycle and at full core level was accomplished with an ERANOS-based EQL3D procedure (Křepel et al., 2013). A hybrid spectrum MSR core was evaluated (Křepel et al., 2014a), the simplified reprocessing scheme assessed (Křepel et al., 2014b), and the continuous and batchwise reprocessing schemes compared in Křepel et al. (2015).

## 26.18.5 Fuel behavior at nominal and accidental conditions

MSR fuel behavior at nominal and accidental conditions can be analyzed by the thermochemistry of molten salts. The variety of possible salt composition calls for a tool able to predict physical and thermodynamic properties of a wide range of mixtures. The PSI in-house open-source Gibbs Energy Minimization Software (GEMS) (Kulik et al., 2004–2014) thus may play a vital role (see Fig. 26.18.3).

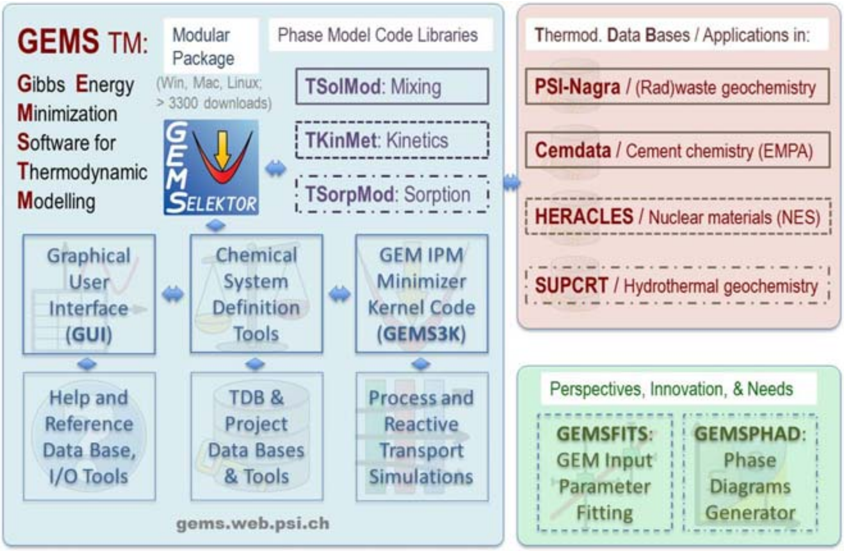

**Figure 26.18.3** Structure of the collaborative project GEMS (Kulik et al., 2015).

The PSI activities grouped in this area are financed via the EU projects ACSEPT, SACSESS, and SAMOFAR, and through an internal MSR project.

The utmost interest for safety evaluations is the physical properties pertaining to accidental conditions such as phase changes (freezing or boiling). Moreover, the behavior of specific fission products such as $^{99}$Mo can be of interest for medical isotope production. The GEMS code with the extended HERACLES database (Shcherbina et al., 2012) can be applied to model the above-mentioned MSR thermodynamic properties. GEMS has a modular and flexible database and user interface built around an efficient open-source GEMS3K numerical kernel code (Kulik et al., 2013) for solving phase equilibria in complex nonideal systems that can be coupled with transport- or multiphysics codes. It has been developed at NES since 2000 under the lead of D.A. Kulik.

GEMS3K also contains a TSolMod code library (Wagner et al., 2012) with >25 state-of-the-art mixing models for aqueous, gaseous, and solid solutions and melts. This gives GEMS a broad applicability to various types of materials, e.g., fused salts, if extended with the necessary datasets for phases and their components. The input thermodynamic functions and interaction parameters of mixing are kept in the database and consistently extended, as required. The accomplished and planned tasks in this topical area are:

- Thermodynamic modeling of salt melts. Mo behavior in alkali chloride melt (LiCl-KCl) was studied based on its speciation in the selected melts and standard Gibbs energies of different species (Nichenko and Streit, 2015).

- Molecular dynamics (MD) application to MSR chemistry. MD and DFT simulations will be used to provide novel data for improvement/extension of a thermodynamic database of the key MSFR fuel systems including $PuF_3$ and $ThF_4$. Properties that will be simulated are, for instance, specific heat, melting behavior, and diffusion coefficients.
- GEMS modification for MSR applications, thermodynamic database HERACLES extension with relevant data and models of fused salts and their mixtures to enable the GEMS for efficient simulations of their thermodynamic properties and processes.
- Extension of GEMS by a GEMSPHAD module for generating and plotting phase diagrams; amendments of GEMS3K kernel for efficient coupling with OpenFOAM.

Optionally, the results obtained by the GEMS code can be employed for precipitation and vaporization simulation under accidental conditions with the in-house code Parallel SImulator of BOILing (PSI-BOIL) (Niceno et al., 2010). It can simulate the solidification process of single crystals, and assess the feasibility of vaporization or freezing methods in the purification of waste salts. Similar simulations have already been carried out in Badillo and Beckermann (2006) and Badillo (2015), where a phase-field model was used to predict the morphology and concentration distribution around a growing crystal.

The information on excess Gibbs energy for binary systems together with the information on thermophysical properties of pure compounds can be used to study complex systems. Such an approach allows to study the speciation in selected melts, and to determine the standard Gibbs energies of various species in melts. The information on standard Gibbs energies is used to assess the standard chemical potentials of different species melts, as well as for constructing the E-p$O^{2-}$ stability diagrams, such as those developed for Mo in LiCl-KCl (Fig. 26.18.4; Nichenko and Streit, 2015). Among the stable Mo species in the LiCl-KCl system in this case are: $MoCl_3$, $MoO_2$, and $MoO_3$. Higher chlorides and oxychlorides are unstable and thus are not present in the melt. This information can support an experimental study on CERMET fuel electrochemical reprocessing in the presented melts.

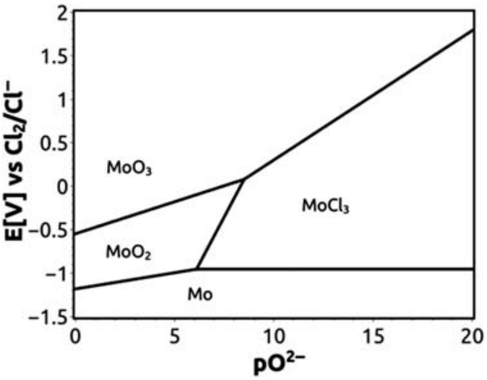

**Figure 26.18.4** The E-p$O^{2-}$ diagram for the Mo-O-Cl system in LiCl-KCl eutectic at 750K.

## 26.18.6 Transient behavior and decay heat removal system

The activities grouped in this topic are based on MSc and PhD studies. They are financed through the NES internal MSR project and EU projects SAMOFAR. The development of two different approaches for MSR transient analysis was launched. They are based on the coupled system code TRACE-PARCS (Kim, 2015; Zanetti et al., 2015) and on the OpenFOAM high-fidelity solver GeN-Foam (Fiorina et al., 2015, 2016; Fiorina and Mikityuk, 2015). MSR thermal-hydraulics is peculiar from several points of view:

- The liquid fuel is acting at the same time as a coolant.
- The solid moderator, if used, is cooled by the liquid fuel.
- The delayed neutron precursors drift with the salt flow.
- The heat from fast-decaying fission products is spatially distributed in the salt.
- The heat from slower-decaying fission products is equally distributed in the salt volume.
- Since the salt is volumetrically heated, the bulk salt temperature has a different meaning for the heat exchange with solid walls than in the classical case.

These features make the simulation of MSRs a very interesting research topic. There are only a few available codes which can simulate several of these peculiarities. Especially, the heat exchange between volumetrically heated liquids and solid surfaces is a scientifically challenging issue, which can have a strong relevance to safety. The accomplished and planned tasks in this topical area are:

- Salt properties inclusion in the TRACE code and pre-evaluation of the heat exchangers (Ariu, 2014).
- TRACE-point kinetics modification for delay neutron precursors drift (Zanetti et al., 2015).
- TRACE-PARCS modification for delay neutron precursors drift and its application to MSRE transients (Kim, 2015).
- Assessment of decay heat distribution in the fuel stream (Choe, 2015).
- Development of GeN-Foam solver for OpenFOAM field solver (Fiorina et al., 2015, 2016; Fiorina and Mikityuk, 2015) and GeN-Foam modification for delay neutron precursors drift.
- In the frame of semester work, the GeN-Foam solver was applied to various simplified layouts of fast MSR geometries in 2015 (Bao, 2015).
- In 2016, two MSc studies were planned and one PhD study was due to be launched. The GeN-Foam solver and the TRACE-PARCS coupled code should be applied to the molten salt reactor experiment (MSRE) and MSFR.
- Other planned tasks may cover molten salt instrumentation (Doppler velocimetry), refined thermal-hydraulics design of the core and DHR system, and possibly also derivation of a new Nusselt number formula for volumetrically heated liquids.

As an example of the TRACE-PARCS application, the response of the MSRE core at 1 MW power level to a 24 pcm reactivity insertion (adopted from Zanetti et al., 2015) is shown in Fig. 26.18.5. The power increase after the insertion is relatively strong; however, the average salt and graphite temperatures at the end of the

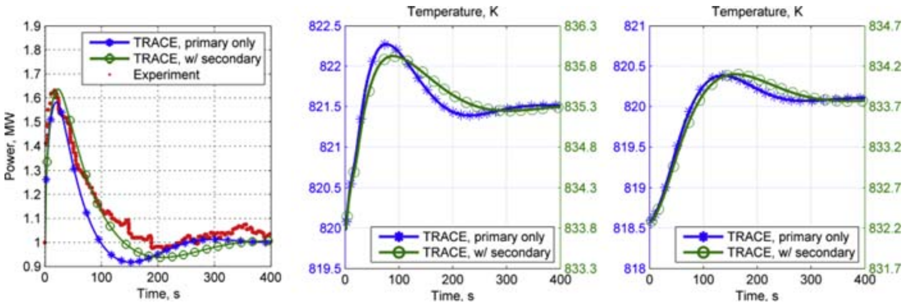

**Figure 26.18.5** Response of the MSRE core at 1 MW power level to the 24 pcm reactivity insertion: power (left), average salt temperature (center), and average graphite temperature (right).

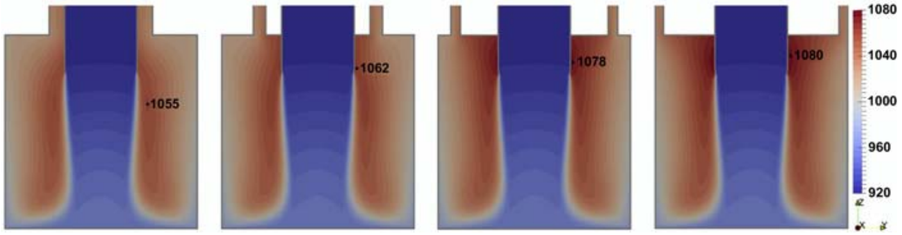

**Figure 26.18.6** Temperature distribution for MSR layout with central "cold jet" and four different locations of the outlet pipe.

transient are only slightly increased. Furthermore, the power stabilizes to the original level. Another illustrative result (Bao, 2015) shows in Fig. 26.18.6 a basic parametric study related to a cold jet-driven MSR. It was assumed that the cold salt in the center of the core can have a stronger reactivity value and thus that it can be used more efficiently to control the power. Four different locations for the salt outlet have been evaluated from the maximal temperature point of view. Generally, it was concluded that the impact of spatial temperature distribution on the reactivity is low and does not provide strong advantages.

## 26.18.7 Safety, fuel stream, and relevant limits

The evaluation of MSR safety should be the main long-term aim of the NES division. It is a very broad topic and the other three research areas should thus provide key inputs to support it. Since MSR safety strongly depends on the fuel treatment, the design and safety evaluation of the off-gas system and reprocessing unit may belong here. MSR safety is also strongly design-dependent and only few general studies can be accomplished without knowledge of the detailed design.

One of these tasks could be aerosol formation and migration in the containment atmosphere. Fission products may be present there, either in the gas phase or as aerosols. They undergo transformations depending on the concentration of the different species as well as the containment temperature and pressure. The formation of aerosols from the gas phase species will be calculated taking into account the formation by homogeneous and heterogeneous nucleation and growth by condensation, coagulation, and agglomeration (Bosshard et al., 2013). Transport of aerosols will be simulated based on the containment thermal-hydraulic conditions and deposition on the walls and other structures will be estimated. The transport of gas-phase species will be assessed based on available models implemented in severe accident codes. As a result, the source term in the containment will be assessed.

Another example is the simplified level-3 Probabilistic Safety Assessment (PSA). This will be applied to MSR to address the consequences of a hypothetical accident in the nuclear energy chain. At the core of this activity is PSI's Energy-related Severe Accident Database (ENSAD). For background information and more details on the simplified PSA employed compare the report of the EU project NEEDS (Burgherr et al., 2008).

### 26.18.8 Summary

Switzerland, and especially the NES division of PSI, is involved in many research areas related to MSR and it is a member of the SAMOAR project consortium. Safety is the key point and the main long-term interest of the MSR research at NES. At the current stage, the program focuses on several specific and independent studies in four research areas.

## References

Ariu, V., 2014. Heat Exchanger Analysis for Innovative Molten Salt Fast Reactor (M.Sc. thesis). EPFL ETHZ joint MSc. in Nuclear Engineering, Switzerland.

Badillo, A., 2015. Quantitative phase-field modeling for wetting phenomena. Phys. Rev. E. 91, 033005.

Badillo, A., Beckermann, C., 2006. Phase-field simulation of the columnar-to-equiaxed transition in alloy solidification. Acta Mater. 56, 2015.

Bao, J., 2015. Assessment of MSR with Cold Jet at the Core Center. Semester work, EPFL ETHZ joint MSc. in Nuclear Engineering, Switzerland.

Bosshard, C., et al., 2013. Large eddy simulation of the differentially heated cubic cavity flow by the spectral element method. Comput. Fluids. 86, 210–227.

Burgherr, P., Hirschberg, S., Cazzoli, E., 2008. Final report on quantification of risk indicators for sustainability assessment of future electricity supply options. NEEDS Deliverable no D7.1 – Research Stream 2b. NEEDS project "New Energy Externalities Developments for Sustainability", Brussels, Belgium.

Choe, J., 2015. Empirical Decay Heat Correlation and Fission Product Behavior in MSR (M.Sc. thesis). EPFL ETHZ joint MSc. in Nuclear Engineering, Switzerland.

Fiorina, C., Mikityuk, K., 2015. Application of the new GeN-Foam multi-physics solver to the European Sodium Fast Reactor and verification against available codes. In: Proceedings of ICAPP 2015. May 03-06, 2015, Nice, France, Paper 15226.

Fiorina, C., et al., 2013. Investigation of the MSFR core physics and fuel cycle characteristics. Prog. Nucl. Energy. 68 (2013), 153−168.

Fiorina, C., et al., 2015. GeN-Foam: a novel OpenFOAM® based multi-physics solver for 2D/3D transient analysis of nuclear reactors. Nucl. Eng. Des. 294 (2015), 24−37.

Fiorina, C., et al., 2016. Development and verification of the neutron diffusion solver for the GeN-Foam multi-physics platform. Ann. Nucl. Energy. 96, 212−222.

Hombourger, B., et al., 2015a. Parametric lattice study of a graphite-moderated molten salt reactor. J. Nucl. Eng. Rad. Sci. 1, 011009.

Hombourger, B., et al., 2015b. Fuel cycle analysis of a molten salt reactor for breed-and-burn mode. In: ICAPP 2015. May 03-06, Nice, France.

Hombourger, B., et al., 2016. The eql0d procedure for fuel cycle studies in molten salt reactors. In: ICAPP 2016. April 17-20, San Francisco, USA.

Kim, H., 2015. Static and Transient Analysis of Molten Salt Reactor Experiment Using Serpent/TRACE/PARCS Codes (M.Sc. thesis). EPFL ETHZ joint MSc. in Nuclear Engineering, Switzerland.

Křepel, J., et al., 2013. Fuel cycle advantages and dynamics features of liquid fueled MSR. Ann. Nucl. Energy. 64, 380−397.

Křepel, J., et al., 2014a. Hybrid spectrum molten salt reactor. In: Physor 2014. Kyoto, Japan, September 28−October 3.

Křepel, J., et al., 2014b. Molten salt reactor with simplified fuel recycling and delayed carrier salt cleaning. In: Icone 22. July 7−11, 2014, Prague, Czech Republic.

Křepel, J., et al., 2015. Comparison of several recycling strategies and relevant fuel cycles for molten salt reactor. In: ICAPP 2015. May 03-06, Nice, France.

Kulik, D.A., Dmytrieva, S.V., Miron, G.D., Leal, A.M.M., Wagner, T., Kosakowski, G., et al., 2015. GEMS: Gibbs energy minimization software for geochemical modeling.

Kulik, D.A., Dmytrieva, S.V., Wagner, T., Kosakowski, G., Thoenen, T., Berner, U., et al., 2004−2014. Gibbs Energy Minimization Software (GEMS). <http://gems.web.psi.ch>.

Kulik, D.A., Wagner, T., Dmytrieva, S.V., Kosakowski, G., Hingerl, F.F., Chudnenko, K.V., Berner, U., 2013. GEM-Selektor geochemical modeling package: revised algorithm and GEMS3K numerical kernel for coupled simulation codes. Comput. Geosci. 17, 1−24.

Niceno, B., Sato, Y., Badillo, A., Andreani, M., 2010. Multi-scale modeling and analysis of convective boiling: towards the prediction of CHF in rod bundles. Nucl. Eng. Technol. 42 (N 6), 620−635.

Nichenko, S., Streit, M., 2015. Thermodynamic modelling of molybdenum behaviour in chloride molten salt. In: Proceedings of TopFuel2015. 13−17 September 2015, Zurich, Switzerland.

Shcherbina, N., Kivel, N., Günther-Leopold, I., Kulik, D.A., Bertsch, J., 2012. HERACLES project and thermodynamic database. <http://www.psi.ch/heracles/heracles>.

Taube, M., et al., 1978. Fast Reactors Using Chloride Salts as Fuel, Final Report (1972−1977). EIR-Bericht Nr. 332. Eidgenössisches Institut für Reaktorforschung, Würenlingen, Switzerland.

Wagner, T., Kulik, D.A., Hingerl, F.F., Dmytrieva, S.V., 2012. GEM-Selektor geochemical modeling package: TSolMod library and data interface for multicomponent phase models. Can. Mineral. 50, 1173−1195.

Zanetti, M., et al., 2015. Extension of the FAST code system for the modelling and simulation of MSR dynamics. In: Proceedings of ICAPP 2015. May 03-06, 2015, Nice, France, Paper 15226.

# 26.19 Turkey

*L. Berrin Erbay*
Eskişehir Osmangazi University, Eskişehir, Turkey

## 26.19.1 Goals

Nuclear studies were started in Turkey in 1955, after agreement between the Republic of Turkey and the United States of America for cooperation in the field of research in the peaceful uses of atomic energy was approved. The Turkish Atomic Energy Commission (TAEK) was established in 1956 and a 1 MW swimming pool type of research reactor was established at Küçük Çekmece, İstanbul. Studies of uranium and thorium exploration and research in Turkey come under the responsibility of the Mineral Research and Exploration Institute (MTA), which was founded by M. Kemal Atatürk in 1935 (Erbay, 1985a). MTA established a pilot plant beneficiation plant for the production of yellow cake and to educate qualified personnel in 1974 (Erbay, 1985b).

The exploration studies continued up to the end of 1990, and 9129 tons of uranium reserve were determined (MENR, 2016). The thorium resources have already been confirmed at about 380,000 tons reasonably achievable and 500,000 additional tons were estimated, totaling 880 kton. Turkey has about 21.4% of the world total. The first nuclear power plant (NPP) in Turkey, Akkuyu NPP, is under construction, for which the investment cost is about 20 billion dollars.

The Ministry of Energy and Natural Resources (MENR) strategic plan for 2015−19 goals are to:

1. Deploy indigenous and renewable energy sources at the maximum level;
2. Support the reduction of energy intensity;
3. Use nuclear energy in electricity generation;
4. Minimize waste and environmental impacts of the energy;
5. Reach a competitive energy system, strengthening the country's strategic position in international energy trade (MENR, 2016).

The coordinators for objective 4 are the Nuclear Energy Project Implementation Department (NEPUD) and the General Directorate of Energy Affairs (EIGM). The Turkish Atomic Energy Authority (TAEK), Electricity Generation Company (EUAS), Turkish Electricity Transmission Corporation (TEIAS), and Energy Market Regulatory Authority (EPDK) are the responsible bodies.

The performance indicators for this objective are:

- Completion of electricity transmission lines for Akkuyu NPP by the end of 2018;
- Start-up of Akkuyu NPP for electricity generation (test generation);
- Start-up of construction for Sinop NPP;
- Determination of the field for the third NPP in line with technical, economic, and environmental criteria;

- The initiation of prefeasibility and investment preparations;
- The completion of studies for the determination of investors;
- Determination of domestic uranium and thorium resources;
- Determination of the domestic nuclear industry policy based on these sources;
- Preparation of a road map by the end of 2019.

Objective 11 in goal 2 is about domestic uranium and thorium resources that shall be explored and developed for fuel in NPPs. Under the coordination of NEPUD, the General Directorate of Mining Affairs (MIGEM), General Directorate of Mineral Research and Exploration (MTA), and ETI Maden General Directorate (ETI MADEN) are the responsible bodies (MENR, 2016). The completion of reserve determination studies of uranium and thorium resources and the preparation of production feasibility studies will be completed by the end of 2019.

Investigations of molten salt reactors and thorium are reported in the literature by individual researchers at universities in Turkey. The interests of academicians have been directed toward the theoretical scientific studies. Generally, thorium as an additive fuel has been considered through neutronic calculations, and some systems such as heat exchangers have been studied.

An extensive study carried out by Energy Frontiers (ITMSF, 2016) with international contributions including L. Berrin Erbay, considers the thorium molten-salt nuclear energy synergetic system (THORIMS-NES). Furukawa et al. (Erbay et al., 1994; Furukawa et al., 1994, 1995, 2008, 2011, 2012; Erbay, 1997, 2012a; Furukawa and Erbay, 1997, 2010) described THORIMS-NES as a symbiotic system which is based on the thorium—uranium-233 cycle; the energy is produced in molten-salt reactors and fissile U-233 is produced by spallation in a breeder accommodated in regional centers.

## 26.19.2 THORIMS-NES and FUJI

The thorium molten salt nuclear energy system (THORIMS-NES) is a radically different fuel cycle concept which departs from current fuel cycles:

1. It uses a liquid fuel instead of solid fuel elements;
2. It uses thorium instead of uranium as the fertile element to breed the fissile isotope U-233;
3. It separates the nuclear power production from the nuclear fuel breeding by proposing a simple thorium molten salt reactor (Th-MSR) devoted exclusively for energy generation by burning initially U-235 or Pu-239 and eventually U-233;
4. It proposes an accelerator molten salt breeder (AMSB) devoted exclusively to the production of fissile U-233;
5. It will incorporate fuel reprocessing in regional centers.

It is a “symbiotic” system with each function optimized by its simplicity. The THORIMS-NES concept includes a planned timetable beginning with the construction of the mini FUJI, a 10 MWe small power reactor, whose purpose is to recover the know-how that the Oak Ridge National Laboratory (ORNL) obtained in 1964—69 with the molten salt reactor experiment (MSRE).

The rational thorium breeding fuel-cycle system called THORIMS-NES (thorium molten-salt nuclear energy synergetics) can reduce the quantity of transuranium elements and recycling fuels produced by all kinds of military, research, and industrial reactors. A system for the realization of THORIMS-NES has been introduced by the explanation of relations between facilities. The status of groups working on Th and the Th fuel cycle has been summarized. The development and launching of THORIMS-NES requires the following three programs during the next three decades (Erbay et al., 1994; Furukawa et al., 1994, 1995, 2008, 2011, 2012; Furukawa and Erbay, 1997, 2010; Erbay, 1997, 2012a):

1. Pilot-plant: miniFUJI (7−10 MWe);
2. Small power reactor: FUJI-Pu (100−300 MWe);
3. Fissile producer: AMSB for globally deploying THORIMS-NES.

The replacement of the present fossil fuel industry by a fission industry needs to be achieved in the next 30−50 years. The fission industry should grow with a 5−7-year doubling time. Such a growth rate will never be achieved by any kind of classical "fission breeding power station" concept. Now a symbiotic system coupling fission with spallation (or D/T fusion, but not yet proven) should be considered, because fission is energy-rich but neutron-poor, and spallation is energy-poor but neutron-rich (Furukawa et al., 2011). The new fission−spallation coupled energy technology should be sufficiently safe to eliminate the chances of a "severe accident."

A new, more simplified, highly efficient, economical, and safe molten salt nuclear power station (MSR) named FUJI is presented, initially constructed from the smaller reactor mini FUJI (Furukawa et al., 2008). The energy is produced in molten-salt reactors (FUJI) and fissile U-233 is produced by spallation in accelerator molten-salt breeders (AMSB). FUJI is size-flexible, and can use all kinds of fissile material, achieving a nearly fuel self-sustaining condition without continuous chemical processing of fuel salt and without core-graphite replacement for the life of the reactor. The AMSB is based on a single-fluid molten-salt target/blanket concept. Several AMSBs can be accommodated in regional centers for the production of fissile U-233, with batch chemical processing including radioactive waste management. The FUJI reactor and the AMSB can also be used for the transmutation of long-lived radioactive elements in the waste, and it has a high potential for producing hydrogen fuel in molten-salt reactors (Furukawa et al., 2008). This system uses the multifunctional "single-phase molten-fluoride" circulation system for all operations. There are no difficulties relating to "radiation-damage," "heat-removal," and "chemical processing" owing to the simple "idealistic ionic liquid" character of the fuel.

## 26.19.3 Stirling engines

Power generation by the Stirling heat engine with molten salt reactors has been proposed and examined by Erbay (1999). In the standard designs of MSRs, the classical steam cycle is considered for the heat removal system. In her study, the steam-turbine is replaced with a Stirling heat engine. The hot molten-salt fuel transfers heat through a heat exchanger (HX) which constitutes the heater (hot-end head) of the

Stirling engine. The flexibility in size of MSRs makes the use of a Stirling engine possible instead of the salt/steam cycle. The special properties of the small molten-salt nuclear reactors and the available designs for Stirling heat engines have been presented to yield the present capacities and the possibility of an MSR–Stirling combination has been discussed (Erbay, 1999). The proposed MSR–Stirling system yields a good match for power production from the nuclear source, and therefore gains higher public acceptance than other nuclear systems, with little maintenance.

The standard design of FUJI-series molten-salt reactors is completed with the supercritical steam-turbine for electric generation with a thermal efficiency of around 45%. On the other hand a Stirling (Str) engine works on the principle of closed operating chambers, necessities long life designs with minimum maintenance and requires high temperatures for high efficiencies. When a small MSR is used as a continuous high-temperature heat source, the combined system turns out to be a prosperous closed power-producing system. A dish Str engine with a directly illuminated tube-type receiver has been considered in the figures in which the receiver is replaced with an HX (Erbay, 1999).

The figures of merit for the proposed MSR–Str combination are summarized as follows (Erbay, 1999):

1. The pressure of the system is maintained as low as possible throughout the plant. In the standard design the steam turbine pressure is around 30 MPa. To maximize power, Stirling engines typically operate at pressure in the range of 5–20 MPa, which is lower than that of a standard steam cycle. The achievable temperature is higher in the proposed Str.
2. The system maintenance and operation are simple and practical, as the Stirling engine is a single closed unit.
3. The flexibility of the power size is ensured by using parallel Stirling engine sets in the proposed system.
4. The MSR–Str combination utilizes MSR benefits:
   a. Reduced radiation damage in the liquid molten-salt fuel and blanket
   b. Physicochemical behaviors of molten salts have high predictability
   c. The configuration of the reactor is a simple tank
   d. The fuel handling is easy
   e. There is no core melt down accident;
5. The system directly imports the advantages of Stirling engines, which are the most efficient heat engines, closed operating systems, operate quietly, and require little maintenance.
6. The proposed system constitutes an almost completely closed power unit, since the MSR has self-sustaining fuel characteristics without continuous fuel processing, and the Stirling engine is also a single unit with a closed cycle.

The MSR–Str combination merits further development for stationary electricity-generating plants. The plant thermal performance is limited by the molten-salt fuel outlet temperature. The required molten-salt fuel outlet temperature depends on the working fluid type of the Stirling heat engine. He gas is chosen as the working fluid. The thermal cycle can be considered as a single loop for initial designs, with the possibility of a two-loop cycle (Erbay, 1999). As the power level increases, the intense radioactivity of the fuel requires the use of a secondary loop. When the

MSR−Str combined system has two loops, the primary loop exchanges heat with molten-salt coolant flowing in the secondary loop. In previous studies, the coolant salt in the secondary loop was NaF-$NaBF_4$ (8−92 mol%). When low power levels of Str heat engine designs are considered, a single loop is sufficient.

Since the power level of the MSR is dictated by the heat transfer rate and fuel is removed outside the reactor by circulation, the design of the hot-end head HX has particular importance (Erbay, 1999). The heater should have a low volume in order to minimize the hold-up of fuel salt. Therefore a counterflow compact U-tube arrangement is preferred (Erbay, 1999). A large heater head has been replaced by the proposed system with a specialized compact HX. Helium, the working fluid of the Stirling heat engine, flows inside the tubes of the heater HX and the molten-salt fuel flows through the shell-side due to the possibility of fission product deposition. Fouling of the tube walls by fission products should be examined seriously. The heater is designed to provide good drainage to avoid the accidental freezing of the molten-salt fuel.

The analysis of alternative combinations for the conceptual design of a power plant consisting of a molten-salt nuclear reactor (MSR) and Stirling engine has been discussed by Erbay (2001).

The system has the following problems to be studied in detail (Erbay, 2001):

1. The oscillatory nature of the flow in the heater-head affecting the flow of the liquid in the secondary loop;
2. Radioactivity of the fluid fuel flowing in the primary loop;
3. Heat exchanger sizing for preventing the hold-up problem;
4. Heater-head design as a heat exchanger for the flows of a molten-salt (Flibe) and He gas working in the engine;
5. The present power limit of Stirling engines;
6. U-233 production as a fuel for the molten-salt nuclear reactor.

## 26.19.4 Heat exchangers

The design of the heat exchanger offers solutions for the FUJI—Th-MSR as a safe reactor (Erbay, 2012b). The design methodology already developed for normal fluids can be applicable to FUJI. For molten salts flowing in the mini-microchannels the flow still can be considered as Newtonian; and Navier-Stokes equations can be applicable by considering the Knudsen number (Erbay, 2012b). The ASME Boiler and Pressure Vessel Codes and Standards of Tubular Exchanger Manufacturers Association (TEMA) are applicable to HXs. The compact arrangements can help reduce the fuel and salt inventory, but the problems of thermal expansion may intensify (Erbay, 2012b). A careful vision is established by considering the decrease in the flexibility of mechanical design. The FUJI system pressure is lower than 0.5 MPa. The FUJI reactor vessel and all mechanical components in contact with the molten salts use Hastelloy N and graphite.

The fundamental design methods are summarized by Kaçar and Erbay (2013). Thermodynamic analysis of an HX is presented in terms of irreversibilities and entropy generation. The irreversibilities are important for HX optimization (Yılmaz et al., 2013). The effect of internal temperature crossing on the heat transfer and entropy generation is examined by tackling the 1−2 TEMA-J shell-and-tube HX (Yılmaz et al., 2013). The effect of the inlet temperature of the cold fluid on the thermal performance of two minichannel flat-tubes with multilouvered fin compact HXs has been studied experimentally by Doğan and Erbay (2016).

In general, studies carried out by researchers have the purpose of thorium utilization in a hybrid reactor or a symbiotic system due to environmental concerns as well as to energy economics.

## 26.19.5 Fusion−fission hybrid reactors and nonproliferation

The potential of a moderated fusion−fission hybrid reactor fueled with $ThC_2$ or $ThF_4$ is investigated by Yapıcı et al. (2000) assuming a plant factor (PF) of 75% under a first wall fusion neutron current load of 5 $MW/m^2$. LWR (light water reactor) fuel rods containing $ThC_2$ or $ThF_4$ are placed in the fissile fuel zone of the hybrid reactor. The behavior of the neutronic is observed for 4 years. At the end of the operation period, the cumulative fissile fuel enrichment (CFFE) values varied between 3.55% and 7% depending on the fuel and coolant type. Yapıcı et al. (2000) indicated that the best neutronic performance is obtained with FliBe, followed by air and natural lithium coolants; after 48 months, the maximum CFFE value is 7% in the $ThF_4$ fuel and FliBe coolant mode, and the lowest CFFE value 3.55% is in the $ThC_2$ fuel and natural lithium coolant mode. Consequently, these enrichments would be sufficient for LWRs, and the lowest radial neutron leakage out of the blanket is with the FLiBe coolant modes.

In a thorium fusion breeder the production of denaturated fissile fuel by mixing the fertile fuel with natural-$UO_2$ and LWR spent nuclear fuel has been investigated by Şahin et al. (2001). Four different coolants (helium, Flibe, natural lithium, and $Li^{17}Pb^{83}$ eutectic) are considered. In order to obtain a power flattening in the fissile-fertile zone, the $UO_2$-fraction or the spent fuel fraction in the mixed oxide (MOX) fuel has been gradually increased in radial direction. Power plant operation periods between 13 and 29 months are evaluated. Şahin et al. (2001) concluded that the U-238 component of natural-$UO_2$ can provide a limited proliferation hardening only for the U-233 component, whereas, the homogeneous mixture of $ThO_2$ with a small quantity of ($>$4%) LWR spent nuclear fuel remains nonproliferational for both uranium and plutonium components.

Şahin et al. (2002) have performed a neutronic analysis for a thorium fusion breeder to burn minor actinides and to produce U-233, Pu-238, Am-242, and Cm-245 for spacecraft application. Natural lithium has been selected as the fuel zone coolant. Minor actinides from 5 to 10 units of LWRs per meter of blanket height have been mixed with $ThO_2$. This has significant advantages with respect to plant operation and uniform utilization of the nuclear fuel in the fissile zone. A neutronic analysis has been performed by Şahin et al. (2004) to assess a prospective utilization of light-water reactor (LWR) spent fuel in deuterium uranium reactors mixed with thoria ($ThO_2$), hence to open the extended utilization of worldwide disposed spent nuclear fuel from CANDU reactors.

Yapıcı and Bayrak (2005) have studied how to denature nuclear weapon-grade plutonium in a thorium fusion breeder. Ten fuel rods containing a mixture of $ThO_2$ and $PuO_2$ are placed in the radial direction in the fissile zone where $ThO_2$ is mixed with variable amounts of $PuO_2$ to obtain a quasiconstant nuclear heat production density. The plutonium composition volume fractions in the fuel rods are gradually increased from 0.1% to 1% in 0.1% increments. The fissile fuel zone is cooled with the four coolants with a volume fraction ratio of 1. Yapıcı and Bayrak (2005) noted that the energy multiplication factor M changed between 2.1731 and 6.6241 depending on coolant type during the operation period.

Some quantities of plutonium have been accumulated in the nuclear waste of civilian LWRs and CANDU reactors. Şahin et al. (2006) indicated that reactor-grade plutonium can be used as a booster fissile fuel material in the form of mixed $ThO_2/PuO_2$ fuel in a CANDU fuel bundle, in order to assure reactor criticality. They investigated the prospects of exploiting the rich world thorium reserves in CANDU reactors. In the study two different fuel compositions were selected for investigations: (1) 96% thoria ($ThO_2$) + 4% $PuO_2$ and (2) 91% $ThO_2$ + 5% $UO_2$ + 4% $PuO_2$. The latter is used for the purpose of denaturing the new $^{233}U$ fuel with U-238. They observed the behavior of the reactor criticality $k_\infty$ and the burn-up values of the reactor during full-power operation for $> \sim 8$ years; the reactor starts with $k_\infty = \sim 1.39$ and decreases asymptotically to values of $k_\infty > 1.06$, which are still tolerable and useable in a CANDU reactor. The reactor criticality $k_\infty$ remains nearly constant between the fourth and seventh years of plant operation, and then, a slight increase is observed thereafter, along with a continuous depletion of the thorium fuel. After the second year, the CANDU reactor begins to operate practically as a thorium burner; very high burn-up can be achieved with the same fuel ($>$160,000 MW D/MT). The reactor criticality would be sufficient until a great fraction of the thorium fuel is burned up, provided that the fuel rods could be fabricated to withstand such high burn-up levels. Fuel fabrication costs and nuclear waste mass for final disposal per unit energy could be reduced drastically.

A new fusion reactor APEX uses a liquid wall between the fusion plasma and the solid first wall for either tritium breeding or energy transfer. This liquid wall also allows using high neutron wall loads and reduces the radiation damage at the first wall to obtain high performance for the reactor. High quality of fissile fuel U-233 production has been studied by Übeyli and Yalçın (2008) to get an additional improvement in APEX. This can be obtained by using salts containing fissionable isotopes as a liquid wall in fusion blankets with respect to energy multiplication and fissile fuel breeding.

For a new reactor type, a so-called fixed bed nuclear reactor (FBNR), Şahin et al. (2009) investigated prospective fuels including Th with respect to reactor criticality. The reactor criticality has lower values with uranium fuel, and there is increased production of minor actinides, reactor-grade plutonium, and weapon-grade plutonium, as expected.

A pebble bed modular reactor (PBMR) was also considered for different fuels including thorium compounds. Acır and Coşkun (2012) have investigated the time evolution of criticality and burn-up grades of the PBMR for reactor-grade plutonium and minor actinides in the spent fuel of LWRs mixed with thoria. First the plutonium–thorium and minor actinides–thorium ratios were determined using the initial $k_{\text{eff}}$ value of the original uranium fuel design. Then the time-dependent neutronic behavior of the reactor-grade plutonium and minor actinides and original fuels in a PBMR-400 reactor was calculated. The core lives for the original, the reactor-grade plutonium/thorium, and the minor actinide/thorium fuels were calculated by Acır and Coşkun (2012) at ~3.2, ~6.5, and ~5.5 years, whereas the corresponding burn-ups came out to be 99,000, ~190,000, and ~166,000 MWD/T, respectively, for an end of life $k_{\text{eff}}$ set equal to 1.02.

Different types of nuclear fuels including thorium have been studied in a gas turbine-modular helium reactor (GTMHR). Şahin and Erol (2012) have considered two different types of nuclear fuels acquired from the reactor operations combined with thorium, and also considered a GTMHR. Performances were compared with the uranium fuel designed for this reactor. Nuclear fuels are 50% $ThO_2$–50% $RGrPuO_2$ and 10% $ThO_2$–90% $RGrPuO_2$ uranium (original) fuel. Operation time (i.e., the time passed until the $k_{\text{eff}}$ value reached a level of 1.02 for original fuel), MA, 50% $ThO_2$–50% RGrPu and 10% $ThO_2$–90% RGrPu mixtures were found by Şahin and Erol (2012) to be 515, 565, 765, and 2315 days with burn-up values of 47.7, 71.94, 75.1, and 213.4 GWd/MTU, respectively.

Lawrence Livermore National Laboratory studied a laser inertial confinement fusion fission energy (LIFE) hybrid fusion–fission nuclear energy system to generate power and burn nuclear waste. Şahin et al. (2014) investigates the main parameters of a LIFE-driven thorium breeder. A blanket similar to the LIFE engine design is chosen in order to allow mutual feedback between the two geographically separated teams towards a more advanced and improved design with independent views. $ThO_2$ has been suspended in the form of microsize tristructural-isotropic (TRISO) particles in the lithium coolant for U-233 breeding. The blanket energy multiplication $M$ increases with thorium volume fraction, namely as $M = 1.2206$, 1.2322, 1.2426, 1.2536, 1.2636, 1.3112 for respective TRISO volume fractions due to the contribution of fission energy. Fissile fuel productions in the blanket were calculated as 17.23, 33.09, 48.66, 64.21, 79.77, and 159.71 $^{233}U$ (kg/year), respectively, by Şahin et al. (2014).

Accelerators can be used to produce fissile isotope U-233 from thorium. Şahin et al. (2015) have analyzed the integral U-233 and $^{239}Pu$ breeding rates, neutron multiplication ratio through (nxn)- and fission-reactions, heat release, energy multiplication, and consequently the energy gain factor in infinite size thorium and uranium as breeder material in accelerator driven systems (ADS). The irradiation is supplied by a 1-GeV proton source. Fissile fuel material production is calculated as 53 $^{232}Th$(n,g) U-233, 80.24 and 90.65 $^{238}U$(n,g) $^{239}Pu$ atoms per incident proton, respectively. They noted that the neutron spectrum maximum is by ~1 MeV and lower energy neutrons $E < 1$ MeV have a major contribution to fissile fuel material breeding (>97.5%), where as the share on energy multiplication is negligible (0.2%) for thorium, depleted uranium.

## References

Acır, A., Coşkun, H., 2012. Neutronic analysis of the PBMR-400 full core using thorium fuel mixed with plutonium or minor actinides. Ann. Nucl. Energy. 48, 45–50.

Doğan, B., Erbay, L.B., 2016. Experimental analysis of the effect of cold fluid inlet temperature on the thermal performance of a heat exchanger. J. Therm. Eng. 2 (1), 583–592.

Erbay, L.B., 1985a. Uranium deposits and possible uranium resources of Turkey. J. Eng. Fac. Anadolu Univ. 2, 163–173.

Erbay, L.B., 1985b. Nuclear fuel element production facilities in Turkey. J. Eng. Fac. Anadolu Univ. 2, 101–109.

Erbay, L.B., 1997. Thorium deposits and related studies in Turkey. In: The International Conference on Thorium Molten—Salt Reactor Development LA.

Erbay, L.B., 1999. Examining the power generation by the Stirling heat engine combined with the molten—salt reactor. In: International Symposium ECOS'99, pp. 429–434.

Erbay, L.B., 2001. A discussion for the MSR—stirling power system. In: IECEC'01 36th Intersociety Energy Conversion Engineering Conference, IECEC2001-CT-19.

Erbay, L.B., 2012a. The future of nuclear I: fuel cycles and thorium in the memory of Furukawa. In: III. International Conference NuRER 2012, p. 106.

Erbay, L.B., 2012b. Knowhow of Th-MSR heat exchange system. In: 11th International Conference on Sustainable Energy Technologies.

Erbay, L.B., et al., 1994. From Turkish point of view: THORIMS-NES. In: International Symposium on All Aspects of Energy in the 21st Century, pp. 150–158.

Furukawa, K., Erbay, L.B., 1997. A proposal for rational thorium usage: THORIMS—NES. In: I. National Nuclear Fuel Technology Symposium, ÇNAEM 2, pp. 475–484.

Furukawa, K., Erbay, L.B., 2010. A study on a global scale symbiotic thorium breeding fuel cycle. In: Proceedings of the 2nd International Conference on Nuclear and Renewable Resources NURER 2010, July 4–7, 2010, pp. 255–261.

Furukawa, K., et al., 1994. Clean and safe nuclear energy. J. Eng. Mach. 35, 410.

Furukawa, K., et al., 1995. Rational Pu-disposition for $^{233}$U-production by THORIMS-NES. IAEA—TECDOC. 840, 169–181.

Furukawa, K., et al., 2008. A road map for the realization of global-scale thorium breeding 3 fuel cycle by single molten-fluoride flow. Energy Convers. Manage. 49 (7), 1832–1848.

Furukawa, K., et al., 2011. New sustainable secure nuclear industry based on thorium molten-salt nuclear energy synergetic (THORIMS-NES). Nuclear Power—Deployment, Operation and Sustainability. InTech, Rijeka, Croatia.

Furukawa, K., et al., 2012. A study on a symbiotic thorium breeding fuel-cycle: THORIMS-NES through FUJI. Energy Convers. Manage. 63, 51–54.

ITMSF, 2016. Web site of International Thorium Molten-Salt Forum. <http://msr21.fc2web.com/english.htm>.

Kaçar, E.N., Erbay, L.B., 2013. A design review for heat exchangers. Eng. Mach. 54 (644), 14–43.

MENR, 2016. Web site of Republic of Turkey, Ministry of Energy and Natural Resources. <http://www.enerji.gov.tr/en-US/Strategic-Plan>.

Şahin, H.M., Erol, Ö., 2012. Utilization of thorium in a Gas Turbine-Modular Helium Reactor with alternative fuels. Energy Convers. Manage. 53, 224−229.

Şahin, S., et al., 2001. Neutronic performance of proliferation hardened thorium fusion breeders. Fusion Eng. Des. 54, 63−77.

Şahin, S., et al., 2002. Power flattening and minor actinide burning in a thorium fusion breeder. Energy Convers. Manage. 43, 799−815.

Şahin, S., et al., 2004. An assessment of thorium and spent LWR-fuel utilization potential in CANDU reactors. Energy Convers. Manage. 45, 1067−1085.

Şahin, S., et al., 2006. Investigation of CANDU reactors as a thorium burner. Energy Convers. Manage. 47, 1661−1675.

Şahin, S., et al., 2009. Criticality investigations for the fixed bed nuclear reactor using thorium fuel mixed with plutonium or minor actinides. Ann. Nucl. Energy. 36, 1032−1038.

Şahin, S., et al., 2014. Neutronic investigations of a laser fusion driven lithium cooled thorium breeder. Prog. Nucl. Energy. 73, 188−196.

Şahin, S., et al., 2015. Energy multiplication and fissile fuel breeding limits of accelerator-driven systems with uranium and thorium targets. Int. J. Hydrogen Energy. 40, 4037−4046.

Übeyli, M., Yalçın, Ş., 2008. Neutronic study on a magnetic fusion reactor using protective liquid wall of thorium molten salts. Energy Convers. Manage. 49, 947−952.

Yapıcı, H., Bayrak, M., 2005. Neutronic analysis of denaturing plutonium in a thorium fusion breeder and power flattening. Energy Convers. Manage. 46, 1209−1228.

Yapıcı, H., et al., 2000. Investigation of neutronic potential of a moderated (D-T) fusion driven hybrid reactor fueled with thorium to breed fissile fuel for LWRs. Energy Convers. Manage. 41, 435−447.

Yılmaz, H., et al., 2013. Entropy generation and temperature cross phenomena at heat exchangers. Eng. Mach. 54 (645), 38−59.

## 26.20 United Kingdom

*Ian Scott*[1] *and Zara Hodgson*[2]

[1]Moltex Energy LLP, London, United Kingdom, [2]National Nuclear Laboratory, Warrington, United Kingdom

The UK started a program on molten salt reactors around 1970, inspired by the US MSRE program. There was close contact with the US group and opportunities to collaborate with France were explored. The program culminated in an extraordinarily ambitious conceptual design for a reactor as follows:

- Pumped molten salt system operating without moderator in a fast spectrum;
- Uranium/plutonium/sodium chloride fuel system with uranium/sodium chloride breeding blanket;
- Electrical power of 2500 MW;
- Output temperature from the core of 1050°C;
- Helium as secondary coolant linked to gas turbine systems for power generation.

Substantial work was also carried out on the fuel cycle, materials requirements, and other aspects. The reports are available for inspection at the UK National Archives at Kew. The key report is AEEW R1059 "Conceptual design and assessment of a helium cooled, 2500 MWe molten salt fast reactor with integrated gas turbine plant," which is located in AB 35/72. Further useful documents are available in the National Archive.

The original program was terminated about the same time as the US MSR program and no further work on molten salt reactors took place in the UK until Moltex Energy began development of reactors based on static molten salt fuels in 2013 (see Chapter 14: Static liquid fuel reactors and Chapter 21: Stable salt fast reactor).

The only UK government-funded project relating to molten salt reactors in recent times was a study on MSRs completed in July 2015 by Energy Process Developments. The report (http://www.energyprocessdevelopments.com/uploads/EPD%20MSR%20Review%20Feasibility%20Study%20July%202015%201.02.pdf) summarizes MSR activity internationally. It looks at the feasibility of developing a pilot-scale demonstration MSR in the UK. A review of potential UK sites is given along with an insight into the UK regulatory process for innovative reactor technology. The technical review of six MSR designs led to the selection of the stable salt reactor, designed by Moltex Energy, as most suitable for UK implementation (http://www.energyprocessdevelopments.com/uploads/Selection_of_Moltex_SSR.pdf).

While government-funded work on molten salt reactors ended in the mid-1970s, work on nuclear fuel reprocessing using molten salts did continue. In the 1960s there was an active program on electrowinning of uranium from spent Magnox fuel. Through the 1970s and 1990s small laboratory-scale projects were carried out at British Nuclear Fuels Ltd (BNFL), generally in the context of larger European collaborations, and with a focus on the pyro-processing concepts developed at Argonne National Laboratory. In the early 2000s and prior to the UK withdrawal from active engagement within the Generation IV International Forum in 2006, the UK had a significant program of research on molten salt electrorefining process technology that included engineering, fundamental science, and experimental infrastructure investment; key to this was a Molten Salts Dynamics Rig (MSDR) that is no longer operational (Banfield et al., 2005). The MSDR was a one-of-a-kind pilot-scale test facility fitted with three pumping options and a lithium chloride-potassium chloride eutectic (LKE) salt inventory of approximately 120 kg.

Since 2006, the UK, through the National Nuclear Laboratory (NNL) and University of Manchester, has maintained skills and expertise in molten salt-based recycling technology through collaborative European projects, such as ACSEPT, SACSESS, and ASGARD (Bourg et al., 2011, XXXX; Roadmap-Actinide Separation Processes 2015). In 2011, a 4-year UK EPSRC (Engineering and Physical Sciences Research Council)-sponsored program commenced focusing on direct electrochemical reduction, electrorefining, and speciation and analysis: this REFINE program was the largest program of molten salts work in the UK up to 2016, led by the University of Edinburgh with partners from the Universities of Manchester, Nottingham, Cambridge, and University College London and NNL. A review of the status as of 2011 is available as IAEA Nuclear

Energy Series NF-T-4.2 “Status of developments in the back end of the fast reactor fuel cycle.”

In 2013, the UK government published its Nuclear Industry Strategy with a vision for nuclear energy in the UK to play a significant role in delivering a secure, sustainable and affordable low-carbon energy future, and in 2014 established the Nuclear Innovation and Research Advisory Board (NIRAB) to advise on the approach and coordination of nuclear innovation, research, and development that will keep future energy options open and enable commercial opportunities to be realized. NIRAB have concluded that there is a clear gap in the UK’s R&D activity into next-generation nuclear reactor technologies, including SMRs and Generation IV reactors, and their associated fuel cycles. The government announced that it intended to re-invigorate the UK nuclear fission research capability, and £250 million was earmarked for this purpose in 2015. The NIRAB recommendations suggested development of UK skills and capabilities for a range of advanced reactor systems (http://www.nirab.org.uk/media/6233/uk-nuclear-innovation-and-research-programme-recommendations.pdf).

In 2016, the UK government announced a “small modular reactor” competition aimed at selecting a new nuclear technology, in which the UK could take a leading development role. While the competition was originally conceived as relating to small modular PWRs, a number of molten salt reactors were entered into the competition.

In early 2017, UK activity in the molten salt reactor field is most significant in the private sector through Moltex Energy LLP, though a number of universities, including the Universities of Manchester and Cambridge, have started academic programs focused around the new concept of static molten salt fuels.

- Actinide reCycling by SEParation and Transmutation (ACSEPT)
- Safety of ACtinide Separation proceSSes (SACSESS)
- Advanced fuelS for Generation IV reActors: Reprocessing and Dissolution (ASGARD)
- REduction of spent Fuel vital In a closed loop Nuclear Energy cycle (REFINE)

## References

Banfield, Z., Cogan, J., Farrant, D., Gaubert, E., Hopkins, P., Lewin, B., 2005. Development of Pyrochemical Spent fuel Management in the UK. ENC 2005, Versailles, France.

Bourg S. et al., Advanced reprocessing developments in Europe status on European projects ACSEPT and ACTINET-13. Proc. Chem. 7, 166–171.

Bourg, S., et al., 2011. ACSEPT–partitioning technologies and actinide science: towards pilot facilities in Europe. Nucl. Eng. Des. 241, 3427–3435.

Roadmap-Actinide separation processes 2015. SACSESS. Available at: < http://www.sacsess.eu/Docs/SACSESS.pdf > , < www.sacsess.eu/Docs/SACSESS.pdf > .

http://www.nirab.org.uk/media/6233/uk-nuclear-innovation-and-research-programme-recommendations.pdf.

# 26.21 Ukraine

*A.S. Bakai*
National Academy of Sciences of Ukraine, Kharkiv, Ukraine

## 26.21.1 Introduction

From the USSR, Ukraine has inherited a huge amount of nuclear weapons, the ruined fourth unit of the Chernobyl Nuclear Power Plant, and 16 PWR units that provide half of the electric power in the country. While the nuclear weapons were transferred abroad under the guarantee of security, Chernobyl is in the process of becoming a nuclear waste storage site. The planned decommissioning of the majority of PWR units (mainly of generation II) is expected before 2030. Taking into account that many institutions and plants in Ukraine were involved in the nuclear projects of the USSR, that one-sixth of explored world uranium reserves and a lot of other raw materials for the nuclear construction materials belong to Ukraine, we are not an ordinary user of nuclear technologies. Ukraine has good prospects for nuclear industrial development as a partner in the world community. The explored uranium reserves would be sufficient to provide the PWR fuel for the next 150 years. Therefore it was proposed (Paton et al., 2008) to develop a two-level nuclear engineering structure in Ukraine during the transition to Gen-IV. The PWR units constitute the first level. The second level is heavy water reactors (HWR) with the fuel cycles oriented towards burning the spent nuclear fuel of PWRs and incinerating radiotoxic isotopes. Later, when MSR technologies are developed, they will be implemented in Ukraine. Since the MSR technologies are more promising but less advanced compared with the HWR technologies, they need a long-term R&D program, which currently is being formed by the world community.

Structural materials for MSR is one of the key problems of this program. Since there are many institutions and experts working in this field in Ukraine, the project "Research and development of fuel and construction materials for accelerator-driven plutonium disposal and nuclear waste transmutation systems using molten salt fluoride blankets" was proposed by the researchers at the National Science Center Kharkiv Institute of Physics and Technology in partnership with the Pacific Northwest National Laboratory (USA). This project was approved for financing by the STCU in 2003.

As a rule, promising construction materials have to be tested in reactors using special loops reproducing all the conditions of a real MSR. Experiments of this type take a lot of time and need special techniques and testing procedures. The idea of the project was to imitate the reactor conditions of material corrosion using electron irradiation. The important point is the relevance of the data obtained in the simulation experiments to the behavior of the material in reactor conditions. This problem needs special investigations, which were performed within the project framework. These investigations are based on the fact that the nature of kinetic processes induced, modified, and activated by irradiation is very similar on the microscopic level regardless of the type of irradiation. For this reason, the investigation of the kinetic processes under electron irradiation gives valuable information, which can be used for prediction of materials behavior in reactors, using the proper rescaling of the kinetic coefficients.

A special remark concerning the corrosion kinetics in surface layers has to be made. The corrosion is controlled by chemical reactions. The reaction rate is sensitive to the local energy deposition due to irradiation. The irradiation excites the electron states and can produce atomic replacements and displacements. These radiation-induced elementary processes need excitation energy from one to tens of electron-volt per atom. Accelerated electrons and $\gamma$-quanta are ideal agents for activation of the corrosion kinetics at a comparatively low rate of replacements and displacements of atoms. Therefore an electron accelerator of proper energy (10 MeV/electron) was chosen to imitate the impact of the reactor irradiation on the corrosion kinetics. Concurrently, the electron irradiation impacts diffusion and phase transformations in the bulk and, especially, within the grain boundaries.

The corrosion tests in metallic melts and salts without irradiation provide a reference database and allow estimating of thermodynamic driving forces controlling the corrosion and aging kinetics.

## 26.21.2 Methodology

### *26.21.2.1 Electron irradiation test facility (EITF)*

Some helpful features of the electron irradiation are:

1. Since the energetic thresholds of nuclear reactions induced by electrons and $\gamma$-rays are nearly 10 MeV or somewhat less, the use of electron beams with the energy of 10 MeV avoids considerable radioactivity of the irradiated materials, so hot cells are not needed in postirradiation investigations of the materials.
2. The penetration length of electrons with an energy of 10 MeV is of some centimeters. On this length scale the electron energy decreases from 10 to 1 MeV or even less due to the bremsstrahlung and other inelastic processes. This means that, on the one hand, the test ampoules can have reasonable size to mimic large-scale experiments and, on the other hand, the irradiation conditions are dramatically changing on a comparatively small length. Therefore we can use many metallic specimens of submillimeter thickness within one ampoule to investigate the dependence of corrosion and radiation damage processes versus energy deposited by e- and $\gamma$-fields.
3. The electron beam can be used as an efficient heater of the irradiated target to maintain the needed temperature if the electron beam power, target geometry, and construction are properly chosen.

The irradiation cell and general view of the EITF are represented in Figs. 26.21.1 and 26.21.2. The construction of the irradiated ampoule with tested specimens immersed into molten salt is also shown. The surface layers of the specimens S1, S2, S3, S4, S5, and S6 are indicated.

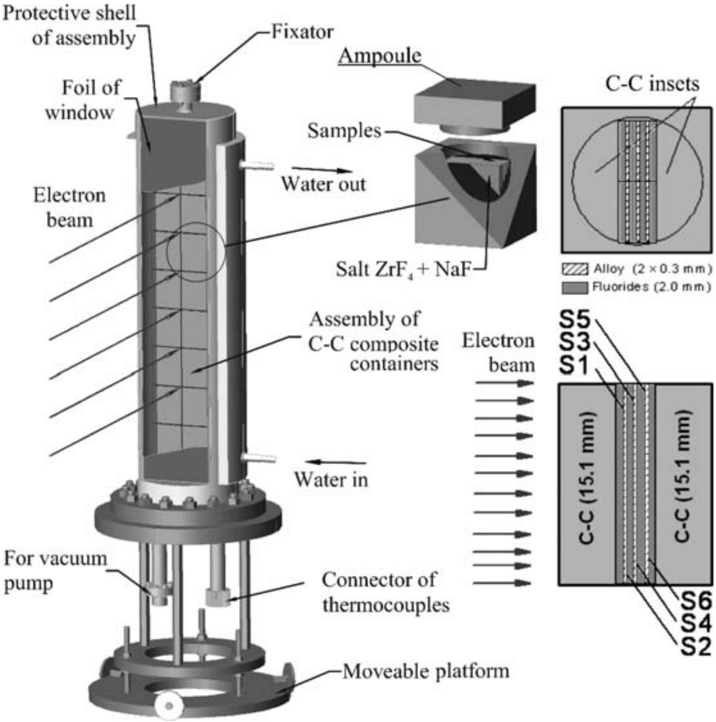

**Figure 26.21.1** Construction of the irradiation cell of the EITF-KIPT. On the later section of the specimens their surfaces are marked by symbols S1−S6. Due to stopping of electrons the deposited energy within the surface layer considerably decreases with the layer number increasing. In particular, the deposited S1 energy is 50 times larger than that in the layer S6.

**Figure 26.21.2** General view of the EITF. The accelerator outlet is on the left.

Surface layers of the specimens are marked by letters S1−S6. Due to the gradual stopping of the electron beam, the deposited energy, $E_\mathrm{d}$ (S1), in the first surface layer is much larger than that in the last layer, $E_\mathrm{d}$ (S6). Computer simulations (Bakai and Garner, 2005) show that during a 700-hour experiment $E_\mathrm{d}$ (S1) $\approx$ 6200 eV/atom, while $E_\mathrm{d}$ (S6) $\approx$ 120 eV/atom. In layers S2−S5 this quantity assumes intermediate values. Such ampoule construction allows one to investigate corrosion kinetics over a wide range of irradiation rates in just one irradiation session.

### 26.21.2.2 Simulations of the e- and $\gamma$-fields and the deposited energy distribution

The electron and $\gamma$-radiation field magnitudes, the spatial profiles of energy deposition onto the molten salt and the samples, as well as the rates of point defect generation in the specimens have been evaluated by means of numerical simulations of radiation transport in the test bench geometry. The results of such simulations may be used to optimize the ampoule construction and provide quantitative predictions for the specimen properties versus the irradiation dose.

### 26.21.2.3 Temperature distribution

The equation of heat balance that takes into account the total deposited energy and the radiation heat losses from the ampoule's surface was used to estimate the thermal balance inside of the irradiated target. To calculate the temperature distribution within the ampoule, the spatial density of the deposited energy was used as an input and then the heat transport equation was solved. The calculations performed show that the temperature variance within the ampoules is very small.

### 26.21.2.4 Mechanical tests

The changes of the macroscopic mechanical properties due to the presence of the molten fluoride salts or metallic coolants were revealed by standard mechanical tests including nanoindentations. Indentation is an informative tool providing information about the changes to the mechanical properties of the corroded surface layers of the irradiated specimens.

Additionally, investigations of the impact of the ultrasonic vibrations on the tested material were performed and provided information on the inner friction and materials' sensitivity to high-frequency fatigue.

### 26.21.2.5 Structural and compositional analysis

The compositional, structural, and phase changes were investigated by means of advanced diffraction and microscopy techniques that reveal structure, composition, and precipitation on the macroscopic, mesoscopic, and microscopic scales.

### 26.21.2.6 Corrosion tests

Corrosion of alloys and their constituents in a molten eutectic NaF-$ZrF_4$ fluoride mixture has been studied by cyclic voltammetry, X-ray analysis, scanning electron microscopy, and metallography. The corrosion rates of the samples exposed in salt at 650°C for different times were measured afterwards in a fresh molten salt by the volt-ampere method. This way the impact of the electron irradiation on the corrosion rate of the alloys in molten fluorides has been measured.

### 26.21.2.7 X-ray spectroscopy

After irradiation by 10 MeV electrons a small number of nuclear reactions occur, leading to the formation of $\gamma$-active nuclei. This gives a possibility to register the products of the alloys corrosion in the molten salt by performing $\gamma$-spectroscopy of the used salt. Although this method does not produce a proper quantitative compositional analysis, it gives a semiquantitative and qualitative information about the solubility of alloy components in the molten salt.

### 26.21.2.8 Theoretical models

Quantitative analysis of the experimental data calls for the development of appropriate theoretical models. The main goal is to describe the corrosion and phase transformation kinetics under the impact of electron irradiation. To the author's knowledge, this problem has not yet been solved.

### 26.21.2.9 Thermodynamics of Zr in alkali halide melts

Equilibrium constants determine the thermodynamic forces responsible for chemical reactions and dissolution of alloys. Since Zr and alkali metals are the basic elements of all fluoride salts used in MSR, it is important to know their thermodynamic characteristics. Investigations of the thermodynamics of Zr in alkali melts were performed within the framework of this project.

## 26.21.3 Materials

### 26.21.3.1 Fluoride salt

The fluoride salt NaF-$ZrF_4$ was used in the experiments.

### 26.21.3.2 Hastelloys

Ni-Mo alloys (Hastelloys), similar to those that had already shown satisfactory corrosion resistance in contact with molten fluoride salts NaF-$ZrF_4$ and $ZrF_4$-LiF-BeF at temperatures of 600−800°C in earlier experiments, were prepared and used.

**Table 26.21.1** Nominal compositions of Alloys A and B

| Element | Alloy A | Alloy B |
|---|---|---|
| Nickel | 78.2 | 78.2 |
| Molybdenum | 11.7 | 11.7 |
| Chromium | 6.7 | 6.2 |
| Titanium | 0.5 | 0.5 |
| Aluminum | 0.8 | 0.8 |
| Iron | 1.5 | 1.5 |
| Manganese | 0.5 | 0.5 |
| Silicon | 0.15 | 0.15 |
| Niobium | – | 0.5 |
| Yttrium | – | 0.05 |
| Carbon | – | – |
| Sulfur | – | – |

Since comparatively small compositional changes of alloys can lead to a considerable decrease or increase in the corrosion resistance, two compositions of the Ni-Mo alloys (Alloy A and Alloy B) were chosen after some analysis of the corrosion data previously obtained by others. The nominal compositions of these alloys are shown in Table 26.21.1. It is noteworthy that yttrium was added to Alloy B to improve the grain boundary corrosion resistance. Compounds of high purity were used to exclude the impact of uncontrolled impurities.

### 26.21.3.3 Carbon–carbon composite

C–C composites with good mechanical properties and low chemical activity in contact with fluoride salts were chosen as materials for the ampoules. Tests of the corrosion resistance of these materials in molten salts under irradiation in EITF provided quantitative results on their corrosive properties.

## 26.21.4 Results

### 26.21.4.1 Results of the C–C composite tests

Tests show that exposure to the molten salt, with or without e-irradiation at 650°C, does not change the properties and composition of the tested specimens and ampoules. It looks like the test conditions were not "hard" enough to initiate destruction of this material.

### 26.21.4.2 *Impact of the NaF-ZrF$_4$ molten salt and e-irradiation on the properties of alloys A and B*

Our data show that:

- Irradiation heavily impacts the corrosion rate;
- Corrosion resistivity is rather sensitive to small compositional changes. Alloys A and B have minor compositional differences but their corrosion resistivities with and without irradiation are considerably different. Besides, the corrosion rate of Alloy B is more sensitive to the deposited energy $E_d$;
- Impurities of La in the NaF-ZrF$_4$ molten salt enhance the corrosion of Alloy A, even without irradiation.

The corrosion rates of Alloy A and Alloy B versus the exposure time and deposited energy $E_d$ are given in Fig. 26.21.3.

As can be seen, the corrosion rate of Alloy B under irradiation increases $\sim 10^3$ times, while in the case of Alloy A the energy deposition rate does not play such a significant role.

In the bremsstrahlung X-ray spectrum of electrons with energy of the order of 10 MeV the comparatively soft $\gamma$-quanta with energy less than 1 MeV dominate. Therefore, the generation of point defects is weak even at high levels of deposited energy. Calculations show that at $E_d = 6200$, $-120$ eV/atom, atomic displacements range from $\sim 10^{-2}$ to $10^{-3}$ per atom (Bakai and Garner, 2005).

The energy deposited in the fluoride salt is several times smaller than that in the Hastelloy specimens. Nevertheless, it is large enough to impact the chemical

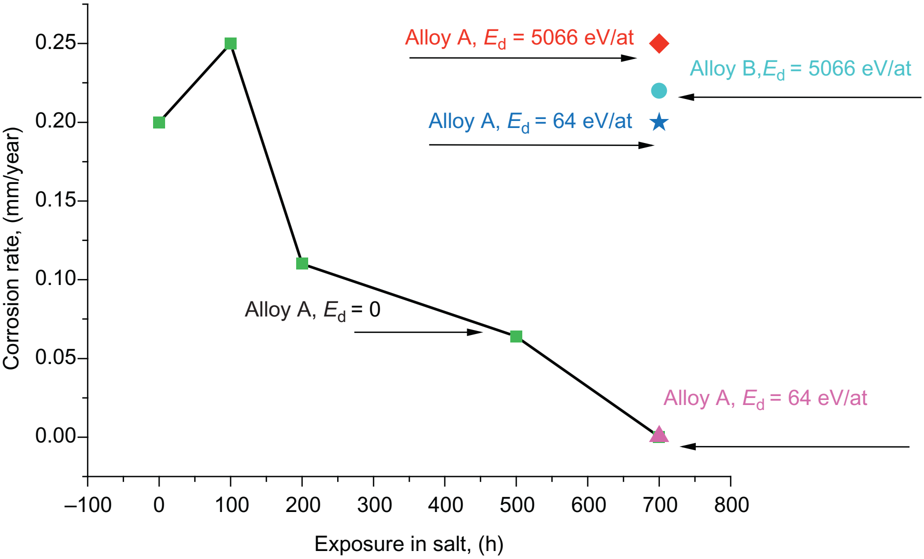

**Figure 26.21.3** The corrosion rates of Alloy A and Alloy B versus the exposure time and $E_d$.

reaction rates. Apparently ionization and activation of atoms under irradiation within and near the surface layers of the alloy are the main cause of the acceleration of corrosion kinetics.

Different sensitivities of Alloys A and B to the deposited energy rate show that the alloying additions (like yttrium and niobium) have an essential impact on the corrosion resistance. Therefore, the search for optimal compositions of the Ni-based structural alloys has to be continued in varied environments and at a range of irradiation intensities.

Postirradiation mechanical tests of the samples prove their high strength and plasticity. Microanalysis reveals Cr depletion and Ti enrichment in the surface layers, as well as penetration of zirconium and sodium into the samples. The thickness of the layers with considerable changes in composition is about 40 μm.

Our tests have demonstrated that the corrosion resistance of both alloys is acceptable but that Alloy B shows better properties.

## 26.21.5 Summary

At least 100 experts from a number of labs in Ukraine and abroad were involved in the EITF tests of the materials for MSR, investigations of their properties before and after irradiation, and attempts to design better material compositions. Results of their efforts are published in Paton et al. (2008), Bakai and Garner (2005), Bakai (2008), Wanderka et al. (2007), Volkov et al. (2006), and other papers. This work was stopped due to lack of funds caused by comparatively slow progress in the development of the overall MSR program. However, the methodology of the MSR structural materials assessment developed in the KIPT-EITF project proved to be remarkably efficient. It is fast, cheap in comparison with the traditional in-pile tests, and surely deserves further development and use in combination with other approaches in the R&D of MSR structural materials.

## References

Bakai, A.S., 2008. Combined effect of molten fluoride salt and irradiation on Ni-based alloys. In: Proceedings of the NATO Advanced Study Institute on Materials Issues for Generation IV Systems: Status, Open Questions and Challenges. Cargese, Corsica, France, September 24–October 6, 2007, vol. XV. Springer, Netherlands, pp. 537–557.

Bakai, A.S., Garner, F.A., 2005. Materials for molten salt reactors. Probl. Atom. Sci. Technol. Ser. Radiat. Damage Phys. Radiat. Mater. Sci. 4 (87). Available from: <http://vant.kipt.kharkov.ua>.

Paton, B.E., Bakai, A.S., Baryakhtar, V.G., Nekludov, I.M., 2008. On Development Strategy of the Nuclear Power Engineering in Ukraine. National Academy of Science of Ukraine, Kiev, Ukraine (in Ukrainian and in Russian).

Volkov, S., Omelchuk, A., Azhazha, V., Bakai, A., 2006. Corrosion stability of irradiated Hastelloy-type alloys in molten NaF-$ZrF_4$ mixture. J. New. Mat. Electrochem. Syst. 9, 311–315.

Wanderka, N., Bakai, A., Abromeit, C., Laheim, D., Seidman, D.N., 2007. Effects of 10 MeV electron irradiation at high temperature of a Ni–Mo-based Hastelloy. Ultramicroscopy. 107, 786–790.

# 26.22 United States of America

*Vince Lackowski and John Kutsch*
Thorium Energy Alliance, Harvard, IL, United States

## 26.22.1 Introduction

MSR development efforts in industry, national laboratories, and universities are growing, due to the urgent need for safe, clean sources of power generation. This research is encouraged by the successful MSRE experiment at Oak Ridge National Laboratory (ORNL) in the 1960s. This section includes the following items:

Introduction
Oak Ridge National Laboratory—David Holcomb and Kun Chen
CRADA
Massachusetts Institute of Technology— Charles Forsberg
University of California–Berkeley (UCB)—Per Peterson
University of Wisconsin–Madison (UW)
University of New Mexico
Thermal-Fluids Lab—Edward Blandford
Ohio State University—Jinsuo Zhang
University of Tennessee Knoxville—Ondrej Chvala
University of Utah—Michael Simpson
Missouri University of Science and Technology (MUST)—Dustin Gage Green
TerraPower and Southern Company Services
ThorCon (Martingale)
Transatomic Power
Flibe Energy
Elysium Industries

## 26.22.2 Oak Ridge National Laboratory

*David Holcomb and Kun Chen*

> *Oak Ridge National Laboratory marked the 50th anniversary of the startup of its Molten Salt Reactor Experiment with a workshop on molten salt reactor technologies Oct. 15–16, 2015, bring together government representatives, U.S. and international researchers, regulators, utilities and reactor design firms for technical discussions*

> *and a reception honoring the pioneers of MSR technology. The MSRE, designed to assess the viability of liquid fuel reactor technologies for use in commercial power generation, operated from January 1965 through December 1969, logging more than 13,000 hours at full power during its four-year run.*

Researchers at ORNL will participate in two new DOE-funded \$6 million projects to develop advanced nuclear reactor technologies. Industry-led teams will include participants from universities and national laboratories.

## 26.22.3 CRADA

The Chinese Academy of Science's (CAS) Shanghai Institute of Applied Physics (SINAP) and the US Department of Energy's (DOE) Oak Ridge National Laboratory (ORNL) have recently entered into a Cooperative Research and Development Agreement (CRADA) to accelerate the development of fluoride salt-cooled high-temperature reactors (FHRs). The CRADA evolved from US–China interactions under a Memorandum of Understanding between the DOE and the CAS on Cooperation in Nuclear Energy Sciences and Technologies. The DOE-NE Office of Advanced Reactor Technologies (ART) is currently supporting FHR development primarily through its nuclear energy university program (NEUP).

The CRADA supports and is funded by SINAP's thorium molten salt reactor (TMSR) program. The overall purpose for SINAP's TMSR program is to develop molten salt reactor technology to supply energy to the growing Chinese economy. The CRADA is limited to solid-fueled MSRs, but recognizes that nearly all of the technology developed will be applicable to liquid fuel MSRs. The FHR test reactors currently being planned will use low-enriched uranium fuel.

Developing a common understanding of the safety characteristics and consequent regulatory requirements decreases the development risk. The approved first phase tasks of the CRADA are:

1. To commission ORNL's liquid salt test loop and use it for pebble bed heat transfer testing;
2. To perform component evaluation and testing;
3. To provide analysis software support;
4. To develop and participate in international FHR training activities;
5. To exchange technical information on FHR supportive technologies.

*Source*: https://www.ornl.gov/news/ornl-supports-new-projects-develop-advanced-nuclear-technologies.

## 26.22.4 Massachusetts Institute of Technology

*Charles Forsberg*

MIT has been developing a fluoride-salt-cooled high-temperature reactor (FHR) with a nuclear ir-Brayton combined cycle (NACC) and firebrick resistance-heated energy storage (FIRES). The goals are to:

1. Improve nuclear power plant economics by 50%−100% relative to a base-load nuclear power plant;
2. Develop technology for a zero-carbon nuclear/renewables electricity grid by providing dispatchable power;
3. Eliminate major fuel failures and consequent potential for major offsite radionuclide releases in a beyond-design basis accident.

The concept of the FHR is more than a decade old (Gat et al., 1992). An integrated research project led by the author at the Massachusetts Institute of Technology (MIT) and including the University of California at Berkeley (UCB), and the University of Wisconsin (UW) has completed a 3-year study (analysis and experiments) to develop the concept and develop a pathway to commercialization. Since the FHR inception there has been growing interest at universities and national laboratories—and a decision by the Chinese Academy of Science to build a 10 MWt test reactor by 2020.

It is the coupling of high-temperature nuclear reactor and gas turbine technologies that results in the transformational characteristics of an FHR with NACC and FIRES. MIT, UCB, and UW have developed an FHR path forward including a commercialization strategy (Sorensen, 2014), an FHR point design—a Mark-1 pebble-bed FHR (Mk1 PB-FHR) (Chvala, 2014), and a test reactor strategy (http://web.utk.edu/~ochvala/MSR/Seminars/). Fig. 26.22.1 shows the Mk1 PB-FHR and its NACC power conversion system.

The pebble-bed fuel is similar to that originally developed in Germany and now used in China for their HTGRs, but the pebble size has been reduced to 3-cm diameter spheres to enable a higher power density. Like the HTGR pebble bed reactors,

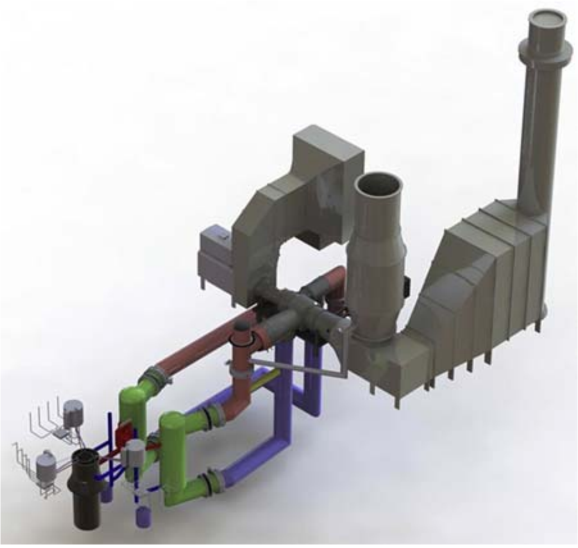

**Figure 26.22.1** Mk1 PB-FHR plant layout, showing coupling to NACC power conversion.

the pebbles flow through the reactor core to allow online refueling. The coolant is Flibe ($^7Li_2BeF_4$), the same coolant proposed for many molten-salt reactors (MSRs) except in an FHR it is clean salt, to minimize corrosion and radiation doses in coolant piping. The solid fuel FHR concept is discussed in Chapter 13, Solid fuel, salt-cooled reactors; the NACC and FIRES concepts are described in Chapter 2, Electricity production; and the Chinese TMSR is described in Chapter 17, Thorium molten salt reactor nuclear energy system (TMSR).

## 26.22.5 University of California—Berkeley (UCB)

*Per Peterson*

The Compact Integral Effects Test (CIET 1.0) facility is a primary component of the UCB Thermal Hydraulics Laboratory's (TH Lab's) mission to develop the scientific and technical basis to design and license fluoride-salt-cooled, high-temperature reactors (FHRs). Along with the other experiments and projects in the UCB TH Lab, the CIET 1.0 facility is part of an experimental test program to validate simulation codes for applications to FHRs. The capability to validate integral transient response models is a key issue for licensing new reactor designs, and CIET 1.0 as well as future iterations of the facility will be critical for providing the validation data to accomplish this.

Currently, the three key missions of the CIET facility are:

1. To provide experimental validation data for system-level thermal hydraulic codes that are used by the NRC and other nuclear regulatory agencies for licensing;
2. To serve as an advanced reactor test bed for advanced reactor control strategies, particularly for cybersecurity strategy;
3. To provide a high-quality user experience to train operators, designers, and regulators on the safe construction and operation of FHRs.

CIET 1.0 is the first integral effects test (IET) facility to study FHRs, and is designed and constructed to reproduce the integral transient thermal hydraulic response of FHRs (Fig. 26.22.2) under forced and natural circulation operation. CIET 1.0 provides data to validate simulation codes for direct reactor auxiliary cooling systems (DRACS), used for natural-circulation-driven decay heat removal in FHRs. CIET 1.0 is designed to replicate an FHR transient response for a wide range of licensing basis events (LBEs).

The CIET 1.0 facility uses Dowtherm A oil as a simulant fluid for fluoride salts, because at relatively low temperatures (50−120°C), Dowtherm can match the Prandtl, Reynolds, and Grashof numbers of the major liquid salts simultaneously, at approximately 50% geometric scale and heater power under 2% of prototypical conditions. CIET 1.0 was scaled based on the earlier design of a 900-MWth channel-type pebble bed advanced high-temperature reactor. Subsequently, UCB developed a new, preconceptual design of a 236-MWth Mark 1 pebble bed FHR (Mk1 PB-FHR), after the scaling and design of CIET 1.0 were finalized. The scaled elevations of the main heat sources and sinks in CIET 1.0 and the Mk1 PB-FHR design have reasonable agreement, as shown below.

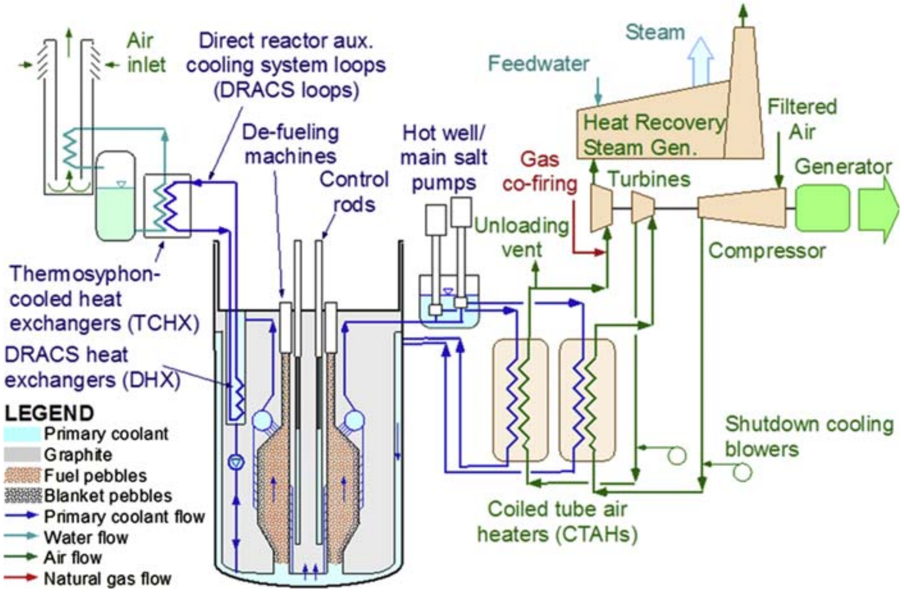

**Figure 26.22.2** MK1 PB-FHR flow schematic (CIET Lab—UC Berkeley).

Key phenomena include heat transfer, phase change, and single and multiphase flows in water, gas, molten salt, and liquid metal coolants for advanced fission and fusion systems, as well as transport and mixing processes that occur inside reactor containment structures and in environmental systems. Experimental facilities include the CIET; the X-ray Pebble Recirculation Experiment, which performs 3-D X-ray tomography of pebble beds; and smaller separate effect tests studying convective heat transport and thermo-photovoltaic power conversion.

*Sources*:

https://public.ornl.gov/conferences/MSR2015/pdf/5Laufer_UCB_CIET_Mike%20Laufer.pdf.
http://fhr.nuc.berkeley.edu/.
http://fhr.nuc.berkeley.edu/fhr-research-areas/compact-integral-effects-test-ciet/.

## 26.22.6 University of Wisconsin—Madison (UW)

UW investigates the transport of tritium and other radioisotopes in molten fluoride salts and graphite fuel elements. They study freezing transients of fluoride salt coolants, nuclear reactor transients, safety analysis, thermal-hydraulic scaling analysis, safety analysis, code verification and validation, and engineering ethics. Fig. 26.22.3 shows the phase diagram of Flibe.

These studies contribute to thermal-hydraulic and mass transport studies for FHRs (Chapter 13: Solid fuel, salt-cooled reactors).

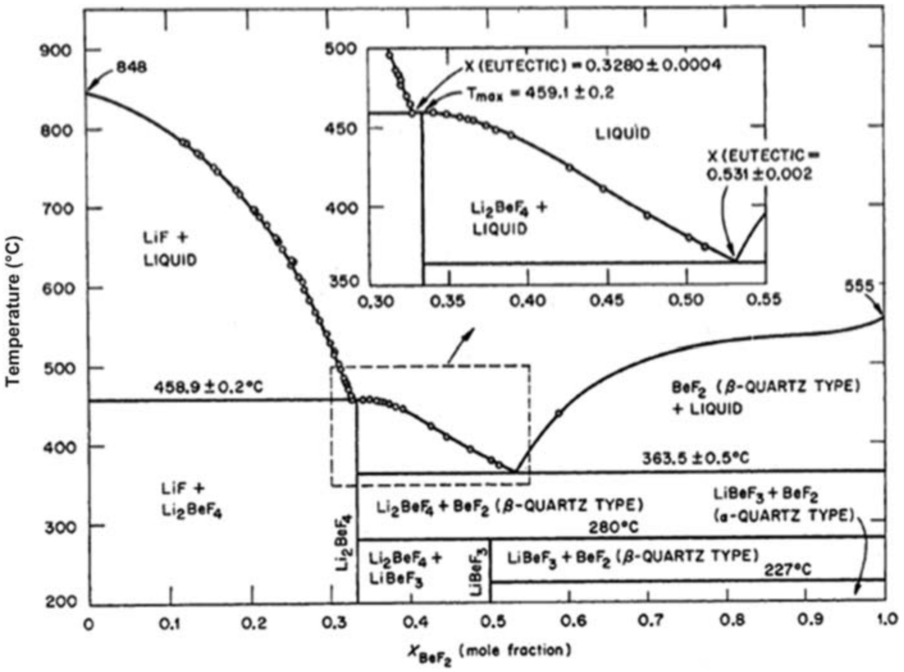

**Figure 26.22.3** Phase diagram of LiF-BeF$_2$ (Flibe), the primary coolant of the FHR nuclear reactor.
*Source*: Romberger, K.A., Braustein, J., Thoma, R.E., 1972. New electrochemical measurements of the liquidus in the lithium fluoride-beryllium fluoride system. Congruency of lithium beryllium fluoride (Li$_2$BeF$_4$). J. Phys. Chem. 76 (8), 1154–1159.

This research has applications beyond the FHR, including pyro-processing separations for nuclear spent fuel recycling, fusion technologies, solar thermal systems, and thermal energy storage.

*Source*: https://heatandmass.ep.wisc.edu/.

## 26.22.7 University of New Mexico Thermal-Fluids Lab

*Edward Blandford*

The UNM research group uses both simulation and experiments to study nuclear safety and fundamental thermal-fluids for existing reactor technologies and advanced concepts. They are interested in best-estimate code validation and verification; various topics in heat and mass transfer, fluid dynamics, and phase change; electrochemical separation facility safeguards modeling; and developing advanced process monitoring technologies.

*Source*: http://blandford.unm.edu/.

## 26.22.8 Ohio State University

*Jinsuo Zhang*

The OSU Molten Salt Laboratory is equipped with two argon-filled glovebox systems and corresponding high-temperature electrochemcial cells. They measured the solubility of lanthanides and alkali metals (Na and Cs) in molten salts. The high-temperature electrochemical molten salt system is designed to determine thermodynamics and transport properties of lanthanides in molten salts for molten salt recycling, and it can also be used to characterize molten salt corrosion. The experiment uses a three-electrode system for cyclic voltammetry and chronopotentiometry to determine apparent potential, activity coefficient, and diffusion coefficient of lanthanides in molten salt at $T \sim 723$ K.

*Source*: https://nmfc.engineering.osu.edu/facilities/molten-salt-laboratory.

## 26.22.9 University of Tennessee Knoxville

*Ondrej Chvala*

The Nuclear Engineering (NE) department of the University of Tennessee at Knoxville (UTK) has historical ties to MSR research at ORNL (Gat et al., 1992; Sorensen, 2014). UTK carried out a parameter scan of possible lattice configurations and salt selections (Chvala, 2014) and explored the dynamic stability of finite DMSR cores (http://web.utk.edu/~ochvala/MSR/Seminars/). They are modeling the fuel cycle of LEU-fueled DMSR without reprocessing, and checking the dynamical stability of the core as a function of burn-up. They estimated the levelized unit of electricity cost of the IMSR and the AP-1000 (Samalova et al., 2017).

## 26.22.10 University of Utah

*Michael Simpson*

The University of Utah's Metallurgical Engineering Department studies pyroprocessing of nuclear fuel with projects in safeguards, actinide separations, and waste management for fuel cycles of the uranium–plutonium metal fuel-based integral fast reactor (IFR) and the thorium–uranium fluoride salt fuel-based molten salt reactor. In the MSR, thorium fluoride is dissolved in LiF-$BeF_2$ (Flibe) and is transmuted to protactinium fluoride, which decays to U-233. The Utah group specializes in studying electrochemical and pyrochemical processes with these salts, developing technology to monitor the composition of the salts in real time; conceptual safeguard approaches to virtually eliminate the potential for diversion of plutonium from nuclear fuel processing facilities; and compact, durable waste forms to enable safe permanent disposal of waste from nuclear reactors.

## 26.22.11 Penn State University

*Hojong Kim*

Penn State researchers study electrochemical separation of alkali/alkaline-earths (Ba, Sr, and Cs) in liquid metals. One key challenge is the accumulation of fission products (e.g., alkali/alkaline-earth and rare-earth elements) in the molten salt electrolyte, which changes the electrolyte properties and diminishes the performance efficiency of an electrorefiner. The accumulation of the alkali/alkaline-earth elements (e.g., Cs and Sr) with short half-lives ($\sim 30$ years) can cause high decay power densities and costly thermal management storage solutions. Advanced separation methods for fission product removal are needed to minimize the nuclear waste volume and decay heat. Electrochemical separation of these alkali/alkaline-earth elements from the molten salt electrolyte may use liquid metal electrodes (e.g., Bi) that can selectively dissolve alkali/alkaline-earth metals (Cs, Sr, and Ba) by utilizing strong atomic interactions between these fission products and liquid metal electrodes. The goal is to enable salt recycling by electrochemical separation of fission products and reduce the volume of the nuclear waste by concentrating alkali/alkaline-earths into chloride-free, metallic form which can be easily converted to oxides for storage.

## 26.22.12 Missouri University of Science and Technology (MUST)

*Dustin Green*

MUST is studying initial fuel possibilities for the TMSR. Considering the possibility of diverting $^{233}$U fissile material, the research will benchmark $^{233}$U as a main fuel for MSRs using the TMSR. U-235 and Pu-239 will then be tested as suitable initial fuels for the first fleet of TMSRs. These fuels are compared to the reference data based on neutron flux spectra and breeding capabilities.

Using MCNP, a TMSR using U-233 for the initial and operating fuel was benchmarked, based on the data presented by Billebaud Annick and her team at the Laboratory for Subatomic Particles and Cosmology in France. The neutron energy spectrum of U-233 was compared with those of U-235 and Pu-239 to analyze nonproliferation concerns. In addition to the reduction of nuclear warhead stockpiles, incorporating U-235 and Pu-239 into the first fleet of TMSRs will facilitate startup without an initial load of U-233.

*Source*: http://scholarsmine.mst.edu/masters_theses/7398/.

## 26.22.13 Thorium Energy Alliance (Nonprofit)

*John Kutsch*

The Thorium Energy Alliance (TEA) is a charitable foundation, founded in 2006 to provide educational outreach to decision-makers, educators, and the public. It supports basic research, such as classification of molten salt reactor waste, and has been organizing and disseminating educational curriculum materials for high school through graduate levels. The TEA has organized eight international conferences with significant global attendance and has been a catalyst for gathering many MSR business leaders together.

## 26.22.14 TerraPower and Southern Company Services

TerraPower and Southern Company Services, in cooperation with ORNL, the Electric Power Research Institute, and Vanderbilt University, are developing molten chloride fast reactors (MCFRs) with liquid fuel. This design (Fig. 26.22.4) offers advantages of simplicity, closed fuel cycle, and efficiency, with enhanced operational performance, safety, security, and economic value.

In January 2016 the US DOE awarded a Gateway for Accelerated Innovation in Nuclear (GAIN) grant to the project, worth up to $40 million. ORNL technical support will focus on the development of reactor systems and technology, safety assessment and licensing strategy, materials assessment and fabrication methods, chlorine isotope separation methodology, and salt purification and property measurement.

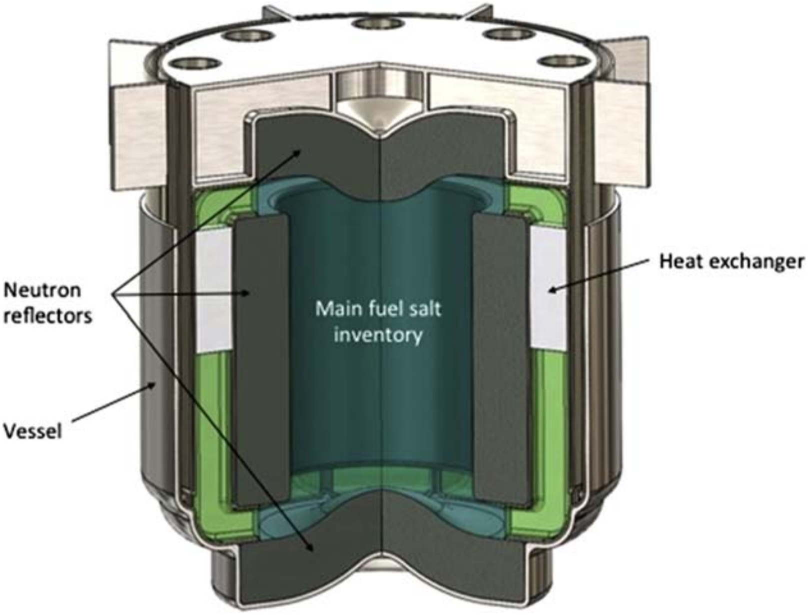

**Figure 26.22.4** The MCFR core is composed of the reactor vessel, fuel salt, neutron reflectors, and primary heat exchangers.
*Source*: Image courtesy of TerraPower.

TerraPower is a spin-off of Intellectual Ventures, the technology investment firm founded by Microsoft cofounder Nathan Myhrvold. Bill Gates is an investor and promoter of the company. (TerraPower is also pursuing a "traveling wave reactor.")

*Sources*:

"Terra Power Quietly Explores New Nuclear Reactor Strategy" MIT Technology Review, Richard Martin 2015.10.21.
https://www.technologyreview.com/s/542686/terrapower-quietly-explores-new-nuclear-reactor-strategy/.
http://www.world-nuclear.org/information-library/current-and-future-generation/molten-salt-reactors.aspx.

## 26.22.15 ThorCon (Martingale)

Martingale Company is designing the ThorCon MSR, which is a 250 MWe single-fluid graphite-moderated thorium converter reactor with Flibe salt. It is described in Chapter 19, ThorCon reactor.

*Sources*:

http://www.world-nuclear.org/information-library/current-and-future-generation/molten-salt-reactors.aspx
http://thorconpower.com

## 26.22.16 Transatomic Power

Transatomic Power Corp is developing a single-fluid MSR using very low-enriched uranium fuel (1.8%), which can safely burn all the used LWR fuel, reducing the need for underground disposal. The TAP reactor has an efficient ZrH moderator (as used in TRIGA research reactors and TOPAZ and SNAP reactors for space program) and a LiF-based fuel salt bearing the $UF_4$ and actinides, hence a very compact core. The secondary coolant is FLiNaK salt (LiF-KF-NaF), which drives a steam generator. This reactor is described in Chapter 22, Transatomic power.

*Source*: http://www.world-nuclear.org/information-library/current-and-future-generation/molten-salt-reactors.aspx.

## 26.22.17 Flibe Energy

"The objective of the liquid-fluoride thorium reactor (LFTR) design proposed by Flibe Energy is to develop a power-generating nuclear reactor that will produce electrical energy at low cost by efficiently consuming thorium, the Earth's greatest natural stored energy resource. A graphite-moderated, thermal-spectrum reactor with solutions of liquid fluoride salts containing both fissile and fertile materials appears to be the best way to realize this objective."

*Source*: http://flibe-energy.com/.

### 26.22.18 Elysium Industries

"Elysium Industries plans to develop a thorium-fueled molten salt reactor, aiming to help meet the majority of the world's future energy demand in a safe, cost-effective, and carbon-free manner."

*Source*: http://www.elysiumindustries.com/.

## References

Chvala, O., 2014. MSR lattice optimization for economic salts with LEU fuel. In: Proc. ICAPP 2014, paper 14187, Charlotte, NC, April 6−9, 2014.

Gat, U., Engel, J.R., Dodds, H.L., 1992. Molten salt reactors for burning sismantled weapons fuel. Nucl. Technol. 100, 390−394.

<http://web.utk.edu/~ochvala/MSR/Seminars/>

Samalova, L., Chvala, O., Maldonado, G.I., 2017. Comparative economic analysis of the Integral Molten Salt Reactor and an advanced PWR using the G4-ECONS methodology. Ann. Nucl. Energy. 99, 258−265.

Sorensen, K., 2014. Thorium research in the Manhattan project era. MS Thesis. <http://trace.tennessee.edu/utk_gradthes/2758/>.

# 26.23 Venezuela

*Eduardo D. Greaves*[1] *and Laszlo Sajo-Bohus*[1,2]

[1]Simón Bolívar University, Caracas, Venezuela, [2]University of Padova, Padova, Italy

### 26.23.1 Introduction

Nuclear physics began in Venezuela with the Eisenhower program "Atoms for Peace" within which a nuclear research reactor RV 1 was contracted and built (1956−60) during the dictatorship of General Marcos Perez Jimenez and the following transition to democratic government in 1958. The reactor was operated in the Instituto Venezolano de Investigaciones Cientificas (IVIC) as a service facility for a mainly biology and medically oriented institute with no real interest or vocation for nuclear physics. However, the institute's library was designated a repository of US Atomic Energy Agency publications, becoming a valuable source of information. However, after successive ups and downs in the policy towards nuclear physics by the institute's directors, the reactor was finally shut down (1991) in a "reversible manner" and the core fuel, 20% enriched uranium, was dismantled and returned to the US. In spite of the closure of an important sector with the decommissioning of the Venezuela Research reactor RV 1, there has been renewed interest in accelerators for medical uses and applications of nuclear techniques for industrial purposes. These activities were also reinforced by technical cooperation agreements with the International Atomic Energy Agency (IAEA) in Vienna, Austria.

During the 1970s the official interest in atomic energy was expressed by the creation of the "Consejo Nacional Nuclear" (CONAN), later converted to "Consejo Nacional para Desarrollo de la Industria Nuclear" (CONADIN) and eventually to the present DEA or "Dirección de Energia Atomica." This institution became the Venezuelan counterpart of the IAEA. It had plans for the introduction of atomic power in Venezuela by the mid-1990s. It carried out modest surveying activities in the search for uranium deposits in the country, which yielded no results. However, a large deposit, Cerro Impacto (Aarden et al., 1973) containing thorium, niobium, rare earths, and other elements was discovered, placing the country in seventh place worldwide in thorium resources (World Nuclear Association, 2015). Nuclear power introduction plans were abandoned with the world's nuclear power cooling after the Three Mile Island and Chernobyl accidents.

A revival of interest in nuclear power came with the election of Hugo Chavez as president in 1998. The new government engaged in deep reform of the political and economic system of the country, including the initiative to launch a nuclear program for peaceful applications. Venezuela had signed the Tlatelolco agreement as a non-nuclear weapons state (UN Office for Disarmament's Affairs, 1967). It signed two agreements with Russia dealing with nuclear science and technology. The first on October 15, 2010 (Gaceta Oficial, 2009) was mainly a mutual collaboration agreement. The second (Gaceta Oficial, 2010) considered the purchase and installation of two nuclear reactors in the country: a research reactor to be used for medical, industrial, and scientific purposes and a nuclear power plant. The agreements included plans for the training of students in Russia to build the necessary manpower.

The tsunami at Japan and ensuing damage to the four Fukushima nuclear power reactors on March 11, 2011 (Fukushima Daiichi, 2016), as well as the following world media campaign against nuclear power, determined a presidential declaration putting a stop to the plans for the Russian nuclear reactors. However, the personal training program continued in a modest way with a number of students completing their postgraduate degrees in Russia. This student training program was still active in 2017.

Modest nuclear science activities are carried out at Venezuelan universities and at IVIC as part of the physics departments. This is mainly concentrated at the Dosimetry Laboratory at IVIC and at the Nuclear Physics Laboratory of the Universidad Simón Bolívar (USB). This laboratory, founded in 1979, has produced the majority of the research into the science, technology, and personal training in nuclear science in Venezuela (Laboratorio de física Nuclear, 2016).

In 2009, Kazuo Furukawa and Takashi Kamei paid a 1-week visit to USB during which they gave a course in thorium molten salt reactors (MSR) after a presentation at the ANFM2009 meeting (Kamei et al., 2009). This visit marks the beginning of the interest in thorium MSR of the research group of the Nuclear Physics Laboratory of the Universidad Simón Bolívar. Some of the group research areas are related to neutron production by spallation, neutron transport, and interactions in the core. In what follows we present some of the background activities in the field of molten salts, we describe a radioisotope excited subcritical liquid fuel assembly and a contribution to accelerator-driven MSR (AD MSR). A further contribution to AD MSR is included in Chapter 15, Accelerator-driven systems.

## 26.23.2 Background activities

Venezuela has a large experience in the industrial use of molten salt. This is an experience which can contribute modestly to the use of molten salts in the nuclear field. The aluminum industry (Alcasa and Venalum) reduce alumina ($Al_2O_3$) to pure aluminum in Hall-Herauld cells that contain molten cryolite ($Na_3AlF_6$) at 950°C. Very large cells handling currents as high as 350,000 A have been developed (Club Ensayos, 2016). The need to streamline the analysis of cryolite in order to diagnose the state of operation of the aluminum production cells and to optimize the operation of the plant resulted in the design of an isotope excited neutron activation procedure for the analysis of the fluoride molten salt (Greaves et al., 2005). This work resulted in first-hand experience with handling high-temperature fluoride molten salts in Venezuela.

As mentioned previously the invitation in 2009 to Kazuo Furukawa and Takashi Kamei to spend a week in USB resulted in close collaboration with the Japanese MSR movement and the publication of review articles (Furukawa et al., 2011; Greaves et al., 2012). The capacity of the molten salt nuclear fuel to be processed for the removal of nuclear waste and generation of fissile (Delpech et al., 2011) as well as the processing of alumina, created the idea of using molten salts for the reduction and production of elements from the refractory mineral columbite–tantalite (niobium and tantalum mineral) from Venezuelan deposits. The work carried out in Orsay, France, by E.D. Greaves with developments in the laboratory of Dr. Silvie Delpech (2013) involved three molten chloride systems: $ZnCl_2$–NaCl, LiCl–KCl, and NaCl–$CaCl_2$ and one fluoride system: FLiNaK, ternary eutectic alkaline metal fluoride salt mixture LiF–NaF–KF (46.5–11.5–42 mol%) that has a melting point of 454°C and a boiling point of 1570°C. The work resulted in additional experience with the use of molten salts and an opportunity for fostering the idea of the thorium MSR (Greaves, 2013a, 2013b).

## 26.23.3 Radioisotope excited subcritical liquid fuel assembly

A subcritical liquid fuel reactor project is in progress at USB. It has as its purpose the acquisition of expertise in the operation of liquid fuel reactors, the testing of modeling results, and training of students. The project contemplates the simplest configuration possible to keep costs and development time at very low levels. Operation is at room temperature for which the reactor's fuel (fertile and (eventually) fissile isotopes) are dissolved in aqueous media such as uranyl nitrate and thorium nitrate solutions. The facility is built around an existing radioisotope neutron irradiator developed as a cryolite ($F_6AlNa_3$) analyzer to serve the Venezuelan aluminum industry (Greaves et al., 2005) as shown in Fig. 26.23.1. The reactor contains a radioactive neutron source consisting of a californium $^{252}$Cf source and an americium-beryllium $^{241}$Am-Be source located in the center of a lead container that serves the purpose of shielding the high-intensity gamma radiation of the californium source between 1 and 10 MeV. The fission neutrons produced by the $^{252}$Cf source are of high energy (on average 2 MeV) so that the source is surrounded by a graphite moderator. The whole assembly has a biological shield consisting of lithium-loaded high-density polyethylene as well as lithium-loaded paraffin blocks. As shown in Fig. 26.23.1, there is an irradiation port which transverses the graphite lengthwise, where the liquid fuel reactor core is located. The core consists of a 3/16-in. polyethylene tube rolled around a graphite frame with a number of turns that is located in the center of the irradiation port. The core has an entrance and exit for the flow of the liquid fuel. The fuel solution is made to circulate in and out of the core by a peristaltic pump at a controlled flow that determines the fuel residence time in the core. Due to the limited thermal neutron flux produced by the radioactive sources, monitoring of reactions taking place is accomplished in-line by a detector, but mainly by off-line measurements of the radioactivity of the liquid fuel. For off-line measurements, these are done before and after irradiation with a high-resolution very low-level gamma ray spectrometer fitted with a solid-state detector (LEGE HPGe Camberra GL2020L) normally intended for environmental measurements. The facility is used for neutron activation experiments in the "Advance Laboratory" practicals of the physics undergraduate curricula at USB using nuclear electronics for energy spectra and lifetime

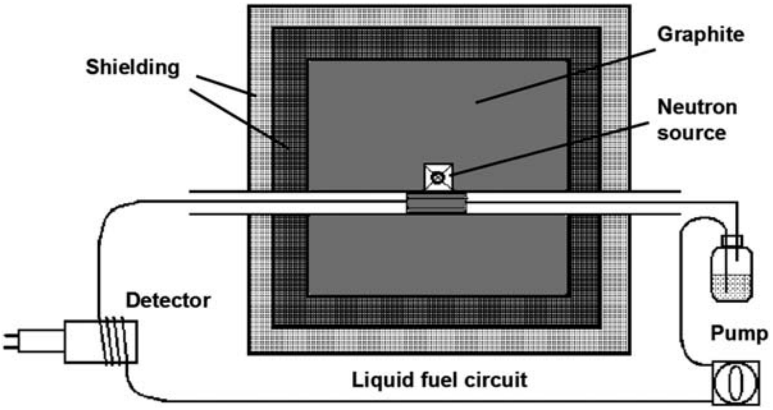

**Figure 26.23.1** Schematic diagram of the subcritical liquid fuel assembly facility showing the graphite moderator, surrounding shielding, and liquid fuel circulation.

measurements in the identification of nuclear isotopes. Open source Monte Carlo software packages such as FLUKA (FLUKA Home, 2016) and GEANT4 (GEANT4, 2016) are taught to advanced MSc and PhD candidates in nuclear technology projects. The modeling of the operation of the liquid fuel subcritical assembly constitutes a challenging proposal to train them in current nuclear energy tasks.

## 26.23.4 Accelerator-driven MSR (AD MSR) simulation

An AD MSR operates as a subcritical assembly and the chain reaction is maintained by an external neutron source. This can be accomplished by different technologies, for example, with a radio-isotopic neutron source ($^{252}$Cf, Ra-Be, Am-Be, or others) as described above or by an accelerator-related source that generates neutrons by gamma ray or particle beam nuclear reactions (Kamei, 2014). Earlier proposals on spallation reaction target design have been considered for running nuclear reactors (Furukawa et al., 1991; Rubbia et al., 1995) that operates close to the critical value. Today's important technological progress could be advantageously employed for this purpose.

As part of an extensive study we considered the on-going EURISOL project (2009) as a possible neutron source for an AD MSR device. Essentially it is an accelerator with a technologically advanced ion source producing a 1 GeV high energy proton beam impinging on the AD MSR device. The system is considered with power between 1 and 10 MW depending on the choice of reactor, effective multiplication factor $k_{\mathrm{eff}}$ value ($\sim k = 0.98$), and desired output power. It is usual to employ $E_{\mathrm{beam}} \geq 800$ MeV, targeting on fuel in the reactor core. In our case this is liquid fuel flowing in the reactor core. This is a target station where spallation neutrons are generated in large numbers, between 30 and 40 neutrons per reaction, that in turn interact with the thorium−uranium fuel providing transmutation and fission. The fertile-fissile nuclei, located by design in a large tank lined with graphite, circulate at high temperature and relatively low speed in a closed loop from the core to the heat exchanger. The target station therefore hosts the spallation neutron source and fissile fuel, including $^{235}$U-rich and $^{232}$Th molten salt mixture. The latter contains $ThF_4$ dissolved in the molten salt (FLiBe) being the fertile fuel to produce fissile fuel $^{233}$U. The target area is a modification of that proposed for the EURISOL neutron source with the important modification that the spallation reaction takes place directly in molten fuel salt. The geometry of the device is shown in Fig. 26.23.2.

Surrounding the target is a graphite moderator with cylindrical geometry providing the thermal neutrons and at the same time a duct for fuel transport. Further from the target (not shown) the fuel flows in a graphite-lined vessel that by reflection improves the neutron economy. As a last radiation barrier a concrete wall provides shielding and structural support for the whole assembly. All of these details have been included in a simulation using the FLUKA code (2016) (Battistoni et al., 2016). The composition of the molten salt and relevant technical details are given elsewhere (Bermudez et al., 2011).

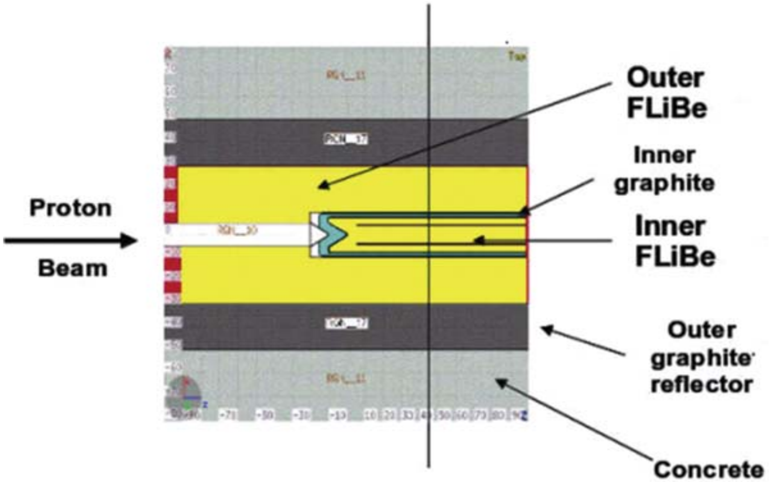

**Figure 26.23.2** Longitudinal section of the model core of AD MSR, showing the area where the proton beam interacts with Th/U + FLiBe fuel.

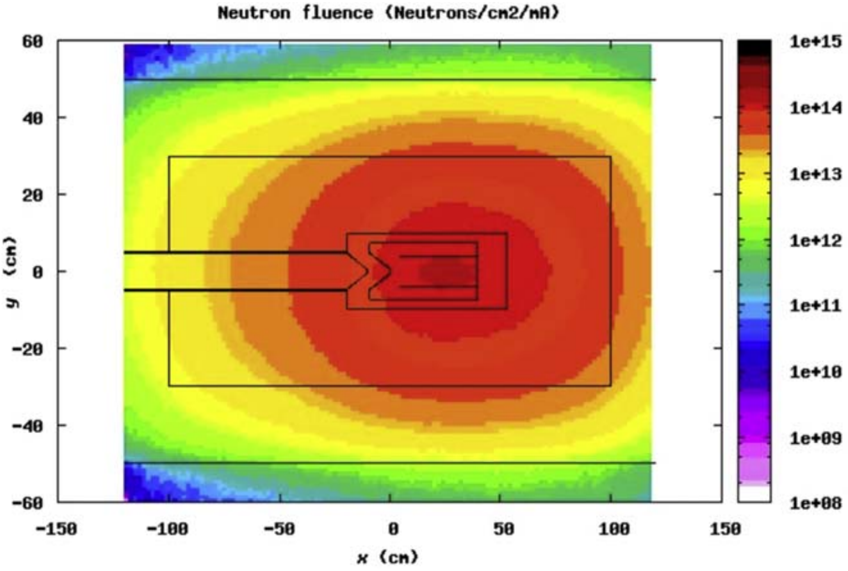

**Figure 26.23.3** Neutron fluence distribution in the core (neutrons/cm$^2$/mA). The results are shown for a proton beam of 1 GeV and a current of 1 mA (Bermudez et al., 2011).

The results of the modeling of the target station for a proton beam of 1 GeV and a current of 1 mA indicate that a specific density of neutrons/cm$^2$/mA is attainable. An example is shown in Fig. 26.23.3.

The distribution of the power density in the core of the reactor follows approximately, as expected, the 3D-Bragg curve. Energy produced by fission in the molten

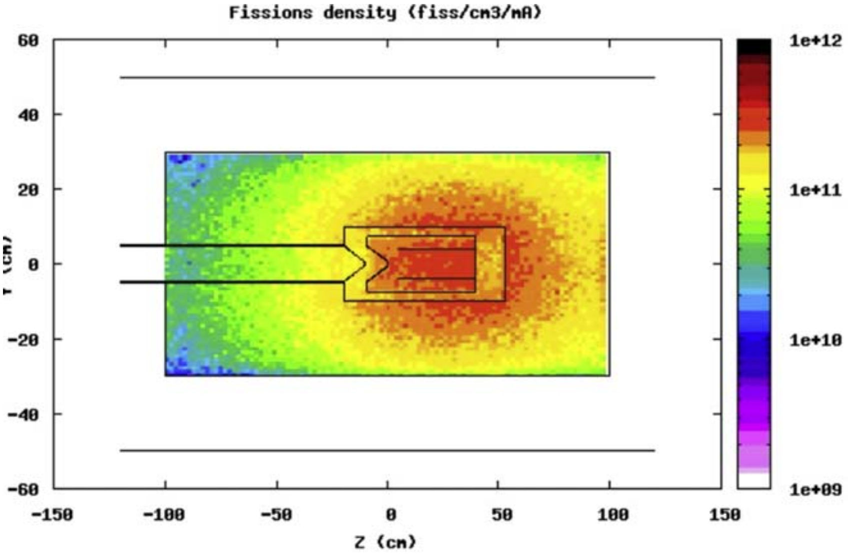

**Figure 26.23.4** Fission density distribution at the target station (Bermudez et al., 2011).

salt has a strong heat gradient toward the surrounded graphite reflector and structural concrete. The system is conceived for an operational power of 10 MW. The distribution of fissions in the fuel as a result of spallation neutrons and of fission neutrons indicates an asymmetry of the neutron fluence, power density, and fission density in the forward direction of the impinging proton beam. The fission density distribution is indicated in Fig. 26.23.4.

Predictions by FLUKA show spectra that depend on a graphite moderator, fuel, reflector, and concrete wall shape and mass. Specific spectra are obtained for the various zones. These have an important consequence on the reactor's effective multiplication factor $k_{\text{eff}}$. In fact, the spallation-related neutron energy distribution departs strongly from the fission spectrum. This in turn will superimpose to the existing in-core neutron spectrum and influences the neutron economy. One of these results is shown in Fig. 26.23.5 in comparison with the fission spectra. It has been observed that, in the nonfission multiplication case, fast neutrons produce a relatively large number of $(n, xn)$, $X = 1,2,3\ldots$ reactions due to the spallation spectra which contain a large portion of fast neutrons in the high-energy region.

The EURISOL AD MSR is characterized by the energy gain $G$ (i.e., energy produced/energy injected) which is expressed by the relation:

$$(\text{Energy}/\text{fission}) \times (N_o\,\text{number of neutrons per protons absorbed})/(\boldsymbol{\nu}(1-k_s)E_{\text{beam}})$$

In that $\boldsymbol{\nu}$ represents the number of neutrons released during fission or

$$G = (0.18N_ok_s)/(\nu(1-k_s)E_{\text{beam}}) = G_o/((1/k_s)-1)$$

For uranium $G_o \sim 3$ and since $k_s$ is very close to unity $G = 3/(1/k_s)$

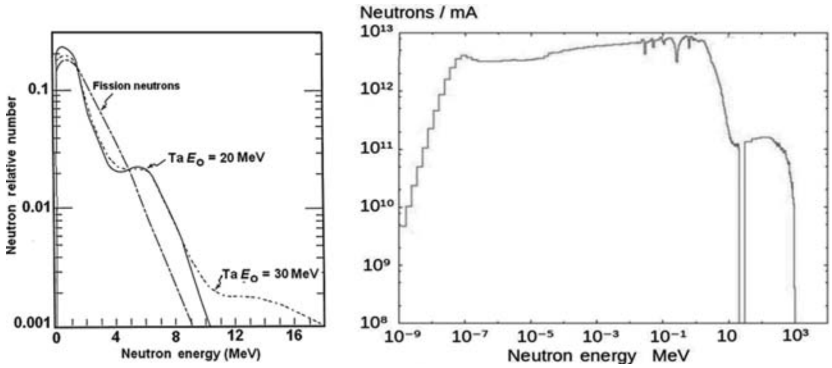

**Figure 26.23.5** (Left) Fission spectra. (Right) Specific neutron spectrum predicted by the AD MSR simulation around the fuel target station (Bermudez et al., 2011).

## 26.23.5 General conclusions

The radioisotope excited subcritical liquid fuel assembly described shows how a facility may be operated with very simple and economical means, without the need for highly radioactive materials which require extensive and lengthy certification procedures. The facility allows the acquisition of knowledge of the important features of liquid fuel reactors. Furthermore, it offers at the same time technical knowledge and the necessary expertise in the use of powerful modeling programs that condense substantial nuclear physics and important data on how these tools may be used for the design of the nucleonic aspects of MSR.

The work carried out in Monte Carlo modeling of the EURISOL type neutron source shows that it is indeed possible to use this technology for a high energy proton accelerator-driven MSR. However, further work is needed in refinement in respect to the size, scaling, fissile concentration, and the requirement of a more realistic geometry.

## Acknowledgments

The authors thank Dr Takashi Kamei for critical reading of and suggestions to the manuscript. They also thank Prof. Rubén Machado, Director of the Dirección de Energía Atómica of the Venezuelan government, for valuable help given to our group in liaison with the International Atomic Energy Agency.

## References

Aarden, H.M., Arozena, J.M., Moticska, P., Navarro, J., Pasquali, J., Sifontes, R.S., 1973. El complejo geológico del area de Impacto, Distrito Cedeño, Estado Bolívar, Venezuela. Ministerio de Minas e Hidrocarburos, Dirección de Geología. Mayo de 1973.

Battistoni, G., Cerutti, F., Fasso, A., Ferrari, A., Muraro, S., Ranft, J., et al., 2016. The FLUKA code: description and benchmarking. <http://www.fluka.org/content/publications/2007_fermilab.pdf> (accessed January 2016).

Bermudez, J., Sajo-Bohus, L., Tecchio, L., Palfalvi, J.K. Palacios, D., 2011. Target design for a thorium Accelerator-Driven Molten Salt Reactor (AD-MSR). 2011 Phys. Research Int'l ID 796318, pp. 1−7 <http://dx.doi.org/10.1155/2011/796318>.

ClubEnsayos.com, 22 de Mayo de 2015. La Celda V-350 (in Spanish). <https://www.clubensayos.com/Tecnolog%C3%ADa/La-Celda-V-350-Representa-El-Punto-De-Partida/2540365.html> (accessed January 2016).

Delpech, S., 2013. Possible routes for pyrochemical separations: focus on the reductive extraction in fluoride media. Pure Appl. Chem. 85 (1), 71−87.

Delpech, S., Merle-Lucotte, E., Heuer, D., Slim, C., 2011. Liquid fuel for nuclear energy: The Molten Salt Fast Reactor (MSFR) concept. Chapter of "Liquid Fuels: Types, Properties and Production" of the series: "Energy Science, Engineering and Technology". Nova Science Publishers (2011).

EURISOL Project, 2009. Multi-MW proton-to-neutron converter. EURISOL Design study, multi-MW proton-to-neutron converter. Accessed January 2016. <http://www.eurisol.org/>.

FLUKA home, 2016. The official FLUKA site. <http://www.fluka.org/fluka.php> (accessed January 2016).

Fukushima Daiichi Nuclear Power Plant, Accessed January 2016. <https://en.wikipedia.org/wiki/Fukushima_Daiichi_Nuclear_Power_Plant>.

Furukawa, K., Lecocq, A., Kato, Y. Mitachi, K., 1991. Radiowaste management in global application of Thorium Molten-Salt Nuclear Energy Synergetics with Accelerator Breeders. Saltsjobaden, SWEDEN, LA-12205-C, 686, June, 1991; UC-940, p. 686 (1991).

Furukawa, K., Greaves, E.D., Erbay, L.B., Hron, M., Kato, Y., 2011. New sustainable secure nuclear industry based on thorium molten-salt nuclear energy synergetics (THORIMS-NES) in nuclear power, Book 1, INTECH Pubs. Pavel Tsvetkov Ed. pp. 407−444 (39p) ISBN 978-953-307-185-5 (2011) <http://j.mp/s4yNYh>.

Gaceta Oficial, 2009. Ley Aprobatoria del Convenio entre el Gobierno de la República Bolivariana de Venezuela y el Gobierno de la Federación de Rusia, sobre la Cooperación en el Área del Uso de la Energía Nuclear con Fines Pacíficos (Law approving the Agreement between the Government of the Bolivarian Republic of Venezuela and the Government of the Russian Federation on Cooperation in the Area of Uses of Nuclear Energy for Peaceful Purposes) 10th March 2009 Gaceta Oficial No 39170 04/05/2009. <http://www.pgr.gob.ve/dmdocuments/2009/39170.pdf> (accessed 23.01.16).

Gaceta Oficial, 2010. No. 39.558 del 23 de noviembre de 2010. Ley Aprobatoria del Acuerdo entre el Gobierno de la República Bolivariana de Venezuela y el Gobierno de la Federación de Rusia Sobre la Cooperación para el Desarrollo del Programa Nucleoeléctrico en la República Bolivariana de Venezuela, la Construcción y Operación de un Reactor de Investigación para la Producción de Radioisótopos de Usos Pacíficos en Medicina e Industria y de una Central Nucleoeléctrica en el Territorio de la República Bolivariana de Venezuela. <http://www.mp.gob.ve/c/document_library/get_file?p_l_id=29938&folderId=108950&name=DLFE-2160.pdf> (accessed February 2016).

GEANT 4, 2016. <http://www.geant4.org/geant4/> (accessed January 2016).

Greaves, E.D., 2013a. A new Paradigm: thorium as nuclear fuel in the molten salt reactor. (Frankfurt, Germany, 2013). <http://www.youtube.com/watch?v=vBIyZZuQl4A

&list=PLoHwt4KyUk5BNBJ_NtTruKKOFuDWjMgRl&index=7> (accessed January 2016).

Greaves, E.D., 2013b. Entrevue de Karel Vereycken avec le Professeur Eduardo Greaves. <https://www.youtube.com/watch?v=OJqyld66lE4> (accessed January 2016).

Greaves, E.D., Sajo-Bohus, L., Manrique, M., DeArriba, C., 2005. Radioisotope neutron activation analysis of cryolite-alumina solution. Acta Phys. Chim. Debrecina. 38–39 (2005), 175–183.

Greaves, E.D., Furukawa, K., Sajo-Bohus, L., Barros, H., 2012. The case for the thorium molten salt reactor. Proceedings IX Latinamerican Symposium on Nuclear Physics and Applications. Quito, Ecuador. 18–22 July 2011. AIP Conf. Proc. 1423, 453–460, doi:10.1063/1.3688845. <http://proceedings.aip.org/resource/2/apcpcs/1423/1/453_1?isAuthorized=no>.

Kamei, T., 2014. A newly developed accelerator to convert thorium to uranium-233. In: International Symposium on Uranium Raw Material for the Nuclear Fuel Cycle (URAM-2014) June 23–27, 2014, Vienna, Austria.

Kamei, T., Kato, Y., Mitachi, K., Shimazu, Y., Furukawa, K., 2009. Thorium molten-salt nuclear energy synergetics for the huge size fission industry. In: Proceedings of ANFM 2009, Pittsburgh, USA, April 12–15, 2009.

Laboratorio de física Nuclear, 2016. Universidad Simón Bolívar, Caracas Venezuela. <http://www.nuclear.fis.usb.ve/> (accessed January 2016).

Rubbia, C., Rubio, J.A., Buono, S., Carminati, F., Fiétier, N., Galvez, J., et al., 1995. Conceptual design of a fast neutron operated high power energy amplifier CERN/AT/95-44 (ET) (1995). <http://www.mipp.fnal.gov/raja/energy_amplifier/cer-0210391.pdf> (accessed January 2016).

UN Office for Dissarment Afairs, 1967. Treaty for the Prohibition of Nuclear Weapons in Latin America and the Caribbean, Opened for signature at Mexico City: 14 February 1967. Venezuela ratification: 23 March 1970. Text available at: <http://disarmament.un.org/treaties/t/tlatelolco> (accessed January 2016).

World Nuclear Association, 2015. Thorium. <http://www.world-nuclear.org/info/current-and-future-generation/thorium/> (accessed January 2016).

# Issues and conclusions

# 27

*Thomas J. Dolan*
University of Illinois at Urbana—Champaign, Champaign, IL, United States

**Chapter Outline**

The world needs widespread use of nuclear energy to promote universal prosperity, to provide fresh water to dry regions, to prevent wars over fossil fuels, to complement intermittent energy sources, and to mitigate climate change. Widespread use requires better utilization of uranium and thorium, hence consideration of breeding with accelerators, fusion reactors, or high conversion ratio fission reactors. Molten salts are useful for all these applications.

## 27.1 Achievements

Molten salt coolants do not evaporate at reactor temperatures, no water or steam is present in a molten salt reactor (MSR) core, and no hydrogen is generated, so the use of low-pressure molten salt instead of high-pressure water could have prevented the Three Mile Island, Chernobyl, and Fukushima accidents. Recognizing the inherent safety advantages, many countries are now engaged in MSR research and in thorium energy development. MSRs could produce energy safely at costs competitive with fossil fuels, if excessive regulatory requirements and delays did not interfere.

Some MSR features and achievements cited in this book are:

- Some MSR development company designs might satisfy the investors' economic, regulatory, and public acceptance requirements for new power plants better than most other reactors (see Chapters 1: Introduction and 17–25).
- The nuclear air-cooled Brayton combined cycle promises high-efficiency, thermal energy storage, and potential deployment in dry climates. Even if the Rankine cycle with current supercritical steam turbine is applied, the MSR has higher efficiency than current light water reactors (LWRs) (see Chapter 2: Electricity production).
- In addition to electrical power generation, MSRs could provide high-temperature chemical production (such as hydrogen, ammonia, and ethylene), actinide waste incineration, desalination of water, space propulsion, and medical isotope production (see Chapter 3: Chemical fundamentals and other applications).

**Molten Salt Reactors and Thorium Energy. DOI: http://dx.doi.org/10.1016/B978-0-08-101126-3.00027-0**

- The reactor physics of moving precursors is being studied: simulation codes to help understand the transport of delayed neutron precursors in the core, delayed neutron emission outside the core, and of fluid flow with heat sources in both the fluid and the graphite (see Chapters 5: Kinetics, dynamics and neutron noise in stationary MSRs and 6: Thermal hydraulics of liquid-fueled MSRs).
- Materials selection, new materials development, and redox potential control can limit corrosion to acceptable values (see Chapter 7: Materials).
- On-line or batch processing can separate uranium, plutonium, other actinides, and fission products from the fuel, breeder, and coolant salts (see Chapters 3: Chemical fundamentals and other applications, 8: Chemical processing of liquid fuel, 11: Liquid fuel, thermal neutron spectrum reactors).
- Most of the fission products decay within 300 years, and the actinides are responsible for the longer-term radioactivity. MSRs could remove the actinides online, or incinerate actinides from LWRs, so that the fuel would not need to be treated as radioactive waste, and it could even be recycled after 300 years (see Chapter 9: Environment, waste, and resources).
- Ways to improve the proliferation resistance of MSR fuel cycles have been identified. The safeguarding of liquid fuel will require changes in the accounting methodology. Efficient incineration of plutonium by thorium MSRs would reduce the proliferation risk, which is a concern for the current U–Pu fuel cycle (see Chapters 10–12).
- The 200-MWe FUJI-U3 thermal spectrum MSR can operate with a fissile mass inventory $\sim$ 1.1 ton, relatively flat power density profile, and conversion ratio $\sim 1$ without online reprocessing, keeping the graphite and liquid fuel in the core for 30 years, and producing only 4% as much actinides as a Boiling water reactor (BWR) (see Chapter 11: Liquid fuel, thermal neutron spectrum reactors).
- Safety issues have been addressed and general design criteria for MSRs have been proposed (see Chapter 11: Liquid fuel, thermal neutron spectrum reactors).
- Due to recent observation of the high solubility of $PuF_3$, $UF_4$, and $AmF_3$ in the eutectic LiF-NaF-KF, three ideas can be combined: liquid fuel, fast neutron spectrum, and U–Pu fuel cycle (see Chapter 12: Fast spectrum, liquid fueled reactors).
- Solid fuel fluoride-salt cooled high-temperature reactors (FHRs) and static liquid fuel reactors might be deployed earlier than liquid fuel-cooled MSRs, providing dispatchable power to complement fluctuating solar and wind power, and perhaps serving as a stepping stone to liquid fuel-cooled molten salt reactors (see Chapters 13: solid fuel, salt-cooled reactors and 14: Static liquid fuel reactors).
- A static liquid fuel reactor with molten salt fuel in conventional fuel tubes and assemblies would avoid the need to pump and valve highly radioactive fluid, avoid the complexity of combining the fuel and primary coolant, and avoid the need for online reprocessing and chemical treatment (see Chapter 14: Static liquid fuel reactors).
- Assuming 80% load factor in an accelerator-driven molten salt breeder, the net production rate of $^{233}U$ is about 800 kg/year, which can be used to start one 1-GWe FUJI-MSR every 2 years. Accelerator-driven systems could incinerate about 300 kg of LWR actinide wastes per GWth-year of Accelerator driven system (ADS) operation (see Chapter 15: Accelerator-driven systems).
- A fusion–fission hybrid neutron source power of 1 GWth could breed $\sim$ 3000 kg/year of U-233, enough to provide fuel for 15 fission reactors (see Chapter 16: Fusion–fission hybrids).
- Nine organizations describe the advantages of their reactor designs (see Chapters 17–25).
- A solid fuel MSR and a liquid fuel MSR are under construction in China (see Chapter 17: Thorium molten salt reactor nuclear energy system (TMSR)).
- Twenty-three countries are engaged in MSR or thorium energy research (see Chapter 26: Worldwide Activities).

## 27.2 Reactor development

The main technology issues are:

- Structure and clad (if solid fuel) resistance against neutron irradiation;
- Corrosion resistance at high-temperature;
- Graphite lifetime (if thermal reactor);
- Tritium inventory measurement and control;
- High fissile nuclide conversion ratio;
- Pumps, valves, and heat exchanger development;
- Fission product separation and use or disposal;
- Startup fissile fuel load sources;
  - MSR breeder reactors with a short doubling time,
  - U-235 from isotope separation systems (expensive, usable for proliferation),
  - Accelerator-driven systems with breeder blankets,
  - Fusion—fission hybrid blankets,
  - Pu-239 from dismantled weapons, or
  - Used LWR fuel.

## 27.3 Societal issues

Some additional issues are:

- Fissile isotope security and inventory control;
- New safety criteria;
- Simplified, efficient, affordable licensing procedures;
- Public education and acceptance of MSRs.

## 27.4 Conclusions

This book shows the good progress that is being made on these issues, building on the valuable MSRE experience. Liquid fuel MSRs afford significant advantages over solid fuels (see Chapter 1: Introduction), but reactors that do not require online processing of liquid fuels might be deployed earlier.

*We envision a world where almost every country has affordable molten salt reactors burning thorium, uranium, and spent fuel actinides, producing electricity, hydrogen, and desalinized water with no serious accidents.*

# Appendix A: Abbreviations

| | |
|---|---|
| **0-D** | Zero-dimensional |
| **1-D** | One-dimensional |
| **2-D** | Two-dimensional |
| **3-D** | Three-dimensional |
| **AAEC** | Australian Atomic Energy Commission (AAEC) |
| **ABWR** | Advanced boiling water reactor |
| **ACSEPT** | Actinide recycling by SEParation and Transmutation |
| **ADE** | adiabatic detachment energy |
| **ADS** | Accelerator-driven system |
| **ADTT** | Accelerator-driven transmutation technology |
| **AECL** | Atomic Energy of Canada Limited |
| **AHTR** | Advanced high-temperature reactor |
| **ALARP** | As low as reasonably practical |
| **ALC** | American Locomotive Company |
| **ALI** | Annual limit for intake |
| **ALISIA** | Assessment of LIquid Salts for Innovative Applications |
| **AMD** | Atomic Minerals Directorate for Exploration and Research |
| **AMSB** | Accelerator molten salt breeder |
| **An** | Actinide |
| **ANL** | Argonne National Laboratory |
| **ANS** | American Nuclear Society |
| **ANSTO** | Australian Nuclear Science and Technology Organisation |
| **AOO** | Anticipated operational occurrences |
| **AOT** | Abnormal operating transients |
| **AP** | Additional Protocol |
| **ARC** | Advanced recycling center |
| **ARE** | Aircraft Reactor Experiment |
| **ARP** | Aircraft nuclear propulsion |
| **ART** | Aircraft reactor test |
| **ART** | Office of Advanced Reactor Technologies |
| **ASME** | American Society of Mechanical Engineers |
| **ASGARD** | Advanced fuelS for Generation IV reActors: Reprocessing and Dissolution |
| **ATS** | Automation system |
| **ATWS** | Anticipated Transient Without SCRAM |
| **AVLIS** | Atomic vapor laser isotope separation |
| **BAPETEN** | National Nuclear Energy Regulatory Agency of Indonesia |
| **BARC** | Bhabha Atomic Research Center |
| **BATAN** | The National Nuclear Energy Agency |
| **BC** | Betavoltaic cell |
| **BCC** | Body-centered cubic |

| | |
|---|---|
| **B-DBA** | Beyond design-basis accidents |
| **BDBE** | Beyond design basis event |
| **BNFL** | British Nuclear Fuels, Limited |
| **BNL** | Brookhaven National Laboratory |
| **BR** | Breeding ratio |
| **BREST** | Inherently safe lead cooled fast reactor |
| **BWR** | Boiling water reactor |
| **CA** | Copenhagen Atomics |
| **CANDU** | CANada Deuterium Uranium |
| **CAPEX** | Capital expenditure |
| **CAS** | Chinese Academy of Sciences |
| **CCGT** | Combined cycle, Brayton and Rankine together |
| **CCP** | Cubic close packing |
| **CEA** | Commissariat a l'Energie Atomique et aux Energies Alternatives |
| **CED** | Cumulative energy demand |
| **CEDE** | Committed effective dose equivalent |
| **CEO** | Chief Executive Officer |
| **CERN** | Centre Européen de la Recherche Nucleaire |
| **CFD** | Computational fluid dynamics |
| **CFFE** | Cumulative fissile fuel enrichment |
| **CHTR** | Compact high-temperature reactor |
| **CIET** | Compact Integral Effects Test |
| **Cinsf1D** | Computer program |
| **CINVESTAV** | Centro de Investigación y de Estudios Avanzados del Instituto Politécnico Nacional |
| **CIRTEN** | Consorzio Interuniversitario per la Ricerca Technologica Nucleare |
| **CNFC** | Closing nuclear fuel cycle |
| **CNRS** | Centre National de la Recherche Scientifique |
| **CNS** | Chassigny Nakhla Shergotty |
| **CNSC** | Canadian Nuclear Safety Commission |
| **COLEX** | Column exchange |
| **CONADIN** | Consejo Nacional para Desarrollo de la Industria Nuclear |
| **CONAN** | Consejo Nacional Nuclear |
| **CRADA** | Cooperative Research and Development Agreement |
| **CRIEPI** | Central Research Institute of Electric Power Industry |
| **CR** | Conversion ratio |
| **CRP** | Coordinated research project |
| **CSP** | Concentrated solar power |
| **CTAH** | Coiled tube air heater |
| **CTHX** | Coiled-tube heat exchanger |
| **CtL** | Coal to liquid fuel |
| **CVD** | Carbon vapor deposition |
| **DAE** | Department of Atomic Energy |
| **DBA** | Design basis accidents |
| **DCF** | Dose conversion factor |
| **DEA** | Dirección de Energía Atómica |
| **DEEP** | Desalination Economic Evaluation Program |
| **DEM** | Discrete element method |
| **DE-TOP** | Desalination Thermodynamic Optimization Program |

| | |
|---|---|
| **DFR** | Dual fluid reactor |
| **DFT** | Density functional theory |
| **DHX** | DRACS heat exchanger |
| **DMSR** | Denatured molten salt reactor |
| **DNBR** | Departure from nucleate boiling ratio |
| **DOE** | Department of Energy, USA |
| **dpa** | Displacments per atom |
| **DPRK** | Democratic People's Republic of Korea |
| **DRACS** | Direct reactor auxiliary cooling system |
| **DSC** | Differential scanning calorimetry |
| **DTU** | Technical University of Denmark |
| **DYN1D-MSR** | Computer program by Forschungszentrum Rossendorf, Germany |
| **DYN3D-MS** | Computer program by Forschungszentrum Rossendorf, Germany |
| **DYNASTY** | DYnamics of NAtural circulation for molten SalT internallY heated |
| **EBR** | Experimental breeder reactor |
| **ECCS** | Emergency core cooling system |
| **ED** | Electrodialysis |
| **EDF** | Electricité de France |
| **EFPD** | Effective full power days |
| **EFPY** | Effective ull power years |
| **EIGM** | General Directorate of Energy Affairs |
| **EIR** | Eidgenössisches Institut für Reaktorforschung |
| **EITF** | Electron irradiation test facility |
| **ENDF** | Evaluated Nuclear Data File |
| **ENSAD** | Energy-related Severe Accident Database |
| **EOC** | End of cycle |
| **EOS** | Equations of state |
| **EPA** | Environmental Protection Agency |
| **EPDK** | Energy Market Regulatory Authority |
| **EPR** | European pressurized water reactor |
| **EPSS** | Electrical power supply system |
| **EROI** | Energy return on investment |
| **ESS** | European Spallation Source |
| **ETI MADEN** | ETI Maden General Directorate |
| **EUA** | Excessive use of abbreviations |
| **EUAS** | Electricity Generation Company |
| **EURATOM** | EURopean ATOMic Energy Community |
| **EURISOL** | European Isotope Separation On-Line |
| **EVOL** | Evaluation and Viability Of Liquid Fuel Fast Reactor (EU project) |
| **FBNR** | Fixed bed nuclear reactor |
| **FBR** | Fast breeder reactor |
| **FBTR** | Fast breeder test reactor |
| **FCC** | Face-centered cubic |
| **FHRs** | Fluoride-salt-cooled high-temperature reactors |
| **FHSS** | Fuel handling and storage system |
| **FHTR** | FHR test reactor |
| **FIRES** | Firebrick resistance heated energy storage |
| **FIRM** | Fuel inside radial moderator |
| **FLiBe** | LiF-BeF2 or Lithium Beryllium Fluoride salt |

| | |
|---|---|
| **FLiNaK** | Eutectic LiF-NaF-KF |
| **FLUKA** | Fluctuating Kascade Monte Carlo program |
| **FMSR** | Fast molten salt reactor |
| **FP** | Fission Products |
| **FP** | Framework Program of the EU |
| **FT** | Fischer-Tropsch |
| **FUJI** | Name of a Japanese MSR design |
| **FUM** | Fuel unloading machines |
| **GAIN** | Gateway for Accelerated Innovation in Nuclear |
| **GCR** | Gas-cooled reactor |
| **GDC** | General Design Criteria |
| **GDR** | Giant dipole resonance |
| **GEMS** | Gibbs Energy Minimization Software |
| **GENIUS** | Generation IV research in universities of Sweden (Research project supported by the Swedish Research Council) |
| **Gen-IV** | Generation IV nuclear systems |
| **GFR** | Gas-cooled fast reactor |
| **GIF** | Generation IV International Forum |
| **Gr** | Grashof number |
| **GT** | Gas turbine |
| **GTMHR** | Gas turbine-modular helium reactor |
| **GWd/tonne** | Power yield per tonne heavy metal in nuclear fuel |
| **GWd/t-U** | Giga Watt day per a metric ton of uranium |
| **GWth** | Giga Watt thermal |
| **HCP** | Hexagonal close packing |
| **HEU** | Highly enriched uranium |
| **HFE** | Human Factors Engineering |
| **HHHC** | Horizontal heater−horizontal cooler |
| **HM** | Heavy metal |
| **HOMO** | Occupied molecular orbitals |
| **HP** | High pressure |
| **HRE** | Homogeneous Reactor Experiment |
| **HRSG** | Heat recovery steam generator |
| **HTC** | High temperature containment |
| **HTDF** | High-temperature DRACS test facility |
| **HTGRs** | High-temperature gas-cooled reactors |
| **HTMR** | High-temperature modular reactor |
| **HTRE** | Heat Transfer Reactor Experiments |
| **HVAC** | Heating, ventilation and air conditioning |
| **HWMSR** | Heavy water moderated molten salt reactor |
| **HWR** | Heavy water reactor |
| **HX** | Heat exchanger |
| **IABAT** | Impact of Accelerator-BAsed Technologies on nuclear fission safety |
| **IAEA** | International Atomic Energy Agency |
| **ICBM** | Intercontinental ballistic missile |
| **ICRP** | International Commission on Radiological Protection |
| **IET** | Integral effects test |
| **IFR** | Integral fast reactor |
| **IGCAR** | Indira Gandhi Centre for Atomic Research |

| | |
|---|---|
| **IHG** | Internal heat generation |
| **IHTR** | Innovative high-temperature reactor |
| **IHX** | Intermediate heat exchanger |
| **ILW** | Intermediate level waste |
| **IME** | Institute of Materials Engineering |
| **IMSBR** | Indian Molten Salt Breeder Reactor |
| **IMSR** | Integral molten salt reactor |
| **INL** | Idaho National Laboratory |
| **IPCC** | Intergovernmental Panel on Climate Change |
| **IPE** | Intermolecular potential energy |
| **IPPE** | Institute of Physics and Power Engineering, Obninsk |
| **IRSN** | Institut de Radioprotection et de Sûreté Nucléaire |
| **ITB** | Bandung Institute of Technology |
| **ITE** | Institute for Transuranium Elements |
| **ITEP** | Institute of Theoretical and Experimental Physics, Moscow |
| **IThEO** | International Thorium Energy Organization |
| **ITMSF** | International Thorium Molten-Salt Forum |
| **IVIC** | Instituto Venezolano de Investigaciones Científicas |
| **JAEC** | Japan Atomic Energy Committee |
| **JEFF** | Joint Evaluated Fission and Fusion File |
| **JENDL** | Japanese Evaluated Nuclear Data Library |
| **JPL** | Jet Propulsion Laboratory |
| **JRC** | Joint Research Centre |
| **JRC-ITU** | Joint Research Center—Institute for Transuranic Elements |
| **KAPF** | Korean Advanced Processing Facility |
| **KEMA** | Research center in Arnhem, Netherlands |
| **KIPT** | Kharkiv Institute of Physics &Technology |
| **KIT** | Karlsruher Institut für Technologie |
| **KSTR** | KEMA Suspension Test Reactor |
| **KTH** | Royal Institute of Technology, Stockholm |
| **LAM** | Laser Additive Manufacturing |
| **LBE** | Lead-bismuth eutectic |
| **LBE** | Licensing basis events |
| **LBLOCA** | Large break loss of coolant accident |
| **LCA** | Life cycle assessment |
| **LET** | Linear energy transfer |
| **LEU** | Low-enriched uranium |
| **LHF** | Localized heat flux |
| **LIBS** | Laser-induced breakdown spectroscopy |
| **LIFE** | Laser-induced fusion energy |
| **LINAC** | Linear accelerator |
| **LKP** | Lee-Kesler-Plocker |
| **LMFBR** | Liquid metal cooled fast breeder reactor |
| **LMR** | Liquid metal reactors |
| **Ln** | Lanthanide |
| **LOCA** | Loss of coolant accident |
| **LOFC** | Loss of forced circulation |
| **LOHS** | Loss of heat sink |
| **LP** | Low pressure |

| | |
|---|---|
| **LRS** | Laboratory for Reactor Physics and System Behaviour |
| **LS-VHTR** | Liquid salt very high temperature reactor |
| **LTDF** | Low-temperature DRACS test facility |
| **LUMO** | Unoccupied molecular orbitals |
| **LWR** | Light-water reactor |
| **M** | Madelung constant |
| **M** | Metal |
| **MA** | Minor actinides |
| **MAFL** | Molten active fluoride salt loop |
| **MAPS** | Madras Atomic Power Station |
| **MCFRs** | Molten chloride fast reactors |
| **MCNP** | MonteCarlo N Particle neutronics code |
| **MCRP** | Minimum critical power ratio |
| **MD** | Molecular dynamics |
| **MED** | Multi-effect distillation |
| **MENR** | Ministry of Energy and Natural Resources |
| **MEPHI** | Moscow Engineering Physics Institute |
| **MFT** | Mean field theory |
| **MHD** | Magnetohydrodynamic |
| **MIGEM** | General Directorate of Mining Affairs |
| **MIMOSA** | EU research project title: “Materials Investigations for MOlten SAlt reactor technology development” |
| **MIT** | Massachusetts Institute of Technology |
| **Mk 1 PB-FHR** | Mark 1 PB-FHR |
| **MOSART** | Molten Salt Actinide Recycler and Transmuter, Russia |
| **MOSEL** | Molten Salt ExperimentaL or Molten Salt EpithermaL |
| **MOST** | MOlten Salt Technology (EU project) |
| **MOX** | Mixed oxide fuel |
| **MP** | Medium pressure |
| **MPDT** | Magnetoplasmadynamic Thrusters |
| **MPM** | Multi-physics modeling |
| **MPP** | Maximum possible production |
| **MPSS** | Main power supply system |
| **MRE** | Homogeneous Reactor Experiment |
| **MS** | Mitigation system |
| **MSBR** | Molten salt breeder reactor |
| **MSBRDF** | Molten salt breeder reactor development facility |
| **MSCR** | Molten salt converter reactor |
| **MSF** | Multistage slash |
| **MSFBR** | Molten-salt fast breeder reactor |
| **MSFR** | Molten salt fast reactor |
| **MSHT** | Molten Salt Hybrid Tokamak |
| **MSR** | Molten salt reactor |
| **MSR-B** | Fast spectrum molten salt reactor burner |
| **MSRE** | Molten Salt Reactor Experiment |
| **MSTW** | Molten Salt Thermal Wasteburner |
| **MTA** | Mineral Research and Exploration Institute |
| **MTHM** | Metric tons of heavy metal |
| **MUST** | Missouri University of Science and Technology |

| | |
|---|---|
| **MWd/t-HM** | Mega Watt day per a metric ton of heavy metal |
| **NACC** | Nuclear Air-Brayton Combined Cycle |
| **NAS** | National Academy of Sciences |
| **NASA** | National Aeronautics and Space Administration |
| **NCL** | Natural circulation loop |
| **NE** | Nuclear Engineering |
| **NEA** | Nuclear Energy Agency |
| **NED** | Nuclear explosive device |
| **NEPUD** | Nuclear Energy Project Implementation Department |
| **NES** | Nuclear Energy and Safety |
| **NEUP** | Nuclear energy university program |
| **NFC** | Nuclear fuel complex |
| **NGCC** | Natural gas combined cycle |
| **NGNP** | Next-generation nuclear power plant |
| **NIFS** | National Institute for Fusion Science |
| **NIRAB** | Nuclear Innovation and Research Advisory Board |
| **NIST** | National Institute of Standards and Technology |
| **NNL** | National Nuclear Laboratory |
| **NNN** | Next-nearest neighbor |
| **NNWS** | Non-nuclear weapons states |
| **NOLSTA** | Nonlinear Stability Analysis Code |
| **NPL** | Nuclear pumped lasers |
| **NPP** | Nuclear power plant |
| **NPT** | Treaty on the Non-Proliferation of Nuclear Weapons |
| **NPV** | Net present value |
| **NRC** | Nuclear Regulatory Commission (USA) |
| **NRI** | National Research Institute |
| **NSA** | Nonstate actors |
| **NSA** | National Security Agency (USA) |
| **NSSS** | Nuclear steam supply system |
| **NTD** | Nuclear track detector |
| **NtL** | Nitrogen to liquid fuel |
| **NTM** | Nuclear Track Detector Methodology |
| **NWS** | Nuclear weapons states |
| **ODE** | Ordinary differential equation |
| **ODS** | Oxide dispersion strengthened |
| **OECD** | Organization of Economic Cooperation and Development |
| **OPEX** | Operational expenditure |
| **ORIGEN** | Computer code that calculates isotopic abundances vs. time |
| **ORNL** | Oak Ridge National Laboratory |
| **OSU** | Ohio State University |
| **OTTO** | Once through then out |
| **P&T** | Integral fast reactor |
| **P&T** | Partitioning and transmutation |
| **PADC** | Poly-allyl-diglicol-carbonate |
| **PB** | Pebble bed |
| **PB-AHTR** | Pebbl bed advanced high-temperature reactor |
| **PB-FHR** | Pebble bed fluoride-salt-cooled high-temperature reactor |
| **PBMR** | Pebble bed modular reactor |

| | |
|---|---|
| **PBR** | Pebble bed reactor |
| **PCHE** | Printed circuit heat exchanger |
| **PCMSR** | Passive, compact molten salt reactor |
| **PCS** | Power conversion system |
| **PDE** | Partial differential equation |
| **PD-MSR** | Photo driven molten salt reactor |
| **PDR** | Pygmy dipole resonance |
| **PHWR** | Pressurized heavy water reactor |
| **PHX** | Primary heat exchanger |
| **PKE** | Point kinetic equation |
| **Polimi** | Politecnico di Milano |
| **Polito** | Politecnico di Torino |
| **PPU** | Pyroprocessing unit |
| **PRA** | Probabilistic risk assessment |
| **PRISM** | Power Reactor Innovative Small Module |
| **PSA** | Probabilistic safety assessment |
| **PSEL** | Project and Study Fund of the Electricity Industry |
| **PSI** | Paul Scherrer Institut (Switzerland) |
| **PSI-BOIL** | Parallel SImulator of BOILing |
| **PUREX** | Plutonium Uranium Redox EXtraction |
| **PWAR** | Pratt and Whitney Aircraft Reactor |
| **PWR** | Pressurized water reactor |
| **R&D** | Research & development |
| **Ra** | Rayleigh number |
| **RB** | Reactor building |
| **RBWR** | Reduced-moderation BWR |
| **RCCS** | Reactor cavity cooling system |
| **Re** | Reynolds number |
| **REDOX** | Reduction oxidation |
| **REFINE** | REduction of spent Fuel vital In a closed loop Nuclear Energy cycle |
| **RELAP5** | Reactor Excursion and Leak Analysis Program |
| **Ri** | Richardson number |
| **RI** | V.G. Khlopin Radium Institute, St Petersburg |
| **RIA** | Reactivity initiated Aacident |
| **RIAR** | Research Institute of Atomic Reactors, Dimitrovgrad |
| **RO** | Reverse osmosis |
| **RPS** | Remote power sources |
| **RPS** | Reactor protection system |
| **RPSS** | Reactor power supply system |
| **RPV** | Reactor pressure vessel |
| **RTG** | Radioisotope thermoelectric generators |
| **RTIL** | Room-temperature ionic liquids |
| **RW** | Radioactive waste |
| **SA** | Severe accident |
| **SACSESS** | Safety of ACtinide SEparation proceSSes |
| **SAGD** | Steam-assisted gravity drainage |
| **SAMOFAR** | SAfety with the MOlten salt FAst Reactor |
| **SBD** | Safeguards-by-design |
| **SBO** | Station blackout |

| | |
|---|---|
| **SCBC** | Supercritical $CO_2$ Brayton cycle |
| **S-CO2** | Supercritical carbon dioxide |
| **SCRAM** | To shut down a reactor quickly, or to flee. Maybe “Safety Control Rods Activation Method” (A legend says that it means “Safety Control Rod Axe Man” because of the Chicago Pile having a man standing by to cut a rope with an ax to drop the control rod in place.) |
| **SDC** | Safety design criteria |
| **SF** | Spent fuel |
| **SFR** | Molten salt fast reactor |
| **SG** | Steam-generator |
| **SHX** | Secondary heat exchanger |
| **SIMMER-III** | Computer program |
| **SINAP** | Shanghai Institute of Applied Physics |
| **SKC** | Swedish Centre for Nuclear Technology |
| **SmAHTR** | Small modular advanced high-temperature reactor |
| **SMR** | Small modular reactor |
| **SNF** | Spent nuclear fuel |
| **S-PRISM** | Super Power Reactor Innovative Small Module |
| **SS** | Stainless steel |
| **SSC** | System structure and components |
| **SSEOS** | Soft Sphere Equation of State |
| **SSR** | Stable salt reactor |
| **Str** | Stirling engine |
| **SVF** | Salt volume fraction |
| **TAEK** | The Turkish Atomic Energy Commission |
| **TAP** | Transatomic Power |
| **TASL** | Track Analysis System Ltd |
| **TBP** | Tributyl phosphate |
| **TDS** | Total dissolved solids/salts |
| **TEA** | Thorium Energy Alliance |
| **TECDOC** | Technical document |
| **TEDE** | Total effective dose equivalent |
| **TEIAS** | Turkish Electricity Transmission Corporation |
| **TEMA** | Tubular Exchanger Manufacturers Association |
| **TFM** | Transient fission matrix |
| **TGA** | Thermogravimetric analysis |
| **Th-MSR** | Thorium molten salt reactor |
| **THORIMS-NES** | Thorium Molten Salt Nuclear Energy Synergetic System |
| **THORIMS-NES** | Thorium Molten Salt Nuclear Energy System |
| **TMFT** | Time-dependent Mean Field Theory |
| **TMI** | Three Mile Island |
| **TMSF-SF0** | Electrically heated simulator for TMSR-SF1 |
| **TMSR** | Thorium molten salt reactor |
| **TMSR-SF** | Thorium molten salt reactor—solid fuel |
| **TMSR-SF1** | TMSR-SF experimental test reactor |
| **TRIGA** | Training, research, isotopes, general atomics |
| **TRISO** | Tristructural-isotropic fuel particles |

| | |
|---|---|
| **TRU** | Trans uranium elements |
| **TSO** | Technical support organizations |
| **TU** | Technical University |
| **TU-Delft** | Technical University—Delft |
| **TWR** | Travelling wave reactor |
| **UCB/UC Berkeley** | University of California Berkeley |
| **UED** | Uranium Extraction Division |
| **UGM** | University of Gadjah Mada |
| **UNIST** | Ulsan National Institute of Science and Technology |
| **UNM** | University of New Mexico |
| **UNOMI** | Universally operable molten-salt reactor integrated |
| **U-Pu FMSR** | Fast molten salt reactor with U-Pu fuel |
| **US** | United States |
| **USNRC** | United States Nuclear Regulatory Commission |
| **UTK** | University of Tennessee Knoxville |
| **UU** | University of Utah |
| **UW-MAD** | University of Wisconsin—Madison |
| **V&V** | Validation and verification |
| **VHHC** | Vertical heater−horizontal cooler |
| **VHTR** | Very high-temperature reactor |
| **VNIIEF** | Research Institute of Experimental Physics, Sarov |
| **VNIIKHT** | Leading Research Institute of Chemical Technology, Moscow |
| **VNIINM** | A.A. Bochvar Institute of Inorganic Materials, Moscow |
| **VNIITP** | Research Institute of Technical Physics, Snezhinsk |
| **VSE** | Association of Swiss Electricity Producers |
| **VTT** | Valtion Teknillinen Tutkimuskeskus (State Technical Research Center, in Finnish) |
| **VVER** | Russian pressurized water reactor |
| **WGPu** | Weapons-grade plutonium |
| **XPREX** | X-ray pebble recirculation experiment |

# Index

*Note*: Page numbers followed by "*f*" and "*t*" refer to figures and tables, respectively.

WOODHEAD PUBLISHING SERIES IN ENERGY

*Molten Salt Reactors and Thorium Energy* is a comprehensive reference on the status of molten salt reactor (MSR) research and thorium fuel utilization.

There is growing awareness that nuclear energy is needed to complement intermittent energy sources and to avoid pollution from fossil fuels. Light water reactors are complex, expensive, and vulnerable to core melt, steam explosions, and hydrogen explosions, so better technology is needed. MSRs could operate safely at nearly atmospheric pressure and high temperature, yielding efficient electrical power generation, desalination, actinide incineration, hydrogen production, and other industrial heat applications.

**Coverage includes:**

- Motivation -- why are we interested?
- Technical issues – reactor physics, thermal hydraulics, materials, environment, ...
- Generic designs -- thermal, fast, solid fuel, liquid fuel, ...
- Specific designs – aimed at electrical power, actinide incineration, thorium utilization, ...
- Worldwide activities in 23 countries
- Conclusions

This book is a collaboration of 58 authors from 23 countries, written in cooperation with the International Thorium Molten Salt Forum. It can serve as a reference for engineers and scientists, and it can be used as a textbook for graduate students and advanced undergrads.

*Molten Salt Reactors and Thorium Energy* is the only complete review of the technology currently available, making this an essential text for anyone reviewing the use of MSRs and thorium fuel, including students, nuclear researchers, industrial engineers, and policy makers.

**Professor Dolan** has worked on nuclear technology and international relations issues for three universities, five national laboratories, and in China, India, Japan, Korea, and Russia. He has worked in industry (Phillips Petroleum) and served as Physics Section Head at the International Atomic Energy Agency in Vienna, where he facilitated international cooperation on research reactors, low energy accelerators, nuclear instrumentation, and nuclear fusion research, including organization of the semi-annual IAEA Fusion Energy Conferences. He has published textbooks on Fusion Research (Pergamon 1982) and Magnetic Fusion Technology (Springer 2013).

*Cover picture: Generic molten salt reactor diagram, showing graphite core (upper left), fuel tubes (yellow), drain tanks (lower left), intermediate salt loop (center), and energy conversion system (right). From Alvin Weinberg, Oak Ridge National Laboratory, 2004.*

ISBN 978-0-08-101126-3

9 780081 011263

ELSEVIER

WP
WOODHEAD
PUBLISHING
An imprint of Elsevier • elsevier.com